

Published in Journals: Energies, International Journal of Environmental Research and Public Health, Processes, Buildings and Atmosphere

Topic Reprint

Energy Efficiency, Environment and Health

Volume III

Edited by
Roberto Alonso González Lezcano,
Francesco Nocera and Rosa Giuseppina Caponetto

www.mdpi.com/topics



Energy Efficiency, Environment and Health—Volume III

Energy Efficiency, Environment and Health—Volume III

Editors

Roberto Alonso González Lezcano

Francesco Nocera

Rosa Giuseppina Caponetto

MDPI • Basel • Beijing • Wuhan • Barcelona • Belgrade • Manchester • Tokyo • Cluj • Tianjin



Editors

Roberto Alonso
González Lezcano
Departamento de
Arquitectura y Diseño,
Escuela Politécnica Superior,
Universidad CEU San Pablo,
Madrid, Spain

Francesco Nocera
Department of Civil
Engineering and Architecture,
University of Catania,
Catania, Italy

Rosa Giuseppina Caponetto
Department of Civil
Engineering and Architecture,
University of Catania,
Catania, Italy

Editorial Office

MDPI
St. Alban-Anlage 66
4052 Basel, Switzerland

This is a reprint of articles from the Topic published online in the open access journals *Energies* (ISSN 1996-1073), *International Journal of Environmental Research and Public Health* (ISSN 1660-4601), *Processes* (ISSN 2227-9717), *Buildings* (ISSN 2075-5309), and *Atmosphere* (ISSN 2073-4433) (available at: https://www.mdpi.com/topics/energy_health).

For citation purposes, cite each article independently as indicated on the article page online and as indicated below:

LastName, A.A.; LastName, B.B.; LastName, C.C. Article Title. <i>Journal Name</i> Year , <i>Volume Number</i> , Page Range.
--

Volume I

ISBN 978-3-0365-8226-9 (Hbk)

ISBN 978-3-0365-8227-6 (PDF)

Volume I-III

ISBN 978-3-0365-8220-7 (Hbk)

ISBN 978-3-0365-8221-4 (PDF)

© 2023 by the authors. Articles in this book are Open Access and distributed under the Creative Commons Attribution (CC BY) license, which allows users to download, copy and build upon published articles, as long as the author and publisher are properly credited, which ensures maximum dissemination and a wider impact of our publications.

The book as a whole is distributed by MDPI under the terms and conditions of the Creative Commons license CC BY-NC-ND.

Contents

About the Editors ix

Wojciech Krasodomski and Zygmunt Burnus

BTEX Emissions in the Logistics of Middle Distillates: Diesel Oil
Reprinted from: *Energies* **2022**, *15*, 3776, doi:10.3390/en15103776 1

Wei Xu, Jiahui Yi and Jinhua Cheng

The Heterogeneity of High-Quality Economic Development in China’s Mining Cities: A Meta Frontier Function
Reprinted from: *Int. J. Environ. Res. Public Health* **2022**, *19*, 6374, doi:10.3390/ijerph19116374 . . . 13

Adel Naseeb, Ashraf Ramadan and Sultan Majed Al-Salem

Economic Feasibility Study of a Carbon Capture and Storage (CCS) Integration Project in an Oil-Driven Economy: The Case of the State of Kuwait
Reprinted from: *Int. J. Environ. Res. Public Health* **2022**, *19*, 6490, doi:10.3390/ijerph19116490 . . . 37

Wenxiao Han, Xiaohua Chu, Sui Shi, Ling Zhao and Zhen Zhao

Practical Application-Oriented Energy Management for a Plug-In Hybrid Electric Bus Using a Dynamic SOC Design Zone Plan Method
Reprinted from: *Processes* **2022**, *10*, 1080, doi:10.3390/pr10061080 57

Xuechao Xia, Hui Sun, Zedong Yang, Weipeng Yuan and Dianyuan Ma

Decoupling Analysis of Rural Population Change and Rural Electricity Consumption Change in China
Reprinted from: *Int. J. Environ. Res. Public Health* **2022**, *19*, 6676, doi:10.3390/ijerph19116676 . . . 71

Yong Chen, Yaqi Liang, Hao Zhou, Qiaozhi Wang and Yanzhong Liu

Farmers’ Adaptive Behaviors to Heavy Metal-Polluted Cultivated Land in Mining Areas: The Influence of Farmers’ Characteristics and the Mediating Role of Perceptions
Reprinted from: *Int. J. Environ. Res. Public Health* **2022**, *19*, 6718, doi:10.3390/ijerph19116718 . . . 91

Bing Xia, Suocheng Dong, Zehong Li, Minyan Zhao, Dongqi Sun, Wenbiao Zhang and Yu Li

Eco-Efficiency and Its Drivers in Tourism Sectors with Respect to Carbon Emissions from the Supply Chain: An Integrated EEIO and DEA Approach
Reprinted from: *Int. J. Environ. Res. Public Health* **2022**, *19*, 6951, doi:10.3390/ijerph19116951 . . . 109

Chengju Wang, Juan Wang and Dan Norbäck

A Systematic Review of Associations between Energy Use, Fuel Poverty, Energy Efficiency Improvements and Health
Reprinted from: *Int. J. Environ. Res. Public Health* **2022**, *19*, 7393, doi:10.3390/ijerph19127393 . . . 135

Kayra Kurşun, Levent Özdemir and Hakan Ersoy

Performance Identification of a Steam Boiler Burner via Acoustic Analysis
Reprinted from: *Processes* **2022**, *10*, 1223, doi:10.3390/pr10061223 165

Zehong Li, Wenbiao Zhang, Bing Xia and Chunying Wang

Comparison of Life Cycle Environmental Impact between Two Processes for Silver Separation from Copper Anode Slime
Reprinted from: *Int. J. Environ. Res. Public Health* **2022**, *19*, 7790, doi:10.3390/ijerph19137790 . . . 177

Mengyao Lyu, Som V. Thomas, Heng Wei, Julian Wang, Tiina A. Reponen, Patrick H. Ryan and Donglu Shi Entrapment of Airborne Particles via Simulated Highway Noise-Induced Piezoelectricity in PMMA and EPDM Reprinted from: <i>Energies</i> 2022 , <i>15</i> , 4935, doi:10.3390/en15144935	189
Baofeng Su, Jiangbi Hu, Juncheng Zeng and Ronghua Wang Traffic Safety Improvement via Optimizing Light Environment in Highway Tunnels Reprinted from: <i>Int. J. Environ. Res. Public Health</i> 2022 , <i>19</i> , 8517, doi:10.3390/ijerph19148517 . . .	203
Shuang Wang, Yucheng Yan, Xueying Gao, Hefeng Zhang, Yang Cui, Qiusheng He, et al. Emission Characteristics and Health Risks of Volatile Organic Compounds (VOCs) Measured in a Typical Recycled Rubber Plant in China Reprinted from: <i>Int. J. Environ. Res. Public Health</i> 2022 , <i>19</i> , 8753, doi:10.3390/ijerph19148753 . . .	223
Wenbin Zhao, Fangshun Liu, Bo Liu, Yang Liu, Huaisheng Cao, Qing Tan and Jinfeng Wang Study on Permeability and Flame Retardancy of Coal Aerosol Atomized by Ultrasonic Wave Reprinted from: <i>Atmosphere</i> 2022 , <i>13</i> , 1415, doi:10.3390/atmos13091415	239
Yanfeng Xue, Yanyan Chen, Linxia Shi, Haotian Wu, Chao Zhang, Minghuang Cheng, et al. Lignite-Based N-Doped Porous Carbon as an Efficient Adsorbent for Phenol Adsorption Reprinted from: <i>Processes</i> 2022 , <i>10</i> , 1746, doi:10.3390/pr10091746	255
Jana Gerta Backes, Pamela Del Rosario, Dino Petrosa, Marzia Traverso, Tobias Hatzfeld and Edeltraud Günther Building Sector Issues in about 100 Years: End-Of-Life Scenarios of Carbon-Reinforced Concrete Presented in the Context of a Life Cycle Assessment, Focusing the Carbon Footprint Reprinted from: <i>Processes</i> 2022 , <i>10</i> , 1791, doi:10.3390/pr10091791	273
Xuyang Zhong, Zhiang Zhang, Wei Wu and Ruijun Zhang Estimating Space-Cooling Energy Consumption and Indoor PM _{2.5} Exposure across Hong Kong Using a City-Representative Housing Stock Model Reprinted from: <i>Buildings</i> 2022 , <i>12</i> , 1414, doi:10.3390/buildings12091414	291
John M. Polimeni, Mihaela Simionescu and Raluca I. Iorgulescu Energy Poverty and Personal Health in the EU Reprinted from: <i>Int. J. Environ. Res. Public Health</i> 2022 , <i>19</i> , 11459, doi:10.3390/ijerph191811459 . .	327
Agnieszka Czachura, Niko Gentile, Jouri Kanters and Maria Wall Identifying Potential Indicators of Neighbourhood Solar Access in Urban Planning Reprinted from: <i>Buildings</i> 2022 , <i>12</i> , 1575, doi:10.3390/buildings12101575	349
Bin Xu How to Efficiently Reduce the Carbon Intensity of the Heavy Industry in China? Using Quantile Regression Approach Reprinted from: <i>Int. J. Environ. Res. Public Health</i> 2022 , <i>19</i> , 12865, doi:10.3390/ijerph191912865 . .	375
Riyadh Almkhtar, Sally I. Hammoodi, Hasan Shakir Majdi and Khalid A. Sukkar Managing Transport Processes in Thermal Cracking to Produce High-Quality Fuel from Extra-Heavy Waste Crude Oil Using a Semi-Batch Reactor Reprinted from: <i>Processes</i> 2022 , <i>10</i> , 2077, doi:10.3390/pr10102077	399
Juan M. Ros-García The Study of Quality of Life as a Guide to Urban Regeneration Analysis of Estepona's New City Hall as a Sustainable Model Reprinted from: <i>Buildings</i> 2022 , <i>12</i> , 1699, doi:10.3390/buildings12101699	415

Xin Yu, Ling Zhao, Kun Zhang and Hongqiang Guo A Shift Schedule to Optimize Pure Electric Vehicles Based on RL Using Q-Learning and Opt LHD Reprinted from: <i>Processes</i> 2022 , <i>10</i> , 2132, doi:10.3390/pr10102132	443
Xingyuan Wang, Yingying Du, Yun Liu and Shuyang Wang Telling You More Fluently: Effect of the Joint Presentation of Eco-Label Information on Consumers' Purchase Intention Reprinted from: <i>Int. J. Environ. Res. Public Health</i> 2022 , <i>19</i> , 13713, doi:10.3390/ijerph192013713 .	465
Ewa Kochanska, Katarzyna Wozniak, Agnieszka Nowaczyk, Patrícia J. Piedade, Marilena Lino de Almeida Lavorato, Alexandre Marcelo Almeida, et al. Global Ban on Plastic and What Next? Are Consumers Ready to Replace Plastic with the Second-Generation Bioplastic? Results of the Snowball Sample Consumer Research in China, Western and Eastern Europe, North America and Brazil Reprinted from: <i>Int. J. Environ. Res. Public Health</i> 2022 , <i>19</i> , 13970, doi:10.3390/ijerph192113970 .	485
Sayahnya Roy, Alexei Sentchev, Marc Fourmentin and Patrick Augustin Machine Learning and Deterministic Methods for Detection Meteorological Phenomena from Ground Measurements: Application for Low-Level Jet and Sea-Breeze Identification in Northern France Reprinted from: <i>Atmosphere</i> 2022 , <i>13</i> , 1873, doi:10.3390/atmos13111873	511
Zhiqun Sun, Yanbo Wu, Hao Sun, Dian Zhou, Yang Lou and Lei Qin The Impact of Building Clean Energy Consumption on Residents' Subjective Well-Being: Evidence from China Reprinted from: <i>Buildings</i> 2022 , <i>12</i> , 2037, doi:10.3390/buildings12112037	525
Yu Zhang and Meiqi Dai Analysis of the Cooling and Humidification Effect of Multi-Layered Vegetation Communities in Urban Parks and Its Impact Reprinted from: <i>Atmosphere</i> 2022 , <i>13</i> , 2045, doi:10.3390/atmos13122045	543
Vasyl Mateichyk, Nataliia Kostian, Mirosław Smieszek, Jakub Mosciszewski and Liudmyla Tarandushka Evaluating Vehicle Energy Efficiency in Urban Transport Systems Based on Fuzzy Logic Models Reprinted from: <i>Energies</i> 2023 , <i>16</i> , 734, doi:10.3390/en16020734	557
Xianning Wang, Zhengang Ma, Jiusheng Chen and Jingrong Dong Can Regional Eco-Efficiency Forecast the Changes in Local Public Health: Evidence Based on Statistical Learning in China Reprinted from: <i>Int. J. Environ. Res. Public Health</i> 2023 , <i>20</i> , 1381, doi:10.3390/ijerph20021381 . . .	579
Eugene Seo and Wanseok Yang Evaluating Smart Home Services and Items: A Living Lab User Experience Study Reprinted from: <i>Buildings</i> 2023 , <i>13</i> , 263, doi:10.3390/buildings13010263	599
Miroslava Sinčák and Jana Sedlakova-Kadukova Hypomagnetic Fields and Their Multilevel Effects on Living Organisms Reprinted from: <i>Processes</i> 2023 , <i>11</i> , 282, doi:10.3390/pr11010282	621
Junjian Wang, Zijun Li, Gang Li and Yu Xu Heat Hazard Control in High-Temperature Tunnels: Experimental Study of Coupled Cooling with Ventilation and Partial Insulation for Synergistic Geothermal Extraction Reprinted from: <i>Int. J. Environ. Res. Public Health</i> 2023 , <i>20</i> , 1941, doi:10.3390/ijerph20031941 . . .	635

About the Editors

Roberto Alonso González Lezcano

Accredited as full professor by AQU Catalunya (March 2023). Extraordinary Doctorate Award. San Pablo CEU University Tenured Professor at the Department of Architecture and Design, the area of Building Systems, within the Institute of Technology of Universidad CEU San Pablo. Coordinator of the Mechanical Systems area. Professor Accredited by ANECA in the position of Tenured Professor. Two six-year research periods at CNEAI (last period 2016–2021). Coordinator of the post-graduate degree of Energy Efficiency and Mechanical Systems in Buildings and Coordinator of the Laboratory of Building Systems within Universidad CEU San Pablo. Member of the PhD Program in “Health Science and Technology” and the PhD Program “Composition, History and Techniques pertaining to Architecture and Urbanism”, where he is the Coordinator of the Construction, Innovation and Technology line and Coordinator of the complementary training program “Methodology of technical and statistical experimentation”. Ángel Herrera Award for the best research work in the areas of Architecture and Engineering for the year 2020/2021 in the XXV Edition of the Ángel Herrera Awards of the CEU San Pablo University. Coordinator of the Wind Energy Section within the master’s course in Renewable Energy of the Institute of Technology (Universidad CEU San Pablo).

Architecture and Solidarity Award (2019) of the 1st Housing Excellence Awards of the newspaper La Razón for the VEM Project financed by Airbus Defense and Space and developed at the CEU San Pablo University. Award won due to the VEM project developed with the AIRBUS company, 2015. Member of the Team Crew and Advisor of the Universidad Autónoma de Occidente and Universidad de San Buenaventura in the MIHOUSE Project team in the Solar Decathlon Latin American and Caribbean 2015.

Francesco Nocera

Qualified as a Full Professor through the Italian National Scientific Qualification, sector 09/C2—Building Physics and Energy Systems in the year 2020. He is the author of more 200 research papers dealing with several research topics experimentally as well as numerically and analytically, including basic thermodynamics, thermo-fluid dynamics, heat transmission, lighting, acoustics, the rational use of energy, the use of renewable energy sources, buildings energy analysis, IEQ, UHI, and HVAC systems.

He was a postdoctoral researcher in Fluid Dynamics Modeling of Aeraulic Ducts, University of Catania (01-10-2007–31-10-2007) and gained a Ph.D. in Applied Environmental Physics, University di Palermo (01-10-2003–10-02-2006).

Scientist responsible for the Computer Laboratory at Special Didactic Structures of Architecture Siracusa (2010–) and responsible for the Energetic Sustainability and Environmental Control (SECA) Laboratory at Special Didactic Structures Architecture (2020–). Rector’s Delegate for the UN Sustainable Development Solutions Network (SDSN) (17-05-2018; 02-07-2019). Member of the Quality Management Board of the Architecture Degree Course, University of Catania (2018–2019) Member of the Joint Committee of the DICAR Department, the University of Catania (2020–). Secretary of Special Didactic Structure of Architecture, University of Catania (2020–2021). Visiting Professor at the University of Valladolid (2020) Scientific Responsible of Memorandum of understanding, cooperation agreement of general interest: CEU Cardenal Herrera University (Spain), Faculty of Urban Construction and Environmental Engineering of Chongqing University (China), Applied Science and Arts of Southern Switzerland University (SUPSI), Lega Ambiente, EURAC center.

Member of International Building Physics Association—IABP (2018). Member of the International Commission on Illumination (CIE)—UNI/CT 023/GL 02 Lighting of Work Places and Schools.

Rosa Giuseppina Caponetto

Qualified as a Full Professor through the Italian National Scientific Qualification, sector 08/C1—Design and Technological Architecture Design, in the year 2022. Her main research topics are: materials and technologies for sustainable construction; the durability of building materials and components; the experimental assessment of building materials' performance; self-build; knowledge of local building tradition and innovative scenarios; the assessment of buildings' sustainability; and energy and seismic upgrading of existing buildings.

She is the scientific director of the LaTPrE laboratory, Laboratory of Building Production Technologies (University of Catania). She is a member of the "Smart Cities & Communities" National Laboratory by CINI (focus group: "ICT for Smart Energy & Smart Buildings"). She is the head of operations management and a member of the scientific committee of "MuRa", Museum of Representation (University of Catania), as well as a member of the "Technical College for Building Consultancy" (University of Catania).

She is the co-inventor of the patent idea entitled "Anti-seismic construction system: technology and production process". She has developed several research works in collaboration with national research institutes (e.g., CNR) and/or with some municipalities (cooperative agreements).

She has been involved in the following projects: the VVITA project "Modernizing Learning and Teaching for Architecture through Smart and Long-lasting Partnerships leading to sustainable and inclusive development strategies to Vitalize Heritage Villages through Innovative Technologies", ERASMUS + KA2 program funded by the European Community (2016–2019), U.O Scientific Responsible; the EWAS project "An Early Warning System for cultural-heritage", funded by the PNR program (2017–2022).

BTEX Emissions in the Logistics of Middle Distillates: Diesel Oil

Wojciech Krasodowski * and Zygmunt Burnus

The Oil and Gas Institute-National Research Institute, Lubicz 25A, 31-503 Kraków, Poland; burnus@inig.pl

* Correspondence: wojciech.krasodowski@inig.pl

Abstract: Besides technological processes; logistics; and the use of petrol and light solvents, which are widely known as pollutants, the sources of BTEX hydrocarbon contributing to air pollution may also include other petroleum products and fuels that feature higher boiling points and that have not yet been associated with this issue. In this study, the contents of benzene; toluene; ethylbenzene; and o-, m-, and p-xylene were evaluated in 25 commercial samples of diesel oils; the gaseous phase in thermodynamic equilibrium with liquid diesel oil at 40 °C was then evaluated. Based on the experimental results, it was found that benzene concentration in the gaseous phase is five to more than fifteen times higher than the limits set by regulations for benzene concentration in the air at a work place (1.6 mg/m³) and cannot be compared with the limits set by regulations for annual average basal levels of benzene concentration in the air (5 µg/m³). The research revealed that diesel oil is a potential source of environmental contamination from BTEX hydrocarbons, in particular benzene.

Keywords: diesel oil; BTEX emission; air pollution

Citation: Krasodowski, W.; Burnus, Z. BTEX Emissions in the Logistics of Middle Distillates: Diesel Oil. *Energies* **2022**, *15*, 3776. <https://doi.org/10.3390/en15103776>

Academic Editors: Francesco Nocera, Roberto Alonso González Lezcano and Rosa Giuseppina Caponetto

Received: 27 April 2022

Accepted: 18 May 2022

Published: 20 May 2022

Publisher's Note: MDPI stays neutral with regard to jurisdictional claims in published maps and institutional affiliations.



Copyright: © 2022 by the authors. Licensee MDPI, Basel, Switzerland. This article is an open access article distributed under the terms and conditions of the Creative Commons Attribution (CC BY) license (<https://creativecommons.org/licenses/by/4.0/>).

1. Introduction

In Europe, air pollution is perceived to be the second biggest environmental problem after climate change [1]. The directives related to air quality presented by the European Commission [2,3], the European Parliament [4], and national documents [5] set the expectations for effective measures that abate air pollution and its effects. The emission of VOC hydrocarbons, in particular benzene, toluene, ethylbenzene, and xylene (BTEX), to the atmosphere is an especially important issue. In the European Union, benzene emissions are monitored by the European Environment Agency (EEA) [6], while in Poland, the Chief Inspectorate of Environmental Protection is responsible for their monitoring [7].

In Poland, this issue is regulated by a few pieces of legislation, the first of which is an act [8] that specifies the general requirements. Subsequent regulations have specified a threshold limit value (TLV) of benzene concentration in the air [9], with an annual average basal level of 5 µg/m³ and with an average level in a place of work of 1.6 mg/m³ [10,11].

Monoaromatic hydrocarbons such as benzene, toluene, ethylbenzene, and xylenes (also known as BTEX) are the source of many adverse health effects, such as asthma; dizziness; tiredness; and irritation of the eyes, nose, and throat. Contact with these substances can also cause nausea and other non-specific health symptoms [12]. Negative health effects from BTEX may be significant even at low concentrations in the case of prolonged exposure [13]. Benzene is considered a special case. The International Agency for Research on Cancer (IARC) classified benzene as a ‘carcinogen for people’ (group 1) [14] based on confirmed evidence that this compound causes acute granulocytic leukaemia. Contrary to benzene, toluene was classified under group 3 (not classified due to its carcinogenic nature for people).

The most frequent case of exposure to BTEX is the inhalation of vapours, which is facilitated by the physical properties of these compounds, in particular their low boiling points and high vapour pressures under standard environmental conditions [15].

BTEX hydrocarbons, xylenes in particular, are environmental pollutants as well as ozone precursors contributing to adverse atmospheric warming [16]. In the atmosphere, BTEX is subject to degradation, mainly as a result of photolysis and/or chemical reactions with reactive structures, such as OH• radicals ('day reactions') and NO• nitrate radicals ('night reactions'). Other free radicals are formed in both reactions, such as organic peroxide (ROO•) and hydrogen peroxide (HOO•) radicals, which promote the formation of nitrogen oxides (NO_x), which are ozone precursors that contribute to increased amount of tropospheric ozone. BTEX also plays a very important role in other chemical processes that occur in the atmosphere. They are considered precursors of other strongly oxidising substances, such as peroxyacetyl nitrate (PAN); they also contribute to the formation of secondary organic aerosols (SOA) [17,18].

A few main sources may be assigned to BTEX emissions into the air. The first type of source is stationary, such as fuel stations, petrol stations, vehicle service workshops, industrial plants, and refineries; the second source is strictly related to transport and traffic [19]. The combustion processes of raw materials such as petroleum and gas as well as forest fires may be defined as a separate group [20].

Benzene exists naturally in fossil fuels and is produced as a result of natural processes or human activity related to the combustion of organic matter, such as wood, coal, and petroleum products. The natural sources of benzene emissions are estimated to be 3–5%, while anthropogenic sources account for more than 90% (petrol vapours, exhaust gas, paints, and chemical production) [21].

Toluene exists naturally as a component of petroleum and is the main aromatic component of petrol, which contains approx. 5–7 wt.% of toluene. It is released during the production of petrol and other fuels from petroleum, during the production of coke from coal, and as a by-product of styrene production. It is used as a semi-finished product in the petrochemical industry [21].

Ethylbenzene is naturally present in petroleum. It is also a by-product of biomass combustion. Ethylbenzene is almost exclusively (>99%) used as a semi-finished product in the production of styrene monomer. Ethylbenzene emissions are related to the logistics of fuels and solvents, and to petrol combustion [21].

Xylenes exist in the environment as a mixture of *ortho*, *meta*, and *para* isomers. Xylenes exist naturally in petroleum and coal tar. Xylenes are released to the atmosphere primarily as emissions from industrial sources (e.g., refineries, or petrochemical and chemical plants) and emissions from internal combustion engines in cars [21].

Besides technological processes; logistics; and the use of petrol and light solvents, which are widely known as pollutants, the sources of VOC pollution may also include other petroleum products and fuels that feature higher boiling points and that have not yet been associated with this issue. It is necessary to recognize the scale of the problem to start effectively monitoring this problem and to develop prevention methods.

Hydrocarbon fractions with a declared initial boiling point above 150 °C contain small amounts of lighter fractions. This causes the gaseous phase remaining in equilibrium with the liquid phase (e.g., in tanks) to be enriched with these components. This results from Raoult's law.

Because of the range of the boiling point, no study has yet considered the potential threat of BTEX hydrocarbons from diesel oil, for which the typical range of boiling points is 160–360 °C, in detail.

2. Materials and Methods

Table 1 presents the selected properties of the 25 samples of commercial diesel oils used in the experiments.

Table 1. Properties of the studied diesel oils (measured by INIG-PIB).

Determined Parameter	Unit	Diesel Oil																									
		1	2	3	4	5	6	7	8	9	10	11	12	13	14	15	16	17	18	19	20	21	22	23	24	25	
Cetane number	-	51.5	53.1	51.7	52.3	52.0	52.3	52.0	52.4	52.9	54.1	52.5	52.5	51.7	52.0	51.8	52.1	51.7	52.4	51.9	51.8	51.5	51.8	52	52.4	52.3	
Density at 150 °C	kg/m ³	835.7	832.6	829.0	829.9	837.5	833.9	829.4	830.7	835.6	832.8	831.4	832.6	835.8	835.7	835.5	828.2	834.2	836.0	835.9	835.0	836.4	835.8	835.9	831.3	832.9	
Ignition temperature	°C	62.0	64.0	64.0	58.0	64.5	61.5	60.5	61.5	62.5	59.5	60.5	62.5	61.5	63.5	59.5	60.5	64.5	64.5	62.5	63.5	62.5	62.5	62.5	59.5	61.5	
FAME content	%(V/V)	5.9	6.9	6.8	6.7	6.4	6.4	6.3	6.4	6.5	<0.05	6.7	6.6	6.7	6.7	6.6	2.63	3.9	6.4	6.6	6.7	6.6	6.7	6.7	6.4	6.2	
Fractional composition:																											
up to 250 °C distils	%(V/V)	37.6	37.0	41.2	37.1	37.3	37.7	39.5	38.8	36.2	39.8	36.1	37.8	39	38.7	39.1	40.3	37.6	36.1	38.5	38.4	37.7	38.5	38.5	38.3	39.2	
up to 350 °C distils	%(V/V)	94.4	93.5	94.2	91.4	94.2	92.6	91.9	92.4	93.6	93.5	91.4	92.8	93.4	93.3	93.6	91.6	93.7	93.9	93.3	93.6	94.9	93.4	93.4	92.2	93.2	
95 % (V/V) distils up to	°C	351.9	354.5	353.8	359.8	352.8	359.3	360.7	358.9	354.2	355.7	363.3	359.4	355.6	356.7	354.9	363	355.4	353.9	356.2	354.7	357	356.4	356.3	359.4	365.3	

The analysis was carried out on a Clarus 500 gas chromatograph with a mass detector (GCMS) (PerkinElmer, Waltham, MA, USA) equipped with a Phenomenex polar capillary column Zebron ZB-50 0.25 μm that was 30 m long with a 0.25 mm inner diameter, with a 50% phenyl/50% dimethylpolysiloxane stationary phase and a quadruple mass detector.

The tests were carried out in accordance with the following procedure.

Approximately 4 cm^3 of the tested diesel oil was introduced to a 9 cm^3 test tube and tightly closed with a plastic septum. The test tube was conditioned at 40 $^\circ\text{C}$ for 2 h; a gas syringe was then used to collect 200 μL of the sample in the gaseous phase, which was analysed on the Clarus 500 GCMS chromatograph. The temperature programme of the separation maintained an initial temperature of 40 $^\circ\text{C}$ for 10 min before the column was heated to 220 $^\circ\text{C}$ at a rate of 15 $^\circ\text{C}/\text{min}$; the final temperature was maintained for another 10 min. Helium 5.0 was used as the carrier gas. The mass detector worked in the selected ion recording (SIR) mode, recording selected molecular weights with the summary signal originating from three ions—78 Da (benzene), 92 Da (toluene, xylenes, and ethylbenzene), and 106 Da (xylenes and ethylbenzene)—or in the total ion chromatogram (TIC) mode, recording all weights from a specified range. The ion weights recorded in the experiment ranged from 5 to 450 Da.

3. Results

The following plan for the experiments was selected based on a literature review.

The contents of benzene and toluene, and the total amounts of ethylbenzene and the o-, m- and p-xylenes were evaluated in 25 samples of various commercial diesel oils. The gaseous phases of those samples were then analysed in thermodynamic equilibrium with the liquid phase at 40 $^\circ\text{C}$. The potential threat of BTEX emission during diesel oil use and during logistics was assessed with an analysis of the results.

Examples of the chromatograms of the gaseous phase sample collected from diesel oil no. 16 are presented below; they were recorded in TIC mode (Figure 1) and SIR mode (Figure 2). The retention times for the compounds in question (Figure 2) were 4.22 min, 8.33 min, 12.89 min, 13.04 min, and 13.82 min for benzene, toluene, ethylbenzene, m-xylene, p-xylene, and o-xylene, respectively. For the purpose of this study, due to partial overlap in the peaks of ethylbenzene and the m- and p-xylenes, the total contents of ethylbenzene and all xylenes were evaluated. The peaks originating from benzene and toluene are not visible in the chromatogram recorded in TIC mode (Figure 1). In the case of benzene, it was obscured by the peaks of isomeric octanes with retention times of 4.15 min and 4.33 min. In both cases, in the summary spectrum of masses for these chromatographic peaks (Figures 3 and 4)—in addition to signals of fragmentation ions characteristic of octanes and the signal of molecular octane ion (114 Da)—weak signals were observed to originate from the ion of molecular benzene (78 Da).

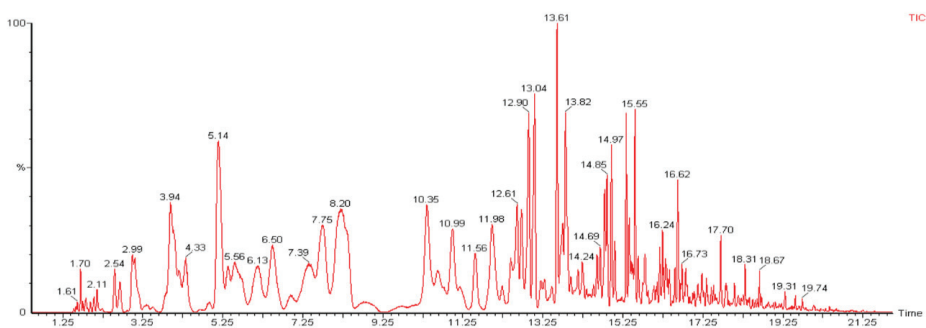


Figure 1. Chromatogram of a sample of diesel oil no. 16, recorded in TIC mode.

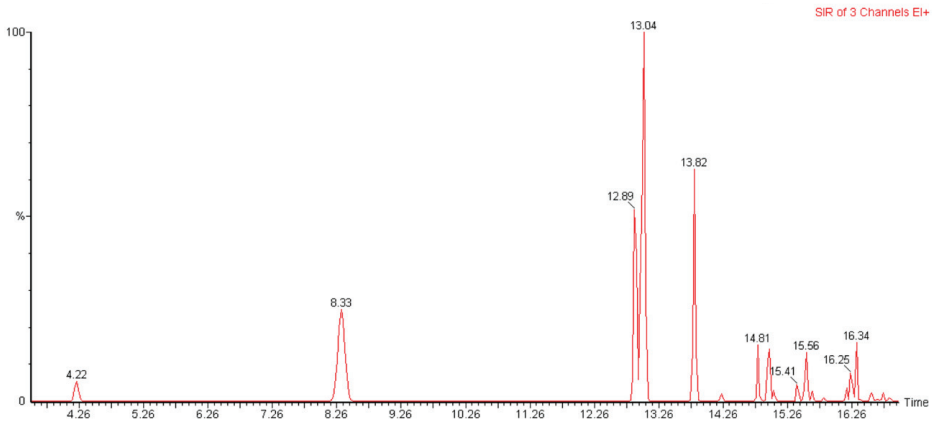


Figure 2. Chromatogram of a sample of diesel oil no. 16, recorded in SIR mode, for three masses: 78 Da, 92 Da, and 106 Da.

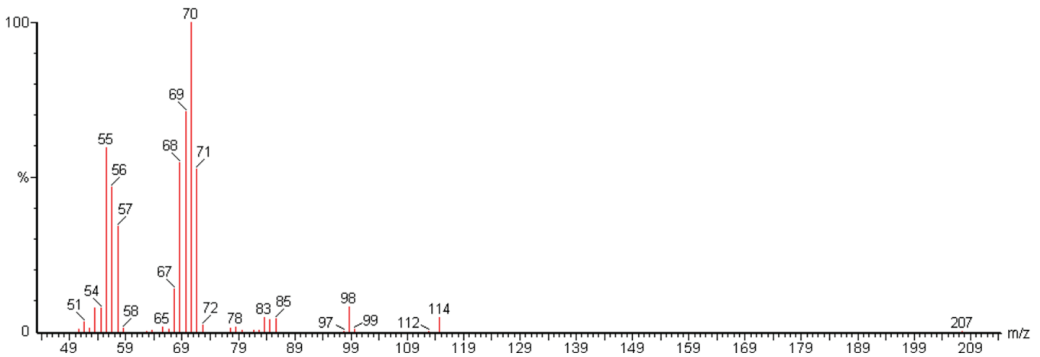


Figure 3. MS spectrum for the peak with a retention time of 4.15 min.

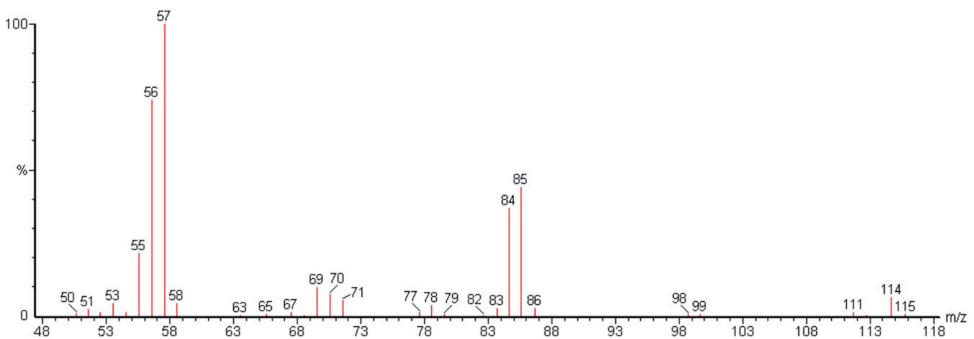


Figure 4. MS spectrum for the peak with a retention time of 4.33 min.

In the case of toluene, the chromatographic peak originating from it was obscured by a broad peak originating from one or more nonane isomers (retention time of 8.20 min). In the summary mass spectrum (Figure 5) for this chromatographic peak—apart from the signals of fragmentation ions characteristic of nonane and the signal of a molecular ion (128 Da)—a weak signal was observed to originate from a molecular ion of toluene (92 Da).

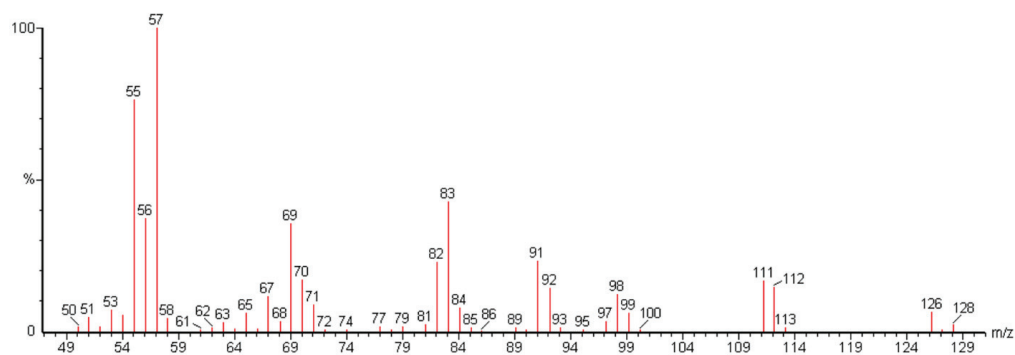


Figure 5. MS spectrum for the peak with a retention time of 8.20 min.

On the chromatogram recorded in TIC mode, for retention times ranging from 12 to 14 min, four peaks were clearly visible, of which three corresponded to the retention times of ethylbenzene, a mixture of *m*- and *p*-xylene, and *o*-xylene. The summary mass spectra (Figures 6–8) confirm the good separation of those compounds from other components in the hydrocarbon matrix. In addition, for retention times between 12 and 14 min, a clear peak of another hydrocarbon was observed for a retention time of 13.61 min. The MS spectrum (Figure 9) shows that it originated from a branched decane.

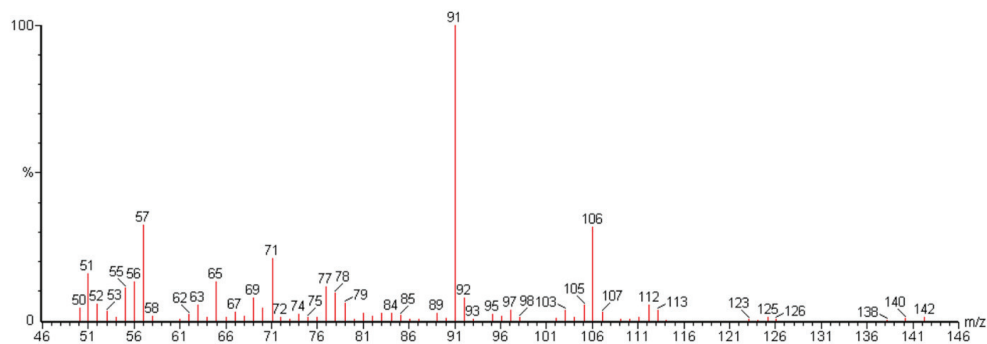


Figure 6. MS spectrum for the peak with a retention time of 12.89 min.

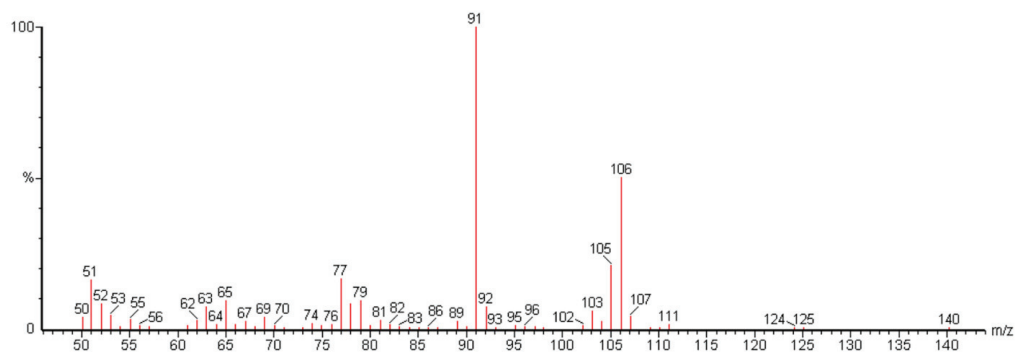


Figure 7. MS spectrum for the peak with a retention time of 13.04 min.

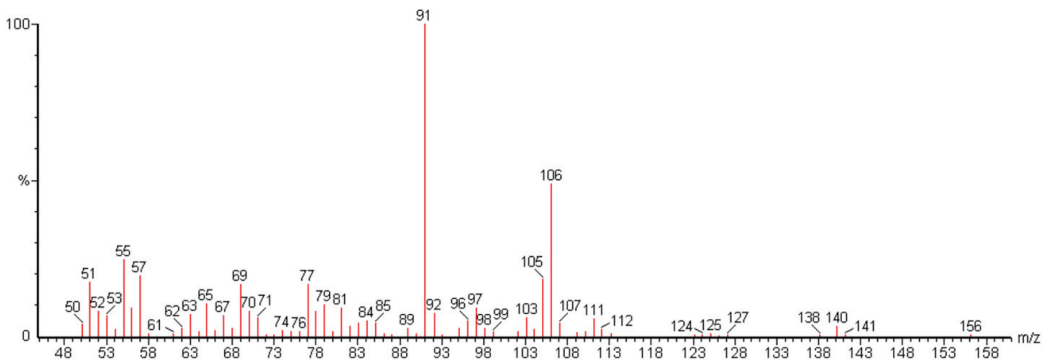


Figure 8. MS spectrum for the peak with a retention time of 13.82 min.

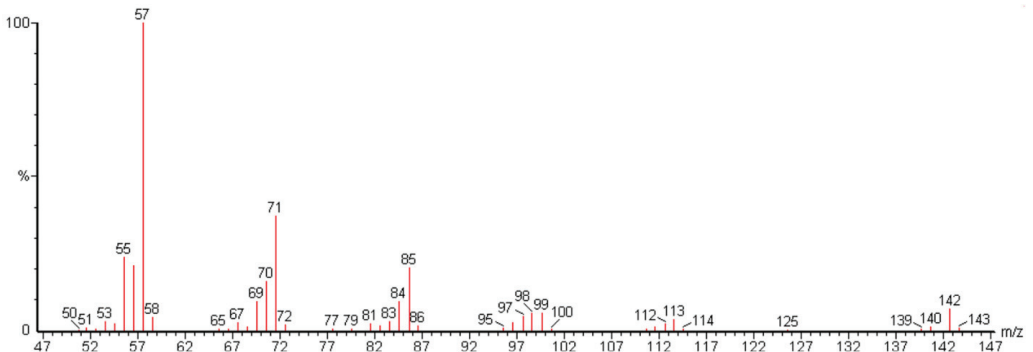


Figure 9. MS spectrum for the peak with a retention time of 13.61 min.

Table 2 presents the measurements of BTEX concentrations in the liquid and gaseous phases of diesel oil in equilibrium at a temperature of 40 °C. In the case of benzene, the concentration present in the liquid phase of the samples ranged from approx. 8 to approx. 27 mg/dm³, while that in the gaseous phase ranged from approx. 7 to approx. 25 mg/m³.

In the case of toluene, its concentration in the liquid phase of the samples ranged from approx. 140 to more than 600 mg/dm³, while that in the gaseous phase ranged from approx. 90 to approx. 230 mg/m³.

The total xylene and ethylbenzene content of the liquid phase in the samples ranged from approx. 1600 to approx. 3500 mg/dm³, while that in the gaseous phase ranged from approx. 220 to more than 500 mg/m³.

Raoult's and Dalton's laws control the composition of a gaseous phase in equilibrium with mixtures of liquids that do not react with each other. For a perfect solution, the partial pressure of a single component is described by the following formula:

$$p_i = x_i * p_i^*$$

where p_i is the partial pressure of component i in the gaseous phase in equilibrium with the liquid phase, x_i is the mole fraction of component i in the liquid phase (solution), and p_i^* is the equilibrium pressure of a pure component's vapours at a given temperature.

When the components of the solution reach thermodynamic equilibrium, the total vapour pressure above the solution p may be described by the following formula:

$$p = \sum_i x_i * p_i^*$$

Table 2. BTEX concentrations in liquid and gaseous phases of diesel oil in equilibrium at a temperature of 40 °C.

Diesel Oil	Benzene		Toluene		Xylenes + Ethylbenzene	
	Liquid Phase	Gaseous Phase	Liquid Phase	Gaseous Phase	Liquid Phase	Gaseous Phase
	mg/dm ³	mg/m ³	mg/dm ³	mg/m ³	mg/dm ³	mg/m ³
1	18.0	11.9	310	108	1906	227
2	14.2	19.5	242	157	1819	319
3	18.1	24.5	386	203	2474	402
4	11.7	15.4	154	148	2378	521
5	25.7	23.5	448	163	2474	291
6	14.4	24.6	632	201	3213	225
7	14.5	9.3	157	87	2697	352
8	11.4	12.4	151	116	2337	322
9	18.0	23.6	308	177	1643	321
10	22.3	23.6	346	203	2440	364
11	8.2	6.7	141	116	2469	460
12	16.8	15.4	271	155	2500	391
13	26.5	15.4	459	131	2439	243
14	14.3	20.6	302	234	1817	404
15	18.1	22.8	423	211	2185	357
16	11.6	8.2	221	132	3513	514
17	16.7	16.5	211	155	3513	313
18	15.4	14.8	254	155	1748	300
19	23.6	21.2	567	209	3073	287
20	27.8	17.9	634	192	3505	340
21	20.5	18.9	393	189	2622	344
22	20.5	17.7	421	188	2139	321
23	22.3	19.8	452	212	2688	389
24	11.9	8.1	237	107	2848	317
25	15.7	13.4	245	151	2307	360

Table 3 presents the equilibrium pressures of pure BTEX vapours p_i^* for the temperature at which the experiment was carried out, and for 10 °C and 25 °C, which are typical of the Central European climate.

Table 3. Equilibrium vapour pressures of pure BTEX components at given temperatures.

Pressure of Pure Hydrocarbon Vapours Being in Equilibrium with Liquid Phase *						
Temp. (°C)	Benzene (kPa)	Toluene (kPa)	O-Xylene (kPa)	M-Xylene (kPa)	P-Xylene (kPa)	Ethylbenzene (kPa)
10	6.807	1.678	0.344	0.451	0.472	0.502
25	12.196	3.827	0.883	1.118	1.186	1.269
40	24.826	7.935	2.051	2.529	2.679	2.875

* calculated from the Antoine equation ($\log_{10}(P) = A - (B/(T + C))$) based on data from the National Institute of Standards and Technology (NIST) [22–26].

Diesel oil is a complex mixture of a large number of hydrocarbons at various concentrations, and therefore, the above description cannot be easily translated into an assessment of correlations between BTEX concentrations in the diesel oils under study and their concentrations in the accompanying gaseous phase.

Figures 10–12 depict the correlations between the composition of a gaseous phase in equilibrium with different mixtures of liquids.

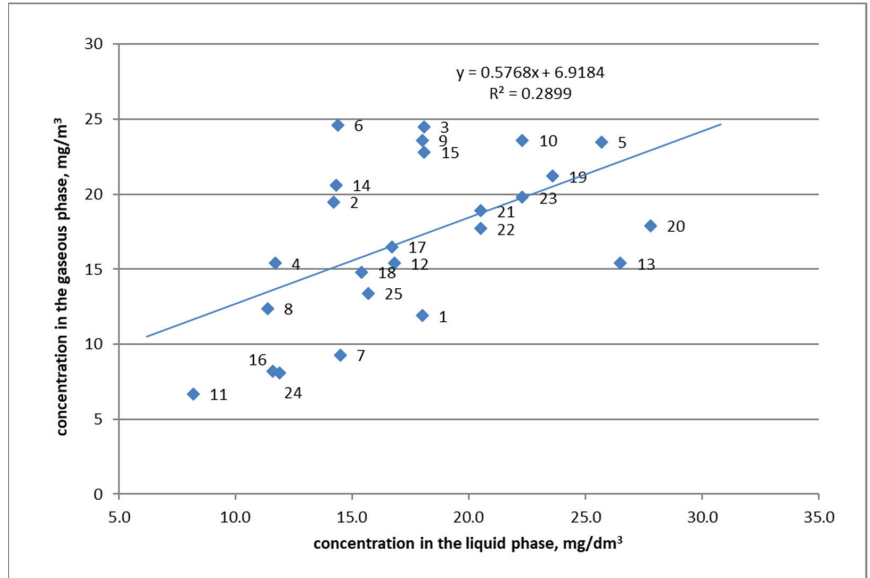


Figure 10. Concentration of benzene in the liquid and gaseous phases of diesel oil in equilibrium.

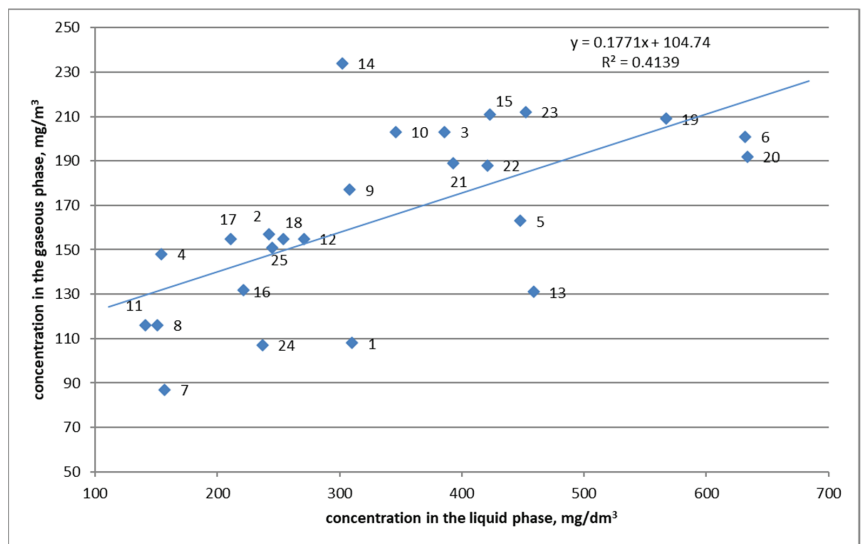


Figure 11. Concentration of toluene in the liquid and gaseous phases of diesel oil in equilibrium.

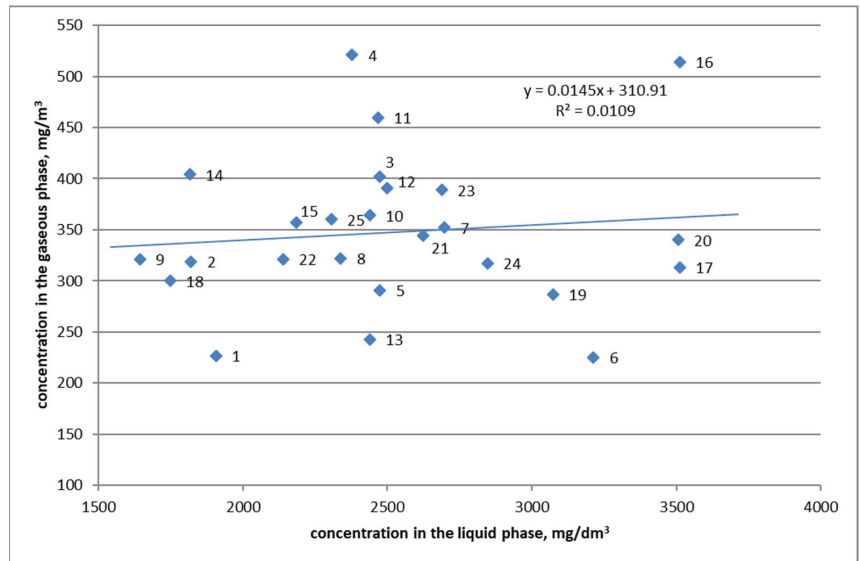


Figure 12. Total concentration of xylenes and ethylbenzene in the liquid and gaseous phases of diesel oil in equilibrium.

For benzene and toluene, a weak relationship was observed (Figures 10 and 11) between their concentrations in the liquid and gaseous phases: an increase in the hydrocarbon concentration in the liquid phase results in an increased concentration in the gaseous phase. In the case of benzene, the slope (coefficient a) is about 0.6, and in the case of toluene, the slope is about 0.2. The coefficients of determination R^2 are 0.3 and 0.4 accordingly. However, for the total xylene and ethylbenzene, practically no systematic relationship was observed (Figure 12); the slope is lower than 0.015; and R^2 is about 0.0, which was most likely related to the presence of varying amounts of other hydrocarbon components with similar equilibrium pressures in the studied diesel oils.

4. Discussion

In these experiments, the benzene concentration in the gaseous phase in equilibrium with diesel oil was found to be from five to more than fifteen times higher than the TLV of benzene concentration in the air for a place of work, which is 1.6 mg/m^3 , and cannot be compared with the TLV of benzene concentration in the air on an annual average basis, which is $5 \text{ }\mu\text{g/m}^3$.

This research revealed that diesel oil is a potential source of environmental contamination with BTEX hydrocarbons, in particular with benzene. In the literature, the combustion processes of middle distillate fuels as a source of BTEX emissions into the air have been described as a concern. No work on such emissions in logistics and the storage of middle distillate fuels was found. The above observations should draw the attention of the authorities involved in environmental protection and in occupational health and safety to the necessity of considering the issue of VOC emission (including BTEX) accompanying the logistics of middle-distillate fuels, including diesel oil.

Author Contributions: Conceptualization, W.K.; methodology, W.K. and Z.B.; validation, Z.B.; formal analysis, W.K. and Z.B.; investigation, W.K. and Z.B.; writing—original draft preparation, W.K.; writing—review and editing, W.K.; visualization, W.K. All authors have read and agreed to the published version of the manuscript.

Funding: This research received no external funding.

Institutional Review Board Statement: Not applicable.

Informed Consent Statement: Not applicable.

Data Availability Statement: Not applicable.

Acknowledgments: This research was financially supported by the Polish Ministry of Education and Science within statutory funding for the Oil and Gas Institute-National Research Institute, project no. 0102/TA/21.

Conflicts of Interest: The authors declare no conflict of interest.

References

1. A Clean Planet for All—A European Strategic Long-Term Vision for a Prosperous, Modern, Competitive and Climate Neutral Economy. Available online: <https://eur-lex.europa.eu/legal-content/EN/TXT/PDF/?uri=CELEX:52018DC0773> (accessed on 7 December 2021).
2. EU Directive 2004/107/WE. Available online: <https://eur-lex.europa.eu/LexUriServ/LexUriServ.do?uri=OJ:L:2005:023:0003:0016:PL:PDF> (accessed on 7 December 2021).
3. EU Directive 2008/50/WE. Available online: <https://eur-lex.europa.eu/legal-content/PL/TXT/PDF/?uri=CELEX:32008L0050&from=PL> (accessed on 7 December 2021).
4. Implementation of the Ambient Air Quality Directives P9_TA(2021)0107. Available online: <https://eur-lex.europa.eu/legal-content/EN/TXT/HTML/?uri=CELEX:52021IP0107&from=PL> (accessed on 7 December 2021).
5. Krajowy Program Ograniczania Zanieczyszczenia Powietrza. Available online: <https://bip.mos.gov.pl/strategie-plany-programy/krajowy-program-ograniczania-zanieczyszczenia-powietrza/> (accessed on 7 December 2021).
6. Air Quality in Europe—2020 Report; EEA Report No 09/2020. Available online: <https://www.eea.europa.eu/publications/air-quality-in-europe-2020-report> (accessed on 7 December 2021).
7. Stan Środowiska w Województwie Małopolskim Raport 2020. Available online: https://www.gios.gov.pl/images/dokumenty/pms/raporty/stan_srodowiska_2020_malopolskie.pdf (accessed on 7 December 2021).
8. Prawo Ochrony Środowiska Dz.U. z Dnia Dz. U. 2021 r. poz. 1973. Available online: <http://isap.sejm.gov.pl/isap.nsf/download.xsp/WDU20210001973/O/D20211973.pdf> (accessed on 7 December 2021).
9. Obwieszczenie Ministra Klimatu i Środowiska w Sprawie Ogłoszenia Jednolitego Tekstu Rozporządzenia Ministra Środowiska w Sprawie Poziomów Niektórych Substancji w Powietrzu Dz.U. 2021 poz. 845. Available online: <https://isap.sejm.gov.pl/isap.nsf/download.xsp/WDU20210000845/O/D20210845.pdf> (accessed on 7 December 2021).
10. Obwieszczenie Ministra Zdrowia w Sprawie Ogłoszenia Jednolitego Tekstu Rozporządzenia Ministra Zdrowia w Sprawie Bezpieczeństwa i Higieny Pracy Związanej z Występowaniem w Miejscu Pracy Czynniki Chemicznych Dz.U. 2016 poz. 1488. Available online: <http://isap.sejm.gov.pl/isap.nsf/download.xsp/WDU20160001488/O/D20161488.pdf> (accessed on 7 December 2021).
11. Obwieszczenie Ministra Rodziny, Pracy i Polityki Społecznej w Sprawie Najwyższych Dopuszczalnych Stężeń i Natężeń Czynniki Szkodliwych Dla Zdrowia w Środowisku Pracy Dz.U. 2017 poz. 1348. Available online: <https://isap.sejm.gov.pl/isap.nsf/download.xsp/WDU20170001348/O/D20171348.pdf> (accessed on 7 December 2021).
12. Wilbur, S.; Bosch, S. Interaction Profile for: Benzene, Toluene, Ethylbenzene, and Xylenes (BTEX). U.S. Department of Health and Human Services; Public Health Service, Agency for Toxic Substances and Disease Registry (ATSDR) 2004. Available online: <https://www.atsdr.cdc.gov/interactionprofiles/ip-btex/ip05.pdf> (accessed on 7 December 2021).
13. Masih, A.; Lall, A.S.; Taneja, A.; Singhvi, R. Inhalation exposure and related health risks of BTEX in ambient air at different microenvironments of a terai zone in north India. *Atmos. Environ.* **2016**, *147*, 55–66. [CrossRef]
14. IARC Working Group on the Evaluation of Carcinogenic Risks to Humans. *Benzene*; IARC Monographs on the Evaluation of Carcinogenic Risks to Humans; The International Agency for Research on Cancer: Lyon, France, 2018; Volume 120. Available online: https://publications.iarc.fr/_publications/media/download/6043/20a78ade14e86cf076c3981a9a094f45da6d27cc.pdf (accessed on 7 December 2021).
15. Ramírez, N.; Cuadras, A.; Rovira, E.; Borrull, F.; Marce, R.M. Chronic risk assessment of exposure to volatile organic compounds in the atmosphere near the largest Mediterranean industrial site. *Environ. Int.* **2012**, *39*, 200–209. [CrossRef] [PubMed]
16. Finlayson-Pitts, B.J.; Pitts, J.N. Atmospheric chemistry of tropospheric ozone formation: Scientific and regulatory implications. *J. Air Waste Manag. Assoc.* **1993**, *43*, 1091–1100. [CrossRef]
17. Monod, A.; Sive, B.C.; Avino, P.; Chen, T.; Blake, D.R.; Rowland, F.S. Monoaromatic compounds in ambient air of various cities: A focus on correlations between the xylenes and ethylbenzene. *Atmos. Environ.* **2001**, *35*, 135–149. [CrossRef]
18. Avino, P.; Manigrasso, M. Ten-year measurements of gaseous pollutants in urban air by an open-path analyzer. *Atmos. Environ.* **2008**, *42*, 4138–4148. [CrossRef]
19. Edgerton, S.A.; Holdren, M.W.; Smith, D.L.; Shah, J.J. Inter-urban comparison of ambient volatile organic compound concentrations in U.S. cities. *J. Air Waste Manag. Assoc.* **1989**, *39*, 729–732. [CrossRef] [PubMed]
20. Hoshi, J.; Amano, S.; Sasaki, Y.; Korenaga, T. Investigation and estimation of emission sources of 54 volatile organic compounds in ambient air in Tokyo. *Atmos. Environ.* **2007**, *42*, 2383–2393. [CrossRef]

21. Air Monitoring Survey of Hydrocarbon Compounds (BTEX) in the Taranaki Region 2019 Tkachenko V. Document 2321405. Available online: <https://trc.govt.nz/assets/Documents/Environment/Monitoring-SOE/Air/BTEX19-web.pdf> (accessed on 7 December 2021).
22. NIST Chemistry WebBook, SRD 69—Benzene. Available online: <https://webbook.nist.gov/cgi/cbook.cgi?ID=C71432&Mask=4> (accessed on 7 December 2021).
23. NIST Chemistry WebBook, SRD 69—Toluene. Available online: <https://webbook.nist.gov/cgi/cbook.cgi?ID=C108883&Mask=4> (accessed on 7 December 2021).
24. NIST Chemistry WebBook, SRD 69—O-Xylene. Available online: <https://webbook.nist.gov/cgi/cbook.cgi?ID=C95476&Mask=4> (accessed on 7 December 2021).
25. NIST Chemistry WebBook, SRD 69—M-Xylene. Available online: <https://webbook.nist.gov/cgi/cbook.cgi?ID=C108383&Mask=4> (accessed on 7 December 2021).
26. NIST Chemistry WebBook, SRD 69—P-Xylene. Available online: <https://webbook.nist.gov/cgi/cbook.cgi?ID=C106423&Mask=4> (accessed on 7 December 2021).



Article

The Heterogeneity of High-Quality Economic Development in China's Mining Cities: A Meta Frontier Function

Wei Xu, Jiahui Yi and Jinhua Cheng *

School of Economics and Management, China University of Geosciences, Wuhan 430074, China; 2201810262@cug.edu.cn (W.X.); anitayjh@gmail.com (J.Y.)

* Correspondence: chengjinhua100@126.com

Abstract: The transformation of mining cities and the realization of high-quality economic development are complicated processes. The objective existence of abundant resource factor endowment in mining cities does not mean that resource allocation is in the optimal state and can play the greatest role. The optimal allocation of factors for the high-quality economic development of mining cities is more important than the resource factors. The input–output allocation efficiency of high-quality economic development under the common frontier and group frontier of 99 mining cities in China from 2006 to 2019 is calculated by using the data envelopment analysis method and common frontier model, and the pure technical efficiency and scale efficiency are decomposed. The results show that (1) the comprehensive technical efficiency values under both common frontiers and group frontiers show that the factor allocation efficiency in the process of high-quality economic development of different mining cities shows obvious heterogeneity. (2) The growth of the input–output allocation efficiency of the high-quality economic development of mining cities has significant spatial convergence characteristics, but the convergence speed is different. (3) The high-quality development path of the mining city's economy should not only focus on comprehensively improving the ability of resource element input and output allocation but also improve the group environment.

Keywords: mining city; high-quality economic development; input-output allocation efficiency; meta-frontier method

Citation: Xu, W.; Yi, J.; Cheng, J. The Heterogeneity of High-Quality Economic Development in China's Mining Cities: A Meta Frontier Function. *Int. J. Environ. Res. Public Health* **2022**, *19*, 6374. <https://doi.org/10.3390/ijerph19116374>

Academic Editors: Francesco Nocera, Roberto Alonso González Lezcano and Rosa Giuseppina Caponetto

Received: 19 March 2022

Accepted: 5 May 2022

Published: 24 May 2022

Publisher's Note: MDPI stays neutral with regard to jurisdictional claims in published maps and institutional affiliations.



Copyright: © 2022 by the authors. Licensee MDPI, Basel, Switzerland. This article is an open access article distributed under the terms and conditions of the Creative Commons Attribution (CC BY) license (<https://creativecommons.org/licenses/by/4.0/>).

1. Introduction

The mineral resource industry has made and is currently an important contribution to the development of the national economy. Mining cities, which rise and develop due to the development of mineral resources, become the main body of mineral resource supply and is the resource production, transfer and reserve hub of China's industrialization, directly providing raw materials for industrialization. China's resource-based cities are numerous and widely distributed, with great historical contributions and have a prominent status. Since the founding of the People's Republic of China, resource-based cities have produced 52.9 billion tons of raw coal, 5.5 billion tons of crude oil, 5.8 billion tons of iron ore, and 2 billion cubic meters of wood. During the First Five-Year Plan period, 53 of the 156 national key construction projects were distributed in resource-based cities, accounting for nearly 50% of the total investment, making historic contributions to the establishment of an independent and complete industrial system and the promotion of national economic development.

At present, international political and economic uncertainty and instability are rising, and the unbalanced, uncoordinated and unsustainable challenges in domestic economic development are prominent. Due to the superposition of internal and external factors and the interweaving of new and old contradictions, the sustainable development of mining resource-based cities faces severe challenges, and the task of accelerating the transformation of the economic development mode is very arduous [1]. The historical legacy of mining resource-exhausted cities is still serious, and the endogenous power of transformation and

development is currently weak [1–3] Dan et al., 2019. There are still nearly 70 million square meters of shantytowns to be renovated, approximately 140,000 hectares of subsidence areas to be treated, more than 600,000 unemployed miners, and more than 1.8 million urban subsistence allowances. Industrial development is still highly dependent on resources, with extractive industries accounting for more than 20% of secondary industries, and modern manufacturing and high-tech industries are in the initial stages. The talent, capital and other elements of the mining resources city have weak agglomeration capacity and low allocation level such that the support and guarantee capacity for further development of alternative industries is seriously inadequate [4–6].

However, the level of technological progress and the quality of economic development represented by total factor productivity and technological efficiency do not show an obvious trend of growth or improvement. Some of the important reasons is that the resource allocation structure is not good, the efficiency is not high, and the overall efficiency of the national and regional urban resource allocation system is not high. In short, the input–output allocation of resource elements is a complicated process, especially for mining resource-based cities, and the input of resource elements is only a necessary condition. Whether the input of resource elements can improve the level of economic development and promote the high-quality development of the economy depends on whether the allocation of input resource elements can be optimized. The input–output allocation of high-quality economic development is a dynamic process of searching and obtaining, distributing and managing, integrating and utilizing, maintaining and updating various material or nonmaterial resource elements in a certain time and mining resource city by government, enterprises, colleges and universities, science and technology intermediary service institutions and nonprofit organizations. Therefore, it is of great significance to promote the sustainable development of mining resource-based cities to promote new industrialization and urbanization and to build a resource-saving and environmentally friendly society. Based on the perspective of the input–output efficiency of resource element allocation in mining cities in China, this paper intends to reveal the internal causes of the deviation of the input and output of resource elements in mining cities and the increasingly obvious and unbalanced spatial agglomeration.

2. Literature Review

With the deepening of resource-based cities, scholars have gradually realized the complexity of the economic growth of mining resource-based cities, and an increasing number of studies have also shown that the realization of mining resource-based cities needs to integrate and reuse the input–output resource elements in the process of economic growth [2,7–10].

With regard to the research on the input–output efficiency of high-quality economic development of mining resource-based cities in China, scholars have calculated and analyzed the effect or efficiency of input–output allocation with different evaluation indices and methods around different dimensions. Application of the statistical management method, Bui et al. (2020) [11] discusses the economic efficiency of the urban waste management system through the AHP-IPA method, Yuan et al. (2019) [12] discusses the spatial-temporal distribution characteristics of the land use efficiency of mining cities using the index decomposition method, and [13] studies the transition development level of Shaanxi, Shanxi and Inner Mongolia resource cities based on the structure decomposition model.

The most literature discuss the eco-environmental, energy and economic efficiency of resource-based cities through the stochastic frontier analysis model (SFA) and data envelopment method (DEA). Representative studies, such as Chen et al. (2019) [7], used the DEA method to study the industrial land use efficiency of 109 resource-based cities in China from 2006 to 2015. Yu et al. (2019) [14] discussed the ecological efficiency of resource-based cities under heterogeneous conditions through a DEA model, and Yin et al. (2020) [15] studied the green transformation efficiency of mining resource-dependent cities through a three-stage DEA model. In terms of econometric application, Yan et al. (2019) [2]

used the nonparametric method to estimate the total factor energy efficiency (TFEE) of 105 resource-based cities in China from 2010 to 2016 and analyzed the temporal and spatial characteristics of the change energy efficiency.

The results show that the input–output efficiency of natural, environmental, ecological and transformation of mining resource-based cities is not ideal, and the development level difference between cities is gradually expanding. According to the level of factor allocation and its related influencing factors, the input and output indices of the economic development of mining resource-based cities are redundant. There is still room for further improvement in the existing relevant research, which is mainly reflected in the following aspects: first, the impact of resource input is ignored, and such output indicators are rarely involved; second, in terms of calculation methods, whether using the DEA or SFA method, it is assumed that all regions have the same technology set, obviously the technical gap between different types of mining cities is not considered, and the reason for efficiency loss cannot be determined. In view of this, on the one hand, the paper considers the impact of resource factor input on the input–output efficiency of high-quality economic development of mining resource-based cities and introduces the industrial agglomeration index into the measurement model of input–output efficiency of high-quality economic development of mining resource-based cities to avoid single factor resource input measurement; on the other hand, in view of the heterogeneity characteristics of different types of mining cities, the paper introduces the production function of the common frontier and comprehensively uses the meta-frontier model to calculate the input–output efficiency of high-quality economic development of mining resource-based cities under the common frontier and group frontier. This paper discusses the characteristics of the high-quality economic development of mining resource cities.

3. Research Design

3.1. Model

The requirements for high-quality economic development of China's mining cities can generally be divided into five categories: human resources, financial resources, material resources, technology and information. The process of high-quality economic development of China's mining cities is complex and malleable, and a single index cannot accurately measure it, while the efficiency of input–output allocation in the process of economic development of China's mining cities can reflect the level of high-quality economic development to a certain extent. When the DEA method is used to measure the high-quality economic development of mining cities in different regions of China, the potential hypothesis is that the evaluated decision-making unit (DMU) has a similar technical level. However, with the existence of regional heterogeneity, it is impossible to accurately measure the allocation efficiency of the real high-quality economic development factors of each mining city by using the population sample only. Battese and Rao (2002) [16] and O'Donnell, Rao and Battese (2008) [17] proposed a common boundary production function analysis framework, using the stochastic frontier analysis method to construct a common frontier and group frontier, and finally measuring the technical gap ratio (TGR) between the two frontiers can make up the input–output efficiency under the condition that traditional DEA cannot measure heterogeneity. Common frontier approaches based on DEA are briefly described below [18,19].

(1) First, according to the National Sustainable Development Plan for Resource-based Cities (2013–2020) issued by the Chinese government, there are 262 resource-based cities in the country, including 126 prefecture-level administrative regions (these include prefecture-level cities, regions, autonomous prefectures, alliances, etc.), 62 county-level cities, 58 counties (including autonomous counties, forest regions, etc.), and 16 municipal districts (development zones, management zones). They are divided into four types: growth type (31), mature type (141), recession type (67) and regeneration type (23). Due to the large gap in resource endowment, factor input, output and allocation capacity of mature, regenerative, declining and growing mining cities and the large difference in

macroeconomic level, mining city policy environment, opening level and other influencing factors, different types of mining cities face different production levels, and the internal difference of each type is smaller than the whole, so the research sample is divided into four groups: mature, regenerative, declining and growing four groups.

(2) According to the common frontier model of Battese and Rao (2002) [16], Zhang et al. (2013) [1], He et al. (2021) [20] let $input \in R^m, output \in R^n$ is the $input$ and $output$ vector, and the common technology set (TE^{meta}) including all $inputs$ and $outputs$ is:

$$TE^{meta} = \{(input, output) \mid input, output \geq 0; input \rightarrow output\} \tag{1}$$

where $input$ is the $input$ vector and $output$ is the $output$ vector, which means the conditions that the required $input$ satisfies under the technology set TE^{meta} to obtain a certain $output$ $product^{meta}$. The set of production possibilities (common boundary) is:

$$product^{>meta}(input) = \{output \mid (input, output) \in TE^{meta}\} \tag{2}$$

Common Frontier Distance Function (DDF^{meta}) of Meta Technical Efficiency can be expressed as Formula (3), where $0 \leq DDF^{meta}(input, output) \leq 1$.

$$DDF^{meta}(input, output) = \inf_{\theta > 0} \{ \theta \mid (\frac{output}{\theta}) \in product^{meta}(input) \} = MTE(input, output) \tag{3}$$

The four clusters of mature, renewable, declining and growing technologies ($TE^{(i)}$) are:

$$TE^{(i)} = \{(input_i, output_i) \mid input_i, output_i \geq 0; input_i \rightarrow output_i\} \tag{4}$$

The production probability (i) is:

$$product^{(i)}(input_i) = \{output_i \mid (input_i, output_i) \in TE^{(i)}\} \tag{5}$$

Group Technical Efficiency (GTE) equivalent to Group Leading Edge Distance Function ($DDF^{(i)}$), as shown in Formula (6), where $0 \leq DDF^{(i)}(input_i, output_i) \leq 1$:

$$DDF^{(i)}(input_i, output_i) = \inf_{\theta > 0} \{ \theta \mid (\frac{output_i}{\theta}) \in product^{(i)}(input_i) \} = GTE(input_i, output_i) \tag{6}$$

(4) Define the Technological Gap Ratio (TGR). TGR reflects the gap between common frontier and group frontier technology level. The higher the value, the closer the actual production efficiency is to the potential production efficiency [19], which means the higher the technology level [18]. When the input–output combination is $(input_i, output_i)$, TGR can be shown in Formula (7), where $0 \leq TGR(input_i, output_i) \leq 1$.

$$TGR_{(input_i, output_i)} = \frac{DDF^{meta}(input, output)}{DDF^{(i)}(input_i, output_i)} = \frac{MTE(input, output)}{GTE(input_i, output_i)} \tag{7}$$

Relationship between common frontier technology efficiency, group frontier technology efficiency and technology gap ratio can be expressed as:

$$MTE = GTE \times TGR \tag{8}$$

3.2. Variables Selection

3.2.1. Input Variables

First, the labor factor. Labor input is an important part of urban economic and social development and plays a decisive role in improving the efficiency of resource allocation for the high-quality development of the mining city economy. Therefore, the total labor wage of mining cities is selected as the proxy variable of labor input.

The second is capital elements. Capital factors include land and plants, production equipment, mining-transportation-processing equipment, etc. Capital investment has a

direct impact on the economic growth and resource allocation of mining cities. Usually, under certain conditions, the more capital factor resources are invested, the more productive activities there are, which is more conducive to improving the efficiency of resource factor allocation and promoting economic growth. Considering the availability of data, the gross fixed capital of mining cities is selected as the proxy variable of capital elements.

The third is resource elements. Resource input plays an important role in the development of mining cities, and resource input is the main way to obtain technical progress [13,15]. Based on the single method of processing the quantity of resource factors, this paper shows the input of resource factors by calculating the industrial concentration level of mining resource-based cities.

3.2.2. Output Variables

The allocation of resource factors in the process of economic development of mining cities can not only bring economic output but also affect the input–output efficiency through the negative effect on the environment. The reason is that in the process of economic development of mining cities, the allocation capacity will be constantly adjusted, which can improve the technical level of resource and energy development and utilization and environmental governance capacity and play an important supporting role in resource reservation and environmental protection. It is an important way to solve the contradiction between population, resources and the environment and improve the carrying capacity of resources and the environment of mining cities to provide for sustainable growth and high-quality development of mining cities. Therefore, the output of resource allocation is further divided into economic output and environmental output.

First, economic output. The indicators of urban economic growth selected by the existing research are very rich, often involving multiple dimensions. By comparison, considering the representativeness and accessibility of indicators, the gross domestic product (GDP) of urban areas can more directly reflect the final output of the economic category.

The second is environmental outputs. Since the generation and discharge of pollutants have a large correlation with the economic level of the region, in terms of the selection of environmental indicators, the pollutant discharge indicators include production and living from the point of view of the pollution source, and there are gas pollution discharge, liquid pollution discharge and solid waste from the perspective of the material form. The environmental quality index is a composite value of environmental quality parameters and environmental quality standards. It also considers the emission and treatment of production and living pollution and is widely used to evaluate the treatment effect of environmental pollution. Therefore, considering the lack of data on solid waste, sulfur dioxide and wastewater discharge per capita are selected to measure environmental output.

3.2.3. Data Sources and Descriptive Statistics of Variables

In view of the availability of data, the sample data of mining-type cities used in this paper was selected from the list of resource-based cities (Schedule 1), and this study uses panel data from 99 mining cities in China (The list of resource-based cities is dynamically assessed and adjusted in combination with resource reserve conditions, development and utilization conditions, etc., and finally 99 representative cities are selected for analysis) (excluding Tibet, Hong Kong, Macao and Taiwan) from 2006 to 2019 for relevant statistics and quantitative analysis. Relevant data mainly come from China Urban Statistics Yearbook, China Macroeconomic Database, China Financial Statistics Database, China Urban Environment Database, etc. Detailed descriptive statistics and correlation analysis were conducted on the characteristics of relevant data samples, and the results are shown in Table 1 and Figure 1. It can be seen that the average values of human resources, financial resources, capital accumulation, industrial agglomeration, GDP and environmental output are 5.7569, 10.1789 and -0.4176 respectively after the logarithm is taken. Compared with the maximum and minimum values, the results show that the sample characteristics are close to the non-normal distribution. According to the standard deviation of sample data,

the standard deviation of information resources and innovation output is 0.3473 and 0.1232 respectively, which indicates these variables data are characterized by relative concentration. The results show that there is no significant Multicollinearity between the main variables in Figure 1, which meets the operational requirements of the DEA model.

Table 1. The summary statistics.

Var	Name	Obs	Mean	SD	Min	Median
logasset	Fixed assets (based 2000)	1386	5.7569	1.064	2.782	5.852
logpcwage	Per capita salary	1386	10.1789	0.589	2.283	10.25
loggather	Industrial agglomeration	1386	-0.4176	0.585	-3.391	-0.3417
logpcgdp	Per GDP	1386	9.3490	0.593	3.943	9.298
logwater	Per wastewater discharge	1386	2.5903	0.816	-0.07886	2.59
logso2	Per SO ₂ emissions	1386	-4.1559	1.024	-7.627	-4.072

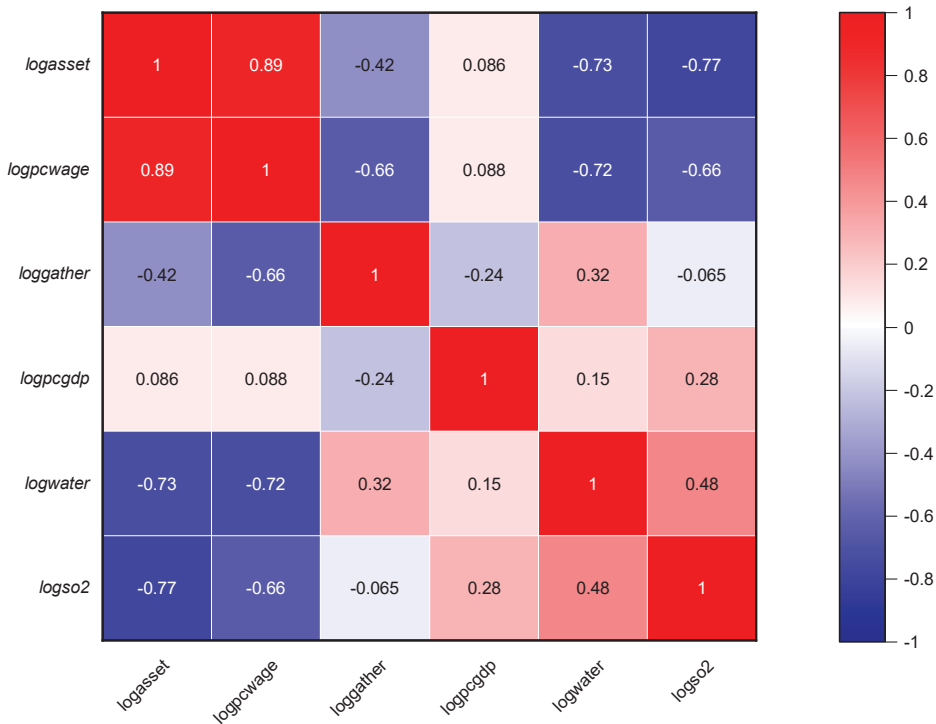


Figure 1. Correlation coefficient Note: Lower-triangular cells report Pearson’s correlation coefficients, upper-triangular cells are Spearman’s rank correlation.

4. Analysis of Empirical Results

According to the constructed index system of high-quality input–output allocation efficiency of the mining city economy, the DEA-Meta-frontier model is comprehensively used to calculate the input–output allocation MTE, GTE and technology gap ratio TGR of the high-quality development of the mining resource-based city economy under the common frontier and the group frontier and to analyze the evolution characteristics of time-space differences. The descriptive statistics calculated by MaxDEA7.16 software are shown in Table 2.

Table 2. Statistical description of regional innovation resource allocation efficiency from 2006 to 2019.

City Type	MTE					GTE					TGR				
	Mean	Min	S.D.	Max	Range	Mean	S.D.	Min	Max.	Range	Mean	S.D.	Min	Max	Range
Mature type	0.4738	0.1740	0.4126	1	0.8260	0.5566	0.2053	0.5019	1	0.7947	0.8432	0.4917	0.8418	1	0.5083
Regenerative	0.5231	0.2191	0.4757	1	0.7809	0.6609	0.2276	0.6236	1	0.7724	0.7951	0.4396	0.7866	1	0.5605
Decay type	0.5205	0.1680	0.4602	1	0.8320	0.8127	0.3757	0.8328	1	0.6243	0.6267	0.2919	0.5778	1	0.7081
Growth	0.6374	0.2240	0.6747	1	0.7760	0.7935	0.2668	0.8890	1	0.7332	0.7885	0.3242	0.7990	1	0.6758
National	0.5046	0.1680	0.4434	1	0.2806	0.6420	0.2053	0.6070	1	0.4082	0.7899	0.2919	0.8146	1	0.1672

Note: 1. S.D. is Standard deviation. 2. Summarize and sort according to the calculation results of MaxDEA7.16 software.

4.1. Comprehensive Efficiency Analysis

4.1.1. MTE and GTE

From the comparison of common frontier technology efficiency (MTE) and group frontier technology efficiency (GTE) in different regions (as shown in Table 2), MTE and GTE are distance function values of DMU based on the common and group boundaries, respectively, reflecting the distance from actual output to the common and group boundary output under the same input level [21].

First, the efficiency of high-quality input–output allocation of regional mining cities in China under the common frontier and group frontier is 0.5046 and 0.2806, respectively, indicating that the input factors of high-quality input–output allocation of China’s mining resource-based cities still have 49.54% saving space if the national optimal technology is used as a reference, and the saving space is as high as 71.94% if the regional optimal technology is taken as reference. The difference in the results is mainly due to the difference in the technical reference set between the two. The common frontier takes the potential optimal input–output allocation efficiency of all samples as the reference structure front, while the group frontier takes the mature, growth, regeneration and decline types as the grouping of the high-quality input–output allocation efficiency of the mining city economy.

Second, the MTE of growth is 0.6374, which indicates that there will be 36.26% efficiency improvement space for growing mining cities and 47.69%, 47.95% and 52.62% efficiency improvement space for growing mining cities. It can be seen that, in comparison, the high-quality input–output allocation efficiency of the regenerative, recession and mature mining cities is still low, which indicates that the elements of these three types of mining resource-based cities are relatively extensive, and the effective development and utilization are insufficient. At the same time, there may be a certain problem of "resource waste" or insufficient input of resource elements.

Third, the mean value of GTE from high to low was the recession type, growth type, regenerative type and mature type, with efficiency improvement spaces of 18.73%, 20.65%, 33.91% and 44.34%, respectively. The calculation results of GTE show that there is significant heterogeneity in the distance between the input–output efficiency of four different types of mining cities and their respective boundaries. Unlike the MTE calculation results, the input–output efficiency of the declining mining cities is relatively average, while the input–output efficiency of the mature mining cities with high-quality economic development varies greatly. The efficiency of the four types of mining city groups needs to be improved less than that of the common frontier efficiency, which indicates that from the perspective of groups, the input scale of resource elements within each group is more appropriate, but the balance of input and output allocation between groups is still needed.

Finally, compared with the two frontiers (MTE and GTE), the high-quality input–output allocation efficiency of the growing mining cities has little difference, while the two frontiers of the mature mining cities have the largest difference. In terms of the ranking of different frontier types, the ranking of the economic high-quality input–output allocation efficiency of growth and mature mining cities has not changed, but the ranking of the input–output allocation efficiency of declining and regenerative mining cities has undergone significant changes. The reason for this phenomenon may be that the resource input,

innovation ability, macroeconomic level and educational development level of the growing and mature mining cities are superior to other types, which represents the national optimal level and the attraction ability is higher than other areas, and the technology collection under the two frontiers is basically the same, while the technology collection under the two frontiers of the declining and regenerative mining cities is significantly different, and the distance between the frontiers of the two types changes greatly.

4.1.2. TGR

In terms of TGR, TGR reflects the gap between the technical level of the group and the technical level of the potential common boundary caused by the specific group institutional environment. The higher the TGR is, the closer the actual technical level of the DMU is to the common boundary technical level, that is, the higher the technical level under the corresponding institutional environment conditions. According to the mean value of TGR of population, mature type, regenerative type, declining type and growing mining cities in the sample period (as shown in Table 2), the mean value of TGR of four types of mining cities is less than 1, among which the mean value of TGR of mature mining cities in the sample period is 0.8432, close to 1, at a higher level, indicating that the technical level of mature mining cities is close to the common technical frontier, and reaches the potential common boundary technical level, which is 84.32% of the potential input–output allocation efficiency; However, the mean value of TGR of regenerative, declining and growing mining cities is below 0.8, which is relatively far away from the common technological frontier. Among them, the mean value of TGR of declining mining cities is 0.6267, indicating that it only reaches 62.67% of the potential input–output allocation efficiency, and there is still 37.33% of efficiency improvement space. At the same time, the differences in the TGR means of the four types of mining cities also explain the rationality of group division in this study.

As a whole, on the one hand, the efficiency of input–output allocation of high-quality economic development of the overall national mining cities and four types of mining cities under the common frontier is not as effective as DEA, and there is certain space for efficiency improvement; on the other hand, the efficiency of MTE and GTE of four types of mining cities is the best performance is growth, and the worst is mature type. This indicates that the growing mining cities have the strongest ability of high-quality input–output allocation and the highest degree of effective use of resource elements under the framework of sustainable development. Comparatively speaking, mature mining cities need to improve the ability of input–output allocation to avoid resource waste.

4.1.3. Differences Types of Mining City

Third, from the comparison of the average value of high-quality input–output allocation efficiency of the four types of mining cities (as shown in Appendix A Table A1), the comprehensive efficiency of high-quality input–output allocation of mature mining cities is the best in Daqing and Dongying, the high-quality input–output allocation efficiency of Daqing and Dongying under the common frontier and group frontier is the first, and Daqing and Dongying are also the provinces and cities with the highest MTE average value among 99 mining resource-based cities, reaching 0.93461 and 0.9108, close to DEA efficiency. The worst performance in the common frontier was Yuncheng city and Baise city, with MTEs of 0.25953 and 0.29452, respectively, ranking last and second; that is, compared with the common boundary technology level of all samples, Yuncheng city and Baise city still had 74.047% and 70.548% efficiency improvement space. Yuncheng city and Baise city still had the worst performance in the group, with mean GTEs of 0.31539 and 0.34009, respectively. That is, mature mining cities have the highest input–output allocation efficiency of mining cities and have the lowest economic high-quality development input–output allocation efficiency. By analogy, the high-quality input–output allocation efficiency of regenerative, recession and growing mining cities can also be further analyzed.

4.1.4. Time Change Trend

First, under the common front (as shown in Figure 2), the high-quality input–output allocation efficiency (MTE) of the four types of mining cities all shows the V-shaped change trend of decreasing first and then gradually increasing, but the decreasing range is distinct. Among them, the decline range of annual MTE change trend of mature mining cities is 2006–2016, with a slight recovery in the middle, and the bottom is 2016; the decline range of the annual MTE change trend of regenerative mining cities is 2006–2018, and the bottom is 2018; the annual MTE change trend of recession mining cities is consistent with that of regenerative mining cities, and the decline range coincides with that of regenerative mining cities; the decline range of the MTE annual average change trend of growing mining cities is 2006–2010 and 2013–2018, with a slight recovery in the middle, and the bottom is 2018. Basically, the average MTE of three types of mining cities, mature, regenerative and declining mining cities, began to show a certain degree of improvement at the end of the “Eleventh Five-Year Plan” period, but during the “12th Five-Year Plan” period, there was a general downward trend, while in the “13th Five-Year Plan” period, there was a significant degree of improvement. Unlike the above three types of mining city MTE changes, the growing mining city MTE in the “12th Five-Year Plan” presents a certain upward trend. The change trend of the annual mean value of MTE in the 12th Five-Year Plan may be related to the sustainable development of resource-based cities in 2013.

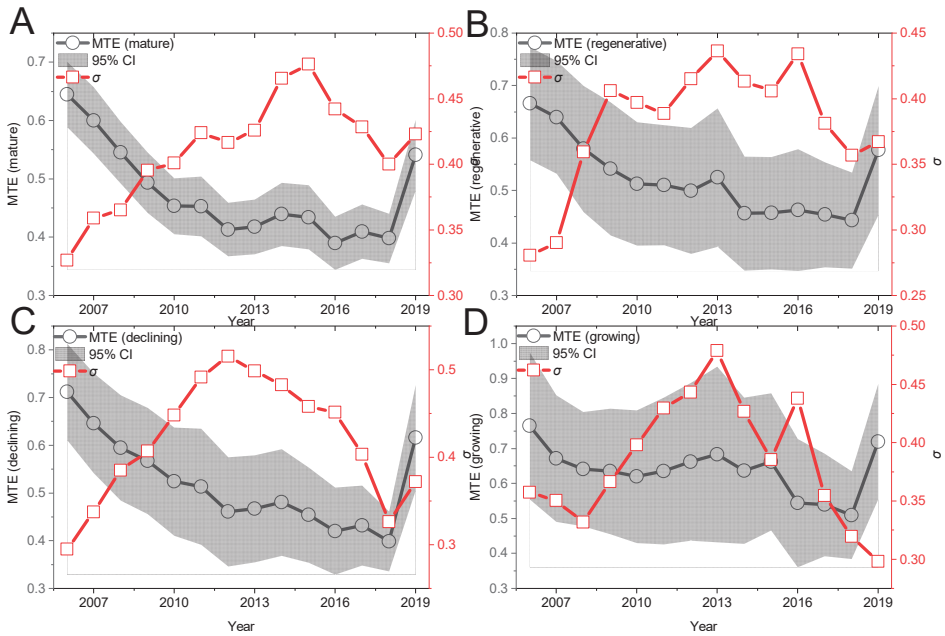


Figure 2. The trend of MTE in four types of mining cities from 2006 to 2019. Note: (A–D) represent mature, renewable, declining and growing mining cities respectively. The shaded area represents the 95% confidence interval (CI). σ Represents the convergence trend of MTE annual mean [22].

Second, under the front of the group (as shown in Figure 3), the change law of GTE of the four types of mining cities shows similar change characteristics. Among them, the GTE of mature, renewable, declining and growing mining cities showed obvious fluctuation and decline trends before 2018; the GTE of mature and declining mining cities rebounded in 2011–2014; the GTE of renewable mining cities rose in 2014–2017; and the GTE of growing mining cities rebounded slightly in 2016–2017.

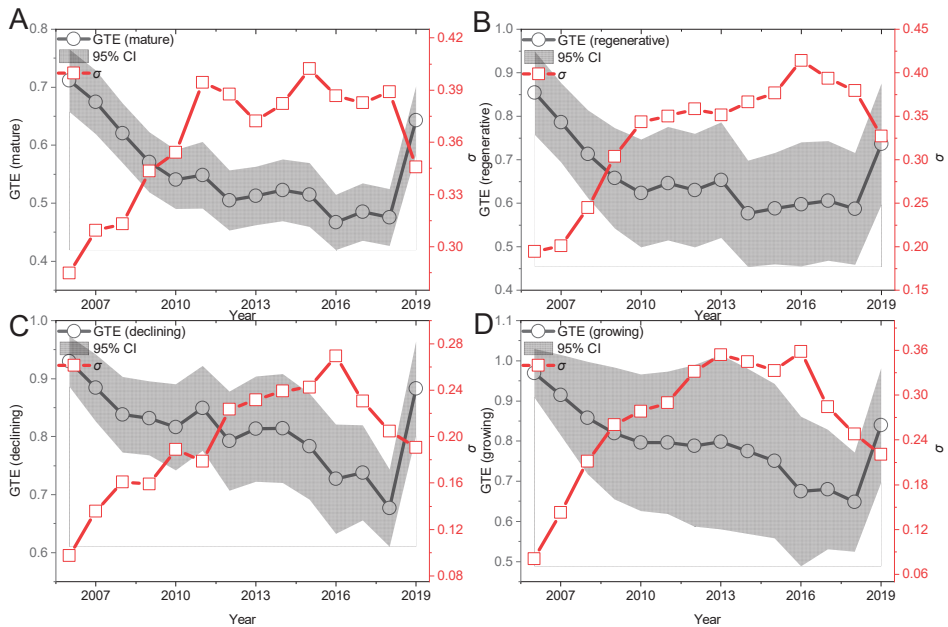


Figure 3. The Trend of GTE in Four Types of Mining Cities from 2006 to 2019. Note: (A–D) represent mature, renewable, declining and growing mining cities respectively. The shaded area represents the 95% confidence interval (CI). σ Represents the convergence trend of MTE annual mean [22].

Finally, from the change trend of TGR of mature, regenerative, recession and growth type in the sample period (Figure 4), the TGR value of regenerative mining cities in 2006–2019 basically remains unchanged, with slight fluctuation in the middle and obvious “m” shape, indicating that the distance between the production front of input–output allocation and the common front in the high-quality economic development of regenerative mining cities basically remains unchanged. The mean value of the TGR of mature and declining mining cities mainly show a downward trend, and the change trend is consistent with the MTE change trend in Figure 2, indicating that the mature and declining mining cities are mainly caused by changes in MTE. The above two types of TGR indicate that the distance between the production frontier and the common frontier in the economic growth process of mining cities has been expanded to a certain extent, that is, the gap between the high-quality input–output allocation efficiency of the mining city economy and the potential high-quality input–output allocation efficiency of the mining city economy is expanding. The TGR value of the growing mining cities shows an obvious rising trend, which indicates that the distance between the production frontier and the common frontier in the process of high-quality economic development of the growing mining cities has a certain narrowing, that is, the gap between the high-quality input–output allocation efficiency of this type of mining cities and the potential high-quality input–output allocation efficiency of the mining cities is narrowing, and the high-quality input–output allocation efficiency of the growing mining cities has a catching-up effect on the high-quality economic growth of mature and regenerative mining cities.

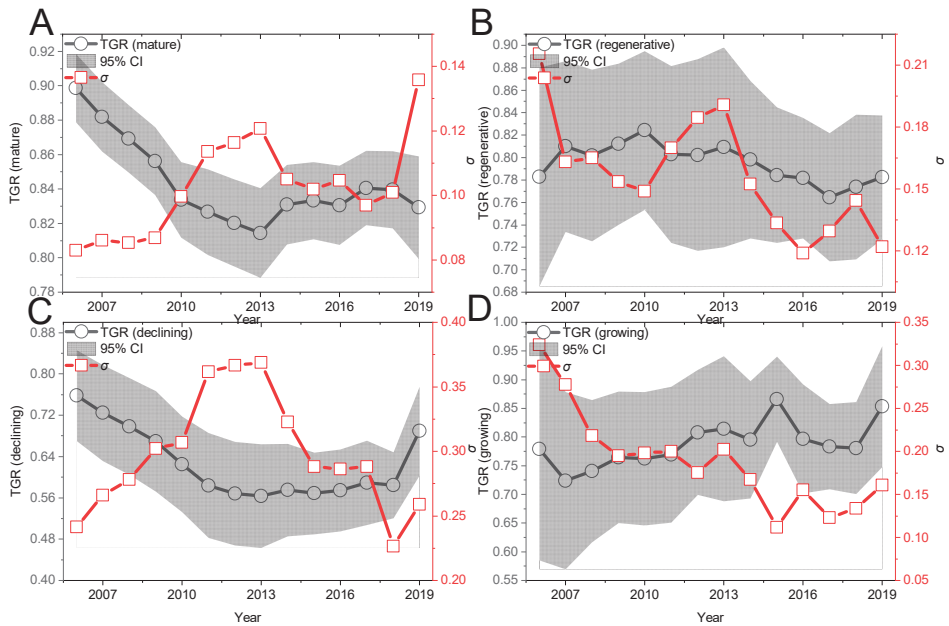


Figure 4. The trend of TGR of four types of mining cities from 2006 to 2019. Note: (A–D) represent mature, renewable, declining and growing mining cities respectively. The shaded area represents the 95% confidence interval (CI). σ Represents the convergence trend of MTE annual mean [22].

4.2. Convergence Analysis

The convergence of economic development means that the difference in economic development shows a trend of gradually narrowing with time. To investigate the evolution trend of high-quality economic development differences of mining cities represented by MTE, GTE and TGR, the convergence model is used to test the convergence of MTE, GTE and TGR. Convergence is divided into σ and β convergence. The main principle of the σ convergence method is to judge the convergence by observing the distribution of the standard deviation of a variable between regions. The standard deviation decreases with time, which means that the difference in the variable between regions decreases, and there is σ convergence between regions. β convergence is developed from the convergence theory in the neoclassical growth model [23], and it is divided into absolute β convergence and conditional β convergence according to whether there are restrictions. The absolute β convergence assumes that each region has the same base of economic conditions, and a certain variable among regions will eventually reach the same steady growth rate and level. The conditional β convergence assumes that after considering the different economic basis conditions of each region, each region develops along its own steady growth path and finally reaches the steady growth rate and level. The main method of absolute β and conditional β convergence is to observe whether the efficiency change rate is related to the initial input–output allocation efficiency level by constructing a metrological equation. If there is a significant negative relationship, the regression coefficient β value is less than 0, indicating that the efficiency change rate is negatively related to the initial input–output allocation efficiency level. The higher the initial input–output allocation level is, the lower the efficiency change rate, or the lower the initial input–output allocation efficiency level is, the higher the rate of change. Mining cities with higher economic development input–output allocation efficiency levels have better development space. There is a faster growth rate than other mining cities at the early stage of development, and this type of β convergence exists in the high-quality economic development of mining cities.

4.2.1. Space Inspection

Considering that the economic development of mining resource-based cities is not independent but has mutual influence, this paper tests the spatial agglomeration and spatial dependence degree [24] of common frontier efficiency, group frontier efficiency and the technical drop ratio of high-quality economic development of mining cities by measuring the overall Moran's I index, and the specific calculation formula is as follows:

$$\text{Moran's I} = \frac{n}{\sum_{i=1}^n \sum_{j=1}^n w_{ij}} \frac{\sum_{j=1}^n w_{ij}(x_i - \bar{x})(x_j - \bar{x})}{\sum_{i=1}^n (x_i - \bar{x})^2} \quad (9)$$

where n is the total number of mining cities, w_{ij} is the spatial weight matrix (using the spatial adjacency weight matrix, the adjacency is 1, and the nonadjacency is 0), and x_i and \bar{x} are the input–output allocation efficiency (MTE, GTE and TGR) and their mean values. According to the formula, the value range of Moran's I index is $[-1,1]$. If Moran's I is greater than 0, it indicates a positive correlation (adjacent mining cities with high economic quality development input–output allocation efficiency or adjacent mining cities with low economic quality development input–output allocation efficiency). A larger value indicates that the spatial correlation of economic development allocation efficiency of mining cities is stronger. If it is less than 0, it indicates a negative correlation (adjacent mining cities with high economic quality development input–output allocation efficiency and adjacent mining cities with low economic quality development input–output allocation efficiency). A smaller value indicates that the difference between the economic development allocation efficiency of mining cities is greater. If Moran's I index tends to 0, it indicates that the economic development of mining cities has no spatial correlation.

As a result, the spatial Moran's I indices of MTE, GTE and TGR are calculated, and the results are shown in Figures 5–7. Figure 5 shows the global spatial autocorrelation of MTE in mining cities from 2006 to 2019 (Moran's I). The results show that Moran's I index is positive in the sample period, the fluctuation range is 0.0001–0.008, and all have passed the significance test, indicating that the common frontier efficiency of economic development among mining cities has a positive correlation during the sample period, demonstrating the phenomenon of spatial concentration on the whole; that is, the common technological frontier of high-quality economic development of mining cities is affected by the adjacent mining cities, the mining cities with high MTE are neighbors, and the cities with low MTE are neighbors. According to the temporal trend of Moran's I index, the Moran's I index of MTE showed a downward trend as a whole, but there was a slight fluctuation in the middle.

Figure 6 shows the global spatial autocorrelation value (Moran's I) of the GTE of mining cities in 2006–2019. The results show that Moran's I index is positive during the sample period, the variation trend is consistent with MTE, and the fluctuation range is 0.00001–0.004. All of them pass the significance test, which demonstrates that the group frontier efficiency of economic development among mining cities has a positive correlation in the sample period and shows the phenomenon of spatial agglomeration on the whole; that is, the technical frontier of the high-quality economic development group of mining cities is affected by the adjacent mining cities. Moreover, the mining cities with higher GTEs are neighbors to each other, and the cities with lower GTEs are neighbors to each other. According to the temporal trend of the Moran's I index, the whole Moran's I index of GTE shows a downward trend, but there is a slight fluctuation in the middle.

Figure 7 shows the global spatial autocorrelation value (Moran's I) of the TGR of mining cities in 2006–2019. The results show that Moran's I index fluctuates in the range of -0.003 – 0.004 during the sample period, and all of them pass the significance test, showing a significant downward trend. The Moran's I index of TGR decreased from 0.004 in 2006 to 0.0001 in 2010, indicating that the technological gap of economic development between mining cities decreased compared with the phenomenon of spatial agglomeration in 2006–2010; the Moran's I index of TGR in 2011–2019 was negative, that is, the technological gap of

high-quality economic development of mining cities (catch-up trend) was affected by the neighboring mining cities, and mining cities with higher TGR and mining cities with lower TGR are neighbors to each other.

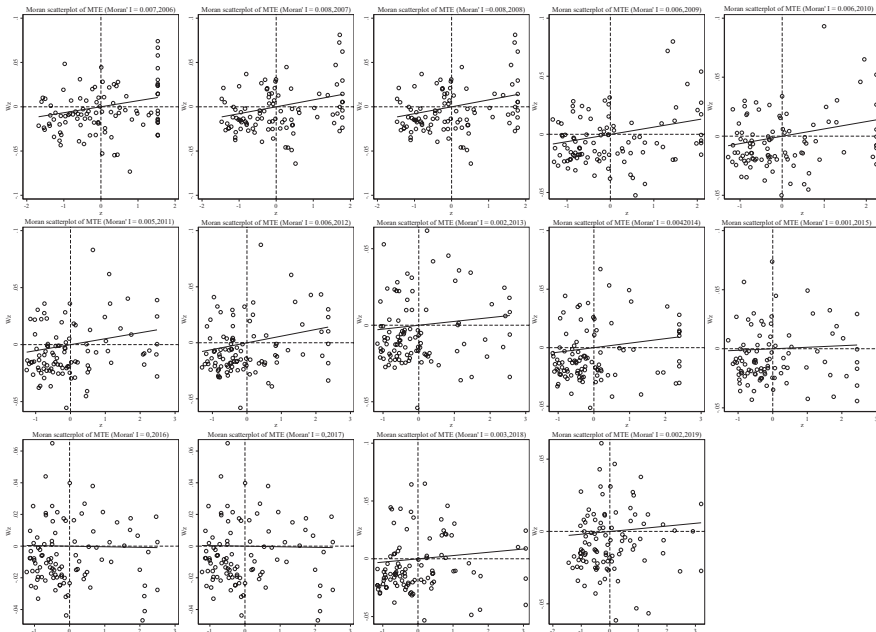


Figure 5. Distribution change of MTE Moran's I scatter plot from 2006 to 2019.

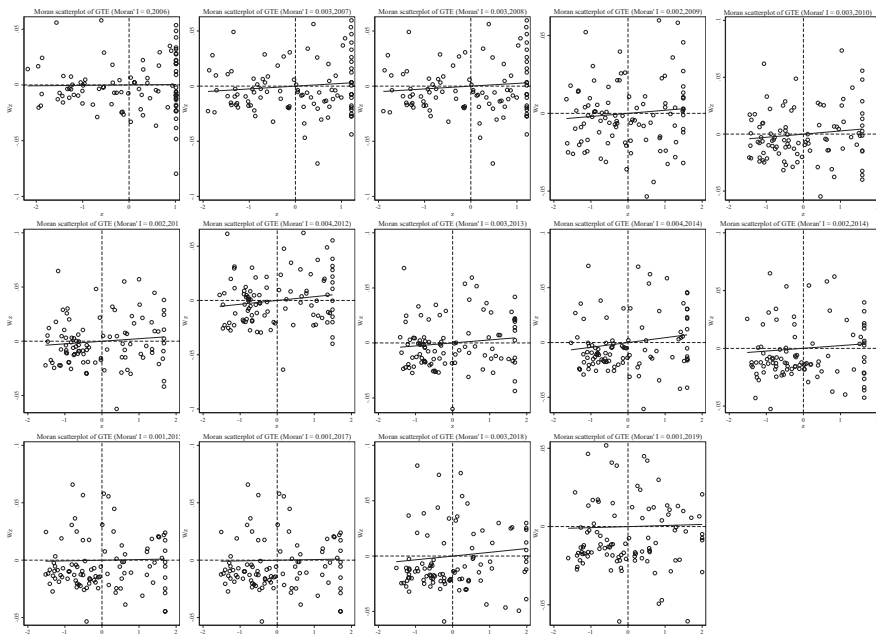


Figure 6. Distribution Change of GTE Moran's I Scatter plot from 2006 to 2019.

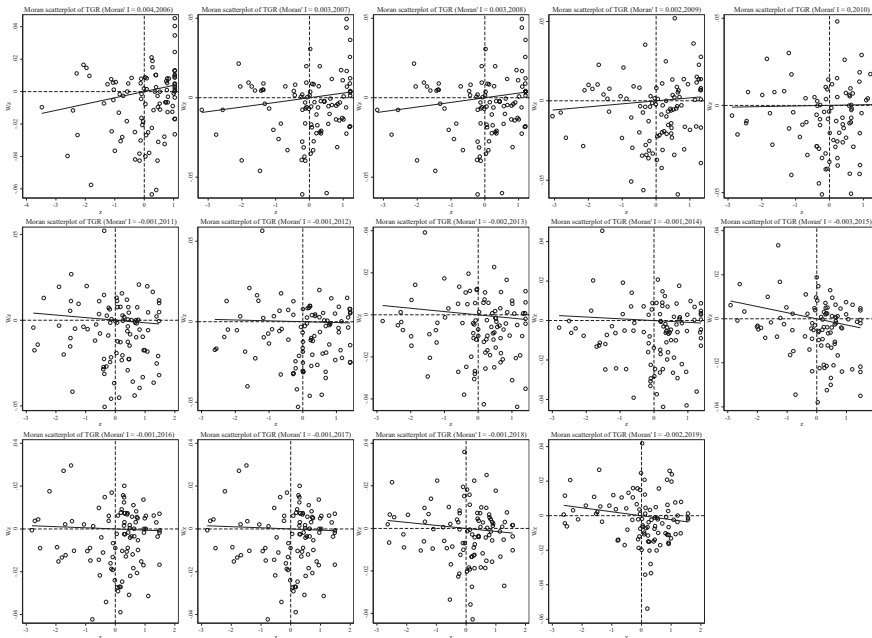


Figure 7. Distribution Change of TGR Moran's I Scatter plot from 2006 to 2019.

4.2.2. σ . Convergence Analysis

Figures 2–4 all discuss the change trend of general σ convergence, and the results do not reach a clear conclusion that there is general σ convergence in the input–output allocation efficiency of high-quality development of the mining city economy. Considering the spatial autocorrelation among MTE, GTE and TGR, the spatial σ convergence characteristics of three kinds of efficiency are discussed in detail. Unlike the general σ convergence model calculation formula and process [22], spatial σ convergence needs to be transferred into the spatial weight matrix (the spatial weight edge is used to calculate the spatial weight of Moran's I index). By deleting the missing value, the maximum likelihood estimation of the difference term and the lag of the variable is carried out. Finally, the standard deviation of the residual error of the regression result is calculated according to the time, and the change trend shown in Figure 8 is drawn. Figure 8 shows the temporal evolution trend of MTE, GTE and TGR standard deviations of input–output for high-quality economic development of mining cities to describe the spatial σ convergence of the mean value of input–output allocation efficiency for high-quality economic development of mining cities. As a whole, the standard deviation of the σ convergence of MTE, GTE and TGR in the sample period from 2006 to 2019 shows a downward trend. That is, there is significant spatial σ convergence in the growth of the input–output allocation efficiency of the high-quality economic development of mining cities, which cannot offset the internal downward trend, although some years have recovered. Specifically, the standard deviation of σ convergence in MTE, GTE and TGR space is relatively concentrated between [0.02,0.07], and the internal gap is in a slow narrowing trend: using 2013 as the watershed, the standard deviation of σ convergence in MTE, GTE and TGR space tends to decrease rapidly before 2013, and the internal gap is narrowed; after 2013, the standard deviation of σ convergence in MTE, GTE and TGR space rises slowly and then falls, and the internal gap is still in a narrowing trend. Figure 8D also shows that in 2006–2019, the highest standard deviation of the spatial σ convergence of mining resource-based cities is GTE, and the lowest is TGR, which shows that the gap between the technical drop ratio and mining cities is smaller, and the gap in GTE growth is gradually expanding.

Since MTE, GTE and TGR have spatial σ convergence in 2006–2019, this paper will conduct a β test on MTE, GTE and TGR to determine the convergence of input–output allocation efficiency in the process of high-quality economic development of mining cities.

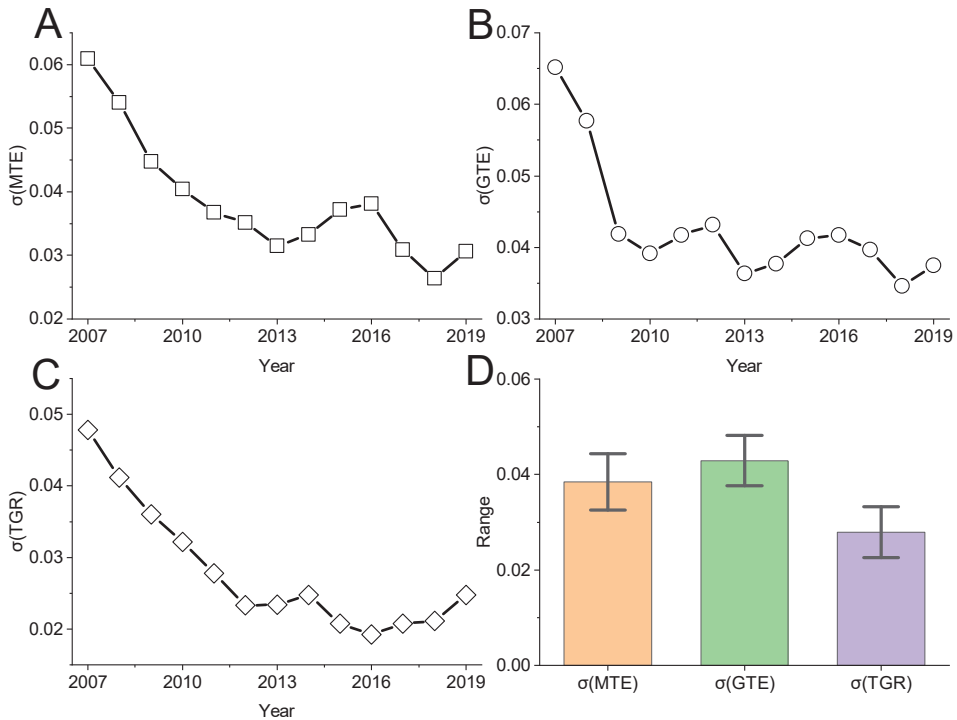


Figure 8. Annual trend of spatial σ convergence and descriptive statistical results. (A–C) represent σ convergence of MTE, GTE, TGR respectively. (D) represents the mean of σ convergence and its 95% confidence interval.

4.2.3. β . Convergence Analysis

Assuming that the macroeconomic development environment, regional policy, financial environment and industrial structure faced by mining cities are consistent, the economic development level of the four different types of mining cities gradually converges to the same development level over time in the sample period, which is called absolute β convergence. Then, the general expression of the absolute β convergence test can be obtained (10):

$$\frac{1}{T} \ln\left(\frac{x_{i,t}}{x_{i,t-1}}\right) = \alpha + \beta \ln(x_{i,t-1}) + \varepsilon \quad (10)$$

where $x_{i,t}$, $x_{i,t-1}$ represent the input–output allocation efficiency of high-quality economic development of mining cities in t and $t - 1$, respectively; α represents the constant term; β represents the convergence coefficient; and ε represents the error term. The formula for measuring the convergence of β is shown in (11):

$$\beta = -\frac{1 - e^{-\lambda T}}{T} \quad (11)$$

where λ is the rate of convergence. If $\beta < 0$, it means that there is convergence in the input–output allocation efficiency of the high-quality economic development of the mining city, that is, the development of the input–output allocation efficiency of the high-quality economic development of the mining city is converging; if $\beta > 0$, it means that the efficiency

of input–output allocation for high-quality economic development of mining cities does not have convergence. Because the spatial test results show that the input–output allocation efficiency of the high-quality economic development of mining cities has global spatial autocorrelation, due to the economic development of each mining city is not isolated but will be affected by the economic development of external regions, it is necessary to introduce the concept of spatial correlation to analyze the convergence of the input–output allocation efficiency of the high-quality economic development of mining cities. According to Formula (10), this paper constructs a spatial panel regression model with spatial absolute β convergence. The specific expression is as follows:

$$\frac{1}{T} \ln \left(\frac{x_{i,t}}{x_{i,t-1}} \right) = \alpha + \beta \ln(x_{i,t-1}) + \beta w_{i,j} \ln \left(\frac{x_{i,t}}{x_{i,t-1}} \right) + \varepsilon \quad (12)$$

where, $\ln \left(\frac{x_{i,t}}{x_{i,t-1}} \right)$ represents the allocation efficiency growth rate of mining city i in period t , ρ is the spatial regression coefficient, and $W_{i,j}$ is the spatial weight matrix. Therefore, it can reflect the efficiency of input–output allocation for the high-quality development of the mining city economy. The expression for the convergence rate is:

$$\gamma = -\frac{1}{T} \ln(1 + \beta) \quad (13)$$

For the accuracy of the model, the parameter estimation method adopted in this paper is the maximum likelihood method. When the spatial error model (SEM) or the spatial lag model (SLM) is selected, the test method is the LM test. SLM or SEM is determined by comparing IMlag and LMerr statistics. Because the LMlag statistics calculated by each mining city in this paper are higher than LMerr statistics, the results of the Hausmann test also point to the use of fixed effects. Therefore, the fixed-effect spatial lag model (SLM) is used to investigate the convergence characteristics of the input–output allocation efficiency of high-quality economic development in the mining cities. Table 3 shows the absolute β convergence results of the OLS model and the spatial lag model for the high-quality development input–output allocation efficiency of the mining city economy in 2006–2019.

Table 3 shows that the regression coefficient β of the input–output allocation efficiency of the high-quality development of the mining city economy is negative and significant at the 1% level when all research samples are tested for convergence, which indicates that the input–output allocation efficiency of the high-quality development of the mining city economy converges significantly during the sample period, there is an absolute convergence trend on the whole, and the growth gap of the input–output allocation efficiency of the high-quality development of the mining city economy gradually narrows. In terms of classification, the β values of the input–output allocation efficiency of the high-quality development of mature, regenerative, declining and growing mining cities are significantly negative and are all significant at the 1% level, indicating that the internal gap in the input–output allocation efficiency of the high-quality development of the four types of mining cities has a narrowing trend. The conclusion of the absolute β convergence test shows that the gap in the input–output allocation efficiency of high-quality economic development in mining cities is gradually narrowing. From a more accurate point of view, we can think that the efficiency of input–output allocation of high-quality economic development of mining cities presents the characteristics of “convergence”, and the growth gap of input–output allocation efficiency of four types of high-quality economic development of mining cities is gradually narrowing.

From the national level, the difference in the input–output allocation efficiency of the high-quality development of the mining city economy generally narrows, but the convergence speed is very slow, 0.0308, 0.0343 and 0.0271. From the perspective of the four types of mining cities, the common frontier efficiency of input–output allocation of high-quality development of mature, regenerative, declining and growing mining city economy (MTE) passes the absolute β convergence test, and the convergence speed is significantly

different, 0.0481, 0.0281, 0.0324 and 0.0294, respectively. Consistent with the convergence change of MTE, the convergence speed of GTE is 0.0477, 0.0299, 0.0448, 0.0345, and the convergence speed of TGR is not much different. The convergence speed of the TGR of the high-quality input–output configuration of the four types of mining cities is 0.0330, 0.0326, 0.0205, and 0.0277. Therefore, the high-quality input–output allocation efficiency of the overall and four types of mining cities will eventually converge to the same value.

Table 3. Summary of absolute β convergence results of input-output allocation efficiency space for high-quality economic development of mining cities.

Vars	(1) OLS	(2) FE	(3) RE	(4) FE	(5) FE	(6) FE	(7) FE
	Overall	Overall	Overall	Growth	Mature	Decay	Regenerative
Panel A							
l.MTE	−0.129 *** (0.0128)	−0.350 *** (0.0212)	−0.129 *** (0.0128)	−0.490 *** (0.0783)	−0.325 *** (0.0267)	−0.365 *** (0.0500)	−0.337 *** (0.0605)
Constant	0.0570 *** (0.00699)	0.167 *** (0.0109)	0.0570 *** (0.00699)	0.306 *** (0.0504)	0.144 *** (0.0130)	0.180 *** (0.0265)	0.168 *** (0.0320)
λ	0.0099	0.0308	0.0099	0.0481	0.0281	0.0324	0.0294
Obs	1287	1287	1287	117	741	247	182
R2	0.073	0.186		0.268	0.178	0.190	0.156
Panel B							
l.GTE	−0.122 *** (0.0131)	−0.381 *** (0.0218)	−0.122 *** (0.0131)	−0.487 *** (0.0699)	−0.342 *** (0.0287)	−0.466 *** (0.0555)	−0.383 *** (0.0527)
Constant	0.0715 *** (0.00887)	0.236 *** (0.0142)	0.0715 *** (0.00887)	0.375 *** (0.0559)	0.183 *** (0.0162)	0.373 *** (0.0453)	0.242 *** (0.0354)
λ	0.0093	0.0343	0.0093	0.0477	0.0299	0.0448	0.0345
Obs	1287	1287	1287	117	741	247	182
R2	0.063	0.204		0.312	0.172	0.237	0.241
Panel C							
l.TGR	−0.108 *** (0.0119)	−0.316 *** (0.0210)	−0.108 *** (0.0119)	−0.370 *** (0.0728)	−0.366 *** (0.0296)	−0.249 *** (0.0464)	−0.321 *** (0.0504)
Constant	0.0814 *** (0.00956)	0.246 *** (0.0167)	0.0814 *** (0.00956)	0.296 *** (0.0575)	0.303 *** (0.0251)	0.150 *** (0.0293)	0.255 *** (0.0404)
λ	0.0082	0.0271	0.0082	0.0330	0.0326	0.0205	0.0277
Obs	1287	1287	1287	117	741	247	182
R2	0.060	0.160		0.195	0.182	0.112	0.195

Note: Values in brackets are standard error values, Panel A represents sample data of MTE, Panel B represents sample data of GTE and Panel C represents sample data of TGR. *** indicate statistical significance at 1%.

4.3. Decomposition of High-Quality Input-Output Allocation Inefficiency of Mining Cities in Different Regions

Although the Meta-Frontier method is used to estimate the common frontier efficiency MTE, group efficiency GTE and technical gap ratio TGR of high-quality input–output allocation of regional mining cities, it is impossible to determine the efficiency difference and the true root of inefficiency among the mining cities and by the mining city type. However, the numerical difference in TGR provides a solution for distinguishing the root causes of the high-quality input–output allocation inefficiency of different mining cities [25,26]. Some scholars have found that the main reasons for the current efficiency loss are the gap in cutting-edge technology and the management inefficiency caused by group management decisions. Based on the research ideas of [10], the inefficiency of high-quality input and output allocation of 99 mining cities is decomposed into the inefficiency of the production technology gap caused by the group and common frontier TGRI (Technology Gap Ratio Inefficiency, TGRI) and the inefficiency of management within the group Group-specific Managerial Inefficiency (GMI). TGRI and GMI together constitute

the total inefficiency loss meta-frontier total inefficiency (MTI), as shown in Formulas (14)–(16), and the results are shown in Appendix A Table A2.

$$TGRI_n^i = GTE_n^i \times (1 - TGR_n^i) \quad (14)$$

$$GMI_n^i = 1 - GTE_n^i \quad (15)$$

$$MTI_n^i = TGRI_n^i + GMI_n^i \quad (16)$$

It needs to be explained that, in combination with the actual characteristics of high-quality input–output allocation of the mining city economy and referring to the research idea of [26], when the proportion of TGRI is obviously higher (more than 70%), it needs to improve the efficiency of regional investment allocation by improving the group environment, while when the proportion of GMI is higher (more than 70%), it needs to improve the efficiency level by improving the high-quality input–output allocation capacity of the regional mining city economy. When the proportion of TGRI and GMI is equal, it indicates that the group needs to improve the innovation environment and improve the high-quality input–output allocation capacity of regional mining cities [27].

First, from the point of view of type, the loss of invalidity rate and improvement path of different groups have obvious heterogeneity. From 2006 to 2019, the contribution degree of mature mining cities was 12.8400% for TGRI, 44.3448% for GMI and 57.1847% for MTI, which indicates that the key to improving the efficiency of input–output allocation is to further improve the allocation capacity of mining cities. The average contribution degrees of the TGRI, GMI and MTI of regenerative mining cities are 13.2444%, 33.9072% and 47.1516%, respectively, which also indicates that the optimization of input and output factors is the most important for the high-quality development of regenerative mining cities. The average contribution degrees of the TGRI, GMI and MTI of declining mining cities are 10.9328%, 18.7332% and 29.6660%, respectively. The results show that the contribution degrees of TGRI and GMI have little difference, which is very important for the high-quality economic development of declining mining cities, the overall improvement of resource factor input–output allocation capacity and the improvement of the group environment. The results of the growing mining cities are similar to those of the regenerative and mature ones, but the contribution of TGRI and GMI of the growing mining cities is not distinct, that is, in the process of high-quality economic development of the growing mining cities, it is mainly to optimize the input–output allocation capacity of resource elements, but it is necessary to improve the group environment.

Second, from the perspective of urban distribution, there is obvious heterogeneity in the loss of urban inefficiency and the improvement path. The contribution degree of TGRI and GMI is lower than 70%, but the ineffective loss degree of some mining cities is close to 70%. From the mean, the contribution of TGRI is much lower than that of GMI. The cities whose GMI contribution is close to 70% are Yuncheng, Baise, Zhangjiakou, Xingtai, Weinan, Hechi and Changzhi. These mining cities are mature, and the key to improving the efficiency of high-quality input–output allocation is the ability of input–output allocation. The cities with similar contribution ratios of GMI and TGRI include Baoshan, Chizhou, Daqing, Datong, Handan, Jixi, Jincheng, Loudi and Yichun, Ordos, Nanchong, Shuozhou and Yulin, Hegang, Puyang and Wuhai, Baotou, Huludao, Lijiang, Tonghua and Xuzhou. These TGRI and GMI are basically the same degree of inefficiency, belonging to provinces and cities that need to improve the regional innovation environment and improve the high-quality input–output allocation capacity of regional mining cities.

5. Conclusions

With the in-depth implementation of the National Sustainable Development Plan for Resource-based Cities (2013–2020), the scale, structure and intensity of high-quality input–output allocation of China’s mining cities have been improved to a certain extent. However, there are also some phenomena and problems in which the efficiency of resource allocation is not high, which restricts the sustainability of high-quality economic development. In

this paper, the DEA meta-frontier method is used to estimate the allocation efficiency of high-quality input and output under the common frontier and group frontier of 99 mining cities in China from 2006 to 2019, and the convergence of the allocation efficiency and the future improvement path are discussed. The results show the following (This conclusion is accurate in China, but it may be the opposite in other countries. We will discuss the high-quality development of mining cities in a larger scale for further research).

First, in terms of the efficiency and technology gap ratio of the common frontier and group frontier, (1) the input factors of the high-quality input–output allocation of national regional mining cities under the common frontier and group frontier has 49.54% and 71.94% saving space, respectively. (2) Under the common frontier, the average value of MTE from high to low is growth, regenerative, declining, and mature. In comparison, regenerative, declining, and mature mining cities still have low economic high-quality input–output allocation efficiency. There may be a certain “resource waste” problem or there may be insufficient input of resource elements.

Second, the common frontier efficiency of economic development among mining cities has a positive correlation in the sample period, and it shows the phenomenon of spatial agglomeration on the whole. The standard deviation of the spatial σ convergence of MTE, GTE and TGR in the sample period from 2006 to 2019 shows a downward trend; that is, there is a significant spatial σ convergence in the increase in the input–output allocation efficiency of high-quality economic development of mining cities. Although some years have a rise, it cannot offset the internal downward trend. From the national level, the difference in the input–output allocation efficiency of high-quality economic development in mining cities is narrowing on the whole, but the convergence speed is very slow; the convergence speed of the input–output allocation efficiency of high-quality economic development in mature, regenerative, declining and growing mining cities is quite different.

Third, in view of the high quality of mature mining city economy, the key to improving the efficiency of input–output allocation is to further improve the allocation capacity of the mining city; optimizing the allocation of the input–output factors is the most important to achieve high-quality development of regenerative type; for recession type, it is very important to comprehensively improve the allocation capacity of input–output of resource factors and improve the group environment; in the process of high-quality development of growing mining city economy, it is mainly to optimize the allocation capacity of input–output of resource factors, but it is necessary to improve the group environment.

Combined with the characteristics of high-quality input–output allocation of mining cities, the policy implications include the following:

One is to comprehensively strengthen cross-regional sustainable cooperation among mature, renewable, declining and growing mining cities. We should give full play to the leading radiation and source supply role of the national mining city regeneration demonstration zone, explore the establishment of a long-term mechanism to improve win–win cooperation, and improve the level and level of cross-mining city type cooperation. Efforts should be made to promote the construction of a cross-regional system of recession-type and regeneration-type key mining cities and growing mining cities and to explore the benefit-sharing mechanism and win–win cooperation mode of the orderly transfer of resource elements along four types of plate gradients.

The second is to build a mining city policy consortium around the common scientific issues of sustainable development. On the one hand, we will adhere to the combination of central planning and local responsibilities, fully mobilize local authorities to optimize the high-quality economic development environment of mining cities and improve the allocation capacity of input and output factors; on the other hand, we will promote the establishment of joint research centers and other resource condition platforms among mining cities, carry out joint tackling of key technologies common to the sustainability of mining cities, and encourage and support the formulation of joint sustainability policies and measures among regions.

The third is to coordinate the high-quality input–output allocation of mature, renewable, declining and growing mining cities. On the one hand, it is necessary to improve the development and utilization efficiency of resource elements of different types of mining cities and accelerate the conversion of new and old kinetic energy. On the other hand, at the top-level design level, the allocation of high-quality input and output of the mining city economy needs to be prioritized to declining cities, adhere to the combination of “blood supply” and “hematopoiesis”, and continuously improve the resource agglomeration function and ecological environment of declining mining cities to improve the economic high-quality input–output allocation capacity of declining mining cities.

Finally, it is necessary to optimize the mutual aid mechanism of different types of mining cities and explore and establish a perfect support mechanism of mature mining cities to grow and regenerate mining cities in order to promote the reasonable flow of talent, technology and funds to grow declining mining cities.

Author Contributions: Conceptualization, J.Y.; Data curation, W.X. and J.Y.; Formal analysis, W.X.; Funding acquisition, J.C.; Methodology, W.X.; Project administration, J.C.; Supervision, J.C.; Visualization, J.Y.; Writing–original draft, W.X.; Writing–review & editing, J.Y. All authors have read and agreed to the published version of the manuscript.

Funding: This research was funded by National Natural Science Foundation of China (No. 71991482).

Institutional Review Board Statement: Not applicable.

Informed Consent Statement: Not applicable.

Data Availability Statement: Publicly available datasets were analyzed in this study. These datasets can be found here: <https://data.stats.gov.cn/> (accessed on 18 March 2022).

Acknowledgments: We are grateful the Major Program of the National Natural Science Foundation of China (NSFC) (No. 71991482).

Conflicts of Interest: The authors declare no conflict of interest.

Appendix A

Table A1. Statistical description of input-output allocation efficiency of mining cities from 2006 to 2019.

Sort	City	MTE	Rank	GTE	Rank	TGR	Rank	Sort	City	MTE	Rank	GTE	Rank	TGR	Rank
Mature	Anshun	0.5275	32	0.5488	63	0.7239	76	Mature	Yichun	0.3993	65	0.4507	80	0.4938	96
Mature	Baise	0.2945	97	0.3401	98	0.8031	60	Mature	Yunfu	0.3472	84	0.4208	90	0.8506	35
Mature	Baoji	0.3509	83	0.4155	91	0.6997	80	Mature	Yuncheng	0.2595	99	0.3154	99	0.7176	78
Mature	Baoshan	0.4395	54	0.5367	67	0.6034	88	Mature	Zhangjiakou	0.2953	96	0.3656	97	0.8142	51
Mature	Benxi	0.4911	41	0.5585	60	0.7987	61	Mature	Changzhi	0.3140	93	0.3962	93	0.8312	40
Mature	Bozhou	0.6501	21	0.7941	29	0.7778	68	Mature	Chongqing	0.3343	90	0.4112	92	0.6899	83
Mature	Chenzhou	0.4487	52	0.5512	61	0.7202	77	Mature	Zigong	0.5809	25	0.6294	45	0.8318	39
Mature	Chengde	0.3970	68	0.5383	66	0.8147	50	Growth	Erdos	0.8338	9	0.9380	7	0.8096	55
Mature	Chizhou	0.4319	57	0.4904	73	0.4360	99	Growth	Hezhou	0.4788	44	0.6455	41	0.7924	66
Mature	Chifeng	0.4718	46	0.5967	53	0.8262	43	Growth	Hulunbeier	0.6646	19	0.8336	24	0.8240	45
Mature	Chuzhou	0.5067	36	0.5845	55	0.7967	64	Growth	Liupanshui	0.2970	95	0.4255	86	0.8107	53
Mature	Dazhou	0.4795	43	0.5817	56	0.8105	54	Growth	Nanchong	0.8793	6	0.9179	13	0.9790	2
Mature	Daqing	0.9346	2	0.9538	4	0.7981	63	Growth	Shuozhou	0.7055	15	0.9739	2	0.8710	22
Mature	Datong	0.3650	77	0.4291	85	0.4506	98	Growth	Songyuan	0.8204	11	0.9378	8	0.7505	73
Mature	Dongying	0.9108	4	0.9202	12	0.8346	37	Growth	Xianyang	0.3384	88	0.5968	52	0.8253	44
Mature	Ezhou	0.5724	26	0.6319	44	0.7363	74	Growth	Yulin	0.7193	14	0.8723	18	0.9616	6

Table A1. Cont.

Sort	City	MTE	Rank	GTE	Rank	TGR	Rank	Sort	City	MTE	Rank	GTE	Rank	TGR	Rank
Mature	Ganzhou	0.4150	62	0.4613	77	0.5921	89	Decay	Baishan	0.5235	33	0.8642	21	0.8619	29
Mature	Guang'an	0.8861	5	0.9167	14	0.8600	30	Decay	Fushun	0.4578	50	0.8732	17	0.8923	14
Mature	Guangyuan	0.6178	23	0.6583	39	0.7948	65	Decay	Fuxin	0.4756	45	0.7297	33	0.8400	36
Mature	Handan	0.3827	71	0.4947	72	0.4836	97	Decay	Hegang	0.8140	12	0.9093	16	0.8924	13
Mature	Hechi	0.3360	89	0.3956	94	0.9685	4	Decay	Huaibei	0.4257	59	0.6241	47	0.7987	62
Mature	Hebi	0.3852	70	0.4567	78	0.5908	90	Decay	Huang	0.3443	85	0.6998	36	0.8176	48
Mature	Heihe	0.8431	8	0.8694	19	0.9346	9	Decay	Jiaozuo	0.3721	74	0.8423	23	0.9638	5
Mature	Hengyang	0.3650	76	0.4414	82	0.9709	3	Decay	Jingdezhen	0.3398	87	0.6645	38	0.8043	59
Mature	Huzhou	0.3928	69	0.4530	79	0.8916	15	Decay	Liaoyuan	0.6839	16	0.9666	3	0.8327	38
Mature	Huainan	0.3815	72	0.4435	81	0.6896	84	Decay	Luzhou	0.3776	73	0.7363	31	0.8068	57
Mature	Jixi	0.7507	13	0.8107	27	0.9226	10	Decay	Pingxiang	0.4140	63	0.7009	35	0.8809	18
Mature	Jilin	0.4166	61	0.5129	71	0.6891	85	Decay	Puyang	0.5388	30	0.9163	15	0.9901	1
Mature	Jining	0.3702	75	0.4775	75	0.7037	79	Decay	Qitaihe	0.8247	10	0.9207	11	0.8699	24
Mature	Jincheng	0.4478	53	0.5248	68	0.5176	94	Decay	Shaoguan	0.2751	98	0.5494	62	0.9552	7
Mature	Laiwu	0.5073	35	0.6356	43	0.6438	87	Decay	Tongling	0.6576	20	0.9323	10	0.7921	67
Mature	Lincang	0.4248	60	0.5620	59	0.7346	75	Decay	Wuhai	0.9535	1	0.9788	1	0.9529	8
Mature	Linfen	0.3546	81	0.4252	87	0.6929	82	Decay	Xinyu	0.4361	55	0.8501	22	0.8235	46
Mature	Longyan	0.4977	39	0.5696	57	0.9156	11	Decay	Yichun	0.6104	24	0.8666	20	0.7760	69
Mature	Loudi	0.3972	67	0.4391	83	0.5219	93	Decay	Zaozhuang	0.3647	78	0.8157	26	0.8648	28
Mature	Mudanjiang	0.4983	38	0.6118	49	0.8716	20	Regenerative	Anshan	0.5059	37	0.6218	48	0.8695	25
Mature	Nanping	0.4534	51	0.5232	69	0.6605	86	Regenerative	Baotou	0.6396	22	0.9341	9	0.8710	21
Mature	Panzhihua	0.5220	34	0.6534	40	0.8115	52	Regenerative	Huludao	0.3516	82	0.4830	74	0.5074	95
Mature	Pingdingshan	0.3342	91	0.4219	89	0.8966	12	Regenerative	Lijiang	0.8443	7	0.9408	6	0.8048	58
Mature	Qijing	0.3550	80	0.4361	84	0.6946	81	Regenerative	Linyi	0.4604	49	0.5468	64	0.8699	23
Mature	Sanmenxia	0.4121	64	0.5206	70	0.8880	17	Regenerative	Luoyang	0.4357	56	0.6259	46	0.8551	34
Mature	Sanming	0.3579	79	0.4251	88	0.7694	71	Regenerative	Ma'anshan	0.3989	66	0.5950	54	0.8095	56
Mature	Shaoyang	0.5286	31	0.8210	25	0.8655	27	Regenerative	Nanyang	0.4948	40	0.5996	51	0.8691	26
Mature	Suzhou	0.5499	29	0.7324	32	0.7579	72	Regenerative	Panjin	0.9199	3	0.9461	5	0.8756	19
Mature	Taian	0.5652	28	0.6822	37	0.8563	33	Regenerative	Suqian	0.5714	27	0.7100	34	0.8571	31
Mature	Weinan	0.3232	92	0.3753	95	0.8148	49	Regenerative	Tangshan	0.4636	48	0.6040	50	0.8292	41
Mature	Xingtai	0.3033	94	0.3748	96	0.7717	70	Regenerative	Tonghua	0.3440	86	0.4622	76	0.5223	92
Mature	Xuancheng	0.4855	42	0.5627	58	0.8903	16	Regenerative	Xuzhou	0.4275	58	0.5440	65	0.5890	91
Mature	Ya'an	0.6728	17	0.7667	30	0.8570	32	Regenerative	Zibo	0.4663	47	0.6398	42	0.8269	42
Mature	Yangquan	0.6680	18	0.8078	28	0.8186	47								

Table A2. Main paths of inefficient decomposition of high-quality input-output allocation and improvement of efficiency in mining cities.

Category	City	TGRI	GMI	MTI	Improved Group Technology	Improve Management Level	Category	City	TGRI	GMI	MTI	Improved Group Technology	Improve Management Level
Mature	Anshun	15.1510%	45.1210%	60.2720%			Mature	Yichun	22.8149%	54.9300%	77.7449%	△	△
Mature	Baise	6.6974%	65.9910%	72.6884%		△	Mature	Yunfu	6.2855%	57.9230%	64.2085%		
Mature	Baoji	12.4792%	58.4510%	70.9302%			Mature	Yuncheng	8.9069%	68.4610%	77.3679%		△
Mature	Baoshan	21.2818%	46.3340%	67.6158%	△	△	Mature	Zhangjiakou	6.7936%	63.4420%	70.2356%		
Mature	Benxi	11.2415%	44.1470%	55.3885%			Mature	Changzhi	6.6868%	60.3840%	67.0708%		

Table A2. Cont.

Category	City	TGRI	GMI	MTI	Improved Group Technology	Improve Management Level	Category	City	TGRI	GMI	MTI	Improved Group Technology	Improve Management Level
Mature	Bozhou	17.6493%	20.5880%	38.2373%	△	△	Mature	Chongqing	12.7538%	58.8760%	71.6298%		
Mature	Chenzhou	15.4206%	44.8850%	60.3056%			Mature	Zigong	10.5843%	37.0620%	47.6463%		
Mature	Chengde	9.9744%	46.1660%	56.1404%			Growth	Erdos	17.8593%	6.2010%	24.0603%	△	△
Mature	Chizhou	27.6574%	50.9620%	78.6194%	△	△	Growth	Hezhou	13.3986%	35.4500%	48.8486%		
Mature	Chifeng	10.3710%	40.3280%	50.6990%			Growth	Hulunbeier	14.6677%	16.6420%	31.3097%	△	△
Mature	Chuzhou	11.8856%	41.5510%	53.4366%			Growth	Liupanshui	8.0563%	57.4530%	65.5093%		
Mature	Dazhou	11.0205%	41.8350%	52.8555%			Growth	Nanchong	1.9239%	8.2120%	10.1359%	△	△
Mature	Daqing	19.2546%	4.6190%	23.8736%	△	△	Growth	Shuozhou	12.5621%	2.6120%	15.1741%	△	△
Mature	Datong	23.5753%	57.0930%	80.6683%	△	△	Growth	Songyuan	23.3950%	6.2250%	29.6200%		
Mature	Dongying	15.2171%	7.9760%	23.1931%			Growth	Xianyang	10.4266%	40.3240%	50.7506%		
Mature	Ezhou	16.6618%	36.8080%	53.4698%			Growth	Yulin	3.3498%	12.7660%	16.1158%	△	△
Mature	Ganzhou	18.8174%	53.8710%	72.6884%			Decay	Baishan	11.9393%	13.5770%	25.5163%	△	△
Mature	Guang'an	12.8356%	8.3300%	21.1656%	△	△	Decay	Fushun	9.4038%	12.6770%	22.0808%	△	△
Mature	Guangyuan	13.5062%	34.1740%	47.6802%			Decay	Fuxin	11.6737%	27.0350%	38.7087%		
Mature	Handan	25.5493%	50.5290%	76.0783%	△	△	Decay	Hegang	9.7875%	9.0720%	18.8595%	△	△
Mature	Hechi	1.2450%	60.4380%	61.6830%			Decay	Huaibei	12.5642%	37.5940%	50.1582%		
Mature	Hebi	18.6894%	54.3270%	73.0164%			Decay	Huang	12.7652%	30.0190%	42.7842%		
Mature	Heihe	5.6874%	13.0630%	18.7504%	△	△	Decay	Jiaozuo	3.0476%	15.7660%	18.8136%		
Mature	Hengyang	1.2827%	55.8590%	57.1417%			Decay	Jingdezhen	13.0055%	33.5540%	46.5595%		
Mature	Huzhou	4.9125%	54.6980%	59.6105%			Decay	Liaoyuan	16.1688%	3.3370%	19.5058%		
Mature	Huainan	13.7679%	55.6460%	69.4139%			Decay	Luzhou	14.2279%	26.3720%	40.5999%	△	△
Mature	Jixi	6.2764%	18.9300%	25.2064%	△	△	Decay	Pingxiang	8.3512%	29.9100%	38.2612%		
Mature	Jilin	15.9454%	48.7120%	64.6574%			Decay	Puyang	0.9080%	8.3740%	9.2820%	△	△
Mature	Jining	14.1464%	52.2550%	66.4014%			Decay	Qitaihe	11.9816%	7.9330%	19.9146%	△	△
Mature	Jincheng	25.3164%	47.5210%	72.8374%	△	△	Decay	Shaoguan	2.4614%	45.0590%	47.5204%		
Mature	Laiwu	22.6440%	36.4360%	59.0800%	△	△	Decay	Tongling	19.3833%	6.7660%	26.1493%		
Mature	Lincang	14.9152%	43.7970%	58.7122%			Decay	Wuhai	4.6080%	2.1240%	6.7320%	△	△
Mature	Linfen	13.0564%	57.4850%	70.5414%			Decay	Xinyu	15.0056%	14.9920%	29.9976%	△	△
Mature	Longyan	4.8077%	43.0440%	47.8517%			Decay	Yichun	19.4123%	13.3380%	32.7503%	△	△
Mature	Loudi	20.9915%	56.0940%	77.0855%	△	△	Decay	Zaozhuang	11.0289%	18.4310%	29.4599%	△	△
Mature	Mudanjiang	7.8532%	38.8190%	46.6722%			Regenerative	Anshan	8.1150%	37.8210%	45.9360%		
Mature	Nanping	17.7634%	47.6840%	65.4474%			Regenerative	Baotou	12.0467%	6.5930%	18.6397%	△	△
Mature	Panzhihua	12.3170%	34.6650%	46.9820%			Regenerative	Huludao	23.7931%	51.7010%	75.4941%	△	△
Mature	Pingdingshan	4.3632%	57.8110%	62.1742%			Regenerative	Lijiang	18.3619%	5.9230%	24.2849%	△	△
Mature	Qijiang	13.3212%	56.3870%	69.7082%			Regenerative	Linyi	7.1122%	45.3200%	52.4322%		
Mature	Sanmenxia	5.8291%	47.9450%	53.7741%			Regenerative	Luoyang	9.0703%	37.4120%	46.4823%		
Mature	Sanming	9.8013%	57.4910%	67.2923%			Regenerative	Ma'anshan	11.3359%	40.4970%	51.8329%		
Mature	Shaoyang	11.0470%	17.8970%	28.9440%	△	△	Regenerative	Nanyang	7.8475%	40.0450%	47.8925%		
Mature	Suzhou	17.7324%	26.7560%	44.4884%	△	△	Regenerative	Panjin	11.7662%	5.3860%	17.1522%	△	△
Mature	Taian	9.8022%	31.7820%	41.5842%			Regenerative	Suqian	10.1492%	28.9970%	39.1462%		
Mature	Weinan	6.9498%	62.4680%	69.4178%			Regenerative	Tangshan	10.3168%	39.6040%	49.9208%		
Mature	Xingtai	8.5563%	62.5200%	71.0763%			Regenerative	Tonghua	22.0770%	53.7810%	75.8580%	△	△
Mature	Xuancheng	6.1716%	43.7260%	49.8976%			Regenerative	Xuzhou	22.3566%	45.5990%	67.9556%	△	△
Mature	Ya'an	10.9657%	23.3330%	34.2987%			Regenerative	Zibo	11.0727%	36.0220%	47.0947%		

△ reflects main path of improvement of efficiency in mining cities.

References

1. Zhang, N.; Zhou, P.; Choi, Y. Energy efficiency, CO₂ emission performance and technology gaps in fossil fuel electricity generation in Korea: A meta-frontier non-radial directional distance function analysis. *Energy Policy* **2013**, *56*, 653–662. [[CrossRef](#)]
2. Yan, D.; Kong, Y.; Ye, B.; Shi, Y.; Zeng, X. Spatial variation of energy efficiency based on a Super-Slack-Based Measure: Evidence from 104 resource-based cities. *J. Clean. Prod.* **2019**, *240*, 117669. [[CrossRef](#)]
3. Jing, Z.; Wang, J. Sustainable development evaluation of the society–energy–environment in a resource-based city of China: A complex network approach. *J. Clean. Prod.* **2020**, *263*, 121510. [[CrossRef](#)]
4. Liu, X.; Meng, X. Evaluation and empirical research on the energy efficiency of 20 mining cities in Eastern and Central China. *Int. J. Min. Sci. Technol.* **2018**, *28*, 525–531. [[CrossRef](#)]
5. Ruan, F.; Yan, L.; Wang, D. The complexity for the resource-based cities in China on creating sustainable development. *Cities* **2020**, *97*, 102571. [[CrossRef](#)]
6. Song, M.; Zhao, X.; Shang, Y. The impact of low-carbon city construction on ecological efficiency: Empirical evidence from quasi-natural experiments. *Resour. Conserv. Recycl.* **2020**, *157*, 104777. [[CrossRef](#)]
7. Chen, W.; Chen, W.; Ning, S.; Liu, E.; Zhou, X.; Wang, Y.; Zhao, M. Exploring the industrial land use efficiency of China's resource-based cities. *Cities* **2019**, *93*, 215–223. [[CrossRef](#)]
8. Deng, W. Evaluating Transformation Efficiency of Resource-based Coastal Cities: An AHP and DEA Based Analysis. *J. Coast. Res.* **2019**, *94* (Suppl. S1), 878–882. [[CrossRef](#)]
9. Hu, Y.; Yan, T.; Chen, F. Energy and Environment Performance of Resource-Based Cities in China: A Non-Parametric Approach for Estimating Hyperbolic Distance Function. *Int. J. Environ. Res. Public Health* **2020**, *17*, 4795. [[CrossRef](#)]
10. Xiao, H.; Wang, D.; Qi, Y.; Shao, S.; Zhou, Y.; Shan, Y. The governance-production nexus of eco-efficiency in Chinese resource-based cities: A two-stage network DEA approach. *Energy Econ.* **2021**, *101*, 105408. [[CrossRef](#)]
11. Bui, T.-D.; Tsai, F.M.; Tseng, M.-L.; Wu, K.-J.; Chiu, A.S. Effective municipal solid waste management capability under uncertainty in Vietnam: Utilizing economic efficiency and technology to foster social mobilization and environmental integrity. *J. Clean. Prod.* **2020**, *259*, 120981. [[CrossRef](#)]
12. Yuan, J.; Bian, Z.; Yan, Q.; Pan, Y. Spatio-Temporal Distributions of the Land Use Efficiency Coupling Coordination Degree in Mining Cities of Western China. *Sustainability* **2019**, *11*, 5288. [[CrossRef](#)]
13. Zhang, H.; Shen, L.; Zhong, S.; Elshkaki, A. Economic Structure Transformation and Low-Carbon Development in Energy-Rich Cities: The Case of the Contiguous Area of Shanxi and Shaanxi Provinces, and Inner Mongolia Autonomous Region of China. *Sustainability* **2020**, *12*, 1875. [[CrossRef](#)]
14. Yu, Y.; Huang, J.; Zhang, N. Modeling the eco-efficiency of Chinese prefecture-level cities with regional heterogeneities: A comparative perspective. *Ecol. Model.* **2019**, *402*, 1–17. [[CrossRef](#)]
15. Yin, Q.; Wang, Y.; Wan, K.; Wang, D. Evaluation of green transformation efficiency in Chinese mineral resource-based cities based on a three-stage DEA method. *Sustainability* **2020**, *12*, 9455. [[CrossRef](#)]
16. Battese, G.E.; Rao, D.S.P. Technology gap, efficiency, and a stochastic metafrontier function. *Int. J. Bus. Econ.* **2002**, *1*, 87.
17. O'Donnell, C.J.; Rao, D.S.; Battese, G.E. Metafrontier frameworks for the study of firm-level efficiencies and technology ratios. *Empir. Econ.* **2008**, *34*, 231–255. [[CrossRef](#)]
18. Liu, W.B.; Zhang, D.Q.; Meng, W.; Li, X.X.; Xu, F. A study of DEA models without explicit inputs. *Omega* **2011**, *39*, 472–480. [[CrossRef](#)]
19. Wang, D.; Li, S.; Sueyoshi, T. DEA environmental assessment on US Industrial sectors: Investment for improvement in operational and environmental performance to attain corporate sustainability. *Energy Econ.* **2014**, *45*, 254–267. [[CrossRef](#)]
20. He, J.H.; He, C.H.; Sedighi, H.M. Evans model for dynamic economics revised. *AIMS Math.* **2021**, *6*, 9194–9206. [[CrossRef](#)]
21. Liu, Y. Analysis of the Efficiency of Environmental Regulation on the Transformation of the Resource-based Cities. *IOP Conf. Ser. Earth Environ. Sci.* **2020**, *598*, 012038. [[CrossRef](#)]
22. Peng, J.; Wen, L.; Fu, L.; Yi, M. Total factor productivity of cultivated land use in China under environmental constraints: Temporal and spatial variations and their influencing factors. *Environ. Sci. Pollut. Res.* **2020**, *27*, 18443–18462. [[CrossRef](#)] [[PubMed](#)]
23. Baumol, W.J. Productivity Growth, Convergence, and Welfare: What the Long-Run Data Show. *Am. Econ. Rev.* **1986**, *76*, 1072–1085.
24. Anselin, L. Lagrange multiplier test diagnostics for spatial dependence and spatial heterogeneity. *Geogr. Anal.* **1988**, *20*, 1–17. [[CrossRef](#)]
25. Qunwei, W.; Peng, Z.; Dequn, Z. Heterogeneity of production technology, carbon dioxide emission and performance lose: An international comparison based on meta-frontier. *Sci. Res. Manag.* **2014**, *35*, 41.
26. Chiu, Y.H.; Huang, K.Y.; Chang, T.H.; Lin, T.Y. Efficiency assessment of coal mine use and land restoration: Considering climate change and income differences. *Resour. Policy* **2021**, *73*, 102130. [[CrossRef](#)]
27. Xiao, W.; Zhang, H.Y.; Zhang, J.Y. GIS-based Analysis of LS Factor under Coal Mining Subsidence Impacts in Sandy Region. *J. Eng. Sci. Technol. Rev.* **2014**, *7*, 4. [[CrossRef](#)]



Article

Economic Feasibility Study of a Carbon Capture and Storage (CCS) Integration Project in an Oil-Driven Economy: The Case of the State of Kuwait

Adel Naseeb ¹, Ashraf Ramadan ² and Sultan Majed Al-Salem ^{2,*}

¹ Techno-Economics Department, Science and Technology Sector, Kuwait Institute for Scientific Research (KISR), P.O. Box 24885, Safat 13109, Kuwait; ajnaseeb@kisir.edu.kw

² Environment and Life Sciences Research Centre, Kuwait Institute for Scientific Research (KISR), P.O. Box 24885, Safat 13109, Kuwait; aramadan@kisir.edu.kw

* Correspondence: ssalem@kisir.edu.kw

Abstract: The rapid growth and urbanization rate, coupled with hot climate and scarce rainfall, makes it essential for a country like Kuwait to have several power and desalination plants with high-generating capacity. These plants are entirely reliant on burning fossil fuels as a source of thermal energy. These plants are also universally accepted to be the largest CO₂ emitters; hence, they present a potential for carbon capture and storage (CCS). Having established the suitability of the existing conditions for post-combustion CCS, a techno-economic-based feasibility study, which took into consideration local power generation technologies and economic conditions, was performed. Relying on fifteen case study models and utilizing the concept of levelized cost of electricity (LCOE), the statistical average method (SAM) was used to assess CCS based on realistic and reliable economic indicators. Zour power station, offering the highest potential CO₂ stream, was selected as a good candidate for the analysis at hand. Heavy fuel oil (HFO) was assumed to be the only fuel type used at this station with affixed price of USD 20/barrel. The analysis shows that the internal rate of return (IRR) was about 7%, which could be attributed to fuel prices in Kuwait and governmental support, i.e., waived construction tax and subsidized workforce salaries. Furthermore, the net present value (NPV) was also estimated as USD 47,928 million with a 13-year payback period (PBP). Moreover, 1–3% reductions in the annual operational cost were reflected in increasing the IRR and the NPV to 9–11% and USD 104,085–193,945 million, respectively, and decreasing the PBP to 12–11 years. On the contrary, increasing the annual operational cost by 1% made the project economically unfeasible, while an increase of 3% resulted in negative IRR (–1%), NVP (–USD 185,458 million) and increased PBP to 30 years. Similarly, increasing the HFO barrel price by USD 5 resulted in negative IRR (–10%) and NVP (–USD 590,409); hence, a CCS project was deemed economically unfeasible. While the study considered the conditions in Kuwait, it is expected that similar results could be obtained for other countries with an oil-driven economy. Considering that around 62% of the fossil fuel blend in Kuwait is consumed by electricity and water generation, it is inevitable to consider the possibility and practicality of having a carbon network with neighboring countries where other oil-driven economies, such as Kingdom of Saudi Arabia and Iraq, can utilize a CCS-based mega infrastructure in Kuwait. The choice of Kuwait is also logical due to being a mid-point between both countries and can initiate a trading scheme in oil derivatives with both countries.

Citation: Naseeb, A.; Ramadan, A.; Al-Salem, S.M. Economic Feasibility Study of a Carbon Capture and Storage (CCS) Integration Project in an Oil-Driven Economy: The Case of the State of Kuwait. *Int. J. Environ. Res. Public Health* **2022**, *19*, 6490. <https://doi.org/10.3390/ijerph19116490>

Academic Editors: Roberto Alonso González Lezcano, Francesco Nocera and Rosa Giuseppina Caponetto

Received: 21 April 2022

Accepted: 24 May 2022

Published: 26 May 2022

Publisher's Note: MDPI stays neutral with regard to jurisdictional claims in published maps and institutional affiliations.



Copyright: © 2022 by the authors. Licensee MDPI, Basel, Switzerland. This article is an open access article distributed under the terms and conditions of the Creative Commons Attribution (CC BY) license (<https://creativecommons.org/licenses/by/4.0/>).

Keywords: levelized cost of electricity; CCS; heavy oil; Kuwait; NPV; IRR

1. Introduction

The recently published report of Working Group III of the Intergovernmental Panel on Climate Change (IPCC) still sets a core concept to reach net-zero carbon dioxide (CO₂) emissions when anthropogenic carbon emissions are balanced globally by anthropogenic CO₂ removals [1]. This is achieved by diversifying energy baskets, reducing existing carbon

emissions from various industrial sources, and aligning efforts to reach the set target of having a 77% increase in electricity production from renewable energy feedstock. There are also various schemes set in place to regulate carbon emissions from various anthropogenic sources, such as the European Commission's (EC) emission trading system (ETS) with measurable targets till the year 2050 [2]. Various countries within the developed world have also committed themselves to measurable targets to keep global warming temperatures well below the 2 °C mark by signing the Paris Agreement on Climate Change [3]. To achieve such goals, especially considering existing industrial infrastructure for developed and developing countries alike, carbon capture and storage (CCS) offers itself as solution to mitigate carbon emission strength from various sectors. Presently, there are 74 operational CCS projects which have successfully utilized different technologies and 43 are under construction due to go into operation as of late 2018 [4,5]. It is also well established that the largest CO₂ emitter around the globe is the power sector, namely utilizing coal, natural gas, and fuel oil as a source to its gas/steam turbines with an average emission strength 3.94, 0.77–1.01, and 0.55–1.27 MtCO₂ per source [6]. Table S1 in the Supplementary Materials depicts the total estimated emissions around the globe from the power sector and the number of each source by fuel type. The reader is also referred to Table S2 for other anthropogenic sources by type and emission strength around the globe. We bring the kind attention of the reader that the letter S used prior to the number of figures and tables stands for material presented in the Supplementary Materials presented electronically to compliment this article.

CCS technologies vary significantly in terms of their capture techniques used. In fact, not all carbon streams are appropriate for capture technologies and the logistics for storing the carbon on- or off-site also present a logistical burden. The typical carbon stream captured should have a partial pressure of 0.1 MPa and a CO₂ concentration (by vol.%) of 3 to 4% [7]. Table S3 shows the different carbon streams that could be captured from various streams within a power plant and their properties. In addition, CCS technologies are summarized in Table S4, depicting the main commercial technologies of market maturity and the principle behind each technique. It should be noted that based on the review conducted and depicted in the aforementioned table, amine absorption in post-combustion technology was noted to be the most mature and popular amongst other options. Although studies within new materials and configurations used in CCS have been published as of late, there seems to be a gap in literature concerning the economic feasibility of projects, such as CCS, namely utilized for power stations which are considered to be the main carbon emitter amongst industrial sources. Furthermore, literature is quite scant for feasibility studies considering regions with an altered economy in Europe or China, such as oil-driven ones where prices vary along with fuel and infrastructure. In a fairly recent study by Koelbl et al. [8], two scenarios were studied in detail using a trade-linked model to analyze the upstream economic behavior for the Netherlands. These scenarios were (i) an 80% emission reduction scheme by 2050 in comparison to the 1990 carbon levels; and (ii) a renewable energy basket strategy for the power sector. It was concluded that the CCS-exclusive scenario for the power sector was less favorable for gross value added (GVA) and energy security when compared to a renewable basket of energy with a biomass focus. Nonetheless, it should be noted that such scenarios consider various imports from outside country borders and favor nuclear power (consequently uranium) imports [9]. In addition, CCS, in the case of the Netherlands as a non-oil dependent economy, may also become dependent on natural gas and fuel imports for the power sector. Al-Qayim et al. [10] have evaluated the techno-economic performance of biomass fuel for combustion power plants, both with and without CCS in the UK, with different coal used as a fuel. Two CCS technologies were applied, resulting in different performances. On the other hand, using biomass has produced negative-emissions of carbon in general. Oxy-fuel CC resulted in a 14% higher efficiency and 6% lower cost of electricity (COE) than post-combustion CC. In order to boost biomass CCS, a critical price of GBP 55.2 per ton was projected in the study. Fan et al. [11] has demonstrated that retrofitting CCS projects did not achieve the optimal

investment value till the year 2027, when compared with renewable strategies in China and after studying total investment value (TIV) with respect to each scenario's net present value (NPV). On the other hand, Xianzheng et al. [12] studied a model of wind power and coal fired power plant to analyze their economic performance. The NPV decreased along with the COE and carbon avoided cost with wind power, indicating worse financial performance in Northwest China. In this work, we consider the largest power plant within the State of Kuwait and conduct a detailed feasibility study for a CCS project that utilizes post-combustion as a technology to capture the carbon being emitted. The work is quite unique based on the fact that it carries detailed analysis in an oil-driven economy with various advantageous options to have such projects commissioned. This is due to their economic and environmental benefits. The article is divided into a number of sections to ease the flow of technical information for the reader. It starts with a general introduction section, detailing the main theme of the research work and a background/literature survey. The section that follows shows the detailed methodology carried out after describing the main characteristics of the country and power plant stations considered. The methods section includes the carbon capture and storage technology selection process, the market size and drivers of cost analysis, as well as economic and sensitivity analysis. After which, a dedicated section is presented to detail the results and discuss its relevance, whilst final conclusions are drawn from the work and presented in a separate section towards the end.

2. Methods

2.1. Country Description and Power Sector's Carbon Strength

The State of Kuwait is located on the Western Arabian Peninsula (29°30' N lat. And 47°45' E long.), noted to be one of the highest countries in the world in terms of gross domestic product (GDP) [13]. It is also an oil-dependent nation that is a member of both the Organization of the Petroleum Exporting Countries (OPEC) and the Organization of Arab Petroleum Exporting Countries (OAPEC), and ranks within the top ten countries of crude oil production and its reserves. The power and energy sector is operated mainly using fossil fuels derived from crude oil downstream activities within its borders. Past efforts in terms of quantifying and identifying carbon emissions and sources in the State of Kuwait with the aim of its future capture and sequestration are quite minimal [14–19]. These studies concluded a number of essential technical points: (i) that enhanced oil recovery (EOR) is not possible in Kuwait due to logistical reasons, scattering of sources, and dilution of carbon concentrations; and that (ii) the highest source of carbon is the power sector [20–22]. A full-carbon Atlas has also been published for Kuwait, quantifying all carbon sources to date [18]. There are also no regulations declared by governing bodies with regards to CCS in Kuwait, and it should also be noted at this stage that the recent International Energy Agency (IEA) reports show that Kuwait, on average, consumes more primary energy (577 BTU per Capita) than the world (75 BTU per Capita), Europe (134 BTU per Capita), and the Middle East (142 BTU per capita) [23,24]. This shows that the associated carbon footprint of Kuwait, with regards to its various carbon sources previously discussed in Al-Salem [19] and Al-Mutairi et al. [18], is somewhat justified since all of such sources are dependent on combusting crude oil derivatives and emit CO₂ to the atmosphere.

The power sector is owned and managed by the Ministry of Electricity and Water (MEW), which on the other hand subsidizes the electricity prices for residents to (USD 0.016 per kWh) as of the year 2017 [25]. This shows that the average resident pays some 5% of the actual utility price. Furthermore, all power stations in Kuwait are operated using fossil fuels and are combined with water desalination units. Both climatic conditions (e.g., reliance on air conditioning for cooling) and rapid population growth (3.3%) are considered to be the main influencing factors for high energy demand in Kuwait [18,20]. The IPCC has set various guidelines and methods to estimate carbon emissions, namely from the power sector. These methods are appropriate for stationary sources and could be summarized as a reference approach, a sectoral approach (Tier 1), and a bottom-up approach (Tier 2) [6]. The latter is considered to be the most common and reliable approach as it relies on technology

assessment of end-user based on the different scenarios considered. There are seven power stations in Kuwait that consume natural gas, heavy and gas oil, and heavy crude, and its derivatives constitute a share of 82% of the total consumption [26]. Other than the major concern of burning crude oil in power stations to compensate high demand in summer months, thermal steam turbines make up 85% of the ones used for operation, which are also associated with higher carbon emissions when compared to gas turbines [27]. The power stations, as well as their declared capacity and primary fuel used, are shown in Table S5. A breakdown of each station by capacity of each turbine type is also shown in Table S6 for the reader's consideration. A previous assessment for Kuwait based on the IPCC Tier 2 approach shows that the 41.636 MtCO₂ y⁻¹ is emitted from the power sector using the emission factors (EFs) depicted in Table S6 for each turbine/station. The power sector is responsible for 41.6% of total carbon strength of the country and a breakdown by station is drawn for the reader's consideration and shown in Figure 1 along with total fuel consumed in Table S7. Further details could be found elsewhere in Al-Mutairi et al. [18]. An assessment study based on the method used and a sensitivity analysis is also carried out and illustrated in Annex in the Supplementary Materials using the latest version of the IPCC inventory software (i.e., V2.54; IPCC, Geneva, Switzerland). This is carried out to provide a comprehensive overview of the case of Kuwait for each power station considered.

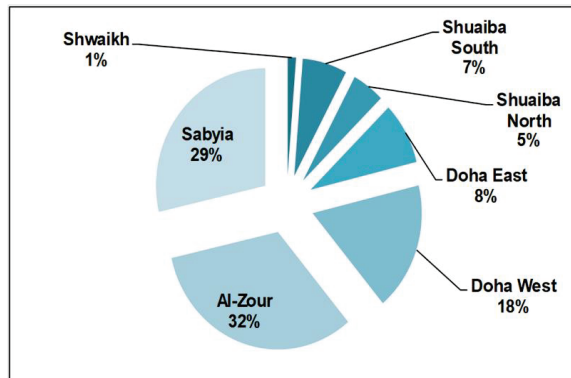


Figure 1. Breakdown (percentile) of power stations in Kuwait by carbon strength.

2.2. Economic Analysis, Process Evaluation, and Technical Considerations

The objective of this work is to demonstrate the viability on an economic basis for CCS in an oil-driven market. As previously shown in Table S5, there are seven power stations in Kuwait with a total installed capacity of around 18 thousand MW. The smallest PS is Shuwaikh with (250 MW); additionally, the largest PS is Al-Zour with installed capacity of 5306.7 MW. Furthermore, the average installed capacity of all stations is around 2200 MW of electricity, which is very similar to station Doha West, in terms of production capacity. Therefore, Doha West is presented as a viable and ideal candidate to represent a stream of CO₂ suitable for CCS based on average capacity [28]. Al-Zour is also considered in the first stages of assessment as the largest station in terms of capacity. The fuel consumed and capacity are shown in Table S7.

2.2.1. Carbon Capture and Storage Technology Selection

Several CCS technologies are available for deployment around the world. However, some factors can affect the selection process of the CCS technology, such as the CO₂ concentration in the gas streams, technology maturity, and fuel types. Accordingly, there are three CCS systems suitable for implementation in the State of Kuwait post-combustion, pre-combustion, and oxy-combustion [6,29]. Pre-combustion techniques can capture the carbon stream after separating the syngas stream post-reforming (Table S4). In other words,

the pre-combustion system processes the fuel with pure oxygen or air steam to produce synthesis gas or syngas. Moreover, the key components of this syntheses gas/syngas are carbon monoxide (CO) and hydrogen gas (H₂). Although this system is ideal for separating high concentrations of CO₂ in gas streams, the processes are considered to be elaborate and costly in power stations [6]. Oxy-combustion systems require large amounts of energy to complete the separation process. Additionally, once the process of oxy-combustion system is finalized, two new components are generated (water and CO₂), which are added to the separation costs and storage. In technical terms, post-combustion systems capture the CO₂ from flue gases that are produced by combustion of fossil fuels. Additionally, the remaining fuel gas is passed through a separation process, by injecting liquid or solid absorbents which can capture the CO₂. Therefore, the CO₂ can be injected into an oil reservoir (RO) for storage, and the remaining flue gas is discharged to the atmosphere. Furthermore, this system is considered to be economically feasible due to several factors, such as technological similarities with the power stations and market maturity; thus, it is selected for the case at hand.

2.2.2. Market Size and Cost Drivers

Around the globe, China has the most substantial electricity demand, reaching up to 5320 terawatt per hour (TWh). Additionally, in the projected year of 2040, electricity demand is estimated to increase by 3910 TWh and to reach around 9230 TWh. Furthermore, the second largest country in electricity demand is the United States, reaching approximately 3886 TWh in 2016, and is projected to reach about 4570 TWh in 2040 [30]. Locally within Kuwait, the government provides energy and desalinated water to households, as well as commercial and industrial sectors. Table 1 illustrates the State of Kuwait demand and supply of power as declared by the state. Moreover, the production of electricity in 2016 is augmented to reach 18,870 MW. Additionally, these increments in electricity over the past few decades are attributable to several factors, such as population growth, economic prosperity, and technological innovations. Table 2 below shows the global and local prices of each fuel source utilized in the State of Kuwait which are considered in this work [31]. The cost of HO is between USD 20–38 per barrel internationally, and locally it is around USD 35 per barrel. Furthermore, the natural gas (NG) prices locally and globally are very similar at USD 3.55 and USD 3 million British thermal unit (MMBTU), respectively. Additionally, the international price of CO is around USD 51 per barrel, while locally is around USD 40 per barrel. Correspondingly, the prices of gas oil (GO) internationally and domestically are both at around USD 53 per barrel. Therefore, this comparison process indicates that MEW fuel costs behavior is driven by international markets prices (Table 2).

Table 1. State of Kuwait power generation demand and supply for the period 1986–2016. Source: MEW [32].

Year	Peak Demand (MW)	Installed Capacity (MW)
1986	3480	5386
1996	5200	6898
2006	8900	10,229
2016	13,390	18,870

Table 2. International market prices and Kuwait’s MEW cost prices of fuels used in power stations for the year 2016. Source: IEA [30], MEW [32], and Lazard [33].

Fuel Category	International Market Price (USD)	Kuwait MEW Cost (USD)	Unit
Heavy Oil	20–38	35	Barrel (based on API)
Natural Gas	3.55	3	MMBTU
Crude Oil	51	40	Barrel *
Gas Oil	53.3	53	Barrel

* Conversion factor of OPEC (1 ton: 7.33 barrel) is used to convert gas oil price USD 390.61/MT to USD 53.3/barrel.

2.2.3. Pricing Method and Carbon Market

There are various factors that affect the cost of electricity, such as fuel prices fluctuating, different power generation technologies and their efficiencies, and power transmission losses. Therefore, a more stable cost calculation method is required to unify the different cost approaches used in the power generation (PG) industry [34]. Consequently, a leveled cost of electricity (LCOE) is developed in this work, consisting of an average revenue received per unit of the energy’s output, for the first year of operation with an annual rate of null (zero). In other words, the LCOE can be defined either by the energy price of electricity or by the net present value (NPV) with a zero investment rate [35]. NPV analysis is chosen as it presents a number of advantages, namely accounting for the future depreciation of investment, the possibility of future investment return analysis, and the fact that it can take account of actual value assets (such as capital costs). The LCOE of different conventional PG teleology’s price ranges, which can be utilized for the recommended technologies and adapted from Lazard [33]. Furthermore, the CO₂ market is divided into several segments, including oil and gas industries, food and beverage industries, medical industries, and fire-fighting industries [36]. Additionally, the worldwide demand of CO₂ is around 80 Mtpa, and the major share of the market is enhanced oil recovery (EOR), representing 63% [37]. In addition, the current price of CO₂ is around USD 40 per ton of CO₂ equivalent—an estimate set by the market’s economical behavior. Furthermore, it is expected that this current price may increase in the near future and reach USD 80 per ton of CO₂ equivalent. Therefore, the growth of the carbon market, especially in the Middle East, allows governments to invest into technologies such as CCS for the purpose of cost reduction or revenue generation [36].

2.3. Techno-Economic Assessment and Evaluation

In order to conduct a feasibility study based on a techno-economic evaluation, three prior consecutive steps that could be treated as individual studies must be completed by selecting a CCS system, a PS system, and the case models, as depicted in Figure 2, showing the tree structure for the methodology followed. The CCS system is chosen by applying the statistical average method on the low-cost accounting technique (SAMLCAT). In other words, multiple case study models (CSMs) of the selected systems mentioned for the CCS are presented, and the system with the lowest average cost (LAC) is chosen as the primary system. Therefore, the assessment is conducted on sound grounds, and the power station and the CCS project based on economic indicators is evaluated, resulting in the most realistic evaluation, as encompassed in Figure 2. Moreover, in the second step, a power station system is selected, based on the power generation technologies and economic conditions that are applicable for MEW in the State of Kuwait. Additionally, in the third consecutive step, a CSM is selected for two entities—the power station installed capacity (PSIC) and the CCS facility (CCSF)—based on the literature review and statistical average methods (Figure 2) [38]. Furthermore, and once completed, the feasibility study is used to evaluate the above selected CSMs. Moreover, and as shown in the tree methodology depicted, there are two feasibility studies—one for the power station case model (PSCM) and the other for the CCSF case model (CCSFCM). Additionally, the first feasibility study has three sections—cost analysis, financial estimation, and economic indicators. Similarly,

the second feasibility study contains four sections—cost analysis, financial estimation, economic indicators, and sensitivity analyses for the CCS project.

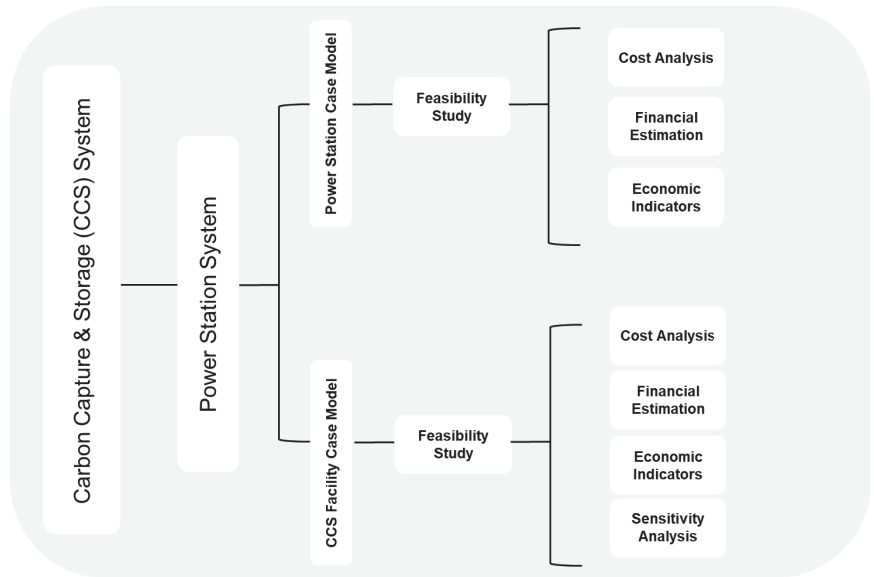


Figure 2. Methodology followed to conduct feasibility study based on techno-economic evaluation.

Additionally, the process of SAMLCAT depends on fifteen CSMs, distributed equally between the systems. Furthermore, once the calculation process of SAMLCAT is completed, the LAC method is selected for this feasibility study [31]. A selection process is instigated for the appropriate power technology that can be adapted with the suggested CCS technology [32].

To select the superlative PSCM that can be applied to its related feasibility study, two processes are used—the PSIC selection process and the PSCM selection process. Accordingly, the PSIC selection process is based upon a statistical average method of Kuwait’s PSIC’s in the year 2016 [18]. By way of explanation, the average PSIC is calculated from Table S6, and consequently the selection process method is based on the nearest Kuwait’s PSIC to the calculated average PSIC. Additionally, in the second process of this section, several CSMs are presented from the literature review. Moreover, each CSM contains a financial statement (FLS), displaying the cost of construction and operation of PS with CCSF. Furthermore, the total cost (TC) of each FLS in its related CSM is collected and arranged, as shown in Table 3. Furthermore, the average cost (AC) of the arranged TCs is calculated; therefore, the FLS that contains the nearest TC value to the AC is selected as the basis for its FS. In addition, the FLS structure of the selected CSM is based on the methodology previously depicted [31].

2.4. Carbon Capture and Storage (CCS) Facility Case Model

The TC of the selected FLS related to CM is evaluated, and the AC calculation method is initiated. Moreover, the TC with the nearest value to the AC is chosen; therefore, its FLS acts as the basis, as shown in Table 4 [38].

Table 3. Total cost of the selected CSMs for the power station. Source: NETL [39–41].

Category	MW-Net	TASC	OM	TS&M	TC
U1	543.3	USD 2,530,832	USD 231,344	USD 138,109	USD 2,900,285
U2	473.6	USD 940,497	USD 208,460	USD 57,448	USD 1,206,405
C1	471.6	USD 2,286,707	USD 126,685	USD 120,670	USD 2,534,062
C2	500.1	USD 2,495,874	USD 135,120	USD 131,550	USD 2,762,544
C3	460.9	USD 1,939,291	USD 109,389	USD 102,434	USD 2,151,114
C4	445.3	USD 2,191,925	USD 121,312	USD 115,662	USD 2,428,899
C5	466.5	USD 2,355,769	USD 127,483	USD 124,163	USD 2,607,415
C6	515.1	USD 2,261,041	USD 138,146	USD 119,959	USD 2,519,146
CB1	497.0	USD 2,784,423	USD 228,275	USD 150,635	USD 3,163,333
CB2	514.0	USD 2,567,836	USD 231,281	USD 139,956	USD 2,939,073
Average	489	USD 2,235,420	USD 165,749	USD 120,058	USD 2,521,227

Table 4. Total cost of the selected CSMs for the CCSF. Source: NETL [39–41].

Cases	CP	OM	TC	%
U1	USD 304,043	USD 68,793	USD 372,836	17%
U2	USD 311,405	USD 66,436	USD 377,841	43%
C1	USD 206,132	USD 49,562	USD 255,694	13%
C2	USD 226,868	USD 54,295	USD 281,163	13%
C3	USD 171,819	USD 41,250	USD 213,069	13%
C4	USD 255,542	USD 59,592	USD 315,134	16%
C5	USD 248,993	USD 58,455	USD 307,448	15%
C6	USD 249,337	USD 58,242	USD 307,579	16%
CB1	USD 264,007	USD 71,300	USD 335,307	14%
CB2	USD 335,462	USD 86,459	USD 421,921	19%
Average	USD 246,767	USD 57,078	USD 303,846	18%

2.4.1. Cost Estimation

The foundation of the feasibility method is based on determining the appropriate TC and the cost of electricity (COE) of the PSCM and the CCSFCM. These are conducted on the basis of following costs combined:

- Raw materials: This cost sums the annual raw materials required to construct, operate, and produce the finished product.
- Equipment: This cost group consists of the annual cost of equipment required to construct, operate, and produce the finished product.
- Labor: This cost group encompasses the annual administrative and operational labor cost for constructing, operating, and producing the finished product.
- Utilities: This cost group covers the annual services cost, such as electricity, water, and oil associated with constructing, operating, and producing the finished product.
- Buildings and structures: This cost group includes the annual costs for building and structures that are required to construct, operate, and produce the finished product.
- Fixed assets: This cost group consists of the cost of the above two cost groups, as well as the building equipment and structures, which are used to construct the essence of the power plant and the CCSF.

- Amortization and depreciation: This cost group involves the depreciation calculation cost for the fixed assets that are utilized in the construction and operation of the power plant and CCSF.
- Total cost: This cost group includes the aggregated totals of all of the above cost groups, as well as other costs that can affect the outcome of the final product. Additionally, the above costs groups are then restructured and reorganized based on the total cost methodology of (TCM).
- Cost of electricity (COE): Once all of the above are calculated, the final cost is estimated for COE, as per the following [42].

$$COE = \frac{(TOC + OCFIX + OCVAR)}{AnnualNetMWhGenerated} = \frac{TotalCost}{TotalProduction} \quad (1)$$

where TOC stands for the first-year capital costs (charges) (USD), OCFIX is the first-year operating costs (USD), and OCVAR is the first-year variable operating costs (USD) (see Tables S10–S18).

2.4.2. Financial Estimation

In order to estimate the financial costing for the power generated in the power plant, as per the followed methodology, four previously mentioned components are calculated as per the following (Figure 1).

- Pre-production cost: To construct the power plant or CCSF and monitor the construction process, an administrative headquarters setup is required. This cost group, due to calculation process position significance, is aligned to this financial group. Furthermore, the components of this financial group are shown in Table S19.
- Revenue: This is the first financial group that is considered as the basis of the other groups. This category is the result of a multiplication process between price and quantity, as shown [31,43].

$$Revenue = Price \times ProductionQuantity(PQ) \quad (2)$$

A variation of the above formula is derived to be applicable in this feasibility study; therefore, the new revenue formula is a multiplication process between LOCE, representing the price, and the power plant output (PPO), representing the quantity of production.

$$Revenue = LOCE \times PPO \quad (3)$$

- Working capital: The objective of this financial group is to calculate the required amount for the purpose of operating the project. In addition, this financial group consists of three main cost groups (salaries, raw materials, and utilities), as shown and estimated in Table S18.
- Initial investment: This is the third financial group which includes a mixture of cost and financial groups to allow in the construction and operation of the project, as illustrated in Table S19.
- Net cash flow: This is the final financial group which calculates the net cash flow (NCF) of the project for the duration of its life span, taken as 30 years. In other words, the purpose of this financial group is to calculate the profits or losses, as depicted below.

$$NCF = Cash-In - Cash-Out \quad (4)$$

Additionally, in the adjusted version of the formula above, the cash-in is replaced by revenue and cash-out is replaced by operational cost, as shown in the formula below [44].

$$NCF = Revenue - Operational Cost \quad (5)$$

2.4.3. Economic Indicators

The economic indicators considered in the feasibility study are summarized below and are aimed at determining the profitability of the project after setting up the initial

investment costs above. To estimate the net present Value (*NPV*) in today's money, the formula below is used [45].

$$NPV = \sum_{t(\text{year})=1}^n \frac{NCF_t}{(1+r)^t} - CF_0 \quad (6)$$

Furthermore, the internal rate of return (*IRR*) is estimated as it represents the compound interest of the present values for the in-flow (revenue), equaling the current value of cash out-flow (expenses). By way of explanation, the *IRR* is the present value of in-flows equaling the investment value when *NPV* is zero [45,46].

$$IRR = \sum_{t(\text{year})=1}^n \frac{CF_t}{(1+IRR)^t} - CF_0 \quad (7)$$

As for the payback period (*PBP*), which signifies the period or length of time required to return the capital investment of the project, it is estimated as the following [45]. The return on investment (*ROI*) is also subsequently calculated [47].

$$PBP = \frac{\text{Investment Value}}{\sum NCF} \quad (8)$$

$$ROI = \frac{NPV}{\text{Initial Investment}} \times 100 \quad (9)$$

3. Results and Discussion

In this section, we present the results of the CSM related to the power station and the CCSF. The selection process for the PSCM and the CCSM is based on the calculations performed using the SAMLCAT and the AC. An adjustment is also performed by replacing the PSIC in the FLS to fit the case at hand for the State of Kuwait. Moreover, the fuel source in FLS is replaced with the Kuwaiti heavy oil (HO) fuel source (Table S7). Furthermore, the consumption capacity is changed, depending on the selected Kuwait's PS-HO consumption capacity, leading to a change in the annual fuel cost variable. The IGCC-PS is the most compatible technology for the sustainability of the CCSF, based on the available information allocated from MEW and the reviewed literature. Moreover, the calculated AC amount from the applied statistical method is around USD 2.5 billion, based on the results depicted in detail within Tables S9–S18. According to the study conducted by the NETL [48], the cost is within the average of CSM for such a project. Hence, to accommodate the largest plant with potential carbon stream appropriate for CCS, we select the Al-Zour station with an installed capacity of 5805.80 MW annually so that the integrated plant can consider its facility. Additionally, the selected fuel source for this FLS is HO, with an average price of USD 34 per barrel, which is very similar to MEW cost (Table S20). Moreover, the selected LCOE price considered is USD/MW 175, and the T and S cost is 5% from TC [48].

3.1. CCSF Selection Process

The objective of this section is to select the CSM for the CCSF applied in the integrated plan for the power station (Al-Zour). By way of explanation, the expected life span of power stations is around 30–35 years (Table S14). This surpasses stations available in Kuwait within the MEW. Therefore, an assumption is made to eliminate the construction cost of a power plant with a CCSF and calculate the TC of a CCSF for an existing MEW-PS instead, which are adapted and calculated based on the data extracted from NETL [35]. The calculated AC of the above CSMs is around USD 303 million, which is in line with previous findings (NETL, 2001). It should also be kept in mind that both feasibility studies in this work aim to assess the power station and the CCS project integrated with it, which have an investment rate of 6% [20].

3.2. Cost Analysis

The first cost group to be estimated is the raw materials (RMs) which amounts to USD 93 million. The second cost group is the equipment cost required to construct and operate the station instead of a retrofitting project which sums to around USD 821 million since the station surpasses its life expectancy and requires more money to maintain it, rather than constructing a new one with modified specifications and applicability for CCS (Tables S9 and S10). Additionally, the third group in this category is labor, where its annual cost is used to construct and operate the station (USD 323 million). Utility costs subsidized at the governmental rate is the fourth cost group, amounting to roughly USD 3.5 thousand. Fixed assets, which sum the two cost groups amounting to USD 840 million, is also considered (Table S14). Furthermore, depreciation and amortization also strictly show the depreciation of the total assets over the project's life span (i.e., 30 years) (Table S15). The TC is estimated at USD 905 million in the first production year, as shown in Table S16. Additionally, this amount fluctuates over the years and stabilizes in year twelve at USD 885,712 million over the remaining life span of the project. Table 5 shows the summary of the cost outputs considered for the Al-Zour power station which is also applicable for constructing a new station to substitute the old one, instead of retrofitting the existing power plant and desalination plant in Kuwait. The CCS project can accommodate 1.7 Mtpa of CO₂ produced from the station, with an amine absorption-based unit (see variation of carbon calculation in Annex in the Supplementary Materials).

Table 5. A summary for cost outputs for the PS-CSM.

Project	Cost (USD/Mill)	Production (MW)	COE (USD/MW)
Case Study Model	905,405	5806	155.95

3.3. Financial Estimation

The pre-production cost is assessed to accommodate the cost requirements of the administration buildings. The total amount that is required to construct and operate the headquarters is around USD 53 million, as per the calculated categories depicted in Table S16. The initial investment is estimated as USD 840 million, and the pre-production and the working capital costs amount to USD 420 and USD 53 million, respectively. Therefore, the total amount of this financial group is around USD 1.3 billion. The revenues from the power station are estimated with a LCOE of 175 USD/MW. The feasibility study associated with the power station yields USD 1 billion; an annual breakdown is given in Table S22. The LCOE is sensitive to various variables, such as the plant capacity, capital investment, and fuel cost [49]. These are investigated and discussed in the sensitivity analysis section, whilst the capacity is kept fixed to accommodate the carbon captured in the considered station (e.g., Al-Zour). Additionally, in the first few years of operations, the NCF project is worth around USD 135 million (Table S21). Furthermore, the NCF increases slightly over the years to reach an amount of USD 144 million. Moreover, the NCF in year twelve stabilizes at USD 187 million for the remaining production year. As for the economic indicators related to the constructed CCS project working on an amine absorption principle, Table 6 summarizes the feasibility study results for the project. Therefore, the COE of the CCSF is around 168 USD/MW. Furthermore, in comparing the feasibilities both COEs, it is realized that the COE-PS is much lower than COE-CCSF; in fact, it is even lower than the LCOE selected for this feasibility. Moreover, one of the reasons for difference in the COE values is due to the PSIC in both FSs.

Table 6. A summary of cost outputs for the CCSF-CSM.

Project	Cost (USD/Mill)	Production (MW)	COE (USD/MW)
Case Study Model	378,120	2246	168.38

As for the economic indicators for the CCS project, the IRR is estimated to be 7%, presenting a lucrative ratio for such projects. This can be attributed to the fuel prices in Kuwait and, moreover, the government subsidies for such projects, which are considered in this work, such as elimination construction tax, supporting labor salaries. The NPV is also estimated as USD 47,928 million, and the PBP is estimated as 13 years and 1 month with an ROI equaling at 20%.

3.4. Sensitivity Analysis for CCS Project

The sensitivity analysis presented in this section is aimed at showing the reliance of this project against changes anticipated within the work and the local market. A baseline scenario is chosen for the LCEO at 175 USD/MW, PSIC at 2541 MW, and HO (Kuwaiti crude), with a price of USD 20 per barrel representing the lower end of the price spectrum when compared with average oil prices. Table 7 illustrates seven hypothetical calculated cost adjustment scenarios for the CCSF-FS. Additionally, the first scenario in the middle is the base study which displays the economic indicators aforementioned. Moreover, the remaining six scenarios are divided into two segments—three with an increase in operational cost and three with a decrease in the same category, which represents the group that could be most influenced by changes in the market. Therefore, in the first scenario, for the above, the operational cost is in the decreasing segment, reaching 1% over the life span of the project. Accordingly, the IRR shows a profitable ratio at 9%, and NPV at USD 104,085 million, which signifies a valuable approach for such projects in Kuwait. Furthermore, the PBP is 12 years and the ROI is 44%, demonstrating a beneficial financial outcome as well. Consequently, in the second and third scenarios of the operational costs, the reduced ratios are 2% and 3%, respectively, leading to an IRR of 10% and 11, correspondingly. Likewise, the NPV of both scenarios is USD 152,327 million and USD 193,945 million, respectively, while the PBP for both scenarios is 11 years. Therefore, the above operational cost reduction scenarios show a favorable financial outcome. Additionally, in the second segment of the scenarios, the operational costs are increased to show a different outcome. However, in the first scenario, the operational cost is increased by 1%, which leads to a significant decrease in the economic indicators. Moreover, in the first indicator, the IRR is reduced to 5%, and the NPV is also decreased, reaching USD 17,713 million. Additionally, the PBP is 15 years and the ROI is -7%; therefore, this scenario economic indicators all display the unfeasibility of the project (highlighted in Table 7). Furthermore, in the second scenario, the operational cost increases by 2%, leading to a 1% decrease in the IRR, thus indicating an unfeasible project. In addition, the NPV, PBP, and ROI are all reduced to reach negative USD 94,738 million across 19 years, i.e., a -40% decrease, respectively. Correspondingly, in the third scenario, the operational cost increases by 3%, which results in a negative IRR, thus indicating unfeasible outcomes of the projects. Moreover, the remaining economic indicators of this scenario present an unfeasible result concerning the project. Therefore, any increase in the operational cost for the base study scenario can lead to a significant decrease in the project’s profitability outcome.

Table 7. Cost adjustment (sensitivity analysis) scenarios for the CCSF.

No	Scenarios (+/−) Operational Cost (USD 856,256 per Annum)	IRR	NPV	ROI	Payback Period
3	−3%	11%	193,945	81%	11.15
2	−2%	10%	152,327	64%	11.15
1	−1%	9%	104,085	44%	12.13
	Baseline (business as usual) scenario	7%	47,928	20%	13.11
4	+1%	5%	−17,713	−7%	15.08
5	+2%	1%	−94,738	−40%	19.04
6	+3%	−1%	−185,458	−78%	30

Table 8 illustrates the price adjustment scenarios in the HO for the CCSF-FS, containing three base study scenarios (business as usual baseline), including A-15 and A-25. In the A-15 scenario, the price of HO is decreased to USD 15 per barrel, while the price of HO increases to USD 25 per barrel in the A-25 scenario. In addition, in the A-15 scenario, the IRR is 41%, the NPV is USD 1164 billion, and the PBP is 2 years, while the ROI is a very high ratio of 487%, indicating a highly feasible project, as shown in Table 8. Additionally, in the second scenario, the price of HO increases up to 25 USD/barrel, which is very similar to its cost in MEW. Therefore, by applying this price, an increase in HO in this scenario can result in adverse economic outcomes. The first economic indicator is IRR, showing a negative 10%; likewise, the NPV shows a negative value of USD 590,409 million. Additionally, the PBP displays a period over 30 years, and the ROI has an unfavorable ratio of -447% . Therefore, any increase in the HO prices beyond the baseline can result in an unfeasible project, as demonstrated. It should be noted that the results may demonstrate a certain tendency to showcase a non-feasible project with any increase expected in the local market for crude oil prices (fuel derivatives), which might lead to neglecting CCS projects in an economy, such as Kuwait. However, the background must be discussed and considered here in detail to deliver a realistic viewpoint. There is a key limitation in conducting sensitivity scenarios for such work, where the focus is on constructing and operating a CCS plant devoted for the power sector as a standalone carbon emitter in Kuwait. In reality, the assumption that the CCS can withstand Al-Zour's plant carbon emission and can also accommodate additional carbon streams from nearby refineries, namely the new refinery project in the same area [19]. Conducting sensitivity analysis on HO prices can exclusively neglect other impacts on various sectors in Kuwait which contribute to carbon sources. The exclusion of energy-saving measures and carbon crediting is also another limitation here and is also indicated in other previous studies [8]. In order to avoid an increase in COE and alterations in IRR with the HO process, carbon crediting schemes can take effect in Kuwait when implemented by governmental bodies, such as the Kuwait Environment Public Authority (KEPA). An allowance proved to be highly useful in the previous study of Bellotti et al. [50], in order to avoid COE increases.

Table 8. Price adjustment scenarios A for the CCSF.

No	Sensitivity Scenarios	IRR	NPV	ROI	Payback Period
1	A-15	41%	1,164,774	487%	2.34
	Base Study	7%	47,928	20%	13.11
2	A-25	-10%	$-590,409$	-247%	30

As previously pointed, the bulk of carbon emissions in Kuwait are associated with the power sector essentially yielded from combusting fossil fuels. The commonly used fuel types in MEW P&D plants are gas oil, lean gas, fuel gas, and crude, depending on type of turbines. This might be of concern for future mitigation plans, where lesser carbon intense sources should be considered as turbines relying on natural gas rather than HO. The four most applicable technologies for CO₂ capture from P&D plants include post-combustion, pre-combustion, oxy-fuel combustion, and chemical looping, which are also reviewed for the benefit of this study. Post-combustion is chosen as a mature choice in the market; however, the study might be extended to assess the feasibility of operating more than one choice in the future or more than one station to overcome logistical issues in storage and transport. Futuristic scenarios of direct extraction from air are also a possibility, namely for integration purposes with a CCS project in Kuwait, such as those presented in this study. This is essential in order to overcome the impracticality of extracting ambient CO₂ concentrations (i.e., ~400 ppm), which are not feasible and require additional operating expenses [51].

From a macro point of view considering the region as a whole, the majority of the power generation in Middle East utilizes oil-fired power and desalination plants. Sixty percent of the world desalination capacity exists in the Middle East, particularly in the Gulf

Cooperation Council (GCC) countries [52]. In the GCC countries, about 58% of the energy consumption is attributed to air conditioning and water desalination [23]. In Kuwait, over 80% of the blend of fossil-fuel-based primary energy is consumed via thermal conversion processes. Around total 62% of this amount is consumed by both electricity and water generation ($\approx 52\%$ for electricity production) and about ($\approx 10\%$) for desalination freshwater production. This poses a direct question of possibility and practicality of having a carbon network with neighboring countries where other oil-driven economies, such as Saudi and Iraq, can utilize a CCS-based mega infrastructure in Kuwait. The choice of Kuwait is also logical due to being a mid-point between both countries and can initiate a trading scheme in oil derivatives with both countries. It should be noted herein that there is a policy gap in terms of most effective CCS technology and implementation policy in Kuwait, where no clear and published targets are put in place to accommodate the country's status. It is quite common in developed nations to tax fossil fuel energy sources as one of the most common policy options to mitigate and control carbon emissions [53]. However, in Kuwait, where the sole means of energy is fossil-fuel-based, this seems to be a hindering step that requires proper infrastructure for renewables (e.g., waste to energy, solar, wind, etc.) and such projects are yet still not in their right stature to produce what is expected of them for the national grid. Therefore, this stage of country's development requires more incentives for energy projects that can utilize renewable sources in order to reduce carbon emissions. Furthermore, judging from the baseline scenario (IRR of 7%), the right choice of CCS technology can be a lucrative option that can become economically self-sustaining with time. The emission issue can be solved with time and can be reduced as the project takes place in other parts of the world, as described by Duan et al. [53]. An internal policy of governmental based carbon taxing seems to be a viable step as well, especially on the oil and power sectors where such a policy implementation can definitely set a true course for action for commissioning CCS plants. KEPA is a regulatory body within the state similar to other parts of the world where a governmental body is responsible for monitoring the emissions of various sectors. With time, large-scale CCS may require policy implementation to accommodate large-scale plants, as well as initiatives to foster entrepreneurial activity and market formation, which can also extend to neighboring countries as well based on our study [54]. Such policies should also accommodate a no cap policy for storage in a similar fashion to the Q45 policy for carbon credits [55]. This is used to accommodate the case of oil-driven economies such as Kuwait at initial stages of technology implementation. There are also a number of conclusions that can be drawn based on the empirical analysis conducted in this work, namely a comparative assessment with other Middle Eastern countries. As of the year 2022, the Middle East is in the lowest region in terms of CCS projects [56]. This should not be confused with the sheer amount of carbon captured, as the region has 11 CCS operational projects located in Saudi, Qatar, and the Emirates, which are responsible for 10% of global CO₂ captured annually (capacity extending 3.8 Mt per annum in some cases), i.e., double that of Europe. The focus of these projects is associated with gas processing plants ($\approx 26\%$ captured globally, 42.6 Mt per annum). Compared to Kuwait, which has no CCS plants as of yet, a good start may be to concentrate efforts on associated gas plants with the oil sector, as described elsewhere [19,20]. However, the power sector remains the largest in Kuwait as a prime emitter of carbon, as depicted earlier in this work (41.636 Mt per annum, 41.6%), which can also provide a good start for such CCS future plans. This is especially true when considering capital scaling and electrical power subsidies provided in the Middle East region, as previously depicted by Paltsev et al. [57]. Currently, the Emirates are ranked first in CCS projects in the region [58]. A carbon network can also offer a good start in Gulf countries between Kuwait, Saudi, and the Emirates.

During the years 2020–2021, the global COVID-19 pandemic has drastically altered energy policies around the world. This was due to a number of factors, namely general lockdowns which, on the other hand, reduced transportation and demand on fuels following boarder closures between countries. Daily carbon emissions reduced by 17%, as of early April 2020, when compared to the average of 2019 [59]. It should be noted that the drop

in CO₂ emissions had no detectable impact on atmospheric CO₂ or climate change [60]. Therefore, it is estimated that CCS projects and future plans can recover as the Russian–Ukrainian conflict drives oil markets to new highs and the original demand shows to gain strength similar to before the pandemic. As of late, the issue of air quality, namely over the past three years, has been a focus of many health agencies where relevant. This is due to proven health effects of major pollutants on the general wellbeing of populations around the globe. Based on the transport sector data, Huang et al. [61] proposed a novel nonlinear multivariate grey model (ENGM (1,4)) based on an environmental Kuznets curve. This new tool was validated against the results from the US, Japan, and China, and during the years 2019–2025, an average increase in carbon emissions from the transport sector in China and the USA was 2.837% and 2.394%, respectively. The results of Japan show a downward trend with an average decline rate of 1.2231%. Therefore, the transport sector in mega populated cities (with largely dense countries) could benefit from such models to estimate and subsequently monitor their carbon emissions. The same principle could also be applied on different sectors and could be transferred to oil-driven economies, such as Kuwait. These sectors can also include industry [62], new emerging transport technologies [63], and pollution during the past pandemic [64].

4. Conclusions

The results have a certain tendency to showcase a non-feasible project with any increase expected in the local market for crude oil prices (fuel derivatives), which might lead to neglecting CCS projects in an economy such as Kuwait. However, there is a key limitation in conducting sensitivity scenarios for such work, where the focus is on constructing and operating a CCS plant devoted for power sectors as a standalone carbon emitter in Kuwait. In reality, there is an assumption that the CCS can withstand the carbon emissions of Al-Zour's plant and can also accommodate additional carbon streams from nearby refineries (Kuwait's fourth refinery is in the proximity of Al-Zour's plant). Furthermore, conducting sensitivity analysis on HO prices exclusively neglects other impacts on various sectors in Kuwait that contribute to carbon sources. The exclusion of energy-saving measures and carbon crediting is also another limitation here, as indicated by other previous studies. In order to avoid an increase in COE and alterations in IRR with the HO process, carbon crediting schemes might take effect in Kuwait when implemented by governmental bodies, e.g., Kuwait Environment Public Authority (KEPA). As previously pointed, the bulk of carbon emissions in Kuwait are associated with the power sector essentially yielded from combusting fossil fuels. The commonly used fuel types in MEW P&D plants are gas oil, lean gas, fuel gas, and crude, depending on the type of turbines. This may present a concern for future mitigation plans where lesser carbon intense sources should be considered, as turbines rely on natural gas rather than HO. Post-combustion CCS is chosen as a mature choice in the market; however, the study might be extended to assess the feasibility of operating more than one choice in the future or more than one station to overcome logistical issues in storage and transport. Futuristic scenarios of direct extraction from air are also a possibility, namely for integration purposes with a CCS project in Kuwait, such as those depicted in this study. Considering that around 62% of the fossil fuel blend in Kuwait is consumed by electricity and water generation, it is inevitable to consider the possibility and practicality of having a carbon network with neighboring countries where other oil-driven economies, such as the Kingdom of Saudi Arabia and Iraq, can utilize a CCS-based mega infrastructure in Kuwait. The choice of Kuwait is also logical due to being a mid-point between both countries and can initiate a trading scheme in oil derivatives with both countries.

Supplementary Materials: The following supporting information can be downloaded at: <https://www.mdpi.com/article/10.3390/ijerph19116490/s1>. References [4,18–20,39–41,65–79] are cited in the supplementary materials.

Author Contributions: A.N.: data curation, formal analysis, and review and editing; A.R.: data curation, formal analysis, and review and editing; S.M.A.-S.: conceptualization, formal analysis, writing—original draft, and review and editing. All authors have read and agreed to the published version of the manuscript.

Funding: This research received no external funding; it is the derived work from a previous funded project EC093C.

Institutional Review Board Statement: Not applicable.

Informed Consent Statement: Not applicable.

Data Availability Statement: Not applicable.

Acknowledgments: The authors would like to thank the Kuwait Institute for Scientific Research (KISR) for their support. The work in this article is derived from the conceptual work and extended analysis related to completed Project (EC093C) funded by the Ministry of Electricity and Water (MEW) State of Kuwait.

Conflicts of Interest: The authors of this communication declare that they have no known competing interests or personal relationships that could influence the work in any shape or form.

Abbreviations

AC	average cost
BTU	British thermal unit
CCS	carbon capture and storage
CCSFCM	carbon capture and storage facility case model
CO ₂	carbon dioxide
COE	cost of electricity
CSM	case study models
FS	feasibility study
GO	gas oil
HO	heavy oil
IRR	internal rate of return
Kwh	kilowatt per hour
LAC	lowest average cost (USD)
LCOE	levelized cost of electricity (USD/MW)
Mtpa	million tons per annum
MW	megawatt
NPV	net present value (USD)
OCFIX	first-year operating costs (USD)
OCVAR	first-year variable operating costs (USD)
PBP	payback period (year)
PSCM	power station case model
PSIC	power station installed capacity (MW)
SAMLCAT	statistical average method on the low-cost accounting technique
TC	total cost (million USD)
TOC	first-year capital costs (charges) (USD)

References

1. Intergovernmental Panel on Climate Change (IPCC). *Global Warming of 1.5 °C: An IPCC Special Report on the Impacts of Global Warming of 1.5 °C above Pre-Industrial Levels*; IPCC: Geneva, Switzerland, 2018.
2. European Commission. EU Emission trading System (ETS) Low Carbon Fuel Standards. 2014. Available online: http://ec.europa.eu/clima/policies/transport/fuel/index_en.htm (accessed on 23 May 2022).
3. United Nations Framework Convention on Climate Change. *Adoption of the Paris Agreement: Proposal by the President; Draft decision -/CP21*; United Nations Framework Convention on Climate Change: Paris, France, 2015.
4. Johansson, D.; Franck, P.; Berntsson, T. CO₂ capture in oil refineries: Assessment of the capture avoidance costs associated with different heat supply options in a future energy market. *Energy Convers. Manag.* **2013**, *66*, 127–142. [CrossRef]
5. Merchant, E.F. With 43 Carbon-Capture Projects Lined Up Worldwide, Supporters Cheer Industry Momentum. 2018. Available online: <https://www.greentechmedia.com/articles/read/carbon-capture-gains-momentum> (accessed on 23 May 2022).

6. Intergovernmental Panel on Climate Change. *Special Report on Carbon Dioxide Capture and Storage*; IPCC: Geneva, Switzerland, 2005.
7. International Energy Agency and Organization for Economic Cooperation and Development. *Prospects for CO₂ Capture and Storage: Energy Technology Analysis*; OECD Publishing: Paris, France, 2004.
8. Koelbl, B.S.; van den Broek, M.; Wilting, H.C.; Sanders, M.W.; Bulavskaya, T.; Wood, R.; Faaij, A.P.; van Vuuren, D.P. Socio-economic impacts of low-carbon power generation portfolios: Strategies with and without CCS for the Netherlands. *Appl. Energy* **2016**, *183*, 257–277. [CrossRef]
9. Tertrais, B. DIIS Policy Brief: Uranium from Niger: A Key Resource of Diminishing Importance for France. Danish Institute for International Studies (DIIS). 2014. Available online: <https://www.ciaonet.org/attachments/25248/uploads> (accessed on 23 May 2022).
10. Al-Qayim, K.; Nimmo, W.; Pourkashanian, M. Comparative techno-economic assessment of biomass and coal with CCS technologies in a pulverized combustion power plant in the United Kingdom. *Int. J. Greenh. Gas Control* **2015**, *43*, 82–92. [CrossRef]
11. Fan, J.; Wei, S.; Zhang, X.; Yang, L. A comparison of the regional investment benefits of CCS retrofitting of coal-fired power plants and renewable power generation projects in China. *Int. J. Greenh. Gas Control* **2020**, *92*, 102858. [CrossRef]
12. Xianzheng, H.; Yong, S.; Zhaofeng, X.; Yalia, X.; Zhea, W.; Hongyi, C. Techno-economic performance of wind and coal-fired power with CCS joint planning. *Energy Procedia* **2017**, *114*, 6677–6684. [CrossRef]
13. Kaza, S.; Yao, L.C.; Bhada-Tata, P.; Van Woerden, F. *What a Waste 2.0: A Global Snapshot of Solid Waste Management to 2050*; World Bank: Washington, DC, USA, 2018.
14. Japan National Oil Corporation. *Investigation of CO₂ Sources in Kuwait*; Final Report; Japan National Oil Corporation: Tokyo, Japan, 1998.
15. Salman, M.; Oskui, R. *Selected Processes for Recovery of Crude Oils in Kuwait. Phase I: Preliminary Study*; Final Report No. KISR 7238; Kuwait Institute for Scientific Research: Safat, Kuwait, 2004.
16. Al-Salem, S.M.; Ma, X.; Mujaiabel, M.M. Assessment of CO₂ emission sources from the petroleum sector in Kuwait. In Proceedings of the 21st International Petroleum Environmental Conference (IPEC), Houston, TX, USA, 14–16 October 2014; p. 54.
17. Al-Salem, S.M. Investigating the global and specific carbon dioxide (CO₂) emissions from the petroleum downstream industry of Kuwait. In Proceedings of the 5th Technological Innovations Conference and Exposition, Kuwait City, Kuwait, 2 November 2014.
18. Al-Mutairi, A.; Smallbone, A.; Al-Salem, S.M.; Roskilly, A.P. The first carbon atlas of the state of Kuwait. *Energy* **2017**, *133*, 317–326. [CrossRef]
19. Al-Salem, S. Carbon dioxide (CO₂) emission sources in Kuwait from the downstream industry: Critical analysis with a current and futuristic view. *Energy* **2015**, *81*, 575–587. [CrossRef]
20. Al-Salem, S.; Ramadan, A.; Al-Mourad, M.; Naseeb, A.; Dashti, B. *Measurement of CO₂ Emissions from Power and Desalination Plants in Kuwait and Possibility of Carbon Capture and Storage*; KISR Final Report, EC093C; KISR: Safat, Kuwait, 2020.
21. Kam, E.; Mirza, Y.; Chehadeh, D.; Ashkanani, A.; Marouf, R.; Al-Muhareb, E. *KNPC Air Emissions Inventory Development, Air Module Implementation and Risk Assessment*; Report No. KISR 7629; Kuwait Institute for Scientific Research: Safat, Kuwait, 2005.
22. Chehadeh, D.; Kam, E.; Mirza, Y.; Al-Shumari, B. *Experience in Air Emission Inventory Development for Refineries of the Kuwait National Petroleum Company*; KISR: Safat, Kuwait, 2004.
23. International Energy Agency and Organization for Economic Cooperation and Development. *World Energy Outlook*; IEA: Paris, France, 2008.
24. International Energy Agency and Organization for Economic Cooperation and Development. *World Energy Outlook*; IEA: Paris, France, 2016.
25. *Statistical Yearbook of Electrical Energy, State of Kuwait: Statistics Department and Information Center*; Ministry of Electricity and Water: Kuwait City, Kuwait, 2011.
26. Alotaibi, S. Energy consumption in Kuwait: Prospects and future approaches. *Energy Policy* **2011**, *39*, 637–643. [CrossRef]
27. Aljohani, T.M.; Alzahrani, A.M. The Operation of the GCCIA HVDC Project and Its Potential Impacts on the Electric Power Systems of the Region. *Int. J. Electron. Electr. Eng.* **2014**, *2*, 207–213. [CrossRef]
28. *Statistical Yearbook of Electrical Energy, State of Kuwait: Statistics Department and Information Center*; Ministry of Electricity and Water: Kuwait City, Kuwait, 2010.
29. Global CCS Institute. *The Costs of CCS and Other Low-Carbon Technologies in the United States: 2015 Update*. Available online: <https://www.globalccsinstitute.com/publications/costs-ccs-and-other-low-carbon-technologies-2015-update> (accessed on 23 May 2022).
30. International Energy Agency. *World Energy Outlook (WEO) 2017*; International Energy Agency: Paris, France, 2017; Available online: <http://www.iea.org/weo2017/> (accessed on 23 May 2022).
31. Horngren, C.T.; Sundem, G.L.; Stratton, W.O.; Burgstahler, D.; Schatzberg, J. *Introduction to Management Accounting*; Pearson Prentice Hall: Hoboken, NJ, USA, 2008; ISBN 9780132405690.
32. *Statistical Yearbook of Electrical Energy, State of Kuwait: Statistics Department and Information Center*; Ministry of Electricity and Water: Kuwait City, Kuwait, 2017.
33. Lazard. 2018. Available online: <https://www.lazard.com/perspective/levelized-cost-of-energy-2017/> (accessed on 4 December 2018).
34. Penn State, Penn State College of Earth and Mineral Sciences—John A. Dutton E-Education Institute. 2018. Available online: <https://www.e-education.psu.edu/eme801/node/560> (accessed on 23 May 2022).

35. National Energy Technology Laboratory. *Cost and Performance Baseline for Fossil Energy Plants Volume 3a: Low Rank Coal to Electricity: IGCC Cases*; US Department of Energy: Washington, DC, USA, 2001.
36. Global CCS Institute. The CO₂ Market. 2018. Available online: <https://hub.globalccsinstitute.com/publications/accelerating-uptake-ccs-industrial-use-captured-carbon-dioxide/2-co2-market> (accessed on 23 May 2022).
37. Grand View Research. Market Research Report-Industry Insights. 2018. Available online: <https://www.grandviewresearch.com/industry-analysis/carbon-dioxide-market> (accessed on 23 May 2022).
38. Anderson, D.R.; Sweeney, D.J.; Williams, T.A.; Freeman, J.; Shoosmith, E. *Statistics for Business and Economics*; South-Western Cengage Learning: Boston, MA, USA, 2009; ISBN 9781844803132.
39. National Energy Technology Laboratory (NETL). *Cost and Performance for Low-Rank Pulverized Coal Oxy-Combustion Energy Plants September*; US Department of Energy: Washington, DC, USA, 2010.
40. National Energy Technology Laboratory (NETL). *Cost and Performance Baseline for Fossil Energy Plants Volume 3 Executive Summary: Low Rank Coal and Natural Gas to Electricity*; US Department of Energy: Washington, DC, USA, 2011.
41. National Energy Technology Laboratory (NETL). *Cost and Performance Baseline for Fossil Energy Plants Volume 1b: Bituminous Coal (IGCC) to Electricity, Revision 2b*; US Department of Energy: Washington, DC, USA, 2015.
42. David, J.; Herzog, H. The Cost of Carbon Capture, Greenhouse Gas Control Technologies. In Proceedings of the 5th International Conference on Greenhouse Gas Control Technologies, Cairns, QLD, Australia, 13–16 August 2000; CSIRO Publishing: Clayton, Australia, 2001. ISBN 0643066721.
43. Behrens, W.; Hawranek, P.M. *Manual for the Preparation of Industrial Feasibility Studies*; UNIDO: Vienna, Austria, 1991; ISBN 9211062691.
44. Amling, R. *Investments an Introduction to Analysis and Management*; Prentice Hall: Hoboken, NJ, USA, 1989; ISBN 0135043417.
45. The Economist. *Number Guide the Essentials of Business Numeracy*; The Economist Books Ltd.: London, UK, 2003; ISBN 9781861975157.
46. Al-Salem, S.M.; Papageorgiou, L.G.; Lettieri, P. Techno-economic assessment of thermo-chemical treatment (TCT) units in the Greater London area. *Chem. Eng. J.* **2014**, *248*, 253–263. [[CrossRef](#)]
47. Gitman, L.J. *Principles of Managerial Finance*; Pearson Prentice Hall: Hoboken, NJ, USA, 2009; ISBN 0321555287.
48. National Energy Technology Laboratory. *Cost and Performance Baseline for Fossil Energy Plants Volume 3a: Low Rank Coal to Electricity: IGCC Cases*; US Department of Energy: Washington, DC, USA, 2011.
49. Emenike, O.; Michailos, S.; Finney, K.N.; Hughes, K.J.; Ingham, D.; Pourkashanian, M. Initial techno-economic screening of BECCS technologies in power generation for a range of biomass feedstock. *Sustain. Energy Technol. Assess.* **2020**, *40*, 100743. [[CrossRef](#)]
50. Bellotti, D.; Sorce, A.; Rivarolo, M.; Magistri, L. Techno-economic analysis for the integration of a power to fuel system with a CCS coal power plant. *J. CO₂ Util.* **2019**, *33*, 262–272. [[CrossRef](#)]
51. Hondo, H. Life cycle GHG emission analysis of power generation systems: Japanese case. *Energy* **2005**, *30*, 2042–2056. [[CrossRef](#)]
52. United Nations Environment Programme. *Environmental Impacts of the Arab Oil and Gas Sector*; Regional Office for West Asia: Nairobi, Kenya, 2007.
53. Duan, H.; Fan, Y.; Zhu, L. What's the most cost-effective policy of CO₂ targeted reduction: An application of aggregated economic technological model with CCS? *Appl. Energy* **2013**, *112*, 866–875. [[CrossRef](#)]
54. Machado, P.G.; Hawkes, A.; de Oliveira Ribeiro, C. What is the future potential of CCS in Brazil? An expert elicitation study on the role of CCS in the country. *Int. J. Greenh. Gas Control* **2021**, *112*, 103503. [[CrossRef](#)]
55. Fan, J.; Xua, M.; Wei, S.; Zhong, P.; Zhang, X.; Yang, Y.; Wang, H. Evaluating the effect of a subsidy policy on carbon capture and storage (CCS) investment decision-making in China—A perspective based on the 45Q tax credit. *Energy Procedia* **2018**, *154*, 22–28. [[CrossRef](#)]
56. Hong, W.Y. A techno-economic review on carbon capture, utilisation and storage systems for achieving a net-zero CO₂ emissions future. *Carbon Capture Sci. Technol.* **2022**, *3*, 100044. [[CrossRef](#)]
57. Paltsev, S.; Morris, J.; Kheshgi, H.; Herzog, H. Hard-to-Abate Sectors: The role of industrial carbon capture and storage (CCS) in emission mitigation. *Appl. Energy* **2021**, *300*, 117322. [[CrossRef](#)]
58. Loria, P.; Bright, M.B.H. Lessons captured from 50 years of CCS projects. *Electr. J.* **2021**, *34*, 106998. [[CrossRef](#)]
59. Le Quéré, C.; Jackson, R.B.; Jones, M.W.; Smith, A.J.P.; Abernethy, S.; Andrew, R.M.; De-Gol, A.J.; Willis, D.R.; Shan, Y.; Canadell, J.G.; et al. Temporary reduction in daily global CO₂ emissions during the COVID-19 forced confinement. *Nat. Clim. Change* **2020**, *10*, 647–653. [[CrossRef](#)]
60. Friedlingstein, P.; Le Quéré, C.; Canadell, P.; Jackson, R.; Peters, G. Impact of COVID-19 on CO₂ Emissions. Global Carbon Project UNFCC. 2022. Available online: https://unfccc.int/sites/default/files/resource/1.GCP_.pdf (accessed on 6 May 2022).
61. Huang, S.; Xiao, X.; Guo, H. A novel method for carbon emission forecasting based on EKC hypothesis and nonlinear multivariate grey model: Evidence from transportation sector. *Environ. Sci. Pollut. Res.* **2022**; online ahead of print. [[CrossRef](#)]
62. Gao, M.; Yang, H.; Xiao, Q.; Goh, M. A novel method for carbon emission forecasting based on Gompertz's law and fractional grey model: Evidence from American industrial sector. *Renew. Energy* **2022**, *181*, 803–819. [[CrossRef](#)]
63. Li, X.; Xiao, X.; Guo, H. A novel grey Bass extended model considering price factors for the demand forecasting of European new energy vehicles. *Neural Comput. Appl.* **2022**; in press. [[CrossRef](#)]

64. Gao, M.; Yang, H.; Xiao, Q.; Goh, M. COVID-19 lockdowns and air quality: Evidence from grey spatiotemporal forecasts. *Socio-Economic Plan. Sci.* **2022**; 101228, *in press*. [[CrossRef](#)]
65. Darwish, A.; Darwish, M. Energy and water in Kuwait: A sustainability viewpoint, Part II. *Desalination* **2008**, *230*, 140–152. [[CrossRef](#)]
66. Darwish, M.; Abdulrahim, H.; Amer, A. On better utilization of gas turbines in Kuwait. *Energy* **2008**, *55*, 571–588. [[CrossRef](#)]
67. Darwish, M.; Al-Awadhi, F.; Darwish, A. Energy and water in Kuwait. A sustainability viewpoint, Part I. *Desalination* **2008**, *225*, 341–355. [[CrossRef](#)]
68. Darwish, M.; Al-Najem, N. The water problem in Kuwait. *Desalination* **2005**, *177*, 167–177. [[CrossRef](#)]
69. Darwish, M. Towards energy conservation in Qatar. *Open J. Energy Effic.* **2013**, *2*, 176–191. [[CrossRef](#)]
70. Ferguson, S.; Stockle, M.; Stamateris, B. Reducing CO₂ carbon capture options applied to the refining industry. In Proceedings of the ERTC Annual Meeting, Barcelona, Spain, 29 November–1 December 2011.
71. IEA. *Prospects for CO₂ Capture and Storage. Energy Technology Analysis*; International Energy Agency; Organization for Economic Cooperation and Development: Paris, France, 2004.
72. Ishida, M.; Jin, H. A novel combustor based on chemical-looping combustion reactions and its reactions kinetics. *J. Chem. Eng. Jpn.* **1994**, *27*, 296–301. [[CrossRef](#)]
73. Ishida, M.; Zheng, D.; Akehata, T. Evaluation of a chemical-looping-combustion power-generation system by graphic exergy analysis. *Energy* **1987**, *12*, 147–154. [[CrossRef](#)]
74. Johansson, D.; Sjöblom, J.; Bernstsson, T. Heat supply alternatives for CO₂ capture in the process industry. *Int. J. Greenh. Gas Control* **2012**, *8*, 217–232. [[CrossRef](#)]
75. Johansson, D.; Rootzen, J.; Bernstsson, T.; Johnsson, F. Assessment of strategies for CO₂ abatement in the European petroleum refining industry. *Energy* **2012**, *42*, 375–386. [[CrossRef](#)]
76. Johansson, D.; Franck, P.; Pettersson, K.; Bernstsson, T. Comparative study of Fischer–Tropsch production and post-combustion CO₂ capture at an oil refinery: Economic evaluation and greenhouse gas emissions (GHG) balances. *Energy* **2013**, *59*, 387–401. [[CrossRef](#)]
77. Markström, P.; Linderholm, C.; Lyngfelt, A. Chemical-looping combustion of solid fuels—Design and operation of a 100 kW unit with bituminous coal. *Int. J. Greenh. Gas Control* **2013**, *15*, 150–162. [[CrossRef](#)]
78. MEW. *Statistical Yearbook of Electricity Energy*; Statistics Department and Information Center, Ministry of Electricity and Water, MEW: Kuwait City, Kuwait, 2014.
79. Thernesz, A.; Szalmas, G.; Dinka, P.; Simon, T. CO₂ Capture-new challenge in refinery industry. *MOL Sci. Mag.* **2008**, *3*, 12–24.

Article

Practical Application-Oriented Energy Management for a Plug-In Hybrid Electric Bus Using a Dynamic SOC Design Zone Plan Method

Wenxiao Han, Xiaohua Chu *, Sui Shi, Ling Zhao and Zhen Zhao

School of Mechanical & Automotive Engineering, Liaocheng University, Liaocheng 252059, China; hanwenxiao68@126.com (W.H.); shisui_2021@163.com (S.S.); zhaoling@lcu.edu.cn (L.Z.); zhaozhen@lcu.edu.cn (Z.Z.)

* Correspondence: chuxiaohua@lcu.edu.cn

Abstract: The main problem in current energy management is the ability of practical application. To address the problem, this paper proposes a reinforcement learning (RL)-based energy management by combining Tubule Q-learning and Pontryagin's Minimum Principle (PMP) algorithms for a plug-in hybrid electric bus (PHEB). The main innovation distinguished from the existing energy management strategies is that a dynamic SOC design zone plan method is proposed. It is characterized by two aspects: ① a series of fixed locations are defined in the city bus route and a linear SOC reference trajectory is re-planned at fixed locations; ② a triangle zone will be re-planned based on the linear SOC reference trajectory. Additionally, a one-dimensional state space is also designed to ensure the real-time control. The off-line trainings demonstrate that the agent of the RL-based energy management can be well trained and has good generalization performance. The results of hardware in loop simulation (HIL) demonstrate that the trained energy management has good real-time performance, and its fuel consumption can be decreased by 12.92%, compared to a rule-based control strategy.

Keywords: plug-in hybrid electric bus; energy management; Q-learning; dynamic SOC design zone; hardware in loop simulation

Citation: Han, W.; Chu, X.; Shi, S.; Zhao, L.; Zhao, Z. Practical Application-Oriented Energy Management for a Plug-In Hybrid Electric Bus Using a Dynamic SOC Design Zone Plan Method. *Processes* **2022**, *10*, 1080. <https://doi.org/10.3390/pr10061080>

Academic Editors: Roberto Alonso González Lezcano, Francesco Nocera and Rosa Giuseppina Caponetto

Received: 27 April 2022

Accepted: 24 May 2022

Published: 27 May 2022

Publisher's Note: MDPI stays neutral with regard to jurisdictional claims in published maps and institutional affiliations.



Copyright: © 2022 by the authors. Licensee MDPI, Basel, Switzerland. This article is an open access article distributed under the terms and conditions of the Creative Commons Attribution (CC BY) license (<https://creativecommons.org/licenses/by/4.0/>).

1. Introduction

The environmental pollution caused by the rapid development of the transportation industry cannot be ignored, and the electric vehicle is expected to solve this dilemma [1]. Plug-in hybrid electric vehicles (PHEVs), characterized by combining an electric motor and an internal combustion engine, can reduce gas emissions [2]. In practice, at least two power sources are deployed in the PHEV, that is, at least two degrees of freedom will be introduced into the energy management [3]. Therefore, energy management is the most important issue for the PHEVs [4,5].

Many energy management strategies such as rule-based, optimization-based, prediction-based, and reinforcement learning (RL)-based methods have been proposed. Nevertheless, no matter what methods are proposed, how to realize the real-time and economic control in real world is the objective of these methods. The rule-based energy management can easily realize real-time control in the real world. However, only when the key parameters are elaborately designed can the control performance improve. For example, Ding N. et al. proposed a hybrid energy management system based on a rule-based control strategy and genetic algorithm to improve the fuel economy and overcome the battery limitations [6]. Li P. et al. proposed an intelligent logic rule-based energy management method by optimizing the working area of the engine [7]. The optimization-based energy management can realize better economic control in the real world, although the real-time control performance may be sacrificed. For example, Hassanzadeh M. et al. proposed an energy management strategy based on PMP to improve the fuel economy and battery life in the uncertain

traffic condition [8]. Wang W. et al. proposed an economic method based on dynamic programming (DP) and a feedback energy management system, which can maintain the state of charge of the battery (SOC) within the desired range [9]. Geng S. et al. compared various prediction methods and equivalent consumption minimization strategy (ECMS) implementations to evaluate the fuel consumption [10]. The prediction method-based energy management can realize real-time control in the real world, while the prediction precision should be well controlled. For example, Lian J. et al. proposed a predictive control algorithm by combining the long short-term memory network (LSTM) and the model predictive control (MPC) strategy to reduce fuel consumption under the constraints of SOC trajectory [11]. Liu Y J. et al. proposed a robust design method based on the Taguchi robust design method, where a nonlinear model predictive control (NMPC) is deployed to realize the real-time energy management [12]. In contrast, the RL-based energy management may be a promising method to realize real-time and economic control in the real world because it can realize self-learned control, thereby enhancing the control performance. For example, Lin X. et al. proposed an intelligent energy management strategy based on an improved RL algorithm with exploration factor to enhance the adaptability and improve the fuel economy [13]. Zhang H. et al. proposed a novel RL-based energy management method named Coach-Actor-Double Critic with a bi-level onboard controller to improve the self-learning ability and adaptability [14]. However, the RL-based energy management also has some disadvantages that may hinder its practical application.

The RL-based energy management is mainly focused on the Q-learning (QL) algorithm. The easy implementation and good real-time control performances make the Tabular QL-based strategy the most popular method [15,16]. However, the problem of the “curse of dimensionality” is difficult to be avoided, once the state space is sufficiently large. Moreover, it can only solve the problem of discrete state and action. The key problem of RL-based energy management is to accurately identify the optimal action based on current state. As SOC should decline to the expected value at the destination, the best action may have a strong relationship with required power, velocity, and travelled distance for PHEV. Moreover, only when the state is adequately discrete can the action catch the best action [17]. Therefore, more than three states may be defined to ensure the strategy has good generalization performance. In this case, if every state is a discrete 100 segments, 1,000,000 states may be generated in the Q-table. This may lead to the “curse of dimensionality” problem, once the strategy is implemented into the currently used vehicle controller. Deep QL (DQL) based strategies can solve the continuous state space problem, which can avoid the “curse of dimensionality” problem by substituting the Q-table by a neural network model (NN) [18,19]. However, the control performance may deteriorate once the fitting precision of neural network (NN) is low. In contrast, Ref. [20] proposed an Action-Critic control framework (AC) to solve the problem of continuous state and action space. However, multiple NNs should be designed in the strategy. Therefore, it is difficult to implement into currently used controllers in order to realize real-time control, because the computation burden will be greatly increased. Similarly, Ref. [21] further proposed a deep deterministic policy gradient (DDPG) framework which considers the traffic information. However, it also has the similar problems as AC.

Thanks to the instantaneous optimization performance of Pontryagin’s Minimum Principle (PMP) and its easy implementable performance for the current vehicle controller, it is a feasible method to be used in real-world, once the co-state can be dynamically recognized [22,23]. So, if we combine the QL and the PMP as the recognition algorithm in a dynamical and uncertain traffic environment, the control performance may be enhanced. However, the “curse of dimensionality” problem should be avoided, if the real-time energy management control is to be satisfied. To solve this problem, Ref. [24] proposed a feasible method by designing the state as the difference between the feedback SOC and the reference SOC. Here, the SOC reference trajectory is designed by the optimal SOC trajectories calculated by a series of historical driving conditions. Inspired by this method, this paper proposes an RL-based energy management together with a similar state variable design

method. In particular, the main difference between Ref. [24] and our work is that a dynamic linear SOC reference trajectory is planned at fixed locations based on the feedback SOC, and a triangle zone will be re-planned based on the reference SOC trajectory. The main advantage of this method is that the dynamic triangle zone can provide a margin for the fuel economy improvement, and can guide the feedback SOC reach the objective SOC.

The remainder of this paper is structured as follows. The modeling of the PHEB is introduced in Section 2. The RL-based energy management is detailed in Section 3. The results and discussion are presented in Section 4, and the conclusions are drawn in Section 5.

2. The Description of the PHEB

Figure 1 shows the layout of the PHEB. It is constituted by an engine, a clutch, an electric motor (EM), and a 6-speed automated mechanical transmission (AMT). The gears used in this paper are from 2 to 6, without considering the climbing driving conditions. Many working modes such as engine driving, hybrid driving, motor driving, and regenerative braking can be realized based on the driving demand and energy management.

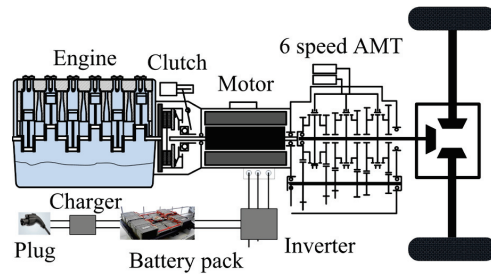


Figure 1. The structure of the PHEB.

An engine model that can satisfy the energy management requirement is indispensable. Based on the fuel consumption rate MAP of the engine (Figure 2), the instantaneous fuel consumption of the engine is formulated by

$$m_e = \frac{T_e \cdot n_e}{9500} \cdot \frac{b_e(T_e, n_e)}{3600} \cdot \Delta t \quad (1)$$

where m_e denotes the instantaneous fuel consumption of the engine; T_e denotes the torque of the engine; n_e denotes the speed of the engine; and $b_e(T_e, \omega_e)$ denotes the fuel consumption rate of the engine.

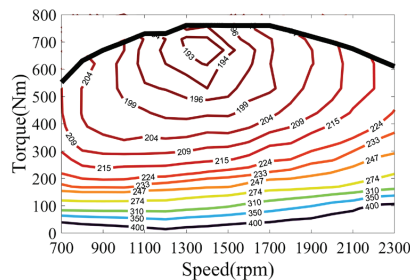


Figure 2. The fuel consumption rate MAP of the engine.

Similarly, the motor is formulated by

$$\begin{cases} P_m = n_m \cdot T_m \cdot \eta_m^{-\text{sgn}(T_m)} / 9550 \\ \text{sgn}(T_m) = \begin{cases} 1 & \text{if } T_m \geq 0 (\text{motoring mode}) \\ -1 & \text{if } T_m < 0 (\text{generating mode}) \end{cases} \end{cases} \quad (2)$$

where P_m denotes the power of the motor; η_m denotes the efficiency of the motor, which can be interpolated by a look-up table formulated by the efficiency map of the motor (Figure 3); and n_m and T_m denote the speed and the torque of the motor, respectively.

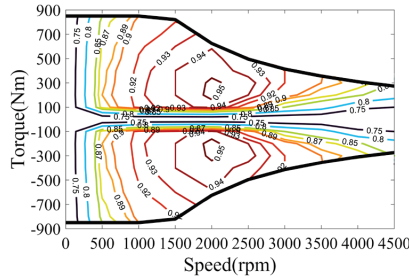


Figure 3. The efficiency MAP of the motor.

As shown in Figure 4, the battery is formulated as a Rint model; it is described as

$$\begin{cases} \dot{SOC} = -\frac{1}{Q_b} I_b \\ I_b = \frac{1}{2R_b} (V_b - \sqrt{V_b^2 - 4R_b P_b}) \end{cases} \quad (3)$$

where V_b denotes the battery voltage; P_b denotes the battery power; R_b denotes the internal resistance; and Q_b denotes the battery capacity.

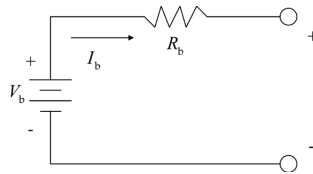


Figure 4. The Rint model of the battery.

3. The Formulation of the RL-Based Energy Management

3.1. The Formulation of PMP

In this paper, an economic gear shift strategy is executed during shift process. In consideration of minimizing the fuel consumption, the objective function is described as

$$\min J = \int_{t_0}^{t_f} [m_e(u(t))] dt \quad (4)$$

where J denotes the performance index function and $u(t)$ denotes the control vector, which is the throttle of the engine ($u(t) = [th(t)]$). Here, the throttle of the engine is denoted by $th(t)$, which ranges from 0 to 1.

Inspired by Ref. [25], the energy management can be converted into instantaneous optimization problem by minimizing the Hamiltonian function, which can be described as

$$\begin{cases} H(x(t), u(t), \lambda(t), t) = m_e(u(t)) + \lambda(t) \cdot \dot{SOC}(t) \\ u^*(t) = \arg \min \{ H(x(t), u(t), \lambda(t), t) \} \\ \dot{SOC}(t) = -\frac{V_b(x(t)) - \sqrt{V_b^2(x(t)) - 4R_b(x(t))P_b(u(t))}}{2R_b(x(t))Q_b} \end{cases} \quad (5)$$

where $u^*(t)$ denotes the optimum control solution; $H(x(t), u(t), \lambda(t), t)$ denotes the Hamiltonian function, whereby the first term is the instant fuel consumption, and the second term is the delta SOC which is multiplied by co-state; and $\lambda(t)$ denotes the co-state.

Theoretically, the co-state is the only key parameter to influence the optimization performance and is a time-varied value. It can be also approximately recognized as constant over the whole trip, based on Refs. [22,23]. Moreover, it can also be adapted in real-time, based on the driving conditions [26].

Furthermore, some constraints, with respect to the physical components of the PHEB, are also indispensable, which is described as

$$\text{S.t.} \begin{cases} \omega_{e_min} \leq \omega_e(t) \leq \omega_{e_max} \\ \omega_{m_min} \leq \omega_m(t) \leq \omega_{m_max} \\ P_{e_min}(\omega_e(t)) \leq P_e(t) \leq P_{e_max}(\omega_e(t)) \\ P_{m_min}(\omega_m(t)) \leq P_m(t) \leq P_{m_max}(\omega_m(t)) \end{cases} \quad (6)$$

where $\omega_e(t)$ and $\omega_m(t)$ denote the rotate speeds of the engine and the motor, respectively; ω_{e_min} , ω_{e_max} and ω_{m_min} , ω_{m_max} denote the corresponding rotate speed boundaries; $P_e(t)$ and $P_m(t)$ denote the powers of the engine and the motor, respectively; and P_{e_min} , P_{e_max} and P_{m_min} , P_{m_max} denote the corresponding power boundaries.

3.2. The Design of the Dynamic SOC Design Zone

In this paper, only one state for the difference between the feedback SOC and reference SOC trajectory is designed for the RL-based energy management. Therefore, the SOC reference trajectory becomes the key issue. As shown in Figure 5, a novel dynamic SOC design zone plan method is proposed. The basic principle is that a linear SOC reference trajectory will be firstly planned at the fixed location, and simultaneously a dynamic reference SOC zone will be defined based on the linear SOC reference trajectory. There are two advantages to this method.

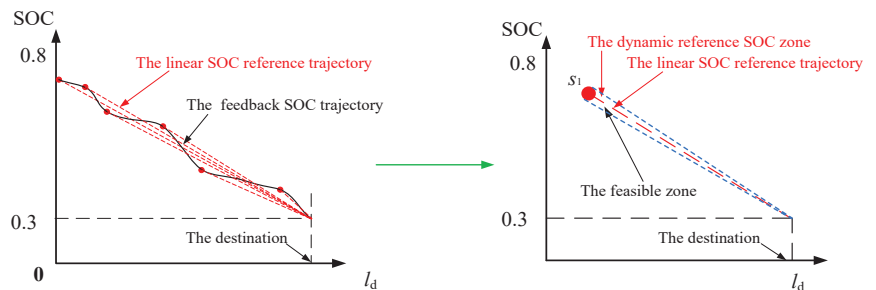


Figure 5. The principle of the dynamic SOC design zone method.

(1). The state of the difference of SOC between the dynamic reference SOC and the feedback SOC is only defined. In this case, only a Q-matrix with 100 rows and 27 columns is designed, which can ensure the real-time control of the strategy.

(2). In practice, the real driving conditions cannot be completely predicted, so the optimal SOC trajectory is usually not completely predicted. In this case, taking the optimal SOC trajectory as reference trajectory is infeasible. However, if a feasible zone (the floating value is designed as 0.02) is defined based on the linear SOC reference trajectory, the feedback SOC may be controlled within a feasible zone, and a great margin for the fuel economy improvement may be provided. This is also the most important innovation in this paper.

The main difference between the proposed method and the existing methods are listed as follows.

(1). In Ref. [24], only a SOC reference trajectory is designed, based on a series of optimal SOC trajectories. In terms of our method, the SOC reference trajectory is only based

on the fixed location. Moreover, a triangle zone will be also defined to improve the fuel economy of the PHEB.

(2). In Ref. [25], only an efficient zone is defined based on a series of optimization SOC trajectories, and no dynamic reference SOC trajectory is planned. Moreover, three states should be designed, and the efficient zone is designed off-line.

In addition, the dynamic SOC design zone plan method can be described as

$$\begin{cases} SOC_{ref} = \frac{SOC_T - SOC_{fnl}}{D_T - D_{fnl}} \cdot (D_{ref} - D_{fnl}) + SOC_{fnl} \\ SOC_{upper} = \frac{SOC_T + 0.02 - SOC_{fnl}}{D_T - D_{fnl}} \cdot (D_{ref} - D_{fnl}) + SOC_{fnl} \\ SOC_{lower} = \frac{SOC_T - 0.02 - SOC_{fnl}}{D_T - D_{fnl}} \cdot (D_{ref} - D_{fnl}) + SOC_{fnl} \end{cases} \quad (7)$$

where SOC_{ref} and D_{ref} denote the reference SOC and travelled distance at current time step, respectively; SOC_T and D_T denote the dynamic value of target SOC and the travelled distance, respectively, which are updated after fixed distance step; and SOC_{fnl} and D_{fnl} denote the value of target SOC and travelled distance at destination, respectively.

3.3. The Formulation of the RL-Based Energy Management

QL is one of the most important RL methods, based on the Temporal-Difference (TD) method. The update process of the Q value can be described as

$$Q(s_t, a_t) \leftarrow Q(s_t, a_t) + \alpha \left[r_{t+1} + \gamma \max_a Q(s_{t+1}, a) - Q(s_t, a_t) \right] \quad (8)$$

where α denotes the learning rate, which is defined as 0.95 in this paper; γ denotes the discount factor, which is defined as 0.8 in this paper; r_{t+1} denotes the immediate reward at time t ; and $\max_a Q(s, a)$ denotes the maximum Q value in the next state.

As shown in Figure 6, at every time step, the agent will obtain a state S_t from the environment, and an action a_t will be evaluated by the agent. Then, a state of the environment s_{t+1} will be adapted, and a corresponding reward r_{t+1} will be transmitted to the agent.

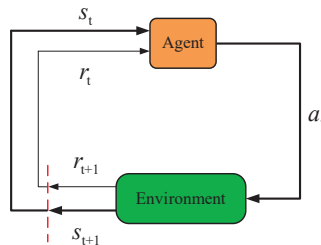


Figure 6. The principle of the reinforcement learning.

As an instantaneous optimization algorithm, PMP-based energy management has good real-time control performance. The only challenge is to recognize the co-state for the unrepeatable, stochastic driving conditions. In addition, QL is widely regarded as an intelligent algorithm that can adapt well to uncertain circumstances. Motivated by this, an RL-based energy management, combining PMP and RL, is proposed. As shown in Figure 7, at every time step, the agent will evaluate an action based on the states, and the states of PHEB will be adapted based on the action, then a reward will be generated and transmitted to the agent.

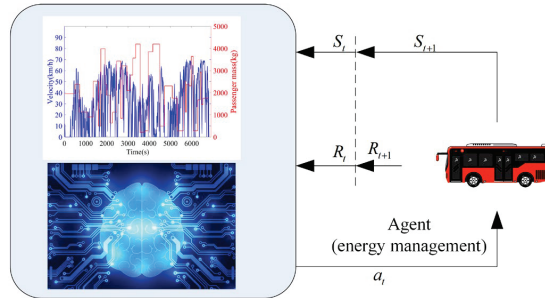


Figure 7. The principle of the RL-based energy management.

(1) The state

As stated above, the difference between the feedback SOC and the reference SOC is defined as the sole state, which is described as

$$s_t = SOC_f - SOC_{ref} \quad (9)$$

where SOC_f denotes the feedback SOC. The state s_t ranges from -0.04 to 0.04 , and is sampled by 100 points. That is to say, the number of rows is only 100, which provides a basis to reduce the dimensionality of the Q and R tables.

(2) The action

The co-state is defined as the only action, which ranges from -2800 to -4000 . Specifically, the action space is

$$a_t = \begin{bmatrix} -2800, -2900, -3000, -3100, -3200, -3250, -3275, -3300, -3325, -3350, -3375, -3390, -3400, \\ -3410, -3425, -3450, -3475, -3500, -3525, -3550, -3575, -3600, -3650, -3700, -3800, -3900, -4000 \end{bmatrix} \quad (10)$$

(3) The reward

As stated above, the reward is defined as Equation (11). Specifically, if the feedback SOC at time step $t + 1$ is larger than the upper boundary, then a punishment will be provided to the Q-value function. Moreover, the further the deviation is, the greater the punishment will be; if the feedback SOC at time step $t + 1$ is lower than the lower boundary, then a punishment will be provided to the Q-value function. Moreover, if the feedback SOC at time step $t + 1$ located in the feasible zone (between the lower and upper boundaries), a reward will be provided to the Q-value function, and the closer the feedback SOC to the reference, the greater the reward will be.

$$r_t = \begin{cases} -abs(SOC_f(t+1) - SOC_{upper}(t+1)) & SOC_f(t+1) > SOC_{upper}(t+1) \\ -abs(SOC_f(t+1) - SOC_{lower}(t+1)) & SOC_f(t+1) < SOC_{lower}(t+1) \\ \frac{10}{1+100*abs(SOC_f(t+1)-SOC_r(t+1))} & SOC_{lower}(t+1) \leq SOC_f(t+1) \leq SOC_{upper}(t+1) \end{cases} \quad (11)$$

(4) The ϵ -greedy algorithm

To realize the self-learning control, the ϵ -greedy algorithm is deployed, which is formulated by

$$\pi^*(a|s) = \begin{cases} a = \text{random}(A) & \text{if } r_n < \epsilon \\ a = \text{max}Q(s, a) & \text{if } r_n \geq \epsilon \end{cases} \quad (12)$$

where r_n is the random number, which ranges from 0 to 1.

(5) The RL-based energy management algorithm

- 1: initializing the Q and R tables with null matrix
- 2: **for** episode = 1, M **do**
- 3: **for** $t = 1, T$ **do**
- 4: observing the current state s_t ($s_t = SOC_t - SOC_{ref}$)
- 5: selecting the action a_t with ϵ -greedy algorithm
- 6: executing the action(a_t) and observing the next state
- 7: calculating the immediate reward based on Eq. (11)
- 8: updating the Q-Table by:

$$Q(s_t, a_t) \leftarrow Q(s_t, a_t) + \alpha [r_{t+1} + \gamma \max_a Q(s_{t+1}, a) - Q(s_t, a_t)]$$
- 9: **end**
- 10: **if** the feedback SOC is bigger than 0.85 or lower than 0.25 or abs($s(t)$) is bigger than 0.04
- 11: continue;
- 12: **end**
- 13: **end**
- 14: **end**

As shown in Figure 8, the design process is divided into three steps: off-line training, off-line verification, and hardware in the loop (HIL) with controller.

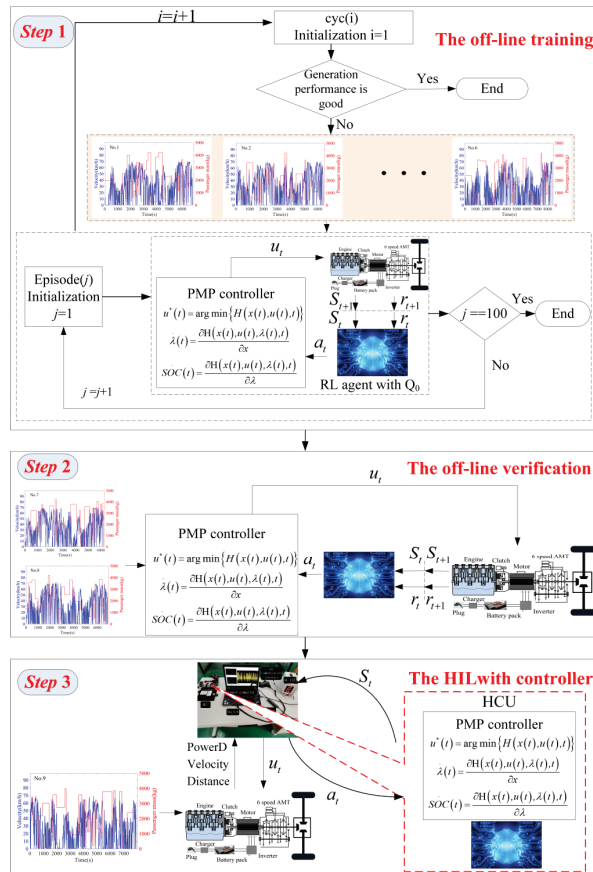


Figure 8. The design process of the RL-based energy management.

4. Result Discussions

A series of historical driving cycles of the PHEB are deployed for training and testing. The total length of route is about 50 km and has 39 bus stops; the number of passengers at

per station is assumed to be random. Moreover, as shown in Figure 9, a series of combined driving cycles, including driving cycle and passenger mass, are designed in this paper.

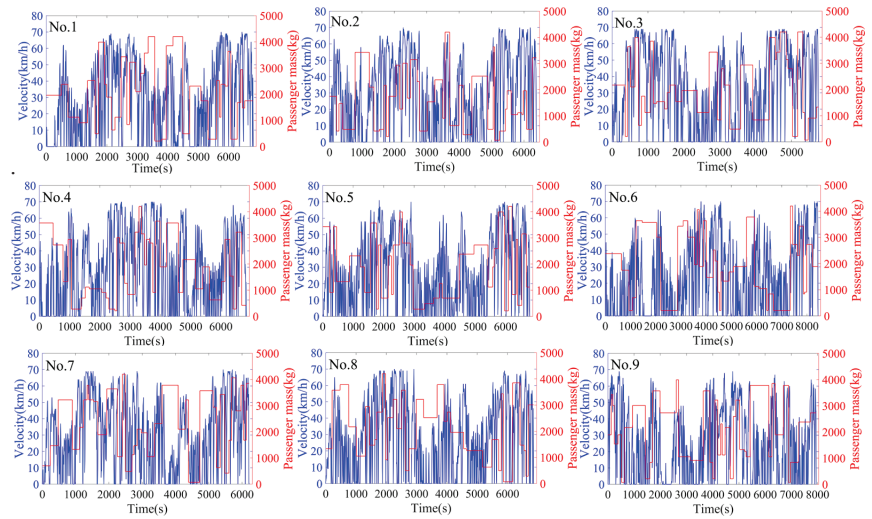


Figure 9. The combined driving cycles.

4.1. The Training Process

To ensure the RL-based energy management has better control performance, a well-trained Q-table of the reinforcement learning is indispensable. Therefore, six combined driving cycles are firstly designed to train the Q-table. The Q-table is continually trained one by one based on the combined driving cycles, and will be trained 100 times for each combined driving cycle based on different ϵ value. Specifically, the training is divided into three stages; in the first stage, the ϵ is designed as 0.5 before episode 45, which implies that the action is randomly selected by the probability of 50%; in the second stage, the ϵ is designed as 0.15 between the episode 46 and episode 75, which implies that the action is randomly selected by the probability of 15%; in the third stage, the ϵ is designed as 0 between the episode 76 and episode 100, which implies that the action is selected by the trained Q-table.

As shown in Figure 10, the combined driving cycle 1 is firstly selected to train the Q-table (named Q-table 1). In the first stage, the agent strives to probe the possible action. In this case, the final SOC is higher than 0.6, which implies that the Q-table 1 is not well trained; in the second stage, the RL will partly select the action based on the trained Q-table 1, whilst trying to probe possible actions by the ϵ -greedy algorithm. In this case, the SOC will be fluctuated around 0.3, which implies the Q-table 1 has been better trained. In the third stage, the final SOC can easily reach the objective value, and the feedback SOC trajectory can easily follow the reference SOC trajectory. This implies that the Q-table 1 has been well trained for the combined driving cycle 1.

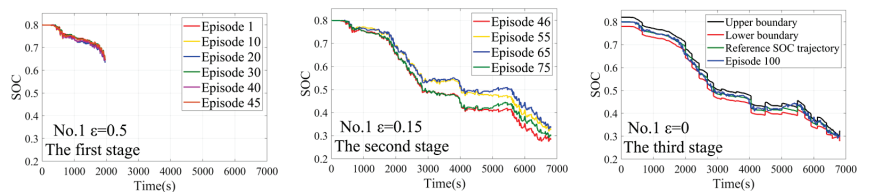


Figure 10. The training process of combined driving cycle 1.

As shown in Figure 11, the combined driving cycle 2 is deployed to continually train the Q-table (Q-table 2), based on Q-table 1. The RL will still be terminated in advance in the first stage. Moreover, the final SOCs are higher than 0.5, which are lower than the final SOCs in Figure 10. In the second stage, the final SOCs can satisfy the control object, and has good control performance. In the third stage, the Q-table has been well trained, the final SOC can satisfy the control object, and the SOC trajectory can better follow the reference SOC trajectory well. This implies that the Q-table 2 has been better trained compared to the Q-table in Figure 10.

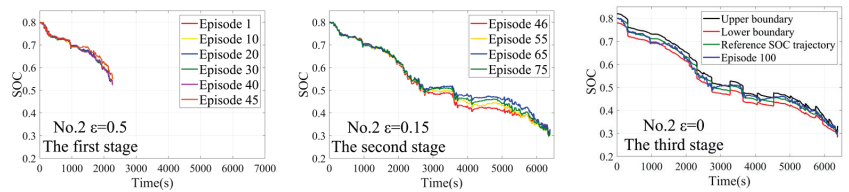


Figure 11. The training process of combined driving cycle 2.

As shown in Figure 12, the combined driving cycle 3 is deployed to continually train the Q-table (Q-table 3), based on the well trained Q-table 2. In the first stage, the control performance has been greatly improved, compared to the first stage for Q-table 1 and 2. However, the final SOCs still do not satisfy the control object. In contrast, the control preference is deteriorated in stage 2 compared to the Q-table 2. This implies that the driving conditions may be different from the combined driving cycle 2, and the generalization performance of the Q-table should be further improved. Nevertheless, the control preference can satisfy the control objective during the third stage, and it is recognized that the Q-table 3 has been well trained.

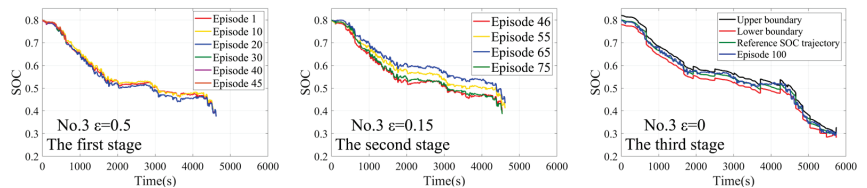


Figure 12. The training process of combined driving cycle 3.

As shown in Figure 13, the combined driving cycle 4 is deployed to continually train the Q-table (Q-table 4), based on the well trained Q-table 3. Similar to the first stage in Figure 12, the Q-table 4 is also not well trained, because the final SOCs do not reach 0.3. However, the control performance is greatly improved in the second stage, and the control performance can satisfy the control objective in the stage 3. This implies that Q-table 4 has been well trained.

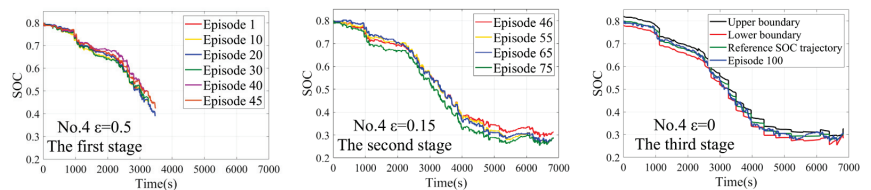


Figure 13. The training process of combined driving cycle 4.

It can be seen from Figures 14 and 15 that the Q-table 4 has been well trained, because the control performance can be well satisfied in three stages, no matter the ϵ value. This implies that the generalization performance of the Q-table 4 has been greatly improved, and

can satisfy the control performance. On the other hand, the generalization performance of the Q-table 4 will be further improved based on the trainings of the two combined driving cycles. In addition, Q-table 6 can be taken as the well trained Q-table being after continually trained by combined driving cycle 5 and 6.

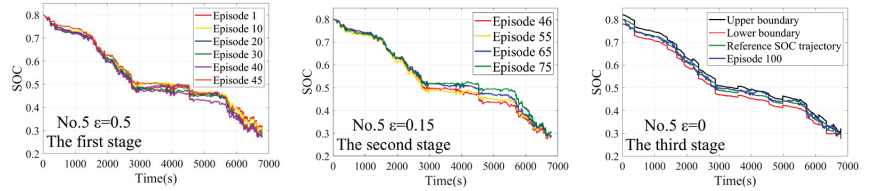


Figure 14. The training process of combined driving cycle 5.

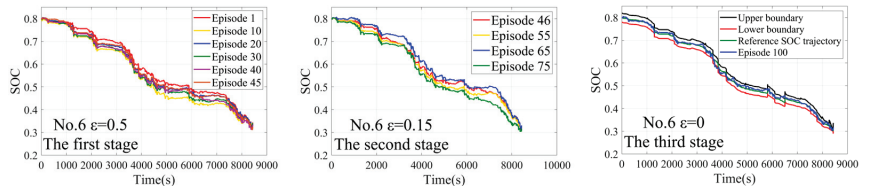


Figure 15. The training process of combined driving cycle 6.

4.2. The Off-Line Verification

To verify the generalization and reliable performances of the Q-Table 6, the combined driving cycle 7 (denoted by No.7) and combined driving cycle 8 (denoted by No.8) are deployed. From Figure 16, it can be seen that the co-state can be well adjusted, based on the driving cycles and the Q-Table 6. Moreover, the final SOC values can satisfy the control object, and the SOC trajectories locate the designed boundary and can easily follow the SOC reference trajectories. This implies that the RL-based strategy has great potential for practical application. In addition, a rule-based energy management is also deployed to evaluate the fuel economy of the RL-based energy management method. From Table 1, it can be seen that the fuel consumption of conditions 7 and 8 can be reduced by 10.95% and 11.78%, respectively.

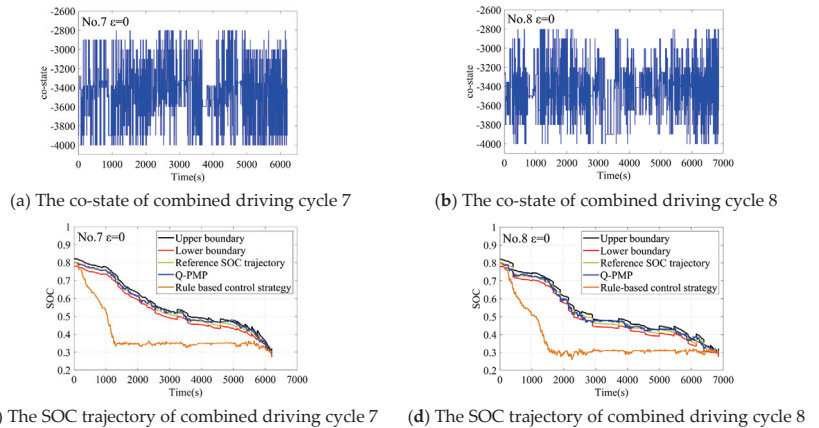


Figure 16. Offline verification results of combined driving cycles 7 and 8.

Table 1. The fuel consumptions of the off-line verification.

Combined Driving Cycle	RL-Based (L/100 km)	Rule-Based (L/100 km)	Fuel Consumption Comparison
No.7	16.8738	18.9497	−10.95%
No.8	16.6673	18.8939	−11.78%

4.3. The Hardware in Loop Simulation Verify

As shown in Figure 17, a HIL test system mainly includes HCU, switch, Upper computer, CAN communication interface, DC 12 V, and Kvaser, built to verify the real-time and reliability of RL-based energy management. Here, the upper computer transmits CAN signals to the HCU through Kvaser.

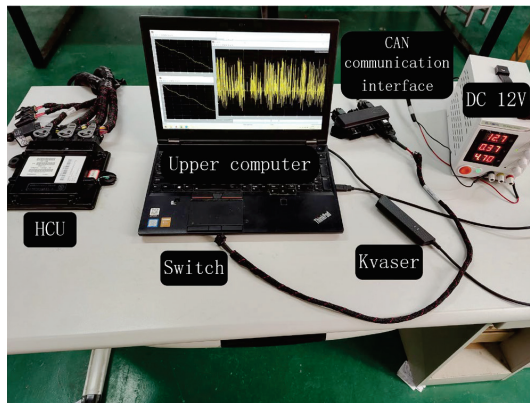


Figure 17. The HIL test system.

As shown in Figure 18, a HIL simulation model is built based on D2P rapid prototyping control system and the well trained strategy. It mainly includes three modules: Input, HCU, and Output, where HCU is used to embed the RL-based energy management.

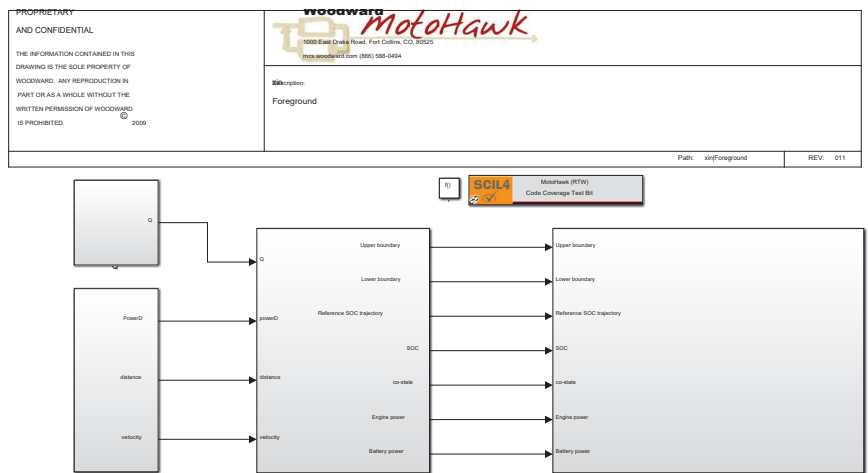


Figure 18. The composition of HIL.

Additionally, the combined driving cycle 9 (denoted by No.9) is also deployed. From Figure 19, it can be seen that the co-state can be adjusted in real-time based on the well-trained strategy, and the control performance can be sufficiently satisfied. Moreover, the

fuel consumption can be decreased by 12.92% compared to the rule based strategy as shown in Table 2.

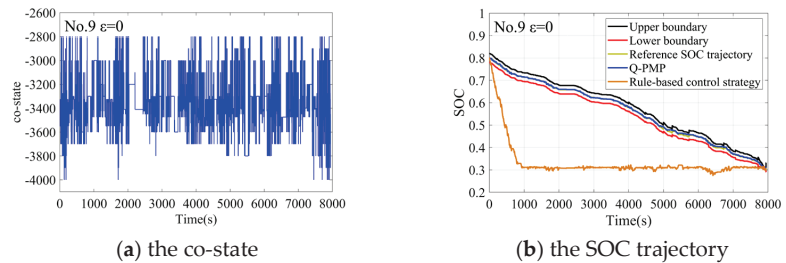


Figure 19. The HIL test results of combined driving cycle 9.

Table 2. The fuel consumption of the HIL.

Combined Driving Cycle	RL-Based (L/100 km)	Rule-Based (L/100 km)	Fuel Consumption Comparison
No.9	15.2956	17.5642	−12.92%

5. Conclusions

This paper proposes an RL-based energy management method based on a novel dynamic SOC design zone plan. The main conclusions are summarized as follows.

Firstly, the proposed dynamic SOC design zone plan method is feasible and applicable. The fuel consumption can be greatly decreased compared to the rule-based energy management.

Secondly, the agent of RL-based energy management can be well trained, and has good generalization performance. Moreover, the trained strategy can be easily embedded into the controller, and the real-time control performance can be satisfied well. It has great potential to be used in practice.

Future work will focus on the further verification of the RL-based energy management in the real vehicles.

Author Contributions: Investigation, X.C.; methodology, W.H. and X.C.; software, S.S. and Z.Z.; supervision, L.Z.; validation, S.S. and Z.Z.; writing-original draft, W.H. All authors have read and agreed to the published version of the manuscript.

Funding: This research received no external funding.

Institutional Review Board Statement: Not applicable.

Informed Consent Statement: Not applicable.

Data Availability Statement: Not applicable.

Conflicts of Interest: The authors declare no conflict of interest.

References

- Ajanovic, A.; Haas, R.; Schrödl, M. On the historical development and future prospects of various types of electric mobility. *Energies* **2021**, *14*, 1070. [\[CrossRef\]](#)
- Plötz, P.; Moll, C.; Bieker, G.; Mock, P. From lab-to-road: Real-world fuel consumption and CO₂ emissions of plug-in hybrid electric vehicles. *Environ. Res. Lett.* **2021**, *16*, 054078. [\[CrossRef\]](#)
- Zhang, F.; Hu, X.; Langari, R.; Cao, D. Energy management strategies of connected HEVs and PHEVs: Recent progress and outlook. *Prog. Energy Combust. Sci.* **2019**, *73*, 235–256. [\[CrossRef\]](#)
- Huang, Y.; Wang, H.; Khajepour, A.; Li, B.; Ji, J.; Zhao, K.; Hu, C. A review of power management strategies and component sizing methods for hybrid vehicles. *Renew. Sustain. Energy Rev.* **2018**, *96*, 132–144. [\[CrossRef\]](#)
- Biswas, A.; Emadi, A. Energy Management Systems for Electrified Powertrains: State-of-The-Art Review and Future Trends. *IEEE Trans. Veh. Technol.* **2019**, *68*, 6453–6467. [\[CrossRef\]](#)

6. Ding, N.; Prasad, K.; Lie, T.T. Design of a hybrid energy management system using designed rule-based control strategy and genetic algorithm for the series-parallel plug-in hybrid electric vehicle. *Int. J. Energy Res.* **2021**, *45*, 1627–1644. [[CrossRef](#)]
7. Li, P.; Li, Y.; Wang, Y.; Jiao, X. An intelligent logic rule-based energy management strategy for power-split plug-in hybrid electric vehicle. In Proceedings of the 2018 37th Chinese Control Conference (CCC), Wuhan, China, 25–27 July 2018; pp. 7668–7672.
8. Hassanzadeh, M.; Rahmani, Z. Real-time optimization of plug-in hybrid electric vehicles based on Pontryagin's minimum principle. *Clean Technol. Environ. Policy* **2021**, *23*, 2543–2560. [[CrossRef](#)]
9. Wang, W.; Cai, Z.; Liu, S. Study on Real-Time Control Based on Dynamic Programming for Plug-In Hybrid Electric Vehicles. *SAE Int. J. Electrified Veh.* **2021**, *10*, 167. [[CrossRef](#)]
10. Geng, S.; Schulte, T.; Maas, J. Model-Based Analysis of Different Equivalent Consumption Minimization Strategies for a Plug-In Hybrid Electric Vehicle. *Appl. Sci.* **2022**, *12*, 2905. [[CrossRef](#)]
11. Lian, J.; Wang, X.R.; Li, L.H.; Zhou, Y.F.; Yu, S.Z.; Liu, X.J. Plug-in HEV energy management strategy based on SOC trajectory. *Int. J. Veh. Des.* **2020**, *82*, 1–17. [[CrossRef](#)]
12. Liu, Y.J.; Sun, Q.; Han, Q.; Xu, H.G.; Han, W.X.; Guo, H.Q. A Robust Design Method for Optimal Engine Operating Zone Design of Plug-in Hybrid Electric Bus. *IEEE Access* **2022**, *10*, 6978–6988. [[CrossRef](#)]
13. Lin, X.; Zhou, K.; Mo, L.; Li, H. Intelligent Energy Management Strategy Based on an Improved Reinforcement Learning Algorithm With Exploration Factor for a Plug-in PHEV. *IEEE Trans. Intell. Transp. Syst.* **2021**, 1–11. [[CrossRef](#)]
14. Zhang, H.; Peng, J.; Tan, H.; Dong, H.; Ding, F. A Deep Reinforcement Learning-Based Energy Management Framework With Lagrangian Relaxation for Plug-In Hybrid Electric Vehicle. *IEEE Trans. Transp. Electrif.* **2020**, *7*, 1146–1160. [[CrossRef](#)]
15. Liu, T.; Hu, X.; Hu, W.; Zou, Y. A Heuristic Planning Reinforcement Learning-Based Energy Management for Power-Split Plug-in Hybrid Electric Vehicles. *IEEE Trans. Ind. Inform.* **2019**, *15*, 6436–6445. [[CrossRef](#)]
16. Chen, Z.; Hu, H.; Wu, Y.; Zhang, Y.; Li, G.; Liu, Y. Stochastic model predictive control for energy management of power-split plug-in hybrid electric vehicles based on reinforcement learning. *Energy* **2020**, *211*, 118931. [[CrossRef](#)]
17. Guo, H.Q.; Wei, G.; Wang, F.; Wang, C.; Du, S. Self-Learning Enhanced Energy Management for Plug-in Hybrid Electric Bus With a Target Preview Based SOC Plan Method. *IEEE Access* **2019**, *7*, 103153–103166. [[CrossRef](#)]
18. Qi, C.; Zhu, Y.; Song, C.; Cao, J.; Xiao, F.; Zhang, X.; Xu, Z.; Song, S. Self-supervised reinforcement learning-based energy management for a hybrid electric vehicle. *J. Power Sources* **2021**, *514*, 230584. [[CrossRef](#)]
19. Wu, Y.; Tan, H.; Peng, J.; Zhang, H.; He, H. Deep reinforcement learning of energy management with continuous control strategy and traffic information for a series-parallel plug-in hybrid electric bus. *Appl. Energy* **2019**, *247*, 454–466. [[CrossRef](#)]
20. Tan, H.; Zhang, H.; Peng, J.; Jiang, Z.; Wu, Y. Energy management of hybrid electric bus based on deep reinforcement learning in continuous state and action space. *Energy Convers. Manag.* **2019**, *195*, 548–560. [[CrossRef](#)]
21. He, W.; Huang, Y. Real-time Energy Optimization of Hybrid Electric Vehicle in Connected Environment Based on Deep Reinforcement Learning. *IFAC-PapersOnLine* **2021**, *54*, 176–181. [[CrossRef](#)]
22. Kim, N.; Jeong, J.; Zheng, C. Adaptive energy management strategy for plug-in hybrid electric vehicles with Pontryagin's minimum principle based on daily driving patterns. *Int. J. Precis. Eng. Manuf.-Green Technol.* **2019**, *6*, 539–548. [[CrossRef](#)]
23. Xie, S.; Hu, X.; Xin, Z.; Brighton, J. Pontryagin's minimum principle based model predictive control of energy management for a plug-in hybrid electric bus. *Appl. Energy* **2019**, *236*, 893–905. [[CrossRef](#)]
24. Guo, H.; Du, S.; Zhao, F.; Cui, Q.; Ren, W. Intelligent Energy Management for Plug-in Hybrid Electric Bus with Limited State Space. *Processes* **2019**, *7*, 672. [[CrossRef](#)]
25. Guo, H.; Zhao, F.; Guo, H.; Cui, Q.; Du, E.; Zhang, K. Self-learning energy management for plug-in hybrid electric bus considering expert experience and generalization performance. *Int. J. Energy Res.* **2020**, *44*, 5659–5674. [[CrossRef](#)]
26. Onori, S.; Tribioli, L. Adaptive Pontryagin's Minimum Principle supervisory controller design for the plug-in hybrid GM Chevrolet Volt. *Appl. Energy* **2015**, *147*, 224–234. [[CrossRef](#)]



Article

Decoupling Analysis of Rural Population Change and Rural Electricity Consumption Change in China

Xuechao Xia ^{1,2}, Hui Sun ^{1,2,*}, Zedong Yang ^{1,2}, Weipeng Yuan ^{1,2} and Dianyuan Ma ^{1,2}

¹ Center for Innovation Management Research of Xinjiang, No.666 Shengli Road, Urumqi 830046, China; xiaxuechao99@163.com (X.X.); 15066198893@163.com (Z.Y.); ywpywp@163.com (W.Y.); madianyuan2022@163.com (D.M.)

² School of Economics and Management, Xinjiang University, No.666 Shengli Road, Urumqi 830046, China

* Correspondence: shui@xju.edu.cn

Abstract: With the accelerated development of urbanization in China, rural permanent population has declined, while rural electricity consumption has increased, resulting in a significant waste of electricity resources. Based on the provincial panel data of China from 2007 to 2020, this paper comprehensively used the decoupling model and the coordination degree model to analyze the temporal change characteristics, spatial distribution characteristics, and the degree of deviation of rural permanent population and rural electricity consumption. Firstly, according to the decoupling model, the type of decoupling between rural electricity consumption and rural permanent population was strong negative decoupling. At the provincial level, Beijing and Tibet belonged to expanding negative decoupling. Tianjin and Liaoning belonged to recession link. The other 27 provinces, including Hebei, Shanxi, and Shandong, belonged to strong negative decoupling. Secondly, according to the coordination degree model, the coordination type of the national rural permanent population and rural electricity consumption was uncoordinated. The areas that can be coordinated include 20 provinces, including Shanghai, Inner Mongolia, Jilin, Jiangsu, Anhui, Fujian, and Jiangxi. The basic coordination areas included Beijing and Tibet. Finally, according to the comprehensive measurement model, the provinces with strong negative decoupling included Shanxi, Zhejiang, and Chongqing. Sichuan, Hebei, Shandong, and Shaanxi belonged to moderately strong negative decoupling groups.

Keywords: rural permanent population; electricity consumption; decoupling; coordination

Citation: Xia, X.; Sun, H.; Yang, Z.; Yuan, W.; Ma, D. Decoupling Analysis of Rural Population Change and Rural Electricity Consumption Change in China. *Int. J. Environ. Res. Public Health* **2022**, *19*, 6676. <https://doi.org/10.3390/ijerph19116676>

Academic Editors: Francesco Nocera, Roberto Alonso González Lezcano and Rosa Giuseppina Caponetto

Received: 23 April 2022

Accepted: 28 May 2022

Published: 30 May 2022



Copyright: © 2022 by the authors. Licensee MDPI, Basel, Switzerland. This article is an open access article distributed under the terms and conditions of the Creative Commons Attribution (CC BY) license (<https://creativecommons.org/licenses/by/4.0/>).

1. Introduction

Since China's reform and opening up in 1978, China has accelerated the process of urbanization, and rural population has been pouring into cities. According to the seventh national census data of 11 May 2021, the urbanization rate in China was 63.89% by 2020. Urbanization has promoted social development in China, but it also led to a rapid decline in the rural population [1]. According to China Statistical Yearbook 2007 and China Statistical Yearbook 2020, the permanent population in China's rural areas decreased from 714.96 million in 2007 to 509.92 million in 2020, a decrease of 200.54 million, accounting for 28% of the number of rural permanent population.

Population mobility and agglomeration are often accompanied by changes in energy consumption patterns [2,3]. Electricity, as an essential energy closely related to people's lives, cannot be ignored in the process of urbanization in China [4]. According to China Energy Statistical Yearbook 2007 and China Energy Statistical Yearbook 2020, China's rural electricity consumption has increased from 550.99 million kWh in 2007 to 971.72 million kWh in 2020. This shows that China's rural areas have not reduced electricity consumption due to the decline of the permanent population, and even the phenomenon of "increasing electricity after people leave" has resulted in a serious waste of electricity resources. Generally speaking, electricity consumption increased with the increase of

population [5–7], but there was a serious imbalance between the permanent population and electricity consumption in China’s rural areas. In addition, due to the wide variation of rural areas in China, changes in rural permanent population and rural electricity consumption varied from province to province. Therefore, what were the specific trends in the permanent population and electricity consumption in China’s rural areas? What were the types of decoupling between rural permanent population and electricity consumption in different regions? What were the background causes of changes in rural resident population and changes in electricity consumption in each region? In the context of global energy shortages and inequitable distribution of energy [8,9], it is essential to explore the decoupling relationship between rural permanent population and electricity consumption in various provinces, which not only reveal the relationship between the two, but also help to provide policy recommendations for the government to formulate reasonable power resource policies. Therefore, this paper used geographic information system (GIS) technology, combined with quantitative analysis decoupling model and coordination degree model, to analyze the degree of decoupling between China’s rural permanent population and rural electricity consumption. Next, we verified and supplemented the research content of population and power energy, which enriched the research methods of the relationship between rural permanent population and rural electricity. Specifically, the research contributions of this paper are that we: (1) revealed the temporal variation characteristics and spatial distribution characteristics of China’s rural permanent population and rural electricity consumption, (2) evaluated and analyzed the decoupling relationship between China’s rural population and rural electricity consumption, and (3) analyzed the coordination relationship between rural population and rural electricity consumption according to the coordination degree model. The rest of this paper is structured as follows. The second part is the current research status of China’s rural population change and electricity consumption change, and comprehensively analyzes the progress and shortcomings of existing research. The third part introduces the data sources and the decoupling and coordination models used in this paper. The fourth part reports the temporal and spatial characteristics of China’s rural permanent population and rural electricity consumption, as well as the types of decoupling and coordination between rural permanent population and rural electricity consumption, and discusses the background reasons for the formation of the results. The fifth part is the conclusion and policy recommendations.

2. Literature Review

2.1. Research of Rural Population Outflow

Due to various reasons, the rural population continues to enter the cities for life and employment, which has a very important impact on rural development. Existing literature summarized the main reasons for rural population outflow as urbanization, high income, and the pursuit of better living conditions. In the process of urbanization, part of the rural population was directly transformed into urban population, and their living land was classified as urban land [10–13]. In addition, some areas have been urbanized by migrating rural population to urban areas, which has also reduced the number of permanent residents in rural areas [14–16]. On the other hand, urban areas have more employment opportunities than rural areas, and wages in urban areas are higher than in rural areas [17]. Income level not only affects quality of life and well-being, but also affects people’s social status [18]. In order to obtain high incomes, some rural people moved to cities to work and settle down, which was an important reason for the decrease in the majority of the permanent population in China’s rural areas [19,20]. In addition, urban medical care, education, transportation, and other conditions were significantly better than rural areas, so part of the rural population moved to cities to enjoy a better quality of life [20–23]. Some scholars have also found that geographical conditions have an impact on the flow of population [24]. Superior traffic conditions have reduced the cost of population mobility, thereby promoting rural population mobility [9,25].

Existing scholars have also analyzed the impact of rural population outflow. More scholars paid attention to the impact of rural population exodus on land. For example, Huang et al. (2020) took the rural areas around the Ganjiang River Basin as the research object, and pointed out that due to the outflow of rural population, a large number of rural land was idle, resulting in a waste of land resources [26]. Zhao et al. (2018) took the rural areas of Shandong as the research object. They found that due to urbanization, the rural population in Shandong Province has been greatly reduced, and the available arable land in rural areas has also decreased. However, urbanization has accelerated the innovation and dissemination of agricultural technology, which has contributed to the growth of agricultural output in Shandong [27]. Some scholars have also found that population was not only an important factor in production but also the impact of rural population loss on rural economic development. For example, Feng (2019) pointed out that due to the siphon effect of urbanization, rural labor transferred to cities, which reduced the level of resource accumulation in rural areas and led to slow rural economic development. In addition, some scholars have found that although urbanization has led to a decrease in the rural population, the technological progress effect brought about by urbanization can promote the reduction of per capita energy consumption and improve the conversion of people from traditional fuels to commercial fuels [28,29].

2.2. Research of Rural Electricity Consumption

Existing literature points out that the main reasons for the increase in rural electricity consumption can be summarized as improvements in power supply infrastructure, increases in rural population income, and the spread of household appliances. Good power supply infrastructure is a prerequisite for electricity. Wang et al. (2022) pointed out that the lighting area in rural China is vast, but the government and enterprises have long ignored the development of available lighting resources in rural China. In recent years, the rapid development of photovoltaic power generation technology has prompted China to accelerate the construction of photovoltaic power supply infrastructure [30]. In order to reduce poverty, the Chinese government has implemented a photovoltaic poverty alleviation policy in rural areas, which has changed the power supply conditions in rural areas, thereby promoting an increase in rural electricity consumption. Agrawal S (2020) found that rural electricity consumption in rural India increased rapidly due to the improvement of the power supply system in rural India. The improvement of income level was also an important prerequisite for the increase of electricity consumption in China's rural areas. For a long time, due to the single source of income in China's rural areas, the income level of farmers was relatively low and the rural electricity price was relatively high, so the rural electricity consumption was relatively low [31]. The Chinese government has increased the income of the rural population through poverty alleviation policies and agricultural subsidies, which provides an important guarantee for the rural population to use electricity [30]. In addition, in order to improve the living standards of the rural population, the Chinese government has implemented a number of policies that benefit the people, such as home appliance subsidies and home appliances to the countryside, which encouraged the rural population to buy home appliances at low cost, thus boosting the rural population's electricity consumption [32].

2.3. Research on the Relationship between Rural Population and Electricity Consumption

Existing literature has also done some research on the relationship between the rural permanent residents and the rural electricity consumption. Most scholars build linear regression models to investigate the impact of rural population changes on electricity consumption from an empirical perspective. Yang et al. (2019) found that China's rural population was rapidly moving to towns due to urbanization, which reduced the number of the rural population. However, urbanization promoted technological progress through factor agglomeration, which was conducive to promoting infrastructure improvement. Rural electricity consumption in China has long been constrained by backward power supply in-

frastructure. In order to improve the living conditions of rural population, the government has been promoting the construction of power supply infrastructure in new rural areas. The National Development and Reform Commission has clearly proposed water, electricity, and road co-construction projects, which has greatly improved the rural power supply and adultery, thus promoting the growth of rural power consumption [3]. Michieka et al. (2020) studied the relationship between rural and urban populations on electricity consumption in five sub-Saharan countries from 1971 to 2013 and found that the impact of rural population changes on electricity consumption in different countries is not heterogeneous [33]. There was a negative relationship between population and electricity consumption in rural areas of the Republic of Congo, but rural population changes in Kenya and South Africa have no significant impact on rural electricity consumption. Han et al. (2021) studied the social structural factors of electricity consumption in Egypt from 1997 to 2018 and also found that an increase in the rural population reduced electricity consumption [34]. Bekhet et al. (2011) analyzed the elasticities of electricity consumption for rural and urban areas in Malaysia from 1980–2009. The results showed that rural electricity consumption was inelastic due to their low income level and low appliance penetration rate. However, the regression results were not significant, indicating that electricity changes were less sensitive to rural population changes in rural areas [35].

We found that scholars have made some research results on the relationship between rural permanent population and electricity consumption in China, India, Africa, Southeast Asia, etc. However, most literature uses classical linear models for qualitative analysis, but lacks quantitative thinking. In addition, the existing literature examining the relationship between rural resident population and rural electricity consumption is scarce. Due to the significant differences in the level of economic development and natural conditions among provinces in China, it is still necessary to further investigate the relationship between changes in rural population in China and changes in rural electricity consumption.

3. Data and Methods

3.1. Data

China's rural population data come from China Statistical Yearbook (2007–2020). China's rural electricity consumption data come from China Energy Statistics Yearbook (2007–2020).

3.2. Methods

3.2.1. Decoupling Model

Based on the decoupling theory, this study employed the decoupling index calculation model and Tapio's [36] decoupling coefficient definition table to construct a decoupling model represented by the ratio of the average annual growth rate of rural electricity consumption to the average annual growth rate of rural permanent population. The relationship between rural electricity consumption and rural permanent population from 2007 to 2020 was analyzed. The decoupling coefficient was used to reflect whether rural electricity consumption is in line with the transition of rural permanent population. The formula is as follows:

$$\alpha_{(n+1)} = \frac{(E_{(n+1)} - E_n)/E_n}{(L_{(n+1)} - L_n)/L_n} \quad (1)$$

where n is the n th year; $\alpha_{(n+1)}$ is the decoupling coefficient in $n + 1$ years; $E_{(n+1)}$ is the rural electricity consumption in $n + 1$ years; E_n is the rural electricity consumption in n years; $L_{(n+1)}$ is the number of rural permanent residents in $n + 1$ years; L_n is the number of rural permanent residents in year n .

According to Li et al. [37] and Tapio, the decoupling system values of 0.8 and 1.2 can be used as the basis for dividing the decoupling state, and the evolution characteristics of the second electricity consumption in each province can be divided into eight categories (Table 1):

- (1) Strong decoupling refers to the increase of rural permanent population and the decrease of rural electricity consumption;
- (2) Weak decoupling means that the number of rural permanent population and rural electricity consumption have increased, and the growth rate of rural electricity consumption is lower than that of rural permanent population;
- (3) Expanding linkage refers to the similar increase in rural electricity consumption and rural population;
- (4) The negative decoupling of expansion refers to the increase of rural electricity consumption and rural population, and the growth rate of rural electricity consumption was faster than that of rural permanent population;
- (5) Strong negative decoupling refers to the decrease of rural permanent population and the increase of rural electricity consumption;
- (6) Weak negative decoupling means that both the number of rural permanent households and rural electricity consumption were decreasing, and the reduction rate of rural electricity consumption was slower than that of rural permanent residents;
- (7) Recession linkage refers to the reduction of rural electricity consumption and the rural permanent population to a similar extent;
- (8) Recession decoupling means that the number of permanent residents in rural areas and rural electricity consumption decrease, and rural electricity consumption decreases faster than the population. The decoupling classification is shown in the following table:

Table 1. Definition of degree of decoupling.

Decoupling State		RE	RL	α
Negative decoupling	Expansion and negative decoupling	>0	>0	>1.2
	Strong negative decoupling	>0	<0	<0
	Weak negative decoupling	<0	<0	$0 < \alpha < 0.8$
Decoupling	Weak decoupling	>0	<0	$0 < \alpha < 0.8$
	Strong decoupling	<0	>0	<0
	Recession decoupling	<0	<0	>1.2
Link	Expansion contact	>0	>0	$0.8 < \alpha < 1.2$
	Recession contact	<0	<0	$0.8 < \alpha < 1.2$

3.2.2. Coordination Degree Model

This paper adopted the coordination degree model to reflect the coordination degree within the system, which can reflect the trend from disorder to order. The coordination degree between rural electricity consumption and rural permanent population is an index to measure the coordination degree. This study introduced a coordination model to analyze the coordination relationship between rural electricity consumption and rural research population in China. The coordination model is as follows:

$$C_{xy} = (x + y) / \sqrt{x^2 + y^2} \tag{2}$$

where x is the annual average change rate of rural electricity consumption; y is the annual average change rate of rural permanent population; C_{xy} is the coordination degree between rural electricity consumption and rural permanent population. The C_{xy} value is between -1.414 and 1.414 . The types of coordination degree between rural electricity consumption and rural permanent population are shown in Table 2 below.

Table 2. The Type of Coordination Degree.

C_{xy}	x, y	Coordination Degree Type
$C_{xy} = 1.414$	$x = y$, and $x > 0, y > 0$	More coordinated
$1.2 \leq C_{xy} < 1.414$	$x \approx y$	Coordinated
$1.0 \leq C_{xy} < 1.2$	$x > 0, y > 0$ and $x > y$	Basically coordinated
$0.5 \leq C_{xy} < 1.0$	$x > 0, y < 0$	Reconcilable
$-1.414 \leq C_{xy} < 0$	$x < 0, y < 0$, or $x > 0$, and $y < 0$	Uncoordinated

4. Results and Discussion

4.1. Temporal Change in Rural Permanent Population and Electricity Consumption from 2007 to 2020

From 2007 to 2020, China’s rural permanent population showed a downward trend (Figure 1). The rural permanent population dropped from 972 million in 2007 to 551 million in 2020, a total decrease of 421 million, an average annual decrease of 32.38 million, an average annual decrease of 4.21%. In different periods, the reduction rate of rural permanent population was different. Rural permanent population decline was slow from 2007 to 2014. The number of permanent residents in rural areas decreased by an average of 16.71 million per year, with an average annual decline rate of 1.80%. After 2014, the reduction of rural permanent population accelerated, and the rural permanent population decreased by 50.66 million, with an annual average decline rate of 6.56%. There were multiple reasons that have shaped the continued decline of China’s rural permanent population from 2007–2020. Urbanization, obtaining high income, and enjoying high-quality living conditions in cities were important reasons for the continuous decline of the rural population [38–41]. In addition, the accelerated pace of China’s agricultural reform, such as the promotion and application of mechanized production, has generated a large number of idle farmers, which has forced the rural permanent population to move into urban areas for employment [42,43]. The reason for the accelerated decline in the rural population in China in 2014 was the separation of rural land ownership, contract rights, and management rights promulgated by the central government. The “separation of powers” made the rural land enter the market economy to participate in competition, which activated the vitality of rural land and increased the direct income and leisure time of rural areas [44–46]. Therefore, the rural population was more willing to contract out the land, and entered the city for employment.

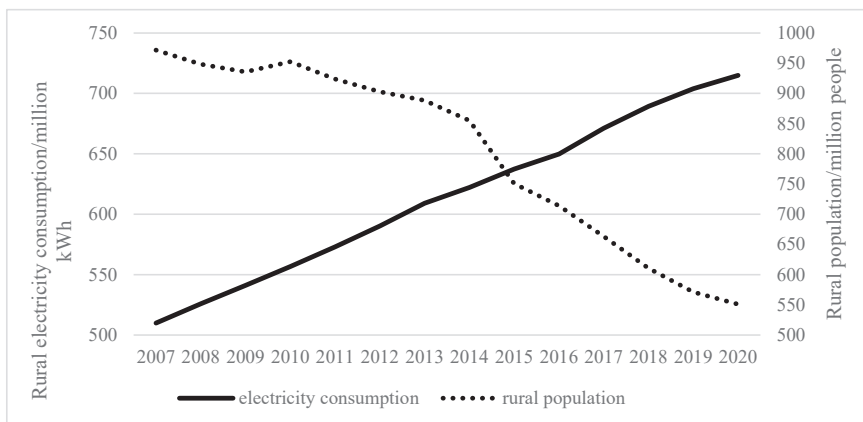


Figure 1. Change trend of rural permanent population and electricity consumption from 2007 to 2020.

Electricity consumption in rural areas continued to grow from 2007 to 2020. The electricity consumption in rural areas increased from 550.99 million kWh to 971.720 million kWh, a

total increase of 205.04 million kWh, an average annual increase of 15.77 million kWh, an average annual increase of 2.64%. Although China has been accelerating its urbanization process, the rural population has been pouring into the cities. However, rural electricity consumption did not decrease due to the reduction of rural population, but instead showed an upward trend. The reasons for this phenomenon were also diverse. On the one hand, the Chinese government has implemented policies that benefit farmers, such as land transfer and agricultural subsidies, which have increased the income of China’s rural permanent population, thereby enhancing the purchasing power of rural electricity [47,48]. On the other hand, China’s rural power supply infrastructure has been continuously improved, which provides the basic conditions for rural electricity consumption [49]. In addition, the Chinese government has continued to increase subsidies for the purchase of electrical appliances, which have contributed to the increasing popularity of home appliances in rural areas [50]. The above-mentioned reasons have formed an unbalanced state of China’s declining rural permanent population and rising rural electricity consumption, indicating a significant waste of power resources.

4.2. Spatial Changes in Rural Permanent Population and Electricity Consumption from 2007 to 2020

From 2007 to 2020, except Beijing and Tibet, China’s rural permanent population has been declining. This paper used the natural breakpoint method that comes with ArcGIS to divide the rural permanent population reduction of 31 provinces in China into five groups. Figure 2 shows:

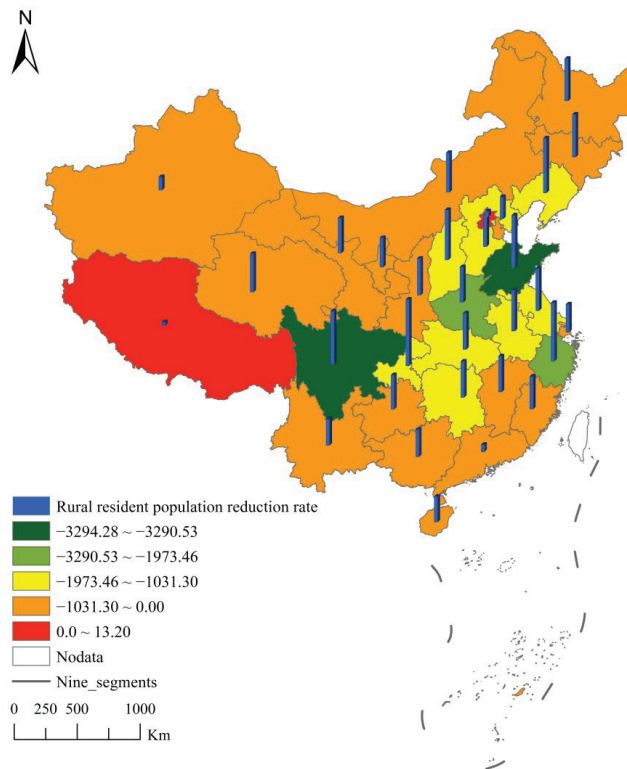


Figure 2. Spatial pattern of absolute increase and average annual decrease rate of rural permanent population from 2007 to 2020.

Rural permanent populations in Shandong and Sichuan have fallen sharply, ranking first echelon. In the past 13 years, Shandong's rural permanent population has decreased by 32.9428 million, and Sichuan's rural permanent population has decreased by 32.9053 million. The cumulative reduction of the two rural permanent population account for 25.32% of the total reduction of the national rural permanent population. Urbanization and the pursuit of better living conditions were traditional reasons for rural population decline in Shandong and Sichuan provinces [51,52]. Out-of-home employment was the main reason for the decrease in the rural permanent population [53]. Both Shandong and Sichuan had a population of more than 100 million, with a high proportion of rural population and a large base of resident population in rural areas. Shandong and Sichuan were also provinces with developed agriculture. During the process of agricultural reform, farmers in these two provinces were first affected. The mechanization of agricultural production has prompted the production of a large number of idle labor in these two provinces. Shandong is located in the eastern part of China, and the rural transportation conditions are convenient, which reduces the cost of the rural population going out for employment. As a consequence, the rural population in Shandong Province has decreased the most. In recent years, the government has continuously improved the traffic conditions in rural areas, which has prompted more and more Sichuan rural people to go to the eastern coast for employment.

The rural permanent population of Henan and Zhejiang has decreased significantly, ranking second echelon. In the past 13 years, the rural permanent population in Henan has decreased by 20.51 million, and the rural permanent population in Zhejiang has decreased by 19.7346 million. The cumulative reduction of the two rural permanent residents accounted for 14.38% of the total reduction of the national rural permanent population. The reasons for the decrease in the rural permanent population in the two provinces were different. Henan was a province with a population of more than 100 million, and its rural population base was large. Since the development of the rural economy in Henan mainly relies on the agriculture, there were relatively few jobs in rural areas. In recent years, Henan has intensified its agricultural reforms, such as speeding up agricultural mechanized production, which has further produced a large number of idle farmers. In order to obtain incomes, a number of rural people in Henan had to go out to work in coastal provinces. In recent years, Henan has also accelerated the process of urbanization, which has prompted some rural population to migrate to cities. The reasons for the decline of rural population in Zhejiang were different from those in Henan. For a long time, in order to promote people's common prosperity, Zhejiang has established small workshop-style enterprises to promote employment and increase people's income, which has accelerated the process of urbanization. Therefore, rural permanent population of Zhejiang has been greatly reduced.

Provinces with a moderate decrease in the rural permanent population include Liaoning, Hebei, Shanxi, Jiangsu, Anhui, Hubei, and Hunan, ranking third echelon, which decreased by 11.365 million, 11.69 million, 10.6018 million, 13.6343 million, 14.68 million, 10.313 million, and 13.1253 million, respectively. The population reduction in the five provinces accounted for 26.45% of the national rural population reduction. The reduction of rural population in these provinces ranks third echelon in the reduction of rural permanent population in China. Urbanization and the pursuit of a high quality of life in cities were part of the reason for the decline in the rural permanent population in these provinces. Out-of-home employment was an important reason for the decline of the rural permanent population in these provinces. On the one hand, there were many jobs in the urban areas of these provinces, which absorbed part of the rural population. On the other hand, these provinces are adjacent to the eastern provinces, which are the most market-oriented regions in China with a large number of jobs. In addition, the rural areas of these provinces have convenient transportation, so many rural people go out to work.

The fourth echelon is the provinces with a soft decrease in the rural permanent population, including Tianjin, Inner Mongolia, Jilin, Heilongjiang, Shanghai, Fujian, Jiangxi, Guangdong, Guangxi, Hainan, Chongqing, Guizhou, Yunnan, Shaanxi, Gansu, Qinghai, Ningxia, Xinjiang, which decreased by 520,000, 4.288 million, 5.5596 million, 6.679 million,

892.3 thousand, 5.39 million, 8.417843 million, 2.25 million, 7.44 million, 1.2039 million, 14.3495 million, 7.9932 million, 7.296 million, 7.26 million, and 5.48 million, accounting for 31.67% of the decrease in China's rural permanent population. Inner Mongolia, Jilin, Heilongjiang, Fujian, Jiangxi, Guangxi, Hainan, Chongqing, Guizhou, Yunnan, Shaanxi, Gansu, Qinghai, Ningxia, and Xinjiang had backward rural economies, and most of the rural population was mainly engaged in agriculture. One of the important characteristics of the rural areas in these provinces was the backward traffic conditions, which not only restricted the travel of the rural population but also led to asymmetric employment information, so there were fewer people going out for employment. On the contrary, Tianjin, Shanghai, and Guangdong are located in the eastern region with a small rural permanent population base. Many enterprises in these provinces settled in the suburbs in order to reduce the cost of land use, and the rural population can be employed on the spot. Therefore, the reduction of the rural population was small. It is worth mentioning that the rural permanent population in China's Beijing and Tibet has experienced positive growth. Beijing's rural permanent population increased by 132,000, while Tibet's rural permanent population increased by 72,700. Beijing had excellent conditions in many aspects, such as developed economy and small urban-rural gap. However, Beijing's urban areas are characterized by high housing prices and congested traffic, while housing prices in rural areas are low. The distance between urban and rural areas is close and the transportation is very convenient. As a result, more and more people immigrated to live in rural areas, leading to an increase in the number of the permanent population in Beijing's rural areas. On the contrary, the transportation in rural areas of Tibet was very backward, and the traffic cost of the rural population was very high, which restricted the flow of the rural permanent population. The natural conditions in Tibet were harsh, and most of the rural population were engaged in animal husbandry for income. There were less employment opportunities in urban areas of Tibet, which led to the rural population being more willing to stay in rural areas. In addition, the rural population had a tradition of "living together with families", which also contributed to the continuous growth of the rural population in Tibet.

From 2007 to 2020, except Liaoning and Tianjin, rural electricity consumption in most provinces of China continued to grow. The increase in electricity consumption varied from province to province. As shown in Figure 3, the areas with serious increase in rural electricity consumption were Jiangsu and Shanghai. From 2007 to 2020, Jiangsu's rural electricity consumption increased by 85.2 trillion kWh, accounting for 20.24% of the national rural electricity consumption increase. Jiangsu was an important technology industry province and the largest industrial province in China. Both the high income of Jiangsu's rural population and the increase in the penetration of household appliances were important reasons for Jiangsu's rural electricity consumption. In addition, due to the limitation of urban areas, some enterprises gradually moved to rural areas, which not only promoted employment in rural areas but also led to a rapid increase in rural electricity consumption. From 2007 to 2020, Shanghai's rural electricity consumption increased by 91.51 trillion kWh, accounting for 21.74% of the national rural electricity consumption increase. Both the high income of the rural population in Shanghai and the high penetration rate of household appliances have increased the consumption of electricity in the rural areas of Shanghai. In addition, Shanghai was the economic center of China and an important gathering place for foreign companies. The land price in Shanghai was very high. Therefore, most enterprises turned to Shanghai's rural areas and parishes, which directly increased the electricity consumption in Shanghai's rural areas.

The added value of rural electricity consumption in Zhejiang and Guangdong ranked second. Electricity consumption in rural areas in Zhejiang increased by 38.81 trillion kWh, accounting for 9.221% of the added value of rural electricity consumption in the country. Zhejiang was a model province of common prosperity in China, where the income of the rural population continued to increase, resulting in the increasing purchasing power of electricity for the rural population. The penetration rate of household appliances in rural areas in Zhejiang was high, so rural electricity consumption had increased. Electricity

consumption in rural areas of Guangdong increased by 53.05 billion kwh, accounting for 12.60% of the added value of rural electricity consumption in the country. Since Guangdong was a major manufacturing province of household appliances in China, the penetration rate in rural areas of Guangdong had grown rapidly, which directly increases the electricity consumption in rural areas. In addition, in order to achieve economic growth, Zhejiang and Guangdong have implemented a number of policies to encourage innovation of small companies and mass company. Therefore, there were a large number of small manufacturing enterprises in Zhejiang and Guangdong. Due to the low price and high labor cost in urban areas, small and medium-sized enterprises were mostly distributed in rural areas, which greatly increased the electricity consumption in rural areas.

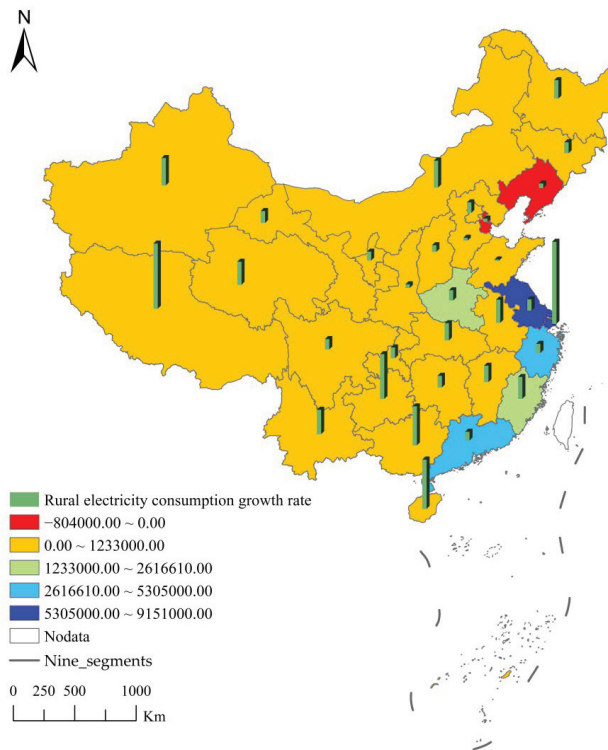


Figure 3. Spatial pattern of the absolute growth rate and the average annual growth rate of rural electricity consumption from 2007 to 2020.

Henan’s rural electricity consumption ranked third in the added value of rural electricity consumption. From 2007 to 2020, Henan’s electricity consumption increased by 149.77 million kWh, accounting for 3.56% of the added value of rural electricity consumption in the country. Henan had relatively developed agriculture and was an important grain producing area in China. With the development of China’s agricultural science and technology in recent years, Henan’s agricultural production had gradually been modernized, and agricultural electricity consumption had increased rapidly.

The added value of rural electricity consumption in 22 provinces, including Heilongjiang, Jilin, Shandong, Hebei, and Anhui, ranked fourth echelon in China. A total of 161,495,770,000 kwh increased, accounting for 38.37% of the national rural electricity consumption. Most of these provinces are located in the central and western regions with large rural populations. These provinces were also large agricultural provinces, but the growth in electricity consumption was the smallest. Most of these provinces are located in the

central and western regions, where the income level of the rural population grows slowly and the penetration rate of household appliances is low. Therefore, the rural electricity consumption increased slowly.

It is worth noting that the rural electricity consumption in Liaoning and Tianjin had been decreasing from 2007 to 2020. The rural electricity consumption in Liaoning decreased by 8.04 billion kWh, and the rural electricity consumption in Tianjin had decreased by 1152.2 million kWh. With the acceleration of urbanization, Tianjin's rural areas had been gradually incorporated into urban construction, and some rural areas had become urban areas, which reduces rural electricity consumption. Liaoning was an important province for brain drain in China. In particular, the rural population had entered the city for employment and settlement, which greatly reduced the electricity consumption in the countryside. In addition, the "new rural construction" strategy in Tianjin and Liaoning concentrates on the rural population and optimizes the rural power grid installation, which also reduces rural power consumption.

4.3. The Relationship between Rural Electricity Consumption and Rural Permanent Population from 2007 to 2020

In order to understand the relationship between rural permanent population and electricity consumption in China, this paper established a decoupling model and a coordination model between rural electricity consumption and rural permanent population. By reporting and discussing the results of the two models, the decoupling relationship between them can be fully reflected. According to the decoupling model and coordination model, the decoupling coefficient and coordination degree between rural electricity consumption and rural permanent population from 2007 to 2020 were calculated, as shown in the following table.

According to the decoupling theoretical model, from 2007 to 2020, the changes in the decoupling relationship between rural electricity consumption and rural permanent population showed three states: expanding negative decoupling, recession link, and strong negative decoupling. From a national perspective, the decoupling coefficient between rural permanent population and rural electricity consumption in 2007–2020 was -0.6168 (Table 3), which was a strong negative decoupling, indicating that the total rural population was declining and electricity consumption was increasing. The reduction rate of rural permanent population was greater than the growth rate of rural electricity consumption. At the provincial level, Beijing and Tibet belonged to the expanding negative decoupling. The rural permanent population and rural electricity consumption were both increasing, and the growth rate of rural electricity consumption was greater than that of the rural permanent population. However, the reasons for the expanding negative decoupling in the two places were indeed different. Beijing's economy was very developed, housing prices were high, and the urban area was densely populated, resulting in the phenomenon of "anti-urbanization". On the contrary, Tibet was economically backward, with poor natural conditions and inconvenient transportation, which reduces the mobility of the rural population. Tianjin and Liaoning belonged to the recession link. Both rural permanent population and rural electricity consumption were decreasing, but the reduction rate of the former was slower than that of the latter. The other 27 provinces, including Hebei, Shanxi, and Shandong, were strong negative decoupling areas. In conclusion, the rural electricity consumption coordination areas and the rural permanent population coordination areas in 27 provinces showed strong negative decoupling to varying degrees. In fact, with the rapid reduction of the rural permanent population, rural electricity consumption was increasing, resulting in a serious waste of power resources.

According to the coordination degree model, the coordination degree between national rural permanent population and rural electricity consumption was -0.3262 . National rural permanent population showed negative growth, and the rural electricity consumption showed positive growth, which was uncoordinated. Focusing on the provincial level, there were three types across the country: reconcilable, basically coordinated, and uncoordinated.

Table 3. Decoupling coefficient and coordination between rural electricity consumption and rural residents.

Province	Rural Permanent Population Growth Rate (%)	Growth Rate of Electricity Consumption (%)	Decoupling Coefficient	Type of Decoupling	Coordination Degree C_{xy}	Type of Coordination	Comprehensive Type
Nationwide	-0.0427	0.0263	-0.6168	Strong negative decoupling	-0.3262	Uncoordinated	Strong negative decoupling and Uncoordinated
Beijing	0.0038	0.0410	10.7236	Expanding negative decoupling	1.0885	Basically coordinated	Expanding negative decoupling and Basically coordinated
Tianjin	-0.0167	-0.0189	1.1278	Recession link	-1.4117	Uncoordinated	Recession link and Uncoordinated
Hebei	-0.0251	0.0132	-0.5242	Strong negative decoupling	-0.4214	Uncoordinated	Strong negative decoupling and Uncoordinated
Shanxi	-0.0446	0.0283	-0.6348	Strong negative decoupling	-0.3083	Uncoordinated	Strong negative decoupling and Uncoordinated
Inner Mongolia	-0.0331	0.0807	-2.4389	Strong negative decoupling	0.5459	Reconcilable	Strong decoupling and Reconcilable
Liaoning	-0.0504	-0.0274	0.5447	Recession link	-1.3565	Uncoordinated	Recession link and Uncoordinated
Jilin	-0.0364	0.0424	-1.1655	Strong negative decoupling	0.1077	Reconcilable	Strong decoupling and Reconcilable
Heilongjiang	-0.0360	0.0621	-1.7258	Strong negative decoupling	0.3639	Reconcilable	Strong decoupling and Reconcilable
Shanghai	-0.0220	0.1524	-6.9245	Strong negative decoupling	0.8468	Reconcilable	Strong decoupling and Reconcilable
Jiangsu	-0.0358	0.0433	-1.2105	Strong negative decoupling	0.1341	Reconcilable	Strong decoupling and Reconcilable
Zhejiang	-0.0554	0.0367	-0.6618	Strong negative decoupling	-0.2821	Uncoordinated	Strong negative decoupling and Uncoordinated
Anhui	-0.0344	0.0731	-2.1235	Strong negative decoupling	0.4787	Reconcilable	Strong decoupling and Reconcilable
Fujian	-0.0264	0.0706	-2.6767	Strong negative decoupling	0.5868	Reconcilable	Strong decoupling and Reconcilable
Jiangxi	-0.0292	0.0574	-1.9640	Strong negative decoupling	0.4374	Reconcilable	Strong decoupling and Reconcilable
Shandong	-0.0473	0.0068	-0.1438	Strong negative decoupling	-0.8475	Uncoordinated	Strong negative decoupling and Uncoordinated
Henan	-0.0288	0.0403	-1.3953	Strong negative decoupling	0.2303	Reconcilable	Strong decoupling and Reconcilable
Hubei	-0.0298	0.0597	-2.0038	Strong negative decoupling	0.4482	Reconcilable	Strong decoupling and Reconcilable
Hunan	-0.0297	0.0446	-1.5042	Strong negative decoupling	0.2791	Reconcilable	Strong decoupling and Reconcilable
Guangdong	-0.0051	0.0351	-6.8529	Strong negative decoupling	0.8451	Reconcilable	Strong decoupling and Reconcilable
Guangxi	-0.0214	0.1019	-4.7727	Strong negative decoupling	0.7737	Reconcilable	Strong decoupling and Reconcilable

Table 3. Cont.

Province	Rural Permanent Population Growth Rate (%)	Growth Rate of Electricity Consumption (%)	Decoupling Coefficient	Type of Decoupling	Coordination Degree C_{xy}	Type of Coordination	Comprehensive Type
Hainan	-0.0200	0.1167	-5.8379	Strong negative decoupling	0.8168	Reconcilable	Strong decoupling and Reconcilable
Chongqing	-0.0671	0.0418	-0.6232	Strong negative decoupling	-0.3198	Uncoordinated	Strong negative decoupling and Uncoordinated
Sichuan	-0.0485	0.0404	-0.8334	Strong negative decoupling	-0.1280	Uncoordinated	Strong negative decoupling and Uncoordinated
Guizhou	-0.0278	0.1104	-3.9753	Strong negative decoupling	0.7258	Reconcilable	Strong decoupling and Reconcilable
Yunnan	-0.0205	0.0757	-3.6903	Strong negative decoupling	0.7036	Reconcilable	Strong decoupling and Reconcilable
Tibet	0.0024	0.1356	55.7806	Expanding negative decoupling	1.0178	Basically coordinated	Expanding negative decoupling Basically coordinated
Shaanxi	-0.0303	0.0169	-0.5571	Strong negative decoupling	-0.3869	Uncoordinated	Strong negative decoupling and Uncoordinated
Gansu	-0.0286	0.0453	-1.5817	Strong negative decoupling	0.3109	Reconcilable	Strong decoupling and Reconcilable
Qinghai	-0.0319	0.0730	-2.2926	Strong negative decoupling	0.5168	Reconcilable	Strong decoupling and Reconcilable
Ningxia	-0.0231	0.0359	-1.5502	Strong negative decoupling	0.2982	Reconcilable	Strong decoupling and Reconcilable
Xinjiang	-0.0096	0.0816	-8.4583	Strong negative decoupling	0.8757	Reconcilable	Strong decoupling and Reconcilable

The reconcilable provinces included Shanghai, Inner Mongolia, Jilin, Jiangsu, Anhui, Fujian, Jiangxi, Heilongjiang, Henan, Hubei, Hunan, Guangdong, Guangxi, Hainan, Guizhou, Yunnan, Gansu, Qinghai, Ningxia, and Xinjiang. The resident rural population in these provinces has decreased, while rural electricity consumption has increased. The rate of decrease in the rural resident population was higher than the growth rate of rural electricity consumption, but the reasons varied from province to province. Urbanization in Shanghai and Jiangsu has played a large role in reducing the rural population. Both Jiangsu and Shanghai have been expanding their urban areas by incorporating rural areas and converting rural populations into urban populations, which has significantly reduced the resident rural population. A remarkable fact was that Shanghai and Jiangsu are located in the Yangtze River Delta metropolitan area with more employment opportunities in urban areas, and the rural population was willing to move to the city for stable jobs to increase income. In addition, the transportation in Shanghai and Jiangsu was very developed and the level of marketization was relatively high, which reduced the transportation cost and information search cost of rural population transferring to urban areas. Therefore, rural permanent population was more willing to transfer to urban areas. However, despite rural electricity consumption in these two regions having increased significantly due to the popularity of household appliances and the rise in income levels of the rural population, the growth rate of electricity consumption was smaller than the reduction rate of rural population, which leads to the current situation of reconciliation between rural population and electricity consumption. For the other provinces, although urbanization played a weak role in reducing the rural resident population, out-migration for employment significantly

reduced the number of rural residents in these provinces. However, the rugged terrain in rural areas of these provinces was not conducive to building electricity supply infrastructure, which limited access to electricity. In addition, the slow growth of farmers' income levels in these provinces had resulted in low purchasing power in rural areas of these provinces and slow growth of electricity consumption in these areas. As a result, the resident population in rural areas was decreasing faster than the increase in electricity consumption.

The basic coordination areas included Beijing and Tibet. The growth rate of Beijing's rural permanent population from 2007 to 2020 was lower than that of rural electricity consumption. The average annual growth rate of Beijing's rural permanent population was 0.38%, and the average annual growth rate of rural electricity consumption was 4.1%. The coordination degree was 1.0885. The growth rate of rural permanent residents in Tibet from 2007 to 2020 was lower than that of rural electricity consumption. The growth rate of the rural permanent population in the Tibet was 0.24%, the average annual growth rate of rural electricity consumption was 13.56%, and the coordination degree was 1.0178. Although the coordination degree between Beijing and Tibet was close, they represented completely different types of regions. There were obviously differences in many aspects such as economic development level, production level, and lifestyle. The growth rate of rural permanent population in Beijing was 1.58 times that of Tibet. However, the growth rate of rural permanent population in Beijing was much higher than that in Tibet. The growth rate of electricity consumption in rural Tibet was 56.5 times that of Beijing, but the growth rate of electricity consumption in Beijing was higher than that in Tibet. Beijing has a developed economy with an urbanization level of 86.60%, ranking first in China. In recent years, due to the gradual shrinking of the usable range in cities and towns, scientific research institutions and productive enterprises have moved to suburban areas and rural areas. This has not only led to the transfer of some population to rural areas, resulting in an increase in the number of rural populations, but also increased rural electricity consumption. On the contrary, Tibet was economically backward and has a low level of urbanization. Animal husbandry was an important source of income in Tibet. The rural areas of Tibet had vast usable land and grasslands. Therefore, the majority of the population remained in rural areas. In addition, Tibet's high altitude and poor natural conditions in most areas further reduced the flow of people. In recent years, the government had not only stepped up poverty alleviation efforts in rural areas of Tibet to increase their income, but also continuously improved the construction of electricity infrastructure in rural areas of Tibet. The number of household appliances in rural areas of Tibet has increased rapidly. As a result, electricity consumption in rural Tibet has increased rapidly.

The uncoordinated regions included Tianjin, Hebei, Shanxi, Liaoning, Zhejiang, Shandong, Sichuan, Chongqing, and Shaanxi. The rural permanent population in these provinces decreased, while rural electricity consumption increased. However, the reduction rate of the rural permanent population was less than the growth rate of rural electricity consumption. The reasons for the change varied from province to province. Urbanization is an important reason for the decrease in the rural resident population in Tianjin and Liaoning. In addition, due to the convenient transportation in Tianjin and Liaoning, the rural population has been employed outside the countryside, which has further reduced the rural resident population. At the same time, Tianjin and Liaoning accelerated the implementation of the "new rural construction" strategy and concentrated on the resettlement of the rural population, which led to more efficient use of electricity and thus reduced rural electricity consumption. The rate of reduction in rural resident population is not consistent with the rate of reduction in rural electricity consumption, resulting in a mismatch between rural population and electricity consumption in the two provinces. Coal-fired and hydroelectric power generation are the main methods of electricity generation in China. Abundant coal resources in Shanxi, Shaanxi, Shandong, and Hebei, and abundant hydro resources in Zhejiang, Sichuan, and Chongqing provide the prerequisites for rural electricity supply. In addition, Zhejiang, Shandong, and Hebei have developed rural economies with increasing penetration of household appliances. As the income level of the rural

population increases, rural electricity consumption is rapidly increasing. Shanxi, Shaanxi, Sichuan, and Chongqing have a large rural poverty population and are key regions for the government to implement poverty alleviation measures. The government set up special poverty alleviation funds for these regions to increase the income of the poor in the form of direct subsidies, which expanded the purchasing power of the rural population for electricity and led to a rapid increase in rural electricity consumption. As a result, the reduction rate of rural population is smaller than the growth rate of rural electricity, which appears incongruous.

Combining the decoupling model and the coordination degree model can more accurately analyze the coordination degree of rural population and electricity consumption. This paper used the natural discontinuity method to divide the strong negative decoupling and non-coordinated provinces into high quality strong non-coordinated provinces and moderate to mildly strong non-decoupling non-coordinated provinces and explored the degree of strong negative decoupling in these 10 provinces. The results show:

(1) Strong negative decoupling provinces, including Shanxi, Zhejiang, Chongqing, and Sichuan provinces and regions, showed strong negative decoupling. The average reduction rate of permanent rural populations in these provinces was 5.39%, much higher than the national average reduction rate (4.27%). The average annual electricity consumption growth rate in these provinces was 3.68%, up from the whole country's 2.68%. The large loss of rural permanent population and the growth of rural electricity consumption were the main reasons for the disharmony between rural population and electricity consumption in these provinces.

(2) Hebei, Shandong, and Shaanxi belonged to the medium strong negative decoupling groups. The average reduction rate of rural permanent population in these three provinces is 3.70%, lower than the national average of 4.27%. The average annual electricity consumption growth rate in these provinces was 1.09%, down from the national 2.68%. The deviation between the growth rate of rural electricity consumption and the growth rate of national average electricity consumption was greater than that of rural population growth rate, which was the most important reason for the high negative decoupling between rural population and electricity consumption in these provinces.

There were multiple reasons that shaped the change in China's rural resident population and rural electricity consumption from 2007 to 2020. The combination of diversified causes shaped an imbalance between the decrease in rural resident population and the increase in rural electricity consumption in China. From a provincial perspective, diversified causes also played different roles in reducing the rural permanent population and increasing rural electricity consumption, which created heterogeneity across provinces in terms of decreasing rural permanent population and increasing rural electricity consumption, leading to different types of decoupling and coordination across provinces.

By further analyzing and summarizing the causes of urbanization and urban employment in each province, this paper found that the attributes of these causes were influenced by the macro conditions of the rural areas themselves and thus affected the changes in the rural population. For example, the population base and geographical conditions determine the different roles played by these causes. In terms of the rural population base, the provinces with more rural populations were those with more decreasing rural resident population, such as Sichuan, Henan, Shandong, and Zhejiang. Agricultural reform affected the large rural population provinces first by reducing the use of farmers. The rural population in these areas moved to the cities for employment in order to obtain higher income. Provinces with easy access to rural transportation were those with a higher reduction of rural population, such as Shandong, Hebei, Liaoning, Jiangsu, and Zhejiang, the central and eastern provinces of China. Developed transportation conditions not only reduced the asymmetry of employment information, but also reduced the transportation costs of the rural population. Similarly, the reasons affecting the changes in rural electricity consumption were influenced by rural macro conditions. From the perspective of power generation resource endowment, abundant coal and hydro resources provided the basic conditions

for rural electricity supply in these provinces. Electricity consumption in rural areas was higher in provinces rich in coal and hydro resources, such as Shaanxi, Shanxi, Shandong, Hebei, and Zhejiang. Areas with high income levels of rural population had greater growth in electricity consumption, for example, Jiangsu, Zhejiang, Shanghai, and Guangdong. The growth of electricity consumption is higher in rural areas with high penetration of home appliances, for example, Jiangsu, Shanghai, Zhejiang, and Guangdong. The macro conditions in rural areas determine the causes of changes in rural resident population and changes in electricity consumption, thus affecting the decoupling and harmonization relationship between rural population and electricity consumption. It is worth noting that the role of China's "agriculture, rural areas, and farmers" policy (Three rural policies) in rural China cannot be ignored. In order to improve the income levels and life satisfaction of the rural population, the Chinese government is constantly improving its "Three rural policies". It is clear that China's "Three rural policies" have had a large impact on rural population and electricity consumption. Agricultural production reforms have generated a large number of idle farmers, agricultural subsidies have increased farmers' income, and subsidies for home appliance purchases have increased the rural population's demand for electricity consumption. As a result, China's "Three rural policies" affected the coupled relationship between rural resident population and electricity consumption by influencing changes in the population and changes in electricity consumption.

5. Conclusions and Suggestions

Based on the comprehensive perspective of the relationship between rural permanent population and rural electricity consumption, this study used decoupling model and coordination model to analyze the temporal change characteristics, spatial variation characteristics, and coupling coordination relationship between the national and provincial rural permanent population and electricity consumption. The main conclusions are as follows: (1) Time-Wise, from 2007 to 2020, China's rural permanent population continued to decrease, while the rural electricity consumption continued to increase. Spatially, the rural permanent population continued to decrease in all provinces except Beijing and Tibet. Rural electricity consumption continued to increase in all provinces except Tianjin and Liaoning. (2) In terms of the type of decoupling, there was a negative decoupling between China's rural permanent population and rural electricity consumption. At the provincial level, Beijing and Tibet belonged to the expanding negative decoupling, Tianjin and Liaoning belonged to the recession link, and the other 27 provinces, such as Hebei, Shanxi, Shandong, etc., were strong negative decoupling. (3) In terms of the coordination type, China's rural permanent population and rural electricity consumption was uncoordinated. At the provincial level, the regions that can be coordinated include 20 provinces, including Shanghai, Inner Mongolia, Jilin, Jiangsu, Anhui, Fujian, and Jiangxi, etc. The basic coordination areas included Beijing and Tibet. The uncoordinated regions included Tianjin, Hebei, Shanxi, Liaoning, Zhejiang, Shandong, Sichuan, Chongqing, and Shaanxi. (4) In terms of the comprehensive degree of decoupling and coordination, Shanxi, Zhejiang, Chongqing, and Sichuan showed extremely strong negative decoupling, while Hebei, Shandong, and Shaanxi belonged to moderately strong negative decoupling groups.

China's rural population continued to flood into cities for settlement and employment, which contributed to social and economic development. However, rural electricity consumption had not decreased with the reduction of rural permanent population. There was a certain harm in the phenomenon of "people decrease and electricity increase" in China's rural areas. First, most of the electricity supply was coal-fired, which further exacerbated the consumption of conventional natural energy and may pollute the environment. Second, the increase in rural electricity consumption had also intensified government investment in infrastructure in rural areas, which may crowd out other uses of resources, increase resource misallocation, and lead to unfair resource allocation. Various regions in China are faced with the task of energy conservation and emission reduction, which raises the requirements for electricity usage in various regions. Some recommendations are suggested as follows:

(1) The government should strengthen the supervision of electricity consumption in rural areas and establish the ladder price of rural electricity to prevent waste of power resources. (2) Accelerate the construction of rural power infrastructure, especially photovoltaic power generation infrastructure, to provide clean power supply sources for rural areas. (3) Considering that the Chinese government has continuously implemented the policy of sending home appliances to the countryside, the government should encourage enterprises to develop household appliances with low power consumption and high performance, and increase their promotion in rural areas to save the use of power resources. (4) Considering that the rural population has little awareness of saving electricity, the government should strengthen the publicity and education of saving electricity, thus cultivating the habit of saving electricity.

Limitations

Although this paper analyzed the decoupling and coordination of rural permanent population and rural electricity consumption in each province of China, there are still some shortcomings. On the one hand, the research method of this paper is relatively simple. There are many research methods on the coupling coordination relationship in the existing literature. The changes between rural population and rural electricity consumption can be further verified by selecting other suitable coupling coordination methods. On the other hand, the rural electricity consumption in this paper is the overall rural electricity consumption. However, electricity use in rural areas can be divided into industrial and residential electricity. Due to the limitation of data, this paper cannot distinguish rural residential electricity consumption from industrial electricity consumption. The above is also the direction for further improvement by the author in the future.

Author Contributions: X.X.: Writing, data processing. H.S.: Project management, Funding support. Z.Y.: Drawing. W.Y.: Supervision. D.M.: Editing. All authors have read and agreed to the published version of the manuscript.

Funding: This work was supported by National Natural Science Foundation of China (No. 71963030), The third Xinjiang scientific expedition program (No.SQ2021xjkk01800), Autonomous Region Social Science Fund Project (No.21BJY050).

Conflicts of Interest: The authors declare no conflict of interest.

References

1. Chen, M.; Gong, Y.; Lu, D.; Ye, C. Build a people-oriented urbanization: China's new-type urbanization dream and Anhui model. *Land Use Policy* **2019**, *80*, 1–9. [\[CrossRef\]](#)
2. Dong, X.-Y.; Hao, Y. Would income inequality affect electricity consumption? Evidence from China. *Energy* **2018**, *142*, 215–227. [\[CrossRef\]](#)
3. Yang, Y.; Liu, J.; Lin, Y.; Li, Q. The impact of urbanization on China's residential energy consumption. *Struct. Chang. Econ. Dyn.* **2019**, *49*, 170–182. [\[CrossRef\]](#)
4. Yu, M.; Yang, Y.; Chen, F.; Zhu, F.; Qu, J.; Zhang, S. Response of agricultural multifunctionality to farmland loss under rapidly urbanizing processes in Yangtze River Delta, China. *Sci. Total Environ.* **2019**, *666*, 1–11. [\[CrossRef\]](#) [\[PubMed\]](#)
5. Mazur, A. How does population growth contribute to rising energy consumption in America. *Popul. Environ.* **1994**, *15*, 371–378. [\[CrossRef\]](#)
6. Saidi, K.; Toumi, H.; Zaidi, S. Impact of Information Communication Technology and Economic Growth on the Electricity Consumption: Empirical Evidence from 67 Countries. *J. Knowl. Econ.* **2015**, *8*, 789–803. [\[CrossRef\]](#)
7. Pyrgou, A.; Santamouris, M. Macroeconomic, demographic and climatic indicators for household electricity consumption model in Cyprus. *Int. J. Sustain. Energy* **2021**, *41*, 205–214. [\[CrossRef\]](#)
8. Salameh, M.G. Can renewable and unconventional energy sources bridge the global energy gap in the 21st century? *Appl. Energy* **2003**, *75*, 33–42. [\[CrossRef\]](#)
9. Lai, B.; Yi, P.; Sui, Y.; Zhang, Q. Energy distribution in EV energy network under energy shortage. *Neurocomputing* **2021**, *444*, 179–188. [\[CrossRef\]](#)
10. Qiu, B.; Li, H.; Tang, Z.; Chen, C.; Berry, J. How cropland losses shaped by unbalanced urbanization process? *Land Use Policy* **2020**, *96*, 104715. [\[CrossRef\]](#)
11. Johnson, K.M.; Lichter, D.T. Metropolitan Reclassification and the Urbanization of Rural America. *Demography* **2020**, *57*, 1929–1950. [\[CrossRef\]](#) [\[PubMed\]](#)

12. Li, Y.; Jia, L.; Wu, W.; Yan, J.; Liu, Y. Urbanization for rural sustainability—Rethinking China’s urbanization strategy. *J. Clean. Prod.* **2018**, *178*, 580–586. [[CrossRef](#)]
13. Liu, Y.; Yang, Y.; Li, Y. Conversion from rural settlements and arable land under rapid urbanization in Beijing during 1985–2010. *J. Rural Stud.* **2017**, *51*, 141–150. [[CrossRef](#)]
14. Wang, X.-R.; Hui, E.C.-M.; Sun, J.-X. Population migration, urbanization and housing prices: Evidence from the cities in China. *Habitat Int.* **2017**, *66*, 49–56. [[CrossRef](#)]
15. Wojewódzka-Wiewiórska, A.; Kłoczko-Gajewska, A.; Sulewski, P. Between the Social and Economic Dimensions of Sustainability in Rural Areas—In Search of Farmers’ Quality of Life. *Sustainability* **2019**, *12*, 148. [[CrossRef](#)]
16. Liao, T.F. Income Inequality, Social Comparison, and Happiness in the United States. *Socius Sociol. Res. A Dyn. World* **2021**, *7*, 237802312098564. [[CrossRef](#)]
17. Sato, Y.; Zenou, Y. How urbanization affect employment and social interactions. *Eur. Econ. Rev.* **2015**, *75*, 131–155. [[CrossRef](#)]
18. Dilshad Ahmad, S.Z.A.S. Economic Violence against Women in Punjab Dimensions, Determinants and its Implications on Women Social Status in Society. *J. Bus. Soc. Rev. Emerg. Econ.* **2022**, *8*, 13–24.
19. Unger, J.; Siu, K. Chinese migrant factory workers across four decades: Shifts in work conditions, urbanization, and family strategies. *Labor Hist.* **2019**, *60*, 765–778. [[CrossRef](#)]
20. Li, X. Rural Depopulation in China: A Comparative Perspective. *Int. Multidiscip. J. Soc. Sci.* **2015**, *4*, 149. [[CrossRef](#)]
21. Heshmati, A.; Rashidghalam, M. Measurement and Analysis of Urban Infrastructure and Its Effects on Urbanization in China. *J. Infrastruct. Syst.* **2020**, *26*, 04019030. [[CrossRef](#)]
22. Gordon, G.L.; Wu, X.; Chaoyang, P.; Fu, A.Z. Urbanization and health care in rural China. *Contemp. Econ. Policy* **2008**, *21*, 11–24. [[CrossRef](#)]
23. Wang, C.; Zhang, Y.; Yang, Y.; Yang, Q.; Hong, J. What is driving the abandonment of villages in the mountains of Southeast China? *Land Degrad. Dev.* **2019**, *30*, 1183–1192. [[CrossRef](#)]
24. Kruszyna, M.; Śleszyński, P.; Rychlewski, J. Dependencies between Demographic Urbanization and the Agglomeration Road Traffic Volumes: Evidence from Poland. *Land* **2021**, *10*, 47. [[CrossRef](#)]
25. Deng Wei, Z.S. Spatiotemporal characteristics of rural labor migration in China evidence from the migration stability under new-type urbanization. *Chin. Geogr. Sci.* **2020**, *30*, 749–764. [[CrossRef](#)]
26. Huang, L.; Ye, A.; Tang, C.; Duan, Q.; Zhang, Y. Impact of rural depopulation and climate change on vegetation, runoff and sediment load in the Gan River basin, China. *Hydrol. Res.* **2020**, *51*, 768–780. [[CrossRef](#)]
27. Chao, Z.; Zhang, P.; Wang, X. Impacts of Urbanization on the Net Primary Productivity and Cultivated Land Change in Shandong Province, China. *J. Indian Soc. Remote Sens.* **2018**, *46*, 809–819. [[CrossRef](#)]
28. Wang, Q. Effects of urbanisation on energy consumption in China. *Energy Policy* **2014**, *65*, 332–339. [[CrossRef](#)]
29. Pachauri, S. An analysis of cross-sectional variations in total household energy requirements in India using micro survey data. *Energy Policy* **2004**, *32*, 1723–1735. [[CrossRef](#)]
30. Wang, Z.; Wang, Y.; Huang, F.; Shuai, C.; Li, J.; Ding, L.; Cheng, X. The environmental impact of household domestic energy consumption in rural areas: Empirical evidence from China’s photovoltaic poverty alleviation regions. *Sustain. Prod. Consum.* **2022**, *30*, 1019–1031. [[CrossRef](#)]
31. Shiu, A.; Lam, P.-L. Electricity consumption and economic growth in China. *Energy Policy* **2004**, *32*, 47–54. [[CrossRef](#)]
32. Feng, K.; Li, Q.; Huang, B.; Yan, H. Research on the Domain and Potential for Further Electrification of Rural Domestic Energy Consumption. *IOP Conf. Ser. Mater. Sci. Eng.* **2020**, *768*, 062055. [[CrossRef](#)]
33. Michieka, N. An empirical analysis of the role of rural population growth on electricity consumption in Sub-Saharan Africa. *Int. J. Energy Technol. Policy* **2020**, *16*, 302–325. [[CrossRef](#)]
34. Hongyun, H.; Radwan, A. Economic and social structure and electricity consumption in Egypt. *Energy* **2021**, *231*, 120962. [[CrossRef](#)]
35. Othman, N.S.b.; Bekhet, H.A. Assessing the Elasticities of Electricity Consumption for Rural and Urban Areas in Malaysia_ A Non-linear Approach. *Int. J. Econ. Financ.* **2011**, *3*, 11–17. [[CrossRef](#)]
36. Tapio, P. Towards a theory of decoupling: Degrees of decoupling in the EU and the case of road traffic in Finland between 1970 and 2001. *Transp. Policy* **2005**, *12*, 137–151. [[CrossRef](#)]
37. Zhang, J.; Fan, Z.; Chen, Y.; Gao, J.; Liu, W. Decomposition and decoupling analysis of carbon dioxide emissions from economic growth in the context of China and the ASEAN countries. *Sci. Total Environ.* **2020**, *714*, 136649. [[CrossRef](#)]
38. Arouri, M.; Ben Youssef, A.; Nguyen, C. Does urbanization reduce rural poverty? Evidence from Vietnam. *Econ. Model.* **2017**, *60*, 253–270. [[CrossRef](#)]
39. Addanki, S.C.; Venkataraman, H. Greening the economy: A review of urban sustainability measures for developing new cities. *Sustain. Cities Soc.* **2017**, *32*, 1–8. [[CrossRef](#)]
40. Su Yaqin, P.T. Where are the migrants from Inter-vs. intra-provincial rural-urban migration in China. *China Econ. Rev.* **2017**, *47*, 142–155.
41. Liu, Z.; Liu, S.; Jin, H.; Qi, W. Rural population change in China: Spatial differences, driving forces and policy implications. *J. Rural Stud.* **2017**, *51*, 189–197. [[CrossRef](#)]
42. Wang, X.; Huang, J.; Rozelle, S. Off-farm employment and agricultural specialization in China. *China Econ. Rev.* **2017**, *42*, 155–165. [[CrossRef](#)]

43. Che, Y. Off-farm employments and land rental behavior: Evidence from rural China. *China Agric. Econ. Rev.* **2016**, *8*, 37–54. [[CrossRef](#)]
44. Chen, X. The core of China's rural revitalization: Exerting the functions of rural area. *China Agric. Econ. Rev.* **2019**, *12*, 1–13. [[CrossRef](#)]
45. Zhou, Y.; Li, Y.; Xu, C. Land consolidation and rural revitalization in China: Mechanisms and paths. *Land Use Policy* **2020**, *91*, 104379. [[CrossRef](#)]
46. Wang, Q.; Zhang, X. Three rights separation: China's proposed rural land rights reform and four types of local trials. *Land Use Policy* **2017**, *63*, 111–121. [[CrossRef](#)]
47. Liu, Z.; Rommel, J.; Feng, S.; Hanisch, M. Can land transfer through land cooperatives foster off-farm employment in China? *China Econ. Rev.* **2017**, *45*, 35–44. [[CrossRef](#)]
48. Zhou, Z.; Wu, W.; Chen, Q.; Chen, S. Study on sustainable development of rural household energy in northern China. *Renew. Sustain. Energy Rev.* **2008**, *12*, 2227–2239. [[CrossRef](#)]
49. He, L.-Y.; Hou, B.; Liao, H. Rural energy policy in China: Achievements, challenges and ways forward during the 40 year rural reform. *China Agric. Econ. Rev.* **2018**, *10*, 224–240. [[CrossRef](#)]
50. Zheng, X.; Wei, C.; Qin, P.; Guo, J.; Yu, Y.; Song, F.; Chen, Z. Characteristics of residential energy consumption in China: Findings from a household survey. *Energy Policy* **2014**, *75*, 126–135. [[CrossRef](#)]
51. Wang, M.; Yang, S.; Gao, H.; Abudu, K. The Characteristics, Influencing Factors, and Push-Pull Mechanism of Shrinking Counties: A Case Study of Shandong Province, China. *Sustainability* **2021**, *13*, 2402. [[CrossRef](#)]
52. Xu, D.; Guo, S.; Xie, F.; Liu, S.; Cao, S. The impact of rural laborer migration and household structure on household land use arrangements in mountainous areas of Sichuan Province, China. *Habitat Int.* **2017**, *70*, 72–80. [[CrossRef](#)]
53. Liu, K.; Wang, J.; Kang, X.; Liu, J.; Xia, Z.; Du, K.; Zhu, X. Spatio-Temporal Analysis of Population-Land-Economic Urbanization and Its Impact on Urban Carbon Emissions in Shandong Province, China. *Land* **2022**, *11*, 266. [[CrossRef](#)]



Article

Farmers' Adaptive Behaviors to Heavy Metal-Polluted Cultivated Land in Mining Areas: The Influence of Farmers' Characteristics and the Mediating Role of Perceptions

Yong Chen ^{1,2,3}, Yaqi Liang ^{1,2}, Hao Zhou ^{1,2,*}, Qiaozhi Wang ^{1,2} and Yanzhong Liu ^{1,2}

- ¹ College of Resource and Environmental Engineering, Wuhan University of Science and Technology, No.947 Heping Avenue, Wuhan 430080, China; chenyong68@wust.edu.cn (Y.C.); lyq1791933149@163.com (Y.L.); wangqiaozhi@wust.edu.cn (Q.W.); liuyanzhong@wust.edu.cn (Y.L.)
 - ² National Key Laboratory of Environmental Protection Mining and Metallurgy Resource Utilization and Pollution Control, Wuhan 430080, China
 - ³ Hubei Provincial Key Laboratory of Efficient Utilization and Agglomeration of Metallurgical Mineral Resources, Wuhan 430080, China
- * Correspondence: areshao1210@foxmail.com; Tel.: +86-18986258297

Abstract: Heavy metal pollution in cultivated land poses a serious threat to environmental health and farmers' livelihoods. As the direct user of cultivated land, understanding farmers' adaptive behavior to heavy metal pollution, and its influencing factors, can provide insight and information relevant for decision-making, so as to better manage the hazards and risks of heavy metal pollution. We proposed a conceptual framework of "farmers' characteristics-perceptions-adaptive behaviors". Factor analysis and mediation effect analysis were used to explore the influence of characteristics and perceptions on adaptive behaviors. The data of 278 farmers in a typical mining area in Daye, China, show that local farmers perceive the hazards of heavy metal pollution, but their adaptive behaviors are hindered to a certain extent. The results of the mediation effect analysis show that perceptions of health impact, self-efficacy, and adaptive cost play a partial mediating role in the impact of characteristics on adaptive behaviors. In addition, the influence of the "factor of dependence on farmland" and the "factor of obstacles to action" on adaptive behavior have no significant relationship with perception levels. By comparing the influencing factors, we found that although farmers' perceptions have mediating effects between characteristics and adaptive behaviors, characteristics still play a decisive role in adaptive behaviors.

Keywords: farmers' adaptive behaviors; heavy metal pollution; mediating effect; factor analysis; hierarchical regression

Citation: Chen, Y.; Liang, Y.; Zhou, H.; Wang, Q.; Liu, Y. Farmers' Adaptive Behaviors to Heavy Metal-Polluted Cultivated Land in Mining Areas: The Influence of Farmers' Characteristics and the Mediating Role of Perceptions. *Int. J. Environ. Res. Public Health* **2022**, *19*, 6718. <https://doi.org/10.3390/ijerph19116718>

Academic Editors: Roberto Alonso González-Lezcano, Francesco Nocera and Rosa Giuseppina Caponetto

Received: 8 May 2022
Accepted: 28 May 2022
Published: 31 May 2022



Copyright: © 2022 by the authors. Licensee MDPI, Basel, Switzerland. This article is an open access article distributed under the terms and conditions of the Creative Commons Attribution (CC BY) license (<https://creativecommons.org/licenses/by/4.0/>).

1. Introduction

Heavy metal pollution (HMP) of cultivated land is becoming a severe ecological and social problem in China [1,2]. According to the National Soil Pollution Survey Bulletin, the over-standard rate of heavy metals in cultivated land in China is as high as 19.4% [3]. Due to HMP, more than 10 million tons of grain production are reduced, and 12 million tons of grains contaminated, each year [4]. HMP has the characteristics of accumulation, persistence, and irreversibility [5,6]. When heavy metals accumulate in the soil to a certain level, it not only reduces the quality of cultivated land and affects crop growth, but also threatens human health and well-being through the food chain [7,8]. Thus, widespread public concern about food safety and health risks are aroused [9].

Mineral resources are an important material basis for social and economic development [10]. As one of the world's largest metal producers and consumers, China has diversified and large-scale mineral resources. The proven reserves of mineral resources account for 12% of the world's total mineral resources [11]. Chinese scholars identified that the main sources

of soil HMP in China were sewage irrigation, sludge application, and mining and smelting of minerals [1]. Among them, the mining industry was considered to be one of the most important sources of HMP. Heavy metals produced in the process of mining, beneficiation, and smelting often cause large-scale soil pollution in the region, through the atmosphere, surface runoff, and groundwater [12].

Strict measures were taken by the Chinese government to alleviate HMP in soil. During the “Twelfth Five-Year Plan” period (2011–2015), more than RMB 21 billion was invested in the treatment of HMP. In 2016, the “Action Plan for Soil Pollution Prevention and Control” was issued. It proposed that the safe utilization rate of polluted cultivated land will reach more than 95% by 2030, and the pilot of cultivated land fallow compensation will be carried out in some areas with serious pollution [13]. However, the implementation of the work was restricted, due to the large area of polluted cultivated land, the high cost, and the long period of remediation. By 2020, only about 6.67 thousand km² of cultivated land polluted by heavy metals were improved. The actual effect of cultivated land fallow was not satisfactory either, and the scale of fallow land was far from reaching the government’s goal [14]. Part of the heavy metal-contaminated farmland is still used.

The existing research on soil HMP focuses on the evaluation of pollution status and remediation technology. However, there is a lack of research on farmers. In China, farmers are the main micro-organizational agents of agricultural production. Since the implementation of the “household contract responsibility system”, the right to use cultivated land was decentralized to farmers [15]. Farmers became the direct users of cultivated land, and the direct bearers of risk control. Understanding their adaptive behaviors toward heavy metal-polluted cultivated land, and the influencing factors, can provide insights and information relevant for decision-making to better manage the hazards and risks of HMP in cultivated land. It is also very crucial in reducing the vulnerability of farmers, securing their livelihood, and formulating future strategies to control heavy metal-polluted cultivated land. But there are few scientific studies on farmers’ living or production behaviors on heavy metal-contaminated land.

In this paper, 278 farmers in the cultivated land polluted by heavy metals in typical mining areas of Daye, China were considered as the research population. We studied the adaptive behaviors of farmers under the threat of HMP and its influencing factors, to make two contributions to the current research. First, our study provides a new case for the study of adaptation to global environmental change, and gives a support basis for the Chinese government to formulate the management policy of heavy metal-contaminated farmland at the farmer level. Second, we proposed a conceptual framework of “farmers’ characteristics-perceptions-adaptive behaviors”, and examined the influence of characteristics and perceptions on adaptive behaviors.

2. Materials and Methods

2.1. Conceptual Framework

Adaptation refers to the process by which people make adjustments according to actual or expected environmental changes, and their impacts to reduce or avoid harm, or exploit beneficial opportunities [16]. With the intensification of conflicts between humans and the environment, the study of adaptive behaviors has become a frontier area and a core component of environmental change research [17–19]. Akcaoz and Ozkan indicate that agriculture is a uniquely high-risk and uncertain industry. Farmers must make decisions in an environment where risks are constantly changing [20]. Understanding the key factors affecting farmers’ adaptation process can help governments formulate adaptation policies to ensure sustainable agricultural development [21,22]. In recent years, more attention was paid to the adaptive behaviors of farmers in response to climate change, and primarily focused on climate change perception, adaptive capacity, and adaptive measures [23–25]. Moreover, because adaptation is a complex and multidimensional process [26], the current understanding of farmers’ adaptation to environmental changes, and the factors that affect them, is still very limited [27,28].

Perception is considered to be the basis of adaptation [29,30]. Deressa et al. divide the adaptation process of farmers to environmental change into two stages: perceiving environmental change and adopting adaptation measures [31]. Lorenzoni et al. propose a three-stage theory, which postulates that the behavioral–psychological process of individual involvement in environmental matters consists of three stages: perceiving environmental change, perceiving the effects of change, and adapting through appropriate behaviors [32]. Bohensky et al. argue that there are three stages for individuals to adapt to environmental changes: observation, perception, and action. The latter stage must be based on the previous stage [33]. Different levels of perception lead to differences in adaptation strategies, so farmers with more obvious perceptions of environmental changes and risks are more likely to take action [34]. However, some scholars found that higher levels of risk perception does not always translate into positive adaptive behaviors [35]. Farmers’ assessments of self-efficacy, adaptive costs, and other factors are mediating factors that impede the transformation of risk perception into adaptive behavior [36]. Grothmann and Patt developed the model of private proactive adaptation to climate change (MPPACC) and define two perceived psychological process variables in the model: risk appraisal and adaptation appraisal. They believe that the two variables are affected by factors such as farmer’s characteristics and social background [37]. Age, race, education, living area, income level, agricultural experience, and other characteristics may affect farmers’ environmental risk perceptions [38–40].

Above all, there is a complex nonlinear relationship between farmers’ characteristics, perceptions, and adaptive behaviors. Nevertheless, existing studies mainly discuss the impact of farmers’ perceptions on adaptive behaviors, or take the unity of farmers’ characteristics and perceptions as independent variables to explore the influence of characteristics and perceptions on adaptive behaviors [27,41–44]. Few studies focus on the mediating role of farmers’ perception between their characteristics and adaptive behavior. Therefore, we constructed a conceptual framework of “farmers’ characteristics-perceptions-adaptive behaviors”, as shown in Figure 1. Then, we hypothesized that farmers’ characteristics have a direct effect on adaptive behaviors, while perceptions mediate the relationship between them. A further explanation of the framework is shown below.

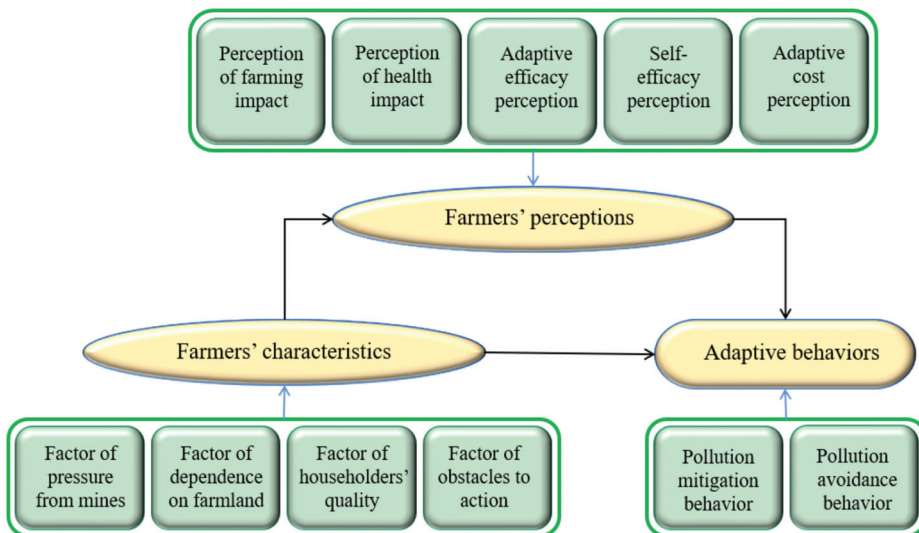


Figure 1. Conceptual framework of “farmers’ characteristics-perceptions-adaptive behaviors”.

2.2. Study Area and Survey Process

2.2.1. Study Area

Three villages seriously affected by HMP in Daye, China were selected as the study areas (Figure 2). Daye is a famous mining city in China, with more than 3000 years of mining and smelting history. In 2012, it was listed as a national key demonstration zone for HMP remediation by the Ministry of Environmental Protection. As early as the 1980s, the problem of HMP in Daye City emerged, such as deterioration of water quality, crop yield reduction (or even no harvest), variation in the quality of agricultural products, and an increase in tumor patients. Over the past 30 years, rapid economic development led to a continuous increase in the demand for mineral resources. High-intensity and extensive mining and smelting of mineral resources aggravated the HMP of soil, water, and agricultural products around the mining area [45]. The agricultural production and physical health of farmers are seriously affected [46].

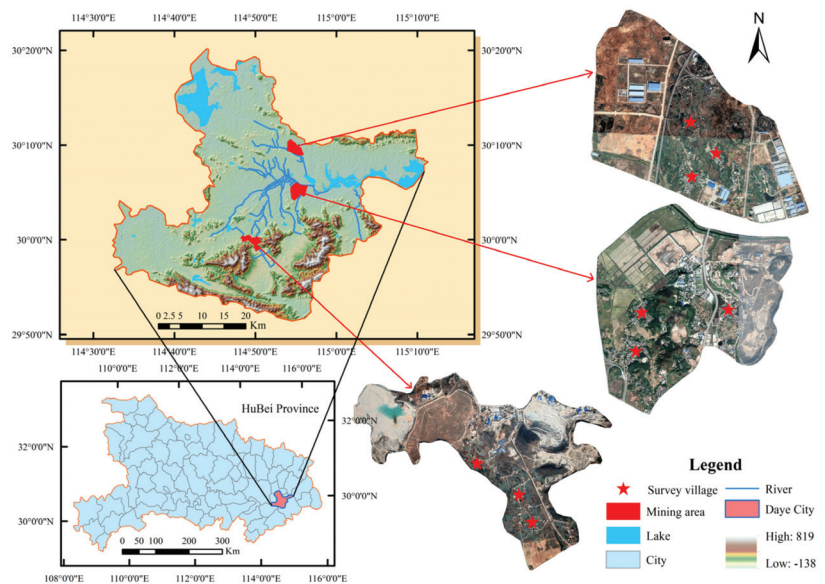


Figure 2. The location of the study areas.

2.2.2. Survey Process

In China, farmers' cultivated land is often located around their residences. We selected 11 villages in Daye City that were relatively seriously affected by HPM. Participatory rural appraisal (PRA) was used to investigate farmers. Two pre-surveys were conducted in October and November 2020, to identify common behaviors adapted to HMP of cultivated land. To ensure that the questionnaire was in line with the actual situation and easily understood by the farmers, we supplemented and improved the questionnaire in accordance with the pre-surveys. The formal survey was conducted in January 2021. According to the stratified sampling method, the household survey was carried out with households as units. To make the results reliable, we provided assistance to each respondent during the survey, and provided them with a return of 30 RMB after answering the questions. A total of 300 questionnaires were collected and the final sample size was 278, with an effective rate of 92.67%.

2.3. Farmers' Adaptive Behaviors

By visiting farmers and consulting experts familiar with the local environment, this research identified six categories of relatively common adaptive behaviors for HMP on cultivated land, as shown in Table 1. From the perspective of cultivated land utilization, we called the four types of adaptive behaviors (i.e., plowing or reshaping the soil, adjusting irrigation patterns, adjusting crop varieties, and changing land-use patterns) pollution mitigation behaviors (Behav-M). These behaviors mean that farmers are still trying to alleviate and utilize the cultivated land polluted by heavy metals. Abandoning farming and trying to move away were named pollution avoidance behaviors (Behav-A), because adopting these behaviors means that farmers are not going to mitigate and use cultivated land polluted by heavy metals.

Table 1. Farmers' adaptive behaviors toward heavy metal-polluted cultivated land.

Adaptive Behaviors		Description
Pollution mitigation behaviors (Behav-M)	Plow or replace the soil (Behav-M1)	Plow or change the soil eroded by sewage or tailings
	Adjust irrigation patterns (Behav-M2)	Irrigate or find new water sources by observing the water regime
	Adjust crop varieties (Behav-M3)	Select heavy metal pollution-tolerant varieties according to experience or media publicity
	Change land-use patterns (Behav-M4)	Planting trees or fish ponds instead of crops
Pollution avoidance behaviors (Behav-A)	Try to move away (Behav-A1)	Abandoning crop cultivation because of the perception of severe pollution
	Abandon farming (Behav-A2)	Trying to move out because of the feeling of serious pollution

2.4. Selection of Farmers' Characteristics and Perceptions

2.4.1. Farmers' Characteristics

Farmers' characteristics were primarily considered from the perspective of the individual and household characteristics. Unlike in the traditional Chinese household registration, the householder in this paper refers to the person who determines a household's agricultural production and livelihood preferences, to a certain extent [47]. Individual characteristics primarily cover the age and education level of the householder, which can reflect their non-agricultural employment ability and information acquisition ability [48]. Household characteristics reflect the socioeconomic base and agricultural production conditions. Referring to relevant research [44,49,50], we selected 9 indicators, including the age and education level of the householder, family size, population dependency ratio, agricultural income share, nonfarm labor force share, arable land per capita (m²), distance from the pollution source (Km), and pollution time (year), as shown in Table 2. Among them, the distance from the pollution source and the pollution time are assigned a value of 1, 2, or 3, according to the distance between the farmer's group and the mine pollution source and the mining time, respectively.

Table 2. Descriptive statistics of respondents' basic information.

Farmers' Characteristics	Class	QTY	PCT(%)	S.D.
Gender	Female	120	43.17	0.50
	Male	158	56.83	
Age	≤45	70	25.18	10.74
	45~60	134	48.20	
	>60	74	26.62	
Education level	Primary school	111	39.93	0.76
	Junior high school	119	42.81	
	High school and above	48	17.26	

Table 2. Cont.

Farmers' Characteristics	Class	QTY	PCT(%)	S.D.
Family size	≤3	55	19.78	1.97
	3~5	126	45.33	
	>5	97	34.89	
Population dependency ratio	≤0.5	84	30.22	0.53
	0.5~1	120	43.17	
	>1	74	26.62	
Agricultural income share	≤20%	163	58.63	0.95
	20~40%	60	21.58	
	>40%	55	19.78	
Nonfarm labor force share	≤20%	79	28.42	0.32
	20%~60%	115	41.37	
	>60%	84	30.22	
Arable land per capita	≤200	93	33.45	0.43
	200~466.67	101	36.33	
	>466.67	84	30.22	
Distance from pollution source	≤1	114	41.01	0.19
	1~2	115	41.37	
	>2	49	17.63	
Pollution time	≤10	88	31.65	0.89
	10~20	43	15.47	
	>20	147	52.88	

2.4.2. Farmers' Perceptions

According to the MPPACC model [37], we investigated farmers' risk perception and adaptation perception of HMP, as shown in Table S1. The risk perceptions in the MPPACC model include possibility perception and severity perception. Since the study areas have been polluted by heavy metals for a long time, farmers hold a very positive and consistent view on the possibility of HMP. In the survey, we found that farmers mainly paid attention to the impact of HMP on agricultural production and health. Therefore, the risk perception of farming (Risk-F) and health (Risk-H) are considered as the risk perceptions in this study. Adaptive perceptions include adaptive efficacy perception (Adapt-A), self-efficacy perception (Adapt-S), and adaptive cost perception (Adapt-C) [37]. It is difficult for farmers to accurately express their adaptive cost perceptions due to the lack of professional knowledge and skills in mitigating heavy metal pollution on cultivated land. The development of urbanization in China since the reform and opening up (reform and opening up is a policy of domestic reform and opening up that China began to implement at the Third Plenary Session of the Eleventh Central Committee in December 1978) provided farmers with a great number of higher-income and non-farm employment opportunities, so farmers no longer considered the direct costs of production when simply making agricultural decisions. Our study drew on the concept of opportunity cost in economics to investigate adaptive cost perception [51]. We quantified farmers' adaptive cost perception in terms of their willingness to spend time and money to mitigate HMP. The stronger the willingness, the lower the adaptive cost perception. For farmers' perceptions, we set five questions, as shown in Table S1. For the closed-ended questions, they were quantified according to a five-point Likert scale.

2.5. Mediation Effect Analysis Method

According to the mediating effect model developed by Baron and Kenny [52], we used hierarchical regression to explore the mediating effects of farmers' perceptions between characteristics and adaptive behaviors. The first stage (Equation (1)): testing the effect of characteristics on adaptive behaviors. If δ_1 is significant, we proceed to the second stage;

(Equation (2)): exploring the influence of characteristics on perceptions. If β_1 is significant, go to the third stage; (Equation (3)): estimating whether characteristics and perceptions are related to adaptive behaviors. If both γ_1 and γ_2 are significant, there is a partial mediating effect, and if γ_2 is significant but γ_1 is not, there is a full mediating effect. Otherwise, there is no mediating effect.

$$\text{AdaptB} = \delta_0 + \delta_1 \text{FarC} + \varepsilon_1 \quad (1)$$

$$\text{FarP} = \beta_0 + \beta_1 \text{FarC} + \varepsilon_2 \quad (2)$$

$$\text{AdaptB} = \gamma_0 + \gamma_1 \text{FarC} + \gamma_2 \text{FarP} + \varepsilon_3 \quad (3)$$

where *AdaptB* denotes farmers' adaptive behaviors, *FarC* denotes farmers' characteristics, and *FarP* denotes farmers' perceptions. Since *AdaptB* is a binary categorical data, logistic regression is more applicable to Equations (1) and (3) than least squares (OLS), so Equations (1) and (3) are rewritten as Equations (4) and (5), respectively [53].

$$\text{AdaptB} = \text{LogitP}(\text{AdaptB} = 1 | \text{FarC}) = \ln \frac{P(\text{AdaptB} = 1 | \text{FarC})}{P(\text{AdaptB} = 0 | \text{FarC})} = \delta_0 + \delta_1 \text{FarC} + \varepsilon_1 \quad (4)$$

$$\text{AdaptB} = \text{LogitP}(\text{AdaptB} = 1 | \text{FarP}, \text{FarC}) = \ln \frac{P(\text{AdaptB} = 1 | \text{FarP}, \text{FarC})}{P(\text{AdaptB} = 0 | \text{FarP}, \text{FarC})} = \gamma_0 + \gamma_1 \text{FarC} + \gamma_2 \text{FarP} + \varepsilon_3 \quad (5)$$

Generally, the value of mediating effect can be expressed as $\beta_1 * \gamma_2$. However, Equations (2) and (3) in this paper were estimated by ordinary least squares (OLS) and logistic regression, respectively, leading to β_1 , and γ_2 on different scales. The regression coefficients of the original equation need to be standardized to quantify the mediating effects [54]. Therefore, we used Mplus to construct the mediating effects model to obtain the standardized coefficients.

3. Results

3.1. Descriptive Statistics

Among the 278 valid questionnaires, we conducted statistical analysis on the basic information of the respondents, as shown in Table 2. Among them, 56.83% are male and 74.28% are over 45 years old. Only 17.27% of farmers received a high school education or above. The majority of farmers have a household size of three or above, and the labor force in the household is under heavy pressure to raise children and the elderly. Over half of them have less than 20% of agricultural income. Nearly 30% of families have a non-farm labor force of more than 60%. Approximately 33% of the respondents have less than 200 m² arable land, which is lower than the average level of Daye City. In addition, about 41% of farmers' cultivated land is less than 1 km away from the pollution source, and more than half of the cultivated land has been polluted for more than 20 years. The basic information of the respondents is in line with the characteristics of rural China. It reflects the situation of farmers in the study area.

3.1.1. Adaptive Behaviors

As shown in Figure 3, statistics show that 60.8% of farmers take at least one adaptive behavior, 44.2% take pollution mitigation behaviors (Behav-M), and 27.3% adopt pollution avoidance behaviors (Behav-A). As Figure 4 shows, the adoption rate of each adaptive behavior is not high. Among the mitigation behaviors, the adoption rates of plowing or reshaping the soil (Behav-M1), adjusting irrigation mode (Behav-M2), and adjusting crop variety (Behav-M3) are less than 20%, and the adoption rate of changing land-use patterns (Behav-M4) is only 8.99%. On the contrary, the adoption rate of trying to move away (Behav-A1) is the highest, reaching 23.38%, indicating that farmers have a strong willingness to escape in the face of HMP in cultivated land.

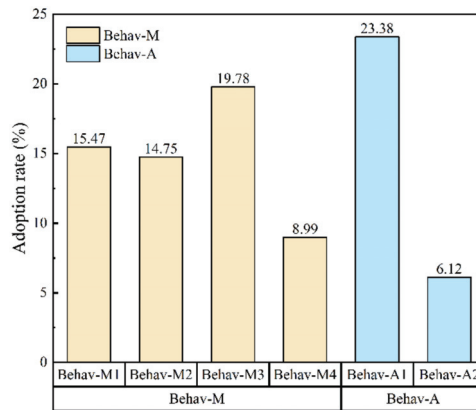


Figure 3. Farmers’ adaptive behaviors to heavy metal pollution in cultivated land.

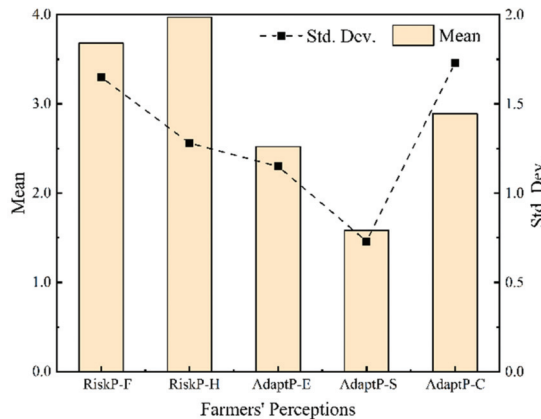


Figure 4. Levels of perceptions on HMP in cultivated land.

3.1.2. Farmers’ Characteristics

In this study, nine variables of farmers’ characteristics were selected. We used factor analysis (FA) to extract common factors. Based on SPSS 24.0, data were tested by KMO and Bartlett tests [55,56]. Then, principal component analysis and maximum variance rotation were used to complete the factor analysis, as shown in Table 3.

Table 3. Results of factor analysis of farmers’ characteristics.

Farmer Characteristics	Characteristic Factors				Data Inspection
	Factor 1	Factor 2	Factor 3	Factor 4	
Age	0.159	−0.104	0.806	−0.155	KMO = 0.61 Sig. = 0.000
Education level	0.029	0.115	0.861	0.063	
Family size	−0.150	−0.086	−0.204	0.782	
Population dependency ratio	0.039	−0.034	−0.051	0.865	
Agricultural income	0.096	0.909	−0.014	−0.012	
Nonfarm labor share	−0.149	−0.217	0.150	0.563	
Arable land per capita(mu)	0.045	0.828	0.043	−0.297	
Distance from the pollution source	0.890	0.050	0.069	−0.069	
Pollution time	0.877	0.094	0.119	−0.127	

Factor 1 focuses on the pollution time and the distance from the pollution source, so it is named the “factor of pressure from mines”. The proportion of agricultural income and arable land per capita have higher loads on factor 2, which reflects the importance of agricultural production in households, and it is called the “factor of dependence on farmland”. Factor 3 primarily reflects the learning ability and adaptability of farmers, so it is designated as the “factor of householder’s quality”. Factor 4 refers to the family size and nonfarm labor share. The higher the score, the greater the pressure in life, which is entitled the “factor of obstacles to action”.

3.1.3. Farmers’ Perceptions

From Figure 4, it can be seen that farmers’ risk perceptions are relatively strong. Both the perceptions of farming impact (RiskP-F) and health impact (RiskP-H) of HMP in cultivated land are at a high level, and the latter is more prominent. The overall levels of adaptive perceptions are moderate or low. Among them, the level of adaptive cost perception (AdaptP-C) is the highest, and there are large fluctuations among individuals (standard deviation = 1.73). The level of self-efficacy perception (AdaptP-S) is the lowest and relatively stable (standard deviation = 0.97), indicating that farmers have insufficient confidence in self-adapting to HMP in cultivated land.

3.2. The Mediating Effect of Perception

3.2.1. Hierarchical Regression

According to the method in Section 2.4, we tested the mediating effect of farmers’ perceptions, as shown in Table 4. First, we tested the effect of farmers’ characteristics on adaptive behaviors (including mitigation and avoidance behaviors). The results are shown in models 1 and 2. Second, in models 3–7 we examine the influence of farmers’ characteristics on perceptions. Finally, the impacts of farmers’ perceptions and characteristics on adaptive behaviors are shown in models 8 and 9.

Table 4. The mediating effect of perceptions between characteristics and behaviors.

Variables	First Stage		Second Stage					Third Stage	
	Model 1: Behav-M	Model 2: Behav-A	Model 3: RiskP-F	Model 4: RiskP-H	Model 5: AdaptP-E	Model 6: AdaptP-S	Model 7: AdaptP-C	Model 8: Behav-M	Model 9: Behav-A
Factor 1	0.287 ** (0.129)	0.379 ** (0.151)	0.087 (0.099)	0.112 *** (0.076)	−0.064 (0.068)	0.174 *** (0.043)	0.029 (0.103)	0.237 * (0.134)	0.278 * (0.156)
Factor 2	0.427 *** (0.130)	−0.079 (0.141)	−0.050 (0.099)	−0.123 *** (0.076)	−0.14 ** (0.068)	−0.016 (0.043)	−0.039 (0.103)	0.474 *** (0.137)	−0.052 (0.147)
Factor 3	0.173 (0.125)	0.437 *** (0.140)	0.094 (0.099)	0.076 (0.076)	0.177 *** (0.068)	0.204 *** (0.043)	0.169 *** (0.103)	0.083 (0.132)	0.362 ** (0.149)
Factor 4	−0.138 (0.125)	−0.370 *** (0.144)	0.018 (0.099)	−0.021 (0.076)	0.003 (0.068)	0.033 (0.043)	0.095 (0.103)	−0.170 (0.129)	−0.402 *** (0.149)
RiskP-F								0.153 * (0.091)	0.025 (0.101)
RiskP-H								−0.048 (0.117)	0.239 * (0.141)
AdaptP-E								0.091 (0.120)	−0.160 (0.138)
AdaptP-S								0.351 * (0.190)	0.329 (0.204)
AdaptP-C								0.028 (0.075)	0.151 * (0.087)
Pseudo R ²	0.091	0.116	0.019	0.034	0.055	0.073	0.040	0.134	0.165

Note: (1) Standard errors are in parentheses; (2) ***, **, * denote statistical significance at the 1%, 5%, and 10%, respectively.

For pollution mitigation behaviors (Behav-M), in the first stage, we find that the “factor of pressure from mines” (Factor 1) and the “factor of dependence on farmland” (Factor 2) have significant effects on Behav-M. In the second stage, from model 6, we observe a significant and positive effect of Factor 1 on self-efficacy perception (AdaptP-S). According to the third stage, in model 8, there are significant positive effects of Factor 1 and AdaptP-S on Behav-M. In addition, risk perception of farming (RiskP-F) has a positive effect on Behav-M. It is revealed that Factor 2 and RiskP-F have direct positive effects on Behav-M, and AdaptP-S plays a partially mediating role in the relationship between Factor 1 and Behav-M.

For pollution avoidance behaviors (Behav-A), in the first stage, we identify significant effects of the “factor of pressure from mines” (Factor 1), the “factor householder’s quality” (Factor 3), and the “factor of obstacles to action” (Factor 4) on Behav-A. In the second stage, model 6 shows that there is a significant positive effect of Factor 1 on the perception of health impact (RiskP-H). From model 7, it is known that there is a significant and positive effect of Factor 3 on the adaptive cost perception (AdaptP-C). According to the third stage, in model 9, Factor 1 and RiskP-H have significant positive effects on Behav-A. In addition, risk perception of health (RiskP-H) has a positive effect on Behav-A. It is shown that Factor 4 has a significant negative effect on Behav-A and RiskP-H has a significant positive effect on Behav-A; RiskP-H partially mediates the relationship between Factor 1 and Behav-A; and AdaptP-C plays a partially mediating role in the relationship between Factor 3 and Behav-A.

Mplus was used to calculate the effect values of the three mediating paths, as shown in Table 5. The mediating effect of AdaptP-S is 0.031, accounting for 20.38% of the total effect. That means that 20.38% of the effect of Factor 1 on Behav-M is via AdaptP-S. The mediating effects of RiskP-H and AdaptP-C are 0.019 and 0.023, accounting for 11.04% and 11.42% of the total effect, respectively.

Table 5. The calculation of mediating effects and Bootstrap test.

Mediation Path	Indirect Effect	Direct Effect	The Proportion of Mediation Effect	Bootstrap Confidence Interval			
				Lower 2.5%	Lower 5%	Upper 5%	Upper 2.5%
Factor 1-AdaptP-S-Behav-M	0.031 **	0.121	20.38%	0.004	0.008	0.071	0.079
Factor 1-RiskP-H-Behav-A	0.019 *	0.153	11.04%	0.000	0.003	0.055	0.063
Factor 3-AdaptP-C-Behav-A	0.023 *	0.178	11.42%	-0.002	0.002	0.062	0.072

Note: **, * denote statistical significance at the 5%, and 10%, respectively.

In addition, we took the Bootstrap test to further examine the reliability of the mediating effects [57,58]. Table 4 indicates that the three mediating effects are significant at the 5% and 10% levels, respectively, revealing that there are indeed mediating effects for these three farmer perceptions.

3.2.2. Robustness Check

To test the robustness of the results, the logistic regression model was converted into the OLS regression model. As shown in Table 6, the two regression models passed the same variables and the signs of the coefficients are identical, indicating that the results are robust.

Table 6. The robustness check of the regression.

Variables	Behav-M		Behav-A	
	Model 10	Model 11	Model 12	Model 13
Factor 1	0.066 **(0.029)	0.054 *(0.150)	0.066 **(0.026)	0.049 *(0.026)
Factor 2	0.100 *** (0.029)	0.105 *** (0.030)	-0.018 (0.026)	-0.013 (0.026)
Factor 3	0.040 (0.029)	0.019 (0.029)	0.082 *** (0.026)	0.066 ** (0.027)
Factor 4	-0.032 (0.029)	-0.036 (0.030)	-0.066 ** (0.026)	-0.071 *** (0.026)

Table 6. Cont.

Variables	Behav-M		Behav-A	
	Model 10	Model 11	Model 12	Model 13
Risk-F		0.034 *(0.029)		0.004(0.018)
Risk-H		−0.010(0.020)		0.039 *(0.023)
AdaptP-E		0.019(0.026)		−0.028(0.024)
AdaptP-S		0.078 *(0.027)		0.061(0.038)
AdaptP-C		−0.006(0.043)		−0.027 *(0.015)
Constant	0.442 ***(0.029)	0.219(0.017)	0.273 ***(0.026)	0.234 *(0.134)

***, **, * denote statistical significance at the 1%, 5%, and 10%, respectively.

4. Discussion

4.1. Strong Risk Perception and Low Self-Efficacy Perception

In the study areas, farmers have strong risk perceptions on HMP, including RiskP-F and RiskP-H. In the survey, we found that only 19.4% of farmers obtained information about HMP through the government. Their knowledge about HMP mainly came from farming experience, neighborhood discussion, and the media. These make it easy to form a relatively consistent view of HMP, and its risks within a village. The phenomenon that crops did not germinate, grow, or even die was common in the polluted cultivated land, which made farmers firmly believe that HMP has a great impact on farming. In comparison, RiskP-H is stronger. On the one hand, mining activities were carried out there for more than 20 years. In recent years, the incidence of cancer increased, and the incidence of the population started to be younger. The reports about “cancer villages” make them link cancer with HMP, which makes them very worried. On the other hand, with the development of China’s rural economy, the material living standards of farmers greatly improved. The majority of people’s thoughts changed from “solving adequate food and clothing” to “pursuing a better and healthy life”. Farmers are particularly concerned about health problems.

The AdaptP-S is generally low. In areas rich in mineral resources, mining is often the pillar industry of local development, which not only brings huge financial revenue to local governments, but also creates a large number of employment opportunities (Antoci et al., 2019). Local governments seek a balance between environmental protection and economic development (Ranängen and Lindman, 2018). To avoid conflicts between farmers and mining enterprises, local governments rarely disclose HMP to the public. There is a greater lack of corresponding knowledge and skills training. Low AdaptP-S discourages farmers from proactively adopting adaptive behaviors [59,60]. The lack of knowledge and skills makes local farmers negative and helpless when facing HMP. They want to seek help. So, 16.2% of farmers have the experience of seeking compensation from mining enterprises, and 30.6% seek compensation from local government.

4.2. Passive and Barely Ineffective Adaptive Behavior

Although 44.2% of farmers took Behav-M, and were still trying to mitigate and utilize the cultivated land polluted by heavy metals, due to the invisibility of HMP [2], it cannot be observed such as water eutrophication and other pollution. The lack of knowledge and skills makes farmers’ behaviors often passive, empirical, and constrained by natural environmental conditions. It is usually spread by word of mouth, based on the experience of residents in the village, and is not widely disseminated. The regional natures of behaviors result in the low adoption rate of each behavior.

It is found in the survey that the behavior of plowing or replacing the soil generally occurs on the cultivated land eroded by tailings or mine sludge. The black tailings or sludge makes farmers intuitively feel that the growth of crops would be affected. Changing the irrigation mode generally occurs in the cultivated land near polluted rivers. Long-term experience taught them that using the polluted river for irrigation makes the crops unable to grow normally, or even die. To this end, farmers tried to find new sources of water,

such as diverting water from farther places, or building ponds. Limited by the natural environment, not all farmers could find suitable water sources. In this case, some of them could only try to plant different crops, adjust the utilization of land to plant trees, or build fish ponds to raise fish. However, due to the HMP caused by mining and metallurgical fume, farmers had no choice but to report to the government. In the study areas, due to the massive expropriation of farmers' land for the development of mineral resources, the per capita cultivated land area of many farmers is less than 300 m². For the sake of livelihood, farmers with high-dependence on cultivated land have to try to use the land with serious HMP, although they know that the output of the cultivated land is very low, and may even fail to harvest.

According to our investigation, the effect of mitigation behaviors is not ideal. Due to the accumulation and irreversibility of HMP [6], the cultivated land that was plowed or had an adjusted irrigation mode still had a low yield and high production cost. Even if the land was used for planting trees, the growth of seedlings was slow, and the mortality was high. We tested and evaluated a random sample of crops in the study areas. The results show that the comprehensive carcinogenic risk coefficients of heavy metals ingested by adults and children through staple food (rice) and vegetables are higher than the safety value. It means farmers' daily consumption of self-produced agricultural products will pose the carcinogenic risk of heavy metals.

4.3. The Mediation role of Perception and the Determinant Role of Characteristics

The results of the hierarchical regression indicate that both farmers' characteristics and perceptions have important influences on their adaptive behaviors to HMP on cultivated land.

From the perspective of farmers' characteristics, the "factor of pressure from mines" (Factor 1) has a significant positive effect on both Behav-M and Behav-A. It is related to the socioeconomic background of the "mining-agricultural combination area". The stress of mining on agricultural development has gradually become prominent, and farmers have to try to adjust production decisions to adapt to the changes in the agricultural environment [61]. While farmers in good condition will choose to abandon farming or even move away from polluted areas, similar to Factor 1, the "factor of dependence on farmland" (Factor 2) also has a significant positive effect on Behav-M. For farmers with a high-dependence on cultivated land, agriculture is often the economic pillar of their families. These families lack means of livelihood other than agricultural production. When they face HMP, they have to take measures to maintain agricultural production, and the basic livelihood of households. As can be seen from model 8 (Table 4), the coefficient of Factor 2 has the largest effect on Behav-M, indicating that the dependence on cultivated land is the most important factor promoting the adoption of Behav-M by farmers. The "factor of householder's quality" (Factor 3) has a significant positive effect on Behav-A. Younger and better-educated people have more non-farm employment opportunities. In the context of rapid urbanization, some Chinese farmers prefer to work, or even live, in the cities [62]. Moreover, this trend is exacerbated in mining areas [63]. Confronted with the HMP of cultivated land, householders with high-quality learning ability and adaptability are more likely to abandon agricultural production, or move away from their current residence, because they have the economic basis to support these behaviors [64]. The "factor of obstacles to action" (Factor 4) has a significant negative effect on Behav-A, which is opposite to Factor 3. Households with larger action damping have more elders and children. It negatively affects the average income of family members, and reduces the marginal income of the labor force [65]. From model 9 (Table 4), we can see that the coefficient of Factor 4 has the largest effect on Behav-A, indicating that it is the most important factor that hinders Behav-A.

In terms of farmers' perceptions, farming impact perception (RiskP-F), health impact perception (RiskP-H), self-efficacy perception (AdaptP-S), and adaptive cost perception (AdaptP-C) all have a positive and significant impact on farmers' adaptive behaviors. RiskP-F promotes Behav-M; when farmers perceive a threat to their production, they try to take measures to mitigate the current situation. RiskP-H plays a mediating role between factor 1 and Behav-A; farmers gradually perceive the health hazards of HMP with the aggravation of pollution [66], which makes them have the idea of staying away from pollution. AdaptP-S plays a mediating role between factor 1 and Behav-M; long-term experience with heavy metal-polluted cultivated land enables farmers to conclude certain countermeasures, such as adjusting crop varieties and finding new sources of irrigation. These measures can increase their confidence in the face of HMP. Even though the effects of these measures are not clear to farmers, it does not prevent them from improving their perception of self-efficacy, then promoting the adoption of Behav-M. AdaptP-C plays a mediating role between factor 3 and Behav-A; householders with high-quality learning ability and adaptability can earn a much higher income than agricultural production in cities, and they have a higher opportunity cost to adopt mitigation behaviors. So, they are more inclined to adopt Behav-A.

Surprisingly, the effects of tillage dependence factors and action resistance factors on adaptive behavior have no significant relationship with perception level. For the former, as Manalo et al. conclude: those who are firmly committed to their identity as rice farmers will find ways to continue growing rice anyway, while those who are not firmly committed to their identity as rice farmers may leave the rice fields if they find it impossible to grow them due to drought [67]. For the latter, currently, the cost of education for children in China is increasing year by year, and the rural retirement system is still inadequate [68]. The economic pressure of supporting the elderly and raising children makes them incapable of abandoning farming. Meanwhile, there are no more funds to support relocation. Except for economic pressure, there is another important factor that hinders their avoidance behaviors, which is called "old farmer's homeland attachment" in this paper. In rural China, some old farmers are reluctant to leave their long-established places and abandon their farmland. They prefer to maintain their current living conditions rather than take the "uncertain" risk of heavy metal pollution.

The factors affecting farmers' adaptive behaviors are complex. This study focuses on the effects of farmers' characteristics on adaptive behaviors, and the impact of farmers' perceptions on this relationship. Farmers' characteristics can reflect household resources and production endowments. They play a decisive role in farmers' adaptation to HMP in cultivated land. Farmers' perceptions reflect farmers' psychological factors. The results show that the perceptions of health impact, self-efficacy, and adaptation cost play a partial mediating role in the influence of farmers' characteristics on adaptive behaviors.

5. Conclusions

To explain the mechanism of farmers' adaptive behaviors towards heavy metal-polluted cultivated land in mining areas, we proposed a conceptual framework of "farmers' characteristics-perceptions-adaptive behaviors". Based on 278 farmers' data in the mining areas of Daye, China, a hierarchical regression approach was used to analyze the influence of farmers' characteristics and perceptions on adaptive behaviors, and the mediating role of farmers' perceptions between farmers' characteristics and adaptive behaviors.

Results show that farmers can perceive the harm of HMP in cultivated land, and have strong perceptions of farming impact and health impact, but farmers' self-efficacy perception is very low, because they have very limited access to HMP knowledge and skills. A total of 60.8% of farmers adopt at least one adaptive behavior; 44.2% of farmers adopt pollution mitigation behavior; and 27.3% of them adopt pollution avoidance behavior, and the adoption rate of each adaptive behavior is not high. From the results of hierarchical regression, self-efficacy perception mediates the relationship between the "factor of pressure from mines" and pollution mitigation behaviors; health impact perception mediates

the relationship between the “factor of pressure from mines” and pollution avoidance behaviors; and adaptive cost perception mediates the relationship between the “factor of householder’s quality” and pollution avoidance behaviors. The “factor of dependence on farmland” and the “factor of obstacles to action” are the most important influences on pollution mitigation behaviors and pollution avoidance behaviors, respectively. The former has a positive effect and the latter a negative effect. Farmers’ perceptions can affect their adaptive behaviors, and play a mediating role in the impact of farmers’ characteristics on behavior, but farmers’ characteristics play a decisive role. For those farmers who are highly dependent on cultivated land, taking pollution mitigation behavior is only for their need to maintain family livelihood, but has nothing to do with perception.

This study believes that there is an urgent need for comprehensive planning and coordination of the treatment and utilization of heavy metal-polluted cultivated land. First, strengthening the monitoring of HMP, and organizing professional skill training and production guidance, in order to improve farmers’ understanding and adaptability to HMP. Second, to help farmers better adapt, the government should give financial support to effectively mitigate HMP. For seriously polluted villages, it is necessary to organize the conversion of farmland and compensate farmers as soon as possible, or the mining enterprises should compensate in the form of land acquisition. For heavily polluted villages, the overall relocation of villages is the best choice. Third, when formulating relevant measures, differentiated countermeasures should be taken for different groups of farmers. Poor farmers with high-dependence on cultivated land may need the most attention.

This study still has some limitations, in that we only focus on farmers in a typical mining area in central China. In the follow-up study, we will conduct a comparative study in other regions of mining areas, to verify the accuracy and reliability of our findings.

Supplementary Materials: The following supporting information can be downloaded at: <https://www.mdpi.com/article/10.3390/ijerph19116718/s1>, Table S1: Description and measurement of farmers’ perceptions.

Author Contributions: Y.C.: conceptualization, methodology, project administration, funding acquisition; Y.L. (Yaqi Liang): methodology, formal analysis, writing—original draft; H.Z.: investigation, writing—review and editing, validation, visualization; Q.W.: investigation, writing—review and editing; Y.L. (Yanzhong Liu): investigation, data curation. All authors have read and agreed to the published version of the manuscript.

Funding: This research was funded by the National Natural Science Foundation of China [grant number: 41971237], and the National Key Laboratory of Environmental Protection Mining and Metallurgy Resource Utilization and Pollution Control Open Fund [grant number: HB201916].

Institutional Review Board Statement: Not applicable.

Informed Consent Statement: Not applicable.

Data Availability Statement: Data is contained within the article or Supplementary Material.

Conflicts of Interest: All authors declare that they have no known competing interests or personal relationships that could appear to influence the work reported in this paper.

References

1. Chen, H.M.; Zheng, C.R.; Tu, C.; Zhu, Y.G. Heavy Metal Pollution in Soils in China: Status and Countermeasures. *AMBIO J. Hum. Environ.* **1999**, *28*, 130–134.
2. Wang, Q.R.; Dong, Y.; Cui, Y.; Liu, X. Instances of Soil and Crop Heavy Metal Contamination in China. *Soil Sediment Contam.* **2001**, *10*, 497–510.
3. MEP. National Soil Contamination Survey Report. Beijing, China, Ministry of Environmental Protection. Available online: http://www.gov.cn/foot/2014-04/17/content_2661768.htm (accessed on 20 September 2020).
4. Zhao, C.; Zhou, Y.; Jiang, J.; Xiao, P.; Wu, H. Spatial Characteristics of Cultivated Land Quality Accounting for Ecological Environmental Condition: A Case Study in Hilly Area of Northern Hubei Province, China. *Sci. Total Environ.* **2021**, *774*, 145765. [[CrossRef](#)]

5. Hu, B.; Shao, S.; Ni, H.; Fu, Z.; Hu, L.; Zhou, Y.; Min, X.; She, S.; Chen, S.; Huang, M. Current Status, Spatial Features, Health Risks, and Potential Driving Factors of Soil Heavy Metal Pollution in China at Province Level. *Environ. Pollut.* **2020**, *266*, 114961. [[CrossRef](#)]
6. Qin, G.; Niu, Z.; Yu, J.; Li, Z.; Ma, J.; Xiang, P. Soil Heavy Metal Pollution and Food Safety in China: Effects, Sources and Removing Technology. *Chemosphere* **2021**, *267*, 129205. [[CrossRef](#)]
7. Nabulo, G.; Young, S.D.; Black, C.R. Assessing Risk to Human Health from Tropical Leafy Vegetables Grown on Contaminated Urban Soils. *Sci. Total Environ.* **2010**, *408*, 5338–5351. [[CrossRef](#)]
8. Zheng, S.; Wang, Q.; Yuan, Y.; Sun, W. Human Health Risk Assessment of Heavy Metals in Soil and Food Crops in the Pearl River Delta Urban Agglomeration of China. *Food Chem.* **2020**, *316*, 126213. [[CrossRef](#)]
9. He, B.; Yun, Z.; Shi, J.; Jiang, G. Research Progress of Heavy Metal Pollution in China: Sources, Analytical Methods, Status, and Toxicity. *Chin. Bull.* **2012**, *58*, 134–140. [[CrossRef](#)]
10. Li, Z.; Ma, Z.; van der Kuijp, T.J.; Yuan, Z.; Huang, L. A Review of Soil Heavy Metal Pollution from Mines in China: Pollution and Health Risk Assessment. *Sci. Total Environ.* **2014**, *468–469*, 843–853. [[CrossRef](#)]
11. Hu, R.-Z.; Liu, J.; Zhai, M. *Mineral Resources Science and Technology in China: A Roadmap to 2050*; Springer Science & Business Media: Berlin/Heidelberg, Germany, 2011.
12. Liu, X.; Bai, Z.; Shi, H.; Zhou, W.; Liu, X. Heavy Metal Pollution of Soils from Coal Mines in China. *Nat. Hazards* **2019**, *99*, 1163–1177. [[CrossRef](#)]
13. Xie, H.; Wang, W.; Zhang, X. Evolutionary Game and Simulation of Management Strategies of Fallow Cultivated Land: A Case Study in Hunan Province, China. *Land Use Policy* **2018**, *71*, 86–97. [[CrossRef](#)]
14. Yu, Z.; Tan, Y.; Wu, C.; Mao, M.; Zhang, X. Alternatives or Status Quo? Improving Fallow Compensation Policy in Heavy Metal Polluted Regions in Chaling County, China. *J. Clean. Prod.* **2019**, *210*, 287–297. [[CrossRef](#)]
15. Fan, S. Effects of Technological Change and Institutional Reform on Production Growth in Chinese Agriculture. *Am. J. Agric. Econ* **1991**, *73*, 266–275. [[CrossRef](#)]
16. Liu, K.; Huisinigh, D.; Zhu, J.; Ma, Y.; O'Connor, D.; Hou, D. Farmers' Perceptions and Adaptation Behaviours Concerning Land Degradation: A Theoretical Framework and a Case-Study in the Qinghai–Tibetan Plateau of China. *Land Degrad. Dev.* **2018**, *29*, 2460–2471. [[CrossRef](#)]
17. Eriksen, S. Sustainable Adaptation: Emphasising Local and Global Equity and Environmental Integrity. *GECHS Synth. Hum. Secur. Era Glob. Change* **2009**, *2*, 40–44.
18. Smit, B.; Wandel, J. Adaptation, Adaptive Capacity and Vulnerability. *Glob. Environ. Change* **2006**, *16*, 282–292. [[CrossRef](#)]
19. Walther, B.A.; Larigauderie, A.; Loreau, M. Diversitas: Biodiversity Science Integrating Research and Policy for Human Well-Being. In *Coping with Global Environmental Change, Disasters and Securit*; Springer: Berlin/Heidelberg, Germany, 2011; pp. 1235–1248.
20. Akcaoz, H.; Ozkan, B. Determining Risk Sources and Strategies among Farmers of Contrasting Risk Awareness: A Case Study for Cukurova Region of Turkey. *J. Arid. Environ.* **2005**, *62*, 661–675. [[CrossRef](#)]
21. Berry, P.M.; Rounsevell, M.D.A.; Harrison, P.A.; Audsley, E. Assessing the Vulnerability of Agricultural Land Use and Species to Climate Change and the Role of Policy in Facilitating Adaptation. *Environ. Sci. Policy* **2006**, *9*, 189–204. [[CrossRef](#)]
22. Stringer, L.C.; Dyer, J.C.; Reed, M.S.; Dougill, A.J.; Twyman, C.; Mkwambisi, D. Adaptations to Climate Change, Drought and Desertification: Local Insights to Enhance Policy in Southern Africa. *Environ. Sci. Policy* **2009**, *12*, 748–765. [[CrossRef](#)]
23. Huang, J.; Wang, Y.; Wang, J. Farmers' Adaptation to Extreme Weather Events through Farm Management and Its Impacts on the Mean and Risk of Rice Yield in China. *Am. J. Agric. Econ.* **2015**, *97*, 602–617. [[CrossRef](#)]
24. Khanal, U.; Wilson, C.; Hoang, V.; Lee, B. Farmers' Adaptation to Climate Change, Its Determinants and Impacts on Rice Yield in Nepal. *Ecol. Econ.* **2018**, *144*, 139–147. [[CrossRef](#)]
25. Quan, S.; Li, Y.; Song, J.; Zhang, T.; Wang, M. Adaptation to Climate Change and Its Impacts on Wheat Yield: Perspective of Farmers in Henan of China. *Sustainability* **2019**, *11*, 1928. [[CrossRef](#)]
26. Stern, P. New Environmental Theories: Toward a Coherent Theory Of Environmentally Significant Behavior. *J. Soc. Issues* **2000**, *56*, 407–424. [[CrossRef](#)]
27. Truelove, H.B.; Carrico, A.R.; Thabrew, L. A Socio-Psychological Model for Analyzing Climate Change Adaptation: A Case Study of Sri Lankan Paddy Farmers. *Glob. Environ. Change* **2015**, *31*, 85–97. [[CrossRef](#)]
28. Abid, M.; Scheffran, J.; Schneider, U.A.; Elahi, E. Farmer Perceptions of Climate Change, Observed Trends and Adaptation of Agriculture in Pakistan. *Environ. Manag.* **2019**, *63*, 110–123. [[CrossRef](#)] [[PubMed](#)]
29. Bord, R.J.; Fisher, A.; Robert, E.O. Public Perceptions of Global Warming: United States and International Perspectives. *Clim. Res.* **1998**, *11*, 75–84. [[CrossRef](#)]
30. Leiserowitz, A. Climate Change Risk Perception and Policy Preferences: The Role of Affect, Imagery, and Values. *Clim. Change* **2006**, *77*, 45–72. [[CrossRef](#)]
31. Deressa, T.T.; Hassan, R.M.; Ringler, C. Perception of and Adaptation to Climate Change by Farmers in the Nile Basin of Ethiopia. *J. Agric. Sci.* **2011**, *149*, 23–31. [[CrossRef](#)]
32. Lorenzoni, I.; Nicholson-Cole, S.; Whitmarsh, L. Barriers Perceived to Engaging with Climate Change among the Uk Public and Their Policy Implications. *Glob. Environ. Change* **2007**, *17*, 445–459. [[CrossRef](#)]
33. Bohensky, E.L.; Smajgl, A.; Brewer, T. Patterns in Household-Level Engagement with Climate Change in Indonesia. *Nat. Clim. Change* **2013**, *3*, 348–351. [[CrossRef](#)]

34. Toma, L.; Mathijs, E. Environmental Risk Perception, Environmental Concern and Propensity to Participate in Organic Farming Programmes. *J. Environ. Manag.* **2007**, *83*, 145–157. [[CrossRef](#)]
35. Wachinger, G.; Renn, O.; Begg, C.; Kuhlicke, C. The Risk Perception Paradox—Implications for Governance and Communication of Natural Hazards. *Risk Anal.* **2013**, *33*, 1049–1065. [[CrossRef](#)]
36. Sullivan-Wiley, K.A.; Gianotti, A.G.S. Risk Perception in a Multi-Hazard Environment. *World Dev.* **2017**, *97*, 138–152. [[CrossRef](#)]
37. Grothmann, T.; Patt, A. Adaptive Capacity and Human Cognition: The Process of Individual Adaptation to Climate Change. *Glob. Environ. Change* **2005**, *15*, 199–213. [[CrossRef](#)]
38. Janmaimool, P.; Watanabe, T. Evaluating Determinants of Environmental Risk Perception for Risk Management in Contaminated Sites. *Int. J. Environ. Res. Public Health* **2014**, *11*, 6291–6313. [[CrossRef](#)] [[PubMed](#)]
39. Ono, K.; Tsunemi, K. Identification of Public Acceptance Factors with Risk Perception Scales on Hydrogen Fueling Stations in Japan. *Int. J. Hydrogen Energy* **2017**, *42*, 10697–10707. [[CrossRef](#)]
40. Maya, K.A.; Sarker, M.A.R.; Gow, J. Factors Influencing Rice Farmers’adaptation Strategies to Climate Change and Extreme Weather Event Impacts in Bangladesh. *Clim. Change Econ.* **2019**, *10*, 1950012. [[CrossRef](#)]
41. Menapace, L.; Colson, G.; Raffaelli, R. Climate Change Beliefs and Perceptions of Agricultural Risks: An Application of the Exchangeability Method. *Glob. Environ. Change* **2015**, *35*, 70–81. [[CrossRef](#)]
42. Zhai, S.; Song, G.; Qin, Y.; Ye, X.; Leipnik, M. Climate Change and Chinese Farmers: Perceptions and Determinants of Adaptive Strategies. *J. Integr. Agric.* **2018**, *17*, 949–963. [[CrossRef](#)]
43. Islam AR, M.; Shill, B.K.; Salam, R.; Siddik, M.; Alam, N.; Patwary, M.A. Insight into Farmers’ Agricultural Adaptive Strategy to Climate Change in Northern Bangladesh. *Environ. Dev. Sustain.* **2020**, *23*, 2439–2464. [[CrossRef](#)]
44. Guo, R.; Li, Y.; Shang, L.; Feng, C.; Wang, X. Local Farmer’s Perception and Adaptive Behavior toward Climate Change. *J. Clean. Prod.* **2021**, *287*, 125332. [[CrossRef](#)]
45. Du, P.; Xie, Y.; Wang, S.; Zhao, H.; Zhang, Z.; Wu, B.; Li, F. Potential Sources of and Ecological Risks from Heavy Metals in Agricultural Soils, Daye City, China. *Environ. Sci. Pollut. Res. Int.* **2015**, *22*, 3498–3507. [[CrossRef](#)] [[PubMed](#)]
46. Yang, J.; Ma, S.; Zhou, J.; Song, Y.; Li, F. Heavy Metal Contamination in Soils and Vegetables and Health Risk Assessment of Inhabitants in Daye, China. *J. Int. Med. Res.* **2018**, *46*, 3374–3387. [[CrossRef](#)] [[PubMed](#)]
47. Zhang, B.; Fu, Z.; Wang, J.; Tang, X.; Zhao, Y.; Zhang, L. Effect of Householder Characteristics, Production, Sales and Safety Awareness on Farmers’ Choice of Vegetable Marketing Channels in Beijing, China. *Br. Food J.* **2017**, *119*, 1216–1231. [[CrossRef](#)]
48. Dang, H.L.; Li, E.; Nuberg, I.; Bruwer, J. Factors Influencing the Adaptation of Farmers in Response to Climate Change: A Review. *Clim. Dev.* **2019**, *11*, 765–774. [[CrossRef](#)]
49. Funk, C.; Sathyan, A.R.; Winker, P.; Breuer, L. Changing Climate-Changing Livelihood: Smallholder’s Perceptions and Adaption Strategies. *J. Environ. Manag.* **2020**, *259*, 109702. [[CrossRef](#)] [[PubMed](#)]
50. Yang, H.; Cai, W.; Liu, J.; Huo, X. Impact of Internet Information on Apple Growers’ Adaptive Behaviors to Frost Disasters: Theory and Empirical Research from the Perspective of Psychological Perception. *Agriculture* **2021**, *11*, 905. [[CrossRef](#)]
51. Hoskin, R.E. Opportunity Cost and Behavior. *J. Account. Res.* **1983**, *21*, 78–95. [[CrossRef](#)]
52. Baron, R.M.; Kenny, D.A. The Moderator–Mediator Variable Distinction in Social Psychological Research: Conceptual, Strategic, and Statistical Considerations. *J. Personal. Soc. Psychol.* **1986**, *51*, 1173. [[CrossRef](#)]
53. Pan, D.; He, M.; Kong, F. Risk Attitude, Risk Perception, and Farmers’ Pesticide Application Behavior in China: A Moderation and Mediation Model. *J. Clean. Prod.* **2020**, *276*, 124241. [[CrossRef](#)]
54. MacKinnon, D.P. *Introduction to Statistical Mediation Analysis*; Routledge: Abingdon-on-Thames, UK, 2012.
55. Dziuban, C.D.; Shirkey, E.C. When Is a Correlation Matrix Appropriate for Factor Analysis? Some Decision Rules. *Psychol. Bull.* **1974**, *81*, 358. [[CrossRef](#)]
56. Dyer, D.D.; Keating, J.P. On the Determination of Critical Values for Bartlett’s Test. *J. Am. Stat. Assoc.* **1980**, *75*, 313–319. [[CrossRef](#)]
57. Li, Q.; Wang, S. A Simple Consistent Bootstrap Test for a Parametric Regression Function. *J. Econom.* **1998**, *87*, 145–165. [[CrossRef](#)]
58. Preacher, K.J.; Rucker, D.D.; Hayes, A.F. Addressing Moderated Mediation Hypotheses: Theory, Methods, and Prescriptions. *Multivar. Behav. Res.* **2007**, *42*, 185–227. [[CrossRef](#)]
59. Burnham, M.; Ma, Z. Climate Change Adaptation: Factors Influencing Chinese Smallholder Farmers’ Perceived Self-Efficacy and Adaptation Intent. *Reg. Environ. Change* **2016**, *17*, 171–186. [[CrossRef](#)]
60. Niles, M.T.; Brown, M.; Dynes, R. Farmer’s Intended and Actual Adoption of Climate Change Mitigation and Adaptation Strategies. *Clim. Change* **2015**, *135*, 277–295. [[CrossRef](#)]
61. Liu, H.; Zhou, Y. Farmers’ Cognition and Behavioral Response Towards Cultivated Land Quality Protection in Northeast China. *Sustainability* **2018**, *10*, 1905. [[CrossRef](#)]
62. Deng, W.; Zhang, S.; Zhou, P.; Peng, L.; Liu, Y.; Wan, J. Spatiotemporal Characteristics of Rural Labor Migration in China: Evidence from the Migration Stability under New-Type Urbanization. *Chin. Geogr. Sci.* **2020**, *30*, 749–764. [[CrossRef](#)]
63. Qi, W.; Yi, J. Spatial Pattern and Driving Factors of Migrants on the Qinghai-Tibet Plateau: Insights from Short-Distance and Long-Distance Population Migrants. *J. Geogr. Sci.* **2021**, *31*, 215–230. [[CrossRef](#)]
64. Shi, X.; Song, Z. The Silent Majority: Local Residents’ Environmental Behavior and Its Influencing Factors in Coal Mine Area. *J. Clean. Prod.* **2019**, *240*, 118275. [[CrossRef](#)]
65. Chen, J.; Yang, H. Geographical Mobility, Income, Life Satisfaction and Family Size Preferences: An Empirical Study on Rural Households in Shaanxi and Henan Provinces in China. *Soc. Indic. Res.* **2016**, *129*, 277–290. [[CrossRef](#)]

66. Raza, M.H.; Abid, M.; Yan, T.; Naqvi, S.A.A.; Akhtar, S.; Faisal, M. Understanding Farmers' Intentions to Adopt Sustainable Crop Residue Management Practices: A Structural Equation Modeling Approach. *J. Clean. Prod.* **2019**, *227*, 613–623. [[CrossRef](#)]
67. Manalo, J.A.; van de Fliert, E.; Fielding, K. Rice Farmers Adapting to Drought in the Philippines. *Int. J. Agric. Sustain.* **2020**, *18*, 594–605. [[CrossRef](#)]
68. Chen, X.; Hu, L.; Sindelar, J.L. Leaving Money on the Table? Suboptimal Enrollment in the New Social Pension Program in China. *J. Econ. Ageing* **2020**, *15*, 100233. [[CrossRef](#)] [[PubMed](#)]



Article

Eco-Efficiency and Its Drivers in Tourism Sectors with Respect to Carbon Emissions from the Supply Chain: An Integrated EEIO and DEA Approach

Bing Xia ¹, Suocheng Dong ^{1,2,*}, Zehong Li ^{1,2}, Minyan Zhao ³, Dongqi Sun ¹, Wenbiao Zhang ⁴ and Yu Li ^{1,2,*}

- ¹ Institute of Geographic Sciences and Natural Resources Research, Chinese Academy of Sciences, Beijing 100101, China; xiab.16b@igsnrr.ac.cn (B.X.); lizehong@igsnrr.ac.cn (Z.L.); sundq@igsnrr.ac.cn (D.S.)
² College of Resources and Environment, University of Chinese Academy of Sciences, Beijing 100049, China
³ Institute of Tibetan Plateau Research, Chinese Academy of Sciences, Beijing 100101, China; my.z@yeah.net
⁴ Beijing Academy of Social Sciences, 33 North Fourth Ring Middle Road, Chaoyang District, Beijing 100101, China; zhangwenbiaozwb@163.com
* Correspondence: dongsc3@163.com (S.D.); liy@igsnrr.ac.cn (Y.L.)

Abstract: Eco-efficiency analysis can provide useful information about sustainability in the tourism industry, which has an important role in both global economy recovery and Sustainable Development Goals (SDGs), generating considerable indirect carbon emissions with respect to the supply chain due to its significant connections to other industries. This study, from the perspective of tourism sectors, including tourism hotels, travel agencies, and scenic spots, integrated the environmentally extended input–output analysis (EEIO) and data envelopment analysis (DEA) models to develop a research framework, analyzing the indirect carbon emissions of the tourism supply chain, evaluating eco-efficiency with respect to both direct carbon emissions and total carbon emissions (including direct and indirect parts), and exploring the driving factors of eco-efficiency of tourism sectors using Tobit regression models. This study took Gansu as a case, a province in China characterized by higher carbon intensity, an underdeveloped economy, and rapid tourism growth. The results demonstrate that (1) tourism hotels contribute the most carbon emissions in tourism sectors, especially indirectly due to the supply chain, with carbon emissions mainly resulting from the manufacturing of food and tobacco; (2) the eco-efficiency of tourism sectors in Gansu presents a U-shaped curve, which is consistent with Kuznets’ theory; and (3) energy technology is key to improving the eco-efficiency of tourism sectors. The research results provide a clear path for the reduction of carbon emissions and the improvement of eco-efficiency in Gansu tourism sectors. Against the backdrop of global climate change and the post-COVID-19 era, our research framework and findings provide a reference for similar regions and countries who are in urgent need of rapid tourism development to effect economic recovery.

Citation: Xia, B.; Dong, S.; Li, Z.; Zhao, M.; Sun, D.; Zhang, W.; Li, Y. Eco-Efficiency and Its Drivers in Tourism Sectors with Respect to Carbon Emissions from the Supply Chain: An Integrated EEIO and DEA Approach. *Int. J. Environ. Res. Public Health* **2022**, *19*, 6951. <https://doi.org/10.3390/ijerph19116951>

Academic Editors: Francesco Nocera, Roberto Alonso González Lezcano and Rosa Giuseppina Caponetto

Received: 19 April 2022

Accepted: 2 June 2022

Published: 6 June 2022



Copyright: © 2022 by the authors. Licensee MDPI, Basel, Switzerland. This article is an open access article distributed under the terms and conditions of the Creative Commons Attribution (CC BY) license (<https://creativecommons.org/licenses/by/4.0/>).

Keywords: eco-efficiency; tourism sector; carbon emissions; supply chain; environmentally extended input–output analysis (EEIO); data envelopment analysis (DEA)

1. Introduction

Facing a post-COVID-19 era, tourism, which contributes over 10% to global economic growth [1], may play a significant role in economic recovery. However, over the past several years, the tourism industry has seen an increase in the consumption of natural resources and energy [2] as well as significant increases in carbon emissions and the disposal of other types of waste [3]. Because the tourism industry has an extremely complex input–output relationship and involves a large number of intermediate input sectors on its supply chain [4], some scholars have begun to use the input–output method to evaluate carbon emissions in the supply chain of tourism [5,6]; furthermore, scholars have found that global carbon emissions, including indirect emissions from the supply chain, are four times higher

than the direct carbon emissions of tourism [7]. At present, the input–output method based on supply chain is a popular tool in the evaluation of carbon emissions and carbon footprints, especially within economic sectors. The supply chain here refers to all the supply sectors of intermediate inputs needed in the production of goods and the provision of services [8]. For different tourism sectors, there is a wide range of related inputs, such as the intermediate input of tourism hotels, including the food and tobacco needed by catering services, the textile and furniture needed to provide accommodation services, and so on. Hence, assessing tourism carbon emissions from a supply chain perspective is necessary to provide a clear path for the reduction of carbon emissions against the backdrop of global climate change [9]. Some scholars have begun to focus on a more comprehensive accounting of carbon emissions. Sun [10] presents an environmentally extended input–output (EEIO) model to assess the distribution of tourism’s economic and carbon emission effects on bilateral travel between Taiwan and Japan. However, because the tourism industry plays a vital role in achieving all 17 SDGs, specifically, ending poverty (SDG 1), decent work and economic growth (SDG 8) [11], and responsible consumption and protection (SDG 12) [12], only assessing its carbon emissions is inherently biased [13,14], especially due to the urgent demand for economic recovery in the post-COVID-19 era. In sum, facing economic recovery and global carbon emission mitigation pressure, the tourism industry needs to focus on seeking more precise emission reduction objectives—tracking indirect carbon emission sources by using the input–output method, and, moreover, exploring driving factors that will improve the comprehensive benefits of the tourism economy and carbon emission mitigation. Therefore, it is important to comprehensively assess tourism’s dual impacts both on economic growth and global climate change in order to find a path to sustainable development.

Eco-efficiency analysis, as proposed by the World Business Council for Sustainable Development (WBCSD) [15], can provide useful information about the sustainability of the tourism industry. Eco-efficiency in the tourism industry is defined as determining the environmental ecology impact per unit of tourism value and developing a carbon dioxide assessment method [16]. The core concept of eco-efficiency is an optimization scheme, which is a path to achieving economic growth while mitigating the environmental impact of tourism [17]. Against the backdrop of global climate change, carbon emissions are usually selected as the environmental ecology indicator in order to analyze tourism eco-efficiency, combined with data envelopment analysis (DEA), which can include multi-input and -output indicators [17,18]. Pan (2021) calculated tourism carbon emission efficiency based on the super-efficiency Slacks Based Measure (SBM-DEA), which is defined as a compound system that consists of tourism carbon emissions, tourism economic development, and tourism regional innovation [19]. However, there is little existing research integrating EEIO and DEA to analyze the eco-efficiency of tourism using direct and indirect carbon emissions. Zha (2020) used the EEIO method to calculate the carbon emissions of tourism in China and used data envelopment analysis (DEA) to examine the sources of change in tourism CO₂ emissions [20]. However, in Zha’s paper, tourism was taken as a whole industry, despite the fact that the carbon emission process and the economic operation laws of different tourism sectors, such as hotels, tourism agencies, and scenic spots, are significantly different.

Based on the above tourism development background and relevant research progress, this research tries to fill the knowledge gaps with the following hypotheses. The first is in regard to Gansu province, where tourism is developing rapidly: What are the time trajectories and development differences between direct and indirect carbon emissions within different tourism sectors? The second considers the input–output relationship between different tourism sectors and other relevant economic sectors: What are the main sources of indirect carbon emissions? The third is considers the two scenarios of direct carbon emissions and total carbon emissions, including indirect carbon emissions: What is the evolutionary trajectory of eco-efficiency in different tourism sectors? The fourth is: What are the driving factors of eco-efficiency in the tourism sector under different carbon

emission scenarios? The innovations of this research are as follows: the first is integrating EEIO and DEA in order to analyze carbon emissions, including direct and indirect parts of the supply chain in different tourism sectors, and to fully consider their economic growth; the second is analyzing from the perspective of specific tourism sectors, including travel agencies, scenic spots, and hotels, which supply the most tourist production and services in China; the third is putting forward more targeted suggestions with respect to the main, indirect carbon emission contributors in the supply chain and the driving forces of eco-efficiency in specific tourism sectors.

This research built a widely used research framework for the comparative evaluation of carbon emissions and eco-efficiency in different sectors of tourism. It did so in order to apply scientific guidance to the targeting of carbon emission mitigation within the supply chain of various tourism sectors, while also keeping the economy growing as much as possible. The rest of this paper is organized as follows: Section 2 reviews the relevant literature and constructs the research framework, including the research boundary and roadmap and the study area; Section 3 discusses the research methods, including the model and data source; Section 4 presents the research findings, including results and analysis; Section 5 presents discussions and implementations; and conclusions are presented in Section 6.

2. Literature Review and Research Framework

2.1. Literature for Carbon Emissions Evaluation of Tourism

Against the backdrop of global climate change, carbon emissions from the tourism industry have become a hot topic in the increasing number of countries that are experiencing rapid tourism development [21,22], such as China [23], New Zealand [9], Portugal [24], Spain [25,26], Italy [27], Turkey [28], Brazil [29], and so on. Carbon emissions, including within direct and indirect parts of the supply chain, are a topic of discussion among many scholars, who sometimes also include carbon footprint within this subject by incorporating direct and indirect domestic and imported virtual carbon, which are required to satisfy the demand for products by different tourism consumers [30]. Carbon footprint is a part of the ecological footprint concept, which quantifies the consumption and occupation of the ecological environment by human society [31]. In this research, the concept of carbon emission is selected for the comparative analysis of tourism eco-efficiency, including with respect to direct carbon emissions and complete carbon emissions.

Carbon emission assessments are mainly based on a “top-down” perspective on the energy supply side [32] and a “bottom-up” perspective on the energy consumption side [33]. Research on carbon emissions in the tourism industry using the “bottom-up” approach focuses on the consumption side and assesses emissions by studying the energy consumption coefficient per unit of the output of various transportation modes [34], travel hotels [35], and tourist activities [36]. However, as tourism development is closely related to a range of economic sectors, including transportation, trade, food and beverage, and wholesale and retail, only measuring carbon emissions by assessing consumption in tourism will not enable researchers to understand the real situation with regard to tourism’s impact on climate change. Furthermore, using this approach entails a large amount of work, and it is difficult to conduct a timeseries analysis.

As EEIO accounts for interindustry connections, and considering the characteristics of input–output tables, as well as multiple timeseries [37,38], EEIO is an important tool for the assessment of carbon emissions [39,40]. This method has even more advantages in regard to assessing emissions in the tourism industry, and it is able to present a complete scope of direct and indirect greenhouse gas emissions [41]. The approach covers direct emissions produced by tourism sectors and all aspects of indirect effects throughout the supply chain within and outside the destination country [42]. There are three generally agreed upon views within carbon emissions research among existing scholars. First, the carbon emissions of tourism, including indirect carbon emissions, are higher than what is known, a subject that requires attention. Second, although the carbon emissions of tourism

are high, the industry brings great social and economic benefits; thus, it is necessary to explore the coordinated development model of tourism ecology and economy. Third, EEIO is considered to be an effective and comprehensive assessment method to measure carbon emissions in macro tourism sectors.

2.2. Literature for Eco-Efficiency Evaluation of Tourism

Separate carbon emission accounting of tourism sectors has limited policy support and practical guidance for the low-carbon development of the industry; e.g., studies have shown that holiday tourists have far higher carbon emissions than sightseeing tourists (due to increased accommodation emissions) [43], and another study showed that the carbon emissions of long-distance tourists are far higher than short-distance travelers due to increased traffic emissions [44]. However, from the perspective of the tourism economy, holiday tourists and long-distance tourists make more contributions to their destination's economy than sightseeing tourists and short-distance tourists. Therefore, research on tourism eco-efficiency based on carbon emissions has expanded into the field of tourism carbon emissions, and, furthermore, has become the hot spot of tourism eco-efficiency research.

Gossling proposed a way to measure the eco-efficiency of tourism based on carbon emissions [16]. He used a single ratio method to compare the eco-efficiency of tourist destinations in France, Amsterdam in Denmark, Seychelles, Siena in Italy, and the Rocky Mountain National Park in the United States, and he found that there were great differences in carbon emissions efficiency between different sectors of tourism. Besides the single ratio method [45], the indicator method [46] and data envelopment analysis (DEA) method have been widely applied to measure eco-efficiency [47], especially the undesirable output model of a slack-based model (undesirable-SBM) [48].

In the post-COVID-19 era and against the backdrop of aggravating global climate change, scholars have found that building prosperous and resilient low-carbon tourism needs a tool that can estimate the balance between economic benefits and eco-environmental impact [49], such as eco-efficiency [9]. A reduction in tourism carbon emissions is necessary in consideration of tourism's value to the economy and the SDGs, thus, formulate targeted policies will help coordinate economic growth and carbon emission reduction.

2.3. The Research Boundary of Carbon Emissions and the Eco-Efficiency of Tourism

Existing research on carbon emissions and the eco-efficiency of the tourism industry mainly treats the industry as a whole [7,16]. The tourism industry comprises sectors that provide various types of consumption to tourists [4]. Based on the definition of the World Tourism Organization of the United Nations (UNWTO), the tourism industry consists of five major sectors related to travel, including transportation, leisure and entertainment, accommodation, food and beverage, and travel agencies. The products and services supplied by each sector are significantly different. Thus, analyzing the carbon emissions and eco-efficiency of tourism as a whole makes it difficult to identify mechanisms for the reduction of carbon emissions and the improvement of eco-efficiency.

Scenic spots, hotels, and travel agencies—based on the operating and management data collected continuously by the statistics department of China's government [50]—are separate sectors and highly representative of the production and service processes of the tourism industry: Scenic spots are a spatial aggregation form of tourism attractions where tourist activities and carbon emissions occur [51,52]; as a sector that provides packaged tourism products and services, travel agencies almost represent the entire consumption process in tourism [53]; and accommodation and food and beverage services usually represent the most energy consumption and carbon emissions in the tourism industry [54], if not including traffic.

The above three tourism sectors differ significantly from each other in terms of their services, the mode in which they provide services and operate businesses, and their carbon emission processes. As such, this article focuses on scenic spots, hotels, and travel agencies as the main tourism sectors, comparing and analyzing their carbon emissions and eco-

efficiency, as well as the drivers of these three sectors in the comprehensive EEIO and DEA, in order to provide a reference and a research framework for tourism in similar regions.

2.4. The Research Framework

Based on the existing research, it has been found that direct carbon emission estimates obviously underestimate the carbon emissions of tourism. Input–output analysis can measure the carbon emissions of tourism, including the supply chain, and it can even overcome the heavy work of timeseries data due to bottom-up analysis. Furthermore, data envelopment analysis is a more comprehensive evaluation method of eco-efficiency, with multiple inputs and multiple outputs. In the post-COVID-19 era and against the backdrop of increasing global climate change, the study of carbon emissions in tourism is necessary to search for a coordinated development model, balancing carbon emissions and tourism’s economic benefits. Therefore, this article analyzes the eco-efficiency of tourism sectors with respect to direct carbon emissions and total carbon emissions, considering interindustry input–output relationships by integrating data envelopment analysis and input–output analysis. Moreover, considering the differences in economic operation laws and carbon emission paths among different sectors of tourism, this article focuses on the comparative analysis of direct carbon emissions and the indirect carbon emissions of tourism hotels, travel agencies, and scenic spots, as well as eco-efficiency and its drivers both with respect to direct and total carbon emissions.

The specific research framework is as follows (Figure 1):

Step 1: To calculate the direct and total carbon emissions of the three tourism sectors through input–output analysis.

Step 2: To analyze the main sources of indirect carbon emissions in the three tourism sectors through input–output analysis.

Step 3: To estimate eco-efficiency with respect to direct and total carbon emissions in the three tourism sectors through the use of DEA.

Step 4: To reveal the main drivers of the three tourism sectors through the Tobit timeseries regression model.

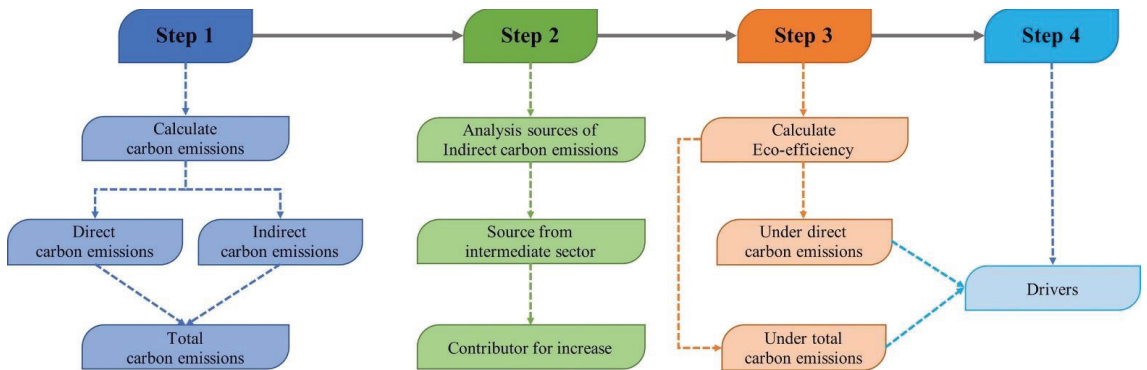


Figure 1. Research framework.

2.5. Study Area

Gansu Province is located in northwest China, where the Mongolian Plateau meets the Qinghai–Tibet Plateau (Figure 2), and is vulnerable to climate change [55]. This area was the core of the ancient Silk Road. The marginalized, transitional geographic location bestows the province with abundant, diversified natural attractions and a cultural heritage that constitute significant, innate advantages for tourism development. In 2012, high-speed train services became available in Gansu, triggering a massive surge in tourism development. From 1997 to 2016, the average growth in total tourism revenue in the province ranked first in China (Figure 2). Tourism has become a new industry that drives regional economic

growth and green development in Gansu, a province that traditionally relied on resources for its economy. Wang et al. (2019) estimated the carbon emissions of each province’s tourism industry between 2001 and 2016 and found that tourism in Gansu generated the highest carbon intensity level across China [56]. Therefore, as a typical province where the tourism industry is facing the dual pressures of economic growth and climate change, Gansu is illustrative for tourism sectors exploring a path to low-carbon, green development with respect to carbon emissions constraints. Herein, tourism hotels, travel agencies, and scenic spots in Gansu Province are taken as study subjects in order to be references to inform the low-carbon development of the tourism industry under the dual pressures of economic recovery and carbon emission reduction.

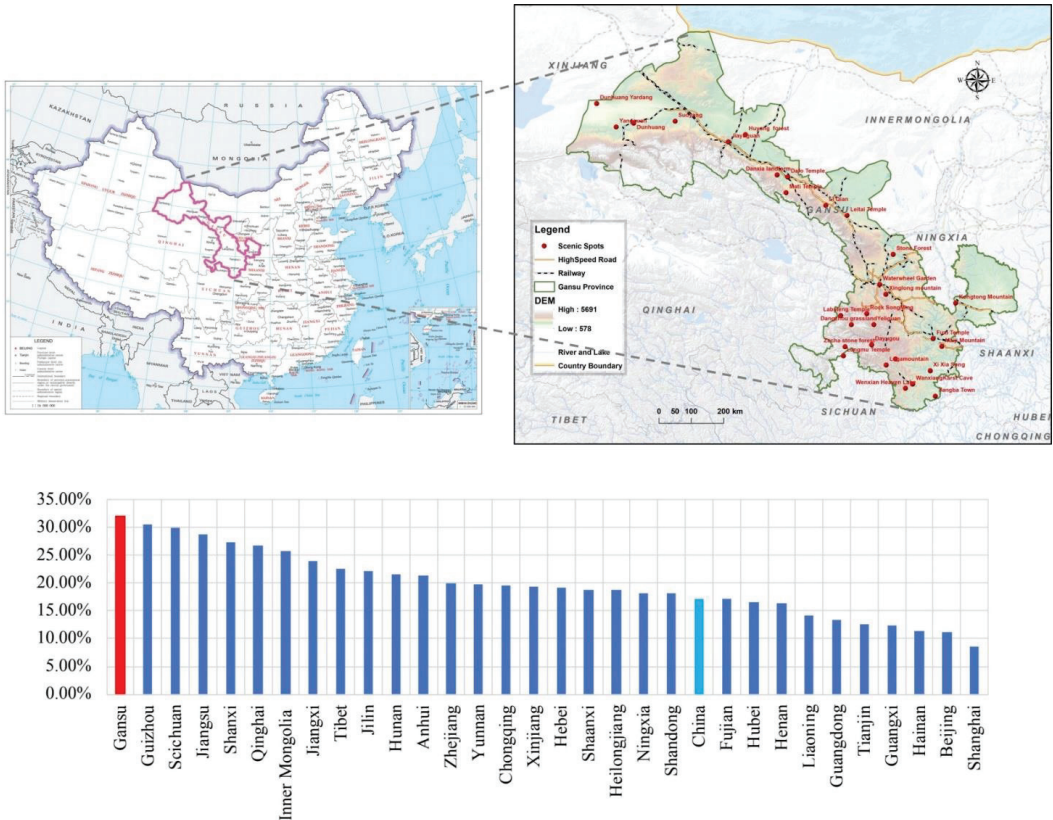


Figure 2. Study area and its economic growth with respect to the tourism industry from 1997 to 2016.

3. Methods

3.1. Calculation of Direct Carbon Emissions

The calculation of direct carbon emissions in tourism sectors is mainly based on the standards set by the Intergovernmental Panel on Climate Change (IPCC). Under these standards, emissions are calculated based on each sector’s revenue and energy emission coefficient, as follows:

$$\eta^{th} = \frac{\sum_{k=1}^r \delta_k \times EC_k^{ac}}{I_{ac}} \quad (1)$$

$$\eta^{ta} = \frac{\sum_{k=1}^r \delta_k \times EC_k^{os}}{I_{os}} \quad (2)$$

$$\eta^{ts} = \frac{\sum_{k=1}^r \delta_k \times EC_k^{os}}{I^{os}} \tag{3}$$

where η^{th} , η^{ta} and η^{ts} denote the energy emission coefficient of hotels, travel agencies, and scenic spots, respectively; δ_k is the total consumption of energy k in Gansu Province ($k = 1, 2, \dots, r$); EC_k^{os} and EC_k^{ac} represent the total consumption of energy k by other economic sectors and the food and beverage sector in Gansu, respectively; and I^{ac} and I^{os} denote the value added from other economic sectors and the food and beverage sector, respectively. Direct carbon emissions of hotels are calculated as follows:

$$CE_{direct}^{th} = \mu \times \eta^{th} \times TR^{th} \tag{4}$$

$$CE_{direct}^{ta} = \mu \times \eta^{ta} \times TR^{ta} \tag{5}$$

$$CE_{direct}^{ts} = \mu \times \eta^{ts} \times TR^{ts} \tag{6}$$

where CE_{direct}^{th} , CE_{direct}^{ta} , and CE_{direct}^{ts} represent the direct carbon emissions of hotels, travel agencies, and scenic spots, respectively, and TR^{th} , TR^{ta} , and TR^{ts} denote the total revenue of hotels, travel agencies, and scenic spots, respectively.

3.2. Calculation of the Total Carbon Emissions of Tourism Sectors Based on EEIO

The structure of the input–output tables for Gansu Province for the years 1997, 2002, 2007, and 2012 is presented in Table 1. The second quadrant where the background is yellow and z^{ij} is denoted represents intermediate inputs and outputs; the first quadrant where the background is blue and f^i is denoted represents final use; and the third quadrant where the background is green l^j is denoted represents value added. The column in red where z^{1j} to z^{nj} are denoted represents the supply chain of sector j (S_j). Specifically, the input–output table includes n production sectors; f^i denotes the final use of sector i ; X^i denotes the total output of sector i ; l^j denotes the value added of sector j ; and Y^j denotes the total input of sector j .

Table 1. Input–output table.

F	Intermediate Use						Final Use	Total Output
	Industrial Sector	S1	...	Sj	...	Sn		
Intermediate input	IS1	z^{11}	...	z^{1j}	...	z^{1n}	f^1	x^1
	⋮	⋮	...	⋮	...	⋮
	ISi	z^{i1}	...	z^{ij}	...	z^{in}	f^i	x^i
	⋮	⋮	...	⋮	...	⋮
	ISn	z^{n1}	...	z^{nj}	...	z^{nn}	f^n	x^n
Value added		l^1	...	l^j	...	l^n		
Total input		x^{1j}	...	x^{jj}	...	x^{jn}		

Note: The part of table in yellow denotes intermediate inputs and outputs, the part of table in blue denotes final use, the part of table in green denotes value added, and the column in red border denotes supply chain.

Within the study period, hotels, travel agencies, and scenic spots belong to different sectors in the input–output table. The proportions that the operating revenues of the above key sectors account for in final use are used to calculate the intermediate use of other sectors using these three sectors, as well as the intermediate input of these three sectors into other sectors. Tourism sector supply chains are represented by the column vectors $z^{i\sim th}$, $z^{i\sim ta}$, and $z^{i\sim ts}$, and can be calculated as follows:

$$z^{i\sim th} = \frac{TR^{th}}{f^{ac}} z^{i\sim ac} \tag{7}$$

$$z^{i\sim ta} = \frac{TR^{ta}}{f^{os}} z^{i\sim os} \tag{8}$$

$$z^{i\sim ts} = \frac{TR^{ts}}{f^{os}} z^{i\sim os} \tag{9}$$

where $z^{i\sim th}$, $z^{i\sim ta}$, and $z^{i\sim ts}$ represent the intermediate use of sector j by sector i in hotels, travel agencies, and scenic spots, respectively; $z^{i\sim ac}$ denotes the intermediate use of sector i by the food and beverage sector, to which hotels belong in the input–output table; $z^{i\sim os}$ denotes the intermediate use of sector i by “other sectors,” to which travel agencies and scenic spots belong in the input–output table; and f^{ac} and f^{os} denote final use of the food and beverage sector and “other sectors.” The intermediate inputs made by hotels, travel agencies, and scenic spots into sector j , and the value added for each sector is obtained in the same manner. The tourism supply chain is column vector $z^{i\sim th}$.

Data for input–output tables are only prepared every five years. To obtain continuous data, based on total carbon emissions calculations, the existing input–output tables were consolidated in accordance with the classification of value added for industries prepared by the National Bureau of Statistics of China.

Based on the input–output tables, the relationship between the total economic output and the total amount of final use can be derived:

$$X = (I - A)^{-1}Y \tag{10}$$

where X denotes the total output matrix of all sectors; Y denotes the final use matrix of all sectors; A denotes the direct consumption coefficient matrix of all sectors; and $(I - A)^{-1}$ is the Leontief inverse matrix.

By replacing Y with the value added matrix denoted by L and transposing the Leontief inverse matrix, the right side of the equation represents the total input for producing a product.

$$X = [(I - A)^{-1}]^T L \tag{11}$$

Let L be the value added matrix of all sectors in a given year; then, X is a $1 \times n'$ matrix, where n' denotes the total number of sectors in the input–output tables. Each of the three tourism sectors—tourism hotels, travel agencies, and scenic spots—belongs to one line in the equation and is denoted by X_i^{th} , X_i^{ta} , and X_i^{ts} , respectively. Total carbon emissions, including indirect emissions by star-rated hotels, travel agencies, and scenic spots, which are denoted by CE_{total}^{th} , CE_{total}^{ta} , and CE_{total}^{ts} , respectively, are calculated as follows:

$$CE_{total}^{th} = \mu \times \eta^{th} \times X^{th} \tag{12}$$

$$CE_{total}^{ta} = \mu \times \eta^{ta} \times X^{ta} \tag{13}$$

$$CE_{total}^{ts} = \mu \times \eta^{ts} \times X^{ts} \tag{14}$$

3.3. Calculation of Indirect Carbon Emissions of Tourism Sectors

According to the input–output tables for 1997 and 2012, the indirect carbon emissions of each sector from other supply chain sectors are calculated according to input proportion. The indirect carbon emissions of each sector are calculated according to the input proportion.

$$CE^{i\sim th} = (CE_{total}^{th} - CE_{direct}^{th}) \times \frac{z^{i\sim th}}{j} \tag{15}$$

$$CE^{i\sim ta} = (CE_{total}^{ta} - CE_{direct}^{ta}) \times \frac{z^{i\sim ta}}{j} \tag{16}$$

$$CE^{i\sim ts} = (CE_{total}^{ts} - CE_{direct}^{ts}) \times \frac{z^{i\sim ts}}{j} \tag{17}$$

3.4. Assessment of the Eco-Efficiency of Tourism Sectors of Gansu Province

DEA has distinct advantages in sustainable development assessments and has been a popular tool in recent years for analyzing eco-efficiency [57]. We built a slack-based measure (SBM) model that includes undesirable outputs [58] in order to estimate the annual eco-efficiency of each sector in Gansu’s tourism industry between 1997 and 2016, and using each sector in each year of this period as a decision-making unit, relative efficiency analysis was performed. Each decision-making unit includes three vectors—input, desirable output, and undesired output—and they are denoted as $xx \in R^p$, $yy^g \in R^{s_1}$, and $yy^b \in R^{s_2}$, respectively. Matrices W , W^g , and W^b are defined as follows: $[XX] = [x_1, \dots, x_q]^T \in R^{p \times q}$, $[Y Y^g] = [yy_1^g, \dots, yy_q^g]^T \in R^{s_1 \times q}$, and $[Y Y^b] = [yy_1^b, \dots, yy_q^b]^T \in R^{s_2 \times q}$, where $XX > 0$, $Y Y^g > 0$, and $Y Y^b > 0$. The production possibility set P is defined as $P = \left\{ (xx, yy^g, yy^b) \mid xx \geq XX\lambda, yy^g \leq Y Y^g \lambda, yy^b \geq Y Y^b \lambda, \lambda \geq 0 \right\}$. The undesirable-SBM model, which varies with returns to scale, is expressed as follows [59]:

$$\begin{aligned}
 EE = \min & \frac{1 - \frac{1}{p} \sum_{d=1}^p \frac{s_i^-}{xx_{i0}}}{1 + \frac{1}{s_1 + s_2} \left[\sum_{r=1}^{s_1} \frac{s_r^g}{yy_{r0}^g} + \sum_{r=1}^{s_2} \frac{s_r^b}{yy_{r0}^b} \right]} \\
 \text{St. } & x_0 = XX\lambda + s^- \\
 & yy_0^g = Y Y^g \lambda - s^g \\
 & yy_0^b = Y Y^b \lambda + s^b \\
 & \lambda \geq 0, s^- \geq 0, s^g \geq 0, s^b \geq 0
 \end{aligned} \tag{18}$$

where s denotes the input and output slack variables and λ is the intensity vector. The objective function, EE , strictly decreases with $s^- \in R^p$, $s^g \in R^{s_1}$, and $s^b \in R^{s_2}$ and $0 \leq EE \leq 1$.

3.5. Input–Output Indicators for Eco-Efficiency Assessments Based on Carbon Emissions

In a traditional economic system, such as in the Cobb–Douglas production function, the input productive factors mainly include labor and capital. As such, in this article, the number of employees, original cost of fixed assets, and operating revenue are taken as the input–output indicators for the economic system, and the direct and total carbon emissions are taken as the undesirable output in order to measure the ecology and climate change impact of tourism sectors (Table 2).

Table 2. Input–output indicators for assessing the eco-efficiency of tourism sectors in Gansu Province based on carbon emissions.

	Indicator	Data Source	Unit
Input	Number of employees	Yearbook of China Tourism Statistics	Count
	Original cost of fixed assets	Yearbook of China Tourism Statistics	10,000 Yuan
Output	Operating revenue	Yearbook of China Tourism Statistics	10,000 Yuan
Undesirable output	Direct carbon emissions/Total carbon emissions	Calculation	10,000 tons

3.6. Analysis of Drivers

The Tobit regression model is proposed by Tobin [60]. It belongs to a regression model with limited dependent variables. It can solve the problem of modeling restricted or truncated dependent variables. The Tobit model has been widely used to investigate the influencing factors of eco-efficiency. Because eco-efficiency evaluated by undesirable-SBM always has a value from 0 to 1, it is not suitable to use ordinary least squares (OLS) for coefficient estimation [61]. Therefore, we selected a timeseries Tobit regression model to identify the driving factors of tourism sector eco-efficiency in Gansu. The model expression is as follows [62]:

$$\begin{aligned}
 ee_t^* &= \alpha zz_t + \varepsilon_t \\
 ee_t &= \begin{cases} ee_t^*, & ee_t^* \geq 0 \\ 0, & ee_t^* \leq 0 \end{cases} \quad t = 1, \dots, NN \\
 \varepsilon_t &\sim NN(0, \sigma^2)
 \end{aligned} \tag{19}$$

where t denotes the year, zz_t is an independent variable, α is a regression coefficient, and ε_t represents a disturbance term.

For eco-economic theory and existing research, industry scale, capita, structure, and low-carbon technology are the main factors that influence the eco-efficiency [63]. Based on the existing research and the characteristics of the tourism sectors of Gansu, indicators that measure scale effect, structure effect, capital effect, and technological effect were selected for econometric regression analysis, and the drivers of tourism sector eco-efficiency were explored.

Scale effect: In the tourism economic system, according to the theory of returns to scale, with an increase in tourist reception, the production scale continues to expand, and the marginal cost may also decrease [64]. Therefore, the scale effect can improve the eco-efficiency of tourism sectors throughout the economic system. With rapid tourist reception expansion, however, a decline in tourism sectors in Gansu with respect to the marginal production costs, driven by scale effect, may not be able to offset rapidly increasing carbon emissions and eco-environmental pressure. Therefore, further discussion is needed via the regression model. The scale effect is presented by each sector's total revenue from tourism and the number of tourists served; the indicators in this category include the revenue of star-rated hotels (HTI), revenue of travel agencies (TTI), revenue of scenic spots (STI), number of guests served by star-rated hotels (HTP), number of tourists served by travel agencies (TTP), and number of visitors to scenic spots (STP).

Structure effect: The optimization of industrial structure can reduce the consumption of resources and energy, improve energy utilization efficiency, reduce carbon emissions, and promote the stability and coordination of the ecological economic system [65]. With the tourism industry structure changed, new linkages will be established between tourism sectors, which might affect carbon emission levels and the eco-efficiency of each sector. As such, in this article, the structure effect is mainly measured by the proportion that each sector's revenue accounts for in the total revenue among the three tourism sectors, including the proportion of the revenue of star-rated hotels (HS), the proportion of travel agency revenue (TS), and the proportion of scenic spot revenue (SS).

Capital effect: As an economic system, the impact of capital input on tourism economic growth is apparent. However, the impact of capital input on the eco-efficiency, or even production efficiency, of tourism is not clear [66]. Whether higher capital input could improve tourism eco-efficiency needs to be further verified. The capital-driven effect is mainly measured using capital input per unit of tourism revenue. This article chooses the original value of fixed capital per unit income in its analysis in order to measure the capital-driven effects of capital investments. The indicators for star-rated hotels, travel agencies, and scenic spots are HRI, TRI, and SRI, respectively.

Technological effect: Low-carbon technology can improve the eco-efficiency of tourism by reducing carbon emissions. The energy efficiency can reflect the carbon efficiency, and

it has been a key index to measure low-carbon technology [67]. The technology effect is mainly measured with energy input per unit of tourism revenue in this article. The indicators for star-rated hotels, travel agencies, and scenic spots are as follows: HEI, TEI, and SEI, respectively.

Meanwhile, based on the drivers of eco-efficiency in the industry, this article selects GDP [68], industry structure [65], urbanization [69], civilization [70], open policy [71], and traffic conditions [72] as control variables outside the tourism eco-economic system. The above control variables are represented by per GDP (PGDP), proportion of tertiary industry (THI), proportion of urban population (UR), number of students in colleges and universities (ED), total investment of foreign enterprises (FR), and road mileage (RO), respectively.

The driver analysis examines direct carbon emission eco-efficiency (HDE, TDE, and SDE) and total carbon emission eco-efficiency (THE, TTE, and STE) for each tourism sector. To avoid data issues brought about by variables of different dimensions, and to reduce the heteroscedasticity of variables and enhance data stability, except for ratios and data results less than 1, all other data are taken as their logarithm. The revenue of each sector is adjusted for inflation based on the consumer price index of Gansu Province, with 1997 being the base year. An ADF unit root test was performed for each variable, and differential processing was performed for variables that did not pass the unit root test. Tobit regression was then conducted based on the processed data. The description of variables is motioned above in Table 3.

Table 3. Description of variables for the analysis of the drivers of tourism sector eco-efficiency in Gansu Province.

Variable	Mean	Standard Deviation	Minimum	Maximum
HDE	0.7936	0.1882	0.3619	1.0000
HTE	0.6014	0.2972	0.2581	1.0000
HS	0.5755	0.0990	0.3243	0.8449
HEI	0.3139	0.0561	0.2464	0.4089
lnHTI	11.5222	0.5330	10.4293	12.1225
lnHTP	9.8961	0.5825	8.7744	10.4335
lnHRI	1.1084	0.3276	0.0000	1.5056
TDE	0.6592	0.2500	0.3227	1.0000
TTE	0.5870	0.2556	0.2835	1.0000
TS	0.2691	0.0631	0.0873	0.3545
TEI	0.2310	0.0419	0.1704	0.3016
lnTTI	10.7397	0.5922	9.5321	11.5509
lnTTP	13.3644	0.5396	12.1093	14.1544
TRI	0.9485	1.2501	0.0680	6.0133
SDE	0.7771	0.2777	0.2175	1.0000
STE	0.6993	0.3128	0.1977	1.0000
SS	0.1554	0.0981	0.0536	0.4709
SEI	0.2310	0.0419	0.1704	0.3016
lnSTI	10.0833	0.9741	8.6770	12.3838
lnSTP	16.3363	1.2287	14.6281	18.3264
SRI	3.2302	2.0131	0.5775	8.1709
lnPGDP	9.0238	0.6053	8.0706	9.8162
THI	0.4075	0.0417	0.3347	0.5141
UR	0.3177	0.0789	0.1839	0.4467
lnED	3.0698	0.7644	1.6233	3.8225
lnRO	1.9817	0.5917	1.2698	2.6603
lnFR	8.1080	0.7943	5.4972	8.9434

Based on the above analyses and assumptions, eco-efficiency models under the direct carbon emission scenario and total carbon emission scenario are constructed for star-rated hotels, travel agencies, and scenic spots as follows:

Model 1: Regression model for the eco-efficiency of star-rated hotels:

$$HDE = \alpha_{10} + \alpha_{11}HS + \alpha_{12}HEI + \alpha_{13}\lnHTI + \alpha_{14}\lnHTP + \alpha_{15}\lnHRI + \alpha_{16}\lnPGDP_{\text{control}} + \alpha_{17}THI_{\text{control}} + \alpha_{18}UR_{\text{control}} + \alpha_{19}\lnED_{\text{control}} + \alpha_{110}\lnRO_{\text{control}} + \alpha_{111}\lnFR_{\text{control}} + \varepsilon \quad (20)$$

Model 2: Regression model for the eco-efficiency of star-rated hotels with respect to the direct carbon emission scenario:

$$HTE = \alpha_{20} + \alpha_{21}HS + \alpha_{22}HEI + \alpha_{23}\lnHTI + \alpha_{24}\lnHTP + \alpha_{25}\lnHRI + \alpha_{26}\lnPGDP_{\text{control}} + \alpha_{27}THI_{\text{control}} + \alpha_{28}UR_{\text{control}} + \alpha_{29}\lnED_{\text{control}} + \alpha_{210}\lnRO_{\text{control}} + \alpha_{211}\lnFR_{\text{control}} + \varepsilon \quad (21)$$

Model 3: Regression model for the eco-efficiency of travel agencies:

$$TDE = \alpha_{30} + \alpha_{31}TS + \alpha_{32}TEI + \alpha_{33}\lnTTI + \alpha_{34}\lnTTP + \alpha_{35}TRI + \alpha_{36}\lnPGDP_{\text{control}} + \alpha_{37}THI_{\text{control}} + \alpha_{38}UR_{\text{control}} + \alpha_{39}\lnED_{\text{control}} + \alpha_{310}\lnRO_{\text{control}} + \alpha_{311}\lnFR_{\text{control}} + \varepsilon \quad (22)$$

Model 4: Regression model for the eco-efficiency of travel agencies with respect to the direct carbon emission scenario:

$$TTE = \alpha_{40} + \alpha_{41}TS + \alpha_{42}TEI + \alpha_{43}\lnTTI + \alpha_{44}\lnTTP + \alpha_{45}TRI + \alpha_{46}\lnPGDP_{\text{control}} + \alpha_{47}THI_{\text{control}} + \alpha_{48}UR_{\text{control}} + \alpha_{49}\lnED_{\text{control}} + \alpha_{410}\lnRO_{\text{control}} + \alpha_{411}\lnFR_{\text{control}} + \varepsilon \quad (23)$$

Model 5: Regression model for the eco-efficiency of tourist agencies:

$$SDE = \alpha_{50} + \alpha_{51}SS + \alpha_{52}SEI + \alpha_{53}\lnSTI + \alpha_{54}\lnSTP + \alpha_{55}SRI + \alpha_{56}\lnPGDP_{\text{control}} + \alpha_{57}THI_{\text{control}} + \alpha_{58}UR_{\text{control}} + \alpha_{59}\lnED_{\text{control}} + \alpha_{510}\lnRO_{\text{control}} + \alpha_{511}\lnFR_{\text{control}} + \varepsilon \quad (24)$$

Model 6: Regression model for the eco-efficiency of scenic spots with respect to the direct carbon emission scenario:

$$STE = \alpha_{60} + \alpha_{61}SS + \alpha_{62}SEI + \alpha_{63}\lnSTI + \alpha_{64}\lnSTP + \alpha_{65}SRI + \alpha_{66}\lnPGDP_{\text{control}} + \alpha_{67}THI_{\text{control}} + \alpha_{68}UR_{\text{control}} + \alpha_{69}\lnED_{\text{control}} + \alpha_{610}\lnRO_{\text{control}} + \alpha_{611}\lnFR_{\text{control}} + \varepsilon \quad (25)$$

3.7. Data Sources

Data on the number of employees, original cost of fixed assets, operating revenue, and number of tourists receipted were obtained from the Yearbook of China Tourism Statistics. The input–output data for calculating total carbon emissions were obtained from input–output tables in the Statistical Yearbook of Gansu Province for the years 1997, 2002, 2007, and 2012. Data on the value added by industry for each year were obtained from the Statistical Yearbook of Gansu Province for the years 1997 to 2017. Per GDP, proportion of tertiary industry, proportion of urban population, number of students in colleges and universities, total investment of foreign enterprises, and road mileage were obtained from the Statistical Yearbook of Gansu Province from 1998 to 2017. Fixed assets, operating revenue, per GDP, and total investment of foreign enterprises were all adjusted for inflation based on the consumer price index of Gansu Province, with 1997 being the base year.

4. Results and Discussion

4.1. The Carbon Emissions of Tourism Sectors' in Gansu Province

The total carbon emissions of the three tourism sectors in Gansu increased from 50.6 kilotons in 1997 to 229 kilotons in 2016, with an average growth of 18.25%, a little higher than that of the 16.01% in China's tourism industry, as evaluated by Zha [73]. The

indirect part of carbon emissions increased from 55.7 kilotons in 1997 to 173.3 kilotons in 2016. Indirect carbon emissions account for 65.9% of total carbon emissions, an increase of 1.93 times more due to direct carbon emissions from tourism industry in 2016. The average ratio of indirect emissions within total carbon emissions has similarities to data in related research. This ratio was 57.5%, 64%, and 52% in China [74], New Zealand [75] and Australia [76], respectively. The growth of indirect emissions was faster than that of direct emissions. The carbon emissions of tourism hotels in Gansu were more than travel agencies and scenic spots; this result is consistent with the situation in China [74] and globally [7]. By 2016, the amount of indirect carbon emissions from tourism hotels was 6.13 times and 14.54 times those of travel agencies and scenic spots, respectively. Scenic spots saw relatively fast growth in direct emissions, slightly higher than those of tourism hotels and travel agencies (Figure 3).

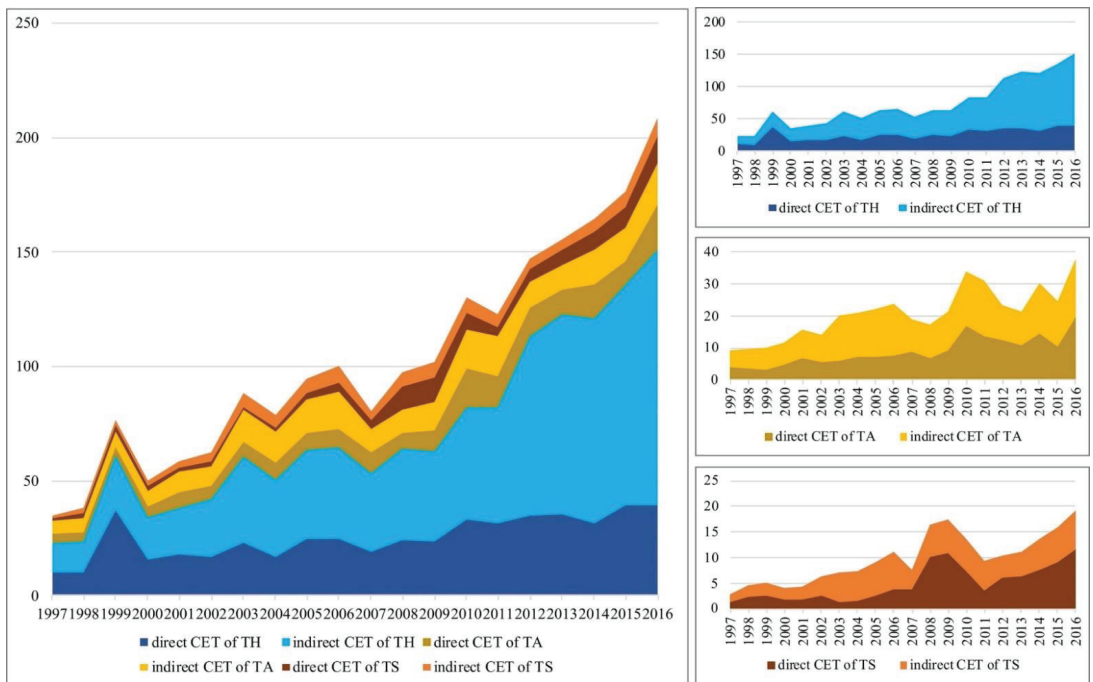


Figure 3. Carbon emissions of tourism sectors in Gansu Province during the 1997–2016 period.

Indirect carbon emissions from tourism hotels grew rapidly during the 1997–2016 period. The evolution of the composition of carbon emissions indicates that a growing number of emissions from tourism hotels were indirect emissions caused by related industries, and that incremental emissions mainly stemmed from intermediate production steps (Figure 3, top right). From 1997 to 2016, the direct carbon emissions of tourism hotels in Gansu increased from 10,200 tons to 39,500 tons, representing an annual growth of 7.4%, which was lower than the average rate of the economic growth (operating revenue), similar to that of Chinese accommodation and food in general with 7.5% [74]. From 1997 to 2016, indirect carbon emissions increased from 13,100 tons to 111,600 tons, representing a growth of 8.5 times across the period, with an annual increase of 11.3%, which was higher than that of China’s general increase of 7.5% [74]. The proportion of indirect carbon emissions from tourism hotels in the total indirect carbon emissions increased from 57.19% in 1997 to 73.84% in 2016. Although carbon emissions from tourism hotels with respect to providing final products did not increase substantially during the study period, emissions from intermediate inputs and outputs increased significantly. In 1997, Gansu Province had 38 tourism

hotels, increasing to 299 as of 2016, six times more than it had in 1997. The scale growth was fast during this period. However, the development of higher tourism hotels was slow. As of 2016, Gansu only had three five-star hotels, and they were all in the provincial capital city of Lanzhou. The lagging development of high-standard hotels may be a main factor leading to high carbon emissions from tourism hotels in Gansu. The high indirect carbon emissions indicate that industries related to hotels had high carbon emissions, and that this phenomenon was related to low-carbon and energy efficiency in Gansu Province being backward [77]. In summary, there is considerable room for hotels and related industries in Gansu to reduce carbon emissions, and there is also a need to comprehensively regulate related industries.

Both direct and indirect carbon emissions from travel agencies in Gansu Province were high and showed a fluctuating pattern. Direct carbon emissions increased from 4000 tons in 1997 to 19,900 tons in 2016, representing an annual growth of 8.8%, which was higher than the annual growth rate of direct carbon emissions from tourism hotels. Indirect carbon emissions increased from 5100 tons in 1997 to 18,100 tons in 2016, an annual increase of 6.5%; this growth was lower than that of the direct emissions of travel agencies and far below the annual growth in the indirect emissions of tourism hotels. The contribution of indirect emissions to the total emissions of travel agencies declined annually. The impact of intermediate production steps on carbon emissions decreased annually, and carbon emissions were increasingly attributed to the production of final products (Figure 3, middle right). Travel agencies in Gansu lagged in terms of developing online services, and they focused on employing traditional offline sale channels to promote local tourist routes. This led to considerably more tourism activities related to traveling to other provinces or countries than those involving coming to Gansu. Therefore, Gansu's travel agencies did not have a high demand for other related industries locally, and they did not require significant local input in their operations. As a result, the carbon emissions of travel agencies via intermediate production steps were not high.

The total carbon emissions of scenic spots were lower than those of tourism hotels and travel agencies, but the growth rate was far above those for the other two sectors, especially with respect to direct carbon emissions. Direct carbon emissions from scenic spots increased from 1200 tons in 1997 to 11,700 tons in 2016, with an annual growth rate of 12.7%. The total carbon emissions of scenic spots increased from 2800 tons in 1997 to 19,400 tons in 2016, representing an annual growth rate of 10.7%. The direct and indirect carbon emissions were both higher than sightseeing carbon emissions in China from 2002 to 2010, with 3.8% and 3%, respectively [74]. In terms of the evolutionary trajectory, carbon emissions from scenic spots peaked in 2008 and 2009 and increased rapidly again in recent years. This was correlated with a significant increase in the number of visitors to Gansu's scenic spots as a result of the development of major scenic spots and high-speed train services; it is also an indication that there was a stronger correlation between the level of carbon emissions and the scale of the tourism industry in the development of scenic spots than in the development of tourism hotels or travel agencies (Figure 3, bottom right). Gansu has few large-scale, high-quality, national scenic spots (e.g., 5A attractions). Coordinated development between scenic spots and other industries is also low. As a result, scenic spots have low indirect carbon emissions. The continuous, rapid increase in direct emissions indicates that, currently, the final products and services of Gansu's scenic spots are provided to visitors without low-carbon technology. In comparison to vacation-oriented tourist destinations that have a strong supply chain effect, for example, Jamaica [8], sightseeing is the major tourist activity in Gansu, and few visitors stay overnight. With the rapid increase in the number of visitors, scenic spots in Gansu had not developed an economic influence on the surrounding regions, and their connections with other industries are weak; this explains why these scenic spots had low indirect emissions but a rapid growth in direct emissions.

4.2. The Sources of Indirect Carbon Emissions from the Supply Chain of Tourism Sectors

Via Equations (15)–(17), the sources of indirect carbon emissions can be obtained. The manufacturing of food and tobacco was the main source of the indirect carbon emissions of tourism hotels in Gansu; furthermore, the contribution of renting, leasing, and business services to the indirect carbon emissions of tourism hotels has increased more obviously in recent years, and they have become the main contribution sectors to the increase in indirect carbon emissions from tourism hotels in Gansu. In 2007, the main source of indirect carbon emissions from tourism hotels in Gansu was from the manufacturing of food and tobacco, accounting for 50%. In 2012, the main source of indirect carbon emissions from tourism hotels was the manufacturing of foods and tobacco, accounting for 34.5% (Figure 4a). From 2007 to 2012, the contribution of indirect carbon emissions from tourism hotels in Gansu mainly came from renting, leasing, and business services; the manufacturing of foods and tobacco; wholesale; retail trade; catering; agriculture; forestry; animal husbandry and fishery; and supplying electric and heat power, contributing increments of 10.1, 9.8, 8.1, 5.4, and 2.5 kilotons, respectively (Figure 4d).

Metal products were the main source of the indirect carbon emissions of travel agencies in Gansu. The contribution of finance has increased in recent years, which became the main contribution sector with respect to the increase in the carbon emissions of travel agencies in Gansu. In 2007, the main source of indirect carbon emissions from travel agencies in Gansu was metal products, accounting for 23.8%. In 2012, the main source of indirect carbon emissions from Gansu travel agencies was metal products, accounting for 31.7% (Figure 4b). From 2007 to 2012, the contribution to the increase in carbon emissions from travel agencies in Gansu mainly came from finance, metal products, wholesale, retail trade, catering, agriculture, forestry, animal husbandry and fishery, and the supplying of water, contributing increments of 1.1 kilotons, 1 kilotons, 0.9 kilotons, 0.8 kilotons, and 0.3 kilotons of indirect carbon emission, respectively (Figure 4e).

Agriculture, forestry, animal husbandry and fishery, and supplying electric and heat power were the main sources of indirect carbon emissions from scenic areas in Gansu, and carbon emissions from supplying electric and heat power have increased obviously in recent years, and have become the main contribution sector with respect to the increase in carbon emissions from scenic areas in Gansu. In 2007, the main sources of indirect carbon emissions in scenic spots in Gansu were agriculture, forestry, and animal husbandry and fishery, accounting for 25%. In 2012, the main source of indirect carbon emissions from scenic spots in Gansu was from supplying electric and heat power, accounting for 30% (Figure 4c). For the years 2007–2012, the indirect carbon emissions increased in Gansu scenic spots mainly due to supplying electric and heat power; household services, repair and other services; renting, leasing, and business services; and other manufacturing industries, transportation, storage, and post, contributing increments of 1.2, 0.3, 0.2, 0.1, and 0.1 kilotons, respectively (Figure 4f).

4.3. Analysis of the Eco-Efficiency of Tourism Sectors in Gansu

During the study period, with the increase in revenue, the eco-efficiency of tourism sectors in Gansu demonstrated a U-shaped development pattern in which eco-efficiency first decreased and then increased. This pattern coincides with the environmental Kuznets curve theory [18]. Some scholars have also found similar results between tourism development and environmental impact [18,78], or in the eco-efficiency of urban [79] and regional [80] development. Considering both the direct carbon emission and total emission scenarios, the ranking of the eco-efficiency of the three sectors is as follows: tourism hotels > travel agencies > scenic spots. The eco-efficiency of these tourism sectors entered an evident trough period from 2002 to 2006. Between 2007 and 2011, the eco-efficiency of tourism hotels, travel agencies, and scenic spots started to recover. After 2012, as a result of the latest round of the province's policy stimulus and high-level infrastructure development, including the construction of a high-speed rail, the eco-efficiency of tourism hotels, travel agencies, and scenic spots returned to a high level (Figure 5).

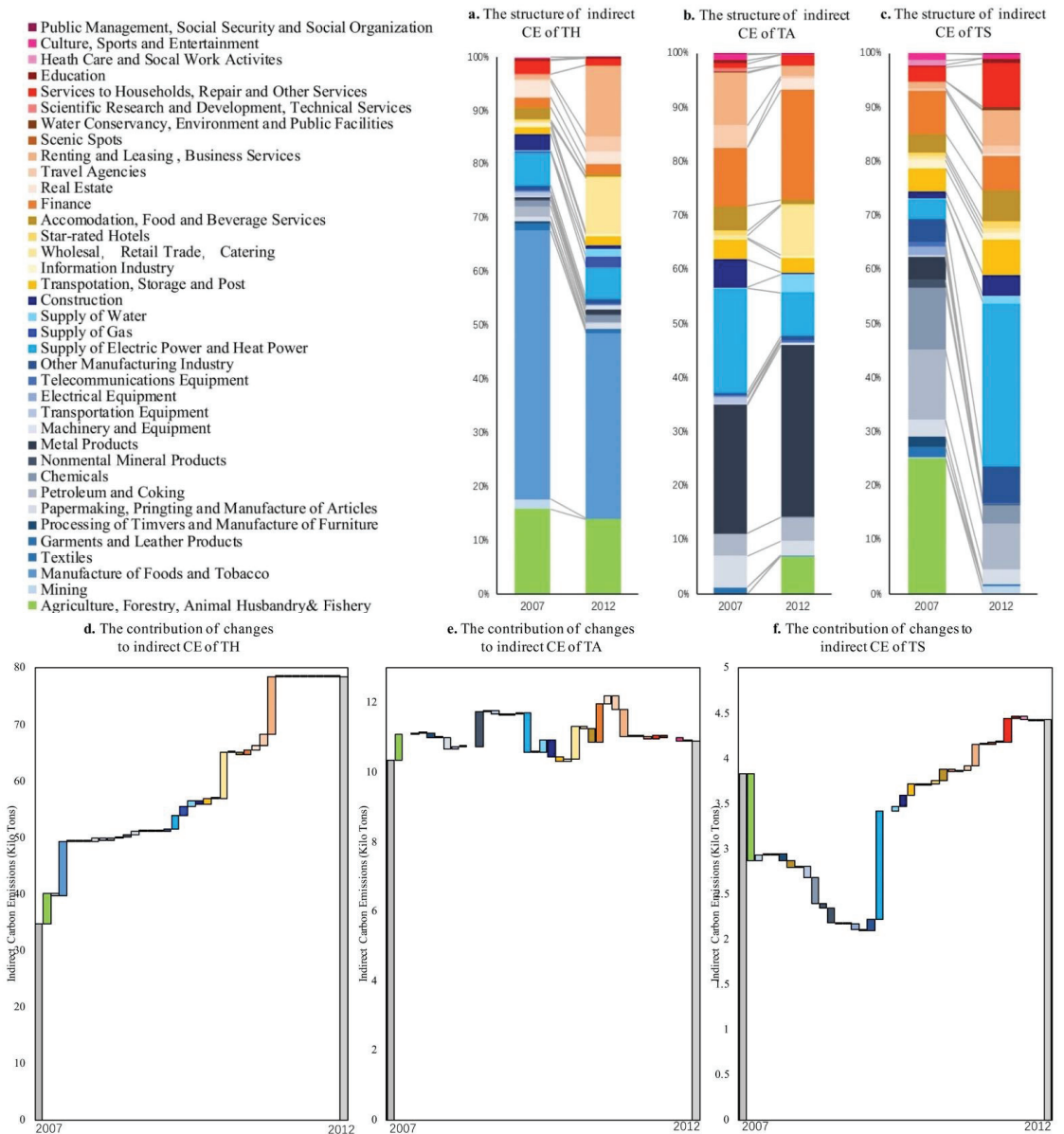


Figure 4. The main sources of indirect carbon emissions from tourism sectors in Gansu Province.

The eco-efficiency of tourism hotels with respect to total carbon emissions demonstrated a distinct U-shaped pattern. In most years during the study period, eco-efficiency with respect to the direct emission scenario was higher than that of the total emission scenario. In 2003 and 2008, eco-efficiency in both scenarios was at the bottom, indicating low eco-efficiency. During these periods, tourism hotels did not experience an evident increase in either direct or total carbon emissions, indicating that carbon emissions did not be constrained, which did not improve the eco-efficiency of tourism hotels. However, in the early stage of tourism development in Gansu, during which tourism hotels had a limited number of guests and, therefore, low economic efficiency, eco-efficiency was low. As

of 2012, the eco-efficiency of tourism hotels with respect to both the direct carbon emission and indirect emission scenarios peaked. At the same time, both direct and total carbon emissions increased somewhat but did not have a major impact on eco-efficiency. As such, the economic contributions of tourism hotels may have compensated for the increase in carbon emissions.

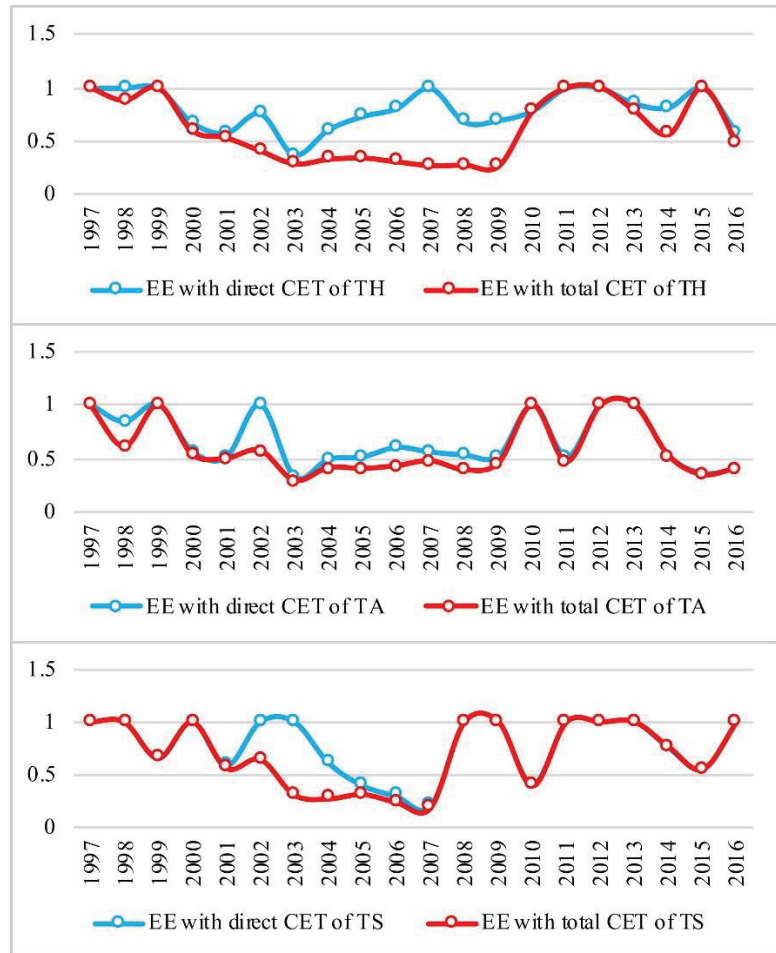


Figure 5. Eco-efficiency of tourism sectors in Gansu Province during the 1997–2016 period.

The eco-efficiency of travel agencies with respect to total carbon emissions displayed a U-shaped development pattern and was at the trough of the U shape during the 2003–2009 period. By 2009, eco-efficiency with respect to the direct and total emission scenarios demonstrated recovering yet fluctuating trends; the two types of eco-efficiency, however, fell into a trough again in both 2011 and 2015. Although the eco-efficiency of travel agencies also peaked in 2012, compared to tourism hotels, travel agencies exhibited more eco-efficiency fluctuations after 2012. This means that the interactive relationship between carbon emissions from travel agencies and economic development is less stable and more complex. The evolutionary trajectory of eco-efficiency with respect to both the direct and total emission scenarios was relatively consistent, and the increase in total carbon emissions did not lead to reduced eco-efficiency for travel agencies. This indicates that travel agencies operated with higher efficiency when they considered their connections to other industries;

that is, with an open strategy, travel agencies may better balance economic growth and carbon emission reduction.

The evolutionary trajectory of scenic spot eco-efficiency with respect to direct and total carbon emissions was consistent and mostly increased after 2007. Between 2002 and 2006, the eco-efficiency of scenic spots under the direct emission scenario was significantly higher than that of the total emission scenario. In comparison with those of tourism hotels and travel agencies, the eco-efficiency of scenic spots was even lower. The development of scenic spots in Gansu lags behind the national level. After 2000, scenic spot development in Gansu gained momentum, because scenic spots that were previously public agencies underwent a systematic transformation, and the reform constituted a rare opportunity to spur economic growth in scenic spots. Moreover, since 2012, due to construction of the high-speed railway, scenic spots in Gansu experienced a growth spurt, especially in the Hexi Corridor area. The abrupt increase in the number of tourists created more economic benefit but also led to increased carbon emissions. As a result, the eco-efficiency of scenic spots with respect to both direct and indirect carbon emissions declined. Moreover, after 2012, the continuous growth of direct carbon emissions instead brought a higher eco-efficiency, which indicates that the provision of scenic spots as a product of the entire tourism industry supply chain is conducive to improvements in eco-efficiency.

4.4. Analysis of the Drivers of Tourism Sector Eco-Efficiency in Gansu

The regression results indicate that both the structure effect and energy technology effect had a significantly positive effect on the eco-efficiency of tourism hotels with respect to total carbon emissions and direct carbon emissions, respectively. An increase of 1% in the revenue of tourism hotels increased their eco-efficiency with respect to direct and total carbon emissions by 1.76 times and 1.84 times, respectively. A reduction of 1% in tourists of tourism hotels increased the eco-efficiency of tourism hotels with respect to direct and total carbon emissions by 1.2 times and 1.36 times, respectively. An increase of 1% in the unit revenue of investment increased the eco-efficiency of tourism hotels with respect to direct and total carbon emissions by 1.68 times and 1.38 times, respectively. A 1% reduction of the unit revenue of energy consumption increased the eco-efficiency of tourism hotels with respect to direct carbon emissions by 3.36. An increase of 1% in the proportion of the revenue of tourism hotels in the total revenue of the three sectors increased the eco-efficiency of tourism hotels with respect to total carbon emissions by 1.52 times (Table 4). Tourism revenue played a more positive role in the eco-efficiency of tourism hotels with respect to total carbon emissions than it did with respect to direct carbon emissions. However, the number of tourist receptions in the scale effect had a significant negative correlation with the eco-efficiency of tourism hotels. This indicates that, because of the relatively lagging development of tourism hotels in Gansu Province, the tourist consumption on tourism hotels was lower. The capital effect was the main driver for the improvement of the eco-efficiency of tourism hotels with respect to both emission scenarios. This is related to the characteristics of high capital investment in tourism hotels [50], and it is also related to the rapid development and large-scale construction of tourism hotels in Gansu Province during the research period.

Table 4. Tobit regression results for factors that drive the tourism eco-efficiency of tourism hotels, travel agencies, and scenic spots in Gansu Province.

	Model 1		Model 2		Model 3		Model 4		Model 5		Model 6	
	Coef.	t	Coef.	t	Coef.	t	Coef.	t	Coef.	t	Coef.	t
HS	0.8167	1.46	1.5175	2.2 *								
D1.lnHTI	1.7599	3.69 ***	1.8436	2.92 **								
D1.lnHTP	-1.2001	-2.77 **	-1.3645	-2.27 *								
D1.HEI	-3.3593	-4.48 ***	-1.5378	-1.67								
D1.lnHRI	1.6817	3.44 **	1.3837	2.43 **								
TS					-3.1697	-2.21 *	-2.2856	-2.7 **				
D1.lnTTI					-0.2767	-1.3	-0.2821	-1.47				
lnTTP					0.7395	1.43	0.7499	1.78				
TEI					-5.2951	-2.62 **	-3.3253	-2.12 *				
TRI					-0.0118	-0.25	-0.0050	-0.13				
SS									16.0436	3.26 **	2.9920	2.39 **
D1.lnSTI	-1.2876	-1.65	0.5526	0.58	2.2572	1.2	0.9559	0.75	-7.7122	-3.49 **	-1.3180	-2.62 **
D1.lnSTP	-2.5387	-0.77	-0.7067	-0.18	-7.1938	-1.65	-8.7556	-2.89 **	3.7003	3.41 **	0.7931	2.23 *
SEI	15.1017	1.68	15.4329	1.04	-3.4939	-0.24	5.2261	0.43	-81.4394	-3.34 **	-9.3551	-2.45 **
SRI	0.0667	0.49	-0.6814	-3.6 ***	-1.1568	-2.63 **	-1.0686	-3.49 **	0.4058	-4.65 ***	-0.0834	-1.72
D2.lnpgdp	0.1216	0.7	0.1952	0.85	-0.3837	-1.38	-0.2979	-1.18	18.9987	3.22 **	-0.6318	-0.42
D1.thirdi	0.3104	1.83	1.1500	5.47 ***	0.7369	0.98	0.8118	1.52	40.0462	3 **	-2.4897	-0.43
lntr	-2.7007	-1.94 *	-7.8254	-4.84 ***	-9.4326	-2.44 **	-11.3842	-3.42 **	-115.4852	-2.57 **	14.4444	0.82
Log likelihood	7.8004		6.0796		4.7628		7.3352		-9.7988	-3.17 **	-1.3673	-2.26 *
									1.8133	3.5 **	0.4618	1.14
									8.1213	3.06 **	1.5389	2.36 *
									-14.0173	-2.25 *	-5.7348	-1.96 *
									3.5624		-1.8279	

Note: *, **, and *** denote significance at the 0.1, 0.05, and 0.01 levels, respectively. D1, and D2, denote first order difference and second difference, respectively.

The structure effect and energy technology effect influenced the eco-efficiency of travel agencies with respect to both direct and total carbon emissions. An increase of 1% in the proportion of the revenue of travel agencies in the total revenue of the three sectors decreased the eco-efficiency of travel agencies with respect to direct carbon emissions and total carbon emissions by 3.16 times and 2.29 times. A 1% reduction in the unit revenue of energy consumption increased the eco-efficiency of travel agencies with respect to direct carbon emissions and total carbon emissions by 5.29 times and 3.33 times (Table 4). The structure of Gansu's tourism industry, which has a significant negative impact on the eco-efficiency of travel agencies, is key to improving the eco-efficiency of this sector. The energy technology effect has a more significant impact on direct carbon emissions, and the elasticity coefficient is also greater; that is, changes in travel agency eco-efficiency with respect to direct carbon emissions are more sensitive to changes in energy technology. This result also indicates that the travel agency sector in Gansu is not well developed—the operation mechanism and processes are still backward, especially for tourists coming to Gansu. A model that focuses on traveling abroad does not make a significant contribution to the development of local tourism. As such, it is imperative to adjust the internal structure of travel agencies and enhance their modernization in order to improve reception capacity and quality. Furthermore, indirect, coordinated interindustry operations can be adopted to increase the influence of tourism hotels and scenic spots on the tourism industry. The energy technology effect had a significant positive impact on the eco-efficiency of travel agencies in Gansu. The main reason is that the distribution of tourism resources in Gansu is relatively scattered, and the mature, international tourism routes along the Silk Road (Tianshui–Lanzhou–Zhangye–Jiayuguan–Dunhuang) have long distances, contributing to increased energy consumption and carbon emissions.

In regard to the structure effect, the scale effect and energy technology effect influence the eco-efficiency of scenic spots with respect to both direct and total carbon emissions. The capital effect has a relatively significant effect on the eco-efficiency of scenic spots with respect to total carbon emissions. An increase of 1% in the proportion of the revenue of scenic spots in the total revenue of the three sectors decreased the eco-efficiency of scenic spots with respect to direct carbon emissions and total carbon emissions by 16.04 times and 2.29 times, respectively. An increase of 1% in the revenue of scenic spots decreased the eco-efficiency of scenic spots with respect to direct and total carbon emissions by 7.71 times and 1.32 times, respectively. An increase of 1% in the tourists of scenic spots increased the eco-efficiency of scenic spots with respect to direct and total carbon emissions by 3.7 times and 0.79%, respectively. A 1% reduction of in the unit revenue of energy consumption increased the eco-efficiency of scenic spots with respect to direct and total carbon emissions by 81.44 times and 9.36 times, respectively. An increase of 1% in the unit revenue of investment increased the eco-efficiency of scenic spots with respect to direct carbon emissions by 19 times (Table 4). The effect of energy technology with respect to direct carbon emissions was particularly prominent. The effect of the scale effect on scenic spots was the opposite of its effect on tourism hotels, which shows that the current per capita consumption level of scenic spots needs to be reduced, since the increase in reception has not improved the eco-efficiency of Gansu scenic spots. This situation should be fully considered due to being in the left half of the environmental Kuznets curve. Therefore, attention should be paid to the development and use of green and low-carbon technologies for tourism products and services in scenic spots given the resilient energy technology effect in order to build a low-carbon and high-quality scenic spot using efficient and guided investment.

5. Discussion

According to Kuznets' environmental theory, the preliminary results of tourism sector low-carbon development have been achieved in Gansu, and the aim of carbon emissions peak is expected to be achieved soon. The growth of indirect emissions was faster than that of direct emissions, which coincided with Gansu's tourism development at that phase: The industry was evolving and maturing, i.e., transitioning from supplying a single product to

providing comprehensive and diversified tourism services [81]. Indirect carbon emissions were 1.93 times that of direct carbon emissions with respect to Gansu tourism, lower than that of the global tourism industry, which is four times larger [7]. Compared with the other industries, such as agriculture and manufacturing, tourism has, relatively, the lowest direct carbon emissions [74]. Moreover, tourism sectors have gained a high eco-efficiency with a faster increase in economic growth compared to carbon emissions as a result of regional policy stimulus, high-level infrastructure development, higher management efficiency, fairer allocation of resources [82]: specific like the construction of high-speed rails, a more efficient and reasonable development of scenic spots. Our results show that the preliminary fruits of each sector's low-carbon development have been achieved, and the aim of carbon emissions peak is expected to soon be achieved in underdeveloped areas in northwest China. In the future, we should adhere to the concept of green development, adhere to promoting the decoupling of tourism carbon emissions from economic growth, scientifically evaluate the development status of tourism sectors, promote the inflection point of the Kuznets curve of carbon emissions with respect to tourism sectors, and strengthen top-level designs.

Tourism hotels being the main contributor of indirect carbon emissions from the supply chain confirms other scholars' research on the increasing food consumption of tourists [83]. The structure of indirect carbon emissions with respect to the tourism sector in Gansu is mostly consistent with the results of Lenzen's study on low-income countries [7]. Based on the existing research, structure changes were an important factor in offsetting indirect carbon emissions in China during 1997–2012 [84]. Therefore, in the new era, China has made efforts to change its economic development mode, targeting high-quality economic growth, i.e., growth driven by higher value added and lower resource intensive inputs [84]. As an important emissions contributor in China, Gansu is taking numerous measures to save energy and reduce carbon emissions. Therefore, industry structural changes, both in tourism and other whole industries, are expected to continue to decrease indirect carbon emissions from the supply chain in the future. The tourism sector should pay attention to coordinated development in the supply chain with respect to indirect carbon emission sources in order to promote carbon emission efficiency.

The drivers of eco-efficiency in the tourism sector are consist with Luo's analysis of the drivers of carbon emissions in China's tourism industry [67]. Moreover, the world is shifting to the use of renewable energy sources [85], and China has taken many effective measures to improve energy efficiency [86]. The structure effect has certain positive effects on tourism hotels and scenic spots, but it has certain negative impacts on travel agencies. Therefore, with the increase in tourism revenue and the share of tourism hotels and scenic spots, and the reduction in the share of travel agency income in all three industries, the structure effect can improve the eco-efficiency of the three sectors. Due to the different effects that the scale effect has on the three sectors, tourism hotels should be able to improve eco-efficiency by improving their per capita income levels, while travel agencies and scenic spots should reduce their per capita consumption levels and expand the reception capacity in order to improve eco-efficiency. Therefore, the green development of tourism sectors in Gansu Province in the future should be driven by improvements in product and service quality, encourage tourism enterprises to provide low-carbon tourism products from the supply side in order to guide green tourism consumption, and avoid blindly expanding the market scale.

6. Conclusions

Taking tourism hotels, travel agencies, and scenic spots in Gansu, China, as study objects, the direct and indirect carbon emissions of the three sectors were measured through EEIO, the eco-efficiency of the three sectors with respect to the direct and total emission scenarios was calculated using the DEA model, and the factors that drive the eco-efficiency of each sector were analyzed. The major conclusions obtained are as follows:

The carbon emissions of Gansu's three tourism sectors continuously increased, especially indirect emissions. The evolution of the eco-efficiency of the three tourism sectors all demonstrated a U-shaped pattern.

Food and tobacco production was the main contributor of indirect carbon emissions from the supply chain of tourism hotels, which contributed the most carbon emissions in the tourism sector, followed by unprocessed food (listed under agriculture, forestry, animal husbandry and fishery).

Energy technology is the key driver in improving the eco-efficiency of the tourism sectors in Gansu. Specifically, the structure effect and energy technology effect had a significantly positive effect on the eco-efficiency of tourism hotels. The structure effect and energy technology effect influenced the eco-efficiency of travel agencies. The structure effect, scale effect, and energy technology effect influence the eco-efficiency of scenic spots with respect to both direct and total carbon emissions.

This research constructs a comprehensive research framework regarding tourism sector carbon emissions and the eco-efficiency in order to evaluate carbon emissions and their sources in the tourism sectors with respect to a supply chain with intermediate input sectors, finding a path to accurately judge tourism sector carbon emissions. This research evaluated eco-efficiency with respect to both the direct and total carbon emission scenarios, applying a multiple input, multiple output model to explore the comprehensive effects and driving factors of the tourism sector on eco-economy and to provide a widely used decision-making analysis tool for tourism sectors facing the pressures of economic recovery in the post-COVID-19 era and global climate change.

Limitations of this study: Gansu's tourism industry is still dominated by mass tourism, and a large part of the carbon emissions from the transportation sector can be reflected through travel agencies, as well as the input-output relationship between scenic spots and hotels. Therefore, this paper does not conduct a separate analysis on traffic carbon emissions, and future research will be required via field work or by taking traffic carbon emissions as a special topic.

Further research: This study takes the whole territory of Gansu as an example. In fact, there are great differences between natural environmental conditions and tourism resource endowments among the 14 cities in Gansu, and there might be spatial differences in tourism carbon emissions and eco-efficiency. Future research will focus on summarizing the spatial differentiation law of tourism eco-efficiency in Gansu, using spatial econometric analysis in order to achieve spatial and precise policy formulation. Moreover, the analysis of direct and indirect carbon emissions and the eco-efficiency of tourism sector at a larger spatial scale will be the focus of future research. For example, the study of spatial differentiation in Mainland China and various provinces will be the main direction of future research.

Author Contributions: Conceptualization, B.X. and S.D.; Data curation, W.Z. and M.Z.; Formal analysis, B.X., Z.L. and W.Z.; Funding acquisition, S.D. and Y.L.; Investigation, D.S.; Methodology, B.X. and D.S.; Resources, Z.L.; Software, W.Z.; Supervision, S.D. and Y.L.; Writing—original draft, B.X.; Writing—review and editing, B.X. and M.Z. All authors have read and agreed to the published version of the manuscript.

Funding: This work was supported by the China Postdoctoral Science Foundation: 2021M703179, the National Natural Science Foundation of China (NSFC-MFST 32161143029), the Strategic Priority Research Program of Chinese Academy of Sciences (XDA20030203), and the Innovation Capability Improvement Project of Colleges and Universities in Gansu Province (2019-A013).

Institutional Review Board Statement: Not applicable.

Informed Consent Statement: Not applicable.

Data Availability Statement: The data presented in this study are available in Yearbook of China Tourism Statistics, and Statistical Yearbook of Gansu Province, it can be found at the website: <https://navi.cnki.net/knavi/yearbooks/index>.

Acknowledgments: The authors would like to thank the editor and reviewers for their insightful comments and suggestions.

Conflicts of Interest: The authors declare no conflict of interest.

Nomenclature

Acronyms

DEA	data envelopment analysis
IOA	input–output analysis
SBM	slacks-based measure of efficiency
EE	eco-efficiency
EC	the consumption of fuel
TR	the total revenue of tourist sector
CE	carbon emissions
HTI	the revenue of star-rated hotels
TTI	the revenue of travel agencies
STI	the revenue of scenic spots
TTP	number of tourists served by travel agencies
STP	number of visitors to scenic spots
HS	the proportion of star-rated hotels’ revenue
SS	the proportion of scenic spots’ revenue
TS	the proportion of travel agencies’ revenue
HRI	the capital input per unit of star-rated hotels revenue
TRI	the capital input per unit of travel agencies’ revenue
SRI	the capital input per unit of scenic spots’ revenue
HEI	the energy input per unit of star-rated hotels revenue
TEI	the energy input per unit of travel agencies’ revenue
SEI	the energy input per unit of scenic spots’ revenue
HDE	direct carbon emissions eco-efficiency of star-rated hotels
TDE	direct carbon emissions eco-efficiency of travel agencies
SDE	direct carbon emissions eco-efficiency of scenic spots
HTE	total carbon emissions eco-efficiency of star-rated hotels
TTE	total carbon emissions eco-efficiency of travel agencies
STE	total carbon emissions eco-efficiency of scenic spots
PGDP	per GDP
THI	proportion of tertiary industry
UR	proportion of urban population
ED	number of students in colleges and universities
FR	total investment of foreign enterprises
RO	road mileage

Notations

X	the total output matrix
Y	the final use matrix
A	the direct consumption coefficient matrix
I	identity matrix
IS	industrial sector
L	the value-added matrix
P	the production possibility set

XX	the input matrix of eco-efficiency
YY	the output matrix of eco-efficiency
NN	the years of eco-efficiency analysis
z	the intermediate input/use
f	the final use
l	the added value
x	the total output
x'	the total input
η	the energy consumption coefficient
δ	the convert coefficient to standard coal
μ	the carbon emissions coefficient
xx	the input of eco-efficiency
yy	the output of eco-efficiency
s	the slack variable
ee	eco-efficiency
zz	the influencing indicators
ϵ	disturbance term
α	regression coefficient of the influencing factors

Subscripts

th	star-rated hotel
ta	travel agency
ts	scenic spot
ac	accommodation and catering sector
os	other services sector
i	the i th industry sector
j	the j th industry sector
n	the number of the industry sectors
m	the number of the regions
r	the number of the types of fuel
k	the k th fuel
g	the good output
b	the bad output
p	the number of the input indicators
q	the years of eco-efficiency analysis
d	the d th input indicator
r	the r th output indicator
λ	the intensity vector in SBM model
t	the t th year
<i>direct</i>	direct carbon emissions
<i>total</i>	total carbon emissions
<i>control</i>	control variables

References

- UNWTO. *Annual Report 2019*; UNWTO: Madrid, Spain, 2020.
- Lee, L.C.; Wang, Y.; Zuo, J. The nexus of water-energy-food in China’s tourism industry. *Resour. Conserv. Recycl.* **2021**, *164*, 9. [[CrossRef](#)]
- Chenghu, Z.; Arif, M.; Shehzad, K.; Ahmad, M.; Oláh, J. Modeling the Dynamic Linkage between Tourism Development, Technological Innovation, Urbanization and Environmental Quality: Provincial Data Analysis of China. *Int. J. Environ. Res. Public Health* **2021**, *18*, 8456. [[CrossRef](#)] [[PubMed](#)]
- UNWTO. *Recommendations for Tourism Statistics 2008*; Department of Economic and Social Affairs: New York, NY, USA, 2010.

5. Whittlesea, E.R.; Owen, A. Towards a low carbon future—The development and application of REAP Tourism, a destination footprint and scenario tool. *J. Sustain. Tour.* **2012**, *20*, 845–865. [[CrossRef](#)]
6. Sun, Y.-Y. A framework to account for the tourism carbon footprint at island destinations. *Tour. Manag.* **2014**, *45*, 16–27. [[CrossRef](#)]
7. Lenzen, M.; Sun, Y.-Y.; Faturay, F.; Ting, Y.-P.; Geschke, A.; Malik, A. The carbon footprint of global tourism. *Nat. Clim. Chang.* **2018**, *8*, 522–528, Correction in *Nat. Clim. Chang.* **2018**, *8*, 544. [[CrossRef](#)]
8. Guan, D.; Wang, D.; Hallegatte, S.; Davis, S.J.; Huo, J.; Li, S.; Bai, Y.; Lei, T.; Xue, Q.; Coffman, D.; et al. Global supply-chain effects of COVID-19 control measures. *Nat. Hum. Behav.* **2020**, *4*, 577–587. [[CrossRef](#)] [[PubMed](#)]
9. Sun, Y.-Y.; Higham, J. Overcoming information asymmetry in tourism carbon management: The application of a new reporting architecture to Aotearoa New Zealand. *Tour. Manag.* **2021**, *83*, 104231. [[CrossRef](#)] [[PubMed](#)]
10. Sun, Y.-Y. Global Value Chains and National Tourism Carbon Competitiveness. *J. Travel Res.* **2018**, *58*, 808–823. [[CrossRef](#)]
11. Matveeva, N.S.; Nazarov, V.S. Legislative Regulation Financial Statement Preparation by Micro Entities: International Experience. *Financ. J.* **2021**, *5*, 125–138. [[CrossRef](#)]
12. UNWTO. *Tourism and the Sustainable Development Goals—Journey to 2030*; UNWTO: Madrid, Spain, 2017.
13. Paiano, A.; Crovella, T.; Lagioia, G. Managing sustainable practices in cruise tourism: The assessment of carbon footprint and waste of water and beverage packaging. *Tour. Manag.* **2019**, *77*, 104016. [[CrossRef](#)]
14. Sun, Y.-Y.; Drakeman, D. Measuring the carbon footprint of wine tourism and cellar door sales. *J. Clean. Prod.* **2020**, *266*, 121937. [[CrossRef](#)]
15. Ehrenfeld, J.R. Eco-efficiency—Philosophy, theory, and tools. *J. Ind. Ecol.* **2005**, *9*, 6–8. [[CrossRef](#)]
16. Gössling, S.; Peeters, P.; Ceron, J.-P.; Dubois, G.; Patterson, T.; Richardson, R. The eco-efficiency of tourism. *Ecol. Econ.* **2005**, *54*, 417–434. [[CrossRef](#)]
17. Sun, Y.-Y.; Lin, P.-C.; Higham, J. Managing tourism emissions through optimizing the tourism demand mix: Concept and analysis. *Tour. Manag.* **2020**, *81*, 104161. [[CrossRef](#)]
18. Papavasileiou, E.F.; Tzouvanas, P. Tourism Carbon Kuznets-Curve Hypothesis: A Systematic Literature Review and a Paradigm Shift to a Corporation-Performance Perspective. *J. Travel Res.* **2021**, *60*, 896–911. [[CrossRef](#)]
19. Pan, Y.; Weng, G.; Li, C.; Li, J. Coupling Coordination and Influencing Factors among Tourism Carbon Emission, Tourism Economic and Tourism Innovation. *Int. J. Environ. Res. Public Health* **2021**, *18*, 1601. [[CrossRef](#)]
20. Zha, J.; Tan, T.; Yuan, W.; Yang, X.; Zhu, Y. Decomposition analysis of tourism CO₂ emissions for sustainable development: A case study of China. *Sustain. Dev.* **2019**, *28*, 169–186. [[CrossRef](#)]
21. Ruan, W.; Li, Y.; Zhang, S.; Liu, C.-H. Evaluation and drive mechanism of tourism ecological security based on the DPSIR-DEA model. *Tour. Manag.* **2019**, *75*, 609–625. [[CrossRef](#)]
22. Zha, J.; Zhu, Y.; He, D.; Tan, T.; Yang, X. Sources of tourism growth in Mainland China: An extended data envelopment analysis-based decomposition analysis. *Int. J. Tour. Res.* **2020**, *22*, 54–70. [[CrossRef](#)]
23. Zhang, J.; Zhang, Y. Assessing the low-carbon tourism in the tourism-based urban destinations. *J. Clean. Prod.* **2020**, *276*, 124303. [[CrossRef](#)]
24. Robaina-Alves, M.; Moutinho, V.; Costa, R. Change in energy-related CO₂ (carbon dioxide) emissions in Portuguese tourism: A decomposition analysis from 2000 to 2008. *J. Clean. Prod.* **2016**, *111*, 520–528. [[CrossRef](#)]
25. Puig, R.; Kiliç, E.; Navarro, A.; Albertí, J.; Chacón, L.; Fullana-I-Palmer, P. Inventory analysis and carbon footprint of coastland-hotel services: A Spanish case study. *Sci. Total Environ.* **2017**, *595*, 244–254. [[CrossRef](#)] [[PubMed](#)]
26. Lee, J.W.; Brahmasrene, T. Investigating the influence of tourism on economic growth and carbon emissions: Evidence from panel analysis of the European Union. *Tour. Manag.* **2013**, *38*, 69–76. [[CrossRef](#)]
27. Bianco, V. Analysis of electricity consumption in the tourism sector. A decomposition approach. *J. Clean. Prod.* **2020**, *248*, 119286. [[CrossRef](#)]
28. Katircioglu, S.T. International tourism, energy consumption, and environmental pollution: The case of Turkey. *Renew. Sustain. Energy Rev.* **2014**, *36*, 180–187. [[CrossRef](#)]
29. Pereira, R.P.T.; Ribeiro, G.M.; Filimonau, V. The carbon footprint appraisal of local visitor travel in Brazil: A case of the Rio de Janeiro-São Paulo itinerary. *J. Clean. Prod.* **2016**, *141*, 256–266. [[CrossRef](#)]
30. Cadarso, M.Á.; Gomez, N.; López, L.A.; Tobarra, M.Á. Calculating tourism’s carbon footprint: Measuring the impact of investments. *J. Clean. Prod.* **2016**, *111*, 529–537. [[CrossRef](#)]
31. Yang, Y.; Li, W. The evolution of the ecological footprint and its relationship with the urban development of megacities in Western China: The case of Xi’an. *J. Environ. Manag.* **2019**, *243*, 463–471. [[CrossRef](#)] [[PubMed](#)]
32. Chen, Q.; Mao, Y.; Morrison, A.M. Impacts of Environmental Regulations on Tourism Carbon Emissions. *Int. J. Environ. Res. Public Health* **2021**, *18*, 12850. [[CrossRef](#)] [[PubMed](#)]
33. Wang, Z.; Yang, Y.; Wang, B. Carbon footprints and embodied CO₂ transfers among provinces in China. *Renew. Sustain. Energy Rev.* **2018**, *82*, 1068–1078. [[CrossRef](#)]
34. Huang, Z.; Cao, F.; Jin, C.; Yu, Z.; Huang, R. Carbon emission flow from self-driving tours and its spatial relationship with scenic spots—A traffic-related big data method. *J. Clean. Prod.* **2017**, *142*, 946–955. [[CrossRef](#)]
35. Tsai, K.-T.; Lin, T.-P.; Hwang, R.-L.; Huang, Y.-J. Carbon dioxide emissions generated by energy consumption of hotels and homestay facilities in Taiwan. *Tour. Manag.* **2014**, *42*, 13–21. [[CrossRef](#)]

36. Luo, F.; Becken, S.; Zhong, Y. Changing travel patterns in China and ‘carbon footprint’ implications for a domestic tourist destination. *Tour. Manag.* **2018**, *65*, 1–13. [[CrossRef](#)]
37. Mi, Z.; Zheng, J.; Meng, J.; Ou, J.; Hubacek, K.; Liu, Z.; Coffman, D.; Stern, N.; Liang, S.; Wei, Y.-M. Economic development and converging household carbon footprints in China. *Nat. Sustain.* **2020**, *3*, 529–537. [[CrossRef](#)]
38. Xu, Z.; Li, Y.; Chau, S.N.; Dietz, T.; Li, C.; Wan, L.; Zhang, J.; Zhang, L.; Li, Y.; Chung, M.G.; et al. Impacts of international trade on global sustainable development. *Nat. Sustain.* **2020**, *3*, 964–971. [[CrossRef](#)]
39. López, L.A.; Cadarso, M.A.; Zafrilla, J.; Arce, G. The carbon footprint of the U.S. multinationals’ foreign affiliates. *Nat. Commun.* **2019**, *10*, 1672. [[CrossRef](#)] [[PubMed](#)]
40. Cheng, H.; Dong, S.; Li, F.; Yang, Y.; Li, S.; Li, Y. Multiregional Input-Output Analysis of Spatial-Temporal Evolution Driving Force for Carbon Emissions Embodied in Interprovincial Trade and Optimization Policies: Case Study of Northeast Industrial District in China. *Environ. Sci. Technol.* **2018**, *52*, 346–358. [[CrossRef](#)]
41. Wiedmann, T.; Minx, J. Definition of Carbon Footprint. In *Ecological Economics Research Trends*; Pertsova, C.C., Ed.; Nova Publishers: Hauppauge, NY, USA, 2008; Volume 1, pp. 1–11.
42. Berners-Lee, M.; Howard, D.C.; Moss, J.; Kaivanto, K.; Scott, W.A. Greenhouse gas footprinting for small businesses—The use of input-output data. *Sci. Total Environ.* **2011**, *409*, 883–891. [[CrossRef](#)]
43. Frampton, S.C. Energy use associated with different travel choices. *Tour. Manag.* **2003**, *24*, 267–277.
44. Kuo, N.-W.; Lin, C.-Y.; Chen, P.-H.; Chen, Y.-W. An inventory of the energy use and carbon dioxide emissions from island tourism based on a life cycle assessment approach. *Environ. Prog. Sustain. Energy* **2009**, *31*, 459–465. [[CrossRef](#)]
45. Gamboa, M.M.; Iribarren, D.; Dufour, J. Environmental impact efficiency of natural gas combined cycle power plants: A combined life cycle assessment and dynamic data envelopment analysis approach. *Sci. Total Environ.* **2018**, *615*, 29–37. [[CrossRef](#)] [[PubMed](#)]
46. AbdelAzim, A.I.; Ibrahim, A.M.; Aboul-Zahab, E.M. Development of an energy efficiency rating system for existing buildings using Analytic Hierarchy Process—The case of Egypt. *Renew. Sustain. Energy Rev.* **2017**, *71*, 414–425. [[CrossRef](#)]
47. Tsaples, G.; Papathanasiou, J. Data envelopment analysis and the concept of sustainability: A review and analysis of the literature. *Renew. Sustain. Energy Rev.* **2020**, *138*, 110664. [[CrossRef](#)]
48. Quintano, C.; Mazzocchi, P.; Rocca, A. Examining eco-efficiency in the port sector via non-radial data envelopment analysis and the response based procedure for detecting unit segments. *J. Clean. Prod.* **2020**, *259*, 120979. [[CrossRef](#)]
49. Gössling, S.; Higham, J. The Low-Carbon Imperative: Destination Management under Urgent Climate Change. *J. Travel Res.* **2020**, *60*, 1167–1179. [[CrossRef](#)]
50. Xia, B.; Dong, S.; Ba, D.; Li, Y.; Li, F.; Liu, H.; Zhao, M. Research on the Spatial Differentiation and Driving Factors of Tourism Enterprises’ Efficiency: Chinese Scenic Spots, Travel Agencies, and Hotels. *Sustainability* **2018**, *10*, 901. [[CrossRef](#)]
51. Yang, Y.; Yao, C.; Xu, D. Ecological compensation standards of national scenic spots in western China: A case study of Taibai Mountain. *Tour. Manag.* **2020**, *76*, 103950. [[CrossRef](#)]
52. Wang, L.; Zhou, X.; Lu, M.; Cui, Z. Impacts of haze weather on tourist arrivals and destination preference: Analysis based on Baidu Index of 73 scenic spots in Beijing, China. *J. Clean. Prod.* **2020**, *273*, 122887. [[CrossRef](#)]
53. W. O. Economics. *2017 Travel & Tourism Economic Impact Research*; W. O. Economics: Oxford, UK, 2017.
54. Koiwanit, J.; Filimonau, V. Carbon footprint assessment of home-stays in Thailand Resource. *Conserv. Recycl.* **2021**, *164*, 105123. [[CrossRef](#)]
55. Zhang, F.; Zhang, M.; Wang, S.; Qiang, F.; Che, Y.; Wang, J. Evaluation of the tourism climate in the Hexi Corridor of northwest China’s Gansu Province during 1980–2012. *Arch. Meteorol. Geophys. Bioclimatol. Ser. B* **2017**, *129*, 901–912. [[CrossRef](#)]
56. Zhang, K.; Liu, X.; Yao, J. Spatial correlation between the agglomeration and CO₂ emissions of China’s tourism industry. *Resour. Sci.* **2019**, *41*, 362–371.
57. Rebolledo-Leiva, R.; Vásquez-Ibarra, L.; Entrena-Barbero, E.; Fernández, M.; Feijoo, G.; Moreira, M.T.; González-García, S. Coupling Material Flow Analysis and Network DEA for the evaluation of eco-efficiency and circularity on dairy farms. *Sustain. Prod. Consump.* **2022**, *31*, 805–817. [[CrossRef](#)]
58. Li, Y.; Zuo, Z.; Xu, D.; Wei, Y. Mining Eco-Efficiency Measurement and Driving Factors Identification Based on Meta-US-SBM in Guangxi Province, China. *Int. J. Environ. Res. Public Health* **2021**, *18*, 5397. [[CrossRef](#)] [[PubMed](#)]
59. Cooper, W.W.; Seiford, L.M.; Tone, K. *Data Envelopment Analysis. A Comprehensive Text with Models, Applications, References and DEA-Solver Software*, 2nd ed.; Springer Science + Business Media, LLC: New York, NY, USA, 2007.
60. McDonald, J.F.; Moffitt, R.A. The Uses of Tobit Analysis. *Rev. Econ. Stat.* **1980**, *62*, 318–321. [[CrossRef](#)]
61. Cheng, Y.; Shao, T.; Lai, H.; Shen, M.; Li, Y. Total-Factor Eco-Efficiency and Its Influencing Factors in the Yangtze River Delta Urban Agglomeration, China. *Int. J. Environ. Res. Public Health* **2019**, *16*, 3814. [[CrossRef](#)] [[PubMed](#)]
62. Chen, Y.; Yin, G.; Liu, K. Regional differences in the industrial water use efficiency of China: The spatial spillover effect and relevant factors. *Resour. Conserv. Recycl.* **2021**, *167*, 105239. [[CrossRef](#)]
63. Ren, Y.; Fang, C.; Li, G. Spatiotemporal characteristics and influential factors of eco-efficiency in Chinese prefecture-level cities: A spatial panel econometric analysis. *J. Clean. Prod.* **2020**, *260*, 120787. [[CrossRef](#)]
64. Zhang, J.; Wang, S.; Yang, P.; Fan, F.; Wang, X. Analysis of Scale Factors on China’s Sustainable Development Efficiency Based on Three-Stage DEA and a Double Threshold Test. *Sustainability* **2020**, *12*, 2225. [[CrossRef](#)]
65. Zhou, Y.; Kong, Y.; Sha, J.; Wang, H. The role of industrial structure upgrades in eco-efficiency evolution: Spatial correlation and spillover effects. *Sci. Total Environ.* **2019**, *687*, 1327–1336. [[CrossRef](#)] [[PubMed](#)]

66. He, L.; Zha, J.; Loo, H.A. How to improve tourism energy efficiency to achieve sustainable tourism: Evidence from China. *Curr. Issues Tour.* **2020**, *23*, 2076–2092. [[CrossRef](#)]
67. Luo, F.; Moyle, B.D.; Moyle, C.-L.J.; Zhong, Y.; Shi, S. Drivers of carbon emissions in China's tourism industry. *J. Sustain. Tour.* **2020**, *28*, 747–770. [[CrossRef](#)]
68. Hu, W.; Guo, Y.; Tian, J.; Chen, L. Eco-efficiency of centralized wastewater treatment plants in industrial parks: A slack-based data envelopment analysis. *Resour. Conserv. Recycl.* **2019**, *141*, 176–186. [[CrossRef](#)]
69. Tang, M.; Li, Z.; Hu, F.; Wu, B. How does land urbanization promote urban eco-efficiency? The mediating effect of industrial structure advancement. *J. Clean. Prod.* **2020**, *272*, 122798. [[CrossRef](#)]
70. Chen, W.; Ning, S.; Chen, W.; Liu, E.-N.; Wang, Y.; Zhao, M. Spatial-temporal characteristics of industrial land green efficiency in China: Evidence from prefecture-level cities. *Ecol. Indic.* **2020**, *113*, 106256. [[CrossRef](#)]
71. Wang, J.; Wang, S.; Li, S.; Cai, Q.; Gao, S. Evaluating the energy-environment efficiency and its determinants in Guangdong using a slack-based measure with environmental undesirable outputs and panel data model. *Sci. Total Environ.* **2019**, *663*, 878–888. [[CrossRef](#)] [[PubMed](#)]
72. Arceo, A.; Biswas, W.K.; John, M. Eco-efficiency improvement of Western Australian remote area power supply. *J. Clean. Prod.* **2019**, *230*, 820–834. [[CrossRef](#)]
73. Zha, J.; Yuan, W.; Dai, J.; Tan, T.; He, L. Eco-efficiency, eco-productivity and tourism growth in China: A non-convex metafrontier DEA-based decomposition model. *J. Sustain. Tour.* **2020**, *28*, 663–685. [[CrossRef](#)]
74. Meng, W.Q.; Xu, L.Y.; Hu, B.B.; Zhou, J.; Wang, Z.L. Quantifying direct and indirect carbon dioxide emissions of the Chinese tourism industry. *J. Clean. Prod.* **2017**, *163*, S401–S409, reprinted in *J. Clean. Prod.* **2016**, *126*, 586–594. [[CrossRef](#)]
75. Becken, S.; Patterson, M. Measuring National Carbon Dioxide Emissions from Tourism as a Key Step Towards Achieving Sustainable Tourism. *J. Sustain. Tour.* **2006**, *14*, 323–338. [[CrossRef](#)]
76. Dwyer, L.; Forsyth, P.; Spurr, R.; Hoque, S. Estimating the carbon footprint of Australian tourism. *J. Sustain. Tour.* **2010**, *18*, 355–376. [[CrossRef](#)]
77. Cheng, Z.; Li, L.; Liu, J. Industrial structure, technical progress and carbon intensity in China's provinces. *Renew. Sust. Energ. Rev.* **2018**, *81*, 2935–2946. [[CrossRef](#)]
78. Zaman, K.; Shahbaz, M.; Loganathan, N.; Raza, S.A. Tourism development, energy consumption and Environmental Kuznets Curve: Trivariate analysis in the panel of developed and developing countries. *Tour. Manag.* **2016**, *54*, 275–283. [[CrossRef](#)]
79. Xue, D.; Yue, L.; Ahmad, F.; Draz, M.U.; Chandio, A.A. Urban eco-efficiency and its influencing factors in Western China: Fresh evidence from Chinese cities based on the US-SBM. *Ecol. Indic.* **2021**, *127*, 107784. [[CrossRef](#)]
80. Haibo, C.; Ke, D.; Fangfang, W.; Ayamba, E.C. The spatial effect of tourism economic development on regional ecological efficiency. *Environ. Sci. Pollut. Res.* **2020**, *27*, 38241–38258. [[CrossRef](#)] [[PubMed](#)]
81. Lu, C.; Li, W.; Pang, M.; Xue, B.; Miao, H. Quantifying the Economy-Environment Interactions in Tourism: Case of Gansu Province, China. *Sustainability* **2018**, *10*, 711. [[CrossRef](#)]
82. Moiseev, N.; Mikhaylov, A.; Varyash, I.; Saqib, A. Investigating the relation of GDP per capita and corruption index. *Entrep. Sustain. Issues* **2020**, *8*, 780–794. [[CrossRef](#)]
83. Li, Y.; Filimonau, V.; Wang, L.-E.; Cheng, S. Tourist food consumption and its arable land requirements in a popular tourist destination. *Resour. Conserv. Recycl.* **2019**, *153*, 104587. [[CrossRef](#)]
84. Yi-Ming, W.; Meng, J.; Guan, D.; Shan, Y.; Song, M.; Wei, Y.-M.; Liu, Z.; Hubacek, K. Chinese CO2 emission flows have reversed since the global financial crisis. *Nat. Commun.* **2017**, *8*, 1712. [[CrossRef](#)]
85. Bushukina, V.I. Specific Features of Renewable Energy Development in the World and Russia. *Financ. J.* **2021**, *13*, 93–107. [[CrossRef](#)]
86. Kranina, E.I. China on the Way to Achieving Carbon Neutrality. *Financ. J.* **2021**, *13*, 51–61. [[CrossRef](#)]



Review

A Systematic Review of Associations between Energy Use, Fuel Poverty, Energy Efficiency Improvements and Health

Chengju Wang *, Juan Wang * and Dan Norbäck

Department of Medical Sciences, Occupational and Environmental Medicine, Uppsala University, 75185 Uppsala, Sweden; dan.norbäck@medsci.uu.se

* Correspondence: chengju.wang.se@gmail.com (C.W.); juan.wang@medsci.uu.se (J.W.)

Abstract: Energy use in buildings can influence the indoor environment. Studies on green buildings, energy saving measures, energy use, fuel poverty, and ventilation have been reviewed, following the guidelines of the Preferred Reporting Items for Systematic Reviews and Meta-Analyses (PRISMA) statement. The database PubMed was searched for articles published up to 1 October 2020. In total, 68 relevant peer-reviewed epidemiological or exposure studies on radon, biological agents, and chemicals were included. The main aim was to assess current knowledge on how energy saving measures and energy use can influence health. The included studies concluded that buildings classified as green buildings can improve health. More efficient heating and increased thermal insulation can improve health in homes experiencing fuel poverty. However, energy-saving measures in airtight buildings and thermal insulation without installation of mechanical ventilation can impair health. Energy efficiency retrofits can increase indoor radon which can cause lung cancer. Installation of a mechanical ventilation systems can solve many of the negative effects linked to airtight buildings and energy efficiency retrofits. However, higher ventilation flow can increase the indoor exposure to outdoor air pollutants in areas with high levels of outdoor air pollution. Finally, future research needs concerning energy aspects of buildings and health were identified.

Keywords: health; asthma; respiratory; indoor air quality; built environment; energy use; energy efficiency buildings; green buildings

Citation: Wang, C.; Wang, J.;

Norbäck, D. A Systematic Review of Associations between Energy Use, Fuel Poverty, Energy Efficiency Improvements and Health. *Int. J. Environ. Res. Public Health* **2022**, *19*, 7393. <https://doi.org/10.3390/ijerph19127393>

Academic Editors: Francesco Nocera, Roberto Alonso González Lezcano and Rosa Giuseppina Caponetto

Received: 4 May 2022

Accepted: 15 June 2022

Published: 16 June 2022



Copyright: © 2022 by the authors. Licensee MDPI, Basel, Switzerland. This article is an open access article distributed under the terms and conditions of the Creative Commons Attribution (CC BY) license (<https://creativecommons.org/licenses/by/4.0/>).

1. Introduction

In modern society, people spend more than 90% of their time in indoor environments, and most of that time is spent at home [1]. Energy is needed to heat or cool buildings, and energy use in buildings is an important issue in contemporary society [2]. The climate change issue, linked to increased greenhouse gases emissions from coal, oil, or gas combustion, has increased the demand to save energy in buildings in different parts of the world [3]. Because of this demand, different measures have been applied to increase energy efficiency in buildings in order to create a sustainable built environment which combines a healthy and energy-efficient indoor environment [4].

There are three main principles of energy efficiency improvements in buildings: reduced energy use, reduced heat transfer, and reduced air leakage [5]. Reduced energy use can reduce emissions and fuel cost, thus reducing exposure to emissions [6]. Furthermore, reduced heat transfer can increase indoor temperature and reduce relative humidity and risk of mould [7]. In contrast, reduced air leakage can increase relative humidity and risk of mould [8]. In practice, common energy saving measures in buildings include increased thermal insulation, installation of central heating or space heating, draught proofing or installation of heat recovery systems [9]. Since energy use in buildings is a complex issue, scientists from many disciplines, as well as stake holders, government officers, and other decision makers need to work together to make updated energy policies [10].

In recent years, there has been an increase of energy-related labelling of buildings, e.g., low energy buildings, zero energy buildings, green buildings, and healthy buildings [11–13].

Green building rating systems have been widely used globally for many years [13]. In the USA, they have created Leadership in Energy and Environmental-Design (LEED) credits to assess green buildings [12]. Other existing green rating systems include BREEAM, CASBEE, Green Star, Enterprise Green Communities, RELi, SITES, Fitwel, Living Building Challenge (LBC), and WELL [11].

However, it should be realized that extreme cold in homes in winter can increase cold-related mortality or morbidity rates [14]. In the UK, fuel poverty is definite as people don't have enough money to heat their home in winter to maintain an acceptable temperature [15]. However, there is also a cost for cooling their homes in extreme heat situations which some people cannot afford [16].

This systematic review included all types of health aspects of energy use, energy saving, and energy efficiency in buildings. The main aim was to summarize the current knowledge on the health impacts of energy saving measures and energy use. The second aim was to collect knowledge on the indoor environment effects of energy-saving measures and energy use. The third aim was to gather knowledge on types of energy saving or energy use that should be promoted from a health perspective.

2. Methods

The guidelines of the Preferred Reporting Items for Systematic Reviews and Meta-Analyses (PRISMA) statement were followed to perform this systematic review [17]. In October 2020, a systematic literature search in PubMed covering articles up to 1 October 2020 was performed. There were ten medical search terms: morbidity, mortality, respiratory, lung function, asthma, rhinitis, eczema, dermatitis, sick building syndrome, building related illness. These medical search terms were combined (any of the ten search terms). In addition, there were eight energy and building related search terms: energy saving, energy use building, energy efficiency building, energy consumption building, energy efficient building, low energy building, energy retrofit, green building. These building and energy-related medical search terms were combined (any of the eight search terms). Then a systematic database search combining any of the ten medical search terms with any of the eight energy and building related search terms was performed. Any medical search term means OR between each search term. Any energy or building related search term means OR between each search term. Combined means AND between the two groups of search terms.

In total, 5776 records were identified from the database searching. Those records were sent to EndNote citation manager for collecting, storing, and organizing. In this reference management software, three reference groups (duplicated group, included group, excluded group) were created. First, 806 duplicated records were removed and added into duplicated group before screening by using the function of EndNote. Then the titles and the abstracts of 4970 articles were screened, to identify articles relevant to the topic of this literature review.

The following three selection criteria were used to include studies in this review:

1. The articles should have studied associations between energy aspects in buildings and health;
2. The articles should be written in English;
3. The articles should not be keynotes, opinions, commentaries, reviews, or modelling studies.

In total, 4882 irrelevant articles were removed. After removal of irrelevant articles, 88 relevant articles were identified. As a next step, keynotes, opinions, commentaries, review articles and modelling articles were removed. Finally, 68 relevant field studies were included in this review, of which 45 were health studies and 23 studies had measured exposure in relation to energy aspects in buildings without investigating health associations. The PRISMA flow diagram of the literature research is shown in Figure 1.

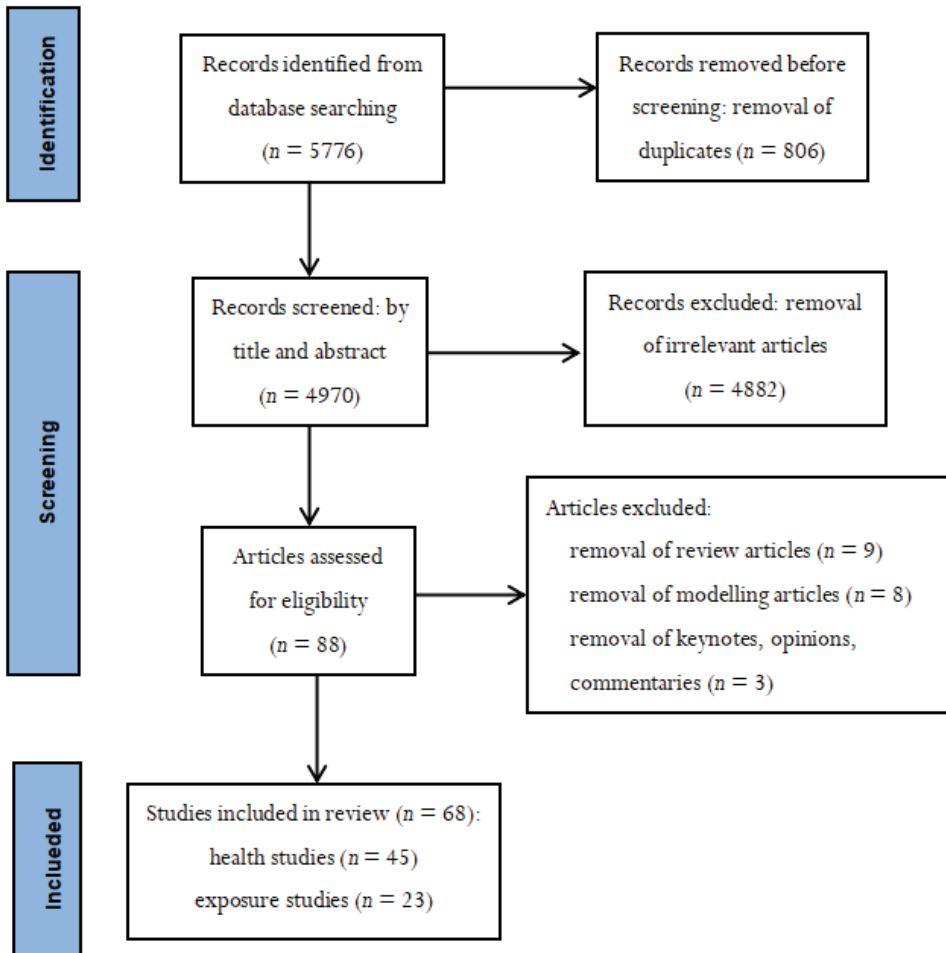


Figure 1. PRISMA flow diagram of literature research.

For each health study, study characteristics on author, year, country, energy aspects, type of study, type of buildings, type of health variables, number of buildings, number of subjects, and main results were extracted. For each exposure study, study characteristics on author, year, country, energy aspects, type of study, type of buildings, measured exposure, changes of measured exposure, number of households, or buildings and main results were extracted. In addition, within the health studies, articles with positive and negative health associations were grouped.

In order to further organize the structure of tables, a thematic classification was made. The studies were divided into four categories: exposure studies, green building health studies, fuel poverty health studies, other energy-related health studies. The exposure studies were divided into three exposure groups, including exposure to radon, exposure to biological agents (mould, bacteria, and house dust mites) and exposure to chemicals. The fuel poverty health studies were divided into three health aspects, including respiratory symptoms, general and mental health, and studies on mortality. Other energy-related health studies were divided into cross-sectional health studies, longitudinal studies, and intervention health studies according to the study design. Details on those thematic tables can be seen in the Appendix A.

The entire process above involved at least two authors to conduct searching to gathering, screening, analyzing, and extracting.

3. Results

3.1. Exposure Studies

In Table 1, associations between energy-related building factors and indoor pollutants among the 23 included exposure studies are summarized. These included 19 studies conducted in Europe, 3 studies conducted in USA, and 1 study conducted in China. Except for one school study [18], 22 exposure studies were conducted in residential buildings (Appendix A).

Table 1. Associations between energy-related building factors and pollutants among the 23 included exposure studies.

No.	References	Country	Pollutant Groups	Improved Ventilation	Thermal Retrofit	Draught Proofing	Green Retrofits	Fuel Poverty	Energy Carrier
1	Collignan et al. 2016 [19]	France	Radon						
2	Symonds et al. 2019 [20]	United Kingdom	Radon		↑				
3	Meyer et al. 2019 [21]	Germany	Radon		↑	↑			
4	Pressyanov et al. 2015 [22]	Bulgaria	Radon		↑	↑			
5	Vasilyev et al. 2017 [23]	Russia	Radon		↑				
6	Yarmoshenko et al. 2014 [24]	Russia	Radon		↑				
7	Vasilyev et al. 2015 [25]	Russia	Radon		↑				
8	Burghele et al. 2020 [26]	Romania	Radon	↓					
9	Pigg et al. 2018 [27]	United States	Radon ¹ , Chemicals ³	↓	↑ ¹ , ↓ ³	↑ ¹ , ↓ ³			
10	Wallner et al. 2015 [28]	Austria	Radon ¹ , Biological agents ² , Chemicals ³	↓ ¹ , ↓ ² , ↓ ³					
11	Du et al. 2019 [29]	Finland Lithuania	Radon ¹ , Biological agents ² , Chemicals ³	↓ ² , ↑ ³	↑ ¹				
12	Hirsch et al. 2020 [30]	Germany	biological agents		↑				
13	Sharpe et al. 2015 [31]	United Kingdom	biological agents					↑	
14	Sharpe et al. 2016 [32]	United Kingdom	biological agents	↓					
15	Spertini et al. 2010 [33]	Switzerland	biological agents	↓					
16	Niculita-Hirzel et al. 2000 [34]	Switzerland	biological agents	↓					
17	Coombs et al. 2018 [35]	United States	biological agents				0		
18	Derbez et al. 2018 [36]	France	Chemicals		↑				
19	Leivo et al. 2018 [37]	Finland Lithuania	Chemicals	↓	↑				
20	Coombs et al. 2016 [38]	United States	Chemicals				↑↓		
21	Yang et al. 2020 [39]	Switzerland	Chemicals		↑				
22	Verriele et al. 2016 [18]	France	Chemicals	↓					
23	Baumgartner et al. 2019 [40]	China	Chemicals						↑↓

↑ means increase, ↓ means decrease, ↑↓ means mixed results, 0 means no associations. ¹ represents radon, ² represents biological agents, ³ represents chemicals.

3.1.1. Radon

There were 11 exposure studies on radon [19–29] (Table 1). Of these, 9 studies reported that energy efficiency thermal retrofitting in homes increased radon concentration [19–25,27,29]. Of these 9 studies, 3 combined thermal insulation with additional air sealing

methods in windows [21,22,27]. There were 6 studies of the 9, in five countries, which reported average radon concentrations above 100 Bq/m³ in rooms [19,20,22,24,25,27]. However, three studies of 11 demonstrated that energy efficiency retrofitting in homes with installation of mechanical ventilation or other measures can reduce radon concentration [26–28]. Other measures included installation of ground covers [26,27] and sub-slab or sump depressurization systems [26].

3.1.2. Biological Agents

There were 8 exposure studies on biological agents [28–35] (Table 2). One study reported that installation of insulated windows and central heating systems increased the concentration of the house dust mites and mould [30]. Another study showed that fuel poverty can increase indoor dampness and mould, regardless of the use of extractor fans [31]. The negative effects may be caused by reduced ventilation [30] and ineffective heating [31]. However, 6 studies of 8 found that energy efficiency improvement in homes with improved ventilation can reduce indoor exposure to mould [28,29,32,34], bacteria [29] and house dust mites [33].

3.1.3. Chemical Substances and Particles

There were 9 exposure studies on chemical substances and particles (Table 3). 4 studies demonstrated that home energy efficiency retrofit can increase indoor air concentrations of certain volatile organic compounds [29,36,38,39] and carbon dioxide levels (CO₂) [39]. CO₂ is an indicator of ventilation flow rate. Those volatile organic compounds included formaldehyde [38,39], aromatics [39], alkanes [39] and alpha-pinene [36], hexaldehyde [36], as well as benzene, toluene, ethyl benzene, and xylene (BTEX) [29]. Alpha-pinene and hexaldehyde could be caused by the use of wood or wood-based products for construction and insulation [36]. However, some studies reported that home energy efficiency improvement combined with mechanical ventilation system can reduce aldehydes [28], formaldehyde [29], total volatile organic compounds (TVOC) [28], CO₂ [18,28,37], carbon monoxide (CO) [27], and black carbon level [38]. One study found that an energy intervention replacing low-polluting semigasifier cooking stoves in rural buildings was associated with decreased exposures to 2.5 (PM_{2.5}) particulate matter and black carbon in winter but higher exposure in summer. The negative effect could be caused by increased use of the cooking stove [40].

3.2. Health Studies

In Table 2, associations between one kind of fuel poverty, improved ventilation, and energy efficiency improvements and health are summarized. There were 28 studies which were conducted in Europe, 10 studies conducted in the USA, and 7 in other countries, including New Zealand (*n* = 3), Japan (*n* = 2), Canada (*n* = 1), and India, (*n* = 1). Except for three office [41–43] and three school studies [44–46], 39 studies were performed in residential buildings (Appendix A).

Table 2. Associations between one kind of fuel poverty, improved ventilation, and energy efficiency improvements and health in all 45 selected health studies.

No.	Reference	Thematic Group	Respiratory Health		General Health	Mental Health	Performance	Satisfaction	Cold-Related Mortality	SBS Symptoms
			Asthma	Other Respiratory Illnesses						
1	Garland et al. 2013 [47]	Green Buildings	+							
2	Singh et al. 2010 [41]	Green Buildings	+	+		+	+			

Table 2. Cont.

No.	Reference	Thematic Group	Respiratory Health		General Health	Mental Health	Performance	Satisfaction	Cold-Related Mortality	SBS Symptoms
			Asthma	Other Respiratory Illnesses						
3	Breyse et al. 2011 [48]	Green Buildings	+	+	+					
4	Breyse et al. 2015 [49]	Green Buildings			+	+				
5	Hedge et al. 2013 [44]	Green Buildings			+		+	+		
6	Hedge et al. 2014 [45]	Green Buildings			+		+	+		
7	Gawande et al. 2020 [42]	Green Buildings								0
8	Rudge et al. 2005 [50]	Fuel Poverty		#						
9	Webb et al. 2013 [51]	Fuel Poverty		#						
10	Sharpe et al. 2015 [52]	Fuel Poverty	#							
11	Poortinga et al. 2017 [53]	Fuel Poverty		+	+/-	+		+/-		
12	Carlton et al. 2019 [54]	Fuel Poverty	-	-						
13	Howden-Chapman et al. 2011 [55]	Fuel Poverty		+	+	+				
14	Howden-Chapman et al. 2007 [56]	Fuel Poverty		+	+					
15	Humphrey et al. 2020 [54]	Fuel Poverty		+						
16	Thomson et al. 2017 [57]	Fuel Poverty			#	#				
17	Ahrentzen et al. 2016 [58]	Fuel Poverty			+	+				
18	Shortt et al. 2007 [59]	Fuel Poverty			+	+				
19	Chapman et al. 2009 [60]	Fuel Poverty			+					
20	Grey et al. 2017 [61]	Fuel Poverty				+		+		
21	Poortinga et al. 2018 [62]	Fuel Poverty				+		+		
22	Pollard et al. 2019 [63]	Fuel Poverty						#		
23	Angelini et al. 2019 [64]	Fuel Poverty							#	
24	Sartini et al. 2018 [65]	Fuel Poverty							+	
25	Peralta et al. 2017 [66]	Fuel Poverty							+/-	
26	Umishio et al. 2019 [67]	Fuel Poverty							#	
27	López-Bueno et al. 2020 [68]	Fuel Poverty							+	
28	Engvall et al. 2003 [69]	Cross sectional								-
29	Smedje et al. 2017 [70]	Cross sectional								+
30	Norback et al. 2014 [71]	Cross sectional		+/-						
31	Wang et al. 2017 [72]	Cross sectional	+							

Table 2. Cont.

No.	Reference	Thematic Group	Respiratory Health		General Health	Mental Health	Performance	Satisfaction	Cold-Related Mortality	SBS Symptoms
			Asthma	Other Respiratory Illnesses						
32	Sharpe et al. 2019 [73]	Cross sectional	+							
33	Sobottka et al. 1996 [74]	Cross sectional								–
34	Bakke et al. 2008 [46]	Cross sectional			#					
35	Kennard et al. 2020 [75]	Cross sectional			#					
36	Wallner et al. 2017 [76]	Longitudinal			+					
37	Somerville et al. 2000 [77]	Intervention	+	+						
38	Barton et al. 2007 [78]	Intervention	+	+						
39	Osman et al. 2010 [79]	Intervention		+						
40	Wilson et al. 2013 [80]	Intervention		+	+			+		
41	Haverinen-Shaughnessy et al. 2018 [81]	Intervention	+					+		
42	Wargocki et al. 2000 [43]	Intervention					+			+
43	Engvall et al. 2005 [82]	Intervention								0
44	Francisco et al. 2017 [83]	Intervention			+					
45	Umishio et al. 2020 [84]	Intervention							+	

Remark: + mean positive result, – means negative result, +/– means mixed results, 0 means no associations, # means fuel poverty issues. SBS: sick building syndrome.

3.2.1. Green Building Health Studies

The green building health studies were conducted in United States ($n = 5$), Canada ($n = 1$), and India ($n = 1$). They were performed in two offices [41,42], two schools [44,45] and three residential buildings (Table 4). Some studies demonstrated that green buildings can reduce self-reported asthma [41,47,48], non-asthmatic respiratory symptoms [41,48], and improve general health [44,45,48,49] and mental health [41,49] as well as performance [41,44,45] and satisfaction [44,45]. One study found no significant association between green buildings and sick building syndrome symptoms (SBS) [42]. Sick building syndrome symptoms include nonspecific symptoms from eyes, skin, upper airways, headache, and fatigue [1].

3.2.2. Fuel Poverty Studies

The fuel poverty studies were conducted in the United Kingdom ($n = 10$), the USA ($n = 3$), New Zealand ($n = 3$), Spain ($n = 2$), Japan ($n = 1$), and multiple countries ($n = 1$). All of the 20 studies were conducted in residential buildings (Tables 5–7). Some studies reported that fuel poverty in low-income homes can increase asthma [52] and respiratory symptoms [50,51] and reduce general health [57] and mental health [57]. Furthermore, low indoor air temperature in low-income homes can increase blood pressure [64,67] and hypertension [67] (linked to cold-related mortality). Besides, lack of insulation [65] and heating systems [68] in low-income homes can increase cold-related mortality. However, one study showed that wearable telemetry (a thermometer with a low-temperature alarm) can raise awareness of the health effects of cold living environments among people living in fuel poverty (linked to psychosocial outcomes) [63].

There were another some studies on the effects of improved ventilation or energy efficiency improvements in low-income homes and health. First, they found that high ventilation rates in low-income urban homes may increase chronic cough, asthma, and asthma-like symptoms, probably caused by infiltration of outdoor air pollutants [54]. However, high infiltration rates in low-income, urban, non-smoking homes can improve lung health [85]. Second, they demonstrated that installation of cavity wall insulation in

social housing without installation of mechanical ventilation can reduce general health outcomes and social outcomes [53]. Energy efficient façade insulation retrofits in public housing can reduce cold-related mortality in women, but can increase cold-related mortality in men. The reason for the gender difference is unclear [66]. However, energy efficiency improvements in low-income homes can improve respiratory symptoms [53,55,56], general health [53,55,58–60] and mental health [53,58] as well as psychosocial outcomes [53,61,62], well-being [55,59,61,62], and sleep [58].

3.2.3. Cross-Sectional Health Studies

The cross-sectional health studies were conducted in Sweden ($n = 4$), the United Kingdom ($n = 2$), Norway ($n = 1$), and Germany ($n = 1$). Except for one school study [46], seven studies were performed in residential buildings (Table 8). Some studies investigated the association between ventilation and health. They reported that higher ventilation rate in homes were associated with less asthma symptoms [72,73]. Furthermore, in multi-family buildings, lack of a mechanical ventilation system was associated with increased prevalence of SBS-related symptoms [69]. Further, buildings with balanced ventilation systems (supply/exhaust ventilation) had a higher prevalence of doctor diagnosed allergies, as compared to buildings with exhaust ventilation only [71].

There were some other investigative studies on the health impacts of energy efficiency in buildings. First, they found that air tightness [69,74] and use of direct electric radiators [69] in residential buildings were associated with increased prevalence of SBS-related symptoms. However, higher insulation level in buildings was associated with less SBS symptoms [70]. Second, buildings using more energy for heating were associated with lower rates of pollen allergies and eczema [71]. Energy efficiency improvements by boiler replacements in homes were associated with less admission rates for asthma and chronic obstructive pulmonary disease (COPD) [73]. Third, lower air temperature in buildings at a university campus was associated with less tear film stability [46]. Higher thermal variety (linked to lower domestic demand temperatures) was associated with fewer morbidities related to cold mortality [75].

3.2.4. Longitudinal Health Studies

A longitudinal study from Austria found that energy efficient buildings combined with installation of mechanical ventilation can improve general health and mental health but increase dry eye symptoms, as compared to conventional buildings with natural ventilation only [76] (Table 9).

3.2.5. Intervention Health Studies

Intervention health studies were conducted in the United Kingdom ($n = 3$), the United States ($n = 2$), Japan ($n = 1$), Sweden ($n = 1$), Denmark ($n = 1$), and multiple countries ($n = 1$). Except for one office study [43], eight studies were performed in residential buildings (Table 10). Some studies reported that energy efficiency intervention in homes can improve asthma [77,78], respiratory symptoms [77–79,81], sinusitis [80], general health [80,83], satisfaction [80,81], and reduce blood pressure [84]. Furthermore, an improved mechanical ventilation rate in office buildings can improve SBS symptoms, productivity, and perceived indoor air quality [43]. In addition, energy saving by reducing ventilation flow to below 0.5 air change rate (ACH) could impair perceived air quality but did not influence SBS [82].

3.2.6. Energy Factors and Health

In Table 3, data on associations between energy factors and any health outcomes among all 45 selected health studies were summarized. Thermal issues, including fuel poverty or low indoor air temperature, were not included in this table. Most studies showed beneficial effects of energy saving.

Table 3. Associations between energy factors and any health outcomes among all 45 selected health studies.

No.	References	Energy Efficiency Improvements (at Least Two Measures)	Green Buildings	More Effective Heating	Thermal Insulation	Draught Proofing	Higher Ventilation Rate	Installation of Mechanical Ventilation
1	Garland et al. 2013 [47]		+					
2	Singh et al. 2010 [41]		+					
3	Breysse et al. 2011 [48]		+					
4	Breysse et al. 2015 [49]		+					
5	Hedge et al. 2013 [44]		+					
6	Hedge et al. 2014 [45]		+					
7	Gawande et al. 2020 [42]		+					
8	Poortinga et al. 2017 [61]	+			–			
9	Carlton et al. 2019 [54]						–	
10	Howden-Chapman et al. 2011 [55]			+	+			
11	Howden-Chapman et al. 2007 [56]				+			
12	Humphrey et al. 2020 [85]						+	
13	Ahrentzen et al. 2016 [58]	+						
14	Shortt et al. 2007 [59]			+	+			
15	Chapman et al. 2009 [60]				+			
16	Grey et al. 2017 [61]	+						
17	Poortinga et al. 2018 [62]	+						
18	Sartini et al. 2018 [65]				+			
19	Peralta et al. 2017 [66]				+/-			
20	López-Bueno et al. 2020 [68]			+				
21	Engvall et al. 2003 [69]			+		–		+
22	Smedje et al. 2017 [70]				+			
23	Norback et al. 2014 [71]			+				
24	Wang et al. 2017 [72]						+	
25	Sharpe et al. 2019 [63]					–		
26	Sobotka et al. 1996 [74]					–		
27	Wallner et al. 2017 [76]	+						
28	Somerville et al. 2000 [77]			+				
29	Barton et al. 2007 [78]	+						
30	Osman et al. 2010 [79]	+						
31	Wilson et al. 2013 [80]	+						
32	Haverinen-Shaughnessy et al. 2018 [81]				+			
33	Wargocki et al. 2000 [43]						+	
34	Engvall et al. 2005 [82]						+	
35	Francisco et al. 2017 [83]				+			
36	Umishio et al. 2020 [84]				+			
	Positive associations (+)	8	7	6	9		4	1
	Negative associations (–)				1	3	1	
	Mixed results (+/–)				1			

Remark: + mean positive result, – means negative result, +/- means mixed results.

4. Discussion

To our knowledge, this review is the first systematic review on associations between different energy aspects of buildings and health. A meta-analysis could not be performed, since there were few articles covering the same energy aspect and the same health variable. However, the current knowledge level and knowledge gaps on the health effects of green buildings, fuel poverty, and energy use as well as energy efficiency improvements in buildings was able to be summarized or described.

In this review, there were three important issues related to exposure studies. Firstly, radon concentration in six studies was above 100 Bq/m³ in mean or in rooms [19,20,22,24,25,27]. In one review with meta-analysis on the risk of radon, the action level of radon for never-smokers and ever-smokers was recommended at 100 Bq/m³ of World Health Organization. They reported that radon exposure is the strongest risk factor for lung cancer for never-smokers [86]. Thus, special concern should be taken around radon exposure when performing home energy efficiency retrofits. In order to reduce radon levels in home energy-efficiency retrofits, installation of ground covers and sub-slab or sump depressurization systems as well as mechanical ventilation could be undertaken. One main source of indoor radon is radon from the ground. It should be ensured that the transmission of radon from the ground into buildings is minimized, especially for buildings in regions with primary geological layers in the underground. Another source of indoor radon is building materials, although it is not the main source. It is highly recommended that the building material for home retrofits works should meet the standards of green buildings. Secondly, installation of insulated windows and central heating systems can increase the indoor concentrations of mould [30]. The health risk of mould had been assessed in a previous review [8]. In many countries, mould and dampness caused by critical thermal bridges is a reason why energy efficiency interventions were performed [87]. Thus, it is important to consider thermal bridges as a cause of indoor mould growth after improving insulation in buildings. Thirdly, home energy efficiency retrofits can increase benzene, toluene, ethyl benzene, and xylene (BTEX) in indoor air [29]. In one previous review, the negative health effects of indoor BTEX had been reported [88]. Thus, it is important to use low-emissions building materials in energy efficiency retrofits.

Moreover, there were four important issues related to health studies.

Firstly, there were negative health effects in buildings with thermal insulation without installation of mechanical ventilation. In most cases, thermal insulation can reduce heat transfer, which will increase indoor temperature and reduce relative humidity and risk of mould. However, since many energy efficiency improvement methods can lead to reduced ventilation rates or air tightness, special concern should be taken to compensate for the reduced natural ventilation rate when working with home energy efficiency improvements. Thus, energy efficiency methods combined with improved ventilation or design should be promoted in airtight homes. In addition, the issue of thermal bridges and mould growth was seldom mentioned in the health studies.

Secondly, there were two negative associations between improved ventilation rate and health. In a fuel poverty study, high ventilation rates in low-income urban homes may increase chronic cough, asthma, and asthma-like symptoms [54]. This could be due to increased infiltration of outdoor air pollutants. Although this knowledge may be well known, the level of outdoor air pollutants had not been evaluated by the current intervention programs of low-income homes we found. In a cross-sectional health study, buildings with balanced ventilation systems (supply/exhaust ventilation) had a higher prevalence of doctor diagnosed allergies, as compared to buildings with exhaust ventilation only [71]. This may be caused by lack of a correct replacement of dirty filters in balanced mechanical ventilation systems. Thus, this knowledge should be addressed to residents in homes with energy efficiency improvements combined with balanced ventilation systems.

Thirdly, four fuel poverty health studies on cold mortality were performed in a longitudinal study design. This means that the cold-mortality effect of fuel poverty has been well known. Thus, fuel poverty behavior should be considered in interventions since it is often linked to reduced ventilation rate and ineffective heating. Except for winter fuel payment and energy intervention policy, wearable telemetry may be a good choice of solution in cold homes [63]. This is because wearable telemetry can increase the occupant's awareness of cold. However, all those studies were based on cold climates. In hot climate zones, there is a need to conduct similar research in low-income homes.

Fourthly, 4 green buildings health studies were conducted in a longitudinal study design. This means that long-term health effects of green buildings were assessed in the

USA. However, those green buildings were assessed by LEED credits of the USA standard. Although there are existing green rating systems in different countries, energy efficiency improvements combined with correct ventilation and renewable energy use have been emphasized in most green rating systems.

This literature review has a number of strengths. The main focus was on epidemiological studies, including intervention studies, cross-sectional studies, and longitudinal studies. However, exposure studies without any reported health data or health associations were also included if they were identified in this literature search. For each included study, the country of the study, type of study, type of buildings, number of buildings and number of subjects were noted in the review. In exposure studies, extra information on the changes of concentrations of major pollutants was collected. In studies with unexpected results or negative impacts of energy use and energy saving, explanations of the results reported by the authors were included.

The studies included in this review had some limitations in their study design. One major limitation was that none of the studies had studied health effects of energy efficiency improvement by the installation of heat recovery to existing mechanical ventilation systems. This may be because many studies had not separated it from combined energy efficiency measures. However, installation of heat recovery to mechanical ventilation systems is a major method nowadays to save energy use and there is a need to assess its health benefits, especially in airtight homes. The second limitation is that many of the intervention studies were based on more than two energy saving improvements. Thus, it is not possible to draw clear conclusions on the health effects of single energy efficiency improvement measures. The third limitation is that there were few prospective health studies on long-term health effects of energy efficiency improvements and energy use. However, many prospective health studies on green buildings and fuel poverty were found. The fourth limitation is that most studies were on residential buildings. Only three studies were on office buildings and only four studies were on school or university buildings.

5. Conclusions

Energy efficiency improvements and green building can have positive effects on asthma, respiratory symptoms, mental health, and general health as well as on performance and satisfaction. Home energy efficiency improvement with mechanical ventilation system can reduce radon, mould, bacteria, and house dust mites, TVOC, CO₂, CO, and black carbon levels as well as some volatile organic compounds. More efficient heating and increased thermal insulation can have positive health impacts in fuel-poverty homes. However, energy savings in airtight buildings and thermal insulation without the installation of mechanical ventilation can impair health. Moreover, health risks linked to energy efficiency retrofits exists. Installation of mechanical ventilation can solve many of the negative effects linked to airtight buildings and energy efficiency retrofits.

For future energy efficiency intervention or retrofit studies, measures of radon and BTEX and other chemicals, as well as levels of thermal bridge and outdoor air pollutants may be needed. In addition, it is important to replace dirty filters in balanced mechanical ventilation systems.

Furthermore, future research needs on this topic were identified. Firstly, the intervention study should measure how much energy they save after energy efficiency measures. Secondly, more studies are needed on the health aspects of energy efficiency improvement by the installation of heat recovery to mechanical ventilation system. Thirdly, future studies should focus on evaluating health effects of single energy efficiency improvement measures, rather than a combination of measures. Fourthly, more prospective health studies on long-term health effects of energy efficiency improvements or energy use are needed. Fifthly, future studies should include offices, schools, and hospital buildings, and should cover different climate zones in the world.

Author Contributions: Conceptualization, C.W., J.W. and D.N.; Methodology, C.W., J.W. and D.N.; Data Curation, C.W., J.W. and D.N.; Writing—Original Draft Preparation, C.W.; Writing—Review & Editing, C.W., J.W. and D.N.; Supervision, J.W. and D.N.; Funding Acquisition, J.W. All authors have read and agreed to the published version of the manuscript.

Funding: The research was supported by the Swedish AFA Insurance (No. 467801100).

Institutional Review Board Statement: Not applicable.

Informed Consent Statement: Not applicable.

Conflicts of Interest: The authors declare no conflict of interest.

Appendix A

Table A1. Exposure Field Studies on Radon.

Author	Year	Country	Energy Aspects	Type of Study	Type of Buildings	Measured Exposure	Changes of Measured Exposure	Number of Households or Buildings	Main Results
Collignan et al. [19]	2016	France	Improved insulation, ventilation and window replacement	One time measurement	Residential buildings	Radon	21% increase (median 147 Bq/m ³)	3233 households or 3233 buildings	Energy efficiency thermal retrofit (linked to reduced air permeability of the building envelope) can increase indoor radon concentration.
Symonds et al. [20]	2019	United Kingdom	Insulation in loft and wall, double glazing	Longitudinal	Residential buildings	Radon	Arith. Mean > 132–159.3 Bq/m ³	470,689 households	Energy efficiency retrofit by improving insulation in loft and wall, and/or double glazing can increase radon concentrations, possibly due to increased airtightness.
Du et al. [29]	2019	Finland and Lithuania	Improved insulation in wall, roof, windows or balconies	Intervention	Residential buildings	Radon	Mean increase of 13.8 Bq/m ³ (<100 Bq/m ³)	336 households or 65 buildings	In homes in Lithuania, energy efficiency retrofits without insulation of mechanical ventilation increased indoor radon concentrations.
Pigg et al. [27]	2018	United States	Weatherization services	Intervention	Residential buildings	Radon	Increased by 0.14 ± 0.13 pCi/L (>100 Bq/m ³ in high zone)	514 households	Energy efficiency weatherization services (retrofits) can increase radon concentration. However, energy efficiency weatherization services with improved ventilation or ground covers can reduce radon concentration.
Meyer et al. [21]	2019	Germany	Air tightness windows and insulation of outer walls	One time measurement	Residential buildings	Radon	40 Bq/m ³ in non-returfished vs. 69 Bq/m ³ in returfished	150 households	Energy efficiency refurbishments of existing buildings without installation of ventilation systems can increase radon concentration, as compared to non-returfished conventional buildings.
Pressyanov et al. [22]	2015	Bulgaria	New energy-efficient windows with plastic joinery	Intervention	Residential buildings	Radon	Rooms with radon increase was 193 Bq/m ³ and rooms with no change was 45 Bq/m ³	20 rooms or 16 buildings	Energy-efficient reconstructions with installation of new energy-efficient windows (linked to air tightness) can increase radon levels.
Vasilyev et al. [23]	2017	Russia	Energy efficiency insulation	One time measurement	Residential buildings	Radon	Arithmetic mean 38 Bq/m ³ in conventional vs. 93 Bq/m ³ in modern buildings	81 buildings	Energy efficiency measures in buildings (linked to low indoor air exchange rate) can increase indoor radon concentration.

Table 1. Cont.

Author	Year	Country	Energy Aspects	Type of Study	Type of Buildings	Measured Exposure	Changes of Measured Exposure	Number of Households or Buildings	Main Results
Yarmoshenko et al. [24]	2014	Russia	Energy efficiency insulation	Before-after	Residential buildings	Radon	Arithmetic mean 42 Bq/m ³ in conventional vs. 133 Bq/m ³ in modern buildings	7 households or 7 buildings	Energy efficiency measures in buildings (linked to low indoor air exchange rate) can increase indoor radon concentration.
Vasilyev et al. [25]	2015	Russia	Energy efficiency insulation	Before-after	Residential buildings	Radon	Arithmetic mean 42 Bq/m ³ in conventional vs. 166 Bq/m ³ in modern buildings	5 rooms or 5 buildings	Energy efficiency measures in buildings (linked to low indoor air exchange rate) can increase indoor radon concentration.
Burghel et al. [26]	2020	Romania	Installation of centralized and decentralized mechanical ventilation with heat recovery	Intervention	Residential buildings	Radon	Reduction was between 25% to 95% (Before >100 Bq/m ³)	10 households or 10 buildings	Sub-slab and sump depressurization, installation of centralized and decentralized mechanical ventilation with heat recovery can reduce radon concentrations.
Wallner et al. [28]	2015	Austria	Existing mechanical ventilation and natural ventilation	Before-after	Residential buildings	Radon	17 Bq/m ³ mechanical ventilation vs. 31 Bq/m ³ natural ventilation	123 households	Energy-efficient buildings with existing mechanical ventilation can reduce radon concentrations, as compared to conventional buildings without installation of mechanical ventilation, especially for radon.

Table 2. Exposure Field Studies on Mould Bacteria and House Dust Mites.

Author	Year	Country	Energy Aspects	Type of Study	Type of Buildings	Measured Exposure	Changes of Measured Exposure	Number of Households	Main Results
Hirsch et al. [30]	2000	Germany	Installation of insulated windows and central heating systems	Intervention	Residential buildings	House dust mite Der f 1 and mould	Der f 1 in carpets 0.65 vs. 1.28 mattresses 1.56 vs. 2.40 µg/g; Aspergillus fumigatus 20 vs. 60 units/g	98 households	Installation of insulated windows and central heating systems (linked to reduced ventilation) increased the concentration of the house dust mite allergen Der f 1 and the mould species Aspergillus fumigatus.
Sharpe et al. [31]	2015	United Kingdom	Fuel poverty	Cross-sectional	Social Residential buildings	Self-reported dampness and mould	No data	671 households	Fuel poverty (linked to ineffective heating and ventilation practices) can increase indoor dampness and mould, regardless of the use of extractor fans.

Table 2. Cont.

Author	Year	Country	Energy Aspects	Type of Study	Type of Buildings	Measured Exposure	Changes of Measured Exposure	Number of Households	Main Results
Sharpe et al. [32]	2016	United Kingdom	Type of heating, glazing, insulation levels, energy efficiency ratings	Cross-sectional	Social Residential buildings	Self-reported allergenic mould	No data	41 households	Energy efficiency improvement combined with increased ventilation flow rate reduced fungal contamination with Aspergillus/Penicillium mould species and Cladosporium spp.
Spertini et al. [33]	2010	Switzerland	Improved insulation, ventilation system with heat recovery and natural ventilation	One time measurement	Residential buildings	Self-reported house dust mites Der f 1	Median 67 vs. 954 ng/g in mattresses and 20 vs. 174 ng/g in carpets	289 households or 11 buildings	Buildings designed for low energy use with installation of mechanical ventilation reduced indoor relative air humidity as well as house dust mite allergen concentration both in mattresses and in carpets, as compared to control buildings.
Niculita-Hrizel et al. [34]	2020	Switzerland	Type of ventilation and energy consumption	One time measurement	Residential buildings	Fungal	Penicillium CFUs was lower	149 households	Installation of mechanical ventilation in buildings reduced the infiltration of outdoor fungal particles, as compared to buildings with natural ventilation only.
Coombs et al. [35]	2018	United States	Green renovation with bathroom fans	Before-after	Residential buildings	Mould	521,826 reads from green homes vs. 726,690 fungal reads from non-green homes	52 households	The concentration of mould in air samples and door dust samples did not differ between green and non-green homes. However, green homes had a lower concentration of mould in bed samples.
Du et al. [29]	2019	Finland and Lithuania	Replacing windows and/or installation of heat recovery to the existing exhaust ventilation system	Intervention	Residential buildings	Airborne mould and bacterial	Fungal 0.6-log; Bacterial 0.6-log in gram-positive and 0.9-log in gram-negative bacterial (reduction in cells/m ³)	336 households or 65 buildings	In homes in Finland, energy efficiency retrofits with installation of mechanical ventilation reduced indoor concentrations of airborne mould and bacterial.
Wallner et al. [28]	2015	Austria	Mechanical ventilation and natural ventilation	Before-after	Residential buildings	Mould	84% of rooms vs. 35% rooms	123 households	Energy-efficient buildings with installation of mechanical ventilation reduced indoor mold spore concentration, as compared to conventional buildings without installation of mechanical ventilation.

Table 3. Exposure Field Studies on Chemicals.

Author	Year	Country	Energy Aspects	Type of Study	Type of Buildings	Measured Exposure	Changes of Measured Exposure	Number of Households or Buildings	Main Results
Derbez et al. [36]	2018	France	Installation of ventilation system or passive stack/hybrid ventilation	Before-after	Residential buildings	VOCs, aldehyde	Hexaldehyde: 37 vs. 17 µg/m ³ in dwellings with/without flooring products	72 households or 43 buildings	Low energy retrofit can increase the air concentration of alpha-pinene and hexaldehyde, possibly caused by the use of wood or wood-based products for the construction and insulation.
Du et al. [29]	2019	Finland and Lithuania	Replacing windows and/or installation of heat recovery to the existing exhaust ventilation system	Intervention	Residential buildings	BTEX and formaldehyde	Mean increase of 2.5 µg/m ³ in BTEX	336 households or 65 buildings	In homes in Finland, energy efficiency retrofits with existing mechanical ventilation increased indoor air concentrations of benzene, toluene, ethyl benzene and xylene (BTEX) but reduced indoor formaldehyde concentrations.
Leivo et al. [37]	2018	Finland and Lithuania	Installation of heat recovery to the existing exhaust ventilation system. Improved thermal insulation in wall, roof, windows or balconies	Intervention	Residential buildings	CO ₂	Median: 775 vs. 956 PPM (1st); Median: 730 vs. 840 PPM (2nd)	290 households or 66 buildings	In homes in Finland, energy efficiency retrofits with existing mechanical ventilation reduced CO ₂ concentration as compared to natural ventilation. In homes in Lithuania, improved insulation without installation of mechanical ventilation increased measured CO ₂ levels.
Coombs et al. [38]	2016	United States	Green renovation	Intervention	Residential buildings	Black carbon, formaldehyde	Black carbon averaging 682 vs. 2364 ng/m ³ ; Formaldehyde 0.03 vs. 0.01 ppm	42 households	Energy efficiency green renovation (linked to reduced ventilation) decreased indoor black carbon level in air from outdoor sources and increased indoor formaldehyde concentration.
Yang et al. [39]	2020	Switzerland	Thermal retrofit of roof, walls and floors; replacement of heating system, installation of mechanical ventilation system	One time measurement	Residential buildings	Aldehydes, VOCs	Formaldehyde 13 vs. 15; Toluene 16 vs. 26; Xylenes 1.4 vs. 58; Acrolein 0.4 vs. 0.6; D-limonene 7.9 vs. 11; Isobutane 3.4 vs. 10; Butane 8.8 vs. 2 (µg/m ³)	169 households	Energy efficiency thermal retrofit without installation of mechanical ventilation increased formaldehyde, aromatics, alkane, and levels of certain volatile organic compounds, as compared to new homes built with installed mechanical ventilation.

Table 3. Cont.

Author	Year	Country	Energy Aspects	Type of Study	Type of Buildings	Measured Exposure	Changes of Measured Exposure	Number of Households or Buildings	Main Results
Verrille et al. [18]	2016	France	Controlled ventilation systems	Before-after	School buildings	CO ₂	Peak Level 1000 ppm vs. 3800–5000 ppm	10 school buildings	Low energy school buildings combined controlled mechanical ventilation systems and an adapted ventilation schedule can reduce CO ₂ levels.
Pigg et al. [27]	2018	United States	Weatherization services	Intervention	Residential buildings	CO	Peak Level 35 ppm vs. 13–20 ppm	514 households	Energy efficiency weatherization services in homes without improved ventilation or ground covers can reduce exposure to CO.
Wallner et al. [28]	2015	Austria	Mechanical ventilation and natural ventilation	Before-after	Residential buildings	CO ₂ , TVOC, aldehydes	CO ₂ : 1360 vs. 1830 ppm and 1280 vs. 1740 ppm; TVOC: 300 vs. 560 µg/m ³ ; aldehydes: 32 vs. 53 µg/m ³ and 18 vs. 33 µg/m ³	123 households	Energy efficient buildings with installation of mechanical ventilation reduced indoor concentrations of CO ₂ , TVOC, aldehydes, and improved the measured indoor air quality in homes, as compared to conventional buildings without installation of mechanical ventilation.
Baumgartner et al. [40]	2019	China	Low-polluting semi gasifier cook stove with chimney, water heater and pelletized biomass fuel	Intervention	Residential buildings	PM _{2.5} , black carbon	PM _{2.5} (46%), black carbon (55%)	205 households	An energy intervention replacing low-polluting semi gasifier cook stove in rural buildings was associated with decreased exposures to PM _{2.5} and black carbon in winter but higher exposures to PM _{2.5} and black carbon in summer, as compared to untreated homes with traditional stoves. The negative effect could be caused by increased use of semi gasifier cook stove.

Table 4. Green Building Health Studies.

Author	Year	Country	Energy Aspects	Type of Study	Type of Buildings	Type of Health Variables	Number of Buildings	Number of Subjects	Main Results
Garland et al. [47]	2013	United States	Green buildings with LEED Credits	Intervention	Residential buildings	Self-reported asthma	1 building	18 children and adults	Green home buildings can reduce self-reported asthma symptoms.
Singh et al. [41]	2010	United States	Green buildings with LEED Credits	Longitudinal	Office buildings	Absenteeism due to self-reported asthma, respiratory allergies, depression and stress, and work productivity	2 office buildings	263 employees	Green office buildings can improve indoor environment quality and reduce absenteeism due to self-reported asthma, respiratory allergies, depression and stress, and moreover improve work productivity.
Breyse et al. [48]	2011	United States	Green efficiency renovation	Longitudinal	Residential buildings	Self-reported asthma, and non-asthma respiratory problems, overall health	1 building	80 children and adults	Among adults, green efficiency renovation in homes can reduce self-reported asthma. Green efficiency renovation in homes can improve self-reported overall health and reduce non-asthmatic respiratory symptoms in adults as well as in children.
Breyse et al. [49]	2015	United States	Green efficiency renovation	Intervention	Residential buildings	Self-reported mental and general physical health	1 building	612 older adults	Green efficiency renovation in homes can improve mental and general physical health.
Hedge et al. [44]	2013	United States	Green buildings with LEED Credits	Longitudinal	University buildings	Overall health, performance and work satisfaction	2 university buildings	44 employees	Green office buildings in a college campus improved health, performance and work satisfaction.
Hedge et al. [45]	2014	Canada	Green buildings with LEED Credits	Longitudinal	University buildings	Overall health, performance and study satisfaction	3 university buildings	319 employees	Green classrooms in an university campus improved health, performance and work satisfaction.
Gawande et al. [42]	2020	India	Green Office Buildings	cross-sectional	Office Buildings	SBS	10 office buildings	148 employees	No significant association between green buildings and sick building syndrome symptoms (SBS), compared with conventional buildings.

Table 5. Fuel Poverty Health Studies on Respiratory Symptoms.

Author	Year	Country	Energy Aspects	Type of Study	Type of Buildings	Type of Health Variables	Number of Households	Number of Subjects	Main Results
Rudge et al. [50]	2005	United Kingdom	Fuel poverty	Longitudinal	Residential buildings	Winter respiratory disease	220 households	460 older adults	Fuel poverty in low-income homes can increase winter respiratory disease.
Webb et al. [51]	2013	United Kingdom	Fuel poverty	Cross-sectional	Residential buildings	Measured respiratory disease	3763 households	3763 older adults	Fuel poverty in low-income homes increase respiratory disease.
Sharpe et al. [52]	2015	United Kingdom	Type of heating, glazing, insulation, energy efficiency ratings	Cross-sectional	Social residential buildings	Doctor diagnosed asthma	706 households	944 adults	Energy efficiency improvement in social housing might increase current adult asthma. This may be due to increased exposure to physical, biological and chemical contaminants linked to inadequate heating, ventilation (fuel poverty behavior).
Poortinga et al. [53]	2017	United Kingdom	Loft insulation, cavity-wall insulation, external wall insulation	Repeated cross-sectional	Social residential buildings	General health, mental health, and social outcomes	Around 9200 households	10,009 individuals	Energy efficiency improvements in social housing can improve respiratory symptoms.
Carlton et al. [54]	2019	United States	Home ventilation rate	Cross-sectional	Residential buildings	Respiratory symptoms	216 households	302 children and adults	High ventilation rates in low-income urban homes may increase chronic cough, asthma and asthma-like symptoms, probably caused by infiltration of outdoor air pollutants.
Howden-Chapman et al. [55]	2011	New Zealand	Improved insulation into existing houses; more effective heating in insulated houses	Intervention	Residential buildings	Respiratory symptoms	1350 households; 409 households	4407 children and adults; 409 children	Energy saving by using more effective heating in insulated low-income homes can improve health status and respiratory symptoms in children with asthma diagnosis.
Howden-Chapman et al. [56]	2007	New Zealand	Installation of a standard retrofit insulation package	Intervention	Residential buildings	Hospital admissions for respiratory conditions	1350 households	4407 children and adults	Energy saving by insulating existing houses in low-income communities can improve indoor environment and reduce hospital admissions for respiratory conditions.
Humphrey et al. [85]	2020	United States	Home ventilation rate	Cross-sectional	Residential buildings	Measured lung function	187 households	253 children and adults	High infiltration rate in low-income, urban, non-smoking homes can improve lung health.

Table 6. Fuel Poverty Health Studies on General and Mental Health.

Author	Year	Country	Energy Aspects	Type of Study	Type of Buildings	Type of Health Variables	Number of Households	Number of Subjects	Main Results
Thomson et al. [57]	2017	32 European Countries	Fuel poverty	Cross-sectional	Residential buildings	General health and well-being	No data	41,560 adults	Fuel poverty in low-income homes can reduce general health and emotional well-being.
Poortgen et al. [53]	2017	United Kingdom	Loft insulation, cavity-wall insulation, external wall insulation	Repeated cross-sectional	Social residential buildings	General health, mental health, and social outcomes	Around 9200 households	10,009 individuals	Energy efficiency improvements in social housing can improve general health, mental health and social outcomes. However, installation of cavity wall insulation without installation of mechanical ventilation can reduce general health outcomes and social outcomes.
Ahrentzen et al. [58]	2016	United States	Insulation of roof and floor, improved thermal, air conditioner heating, cooling system, new ceiling fans, new windows	Intervention	Residential buildings	General health, emotional distress, sleep	53 households	57 older adults	Energy efficiency retrofits in low-income homes can improve general health, emotional distress, and sleep among the older adults.
Shortt et al. [59]	2007	United Kingdom	Installation of central heating systems or improved insulation	Intervention	Residential buildings	General health, well being	100 households	100 individuals	Energy efficiency intervention in fuel poverty homes can improve general health, well-being.
Howden-Chapman et al. [55]	2011	New Zealand	Improved insulation into existing houses; more effective heating in insulated houses	Intervention	Residential buildings	General health and well being	1350 households; 409 households	4407 children and adults; 409 children	Energy saving by improving insulation in low-income homes can improve general health and well-being and reduce hospitalization in children and adults. Energy saving by using more effective heating in insulated low-income homes can improve general health status in children.
Howden-Chapman et al. [56]	2007	New Zealand	Installation of a standard retrofit insulation package	Intervention	Residential buildings	General health and well being	1350 households	4407 children and adults	Energy saving by insulating existing houses in low-income communities can improve indoor environment so that improve self-reported health, wheezing, days off school and work.

Table 6. Cont.

Author	Year	Country	Energy Aspects	Type of Study	Type of Buildings	Type of Health Variables	Number of Households	Number of Subjects	Main Results
Chapman et al. [60]	2009	New Zealand	Installation of a standard retrofit insulation package	Intervention	Residential buildings	General health, well being	1350 households	4407 children and adults	Energy saving by insulating existing houses in low-income communities can improve general health, as well as cost-benefit of general practitioner (GP) visits, hospitalizations, reduced time off work and school.
Grey et al. [61]	2017	United Kingdom	External wall insulation, central heating system, and installation of gas network	Intervention	Residential buildings	Well-being and psychosocial outcomes	774 households	776 individuals	Energy efficiency intervention in low-income homes can increase residential wellbeing and psychosocial-related health.
Poortinga et al. [62]	2018	United Kingdom	External wall insulation, photovoltaics, solar water heating, air source heat pumps, loft/rafter insulation	Intervention	Residential buildings	Well-being and psychosocial outcomes	4968 households	25,908 individuals	Energy efficiency intervention in low-income homes can improve well-being and psychosocial outcomes.
Pollard et al. [63]	2019	United Kingdom	Fuel poverty	Intervention	Residential buildings	Psychosocial outcomes	22 households	22 adults	Wearable telemetry (a thermometer with a low-temperature alarm) can raise awareness of the health effects of cold home among people living in fuel poverty (linked to psychosocial outcomes).

Table 7. Fuel Poverty Health Studies on Cold-related Mortality.

Author	Year	Country	Energy Aspects	Type of Study	Type of Buildings	Type of Health Variables	Number of Households	Number of Subjects	Main Results
Angelini et al. [64]	2019	United Kingdom	Winter fuel payment	Longitudinal	Residential buildings	Cold-related mortality, blood pressure, fibrinogen	11,578 households	18,813 adults	Low indoor air temperature in low-income homes can increase systolic and diastolic blood pressure and fibrinogen levels in blood samples (linked to cold-related mortality).
Sartini et al. [65]	2018	United Kingdom	Fuel poverty types of home insulation and heating	Longitudinal	Residential buildings	Cold-related mortality	1006 households	1402 older men	Lack of insulation in low-income homes can increase cold-related mortality.
Peralta et al. [66]	2017	Spain	Energy efficient façade insulation retrofit	Longitudinal	Social residential buildings	Cold-related mortality	2552 households	2552 individuals	Energy efficient façade insulation retrofit in public housing can reduce cold-related mortality in women, but can increase cold-related total mortality in men. The health outcome for the gender difference is unclear.
Umishio et al. [67]	2019	Japan	Low insulation in cold homes	Cross-sectional	Residential buildings	Blood pressure	1840 households	2900 adults	Low indoor air temperature was higher associated with blood pressure and hypertension (linked to cold-related mortality).
López-Bueno et al. [68]	2020	Spain	Heating systems	Longitudinal	Residential buildings	Cold-related mortality	No data	No data	Districts with higher homes without a heating system had cold-related mortality.

Table 8. Cross-sectional Health Studies.

Author	Year	Country	Energy Aspects	Type of Study	Type of Buildings	Type of Health Variables	Number of Buildings or Households	Number of Subjects	Main Results
Engvall et al. [69]	2003	Sweden	Type of ventilation and heating system, heat pumps, reconstruction and energy-saving measures	Cross-sectional	Residential buildings	Sick building syndrome (SBS) symptoms	231 buildings	3241 adults	In multi-family buildings, lack of a mechanical ventilation system and use of direct electric radiators were associated with increased prevalence of SBS-related symptoms. Major reconstruction and multiple sealing in multi-family buildings were associated with increased prevalence of SBS-related symptoms.
Smedje et al. [70]	2017	Sweden	Type of ventilation system and insulation level	Cross-sectional	Residential buildings	Sick building syndrome (SBS) symptoms	605 buildings	1160 adults	In single-family buildings, a lower U-value (higher insulation level) was associated with less SBS symptoms.
Norback et al. [71]	2014	Sweden	Type of ventilation and energy use for heating	Cross-sectional	Residential buildings	Doctor's diagnosed asthma, allergy and self-reported pollen allergy, eczema	472 buildings	7554 adult	Multi-family buildings with balanced ventilation systems (supply/exhaust ventilation) had a higher prevalence of doctor diagnosed allergy, as compared to buildings with exhaust ventilation only. Buildings using more energy for heating were associated with less pollen allergy and eczema.
Wang et al. [72]	2017	Sweden	Type of ventilation and degree of insulation	Cross-sectional	Residential buildings	Doctors' diagnosed asthma, self-reported asthma	605 buildings	1160 adults	Higher air exchange rate in the single-family residential homes was associated with less current asthma symptoms.
Sharpe et al. [73]	2019	United Kingdom	Energy efficiency ratings	Cross-sectional	Residential buildings	Asthma, chronic obstructive pulmonary disease, cardiovascular disease	No data	No data	Reduced home ventilation rates were associated with more asthma disease. Homes with more energy efficiency improvements may be associated with more admission rates for respiratory and cardiovascular diseases, possibly caused by reduced home ventilation flow rate. Energy efficiency measures can improve health outcomes, especially chronic respiratory illness.

Table 8. Cont.

Author	Year	Country	Energy Aspects	Type of Study	Type of Buildings	Type of Health Variables	Number of Buildings or Households	Number of Subjects	Main Results
Sobotka et al. [74]	1996	Germany	New windows and door, improved insulation and heating system	Cross-sectional	Residential buildings	Sick building syndrome (SBS) symptoms	52 buildings	No data	Energy saving by installing new air-tightness windows and door in homes was associated with more SBS-related health complaints. This may be due to fuel poverty behavior by not airing their flats sufficiently.
Bakke et al. [46]	2008	Norway	Lower air temperature	Cross-sectional	University buildings	Tear film stability, nasal patency	4 university buildings	173 employees	Lower air temperature in buildings at a university campus was associated with less tear film stability and more health problems.
Kennard et al. [75]	2020	United Kingdom	Space heating energy use	Cross-sectional	Residential buildings	Cold-mortality	77,762 households	77,762 adults	Higher thermal variety (linked to lower domestic demand temperatures) was associated with less morbidities related to cold-mortality.

Table 9. Longitudinal Health Studies.

Author	Year	Country	Energy Aspects	Type of Study	Type of Buildings	Type of Health Variables	Number of Buildings	Number of Subjects	Main Results
Wallner et al. [76]	2017	Austria	Mechanical ventilation and natural ventilation	Longitudinal	Residential buildings	General health and dry eye symptoms	123 buildings	575 children and adults	Energy efficient buildings combined with installation of mechanical ventilation can improve self-reported health but increase dry eye symptoms, as compared to conventional buildings with natural ventilation only.

Table 10. Intervention Health Studies.

Author	Year	Country	Energy Aspects	Type of Study	Type of Buildings	Type of Health Variables	Number of Buildings or Households	Number of Subjects	Main Results
Somerville et al. [77]	2000	United Kingdom	the installation of central heating systems	Intervention	Residential buildings	Respiratory symptoms	59 households	72 children with diagnosed asthma	Energy efficiency intervention in homes reduced respiratory symptoms, and reduced missed school days due to asthma in children with diagnosed asthma.
Barton et al. [78]	2007	United Kingdom	Central heating systems, ventilation, rewiring, insulation, and re-roofing	Intervention	Social residential buildings	Asthma, non-asthma-related respiratory disease	119 households	480 children and adults	Energy efficiency intervention in social housing reduced asthma symptoms, and non-asthmatic respiratory disease.
Osman et al. [79]	2010	United Kingdom	Central heating systems, installation of loft, under-floor and cavity wall insulation	Intervention	Residential buildings	Diagnosed chronic obstructive pulmonary disease (COPD)	178 households	178 older adults with COPD	Energy efficiency intervention in homes can improve respiratory health for elderly COPD patients.
Wilson et al. [80]	2013	United States	Insulation, heating equipment and ventilation improvements	Intervention	Residential buildings	Sinusitis, general health, satisfaction	248 households	323 children and adults	Energy efficiency retrofits work in homes can improve sinusitis, general health, satisfaction.
Haavinen-Staughtnessy et al. [81]	2018	Finland and Lithuania	Installation of heat recovery to the existing exhaust ventilation system. Improved thermal insulation in wall, roof, windows or balconies	Intervention	Residential buildings	Respiratory symptoms	66 buildings	283 individuals	Energy efficiency retrofits in homes can improve occupant satisfaction with daily noise nuisance, upper respiratory symptoms, and reduce absence from school or from work due to respiratory infections.
Wargoeki et al. [43]	2000	Denmark	different ventilation rates	Intervention	Office building	Sick building syndrome (SBS) symptoms, work productivity	1 office building	30 female employees	Improved mechanical ventilation rate in office building improve SBS symptoms, work productivity, and perceived indoor air quality.
Engvall et al. [82]	2005	Sweden	different ventilation rates	Intervention	Residential buildings	General health	1 building	44 adults	Energy saving by reducing ventilation flow to below 0.5 ACH could impair perceived air quality but did not influence SBS.
Francisco et al. [83]	2017	United States	Weatherization services	Intervention	Residential buildings	General health	72 households	178 children and adults	Energy efficiency retrofits can improve self-reported health.
Umishio et al. [84]	2020	Japan	installation of outer walls, floor and/or roof insulation and replacement of windows	Intervention	Residential buildings	Blood pressure	1009 households	1685 adults	Energy efficiency insulation retrofitting in homes can reduce home blood pressure and reduce morning home systolic blood pressure of hypertensive patients.

References

1. Norbäck, D. An update on sick building syndrome. *Curr. Opin. Allergy Clin. Immunol.* **2009**, *9*, 55–59. [[CrossRef](#)] [[PubMed](#)]
2. Melikov, A.K. Advanced air distribution: Improving health and comfort while reducing energy use. *Indoor Air* **2016**, *26*, 112–124. [[CrossRef](#)] [[PubMed](#)]
3. Smith, K.R.; Frumkin, H.; Balakrishnan, K.; Butler, C.D.; Chafe, Z.A.; Fairlie, I.; Kinney, P.; Kjellstrom, T.; Mauzerall, D.L.; McKone, T.E.; et al. Energy and human health. *Annu. Rev. Public Health* **2013**, *34*, 159–188. [[CrossRef](#)] [[PubMed](#)]
4. Brennan, M.; O’Shea, P.M.; Mulkerrin, E.C. Preventative strategies and interventions to improve outcomes during heatwaves. *Age Ageing* **2020**, *49*, 729–732. [[CrossRef](#)]
5. Willand, N.; Ridley, I.; Maller, C. Towards explaining the health impacts of residential energy efficiency interventions—A realist review. Part 1: Pathways. *Soc. Sci. Med.* **2015**, *133*, 191–201. [[CrossRef](#)]
6. Barrett, B.; Charles, J.W.; Temte, J.L. Climate change, human health, and epidemiological transition. *Prev. Med.* **2015**, *70*, 69–75. [[CrossRef](#)]
7. Wilkinson, P.; Smith, K.R.; Beevers, S.; Tonne, C.; Oreszczyn, T. Energy, energy efficiency, and the built environment. *Lancet* **2007**, *370*, 1175–1187. [[CrossRef](#)]
8. Peat, J.K.; Dickerson, J.; Li, J. Effects of damp and mould in the home on respiratory health: A review of the literature. *Allergy* **1998**, *53*, 120–128. [[CrossRef](#)]
9. Kolokotsa, D.; Santamouris, M. Review of the indoor environmental quality and energy consumption studies for low income households in Europe. *Sci. Total Environ.* **2015**, *536*, 316–330. [[CrossRef](#)]
10. Carmichael, L.; Prestwood, E.; Marsh, R.; Ige, J.; Williams, B.; Pilkington, P.; Eaton, E.; Michalec, A. Healthy buildings for a healthy city: Is the public health evidence base informing current building policies? *Sci. Total Environ.* **2020**, *719*, 137146. [[CrossRef](#)]
11. Houghton, A.; Castillo-Salgado, C. Associations between Green Building Design Strategies and Community Health Resilience to Extreme Heat Events: A Systematic Review of the Evidence. *Int. J. Environ. Res. Public Health* **2019**, *16*, 663. [[CrossRef](#)] [[PubMed](#)]
12. Allen, J.G.; MacNaughton, P.; Laurent, J.G.; Flanigan, S.S.; Eitland, E.S.; Spengler, J.D. Green Buildings and Health. *Curr. Environ. Health Rep.* **2015**, *2*, 250–258. [[CrossRef](#)] [[PubMed](#)]
13. Cedeno-Laurent, J.G.; Williams, A.; MacNaughton, P.; Cao, X.; Eitland, E.; Spengler, J.; Allen, J. Building Evidence for Health: Green Buildings, Current Science, and Future Challenges. *Annu. Rev. Public Health* **2018**, *39*, 291–308. [[CrossRef](#)] [[PubMed](#)]
14. Liddell, C.; Morris, C. Fuel poverty and human health: A review of recent evidence. *Energy Policy* **2010**, *38*, 2987–2997. [[CrossRef](#)]
15. Howieson, S.G.; Hogan, M. Multiple deprivation and excess winter deaths in Scotland. *J. R. Soc. Promot. Health* **2005**, *125*, 18–22. [[CrossRef](#)]
16. Anderson, M.; Carmichael, C.; Murray, V.; Dengel, A.; Swainson, M. Defining indoor heat thresholds for health in the UK. *Perspect. Public Health* **2013**, *133*, 158–164. [[CrossRef](#)]
17. Page, M.J.; McKenzie, J.E.; Bossuyt, P.M.; Boutron, I.; Hoffmann, T.C.; Mulrow, C.D.; Shamseer, L.; Tetzlaff, J.M.; Akl, E.A.; Brennan, S.E.; et al. The PRISMA 2020 statement: An updated guideline for reporting systematic reviews. *Int. J. Surg.* **2021**, *88*, 105906. [[CrossRef](#)]
18. Verrielle, M.; Schoemaeker, C.; Hanoune, B.; Leclerc, N.; Germain, S.; Gaudion, V.; Locoge, N. The MERMAID study: Indoor and outdoor average pollutant concentrations in 10 low-energy school buildings in France. *Indoor Air* **2016**, *26*, 702–713. [[CrossRef](#)]
19. Collignan, B.; Le Ponner, E.; Mandin, C. Relationships between indoor radon concentrations, thermal retrofit and dwelling characteristics. *J. Environ. Radioact.* **2016**, *165*, 124–130. [[CrossRef](#)]
20. Symonds, P.; Rees, D.; Daraktchieva, Z.; McColl, N.; Bradley, J.; Hamilton, I.; Davies, M. Home energy efficiency and radon: An observational study. *Indoor Air* **2019**, *29*, 854–864. [[CrossRef](#)]
21. Meyer, W. Impact of constructional energy-saving measures on radon levels indoors. *Indoor Air* **2019**, *29*, 680–685. [[CrossRef](#)] [[PubMed](#)]
22. Pressyanov, D.; Dimitrov, D.; Dimitrova, I. Energy-efficient reconstructions and indoor radon: The impact assessed by CDs/DVDs. *J. Environ. Radioact.* **2015**, *143*, 76–79. [[CrossRef](#)] [[PubMed](#)]
23. Vasilyev, A.; Yarmoshenko, I. Effect of energy-efficient measures in building construction on indoor radon in Russia. *Radiat. Prot. Dosim.* **2017**, *174*, 419–422. [[CrossRef](#)]
24. Yarmoshenko, I.V.; Vasilyev, A.V.; Onishchenko, A.D.; Kiselev, S.M.; Zhukovsky, M.V. Indoor radon problem in energy efficient multi-storey buildings. *Radiat. Prot. Dosim.* **2014**, *160*, 53–56. [[CrossRef](#)] [[PubMed](#)]
25. Vasilyev, A.V.; Yarmoshenko, I.V.; Zhukovsky, M.V. Low air exchange rate causes high indoor radon concentration in energy-efficient buildings. *Radiat. Prot. Dosim.* **2015**, *164*, 601–605. [[CrossRef](#)]
26. Burghel, B.D.; Botoș, M.; Beldean-Galea, S.; Cucos, A.; Catalina, T.; Dicu, T.; Dobrei, G.; Florică, Ș.; Istrate, A.; Lupulescu, A.; et al. Comprehensive survey on radon mitigation and indoor air quality in energy efficient buildings from Romania. *Sci. Total Environ.* **2020**, *751*, 141858. [[CrossRef](#)]
27. Pigg, S.; Cautley, D.; Francisco, P.W. Impacts of weatherization on indoor air quality: A field study of 514 homes. *Indoor Air* **2018**, *28*, 307–317. [[CrossRef](#)]
28. Wallner, P.; Munoz, U.; Tappler, P.; Wanka, A.; Kundi, M.; Shelton, J.F.; Hutter, H.P. Indoor Environmental Quality in Mechanically Ventilated, Energy-Efficient Buildings vs. Conventional Buildings. *Int. J. Environ. Res. Public Health* **2015**, *12*, 14132–14147. [[CrossRef](#)]

29. Du, L.; Leivo, V.; Prasauskas, T.; Taubel, M.; Martuzevicius, D.; Haverinen-Shaughnessy, U. Effects of energy retrofits on Indoor Air Quality in multifamily buildings. *Indoor Air* **2019**, *29*, 686–697. [[CrossRef](#)]
30. Hirsch, T.; Hering, M.; Burkner, K.; Hirsch, D.; Leupold, W.; Kerkmann, M.L.; Kuhlisch, E.; Jatzwauk, L. House-dust-mite allergen concentrations (Der f 1) and mold spores in apartment bedrooms before and after installation of insulated windows and central heating systems. *Allergy* **2000**, *55*, 79–83. [[CrossRef](#)]
31. Sharpe, R.A.; Thornton, C.R.; Nikolaou, V.; Osborne, N.J. Fuel poverty increases risk of mould contamination, regardless of adult risk perception & ventilation in social housing properties. *Environ. Int.* **2015**, *79*, 115–129. [[CrossRef](#)] [[PubMed](#)]
32. Sharpe, R.A.; Cocq, K.L.; Nikolaou, V.; Osborne, N.J.; Thornton, C.R. Identifying risk factors for exposure to culturable allergenic moulds in energy efficient homes by using highly specific monoclonal antibodies. *Environ. Res.* **2016**, *144*, 32–42. [[CrossRef](#)]
33. Spertini, F.; Berney, M.; Foradini, F.; Roulet, C.A. Major mite allergen Der f 1 concentration is reduced in buildings with improved energy performance. *Allergy* **2010**, *65*, 623–629. [[CrossRef](#)]
34. Niculita-Hirzel, H.; Yang, S.; Hager Jörin, C.; Perret, V.; Licina, D.; Goyette Pernot, J. Fungal Contaminants in Energy Efficient Dwellings: Impact of Ventilation Type and Level of Urbanization. *Int. J. Environ. Res. Public Health* **2020**, *17*, 4936. [[CrossRef](#)]
35. Coombs, K.; Taft, D.; Ward, D.V.; Green, B.J.; Chew, G.L.; Shamsaei, B.; Meller, J.; Indugula, R.; Reponen, T. Variability of indoor fungal microbiome of green and non-green low-income homes in Cincinnati, Ohio. *Sci. Total Environ.* **2018**, *610–611*, 212–218. [[CrossRef](#)]
36. Derbez, M.; Wyart, G.; Le Ponner, E.; Ramalho, O.; Ribéron, J.; Mandin, C. Indoor air quality in energy-efficient dwellings: Levels and sources of pollutants. *Indoor Air* **2018**, *28*, 318–338. [[CrossRef](#)] [[PubMed](#)]
37. Leivo, V.; Prasauskas, T.; Du, L.; Turunen, M.; Kivistie, M.; Aaltonen, A.; Martuzevicius, D.; Haverinen-Shaughnessy, U. Indoor thermal environment, air exchange rates, and carbon dioxide concentrations before and after energy retro fits in Finnish and Lithuanian multi-family buildings. *Sci. Total Environ.* **2018**, *621*, 398–406. [[CrossRef](#)]
38. Coombs, K.C.; Chew, G.L.; Schaffer, C.; Ryan, P.H.; Brokamp, C.; Grinshpun, S.A.; Adamkiewicz, G.; Chillrud, S.; Hedman, C.; Colton, M.; et al. Indoor air quality in green-renovated vs. non-green low-income homes of children living in a temperate region of US (Ohio). *Sci. Total Environ.* **2016**, *554–555*, 178–185. [[CrossRef](#)]
39. Yang, S.; Perret, V.; Hager Jörin, C.; Niculita-Hirzel, H.; Goyette Pernot, J.; Licina, D. Volatile organic compounds in 169 energy-efficient dwellings in Switzerland. *Indoor Air* **2020**, *30*, 481–491. [[CrossRef](#)]
40. Baumgartner, J.; Clark, S.; Carter, E.; Lai, A.; Zhang, Y.; Shan, M.; Schauer, J.J.; Yang, X. Effectiveness of a Household Energy Package in Improving Indoor Air Quality and Reducing Personal Exposures in Rural China. *Environ. Sci. Technol.* **2019**, *53*, 9306–9316. [[CrossRef](#)]
41. Singh, A.; Syal, M.; Grady, S.C.; Korkmaz, S. Effects of green buildings on employee health and productivity. *Am. J. Public Health* **2010**, *100*, 1665–1668. [[CrossRef](#)] [[PubMed](#)]
42. Gawande, S.; Tiwari, R.R.; Narayanan, P.; Bhadri, A. Indoor Air Quality and Sick Building Syndrome: Are Green Buildings Better than Conventional Buildings? *Indian J. Occup. Environ. Med.* **2020**, *24*, 30–32. [[CrossRef](#)]
43. Wargocki, P.; Wyon, D.P.; Sundell, J.; Clausen, G.; Fanger, P.O. The effects of outdoor air supply rate in an office on perceived air quality, sick building syndrome (SBS) symptoms and productivity. *Indoor Air* **2000**, *10*, 222–236. [[CrossRef](#)] [[PubMed](#)]
44. Hedge, A.; Dorsey, J.A. Green buildings need good ergonomics. *Ergonomics* **2013**, *56*, 492–506. [[CrossRef](#)] [[PubMed](#)]
45. Hedge, A.; Miller, L.; Dorsey, J.A. Occupant comfort and health in green and conventional university buildings. *Work* **2014**, *49*, 363–372. [[CrossRef](#)]
46. Bakke, J.V.; Norback, D.; Wieslander, G.; Hollund, B.E.; Florvaag, E.; Haugen, E.N.; Moen, B.E. Symptoms, complaints, ocular and nasal physiological signs in university staff in relation to indoor environment—temperature and gender interactions. *Indoor Air* **2008**, *18*, 131–143. [[CrossRef](#)] [[PubMed](#)]
47. Garland, E.; Steenburgh, E.T.; Sanchez, S.H.; Geevarughese, A.; Bluestone, L.; Rothenberg, L.; Rialdi, A.; Foley, M. Impact of LEED-certified affordable housing on asthma in the South Bronx. *Prog. Community Health Partnersh. Res. Educ. Act.* **2013**, *7*, 29–37. [[CrossRef](#)]
48. Breyse, J.; Jacobs, D.E.; Weber, W.; Dixon, S.; Kawecki, C.; Aceti, S.; Lopez, J. Health outcomes and green renovation of affordable housing. *Public Health Rep.* **2011**, *126* (Suppl. 1), 64–75. [[CrossRef](#)]
49. Breyse, J.; Dixon, S.L.; Jacobs, D.E.; Lopez, J.; Weber, W. Self-reported health outcomes associated with green-renovated public housing among primarily elderly residents. *J. Public Health Manag. Pract.* **2015**, *21*, 355–367. [[CrossRef](#)]
50. Rudge, J.; Gilchrist, R. Excess winter morbidity among older people at risk of cold homes: A population-based study in a London borough. *J. Public Health* **2005**, *27*, 353–358. [[CrossRef](#)]
51. Webb, E.; Blane, D.; de Vries, R. Housing and respiratory health at older ages. *J. Epidemiol. Community Health* **2013**, *67*, 280–285. [[CrossRef](#)]
52. Sharpe, R.A.; Thornton, C.R.; Nikolaou, V.; Osborne, N.J. Higher energy efficient homes are associated with increased risk of doctor diagnosed asthma in a UK subpopulation. *Environ. Int.* **2015**, *75*, 234–244. [[CrossRef](#)]
53. Poortinga, W.; Jones, N.; Lannon, S.; Jenkins, H. Social and health outcomes following upgrades to a national housing standard: A multilevel analysis of a five-wave repeated cross-sectional survey. *BMC Public Health* **2017**, *17*, 927. [[CrossRef](#)]
54. Carlton, E.J.; Barton, K.; Shrestha, P.M.; Humphrey, J.; Newman, L.S.; Adgate, J.L.; Root, E.; Miller, S. Relationships between home ventilation rates and respiratory health in the Colorado Home Energy Efficiency and Respiratory Health (CHEER) study. *Environ. Res.* **2019**, *169*, 297–307. [[CrossRef](#)]

55. Howden-Chapman, P.; Crane, J.; Chapman, R.; Fougere, G. Improving health and energy efficiency through community-based housing interventions. *Int. J. Public Health* **2011**, *56*, 583–588. [[CrossRef](#)]
56. Howden-Chapman, P.; Matheson, A.; Crane, J.; Viggers, H.; Cunningham, M.; Blakely, T.; Cunningham, C.; Woodward, A.; Saville-Smith, K.; O’Dea, D.; et al. Effect of insulating existing houses on health inequality: Cluster randomised study in the community. *BMJ* **2007**, *334*, 460. [[CrossRef](#)]
57. Thomson, H.; Snell, C.; Bouzarovski, S. Health, Well-Being and Energy Poverty in Europe: A Comparative Study of 32 European Countries. *Int. J. Environ. Res. Public Health* **2017**, *14*, 584. [[CrossRef](#)]
58. Ahrentzen, S.; Erickson, J.; Fonseca, E. Thermal and health outcomes of energy efficiency retrofits of homes of older adults. *Indoor Air* **2016**, *26*, 582–593. [[CrossRef](#)]
59. Shortt, N.; Rugkåsa, J. “The walls were so damp and cold” fuel poverty and ill health in Northern Ireland: Results from a housing intervention. *Health Place* **2007**, *13*, 99–110. [[CrossRef](#)]
60. Chapman, R.; Howden-Chapman, P.; Viggers, H.; O’Dea, D.; Kennedy, M. Retrofitting houses with insulation: A cost-benefit analysis of a randomised community trial. *J. Epidemiol. Community Health* **2009**, *63*, 271–277. [[CrossRef](#)]
61. Grey, C.N.; Jiang, S.; Nascimento, C.; Rodgers, S.E.; Johnson, R.; Lyons, R.A.; Poortinga, W. The short-term health and psychosocial impacts of domestic energy efficiency investments in low-income areas: A controlled before and after study. *BMC Public Health* **2017**, *17*, 140. [[CrossRef](#)] [[PubMed](#)]
62. Poortinga, W.; Rodgers, S.E.; Lyons, R.A.; Anderson, P.; Tweed, C.; Grey, C.; Jiang, S.; Johnson, R.; Watkins, A.; Winfield, T.G. Public Health Research. In *The Health Impacts of Energy Performance Investments in Low-Income Areas: A Mixed-Methods Approach*; Public Health Research; NIHR Journals Library: Southampton, UK, 2018.
63. Pollard, A.; Jones, T.; Sherratt, S.; Sharpe, R.A. Use of Simple Telemetry to Reduce the Health Impacts of Fuel Poverty and Living in Cold Homes. *Int. J. Environ. Res. Public Health* **2019**, *16*, 2853. [[CrossRef](#)] [[PubMed](#)]
64. Angelini, V.; Daly, M.; Moro, M.; Navarro Paniagua, M.; Sidman, E.; Walker, I.; Weldon, M. Public Health Research. In *The Effect of the Winter Fuel Payment on Household Temperature and Health: A Regression Discontinuity Design Study*; Public Health Research; NIHR Journals Library: Southampton, UK, 2019.
65. Sartini, C.; Tammes, P.; Hay, A.D.; Preston, I.; Lasserson, D.; Whincup, P.H.; Wannamethee, S.G.; Morris, R.W. Can we identify older people most vulnerable to living in cold homes during winter? *Ann. Epidemiol.* **2018**, *28*, 1–7.e3. [[CrossRef](#)] [[PubMed](#)]
66. Peralta, A.; Camprubi, L.; Rodriguez-Sanz, M.; Basagana, X.; Borrell, C.; Mari-Dell’Olmo, M. Impact of energy efficiency interventions in public housing buildings on cold-related mortality: A case-crossover analysis. *Int. J. Epidemiol.* **2017**, *46*, 1192–1201. [[CrossRef](#)] [[PubMed](#)]
67. Umishio, W.; Ikaga, T.; Kario, K.; Fujino, Y.; Hoshi, T.; Ando, S.; Suzuki, M.; Yoshimura, T.; Yoshino, H.; Murakami, S. Cross-Sectional Analysis of the Relationship Between Home Blood Pressure and Indoor Temperature in Winter: A Nationwide Smart Wellness Housing Survey in Japan. *Hypertension* **2019**, *74*, 756–766. [[CrossRef](#)]
68. López-Bueno, J.A.; Linares, C.; Sánchez-Guevara, C.; Martínez, G.S.; Mirón, I.J.; Núñez-Peiró, M.; Valero, I.; Díaz, J. The effect of cold waves on daily mortality in districts in Madrid considering sociodemographic variables. *Sci. Total Environ.* **2020**, *749*, 142364. [[CrossRef](#)]
69. Engvall, K.; Norrby, C.; Norback, D. Ocular, nasal, dermal and respiratory symptoms in relation to heating, ventilation, energy conservation, and reconstruction of older multi-family houses. *Indoor Air* **2003**, *13*, 206–211. [[CrossRef](#)]
70. Smedje, G.; Wang, J.; Norback, D.; Nilsson, H.; Engvall, K. SBS symptoms in relation to dampness and ventilation in inspected single-family houses in Sweden. *Int. Arch. Occup. Environ. Health* **2017**, *90*, 703–711. [[CrossRef](#)]
71. Norback, D.; Lampa, E.; Engvall, K. Asthma, allergy and eczema among adults in multifamily houses in Stockholm (3-HE study)—associations with building characteristics, home environment and energy use for heating. *PLoS ONE* **2014**, *9*, e112960. [[CrossRef](#)]
72. Wang, J.; Engvall, K.; Smedje, G.; Nilsson, H.; Norback, D. Current wheeze, asthma, respiratory infections, and rhinitis among adults in relation to inspection data and indoor measurements in single-family houses in Sweden-The BETSI study. *Indoor Air* **2017**, *27*, 725–736. [[CrossRef](#)]
73. Sharpe, R.A.; Machray, K.E.; Fleming, L.E.; Taylor, T.; Henley, W.; Chenore, T.; Hutchcroft, I.; Taylor, J.; Heaviside, C.; Wheeler, B.W. Household energy efficiency and health: Area-level analysis of hospital admissions in England. *Environ. Int.* **2019**, *133*, 105164. [[CrossRef](#)]
74. Sobottka, A.; Thriene, B. Sanitation programmes for living spaces and health risks involved. *Toxicol. Lett.* **1996**, *88*, 365–368. [[CrossRef](#)]
75. Kennard, H.R.; Huebner, G.M.; Shipworth, D.; Oreszczyń, T. The associations between thermal variety and health: Implications for space heating energy use. *PLoS ONE* **2020**, *15*, e0236116. [[CrossRef](#)] [[PubMed](#)]
76. Wallner, P.; Tappler, P.; Munoz, U.; Damberger, B.; Wanka, A.; Kundi, M.; Hutter, H.P. Health and Wellbeing of Occupants in Highly Energy Efficient Buildings: A Field Study. *Int. J. Environ. Res. Public Health* **2017**, *14*, 314. [[CrossRef](#)] [[PubMed](#)]
77. Somerville, M.; Mackenzie, I.; Owen, P.; Miles, D. Housing and health: Does installing heating in their homes improve the health of children with asthma? *Public Health* **2000**, *114*, 434–439. [[CrossRef](#)]
78. Barton, A.; Basham, M.; Foy, C.; Buckingham, K.; Somerville, M.; Torbay Healthy Housing, G. The Watcombe Housing Study: The short term effect of improving housing conditions on the health of residents. *J. Epidemiol. Community Health* **2007**, *61*, 771–777. [[CrossRef](#)] [[PubMed](#)]

79. Osman, L.M.; Ayres, J.G.; Garden, C.; Reglitz, K.; Lyon, J.; Douglas, J.G. A randomised trial of home energy efficiency improvement in the homes of elderly COPD patients. *Eur. Respir. J.* **2010**, *35*, 303–309. [[CrossRef](#)]
80. Wilson, J.; Dixon, S.L.; Jacobs, D.E.; Breyse, J.; Akoto, J.; Tohn, E.; Isaacson, M.; Evens, A.; Hernandez, Y. Watts-to-Wellbeing: Does residential energy conservation improve health? *Energy Effic.* **2013**, *7*, 151–160. [[CrossRef](#)]
81. Haverinen-Shaughnessy, U.; Pekkonen, M.; Leivo, V.; Prasauskas, T.; Turunen, M.; Kiviste, M.; Aaltonen, A.; Martuzevicius, D. Occupant satisfaction with indoor environmental quality and health after energy retrofits of multi-family buildings: Results from INSULAtE-project. *Int. J. Hyg. Environ. Health* **2018**, *221*, 921–928. [[CrossRef](#)]
82. Engvall, K.; Wickman, P.; Norback, D. Sick building syndrome and perceived indoor environment in relation to energy saving by reduced ventilation flow during heating season: A 1 year intervention study in dwellings. *Indoor Air* **2005**, *15*, 120–126. [[CrossRef](#)]
83. Francisco, P.W.; Jacobs, D.E.; Targos, L.; Dixon, S.L.; Breyse, J.; Rose, W.; Cali, S. Ventilation, indoor air quality, and health in homes undergoing weatherization. *Indoor Air* **2017**, *27*, 463–477. [[CrossRef](#)] [[PubMed](#)]
84. Umishio, W.; Ikaga, T.; Kario, K.; Fujino, Y.; Hoshi, T.; Ando, S.; Suzuki, M.; Yoshimura, T.; Yoshino, H.; Murakami, S. Intervention study of the effect of insulation retrofitting on home blood pressure in winter: A nationwide Smart Wellness Housing survey. *J. Hypertens.* **2020**, *38*, 2510–2518. [[CrossRef](#)] [[PubMed](#)]
85. Humphrey, J.L.; Barton, K.E.; Man Shrestha, P.; Carlton, E.J.; Newman, L.S.; Dowling Root, E.; Adgate, J.L.; Miller, S.L. Air infiltration in low-income, urban homes and its relationship to lung function. *J. Expo. Sci. Environ. Epidemiol.* **2020**, *30*, 262–270. [[CrossRef](#)] [[PubMed](#)]
86. Cheng, E.S.; Egger, S.; Hughes, S.; Weber, M.; Steinberg, J.; Rahman, B.; Worth, H.; Ruano-Ravina, A.; Rawstorne, P.; Yu, X.Q. Systematic review and meta-analysis of residential radon and lung cancer in never-smokers. *Eur. Respir. Rev.* **2021**, *30*, 200230. [[CrossRef](#)]
87. Ilomets, S.; Kalamees, T. Evaluation of the criticality of thermal bridges. *J. Build. Pathol. Rehabil.* **2016**, *1*, 11. [[CrossRef](#)]
88. Bolden, A.L.; Kwiatkowski, C.F.; Colborn, T. New Look at BTEX: Are Ambient Levels a Problem? *Environ. Sci. Technol.* **2015**, *49*, 5261–5276. [[CrossRef](#)]

Article

Performance Identification of a Steam Boiler Burner via Acoustic Analysis

Kayra Kurşun ¹, Levent Özdemir ² and Hakan Ersoy ^{1,*}

¹ Department of Mechanical Engineering, Akdeniz University, Antalya 07070, Turkey; kayrakursun@akdeniz.edu.tr

² Technical Directorate of Akdeniz University Hospital, Akdeniz University, Antalya 07070, Turkey; lozdemir@akdeniz.edu.tr

* Correspondence: hakanersoy@akdeniz.edu.tr

Abstract: Almost all systems generate acoustic signals when operating or when a process is being performed. These signals contain certain data related to the operating performance of systems. In this study, acoustic data were used to study the performance and to identify the optimum operating points of natural gas burners that are used in steam boilers. The sound recordings of burners obtained under different operating conditions were examined with acoustic analysis methods. The impact of various operating parameters on acoustic values was determined using time series analysis, frequency spectrum data and then power spectral density values. When the excess air coefficient and emission and efficiency values of boilers were compared with the acoustic data, it was determined that the Yule–Walker algorithm contained distinct and explanatory values. The steam boiler and the natural gas burner within were considered a system for the analysis. Measurement results showed that operating parameters and acoustic analysis results were correlated. Moreover, the results were confirmed with the emission measurement results. Finally, it was deduced that the acoustic values can be used for obtaining the optimum operating points in similar systems where inlet and outlet parameters cannot be measured, and the related principles were revealed.

Keywords: acoustics; steam boiler; steam trap; excess air coefficient; Fourier transformation; spectral analysis; autoregressive method; Yule–Walker

Citation: Kurşun, K.; Özdemir, L.; Ersoy, H. Performance Identification of a Steam Boiler Burner via Acoustic Analysis. *Processes* **2022**, *10*, 1223. <https://doi.org/10.3390/pr10061223>

Academic Editors: Roberto Alonso González Lezcano, Francesco Nocera and Rosa Giuseppina Caponetto

Received: 5 May 2022
Accepted: 13 June 2022
Published: 20 June 2022



Copyright: © 2022 by the authors. Licensee MDPI, Basel, Switzerland. This article is an open access article distributed under the terms and conditions of the Creative Commons Attribution (CC BY) license (<https://creativecommons.org/licenses/by/4.0/>).

1. Introduction

The primary goal of employing time series in system analyses is to determine the state of the physical quantity being observed or investigated over time based on changing parameters, as well as to comprehend the nature of such data. The obtained data allow for predictions about the system's current state and potential future values. Furthermore, by examining and analyzing time series using various methods, it is possible to reach specific conclusions about the system parameters that constitute the time series. Preliminary values for detecting system failure, as well as vital data on the system's operating performance, can be obtained by examining the acoustic time series that occur during the operation. However, obtaining the essential conclusions from these raw data is a challenge. Therefore, significant results can only be obtained by employing specific methods on the measured signals and then conducting appropriate analyses.

In this study, the combustion performance data of the natural gas burner operating in conjunction with the steam boiler were studied by analyzing acoustic signals. Most studies in the literature considered the vibration data of the systems as time series and attempted to reach conclusions for performance and failure prevention in this manner. For instance, gearbox vibration data were used in studies related to detection of gear shaft and gear tooth failure. In these studies, autoregressive methods [1] and parametric methods [2] were used for modeling, and the Yule–Walker algorithm was used for parameter estimation [1,2]. Likewise, parametric methods also provided decent results in the formation and analysis

of impact-induced vibration models [3]. Additionally, the Kolmogorov–Smirnov method is utilized to predict error signals [1,4]. On the other hand, in studies that focus more on steam boilers, combustion chambers or burners for failure detection, it is observed that the main problems of interest are related to leak detection, performance identification and combustion instability. In studies related to leak detection, model-based least squares technique [5] and principal component analysis are used [6]. For the matter of performance identification, acoustic data are used for analysis, and Yule–Walker algorithms are utilized for parameter estimation [7]. Apart from these, issues related to combustion instability are an area of interest in the literature. In this area, the static instability of the plasma arcs [8] and the combustion imbalances in the annulus burners of rotary kiln [9] are studied experimentally for swirl flame. In the case of thermo-acoustic instability [10,11], numerical and experimental methods [12–14], experimental flame transfer functions [15,16], large eddy simulations [17,18], fast random particle method [19] and nonlinear network models [20,21] are used. To provide the passive control of thermo-acoustic instability, the slope confinement method is utilized [22]. In addition, the acoustic emission method, which, in recent years, needs less data [23], is used for failure detection in the tubes of steam generators, boilers and heat exchangers [24]. Moreover, bidirectional long short-term memory recurrent neural networks [25] and the deep learning flexible boundary regression method can be used with acoustic emission signals to enhance leak detection in boiler tubes [26]. Acoustic array global interpolation algorithms have been developed for leak detection during boiler operations of coal-fired power plants [27].

In this study, it has been shown that acoustic methods can be used to obtain optimum operating performance in terms of gas emissions and fuel efficiency. Spectral analysis methods were applied to produce optimum air excess coefficient settings of steam boilers and burners. It was observed that combustion adjustments can be made through acoustic analysis, especially in cases where classical measurement methods cannot be performed.

2. Materials and Methods

The spectral analysis method explains the power distribution of a signal (such as sound and vibration) in a finite data set. This method can be used in various applications such as the detection of embedded signals in a wide band interval. Spectrum analysis in signal processing can be basically classified as parametric and non-parametric methods. In non-parametric methods, power spectrum density (PSD) is directly obtained from the signal itself, and the simplest of these is the periodogram. The developed form of periodogram is based on Welch’s method and the multitaper method. In parametric methods, the PSD is obtained from a linear system. The most commonly known algorithms of this method are the Yule–Walker autoregressive method and the Burg method. These methods try to obtain the parameters (coefficients) of the linear system to determine the PSD. Then, they generate a signal based on the assumption. These methods yield better results than conventional non-parametric methods if the signal duration is short. Moreover, parametric methods can achieve higher resolution values compared to non-parametric methods [28]. Because the data of a system are depicted as X_n , the spectral power density of a random fixed process is related to the correlation series of a discrete Fourier transformation. This expression, in terms of normalized frequency, is as follows.

$$X(\omega) = \frac{1}{2\pi} \sum_{n=-\infty}^{\infty} x(n)e^{-jn\omega} \quad (1)$$

where the normalized frequency is $\omega = 2\pi f/f_s$, f is the physical frequency, and f_s is the sampling frequency.

$$X(f) = \frac{1}{f_s} \sum_{n=-\infty}^{\infty} \frac{x(n)e^{-2\pi jfn}}{f_s} \quad (2)$$

Correlation series can be obtained from the spectral power density using the inverse of the discrete time Fourier transformation.

$$X(n) = \int_{-n}^n (x(\omega)e^{j\omega n})d\omega = \int_{-\frac{fs}{2}}^{\frac{fs}{2}} (x(f)e^{\frac{2\pi jfn}{s}})df \quad (3)$$

The average power of the $X(n)$ series within a certain data range is expressed by the following equation.

$$X(0) = \int_{-\pi}^{\pi} x(\omega)d\omega = \int_{\frac{fs}{2}}^{\frac{fs}{2}} x(f)df \quad (4)$$

The average power of a signal on a certain frequency band, $[\omega_1, \omega_2]$, $0 \leq \omega_1 < \omega_2 \leq \pi$, can be determined by taking the integral of the spectral power density over this band.

$$x_{[\omega_1, \omega_2]} = \int_{\omega_1}^{\omega_2} x(\omega)d\omega + \int_{-\omega_2}^{-\omega_1} x(\omega)d\omega \quad (5)$$

In Equation (5), this expression, which represents the power content of a signal in $x(\omega)$ infinitely low frequency band, is called the spectral power density. In reality, PSDs of signals are symmetrical. Therefore, $x(\omega)$ entirely represents the PSD in the interval $0 \leq \omega < \pi$. Of the spectral estimation methods, the Yule–Walker AR method calculates the AR parameters of a signal generated with the partial prediction of its “autoregressive” function and calculates the forward prediction error with the minimization of the smallest squares. Equation (6) is known as the Yule–Walker equation and forms the basis of many AR prediction methods [29].

$$\begin{bmatrix} r(1) & r(2) & \cdots & r(p) \\ r(2) & r(1) & \cdots & r(p-1) \\ \vdots & \vdots & \cdots & \vdots \\ r(p) & \cdots & r(2) & r(1) \end{bmatrix} \begin{Bmatrix} a(2) \\ a(3) \\ \vdots \\ a(p+1) \end{Bmatrix} = \begin{Bmatrix} -r(2) \\ -r(3) \\ \vdots \\ -r(p+1) \end{Bmatrix} \quad (6)$$

The Yule–Walker AR method generates results like a maximum entropy estimator. Using a method against the autocorrelation function ensures that the autocorrelation matrix in Equation (6) is positive. Therefore, the matrix can be reversed, and it can guarantee an existing solution. Moreover, these calculated AR parameters always result in a stable all-pole model. The Yule–Walker equations make use of the Toeplitz structure, which is an autocorrelation matrix and is efficiently solved using the Levinson algorithm. This is a matrix, and each member, from left to right diagonally, is fixed.

Experimental Setup

Measurements were taken on an industrial-type steam boiler installed in the university hospital. The steam boiler technical specifications were as follows: capacity max. 6800 kW; operating pressure 7 Bar; water volume 25,000 L; burner capacity max. 8000 kW; fuel type, natural gas; motor power, 30 kW. Moreover, the steam boiler uses natural gas as fuel and has an Oertili induflame burner. A Testo 330-2LL (Testo, Istanbul, Turkey) device was used to measure the flue gas emissions. The calibration of this device was set to maximum. A composition of 3% O₂ and 12% CO₂ was used, and a AKG perception 170 cardioid condenser microphone was used for the acoustic data. Data were transferred to the computer via a Behringer-1222 FX preamp (Behringer, Willich, Germany) with 48 V phantom power supply. The Goldwave program (v5.10, St. John’s, NL, Canada) was used in the preprocessing of the data; all other analyses and calculations were made using Matlab (v9.8 Academic, Mathworks, Natick, MA, USA, Source: Akdeniz University, IT Department, Antalya, Turkey). Before beginning the measurements, the boiler was operated for ~40 min, and the system was made to reach a stable state. For the comparability of the measurements, adjustments were made during all measurements, such that the steam

boiler pressure was 6 bars and the frequency value of the primary air fan with frequency inverter was 25.7 Hz (Figure 1).



Figure 1. Boiler under measurement and test set-up.

3. Results

Measurements of the system were made for eight different excess air coefficients at 16 bits. The presence of three sound sources was assumed in the system during the acoustic recordings: the data coming from the primary air fan, the sound of natural gas flow and the acoustic data during burning in the combustion chamber. The acoustic data in the combustion chamber were subjected to acoustic analyses after they were separated from the noise coming from the other two sources. It was observed that the system worked stably during the steady regime; therefore, it was concluded that a measurement interval of 10 s was sufficient. When the acoustic recordings were being made, flue gas emissions and efficiency values of the system were simultaneously determined. Figure 2 shows the time–amplitude values of the acoustic data obtained from the recordings for the eight different excess air coefficients. Here, fluctuations depending on the combustion state are reflected in the graphics. Subsequently, these values were transferred from time domain to frequency domain for each excess air coefficient. Figure 3 shows the expansions of signals on the frequency axis.

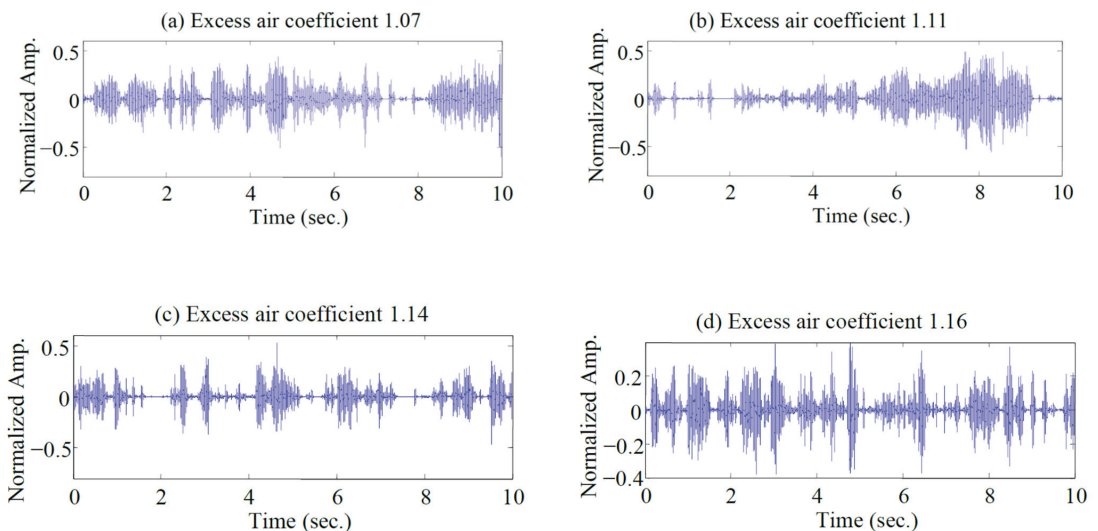


Figure 2. Cont.

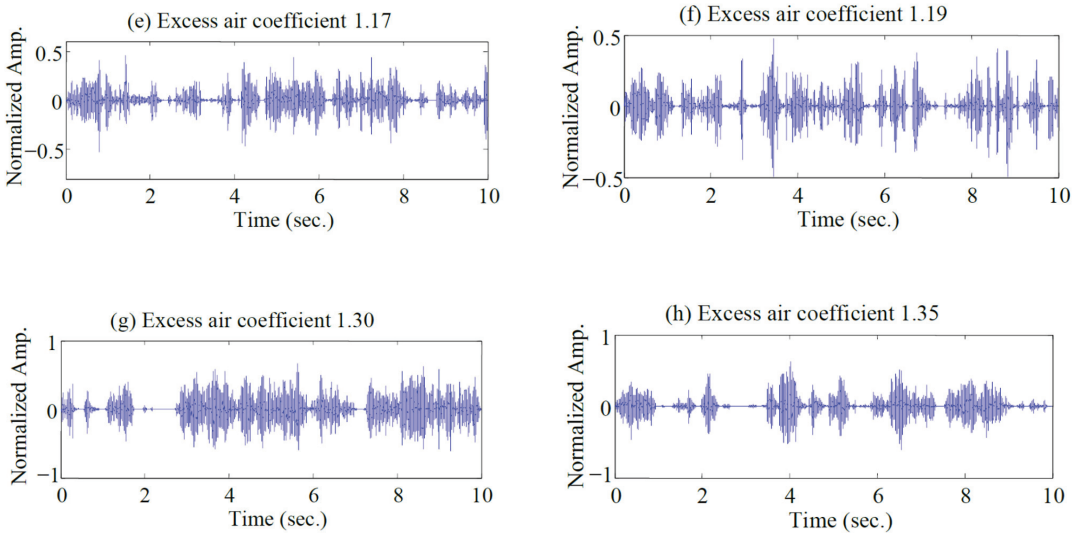


Figure 2. Measurement data obtained for the excess air coefficients.

While recording acoustic data, changes were made in the λ excess air coefficient values and flue gas emissions, and boiler efficiency values were simultaneously measured for each excess air coefficient value. These values are listed in Table 1. When the emission and efficiency values were examined, the measurement number 3 corresponding to $\lambda = 1.14$ value was more balanced compared to other parameters; it was decided that it could be considered a reference. The excess air coefficient of 1.14 of the boiler measured at the third measurement was determined as the excess air coefficient where combustion is the most suitable, as per the criteria set by standards regarding flue gas emissions and efficiency values. When determining this value, an evaluation was made among emission values and efficiency values in Table 1, and the balance between emission and efficiency values was considered. This designated value was considered as a reference for other measurements.

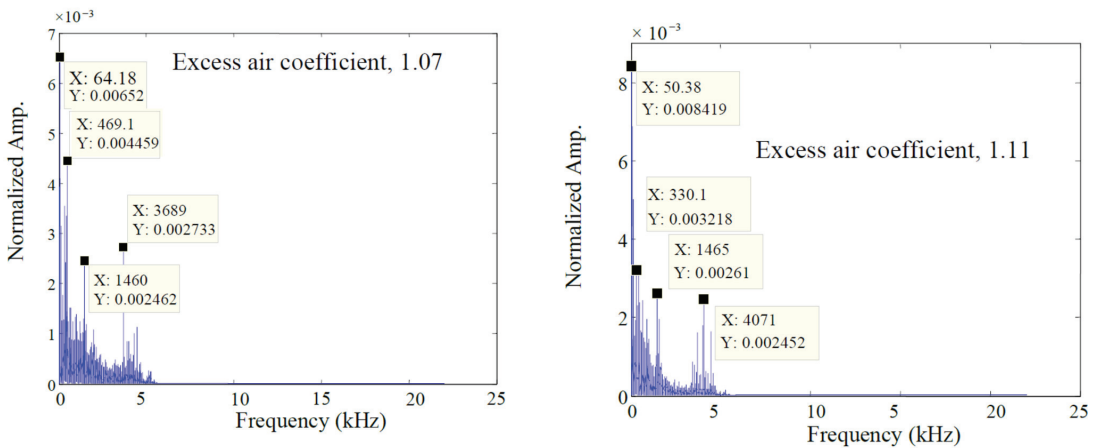


Figure 3. Cont.

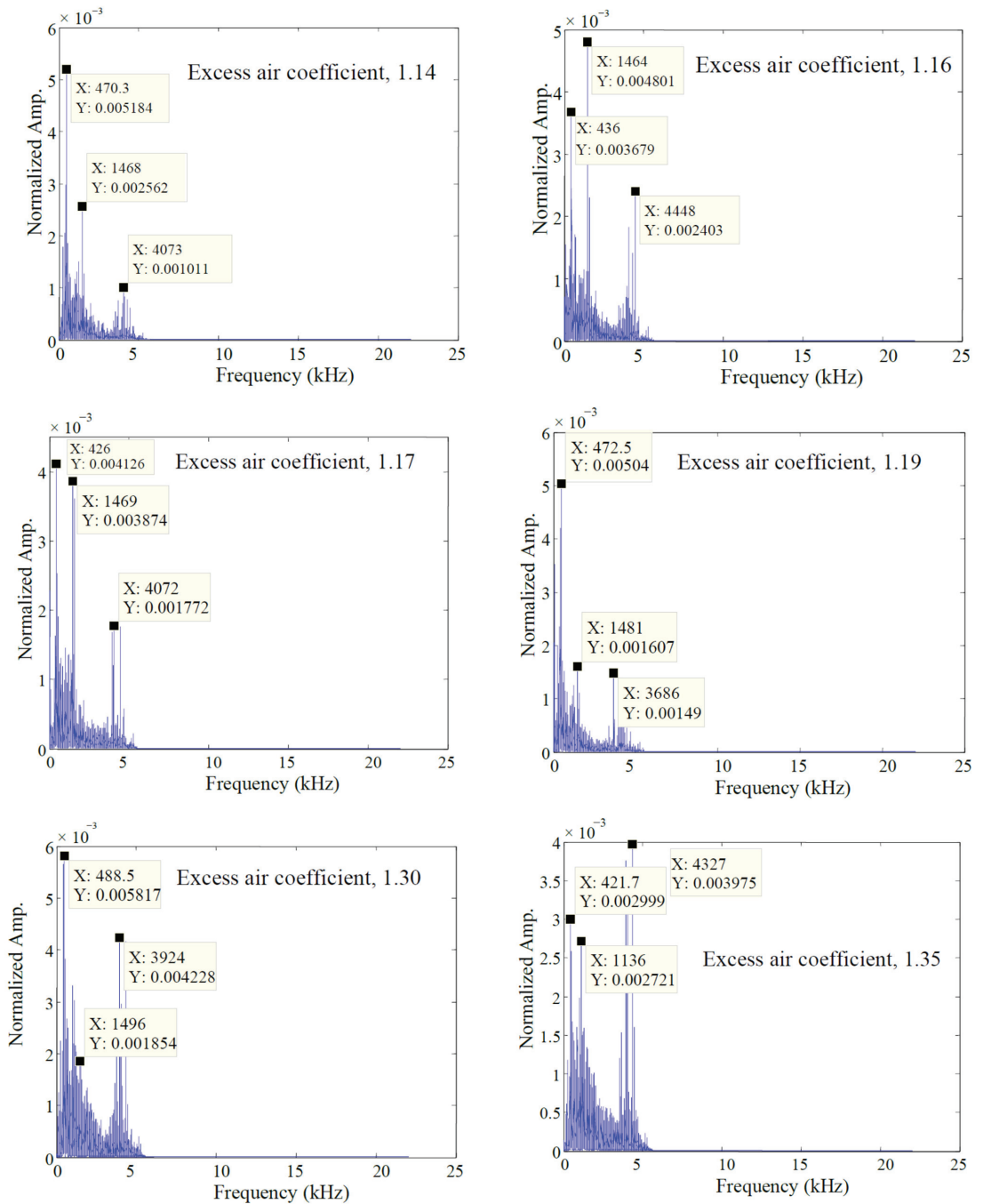


Figure 3. Frequency distributions of measurements taken for the excess air coefficients.

Table 1. Flue gas emission values and boiler efficiency for the excess air coefficient λ values.

Measurement	1	2	3	4	5	6	7	8
λ	1.07	1.11	1.14	1.16	1.17	1.19	1.30	1.35
O ₂ %	1.3	2.0	2.5	2.9	3.1	3.3	4.8	5.5
CO ₂ %	11.26	10.86	10.57	10.34	10.23	10.11	9.26	8.86
CO%	199	81	14	7	4	5	0	0
Efficiency %	93.8	93.8	93.6	93.5	93.4	93.5	93.0	92.6

Yule–Walker power spectral density values with respect to the excess air values are given in Table 2.

Table 2. Yule–Walker power spectral density values corresponding to excess air values.

Measurement	1	2	3	4	5	6	7	8
λ	1.07	1.11	1.14	1.16	1.17	1.19	1.30	1.35
x1	775.1	602.9	689.1	1034.0	947.5	516.8	947.5	1120.0
x2	3962	3962	3704	3962	3962	3962	4048	4048
y1/y2	13.02	22.29	22.77	14.87	2.25	2.84	8.55	4.28

If we consider the acoustic data as a time series, the recordings were made for eight different excess air coefficients in time slices of 10 s (Figure 2). From this data, the distribution in frequency domain was obtained through the fast Fourier transform process (Figure 3). Using the obtained frequency data, the distribution of PSD values in frequency domain was found using the Yule–Walker algorithm (Figure 4). In the PSD graphs, the peak frequencies for normalized values were examined. By making power density calculations, it was determined at which frequencies the data were concentrated (Figure 5).

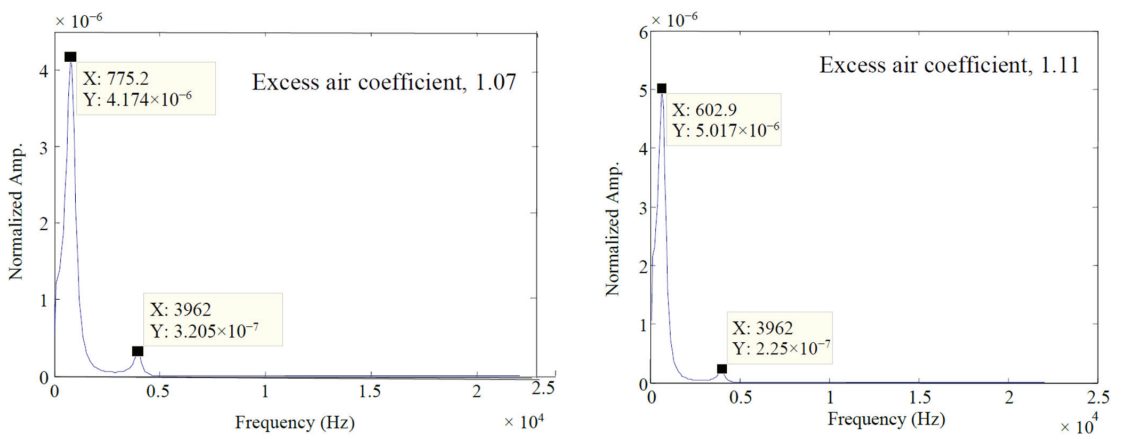


Figure 4. Cont.

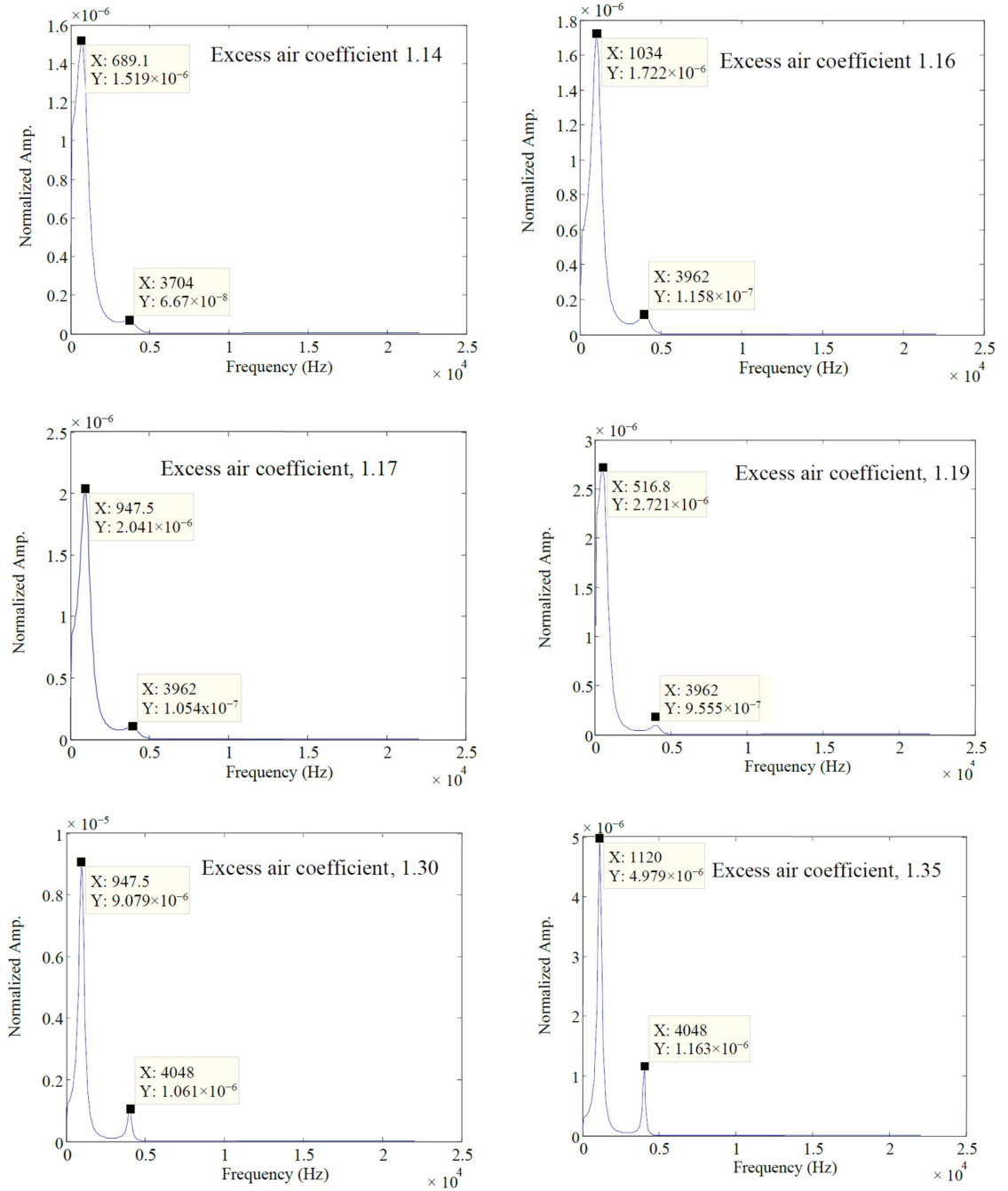


Figure 4. Yule-Walker power spectral density values.

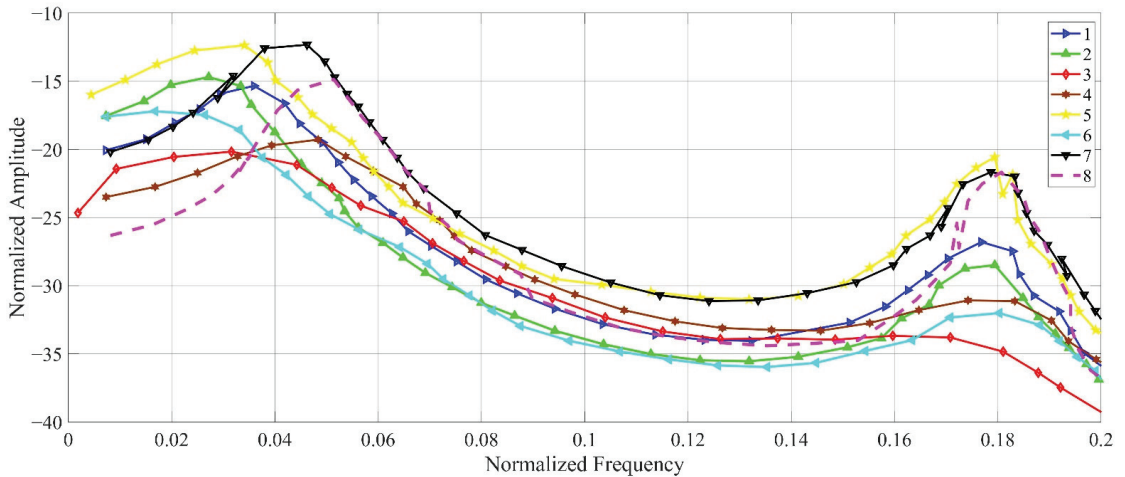


Figure 5. Yule-Walker Power Spectral Density.

4. Discussion

Time graphs of acoustic data were plotted for eight different excess air coefficients, and then their frequency spectra were obtained. PSD values were calculated and plotted for these values. Furthermore, other parametric methods, namely Burg, covariance and modified covariance methods, were also examined. In the data obtained within the scope of the study, it was determined that the “Yule–Walker” method has some advantages over other methods; it is also possible to apply windowing to acoustic signals, and these data can be recorded as larger datasets compared to other methods. When the Figure 5 plot comprising the power spectra of the acoustic signals obtained for each of the eight residual air coefficients was examined, the curve around the first and second peak values showed that the combustion was in the best condition. In other areas of the spectrum, a decrease and a stable situation were observed. Therefore, it was concluded that the Yule–Walker method is more suitable for these data characteristics and analyses, and plots were made using the Yule–Walker method. Table 2 shows the frequencies at which the peak points of PSD values occur for each excess air coefficient and yields the PSD ratios of the two peak points as y_1/y_2 . In the literature, thermoacoustic instability of a large-scale industrial oil furnace was studied using acoustic data, turbulence energy spectrum and Rayleigh parameter, across the domain in [17]. At the maximum continuous rating load, all three methods predict instability with fluctuations of the predicted dominant frequencies in agreement with the observed nondimensional frequency of 0.615. Here, the measurement made for the excess air coefficient of 1.14 stands out from the others with its higher value. Moreover, this value corresponds to the value of 1.14, which may be considered the optimum value compared with the emission and efficiency values in Table 1. When the values obtained with the Yule–Walker algorithm are examined in Figure 5, the curve number 3 belonging to the excess air coefficient of 1.14 stands out because of its lower relative peak points.

5. Conclusions

In this study, the operating parameters of the natural gas boiler’s burner were evaluated along with acoustic data. Law emission values for internal combustion engines are not at points where the engine power and efficiency are at their optimum values, and an optimum operating point must be determined among these values. A similar situation is observed for gas burners. This study has shown that this optimum point can be determined using acoustic data. Acoustic data can be easily used in systems where it is impossible or very difficult to measure operating parameters. Furthermore, analyses can be made in

many systems with acoustic data that can be measured much more easily. Furthermore, in many cases, acoustic data contain considerably more information about the system. In this study, the Yule–Walker PSD values can be applied to the steam boiler with natural gas burner and correlated with the performance values of the boiler such as emission and efficiency; moreover, such analyses can be used for improving the boiler performance. In particular, parametric methods will be an important analysis method for optimizing combustion parameters.

Author Contributions: Conceptualization, K.K. and H.E.; methodology, L.Ö. and H.E.; experimental setup, L.Ö. and K.K.; validation, K.K. and H.E.; formal analysis, K.K.; investigation, K.K. and L.Ö.; resources, K.K. and H.E.; data curation, H.E.; writing—original draft preparation, L.Ö. and K.K.; writing—review and editing, K.K. and L.Ö.; visualization, K.K. and L.Ö.; supervision, H.E.; project administration, L.Ö. and H.E.; funding acquisition, H.E. All authors have read and agreed to the published version of the manuscript.

Funding: This work was supported by The Scientific Research Projects Coordination Unit of Akdeniz University. Project Number: FDK-2021-5619.

Institutional Review Board Statement: Not applicable.

Informed Consent Statement: Not applicable.

Data Availability Statement: The data presented in this study are available on request from the corresponding author.

Conflicts of Interest: The authors declare no conflict of interest.

Nomenclature

$x(n)$	Time series
$X(f)$	Fourier transform
f_s	Sampling frequency
f	Frequency
ω	Angular frequency
$r(p)$	Autocorrelation function

References

1. Wang, X.; Makis, V. Autoregressive model-based gear shaft fault diagnosis using the Kolmogorov–Smirnov test. *J. Sound Vib.* **2009**, *327*, 413–423. [[CrossRef](#)]
2. Ettefagh, M.M.; Sadeghi, M.H.; Rezaee, M.; Chitsaz, S. Latent component-based gear tooth fault detection filter using advanced parametric modeling. *Mech. Syst. Signal Process.* **2009**, *23*, 2260–2286. [[CrossRef](#)]
3. Ettefagh, M.M.; Sadeghi, M.H.; Rezaee, M.; Khoshbakhti, R.; Akbarpour, R. Application of a new parametric model-based filter to knock intensity measurement. *Measurement* **2010**, *43*, 353–362. [[CrossRef](#)]
4. Kar, C.; Mohanty, A.R. Multistage gearbox condition monitoring using motor current signature analysis and Kolmogorov–Smirnov test. *J. Sound Vib.* **2006**, *290*, 337–368. [[CrossRef](#)]
5. Sun, X.; Chen, T.; Marquez, H.J. Efficient model-based leak detection in boiler steam-water systems. *Comput. Chem. Eng.* **2002**, *26*, 1643–1647. [[CrossRef](#)]
6. Sun, X.; Marquez, H.J.; Chen, T.; Riaz, M. An improved PCA method with application to boiler leak detection. *ISA Trans.* **2005**, *44*, 379–397. [[CrossRef](#)]
7. Özdemir, L. Performance Identification of Steam Heating Systems by Acoustic Analyses. Master’s Thesis, Akdeniz University, Antalya, Turkey, 2013.
8. Chen, W.; Jin, D.; Cui, W.; Huang, S. Characteristics of gliding arc plasma and its application in swirl flame static instability control. *Processes* **2020**, *8*, 684. [[CrossRef](#)]
9. Elattar, H.F.; Specht, E.; Fouda, A.; Rubaiee, S.; Al-Zahrani, A.; Nada, S.A. Swirled Jet Flame Simulation and Flow Visualization Inside Rotary Kiln—CFD with PDF Approach. *Processes* **2020**, *8*, 159. [[CrossRef](#)]
10. Gangisetty, G.; Jayachandran, A.T.; Sverbilov, V.Y.; Zubrilin, I.; Matveev, S. Review paper on thermo-acoustic instabilities in a gas turbine burners—Flashback avoidance. *J. Phys. Conf. Ser.* **2019**, *1276*, 012051. [[CrossRef](#)]
11. Beita, J.; Talibi, M.; Sadasivuni, S.; Balachandran, R. Thermoacoustic Instability Considerations for High Hydrogen Combustion in Lean Premixed Gas Turbine Combustors: A Review. *Hydrogen* **2021**, *2*, 33–57. [[CrossRef](#)]
12. Hou, S.-S.; Chung, D.-H.; Lin, T.-H. Experimental and numerical investigation of jet flow and flames with acoustic modulation. *Int. J. Heat Mass Transf.* **2015**, *83*, 562–574. [[CrossRef](#)]

13. Kraus, C.; Harth, S.; Bockhorn, H. Experimental investigation of combustion instabilities in lean swirl-stabilized partially-premixed flames in single- and multiple-burner setup. *Int. J. Spray Combust. Dyn.* **2016**, *8*, 4–26. [[CrossRef](#)]
14. Laera, D.; Camporeale, S.M. A Weakly Nonlinear Approach Based on a Distributed Flame Describing Function to Study the Combustion Dynamics of a Full-Scale Lean-Premixed Swirled Burner. *J. Eng. Gas Turbines Power* **2017**, *139*, 091501. [[CrossRef](#)]
15. Berger, F.M.; Hummel, T.; Hertweck, M.; Kaufmann, J.; Schuermans, B.; Sattelmayer, T. High-Frequency Thermoacoustic Modulation Mechanisms in Swirl-Stabilized Gas Turbine Combustors—Part I: Experimental Investigation of Local Flame Response. *J. Eng. Gas Turbines Power* **2017**, *139*, 071501. [[CrossRef](#)]
16. Weng, F.; Li, S.; Zhong, D.; Zhu, M. Investigation of self-sustained beating oscillations in a Rijke burner. *Combust. Flame* **2016**, *166*, 181–191. [[CrossRef](#)]
17. Kim, D.; Park, Y.; You, D.; Huh, K.Y. Analysis of thermoacoustic instability with corresponding eigenfrequencies in a large scale industrial oil furnace. *J. Mech. Sci. Technol.* **2016**, *30*, 4979–4988. [[CrossRef](#)]
18. Kraus, C.; Selle, L.; Poinot, T.; Arndt, C.M.; Bockhorn, H. Influence of Heat Transfer and Material Temperature on Combustion Instabilities in a Swirl Burner. *J. Eng. Gas Turbines Power* **2017**, *139*, 051503. [[CrossRef](#)]
19. Grimm, F.; Ohno, D.; Noll, B.; Aigner, M.; Ewert, R.; Dierke, J. Broadband Combustion Noise Simulation of the PRECCINSTA Burner Based on Stochastic Sound Sources. *J. Eng. Gas Turbines Power* **2017**, *139*, 011505. [[CrossRef](#)]
20. Bothien, M.R.; Noiray, N.; Schuermans, B. Analysis of Azimuthal Thermo-acoustic Modes in Annular Gas Turbine Combustion Chambers. *J. Eng. Gas Turbines Power* **2015**, *137*, 061505. [[CrossRef](#)]
21. Yang, F.; Guo, Z.; Fu, X.; Yu, D. Computation of acoustic transfer matrices of swirl burner with finite element and acoustic network method. *J. Low Freq. Noise Vib. Act. Control* **2015**, *34*, 169–184. [[CrossRef](#)]
22. Song, H.; Lin, Y.; Han, X.; Yang, D.; Zhang, C.; Sung, C.-J. The thermoacoustic instability in a stratified swirl burner and its passive control by using a slope confinement. *Energy* **2020**, *195*, 116956. [[CrossRef](#)]
23. Vicuña, C.M.; Höweler, C. A method for reduction of Acoustic Emission (AE) data with application in machine failure detection and diagnosis. *Mech. Syst. Signal Process.* **2017**, *97*, 44–58. [[CrossRef](#)]
24. Baofu, L.; Upadhyaya, B.R.; Perez, R.B. Structural integrity monitoring of steam generator tubing using transient acoustic signal analysis. *IEEE Trans. Nucl. Sci.* **2005**, *52*, 484–493. [[CrossRef](#)]
25. Ramezani, M.G.; Hasanian, M.; Golchinfar, B.; Saboonchi, H.; Zonta, D.; Huang, H. Automatic boiler tube leak detection with deep bidirectional LSTM neural networks of acoustic emission signals. In Proceedings of the Sensors and Smart Structures Technologies for Civil, Mechanical, and Aerospace Systems, Online Only, 27 April–9 May 2020.
26. Duong, B.P.; Kim, J.; Kim, C.-H.; Kim, J.-M. Deep Learning Object-Impulse Detection for Enhancing Leakage Detection of a Boiler Tube Using Acoustic Emission Signal. *Appl. Sci.* **2019**, *9*, 4368. [[CrossRef](#)]
27. Zhang, S.; Shen, G.; An, L. Leakage location on water-cooling wall in power plant boiler based on acoustic array and a spherical interpolation algorithm. *Appl. Therm. Eng.* **2019**, *152*, 551–558. [[CrossRef](#)]
28. Şeker, M.; Tokmakçı, M.; Asyali, M.H.; Seğmen, H. Examining EEG signals with parametric and non-parametric analyses methods in migraine patients during pregnancy. In Proceedings of the 2010 15th National Biomedical Engineering Meeting, Antalya, Turkey, 21–24 April 2010; IEEE: Piscataway Township, NJ, USA, 2010; pp. 1–4.
29. Stoica, P.; Moses, R.L. *Spectral Analysis of Signals*; Prentice Hall: Hoboken, NJ, USA, 2005.



Article

Comparison of Life Cycle Environmental Impact between Two Processes for Silver Separation from Copper Anode Slime

Zehong Li ^{1,2}, Wenbiao Zhang ^{3,*}, Bing Xia ¹ and Chunying Wang ^{1,2}

¹ Institute of Geographic Sciences and Natural Resources Research, Chinese Academy of Sciences, 11A Datun Road, Chaoyang District, Beijing 100101, China; lizehong@igsnr.ac.cn (Z.L.); xiab.16b@igsnr.ac.cn (B.X.); wangchunying19@mailsucas.ac.cn (C.W.)

² College of Resources and Environment, University of Chinese Academy of Sciences, 380 Huaibeizhuang, Huairou District, Beijing 100049, China

³ Beijing Academy of Social Sciences, 33 North Fourth Ring Middle Road, Chaoyang District, Beijing 100101, China

* Correspondence: zhangwenbiaozwb@163.com

Abstract: The cost of silver separation is lowered when ammonia and hydrazine hydrate are replaced with sodium thiosulfate and sodium dithionite in the process of extracting of metallic silver from copper anode slime. The overall environmental impact of two types of copper silver separation processes from anode slime has been analyzed using the LCA method. Through the subdivision analysis, we found the raw materials or emission items that should be improved first. The following conclusions are drawn: (1) The life cycle environmental impact of the sodium thiosulfate process is much lower than the existing process; (2) The resource and environmental impacts of the sodium thiosulfate method are mainly in the fields of climate change, photochemical smog, and ionizing radiation, exceeding two-thirds of the impact on all of the resources and environment; (3) In terms of input and output items, the main impact of the new process on the resources and the environment is concentrated on the use of sodium hydroxide, accounting for 33.98% of the total equivalent, followed by sodium thiosulfate and sodium carbonate, respectively. These input–output items are the key fields that need attention in future technology improvement.

Keywords: copper anode slime; silver separation; life cycle assessment; ecological impact; green manufacturing

Citation: Li, Z.; Zhang, W.; Xia, B.; Wang, C. Comparison of Life Cycle Environmental Impact between Two Processes for Silver Separation from Copper Anode Slime. *Int. J. Environ. Res. Public Health* **2022**, *19*, 7790. <https://doi.org/10.3390/ijerph19137790>

Academic Editors: Roberto Alonso González Lezcano, Francesco Nocera and Rosa Giuseppina Caponetto

Received: 8 May 2022
Accepted: 16 June 2022
Published: 24 June 2022



Copyright: © 2022 by the authors. Licensee MDPI, Basel, Switzerland. This article is an open access article distributed under the terms and conditions of the Creative Commons Attribution (CC BY) license (<https://creativecommons.org/licenses/by/4.0/>).

1. Introduction

Copper anode slime is a by-product of crude copper electrorefining, and a substance that deposits at the bottom of the electrolytic cell during the process of copper electrorefining [1]. The mass is generally about 0.2–1.0% of the anode plate. Anode slime is one of the main raw materials for extraction of rare and precious metals, because it contains a large amount of gold, silver, copper, selenium, tellurium, and platinum group metals [2–5]. The annual output of copper anode slime in China is about 71,100 tons [6], which is an important source of metallic silver production. With the rapid increase in China's copper and other non-ferrous metals production [7], the extraction of silver and other precious metals from anode slimes will have increasingly important economic and environmental impacts. The improvement of related extraction technology and its effect on the environment will also attract more and more attention.

The main method to recover silver from anode slime is pyrometallurgy [8,9]. This method usually involves a series of pyrometallurgical processes and consumes a lot of energy [10], and has disadvantages such as high energy consumption, poor silver recovery, and severe air pollution (e.g., SO₂, lead-containing fumes, arsenic, and antimony) [11]. The wet method and semi-wet method are adopted by most companies in China. The ammonia method is mostly used in the silver separation process—i.e., ammonia and hydrazine

hydrate are used as reducing agents to reduce silver ions into elementary substances. However, due to the higher cost and toxicity of hydrazine hydrate, as well as the high volatility of ammonia, the environmental impact is obvious [12].

Semi-hydrometallurgical technology has been developed in order to resolve these disadvantages. The technology includes the following steps: sulfate roasting, sulfuric acid leaching of copper, and sodium sulfite leaching of silver [13,14]. However, this method also has disadvantages, including high consumption of leaching agent and release of harmful gases such as SO₂. During the pretreatment process, the oxidation of sulfide in the anode slime produces SO₂ during the sulfation step of baking, thus possibly inducing pollution due to careless operations. During the leaching process, due to its poor stability, the measured Ag (SO₃)₃²⁻ is easily oxidized by the oxygen dissolved in the aqueous solution [15]. Thus, it is inevitable to use high-concentration sodium sulfite. As a result, the leaching agent is consumed excessively.

The Institute of Process Engineering of the Chinese Academy of Sciences has proposed an efficient hydrometallurgical technology for recovering silver from anode slime, with sodium thiosulfate as the silver leaching agent and sodium hydrosulfite for silver reduction. This method has a high recovery rate of silver of up to 95.4% under the optimal conditions. The technology was tested on site by metallurgical enterprise in Jiangxi, with the ammonia method for silver separation, commonly used in China, transformed into a thiosulfate method. With unchanged existing equipment and fine-tuning of the technology process flow, the direct material cost per ton of gold slag dropped from 1654.04 yuan to 802.90 yuan—a decrease of over 50%—thereby achieving good economic benefits. However, the changes in the environmental impact have not yet been analyzed.

There are relatively few studies on the environmental impact of the extraction of precious metals in anode slime. Tang et al. [16] calculated the waste discharge and emission reduction of copper anode slime utilization through joint process analysis. Chai [17] determined the migration process of major pollutants of the waste copper smelting production line via material flow analysis and identified the emission items of the accumulation of pollutants such as smelting slag, smoke, and dust. Nuss [18] analyzed the flow of tellurium in copper anode mud by means of material flow analysis and put forward suggestions on the environmental impact management of tellurium. Iannicelli-Zubiani et al. [19] used the LCA method to analyze the environmental impact of recycling important metals such as copper and gold from electronic waste and identified industrial processes with greater environmental impact. These studies are more static studies on the environmental effects of the production line, lacking comparison of the environmental effects of different processes, and it is therefore difficult to point out the direction of process improvement. From a methodological point of view, direct process analysis and material flow analysis of a production line are limited to the evaluation of the direct environmental impact of the production line. It is difficult to measure the pollution caused by the production of raw materials and waste treatment in the upstream and downstream industries. Relatively, life cycle assessment traces the source of all input and output items, and evaluates its environmental impact more comprehensively.

Life cycle assessment (LCA) is a process of assessing a product, technology, or activity—i.e., an environmental load-related process throughout the entire life cycle, including raw material collection, production, transportation, sales, utilization, recycle, maintenance, and final disposal. Firstly, it identifies and quantifies the consumption and environmental release of energy and materials throughout the life cycle, then it evaluates the impact of consumption and release on the environment, and finally identifies and evaluates the opportunities to reduce the impact [20]. Usually, LCA is divided into four steps: definition of goals and scope determination, inventory analysis, impact evaluation, and improvement evaluation. This method quantifies and evaluates the resource consumption, ecological pressure, and human health impact of specific substances throughout their entire life cycle. Moreover, it further analyzes the impact of differences between the raw materials or products on the environment [21]. Compared with other environmental impact

evaluation methods that directly evaluate production, it can more completely assess the entire environmental impact of a specific product or process.

In this paper, life cycle assessment (LCA) method is used to analyze the final resource consumption and pollutant emissions per unit output of the main product—metallic silver—in two different silver separation processes, the ammonia method and sodium thiosulfate method. Then, the impact on different aspects of the ecological environment is analyzed to compare the impact intensity and characteristics between the two processes. On the basis of the overall impact analysis, we analyzed the sensitivity of the environmental impact of all input–output items to select the input–output items that have the greatest ecological impact, and then the direction of technology improvement is proposed. The novelty of this paper is the first life cycle environmental impact assessment of silver extraction from copper anode slime. This assessment will help to identify the links and input–output items with greater environmental impact, and provide direction for future process improvement. The structure of this paper is as follows: Section 2 describes the methodology and data sources used in this paper. Part 3 explains and discusses the analytical results. Part 4 presents final conclusions and suggestions according to the result analyzed, explores the disadvantages, and touches upon a further research direction.

2. Methods and Data

2.1. Data Sources

The data used in this paper can be divided into foreground data and background data. The former refers to the material and energy data direct input and output in the production process. The latter is the data on the resource consumption and environmental impact of these materials and energy in their respective production processes. The foreground data used in this paper were mainly provided by a company in Jiangxi, China including the data on all input–output items in the two silver separation processes and the data regarding economic value. The background data come from the Gabi database [22–26].

2.2. Methods

In this paper, the life cycle assessment method is used to evaluate the final resource consumption and pollutant emissions generated in the two different processes of silver separation from copper anode slime. A scope boundary is established for LCA according to the company's input–output process directly related to silver separation; a life cycle inventory is set up for the production processes according to the data obtained from the field survey; Gabi 9.0 is adopted for evaluating the change in the environmental impact of the two silver separation processes using ReCiPe 2016. Different eco-environmental effects—including soil acidification and ozone destruction—are comparatively analyzed at different points of the production processes. Then, the environmental effects of the input and output items of the new process are analyzed, and the input and output substances that have a greater impact on the resources and the environment are found, and the direction for further technological improvement is pointed out. Finally, Monte Carlo analysis is performed on the calculation results to judge the certainty of the calculation results.

2.2.1. Determination of Boundary

The case selected is a metal recycling company located in Jiangxi Province, China. It is a high-tech environmental protection enterprise that specializes in producing black copper, electrolytic copper, nickel sulfate, electrolytic zinc, and precious metals from copper-containing recycling materials such as electronic waste and electroplating sludge; and recovering rare and precious metals, such as gold and silver, from copper anode slime. The company has a designed annual production capacity of 100,000 tons of refined copper and 1500 tons of anode slime, and 90 kg of recovered metallic silver. The production technology is highly representative. This paper introduces the production technology and input–output items of the former ammonia silver separation technology and the new sodium thiosulfate technology developed by the Institute of Process Engineering.

The enterprise adopts the ammonia separation technology originally, by which ammonia is used as a leaching agent to generate silver–ammonia complex ions, and hydrazine hydrate as a reducing agent to generate silver. In the new process, sodium thiosulfate is used as leaching agent to generate silver–thiosulfate complex ions, and sodium dithionite is employed as a reducing agent to generate silver. For a simple technology comparison, we took the dominant product—metallic silver—as the benchmark and determined the functional unit of LCA as 1 kg of metallic silver. Figure 1 shows the flow of materials among all the production links in the process of completing a functional unit.

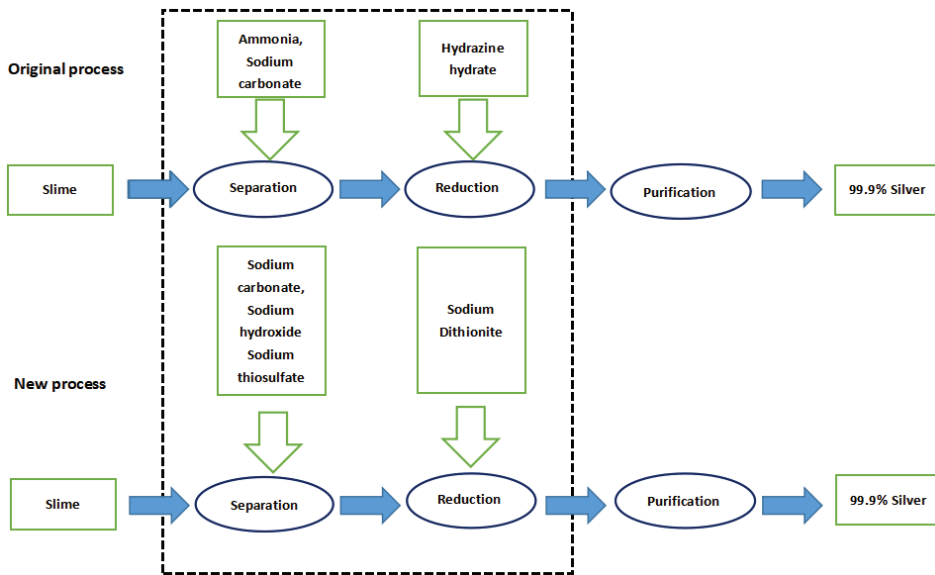


Figure 1. Definition of the LCA scope of the silver separation processes.

As this paper is focused on the environmental impact generated in the production processes, the ‘cradle-to-gate’ model is selected for the research boundary. That is, from the development of various raw materials to the products, as well as the waste disposal during production, the environmental impact of equipment and infrastructure construction is not taken into consideration as the same facilities are used in both processes. As the silver separation process only produces one beneficial product of metallic silver, the distribution of environmental burdens is not discussed in this paper. The energy consumption rates of the new and old processes are almost the same. Since this paper compares the environmental effects of the new and old processes, the energy consumption can be ignored.

2.2.2. Establishment of Life Cycle Inventory

With Gabi 9.0 software (Sphera Solutions GmbH, Leinfelden-Echterdingen, Germany), the direct raw materials used in each production process are associated with the production processes and the emissions to be treated are associated with the treatment process, thereby establishing a complete life cycle inventory. The material input and output in the inventory should be balanced.

The input–output items of original silver separation process include sodium carbonate, liquid ammonia, hydrazine hydrate, and residue of anode slime after gold/copper/selenium separation. The output is metallic silver, residue and wastewater are also generated. Each 1 kg of metallic silver extracted requires 0.95 kg of sodium carbonate, 4.94 kg of ammonia, 4.75 kg of hydrazine hydrate, and 17.09 kg of slime; while 1 kg of crude silver, 15.72 kg of residue, and 11.00 kg of wastewater are produced (Table 1).

Table 1. Material inventory of original silver separation process.

Material	Unit	Quantity	Note
Input			
Sodium carbonate	kg	0.95	
Ammonia	kg	4.94	
Hydrazine hydrate	kg	4.75	
Slime	kg	17.09	Self-produced
Output			
Crude silver	kg	1.00	
Slag	kg	15.72	
Waste water	kg	11.00	

In the new process, the input items include sodium hydroxide, sodium carbonate, sodium thiosulfate, sodium dithionite, and metal residue; while the output items remain as metallic silver, residue, and wastewater. Each 1 kg of metallic silver extracted requires 1.52 kg of sodium hydroxide, 0.67 kg of sodium carbonate, 0.91 kg of sodium dithionite, 2.85 kg of sodium thiosulfate, and 17.09 kg of slime, while 13.56 kg of residue and 8.48 kg of wastewater are generated (Table 2).

Table 2. Material inventory of new silver separation process.

Material	Unit	Quantity	Note
Input			
Sodium hydroxide	kg	1.52	
Sodium carbonate	kg	0.67	
Sodium dithionite	kg	0.91	
Sodium thiosulfate	kg	2.85	
Slime	kg	17.09	Self-produced
Output			
Crude silver	kg	1.00	
Slag	kg	13.56	
Waste water	kg	8.48	

The quality and consistency of all data input are analyzed. The results show that the data used have high technical and temporal representativeness, and slightly lower location representativeness; the input–output mass difference among different links is less than 0.5%, passing the consistency test (Table 3).

Table 3. Data quality assessment of the silver separation processes.

Unit: %	Completely Representative	Partly Representative	Not Representative
Technique	94.4	0	5.56
Location	44.4	50	5.56
Time	94.4	0	5.56

The life cycle inventory analysis could be conducted on the input–output table to acquire data about the classification and sum of the resource consumption and waste emissions generated throughout the production processes. The corresponding data and analysis results are shown in Section 3.1.

2.2.3. Life Cycle Impact Assessment (LCIA)

Through characterization, the impacts of different types of environmental factors are comparatively analyzed and quantified. During the calculation process, characteristic factors are used to convert the results in the life cycle inventory into measurable units for specific environmental impacts. For example, the impact of various substances on global warming is all converted into carbon dioxide equivalent, and various quantitative

indicators of ecological environmental impact are obtained for comparison and analysis. Finally, the characterization results of the life cycle are weighted in order to reveal the overall environmental impact. Weighting assigns various weight coefficients based on value selection to different impact type index results and then combines the weighted results.

Using LCA-ReCiPe 2016 [27] characterization and normalization method system (mid-point and end-point method) weighted addition, the life cycle list is further converted into impact marks in different areas. ReCiPe 2016 can be regarded as a combine of two models: the mid-point indexes of CML and the end-point indexes of eco-indicator are adopted, so the eco-environmental impact of the production processes can be demonstrated by the evaluation results more comprehensively. Compared with the earlier versions, the parameter setting in ReCiPe 2016 shows significant global applicability. The method considers 16 mid-point indexes. On this basis, the 16 mid-point indexes are converted into three categories of end-point indicators through mid-point-to-end-point conversion. Finally, according to the ratio of each indicator value to the global average value, all indicators are normalized to obtain comparable normalized indicator values (Figure 2).

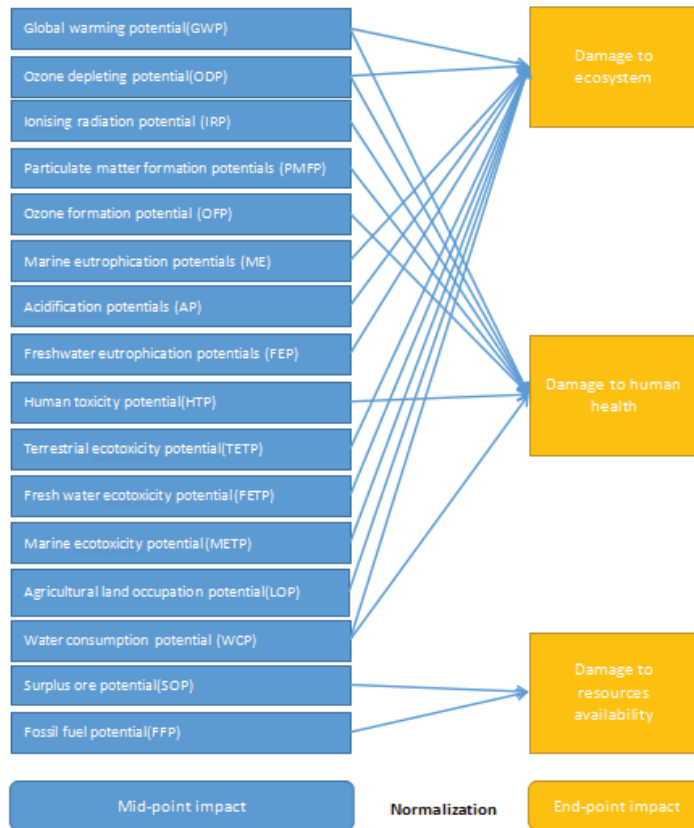


Figure 2. LCA-ReCiPe 2016 life cycle impact assessment process (Huijbregts, Steinmann et al., 2017) [27].

2.2.4. Uncertainty Analysis

Due to the quality of data collection and the error range, the environmental impact results calculated by the LCA method may be uncertain. This paper will use the Monte Carlo analysis method in Gabi software to evaluate the uncertainty of the calculation results. The mean, standard deviation (SD), and coefficient of variation (CV) are used

to quantify the uncertainty. The CV is a parameter that measures the magnitude of the standard deviation relative to the mean. The calculation formula of coefficient of variation is: coefficient of variation $CV = (\text{standard deviation}/\text{mean}) \times 100\%$.

The number of Monte Carlo iterations is set to 1000, and the confidence interval is within 95%.

3. Results and Discussion

3.1. Results and Discussion of Inventory Analysis

In general, 12,847.50 kg of total materials are required for producing 1 kg of metallic silver by the new process, while 13,402.75 kg of total materials are required for producing 1 kg of metallic silver by the original process. This shows that—calculated by mass—the impact on the resources and environment exerted in the new process is less severe. In terms of itemization, the new process has a lower material flow than the original process except for sea water emission. To be specific, the main energy consumption is all non-renewable energy, while most of the resource consumption is in renewable resources. In terms of emissions, the main emission is freshwater emission, followed by emission to air (Table 4).

Table 4. Life cycle resource depletion and emissions comparison of the silver separation processes.

Unit: kg	Original Process	New Process
Flows	13,402.75	12,847.50
Energy resources	6.21	2.17
Non-renewable energy resources	6.21	2.17
Renewable energy resources	0.00	0.00
Material resources	6700.84	6415.41
Non-renewable resources	34.96	15.18
Renewable resources	6665.83	6400.21
Emissions	6695.70	6429.91
Deposited goods	35.63	24.65
Emissions to air	149.85	75.03
Emissions to fresh water	6501.01	6308.29
Emissions to sea water	9.22	21.94
Emissions to agricultural soil	0.00	0.00
Emissions to industrial soil	0.00	0.00

3.2. Results and Discussion of Impact Assessment

The specific number of 16 eco-environmental indicators of the two processes are shown in the table below. The new process is better than the original process in terms of 13 indexes, including GWP, PMFP, FFP, WCP, FETP, FEP, LOP, ME, SOP, OFP, ODP, AP, and TETP. The global warming effect is 4.61 kg CO₂ eq., equivalent to 58.06% of the original process; the particulate matter is 0.004 kg PM_{2.5} eq., equivalent to 49.02% of the original process; the fossil energy consumption is 1.57 kg oil eq., only about 30.43% of the original process. The remaining three indexes—i.e., human toxicity, ionizing radiation, and seawater ecotoxicity—are inferior to the original process, equivalent to 153.45%, 192.31%, and 126.65% of the original process, respectively (Table 5).

Through normalization, the total value of the eco-environmental impact is obtained as follows (Figure 3): The weighted person equivalent in the new process is 2.56, equal to 21.94% of that in the original process. To be specific, the human health impact equivalent is 1.22, the ecological impact equivalent is 1.09, and the resource availability impact equivalent is 0.25. The corresponding values of the original process are 2.67, 1.97, and 1.05. Compared with the new process, the ecological impact decreases the most, to only 13.72% of the original process; followed by resource availability, equal to 23.73% of the original process; even as for the human health impact, it decreases by more than half in the new process, equivalent to 45.78% of the original process. From the perspective of the new process itself, the greatest impact on the resources and environment is the human health impact,

accounting for 47.06% of the total weighted human equivalent, followed by the ecological impact. Furthermore, the impact is mainly divided into climate change, photochemical smog and ionizing radiation, which account for 37.23%, 17.87%, and 13.38% of the total equivalents respectively. The sum of the three items exceeded two-thirds of the total impact on the resources and environment, which is a key area that needs attention in future technology improvement.

Table 5. Comparison of the life cycle impact indicators of the silver separation processes.

Factor	Unit	Original Process	New Process
GWP	kg CO ₂ eq.	7.94	4.61
PMFP	kg PM _{2.5} eq.	8.16×10^{-2}	4.00×10^{-3}
FFP	kg oil eq.	5.75	1.75
WCP	m ³	2.56×10^{-2}	1.90×10^{-2}
FETP	kg 1,4-DB eq.	7.98×10^{-4}	7.29×10^{-4}
FEP	kg P eq.	2.44×10^{-5}	1.28×10^{-5}
HTP	kg 1,4-DB eq.	$1.16 \times 10^{+1}$	$1.78 \times 10^{+1}$
IRP	kBq Co-60 eq. to air	3.12×10^{-1}	6.00×10^{-1}
LOP	Annual crop eq.·y	2.11×10^{-1}	9.08×10^{-2}
METP	kg 1,4-DB eq.	6.98	8.84
ME	kg N eq.	3.59×10^{-4}	1.80×10^{-4}
SOP	kg Cu eq.	9.71×10^{-2}	7.29×10^{-2}
OPF	kg NO _x eq.	2.72×10^{-2}	2.12×10^{-2}
ODP	kg CFC-11 eq.	3.43×10^{-5}	1.71×10^{-6}
AP	kg SO ₂ eq.	6.47×10^{-1}	1.26×10^{-2}
TETP	kg 1,4-DB eq.	2.23	1.76

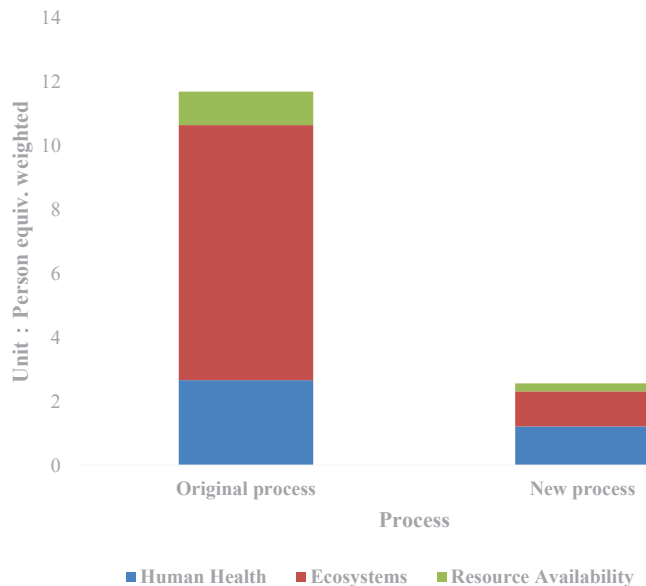


Figure 3. Comparison of the life cycle impact indicators of the silver separation processes.

In terms of each input–output item (Figure 4), it can be seen that sodium hydroxide is the input–output item with the greatest impact on the resources and environment, and the weighted person equivalent reaches 0.87, accounting for 33.98% of the total equivalent, followed by sodium thiosulfate and sodium carbonate, which account for 26.10% and 18.30% of the total equivalent respectively. By classification, sodium hydroxide contributes to the greatest impact on human health, accounting for 42.90% of the total human health impact;

followed by sodium thiosulfate and sodium carbonate, accounting for 22.25% and 14.66% respectively. Sodium thiosulfate contributes to the greatest impact on the ecological and resource availability, accounting for 28.47% and 34.61% of the total respectively, followed by sodium hydroxide and sodium carbonate.

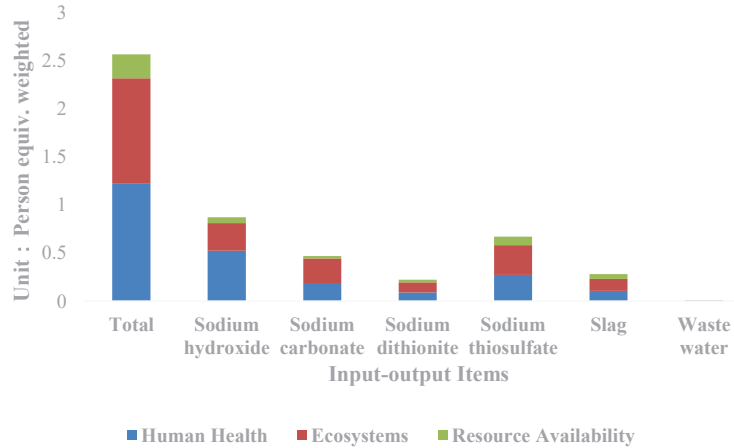


Figure 4. Comparison of the life cycle impact indicators of input–output items of the silver separation processes.

In terms of each impact factor (Figure 5), sodium thiosulfate exerts the greatest impact in the field of GWP, PMF, FFP, WCP, FETP, FEP, METP, OFP, AP, and TETP; sodium hydroxide exerts the greatest impact in the field of ionizing radiation, land use changes, and ozone depletion; solid waste disposal is the largest cause of metal consumption, while wastewater treatment causes the greatest impact on seawater eutrophication.

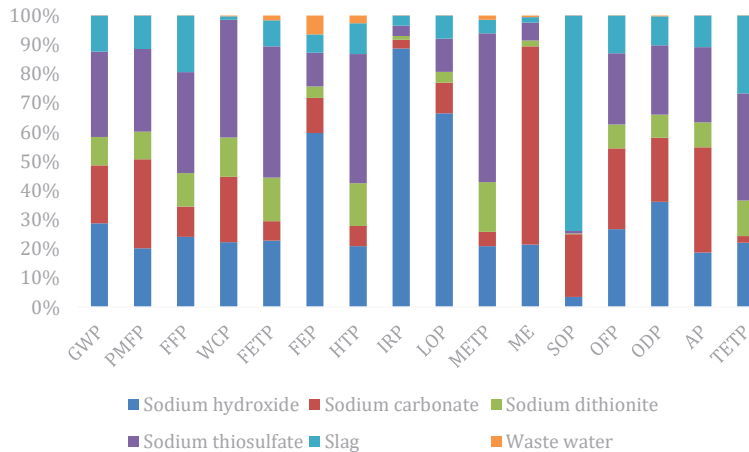


Figure 5. Subdivided end-point indicators of the input–output items of the silver separation processes.

3.3. Uncertainty Analysis

The Monte Carlo analysis module in GaBi software is used to analyze the uncertainty of the calculation results (Table 6). The analysis results show that the CVs of the input–output quality analysis results are 4.61% and 4.60% respectively; that is, the certainty is very significant. In the mid-point data, PMFP (8.79%), FFP (6.83%), METP (6.02%), and TETP (9.37) are significant at the 10% level, and the rest are significant at the 5% level. The CV

value of the end-point data is 2.25%, which is less than 5%, indicating that the calculation results have high reliability.

Table 6. Monte Carlo analysis of the results of the silver dividing processes LCA.

	Unit	Mean	CV
Mass-input	kg	$1.25 \times 10^{+4}$	4.61%
Mass-output	kg	$8.60 \times 10^{+1}$	4.60%
Mid-point-GWP	kg CO ₂ eq.	$7.50 \times 10^{+3}$	4.84%
Mid-point-PMFP	kg PM2.5 eq.	$1.28 \times 10^{+4}$	8.79%
Mid-point-FFP	kg oil eq.	1.53	6.83%
Mid-point-WCP	m ³	3.72×10^{-2}	4.61%
Mid-point-FETP	kg 1,4 DB eq.	$1.92 \times 10^{+2}$	3.58%
Mid-point-FEP	kg P eq.	$2.94 \times 10^{+4}$	4.46%
Mid-point-HTP	kg 1,4-DB eq.	$9.12 \times 10^{+2}$	3.17%
Mid-point-IRP	kBq Co-60 eq. to air	$3.01 \times 10^{+2}$	2.40%
Mid-point-LOP	Annual crop eq.·y	$1.58 \times 10^{+4}$	3.04%
Mid-point-METP	kg 1,4-DB eq.	5.38×10^{-1}	6.02%
Mid-point-ME	kg N eq.	$1.70 \times 10^{+2}$	2.98%
Mid-point-SOP	kg Cu eq.	$2.42 \times 10^{+1}$	4.48%
Mid-point-OFP	kg NOx eq.	$2.39 \times 10^{+1}$	3.94%
Mid-point-ODP	kg CFC-11 eq.	3.60×10^{-2}	3.65%
Mid-point-AP	kg SO ₂ eq.	$6.62 \times 10^{+2}$	3.65%
Mid-point-TETP	kg 1,4-DB eq.	$3.99 \times 10^{+3}$	9.37%
End-point	Weighted person equivalents	$1.25 \times 10^{+4}$	2.25%

4. Conclusions and Recommendation

The life cycle environmental impact of the sodium thiosulfate-based silver separation technology is much lower than that of the original process. The weighted person equivalent is approximately 21.94% of the original process. The ecological impact, human health impact, and resource availability are equal to 13.72%, 45.78%, and 23.73% of the original process respectively. The new process has good environmental and economic benefits and broad application prospects. The new process brings in an additional economic income of 8.12 yuan per kilogram of silver. China has an annual output of 71,100 tons of copper anode slime [6], from which about 4000 tons of metallic silver can be extracted. If the sodium thiosulfate method is adopted for silver separation, an additional economic income of more than 30 million yuan can be generated annually. Meanwhile, greenhouse gas emissions (1.3×10^4 tons of CO₂ equivalent), fossil energy consumption (1.6×10^4 tons of oil equivalent), acidification (2.5×10^3 tons of sulfur dioxide equivalent), and particulate matter emissions (3.1×10^2 tons of PM2.5 equivalent) can be reduced.

The new process has the greatest impact on human health, accounting for 47.06% of the total weighted human equivalent. Subdivided further, the impact is mainly divided into climate change, photochemical smog, and ionizing radiation, which account for 37.23%, 17.87%, and 13.38% of the total equivalents respectively. The sum of the three items exceeded two-thirds of the impact on total resources and environment. In terms of input and output, the main impact of the new process on the resources and environment is concentrated on the use of sodium hydroxide, accounting for 33.98% of the total equivalent, followed by sodium thiosulfate and sodium carbonate, accounting for 26.10% and 18.30% of the total equivalent respectively. These input and output items are the key areas that need attention in future technology improvement.

In this paper, the overall environmental impacts of two copper anode slime silver separation processes were analyzed using the life-cycle assessment method, and the ultimate resource consumption and pollutant emissions arising from the two silver separation processes were evaluated. Additionally, two types of environmental impact in different areas were analyzed through subdivision analysis, revealing the raw materials or emission

items that should be improved first. This conclusion has greater guiding significance for the improvement of the production technology.

This paper has some shortcomings caused by the test progress. First, limited by the shortcoming of technical analysis, this paper fails to further analyze the technology mechanism of the main raw material consumption and waste discharge; second, this article only evaluates the environmental impact of existing production methods, and proposes improvement directions on this basis, but failed to propose a clear technological path for improvement. These issues will be important directions for our further research.

Author Contributions: Z.L.: conceptualization; W.Z.: methodology, writing—original draft preparation; B.X.: English editing; C.W.: software support. All authors have read and agreed to the published version of the manuscript.

Funding: This research was conducted with support from the Key Deployment Project of the Chinese Academy of Sciences, “Evaluation of eco-efficiency of Cu–Ni–Co regenerated metal short process recycling industry chain”, grant no. ZDRWZS201812; the Project of Innovation Academy for Green Manufacturing, Chinese Academy of Sciences grant no. IAGM-2019-A16; the Training Program of the Major Research Plan of the National Natural Science Foundation of China, grant no. 92062111; and the Special Investigation on National Basic Science and Technology Resources, grant no. 2019QZKK040303.

Institutional Review Board Statement: The study did not involve humans or animals.

Informed Consent Statement: Not applicable.

Data Availability Statement: The data presented in this study are available on request from the corresponding author. The data are not publicly available due to business secrets of enterprises.

Conflicts of Interest: The authors declare no conflict of interest.

References

1. Bin, W.; Lu, Y. *Precious Metal Metallurgy*; Central South University Press: Changsha, China, 2011; pp. 33–35.
2. Wang, Y. Progress of the Metallurgical Engineering Technology of Precious Metals in China. *Precious Met.* **2011**, *32*, 59–71.
3. Yldrm, G.; Tokaloglu, S.; Sahan, H.; Patat, S. Preconcentration of Ag and Pd ions using graphite oxide and 2,6-diaminopyridyne from water, anode slime and catalytic converter samples. *RSC Adv.* **2014**, *4*, 18108–18116. [[CrossRef](#)]
4. Ding, Y.; Zhang, S.; Liu, B.; Li, B. Integrated process for recycling copper anode slime from electronic waste smelting. *J. Clean. Prod.* **2017**, *165*, 48–56. [[CrossRef](#)]
5. Wang, S.; Cui, W.; Zhang, G.; Zhang, L.; Peng, J. Ultra fast ultrasound-assisted decopperization from copper anode slime. *Ultrason. Sonochem.* **2017**, *36*, 20–26. [[CrossRef](#)] [[PubMed](#)]
6. Liao, C.; Li, A.; Liu, D.; Jiao, Y. Method for Recycling Tellurium from Copper Anode Slime. China Patent 201310060626.7, 26 February 2013.
7. Zhang, W.; Li, Z.; Dong, S.; Qian, P.; Ye, S.; Hu, S.; Xia, B.; Wang, C. Analyzing the environmental impact of copper-based mixed waste recycling—A LCA case study in China. *J. Clean. Prod.* **2021**, *284*, 125256. [[CrossRef](#)]
8. Hait, J.; Jana, R.; Sanyal, S. Processing of copper electrorefining anode slime: A review. *Min. Process. Extr. Metall. Rev.* **2009**, *118*, 240–252. [[CrossRef](#)]
9. Khanlariana, M.; Rashchia, F.; Saba, M. A modified sulfation-roasting-leaching process for recovering Se, Cu, and Ag from copper anode. *J. Clean. Prod.* **2019**, *261*, 121214.
10. Xu, B.; Yang, Y.; Li, Q.; Yin, W.; Jiang, T.; Li, G. Thiosulfate leaching of Au, Ag and Pd from a high Sn, Pb and Sb bearing decopperized anode slime. *Hydrometallurgy* **2016**, *164*, 278–287. [[CrossRef](#)]
11. Ludvigsson, B.; Larsson, S. Anode slimes treatment: The Boliden experience. *Jom* **2003**, *55*, 41–44. [[CrossRef](#)]
12. Ning, R. Copper Anode Slime Treatment Process Comparison and Suggestions. *Metall. Metall. Eng.* **2018**, *6*, 42–47.
13. Hyk, W.; Kitka, K. Highly efficient and selective leaching of silver from electronic scrap in the base-activated persulfate ammonia system. *Waste Manag.* **2017**, *60*, 601–608. [[CrossRef](#)] [[PubMed](#)]
14. Valiuniene, A.; Baltrunas, G.; Valiunas, R.; Popkirov, G. Investigation of the electroreduction of silver sulfite complexes by means of electrochemical FFT impedance spectroscopy. *J. Hazard. Mater.* **2010**, *180*, 259–263. [[CrossRef](#)] [[PubMed](#)]
15. Baltrunas, G.; Valiuniene, A.; Margarian, Z.; Viselgiene, G.; Popkirov, G. The electroreduction kinetics of silver sulfite complexes. *Electrochim. Acta* **2008**, *53*, 6513–6520. [[CrossRef](#)]
16. Tang, X.; Zhang, S.; Mao, L. Production process and pollution prevention control measures of gold and silver recovery from copper anode mud. *Jiangxi Chem. Ind.* **2017**, 103–108.
17. Chai, Z. *Migration and Transformation of Pollutants in Scrap Copper Smelting Process*; China University of Mining and Technology: Beijing, China, 2014; pp. 21–23.
18. Nuss, P. Losses and environmental aspects of a byproduct metal: Tellurium. *Environ. Chem.* **2019**, *16*, 243–250. [[CrossRef](#)]

19. Iannicelli-Zubiani, E.; Giani, M.; Recanati, F.; Dotellia, G.; Puricellia, S.; Cristiania, C. Environmental impacts of a hydrometallurgical process for electronic waste treatment: A life cycle assessment case study. *J. Clean. Prod.* **2017**, *140*, 1204–1216. [[CrossRef](#)]
20. Santoyo-Castelazo, E.; Azapagic, A. Sustainability assessment of energy systems: Integrating environmental, economic and social aspects. *J. Clean. Prod.* **2014**, *80*, 119–138. [[CrossRef](#)]
21. *ISO 14040*; Environmental Management-Life Cycle Assessment-Principles and Framework. ISO: London, UK, 2006.
22. Eksteen, J.; Oraby, E. The leaching and adsorption of gold using low concentration amino acids and hydrogen peroxide: Effect of catalytic ions, sulphide minerals and amino acid type. *Miner. Eng.* **2015**, *70*, 36–42. [[CrossRef](#)]
23. Speck, R.L. A Comparative Analysis of Commercially Available Life Cycle Assessment Software. Ph.D. Thesis, Michigan State University, East Lansing, MI, USA, 2014.
24. Xiao, H.; Zhang, D.; Tang, Z.; Li, K.; Guo, H.; Niu, X.; Yi, L. Comparative environmental and economic life cycle assessment of dry and wet anaerobic digestion for treating food waste and biogas digestate. *J. Clean. Prod.* **2022**, *338*, 130674. [[CrossRef](#)]
25. Mandavgane, S.A.; Joglekar, S.N.; Kharkar, R.A.; Kulkarni, B.D. Process development of silica extraction from RHA: A Cradle to gate environmental impact approach. *Environ. Sci. Pollut. Res.* **2019**, *26*, 1954.
26. Khalil, Y.F. Comparative environmental and human health evaluations of thermolysis and solvolysis recycling technologies of carbon fiber reinforced polymer waste. *Waste Manag.* **2018**, *76*, 767–778. [[CrossRef](#)] [[PubMed](#)]
27. Huijbregts, M.; Steinmann, Z.; Elshout, P. ReCiPe2016: A harmonised life cycle impact assessment method at midpoint and endpoint level. *Int. J. Life Cycle Assess.* **2017**, *22*, 138–147. [[CrossRef](#)]

Article

Entrapment of Airborne Particles via Simulated Highway Noise-Induced Piezoelectricity in PMMA and EPDM

Mengyao Lyu ¹, Som V. Thomas ¹, Heng Wei ², Julian Wang ³, Tiina A. Reponen ⁴, Patrick H. Ryan ^{4,5,6} and Donglu Shi ^{1,*}

¹ The Materials Science and Engineering Program, Department of Mechanical and Materials Engineering, College of Engineering and Applied Science, University of Cincinnati, Cincinnati, OH 45221, USA; lyumo@mail.uc.edu (M.L.); valicksm@mail.uc.edu (S.V.T.)

² Department of Civil & Transportation Engineering, College of Engineering and Applied Science, University of Cincinnati, Cincinnati, OH 45221, USA; heng.wei@uc.edu

³ Architectural Engineering, Penn State University, State College, PA 16801, USA; jqw5965@psu.edu

⁴ Environmental & Public Health Sciences, Medical School, University of Cincinnati, Cincinnati, OH 45221, USA; reponeta@ucmail.uc.edu (T.A.R.); patrick.ryan@cchmc.org (P.H.R.)

⁵ Department of Pediatrics, University of Cincinnati College of Medicine, Cincinnati, OH 45221, USA

⁶ Division of Biostatistics and Epidemiology, Cincinnati Children's Hospital Medical Center, Cincinnati, OH 45229, USA

* Correspondence: donglu.shi@uc.edu

Abstract: The US highway system features a huge flux of energy transportation in terms of weight, speed, volume, flow density, and noise levels, with accompanying environmental effects. The adverse effects of high-volume traffic cause health concerns for nearby residential areas. Both chronic and acute exposure to PM 2.5 have detrimental effects on respiratory and cardiovascular health, and motor vehicles contribute 25–35% of direct PM 2.5 emissions. In addition to traffic-related pollutants, residing near major roadways is also associated with exposure to increased noise, and both affect the health and quality of life of residents. While regulatory and policy actions may reduce some exposures, engineering means may offer novel and significant methods to address these critical health and environmental issues. The goal of this study was to harvest highway-noise energy to induce surface charge via a piezoelectric material to entrap airborne particles, including PM 2.5. In this study, we experimentally investigated the piezoelectric effect of a polymethyl methacrylate (PMMA) sheet and ethylene propylene diene monomer (EPDM) rubber foam on the entrapment of copper (II)-2,4 pentanedione powder (Cu II powder). Appreciable voltages were induced on the surfaces of the PMMA via mechanical vibrations, leading to the effective entrapment of the Cu II powder. The EPDM rubber foam was found to attract a large amount of Cu II powder under simulated highway noise in a wide range, of 30–70 dB, and at frequencies of 700–1300 Hz, generated by using a loudspeaker. The amount of Cu II powder entrapped on the EPDM rubber-foam surfaces was found to scale with the SPL, but was independent of frequency. The experimental findings from this research provide a valuable base for the design of a robust piezoelectric system that is self-powered by harvesting the wasted sound energy from highway noise and reduces the amount of airborne particles over highways for effective environmental control.

Keywords: piezoelectric; highway noise; particle entrapment; sound energy

Citation: Lyu, M.; Thomas, S.V.; Wei, H.; Wang, J.; Reponen, T.A.; Ryan, P.H.; Shi, D. Entrapment of Airborne Particles via Simulated Highway Noise-Induced Piezoelectricity in PMMA and EPDM. *Energies* **2022**, *15*, 4935. <https://doi.org/10.3390/en15144935>

Academic Editors: Francesco Nocera, Roberto Alonso González Lezcano and Rosa Giuseppina Caponetto

Received: 28 May 2022

Accepted: 5 July 2022

Published: 6 July 2022



Copyright: © 2022 by the authors. Licensee MDPI, Basel, Switzerland. This article is an open access article distributed under the terms and conditions of the Creative Commons Attribution (CC BY) license (<https://creativecommons.org/licenses/by/4.0/>).

1. Introduction

Road traffic is a major source of airborne PM 2.5 (particles <2.5 µm in size) and noise pollution, both of which are recognized contributors to cardiovascular and other adverse health effects [1]. The association between road-traffic noise and public health has become increasingly evident, especially during the last decade [2]. For instance, the increase in weighted noise level 10 dB(A) within the range of approximately 52–77 dB(A) results in an

8% increase in the risk of cardiovascular diseases [3]. There is a 3% increase in the prevalence of hypertension per 5 dB(A) increase in the noise range of 45–75 dB(A) [3,4]. Additionally, residential traffic noise has the potential to worsen related depressive symptoms [5], mental disorders [6], and insomnia [7]. Furthermore, the PM 2.5 is causally associated with cardiovascular and respiratory health outcomes and co-exposures to both PM 2.5 and noise may have synergistic health effects. Approximately 11.3 million people (or 3.7% of the US population) live within 150 m of major highway infrastructures, placing them at risk for increased exposure to traffic air pollution and associated adverse health outcomes [8]. Time-series analyses suggest that exposure to PM 2.5 has detrimental effects on respiratory health, and motor vehicles contribute from 25% to 35% of direct PM 2.5 emissions [9–16]. Infants or elementary students at schools near heavy transportation infrastructures are particularly susceptible to such air pollutants [17–19].

Exposure to traffic pollution has been associated with adverse health effects, including pulmonary, neurological, and cardiovascular mortality and morbidity [20,21]. Specifically, exposure to traffic-related airborne particles (TRAP) has been associated with the exacerbation of existing asthma and the incidence of asthma among young and adolescent children [18,22,23]. In a previous community-based study in Cincinnati, we observed significant associations between the estimated TRAP exposure and adverse respiratory outcomes in children, including early childhood wheezing, persistent wheezing through age 7, and the development of asthma by age [7,17,24]. The threat from COVID-19 is even more alarming as the severity of COVID-19 infection has been associated with increased PM 2.5 exposure [25–28]. This interaction can occur either directly, by compromising the lungs' immune response to the infection, or indirectly, by exacerbating underlying respiratory or cardiovascular diseases [28].

Sound is typically characterized in terms of two main properties: frequency and intensity. The frequency of sound is the objective measure of its pitch (subjective measure). Cars produce noises in the range of 50 to 5000 Hz, while trucks produce noises in the range of 10 to 1000 Hz. In both cases, the typical noise distribution has a broad intensity peak at about 1250 Hz and a broad perceptual peak at about 500 Hz [29]. Noise barriers are designed to block the sound waves in the propagation path from the source to the receiver. The Environmental Impact Assessment and Noise Impact Assessment determined the types of noise barrier, such as reflective noise barriers, absorptive noise barriers or a combination of both [29]. Improving the acoustic performance of a vertical barrier without increasing its height has long been a challenge to the acoustic engineer. The pure reflective types, even with optimal morphological design and parametric analysis, are still not able to resolve this challenge. Based on a literature review, potential solutions can be classified into three types—absorptive, angled, and capped barriers. The notable developments include vegetation barriers [30,31], parallel noise barriers [16], barriers with absorbent/soft/reactive surfaces [32], diffusive noise barriers [33], T-shaped barriers [34], and other hybrid barrier profiles combined with T-, Y-, and inclined types [35–42].

The dispersion of pollutants from traffic emissions has been shown to be affected by near-road obstacles, such as noise barriers, buildings, and vegetation [43–45]. Depending upon the roadway–barrier configuration, concentration deficits of 50% or more have been observed relative to a reference roadway configuration in the absence of a barrier [17]. Previous studies showed that noise barriers can lead to an upward deflection of airflow caused by the structure. Thus, these barriers could increase the apparent release height of the pollutant, leading to more vertical mixing due to the flow separation at the top of the barrier [46–50]. More importantly, as a huge flux of transport energy in terms of weight, speed, volume, and noise, highway systems generate vast amounts of wasted energy due to inefficient consumption, particularly through large-sized-engine vehicles. The energy from both audible noise and the high flux of heavy-vehicular traffic flows is not only entirely wasted, but also results in traffic-related pollution and adverse health effects.

It is possible to address these critical issues by harvesting highway-noise energy and converting it to electricity via a piezoelectrical material with unique structures. The

piezoelectric effect results from the imbalance of the ionic crystal-lattice-based electric dipole moments under mechanical deformation [51,52]. Upon mechanical-pressure-induced deformation, the electric dipole moments are induced for ions on crystal-lattice sites with asymmetric charge surroundings. The noise from highways is a mechanical wave with an oscillation of pressure traveling through a medium. When the sound waves encounter the piezoelectric material with sufficient vibrations, surface charges can be developed on the piezoelectric materials. There are considerable studies on harvesting environmental noise for energy generation. Piezoelectric devices and sensors have been placed within highway structures to harvest noise energy, with significant successes [53]. Field-traffic and sound measurements can be collected in time intervals with the peak hour factor (PHF) to reflect the characteristics of traffic flow. Highway noise is generated from motor vehicles of various sizes and weights, contributing to a spectrum of collective sound energy with an average frequency of road noise of around 1000 Hz [29].

Previous research has mainly concentrated on the areas of noise harvest for energy generation and noise monitoring using piezoelectric materials and devices. No research has been carried out to investigate the possibility of capturing the airborne particles emanating from motor vehicles by using piezoelectric filters. Further, questions remain as to the level of noise that is sufficient to generate enough surface charge for the entrapment of airborne particles of different dimensions, distributions, and weights. In this study, we experimentally investigated the piezoelectric materials of a polymethyl methacrylate (PMMA) sheet and ethylene propylene diene monomer (EPDM) foam for the entrapment of copper (II) 2,4-pentanedionate (Cu II particles) under sound waves of different decibels (dB) and frequencies. Both PMMA and EPDM are known piezoelectric materials with piezoelectric coefficients (d_{33}) of 0.276 pC/N and 1.658 pC/N, respectively. The chosen sound frequencies and decibels are within the range of highway noise levels. Cu II particles are significantly larger and heavier than typical PM 2.5 particles; this allowed us to establish the baseline for the entrapment of most of the airborne particles in terms of size and weight. If a piezoelectric material vibrates in response to highway noise, depending upon the level of vibration, surface charges can be generated that are proportional to the level of noise (in decibels). Most of the airborne particles are surface-charged under various conditions [54–56]. The surface-charged piezoelectric material can therefore electrostatically entrap the airborne particles, including various harmful airborne pollutants, emitted from traffic, such as PM 2.5.

2. Experimental Details

We chose polymethyl methacrylate (PMMA) for the initial particle entrapment. PMMA is a type of piezoelectric material that can convert mechanical energy to electricity (and vice versa) [57]. PMMA is strong, tough, transparent, lightweight, and inexpensive. The density of PMMA is 1.20 g/cm³, which is less than half that of glass, but with much higher impact strength. PMMA is inherently UV-resistant due to its molecular stability. In this study, we used a commercial transparent PMMA sheet with a thickness of 0.15 mm as the piezoelectric material to test the surface charge generated at different sound levels and frequencies.

Figure 1 shows the experimental set-up to generate surface charge on PMMA surfaces by a vibration motor (VM). The measurement path is also included in this figure. Commercial DC 3.0V Micro Coin Vibration Motor (VM) was used in this experiment, which can provide a vibration force of 0.6 g @100 g, drawing less than 80 mA. A DC power supply (HEWLETT PACKARD, E3612A, 60 V, 0.5 A or 120 V, 0.25 A) was used to drive the VM at various voltages (1 V, 2 V, 3 V, 4 V, and 5 V), and corresponding vibrations were recorded by an accelerometer (cell-phone software, VibSensor, was used to measure the acceleration). As shown in Figure 1, five PMMA sheets of 2.54 × 2.54 cm² were stacked in parallel and fixed tightly with adhesive tapes at four edges. Before each measurement, the mass of the clean sample (five layers of PMMA sheets) was weighed. The sample was laid horizontally on the VM (Figure 1). The DC power supply was turned on by increasing the

power-supply input voltage to a constant value at 1 V, 2 V, 3 V, 4 V, and 5 V. The voltage generated by piezoelectric material across the two outer PMMA surfaces was measured by closely attaching two parallel copper tape plates on both sides of the sample, as electrodes that were connected to the Keithley 2400.

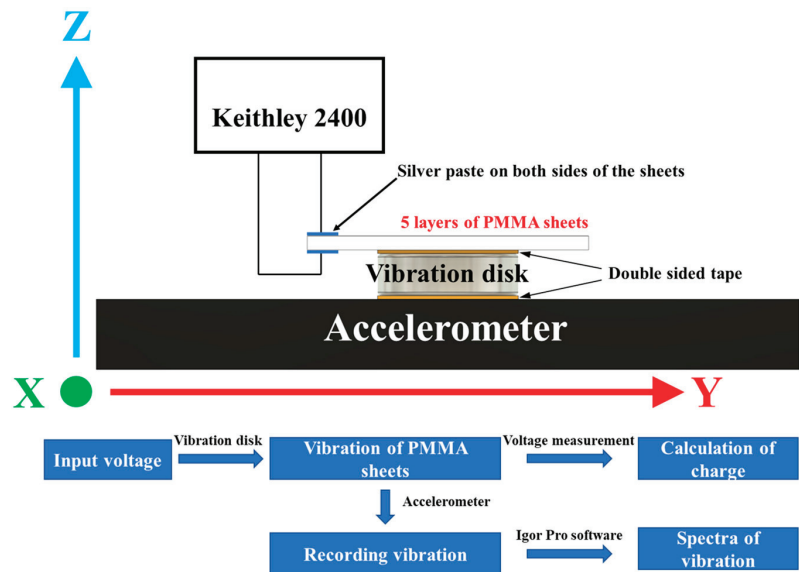


Figure 1. Experiment setup for measuring surface charge and trapped Cu II particles on PMMA.

To simulate the airborne particles, we selected copper (II)-2,4 pentanedionate powder (Cu II powder) for the entrapment experiments. Copper II is used as a catalyst for carbene transfer reactions, coupling reactions, and Michael addition reactions. It is also used as a catalyst for polymerization of olefins and transesterification reactions, as well as a PVC stabilizer. Cu II has a molecular weight of 261.76, which is extremely light, and it is easily absorbed by surface charges created by piezoelectric materials under slight vibrations. The scanning electron microscopy of Cu II particles is shown in Figure 2. As shown in this figure, the Cu II particles exhibit column-like structures, with high aspect ratios. The maximum length of the long axes of the particles was $>10\ \mu\text{m}$. To capture particles of this size, substantial surface charge needed to be induced by the strong piezoelectric effect of the materials. Experiments based on the Cu II powder ensure effective absorption of airborne PM 2.5 particles, which are much smaller and lighter.

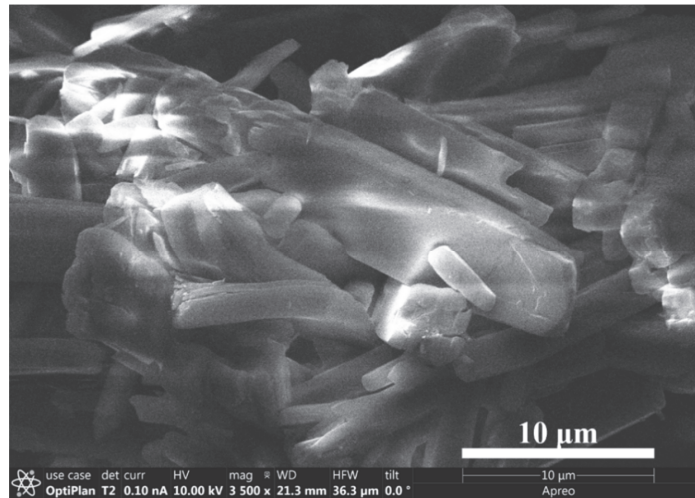


Figure 2. Scanning electron microscopy of the Cu II particles.

3. Results

The PMMA sheets were placed in the set-up, as shown in Figure 1, and the VM was turned on to generate the vibration, whose magnitude was represented by maximum acceleration (m/s^2) at a given voltage (1–5 V). Figure 3 shows the maximum acceleration of the vibration generated by the VM at different voltages: 1 V, 2 V, 3 V, 4 V, and 5 V. As shown in Figure 3a,b, the maximum acceleration of the vibration was rather low; it was below 0.1 m/s^2 when the applied voltage of the vibration motor was 1 V (0.037 m/s^2) and 2 V (0.051 m/s^2). The maximum acceleration of vibration increased to 0.36 m/s^2 at 3 V (Figure 3c), to 0.45 m/s^2 at 4 V (Figure 3d), and to 0.48 m/s^2 at 5 V (Figure 3e), respectively. It should be noted that there was a sharp peak around 14 s at 4 V (Figure 3d), which was disregarded as an anomaly from the background, since it was not sustained enough to affect the particle entrapment.

Figure 4 shows the maximum acceleration vs. the input voltage (Figure 4a), the voltage generated on the PMMA surface vs. the maximum acceleration (Figure 4b), the charge generated on the PMMA surface vs. the maximum acceleration (Figure 4c), and the mass of the trapped Cu II powder on the PMMA surface vs. the voltage. The inset presents a schematic of the Cu II powder attracted on the vertical PMMA surfaces. As shown in Figure 4a, the vibration energy, as indicated by the maximum acceleration, was controlled well by the applied voltage, which could be used to scale with the highway noise level. Due to the piezoelectricity, the vibration induced surface voltage on the PMMA surfaces, as shown in Figure 4b. This figure also shows that the surface voltage induced by the vibration remained quite low, below 10 mV, at the maximum acceleration of the vibration of 0.36 m/s^2 , which appeared to be a threshold value beyond which the induced voltage rapidly increased, up to 981 mV (Figure 4b). The related surface charge as a function of the maximum acceleration of the vibration is shown in Figure 4c. It was calculated based on the surface voltage, $Q = CV$, where Q is the surface charge, C is the capacitance, and V is the voltage. The capacitance is given by $C = k\epsilon_0 A/d$, where k is the dielectric constant of PMMA, ϵ_0 is the permittivity of the vacuum, A is the surface area of the PMMA (two outer surfaces), and d is the total thickness of the PMMA. The charge generated by the PMMA sheets was $4.1 \times 10^{-18} \text{ C}$, $9.2 \times 10^{-18} \text{ C}$, $9.2 \times 10^{-17} \text{ C}$, $1.56 \times 10^{-16} \text{ C}$, and $3.36 \times 10^{-16} \text{ C}$ for 1 V, 2 V, 3 V, 4 V, and 5 V, respectively, as shown in Figure 4c.

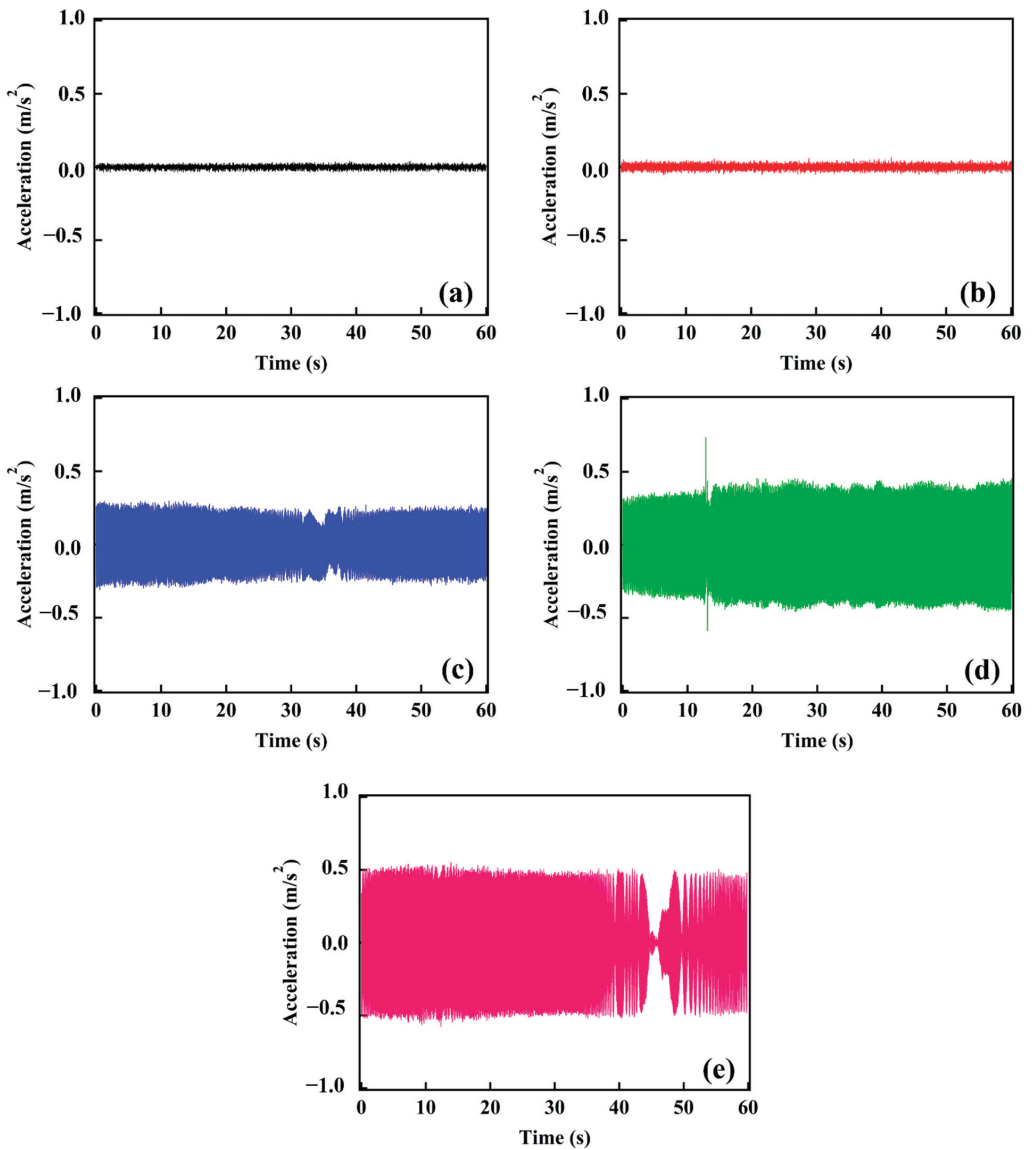


Figure 3. Acceleration of vibration generated by different voltages: (a) 1 V, (b) 2 V, (c) 3 V, (d) 4 V, and (e) 5 V.

The PMMA sheets were placed in the set-up, as shown in Figure 1 and the VM was turned on for 30 s to generate the surface charge at a given voltage (Figure 4b). The VM power supply was then turned off (after 30 s), and the Cu II powder was loosely sprinkled on both surfaces of the PMMA sheets. These PMMA sheets were then positioned vertically to observe the adhered powder on both sides due to the surface charge (inset of Figure 4d). The PMMA sheets with the electrostatically captured powder were weighted using Cole-Parmer Symmetry LA-225.C Analytical Balance to account for the Cu II particles that remained on the two outer surfaces (Figure 4d). As shown in Figure 4d, the mass of the

Cu II powder adhered on the PMMA surfaces increased with the input voltage of the VM, reaching 60 mg, at 5 V.

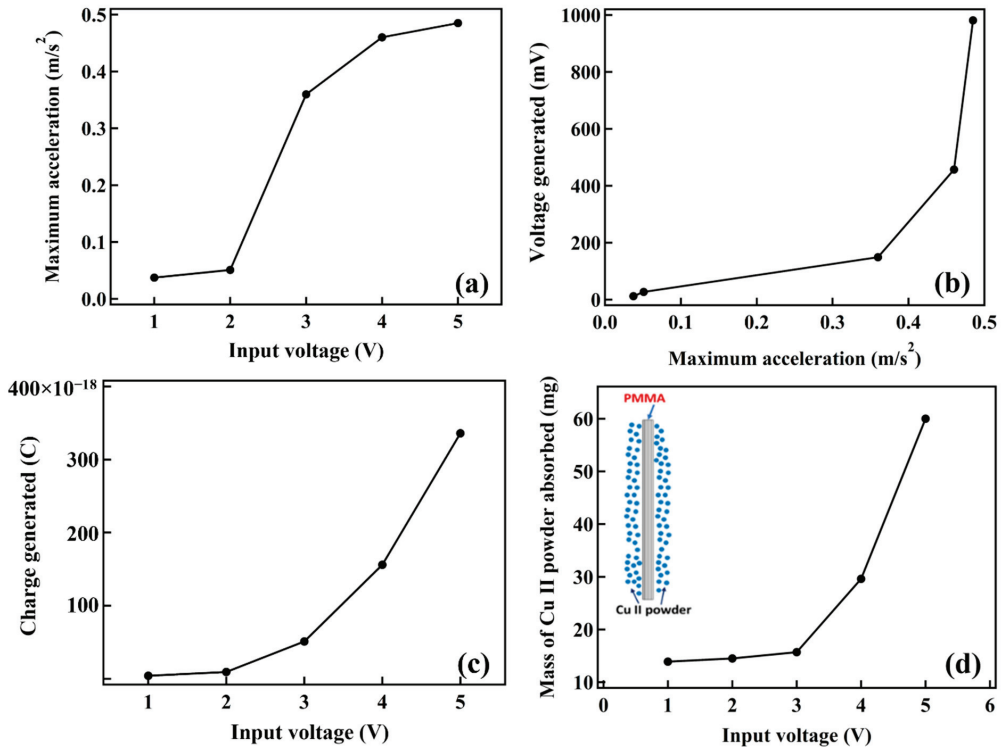


Figure 4. (a) Maximum acceleration generated by different input voltages, (b) voltage generated vs. maximum acceleration of different voltages, (c) charge generated vs. maximum acceleration of different voltages, (d) mass of trapped Cu II powder vs. voltage. Inset: Schematic of Cu II powder adhered on the vertical PMMA surfaces.

Figure 5 shows the photographs of the PMMA sheets with the surface-trapped Cu II powder at different VM input voltages, as indicated. As can be seen in this figure, at low vibration (maximum acceleration), the particles adhered on the surfaces were limited (1–3 V), but at 5 V, a substantial amount of Cu II powder was entrapped on both the outer surfaces of the PMMA sheets, indicating the strong electrical voltages/charges generated by the piezoelectric effect of the PMMA.

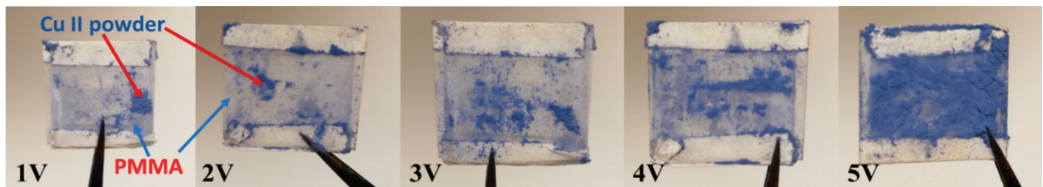


Figure 5. Photographs showing adhered Cu II powder on the PMMA surfaces at different input voltages.

Figure 5 shows the significant electric field on the PMMA surfaces generated by a vibrating motor. However, to entrap the airborne particles via traffic noise, the surface charge on the PMMA surfaces had to be generated directly from sound waves with decibels and frequencies comparable to those of a highway. Levels of highway traffic noise typically range from 70 to 80 dB(A) 15 m from highways. Depending upon the size of the vehicles, the highway-noise spectral content is typically dominated by frequencies from 500 to 1000 Hz.

To simulate a more realistic situation for noise-generated surface charge via a piezoelectric material, an experiment was set up for particle capture, as shown in Figure 6, along with the measurement path. A loudspeaker was used to simulate a background noise in a wide range of frequencies and sound pressure levels (SPL). The required frequencies (700–1300 Hz) were generated by a sound-frequency online tone generator. A JBL Cinema 510 5.1 Home Theater Speaker System with a subwoofer (sound source) was connected to a Yamaha 5.1 Channel 4K Ultra HD A/V home-theater receiver. The sound generated was measured and analyzed by cell-phone software called Sound Spectrum Analysis.

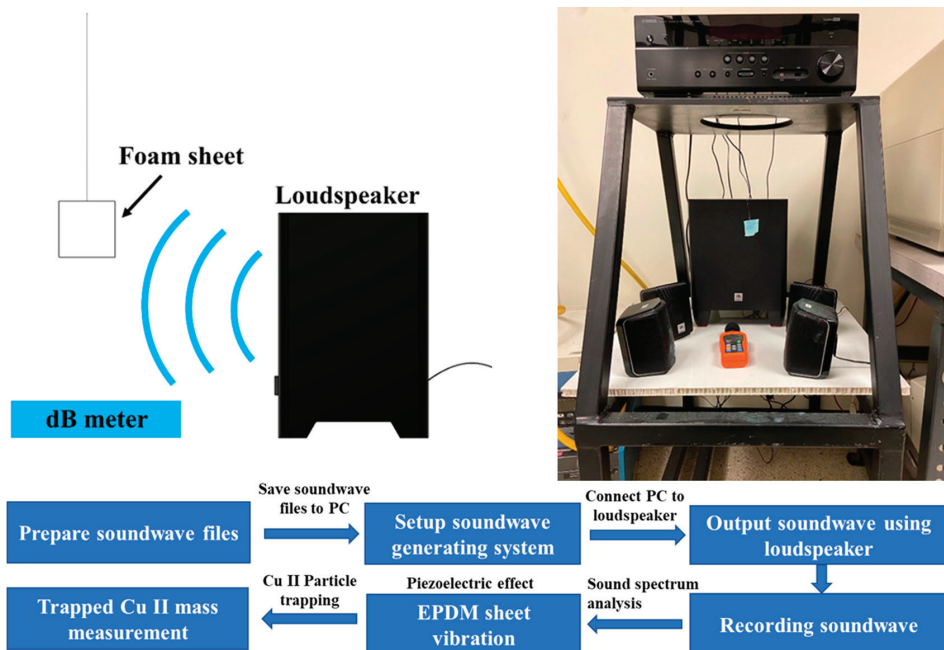


Figure 6. Schematic of experimental set-up for generating sound waves and measurement of particle trapping on EPDM.

For capturing the airborne particles, instead of the PMMA sheets used in the VM vibration experiments, we employed ethylene propylene diene monomer (EPDM) rubber-foam sheets. Ethylene-propylene diene monomer (EPDM) rubber is an excellent sound-absorbing material due to the long-chain structure of the polymer [58]. EPDM also exhibits excellent thermal, mechanical, and electrical properties for a variety of engineering applications [59–62]. EPDM foam has a porous structure that is ideal for the entrapment of airborne particles. Its elastic characteristic enable the efficient absorption of sound waves and conversion to electrical charge on the surfaces.

The EPDM foam sheet was suspended in midair (Figure 6). A Sound Monitor dB Meter (VLIKE LCD Digital Audio Decibel Meter) was positioned adjacent to the EPDM foam sheet that registered the SPL from the sound sources. The distance and the sound

meter between the EPDM foam sheet and the loudspeaker were kept at 25 cm. The speaker was turned on for 30 s at a given SPL and frequency, during which the EPDM foam sheet was vibrated by the sound wave. The speaker was then turned off after 30 s, followed by sprinkling the Cu II powder loosely on both surfaces of the EPDM foam sheet, which was positioned vertically (Figure 6). The EPDM foam sheet with the electrostatically captured Cu II powder was weighed to account for the Cu II particles that remained on the EPDM foam-sheet surfaces (on both sides). The mass of the Cu II particles captured by the EPDM foam sheet was determined under SPL of 30, 40, 50, 60, and 70 dB (referring to sound power intensities of 1, 10, 100, 1000, and 10,000 nW/m², respectively.) At a given SPL, the mass of the captured powder was also determined at various frequencies (700, 800, 900, 1000, 1100, 1200, and 1300 Hz).

Figure 7a shows the mass of the trapped Cu II particles as a function of the SPL at all frequencies (700–1300 Hz). At 900 and 1000 Hz, the amounts of the trapped Cu II particles were the highest, approaching 800 mg, much higher than those recorded using the vibrating motor (VM), as shown in Figure 4d. It was noted that the highway-noise frequency was around 1000 Hz, which was the optimum range tested in this experiment. Figure 7b shows the masses of the Cu II particles trapped as a function of frequency for different levels of SPL. Quite consistently, in a wide frequency range, between 700 Hz and 1300 Hz, the masses of the trapped Cu II particles were highest at 70dB. These relationships (Figure 7) show the pronounced piezoelectric effect of the EPDM foam sheets, indicating an ideal material candidate for making sound-absorbing and airborne particle-trapping filters for highways. Figure 8 shows the photographs of the EPDM foam sheet with the surface-entrapped Cu II particles (blue color) at different SPL. As shown in this figure, consistent with Figure 7a,b, the amount of Cu II particles increased with increasing SPL, as expected.

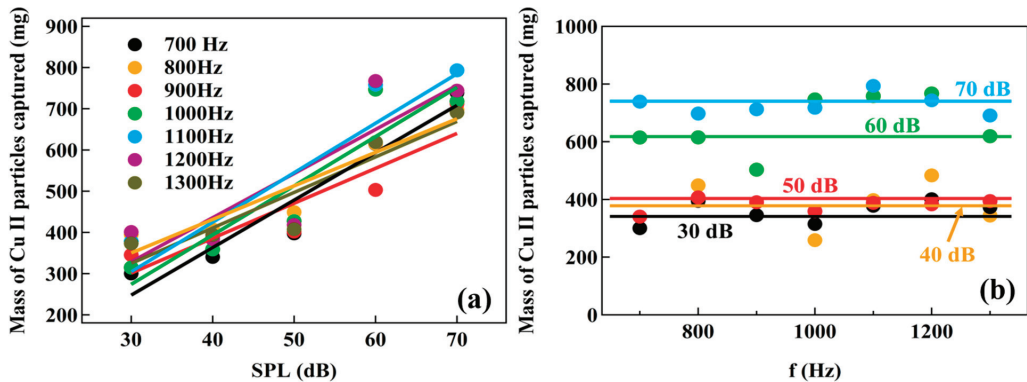


Figure 7. (a) Mass of captured Cu II particle vs. SPL of different frequencies, (b) mass of captured Cu II particle vs. frequency of different SPL.

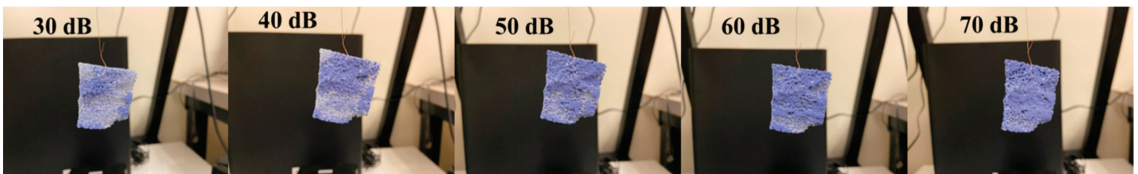


Figure 8. Cu II particles entrapped on the EPDM foam sheet after sound vibration under different SPL (the black box in the background is the loudspeaker).

4. Discussion

There have been extensive studies on airborne-particle captures using various methods. One option to improve the efficiency of mechanical filters is to add electrical charges to the filter material. Examples of these are electret or triboelectric filters. These filters have shown some efficient particle-trapping results, but their efficiency varies with the particle size. Electret filters have been widely used for the filtration of air particles. Since most airborne particles are electrically charged, the capturing mechanism has been typically based on electrostatic interaction. Romay, Liu, and Chae reported on commercially available fibrous electret filters: corona-charged fibrillated split-fiber media, triboelectrically charged mixed-fiber media, and corona-charged melt-blown media [63]. They measured the filtration efficiencies of these filters for different particle sizes and charge states.

Han developed a triboelectric filter for removing PM 2.5 from automobile exhaust fumes using the triboelectrification effect [64,65]. They found that the friction between PTFE (Polytetrafluoroethylene) pellets and electrodes can generate large triboelectric charges and form a space electric field as high as 12 MV/m. By controlling the vibration frequency and fill ratio of the pellets, over 94% of airborne PM 2.5 can be removed using the high electric field in the triboelectric filter. However, the triboelectric filter requires the mounting of the filter in the automobile exhaust system for sufficient mechanical vibrations. The system shown in this study can enable the harvesting of highway noise directly and with much greater sensitivity, making it much simpler, more effective, and more economically viable. In addition, the Cu II power particles are much heavier and larger than the PM 2.5 particles, showing strong electrostatic attraction force on the piezoelectric surfaces.

One of the critical issues in this proof-of-concept study was whether sufficient electrical charge can be generated to create strong enough electrostatic attraction to entrap the Cu II powders and other airborne particles. Although PMMA is a well-known piezoelectric material, the determination of the level of vibration required to generate sufficient surface charge (or voltage) was the first experimental step to be carried out. As shown in Figure 4, even with the small acceleration of vibration, appreciable surface voltages were induced, with a maximum approaching 1000 mV. Within the range of the surface voltage generated, a substantial amount of Cu II particles was captured by the PMMA up to 60 mg, which is quite significant. This correlation between the mechanical vibration/surface charge and the amount of Cu II particles on the PMMA established the baseline and feasibility of airborne entrapment via piezoelectric.

To simulate highway noise, a loudspeaker was employed to generate soundwaves instead of direct mechanical vibration. Sound is typically characterized in terms of two main properties: frequency and sound-pressure levels. For highway traffic, cars produce noise in the range of 50 to 5000 Hz, while trucks produce noise in the range of 10 to 1000 Hz. In both cases, the typical noise distribution has a broad intensity peak at about 1250 Hz and a broad perceptual peak at about 500 Hz [29]. The simulated sound waves used in this study were within the ranges of the highway noise levels (SPL: 30–70 dB, 1 nW/m^2 , frequency: 700–1300 Hz). Successfully, even at the low-noise end of 30 dB in a wide frequency range of 700–1300 Hz, a substantial amount of Cu II powder above 300 mg was captured by the EPDM foam sheet (Figure 7a). The amount of Cu II powder linearly increased with the SPL, up to 800 mg, which is not dependent on frequency (Figure 7b). These experimental results show solid evidence of particle entrapment via sound-generated electrostatic charges using piezoelectric materials. It should be noted that nanoscale piezoelectric materials can be designed and developed with even more airborne particle entrapment.

Another application EPDM foam sheets is to absorb the highway noise in the propagation path from the source to the receiver while harvesting the sound energy for airborne-particle entrapment. EPDM is an excellent soundproofing barrier, especially when it is used on highway edges with high levels of noise. Therefore, EPDM may serve for two purposes: (1) as a sound-insulation barrier to reduce noise pollution, and (2) harvesting noise energy for the entrapment of airborne particles. The Environmental Impact Assessment and Noise Impact Assessment determined different types of noise barrier, such as reflective noise

barriers, absorptive noise barriers, or a combination of both [29]. Improving the acoustic performance of vertical barriers without increasing their height has long been a challenge for acoustic engineers. The pure reflective types, even with optimal morphological designs and parametric analysis, are still not able to resolve this challenge. The system designed in this study could potentially reduce noise levels by engineering the design of acoustic walls with piezoelectric sound absorbers, such as EPDM foam sheets. However, the design of this study is fundamentally different from those of traditional sound barriers, which simply block or reflect highway noise. The EPDM can be utilized to absorb the highway noise and convert the soundwave energy into surface charge via piezoelectricity for the more efficient entrapment of airborne particles of various weights and sizes, including PM 2.5. In this way, the wasted sound energy can be harvested for both noise and airborne-particle reduction.

5. Conclusions

In conclusion, we demonstrated the effective entrapment of Cu II particles by both PMMA and EPDM via the piezoelectric effect. Significant surface charge was generated via mechanical vibrations that enabled the capture of Cu II particles on the PMMA surfaces. The EPDM foam sheets were capable of entrapping Cu II particles effectively in the wide highway-noise ranges of SPL (30–70 dB), sound intensity ($1\text{--}10^4$ nW/m²), and frequency (700–1300 Hz). The experimental outcomes obtained from this study provide the possibility of reducing highway airborne particles via simple piezoelectric materials. Novel nanoscale structures of piezoelectric materials can also be designed and developed for more efficient airborne-particle entrapment based on the physical principles developed in this study.

Author Contributions: Conceptualization, D.S.; Data curation, M.L. and S.V.T.; Formal analysis, D.S., M.L., S.V.T., H.W., J.W., T.A.R. and P.H.R.; Methodology, D.S., M.L. and S.V.T. All authors have read and agreed to the published version of the manuscript.

Funding: This research was funded by the University of Cincinnati CRA Track 1: PILOTS (Fund Number: D700315).

Institutional Review Board Statement: Not applicable.

Informed Consent Statement: Not applicable.

Data Availability Statement: Data available in a publicly accessible repository.

Conflicts of Interest: The authors declare no conflict of interest.

References

- Meier, R.; Cascio, W.E.; Ghio, A.J.; Wild, P.; Danuser, B.; Riediker, M. Associations of short-term particle and noise exposures with markers of cardiovascular and respiratory health among highway maintenance workers. *Environ. Health Perspect.* **2014**, *122*, 726–732. [CrossRef] [PubMed]
- Hammer, M.S.; Swinburn, T.K.; Neitzel, R.L. Environmental noise pollution in the US: Developing an effective public health response. *Environ. Health Perspect.* **2014**, *122*, 115–119. [CrossRef] [PubMed]
- Van Kamp, I.; Babisch, W.; Brown, A.L. Environmental noise and health. In *The Praeger Handbook of Environmental Health*; Friis, R.H., Ed.; ABC-CLIO: Santa Barbara, CA, USA, 2012; Volume 1, pp. 69–93, ISBN 978-0-313-38601-5.
- Babisch, W.; Dutilleul, G.; Paviotti, M.; Backman, A.; Gergely, B.; McManus, B. *Good Practice Guide on Noise Exposure and Potential Health Effects*; EEA Technical report; European Environmental Agency: Copenhagen, Denmark, 2010; Volume 11.
- Orban, E.; McDonald, D.; Sutcliffe, R.; Hoffman, B.; Fuks, K.B.; Dragono, N.; Viehmann, A.; Erbel, R.; Jöckel, K.H.; Pundt, N.; et al. Residential road traffic noise and high depressive symptoms after five years of follow-up. *Environ. Health Perspect.* **2016**, *124*, 578–585. [CrossRef]
- Sygná, K.; Aasvang, G.M.; Aamodt, G.; Oftedal, B.; Krog, N.H. Road traffic noise, sleep and mental health. *Environ. Res.* **2014**, *131*, 17–24. [CrossRef] [PubMed]
- Evandt, J.; Oftedal, B.; Hjertager Krog, N.; Nafstad, P.; Schwarze, P.E.; Marit Aasvang, G. A population-based study on nighttime road traffic noise and insomnia. *Sleep* **2017**, *40*, zsw055. [CrossRef] [PubMed]
- Meyer, P.; Yoon, P.W.; Kaufmann, R.B. Introduction: CDC Health Disparities and Inequalities Report—United States. *MMWR Supplements* **2013**, *62*, 3–5.
- Duhme, H.; Weiland, S.K.; Keil, U. Epidemiological analyses of the relationship between environmental pollution and asthma. *Toxicol. Lett.* **1998**, *102*, 307–316. [CrossRef]

10. Hu, S.; McDonald, R.; Martuzevicius, D.; Biswas, P.; Grinshpun, S.A.; Kelley, A.; Reponen, T.; Lockey, J.; LeMasters, G. UNMIX modeling of ambient PM 2.5 near an interstate highway in Cincinnati, OH, USA. *Atmos. Environ.* **2006**, *40*, 378–395. [[CrossRef](#)]
11. Martuzevicius, D.; Grinshpun, S.A.; Lee, T.; Hu, S.; Biswas, P.; Reponen, T.; LeMasters, G. Traffic-related PM 2.5 aerosol in residential houses located near major highways: Indoor versus outdoor concentrations. *Atmos. Environ.* **2008**, *42*, 6575–6585. [[CrossRef](#)]
12. Brunekreef, B.; Holgate, S.T. Air pollution and health. *Lancet* **2002**, *360*, 1233–1242. [[CrossRef](#)]
13. Baldauf, R.W.; Isakov, V.; Deshmukh, P.; Venkatram, A.; Yang, B.; Zhang, K.M. Influence of solid noise barriers on near-road and on-road air quality. *Atmos. Environ.* **2016**, *129*, 265–276. [[CrossRef](#)]
14. Finn, D.; Clawson, K.L.; Carter, R.G.; Rich, J.D.; Eckman, R.M.; Perry, S.G.; Isakov, V.; Heist, D.K. Tracer studies to characterize the effects of roadside noise barriers on near-road pollutant dispersion under varying atmospheric stability conditions. *Atmos. Environ.* **2010**, *44*, 204–214. [[CrossRef](#)]
15. NAAQS Table. Available online: <https://www.epa.gov/criteria-air-pollutants/naaqs-table> (accessed on 16 July 2021).
16. United States Environmental Protection Agency. *Transportation Conformity Guidance for Quantitative Hot-Spot Analyses in PM 2.5 and PM10 Nonattainment and Maintenance Areas*; United States Environmental Protection Agency: Washington, DC, USA, 2010.
17. Ryan, P.H.; LeMasters, G.K.; Biswas, P.; Levin, L.; Hu, S.; Lindsey, M.; Bernstein, D.I.; Lockey, J.; Villareal, M.; Khurana Hershey, G.K.; et al. A comparison of proximity and land use regression traffic exposure models and wheezing in infants. *Environ. Health Perspect.* **2007**, *115*, 278–284. [[CrossRef](#)] [[PubMed](#)]
18. Brunekreef, B.; Janssen, N.A.; de Hartog, J.; Harssema, H.; Knape, M.; van Vliet, P. Air pollution from truck traffic and lung function in children living near motorways. *Epidemiology* **1997**, *8*, 298–303. [[CrossRef](#)]
19. Heinrich, J. Influence of indoor factors in dwellings on the development of childhood asthma. *Int. J. Hyg. Environ. Health.* **2011**, *214*, 1–25. [[CrossRef](#)]
20. Health Effects Institute. Panel on the Health Effects of Traffic-Related Air Pollution. In *Traffic-Related Air Pollution: A Critical Review of the Literature on Emissions, Exposure, and Health Effects*; Special Report 17; Health Effects Institute: Cambridge, MA, USA, 2010.
21. Salvi, A.; Salim, S. Neurobehavioral consequences of traffic-related air pollution. *Front. Neurosci.* **2019**, *13*, 1232. [[CrossRef](#)]
22. Gauderman, W.J.; Avol, E.; Gilliland, F.; Vora, H.; Thomas, D.; Berhane, K.; McConnell, R.; Kuenzli, N.; Lurmann, F.; Rappaport, E.; et al. The Effect of Air Pollution on Lung Development from 10 to 18 Years of Age. *N. Engl. J. Med.* **2004**, *351*, 1057–1067. [[CrossRef](#)]
23. McConnell, R.; Berhane, K.; Yao, L.; Jerrett, M.; Lurmann, F.; Gilliland, F.; Kuenzli, N.; Gauderman, J.; Avol, E.D.; Thomas, D.; et al. Traffic, susceptibility, and childhood asthma. *Environ. Health Perspect.* **2006**, *114*, 766–772. [[CrossRef](#)]
24. Ryan, P.H.; LeMasters, G.K.; Levin, L.; Burkle, J.; Biswas, P.; Hu, S.; Grinshpun, S.; Reponen, T. A land-use regression model for estimating microenvironmental diesel exposure given multiple addresses from birth through childhood. *Sci. Total Environ.* **2008**, *404*, 139–147. [[CrossRef](#)]
25. Wu, X.; Nethery, R.C.; Sabath, M.B.; Braun, D.; Dominici, F. Air pollution and COVID-19 mortality in the United States: Strengths and limitations of an ecological regression analysis. *Sci. Adv.* **2020**, *6*, eabd4049. [[CrossRef](#)]
26. Tian, T.; Zhang, J.; Hu, L.; Jiang, Y.; Duan, C.; Li, Z.; Wang, X.; Zhang, H. Risk factors associated with mortality of COVID-19 in 3125 counties of the United States. *Infect. Dis. Poverty* **2021**, *10*, 3. [[CrossRef](#)] [[PubMed](#)]
27. Conticini, E.; Frediani, B.; Caro, D. Can atmospheric pollution be considered a co-factor in extremely high level of SARS-CoV-2 lethality in Northern Italy? *Environ. Pollut.* **2020**, *261*, 114465. [[CrossRef](#)] [[PubMed](#)]
28. Travaglio, M.; Yu, Y.; Popovic, R.; Selley, L.; Leal, N.S.; Martins, L.M. Links between air pollution and COVID-19 in England. *Environ. Pollut.* **2021**, *268*, 115859. [[CrossRef](#)] [[PubMed](#)]
29. Donovan, P.R.; Janello, C.J. *Mapping Heavy Vehicle Noise Source Heights for Highway Noise Analysis*; No. Project 25-45; Transportation Research Board: Washington, DC, USA, 2017. [[CrossRef](#)]
30. Van Renterghem, T.; Botteldooren, D.; Verheyen, K. Road traffic noise shielding by vegetation belts of limited depth. *J. Sound Vib.* **2012**, *331*, 2404–2425. [[CrossRef](#)]
31. Lacasta, A.M.; Penaranda, A.; Cantalapiedra, I.R.; Auguet, C.; Bures, S.; Urrestarazu, M. Acoustic evaluation of modular greenery noise barriers. *Urban For. Urban Green.* **2016**, *20*, 172–179. [[CrossRef](#)]
32. Monazzam, M.R.; Fard, S.M.B. Impacts of Different Median Barrier Shapes on a Roadside Environmental Noise Screen. *Environ. Eng. Sci.* **2011**, *28*, 435–441. [[CrossRef](#)]
33. Cianfrini, C.; Corcione, M.; Fontana, L. Experimental verification of the acoustic performance of diffusive roadside noise barriers. *Appl. Acoust.* **2007**, *68*, 1357–1372. [[CrossRef](#)]
34. Oldham, D.J.; Egan, C.A. A parametric investigation of the performance of T-profiled highway noise barriers and the identification of a potential predictive approach. *Appl. Acoust.* **2011**, *72*, 803–813. [[CrossRef](#)]
35. Karimi, M.; Younesian, D. Optimized T-Shape and Y-Shape Inclined Sound Barriers for Railway Noise Mitigation. *J. Low Freq. Noise Vib. Act. Control* **2014**, *33*, 357–370. [[CrossRef](#)]
36. England Health Agent. *The Design Manual for Roads and Bridges*; England Health Agent: London, UK, 2015.
37. Berglund, B.; Hassmén, P.; Job, R. Sources and effects of low-frequency noise. *J. Acoust. Soc. Am.* **1996**, *99*, 2985–3002. [[CrossRef](#)]
38. Twardella, D.; Ndrepepa, A. Relationship between noise annoyance from road traffic noise and cardiovascular diseases: A meta-analysis. *Noise Health* **2011**, *13*, 251. [[CrossRef](#)]

39. Leventhall, H.G. Low frequency noise and annoyance. *Noise Health* **2004**, *6*, 59–72. [[PubMed](#)]
40. Auerbach, M.; Bockstedte, A.; Zaleski, O.; Von Estorff, O. Numerical and experimental investigations of noise barriers with Helmholtz resonators. In Proceedings of the NOISE-CON 2010, Baltimore, MD, USA, 19–21 April 2010.
41. Chintapalli, V.S.N.R.; Padmanabhan, C. An experimental investigation of cavity noise control using mistuned Helmholtz resonators. In *INTER-NOISE and NOISE-CON Congress and Conference Proceedings*; Institute of Noise Control Engineering: Washington, DC, USA, 2014; Volume 249, pp. 1413–1418.
42. Yang, C.; Pan, J.; Cheng, L. A mechanism study of sound wave-trapping barriers. *J. Acoust. Soc. Am.* **2013**, *134*, 1960–1969. [[CrossRef](#)] [[PubMed](#)]
43. Bowker, G.E.; Baldauf, R.; Isakov, V.; Khlystov, A.; Petersen, W. The effects of roadside structures on the transport and dispersion of ultrafine particles from highways. *Atmos. Environ.* **2007**, *41*, 8128–8139. [[CrossRef](#)]
44. Hagler, G.S.; Lin, M.Y.; Khlystov, A.; Baldauf, R.W.; Isakov, V.; Faircloth, J.; Jackson, L.E. Field investigation of roadside vegetative and structural barrier impact on near-road ultrafine particle concentrations under a variety of wind conditions. *Sci. Total Environ.* **2012**, *419*, 7–15. [[CrossRef](#)]
45. Janhäll, S. Review on urban vegetation and particle air pollution—Deposition and dispersion. *Atmos. Environ.* **2015**, *105*, 130–137. [[CrossRef](#)]
46. Amini, S.; Ahangar, F.E.; Schulte, N.; Venkatram, A. Using models to interpret the impact of roadside barriers on near-road air quality. *Atmos. Environ.* **2016**, *138*, 55–64. [[CrossRef](#)]
47. Baldauf, R.; Thoma, E.; Khlystov, A.; Isakov, V.; Bowker, G.; Long, T.; Snow, R. Impacts of noise barriers on near-road air quality. *Atmos. Environ.* **2008**, *42*, 7502–7507. [[CrossRef](#)]
48. Heist, D.K.; Perry, S.G.; Brixey, L.A. A wind tunnel study of the effect of roadway configurations on the dispersion of traffic-related pollution. *Atmos. Environ.* **2009**, *43*, 5101–5111. [[CrossRef](#)]
49. Steffens, J.T.; Heist, D.K.; Perry, S.G.; Zhang, K.M. Modeling the effects of a solid barrier on pollutant dispersion under various atmospheric stability conditions. *Atmos. Environ.* **2013**, *69*, 76–85. [[CrossRef](#)]
50. Lindman, J.K. Effect of a noise wall on snow accumulation and air quality. *Transp. Res. Rec.* **1985**, *1033*, 79–88.
51. Manbachi, A.; Cobbold, R.S.C. Development and Application of Piezoelectric Materials for Ultrasound Generation and Detection. *Ultrasound* **2011**, *19*, 187–196. [[CrossRef](#)]
52. Gautschi, G. *Piezoelectric Sensorics: Force, Strain, Pressure, Acceleration and Acoustic Emission Sensors, Materials and Amplifiers*; Springer Science & Business Media: Berlin, Germany, 2002; ISBN 978-3-662-04732-3.
53. Walubita, L.F.; Sohoulane Djebou, D.C.; Faruk, A.N.; Lee, S.I.; Dessouky, S.; Hu, X. Prospective of Societal and Environmental Benefits of Piezoelectric Technology in Road Energy Harvesting. *Sustainability* **2018**, *10*, 383. [[CrossRef](#)]
54. Jang, G.G.; Wiechert, A.I.; Ladshaw, A.P.; Spano, T.; McFarlane, J.; Myhre, K.; Yiacoumi, S.; Tsouris, C. Surface charge of environmental and radioactive airborne particle. *Atmos. Chem. Phys. Discuss.* **2021**, 1–14. [[CrossRef](#)]
55. Kim, Y.H.; Yiacoumi, S.; Tsouris, C. Surface charge accumulation of particles containing radionuclides in open air. *J. Environ. Radioact.* **2015**, *143*, 91–99. [[CrossRef](#)]
56. Zhang, L.; Gu, Z.; Yu, C.; Zhang, Y.; Cheng, Y. Surface charges on aerosol particles—Accelerating particle growth rate and atmospheric pollution. *Indoor Built Environ.* **2016**, *25*, 437–440. [[CrossRef](#)]
57. Rende, D.; Schadler, L.S.; Ozisik, R. Controlling Foam Morphology of Poly(methyl methacrylate) via Surface Chemistry and Concentration of Silica Nanoparticles and Supercritical Carbon Dioxide Process Parameters. *J. Chem.* **2013**, *2013*, 864926. [[CrossRef](#)]
58. Wang, K.; Yan, X. Performance analysis of ethylene-propylene diene monomer sound-absorbing materials based on image processing recognition. *EURASIP J. Image Video Process.* **2018**, *2018*, 128. [[CrossRef](#)]
59. Athawale, A.A.; Joshi, A.M. Electronic Applications of Ethylene Propylene Diene Monomer Rubber and Its Composites. In *Flexible and Stretchable Electronic Composites*; Ponnamma, D., Sadasivuni, K.K., Wan, C., Thomas, S., AIMa’adeed, M.A.A., Eds.; Springer: Coventry, UK, 2015; pp. 305–333, ISBN 978-3-319-23663-6.
60. Bizhani, H.; Katbab, A.A.; Lopez-Hernandez, E.; Miranda, J.M.; Lopez-Manchado, M.A.; Verdejo, R. Preparation and Characterization of Highly Elastic Foams with Enhanced Electromagnetic Wave Absorption Based On Ethylene-Propylene-Diene-Monomer Rubber Filled with Barium Titanate/Multiwall Carbon Nanotube Hybrid. *Polymers* **2020**, *12*, 2278. [[CrossRef](#)]
61. Dai, C.; Wu, J.; Zhou, G.; Miao, L.; Yin, Y. Effect of AC Electric Field on Space Charge Distribution in Ethylene Propylene Diene Monomer. In Proceedings of the 2019 IEEE Conference on Electrical Insulation and Dielectric Phenomena, Richland, WA, USA, 20–23 October 2019; pp. 450–453.
62. Noh, J.S. Conductive Elastomers for Stretchable Electronics, Sensors and Energy Harvesters. *Polymers* **2016**, *8*, 123. [[CrossRef](#)]
63. Romay, F.J.; Liu, B.Y.; Chae, S.J. Experimental Study of Electrostatic Capture Mechanisms in Commercial Electret Filters. *Aerosol Sci. Technol.* **1998**, *28*, 224–234. [[CrossRef](#)]
64. Han, C.B.; Jiang, T.; Zhang, C.; Li, X.; Zhang, C.; Cao, X.; Wang, Z.L. Removal of Particulate Matter Emissions from a Vehicle Using a Self-Powered Triboelectric Filter. *ACS Nano* **2015**, *9*, 12552–12561. [[CrossRef](#)] [[PubMed](#)]
65. Park, J.H.; Yoon, K.Y.; Noh, K.C.; Byeon, J.H.; Hwang, J. Removal of PM 2.5 entering through the ventilation duct in an automobile using a carbon fiber ionizer-assisted cabin air filter. *J. Aerosol Sci.* **2010**, *41*, 935–943. [[CrossRef](#)]



Project Report

Traffic Safety Improvement via Optimizing Light Environment in Highway Tunnels

Baofeng Su ¹, Jiangbi Hu ^{1,*}, Juncheng Zeng ² and Ronghua Wang ¹

¹ Faculty of Architecture, Civil and Transportation Engineering, Beijing University of Technology, Beijing 100124, China; bfi2087121@hotmail.com (B.S.); wangrh@bjut.edu.cn (R.W.)

² Fujian Expressway Science & Technology Innovation Research Institute Co., Ltd., Fuzhou 350001, China; ulzeng@126.com

* Correspondence: hujiangbi@bjut.edu.cn

Abstract: Driving in tunnel areas depends more heavily on light conditions than that on open roadways. Traditional lighting systems in highway tunnels adjust lighting parameters only caring about outside light luminance, and focus is usually on energy conservation; however, little concern is about drivers' actual physical and psychological needs. How to leverage the enormous research progress of traffic safety, light environment, human factors engineering, and modern lighting sources to create an ideal tunnel light environment that aids with ensuring driving safety and lower interference effects caused by the change of light environment will greatly improve safety level and reduce adverse influence on drivers' visual health in a tunnel area. An intelligent lighting control system designed with multiple influence factors are systematically considered. Based on sensor data from outside natural light conditions, target lighting parameters are determined per each lighting zone requires; then, lighting commands will be transferred and parsed by adaptive lighting controllers and modules, eventually LED lighting properties are altered step by step. This system helps a lot with optimizing tunnel lighting quality and improving drivers' visual performance; as a result, it contributes to lower the fluctuation of drivers' workload and get a smooth traffic flow, and ultimately this technically ensures physical and mental health of drivers in a tunnel area.

Keywords: light environment; tunnel lighting; visual health; traffic safety; intelligent control

Citation: Su, B.; Hu, J.; Zeng, J.; Wang, R. Traffic Safety Improvement via Optimizing Light Environment in Highway Tunnels. *Int. J. Environ. Res. Public Health* **2022**, *19*, 8517. <https://doi.org/10.3390/ijerph19148517>

Academic Editors: Francesco Nocera, Roberto Alonso González Lezcano and Rosa Giuseppina Caponetto

Received: 1 June 2022
Accepted: 28 June 2022
Published: 12 July 2022



Copyright: © 2022 by the authors. Licensee MDPI, Basel, Switzerland. This article is an open access article distributed under the terms and conditions of the Creative Commons Attribution (CC BY) license (<https://creativecommons.org/licenses/by/4.0/>).

1. Background

In recent years, highway tunnel construction is increasing on a global scale. As of 2020, China had 21,316 highway tunnels or 21.9993 million meters, and the scale and number rank first in the world [1]. Table 1 also shows that, from 2011 to 2020, the proportion of long and extra-long tunnels rose year by year from 17.6% and 3.8% to 26% and 6.5%, respectively, and annual growth rates of both types exceeded that of total tunnels.

While improving traffic efficiency, to some extent, tunnels are also possible bottleneck sections of highway network. 2019 annual statistical data of Traffic Management Bureau of Ministry of Public Security of China indicate that the number of casualties caused by tunnel accidents accounts for 0.32% of total casualties caused by road traffic accidents, and direct property loss is about 0.95% of total loss, although tunnel traffic accidents occupy only 0.23% of total count of road traffic accidents [2]. Meanwhile, because tunnel space is relatively closed and there are wide variances between tunnel area and open roadways, this leads to increasing traffic risks in the tunnel area, and tunnel traffic accidents are characterized by complex causes, short disaster time, inconvenient evacuation, and difficult rescue. Moreover, once such a traffic accident occurs, if protection measures are inappropriate, it is easy to cause second accidents resulting in aggravated chain reactions, such as rescue difficulty, economic loss, social impact, etc.

Table 1. Progress of tunnel construction in China (2011–2020).

	2011	2012	2013	2014	2015	2016	2017	2018	2019	2020
Total	8522	10,022	11,359	12,404	14,006	15,181	16,229	17,738	19,067	21,316
Long	1504	1944	2303	2623	3138	3520	3841	4315	4784	5541
Extra-long	326	441	562	626	744	815	902	1058	1175	1394

How to reduce frequency and extent of injury of tunnel traffic accidents has motivated a widespread concern because this directly affects whether tunnel construction and operation can really improve traffic efficiency. Road traffic accidents are caused by synergic effects of people, vehicle, road, and environment. As denoted in Figure 1, traffic accident causes are grouped into three major categories in America, driver related factors dominate, and reliability of drivers has a decisive influence on traffic safety [3]. During the driving process, the road environment greatly affects drivers’ cognition, decision-making and behavior, so road environment is a potentially important factor affecting traffic safety.

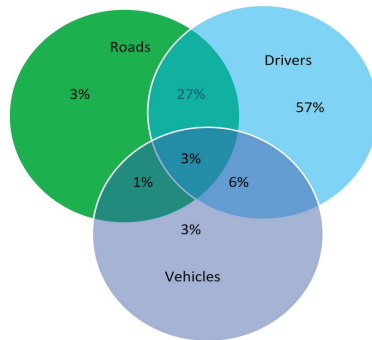


Figure 1. Causes of traffic accidents in America.

Studies show that the major source for drivers to sense road conditions is vision under normal driving conditions [4], and drivers rely on vision to cognize more than 80% of road traffic information in the surroundings [5]. Drivers’ visual condition is closely related to traffic safety. The optical environment in highway tunnels directly influences a lot on visual characteristics of drivers. Highway tunnel is a special road structure which makes internal space semi-isolated from the external environment with entrances or exits as the transition zone between different traffic environments. The inherent nature of tunnel structure makes it a very special road traffic environment, which is characterized by relatively narrow and almost closed space, clear distinction of lighting environment between inside and outside space, low luminance inside the tunnel, slow diffusion of smoke and dust, etc. Driving inside tunnels with bad lighting conditions for a long time will inevitably induce fear, irritability, depression, visual fatigue, and other adverse physiological and psychological reactions, which have a negative effect on driving safety and can easily cause traffic accidents. Research data show about 8% of skilled drivers and 14% of drivers first driving through the tunnel area feel depressed while driving inside [6].

In order to investigate the rationality of light environment of the tunnels in service of a certain province in China, the research team designed a questionnaire for drivers and conducted a large number of questionnaire surveys on the overall lighting conditions of more than 10 highway tunnels. Statistical results indicate that, for all drivers that participated in this survey, 41% feel that overall tunnel lighting conditions are rather dark and 14% feel lighting in the interior zone is too dark as Figure 2, 78% think exit and threshold zones are the most dangerous tunnel zones as Figure 3, and 61% consider 11:00 A.M. to 1:00 P.M. of daytime and nighttime are unsafe periods for tunnel driving as Figure 4.

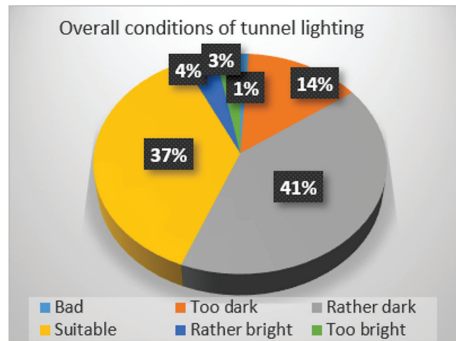


Figure 2. Overall conditions of tunnel lighting.

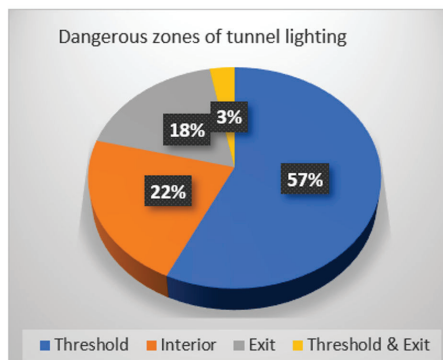


Figure 3. Dangerous zones of tunnel lighting.

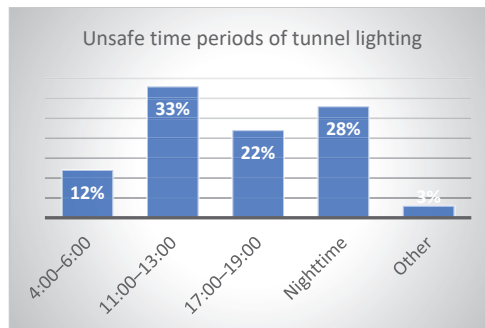


Figure 4. Unsafe time periods of tunnel lighting.

The above study shows that apparent discrepancies of lighting environment existing in entrance or exit and low luminance in interior zone are both major causes resulting in degradation of drivers' visual ability and cognition, eventually to trigger traffic accidents more frequently. However, it is uneconomical and technically unpractical to maintain exactly the same illumination level for the tunnel light environment as outside natural light.

Based on the above analysis of actual tunnel lighting problems, firstly this study is to sum up the theoretical bases, such as light environment theories of highway tunnel, safety and comfort requirements on driving vision in tunnel environment, characteristics and applications of tunnel light sources, and research achievements of tunnel lighting control systems. Then, this research will explore and design an innovative tunnel lighting control system which is able to meet drivers' vision and cognition demand, to operate

with low energy consumption, to make artificial and natural light sources friendly coupled, and eventually to create comfortable conditions to improve driving safety level in the tunnel area.

2. Traffic Safety and Light Environment in Highway Tunnels

2.1. Light Environment in Tunnels: Definition and Objective

Tunnel light environment is the dynamically changing environment which covers certain sections beyond tunnel entrances and exits, is created by multiple factors, such as natural light, artificial light, active or passive lighting signs and marks inside tunnels, light reduction anti-glare facilities, tunnel wall color or decoration and landscape facilities, etc., and is also synthetically affected by light source characteristics such as illuminance, color temperature, and color rendering with their coupling effects. Tunnel light environment is drivers centered, and various light environment characteristics in tunnel influence areas have different effects on drivers' vision and recognition. In order to smoothen the transition of running tunnel light environments, and then to ensure drivers' visual performance and driving comfort, it is necessary to divide tunnel lighting area into several zones according to variances of lighting requirements and drivers' demand in different tunnel locations; doing this will build a comfortable atmosphere for drivers to drive safely through tunnel area with appropriate speed and workload; this also enable drivers to timely obtain requisite information for driving safety in different lighting zones and prevent hidden dangers caused by insufficient visual information.

2.2. Necessity to Improve Tunnel Light Environment

Highway tunnel is a very special road traffic operation environment, which is often confronted with large difference between inside and outside tunnel light environment and low luminance level in the interior zone. The particularity of the tunnel environment requires a driver's higher level of driving skill than that on open roadways, but this is limited by the driver's ability threshold as a person in the dynamic process in which visual information synthesizing and decision-making are continuously taking place. Vision as a decisive factor of this process is affected by physiological function of human eyes and characteristics of external light source.

For different weather conditions and time periods, tunnel light environment varies a lot from natural light environment. When drivers experience the transition zone between natural and artificial light environment, severe light environment discrepancy will lead to white hole or black hole effects with drivers' vision then forming a blind vision period. Therefore, it is particularly necessary to set up reasonable and effective lighting conditions in threshold, exit, and interior zones to meet driving needs in different time periods.

On the other hand, although a variety of standards exist for traditional tunnel lighting, there is no mature and stable technology to detect and control artificial light sources, which brings out high cost on energy consumption. As a result, it is quite difficult to effectively describe and accurately obtain visual requirements for driving in a tunnel light environment, this makes it hard to cooperate with driving behaviors. In view of the mutability of natural light source, tunnel light environment must systematically take into account the requirements of drivers' visual perception, driving safety and comfort, and low energy consumption of artificial light sources.

In the meantime, energy saving should not be at the cost of a lowered safety level of tunnel operation. One widespread adopted method via turning off lights on one side will cause uneven brightness inside tunnels thus forming a Zebra effect, which is prone to causing visual fatigue of drivers. In addition, if locations and angles of lighting fixtures are not reasonably set up, once a glare phenomenon is induced, it will impact drivers' cognition, judgment and decision on vehicles or obstacles in front, thus bringing risks to driving safety.

In addition, how to monitor and control tunnel light environment, how to evaluate natural and artificial light environments, and what criteria and techniques to apply under

different working conditions are all challenging interdisciplinary issues worthy of in-depth study.

In a word, tunnel lighting is targeted to provide a safer, more comfortable and beautiful road environment for different drivers [7]. However, because of the inadequacy of analysis about drivers' physical and psychological requirements, together with insufficient synthesis on the influence factors of tunnel lighting quality, many tunnel lighting control systems in service fail to balance actual tunnel managements and driving demands, this imbalance will make it hard to meet drivers' visual comfort, psychological comfort, and convenience of tunnel maintenance simultaneously.

2.3. Existing Guidelines for Tunnel Lighting Design

Although there is no uniform tunnel lighting standard globally, International Commission on Illumination (CIE) and most countries adopt luminance based evaluation indexes and specifications; however, standard values are of great difference. Most Chinese tunnel lighting designs refer to luminance based technical specifications as developed countries do. Current Guidelines for Design of Lighting of Highway Tunnels [8] divides a tunnel lighting area into threshold zone, transition zone, interior zone, and exit zone, which are respectively managed with daytime and nighttime patterns. However, only a luminance reduction factor for threshold zone and luminance for other zones are used to evaluate tunnel lighting quality; these evaluation indexes are not adequate. There is no comprehensive analysis on the mechanism of drivers' visual needs in the tunnel environment, there is no research on the correlation of driving behavior characteristics with different lighting conditions made from different light sources; in addition, technological progress of modern lighting sources has not been objectively and scientifically adopted to monitor and control the lighting environment design, which should be enhanced to improve tunnel driving safety and comfort level.

3. Theory and Evaluation Indexes on Tunnel Lighting

CIE suggests tunnel lighting safety be judged by determining whether tested drivers could find target obstacles at a distance not less than a stopping sight distance (SSD) [9]. This method can directly reflect physiological and psychological reactions of drivers under various lighting conditions. If visibility impact could be ignored and drivers could find target obstacles in time outside the SSD while entering or leaving tunnels at specified speed, this light environment should be qualified to ensure driving safety.

As for the relationship of target obstacle and SSD, CIE proposed an evaluation method for tunnel lighting based on optical measurements, a gray cube with side length 20 cm and surface reflection coefficient 0.2 is recommended as the reference to evaluate SSD. Although actual obstacles may be of different size or shape, studies show that this recommended cube still applies to evaluate a variety of lighting environments [10].

3.1. Dynamic Visual Recognition Needs

The visual perception and judgment ability of drivers in dynamic driving are obviously different from that in stationary state. According to motor vision psychology, dynamic vision is about 10% to 40% lower than static vision [11]. During dynamic driving, visual observation ability degrades due to decreased visual acuity and narrowed field of vision, and visual cognition is significantly attenuated compared with that under static conditions. Therefore, it is hard to accurately percept and judge abnormal information outside vehicles, thus the risk of driving errors increases. In long tunnels, if mandatory measures could be taken to widen the narrowed field of vision for example changing tunnel landscape, this will prompt drivers to change the field of vision of the fixation point; then, frequency of traffic accidents will be reduced.

Cognitive speed and accuracy not only depend on physiological function of eyes and visual experiences accumulated by brains, but also relate closely to nature of lighting sources in the visual environment. Nature and level of ambient lighting impact drivers'

visual recognition obviously. Luminance enables drivers to sense the change of light and shade from visual environment. When an object is observed under different light source characteristics, seeing the dark from bright needs higher requirements than seeing the bright from dark, and luminance difference has a certain influence on visual recognition of human eyes. If road surface luminance can ensure a driver's visibility, it will also meet his visual requirements to cognize other information conditions.

Speed and reliability of visual recognition are also affected by brightness contrast or color difference between target and background. For low illumination, this speed is very slow. With the increase of illumination, this accelerates, but this speed does not change significantly when illumination exceeds 1000 lx.

Significant differences exist with drivers' awareness for daytime and nighttime; normally, night vision is about 1/2 of day vision; this is because the luminance of obstacles decreases when natural light dims rapidly, but drivers' dark adaptation has not fully built up, weakened contrast between obstacles and ambient background causes drivers' visual cognition dysfunction [12]. Consequently, night driving relies highly on artificial lighting.

3.2. Visual Safety and Comfort Theory

In tunnel entrance and exit area, excessive luminance difference will significantly prolong drivers' visual adaptation and cause short-term impairment of visual cognitive function, then resultant rise of psychological load will affect driving safety greatly.

Human eyes have different visual perception with various light source characteristics (color temperature, color rendering, light intensity, etc.). In the daytime, if artificial light in a threshold zone is close to natural light, drivers could adapt quickly and feel comfortable. At night, drivers have better adaptability to light sources with low color temperature and feel more comfortable. When foggy, light sources with low color temperature favor drivers to recognize tunnel entrances easily.

In the visible spectrum range, human eyes have different sensitivities to distinct light wavelengths. Tunnel lighting should not focus merely on physical light properties, but also a drivers' visual system response to light should be cared about, which is also called dynamic visual sensitivity to a visible spectrum [9].

The color of light source depends on the relative energy ratio of different wavelengths it emits. Spectral composition of light source determines not only its color temperature, but also the color rendering effect of illuminated objects. In the bright environment, human eyes are most sensitive to yellow-green light with a wavelength of 555 nm, and in a dark environment, eyes sense acutely blue-green light with a wavelength of 510 nm. The visual state between above two environmental luminances is called intermediate vision, which is basically equivalent to luminance level of general road lighting [13].

When driving inside tunnels, if intervals of road lamps induce zebra crossings with alternating light and shade, and if this alternation ranges within 2.5 Hz to 15 Hz, drivers will feel a stroboscope effect that maybe causes visual discomfort and psychological interference. In addition, glare caused by tunnel lighting possibly disrupts the adaptation of a visual system to surrounding physical space, and then induces visual discomfort or degradation.

3.3. Light Source versus Driving Safety and Comfort

3.3.1. Characteristics of Natural Light Source

Characteristics of outside natural light mainly relates to longitude and latitude of the tunnel, solar altitude angle, season, weather, time period, cloud, ground reflection ability, atmospheric transparency, etc. In a specific tunnel area, color temperature of natural light is relatively stable, especially when cloudy or foggy. However, when sunny, color temperature changes gently from low to high and then back to low; peak value usually appears at noon. Outside luminance is basically determined by season, weather, time period, direction of tunnel entrance and surroundings, especially by weather conditions; it changes gently when cloudy (coverage exceeds 0.8) and fluctuates a lot when sunny.

3.3.2. Visual Adaption in the Transition Zone

Ahead of threshold zone, drivers’ eyes have adapted to the luminance of the main field of view within a certain driving distance outside the tunnel. This adaptive luminance is generally considered to be the average luminance measured in the field of view of 20° at SSD in front of the tunnel entrance, which is called L_{20} value [8]. This value directly affects tunnel lighting design and is the reference parameter especially for threshold zone. With the characteristic changes of nature light source, lighting parameters (luminance and color temperature) of artificial light source should change accordingly to ensure drivers’ visual recognition of road conditions ahead.

When inside and outside light environments are of great difference, drivers need some time to adapt to the big change of light intensity. When driving at high speed, sudden illumination change possibly induces black hole or white hole effects. In order to reduce the discomfort caused by this, according to geographical location, environmental conditions, entrance forms, and terrain conditions of the tunnel, different forms of light reduction and anti-glare structures, such as sunshade, shading board, vegetation, pergola [14], etc., can be set up to build a light environment transition zone; this helps very much to couple natural light with artificial light in a friendly manner in the process of visual adaptation.

3.3.3. Characteristics of Artificial Light Sources

Tunnel lighting quality depends heavily on reliable light sources. Selection of tunnel light source must be considered comprehensively and rationally, which is limited by special requirements in tunnel scenario, such as illuminance, photochromic properties (color temperature and color rendering), light efficiency, light flux, light attenuation, lifetime and cost, as well as good visibility even in a smoky atmosphere caused by vehicle emissions. Traditionally incandescent, fluorescent, and high pressure sodium lamps (HPSL) are used for tunnel lighting. At present, light sources for tunnel lighting mainly include fluorescent, HPSL, and LED lamps; incandescent lamps are no longer installed. Table 2 compares the technical parameters for HPSL and LED lamps.

Table 2. Comparison of HPSL and LED.

	HPSL	LED
Service Life	Short service life ¹	Long service life ¹
Color Rendering	Low CRI, bad restoration to original color.	High CRI, restoration to original color with minor distortion.
Color Temperature	Narrow range (2000–3000 K).	Wide range (3000–6500 K).
Utilization Factor	Omnidirectional luminescence, 60–80% luminous flux reaches the ground.	Directional luminescence, More than 85% of the luminous flux reaches the ground.
Others	Pollutants (Mercury, lead), Slow startup and restart.	-

Note: ¹ Compared with the same criterion of light attenuation (70%) or damage ratio.

This comparison between HPSL and LED indicates LED is more suitable for tunnel lighting; this conforms to the target of energy saving and emission reduction, also assuring drivers’ safety and comfort of driving cognition.

3.4. Evaluation Indexes of Light Environment in Highway Tunnels

Global research on tunnel light environment mainly builds on tunnel luminance condition; there are three primary methods to evaluate lighting quality via visual effect, namely, visual performance used for short time recognition, visual fatigue used for long duration visual tasks, and subjective evaluation method based on visual psychological satisfaction. In this case, tunnel light environment is usually subdivided into access zone, threshold zone, transition zone, interior zone, and exit zone [8,15], as Figure 5.

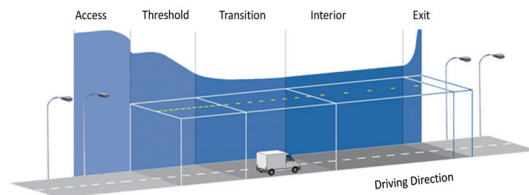


Figure 5. Tunnel zones for light environment.

Research shows that drivers' ability of visual recognition in tunnel lighting zones not only relates to road surface luminance and uniformity of road surface luminance but is affected by characteristics of light source and luminance difference between inside and outside of tunnels. However, there are no relevant regulations on photochromic properties and spectral distribution of light sources in current specifications. Hence, tunnel lighting design firstly needs to abide by the requirements in current lighting guidelines, and it is also desirable to study characteristics of light sources systematically and apply them reasonably; this will contribute to balancing favorable lighting effects and energy saving.

3.4.1. Color Temperature and Color Rendering Index

Warm or cold feelings of light color relates to human physiological and psychological effects. Appropriate color temperature aids in balancing the functions of the central nervous system and autonomic nervous system, and to keep nerves in a relaxed state. Otherwise, it may lead to dysfunction of the central nervous system and even disturb the body's natural balance [16]. Some experiments indicate that different spectral compositions of light source and adaptation level of human eyes influence visual response time greatly, and the radiation spectrum containing more blue and green light will shorten this response time.

Relative spectral power distribution of various wavelengths in light source determines its color rendering index (CRI). Light sources with continuous spectral distribution, wide spectral coverage, and spectral energy characteristics close to natural light have high CRI. CRI directly affects if drivers could recognize colored objects correctly. In a CRI test with small targets, Yamamoto found that, under intermediate visual range, different spectral composition of light sources influences if small colored targets could be correctly recognized a lot. On the premise of meeting the same correct recognition rate of small targets, tunnel light sources with high CRI and high content of short-wave components are more conducive to improving visual recognition [17].

Traditionally, tunnel lighting mainly adopted HPSL, and modern tunnel designs tend to choose LED due to its adjustable color temperature and high CRI. Because various combinations of color temperature and CRI have different influences on drivers' ability of visual recognition, they are important indexes to characterize tunnel light sources.

3.4.2. Luminance Reduction Factor

While driving inside from the outside, visual recognition is impacted not only by road surface luminance of the threshold zone, but by an outside luminance level. Luminance difference between inside and outside is the main index affecting driving behavior characteristics at the threshold zone. Thus, designing appropriate luminance transition between threshold zone and outside is vital to improve drivers' visual recognition. Luminance reduction factor K is defined to describe this difference between threshold zone and outside:

$$K = L_{th}/L_{20} \quad (1)$$

Here, L_{th} is the average road surface luminance at threshold zone, and L_{20} is the average luminance at a safe stopping sight distance with 20° field of view opposite the tunnel entrance.

Similar to the absence of uniform luminance standards, most countries and academic organizations have no uniform provisions on luminance reduction factor in the threshold

zone. Actual reduction factor can be determined appropriately through experiments according to characteristics of natural light source in the access zone during daytime, design speed, traffic volume, and required threshold to satisfy driving safety and comfort, so as to harmonize driving safety with energy saving.

Cognitive and behavioral characteristics of drivers at tunnel entrances and exits indicate that, when driving in the environment with luminance difference between inside and outside at night, if this difference exceeds a certain threshold impacting drivers' visual cognition and even producing a white hole or black hole effect, at this moment, the most common preventive measure drivers tend to take to alleviate the unsafety and discomfort is changing vehicles' speed [18], but this speed shift will further worsen the speed standard deviation and variance among different vehicles, which have a positive correlation with traffic accident rates [15,19]. Therefore, luminance difference between inside and outside is an important index to characterize the validity of visual cognition for a light environment at the tunnel entrance and exit area.

3.4.3. Road Surface Luminance

Drivers' visual perception is closely related to luminance of light environment, but there is a luminance threshold for the self-tuning ability of drivers' visual systems. When driving on the road, it is road surface luminance that drivers feel more real rather than illumination of light source. The luminance method evaluates drivers' visual ability by estimating the luminous flux of light source reflected from road surface into drivers' eyes. Static experiment shows that drivers' ability of visual recognition varies for the same light source with the same photochromic properties but different road surface luminance as Table 3.

Table 3. Visual recognition under different luminance levels.

Color Temperature: 5700 K, CRI: 70								
Luminance (cd/m ²)	5	4.5	4	3.5	3	2.5	2	1.5
Number of frames	9.60	9.60	11.10	13.00	13.38	12.63	13.50	17.57
Found times	10	10	10	8	8	8	8	7
Ratio	100%	100%	100%	100%	100%	100%	100%	87.50%

Road surface luminance is the actual perception of light intensity reflected from road surface to drivers' eyes; it directly affects drivers' recognition on road obstacles, and road situations can not be clearly recognized in case of insufficient luminance. Therefore, this index is a globally accepted indicator to evaluate the validity of visual recognition in a tunnel light environment, and its minimum is prescribed to 1.0 cd/m².

3.4.4. Uniformity of Road Surface Luminance

Because road surface luminance is from the reflected illuminance emitted by an overhead artificial point light source that projects and superimposes on the ground, if uneven superposition or reflection exists, non-uniform dark spots or shadows will appear, then resultant wavy feeling will endanger driving safety more or less. Onaygil and Sennin discussed the influence that luminance uniformity acts on visibility level in road lighting design and took visibility level as an indicator to measure driving comfort and safety [20].

Flicker frequency that resulted from tunnel lamps installation should not be within 2.5–15 Hz to avoid causing visual discomfort and psychological interference to drivers, which is based on the fact that impact on people is negligible when flicker frequency is lower than 2.5 Hz or higher than 15 Hz. The spacing between lamps is larger in an interior zone than that in the threshold zone, so it is difficult to ensure good uniformity in an interior zone. In some areas of the interior zone, there are maybe some dark bands with low luminance, if bright and dark bands appear repeatedly, this resultant zebra effect will

disturb drivers' visual recognition for ahead road conditions. This non-uniformity is to induce negative psychological reactions making drivers feel irritable.

In terms of lighting effect, given the same tunnel environment and lamps, road surface illumination produced by staggered arrangement is slightly better than that by symmetrical arrangement, and total uniformity of road surface luminance is higher than that by symmetrical arrangement.

Stepless dimming advantage of LED light source makes it unnecessary to turn off partially to reduce energy consumption; instead, it is feasible to finely adjust the output power of lamps according to current traffic flow and maintenance factor of lamps, which could reduce energy consumption and ensure the uniformity of road surface luminance.

All of the above analysis shows that uniformity of road surface luminance is an important index to characterize tunnel light environment.

3.4.5. Visual Cognition Distance

When driving in tunnel area, drivers need to clearly recognize the linear conditions, road conditions, signs and markings, vehicles information, obstacles, and landscape conditions within ahead safe distance. Only by ensuring enough safe visual distance can drivers finish the complete process consisting of cognition, judgment, decision-making, and operation to ensure driving safety. In this study, as suggested by CIE, SSD is used to evaluate drivers' visual recognition process to determine if target obstacles can be found at a distance not less than SSD, on which to judge the safety of a tunnel light environment.

3.4.6. Other Indexes

Besides the above indexes for tunnel light environment, in this study, the ways below are used to indirectly evaluate the quality of a tunnel lighting control system:

- (1) With help of actual traffic flow data at peak hours, the average speed of traffic flow, standard deviation, or variance of vehicle speeds are statistically analyzed; this method is able to indirectly indicate the smoothness of tunnel traffic flow at designed speed.
- (2) It can be regarded as another subjective evaluation method of lighting quality through questionnaire collecting real feedback of drivers on tunnel lighting or experience of safety and comfort during tunnel driving.
- (3) Based on data of lighting energy consumption, horizontal comparison results with similar tunnels (similar in geographical location, length, traffic flow, and other properties) can be thought of as an objective index to assess the economy of tunnel lighting.

4. Design of Lighting Control System

4.1. Selection of Light Source and Control Mode

Research of tunnel lighting control mainly includes two aspects, overall architecture of lighting system and control mode of lighting lamps. The lighting control system has gone through several stages, namely centralized control, distributed control, and fieldbus control. Currently, fieldbus control built on industrial Ethernet dominates most newly constructed tunnels. Control mode of tunnel lamps includes roughly three categories, artificial control, time sequence control, and presently the mainstream intelligent control. Meanwhile, stepless dimming has replaced traditional logic switching and becomes the primary control mode because LED lamps can be continuously dimmed within a full range.

With the advance of LED lighting theory and manufacturing technique, LED lighting is being widely used in bridge and tunnel construction. Olijnyk studied the advantages of LED on energy saving as tunnel lighting sources used by TIR Systems Inc. [21]. Guo et al. combined stepless dimming mode with an LED light source, and achieved 57% energy savings through transformation of traditional extensive lighting control [22]. Wang et al. replaced traditional HPSs with LEDs, and reformed lighting control from depending only on luminance to variable color temperature together with stepless dimming, which brought rewards of 18% energy saving [23]. Zhang et al. designed an automatic lighting

control mode (i.e., tunnel lamps switch on when car enters and off after leaves) via PID closed-loop feedback and road surface luminance measurement with image processing [24]. Today, on the Chinese Hongkong-Zhuhai-Macau Bridge, LED lamps and lighting control systems are serving the lighting project, which includes the main project of one 22.9 km bridge connected by one 6.7 km tunnel and branch project composed of multiple artificial islands [25].

4.2. Topology of System and Components

As Figure 6 shows, full consideration is taken on the advantages of distributed system and hierarchical management model, from the perspective of logic functions and control flows, this system is designed into two levels; namely, top-level tunnel system manager and tunnel onsite manager will implement system designed functions as Table 4.

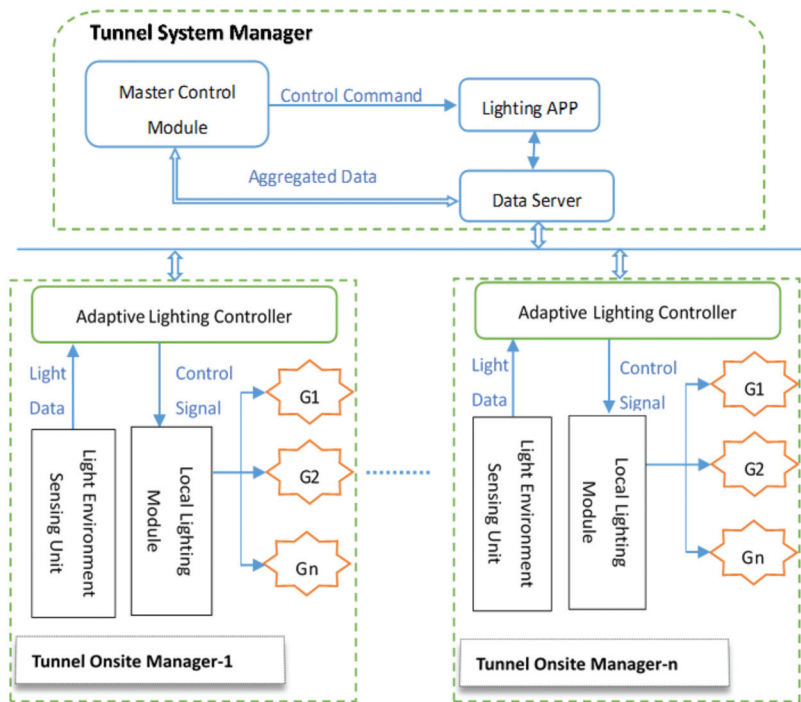


Figure 6. Network topology of the tunnel lighting control system.

Tunnel System Manager deployed in a central control room includes a Master Control Module of this system software, the lighting APP module responsible for running an intelligent dimming strategy, and the Data Server module in charge of transferring data and control instructions amongst different software components. Lighting APP receives periodic data generated by perception layer and transferred by Data Server, such as lighting condition, tunnel facilities, traffic flow, etc. and then decides next-cycle light adjustment parameters, and output control commands through Data Server to Tunnel Onsite Managers.

Tunnel Onsite Manager mainly consists of Adaptive Lighting Controller, Light Environment Sensing Unit, and Local Lighting Module. The Adaptive Lighting Controller mainly realizes two functions. Firstly, it provides the upper Lighting APP module with light sensing data (outside color temperature and luminance) sampled by light sensors located outside of the tunnel entrance. In addition, it addresses lighting control instructions output by upper Lighting APP to corresponding Local Lighting Modules. The Local Lighting Module takes charge of interpreting lighting control signals translated by Adaptive

Lighting Controller and converting them into appropriate voltage values and proportions for yellow and white light, respectively. Then, it sets the power supply modules of specific lamp groups covered by the Local Lighting Module; the lamp groups will produce expected luminance and color temperature. In the current system, Adaptive Lighting Controller and Local Lighting Module can be addressed individually, and lamps are controlled in groups. In addition, if needed, it is also feasible and easily accomplished to adjust lighting parameters for a single lamp in fine granularity by assigning a unique address to each lamp.

Table 4. Functions and components of the lighting control system.

	Master Control Module	Fulfill Top-Level Management of This Lighting Control System
Tunnel System Manager	Lighting APP	<ol style="list-style-type: none"> 1. Module in which predefined intelligent lighting policies resides. 2. Real-time response to data from Light Environment Sensing Unit. 3. Assembly Lighting Adjustment Command.
	Data Server	<ol style="list-style-type: none"> 1. Transfer data and control commands among modules. 2. Databases in charge of tunnel management jobs.
Tunnel Onsite Manager	Adaptive Lighting Controller	<ol style="list-style-type: none"> 1. Collect light data from Light Environment Sensing Unit, and transfer this data to Tunnel System Manager. 2. Parse Lighting Adjustment Command from Lighting App, and transfer to Local Lighting Module in the form of Control Signal.
	Light Environment Sensing Unit	<ol style="list-style-type: none"> 1. Sense outside tunnel light environment. 2. Normalize Light Data (outside color temperature and luminance).
	Local Lighting Module	<ol style="list-style-type: none"> 1. Parse Control Signal from Adaptive Lighting Controller. 2. Distribute appropriate voltage values to covered LED lamps.

4.3. Software Framework Based on System Requirements

As Figure 7 shows, this system consists of four layers, namely, Perception, Transport, Service Management, and Application; this structure is flexible and requirements orientated as Table 5.

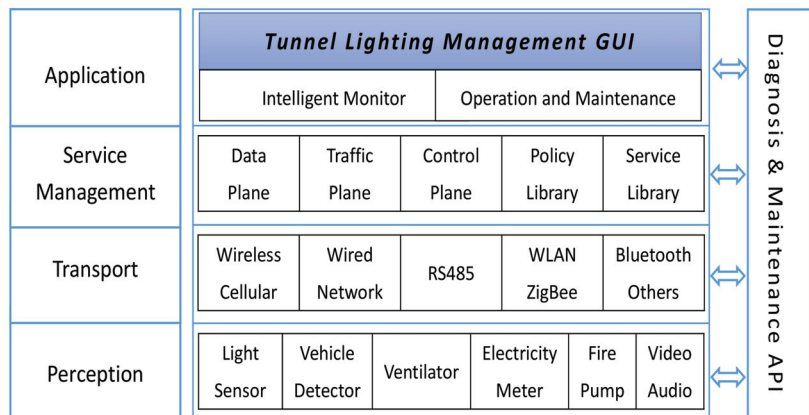


Figure 7. Overall architecture of the tunnel lighting control system.

Perception layer mainly acquires and normalizes all kinds of data from multiple heterogeneous sensors deployed in tunnels, such as light sensor, vehicle detector, ventilator, electricity meter, water pump and fire control facilities, video and audio devices, etc.; these data will feed into the dimming policies residing in Lighting APP.

In order to suit the diversity of perception devices, the transport layer supports several access media, namely wireless cellular, optical network, RS485, and WLAN, providing transparent and reliable links to exchange data between lower and upper layers.

As a key component of this control system, service management layer consists of a data plane in charge of data storage and transfer, traffic plane for routine operations, control plane to handle control commands for different layers and monitor status of lower facilities, policy library to execute lighting strategies, and service library for extra user demands.

Table 5. System layering and assignment of system requirements.

Layer-4	Application	<ol style="list-style-type: none"> 1. Tunnel Lighting Management GUI 2. Real-time monitoring of tunnel light environment. 3. Ease of Software upgrade and maintenance. 	
Layer-3	Service Management	<ol style="list-style-type: none"> 1. Data Plane for storage and transfer. 2. Traffic Plane for routine tunnel lighting operations. 3. Control Plane to deliver lighting control commands and status indications of lower facilities. 4. Policy Library to carry out intelligent lighting strategy. 5. Service Library for extra demands and extensibility. 	Diagnostics and Maintenance API, <ol style="list-style-type: none"> 1. Troubleshooting ports reserved for each layer. 2. Online upgrade and maintenance for any modules.
Layer-2	Transport	Diverse and highly reliable communication links and media to relay sensing data and control flow to and from upper layers.	
Layer-1	Perception	Sample and normalize sensing data from multiple sensors.	

The application layer provides operating personnel with friendly GUI to monitor real-time conditions of tunnel environment via two subsystems. An intelligent monitoring subsystem presents the running states of tunnel facilities, traffic flow, and dimming strategy, tracks if lighting APP effectively responds to changes of outside light conditions, and diagnoses if this system performs well to meet driving safety and comfort requirements. Meanwhile, the operation and maintenance subsystem offers conveniences for manual calibration and correction of system deviation.

Parallel with these four layers, Diagnostics and Maintenance API is reserved to facilitate online detection and trouble-shooting with all lighting equipment and software components during system integration and after deployment.

4.4. Software Process of Lighting APP

The process of intelligent lighting software mainly means how lighting APP outputs specific lighting control commands. This software aims to adjust a tunnel light environment for different design speeds of 40 km/h, 60 km/h, 80 km/h, 100 km/h, 120 km/h, etc., in the meantime, other multiple factors, namely weather, traffic volume, color temperature, and luminance, are considered together. Friendly coupling of internal and external light environments will be achieved through regulating artificial lighting parameters.

Lighting APP is adaptive for four kinds of weather changes outside tunnels:

- (1) Regulation under normal weather conditions;
- (2) Regulation under abnormal weather conditions;
- (3) Regulation when normal weather changes to abnormal weather conditions;
- (4) Regulation when abnormal weather changes to normal weather conditions.

Each of these scenarios matches its own criteria for color temperature and luminance conversion; lighting adjustment is executed in smaller steps of color temperature and

luminance in turn without introducing significant transition of visual comfort. Figure 8 is used to exemplify the basic algorithm and process corresponding to design speed of 80 km/h in the daytime at the threshold zone; this pattern also suits for other design speeds.

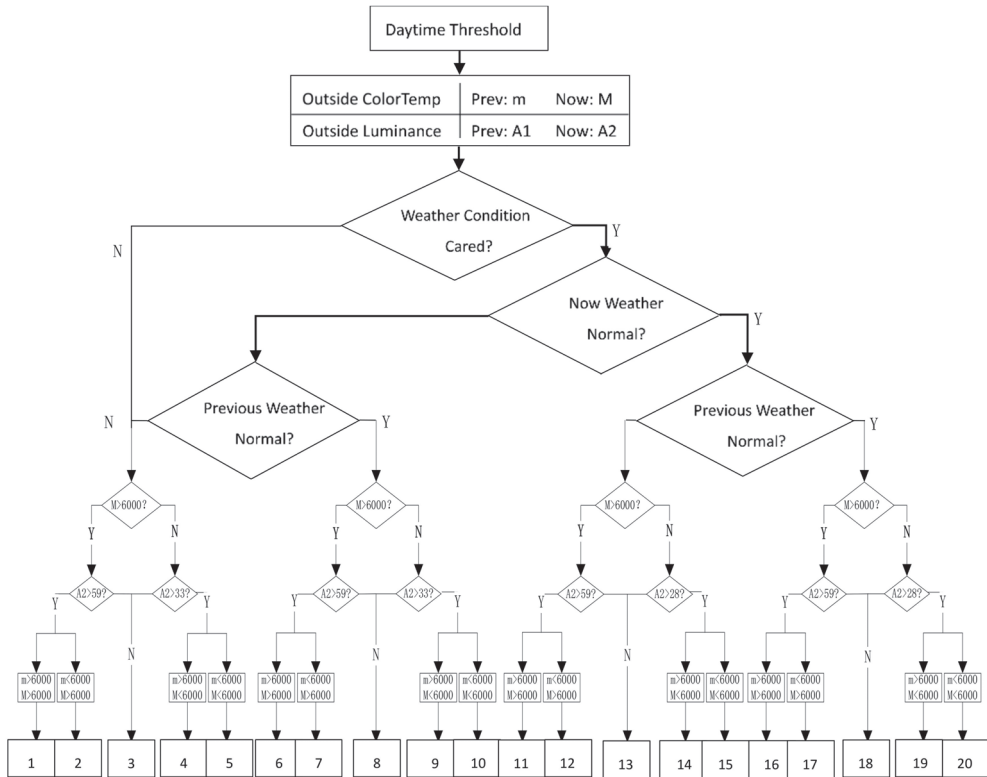


Figure 8. Flowchart of Lighting APP at 80 km/h.

In this figure, acronyms and legends as Table 6 are used to denote decision conditions.

Table 6. Notes and legends used in Figure 8.

A2 > 59	If outside luminance is greater than threshold 59 cd/m ² , luminance transition will take place. Similar to A2 > 33, A2 > 28, etc.
M > 6000	If now outside color temperature is greater than 6000 K, similar to M < 6000. Different color temperate transition pattern, for example m > 6000 and M < 6000, different dimming strategy applies.
Table 1–20	Each table (from 1 to 20) corresponds to one separate dimming strategy. Target light environment parameters are decided by the tuple (weather, outside light condition, tunnel design speed, traffic volume).

The major principle of this lighting strategy is to avoid significant transition of visual comfort, so adjustment of lighting parameters is executed in steps as small as possible for both internal color temperature and luminance, which will make drivers feel no visible change of lighting conditions,

- (1) If color temperature will transition across a span larger than 500 K or luminance transition is greater than 2 cd/m², lighting adjustment should be finished in multiple steps for color temperature or luminance;

- (2) The number of color temperature adjustment steps (*StepCT*) equals the biggest integer of color temperature span,

$$StepCT = Ceiling[Abs(M - m)/500]; \tag{2}$$

- (3) The number of luminance adjustment steps (*StepL*) equals the biggest integer of luminance span,

$$StepL = Ceiling[Abs(A1 - A2)/2]; \tag{3}$$

- (4) If both color temperature and luminance are required to be adjusted in single cycle, color temperature adjustment has higher priority than luminance change.

4.5. Reliability Assurance Aided by FMEA

Failure Mode and Effects Analysis (FMEA) is a systematic procedure to analyze potential failure modes and causes, and their impacts on system performance. It is both a program to assure the quality of system development and a preventive thinking model [26–28]. FMEA can be qualitative or quantitative [29,30], and is often the vital step to study the reliability of a specific system. In this study, before the lighting control system is officially put into operation, system analysis and design aided by FMEA can find potential failures as early as possible and reduce failure risks at lower costs, and eventually enable this system to be reliable and robust to meet required design criteria with a high confidence level.

Based on these system requirements, overall architecture, and network topology, there are mainly the following failure modes:

- (1) Loss of function;
- (2) Functional degradation;
- (3) Intermittent functional failure;
- (4) Function delay;
- (5) Unexpected functions.

The FMEA method determines three parameters for each failure mode caused by a single cause according to predefined grading standards, namely severity (S), occurrence (O) and detection (D), and each ranges from 1 to 10 as Tables 7–9, respectively.

Table 7. Evaluation criteria for FMEA severity (S).

Severity	Evaluation Criteria	Impact
10	All LED lamps within control area go out with no warning.	critical
9	Whole system or some modules are loss of basic functions and cannot be restored.	
8	All LED lamps within control area flicker on and off with no warning.	very serious
7	Abnormal optical sensing data (color temperature or luminance) in a light environment sensing unit.	serious
6	In a certain lighting zone, LED lamps lose control, luminance, and color temperature cannot be adjusted or obviously lagged behind.	
5	In a certain lighting zone, LED lamps cannot be ideally controlled, and luminance or color temperature cannot be adjusted.	
4	In a certain lighting zone, luminance or color temperature of LED lamps are inconsistent with the preset dimming strategy.	medium
3	System functions normally, its performance meets design requirements with occasional status prompt.	
2	System and each module function well as expected with internal prompt messages logged.	low
1	There are no discernible anomalies.	very low

Table 8. Evaluation criteria for FMEA occurrence (O).

Occurrence	Evaluation Criteria	Failure Probability
10	More than 100 times for every 1000 samples.	extremely frequent
9	80 times for every 1000 samples.	
8	50 times for every 1000 samples.	frequent
7	20 times for every 1000 samples.	
6	10 times for every 1000 samples.	occasional
5	5 times for every 1000 samples.	
4	Once for every 1000 samples.	
3	Once for every 2000 samples.	low
2	Once for every 10,000 samples.	
1	Less than once for every 10,000 samples.	Almost never

Table 9. Evaluation criteria for detection (D).

Detection	Evaluation Criteria	Chance
10	Unable to design probe methods.	no chance
9	Weak probe ability, hard to simulate real conditions.	basically undetectable
8	This mode can only be simulated.	extremely low
7	Mode and mechanism can be located empirically.	very low
6	No obvious dimming effect, more than 1 failure mode can be located with testing equipment.	low
5	No obvious dimming effect, 1 failure mode can be located with testing equipment.	general
4	Mode and mechanism can be deduced depending on predefined lighting strategy.	a bit high
3	Obvious inconformity between dimming effect and lighting strategy, more than 1 failure mode can be accurately located.	high
2	Inconformity between dimming effect and lighting strategy, 1 failure mode can be accurately located.	very high
1	Failure does not occur due to leverage of previous high-quality software or hardware modules.	needless

For each failure mode, Risk Sequence Number (RPN) is calculated as Equation (4) by referring to above Tables 7–9, namely product of *S*, *O*, and *D* that ranges from 1 to 1000. In addition, if this *RPN* exceeds 100, measures should be taken to reduce this *RPN*:

$$RPN = S \times O \times D \tag{4}$$

With this process iterates, when *RPN* of each failure mode is small enough (normally less than 20) and its severity is less than 7, failure risk of whole system is fairly low and its reliability is increasing. During this process, preventive and optimization measures need to be filed to provide reference for subsequent development, testing, and maintenance.

5. Application and Evaluation of Lighting Control System

5.1. Application

YanChong highway is the major channel connecting Beijing and Chongli competition areas for 2022 Beijing Winter Olympic Games. It is also listed in the first batch of green road constructions and typical demonstration projects approved by the Chinese Ministry of Transport. As one of the important control projects of YanChong highway, construction and operation of Songshan tunnel should firstly consider the potential factors related to traffic accidents due to its 9.2 km total length; another concern is with ecological environment since it is adjacent to one national nature reserve. Besides these requirements, driving safety and

low-carbon operation should be given more attention. As of today, one intelligent lighting control system conforming to these premises has been deployed after the acceptance test and runs normally with continuous supervision of lighting quality.

As Table 10 shows, a light environment sensing unit at the tunnel entrance mainly consists of a luminance detector and a color temperature thermometer, which are used to sense and collect real-time light conditions and flow the transformed light data into the onsite adaptive lighting controller. This controller is essentially one highly reliable DA-1000 industrial computer driven by the CentOS system; it collects light data and manages local lighting modules. A local lighting module is evolved from CC09TA with adjustable voltages ranging from 0–10 V; it parses control commands from adaptive lighting controller and outputs well-proportioned voltages via RS485 bus to drive the corresponding LED lamp group to emit white and yellow lights separately matching with target color temperature and luminance. These LED lamps with 70 w rated power are voltage adjustable for white and yellow lights individually within 0–10 v, and color temperature ranges 3000–7000 K.

Table 10. Main functional components and hardware entities.

Light Environment Sensing Unit	light luminance detector color temperature thermometer
Adaptive Lighting Controller	industrial computer: DA-1000 operating system: CentOS
Local Lighting Module	centralized controller: CC09TA regulation voltage: 0–10 v
LED Lamps	rated power: 70 w color temperature: 3000–7000 K CRI: 70
RS485 wires	remote control to LED lamps
Upper computers in tunnel station	host computers shared by Master Control Module, Lighting APP, and Data Server

Master control and lighting APP modules reside in upper computers located in a tunnel station; they work as a top-level coordinator for all components inside this system.

5.2. Evaluation

Since its deployment, this system has experienced a variety of working conditions in different seasons and weather, and the research team has conducted a mass of field tests and collected vast amounts of running data.

After periodic load tests and field verification, this system works stably:

- (1) Average road surface luminance and uniformity of road surface luminance meet expected lighting specifications;
- (2) Color temperature and luminance of LED lamps alter as intelligent lighting strategy requires;
- (3) Artificial light environment of each tunnel zone offers adequate visual cognition distance for driving safety and comfort;
- (4) Inside this tunnel, traffic flow runs smoothly and there is no obvious speed variability;
- (5) Feedback from actual drivers through this area indicates that this lighting quality satisfies visual performance, and little visual fatigue is induced.

Figures 9 and 10 are used to exemplify how color temperature and luminance in a threshold zone vary on a 10-min cycle in normal weather with outside light data for consecutive 12 h from 6:00 A.M. to 6:00 P.M.

In Figure 9, there are twice the transitions between 6000 K and 3500 K, 3500 K lasts roughly in the midday duration. During this time window, drivers are prone to struggle with visual fatigue; this transition of color temperature between threshold zone and open space helps a lot with stimulating drivers' excitement and making them concentrate on driving carefully, eventually keeping the driving process safe and smooth in the tunnel area.

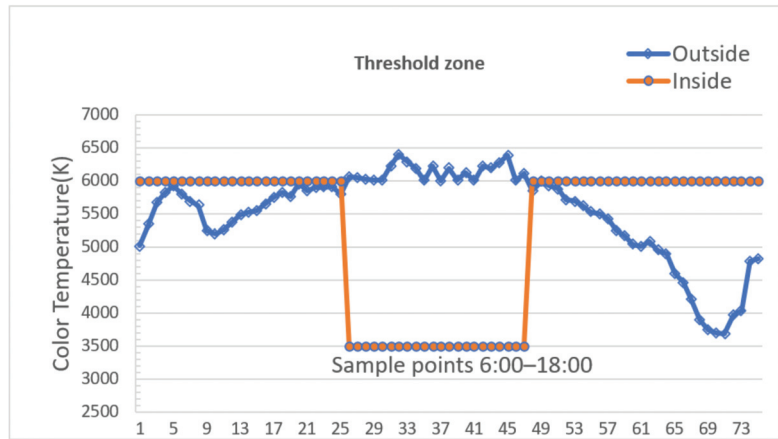


Figure 9. Color temperature curve in a threshold zone.

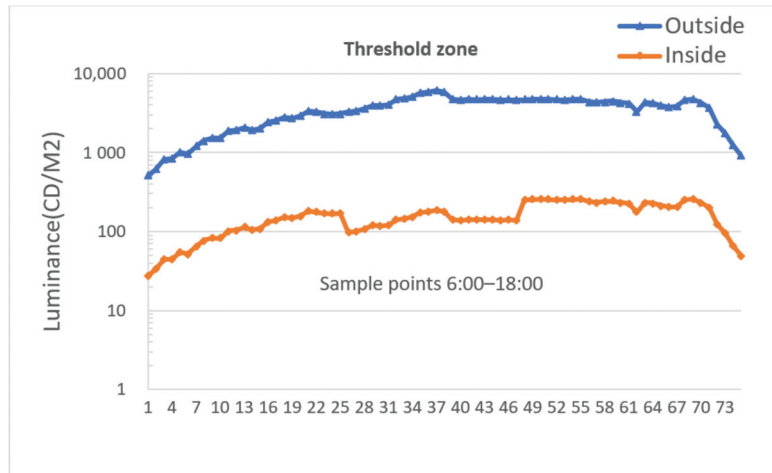


Figure 10. Luminance curve in a threshold zone.

Figure 10 shows that the luminance trend in the threshold zone is basically consistent with that of the outside tunnel, which contributes a lot to reducing visual discomfort caused by a black hole effect while approaching the threshold zone.

However, this luminance curve shifts slightly at the moment when color temperature transitions between 6000 K and 3500 K; this is because different L_{20} luminance reduction factors are assigned in the lighting strategy to make up color temperature fluctuation in the daytime under normal weather. In the meantime, since target lighting parameters are possibly adjusted in multiple steps, a large gradient change of luminance or color temperature is subdivided into several time slices with smaller granularity in each regulation period, which effectively weakens the harm that large gradient luminance or color temperature jitter may cause.

6. Conclusions

Different from many existing lighting control systems, technical means are explored in this system to alleviate visual discomfort from the standpoint of driving safety and comfort requirements in the tunnel light environment, which is theoretically founded on

the correlation research of variable color temperature technology of an LED lighting source with human factor engineering. After its deployment with an actual highway tunnel, this system is serving tunnel users with high lighting quality, which is verified by testing results and actual operation data; this system is adaptive with high reliability, it contributes a lot to optimizing lighting conditions and reducing the fluctuation of driving workload; as a result, driving safety level is somewhat enhanced in return. This indicates that this LED lighting control system is quite practical for promoting visual effects and reducing traffic risks in long and extra-long tunnels.

In view of the potential out-of-limit deviations between actual lighting performance of LED lamps and ideal parameters calculated by an intelligent lighting algorithm, in the long run, it is highly preferred to introduce a feedback link of closed loop control to offset the deficiency of current open loop control. In addition, if an artificial intelligence algorithm could be used to deeply mine the mass data accumulated by this system, it will be of great benefit to optimize the emergency plan and time sequence control mode of tunnel lighting.

Author Contributions: The authors confirm the contributions to the paper as follows: study conception and design, B.S. and J.H.; data collection, B.S. and J.H.; analysis and interpretation of results, B.S. and J.Z.; draft manuscript preparation, B.S., J.H., J.Z. and R.W. All authors have read and agreed to the published version of the manuscript.

Funding: This work was partly supported by the scientific research project of Fujian Expressway Group Co., Ltd., and partly by the Department of Transport of Yunnan Province and partly by the traffic scientific research project of Department of Transport of Shaanxi Province (No. 21-02X).

Institutional Review Board Statement: Not applicable.

Informed Consent Statement: Not applicable.

Data Availability Statement: Data generated in this study are available upon request.

Acknowledgments: The authors would like to thank all of the participants for attending the experiments.

Conflicts of Interest: The authors declare no conflict of interest. The company had no role in the design of the study; in the collection, analyses, or interpretation of data; in the writing of the manuscript, or in the decision to publish the results.

References

1. Ministry of Transport, PRC. Statistics Report of Transportation in China. 2021. Available online: http://www.gov.cn/xinwen/2021-05/19/content_5608523.htm (accessed on 15 May 2021).
2. 2019 Road Traffic Accident Statistical Annual Report of the People's Republic of China; Traffic Management Bureau of the Ministry of Public Security: Beijing, China, 2020.
3. Liu, Y.T. *Manual of Traffic Safety*; Communication Press: Beijing, China, 2004.
4. Babkov, B.X. *Road Conditions and Traffic Safety*; Jing, T.R., Translator; Tongji University Press: Shanghai, China, 1990; Volume 6.
5. Zhang, X.Q.; Hu, J.B. Analysis of theory for highway tunnel lighting set and evaluation method situation. *Highway* **2016**, *61*, 5.
6. Du, K. Research on Drivers' Mentality in Extra-Long Tunnels. Master's Thesis, Chang'an University, Xi'an, China, 2006.
7. Illinois Division of Highways. Bureau of Design and Environment. Chapter fifty-six: Highway lighting. In *Bureau of Design and Environment Manual*; Illinois Division of Highways, Bureau of Design and Environment: Springfield, IL, USA, 2013.
8. JTG/TD70/2-01-2014; Guidelines for Design of Lighting of Highway Tunnels. Communications Press Co., Ltd.: Beijing, China, 2014.
9. CIE Technical Report: 88-2004 Guide for the Lighting of Road Tunnels and Underpasses; CIE: Vienna, Austria, 2004.
10. Zhang, Q.Y.; Tu, Y.; Hu, Y.K. Highway tunnel entrance illumination measurement method based on physiological and psychological Effects. *Zhaoming Gongcheng Xuebao* **2012**, *23*, 8–14.
11. Zhao, B.Q. Driver's dynamical visual character and its effects. *J. Highw. Transp. Res. Dev.* **1998**, *15*, 38–41.
12. Fan, S.R. *Traffic Psychology*; People's Public Security University of China Press: Beijing, China, 2011; Volume 1.
13. Building Electrical Branch of Architectural Society of China. *Architectural Lighting*; Building Industry Press: Beijing, China, 2010; Volume 1.
14. Peña-García, A. The impact of lighting on drivers well-being and safety in very long underground roads: New challenges for new infrastructures. *Tunn. Undergr. Space Technol.* **2018**, *80*, 38–43. [[CrossRef](#)]
15. Shy, B. Overview of traffic safety aspects and design in road tunnels. *IATSS Res.* **2016**, *40*, 35–46.
16. Zhang, Q.W.; Chen, Z.L.; Hu, Y.K. *Study on the Influence of Lighting Source Color Temperature on Visual Performance in Tunnel and Road Lighting*; College of Architecture and Urban Planning, Chongqing University: Chongqing, China, 2008; Volume 19, pp. 24–29.

17. Yamamoto, J.; Kobayashi, S.; Nagasawa, T.; Ito, H. Visibility and color-rendering properties of Light sources in tunnel lighting. In Proceedings of the 26th Session of CIE (Volume 2), Beijing, China, 4–11 July 2007.
18. Hu, J.B.; Jiang, C.; Gao, X.J. Analysis of tunnel lighting brightness in high-altitude area based on driving workload. *Tunn. Constr.* **2020**, *40*, 17–24.
19. Garber, N.J.; Gadiraju, R. Factors affecting speed variance and its influence on accidents. *Transp. Res. Rec. J. Transp. Res. Board* **1989**, *1213*, 64–71.
20. Onaygil, S. The effect of luminance uniformity on visibility level in road lighting. *Lighting Res. Technol.* **2003**, *35*, 199–213.
21. Olijinyk, Z. *Lettherebelight*; Canadian Business: Toronto, ON, Canada, 2003; Volume 76, pp. 151–153.
22. Guo, Y.W.; Fu, D.X. Research on comprehensive energy saving technology of ventilation and lighting linkage in highway tunnel. *Build. Energy Conserv.* **2018**, *45*, 4.
23. Wang, Y.; Qin, H.B.; Hu, Y.Z. Design of tunnel color temperature lighting control system. *Softw. Guide* **2018**, *17*, 5.
24. Zhang, L.D.; Qin, L.; Jiang, H.T. Design and implementation of intelligent monitoring software system for tunnel lighting. *J. Highw. Transp. Res. Dev.* **2017**, *34*, 92–99.
25. Du, J.; Zhou, S.K.; Chen, C.G. LED lighting technology of Hong Kong-Zhuhai-Macao Bridge lighting project. *Zhaoming Gongcheng Xuebao* **2020**, *31*, 11.
26. Tearesa, L.W. The Development of a FMEA Process for Design and Maintenance. Master's Thesis, Western Michigan University Kalamazoo, Kalamazoo, MI, USA, 2000.
27. Li, C.; Liu, Y.Z.; Li, X. *FMEA Method Used in EV Control System*; Automotive Digest: Manhattan Beach, CA, USA, 2021; Volume 8.
28. Song, G.Z.; Meng, Z.Q.; Gao, J. Failure Analysis of domestic PET/MR with FMEA method. *China Instrum.* **2021**, *5*, 34–38.
29. Rausand, M.; Barros, A.; Hoyland, A. *System Reliability Theory: Models, Statistical Methods, and Applications*, 2nd ed.; Wiley: Hoboken, NJ, USA, 2004; p. 88.
30. Tay, K.M.; Lim, C.P. On the use of fuzzy inference techniques in assessment models: Part II: Industrial applications. *Fuzzy Optim. Decis. Mak.* **2008**, *7*, 282–302. [[CrossRef](#)]



Article

Emission Characteristics and Health Risks of Volatile Organic Compounds (VOCs) Measured in a Typical Recycled Rubber Plant in China

Shuang Wang ¹, Yucheng Yan ¹, Xueying Gao ¹, Hefeng Zhang ², Yang Cui ¹, Qiusheng He ^{1,*}, Yuhang Wang ³ and Xinming Wang ⁴

- ¹ School of Environmental Science and Engineering, Taiyuan University of Science and Technology, No. 66 Waliu Road Wanbailin District, Taiyuan 030024, China; s20202301014@stu.tyust.edu.cn (S.W.); yanyucheng1021@163.com (Y.Y.); gaouxueying@sxist.edu.cn (X.G.); cuiyang201110@163.com (Y.C.)
- ² Chinese Research Academy of Environmental Sciences (CRAES), Ministry of Environment Protection (MEP), Beijing 100012, China; zhanghf@craes.org.cn
- ³ School of Earth and Atmospheric Science, Georgia Institute of Technology, Atlanta, GA 30332, USA; yuhang.wang@eas.gatech.edu
- ⁴ State Key Laboratory of Organic Geochemistry, Guangzhou Institute of Geochemistry, Chinese Academy of Sciences, Guangzhou 510640, China; wangxm@gig.ac.cn
- * Correspondence: heqs@tyust.edu.cn; Tel./Fax: +86-(35)-16998326

Abstract: The continued development of the automotive industry has led to a rapid increase in the amount of waste rubber tires, the problem of “black pollution” has become more serious but is often ignored. In this study, the emission characteristics, health risks, and environmental effects of volatile organic compounds (VOCs) from a typical, recycled rubber plant were studied. A total of 15 samples were collected by summa canisters, and 100 VOC species were detected by the GC/MS-FID system. In this study, the total VOCs (TVOCs) concentration ranged from 1000 ± 99 to $19,700 \pm 19,000 \mu\text{g}/\text{m}^3$, aromatics and alkanes were the predominant components, and m/p-xylene ($14.63 \pm 4.07\%$ – $48.87 \pm 3.20\%$) could be possibly regarded as a VOCs emission marker. We also found that specific similarities and differences in VOCs emission characteristics in each process were affected by raw materials, production conditions, and process equipment. The assessment of health risks showed that devulcanizing and cooling had both non-carcinogenic and carcinogenic risks, yarding had carcinogenic risks, and open training and refining had potential carcinogenic risks. Moreover, m/p-xylene and benzene were the main non-carcinogenic species, while benzene, ethylbenzene, and carbon tetrachloride were the dominant risk compounds. In the evaluation results of L_{OH} , m/p-xylene (25.26–67.87%) was identified as the most key individual species and should be prioritized for control. In conclusion, the research results will provide the necessary reference to standardize the measurement method of the VOCs source component spectrum and build a localized source component spectrum.

Keywords: volatile organic compounds; recycled rubber plant; source profiles; health risk assessment; OH radical loss rate

Citation: Wang, S.; Yan, Y.; Gao, X.; Zhang, H.; Cui, Y.; He, Q.; Wang, Y.; Wang, X. Emission Characteristics and Health Risks of Volatile Organic Compounds (VOCs) Measured in a Typical Recycled Rubber Plant in China. *Int. J. Environ. Res. Public Health* **2022**, *19*, 8753. <https://doi.org/10.3390/ijerph19148753>

Academic Editors: Roberto Alonso González Lezcano, Francesco Nocera and Rosa Giuseppina Caponetto

Received: 3 June 2022
Accepted: 13 July 2022
Published: 19 July 2022



Copyright: © 2022 by the authors. Licensee MDPI, Basel, Switzerland. This article is an open access article distributed under the terms and conditions of the Creative Commons Attribution (CC BY) license (<https://creativecommons.org/licenses/by/4.0/>).

1. Introduction

As important substances participating in atmospheric photochemical reactions, volatile organic compounds (VOCs) are the main precursors of secondary organic aerosols (SOA) and tropospheric ozone (O_3), which are also the major factor for photochemical smog and haze [1–6]. Meanwhile, many substances in VOCs, such as benzene, toluene, and other benzene series, are also carcinogenic, teratogenic, and mutagenic and can directly enter the human body through the respiratory tract, skin, and other routes, seriously affecting human health [7–10]. With the rapid development of urban industrialization in the country, the increase in human activities has led to significantly higher anthropogenic

VOC emissions in most areas [11,12]. Furthermore, industrial VOCs account for more than 50% of anthropogenic VOC emissions [13] and have become the key to VOC emission reduction in air pollution prevention and control [14–16].

Previous studies on the emission characteristics of VOCs from industrial sources at home and abroad have mainly focused on industries such as the chemical industry, oil refineries, and solvent use. Dumanoglu et al. [17] analyzed the emission sources of Turkey's heavy industry region and proposed that refineries and petroleum products, petrochemical industry, solvent use, industrial processes, and vehicle exhaust gas were identified as VOC sources, accounting for 56%, 22%, 12%, and 10%, respectively; a study by Saeaw et al. [18] on industrial areas in Thailand pointed out that mobile and industrial sources account for 42% to 57% and 15% to 44% of VOCs concentrations, respectively. He et al. [19] analyzed the composition characteristics and potential tracers of non-coal emission sources, including refueling, solvent use, and industrial and commercial activities. Wei et al. [20] collected samples near different production units in a large oil refinery in Beijing, showing that C₃–C₆ alkanes, C₃–C₄ alkenes, and aromatic hydrocarbons were the most important species.

With the sustained development of the automotive industry, the number of rubber tires has quietly increased, waste tire production will exceed 20 million tons in China, ranking first in the world, and will gradually become a new source of solid-waste pollution, and the problem of "black pollution" is severe. The latest research has shown that burning and energetic "recycling" in cement plants appear to be the dominant usages of old tires; feedstock recycling would be a very beneficial approach in the case of tires and rubber in general [21]. In China, tire recycling is mainly distributed in Hebei, Shandong, Shanxi, and other provinces; most of them are small and medium-sized enterprises, which have backward technology and treatment equipment, and when solving the pollution problem of the waste tire, a large number of complex organic waste gas will be emitted, so the environmental effects and health effects cannot be ignored.

At present, research into the rubber industry mainly focuses on the exhaust gas emission characteristics and terminal treatment technology of raw rubber material treatment [22–25]; there is less literature reporting on the composition and concentration of pollutants emitted by processes from recycled rubber plants [26]. Based on the above background, in this study, we selected VOCs from different processes in a typical recycled rubber plant in Shanxi Province for detection and analysis and then the emission characteristics of VOCs were studied deeply, the industry markers were determined, and the health risks were evaluated. Finally the L_{OH} was calculated to quantify the environmental effects of the industry. The research results help the government to understand the emission characteristics and risk levels of VOCs in the recycled rubber plant better and provide an essential reference for China to standardize the measurement method of VOCs source composition spectrum and build a localized source composition spectrum.

2. Materials and Methods

2.1. Description of the Waste Rubber Tire Recycling Process

There are many ways to recycle waste rubber tires. The principle is that the network structure of waste rubber is destroyed under the comprehensive action of heat, oxygen, mechanical force, and a chemical regeneration agent so that the plasticity of waste rubber can be restored and achieve regeneration [27,28]. Among them, the regeneration process, which uses a dynamic devulcanization tank and rubber mixing, is widely used in North China. In this study, we selected a representative recycled rubber plant in Shanxi province, which used waste tires as the main raw material. The plant had typical recycling processes that could be generally divided into two stages, i.e., rubber powder preparation and recycling.

The detailed processes are described as follows: The collected waste tires are centrally treated and then crushed step by step by the tire crushing equipment (crumb rubber production step), and the main particulate matter can be effectively removed by the gas collection system and the dust collector (more than 99%). After preparation, the crumb

rubber and a certain proportion of chemical additives (coal tar, crude aromatic oil, cracking heavy oil, etc.) are reacted in the dynamic devulcanization tank at a high temperature (210~250 °C) and high pressure (2.0~2.3 MPa), thereby plastic and viscous rubber are regenerated (devulcanization step), and then the devulcanized crumb rubber is transported through the conveyor belt to the cooling yard for cooling (cooling and yarding step), then the cooled crumb rubber enters the mill and refiner machine in turn and is continuously affected by the mechanical shear force of the rotor in the machine, the temperature was raised to about 160 °C (rubber refining step), which can improve the plasticity of the rubber powder to the level of replacing natural rubber; finally, it is pressed into a tablet. The typical process flowchart of waste rubber tire recycling is shown in Figure 1.

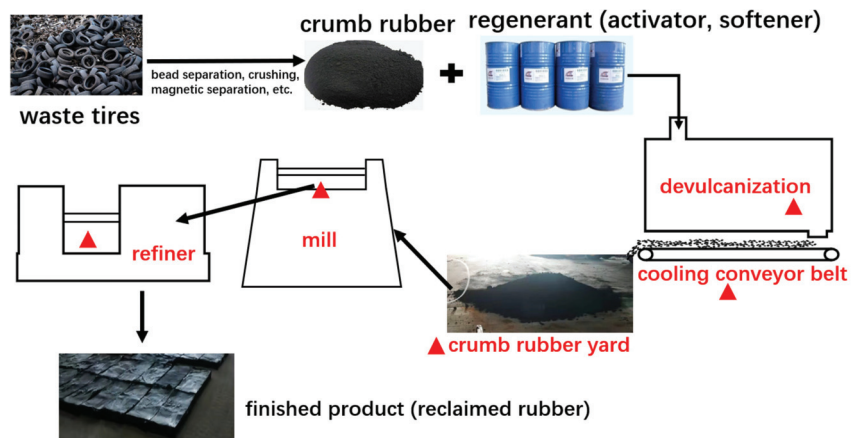


Figure 1. Typical process flowchart of waste rubber tire recycling.

The contaminant emitted from the recycling is usually different from that emitted from crumb rubber production. The production process mainly emits particulate matter, which only involves physical processes, while the recycling process mainly emits organic waste gas (more than 90%) with high temperature and high discharges. The specific reasons for the occurrence of VOCs are expressed as follows: In the devulcanizing step, the production process of the dynamic devulcanization tank equipment is not continuous, and the exhaust gas needs to be discharged intermittently before unloading, which will engender a large amount of organic waste gas, the cooling and yarding step has just undergone a high-temperature state of chemical reaction, and the rubber powder is exposed to the workshop throughout the process; subsequently, a great deal of organic waste gas will be released, the high temperature of the rubber refining process causes low-molecular compounds to be volatilized quickly.

2.2. VOC Sampling and Analysis

In this study, five sampling sites, which could represent the emission characteristics of the processes were selected, including the dynamic devulcanization tank pressure relief port, screw cooling conveyor outlet, crumb rubber yard, mill, and refiner. When collecting samples, in order to ensure the accuracy of samples and reduce accidental errors, three parallel discharge samples were collected at each sampling site by a summa canister (Entech, Malvern, PA, USA) equipped with a restrictor valve (39-RS-x; Entech Instruments), the collection time of each sample was completed within 5–10 min, all of the collected samples were completed within 1 day. The VOC emissions during the one-day sampling period may not be fully representative of the annual emissions from the rubber plant. However, during the sampling period, each facility in the plant was in normal production, and the processes were operating normally, so sampling at this time had preferable representativeness. For the yard and cooling link, our fugitive emission sampling point was set outside the pollution

source at 1 m; for the rest of the process with the gas collection hood, our sampling point was placed at 0.5m directly above the gas collection hood of each production facility. Table 1 shows specific information about sampling. A total of 15 samples from industrial sources were collected (including fugitive and organized emission samples). After sampling, all of the VOC samples were sent back to the laboratory within 20 days for preservation and analysis. Afterward, these samples were injected into the GC/MS-FID system (Agilent 7890A/5975C).

Table 1. Sampling information in each measured sample ($\mu\text{g}/\text{m}^3$).

No. of Samples	Sampling Objective	Sampling Site	Emission Form	Facility Condition
1	Dynamic devulcanization tank pressure relief port	0.5 m above	Organized	Normal
2	Screw cooling conveyor outlet	1 m horizontal	Fugitive	Normal
3	Crumb rubber yard	1 m horizontal	Fugitive	Normal
4	Mill	0.5 m above	Organized	Normal
5	Refiner	0.5 m above	Organized	Normal

The detailed analysis process of the samples is described as follows: Before entering the GC/MS analysis, the collected samples were condensed and enriched, firstly by the three-stage low-temperature cold trap of the atmospheric pre-concentrator (Nutech 8900DS), and the sample was first passed through a primary cold trap composed of glass beads (at a temperature of $-150\text{ }^\circ\text{C}$) to remove water vapor, then the VOCs in the samples were enriched by a secondary cold trap consisting of a Tenax adsorbent (at $-20\text{ }^\circ\text{C}$) while removing nitrogen, oxygen, and carbon dioxide, the desorption temperature and time was $225\text{ }^\circ\text{C}$ and 3 min, respectively, finally, the samples were condensed and concentrated by the third cold trap stage (at $-165\text{ }^\circ\text{C}$) and transferred to the GC/MS system (Agilent 7890A/5975C) for analysis. During the analysis, high-purity helium gas was used as the carrier gas to load the collected air samples into a chromatographic column DB-1 ($60\text{ m} \times 0.32\text{ mm} \times 1\text{ }\mu\text{m}$, Agilent Technology, Santa Clara, CA, USA) for separation. Subsequently, the $\text{C}_2\text{--C}_3$ VOCs were separated on a PLOT-Q column ($30\text{ m} \times 0.32\text{ mm} \times 20\text{ }\mu\text{m}$, Agilent Technology, Santa Clara, CA, USA) and quantified using a flame ionization detector (FID), while the $\text{C}_4\text{--C}_{12}$ compounds (including hydrocarbons, oxygenated VOCs, halocarbons, and other species) were separated on a nonpolar column ($50\text{ cm} \times 0.15\text{ mm}$ (I.D)) and detected using quadrupole mass spectrometry detector (MSD). The oven temperature was initially held at $35\text{ }^\circ\text{C}$ for 5 min, then increased to $150\text{ }^\circ\text{C}$ at $5\text{ }^\circ\text{C}/\text{min}$ for 7 min, and finally increased to $200\text{ }^\circ\text{C}$ at $10\text{ }^\circ\text{C}/\text{min}$ for 4 min, the ion source was electron ionization (EI), and the ion scan mode was selective ion scan. The target compound was identified according to the retention time of the sample and mass spectrum and quantified by the external standard curve method. A total of 100 VOC species were measured in this study, including 11 alkenes, 29 alkanes, 16 aromatics, 36 halocarbons, 6 ether esters, acetylene, and carbon disulfide. Standard curves were prepared by diluting a mixture of photochemical assessment monitoring stations (PAMS) and TO-15 (Spectra Gases, Linde, Stewartsville, NJ, USA) standard gases to corresponding concentrations (5, 10, 20, 50, and 100 ppbv), respectively. A replicate of every 10 samples was analyzed to ensure that the relative standard deviation was less than 30%.

2.3. Analytical Methods

2.3.1. Coefficient of Divergence Method

The coefficient of divergence method can be used to analyze the similarity between VOC composition spectra in different processes [29]. The equation for calculating CD_{ij} is as follows:

$$CD_{jk} = \sqrt{\frac{1}{p} \sum_{i=1}^p \left(\frac{X_{ij} - X_{ik}}{X_{ij} + X_{ik}} \right)^2} \quad (1)$$

where CD_{jk} is the divergence coefficient, j and k are different production processes, X_{ij} and X_{ik} are the content of component i in process j and k , respectively, and p is the number of chemical components involved in the calculation.

The CD values range from 0 to 1. The closer the CD is to 0, the stronger the similarity between the composition profiles, and the closer the CD is to 1 indicates that the content of each component between the composition profiles varies greatly. At present, there is no standard for dividing the similar grades clearly between the compositional profiles in domestic studies. When using this method, Wang et al. believe that two component spectra with divergence coefficients between 0 and 0.2 must be similar, two component spectra between 0.2 and 0.5 may be similar, and two component spectra between 0.5 and 1 must not be similar. This study analyzed the degree of similarity based on this criterion.

2.3.2. Health Risk Assessment

Considering that the rubber regeneration process requires the manual operation of equipment and film trimming, operators are exposed to the unorganized exhaust gas in the factory for a long time, and the exposure to benzene and benzene series will cause potential harm to the nerves and immune system of the body [30]; therefore, the health risks of VOCs emitted from various processes in rubber recycling were evaluated in this study. Exposure to air pollutants by ingestion, inhalation, and dermal contact are vital exposure scenarios for people. In industrial parks, inhalation is generally considered to be the main route of exposure to VOCs for workers [31–33]. In this study, the lifetime cancer risk (LCR) and hazard index (HI) (<https://www.epa.gov/risk/risk-assessment-guidance-superfund-rags-part-f>) (accessed on 12 July 2022) were used to assess the carcinogenic and noncarcinogenic risks of inhaled VOCs for workers. The calculation can be expressed by the following equations:

$$LCR = \frac{C_i \times ET \times EF \times ED}{365 \times AT_{ca} \times 24} \times IUR \quad (2)$$

$$HI = \frac{C_i \times ET \times EF \times ED}{365 \times AT_{nca} \times 24} \times \frac{1}{RfC} \quad (3)$$

where C_i represents the daily environmental concentrations of VOCs ($\mu\text{g}/\text{m}^3$); ET , EF , and ED represent the daily exposure time ($\text{h} \cdot \text{d}^{-1}$), exposure frequency ($\text{d} \cdot \text{a}^{-1}$), and exposure duration (a) for workers successively, take 8 h, 250 d, and 20 a, respectively; AT_{ca} and AT_{nca} represent the average times (a) of carcinogenic and noncarcinogenic effects, take 70 a and 25 a, respectively. The selection of the above parameters refers to national standards and related research reports [34,35]. IUR represents the inhalation unit risk ($\mu\text{g}/\text{m}^3$)⁻¹ of VOCs species used for carcinogenic risk assessment, and RfC represents the reference concentration ($\mu\text{g}/\text{m}^3$) of the VOC species used for noncarcinogenic risk assessment. IUR and RfC values are derived from the U.S. EPA (United States Environmental Protection Agency) (<https://www.epa.gov/fera/risk-assessment-carcinogenic-effects>) (accessed on 12 July 2022) and the U.S. EPA IRIS (United States Environmental Protection Agency Integrated Risk Information System (https://iris.epa.gov/AtoZ/?list_type=alpha)) (accessed on 12 July 2022).

2.3.3. OH Radical Loss Rate (L_{OH}) Calculation Method

In existing studies, the photochemical O_3 creation potential (POCP) method, the maximum incremental reactivity (MIR), and the OH-reactivity-based (L_{OH}) method were created to investigate the contribution of individual VOC species to O_3 formation [36–38].

In this study, the L_{OH} value among each process was calculated. The method used to calculate the L_{OH} of individual VOCs species is described below:

$$L_{iOH} = K_{iOH} \times [VOC]_i \quad (4)$$

where L_{iOH} denotes the OH radical loss rate of VOC species i , $[VOC]_i$ represents the concentration of VOC species i , K_{iOH} denotes the reaction coefficient of VOC species i with OH radicals, and the K_{iOH} values are from Atkinson (2003) [9]. The total L_{OH} of the VOCs are the sum of the each L_{iOH} .

3. Results and Discussion

3.1. Total Concentrations and Component Characteristics of VOCs from Detailed Processes

Considering that the measured concentration of carbon disulfide is too low ($0\text{--}2 \mu\text{g}/\text{m}^3$), its analysis will be ignored. The concentrations of the measured VOC species at various sampling sites for each step are summarized in Table 2. The monitoring data show that the concentration of total VOCs (TVOCs) ranged from 1000 ± 99 to $19,700 \pm 19,000 \mu\text{g}/\text{m}^3$. The TVOCs concentrations for devulcanizing ($19,700 \pm 19,000 \mu\text{g}/\text{m}^3$) and cooling ($10,500 \pm 1600 \mu\text{g}/\text{m}^3$) were obviously higher than those in the open training ($2800 \pm 1500 \mu\text{g}/\text{m}^3$), yarding ($2300 \pm 340 \mu\text{g}/\text{m}^3$), and refining processes ($1000 \pm 99 \mu\text{g}/\text{m}^3$), indicating assuredly that high-intensity VOC concentrations were related to different processes in the recycled-rubber plant. For devulcanizing, the highest concentration was monitored, which used a lot of chemical additives and had the highest temperature among all of the steps; therefore, the organic waste gas was released more. The concentration of alkanes, alkenes, halocarbons, aromatics, ether esters, and acetylene measured in each process are also shown in Table 1. We found that aromatics were detected at the highest level ($500 \pm 180\text{--}12,700 \pm 10,400 \mu\text{g}/\text{m}^3$) in each process, and alkanes were the second group ($120 \pm 70\text{--}4700 \pm 6500 \mu\text{g}/\text{m}^3$) in devulcanizing, cooling, yarding, and refining, except that in the open training, halocarbons ($270 \pm 280 \mu\text{g}/\text{m}^3$) were detected as the second component. The values of alkenes and halocarbons were also higher in the devulcanizing with 1200 ± 1900 and $960 \pm 700 \mu\text{g}/\text{m}^3$. The remaining components as, ether esters, and acetylene were monitored with lower concentrations. The above analysis indicated that the main emission components of each process were shown to be quite similar, aromatics; and alkanes were the predominant components. Considering that the production process of recycled rubber was single, in addition to the use of chemical agents in the devulcanizing step from raw materials and finished products, others were mainly based on high temperature and physical forces.

Table 2. Concentration characteristics of VOCs components in each process ($\mu\text{g}/\text{m}^3$).

Process	Devulcanizing	Cooling	Yarding	Open Training	Refining
Alkanes	4700 ± 6500	1100 ± 200	120 ± 70	230 ± 100	320 ± 80
Alkenes	1200 ± 1900	100 ± 10	30 ± 5	20 ± 4	50 ± 10
Halocarbons	960 ± 700	190 ± 70	50 ± 12	270 ± 280	120 ± 70
Aromatics	$12,700 \pm 10,400$	9000 ± 1300	2100 ± 257	2200 ± 1100	500 ± 180
Ether esters	30 ± 35	20 ± 6	50 ± 8	7 ± 10	5 ± 2
Acetylene	20 ± 8	30 ± 1	4 ± 0	20 ± 0	30 ± 10
TVOCs	$19,700 \pm 19,000$	$10,500 \pm 1600$	2300 ± 340	2800 ± 1500	1000 ± 99

Table 3 compares the dominant components emitted by different rubber industries, in which aromatics were pointed out as the main components in each study, which were consistent with the results of this study. In addition, Gagol et al. [39] measured sulfides as the principal emission in the reclaimed rubber process at $150 \text{ }^\circ\text{C}$; Kamarulzaman et al. [24] determined the exhaust gas emission characteristics of the natural rubber drying process at $30 \text{ }^\circ\text{C}$ and $60 \text{ }^\circ\text{C}$, and detected important components such as pinene; this may be due to the fact that both studies used a different analytical technique (dynamic headspace and gas chromatography-mass spectrometry) than this study, while the raw material measured in the latter study was natural rubber. Qianqian Li et al. [40] studied the characteristics of VOCs emitted in the three main process stages of rubber products and showed that

the concentration of VOCs in the vulcanization stage was second only to the highest spray stage, alkanes and alkenes were the most important components; Huang et al. [41] measured dichloromethane as the major species in the mixing process, C₆–C₈ alkanes were dominant in the shaping process, and sulfides were released from the vulcanization process; Kwon et al. [26] pointed out that the main VOCs released during the heating process of waste rubber tires at 160 °C were alkanes, C₂–C₄ alkenes, etc. The above comparison results showed that marked regional differences occurred in the VOC emission characteristics of the recycled rubber plant, similarities and differences in VOCs emission characteristics were both found between different rubber industries, and the differences might be caused by the different product formulations, analytical techniques, and reaction conditions used in each rubber industry.

Table 3. Comparison of key VOCs components in other rubber industries.

References	Characteristic Components of the Main Process
The study	Aromatics, Alkanes
Huang et al., (2022) [41]	Dichloromethane, C ₆ –C ₈ alkanes, Sulfides, Aromatics
Kamarulzaman et al. (2019) [24]	Alkanes, Aromatics, Pinenes
Qianqian Li et al. (2019) [40]	Alkylene, Aromatics, Sulfides
Gagol et al. (2015) [39]	Aromatics, Sulfides
Kwon et al. (2015) [26]	Alkanes, C ₂ –C ₄ alkenes, Aromatics

3.2. Key Species Compositions of VOC in Process

To analyse the emitted VOC in each process as a whole, the top ten species by concentration proportion for each process were selected, as shown in Figure 2, which accounted for about 68.08 ± 7.07%, 82.20 ± 1.12%, 90.17 ± 1.29%, 83.59 ± 3.65%, and 56.93 ± 7.91% of the TVOCs, respectively. We clearly found that aromatics (49.04 ± 15.20–89.79 ± 1.97%) were the richest component, and m/p-xylene (14.63 ± 4.07–48.87 ± 3.20%) provided the highest contribution, which could be possibly regarded as the VOCs emission marker from the recycled rubber plant. The “Compilation of Air Pollutant Emission Factors” (AP-42) and the Rubber Products Industry Pollutant Emission Standard (GB27632-2011) compiled by the State Environmental Protection Administration both point out that xylene is used as the emission factor, which is consistent with the results of this study. Furthermore, compared with yarding, 1,2,4-trimethylbenzene (5.08 ± 0.07–10.04 ± 4.59%), 1,3,5-trimethylbenzene (3.82 ± 0.08–5.04 ± 2.49%), dodecane (2.31 ± 0.46–7.45 ± 5.07%), 1,2,3-trimethylbenzene (2.24 ± 0.97–4.49 ± 2.47%), and 1-ethyl-3-methylbenzene (2.27 ± 0.11–3.08 ± 1.38%) were detected in a relatively richer proportion in the other four steps that exhibited similar emission characteristics. This result is reasonable for these four steps are carried out at obviously higher temperatures than yarding, and the boiling point of trimethylbenzene and dodecane are higher than benzene and toluene, so only relatively high proportions of toluene (16.78 ± 0.58%) and benzene (15.82 ± 0.39%) were detected in the yarding step. We also found that the proportions of styrene and ethylbenzene in both devulcanizing (4.12 ± 1.93%, 4.02 ± 1.96%) and cooling (3.74 ± 0.48%, 5.39 ± 0.63%) were bigger than other steps, styrene is widely used as raw materials for synthetic rubber.

As mentioned in Section 3.1, the TVOC concentrations in the devulcanizing and cooling were rather higher than those in the other processes. Between these two high-pollution processes, the main differences appeared in the alkenes, halocarbons, and alkanes. In the devulcanizing, the concentrations of alkenes, halocarbons, and alkanes were 10, 5, and four-times higher than those in cooling, respectively, in which n-butene (4.82 ± 3.20%), 2-methylpentane (3.73 ± 2.90%), carbon tetrachloride (1.75 ± 1.04%), and tetrachloroethane (1.68 ± 10.49%) provided higher percentages. For open training, tetrachloroethane (7.60 ± 5.78%) was observed as the second largest contributor, which is used as a non-combustible solvent for rubber in industry and is easy to maintain in rubber use. The main species in refining were dodecane (7.45 ± 5.07%), methylcyclohexane (3.62 ± 4.17%), and acetylene (2.85 ± 1.59%), for both the international standard classifica-

tion and the Chinese standard classification have outlined that dodecane can be used as a chemical additive in rubber products. This result revealed that specific similarities and differences were found in the VOC emission characteristics of each process affected by raw materials, production conditions, and process equipment.

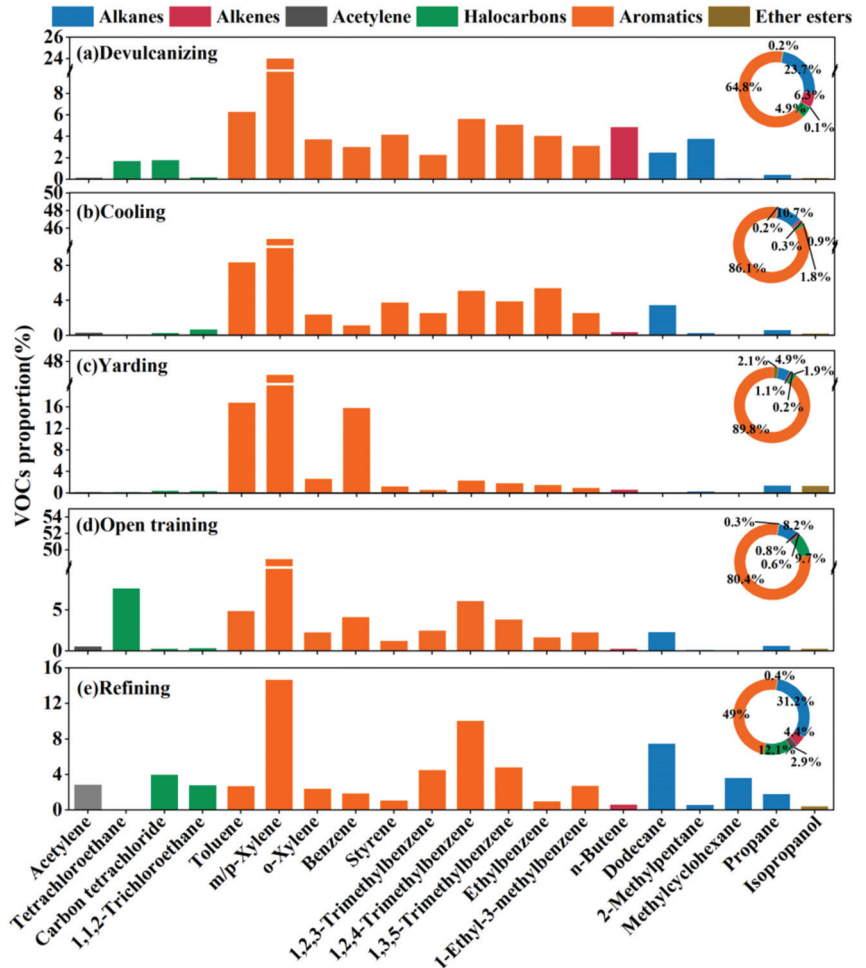


Figure 2. VOCs source profiles for the recycling plant Note: species included in the bar graph were in the top ten of the total concentrations of each profile, while the ring charts contain all measured species.

As noted above, although the main components of VOCs emitted by each process were similar, the content of different species varied greatly. In order to quantitatively compare the differences between the VOCs source profiles of different steps, we also used the coefficient of divergence method to analyze the similar degree, as illustrated in Table 4. Eight species were selected to participate in the calculation, which accounted for more than 5% of each process. We found that the divergence coefficients between the VOCs source profiles of different steps ranged from 0.308 to 0.654, among which the devulcanizing and open training were relatively similar with 0.308; the differences between the yarding and other processes were relatively higher, while the divergence coefficients were more than 0.5, the maximum was 0.654; the divergence coefficients between the other

processes were relatively small, ranging from 0.2 to 0.5, which were judged to be possibly similar. This calculation was consistent with the previous analysis results and could be considered reasonable.

Table 4. Divergence coefficients between the VOCs source profiles in each process.

Process	Devulcanizing	Cooling	Yarding	Open Training	Refining
Devulcanizing	0				
Cooling	0.416	0			
Yarding	0.615	0.654	0		
Open training	0.308	0.465	0.595	0	
Refining	0.489	0.539	0.654	0.490	0

As mentioned in the above analysis, devulcanizing, cooling, open training, and refining were confirmed as the key steps of the recycled rubber plant in this study. Table 5 lists the comparison of TVOC concentrations and characteristic species by the rubber industry in this study and other typical industrial sources. The concentration of TVOCs in the recycling rubber process was significantly lower than that of the coking industry, petrochemical, and pharmaceutical industry. Comparing the main VOCs emitted by various industries, it was found that the main emissions of m/p-xylene, trimethylbenzene, and dodecane from recycling rubber production were significantly different from that emitted by solvent, petrochemical, coking, and pharmaceutical. In addition, the proportion of aromatics was also compared in these industries, which for the rubber plant (49.04–89.79%) was significantly higher than that of other industries except pharmaceutical (67.8–95.3%). Considering the health problems of workshop equipment operators, more attention should be paid to the discharge of pollutants from the rubber industry.

Table 5. Comparison with VOCs emitted by other typical industries.

Emission Source	Concentration of TVOCs	Major Species	The Proportion of Aromatics
This study	1000–19,700 $\mu\text{g}/\text{m}^3$	m/p-Xylene, Trimethylbenzene, Dodecane	49.04–89.79%
Solvent [42]	–	Ethylene, Undecane, Benzene, Ethylbenzene, m/p-Xylene	12.91–47.48%
Petrochemical [43]	99.5–95,253.0 $\mu\text{g}/\text{m}^3$	Undecane, Benzene, Toluene, n-pentane, cis-2-butene	2.8–60.0%
Coking [44]	690.29–62,651.59 $\mu\text{g}/\text{m}^3$	Ethylene, Ethane, Benzene, Toluene, Naphthalene	12.93–93.81%
Pharmaceutical [45]	827–33,700 $\mu\text{g}/\text{m}^3$	Toluene, Dichloromethane, Ethanol, Methanol	67.8–95.3%

3.3. Health Risk Assessment among the Process

Considering the health problems of workers in a rubber factory, the health risks of the VOC species emitted by each process were assessed. In this study, according to the U.S. EPA IRIS database, only seven carcinogenic substances and 11 non-carcinogenic species were detected. The inhalation unit risk (IUR) and reference concentrations (RfC) values of these 18 VOCs are shown in Table 6. Due to carcinogenic VOCs also having non-carcinogenic risks, the carcinogenic risks of seven VOCs and the non-carcinogenic risks of 18 VOCs were evaluated in this study. Both carcinogenic and non-carcinogenic risk values are provided by US EPA. When the carcinogenic risk value LCR is less than 10^{-6} , it is regarded as an acceptable risk level, and if it is between 10^{-6} and 10^{-4} , indicating that there is a potential carcinogenic risk; when it is greater than 10^{-4} , it is regarded as a large carcinogenic risk; when the carcinogenic risk value HI > 1, it indicates that there is a non-carcinogenic health risk, and when HI < 1, it indicates that the risk is negligible (https://www.epa.gov/sites/production/files/2015-09/documents/rags3adt_complete.pdf) (accessed on 12 July 2022).

Table 6. VOCs risk assessment related parameters.

Compounds	IUR ($\mu\text{g}/\text{m}^3$) ⁻¹	RfC ($\mu\text{g}/\text{m}^3$)	Compounds	IUR ($\mu\text{g}/\text{m}^3$) ⁻¹	RfC ($\mu\text{g}/\text{m}^3$)
n-hexane		700	1,2,4-Trimethylbenzene		60
Cyclohexane		6000	1,2,3-Trimethylbenzene		60
1,3-Butadiene	0.00003	2	Trichloroethylene	0.0000041	2
Benzene	0.0000078	30	Chlorobenzene		1000
Toluene		5000	1,2,4-Trichlorobenzene		200
Ethylbenzene	0.0000025	1000	1,3,5-Trimethylbenzene		60
m/p-xylene		100	Vinyl chloride	0.0000088	100
O-xylene		100	Carbon tetrachloride	0.000006	100
Styrene		1000	1,3-Dichlorobenzene	0.000004	20

In the whole process, the HI value exceeded the threshold limit value of 1, indicating that the exhaust gas emitted by the five steps in the park had non-carcinogenic health risks. Among them, the non-carcinogenic risk mean value of the devulcanizing is the highest at 24.71, followed by cooling, reaching 13.98; the values of HI in other steps were relatively low (1.18–4.84). Figure 3 only shows seven substances with a mean HI of non-carcinogenic health risk greater than 1, including 1,2,4-trimethylbenzene, 1,3,5-trimethylbenzene, 1,2,3-trimethylbenzene, benzene, o-xylene, trichloroethylene, and m/p-xylene. For devulcanizing, the HI values of these seven substances were all higher than 1, in which m/p-xylene had the largest value of 8.62 at the mean level. The HI values of m/p-xylene, 1,2,4-trimethylbenzene, and 1,3,5-trimethylbenzene in the cooling were greater than 1, with 8.58, 1.62, and 1.24, respectively. In the yarding, higher HI values were observed for benzene and m/p-xylene (2.25, 1.94). The HI value of m/p-xylene in the opening training was also greater than 1 with the mean value of 2.48, and the HI value of each species in the refining was less than 1, which was within the acceptable risk level. The above results showed that devulcanizing and cooling would cause greater non-carcinogenic health risks; m/p-xylene and benzene were the main contributors to the HI value of the plant.

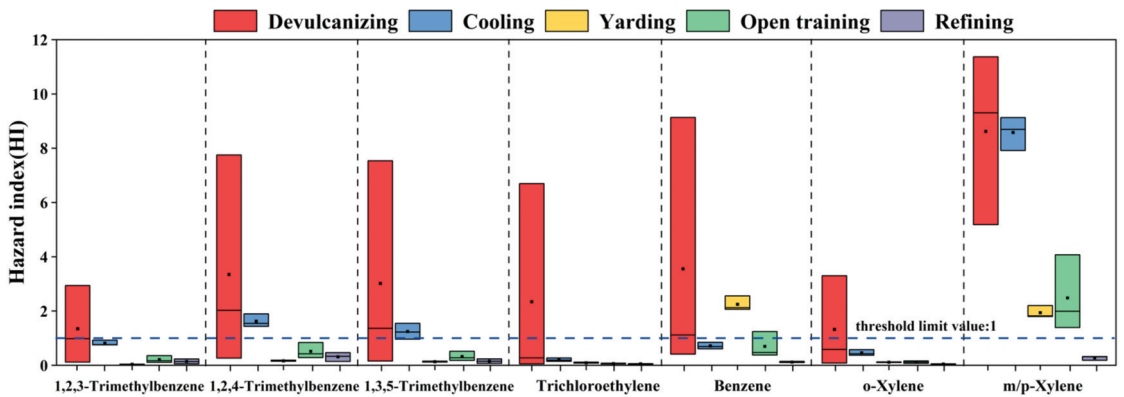


Figure 3. HI value of compounds from each process. The box represented the 25–75th percentiles of HI values. The middle square and middle line represented the mean and the median values of HI values, respectively.

The calculation results of the LCR value are shown in Figure 4, and the values of LCR in the devulcanizing, cooling, and yarding were more than 10^{-4} , which were 5.7×10^{-4} , 1.7×10^{-4} , and 2.0×10^{-4} , respectively, and were confirmed to be of relatively high carcinogenic risk. The mean LCR values of open training and refining were 7.0×10^{-5} and 2.8×10^{-5} , respectively, indicating a potential carcinogenic risk. For devulcanizing, benzene, carbon tetrachloride, and ethylbenzene were the main contributors to the LCR values, with 3.0×10^{-4} , 1.3×10^{-4} , and 1.3×10^{-4} , respectively; meanwhile, trichloroethylene

and 1,3-dichlorobenzene had LCR values between 10^{-6} and 10^{-4} . Benzene (6.0×10^{-5}), ethylbenzene (9.2×10^{-5}), carbon tetrachloride (1.0×10^{-5}), and 1,3-dichlorobenzene (2.6×10^{-6}) in cooling were potential carcinogenic risks. The LCR value of benzene in yarding was higher than 1×10^{-4} , and that of 1,3-butadiene, ethylbenzene, and carbon tetrachloride were between 10^{-6} and 10^{-4} . Both open training and refining had the same characteristic VOC species with LCR values, such as benzene (5.8×10^{-5} , 9.6×10^{-6}), ethylbenzene (7.5×10^{-6} , 1.6×10^{-6}), and carbon tetrachloride (2.9×10^{-6} , 1.6×10^{-5}). T compounds not mentioned in any of the above analyses had LCR values below 10^{-6} and were considered to be within acceptable risk levels. Therefore, devulcanizing, cooling, and yarding in the plant had greater carcinogenic risks, and the others had potential carcinogenic risks. Benzene, ethylbenzene, and carbon tetrachloride were the dominant risk compounds that should be firstly considered to protect the health of workers in the recycled rubber plant.

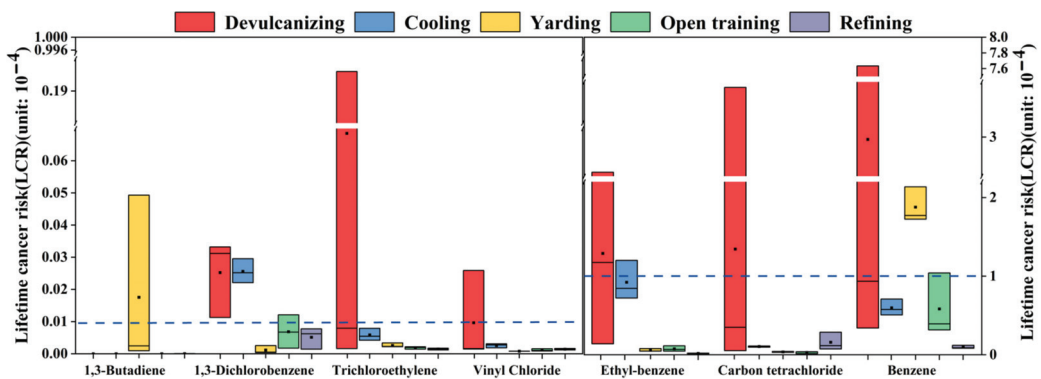


Figure 4. LCR value of compounds from each process. The box represented the 25–75th percentiles of LCR values. The middle square and middle line represented the mean and the median values of LCR values, respectively.

However, due to the exposure parameters, such as IUR, ED, EF, ET, and AT being variable, large uncertainties still exist. These VOC levels were detected over a short time, whereas the assessment was defined as assuming a 25-year and 70-year lifespan of continuous exposure. Additionally, in this study, only inhalation risks were considered, possibly resulting in inaccurate risk assessments.

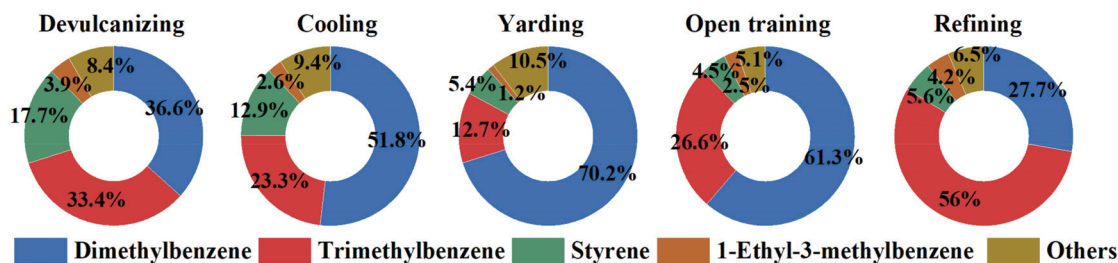
3.4. OH Radical Loss Rate

As is known to all, VOCs are the momentous precursors of ozone, and the OH loss rates (L_{OH}) and ozone formation potential are widely used to assess ozone contribution. In this study, OH radical loss rate method is used to analyze the ozone contribution in different steps in order to evaluate the environmental effects of the rubber plant. Table 7 shows the L_{OH} evaluation results of VOC components. The L_{OH} values of VOCs emitted from different processes were found in the following decreasing order: devulcanizing > cooling > open training > yarding > refining. Devulcanizing and cooling were the largest and second-largest contributors to ozone, accounting for 56.56% and 29.19%, for the superior concentrations of aromatics and alkenes, which had the stronger propensity to ozone formation. Other steps (open training, yarding, and refining) had the lower L_{OH} values due to the low levels of active constituents, such as aromatics and alkenes, accounting for 7.04%, 4.84%, and 2.37%, respectively. The L_{OH} contribution characteristics of different kinds of VOCs were also displayed in Table 7. The clear result was that aromatics were the most abundant component in the whole plants, with the percentage ranging from 72.11% to 93.74%, followed by alkenes (2.81–20.62%) and alkanes (1.69–12.97%). Distinctly, it is essential to focus on the emission of aromatics.

Table 7. The L_{OH} contribution of VOCs from all the recycling processes (s^{-1}).

Process	Alkanes	Alkenes	Aromatics	L_{OH}
Devulcanizing	250 ± 340	720 ± 1100	2500 ± 2200	3500 ± 3700
Cooling	70 ± 16	56 ± 6	1700 ± 240	1800 ± 260
Yarding	5 ± 2	14 ± 2	280 ± 34	300 ± 40
Open training	15 ± 8	12 ± 2	410 ± 220	430 ± 230
Refining	20 ± 4	22 ± 4	110 ± 46	150 ± 44

For this reason, in this study, we conducted a further detailed analysis of the high-contribution species of L_{OH} in aromatics. The contribution proportions (%) for individual species in aromatics with their homologous L_{OH} values are shown in Figure 5. Dimethylbenzene (m/p-xylene and o-xylene), trimethylbenzene (1,3,5-trimethylbenzene, 1,2,4-trimethylbenzene and 1,2,3-trimethylbenzene), and styrene were found to be the main dominant species for almost all processes, accounting for 87.76%, 87.99%, 88.30%, 92.38%, and 89.26%, respectively. Among them, the most key species for L_{OH} were m/p-xylene (25.26–67.87%). Therefore, for the recycled rubber plant in this study, the emission level of aromatics, especially m/p-xylene, should be prioritized for control through L_{OH} activity evaluation. Further work is required for further in-depth study of the mechanism of ozone formation in recycled rubber plants.

**Figure 5.** The L_{OH} contribution of aromatics in each process.

4. Conclusions

A total of 15 samples from the typical recycled rubber plant were collected by summa canisters in a typical recycled rubber plant, and 100 VOC species were detected by the GC/MS-FID system. We observed that aromatics and alkanes were the predominant components in the whole process, followed by halocarbons and alkene. The result of key species compositions of VOC in the process showed that m/p-xylene could be possibly regarded as a VOC emission marker. We also found that specific similarities and differences in VOC emission characteristics in each process were affected by raw materials, production conditions, and process equipment; n-butene provided higher percentages in devulcanizing, for open training, tetrachloroethane was observed as the second largest contributor, dodecane, methylcyclohexane, and acetylene were the main species in refining, these were also confirmed by the coefficient of divergence method. The assessments of health risks showed that the non-carcinogenic risk value of the devulcanizing is the highest, the values of LCR in the devulcanizing, cooling, and yarding were more than 10^{-4} and were confirmed to be of relatively high carcinogenic risk, and open training and refining had potential carcinogenic risks. In the plant, m/p-xylene and benzene were the main non-carcinogenic species, while benzene, ethylbenzene, and carbon tetrachloride were the dominant risk compounds. In the evaluation results of L_{OH} , devulcanizing and cooling steps were the largest and second largest contributor, and aromatics were the most abundant component to ozone formation, in which m/p-xylene was the most key individual species and should be prioritized for control. The key species detected in this study provide important information for the formulation of emission reduction policies.

Author Contributions: Conceptualization, S.W., H.Z., Q.H., Y.W. and X.W.; methodology, S.W., Y.C. and Q.H.; validation, S.W. and Y.Y.; formal analysis, S.W.; investigation, S.W., Y.Y., X.G. and Y.C.; resources, Q.H.; data curation, S.W., Y.Y., X.G., H.Z. and Q.H.; writing—original draft preparation, S.W.; writing—review and editing, Q.H.; visualization, S.W.; supervision, H.Z., Q.H., Y.W. and X.W.; project administration, S.W.; funding acquisition, Q.H. All authors have read and agreed to the published version of the manuscript.

Funding: This research was funded by the Environmental Monitoring Center Station of Taiyuan, the National Natural Science Foundation of China (42077201); the Project Supported by Shanxi Basic Research Program (202103021223300); the Shanxi Applied Basic Research Program Project (201901D111250).

Institutional Review Board Statement: The study did not require ethical approval.

Informed Consent Statement: Informed consent was obtained from all subjects involved in the study.

Data Availability Statement: Data are available from the authors at reasonable written request after authorization by the School of Environmental Science and Engineering, Taiyuan University of Science and Technology, China.

Acknowledgments: We would like to thank Yucheng Yan and Xueying Gao for contributed to the data analysis framework design.

Conflicts of Interest: The authors declare no conflict of interest.

Abbreviations

Abbreviation	Full Name
VOCs	volatile organic compounds
SOA	secondary organic aerosols
O ₃	ozone
FID	flame ionization detector
MSD	mass spectrometry detector
EI	electron ionization
PAMS	photochemical assessment monitoring stations
LCR	lifetime cancer risk
HI	hazard index
ET	exposure time
EF	exposure frequency
ED	exposure duration
AT	average time
IUR	inhalation unit risk
RfC	reference concentration
U.S. EPA	United States Environmental Protection Agency
U.S. EPA IRIS	United States Environmental Protection Agency Integrated Risk Information System
TVOCs	total VOCs

References

- Ding, X.; Wang, X.; Gao, B.; Fu, X.-X.; He, Q.; Zhao, X.-Y.; Yu, J.; Zheng, M. Tracer-based estimation of secondary organic carbon in the Pearl River Delta, south China. *J. Geophys. Res.* **2012**, *117*, 5313. [[CrossRef](#)]
- Guo, S.; Hu, M.; Guo, Q.; Zhang, X.; Zheng, M.; Zheng, J.; Chang, C.C.; Schauer, J.J.; Zhang, R. Primary Sources and Secondary Formation of Organic Aerosols in Beijing, China. *Environ. Sci. Technol.* **2012**, *46*, 9846–9853. [[CrossRef](#)]
- Geng, F.; Tie, X.; Xu, J.; Zhou, G.; Peng, L.; Gao, W.; Tang, X.; Zhao, C. Characterizations of ozone, NO_x, and VOCs measured in Shanghai, China. *Atmos. Environ.* **2008**, *42*, 6873–6883. [[CrossRef](#)]
- Wang, M.; Shao, M.; Lu, S.-H.; Yang, Y.-D.; Chen, W.-T. Evidence of coal combustion contribution to ambient VOCs during winter in Beijing. *Chin. Chem. Lett.* **2013**, *24*, 829–832. [[CrossRef](#)]
- Wang, Q.; Li, S.; Dong, M.; Li, W.; Gao, X.; Ye, R.; Zhang, D. VOCs emission characteristics and priority control analysis based on VOCs emission inventories and ozone formation potentials in Zhoushan. *Atmos. Environ.* **2018**, *182*, 234–241. [[CrossRef](#)]
- Li, J.; Li, H.; He, Q.; Guo, L.; Zhang, H.; Yang, G.; Wang, Y.; Chai, F. Characteristics, sources and regional inter-transport of ambient volatile organic compounds in a city located downwind of several large coke production bases in China. *Atmos. Environ.* **2020**, *233*, 117573. [[CrossRef](#)]

7. Lyu, X.; Guo, H.; Wang, Y.; Zhang, F.; Nie, K.; Dang, J.; Liang, Z.; Dong, S.; Zeren, Y.; Zhou, B.; et al. Hazardous volatile organic compounds in ambient air of China. *Chemosphere* **2020**, *246*, 125731. [[CrossRef](#)]
8. Abas, M.R.B.; Mohamad, S. Hazardous (Organic) Air Pollutants. In *Encyclopedia of Environmental Health*, 2nd ed.; Nriagu, J., Ed.; Elsevier: Oxford, UK, 2011; pp. 405–416.
9. Atkinson, R.; Arey, J. Atmospheric Degradation of Volatile Organic Compounds. *ChemInform* **2004**, *35*, 4605–4638. [[CrossRef](#)]
10. He, Q.; Yan, Y.; Zhang, Y.; Wang, X.; Wang, Y. Coke workers' exposure to volatile organic compounds in northern China: A case study in Shanxi Province. *Environ. Monit Assess* **2015**, *187*, 359. [[CrossRef](#)]
11. Li, B.; Ho, S.S.H.; Li, X.; Guo, L.; Chen, A.; Hu, L.; Yang, Y.; Chen, D.; Lin, A.; Fang, X. A comprehensive review on anthropogenic volatile organic compounds (VOCs) emission estimates in China: Comparison and outlook. *Environ. Int.* **2021**, *156*, 106710. [[CrossRef](#)]
12. Dörter, M.; Odabasi, M.; Yenisoý-Karakaş, S. Source apportionment of biogenic and anthropogenic VOCs in Bolu plateau. *Sci. Total Environ.* **2020**, *731*, 139201. [[CrossRef](#)] [[PubMed](#)]
13. Wu, R.; Bo, Y.; Li, J.; Li, L.; Li, Y.; Xie, S. Method to establish the emission inventory of anthropogenic volatile organic compounds in China and its application in the period 2008–2012. *Atmos. Environ.* **2016**, *127*, 244–254. [[CrossRef](#)]
14. Sun, W.; Shao, M.; Granier, C.; Liu, Y.; Ye, C.; Zheng, J. Long-term Trends of Anthropogenic SO₂, NO_x CO, and NMVOCs Emissions in China. *Earth's Future* **2018**, *6*, 1112–1133. [[CrossRef](#)]
15. Zheng, B.; Tong, D.; Li, M.; Liu, F.; Hong, C.; Geng, G.; Li, H.; Li, X.; Peng, L.; Qi, J.; et al. Trends in China's anthropogenic emissions since 2010 as the consequence of clean air actions. *Atmos. Chem. Phys. Discuss.* **2018**, *18*, 14095–14111. [[CrossRef](#)]
16. Ou, J.; Zheng, J.; Yuan, Z.; Guan, D.; Huang, Z.; Yu, F.; Shao, M.; Louie, P.K.K. Reconciling discrepancies in the source characterization of VOCs between emission inventories and receptor modeling. *Sci. Total Environ.* **2018**, *628–629*, 697–706. [[CrossRef](#)]
17. Dumanoglu, Y.; Kara, M.; Altioik, H.; Odabasi, M.; Elbir, T.; Bayram, A. Spatial and seasonal variation and source apportionment of volatile organic compounds (VOCs) in a heavily industrialized region. *Atmos. Environ.* **2014**, *98*, 168–178. [[CrossRef](#)]
18. Saeaw, N.; Thepanondh, S. Source apportionment analysis of airborne VOCs using positive matrix factorization in industrial and urban areas in Thailand. *Atmos. Pollut. Res.* **2015**, *6*, 644–650. [[CrossRef](#)]
19. He, Q.; Yan, Y.; Li, H.; Zhang, Y.; Chen, L.; Wang, Y. Characteristics and reactivity of volatile organic compounds from non-coal emission sources in China. *Atmos. Environ.* **2015**, *115*, 153–162. [[CrossRef](#)]
20. Wei, W.; Cheng, S.; Li, G.; Wang, G.; Wang, H. Characteristics of volatile organic compounds (VOCs) emitted from a petroleum refinery in Beijing, China. *Atmos. Environ.* **2014**, *89*, 358–366. [[CrossRef](#)]
21. Markl, E.; Lackner, M. Devulcanization Technologies for Recycling of Tire-Derived Rubber: A Review. *Materials* **2020**, *13*, 1246. [[CrossRef](#)]
22. Hoven, V.P.; Rattanakarun, K.; Tanaka, Y. Reduction of offensive odor from natural rubber by odor-reducing substances. *J. Appl. Polym. Sci.* **2004**, *92*, 2253–2260. [[CrossRef](#)]
23. Idris, N.; Kamarulzaman, N.; Mohd Nor, Z. Determination of Volatile Fatty Acids from Raw Natural Rubber Drying Activity by Thermal Desorption-Gas Chromatography. *Chem. Eng. Trans.* **2012**, *30*, 175–180.
24. Kamarulzaman, N.H.; Le-Minh, N.; Fisher, R.M.; Stuetz, R.M. Quantification of VOCs and the development of odour wheels for rubber processing. *Sci. Total Environ.* **2019**, *657*, 154–168. [[CrossRef](#)] [[PubMed](#)]
25. Pajarito, B.B.; Castañeda, K.C.; Jeresano, S.D.M.; Repoquit, D.A.N. Reduction of Offensive Odor from Natural Rubber Using Zinc-Modified Bentonite. *Adv. Mater. Sci. Eng.* **2018**, *2018*, 9102825. [[CrossRef](#)]
26. Kwon, E.E.; Oh, J.-I.; Kim, K.-H. Polycyclic aromatic hydrocarbons (PAHs) and volatile organic compounds (VOCs) mitigation in the pyrolysis process of waste tires using CO₂ as a reaction medium. *J. Environ. Manag.* **2015**, *160*, 306–311. [[CrossRef](#)]
27. Adhikari, B.; De, D.; Maiti, S. Reclamation and recycling of waste rubber. *Prog. Polym. Sci.* **2000**, *25*, 909–948. [[CrossRef](#)]
28. Rajan, V.V.; Dierkes, W.K.; Joseph, R.; Noordermeer, J.W.M. Science and technology of rubber reclamation with special attention to NR-based waste latex products. *Prog. Polym. Sci.* **2006**, *31*, 811–834. [[CrossRef](#)]
29. Wang, K. Study on the Composition Spectrum of Coal Combustion in Power Plants and Risk Assessment of Heavy Metals. Master's Thesis, Taiyuan University of Technology, Taiyuan, China, 2016. (In Chinese).
30. Bolden, A.; Kwiatkowski, C.; Colborn, T. New look at BTEX: Are ambient levels a problem. *Environ. Sci. Technol.* **2015**, *49*, 5261–5276. [[CrossRef](#)]
31. Nie, E.; Zheng, G.; Ma, C. Characterization of odorless pollution and health risk assessment of volatile organic compound emissions in swine facilities. *Atmos. Environ.* **2020**, *223*, 117233. [[CrossRef](#)]
32. Cheng, Z.; Sun, Z.; Zhu, S.; Lou, Z.; Zhu, N.; Feng, L. The identification and health risk assessment of odor emissions from waste landfilling and composting. *Sci. Total Environ.* **2019**, *649*, 1038–1044. [[CrossRef](#)]
33. Jia, H.; Gao, S.; Duan, Y.; Fu, Q.; Che, X.; Xu, H.; Wang, Z.; Cheng, J. Investigation of health risk assessment and odor pollution of volatile organic compounds from industrial activities in the Yangtze River Delta region, China. *Ecotoxicol. Env. Saf.* **2021**, *208*, 111474. [[CrossRef](#)] [[PubMed](#)]
34. Sivret, E.C.; Wang, B.; Parsci, G.; Stuetz, R.M. Prioritisation of odorants emitted from sewers using odour activity values. *Water Res.* **2016**, *88*, 308–321. [[CrossRef](#)] [[PubMed](#)]
35. Durmusoglu, E.; Taspinar, F.; Karademir, A. Health risk assessment of BTEX emissions in the landfill environment. *J. Hazard. Mater.* **2010**, *176*, 870–877. [[CrossRef](#)] [[PubMed](#)]

36. Carter, W.P.L. Development of Ozone Reactivity Scales for Volatile Organic Compounds. *Air Waste* **1994**, *44*, 881–899. [[CrossRef](#)]
37. Chameides, W.L.; Fehsenfeld, F.; Rodgers, M.O.; Cardelino, C.; Martinez, J.; Parrish, D.; Lonneman, W.; Lawson, D.R.; Rasmussen, R.A.; Zimmerman, P.; et al. Ozone precursor relationships in the ambient atmosphere. *J. Geophys. Res. Atmos.* **1992**, *97*, 6037–6055. [[CrossRef](#)]
38. Derwent, R.G.; Jenkin, M.E.; Saunders, S.M. Photochemical ozone creation potentials for a large number of reactive hydrocarbons under European conditions. *Atmos. Environ.* **1996**, *30*, 181–199. [[CrossRef](#)]
39. Gagol, M.; Boczkaj, G.; Haponiuk, J.; Formela, K. Investigation of volatile low molecular weight compounds formed during continuous reclaiming of ground tire rubber. *Polym. Degrad. Stab.* **2015**, *119*, 113–120. [[CrossRef](#)]
40. Li, Q.; Su, G.; Li, C.; Wang, M.; Tan, L.; Gao, L.; Mingge, W.; Wang, Q. Emission profiles, ozone formation potential and health-risk assessment of volatile organic compounds in rubber footwear industries in China. *J. Hazard. Mater.* **2019**, *375*, 52–60. [[CrossRef](#)]
41. Huang, H.; Wang, Z.; Dai, C.; Guo, J.; Zhang, X. Volatile organic compounds emission in the rubber products manufacturing processes. *Environ. Res.* **2022**, *212*, 113485. [[CrossRef](#)]
42. Liu, Z.; Cao, Z.; Zhao, J.; Fang, Y.; Wei, W. Characteristics of VOCs Emission Components in Typical Solvents Source Industries in Tianjin. *IOP Conf. Ser. Earth Environ. Sci.* **2021**, *781*, 032010. [[CrossRef](#)]
43. Lv, D.; Lu, S.; Tan, X.; Shao, M.; Xie, S.; Wang, L. Source profiles, emission factors and associated contributions to secondary pollution of volatile organic compounds (VOCs) emitted from a local petroleum refinery in Shandong. *Environ. Pollut.* **2021**, *274*, 116589. [[CrossRef](#)] [[PubMed](#)]
44. Wang, H.; Hao, R.; Fang, L.; Nie, L.; Zhang, Z.; Hao, Z. Study on emissions of volatile organic compounds from a typical coking chemical plant in China. *Sci Total Environ.* **2021**, *752*, 141927. [[CrossRef](#)] [[PubMed](#)]
45. Cheng, N.; Jing, D.; Zhang, C.; Chen, Z.; Li, W.; Li, S.; Wang, Q. Process-based VOCs source profiles and contributions to ozone formation and carcinogenic risk in a typical chemical synthesis pharmaceutical industry in China. *Sci. Total Environ.* **2021**, *752*, 141899. [[CrossRef](#)] [[PubMed](#)]

Article

Study on Permeability and Flame Retardancy of Coal Aerosol Atomized by Ultrasonic Wave

Wenbin Zhao, Fangshun Liu, Bo Liu, Yang Liu, Huaisheng Cao, Qing Tan and Jinfeng Wang *

School of Safety and Environmental Engineering, Shandong University of Science and Technology, Qingdao 266590, China

* Correspondence: wangjf@sdust.edu.cn

Abstract: In order to analyze the permeability and particle size distribution of atomized aerosol in different coal particle sizes and to explore the inhibition performance of an atomized inhibitor in different atomization times and positions, the following conclusions are obtained by ultrasonic atomization device: The results of permeability experiment show that the particle size of aerosol decreases with the increase of atomization frequency. In addition, with the particle size of the coal sample decreasing from 5 cm to 0.6 cm, the penetration ratio of aerosol in coal decreases from 64.2% to 15.5% due to the interception of large particle size water mist by dense coal. The aerosol with a particle size of 2–4 μm has better permeability in crushed coal. The flame retardant experiment shows that compared with the raw coal, the aliphatic hydrocarbon of the atomized coal decreases by 75.9%, the aromatic hydrocarbon decreases by 57.5%, and the flame retardant effect is good. Meanwhile, the extension of solution atomization time will further enhance the flame retardant ability of ultrasonic atomized aerosol.

Keywords: aerosol; permeability; particle size; functional groups; flame retardant

Citation: Zhao, W.; Liu, F.; Liu, B.; Liu, Y.; Cao, H.; Tan, Q.; Wang, J. Study on Permeability and Flame Retardancy of Coal Aerosol Atomized by Ultrasonic Wave. *Atmosphere* **2022**, *13*, 1415. <https://doi.org/10.3390/atmos13091415>

Academic Editors: Roberto Alonso González Lezcano, Francesco Nocera, Rosa Giuseppina Caponetto and Ian Colbeck

Received: 10 July 2022

Accepted: 30 August 2022

Published: 1 September 2022



Copyright: © 2022 by the authors. Licensee MDPI, Basel, Switzerland. This article is an open access article distributed under the terms and conditions of the Creative Commons Attribution (CC BY) license (<https://creativecommons.org/licenses/by/4.0/>).

1. Introduction

The spontaneous combustion of coal is one of the main threats to coal mine safety. The fires may cause casualties, resulting in economic losses and environmental pollution [1–4]. Many scholars have studied the spontaneous combustion of coal, its prevention, and control technologies. Topics covered include the oxygen consumption rate of the remaining coal as well as the distribution of the temperature field [5–7]. However, the uncertainty of the location of spontaneous combustion in the goaf brings many difficulties to its prevention and control. Commonly used fire-fighting technologies in goaf are grouting, sealing, gel, inert medium injection, two-phase foam, and three-phase foam [8–12]. The traditional fire-fighting technology is mainly based on plugging to prevent oxygen from contacting and reacting with residual coal. However, due to the large area and complex structure of the goaf, the traditional fire prevention measures cannot completely block the air leakage. Under the above background, “inert gas injection fire prevention” came into being, which can penetrate deep into the goaf, reduce the oxygen concentration in the area, and make the residual coal fundamentally lose its spontaneous combustion ability. Unfortunately, due to the influence of gas mobility in the goaf, it is difficult for the inert gas infiltrated into the gob to stay for a long time, resulting in a decrease in the fire-fighting effect [13–16]. Materials containing various flame retardants cannot only reach the inside of the goaf but also adhere to the surface of the coal, which makes us consider using flame retardant materials to suppress the spontaneous combustion of coal effectively.

At present, flame retardant materials can be applied to spontaneous combustion areas in goafs through spraying, foam, aqueous solutions, colloids, slurries, and solids. However, due to the volume of the material itself, the fire-fighting effect is not good [17,18]. In addition, due to the small particle size of the aerosol, it has the advantages of good

diffusivity and adhesion in the void and crevice structure. By atomizing the flame retardant into aerosol and injecting it into the goaf, it is widely used in various fire prevention and control [19]. Scholars started with equipment parameters (such as working frequency and power consumption) and working parameters (such as flow rate and liquid properties) to explore the influencing factors of aerosol atomization parameters to prepare the best aerosol fireproof materials [20,21]. Luo Zhenmin used a 1 m^3 airtight test box to study the inhibitory effect of aerosol fire extinguishing agents on coal fires within a 30-min soaking time. The experimental results showed that the aerosol fire extinguishing agent has a certain inhibitory effect on the combustion of coal and can extinguish the gas-phase combustion flame on the surface of the coal. The aerosol used in the experiment is composed of solid particles with low vapor pressure and slow sedimentation under the action of gravity [22]. Different from traditional atomization, ultrasonic atomization sprays' fine droplets from the liquid film formed on the ultrasonic vibration surface, thereby atomizing to form aerosol particles with controllable and stable particle size distribution. Ultrasonic atomization can be more energy efficient, only the mechanical vibrations generated by the supplied electrical energy are used to generate droplets. Kooij conducted the first systematic study of the droplet size distribution for different nebulizer technologies and showed that median droplet size varied proportionally with capillary wavelength [23]. Kiran A. Ramisetty found that with increasing ultrasonic intensity, the droplet size distribution changed from a narrow range to a wider range [24]. To verify the predictability of the droplet size produced, Dalmoro, A. used three empirical correlations to predict droplet size that took into account feed solution properties/process parameters [25]. Kudo determined the relationship between droplet size distribution and ultrasonic frequency and proposed the generation mechanism of ultrasonic nano-mist based on the amount of water vapor around the liquid column. The mechanism was to affect the number and size distribution of aerosols by changing the solution density and power intensity of the ultrasonic atomizer [26]. Tang used the aerosol prepared by the ultrasonic atomizer to suppress the spontaneous combustion of coal, and the effect was remarkable [27]. Li prepared iron-based composite adsorbents with biochar as a carrier by coprecipitation and sol-gel methods, indicating that the removal of $\text{Hg}0$ by modified biochar mainly includes adsorption and oxidation processes [28].

Ultrasonic atomization technology is an effective method for preparing cold aerosols. The principle is to convert the specific electrical energy generated by the circuit system into ultrasonic wave energy through the high-frequency oscillation of the atomizing vibrator, thereby atomizing to form aerosol particles with controllable and stable particle size distribution. The ejection of droplets from vibrating surfaces has been explained by the capillary wave hypothesis, which posits that the instability of the surface waves of solutions is due to ultrasonic atomization. When the ultrasonic wave of fixed frequency acts on the interface of gas and liquid, the interface will produce high-frequency vibration. When the surface tension wave increases to a certain amplitude, atomization will be generated at the peak position. The atomization model figure is shown in Figure 1.

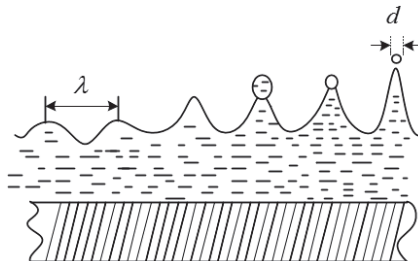


Figure 1. Atomization model diagram.

In Figure 1, λ is the capillary wavelength and d is the average particle size.

In the early ultrasonic atomization research, Lang proposed the ultrasonic capillary wave length formula based on the Kelvin equation [29]:

$$\lambda = \left(\frac{8\pi\sigma}{\rho f^2} \right)^{1/3} \quad (1)$$

Assuming that the instantaneous amplitude of the liquid film atomization is proportional to the wavelength of the capillary wave, the ratio is K , and the expression of d is:

$$d = \frac{3}{4\pi^2 K^2} \left(\frac{\sigma}{\pi^2 \rho f^2} \right)^{1/3} = \text{const.} \cdot \frac{\sigma}{\rho f^2 \lambda^2} \quad (2)$$

where σ is the surface tension, mN/m; ρ is the density, g/cm³; f is the ultrasonic frequency, MHz. It can be seen that the average particle size is related to liquid surface tension, liquid density, ultrasonic frequency, and capillary wave wavelength.

In summary, scholars have demonstrated that aerosols of chemical inhibitors can play a flame retardant role and also obtained the relevant laws of droplet size distribution. However, there are caving voids in the goaf, which will affect the passage of aerosols of different particle sizes in the gob. There are few studies on the penetration and flame retardant effect of aerosols with different particle sizes under different void structures. Therefore, based on the analysis of the atomization mechanism, we used the permeability experimental device to test the permeability of aerosol particles through coal samples with different particle sizes. At the same time, the flame retardant effect of aerosol under the conditions of different flame retardants and atomization time was analyzed by Fourier transform infrared spectroscopy. This paper proves that the ultrasonic atomized aerosol can pass through the gap between the coal bodies to reach the deep part of the goaf and play a flame retardant effect, which is an effective means to suppress the spontaneous combustion of coal in the gob.

2. Experimental Equipment, Materials and Methods

Figure 2 shows the relationship between the three experiments (i.e., the ultrasonic atomization experiment, the permeability experiment, and the flame retardancy experiment) in this paper. Through experiment 1, the MgCl₂ flame retardant solution was atomized into aerosol particles, and then the permeability of the aerosol particles was analyzed through experiment 2. Finally, in experiment 3, the flame retardant properties of aerosol particles on the coal surface were analyzed.

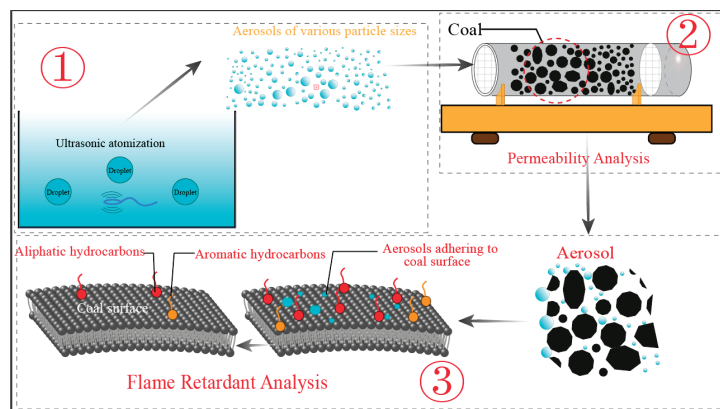


Figure 2. Experimental flow chart. The experiment 1 is the preparation of aerosol; Experiment 2 is aerosol permeability experiment; Experiment 3 is an aerosol flame retardant experiment.

2.1. Preparation of Coal Samples

Bituminous coal from the Jining mining area in the southwest of Shandong Province was selected as the experimental coal sample. According to the coal particle size classification standard (Table 1), a jaw crusher to crush and sieve the coal samples is used. The flame retardant (MgCl_2) used in the experiment was of chemical purity grade (i.e., purity > 99.5%) and was purchased from China Shandong Chemical Reagent Co., Ltd. (Shandong, China).

Table 1. Coal particle size classification.

Serial Number	Particle Size (cm)
1	>10
2	5~10
3	2.5~5
4	1.3~2.5
5	0.6~1.3
6	less than 0.6

2.2. Ultrasonic Atomization

The ultrasonic atomizer used in this experiment is mainly composed of a piezoelectric ceramic vibrator (UL106128AWG) and a small fan (KS-16-3.0BU-PCB). The vibrator (yellow area) atomizes the added flame retardant solution into aerosol particles. The upper left side of the solution is connected to a speed-regulated small fan (driven by a piezoelectric transducer, Shenzhen Youbisheng Technology Co., Ltd., Jinjiang, China), which is used to transfer aerosol particles. The experimental equipment has the function of changing the amplitude of the atomizer and the air volume delivery by adjusting the output power, as shown in Figure 3. The frequency of the ultrasonic atomizer is 3 MHz, according to the previous test.

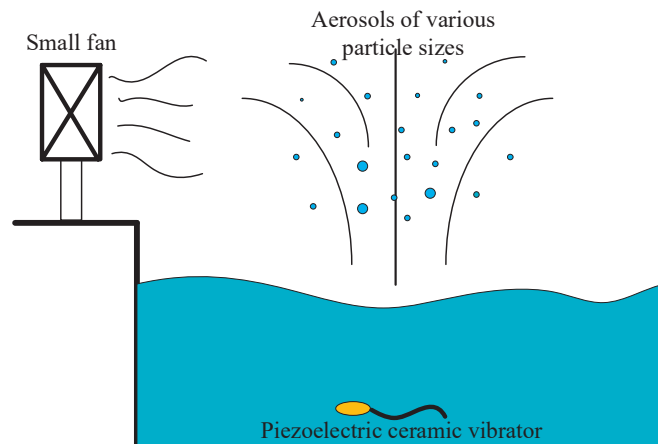


Figure 3. Ultrasonic atomization device.

2.3. Permeability Test

In order to ensure the flame retardant properties of aerosols, it is necessary to pay attention to the permeability of aerosols in the coal void structure in the goaf. The experiment adopts the self-designed device, which is mainly divided into two parts: the permeation device and the flow meter, as shown in Figure 4. The coal sample tube is placed horizontally, the effective length of the filled coal sample is 40 cm, and the diameter is 7 cm. The particle size distribution of the coal sample is shown in Table 1. Both sides of the coal body are fixed with metal mesh screens to prevent the collapse of the coal body structure.

When the aerosol particles generated by the ultrasonic atomization device traveled through the sample tank, some of the aerosol particles were trapped by the coal sample filled inside. By recording the mass of aerosol particles before and after passing through the sample tank, we tested their permeability through coal samples of different particle sizes. So as to avoid the influence of other factors, pure water was selected as the atomization solution, the atomization frequency was 3 MHz, and the atomization time was 10 min.

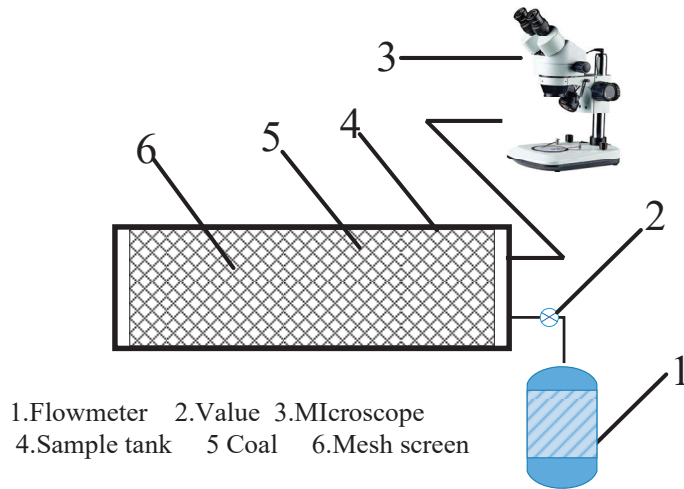


Figure 4. Schematic diagram of the device.

Specific steps are as follows:

- (1) The aerosol produced by the ultrasonic atomizing device was passed through the device shown in Figure 4, and its air tightness was tested;
- (2) Turned on the switch of the atomization device and first tested the particle size of the aerosol droplets in the front and rear of the empty pipe (without coal sample);
- (3) The coal sample was tightly filled into the test section tube, and the two sides were fixed with metal mesh sieves to test the particle size change of aerosol after passing through the coal sample;
- (4) The same group of experiments was tested three times, and the test data were recorded;
- (5) Changed the particle size of the filled coal sample, and tested the particle size of 3.0–2.5, 2.5–2.0, 2.0–1.5, 1.5–1.0, 1.0–0.6, and <0.6, respectively;
- (6) Summarized and organized test data and conducted data analysis.

2.4. CCD Image Acquisition System

In order to determine the changing rule of atomized particle size at different levels, a layer of petroleum jelly was evenly daubed on the glass slide and passed through the aerosol atomization field at a uniform speed at the back of the coal sample tank. Then, the slide was moved to the microscope for observation, and the image was transferred to the computer through the CCD image acquisition system (QA3020CNC (T) including microscope, image acquisition card, and computer), as shown in Figure 5. Image processing using image-Pro Plus software.

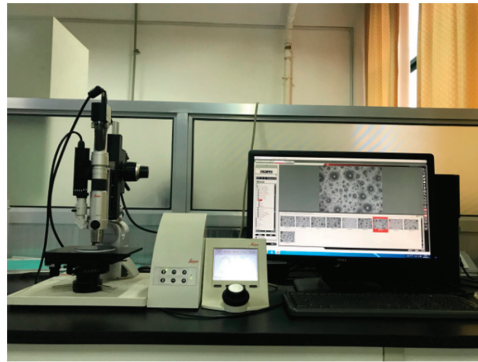


Figure 5. CCD image acquisition system.

Details of how images are processed:

- ① Read image;

Opened Image-Pro Plus software and imported the images to be processed. The image was in tif format with 1600×1200 pixels.

- ② Add ruler;

According to the pixel and size of the picture, it can be calculated that 3.8 pixels correspond to a length of $1 \mu\text{m}$, and the scale parameters were set: the length is $20 \mu\text{m}$, as shown in Figure 6.

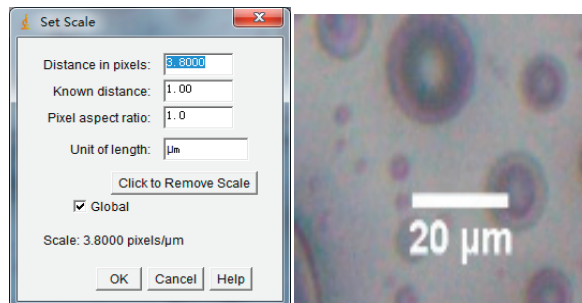


Figure 6. Set the scale.

- ③ Select the area to be processed;

The processing area is selected by calling rectangle, ellipse, and irregular tools. The selected area needs to be fresh and bright, and the color contrast is distinct, which can clearly show the outline of the droplets, as shown in Figure 7.

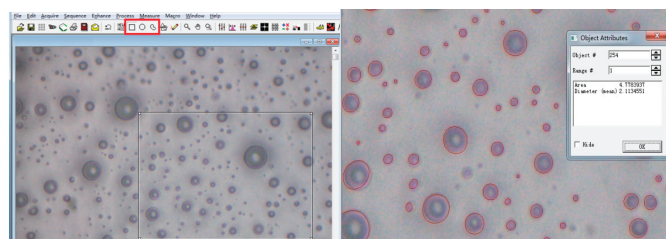


Figure 7. Calling the tool.

④ Droplet boundary selection;

Droplet boundaries were selected by setting a threshold.

⑤ Smooth border;

When the boundary of droplet particle size was selected to be irregular, the boundary can be made regular by smoothing the curve.

⑥ Particle size measurement and output.

2.5. Flame Retardant Test

In order to test the flame retardant properties of the aerosol, 200 mL of $MgCl_2$ solution with a concentration of 15% was selected, and the atomization time was set to 30 min and 60 min, in turn. Since $MgCl_2$ is easily soluble in water and easily atomized by an ultrasonic atomizing device, $MgCl_2$ was selected as the inhibitor in the experiment. The $MgCl_2$ was atomized by an ultrasonic atomizer, and the formed droplets entered the coal sample tank with the help of the airflow of the fan of the atomization device and then were discharged from the outlet of the coal sample tank. The size of the coal sample is 0.5–0.7 cm, and the atomization frequency is 3 MHz. Next, the coal sample was taken from the front and rear ends of the coal sample tank, placed in a vacuum drying oven, dried at 40 °C for 24 h, and then mixed with KBr at a mass ratio of 1:100, dispersed and ground in an agate mortar for about 3 min. The mixture was pressed into flakes under the pressure of 20 MPa, and the pressing time was 1–2 min. Then the knob was rotated to release the pressure, and the coal sample was taken out to obtain a thin sheet with a diameter of 0.9 mm and a thickness of 0.1 mm. The transmission spectrum of the coal sample slices was obtained using a Nicolet iS10 Fourier (Beijing Jinli Tongjian Environmental Technology Co., Ltd., Beijing, China.) transform infrared spectrometer. The analyzer has a standard scan error of 4 cm^{-1} . The obtained spectral range is 400–4000 cm^{-1} , and the number of scans for both background and sample is 64. The flame retardant properties of $MgCl_2$ aerosols were analyzed by the absorption peaks of the obtained spectra.

3. Results

3.1. The Influence of Frequency on Atomized Particle Size

In the experiment, pure water was used as the atomization object, and the ultrasonic atomization device (Figure 3) and CCD image acquisition system (Figure 5) were used to measure the aerosol particle size at different frequencies. The particle size distribution is shown in Figure 8. As shown in the figure, as the atomization frequency increases, the atomization particle size map gradually shifts to the left, the droplet particle size peak gradually decreases, and the distribution range also shrinks.

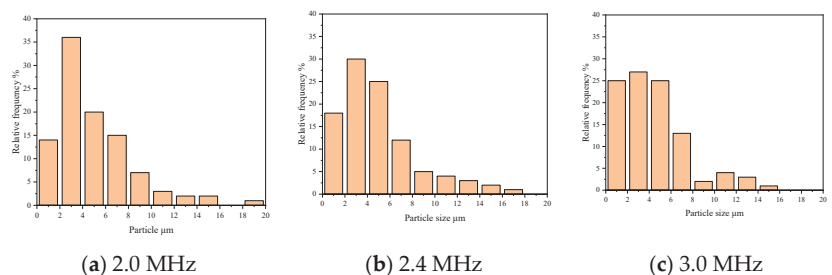


Figure 8. Histogram of frequency particle size distribution. (a) is the atomization frequency of 2.0 MHz; (b) is the atomization frequency of 2.4 MHz; and (c) is the atomization frequency of 3.0 MHz.

According to the particle size distribution histogram, each characteristic particle size was calculated, see Table 2. As the frequency increases from 2.0 MHz to 3.0 MHz, D32, D43,

D10, D50, D90 decrease from 5.35, 7.55, 1.59, 3.73, 10.92 μm to 4.01, 6.24, 1.55, 2.96, 9.4 μm, respectively. It can be seen that the particle size produced by high-frequency microwave atomization was small, and the concentration of the range is conducive to diffusion.

Table 2. Results of particle size.

Frequency MHz	Particle Size μm				
	D32	D43	D10	D50	D90
2.0	5.35	7.55	1.59	3.73	10.92
2.4	4.89	6.96	1.58	3.1	10.59
3.0	4.01	6.24	1.55	2.96	9.4

D represents the diameter of the powder particles, D50 represents the diameter of the cumulative 50% point (or 50% passing particle size), D10 represents the diameter of the cumulative 10% point, D50 is also known as the average particle diameter or median diameter, D43 represents the volume average diameter, and D32 represents the plane average diameter.

3.2. Analysis of Aerosol Permeability

3.2.1. Aerosol Permeation Flow Analysis

By replacing coal samples with different particle sizes for testing, we used a self-designed ultrasonic atomization device (Figure 4) to obtain changes in aerosol permeability and retention rate, as shown in Figure 9.

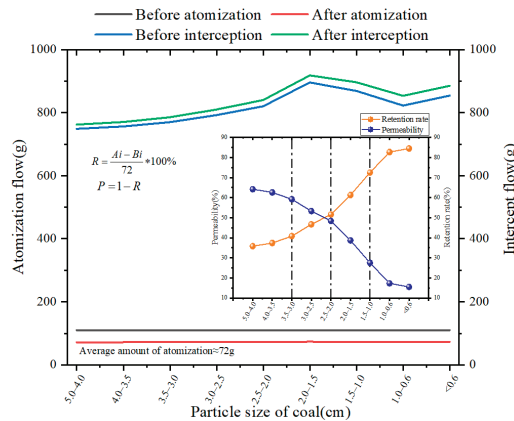


Figure 9. Aerosol diffusion effect diagram.

As can be seen from Figure 9, microwave atomized particles can pass through the pipe smoothly under the condition of an air pipe, and the particle passing rate is 95.6%. These results indicate that microwave atomized aerosol particles have good diffusivity in free space.

As the diameter of filled coal particles in the pipeline decreases from 5 cm to less than 0.6 cm, the diffusion effect of aerosol through the coal particle space becomes worse, and the proportion of aerosol interception increases from 35.8% to 84.5%. The permeability of sol particles decreases greatly due to the influence of the void structure between coal particles.

Among them, under different particle sizes, the penetration rules of atomized particles are as follows:

- (1) The coal sample was composed of middle lump coal with a large void structure, the interception ratio increased from 35.8% to 40.8%, and the infiltration ratio decreased from 64.2% to 59.2%.
- (2) In the process of coal sample accumulation from medium block to small block, the slope of the rejection curve changed rapidly, and the interception ratio increased from 40.8% to 51.6%.

- (3) The coal sample accumulated from small pieces to granular coal, the pore structure decreased sharply, and the space allowing aerosol to pass shrunk. The interception ratio rose from 51.6% to 82.7%. At this stage, the slope of the curve changed fastest, but aerosol can still penetrate.
- (4) At this time, the coal sample was formed by the accumulation of pulverized coal, and the void structure was small. The proportion of interception increased from 82.7% to 84.5%, and the proportion of penetration decreased from 17.3% to 15.5%. Aerosol permeability changed gently.

The void fraction of the goaf changes dynamically with the spatial location, which in turn affects the aerosol passing ability. The atomization device developed in this paper can generate aerosol particles with a controllable particle size distribution, which can penetrate the dense space and attach to the coal to play a role of resistance so that it can achieve a wide range of flame retardants in the goaf.

The void fraction of the goaf changes dynamically with the spatial location, which in turn affects the aerosol passing ability. The atomization device developed in this paper can generate aerosol particles with a controllable particle size distribution so that the large particle size droplets stay in the area with high porosity while the small particle size droplets can enter the deep part of the goaf and attach to the coal, the flame retardant of the goaf can be achieved in a wide range.

3.2.2. Analysis of Aerosol Permeable Particle Size

Considering the influence of microwave atomized particle size on permeability, the difference in particle size distribution at the outlet of the pipe was compared when the air duct was in operation. In the experiment, the CCD image system was used to collect fog droplet images at the inlet and outlet positions by using slides, and the images were transmitted to the computer to test the particle size distribution of fog droplets under different conditions, as shown in Figure 10. Images were analyzed and processed by image-Pro Plus software.

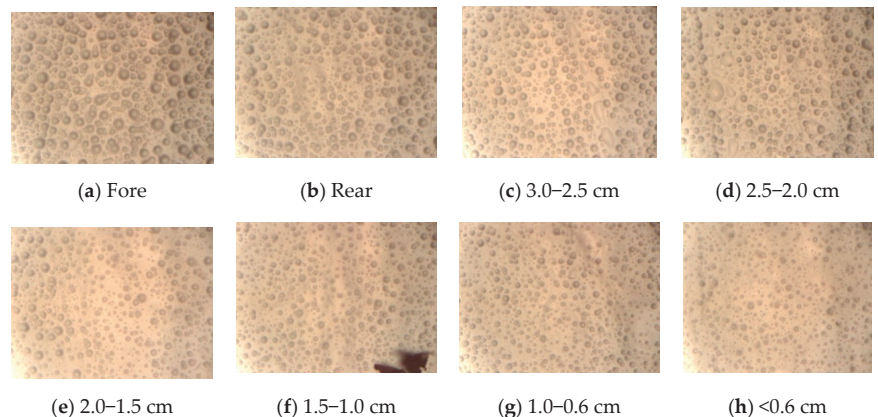


Figure 10. Particle size test diagram. (a) is the droplet at the entrance of the empty pipe; (b) is the droplet at the exit of the empty pipe; (c) is the exit droplet with a particle size of 3.0–2.5 cm; (d) is the exit droplet with a particle size of 2.5–2.0 cm; (e) is the exit droplet with a particle size of 2.0–1.5 cm; (f) is the exit droplet with a particle size of 1.5–1.0 cm; (g) is the exit droplet with a particle size of 1.0–0.6 cm; and (h) is the exit droplet with a particle size of <0.6 cm.

Use Image-Pro Plus software to count the aerosol particle size, as shown in Figure 10. Figure 10a,b is the aerosol particle size distributions at the inlet and outlet in the case of empty pipes, and Figure 10c–h is the aerosol particle size distributions at the outlet with different coal-sample void structures.

- (1) From the particle size distribution (Figures 10a,b and 11a,b), it can be seen that during the movement of the droplets in the free space of the empty tube, the atomized particle size at the inlet was mainly concentrated in the range of $<10 \mu\text{m}$. The particle size increased slightly in the range of $16\text{--}18 \mu\text{m}$, which may be affected by the collision and fusion of glass droplets. After the atomized particles ran for a certain distance in the pipeline, the particle size distribution within the range of $<10 \mu\text{m}$ became more concentrated at the exit, which showed that the particle size at the exit decreased. The particle size of $2\text{--}4 \mu\text{m}$ increased significantly, and the particle size of $>10 \mu\text{m}$ decreased significantly, indicating that the larger particle size was more lost due to gravity sedimentation during the operation of fog droplets above the particle size.

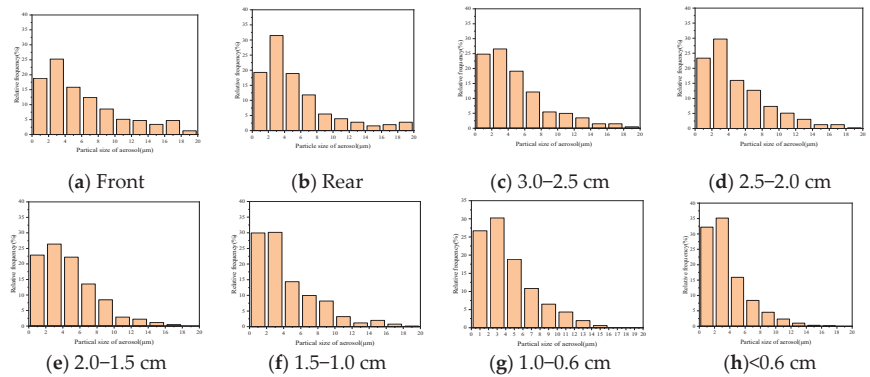


Figure 11. Aerosol particle size distribution under different void structures. (a) is the droplet at the entrance of the empty pipe; (b) is the droplet at the exit of the empty pipe; (c) is the exit droplet with a particle size of $3.0\text{--}2.5 \text{ cm}$; (d) is the exit droplet with a particle size of $2.5\text{--}2.0 \text{ cm}$; (e) is the exit droplet with a particle size of $2.0\text{--}1.5 \text{ cm}$; (f) is the exit droplet with a particle size of $1.5\text{--}1.0 \text{ cm}$; (g) is the exit droplet with a particle size of $1.0\text{--}0.6 \text{ cm}$; and (h) is the exit droplet with a particle size of $<0.6 \text{ cm}$.

- (2) With the decrease of particle size of broken coal filling in the tube, the peak particle size of fog droplets at the exit gradually shifted to the right. The proportion of aerosol particles larger than $8 \mu\text{m}$ decreased from 27.7% to 8.2% , especially those larger than $14 \mu\text{m}$, which decreased from 9.4% to 0.4% . The aerosol particles less than $4 \mu\text{m}$ increased most significantly, from 44.0% to 67.3% .

These results indicate that when the aerosol passes through the dense coal structure, the aerosol particles with larger particle sizes are more likely to be trapped. Affected by the particle size of pulverized coal in the tube, the decrease of aerosol particles is most obvious in the range of $10\text{--}20 \mu\text{m}$. The $0\text{--}4 \mu\text{m}$ aerosol particles increase with the decrease of the particle size of the crushed coal particles in the tube, which indicates that the atomized particles in this range have good permeability, as shown in Figures 11 and 12.

According to the particle size map, the statistical Sauter average particle size and characteristic particle size were mainly D10, D50, and D90, as shown in Figure 13. When aerosol passes through the space where coals of different particle sizes are stacked, the aerosol particle size will change. As a whole, as the particle size of the filled coal decreased, the aerosol particle size decreased accordingly.

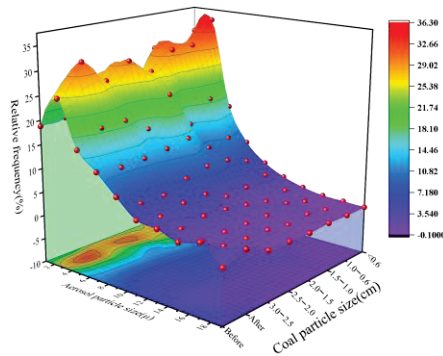


Figure 12. Statistical chart of particle size.

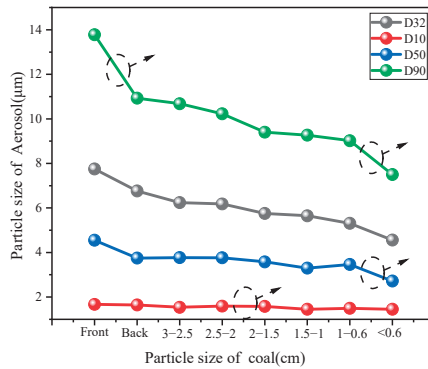


Figure 13. Change of characteristic particle size.

- (1) In the front and rear of the empty tube test particle size, greater than 10 μm aerosol particles due to its sedimentation, more easily deposited on the wall, and smaller particle size aerosols are more likely to float outside the tube.
- (2) From the perspective of particle size classification, the D10 particle size curve does not change with the decrease of coal particle size, indicating that aerosol particles smaller than 2 μm can pass through the denser coal structure without being affected by it.
- (3) The median particle size D50 decreases from 4.55 μm to 2.72 μm with the decrease of coal particle size, showing a downward trend. When the coal particle size is less than 0.6 cm, the downward trend is more obvious. At this time, the spatial structure of the coal is denser, allowing aerosol particles to pass through a narrower space, and large aerosol particles are more easily intercepted.
- (4) With the decrease of the particle size of the piled coal, the D90 particle size changes more obviously. When the coal particle size is less than 0.6 cm, the D90 particle size is reduced from 9.02 μm to 7.50 μm. Due to the dense coal space structure, most of the aerosol particles larger than 7 μm are intercepted by the coal.

3.3. Analysis of Aerosol Resistance

MgCl₂ solution was used as the atomization object, and the wettability and surface tension of the MgCl₂ aqueous solution was decreased. An ultrasonic atomization device was used to generate aerosols and test coal samples. The atomization time was set to 30 min and 60 min, respectively. After atomization, the coal sample was cooled and dried and then tested and analyzed by infrared spectrum, as shown in Figure 14.

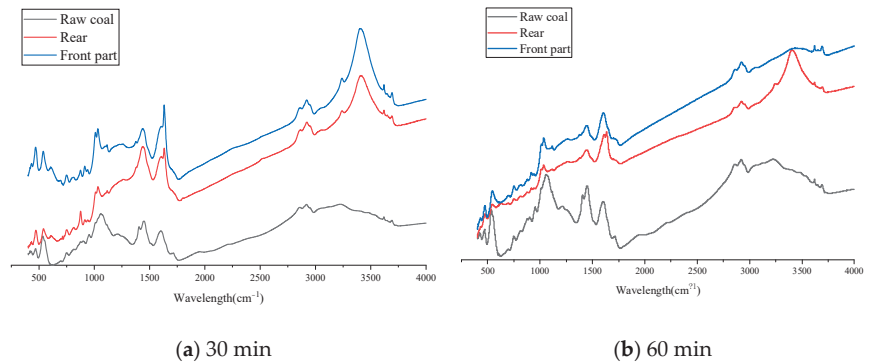


Figure 14. Schematic diagram of infrared spectrum of $MgCl_2$. (a) is the infrared spectrum when the atomization time is 30 min; and (b) is the infrared spectrum when the atomization time is 60 min.

In Figure 14, 3407 cm^{-1} is the attribution peak of hydroxyl, 2858 cm^{-1} and 2923 cm^{-1} are the asymmetric vibration of methyl and methylene, respectively, the stretching vibration of the carboxyl functional group near 1627 cm^{-1} , and the shear vibration of methylene are 1435 cm^{-1} .

Compared with the raw coal sample, the absorption peak of $-OH$ is obviously enhanced. This is because the $MgCl_2$ inhibitor has water absorption and is very easy to absorb water in the air so that the water content in the coal increases and the absorption peak of $-OH$ increases. Methylene and methyl groups are relatively high activity and are easy to react with oxygen to produce unstable intermediate active groups. Due to the substitution of methylene and methyl H^+ , the absorption peaks of the above two groups decreased significantly. The absorbance of the functional group corresponding to $C=O$ is also significantly reduced. This is mainly because Mg^{2+} in the absorbent salt inhibitor $MgCl_2$ is more likely to complex with coal molecules in a high-temperature environment, which reduces the carbonyl group in coal and results in a significant decrease in carbonyl content.

In considering the influence of different atomization positions and atomization time on coal's resistance performance, the functional group analysis of the infrared spectrograph is shown in Figure 15. When the atomization time is 30 min, compared with raw coal, the atomized aliphatic hydrocarbons and aromatic hydrocarbons of coal show a step-type law of decline. In space, the peak area of functional groups of the front coal sample decreased faster than that of the raw coal sample and the rear coal sample. Compared with raw coal fat, the fat and aromatic hydrocarbons in the front coal samples decreased by 75.9% and 57.5%, respectively. Compared with raw coal, aliphatic hydrocarbons and aromatic hydrocarbons in rear coal samples decreased by 32.6% and 14.0%, respectively. This indicates that $MgCl_2$ aerosol has a large amount of intercepting in the front part and a good blocking effect, while at the back of the coal sample tank, due to the short passage time of atomized aerosol and low blocking amount, $MgCl_2$ has a reduced blocking effect on coal and fewer changes in functional groups.

When the atomization time was extended to 60 min, the peak areas of aliphatic hydrocarbons and aromatic hydrocarbons in the coal sample decreased significantly compared with the raw coal sample. Compared with raw coal, aliphatic hydrocarbons and aromatic hydrocarbons of the rear coal sample decreased by 71.3% and 19.6%, respectively. It is speculated that the flame retardant solution is more, and the atomization is not complete in a short time. With the passage of time, the solution can be atomized more thoroughly to produce more aerosol particles, resulting in enhanced flame retardant. This indicates that the longer atomization time will promote the flame retardant solution to produce more aerosol so that it can reach the rear of the coal sample tank through the gap of the coal body and play a role in inhibiting the coal sample.

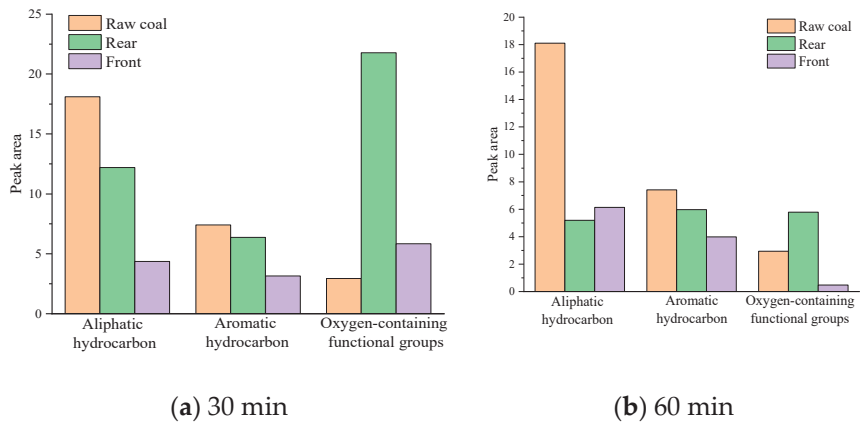


Figure 15. Variation of functional group content. (a) is the functional group content when the atomization time is 30 min; and (b) is the functional group content when the atomization time is 60 min.

4. Conclusions

The permeability and barrier properties of aerosols were investigated. This development not only analyzes the permeability of aerosols under different pore structures and the residence of inhibitors in penetrating coal seams but also obtains the temporal and spatial variation of the resistance. It has been proven that ultrasonic atomized aerosol is an effective means of suppressing spontaneous combustion of coal in goafs. The specific conclusions are as follows:

- (1) As the particle size of the test coal decreases from 5.0 cm to below 0.6 cm, the permeability of microwave atomized droplets decreases from 64.2% to 15.5%. When the coal particles are less than 0.6 cm, the aerosol permeability is less than 15%, and a large number of aerosols are retained in the coal.
- (2) When aerosols passed through the space of coal with different particle sizes, the particle sizes of trapped aerosols differed greatly and generally became smaller with the smaller particle sizes of filled coal. The average particle size D50 decreased with the decrease of coal particle size, and the D10 particle size curve changed little with the decrease of coal particle size, indicating that aerosol particles less than 2–4 μm can pass through the dense coal structure smoothly.
- (3) Infrared spectroscopy analysis showed that the content of functional groups in the coal sample after ultrasonic atomization treatment was greatly reduced compared with the uninhibited raw coal. When the atomization time was extended from 30 min to 60 min, the peak areas of aliphatic hydrocarbons and aromatic hydrocarbons in the rear coal sample decreased significantly compared with the original coal sample. This indicates that the smaller particles can penetrate the broken coal voids well, thus realizing the flame retardancy of the MgCl_2 aerosol on the deep coal body.

Author Contributions: Methodology, W.Z.; software, F.L.; validation, B.L. and Y.L.; formal analysis, F.L.; investigation, H.C.; resources, Q.T.; data curation, B.L.; writing—original draft preparation, B.L.; writing—review and editing, F.L. and B.L.; visualization, F.L.; supervision, W.Z.; project administration, W.Z.; funding acquisition, J.W. All authors have read and agreed to the published version of the manuscript.

Funding: This work was supported by the National Natural Science Foundation (52174193 and 51974179).

Institutional Review Board Statement: The study does not require ethical approval.

Data Availability Statement: Not applicable.

Acknowledgments: We thank Wenbin Zhao for his technical and theoretical guidance on this paper.

Conflicts of Interest: The authors declare that they have no known competing financial interest or personal relationship that could have appeared to influence the work reported in this paper. The funders had no role in the design of the study; in the collection, analyses, or interpretation of data; in the writing of the manuscript, or in the decision to publish the results.

References

1. Lang, L.; Fu-bao, Z. A comprehensive hazard evaluation system for spontaneous combustion of coal in underground mining. *Int. J. Coal Geol.* **2010**, *82*, 27–36. [[CrossRef](#)]
2. Deng, J.; Xiao, Y.; Li, Q.; Lu, J.; Wen, H. Experimental studies of spontaneous combustion and anaerobic cooling of coal. *Fuel* **2015**, *157*, 261–269. [[CrossRef](#)]
3. Xia, T.; Zhou, F.; Wang, X.; Zhang, Y.; Li, Y.; Kang, J.; Liu, J. Controlling factors of symbiotic disaster between coal gas and spontaneous combustion in longwall mining gobs. *Fuel* **2016**, *182*, 886–896. [[CrossRef](#)]
4. Shi, Q.; Qin, B.; Liang, H.; Gao, Y.; Bi, Q.; Qu, B. Effects of igneous intrusions on the structure and spontaneous combustion propensity of coal: A case study of bituminous coal in Daxing Mine, China. *Fuel* **2018**, *216*, 181–189. [[CrossRef](#)]
5. Qin, Y.; Liu, W.; Yang, C.; Fan, Z.; Wang, L.; Jia, G. Experimental study on oxygen consumption rate of residual coal in goaf. *Saf. Sci.* **2012**, *50*, 787–791. [[CrossRef](#)]
6. Cheng, W.; Hu, X.; Xie, J.; Zhao, Y. An intelligent gel designed to control the spontaneous combustion of coal: Fire prevention and extinguishing properties. *Fuel* **2017**, *210*, 826–835. [[CrossRef](#)]
7. Lu, Y. Laboratory Study on the Rising Temperature of Spontaneous Combustion in Coal Stockpiles and a Paste Foam Suppression Technique. *Energy Fuels* **2017**, *31*, 7290–7298. [[CrossRef](#)]
8. Dong, S.; Lu, X.; Wang, D.; Wang, H.; Zheng, K.; Shi, Q.; Chen, M. Experimental investigation of the fire-fighting characteristics of aqueous foam in underground goaf. *Process Saf. Environ. Prot.* **2017**, *106*, 239–245. [[CrossRef](#)]
9. Lu, X.; Zhu, H.; Wang, D.; Hu, C.; Zhao, H.; Huo, Y. Flow characteristic investigation of inhibition foam used for fire extinguishment in the underground goaf. *Process Saf. Environ. Prot.* **2018**, *116*, 159–168. [[CrossRef](#)]
10. Lu, Y.; Shi, S.; Yang, F.; Zhang, T.; Niu, H.; Wang, T. Mo-doping for improving the ZrF₄ coated-Li[Li_{0.20}Mn_{0.54}Ni_{0.13}Co_{0.13}]O₂ as high performance cathode materials in lithium-ion batteries. *J. Alloy. Compd.* **2018**, *767*, 23–33. [[CrossRef](#)]
11. Shan, B.; Wang, G.; Cao, F.; Wu, D.; Liang, W.; Sun, R. Mercury emission from underground coal fires in the mining goaf of the Wuda Coalfield, China. *Ecotoxicol. Environ. Saf.* **2019**, *182*, 109409. [[CrossRef](#)] [[PubMed](#)]
12. Shi, Q.; Qin, B. Experimental research on gel-stabilized foam designed to prevent and control spontaneous combustion of coal. *Fuel* **2019**, *254*, 115558. [[CrossRef](#)]
13. Xu, Y.-L.; Wang, D.-M.; Wang, L.-Y.; Zhong, X.-X.; Chu, T.-X. Experimental research on inhibition performances of the sand-suspended colloid for coal spontaneous combustion. *Saf. Sci.* **2012**, *50*, 822–827. [[CrossRef](#)]
14. Dou, G.; Wang, D.; Zhong, X.; Qin, B. Effectiveness of catechin and poly(ethylene glycol) at inhibiting the spontaneous combustion of coal. *Fuel Processing Technol.* **2014**, *120*, 123–127. [[CrossRef](#)]
15. Tang, Y. Experimental investigation of applying MgCl₂ and phosphates to synergistically inhibit the spontaneous combustion of coal. *J. Energy Inst.* **2018**, *91*, 639–645. [[CrossRef](#)]
16. Xue, D.; Hu, X.; Cheng, W.; Wei, J.; Zhao, Y.; Shen, L. Fire prevention and control using gel-stabilization foam to inhibit spontaneous combustion of coal: Characteristics and engineering applications. *Fuel* **2020**, *264*, 116903. [[CrossRef](#)]
17. Qin, B.; Jia, Y.; Lu, Y.; Li, Y.; Wang, D.; Chen, C. Micro fly-ash particles stabilized Pickering foams and its combustion-retardant characteristics. *Fuel* **2015**, *154*, 174–180. [[CrossRef](#)]
18. Tang, Y.; Wang, H. Experimental investigation on microstructure evolution and spontaneous combustion properties of secondary oxidation of lignite. *Process Saf. Environ. Prot.* **2019**, *124*, 143–150. [[CrossRef](#)]
19. Li, M.; Wang, D.; He, S.; Shao, Z.; Shen, Y. Experimental study on foaming properties of anion-cation compound foaming agent to prevent coal spontaneous combustion. *Colloids Surf. A Physicochem. Eng. Asp.* **2019**, *581*, 123847. [[CrossRef](#)]
20. Sijts, R.; Kooij, S.; Holterman, H.J.; van de Zande, J.; Bonn, D. Drop size measurement techniques for sprays: Comparison of image analysis, phase Doppler particle analysis, and laser diffraction. *Aip Adv.* **2021**, *11*, 15315. [[CrossRef](#)]
21. Im, J.; Park, I.; Shin, D. Effect of atomization methods on the size and morphology of Gd_{0.1}Ce_{0.902}-delta powder synthesized by aerosol flame synthesis. *Ceram. Int.* **2012**, *38*, 2051–2058. [[CrossRef](#)]
22. Min, L.Z.; Zhao, Z.X.; Jun, D.; Ming, C.F. Experimental Study on Aerosol Fire—Extinguishing Agent to Inhibit Coal Combustion. *Saf. Coal Mines* **2010**, *41*, 11–14.
23. Kooij, S.; Astefanei, A.; Corthals, G.L.; Bonn, D. Size distributions of droplets produced by ultrasonic nebulizers. *Sci. Rep.* **2019**, *9*, 6128. [[CrossRef](#)]
24. Ramisetty, K.A.; Pandit, A.B.; Gogate, P.R. Investigations into ultrasound induced atomization. *Ultrason. Sonochem.* **2013**, *20*, 254–264. [[CrossRef](#)]
25. Dalmoro, A.; Barba, A.A.; d’Amore, M. Analysis of Size Correlations for Microdroplets Produced by Ultrasonic Atomization. *Sci. World J.* **2013**, *2013*, 482910. [[CrossRef](#)]

26. Kudo, T.; Sekiguchi, K.; Sankoda, K.; Namiki, N.; Nii, S. Effect of ultrasonic frequency on size distributions of nanosized mist generated by ultrasonic atomization. *Ultrason. Sonochem.* **2017**, *37*, 16–22. [[CrossRef](#)]
27. Tang, Y.; Guo, Q.; Yerman, L. Experimental Investigation on Using Chloride/Hydroxide Aerosol to Control Spontaneous Combustion of Lignite in Underground Coal Mines. *Energy Fuels* **2020**, *34*, 10607–10618. [[CrossRef](#)]
28. Jia, L.; Yu, Y.; Li, Z.P.; Qin, S.N.; Guo, J.R.; Zhang, Y.Q.; Wang, J.C.; Zhang, J.C.; Fan, B.G.; Jin, Y. Study on the Hg(0) removal characteristics and synergistic mechanism of iron-based modified biochar doped with multiple metals. *Bioresour Technol.* **2021**, *332*, 125086. [[CrossRef](#)]
29. Lang, R.J. Ultrasonic atomization of liquids. *J. Acoust. Soc. Am.* **1962**, *34*, 6–8. [[CrossRef](#)]

Article

Lignite-Based N-Doped Porous Carbon as an Efficient Adsorbent for Phenol Adsorption

Yanfeng Xue ^{1,*}, Yanyan Chen ², Linxia Shi ¹, Haotian Wu ¹, Chao Zhang ¹, Minghuang Cheng ¹, Hongbin Li ¹, Wanjun Li ¹ and Yulan Niu ¹

¹ Collaborative Innovation Center of CO₂ Conversion and Utilization, Department of Chemistry and Chemical Engineering, Taiyuan Institute of Technology, Taiyuan 030008, China

² Institute of Coal Chemistry, Chinese Academy of Sciences, Taiyuan 030001, China

* Correspondence: xueyf@tit.edu.cn

Abstract: The treatment of phenolic-containing wastewater has received increased attention in recent years. In this study, the N-doped porous carbons were prepared from lignite with tripolycyanamide as the N source, and their phenol adsorption behaviors were investigated. Results clearly showed that the addition of tripolycyanamide largely improved the surface area, micropore volume, N content and thus the phenol adsorption capacity of lignite-based carbons. The N-doped sample prepared at 700 °C showed a surface area of 1630 m²/g and a phenol adsorption capacity as high as 182.4 mg/g at 20 °C, which were 2.0 and 1.6 times that of the lignite-based carbon without N-doping. Pseudo-second order and Freundlich adsorption isotherm models could better explain the phenol adsorption behaviors over lignite-based N-doped porous carbon. Theoretical calculations demonstrated that phenol adsorption energies over graphitic-N (−72 kJ/mol) and pyrrolic-N (−74 kJ/mol) groups were slightly lower than that over the N-free graphite layer (−71 kJ/mol), supporting that these N-containing groups contribute to enhance the phenol adsorption capacity. The adsorption mechanism of phenol over porous carbon might be interpreted by the π - π dispersion interactions between aromatic-ring and carbon planes, which could be enhanced by N-doping through increasing π electron densities in the carbon plane.

Keywords: lignite; N-doping; phenol; adsorption

Citation: Xue, Y.; Chen, Y.; Shi, L.; Wu, H.; Zhang, C.; Cheng, M.; Li, H.; Li, W.; Niu, Y. Lignite-Based N-Doped Porous Carbon as an Efficient Adsorbent for Phenol Adsorption. *Processes* **2022**, *10*, 1746. <https://doi.org/10.3390/pr10091746>

Academic Editors: Roberto Alonso González Lezcano, Francesco Nocera and Rosa Giuseppina Caponetto

Received: 4 August 2022

Accepted: 30 August 2022

Published: 2 September 2022



Copyright: © 2022 by the authors. Licensee MDPI, Basel, Switzerland. This article is an open access article distributed under the terms and conditions of the Creative Commons Attribution (CC BY) license (<https://creativecommons.org/licenses/by/4.0/>).

1. Introduction

Phenol compounds are prevalently contained in industrial effluents from petroleum refining, coking, plastic, pharmaceutical, dyeing and many other processes, thus leading to a large amount of phenolic wastewater discharging into water streams [1,2]. According to industrial statistics, the concentration of phenol in synthetic concocted wastewater reaches 1000 mg/L [3], while wastewater from petrochemical and coal conversion industries gives a wide phenol concentration ranging from 200 up to 7000 mg/L [4]. Because of the high biotoxicity and carcinogenicity of phenols to humans and ecosystems, phenolic wastewater currently results in serious environmental and ecological problems [5]. Therefore, the removal of phenols from wastewater before discharging has become an urgent problem that needs to be solved. Several approaches have been implemented for the treatment of phenol-containing wastewater, including membrane separation [3,6], electrochemical oxidation [7,8], microbial biodegradation [9], photocatalytic degradation [10], and adsorption [11,12]. Among these methods, adsorption has aroused many concerns because of its advantages of high efficiency, low cost, simplicity, and non-pollution [13–15].

In the adsorption process, a cost-effective adsorbent with high adsorption performance is highly desired. Activated carbon (AC) has been vastly applied presently, especially for wastewater with low adsorbate concentration due to the high surface area, developed pore structure and the presence of varieties of surface functional groups [16,17]. For

instance, activated carbon samples were prepared from oily sludge to remove phenol. The synthesized adsorbent showed a high adsorption capacity of 434 mg/g [18]. Saleh et al., for example, employed waste rubber-derived AC to extract phenol from an aqueous solution, and the produced AC showed a maximum adsorption capacity of 18.12 mg/g [19]. In another study, KOH-activated carbon derived from cattle bone showed a high adsorption capacity of 431 mg/g [20].

Generally, the pore structure of AC has important roles in physical adsorption because it provides accessible adsorption sites and diffusion channels to the adsorbate molecules, while another key factor in controlling adsorption capacity is the surface chemistry [21,22]. The complex nature of surface chemistry mainly depends on the surface functional groups, which determine the acid–base property, hydrophilia-hydrophobicity, and electron density of the carbon surface, further impacting the specific interactions between adsorbate and adsorption sites [23]. To further elucidate the effects of surface chemistry or mechanism of adsorption, the heteroatoms such as O [24], N [25], P [26], and B [27] have been introduced to the functional groups or carbon matrix of AC.

However, the introduction of oxygen atoms by oxidation was found to lead to a decrease in the adsorption capacity of phenols [22,28]. The surface oxygen groups could attract the π -electrons from the basal plane of AC, thus decreasing the interaction between the phenol aromatic-ring and carbon surface [28]. Moreover, the increase in oxygen-containing functional groups, such as carboxylic groups, improves the hydrophilia of AC, thereby enhancing water adsorption and hindering the accessibility and affinity of phenols on adsorption sites [22,28]. In contrast, the N-doped modification of carbons was found to be an effective method of facilitating the adsorption capacity of phenols. The electron-rich nitrogen groups are considered to provide π -electrons to form a π - π bond with the π -electron from the aromatic-ring, thus strengthening the interactions between the phenol and adsorbent [13]. As reported by Yang et al. [16], the AC treated with ammonia at 650 °C gives a 28.9% increase in phenol adsorption. The microporous-dominated N-doped carbons prepared by EDTA-4Na exhibit a large adsorption capacity of 521 mg/g toward bisphenol [23]. Liu et al. [13] further verified with theoretical calculations that the adsorption energy of phenol over the N-doped carbon plane is 12.37 kJ/mol lower than that over N-free graphite carbon. These previous studies demonstrate that N-doped carbon materials are fine candidates for removing the phenols from wastewater. However, the specific mechanisms of the adsorption of phenol on N-doped carbon materials are still fragmentary and not adequately understood, and the interactions between phenols and different N-containing functional groups are still especially ambiguous. Therefore, it is essential to further investigate the phenol adsorption behaviors over N-doped carbon materials.

Low-cost lignite is a kind of mineral coal with rich reserves. It has great potential to be prepared as a pollutant adsorbent for wastewater treatment because of its developed porous structure and abundant functional groups [29]. In addition, varieties of structural defects are irregularly distributed on the carbon matrix of lignite, which makes it possible for nitrogen atoms to be doped into the carbon structures or surface functional groups. Therefore, lignite-based N-doped porous carbon should be a promising adsorbent for treating phenolic wastewater. To the best of our knowledge, however, the preparation of lignite-based N-doped porous carbon and its application for wastewater treatment was rarely reported.

In this study, the lignite-derived N-doped carbons were prepared and applied as the adsorbent for phenol adsorption in simulated phenolic wastewater. The structure and surface chemistry of lignite-based N-doped carbons were systematically characterized by using various characterization techniques. Pseudo-first-order (PFO) and pseudo-second-order (PSO) models were used to investigate the adsorption kinetics, and isotherm adsorption was studied using Langmuir and Freundlich models. The adsorption mechanism of N-doped carbon towards phenol in relation to different N-containing groups was elucidated on the basis of theoretical calculations. The main objectives of this study were to: (1) investigate the modification effects of N-doping on the structural and surface chemistry of

lignite-based porous carbon; (2) evaluate the adsorption performances of lignite-based porous carbons; (3) establish the relationships between the physicochemical properties of lignite-based porous carbon and its phenol adsorption capacity. The findings obtained in this work will provide a better understanding of the preparation of lignite-based N-doped porous carbon and its application in phenol-containing wastewater treatment.

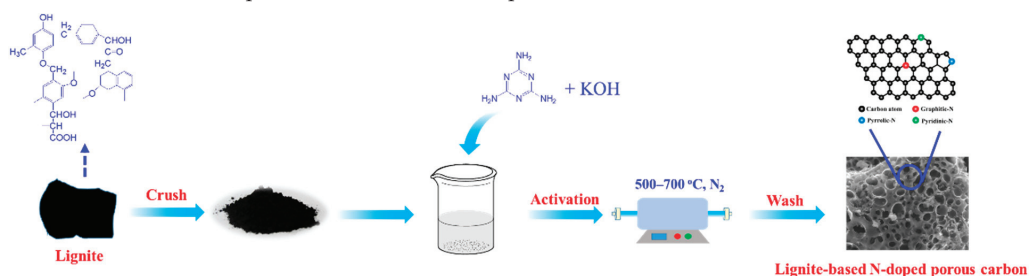
2. Experimental

2.1. Materials

The lignite was supplied by Yunnan Xiaolongtan Mining Bureau. The raw lignite was dried at 60 °C for 12 h, then crushed and passed through a 100-mesh sieve to obtain lignite powder. Phenol, potassium hydroxide (KOH) and tripolycyanamide were purchased from Sinopharm Chemical Reagent Co., Ltd. (Shanghai, China).

2.2. Preparation of Lignite-Based Porous Carbon

The lignite-based porous carbons were synthesized with the chemical activation methods reported in Refs. [30,31]. Typically, 7.0 g of tripolycyanamide was dissolved in 300 mL of deionized water at 80 °C. After stirring for 30 min, 50.0 g lignite powder and 50.0 g KOH were added, and the mixture was stirred at 80 °C for 2 h. After that, the slurry was dried at 100 °C overnight to evaporate water. The sample was activated in 40 mL/min N₂ flow at 500–700 °C for 2 h, then washed with deionized water until the pH value of filtrate reached 7. Finally, the sample was dried at 100 °C for 4 h. The schematic of the fabrication process is described in Scheme 1. For brevity of description, the samples were denoted as L-CN-x, with x representing the activation temperature. For comparison, the lignite-based porous carbon without N-doping was prepared with a similar procedure, except that no tripolycyanamide was added. These samples were denoted as L-x, where x represents the activation temperature.



Scheme 1. Schematic of the preparation of the lignite-based N-doped porous carbon.

2.3. Sample Characterization

Powder X-ray diffraction (XRD) patterns were recorded on a Rigaku MiniFlex II desktop X-ray diffractometer with Cu K α radiation. Scanning electron microscopy (SEM) images were collected with a JEOL JSM-700 microscope at an accelerating voltage of 10.0 kV. The X-ray photoelectron spectra (XPS) were measured on a Krato AXIS Ultra DLD spectrometer with Al K α resource. The elemental compositions of the sample were measured with an Elemntar Vario EL Cube microanalyzer. N₂ sorption analysis was performed at −196 °C on Micromeritics ASAP2460. Before the measurement, the sample was degassed at 300 °C for 4 h. The total surface area, mesopore and micropore volume were obtained by the BET, BJH and *t*-plot methods, respectively. The Raman spectra were measured on a Renishaw inVia Qontor spectrometer using a laser with a wavelength of 532 nm as the excitation source.

2.4. Adsorption Experiments

The adsorption experiments were performed in a conical flask by immersing 20 mg of carbon materials into a 50 mL phenol solution. The flasks were placed on a shaker and then

shaken at 200 rpm at room temperature (20 °C). For the adsorption kinetic experiments, a 133 mg/L phenol solution was used, and the adsorption was performed at set times (10, 15, 20, 30, 50, 70, 90, and 120 min). The adsorption isotherm studies were conducted at 20 °C for 120 min with a series of different initial phenol concentrations ranging from 50 to 275 mg/L. After adsorption, the mixed solution was filtered with a 0.45 µm membrane filter to remove the adsorbent, and then the filtrate was analyzed for the concentration of phenol by an Agilent 1100 series high-performance liquid chromatography (HPLC) system equipped with a C18 column (250 mm × 4.6 mm, 2.5 µm). The mobile phase of HPLC was acetonitrile-water (20/80 in mass ratio), and the flow rate was maintained at 0.8 mL/min. The detection wavelength was 270 nm, and the column temperature was set at 25 °C. The retention time of phenol was 14 min.

The reusability performance of L-CN-700 was investigated at the concentration of 133 mg/L at 20 °C. After adsorption, the used L-CN-700 sample was placed in 50 mL of methanol solvent and stirred for 5 h to desorb phenol. Then, the washed sample was used for six adsorption–desorption cycles to investigate its regeneration performance.

The phenol uptake Q_t (mg/g) of the sample was calculated from the following equation:

$$Q_t = V \times (C_0 - C_t) / m \quad (1)$$

where V (L) is the volume of the phenol solution, C_0 and C_t (mg/L) represent the initial and final phenol concentrations, respectively, m (g) is the mass of the adsorbent.

The PFO and PSO models are widely used for analyzing the adsorption kinetic behaviors of adsorbents [32,33]. The PFO and PSO models are expressed as Equations (2) and (3), as follows:

$$Q_t = Q_e \times (1 - \exp(-k_1 \times t)) \quad (2)$$

$$Q_t = Q_e^2 \times k_2 \times t / (1 + Q_e \times k_2 \times t) \quad (3)$$

where Q_t (mg/g) represents the phenol uptake of the sample, Q_e (mg/g) is the calculated equilibrium adsorption amount, k_1 (min^{-1}) and k_2 (g/mg·min) represent the rate constants of PFO and PSO models, respectively, and t is the adsorption time (min).

The adsorption isotherm data were simulated by the Langmuir and Freundlich models to disclose more information about adsorption behaviors [34,35]. The Langmuir and Freundlich models are usually described by Equations (4) and (5) as follows:

$$Q_e = Q_m \times k_L \times C_e / (1 + k_L \times C_e) \quad (4)$$

$$Q_e = k_F \times C_e^{1/n} \quad (5)$$

where Q_m (mg/g) and C_e (mg/L) are the theoretical maximum adsorption capacity and equilibrium concentration of adsorbate, respectively, k_L (L/mg) is the Langmuir constant, and k_F ($\text{mg}^{1-1/n} \cdot \text{L}^{1/n} \cdot \text{g}$) and n are the Freundlich constants.

2.5. Models and Method

To investigate the phenol adsorption mechanism on N-doped carbons, a theoretical calculation was used to simulate phenol adsorption over different N-containing functional groups. Herein, four cluster models of graphene, including modified graphitic-N, pyrrolic-N, pyridinic-N, and without modification (N-free graphite layer), are built, respectively. The peripheral carbon atoms are saturated by H atoms. All calculations were carried out using the Gaussian 09 package [36]. All atoms are active and relaxed, and the ωB97X-D functional, including dispersion corrections and the 6-31G(d,p) basis set, was used in all geometry optimizations. The adsorption energy (E_{ads}) of phenol is defined as Equation (6), where $E_{(AB)}$, $E_{(A)}$ and $E_{(B)}$ are the complex, adsorbent, and adsorbate single-point energy, respectively.

$$E_{ads} = E_{(AB)} - E_{(A)} - E_{(B)} \quad (6)$$

3. Results and Discussions

3.1. Characteristics of Lignite-Based Porous Carbon

The micro-scale morphology of lignite-based N-doped carbon materials was characterized by SEM measurement. As shown in Figure 1, L-600 and L-CN-600 are irregular blocky solids with a rough and etched surface. A large number of macropores or cavities are formed over the surface of samples due to the harsh activation by KOH at 600 °C [30]. However, the L-CN-600 presents an interconnected three-dimensional hollow morphology, with a larger macropore diameter than that of L-600. By contrast, it is observed that the destruction by KOH etching over L-600 mostly occurs on the surface of lignite. These results indicate that the etching process by KOH is intensified by the introduction of tripoly-cyanamide, probably due to the fact that the decomposition products of tripoly-cyanamide, such as N_2 and NH_3 , contribute to the formation, expansion and connection of pore systems during activation at high temperature (500–700 °C) [37].

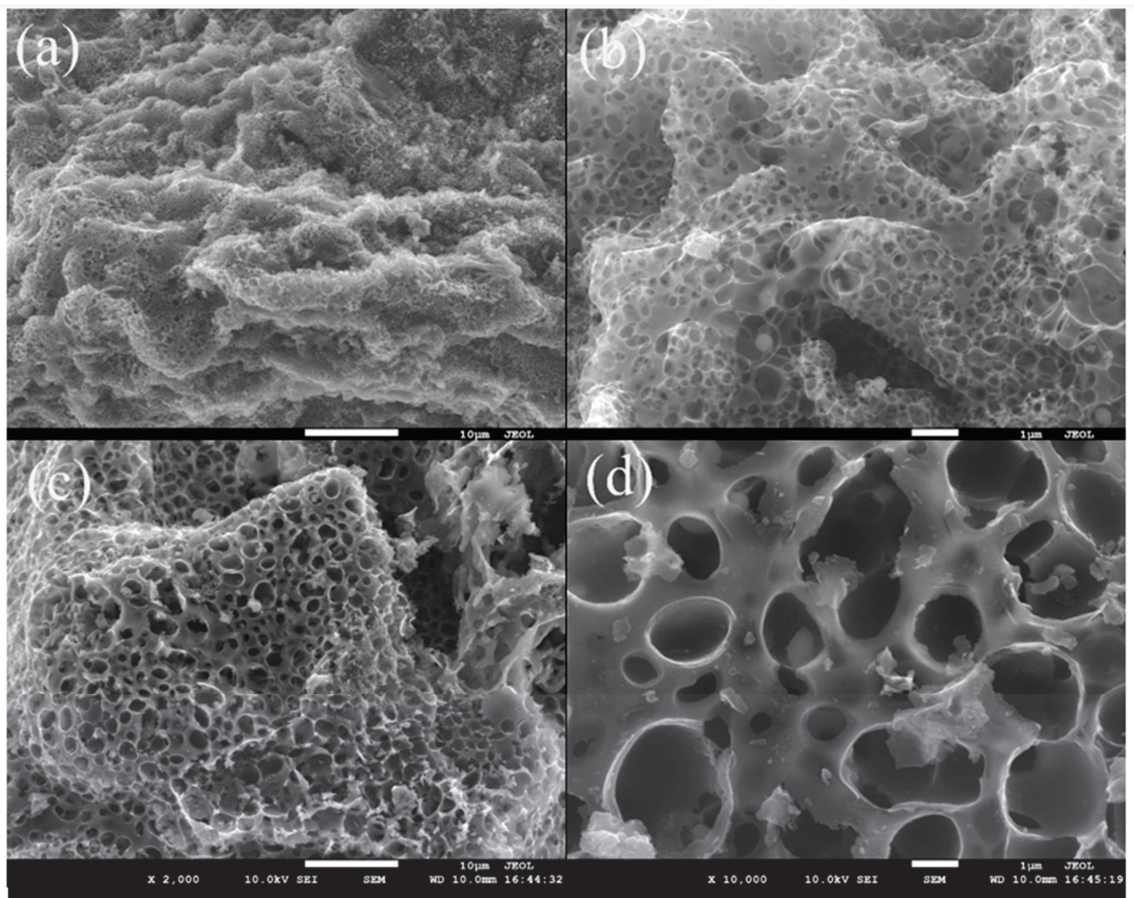


Figure 1. SEM images of L-600 (a,b) and L-CN-600 (c,d) samples.

The textural properties of samples were characterized by an N_2 adsorption–desorption isotherms method, and the results are shown in Figure 2 and Table 1. All the samples show the typical Type-IV isotherms, indicative of their micro-mesoporous structures. The adsorption volume of N_2 rapidly lifts at relative pressures of $P/P_0 < 0.1$ in all the samples, indicating that abundant micropores are formed. In addition, all samples present the

hysteresis loop in the relative pressure P/P_0 of 0.45–1.0, suggesting a distinct formation of mesopores. The BJH pore size distributions of samples are shown in Figure 2c,d, which demonstrates that the pore size of mesopores for all samples is centered at around 4 nm.

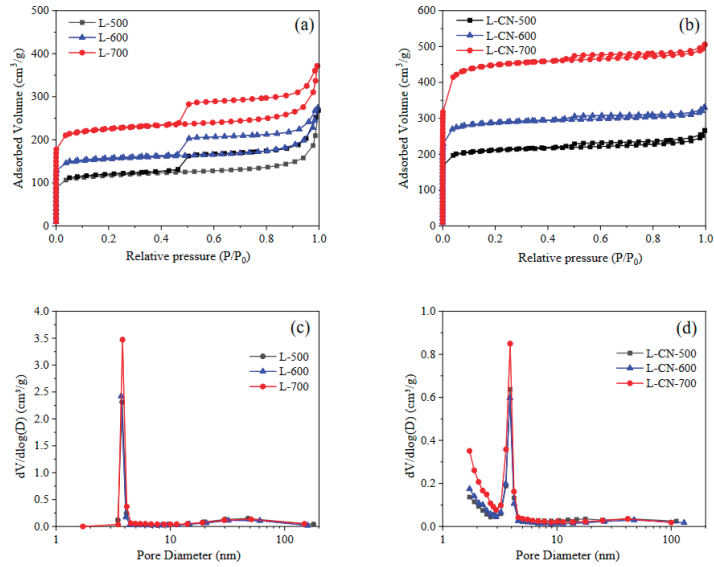


Figure 2. N_2 sorption isotherms (a,b), and pore size distribution curves (c,d) of lignite-based porous carbons.

Table 1. Textural properties of lignite-based porous carbons prepared at different activation temperatures.

Sample	Surface Area (m^2/g)		Pore Volume (cm^3/g)		Pore Size (nm)
	S_{BET}	S_{meso}	V_{micro}	V_{meso}	
L-500	424	59	0.16	0.09	2.37
L-600	561	55	0.22	0.09	2.22
L-700	814	82	0.31	0.12	2.14
L-CN-500	762	58	0.30	0.07	1.93
L-CN-600	1041	59	0.42	0.06	1.85
L-CN-700	1630	89	0.66	0.09	1.83

Table 1 shows that L-500 has a surface area of $424 m^2/g$ and a total pore volume of $0.25 cm^3/g$. A further increase in activation temperature increases the surface area and pore volume, and L-700 gives a surface area of $814 m^2/g$ and a pore volume of $0.43 cm^3/g$. However, with increasing the activation temperature, the average pore size is slightly decreased. The L-CN-500, 600 and 700 samples show a similar trend. Interestingly, the introduction of tripolycyanamide largely improves the surface area and micropore volume (V_{micro}) of lignite-based carbon materials. The L-CN-500, 600 and 700 samples have a surface area of 762, 1041 and $1630 m^2/g$, which are 1.8, 1.9 and 2.0 times that of L-500, 600 and 700, respectively. The total pore volume of L-CN-700 is $0.66 cm^3/g$, which is $0.35 cm^3/g$ larger than L-700. However, Table 1 discloses that the external surface areas (S_{meso}) of L-CN-500, 600 and 700 samples are quite comparable with L-500, 600 and 700, respectively, suggesting that the introduction of tripolycyanamide mainly improves the amounts of micropores. The SEM analysis shows that introduction of tripolycyanamide results in a larger macropore diameter over samples, while the N_2 sorption results reveal that the surface area and micropore volume are largely improved with the assistance of tripolycyanamide. Obviously, this micro-meso-macro hierarchical structure of lignite-based

N-doped carbon is facilitated to reduce the diffusion resistance of adsorbate, thus enhancing the accessibility of phenol molecules to adsorption sites.

The XRD patterns of L-600 and L-CN-600 are shown in Figure 3. One broad diffraction peak located at 2θ of ca. 22.9° corresponding to the (002) plane is observed for both samples, indicating that they are amorphous carbon materials [31,38]. In addition, the (100) diffraction peak (2θ of ca. 42.5°) is also distinct for these two samples, implying that they have a high graphitization degree [39].

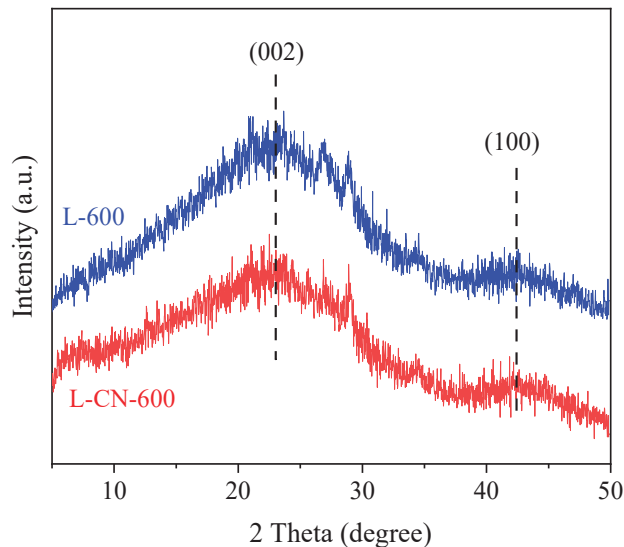


Figure 3. XRD patterns of L-600 and L-CN-600 samples.

In order to obtain further confirmation on the structure of lignite-based carbon, Raman spectra of all samples were collected, as shown in Figure 4. All samples show two distinct bands at 1588 cm^{-1} (G-band, highly ordered graphitic structure) and 1340 cm^{-1} (D-band, disordered structure), indicating that the lignite-based carbon materials are composed of highly ordered graphite and disordered structures, consistent with the XRD results. The intensity ratio of D-band to G-band (I_D/I_G) is often used to estimate the degree of graphitization for carbon materials [40,41]. A higher value of I_D/I_G represents a lower graphitization degree with more disordered structures or topological defects. Figure 4 shows that the I_D/I_G value increases from 0.87 for L-500 to 1.02 for L-700, suggesting that the increase in activation temperature leads to a decline in graphitization degree. This phenomenon can be explained by the fact that a higher activation temperature causes a more serious decomposition of functional groups over the lignite-based carbon materials, thus generating more defects or disordered structures over the carbon matrix.

The chemical compositions of lignite-based porous carbons prepared at different activation temperatures are listed in Table 2. The samples with no addition of tripolycyanamide have a nitrogen content of 0.90–1.75% because the raw lignite itself contains a certain amount of nitrogen. In addition, sulfur is also included in all samples as an impurity of lignite. With increasing the activation temperature, the N, H and S contents distinctly decrease owing to the decompositions of functional groups over the lignite-based carbons. In addition, the introduction of tripolycyanamide strikingly improves the N content in carbon materials, which increases from 1.75%, 1.64% and 0.90% for L-500, 600, and 700 to 3.49%, 3.50% and 1.53% for L-CN-500, 600 and 700, respectively, indicating that N atoms are successfully doped into lignite-based carbons with tripolycyanamide as the N source.

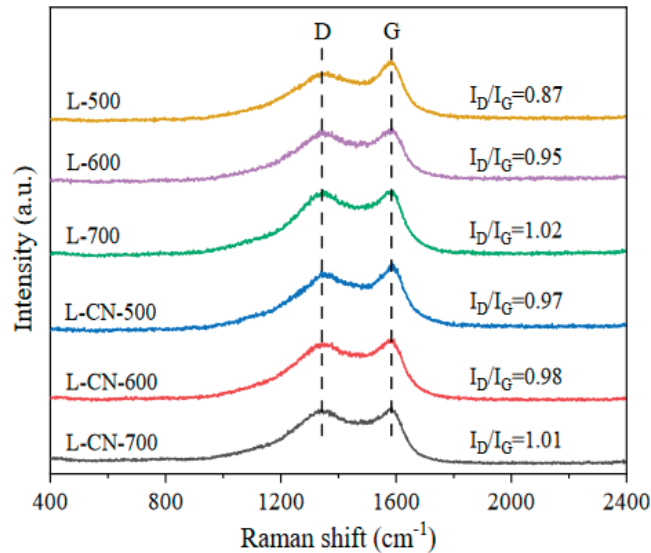


Figure 4. Raman spectra of the lignite-based porous carbons.

Table 2. Chemical compositions of lignite-based porous carbons prepared at different activation temperatures.

Samples	Chemical Compositions (wt%)					N/C ^a	H/C ^a
	N	C	H	S	Other		
L-500	1.75	67.53	2.24	0.38	28.11	0.02	0.40
L-600	1.64	66.62	1.59	0.27	29.88	0.02	0.29
L-700	0.90	65.58	1.41	0.30	31.81	0.01	0.26
L-CN-500	3.49	64.77	2.08	0.29	29.37	0.05	0.39
L-CN-600	3.50	68.37	1.58	0.16	26.39	0.04	0.28
L-CN-700	1.53	75.60	0.85	0.22	21.80	0.02	0.14

^a Molar ratios.

The presence of surface functional groups over lignite-based porous carbon was evidenced by XPS measurement. Figure 5 shows the wide scan of the L-CN-600 sample, and it can be seen that some impurity peaks assigned to Ca and K are observed. Figure 6 shows the N 1s XPS spectra in narrow scans, which can be deconvoluted into three groups depending on the binding energies. The N 1s peaks located at 398.6, 400 and 401 eV are assigned to pyridinic-N, pyrrolic-N and graphitic-N groups, respectively [13,16,42]. Table 3 shows that the relative amounts of graphitic-N and pyrrolic-N increase with the activation temperature, implying that the high activation temperature was favorable to the formation of graphitic-N and pyrrolic-N groups, although the total amount of different types of nitrogen species decreased. In contrast, the relative content of the pyridinic-N group steadily decreases from 29.2% for L-500 to 22.0% for L-700, with activation temperature increasing from 500 to 700 °C, while the relative content of pyridinic-N reaches the maximum value of 41.2% over the L-CN-500 sample, then rapidly declines to 14.1% when activation temperature increases to 700 °C. These results suggest that some of the pyridinic-N groups are unstable at high activation temperatures, probably convert into graphitic-N and pyrrolic-N groups or are decomposed during the activation process. As reported previously [13], these N-containing

groups are important functional groups for phenol adsorption despite the fact that their adsorption mechanisms are not fully elucidated.

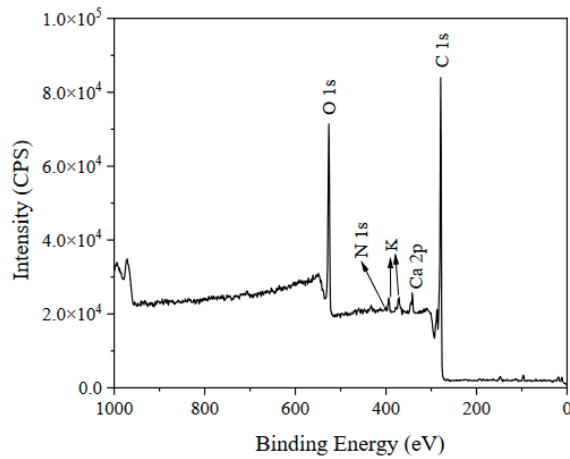


Figure 5. XPS wide scan of the L-CN-600 sample.

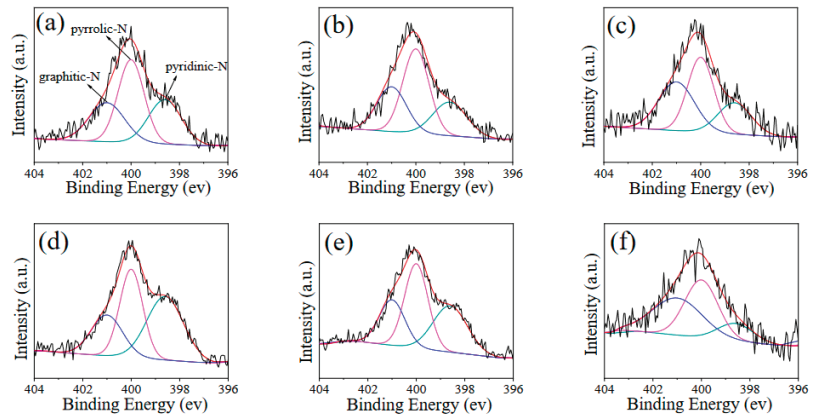


Figure 6. N 1s XPS spectra of L-500 (a), L-600 (b), L-700 (c), L-CN-500 (d), L-CN-600 (e), and L-CN-700 (f) samples.

Table 3. Relative peak areas determined from the N 1s XPS spectra of lignite-based porous carbons.

Sample	Graphitic-N (%)	Pyrrolic-N (%)	Pyridinic-N (%)
L-500	27.6	43.2	29.2
L-600	29.1	49.8	21.1
L-700	36.8	41.2	22.0
L-CN-500	22.8	36.0	41.2
L-CN-600	24.6	41.8	33.6
L-CN-700	42.3	43.6	14.1

3.2. Phenol Adsorption Performance of Lignite-Based Porous Carbons

3.2.1. Adsorption Capacity of Different Lignite-Based Porous Carbons

The increasing concern about the inappropriate discharge of phenolic-containing wastewater in recent years has necessitated a more efficient and viable way for the treatment of phenolic wastewater. Herein, the lignite-based porous carbons prepared in this work

were applied as adsorbents for the removal of phenol from wastewater. According to the results shown in Figure 7, all lignite-based carbons can adsorb a certain amount of phenol due to their high surface area and abundant functional groups. Specifically, with an increase in activation temperature, L-700 exhibits considerably higher adsorption performance than L-500, and the phenol adsorption capacity of the former (114.9 mg/g) is 1.9 times that of the latter (61.3 mg/g). This trend also holds true for L-CN-500, 600 and 700 samples. Meanwhile, it is worth noting that the addition of tripolycyanamide largely improved the phenol adsorption capacity, L-CN-700 showed the highest adsorption capacity (182.4 mg/g) among all the lignite-based porous carbons, which was also at a high level in the reported porous carbon adsorbents (Table 4).

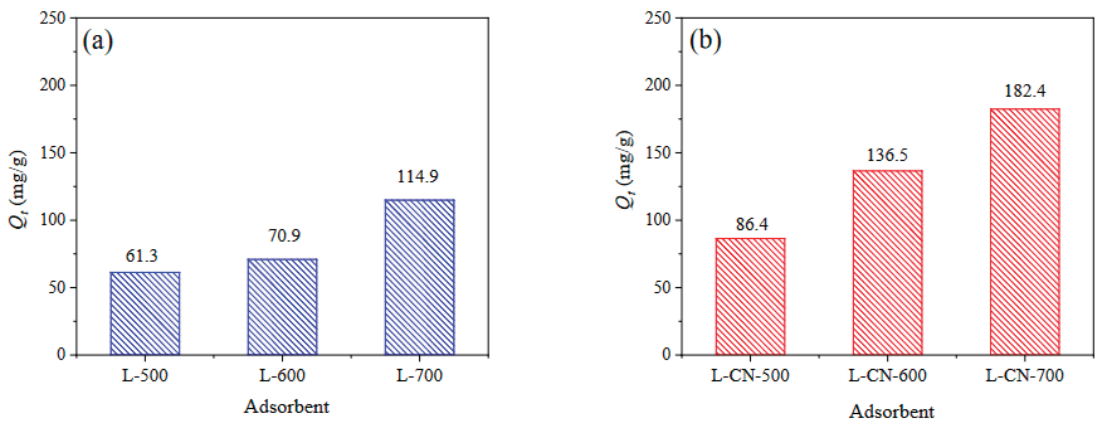


Figure 7. Effect of activation temperature on the adsorption capacities of L-x (a) and L-CN-x (b) samples. Adsorption conditions: $C_0 = 133$ mg/L, $m/v = 0.4$ g/L, 20 °C, $t = 90$ min.

Table 4. Phenol adsorption capacity of adsorbents in some recent reports.

Adsorbent	Phenol Adsorption Capacity, (mg/g)	Reference
Molecularly imprinted composite membrane	51.40	[6]
Nitrogen-doped magnetic mesoporous hollow carbon	55.86	[13]
Oily sludge-based AC	434	[18]
Diethylenetriamine-modified activated carbon	18.12	[19]
Nitrogen-doped hierarchically porous carbon	431	[20]
Activated carbon	96.92	[26]
Graphene	28.26	[34]
Porous carbon from <i>Toona sinensis</i> leaves	325	[43]
Lignite-based N-doped porous carbon	182.4	This work

The regeneration performance of adsorption materials is an important factor in the treatment of wastewater. To verify this, the regeneration performance of L-CN-700 was studied for six cycles at the adsorption temperature of 20 °C. Figure 8 shows that L-CN-700 maintains a stable adsorption capacity after six cycles, indicating that the lignite-based N-doped carbon has good regeneration performance in phenol adsorption.

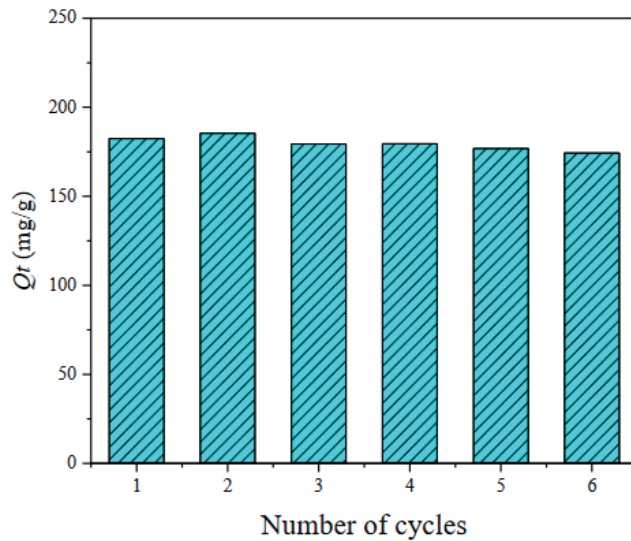


Figure 8. The regeneration cycles for phenol adsorption over the L-CN-700 sample. Adsorption conditions: $C_0 = 133$ mg/L, $m/v = 0.4$ g/L, 20 °C, $t = 90$ min.

It has been reported that the phenol adsorption capacity of carbon materials mainly depends on these factors, such as adsorbent–adsorbate interactions (physical and chemical effects) and pore structures (surface area and pore volume) [23]. The N_2 sorption measurements verified that the addition of tripolycyanamide significantly lifted the surface area of lignite-based porous carbons, which could evidently contribute to the phenol adsorption capacity. Furthermore, the contributions of surface chemical groups, especially the N-containing groups, are considered to be another important factor in determining phenol adsorption performance. At present, there are four adsorption mechanisms, i.e., the π - π dispersion interactions, electron donor–acceptor complex, hydrophobic interactions, and the hydrogen bond effect, which have been proposed to interpret the adsorption process of phenols [21,23,43]. To further understand a deep insight into the adsorption mechanism, the adsorption behaviors, including kinetics and isotherm over lignite-based porous carbons were elaborated on in detail.

3.2.2. Adsorption Kinetics

Figure 9 compares the phenol adsorption capacity of L-CN-600 and L-600 at 20 °C at different contact times. It is found that over 50% of the equilibrium adsorption amount is achieved within the first 10–15 min of the adsorption process for L-600 and L-CN-600. The phenol adsorption capacity of L-CN-600 rapidly increases to 120.7 mg/g with increasing adsorption time to 30 min, while a further increase to 50 min slowly increases the phenol uptake to 132.4 mg/g, then reaches the equilibrium within 70 min. The uptake of phenol over L-600 monotonically rises to 62.3 mg/g with increasing adsorption time to 50 min, which then slowly achieves equilibrium at the contact time of 90 min. Figure 9 reveals the fact that the time to reach the adsorption equilibrium for L-CN-600 is shorter than that of L-600. This is expected because the micropore volume of L-CN-600 is much larger than L-600, which leads to a lower mass transfer resistance when phenol diffuses into the adsorption sites [44,45].

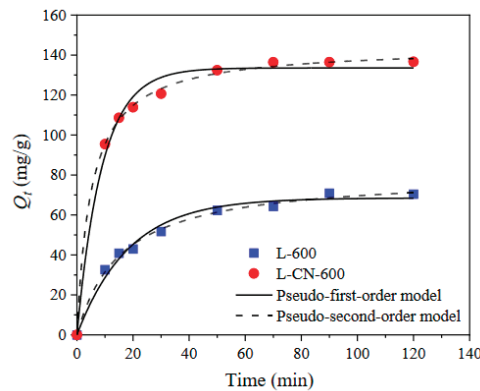


Figure 9. Adsorption kinetic curves of lignite-based porous carbons. Adsorption conditions: $C_0 = 133 \text{ mg/L}$, $m/v = 0.4 \text{ g/L}$, $20 \text{ }^\circ\text{C}$.

With the purpose of understanding the rate-controlling steps in the adsorption process, the phenol adsorption experiment data collected over L-600 and L-CN-600 were fitted by the PFO and PSO models. The kinetics fitting plots and parameters are shown in Figure 9 and Table 5. As listed in Table 5, the correlation coefficients (R^2) for the PSO model of both L-600 and L-CN-600 are higher than that of the PFO model, indicating the sorption process follows the PSO adsorption rate expression. However, it should be mentioned that the calculated values of $Q_{e,cal}$ for the PFO model are closer to the experimental data ($Q_{e,exp}$), while the $Q_{e,cal}$ for the PSO model are higher compared with experimental values, and this gap between the calculated and experimental values might be caused by experimental errors. The results that phenol adsorption obeying the PSO kinetics model over lignite-based carbons are in line with the previous conclusions obtained over the N-doped magnetic mesoporous hollow carbon [13], the activated carbons by thermal modification [21] and biomass-based carbons [43]. As previously mentioned [32], the PSO model is based on the assumption that the rate-limiting step is chemisorption, which is controlled by valency forces via electronic sharing or exchanging between adsorbent and adsorbate. This may support the fact that phenol adsorption on lignite-based porous carbon is mainly caused by the π - π interaction between the aromatic-ring of phenol and the basal plane of porous carbons.

Table 5. The kinetic parameters of phenol adsorption over L-600 and L-CN-600 samples.

Adsorbent	$Q_{e,exp}^a$	Pseudo-First-Order			Pseudo-Second-Order		
		$Q_{e,cal}^b$	k_1	R^2	$Q_{e,cal}^b$	k_2	R^2
L-600	70.44	68.49	0.0541	0.9849	80.44	0.0008	0.9953
L-CN-600	136.64	133.54	0.1112	0.9898	144.19	0.0014	0.9988

^a $Q_{e,exp}$: the equilibrium adsorption amount obtained by experiments. ^b $Q_{e,cal}$: the calculated equilibrium adsorption amount.

3.2.3. Adsorption Isotherms

The isotherm adsorption model is widely used as an effective tool to describe the interaction between adsorbent and adsorbate. Herein, two classical isotherm models, i.e., the Langmuir and Freundlich models, were adopted to analyze the equilibrium adsorption isotherms of phenol over L-CN-600 and L-600 samples at $20 \text{ }^\circ\text{C}$, and the fitting plots and parameters are shown in Figure 10 and Table 6. As shown in Figure 10, the adsorption equilibrium curves of both L-CN-600 and L-600 samples show the typical-I isotherm, where the equilibrium adsorption capacity of samples steadily increases with the phenol concentrations. The equilibrium adsorption capacity of L-CN-600 reaches 171.6 mg/g when the phenol concentration is 203.9 mg/L .

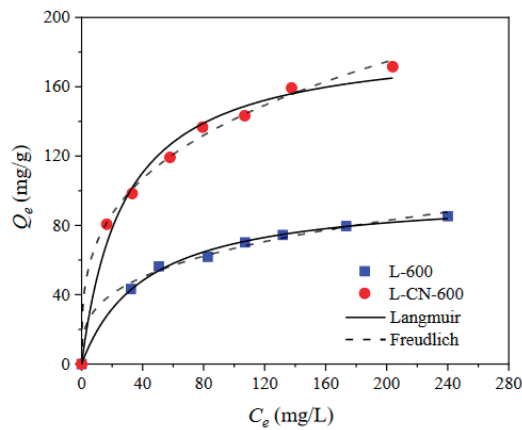


Figure 10. Adsorption isotherm curves of lignite-based porous carbons. Adsorption conditions: $m/v = 0.4$ g/L, 20 °C, $t = 120$ min.

Table 6. Langmuir and Freundlich adsorption isotherm parameters for L-600 and L-CN-600 at 20 °C.

Adsorbent	Langmuir			Freundlich		
	Q_m	k_L	R^2	k_F	n	R^2
L-600	98.65	0.0238	0.9960	15.8861	3.2088	0.9938
L-CN-600	187.73	0.0357	0.9870	34.7823	3.2859	0.9971

Table 6 discloses that Langmuir and Freundlich models both fit well with the experimental results of the L-600 sample because the correlation coefficients of the Langmuir (0.9960) and Freundlich (0.9938) models are very close to 1. The Langmuir model is more applicable for describing the adsorption behavior of phenol because of its higher value of R^2 . This indicates that phenol adsorption over L-600 should obey the monolayer adsorption mechanism, which assumes that adsorbate molecules form a localized and uniform monolayer coverage on the adsorbent [46,47]. On the contrary, a comparison of the correlation coefficient reveals that the Freundlich model is superior to the Langmuir model over L-CN-600, suggesting the occurrence of multi-molecular layers adsorption over L-CN-600, most likely due to its heterogeneous surface and abundant N-containing functional groups as adsorption sites for phenol [23,48,49]. As listed in Table 6, the n value obtained in this work is 3.2859 for L-CN-600, which means that phenol is easily adsorbed on the surface of lignite-based N-doped porous carbon [26].

3.3. Theoretical Calculations and Adsorption Mechanism

With the aim of providing a deep understanding of the adsorption mechanism over lignite-based porous carbon, four theoretical models with different functional groups were established, by which the phenol adsorption energies (E_{ads}) over different adsorption sites were calculated. The graphene was used to simulate the base plane of carbon materials in this work, while three N-containing groups (the graphitic-N, pyrrolic-N, and pyridinic-N) were adopted according to the XPS measurements.

Figure 11 shows the E_{ads} and the optimized geometric structures of phenol adsorbed on these adsorption sites. It can be seen that the adsorption energies between phenol and the N-free graphite layer are as low as -71 kJ/mol (Figure 11a), suggesting that the phenol molecule can be stably adsorbed on the carbon materials. The value of E_{ads} over the N-free layer is higher than those of graphitic-N and pyrrolic-N groups, supporting the fact that the interactions between phenol and these N-containing groups are stronger. Nevertheless, it should be mentioned that despite the fact that the E_{ads} over pyrrolic-N shows the lowest

value, the gap of E_{ads} between pyrrolic-N and N-free graphite layer is only 3 kJ/mol. This means that the adsorption capacity of pyrrolic-N groups is only slightly stronger than the N-free graphite layer. However, the weak advantage of N-containing functional groups should still not be ignored because it could be effectually enlarged by increasing the amount of N-containing groups during application. On the other hand, it should be noted that the value of E_{ads} over pyridinic-N groups is 1 kJ/mol higher than the N-free graphite layer, which indicates that the contribution of pyridinic-N to phenol adsorption should be not obvious or even negative in contrast to the N-free graphite layer.

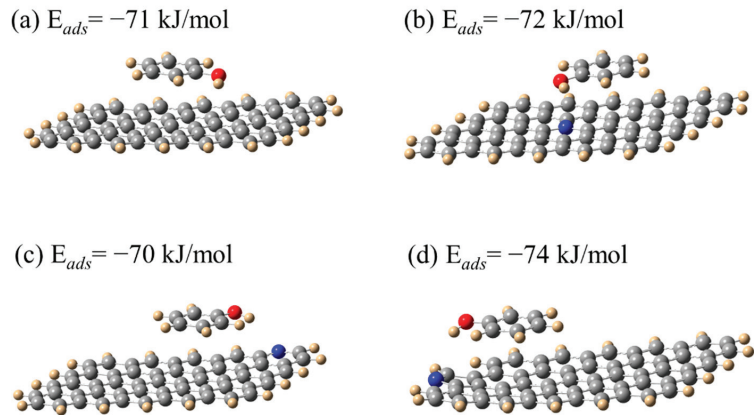


Figure 11. The optimized geometric structures of phenol adsorbed on N-free carbon (a), graphitic-N (b), pyridinic-N (c) and pyrrolic-N (d) functional groups.

It is interesting and worth noting that phenol exhibits different adsorption energies on different N-containing functional groups. The value of E_{ads} for phenol is in the order of pyridinic-N > N-free graphite layer > graphitic-N > pyrrolic-N groups. The nature of phenol adsorption is primarily caused by the π - π dispersion interactions between the π electrons in aromatic rings and those in graphite layers, as supported by the kinetics results and previous studies [13,23]. Thus, it can be inferred that the gaps in the adsorption capacity could be interpreted by the different π electron densities over different functional groups. The pyrrolic-N group should provide the highest π electron density due to its smaller five-membered ring structure. Meanwhile, in comparison to the N-free graphite, the enhanced electron density could be obtained over the graphitic-N group owing to the doping of the electron-rich nitrogen atom. In the case of pyridinic-N groups, the N atom is located at the margin of the carbon plane, where the asymmetrical distribution of the π electron might weaken the π - π conjugated interactions.

In this work, because the specific surface areas and pore volumes of lignite-based porous carbon exhibit wide variation due to the addition of tripolycyanamide, it is inappropriate to only attribute the enhancement of phenol uptakes to the carbon surface chemistry or the presence of N-containing functional groups. In particular, Figure 12 shows the good linear relationships between phenol adsorption capacity and the surface area ($R^2 = 0.9588$) or micropore volume ($R^2 = 0.9523$), suggesting that the micropore properties of lignite-based porous carbon strongly influence the phenol adsorption. In contrast, the correlation coefficients between the N contents and phenol adsorption capacity were only 0.0009–0.1015. Such low correlation coefficients reveal that N-containing groups in the lignite-based porous carbon may not be the dominant factor in the experimental range, despite the fact that it is usually considered the principal factor influencing phenol adsorption [13]. Similar results were reported by Cansado and co-workers related to the removal of 4-chloro-2-methyl-phenoxyacetic acid by ACs containing different N contents [50].

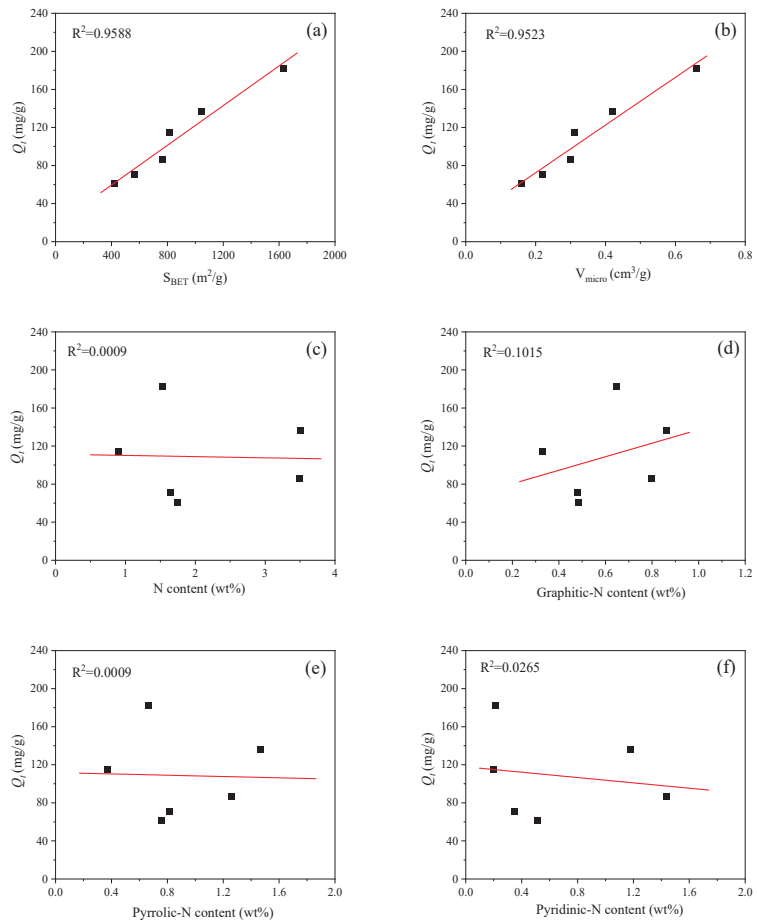


Figure 12. Dependence of phenol adsorption capacity on the specific surface area (a), micropore volume (b), total N content (c), graphitic-N content (d), pyrrolic-N content (e), and pyridinic-N content (f) of the lignite-based porous carbons. Adsorption conditions: $C_0 = 133$ mg/L, $m/v = 0.4$ g/L, 20 °C, $t = 90$ min.

4. Conclusions

In this work, using lignite as the carbon precursor, a series of lignite-based porous carbons were prepared for phenol adsorption in an aqueous solution. It was found that the N-doping with tripolycyanamide as an N source significantly enhanced the etching of lignite by KOH during activation, resulting in an increase in the specific surface area, pore volume, N content, and hence, the phenol adsorption capacity. The equilibrium adsorption capacity over the lignite-based N-doped porous carbon achieves 171.6 mg/g for 203.9 mg/L of phenol at 20 °C. The kinetics adsorption results disclosed that phenol adsorption over lignite-based porous carbon matches well with the PSO model, indicative of the chemical interactions between phenol and adsorbent. The adsorption isotherm over lignite-based N-doped porous carbon is fitted well with the Freundlich model, suggesting that phenol molecules are adsorbed in multiple layers on the surface of carbons. Furthermore, theoretical calculations demonstrate that graphitic-N and pyrrolic-N groups could play positive roles in phenol adsorption, probably attributed to the enhancement of the π - π interaction between the aromatic-ring of phenol and the carbon plane, while the π - π interactions are

essentially influenced by the π electron densities of the functional groups over carbon planes. Finally, the work presented here could provide a valuable reference for fabricating a lignite-based adsorbent to remove phenolic compounds from wastewater.

Author Contributions: Conceptualization, Y.X.; investigation, Y.X. and L.S.; validation, H.W. and C.Z.; formal analysis, M.C. and H.L.; resources, W.L. and Y.N.; writing—original draft preparation, writing—review and editing, Y.X. and Y.C.; project administration, Y.N.; funding acquisition, Y.X. and Y.N. All authors have read and agreed to the published version of the manuscript.

Funding: This research was financially supported by the Natural Science Foundation of Shanxi Province of China under Grant (No. 201901D111321), the Taiyuan Institute of Technology Scientific Research Initial Funding (No. 2022KJ062), the Scientific and Technological Innovation Programs of Higher Education Institutions in Shanxi under Grant (No. 2020L0655) and the Fund for Shanxi “1331” Project (Collaborative Innovation Center of CO₂ Conversion and Utilization).

Institutional Review Board Statement: Not applicable.

Informed Consent Statement: Not applicable.

Data Availability Statement: All of the data are given in the manuscript.

Conflicts of Interest: The authors declare no conflict of interest.

References

- Ghafari, M.; Cui, Y.; Alali, A.; Atkinson, J.D. Phenol adsorption and desorption with physically and chemically tailored porous polymers: Mechanistic variability associated with hyper-cross-linking and amination. *J. Hazard. Mater.* **2019**, *361*, 162–168. [[CrossRef](#)] [[PubMed](#)]
- Liu, B.; Govindan, R.; Muthuchamy, M.; Cheng, S.; Li, X.; Ye, L.; Wang, L.; Guo, S.; Li, W.; Alharbi, N.S.; et al. Halophilic archaea and their extracellular polymeric compounds in the treatment of high salt wastewater containing phenol. *Chemosphere* **2022**, *294*, 133732. [[CrossRef](#)] [[PubMed](#)]
- Adeel, M.; Xu, Y.; Ren, L.; Shao, J.; He, Y. Improvement of phenol separation and biodegradation from saline wastewater in extractive membrane bioreactor (EMBR). *Bioresour. Technol. Rep.* **2022**, *17*, 100897. [[CrossRef](#)]
- Mohd, A. Presence of phenol in wastewater effluent and its removal: An overview. *Int. J. Environ. Anal. Chem.* **2020**, *102*, 1362–1384.
- Zhou, S.; Gu, P.; Wan, H.; Zhu, Y.; Li, N.; Chen, D.; Marcomini, A.; Xu, Q.; Lu, J. Preparation of new triptycene- and pentaptycene-based crosslinked polymers and their adsorption behavior towards aqueous dyes and phenolic organic pollutants. *Sep. Purif. Technol.* **2021**, *278*, 119495. [[CrossRef](#)]
- Qu, Y.; Qin, L.; Guo, M.; Liu, X.; Yang, Y. Multilayered molecularly imprinted composite membrane based on porous carbon nanospheres/pDA cooperative structure for selective adsorption and separation of phenol. *Sep. Purif. Technol.* **2022**, *280*, 119915. [[CrossRef](#)]
- Nady, H.; El-Rabiei, M.M.; Abd El-Hafez, G.M. Electrochemical oxidation behavior of some hazardous phenolic compounds in acidic solution. *Egypt. J. Pet.* **2017**, *26*, 669–678. [[CrossRef](#)]
- Wu, H.; Liu, R.; Sun, Y.; Wen, Y.; Zhao, Q.; Lin, S.; Wang, Y. Effect of MoS₂ on phenol decomposition in water after high-voltage pulse discharge treatment. *Chemosphere* **2022**, *294*, 133808. [[CrossRef](#)]
- Dionisi, D.; Etteh, C.C. Effect of process conditions on the aerobic biodegradation of phenol and paracetamol by open mixed microbial cultures. *J. Environ. Chem. Eng.* **2019**, *7*, 103282. [[CrossRef](#)]
- Wu, Z.; Jing, J.; Zhang, K.; Li, W.; Yang, J.; Shen, J.; Zhang, S.; Xu, K.; Zhang, S.; Zhu, Y. Epitaxial BiP₅O₁₄ layer on BiOI nanosheets enhancing the photocatalytic degradation of phenol via interfacial internal-electric-field. *Appl. Catal. B Environ.* **2022**, *307*, 121153. [[CrossRef](#)]
- Bertoncini, C.; Raffaelli, J.; Fassino, L.; Odetti, H.S.; Bottani, E.J. Phenol adsorption on porous and non-porous carbons. *Carbon* **2003**, *41*, 1101–1111. [[CrossRef](#)]
- Liu, X.; Pinto, N.G. Ideal adsorbed phase model for adsorption of phenolic compounds on activated carbon. *Carbon* **1997**, *35*, 1387–1397. [[CrossRef](#)]
- Liu, H.; Kim, G.E.; Hong, C.O.; Song, Y.C.; Lee, W.K.; Liu, D.; Jang, S.H.; Park, Y.K. Treatment of phenol wastewater using nitrogen-doped magnetic mesoporous hollow carbon. *Chemosphere* **2021**, *271*, 129595. [[CrossRef](#)] [[PubMed](#)]
- Beker, U.; Ganbold, B.; Dertli, H.; Gülbayir, D.D. Adsorption of phenol by activated carbon: Influence of activation methods and solution pH. *Energy Convers. Manag.* **2010**, *51*, 235–240. [[CrossRef](#)]
- Su, F.; Lv, L.; Hui, T.M.; Zhao, X.S. Phenol adsorption on zeolite-templated carbons with different structural and surface properties. *Carbon* **2005**, *43*, 1156–1164. [[CrossRef](#)]
- Yang, G.; Chen, H.; Qin, H.; Feng, Y. Amination of activated carbon for enhancing phenol adsorption: Effect of nitrogen-containing functional groups. *Appl. Surf. Sci.* **2014**, *293*, 299–305. [[CrossRef](#)]

17. Stavropoulos, G.G.; Samaras, P.; Sakellariopoulos, G.P. Effect of activated carbons modification on porosity, surface structure and phenol adsorption. *J. Hazard. Mater.* **2008**, *151*, 414–421. [[CrossRef](#)]
18. Mojoudi, N.; Mirghaffari, N.; Soleimani, M.; Shariatmadari, H.; Belver, C.; Bedia, J. Phenol adsorption on high microporous activated carbons prepared from oily sludge: Equilibrium, kinetic and thermodynamic studies. *Sci. Rep.* **2019**, *9*, 19352. [[CrossRef](#)]
19. Saleh, T.A.; Adio, S.O.; Asif, M.; Dafalla, H. Statistical analysis of phenols adsorption on diethylenetriamine-modified activated carbon. *J. Clean. Prod.* **2018**, *182*, 960–968. [[CrossRef](#)]
20. Du, W.; Sun, J.; Zan, Y.; Zhang, Z.; Ji, J.; Dou, M.; Wang, F. Biomass-derived nitrogen-doped hierarchically porous carbon networks as efficient adsorbents for phenol removal from wastewater over a wide pH range. *RSC Adv.* **2017**, *7*, 46629–46635. [[CrossRef](#)]
21. Zhang, D.; Huo, P.; Liu, W. Behavior of phenol adsorption on thermal modified activated carbon. *Chin. J. Chem. Eng.* **2016**, *24*, 446–452. [[CrossRef](#)]
22. Liu, S.; Wang, R. Modified activated carbon with an enhanced nitrobenzene adsorption capacity. *J. Porous Mater.* **2010**, *18*, 99–106. [[CrossRef](#)]
23. Wang, T.; Cheng, Z.; Liu, Y.; Tang, W.; Fang, T.; Xing, B. Mechanistic understanding of highly selective adsorption of bisphenols on microporous-dominated nitrogen-doped framework carbon. *Sci. Total Environ.* **2021**, *762*, 143115. [[CrossRef](#)] [[PubMed](#)]
24. Sheng, G.D.; Shao, D.D.; Ren, X.M.; Wang, X.Q.; Li, J.X.; Chen, Y.X.; Wang, X.K. Kinetics and thermodynamics of adsorption of ionizable aromatic compounds from aqueous solutions by as-prepared and oxidized multiwalled carbon nanotubes. *J. Hazard. Mater.* **2010**, *178*, 505–516. [[CrossRef](#)] [[PubMed](#)]
25. Wei, J.; Cai, W. One-step hydrothermal preparation of N-doped carbon spheres from peanut hull for efficient removal of Cr(VI). *J. Environ. Chem. Eng.* **2020**, *8*, 104449.
26. Zhang, F.; Zhang, S.; Chen, L.; Liu, Z.; Qin, J. Utilization of bark waste of *Acacia mangium*: The preparation of activated carbon and adsorption of phenolic wastewater. *Ind. Crop. Prod.* **2021**, *160*, 113157. [[CrossRef](#)]
27. Wang, L.; Zhu, D.; Chen, J.; Chen, Y.; Chen, W. Enhanced adsorption of aromatic chemicals on boron and nitrogen co-doped single-walled carbon nanotubes. *Environ. Sci. Nano* **2017**, *4*, 558–564. [[CrossRef](#)]
28. Li, B.; Lei, Z.; Zhang, X.; Huang, Z. Adsorption of simple aromatics from aqueous solutions on modified activated carbon fibers. *Catal. Today* **2010**, *158*, 515–520. [[CrossRef](#)]
29. Liu, X.; Tu, Y.; Liu, S.; Liu, K.; Zhang, L.; Li, G.; Xu, Z. Adsorption of ammonia nitrogen and phenol onto the lignite surface: An experimental and molecular dynamics simulation study. *J. Hazard. Mater.* **2021**, *416*, 125966. [[CrossRef](#)]
30. Song, J.; Shen, W.; Wang, J.; Fan, W. Superior carbon-based CO₂ adsorbents prepared from poplar anthers. *Carbon* **2014**, *69*, 255–263. [[CrossRef](#)]
31. Ge, C.; Song, J.; Qin, Z.; Wang, J.; Fan, W. Polyurethane Foam-Based Ultramicroporous Carbons for CO₂ Capture. *ACS Appl. Mater. Inter.* **2016**, *8*, 18849–18859. [[CrossRef](#)] [[PubMed](#)]
32. Ho, Y.S.; McKay, G. Pseudo-second order model for sorption processes. *Process Biochem.* **1999**, *34*, 451–465. [[CrossRef](#)]
33. Kumar, K.V. Pseudo-second order models for the adsorption of safranin onto activated carbon: Comparison of linear and non-linear regression methods. *J. Hazard. Mater.* **2007**, *142*, 564–567. [[CrossRef](#)] [[PubMed](#)]
34. Li, Y.; Du, Q.; Liu, T.; Sun, J.; Jiao, Y.; Xia, Y.; Xia, L.; Wang, Z.; Zhang, W.; Wang, K.; et al. Equilibrium, kinetic and thermodynamic studies on the adsorption of phenol onto graphene. *Mater. Res. Bull.* **2012**, *47*, 1898–1904. [[CrossRef](#)]
35. Jain, M.; Khan, S.A.; Sahoo, A.; Dubey, P.; Pant, K.K.; Ziora, Z.M.; Blaskovich, M.A.T. Statistical evaluation of cow-dung derived activated biochar for phenol adsorption: Adsorption isotherms, kinetics, and thermodynamic studies. *Bioresour. Technol.* **2022**, *352*, 127030. [[CrossRef](#)]
36. Frisch, M.J.; Trucks, G.W.; Schlegel, H.B.; Scuseria, G.E.; Robb, M.A.; Cheeseman, J.R.; Scalmani, G.; Barone, V.; Mennucci, B.; Petersson, G.A. *Gaussian 09*; Revision E.01; Gaussian, Inc.: Wallingford, CT, USA, 2009.
37. Wang, B.; Gan, F.; Dai, Z.; Ma, S.; Chen, W.; Jiang, X. Air oxidation coupling NH₃ treatment of biomass derived hierarchical porous biochar for enhanced toluene removal. *J. Hazard. Mater.* **2021**, *403*, 123995. [[CrossRef](#)]
38. Franco, D.S.P.; Georgin, J.; Netto, M.S.; Allasia, D.; Oliveira, M.L.S.; Foletto, E.L.; Dotto, G.L. Highly effective adsorption of synthetic phenol effluent by a novel activated carbon prepared from fruit wastes of the *Ceiba speciosa* forest species. *J. Environ. Chem. Eng.* **2021**, *9*, 105927. [[CrossRef](#)]
39. Song, J.; Shen, W.; Wang, J.; Fan, W. Synthesis of novel hollow graphitic vesicle-supported Pt nanoparticles for oxygen reduction reaction. *Carbon* **2016**, *109*, 505–516. [[CrossRef](#)]
40. Xue, Y.; Li, J.; Wang, S.; Cui, X.; Dong, M.; Wang, G.; Qin, Z.; Wang, J.; Fan, W. Co-reaction of methanol with butene over a high-silica H-ZSM-5 catalyst. *J. Catal.* **2018**, *367*, 315–325. [[CrossRef](#)]
41. Urbonaite, S.; Hälldahl, L.; Svensson, G. Raman spectroscopy studies of carbide derived carbons. *Carbon* **2008**, *46*, 1942–1947. [[CrossRef](#)]
42. Shi, R.; Zhao, J.; Liu, S.; Sun, W.; Li, H.; Hao, P.; Li, Z.; Ren, J. Nitrogen-doped graphene supported copper catalysts for methanol oxidative carbonylation: Enhancement of catalytic activity and stability by nitrogen species. *Carbon* **2018**, *130*, 185–195. [[CrossRef](#)]
43. Kong, X.; Gao, H.; Song, X.; Deng, Y.; Zhang, Y. Adsorption of phenol on porous carbon from *Toona sinensis* leaves and its mechanism. *Chem. Phys. Lett.* **2020**, *739*, 137046. [[CrossRef](#)]
44. Lorenc-Grabowska, E.; Diez, M.A.; Gryglewicz, G. Influence of pore size distribution on the adsorption of phenol on PET-based activated carbons. *J. Colloid Interface Sci.* **2016**, *469*, 205–212. [[CrossRef](#)] [[PubMed](#)]

45. Kowalczyk, P.; Deditius, A.; Ela, W.P.; Wiśniewski, M.; Gauden, P.A.; Terzyk, A.P.; Furmaniak, S.; Włoch, J.; Kaneko, K.; Neimark, A.V. Super-sieving effect in phenol adsorption from aqueous solutions on nanoporous carbon beads. *Carbon* **2018**, *135*, 12–20. [[CrossRef](#)]
46. Zhang, J.; Qin, L.; Yang, Y.; Liu, X. Porous carbon nanospheres aerogel based molecularly imprinted polymer for efficient phenol adsorption and removal from wastewater. *Sep. Purif. Technol.* **2021**, *274*, 119029. [[CrossRef](#)]
47. Chen, A.; Li, Y.; Yu, Y.; Li, Y.; Xia, K.; Wang, Y.; Li, S.; Zhang, L. Synthesis of hollow mesoporous carbon spheres via “dissolution-capture” method for effective phenol adsorption. *Carbon* **2016**, *103*, 157–162. [[CrossRef](#)]
48. Wang, T.; Huang, M.; Liu, X.; Zhang, Z.; Liu, Y.; Tang, W.; Bao, S.; Fang, T. Facile one-step hydrothermal synthesis of α -Fe₂O₃/g-C₃N₄ composites for the synergistic adsorption and photodegradation of dyes. *RSC Adv.* **2019**, *9*, 29109–29119. [[CrossRef](#)]
49. Jun, L.Y.; Karri, R.R.; Mubarak, N.M.; Yon, L.S.; Bing, C.H.; Khalid, M.; Jagadish, P.; Abdullah, E.C. Modelling of methylene blue adsorption using peroxidase immobilized functionalized Buckypaper/polyvinyl alcohol membrane via ant colony optimization. *Environ. Pollut.* **2020**, *259*, 113940. [[CrossRef](#)]
50. Cansado, I.P.P.; Mourão, P.A.M. Impact of the use of co-adjuvants agents during chemical activation on the performance of activated carbons in the removal of 4-chloro-2-methyl-phenoxyacetic acid. *Environ. Technol. Inno.* **2021**, *24*, 102058. [[CrossRef](#)]

Article

Building Sector Issues in about 100 Years: End-Of-Life Scenarios of Carbon-Reinforced Concrete Presented in the Context of a Life Cycle Assessment, Focusing the Carbon Footprint

Jana Gerta Backes ^{1,*}, Pamela Del Rosario ¹, Dino Petrosa ¹, Marzia Traverso ¹, Tobias Hatzfeld ^{2,3} and Edeltraud Günther ^{2,3}

- ¹ Institute of Sustainability in Civil Engineering, Faculty of Civil Engineering, RWTH Aachen University, Mies-van-der-Rohe-Str. 1, 52074 Aachen, Germany
- ² Chair of Business Administration esp. Sustainability Management and Environmental Accounting, Faculty of Business and Economics, Technische Universität Dresden, Falkenbrunnen, FAL A 119, Würzburger Straße 35, 01187 Dresden, Germany
- ³ Institute for Integrated Management of Material Fluxes and of Resources (UNU-FLORES), United Nations University, 01067 Dresden, Germany
- * Correspondence: jana.backes@inab.rwth-aachen.de; Tel.: +49-241-800-22765

Abstract: Carbon-reinforced concrete (CRC) has the potential to play a pivotal role in optimizing the built environment and has therefore been experiencing a wave of research and development in the construction industry in recent years. The production of carbon fibers for CRC is energy-intensive, prompting the need to explore circular economy approaches (e.g., recycling at the End-of-Life (EoL)) to optimize the environmental performance of this material. Underdeveloped processes and a resulting lack of primary data regarding the recycling of CRC have hampered a comprehensive sustainability assessment of the novel composite building material. The novelty of this article is the detailed presentation of possible EoL scenarios for CRC and the detailed determination of the respective environmental impacts. This study aims to model EoL options within a Life Cycle Assessment (LCA), focusing on the EoL stage based on ISO 14040/44 using the GaBi ts 10.5.1.124 software and the CML2001 (2016) methodology. The practical relevance of the study lies in the early consideration of the entire life cycle of new materials, such as CRC, already in the design phase. Furthermore, the EoL can have relevant impacts on the environment, and due to an increasing significance of sustainability aspects, this LCA clarifies first approaches for the future of the construction sector in quantitative statements (e.g., CO₂ emissions). All data are literature-based and are explained in detail and calculated for our case study with the functional unit of one kilogram of re-usable material (reusable and fully usable “raw” material for further use/ development) from a double wall. The impact assessment was calculated for 11 midpoint categories and related indicators, although the main focus was on Global Warming Potential (GWP). It was found that the highest-quality recycled options for CRC arise when the individual fractions (concrete matrix and carbon fibers) are first broken up, separated and then individually processed. This study focused mainly on the processing of the carbon fibers contained in CRC, for which pyrolysis and mechanical recycling have the strongest potential for industrial application. For the demolition and separation of both the concrete and the carbon fiber fractions, the conventional transport from the demolition site to the stationary processing plant proved to be the main driver of the GWP (1.4×10^{-3} kg CO₂e). In the subsequent processing of the carbon fibers, pyrolysis showed a higher GWP (9.7×10^{-3} kg CO₂e) than mechanical recycling (3.1×10^{-4} kg CO₂e). In addition, the production of one m³ of concrete (C30/37) was compared to a primary raw material concrete fraction. Concrete can be successfully used as a substitute material for the gravel present in the C30/37 concrete. The use of recycled parts in concrete (originating from the concrete used in carbon-reinforced concrete) as a substitute for primary gravel showed a savings of 6.9 kg CO₂e per m³ of primary concrete, corresponding to a reduction of 22.5%. The results show that the mechanical recycling of carbon fibers is overall the route with the lowest energy input and emissions. However, compared to pyrolysis, the recycled carbon

Citation: Backes, J.G.; Del Rosario, P.; Petrosa, D.; Traverso, M.; Hatzfeld, T.; Günther, E. Building Sector Issues in about 100 Years: End-Of-Life Scenarios of Carbon-Reinforced Concrete Presented in the Context of a Life Cycle Assessment, Focusing the Carbon Footprint. *Processes* **2022**, *10*, 1791. <https://doi.org/10.3390/pr10091791>

Academic Editor: Kian Jon Chua

Received: 1 August 2022

Accepted: 2 September 2022

Published: 5 September 2022



Copyright: © 2022 by the authors. Licensee MDPI, Basel, Switzerland. This article is an open access article distributed under the terms and conditions of the Creative Commons Attribution (CC BY) license (<https://creativecommons.org/licenses/by/4.0/>).

fibers from mechanical recycling have a lower quality. Therefore, despite the higher energy input, pyrolysis is a more promising approach to close the material cycle. Furthermore, recycled aggregate concrete can reduce emissions by a quarter compared to primary concrete. Finally, this work aimed to provide a basis for further life cycle optimization in the construction sector. In subsequent studies, the EoL must be combined with the production and use stages to depict the entire life cycle, identify possible trade-offs and compare the results with conventional construction methods or materials such as steel-reinforced concrete.

Keywords: carbon-reinforced concrete; LCA; end-of-life; recycling; carbon fiber; reinforced concrete

1. Introduction

The construction sector is an important part of the fight against climate change. Current data show that globally, 37% of energy-related CO₂ emissions (incl. use stage), about 7–8% of total CO₂ emissions (excl. use stage), 36% of energy consumption and 40% of raw material consumption are attributable to the construction sector [1–3]. Accordingly, there is an increasing focus on sustainable design and resource-efficient use of building materials [4]. In this context, concrete is the dominant building material, with an estimated global consumption of 8.8 billion tons per year, which is under increasing criticism due to its resource consumption and production-related CO₂ emissions [5–7]. At the same time, both global population growth and urbanization are leading to an increased demand for housing and infrastructure, resulting in increased resource use as well as CO₂ release throughout a building's life cycle [4,8]. Therefore, to counter both a future threat of resource scarcity and increasing CO₂ emissions in the building and construction sector, sustainable innovations are needed to improve potential building sector issues in about 100 years [8–11].

The composite material carbon-reinforced concrete (CRC) has the potential to play a crucial role in optimizing the built environment [8,10]. CRC consists of reinforcement made of carbon fibers and thus substitutes the steel reinforcement of conventional steel-reinforced concrete, which has been the most widely used building material worldwide to date [12–14]. Steel reinforcement has the decisive disadvantage of being susceptible to corrosion—an additional concrete cover serving as corrosion protection is required [8]. In comparison, the carbon reinforcement found in CRC is non-corrosive, which could lead to thinner components and enormous concrete savings as well as ultimately an increase in environmental and economic efficiency [8,12,14]. CRC not only offers the advantage of not corroding but also has an above-average service life of an estimated 100 years [15], which is significantly longer than the service life of reinforced concrete (40–80 years) [8,12,14]. Furthermore, most studies in the construction industry focus on a service life of only 50 years [16,17], which can be exceeded by CRC and by this postpone (emissions) end-of-life challenges to in about 100 years (instead of 50 years).

Currently, End-of-Life (EoL) processes for CRC are underdeveloped and far from ideal from an environmental perspective. These processes lead to downcycling, which is insufficient to significantly reduce resource consumption and associated emissions within a circular economy [4,10]. Moreover, there is a lack of primary data on the recycling of CRC, which until now has hindered a complete sustainability assessment of this innovative composite building material. Developing a suitable reuse and recycling concept for CRC is critical for its environmental sustainability [10]. Consequently, this study aims to identify the currently possible methods for the CRC recycling and determine the associated energy consumption to enable an environmental assessment of CRC at the end of its life cycle. For this purpose, a Life Cycle Assessment (LCA) of the CRC at the end of its service life is carried out.

In the following, we present the State-of-the-Art of CRC and previous LCAs related to CRC. Furthermore, the LCA case study is split into two scenarios: mechanical recycling and pyrolysis. Both scenarios start with identical deconstruction, and it is assumed that the

analyzed material is composed of primary raw material. Finally, we assume concrete to be reused in road construction as a possible second life scenario.

Carbon-Reinforced Concrete

CRC is an innovative composite building material composed of concrete and reinforcement which, in contrast to reinforced concrete, is not made of steel but carbon fibers [8]. In the construction sector, the starting material for the production of carbon fibers is polyacrylonitrile (PAN), obtained from petroleum. The fiber is impregnated and absorbs a predetermined amount of impregnation and water. Depending on the desired stability and flexibility of the reinforcing mesh, the construction industry usually distinguishes between two types of impregnation: epoxy resin (duromers; EP) or styrene-butadiene rubber (elastomers; SBR). To produce the reinforcement, up to 50,000 filaments (individual fibers) are bundled into long fibers and then spun into a roving (yarn) [12].

2. Recycling of CRC

When recycling CRC, a distinction is made between two routes. In the first, the demolition material is separated into individual fractions (concrete matrix and carbon reinforcement) that can be reused individually, and in the second route, the demolition material is not separated into individual fractions, resulting in the recycling of a heterogeneous and non-pure material [12]. Demolition and separation of the CRC components are expected to achieve the highest quality recycling output of the processed raw materials (processed concrete and processed carbon fibers) [12]. For this reason, only this type of recycling is considered in this study. The process for the CRC recycling elaborated by Kortmann (2020a) was used in this study as a model for the LCA. Figure 1 shows a sketch of the modeled and calculated processes.

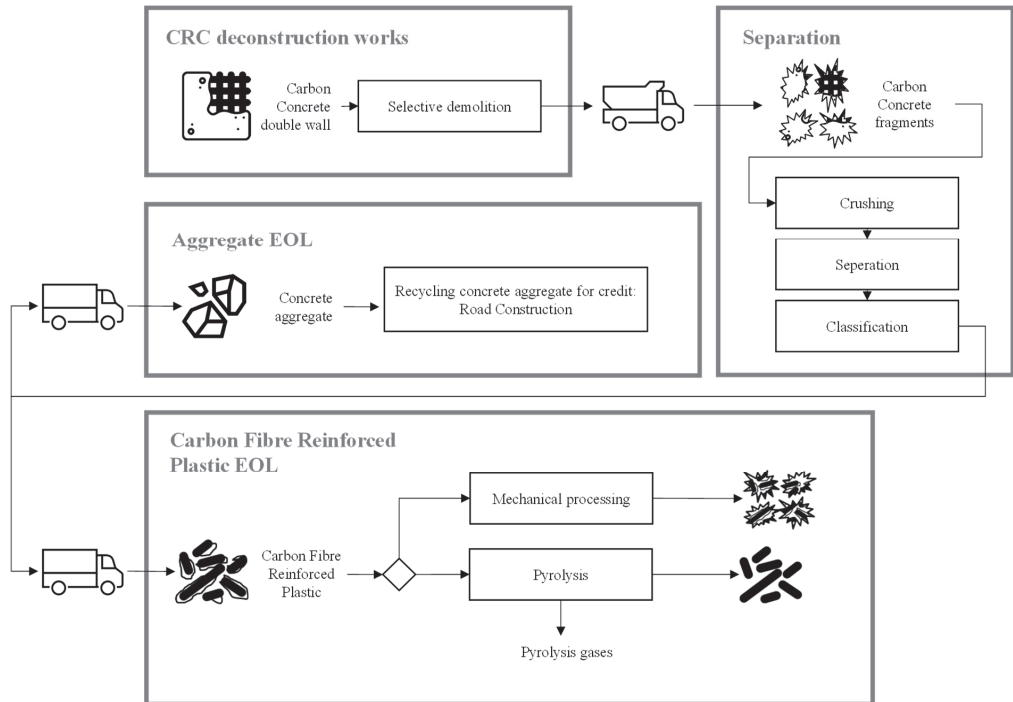


Figure 1. Processes to recycle CRC.

First, the CRC is selectively crushed using a carrier with attachment tools (concrete pulverizer and sorting grab). This step results in pre-crushed, coarser fragments of CRC, where the carbon reinforcement is still present [12]. To separate the reinforcement and continue the preparation process, the pre-crushed CRC is loaded onto a dump truck using a hydraulic excavator and transported to a stationary preparation plant [12]. In the plant, the main crushing of the demolition material is performed by a jaw crusher (or an impact crusher), resulting in a heterogeneous mixture of building materials. This construction material mixture consists of concrete fragments of the grain group 0/56 and exposed carbon roving fragments with an average individual length of 80 mm. In this sub-process, the degree of disintegration of the carbon roving fragments from the concrete matrix is over 99% [12].

In the pre-separation, metallic embedded parts are first removed from the material flow by a stationary magnetic separator. Then, concrete fines (largest grain size of 2 mm), lightweight plastic components (e.g., spacers) and carbon reinforcement with a mass fraction of an estimated 10% are removed by a cross-flow classifier. In addition, the spacers and the carbon reinforcement are separated from the concrete fines by screening, which prepares them for further material recycling steps. The metallic components separated by the magnetic separator are sent to steel scrap recycling. After completing the pre-separation, the material stream contains a heterogeneous accumulation of concrete fragments of grain group 3/56 and exposed carbon roving fragments (average length 80 mm) [12].

A camera-based sorting unit is then used for the main separation of the concrete and carbon roving fragments. According to Kortmann, 97.7% of the carbon roving fragments can be separated in practice with this type of single-grain sorting. A maximum proportion of 2.3% of the carbon reinforcement remains in the concrete recycle and finally reduces the mass fraction of the reinforcement structures from the former 1% to 0.023%. The result of the main separation is thus, on the one hand, the concrete fraction of grain group 3/56 (Aggregate EoL) with a residual carbon fiber content of less than 0.05% and, on the other hand, the separated carbon fiber fraction, including foreign mineral constituents of grain group 0/2. [12] Subsequent screening with a screen diameter of 3 mm allows the carbon fiber fraction to be separated from the foreign mineral constituents in a pure state, to obtain only the fibers themselves [12] (Figure 1). Next, a further fiber processing step, such as mechanical recycling or pyrolysis, follows.

2.1. Recycling of Carbon Fiber Composites

The three main waste management strategies for carbon fibers are (1) landfilling, (2) energy recovery in the form of incineration or co-incineration in a cement kiln [18,19], and (3) recycling [20–22]. Since this study focuses exclusively on carbon fiber recycling, landfilling and energy recovery are not considered. Carbon fiber reinforced plastics (CFRP) waste is currently not suitable for conventional incineration and co-incineration due to the required pre-processing and increased operating temperatures. Moreover, landfilling is a problematic option since carbon fibers are chemically inert and degrade slowly [23].

In general, a suitable recycling method for carbon fibers should be efficient, environmentally friendly, have minimal impact on fiber length and allow interfacial compatibility with new resins [24]. Moreover, an environmentally sound recycling method should cause less overall environmental impact than the production process of primary raw material or other waste management methods [23]. In this regard, there are mainly three recycling methods for carbon fibers: mechanical recycling, thermal recycling and chemical recycling [20,24].

Thermal recycling includes pyrolysis as well as fluidized bed pyrolysis, while chemical recycling includes solvolysis (with near- or supercritical fluid) and acid digestion [25]. Among these methods, pyrolysis and mechanical recycling show a better technological readiness [21] compared to chemical recycling or fluidized bed pyrolysis [20,25]. For mechanical recycling, this is due to the energy efficiency in high production rates and production capacities, as well as the lower costs [25,26]. In the case of pyrolysis, this is

currently the most technologically advanced method for the recycling of carbon fibers and has already proven its economic feasibility in large-scale plants [27]. For these reasons, only mechanical recycling and pyrolysis will be discussed below.

2.1.1. Mechanical Recycling

One advantage of mechanical recycling (Figure 1) is that it can address the growing amounts of carbon fiber waste [25]. This is because, in this method, the fiber composite material is shredded and milled through a multi-stage process [28]). For this purpose, equipment such as multi-shaft shredders and granulators are used, followed by the screening of the fibers to obtain a homogeneous particle size distribution [29,30]. In mechanical recycling, the fibers cannot be completely separated from the matrix (impregnation as EP or SBR) [28,31]. However, recycling can also take place without the separation of these two components [32]. The shredded carbon fibers can be used as fillers in composites, concrete, asphalt and coatings, which would involve downcycling the fibers [29,32–34]. The use of fillers consisting of recycled carbon fibers can increase mechanical (e.g., fatigue and fracture) as well as tribological properties (e.g., friction and wear) of new pure plastics [29,35]. In summary, the rapid processing and ease of scalability are major advantages of this recycling method, but the length of the carbon fibers is greatly reduced and contains resin residues, which in turn affects their recyclability in new products [25]. Technically, the term ‘mechanical recycling’ would also comprise the technologies of electrodynamic and electrohydraulic fragmentation, which separate resin and carbon fiber (CF) under high voltage. However, as they are still at lab-scale, they are excluded from this study [36].

2.1.2. Pyrolysis

Pyrolysis is a recycling method that can produce recycled carbon fibers on a large scale (Figure 1), with an estimated total energy consumption of 5–10% of the total energy required to produce primary fibers [23,25]. Compared to mechanical recycling, a fundamental advantage of pyrolysis is that the polymer matrix (impregnation) can be completely parted from the carbon fibers, thus enabling split recycling of the fibers and polymer matrix [29,32]. These are separated in an inert atmosphere (usually nitrogen) under atmospheric pressure at a controlled temperature of at least 350 °C [24,37,38]. During this process, so-called pyrolysis gases (e.g., H₂, CH₄, CO and CO₂) are emitted from the polymer matrix [39,40]. Due to their high calorific value, these can be reused as fuel to directly support pyrolysis and offset some of the electricity (or natural gas), necessary as inputs for the pyrolysis [12,20,41,42]. Burning off the polymer matrix can cause soot adhesion to the carbon fiber surface, which would prevent the fibers from bonding well with new resin [24,27]. For this reason, subsequent oxidation is necessary, which can remove the carbon black particles but harms the mechanical properties of the carbon fibers (elastic modulus and tensile strength) [40,42–45]. The extent of this damage depends largely on the operating conditions such as pyrolysis and oxidation temperatures, residence time and reaction atmosphere [25]. In this regard, the best mechanical properties (93% of tensile strength and 96% of the elastic modulus) have been obtained at a pyrolysis and oxidation temperature of 500 °C, a pyrolysis time of one hour and an oxidation time of two hours [46]. The oxidation process may additionally enrich the pyrolyzed fibers with oxidized groups, thus serving as a crosslinker between the recycled fibers and new resin [47].

However, it has been reported that the composites made with recycled carbon fibers tend to have lower mechanical properties compared to the composites made with primary fibers [25]. They can be used to increase the strength of plastics in injection molded components as well as further processed into nonwovens [12]. Therefore, the recycled fibers find application only in the field of non-structural composites such as cladding in the automotive and aerospace industries or lightweight sports equipment [12,43,47]. We exclude in our study the technology of microwave-assisted pyrolysis. Although it has lower energy needs, it is still at the laboratory stage, and the quality of the recovered CF is

lower compared to conventional pyrolysis [22]. We also exclude fluidized bed pyrolysis for CF recovery due to its lab stage status too.

2.2. State-Of-The-Art: End-Of-Life Life Cycle Assessment Implementations to CRC

In many scientific articles on environmental assessments of CRC, most notably Stoiber et al. (2021) [48], Laiblová et al. (2019) [49] and Williams Portal et al. (2015) [50], recycling is generally not considered. However, the authors of these works call for an environmental assessment of the EoL, pointing out, on the one hand, the good recyclability of the reinforcement material steel that is already in practice and, on the other hand, the difficult recycling procedures for CRC, which is the aim of the current research [51,52]. An environmental assessment of the recycling of CRC has so far only been performed by Scope et al. (2020) [53] and Hatzfeld et al. (2022) [54]. Scope et al. (2020) [53] conducted a cradle-to-grave Life Cycle Sustainability Assessment (LCSA) on a CRC double wall, encompassing the environmental, economic and social dimension. However, for the EoL, they found that recycling can hardly provide an environmental benefit according to the CML environmental impact categories results. The authors modeled a pyrolysis recycling of the CFRP fraction according to Meng et al. (2018) [55] and crediting for recycled carbon fibers use as a substitute for primary glass fiber in a glass fleece. Nevertheless, this study omits deconstruction and separation processes as well as the mechanical recycling. Inspired by these findings, Hatzfeld et al. (2022) [54] map multiple recycling paths of CRC and its components. For the individual processes, they provide a measure of technological maturity using Manufacturing Readiness Levels (MRL) and state the literature-based GWP values, giving recommendations for a technologically feasible and environmentally sound recycling of CRC [54].

2.2.1. Life Cycle Assessment of Mechanical Recycling and Pyrolysis

There are numerous environmental assessments on mechanical recycling and pyrolysis of CFRP in the scientific literature. Namely, for pyrolysis, the studies by Gopalraj et al. (2021) [18], He et al. (2020) [56], Khalil et al. (2018) [20], Vo Dong et al. (2018) [57], Dieterle et al. (2017) [58], Meng et al. (2018) [55], Pillain et al. (2019) [36] and Nunes et al. (2018) [59] can be highlighted. Studies focusing on the mechanical recycling of carbon fibers are Li et al. (2016) [60], Meng et al. (2018) [55], Shuaib and Mativenga (2017) [61] and Howarth et al. (2014) [26]. All mechanical recycling and pyrolysis studies have consistent findings for the respective technologies. First of all, they show that recycled carbon fiber (rCF) has a better environmental performance than virgin carbon fiber (vCF). The mechanical recycling process is generally found to have the lowest environmental impacts. However, as pyrolysis can recover higher quality recycled CF components by maintaining more of the structural integrity and length of the fibers, it allows for more options to substitute vCF. Hence, if crediting is applied, the pyrolysis achieves better results. If the rCF is used as a substitute for other products, such as glass and steel fibers, environmental performance worsens [53,62].

2.2.2. Life Cycle Assessment of Recycling of Concrete Fragments

Environmental assessment studies on the recycling of concrete in the scientific literature vary heavily in their results, depending on assumptions regarding transport distances, concrete specifications, stationary or mobile recycling, type of recycling processes, country, data sources for the Life Cycle Inventory and application of the recycle. Current common uses for recycling concrete aggregate (RCA) are backfills, road sub-base and base, i.e., downcycling. These recycling routes are modelled in environmental assessments by Guignot et al. (2015) [63], Martínez-Arguelles et al. (2019) [64] and Wei et al. (2013) [65]. Although the use of RCA does not significantly lower GWP, it prevents the depletion of natural aggregates, which are becoming increasingly scarce.

RCA application is as an alternative to natural aggregates in structural concrete, a higher quality application in comparison to its implementation in road construction. There

are many environmental assessments on this recycling route, collected in two LCA studies and reviews by Colangelo et al. (2020) [66], Mostert et al. (2021) [67], Yazdanbakhsh et al. (2018) [68], Guo et al. (2018) [69], Fraj and Idir (2017) [70], Kleijer et al. (2017) [71], Braga et al. (2017) [72], Müller et al. (2015) [73], Serres et al. (2016) [74], Turk et al. (2015) [75], Mettke et al. (2015) [76], Knoeri et al. (2013) [77], Weimann et al. (2013) [78], Heyn and Mettke (2010) [79], Marinković et al. (2010) [80] and Bischof et al. (2010) [81]. In most studies, the results show that the GWP is not significantly lower, as the crushing of the concrete and the transport have high energy needs, and there is still the need to add primary cement to the concrete mix. However, results vary greatly. The GWP of RCA concrete ranges from 20% less to 35% more than natural aggregate concrete. This large variation is due to the different assumptions made in the studies. Furthermore, there is a method that allows a closed-loop recycling of concrete—electrodynamic fragmentation. This method allows for separate reclaiming of the cement fragments and the aggregate fragments. Respective environmental assessments are conducted by Gehring et al. (2015) [82] and Guignot et al. (2015) [63]. However, this technology is still in the laboratory stage, and due to the high energy needs of this method, the environmental impacts are not significantly lower.

3. Methodology

3.1. Goal and Scope

This study aims to present the range of environmental impacts of CRC after its use phase until re-usable material fractions are obtained using LCA. Accordingly, the scope of the study is defined from demolition to waste management (= C1–C3 in DIN EN 15804) [83]. The following scenarios are based on ISO 14040/44 and are modeled with GaBi ts 10.5.1.124 [84,85]. In addition, production in Germany is assumed, which is why any energy supply was modeled with German input processes. The impact categories used are in line with the CML2001 (August 2016) methodology [86]. The Functional Unit (FU) is mass in kg of re-usable material, originating from the CRC double-wall described by Otto and Adam (2019) [87], with dimensions (per wall) of $5 \times 2.5 \times 0.25$ m and a total weight of 1.43 t (of which concrete 1.42 t and 0.0102 t scrim per double-wall) or 0.6 m^3 [87,88]. The reason for kg as a FU is to understand what percentage of the original wall can ultimately be reused and not end up as waste. External joining elements to the double wall, as well as optional insulation materials are not included in the LCA.

3.2. Life Cycle Inventory

This life cycle inventory (Table 1) is based on the process sequence explained in Section 2 (Figure 1). The energy values and the transports including fuel refer exclusively to the functional unit (1 kg of re-usable material) and accordingly not to the complete double-wall. In this context, reference flow for our study is 0.993 kg of concrete and 0.007 kg of carbon reinforcement. The entire life cycle inventory is based on literature data or datasheets from German companies, which were converted to the target value according to justified assumptions. A detailed description of the individual assumptions and calculations made can be found in the Supplementary Material (A.1).

Table 1. Inventory Demolition.

Process	Mass Unit	Input	GaBi Process	Assumption/Reference
Selective demolition with pre-crushing	MJ/kg	0.03382	Modeled process DE: Diesel mix at filling station Sphera	Machinery and related net power: [89,90] Fuel consumption: [91]
Transport of the material to the stationary processing plant	km	17	GLO: Truck, Euro 4, 26–28t gross weight/18.4t payload capacity	[92]
Loading of the demolition material with excavator (in the processing plant)	MJ/kg	0.0047	Modeled process DE: Diesel mix at filling station Sphera	[89]

Table 1. Cont.

Process	Mass Unit	Input	GaBi Process	Assumption/Reference
Main crushing with concrete crusher (jaw crusher or impact mill)	MJ/kg	0.035	Modeled process DE: Diesel mix at filling station Sphera	[89]
Pre-separation with stationary magnetic separator in combination with cross flow sifter	MJ/kg	0.0072	Modeled process DE: Electricity grid mix (2020) ts	[89]
Main separation (camera-based sorting)	MJ/kg	0.0054	Modeled process DE: Electricity grid mix (2020) ts	[93]
Sieving	MJ/kg	0.0000385	Modeled process DE: Diesel mix at filling station Sphera	[89]
Discharge to the bunker with wheel loader	MJ/kg	0.0057	Modeled process DE: Diesel mix at filling station Sphera	[89]
Transport from the processing plant to further recycling	km	100	GLO: Truck, Euro 4, 12–14t gross weight/9.3t payload capacity	Authors' assumption

3.2.1. Recycling Option 1: Mechanical Recycling

Mechanical recycling (Table 2) consumes 0.27 MJ per kg of carbon fiber reinforced composite waste [26,94].

Table 2. Inventory mechanical recycling.

Process	Mass Unit	Input	GaBi Process	Assumption/Reference
Mechanical recycling	MJ/kg	0.00189	Individually modelled process DE: Electricity grid mix (2020) ts	[26,94]

To determine the energy value, Howarth et al. (2014) [26] used the energy equation developed after Gutowski et al. (2006) [95]: $E = (P_0 + kQ)t$ [26,95]. Here, P_0 describes the basic power, k the specific energy for comminution of a given material, Q the rate of study and t the total study time. To determine these parameters, 1 kg of carbon-fiber-reinforced composite sheets with a thickness of 3 mm were fed to an industrial shredding machine. A basic power of 5248 W, specific energy of 0.218 J/mm³ and a required loading time of 6 min was measured for the comminution of 1 kg of carbon-fiber-reinforced composite sheets, and a consequent rate of 10 kg per hour was calculated. Subsequently, these parameters were used in the energy equation and resulted in process energy of 2.03 MJ/kg. It should be noted that, according to the machine manufacturer, steady rates of up to 150 kg per hour are possible. [26] If this rate is used, the energy equation developed by Gutowski et al. (2006) [95] yields process energy of 0.27 MJ/kg [26,95]. Consequently, mechanical recycling at high rates or industrial scale is more energy efficient [26], thus reducing emissions per kg processed material.

The energy consumption of 0.27 MJ per kg of carbon fiber reinforced composite waste reported by Hedlund-Åström (2005) [94] was provided by the Swedish recycling company Jomill AB [94]. This energy consumption was offset against the mass of carbon reinforcement (0.007 kg), resulting in 1.89×10^{-3} MJ. This consumption was modeled in GaBi using the input process “DE: Electricity grid mix (2020) ts”.

3.2.2. Recycling Option 2: Pyrolysis

Pyrolysis (Table 3) consumes 7.6 MJ (from electricity) and 13.2 MJ (from natural gas) per kg of carbon fiber reinforced composite waste [55].

These energy-related inventory data were used from a commercial operation of ELG Carbon Fibre Ltd., according to Meng et al. (2018) [55]. The two energy values were each offset by the mass of carbon reinforcement (0.007 kg), resulting in 0.0532 MJ (electricity) and 0.0924 MJ (natural gas). The energy consumption by the electricity was modeled with the input process “DE: Electricity grid mix (2020) ts” and the energy consumption by the natural gas with the input process “DE: Natural gas mix Sphera”.

Table 3. Inventory pyrolysis.

Process	Mass Unit	Input	GaBi Process	Assumption /Reference
Pyrolysis	MJ/kg	0.0532 0.0924	Individually modelled process DE: Electricity grid mix (2020) ts DE: Natural gas mix Sphera	[55]

4. Life Cycle Impact Assessment Results: Focusing on the Carbon Footprint

In this study, we use the impact categories according to the CML2001 (August 2016) methodology [86]. In this section, we refer primarily to the impact category Global Warming Potential (GWP in kg CO₂e). In the first section (recycling phase 1), the selective demolition up to the transport of the carbon fibers for further recycling is presented as recycling phase 1. Further recycling (mechanical recycling and pyrolysis) is defined as recycling phase 2. A division of the impact assessment into two sections was made, because the recycling process of the carbon concrete up to this limit is independent of the further recycling of the carbon fibers. Future life cycle assessments, which investigate further recycling processes for the carbon fibers contained in the carbon concrete (e.g., solvolysis), are thus offered the possibility of applying the emission values determined in recycling phase 1 for the separation of the concrete from the carbon fibers. Finally, we assume the recycled concrete partly being used for road construction.

4.1. Recycling Phase 1

Figure 2 shows the GWP in kg CO₂e of the recycling process before further recycling (mechanical recycling and pyrolysis), per process. Among all the processes (listed in Table 1), transportation to a stationary processing plant shows the highest GWP value, while screening shows the lowest. The sum of global warming potentials for all processes totals 4.2×10^{-3} kg CO₂e. Among the two processes operated with “DE: Electricity grid mix (2020) ts” (pre-separation and main separation), the pre-separation has the highest GWP with 1.2×10^{-3} kg CO₂e. For the processes operated with “DE: Diesel mix at filling station Sphera”, the main crushing shows the highest GWP with 2.7×10^{-4} kg CO₂e and screening shows the lowest GWP with 3.0×10^{-7} kg CO₂e. Furthermore, transportation to further recycling shows a lower GWP with 8.4×10^{-5} kg CO₂e.

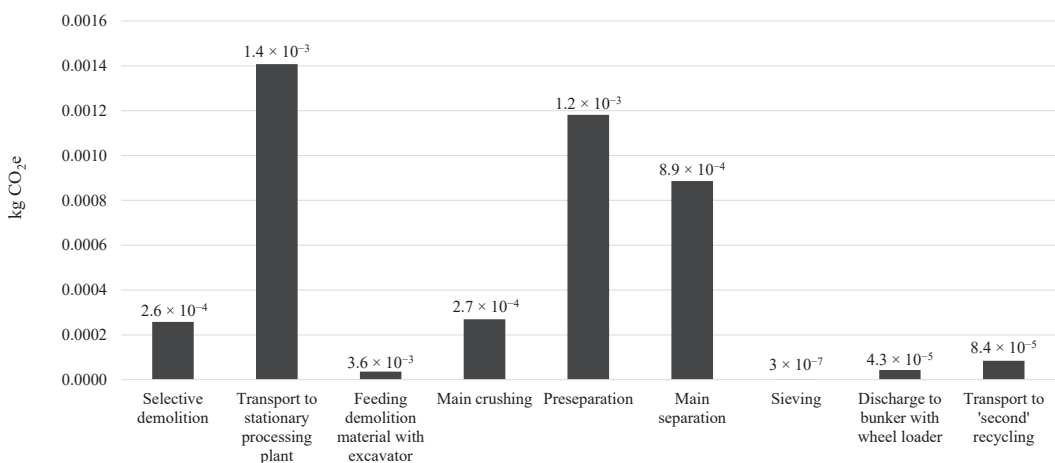


Figure 2. Global warming potential in kg CO₂e of 1 kg re-usable material out of a double wall—recycling phase 1.

4.2. Recycling Phase 2 ('Second' Recycling)

Recycling phase 1 is followed by an impact assessment for further recycling of the carbon fibers contained in the CRC. Figure 3 shows both the GWP of mechanical recycling and the GWP of pyrolysis. Pyrolysis has a higher GWP of 9.7×10^{-3} kg CO₂e than mechanical recycling with 3.1×10^{-4} kg CO₂e.

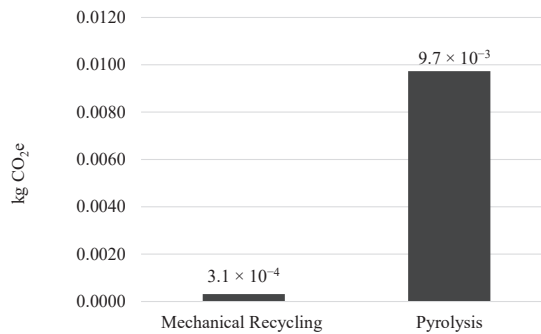


Figure 3. Global warming potential in kg CO₂e of 1 kg re-usable material out of a double wall—recycling phase 2.

Adding the respective GWP of the two recycling processes (mechanical recycling and pyrolysis) to the GWP of 4.2×10^{-3} kg CO₂e calculated in recycling phase 1, we finally obtain a total GWP of 4.5×10^{-3} kg CO₂e from mechanical recycling and 1.4×10^{-2} kg CO₂e from recycling within pyrolysis.

4.3. Use of Recycled Carbon Fiber Fragments

A long residence time of the carbon fibers in the material cycle is the aim since the carbon fibers represent a valuable and energy-intensive material [12]. Mechanical recycling and pyrolysis do not yet include a variant in which the carbon fibers are added back to the material cycle and, for example, a new carbon reinforcement is produced from the recycled carbon fibers. One theoretical solution is to process the recycled carbon fibers into staple fiber yarns [12]. In a carding process, the staple fiber yarns can be processed as hybrid yarns from a proportion of reprocessed carbon fibers and thermoplastic fibers (e.g., polyamide) and then carded, bundled and deposited on bobbins [12]. Hybrid yarns developed at the TU Dresden showed a bond strength of 1100 N/mm², which corresponds to a comparative value of 48% and 55% of the 'primary raw material' strength of the carbon reinforcement of 2300 N/mm² and 2000 N/mm² used in CRC at the beginning [12,96]. Considering that, according to Yang et al. (2015) [45], up to 80% of the tensile strength potential of pyrolyzed fibers is achieved compared to primary fibers, the recycled carbon fibers resulting from pyrolysis could be processed into yarn structures and reprocessed into textile structures (e.g., rods or scrim) as reinforcement in concrete components [12,45].

It should be noted that we do not have exact energy values for the processing procedure nor a quantitative ratio of recycled carbon fibers in the hybrid yarns given. For this reason, no further crediting for recycled carbon fibers is performed.

4.4. Reuse of Concrete Fragments

Compared to the recycling of carbon fibers, a view across the system boundary in terms of the processed concrete fraction is both theoretically and practically feasible. Dwindling resource sources for the extraction of suitable sands and gravels, as well as the rising cost of landfilling waste, have contributed to the fact that the recycling of mineral building materials has long been the focus of practical construction and scientific activities [97]. Moreover, the mineral concrete fraction can be almost completely recycled through single-

variety processing, as well as theoretically reused several times in an ideal recyclable material cycle [31].

It is possible to use the concrete fraction recycled in the stationary processing plant for the production of concrete made of primary raw material. According to Kortmann (2020) [12], the mineral fraction is in the coarse-grained and wide-graded aggregate 3/56 after completion of recycling. For the production of concrete, the mineral fraction should be crushed and classified to the narrow-graded aggregate 2/8 or 8/16. The maximum permissible volume fraction of the recycled concrete fraction that may be added during the production of concrete made of primary raw material is defined in DIN EN 12620 (07/2008) by classification into delivery type 1 or 2 [98]. The two delivery types are defined by DIN 4226-101 (08/2017) [99]. [12] A classification of the recycled concrete fraction into the two delivery types is based on the material composition. According to DIN EN 12620 (07/2008) [98], a volume fraction of up to 45% can be added to delivery type 1 and a volume fraction of up to 35% can be added to delivery type 2 in the production of concrete made of primary raw material [100].

Despite an existing mass fraction of the reinforcement structures of 0.023% within the recycled concrete fraction, the concrete fraction can be assigned to delivery type 1, since the plastic mass fraction is less than 1%. Consequently, no additional separation of the remaining reinforcement structures in the recycled concrete fraction is necessary, and it can be crushed and classified directly for further use as a substitute material for the production of concrete made of primary raw material to a narrow-graded grain size of 2/8 or 8/16 [12].

To investigate a potential emission saving by using the recycled aggregate from the concrete demolition, a comparison to primary raw material concrete is made. For this purpose, it was assumed that the resulting recycled concrete fraction, as described by Kortmann (2020) [12], corresponds to the grain size 3/56 and is first crushed to a narrow-graded grain size 8/16 and 2/8 [12]. Furthermore, it was assumed that the recycled aggregate is transported to another stationary processing plant where it is crushed. In this respect, we follow the process sequence, as well as the results of the research project of the University (BTU) Cottbus, worked on by Mettke and Heyn (2010) [79], which examined the process sequence for the production of the recycled aggregate in a stationary processing plant of the company Scherer + Kohl GmbH and Co. KG concerning the energy consumption [79]. The evaluation in GaBi showed that the preparation of 0.993 kg of concrete fraction has a total GWP of 6.9×10^{-3} kg CO₂e.

To compare the production of concrete without the use of the recycled concrete fraction with the production of concrete with the use of recycled material, a concrete formulation must first be defined. For this purpose, the commonly used concrete C30/37 from the company TBS was used [79] (Figure 4).

Concerning the production of one m³ of common used concrete C30/37, the GWP that arises for the 2/8 and 8/16 gravel is determined below. For this purpose, the input process "DE: Gravel (Grain size 3/32)" was used, according to which the production of 1 kg of gravel has a GWP of 2.8×10^{-2} kg CO₂e. It should be noted that in GaBi no exact differentiation of grain sizes was possible, so it is simplified to assume that the production of 1 kg of gravel shows the same GWP for both grain sizes 2/8 and 8/16. For the production of one m³ of common used concrete C30/37 according to TBS, 363 kg of 2/8 gravel and 729 kg of 8/16 gravel are required [79]. Offsetting the mass of gravel required per m³ of common used concrete C30/37 with the GWP of 1 kg of gravel results in a gravel-derived GWP of 30.6 kg CO₂e per m³ of common used concrete C30/37.

The recycled concrete fraction is assigned to delivery type 1 and can accordingly be added to the production of concrete made of primary raw material up to a volume fraction of 45%. According to the data of Mettke and Heyn (2010) [79], 34.5% of the concrete demolition waste is converted into 8/16 grain size and 13.8% into 2/8 grain size. Consequently, from the 0.993 kg of recycled concrete fraction, a total of 0.343 kg is processed into 8/16 grain size and 0.137 kg into 2/8 grain size. Since for the production of one m³ of common used concrete C30/37 (without the use of the recycled concrete fraction) no

differentiation was possible for the GWP of the different grain sizes of the gravel (2/8 and 8/16), it is also assumed here that both grain sizes have the same GWP. Previously, the GWP for the processing of 0.993 kg of concrete fraction or the resulting recycled 0.137 kg of the 2/8 and 0.343 kg of the 8/16 aggregate was determined to be 6.9×10^{-3} kg CO₂e. Assuming that the GWP is not differentiated for the aggregate sizes, the GWP is 0.014 kg CO₂e per kg of recycled aggregate. If the total gravel required to produce one m³ of standard C30/37 concrete (363 kg of 2/8 gravel + 729 kg of 8/16 gravel = 1092 kg of gravel in total) is composed of 45% recycled aggregate, the GWP is 23.7 kg CO₂e.

Thus, with the use of the recycled aggregate in the production of one m³ of common used concrete C30/37, a total of 6.9 kg CO₂e per m³ of common used concrete C30/37 is saved compared to the production without the use of the recycled aggregate (substitution of gravel), which corresponds to a percentage reduction of 22.5%.

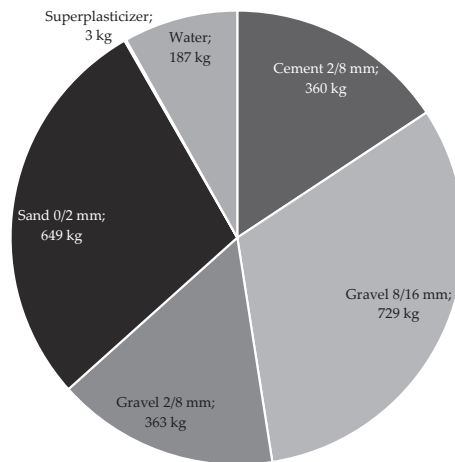


Figure 4. Concrete materials in kg (according to [79]).

5. Discussion and Limitations

In this study, we consider the EoL of CRC. The sustainability assessment of CRC of the EoL is highly relevant, as it enables the environmental impact of the recycling process to be determined at an early stage and can thus address the question of whether CRC has the potential to play a decisive role in improving the built environment given the current climate crisis. This question must be answered as early as possible, since the intended commercialization of CRC, mainly motivated by concrete or cement savings, is accompanied by a large investment in research and development as well as the establishment of new construction guidelines. For these reasons, the LCA of the EoL of CRC must in the future be connected to an analysis of the environmental impacts of the production and use stages to map the complete life cycle of the material. This connection would allow a comprehensive comparison of the environmental performance of CRC with conventional variants, such as steel-reinforced concrete.

Within the system boundaries, the selective demolition and the transport of the carbon fibers for further recycling were defined as recycling phase 1, while the further recycling (mechanical recycling and pyrolysis) as recycling phase 2. For recycling phase 1, transport to the stationary processing plant showed the highest GWP with 1.4×10^{-3} kg CO₂e, and screening showed the lowest GWP with 3.0×10^{-7} kg CO₂e. Transport to the stationary processing plant, as the main driver of GWP, highlights the need for processing plants at a short distance that have the technical implementation capabilities to recycle CRC. It stands out that among the processes taking place in the stationary processing plant, the only two processes powered by electricity, the pre-separation with 1.2×10^{-3} kg CO₂e and the main

separation with 8.9×10^{-4} kg CO₂e, also show the largest GWP. The use of renewable energy sources could lead to further emission savings.

For the subsequent recycling phase 2, pyrolysis showed a higher GWP with 9.7×10^{-3} kg CO₂e than mechanical recycling with 3.1×10^{-4} kg CO₂e. It should be emphasized that although mechanical recycling shows a lower GWP, the inferior quality of the recycled carbon fibers and the resulting lower range of recycling options for new products represent significant disadvantages compared to pyrolysis. The importance of the closed material cycle and the associated preparation of the recycled carbon fibers into a new carbon reinforcement is emphasized in this work. This stems from both the high energy input and the dependence on the non-renewable raw material petroleum for the production of primary carbon fibers. In this respect, mechanical recycling represents the overall process with the lowest energy input but does not have the decisive potential to close the material cycle compared to pyrolysis.

In this work, it was also assumed that the concrete fraction separated from the CRC and subsequently recycled can be successfully used as a substitute material for the production of concrete made of primary raw material. It was determined that with the use of the recycled material in the production of one m³ of common used concrete C30/37, 22.5% of primary raw material concrete GWP could be saved. These results illustrate two important points: first, the emission savings through the use of recycled aggregate and second, the possibility of partially closing the material cycle of the concrete fraction.

The central limitation of our study arises from the fact that CRC is a new type of composite construction material, and no primary data is currently available for the energy consumption of recycling. Consequently, the consumption data used in the life cycle inventory are secondary data not explicitly related to CRC. Therefore, the implemented data only provide reference values for a possible recycling process. The life cycle inventory is also limited by the fact that:

- The consumption data of the selective demolition according to Klingler et al. (2021) [89] refer to weakly reinforced concrete and not CRC [89];
- The calculation of transport distances only represents a theoretical approximation [12,92];
- Energy consumption represents the average electricity consumption of German companies, determined from previous literature [89,93], not measured values;
- Operating conditions such as pyrolysis and oxidation temperatures, residence time and reaction atmosphere of the ELG Carbon Fibre Ltd. pyrolysis plant were not reported by Meng et al. (2018) [55] (only the total energy consumption), and energy consumption may differ significantly compared to other pyrolysis plants [55];
- A variance in energy consumption results from the different machines is possible for mechanical recycling.

These limitations should be optimized in subsequent studies by using primary data from recyclers that explicitly recycled CRC. This requires both details on pyrolysis and any energy consumption. In addition, the consideration of the entire life cycle is relevant, and also the direct comparison with a functionally comparable reinforced concrete component will provide further insights regarding the environmental performance of CRC.

6. Conclusions

This study aimed to assess the environmental performance of the recycling of CRC considering the scenarios of mechanical recycling and pyrolysis and to determine the associated energy consumption to enable an environmental assessment (focusing GWP) of CRC at the end of its life cycle.

To date, articles on CRC have not fully considered recycling in terms of its environmental impact. Very few studies have looked at the EoL of CRC. The novelty of this article is the detailed presentation of possible EoL scenarios for CRC and the detailed determination of the respective environmental scenarios for a double wall of CRC. Especially for practitioners in the construction sector, the relevance of this article is that the entire life cycle of new material such as CRC should be considered, especially during the design

phase. Moreover, the EoL can have relevant impacts on the environmental emissions, and due to an increasing interest in sustainability in the construction sector, our LCA scenarios clarified first approaches for the future of this sector. The determined energy consumption for the elaborated recycling process meets the lack of primary data of CRC recycling and enables future life cycle assessments, which, e.g., investigate further recycling methods for the carbon fibers contained in the CRC to apply the used energy input data, which accrue for the separation of the concrete fraction from the carbon fiber fraction.

The LCA with the system boundary demolition to recyclable material, with the functional unit of 1 kg of recyclable material from a double-wall according to Otto and Adam (2019) [88] was modeled using literature-based data in GaBi ts software and CML2001 (2016) methodology. The main drivers of the GWP represent transport and pyrolysis. For the demolition and separation of both the concrete and the carbon fiber fractions, the conventional transport from the demolition site to the stationary processing plant proved to be the main driver of GWP (1.4×10^{-3} kg CO₂e). In the subsequent processing of carbon fibers, pyrolysis showed a higher GWP (9.7×10^{-3} kg CO₂e) than mechanical recycling (3.1×10^{-4} kg CO₂e). It should be emphasized that although mechanical recycling shows a lower GWP, the inferior quality of the recycled carbon fibers and the resulting lower range of recycling options for new products represent significant disadvantages compared to pyrolysis.

The concrete fraction separated from the CRC and subsequently recycled can be successfully used as a substitute material for the production of concrete made of primary raw material. The use of the recycled material in the production of one m³ of commonly used concrete C30/37 corresponds to a percentage reduction of 22.5% (saving of 6.9 kg CO₂e).

Finally, further studies should consider the entire life cycle of CRC (including construction, life time and EoL) and ensure a direct comparison with a functionally equivalent component made of steel-reinforced concrete.

Supplementary Materials: The following supporting information can be downloaded at: <https://www.mdpi.com/article/10.3390/pr10091791/s1>, Supplementary Material (A.1).

Author Contributions: Conceptualization: J.G.B. and P.D.R.; methodology: J.G.B., P.D.R. and D.P.; formal analysis and investigation: D.P.; writing—original draft preparation: D.P., J.G.B. and P.D.R.; writing—review and editing: J.G.B., P.D.R., T.H., M.T. and E.G.; funding acquisition: M.T., J.G.B., P.D.R. and E.G.; supervision: M.T. and E.G. All authors read and approved the final manuscript.

Funding: This study was funded by the German Research Foundation (DFG), as part of the Sonderforschungsbereich/Transregio 280 (SFB/TRR 280) ‘Konstruktionsstrategien für materialminimierte Carbonbetonstrukturen’/‘Design Strategies for Material-Minimized Carbon Reinforced Concrete Structures’ (Subproject E01, project number 417002380), as well as SFB/TRR 339, Project ID 453596084. The financial support by the German Research Foundation (DFG) is gratefully acknowledged.

Data Availability Statement: The data presented in this study are fully available in this study.

Conflicts of Interest: The authors declare no conflict to interest.

Abbreviations

CF	carbon fiber(s)
CFRP	carbon fiber reinforced plastics
CRC	carbon reinforced concrete
DIN	Deutsches Institut für Normung
EoL	End-of-Life
EP	epoxy resin
FU	Functional Unit
GWP	Global Warming Potential
LCA	Life Cycle Assessment
LCSA	Life Cycle Sustainability Assessment
MRL	Manufacturing Readiness Levels
PAN	polyacrylonitrile

RCA	recycling concrete aggregate
rCF	recycled carbon fiber
SBR	styrene-butadiene rubber
vCF	virgin carbon fiber

References

- Choi, J.-H. Strategy for reducing carbon dioxide emissions from maintenance and rehabilitation of highway pavement. *J. Clean. Prod.* **2018**, *209*, 88–100. [[CrossRef](#)]
- Ding, T.; Xiao, J.; Tam, V.W.Y. A closed-loop life cycle assessment of recycled aggregate concrete utilization in China. *Waste Manag.* **2016**, *56*, 367–375. [[CrossRef](#)] [[PubMed](#)]
- Sameer, H.; Bringezu, S. Life cycle input indicators of material resource use for enhancing sustainability assessment schemes of buildings. *J. Build. Eng.* **2018**, *21*, 230–242. [[CrossRef](#)]
- Elbers, U. Ressourcenschonendes Bauen—Wege und Strategien der Tragwerksplanung. *Bautechnik* **2021**, *99*, 57–64. [[CrossRef](#)]
- Blandini, L. Ressourceneffizientes und klimagerechtes Bauen mit Beton—eine Illusion? *Beton Stahlbetonbau* **2021**, *116*, 717. [[CrossRef](#)]
- Chung, S.-Y.; Abd Elrahman, M.; Stephan, D.; Kamm, P.H. The influence of different concrete additions on the properties of lightweight concrete evaluated using experimental and numerical approaches. *Constr. Build. Mater.* **2018**, *189*, 314–322. [[CrossRef](#)]
- Ramana, P.V.; Agnihotri, A. Fly-ash conjoined ground granulated blast furnace slag proxy for fresh and hardened responses. *Mater. Today Proc.* **2021**, *49*, 1942–1949. [[CrossRef](#)]
- Seifert, W.; Lieboldt, M. Ressourcenverbrauch im globalen Stahlbetonbau und Potenziale der Carbonbetonbauweise. *Beton- und Stahlbetonbau* **2020**, *115*, 469–478. [[CrossRef](#)]
- Guerra, B.C.; Leite, F. Circular economy in the construction industry: An overview of United States stakeholders' awareness, major challenges, and enablers. *Resour. Conserv. Recycl.* **2021**, *170*, 105617. [[CrossRef](#)]
- Kraft, R.; Kahnt, A.; Grauer, O.; Thieme, M.; Wolz, D.S.; Schlüter, D.; Tietze, M.; Curbach, M.; Holschemacher, K.; Jäger, H.; et al. Advanced carbon reinforced concrete technologies for façade elements of nearly zero-energy buildings. *Materials* **2022**, *15*, 1619. [[CrossRef](#)]
- OECD. *Global Material Resources Outlook to 2060. Economic Drivers and Environmental Consequences*; OECD Publishing: Paris, France, 2019.
- Kortmann, J. *Verfahrenstechnische Untersuchungen zur Recyclingfähigkeit von Carbonbeton*; Springer: Berlin/Heidelberg, Germany, 2020. [[CrossRef](#)]
- Monteiro, P.J.M.; Miller, S.; Horvath, A. Towards sustainable concrete. *Nat. Mater.* **2017**, *16*, 698–699. [[CrossRef](#)] [[PubMed](#)]
- Reichenbach, S.; Preinstorfer, P.; Hammerl, M.; Kromoser, B. A review on embedded fibre-reinforced polymer reinforcement in structural concrete in Europe. *Constr. Build. Mater.* **2021**, *307*, 124946. [[CrossRef](#)]
- Spelter, A.; Bergmann, S.; Bielak, J.; Hegger, J. Long-Term Durability of Carbon-Reinforced Concrete: An Overview and Experimental Investigations. *Appl. Sci.* **2019**, *9*, 1651. [[CrossRef](#)]
- Goulouti, K.; Favre, D.; Giorgi, M.; Padey, P.; Galimshina, A.; Habert, G.; Lasvaux, S. Dataset of service life data for 100 building elements and technical systems including their descriptive statistics and fitting to lognormal distribution. *Data Brief* **2021**, *36*, 107062. [[CrossRef](#)]
- Grant, A.; Ries, R. Impact of building service life models on life cycle assessment. *Build. Res. Inf.* **2012**, *41*, 168–186. [[CrossRef](#)]
- Gopalraj, S.K.; Deviatkin, I.; Horttanainen, M.; Kärki, T. Life cycle assessment of a thermal recycling process as an alternative to existing CFRP and GFRP composite wastes management options. *Polymers* **2021**, *13*, 4430. [[CrossRef](#)]
- Stockschläder, J.; Quicker, P.; Baumann, W.; Wexler, M.; Stapf, D.; Beckmann, M.; Thiel, C.; Hoppe, H. Thermal treatment of carbon-fibre-reinforced polymers (Part 2: Energy recovery and feedstock recycling). *Waste Manag. Res. J. Sustain. Circ. Econ.* **2021**, *40*, 685–697. [[CrossRef](#)]
- Khalil, Y. Comparative environmental and human health evaluations of thermolysis and solvolysis recycling technologies of carbon fiber reinforced polymer waste. *Waste Manag.* **2018**, *76*, 767–778. [[CrossRef](#)]
- Rybicka, J.; Tiwari, A.; Leeke, G.A. Technology readiness level assessment of composites recycling technologies. *J. Clean. Prod.* **2016**, *112*, 1001–1012. [[CrossRef](#)]
- Shuaib, N.A.; Mativenga, P. Carbon footprint analysis of fibre reinforced composite recycling processes. *Procedia Manuf.* **2017**, *7*, 183–190. [[CrossRef](#)]
- Witik, R.A.; Teuscher, R.; Michaud, V.; Ludwig, C.; Månson, J.-A.E. Carbon fibre reinforced composite waste: An environmental assessment of recycling, energy recovery and landfilling. *Compos. Part A Appl. Sci. Manuf.* **2013**, *49*, 89–99. [[CrossRef](#)]
- Oliveux, G.; Dandy, L.O.; Leeke, G.A. Current status of recycling of fibre reinforced polymers: Review of technologies, reuse and resulting properties. *Prog. Mater. Sci.* **2015**, *72*, 61–99. [[CrossRef](#)]
- Pakdel, E.; Kashi, S.; Varley, R.; Wang, X. Recent progress in recycling carbon fibre reinforced composites and dry carbon fibre wastes. *Resour. Conserv. Recycl.* **2020**, *166*, 105340. [[CrossRef](#)]
- Howarth, J.; Mareddy, S.S.; Mativenga, P.T. Energy intensity and environmental analysis of mechanical recycling of carbon fibre composite. *J. Clean. Prod.* **2014**, *81*, 46–50. [[CrossRef](#)]

27. Limburg, M.; Quicker, P. Entsorgung von carbonfasern—Probleme des recyclings und auswirkungen auf die abfallverbrennung. *Berl. Abfallwirtsch. Energ.* **2016**, *13*, 135–144.
28. Woidasky, J.; Seiler, E.; Henning, F.; Wolf, M.-A.; Harsch, M. Kunststoffe und bauteile—Umwelt und recycling. In *Polymer Engineering 3*; Springer: Berlin/Heidelberg, Germany, 2020; pp. 89–139. [\[CrossRef\]](#)
29. May, D.; Goergen, C.; Friedrich, K. Multifunctionality of polymer composites based on recycled carbon fibers: A review. *Adv. Ind. Eng. Polym. Res.* **2021**, *4*, 70–81. [\[CrossRef\]](#)
30. Vincent, G.A.; de Bruijn, T.A.; Wijskamp, S.; Rasheed, M.I.A.; van Drongelen, M.; Akkerman, R. Shredding and sieving thermoplastic composite scrap: Method development and analyses of the fibre length distributions. *Compos. Part B Eng.* **2019**, *176*, 107197. [\[CrossRef\]](#)
31. Martens, H.; Goldmann, D. *Recyclingtechnik. Fachbuch für Lehre und Praxis*, 2nd ed.; Springer: Berlin/Heidelberg, Germany, 2016. [\[CrossRef\]](#)
32. Krauklis, A.E.; Karl, C.W.; Gagani, A.I.; Jørgensen, J.K. Composite material recycling technology—State-of-the-art and sustainable development for the 2020s. *J. Compos. Sci.* **2021**, *5*, 28. [\[CrossRef\]](#)
33. Palmer, J.; Savage, L.; Ghita, O.; Evans, K. Sheet moulding compound (SMC) from carbon fibre recycle. *Compos. Part A Appl. Sci. Manuf.* **2010**, *41*, 1232–1237. [\[CrossRef\]](#)
34. Pickering, S. Recycling technologies for thermoset composite materials—Current status. *Compos. Part A Appl. Sci. Manuf.* **2006**, *37*, 1206–1215. [\[CrossRef\]](#)
35. Hornbogen, E. Chemische und tribologische eigenschaften. In *Werkstoffe-Aufbau Und Eigenschaften von Keramik-, Metall-, Polymer- Und Verbundwerkstoffen*; Springer: Berlin/Heidelberg, Germany, 2002; pp. 220–241. [\[CrossRef\]](#)
36. Pillain, B.; Loubet, P.; Pestalozzi, F.; Woidasky, J.; Erriguible, A.; Aymonier, C.; Sonnemann, G. Positioning supercritical solvolysis among innovative recycling and current waste management scenarios for carbon fiber reinforced plastics thanks to comparative life cycle assessment. *J. Supercrit. Fluids* **2019**, *154*, 104607. [\[CrossRef\]](#)
37. Meyer, L.; Schulte, K.; Grove-Nielsen, E. CFRP-recycling following a pyrolysis route: Process optimization and potentials. *J. Compos. Mater.* **2009**, *43*, 1121–1132. [\[CrossRef\]](#)
38. Park, J.-M.; Kwon, D.-J.; Wang, Z.-J.; Gu, G.-Y.; DeVries, K.L. Effect of thermal treatment temperatures on the reinforcing and interfacial properties of recycled carbon fiber–phenolic composites. *Compos. Part A Appl. Sci. Manuf.* **2013**, *47*, 156–164. [\[CrossRef\]](#)
39. Kortmann, J. *Carbon- und Textilbetontage*; TUDALIT e.V.: Dresden, Germany, 2020; p. 17.
40. Naqvi, S.; Prabhakara, H.M.; Bramer, E.; Dierkes, W.; Akkerman, R.; Brem, G. A critical review on recycling of end-of-life carbon fibre/glass fibre reinforced composites waste using pyrolysis towards a circular economy. *Resour. Conserv. Recycl.* **2018**, *136*, 118–129. [\[CrossRef\]](#)
41. Abdallah, R.; Juaidi, A.; Savaş, M.A.; Çamur, H.; Albatayneh, A.; Abdala, S.; Manzano-Agugliaro, F. A Critical review on recycling composite waste using pyrolysis for sustainable development. *Energies* **2021**, *14*, 5748. [\[CrossRef\]](#)
42. López, F.A.; Rodríguez, O.; Alguacil, F.J.; García-Díaz, I.; Centeno, T.A.; García-Fierro, J.L.; González, C. Recovery of carbon fibres by the thermolysis and gasification of waste prepreg. *J. Anal. Appl. Pyrolysis* **2013**, *104*, 675–683. [\[CrossRef\]](#)
43. Onwudili, J.; Miskolczi, N.; Nagy, T.; Lipóczi, G. Recovery of glass fibre and carbon fibres from reinforced thermosets by batch pyrolysis and investigation of fibre re-using as reinforcement in LDPE matrix. *Compos. Part B Eng.* **2016**, *91*, 154–161. [\[CrossRef\]](#)
44. Yang, J.; Liu, J.; Liu, W.; Wang, J.; Tang, T. Recycling of carbon fibre reinforced epoxy resin composites under various oxygen concentrations in nitrogen–oxygen atmosphere. *J. Anal. Appl. Pyrolysis* **2015**, *112*, 253–261. [\[CrossRef\]](#)
45. Zhang, J.; Chevali, V.S.; Wang, H.; Wang, C.-H. Current status of carbon fibre and carbon fibre composites recycling. *Compos. Part B Eng.* **2020**, *193*, 108053. [\[CrossRef\]](#)
46. Nahil, M.A.; Williams, P. Recycling of carbon fibre reinforced polymeric waste for the production of activated carbon fibres. *J. Anal. Appl. Pyrolysis* **2011**, *91*, 67–75. [\[CrossRef\]](#)
47. Mazzocchetti, L.; Benelli, T.; D'Angelo, E.; Leonardi, C.; Zattini, G.; Giorgini, L. Validation of carbon fibers recycling by pyro-gasification: The influence of oxidation conditions to obtain clean fibers and promote fiber/matrix adhesion in epoxy composites. *Compos. Part A Appl. Sci. Manuf.* **2018**, *112*, 504–514. [\[CrossRef\]](#)
48. Stoiber, N.; Hammerl, M.; Kromoser, B. Cradle-to-gate life cycle assessment of CFRP reinforcement for concrete structures: Calculation basis and exemplary application. *J. Clean. Prod.* **2020**, *280*, 124300. [\[CrossRef\]](#)
49. Laiblová, L.; Pešta, J.; Kumar, A.; Hájek, P.; Fiala, C.; Vlach, T.; Kočí, V. Environmental Impact of Textile Reinforced Concrete Facades Compared to Conventional Solutions—LCA Case Study. *Materials* **2019**, *12*, 3194. [\[CrossRef\]](#) [\[PubMed\]](#)
50. Portal, N.W.; Lundgren, K.; Wallbaum, H.; Malaga, K. Sustainable potential of textile-reinforced concrete. *J. Mater. Civ. Eng.* **2015**, *27*, 04014207. [\[CrossRef\]](#)
51. Kimm, M.; Gerstein, N.; Schmitz, P.; Simons, M.; Gries, T. On the separation and recycling behaviour of textile reinforced concrete: An experimental study. *Mater. Struct.* **2018**, *51*, 122. [\[CrossRef\]](#)
52. Merli, R.; Preziosi, M.; Acampora, A.; Lucchetti, M.C.; Petrucci, E. Recycled fibers in reinforced concrete: A systematic literature review. *J. Clean. Prod.* **2019**, *248*, 119207. [\[CrossRef\]](#)
53. Scope, C.; Guenther, E.; Schütz, J.; Mielecke, T.; Mündecke, E.; Schultze, K.; Saling, P. Aiming for life cycle sustainability assessment of cement-based composites: A trend study for wall systems of carbon concrete: Dresden Nexus Conference 2020—Session 4—Circular economy for building with secondary construction materials to minimise resource use and land use. *Civ. Eng. Des.* **2020**, *2*, 143–158. [\[CrossRef\]](#)

54. Hatzfeld, T.; Backes, J.G.; Scope, C.; Guenther, E.; Traverso, M. Environmental assessment of carbon reinforced concrete recycling options. In Proceedings of the Fib Conference, Oslo, Norway, 12–16 June 2022.
55. Meng, F.; Olivetti, E.A.; Zhao, Y.; Chang, J.C.; Pickering, S.J.; McKechnie, J. Comparing life cycle energy and global warming potential of carbon fiber composite recycling technologies and waste management options. *ACS Sustain. Chem. Eng.* **2018**, *6*, 9854–9865. [[CrossRef](#)]
56. He, D.; Soo, V.K.; Kim, H.C.; Compston, P.; Doolan, M. Comparative life cycle energy analysis of carbon fibre pre-processing, processing and post-processing recycling methods. *Resour. Conserv. Recycl.* **2020**, *158*, 104794. [[CrossRef](#)]
57. Dong, P.A.V.; Azzaro-Pantel, C.; Cadene, A.-L. Economic and environmental assessment of recovery and disposal pathways for CFRP waste management. *Resour. Conserv. Recycl.* **2018**, *133*, 63–75. [[CrossRef](#)]
58. Dieterle, M.; Seiler, E.; Viere, T. Application of eco-efficiency analysis to assess three different recycling technologies for Carbon Fiber Reinforced Plastics (CFRPs). *Key Eng. Mater.* **2017**, *742*, 593–601. [[CrossRef](#)]
59. Nunes, A.O.; Viana, L.R.; Guineheuc, P.-M.; Moris, V.A.D.S.; de Paiva, J.M.F.; Barna, R.; Soudais, Y. Life cycle assessment of a steam thermolysis process to recover carbon fibers from carbon fiber-reinforced polymer waste. *Int. J. Life Cycle Assess.* **2017**, *23*, 1825–1838. [[CrossRef](#)]
60. Li, X.; Bai, R.; McKechnie, J. Environmental and financial performance of mechanical recycling of carbon fibre reinforced polymers and comparison with conventional disposal routes. *J. Clean. Prod.* **2016**, *127*, 451–460. [[CrossRef](#)]
61. Shuaib, N.A.; Mativenga, P.T.; Kazie, J.; Job, S. Resource efficiency and composite waste in UK supply chain. *Procedia CIRP* **2015**, *29*, 662–667. [[CrossRef](#)]
62. Abdulkareem, M.; Havukainen, J.; Horttanainen, M. How environmentally sustainable are fibre reinforced alkali-activated concretes? *J. Clean. Prod.* **2019**, *236*, 117601. [[CrossRef](#)]
63. Guignot, S.; Touzé, S.; Von Der Weid, F.; Ménard, Y.; Villeneuve, J. Recycling construction and demolition wastes as building materials: A life cycle assessment. *J. Ind. Ecol.* **2015**, *19*, 1030–1043. [[CrossRef](#)]
64. Martínez-Arguelles, G.; Acosta, M.P.; Dugarte, M.; Fuentes, L. Life cycle assessment of natural and recycled concrete aggregate production for road pavements applications in the Northern Region of Colombia: Case study. *Transp. Res. Rec. J. Transp. Res. Board* **2019**, *2673*, 397–406. [[CrossRef](#)]
65. Wei, K.-Y.; Lin, J.-D.; Yu, I.-H. Assessment of [CO₂] emission reduction in road construction using recycled concrete materials. *Int. J. Pavement Res. Technol.* **2013**, *6*, 423–430. [[CrossRef](#)]
66. Colangelo, F.; Navarro, T.G.; Farina, I.; Petrillo, A. Comparative LCA of concrete with recycled aggregates: A circular economy mindset in Europe. *Int. J. Life Cycle Assess.* **2020**, *25*, 1790–1804. [[CrossRef](#)]
67. Mostert, C.; Sameer, H.; Glanz, D.; Bringezu, S. Climate and resource footprint assessment and visualization of recycled concrete for circular economy. *Resour. Conserv. Recycl.* **2021**, *174*, 105767. [[CrossRef](#)]
68. Yazdanbakhsh, A.; Bank, L.C.; Baez, T.; Wernick, I. Comparative LCA of concrete with natural and recycled coarse aggregate in the New York City area. *Int. J. Life Cycle Assess.* **2017**, *23*, 1163–1173. [[CrossRef](#)]
69. Guo, Z.; Tu, A.; Chen, C.; Lehman, D.E. Mechanical properties, durability, and life-cycle assessment of concrete building blocks incorporating recycled concrete aggregates. *J. Clean. Prod.* **2018**, *199*, 136–149. [[CrossRef](#)]
70. Fraj, A.B.; Idir, R. Concrete based on recycled aggregates—Recycling and environmental analysis: A case study of Paris’ region. *Constr. Build. Mater.* **2017**, *157*, 952–964. [[CrossRef](#)]
71. Kleijer, A.; Lasvaux, S.; Citherlet, S.; Viviani, M. Product-specific life cycle assessment of ready mix concrete: Comparison between a recycled and an ordinary concrete. *Resour. Conserv. Recycl.* **2017**, *122*, 210–218. [[CrossRef](#)]
72. Braga, A.M.; Silvestre, J.D.; de Brito, J. Compared environmental and economic impact from cradle to gate of concrete with natural and recycled coarse aggregates. *J. Clean. Prod.* **2017**, *162*, 529–543. [[CrossRef](#)]
73. Müller, C.; Reiners, J.; Palm, S. *Closing the Loop: What Type of Concrete Re-Use Is the Most Sustainable Option*; Technical Report A-2015/1860; The Concrete Initiative: Brussels, Belgium, 2015.
74. Serres, N.; Braymand, S.; Feugeas, F. Environmental evaluation of concrete made from recycled concrete aggregate implementing life cycle assessment. *J. Build. Eng.* **2016**, *5*, 24–33. [[CrossRef](#)]
75. Turk, J.; Cotič, Z.; Mladenović, A.; Šajna, A. Environmental evaluation of green concretes versus conventional concrete by means of LCA. *Waste Manag.* **2015**, *45*, 194–205. [[CrossRef](#)]
76. Mettke, A.; Schmidt, S.; Jacob, S. *Dokumentation zum Einsatz von Ressourcenschonendem Beton*; Senatsverwaltung für Stadtentwicklung und Umwelt: Berlin, Germany, 2015.
77. Knoeri, C.; Sanyé-Mengual, E.; Althaus, H.-J. Comparative LCA of recycled and conventional concrete for structural applications. *Int. J. Life Cycle Assess.* **2013**, *18*, 909–918. [[CrossRef](#)]
78. Weimann, K.; Matyschik, J.; Adam, C.; Schulz, T.; Linss, E.; Müller, A. *Optimierung des Rückbaus/Abbaus von Gebäuden zur Rückgewinnung und Aufbereitung von Baustoffen unter Schadstoffentfrachtung (insbes. Sulfat) des RC-Materials*; UBA: Dessau-Roßlau, Germany, 2013.
79. Heyn, S.; Mettke, A. *Ökologische Prozessbetrachtung—RC-Beton (Stofffluss, Energieaufwand, Emissionen)*; Brandenburgische Technische Universität Cottbus: Brandenburg, Germany, 2010; Volume 86.
80. Marinković, S.; Radonjanin, V.; Malešev, M.; Ignjatović, I. Comparative environmental assessment of natural and recycled aggregate concrete. *Waste Manag.* **2010**, *30*, 2255–2264. [[CrossRef](#)]

81. Bischof, S.; Sugg, T.; Meister, R.; Grüninger, R.; Kytzia, S.; Lier, S. *Ökobilanzen Rezyklierter Gesteinskörnung für Beton*; Holcim: Zug, Switzerland, 2010.
82. Gehring, F.; Albrecht, S.; Homolka, S.; Leistner, P.; Thome, V.; Seifert, S. Aus Altbeton wird Beton—ein innovativer Recyclingansatz. *Bauphysik* **2015**, *37*, 296–300. [[CrossRef](#)]
83. *DIN EN 15804*; Nachhaltigkeit von Bauwerken—Umweltproduktdeklarationen—Grundregeln für die Produktkategorie Bauprodukte. DIN: Berlin, Germany, 2009.
84. *ISO 14040*; Environmental Management—Life Cycle Assessment—Principles and Framework. ISO: Geneva, Switzerland, 2006.
85. *ISO 14044*; Environmental Management—Life Cycle Assessment—Requirements and Guidelines. ISO: Geneva, Switzerland, 2008.
86. CML—Department of Industrial Ecology. CML-IA Characterisation Factors [WWW Document]. 2016. Available online: <https://www.universiteitleiden.nl/en/research/research-output/science/cml-ia-characterisation-factors> (accessed on 31 July 2022).
87. Otto, J.; Adam, R. Carbonbeton und Stahlbeton im wirtschaftlichen Vergleich/Textile-reinforced concrete and reinforced concrete in an economic comparison. *Bauingenieur* **2019**, *94*, 246–252. [[CrossRef](#)]
88. Backes, J.G.; Traverso, M. Sustainability assessment of a disruptive innovation: Comparative cradle-to-gate life cycle assessment of carbon reinforced concrete. *Int. J. Life Cycle Assess.* **2022**; submitted.
89. Klingler, M.; Savi, D.; Gabor, D. Harmonisierte Ökobilanzen der Entsorgung von Baustoffen—Für die Liste der Ökobilanzdaten im Baubereich. 2021. Available online: www.umweltchemie.ch (accessed on 31 July 2022).
90. Schröder, M.; Pocha, A. *Abbrucharbeiten*, 3rd ed.; Verlagsgesellschaft Rudolf Müller GmbH & Co. KG: Köln, Germany, 2015.
91. Notter, B.; Schmied, M. *Energieverbrauch und Schadstoffemissionen des Non-road-Sektors: Studie für die Jahre 1980–2050*; Bundesamt für Umwelt: Bern, Switzerland, 2015.
92. Müller, A. *Baustoffrecycling-Entstehung-Aufbereitung-Verwertung*; Springer: Wiesbaden, Germany, 2018. [[CrossRef](#)]
93. Manouchehri, H.-R. Application of optoelectronic sorting technique for upgrading minerals and wastes. In Proceedings of the Konferenz i Mineraltechnik, Luleå, Sweden, 7–8 February 2006. Föreningen Mineralteknisk Forskning/Swedish Mineral Processing Research Association.
94. Hedlund-Åström, A. Model for End of Life Treatment of Polymer Composite Materials. Ph.D. Thesis, School of Industrial Engineering and Management (ITM), Stockholm, Sweden, 2005.
95. Gutowski, T.; Dahmus, J.; Thiriez, A. Electrical energy requirements for manufacturing processes. In Proceedings of the 13th CIRP International Conference on Life Cycle Engineering, Leuven, Belgium, 31 May–2 June 2006.
96. Hengstermann, M. *Entwicklung von Hybridgarnen aus Recycelten Carbonfasern und Polyamid 6-Fasern für Thermoplastische Verbundbauteile mit Hohem Leistungsvermögen*; Universität Dresden: Dresden, Germany, 1986.
97. Hartz, A.; Schniedermeier, L.; Saad, S.; Manderla, B. *Mittel- und Langfristige Sicherung Mineralischer Rohstoffe in der Landesweiten Raumplanung und in der Regionalplanung*; MORO Praxis: Berlin, Germany, 2017.
98. *DIN EN 12620*; DAfStb Beton rezyklierte Gesteinskörnung, DAfStb-Richtlinie Beton nach DIN EN 206-1 und DIN 1045-2 mit rezyklierten Gesteinskörnungen Nach. DIN: Berlin, Germany, 2010.
99. *DIN 4226-101*; Deutsches Institut für Normung (DIN) e.V. DIN: Berlin, Germany, 2017.
100. *DIN EN 12620*; Deutsches Institut für Normung (DIN) e.V. DIN: Berlin, Germany, 2008.

Article

Estimating Space-Cooling Energy Consumption and Indoor PM_{2.5} Exposure across Hong Kong Using a City-Representative Housing Stock Model

Xuyang Zhong^{1,2,*}, Zhiang Zhang^{3,*}, Wei Wu⁴ and Ruijun Zhang⁵¹ School of Architecture and Urban Planning, Chongqing University, Chongqing 400045, China² Department of Civil Engineering, Faculty of Engineering, Lishui University, Lishui 323000, China³ Department of Architecture and Built Environment, University of Nottingham Ningbo China, 199 East Taikang Road, Ningbo 315100, China⁴ School of Energy and Environment, City University of Hong Kong, Hong Kong, China⁵ Department of Architecture and Built Environment, The University of Nottingham, Nottingham NG7 2RD, UK

* Correspondence: xuyangz7@hotmail.com (X.Z.); zhiang.zhang@nottingham.edu.cn (Z.Z.)

Abstract: High-quality data on building energy use and indoor pollution are critical to supporting government efforts to reduce carbon emissions and improve the population's health. This study describes the development of a city-representative housing stock model used for estimating space-cooling energy use and indoor PM_{2.5} exposure across the Hong Kong housing stock. Archetypes representative of Hong Kong dwellings were developed based on geographically-referenced housing databases. Simulations of unique combinations of archetype, occupation, and environment were run using EnergyPlus, estimating the annual space-cooling energy consumption and annual average PM_{2.5} exposure concentrations under both non-retrofit and retrofit scenarios. Results show that modern village houses and top-floor flats in high-rise residential buildings, on average, used 19% more space-cooling energy than other archetypes. Dwellings in urban areas had lower exposure to outdoor-sourced PM_{2.5} and higher exposure to indoor-sourced PM_{2.5} compared to those in rural areas. The percentage decrease in space-cooling energy consumption caused by energy efficiency retrofits, including external wall insulation, low-e windows, and airtightening, varied significantly based on archetype. The implementation of external wall insulation in the housing stock led to an average decrease of 3.5% in indoor PM_{2.5} exposure, whilst airtightening and low-e windows resulted in 7.9% and 0.2% average increases in exposure, respectively.

Keywords: building simulation; housing stock modelling; space-cooling energy use; indoor PM_{2.5} exposure; building retrofit

Citation: Zhong, X.; Zhang, Z.; Wu, W.; Zhang, R. Estimating Space-Cooling Energy Consumption and Indoor PM_{2.5} Exposure across Hong Kong Using a City-Representative Housing Stock Model. *Buildings* **2022**, *12*, 1414. <https://doi.org/10.3390/buildings12091414>

Academic Editors: Roberto Alonso González Lezcano, Francesco Nocera and Rosa Giuseppina Caponetto

Received: 10 August 2022

Accepted: 5 September 2022

Published: 8 September 2022



Copyright: © 2022 by the authors. Licensee MDPI, Basel, Switzerland. This article is an open access article distributed under the terms and conditions of the Creative Commons Attribution (CC BY) license (<https://creativecommons.org/licenses/by/4.0/>).

1. Introduction

1.1. Space-Cooling Energy Consumption in Homes

The energy used by homes for space cooling accounted for 5.5% of the total energy use in Hong Kong in 2019 [1], and is expected to increase in the following years due to climate change and the urban heat island effects. For example, according to a tracking report by the International Energy Agency (IEA) [2], electricity demand for space cooling in the residential sector in China and India increased in 2020. Addressing the increasingly high space-cooling energy consumption in homes will first require a deep understanding of the underlying relationship between dwelling characteristics and space-cooling energy demands. Without this insight, the ability of the government to introduce evidence-based policies to seek a significant reduction in space-cooling energy consumption in the residential sector may be compromised [3]. To date, however, such data have been difficult to come by, possibly due to the lack of interest, poor coordination, and lack of

a connection between existing databases. Many studies have identified the key factors that impact the amount of space-cooling energy used by Hong Kong dwellings, including the building geometry [4], building fabric (e.g., building airtightness, window types, and levels of insulation in external walls) [5], natural ventilation potential [6], internal gains from occupants and equipment [7], occupant behaviour [8], the storey level of the flat within the containing building [9], orientation [10], and local environment of the building (e.g., shading from surrounding buildings, terrains, and surrounding microclimates) [11]. There can be a high degree of variation in these factors, as evidenced by the fact that space-cooling energy consumption varies significantly across the Hong Kong housing stock [12]. This means that accounting for the variability in these factors is crucial when examining residential space-cooling energy use.

Given the need for the reduction of carbon emissions, and residential space-cooling energy use being one of the main contributors to carbon emissions, it has been suggested that the Hong Kong government should develop energy efficiency programmes that offer improvements in the energy efficiency of homes [13]. Policies around the world are currently promoting the energy efficiency retrofit of the existing housing stock. In Germany, for example, energy-efficient heating and cooling systems were installed in more than 900 dwellings that were built before 1978 [14]. From the perspective of policy makers, focusing on dwellings with great potential to benefit from a certain energy efficiency intervention is an important strategic objective in order to maximise return on the original investment. Many studies have been undertaken to examine the effect of implementing energy efficiency measures in Hong Kong dwellings, where the estimates of energy savings from an energy efficiency measure were based either on comparisons of pre- and post-measure energy bills of homes [7,15] or on dwelling-specific simulations [16,17]. It is unclear from these studies whether the energy efficiency measure needs to be specific for a dwelling, or whether a ‘one-size-fits-all’ measure can be applied throughout the housing stock. A model that can enable estimates of population-wide energy benefits gained from home energy efficiency measures, and can provide insight into how the energy benefits vary according to the dwelling type, will play an important role in shaping energy efficiency policies for the residential sector.

1.2. Population Exposure to Domestic Indoor PM_{2.5}

The level of outdoor fine particulate matter (PM_{2.5}) in Hong Kong is high due to high volumes of traffic and a dense road network [18]. The relationship between population exposure to PM_{2.5} and negative health effects has increased as a research priority locally, largely due to the increasing burden of healthcare spending [19]. Epidemiological studies, including [20–22], examined health consequences using outdoor PM_{2.5} levels as an estimate of exposure, and there has been significantly less research relating health consequences to indoor PM_{2.5} exposure. In Hong Kong, people spend approximately 85% of their time indoors [23], meaning that indoor PM_{2.5} levels can have a huge impact on personal exposure. In addition, while previous studies have taken into account spatially-distributed outdoor PM_{2.5} levels in estimating health risks [24–26], they have normally ignored the way in which the variation in housing stock may influence the health risks that are associated with indoor PM_{2.5} exposure.

Dwellings, and the way in which they are operated, can significantly impact indoor PM_{2.5} concentrations from outdoor and indoor sources. PM_{2.5} from outdoor sources (e.g., traffic) may infiltrate into the building via cracks and gaps in the envelope of the building, via open windows, and via mechanical ventilation systems. A number of factors can influence PM_{2.5} infiltration, including dwelling geometry [27], dwelling airtightness [28], the storey level of the flat within the containing building [29], location [30], and occupant ventilation behaviour (e.g., window opening or mechanical ventilation systems) [31]. In addition to infiltration, indoor PM_{2.5} concentrations can be influenced by emissions from indoor sources such as cooking, smoking, showering, dusting, and vacuuming [32]. The

level of indoor- or outdoor-sourced $PM_{2.5}$ is also highly dependent on the removal of $PM_{2.5}$ from the indoor air via exfiltration, deposition, or ventilation.

Estimating indoor $PM_{2.5}$ concentrations can be performed using either field measurements or modelling approaches. Many local studies on indoor $PM_{2.5}$ concentrations were carried out based on field measurements [33–36], but there is very little empirical evidence to demonstrate the difference in indoor $PM_{2.5}$ concentrations between different dwelling types. Internationally, the role of dwellings in indoor $PM_{2.5}$ levels has been examined in some modelling studies. An advantage of using modelling approaches is that $PM_{2.5}$ concentrations in a great number of dwellings can be examined quickly at a lower cost compared to field measurements. In the study aiming to develop a nationally-representative model of indoor $PM_{2.5}$ exposure, Fazli and Stephens [37] used infiltration rates for dwellings in different US cities to estimate indoor $PM_{2.5}$ concentrations; the results indicate a significant difference in indoor $PM_{2.5}$ exposure between different dwelling types, but the variation in occupant practices made it difficult to isolate the impact of dwellings. Indoor $PM_{2.5}$ modelling was performed across sets of dwelling types in the UK, showing how flats may have higher exposure to indoor-sourced $PM_{2.5}$ and lower exposure to outdoor-sourced $PM_{2.5}$ compared to houses [27]. A nationally-representative housing stock model developed by Taylor et al. [38] indicates that the permeability of the building envelope could lead to significant differences in exposure to outdoor-sourced $PM_{2.5}$ between different dwellings.

1.3. Objective

The literature review summarised that: (1) accounting for the variability in factors (e.g., dwelling characteristics, occupant behaviour, environment, etc.) that impact the amount of energy used by homes for space cooling is crucial when examining space-cooling energy consumption across the housing stock; (2) there has been little research to produce a model that allows for estimates of the changes to space-cooling energy consumption and indoor $PM_{2.5}$ exposure caused by home energy efficiency retrofits across Hong Kong; (3) previous epidemiological studies have established the relationships between outdoor $PM_{2.5}$ exposure and population's health; however, these relationships might not apply to Hong Kong where the population would spend time largely indoors; and (4) effort is required to estimate population exposure to domestic indoor $PM_{2.5}$ using Hong Kong's housing stock and environmental data.

The objective of this study is to develop a model that can be used to estimate space-cooling energy consumption and exposure to indoor $PM_{2.5}$ across Hong Kong dwellings. The model outcomes associated with the presence of home energy efficiency retrofits can be used by policy makers in devising viable home-energy-efficient and indoor-environmentally-friendly policies. To do this, archetypes broadly representative of the Hong Kong housing stock were developed using geographically-referenced housing databases. The unique combinations of archetype, occupation, and environment were simulated for annual space-cooling energy consumption and annual average exposure concentrations to indoor- and outdoor-sourced $PM_{2.5}$ using EnergyPlus version 8 [39]. The modelled home energy efficiency retrofits included external wall insulation, low-e windows, and airtightening.

2. Methods

2.1. Housing Data

Housing data were taken from three housing databases, including: (1) the Hong Kong Housing Authority (HA) database that contains records of the number of households in the public rental and subsidised home ownership housing [40]; (2) the Home Affairs Department (HAD) database that contains records of the number of households in private permanent housing [41]; and (3) the EMPORIS database that contains up-to-date building information worldwide [42]. EMPORIS was used as the fundamental database of the city-representative housing stock model, as it provided details about the built form, built age, and geographical location of dwellings. The number of residential buildings in the

EMPORIS database (7152) was slightly less than that of the HA and HAD databases combined (7337), indicating good agreement.

Housing types with sufficient information to enable space-cooling energy consumption and indoor PM_{2.5} concentrations to be estimated included high-rise flats, low-rise flats, tenements, and modern village houses. Internal layouts available in the literature [43–45] were assigned to each housing type according to the number of households and built age, leading to 15 different archetypes (Table 1). While dozens of combinations of housing type and internal layout were identified, those having more than ten examples in the housing stock were selected. The modelled archetypes accounted for approximately 1.8 million households, representing 72% of the 2.5 million households in Hong Kong [46]. The example building for each archetype, along with the floor plan, can be seen in Appendix A.

Table 1. The housing type, built form, built age, and proportion of the 15 archetypes.

Archetype	Housing Type	Built Form	Age	% of the Housing Stock ¹
1	Tenement	Four storeys and each storey comprises compact flats	1903–1940	2.4
2	Tenement	Four storeys and each storey comprises two wings that are perpendicular	1903–1940	3.2
3	Low-rise flat	Six storeys and each storey comprises rectangular blocks joining end by end	1941–1961	2.6
4	Low-rise flat	An elongated rectangular block of single-facing flats	1941–1961	4.8
5	Low-rise flat	A central core with units that form wings extending outwards from the core in four directions, being low-rise	1962–1990	1.9
6	High-rise flat	Elongated rectangular blocks joining end by end	1962–1990	2.1
7	High-rise flat	Two rectangular blocks joining corner by corner	1962–1990	3.7
8	High-rise flat	Two H-shaped blocks joining end by end (with external access corridors)	1962–1990	2.5
9	High-rise flat	A central core with flats that form wings extending outwards from the core in three directions	1962–1990	5.3
10	High-rise flat	A central core with flats that form wings extending outwards from the core in two directions	1962–1990	2.3
11	High-rise flat	A Y-shaped block	1991–2018	9.7
12	High-rise flat	Similar branches asymptotic to two mutually perpendicular pairs of lines, in the shape of a cross (16 units per floor)	1991–2018	11.7
13	High-rise flat	Similar branches asymptotic to two mutually perpendicular pairs of lines, in the shape of a cross (8 units per floor)	1991–2018	13.6
14	Modern village house	Three storeys with a compact layout	1998–2018	2.9
15	Modern village house	Four storeys with a T-shaped layout	1998–2018	3.2

¹ The proportion of individual archetypes broken down by district can be seen in Appendix B.

The Window-to-Wall Ratio (known as WWR), which is the fraction of the external wall area that is covered by windows, was estimated using the results from a large-scale housing survey conducted by Wan and Yik [47]. Hong Kong GIS resources [48], in conjunction with the EMPORIS database, were used to determine the footprint, orientation, building height, and ceiling height for individual archetypes. In order to reduce the number of simulations, footprints, building heights, or ceiling heights for the buildings that were classified as the same archetype were averaged. Buildings were assigned to four orientations, North (0°), West (90°), South (180°), and East (270°), based on their actual orientation. For instance, if a building was oriented at 75°, then it was modelled at West. The internal-layout-based method developed by the Buildings Department (BD) [49] was used to assess whether the internal layout for each archetype was sufficient for providing cross ventilation; the detailed assessments can be seen in Appendix C. Dwellings older than 1961 were modelled with external shading devices (i.e., overhangs or side fins), based on the estimated prevalence of

external shading devices in the Hong Kong housing stock [50]. Geometrical characteristics of the 15 archetypes can be seen in Table 2.

Table 2. Geometrical characteristics of the 15 archetypes.

Archetype Number	Footprint ¹ (m ²)	Floor Area of Flat ² (m ²)	Building Height ¹ (m)	Ceiling Height ¹ (m)	WWR (%)	Internal Layout Sufficient for Cross Ventilation? ³
1	139	25	17	3.0	40	Yes
2	417	32	16	3.0	45	No
3	452	35	23	3.0	26	No
4	576	43	34	3.0	32	No
5	1062	49	27	2.8	30	No
6	1125	55	89	2.8	30	No
7	980	59	128	2.8	30	No
8	1020	58	97	2.8	30	Yes
9	983	61	82	2.8	30	No
10	920	56	136	2.8	30	No
11	1093	69	87	2.8	30	Yes
12	1265	63	132	2.8	30	No
13	767	71	139	2.8	30	Yes
14	158	158	11	3.0	50	Yes
15	136	136	18	3.0	45	Yes

¹ Averaged over the buildings that were classified as the same archetype. ² Averaged over the flats of the buildings that were classified as the same archetype. ³ For detailed assessments, refer to Appendix C.

Building fabrics (i.e., external walls, ground floors, roofs, and windows) were modelled with U-values selected from the Hong Kong Building Environment Assessment Method (HK-BEAM) lookup tables based on the built age and fabric type of the dwelling [51]. Dwellings were modelled under the assumption that they had the most commonly seen construction materials according to the surveys of Hong Kong residences [50,52,53]. Information about the thermal conductivity of construction materials was obtained from the BD database [49]; the thickness of individual materials was adjusted to reflect the U-values of building fabrics.

The EnergyPlus AirflowNetwork module was used to calculate infiltration driven by wind and/or by forced air. To take into account the variation in infiltration due to wind pressures, the permeability (i.e., the air leakage rate per hour at a difference of 50 Pa between indoor and outdoor pressure, to the building fabric) was used to replace the infiltration rate. To do this, the infiltration rate for each archetype was estimated based on the methodology outlined in ISO 13790 [54]. An advantage of using the ISO 13790 methodology was that infiltration rates for a large number of dwellings could be estimated quickly at lower costs compared to pressurisation tests. The estimated infiltration rate was then converted to permeability using the volume and surface area of the dwelling. The fabric characteristics of the 15 archetypes are summarised in Table 3. For each archetype, the profile of wind pressure coefficients were determined based on the published data [4,55–61].

Shading due to surrounding buildings was modelled using the Land Cover Mapping database [62]. For instance, if the building was in an area that was classified as compact high-rise (i.e., more than 40% of the land was covered by buildings and the average height of buildings in this area was above 25 m), then it was modelled with block arrays representative of this density. Shading flats in multiple-occupancy buildings were treated as copies of the flats of interest, with no heat transferred in the separating walls.

Table 3. A summary of the fabric characteristics for the modelled 15 archetypes.

Archetype Number	Wall Type and U-Value (W/m ² ·K)	Floor Type and U-Value (W/m ² ·K)	Roof Type and U-Value (W/m ² ·K)	Window Type and U-Value (W/m ² ·K)	Permeability (m ³ h ⁻¹ m ⁻² at 50 Pa)
1	SW1 ¹ (3.5)	SF1 ² (0.60)	IC ³ (0.58)	SCG ⁴ (5.2)	18.9
2	SW1 (3.5)	SF1 (0.60)	IC (0.58)	SCG (5.2)	18.9
3	SW1 (3.3)	SF1 (0.58)	IC (0.51)	SCG (5.0)	11.6
4	SW1 (3.3)	SF1 (0.58)	IC (0.51)	SCG (5.0)	11.6
5	SW2 ⁵ (3.1)	SF1 (0.54)	IC (0.42)	SCG (4.6)	10.1
6	SW2 (3.1)	SF1 (0.54)	IC (0.42)	SCG (4.6)	10.1
7	SW2 (3.1)	SF1 (0.54)	IC (0.42)	SCG (4.6)	10.1
8	SW2 (3.1)	SF1 (0.54)	IC (0.42)	SCG (4.6)	10.1
9	SW2 (3.1)	SF1 (0.54)	IC (0.42)	SCG (4.6)	10.1
10	SW2 (3.1)	SF1 (0.54)	IC (0.42)	SCG (4.6)	10.1
11	SW2 (2.9)	SF1 (0.51)	IC (0.36)	SCG (4.6)	9.2
12	SW2 (2.9)	SF1 (0.51)	IC (0.36)	SCG (4.6)	9.2
13	SW2 (2.9)	SF1 (0.51)	IC (0.36)	SCG (4.6)	9.2
14	SW2 (2.6)	SF2 ⁶ (0.49)	IC (0.30)	STG ⁷ (4.6)	15.8
15	SW2 (2.6)	SF2 (0.49)	IC (0.30)	STG (4.6)	15.8

¹ Solid wall 1: concrete gypsum plasterboard, concrete, gypsum plastering (outside to inside). ² Solid floor 1: slab on ground, screed over insulation. ³ Insulated concrete: asphalt mastic roofing, expanded polystyrene, reinforced concrete, gypsum plastering (outside to inside). ⁴ Single clear glass with a solar heat gain coefficient (SHGC) of 0.76. ⁵ Solid wall 2: mosaic tile, concrete gypsum plasterboard, concrete, gypsum plastering (outside to inside). ⁶ Solid floor 2: suspended concrete floor, granite. ⁷ Single tinted glass with a SHGC of 0.50.

In addition to the 15 archetypes described above, another set of 15 archetypes representative of the possible energy-efficient improvements to the Hong Kong housing stock in the future was developed. Each archetype was given fabric properties reflecting recommended energy efficiency retrofits [63]: (1) external walls were provided with internal insulation, which reduced the U-value of the walls by 40%; (2) low-e coatings were added to the glass panes of windows, resulting in a 30% reduction in SHGC; and (3) permeability of the building envelope was decreased by 3 m³/h/m². The effects of individual home energy efficiency retrofits on space-cooling energy consumption and exposure to indoor PM_{2.5} are examined in Sections 3.1 and 3.2.

2.2. Environmental Data

The weather data, including temperature, relative humidity, wind, atmospheric pressure, cloud cover, and solar radiation, were obtained from the weather dataset published by the Hong Kong Observatory (HKO) [64]. Data on ambient outdoor PM_{2.5} concentrations at ground level were obtained from the air quality monitoring dataset published by the Environmental Protection Department (EPD) [65]. An environment file that contained concurrent weather and outdoor pollution components was created using these two datasets. The dispersion model developed by Chan and Kwok was used to estimate how the ambient outdoor PM_{2.5} concentrations varied at different levels above ground [29]. Weather and outdoor pollution data for the 18 districts in Hong Kong (Figure 1) were used to generate site-specific environment files, assuming that dwellings in the same district were under the same environmental conditions. For districts (i.e., North, Tuen Mun, Tai Po, and Kwai Tsing) where there were some weather or pollution data missing, data from the closest district were used instead. Descriptive statistics of the key environmental variables for individual districts can be seen in Appendix D.

With the location information provided by EMPORIS, dwellings were assigned to the 18 districts and were simulated using the site-specific environment files. Urban/Rural classifications of the Planning Department (PD) were used to classify dwellings into urban or rural category according to their location [66]; simulations were carried out with different wind speed profile coefficients to reflect urban and rural settings [67].



Figure 1. Hong Kong's 18 districts.

2.3. Model Development

Building physics models of the 15 archetypes were developed using EnergyPlus version 8. Methods and assumptions that were used in the development of models are described in Sections 2.3.1–2.3.4

2.3.1. Dwellings

For tenements and low-rise residential buildings (Archetypes 1–5), simulations were carried out only for middle-floor rooms/flats, under the assumption that these rooms/flats could represent the majority of rooms/flats in the building. For high-rise residential buildings (Archetypes 6–13), ground-, middle-, and top-floor flats were modelled to account for differences in obstruction, wind speed, wind pressure, and ambient outdoor $PM_{2.5}$ levels between flats on different floors. The flats of interest and the adjoining flats to the sides, above, and below were assumed to have a net heat, air, and contaminant flow of zero between them. Internal doors were closed, except for the bedroom doors that remained open. The living room and bedroom were chosen as the rooms of interest, given the fact that they were the locations (1) where people spent most of their time when they were at home, and (2) where people most frequently installed and used their air conditioners [50]. The living room and bedrooms were treated as a single well-mixed zone for simplicity.

2.3.2. Occupancy

The occupancy modelled with a family of three (two parents and one child) or two pensioners determined internal heat gains and the periods of exposure to indoor $PM_{2.5}$. The occupancy groups (i.e., the family of three and pensioners) were selected based on their ability to lead to significant changes in space-cooling energy consumption and exposure to indoor $PM_{2.5}$ [52], whilst the number of occupants was determined based on the statistics showing that the average domestic household size was 2.5 [46]. Occupants were assumed to stay in the combined living-room-and-bedroom zone when they were at home. Dwellings with the family occupancy were simulated to be unoccupied between 08:30 and 18:30 on weekdays, and occupied at all other times, while those with the pensioner occupancy were occupied for 24 h per day, 7 days per week. Internal heat gains from occupants (130 W per person), lighting (550 W), and electric equipment (700 W) were modelled as per CIBSE [68]. The net generation rate of moisture inside the home was modelled at 9.8 kg per day [69].

2.3.3. Cooling and Ventilation

Cooling was modelled to a 24 °C set-point during the period from April through October [70,71]. The period of the cooling season was consistent with the results from the surveys of Hong Kong households indicating that people rarely switched air conditioners on during the period from November to March [52,72,73]. The cooling system was a split-type air conditioner, which removed heat from the indoor air without bringing in fresh air from outside. The COP of the split-type air conditioner was set as 2.8, according to the Code of Practice for Energy Efficiency of Building Services Installation [74]. Heating devices and mechanical ventilation systems were not modelled because of their rarity in the Hong Kong domestic sector. Extract fans in the kitchen and bathroom ran during cooking and showering, and were sized in accordance with building regulation requirements [75].

Occupant-controlled window opening was modelled to occur in the combined living-room-and-bedroom zone during the period from November to March (i.e., when the buildings were in a free-running mode). The behavioural model developed by Haldi and Robinson [76], which has been shown to accurately predict occupant window opening behaviour in Hong Kong dwellings [77], was used to capture occupants' window-use patterns. Given the fact that the behavioural model can only work in cases where there is no air conditioning, a rule-based window opening schedule was used for the cooling season. When indoor temperatures were in the range of 18 °C to 24 °C, windows were opened in the combined living-room-and bedroom zone. When indoor temperatures were below 18 °C, windows were closed. In both cases, windows were closed if outdoor temperatures were greater than indoor temperatures, if no one was at home, or if the air conditioning was switched on. The criteria used to determine whether windows could be opened are broadly consistent with the field studies of occupant window opening behaviour [15,78].

2.3.4. PM_{2.5} Transport

EnergyPlus version 8 can model the transport of PM_{2.5} based on the Generic Contaminant transport algorithm [79]. The infiltration of PM_{2.5} from outdoor sources was modelled through cracks in the building envelope (i.e., the external walls, roof, and ground floor) and open windows. Cracks were put at the top and bottom of the external walls of the dwelling, in order to take into account the difference in wind pressure according to the ceiling height. Cracks were assigned air mass flow exponents of 0.66 and the reference air mass flow coefficients were dependent on the dwelling airtightness and surface area [80]. The penetration factor of PM_{2.5} was 0.8 if windows were closed and 1.0 if windows were open [28]. Internal walls were modelled with cracks, allowing the transport of PM_{2.5} between rooms. Indoor-sourced PM_{2.5} were those from cooking in the kitchen (1.6 mg/min) and showering in the bathroom (0.04 mg/min) [81]; the emission schedules of indoor-sourced PM_{2.5} can be seen in Table 4. Smoking was ignored because of the great uncertainty about the emission schedule. PM_{2.5} deposition was modelled at a rate of 0.19 h⁻¹ [82]. Air purifiers (or filters installed in air conditioners) that can help reduce indoor PM_{2.5} concentrations were not modelled due to their rarity in the Hong Kong domestic stock.

Table 4. The periods of PM_{2.5} emissions from indoor sources.

Indoor Source	Period of PM _{2.5} Emission
Cooking in the kitchen	7:40 a.m. to 8:00 a.m. 12:00 p.m. to 12:30 p.m. ¹ 7:00 p.m. to 7:30 p.m.
Showering in the bathroom	9:40 p.m. to 10:00 p.m.

¹ Apply to the pensioners throughout the week, and the family during weekends.

2.4. Simulation and Data Collation

Simulations were carried out for the combinations of variables that included:

- 15 archetypes (31 variants including flats on the ground, middle, and top floors);
- 4 orientations (North, West, South, and East);

- 18 locations (weather and outdoor pollution data for 18 districts);
- 5 types of overshadowing (compact high-rise, compact low-rise, open high-rise, open low-rise, and sparsely built);
- 2 types of terrain (urban and rural);
- 2 occupancy groups (two pensioners and a family of three);
- 3 types of fabric retrofits (external wall insulation, low-e windows, and airtightening).

First, EnergyPlus input files for the 31 archetype variants were created using OpenStudio Sketchup Plug-in [83], which allows users to quickly input building geometry. Next, a python-based simulation tool, jEPlus [84], capable of rapidly editing EnergyPlus input files, was used to generate EnergyPlus input files that contained unique combinations of the variables described above. Finally, simulations were run for each combination for a full year using EnergyPlus's built-in batch file, RunEPlus.bat.

Space-cooling energy consumption was calculated at 10-min intervals and the results output hourly. Indoor PM_{2.5} concentrations were calculated at 10-min intervals and output hourly alongside ambient outdoor PM_{2.5} concentrations. Data collation was carried out using SAS [85], which collated the simulation results, and calculated space-cooling energy consumption (kWh/m²) by dividing space-cooling energy consumption for flats on the same floor by the total floor area of these flats, and determined indoor PM_{2.5} exposure (averaged over the flats on the same floor) by overlaying the occupancy profile on the indoor PM_{2.5} concentration profile. To date, there was a lack of information on occupancy patterns for individual archetype variants. Considering that working people comprised 50% of the population [86], the estimates of space-cooling energy consumption and exposure to indoor PM_{2.5} for each dwelling were made by averaging the family and pensioner occupancy results.

2.5. Model Validation

The robustness of the city-representative housing stock model developed in this study was assessed on two grounds: (1) how accurately EnergyPlus version 8 could predict space-cooling energy use and indoor PM_{2.5} concentrations for a typical Hong Kong dwelling; and (2) whether the simulation results of space-cooling energy consumption and indoor PM_{2.5} concentrations across the housing stock were consistent with public data from the government and other studies. The assessment of the predictive power of EnergyPlus is presented in this section, whilst comparisons between the simulation results and public data can be seen in Section 4.2.

Measurement data on space-cooling energy use and indoor PM_{2.5} levels for a flat located in Kowloon (Figure 2) were used to assess the prediction accuracy of the EnergyPlus model. The flat was composed of a living room, two bedrooms, a bathroom, a kitchen, and a balcony. Fabric U-values were 3.1 W/m²K for external walls, 0.54 W/m²K for the ground floor, 0.42 W/m²K for the roof, and 4.6 W/m²K for windows. The window glass had a SHGC of 0.76. The permeability of the building envelope was 10.1 m³ h⁻¹ m⁻² at 50 Pa. Measurements were carried out in Bedroom 1, which had an air conditioner with a COP of 2.8 and a rated cooling capacity of 1.9 kW. Windows and internal doors were closed. Weather data were collected from a meteorological station nearby.

Measurements of space-cooling energy consumption were taken from 28 September 2017 to 30 September 2017, with the cooling setpoint set as 24 °C. A portable power meter (SP2; BroadLink, Hangzhou, China) was used to measure hourly electrical energy consumption for air conditioning. Measurements of indoor PM_{2.5} levels were conducted from 15 November 2017 to 17 November 2017, during which the air conditioning was switched off. The levels of indoor and ambient outdoor PM_{2.5} were measured every hour using two air pollution monitors (DUSTTRAK 8530EP; TSI, Shoreview, MN, USA), which were newly calibrated and were accurate to ±5% (with a measurement range of 0.001 mg/m³ to 150 mg/m³). One air pollution monitor was placed in the middle of Bedroom 1 for measurements of indoor concentrations, and the other was placed in the stairs for measurements of ambient outdoor concentrations (Figure 2b).

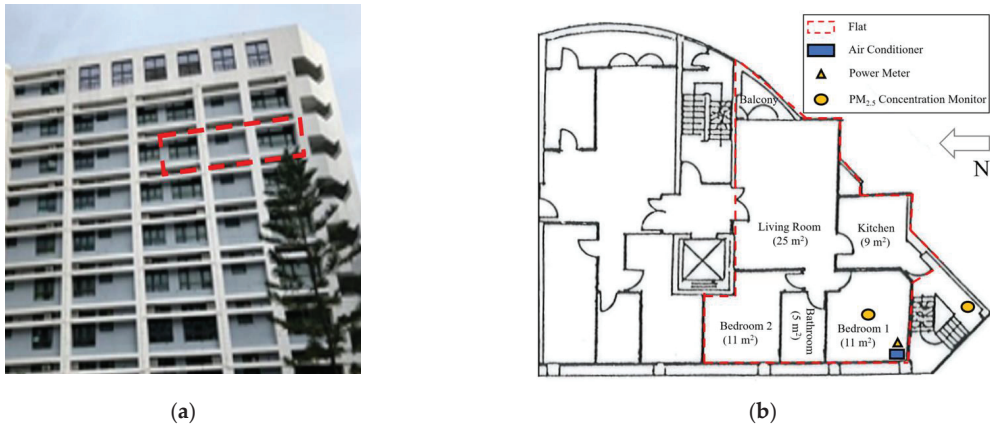


Figure 2. (a) The measured flat; (b) the floor plan of the measured flat.

The measured flat was modelled in EnergyPlus version 8 using the geometry, fabric characteristics, occupancy schedule, weather conditions, ambient outdoor PM_{2.5} levels, and air conditioner as described above. The deposition rate of indoor PM_{2.5} was modelled at 0.19 h^{-1} [82], whilst the penetration factor was assumed to be 0.8 [28]. The measurement and simulation results for 29 September 2017 (electricity use) and 16 November 2017 (PM_{2.5} concentrations) were used for analysis. The simulated amount of electricity consumption for air conditioning was consistent with that obtained from the field measurement (Figure 3), with an average error of 5.2%. The simulated indoor PM_{2.5} levels were also generally in line with the measurements (Figure 4), with an average error of 8.9%. The discrepancy in concentrations was possibly due to the modelled deposition of PM_{2.5} not being very representative of the actual PM_{2.5} deposition seen in the measured flat. In conclusion, EnergyPlus version 8 could be used to accurately estimating space-cooling energy use and indoor PM_{2.5} concentrations for a typical dwelling in Hong Kong; this was fundamental to reasonable estimates of space-cooling energy use and indoor PM_{2.5} levels across the housing stock.

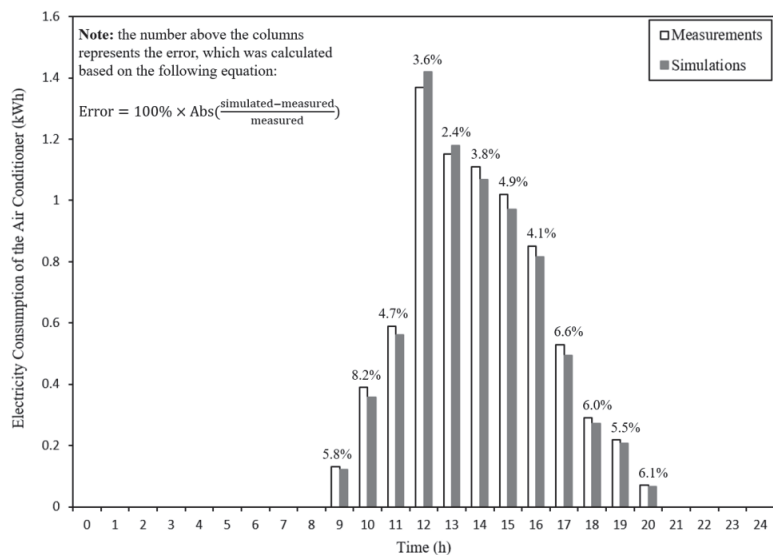


Figure 3. The measured and simulated electricity consumption of the air conditioner.

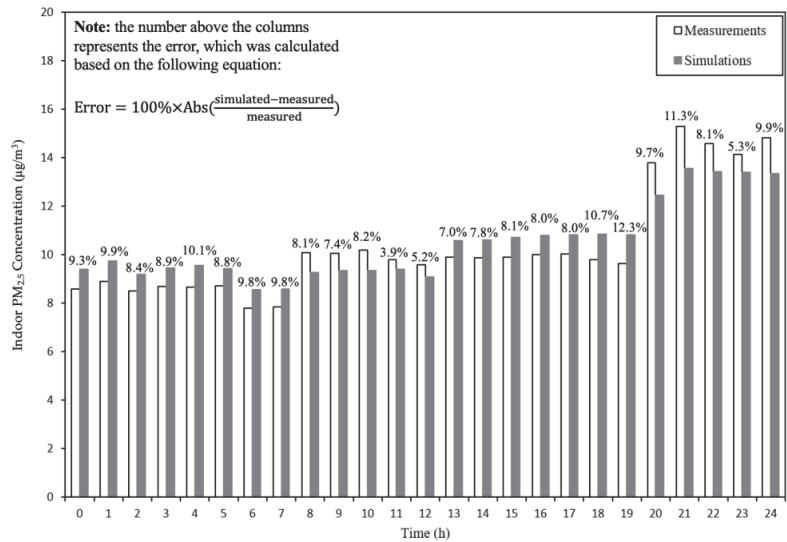


Figure 4. The measured and simulated indoor PM_{2.5} concentrations for the flat.

3. Results

3.1. Space-Cooling Energy Use across the Housing Stock

A simple initial statistical analysis was carried out to compare space-cooling energy consumption between different archetypes (Figure 5). The top-floor flats in high-rise residential buildings (Archetypes 6c–13c) and modern village houses (Archetypes 14–15), on average, used 19% more space-cooling energy than other archetypes. The archetypes that used the lowest amount of space-cooling energy were ground-floor flats in high-rise residential buildings (Archetypes 6a–13a). Comparisons among Archetypes 6–13 show that high-rise flats with an internal layout sufficient for providing cross ventilation (i.e., Archetypes 8, 11, and 13, as described in Table 2), on average, used 7.2% less space-cooling energy than the non-cross-ventilation counterparts. Pensioners had a greater demand for space cooling than the family of three, attributable to their presence inside the home during the daytime. Compared with the pensioner results, the family results show less significant variation in space-cooling energy consumption between different archetypes. A likely explanation for this is that people were not at home during the periods of high solar radiation, in which case the difference in the space-cooling energy use between dwellings caused by shading (which had been taken into account based on the archetype, location, and terrain) was relatively small. Figure 6 shows the spatial trend of space-cooling energy consumption for Archetype 5; other archetypes showed similar spatial trends. As expected, dwellings modelled under the microclimate of Sham Shui Po or Wan Chai (which had a relatively higher annual average outdoor temperature, as described in Appendix D) were seen to have the greatest energy demand for space cooling, while those under the microclimate of Tsuen Wan had the lowest space-cooling energy demand.

The percentage change to space-cooling energy consumption caused by fabric retrofits is shown in Figure 7, in which the negative values mean that there were energy benefits to be had from each retrofit. The trend was the same for each archetype—low-e windows led to the largest reduction in space-cooling energy consumption, then the tightening of the building envelope, and finally the external wall insulation. Compared with low- and high-rise residential buildings (Archetypes 3–13), tenements (Archetypes 1–2) and modern village houses (Archetypes 14–15) saw a greater percentage decrease in space-cooling energy consumption following each fabric retrofit, largely because they had a greater externally exposed surface-area-to-volume ratio and a larger WWR.

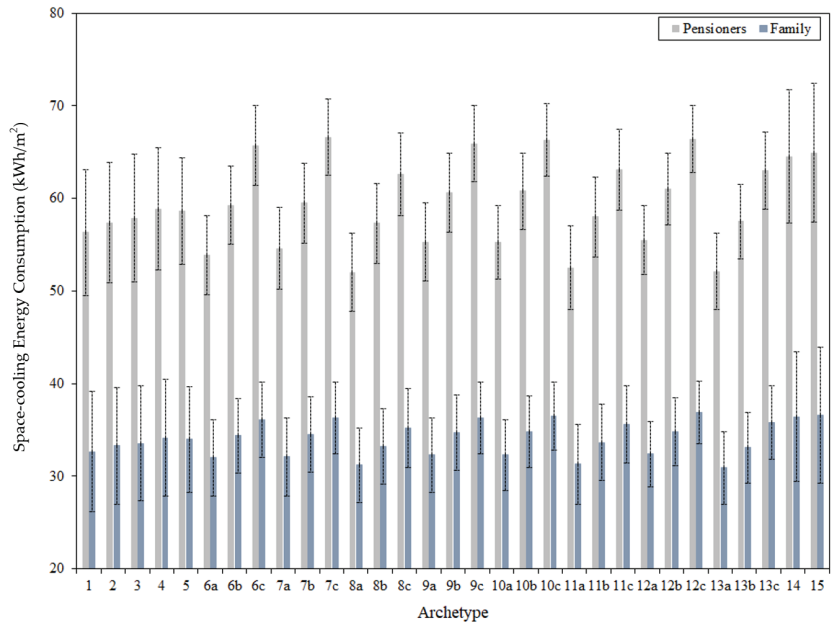


Figure 5. Space-cooling energy consumption for different archetypes (a: ground-floor flats, b: middle-floor flats, and c: top-floor flats) with the pensioner/family occupancy. The error bars indicate ± 1 standard deviation.

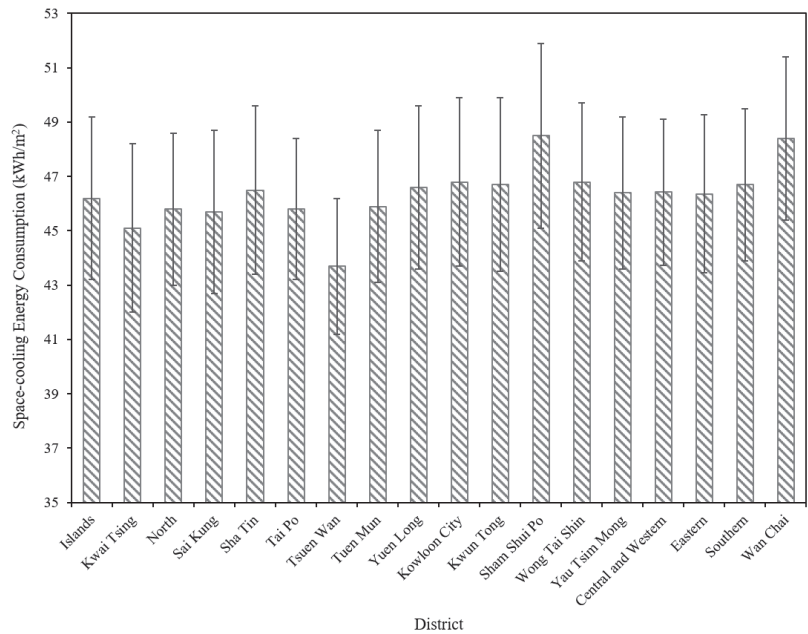


Figure 6. The space-cooling energy consumption for Archetype 5 under different microclimates, averaged over the pensioner and family results. The error bars indicate ± 1 standard deviation.

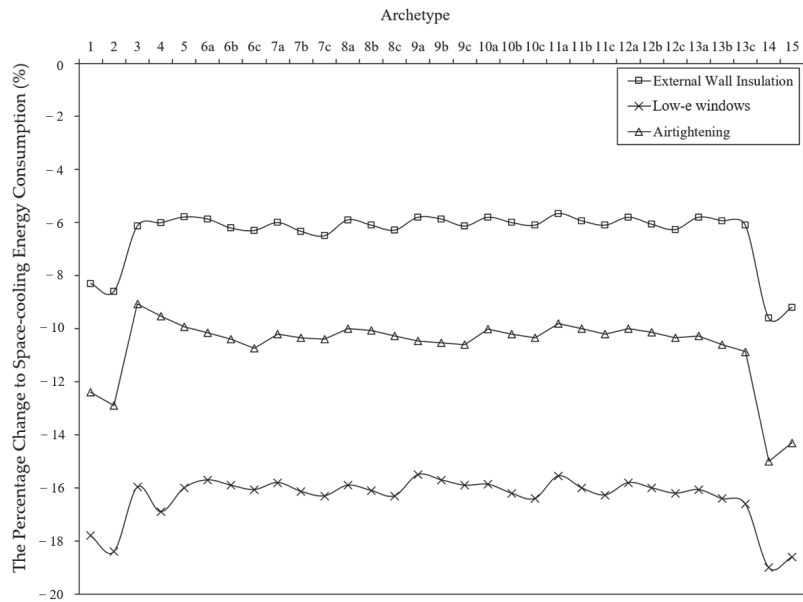


Figure 7. The percentage change to space-cooling energy consumption caused by individual fabric retrofits amongst the modelled archetypes (a: ground-floor flats, b: middle-floor flats, and c: top-floor flats), averaged over the pensioner and family results.

3.2. Indoor PM_{2.5} Exposure across the Housing Stock

The EnergyPlus results show a range of annual average exposure concentrations to PM_{2.5} from different sources across the housing stock (Figure 8). The exposure to PM_{2.5} from outdoor sources was found to be lower in low- and high-rise flats (Archetypes 3–13), and higher in tenements (Archetypes 1–2) and modern village houses (Archetypes 14–15). This supports previous research on the infiltration of PM_{2.5} into buildings [27], suggesting that reducing the permeability of the building envelope or externally exposed surface-area-to-volume ratio could help reduce exposure to outdoor-sourced PM_{2.5} (refer to Table 3 for information about the permeability of individual archetypes). For high-rise residential buildings, middle- and top-floor flats (Archetypes 6b–13b and Archetypes 6c–13c, respectively) had lower exposure to PM_{2.5} from outdoor sources compared to ground-floor flats (Archetypes 6a–13a), attributable to the ambient outdoor PM_{2.5} concentrations outside flats towards the top of the containing building being lower than concentrations at the bottom (Table A3 in Appendix D). Comparisons between Archetypes 6–13 show that high-rise flats with the ability to cross-ventilate (Archetypes 8, 11, and 13) had greater exposure to PM_{2.5} from outdoor sources compared to the non-cross-ventilation counterparts. Dwelling-to-dwelling differences for PM_{2.5} from indoor sources are generally the inverse of those observed for PM_{2.5} from outdoor sources, with tenements and modern village houses exhibiting lower exposure to PM_{2.5} from indoor sources compared to low- and high-rise flats, and high-rise flats with the ability to cross-ventilate showing lower exposure compared to the non-cross-ventilation counterparts. Even with the incorporation of extract fans into the kitchen and bathroom, exposure concentrations to PM_{2.5} from cooking and showering were seen to be larger than those to PM_{2.5} from outdoor sources in most of the dwellings.

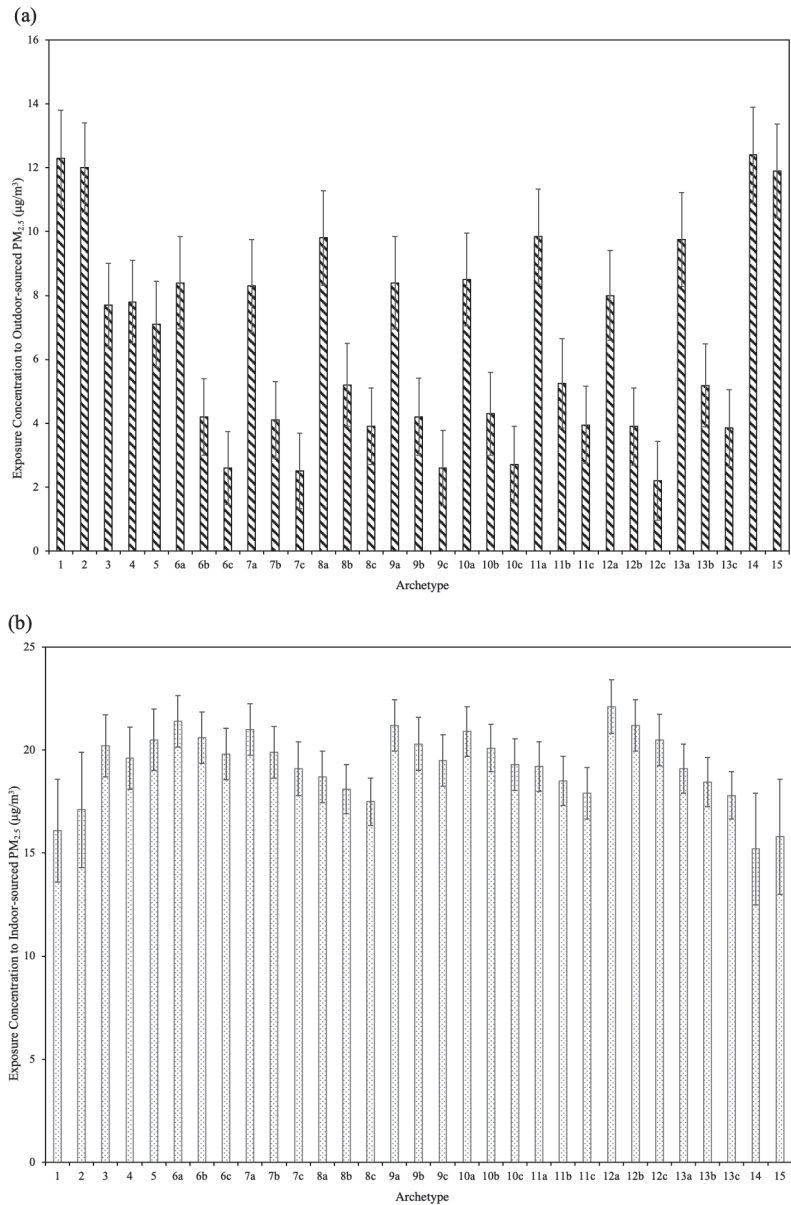


Figure 8. Annual average exposure concentrations to (a) outdoor-sourced PM_{2.5} and (b) indoor-sourced PM_{2.5} for individual archetypes (a: ground-floor flats, b: middle-floor flats, and c: top-floor flats), averaged over the pensioner and family results. The error bars indicate ± 1 standard deviation.

The city-wide trend for exposure to PM_{2.5} from outdoor sources can be seen in Figure 9, where the results were weighted by the proportion of individual archetypes in the same district. Exposure concentrations to outdoor-sourced PM_{2.5} were found to be higher in the Islands, North, and Sai Kung, due to leaky modern village houses (Archetypes 14–15) being the dominant archetype (as described in Appendix B) and greater exposure to wind (i.e., a rural setting for most of the dwellings), and lower in other districts due to the prevalence of airtight low- and high-rise flats (Archetypes 3–13) and lower wind exposure

(i.e., an urban setting for most of the dwellings). This result is in contrast to the data of outdoor $PM_{2.5}$, which show that higher outdoor $PM_{2.5}$ concentrations were generally found in urban areas. Dwellings in Yau Tsim Mong, in which there were busy roads and mainline tracks nearby, were seen to have greater exposure to outdoor-sourced $PM_{2.5}$ in comparison to those in other urban locations. Dwellings in Tsuen Wan exhibited the lowest exposure to $PM_{2.5}$ from outdoor sources. Exposure concentrations to indoor-sourced $PM_{2.5}$ were seen to be the opposite of those to outdoor-sourced $PM_{2.5}$, with lower exposure in areas where there was a large number of leaky dwellings present, higher exposure in areas where there was a large number of airtight dwellings present, and dwellings in Tsuen Wan being the most vulnerable to high $PM_{2.5}$ concentrations from indoor sources.

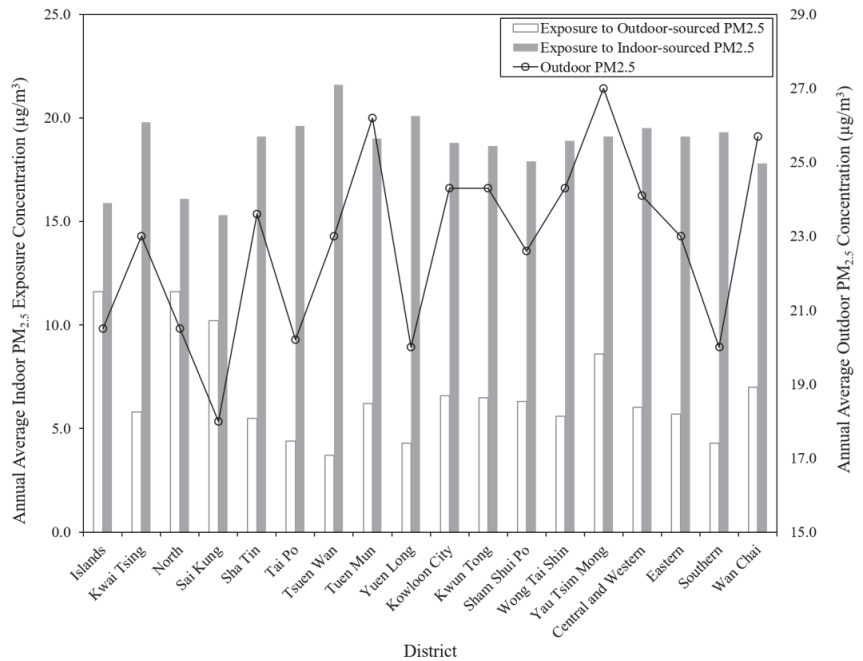


Figure 9. Exposure concentrations to indoor- and outdoor-sourced $PM_{2.5}$ for dwellings across Hong Kong, averaged over the pensioner and family results.

The percentage change to indoor $PM_{2.5}$ exposure caused by individual fabric retrofits across the housing stock can be seen in Figure 10, where the positive and negative values show increased and reduced exposure, respectively. The airtightening of the building envelope helped reduce exposure to outdoor-sourced $PM_{2.5}$, however, at the cost of higher exposure concentrations to $PM_{2.5}$ from indoor sources. The implementation of external wall insulation was observed to increase exposure to $PM_{2.5}$ from outdoor sources and reduce exposure to $PM_{2.5}$ from indoor sources. Compared with airtightening and external wall insulation, the influence of low-e windows on exposure from outdoor and indoor sources was much less significant. The modelled fabric retrofits had a greater influence on exposure to indoor- or outdoor-sourced $PM_{2.5}$ for tenements (Archetypes 1–2) and modern village houses (Archetypes 14–15), largely because of their higher outside exposed surface-area-to-volume ratio and WWR. When combining exposure from outdoor and indoor sources, the modelled archetypes saw 7.9% and 0.2% average increases in exposure from airtightening and low-e windows, respectively, and an average decrease of 3.5% in exposure from external wall insulation.

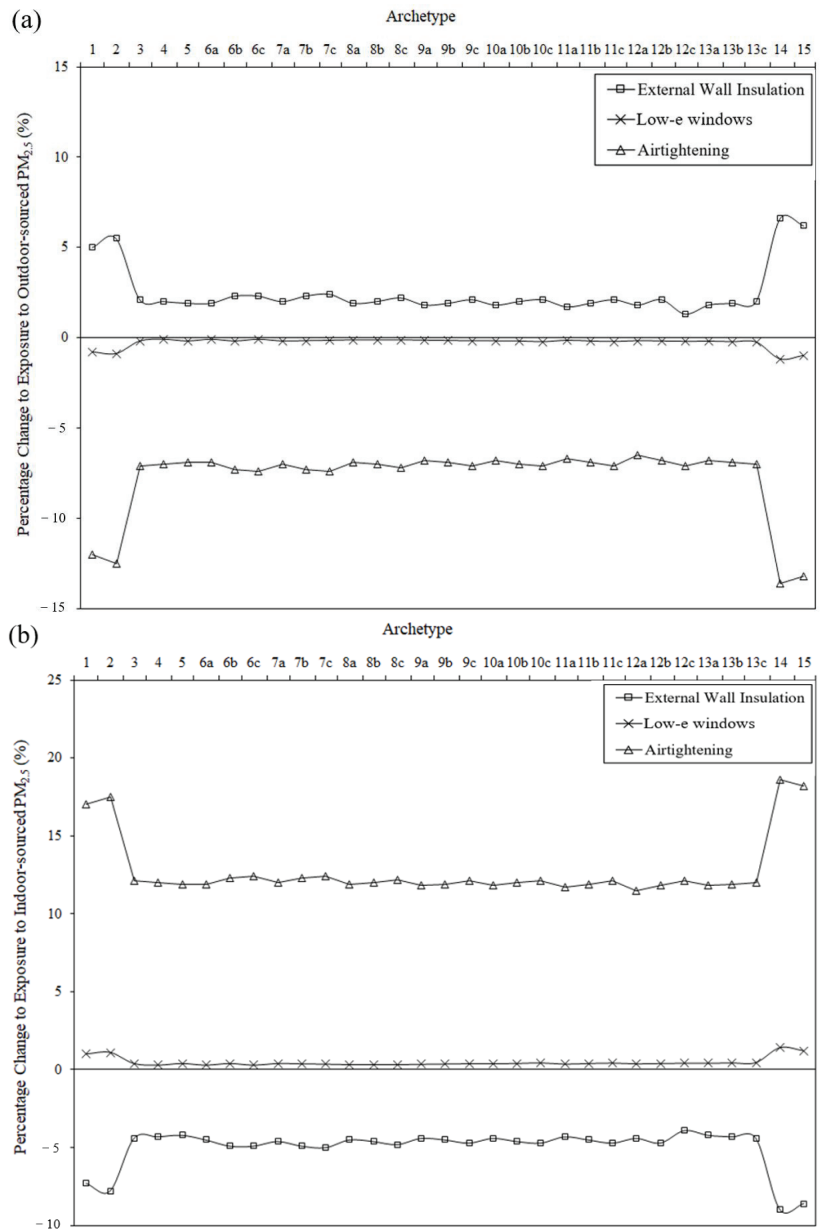


Figure 10. Cont.

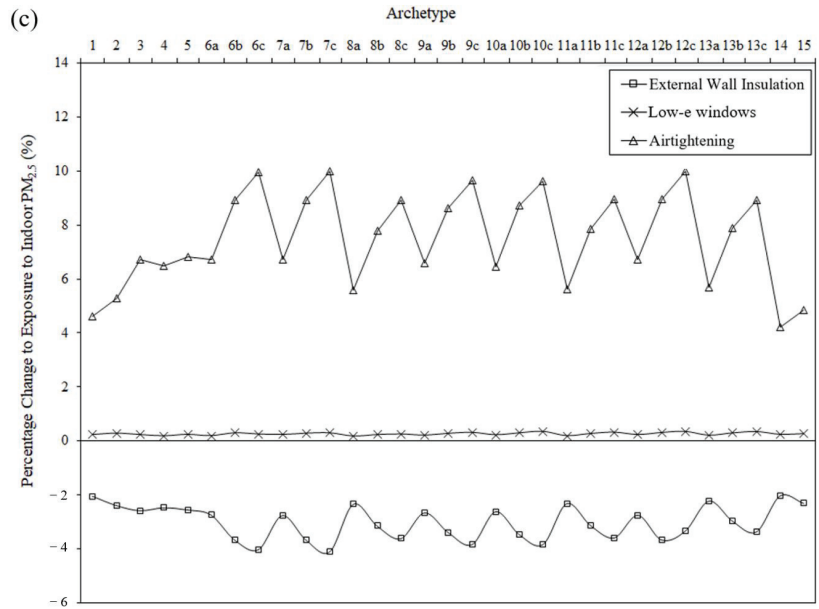


Figure 10. The percentage change to exposure to (a) $PM_{2.5}$ from outdoor sources; (b) $PM_{2.5}$ from indoor sources; and (c) indoor $PM_{2.5}$ caused by each fabric retrofit amongst the 15 archetypes (a: ground-floor flats, b: middle-floor flats, and c: top-floor flats), averaged over the pensioner and family results.

4. Discussion

4.1. The Housing Stock Model

The EMPORIS database that contains detailed building and location data was the most extensive database available when the study was carried out. When compared to the government databases, EMPORIS has shown a good agreement in terms of the number of dwellings. Although extensive, the EMPORIS database lacks information about the built form or built age for 28% of the households in Hong Kong. In addition, EMPORIS does not contain retrofit information across the city, so there is a bias towards the ‘as-built’ dwellings that have not undergone refurbishment (e.g., wall cavity insulation, duct-sealing, or reorganising the internal layout of the dwelling). Not all of the dwellings that have a unique archetype have been modelled, for example, dwellings with a loft or a green roof. Developing archetypes for each dwelling in the housing stock is unrealistic and will require considerable time to simulate via building simulation tools available at the time of the study. However, the archetypes were modelled to represent the majority of dwellings in Hong Kong rather than a specific dwelling, and the deviation of each dwelling from the nominal archetype can be minimised if the results apply to a wide geographical scale—in this case, the whole city.

HVAC systems such as heating systems, mechanical ventilation systems, and air purifiers (or filters in air conditioners) have not been considered because of their relative rarity in the Hong Kong domestic stock. Local shading has been taken into account according to the archetype, location, and terrain, while shading from other sources such as vegetation or signboards (commonly seen in tenements) was not modelled because of a lack of data on building-specific overshadowing. The role of occupants in space-cooling energy consumption and exposure to indoor $PM_{2.5}$ has not been investigated beyond the two occupancy patterns described in Section 2.3.2. There can be a great degree of variation in model outputs due to uncertainty over the occupancy pattern, for example, people who

work overtime in the office being less likely to have high space-cooling energy costs at home, and those who smoke being more vulnerable to great exposure to indoor PM_{2.5}.

4.2. Model Outcomes

By using a city-representative housing stock model, this study has been able to examine space-cooling energy use and exposure to indoor PM_{2.5} across the Hong Kong housing stock, and how energy efficiency retrofits may influence population exposure to domestic indoor PM_{2.5}. The model outcomes (Figure 5) indicate that modern village houses and top-floor flats in high-rise residential buildings used more space-cooling energy than other dwellings. The increasing demand for housing may imply that flats on high floors will become more common in the future, which may result in higher space-cooling demand in the residential sector. High-rise flats with an internal layout that facilitated cross ventilation were found to have a lower space-cooling energy consumption compared to the non-cross-ventilation counterparts. While cross-ventilation via open windows leads to a reduction in the space-cooling energy consumption, this may not be applicable to the entire housing stock, for instance, the dwellings with security concerns. The significant variability of home space-cooling energy use between different districts (Figure 6) indicates that the microclimate is potentially a key factor in determining the space-cooling energy consumption for dwellings, and that modelling studies examining the space-cooling energy consumption across the housing stock should include location-specific weather files. This study did not consider variations in local temperatures caused by the urban heat island effects, even though they are expected to amplify the differences in home space-cooling energy use between urban and rural locations.

Government policies encouraging the uptake of energy efficiency interventions in the Hong Kong housing stock are currently being implemented [87], which means that the number of retrofit dwellings is expected to increase. An examination of the space-cooling energy use in dwellings with fabric retrofits (i.e., external wall insulation, airtightening, and low-e windows) (Figure 7) agrees with previous research showing that retrofit dwellings used less space-cooling energy in comparison to the non-retrofit counterparts [5,63]. This energy benefit could be attributable to a lower rate of heat gain during peak demand hours. The percentage change of space-cooling energy consumption caused by fabric retrofits shows, in some cases, a significant difference between different archetypes, highlighting the necessity of taking into account the modifying effect of archetypes when investigating the energy benefits of home energy efficiency retrofits.

According to the data on the use of energy in Hong Kong [88], the annual electricity used for space cooling for a household in 2018 was 40.9 kWh/m², which is 9.7% lower than the value obtained in this study. There are several likely reasons for this discrepancy, including: (1) the modelled two occupancy patterns (i.e., the family and pensioners) did not account for holidays when people are possibly away from home; (2) giving equal weight to the two occupancy patterns may overestimate the number of dwellings with the pensioner occupancy, which were found to use more space-cooling energy than those with the family occupancy; (3) cooling was modelled to a 24 °C set-point, while the actual cooling set-points may vary across dwellings and can be greater than the modelled ones; (4) the living room and bedrooms of a dwelling were modelled as a single thermal zone and were, therefore, air-conditioned simultaneously, which may not reflect the fact that only the occupied room is air-conditioned; (5) a considerable number of dwellings may be equipped with air conditioners with a COP greater than 2.8; and (6) occupants may occasionally use fans instead of air conditioners for cooling.

The spatial variation in outdoor PM_{2.5} concentrations (Figure 9) indicates that the level of outdoor PM_{2.5} was higher in urban areas (e.g., Tuen Mun, Yau Tsim Mong, and Wan Chai) than in rural areas (e.g., Islands, North, and Sai Kung). However, taking into account the modifying effect of archetypes led to an obvious inversion of the exposure risk. PM_{2.5} infiltration was greatly affected by the exposure to wind, which, when in conjunction with the leaky modern village houses being the dominant dwelling archetype, meant that

high PM_{2.5} concentrations from outdoor sources were seen in rural areas. Compared with those in rural areas, dwellings in urban areas had lower PM_{2.5} concentrations from outdoor sources regardless of the high outdoor concentrations, attributable to the predominance of smaller and more airtight archetypes such as low- and high-rise flats. The exposure to indoor-sourced PM_{2.5} was seen to be the opposite of that to outdoor-sourced PM_{2.5}, with greater exposure for dwellings in urban areas.

By using a behavioural model to simulate occupant-controlled window opening, this work has been able to determine the difference in exposure between dwellings caused by different window-use patterns. Top-floor flats in high-rise residential buildings are generally more susceptible to high indoor temperatures in comparison to ground- and middle-floor flats, meaning that people may open windows at a higher frequency to maintain as comfortable a temperature as possible. Dwellings with a larger amount of window-opening may facilitate the removal of indoor-produced PM_{2.5}. This is supported by Figure 8 showing that top-floor flats had lower exposure to PM_{2.5} from indoor sources in comparison to ground- and middle-floor flats. Similarly, dwellings in Sham Shui Po or Wan Chai showed lower levels of exposure to PM_{2.5} from indoor sources in comparison to those in Tsuen Wan (Figure 9), due to an increase in the amount of window-opening caused by higher outdoor temperatures.

Airtightening was seen to be dangerous for increasing the risk of indoor PM_{2.5} exposure, in line with previous studies [28,30], while the low-e window was seen to be a much less significant factor in determining the exposure risk (Figure 10). External wall insulation could help reduce indoor PM_{2.5} exposure concentrations. One possible reason for this health benefit is that external wall insulation limited heat loss through the building envelope and, therefore, increased indoor temperatures, in which case, people have to ventilate the room more (and therefore, have lower exposure to PM_{2.5} from indoor sources) in order to try to maintain desired levels of thermal comfort.

While there is a lack of data on population exposure to PM_{2.5} in Hong Kong dwellings, the model outcomes (Figure 8) are generally in line with previous studies. The measurements taken in 63 dwellings in the New Territories estimated a range of average indoor PM_{2.5} concentrations of $26.3 \pm 12.0 \mu\text{g}/\text{m}^3$ [33,36], similar to the range of values (20.2 to 29.7 $\mu\text{g}/\text{m}^3$) obtained in this study. The results of cooking-produced PM_{2.5} measurements taken by Wan et al. [89] are similar in terms of magnitude, but are hard to directly compare with the model outcomes due to differences in the way kitchen extract fans operate. Some local studies [34,35] have found infiltration factors (which represent the proportion of outdoor pollutants that penetrate the building and remain suspended) ranging from 0.29 to 0.82, which are also similar to the model outcomes (0.35 to 0.67).

4.3. Limitations and Further Research

There are some simplifications that could impact the model outcomes. In terms of occupant window opening behaviour during the cooling season, the static temperature thresholds for opening and closing windows were selected based on field studies [15,78], however, there can be a significant variation in this behaviour. For example, while an increase in ventilation will be normally required when indoor temperatures exceed 18 °C, it could be the case that windows are opened at a higher indoor temperature due to occupant adaptation to a warmer indoor environment. In addition, temperature is a key factor that influences occupants' window operation, but windows may not be only opened for ventilative cooling, or can be closed for security reasons. Finally, the model assumption that bedroom doors remained open may not reflect the reality that occupants may keep bedroom doors closed, especially those who share a flat.

There are also some uncertainties about indoor PM_{2.5} modelling. Emissions from cooking and showering are likely to vary across dwellings according to the size of the dwelling and the number of occupants, whilst the deposition rate is highly sensitive to the dwelling-specific wall finishes (e.g., tiles or plaster), air speed, and turbulence intensity [90]. The penetration factor is largely dependent on the size of the particle [82], but to simplify

simulations and analyses, PM_{2.5} was treated as a single particle. The penetration factor was assumed to be 1.0 when windows were open, but there is evidence that the penetration factor largely depends on the area of window-opening [91]. The model outcomes indicate that fabrics play an important role in determining indoor PM_{2.5} exposure. However, a single set of fabrics was assigned to individual archetypes. The fabrics may vary across dwellings that are classified as the same archetype, and therefore, can lead to significant variation in exposure to indoor PM_{2.5}. While cooking and showering were considered as the only indoor PM_{2.5} sources, PM_{2.5} can be produced indoors through other indoor activities such as smoking and cleaning. The above-mentioned uncertainties imply that the model outcomes reflect the potential role of dwellings in indoor PM_{2.5} exposure, but may not be representative of the actual differences in indoor PM_{2.5} exposure between different dwellings.

The model validation was based on short-period measurements for a typical Hong Kong flat with a single set of fabrics, and therefore, could not provide enough information about the ability of the model to accurately predict the year-round building performance or the performance of flats with different sets of fabrics. Future work will carry out field measurements for a wider housing stock. By focusing work on the current environment, this study is unable to predict future changes in building performance due to climate change and government policies to reduce PM_{2.5} emissions. Further work will use the foundations of this study to develop an EnergyPlus model that is able to reflect changes in climate and outdoor PM_{2.5} concentrations. Additionally, future work will apply the outcomes of this study towards an epidemiological study, allowing the relationship between the housing and health effects due to domestic indoor PM_{2.5} exposure to be better understood.

5. Conclusions

This study reports the outcomes of a city-representative housing stock model developed for the Hong Kong housing stock, illustrating the role of housing on space-cooling energy consumption and exposure to indoor PM_{2.5}, the areas where households were expected to have higher space-cooling energy costs and greater exposure to indoor- and outdoor-sourced PM_{2.5}, and the impacts of home energy-efficient retrofits on space-cooling energy use and exposure to indoor PM_{2.5} across the housing stock. The main outcomes of this study are:

1. Modern village houses and top-floor flats in high-rise residential buildings, on average, used 19% more space-cooling energy than other dwelling archetypes. Dwellings in Sham Shui Po and Wan Chai were seen to have the greatest energy demand for space cooling, while those in Tsuen Wan had the lowest. High-rise flats with the ability to cross-ventilate, on average, used 7.2% less space-cooling energy than the non-cross-ventilation counterparts;
2. There were considerable energy benefits to be had from the modelled energy efficiency retrofits, including external wall insulation, airtightening, and low-e windows. The reduction in the space-cooling energy consumption caused by individual retrofits shows, in some cases, a significant difference between different archetypes, highlighting the importance of considering the modifying effect of archetypes when investigating the energy benefits of home energy efficiency retrofits;
3. Exposure to indoor PM_{2.5} was found to vary according to the geographical location, with lower exposure to outdoor-sourced PM_{2.5} for dwellings in urban areas due to airtight low- and high-rise flats being the dominant dwelling archetypes, and higher exposure to outdoor-sourced PM_{2.5} for dwellings in rural areas due to the predominance of leaky modern village houses. This variation was in contrast to the profile of outdoor PM_{2.5} concentrations, which showed that outdoor PM_{2.5} concentrations were higher in urban areas than in rural areas. The inverse effect was found for exposure to indoor-sourced PM_{2.5}, with dwellings in urban areas exhibiting greater exposure than those in rural areas;

4. The modelled energy efficiency retrofits had a greater impact on exposure from indoor or outdoor sources for tenements and modern village houses than on exposure from indoor or outdoor sources for flats. When combining exposure to indoor PM_{2.5} from different sources, the housing stock saw 7.9% and 0.2% average increases in exposure from airtightening and low-e windows, respectively, and an average decrease of 3.5% in exposure from external wall insulation.

The outcomes of the housing stock model could be used to help enhance the ability of the government to introduce evidence-based policies (for example, targeting energy efficiency measures to dwellings with a great demand for space cooling, focusing on dwellings with great potential to benefit from a certain energy efficiency retrofit, and taking energy efficiency measures that increase the energy efficiency of the housing stock while reducing indoor PM_{2.5} exposure concentrations) to reduce carbon footprints and improve the population's health.

Author Contributions: Conceptualisation, X.Z., Z.Z. and R.Z.; methodology, X.Z. and Z.Z.; software, Z.Z.; validation, X.Z., Z.Z. and R.Z.; formal analysis, X.Z. and Z.Z.; investigation, X.Z., Z.Z. and W.W.; resources, Z.Z. and W.W.; data curation, Z.Z.; writing—original draft preparation, X.Z. and Z.Z.; writing—review and editing, X.Z., Z.Z., R.Z. and W.W.; visualisation, X.Z. and Z.Z.; supervision, Z.Z. and W.W.; project administration, Z.Z. and W.W.; funding acquisition, Z.Z. All authors have read and agreed to the published version of the manuscript.

Funding: This research was funded by the Ningbo Science and Technology Bureau under the Major Science and Technology Programme, grant number 2022Z161.

Data Availability Statement: The data presented in this study are available on request from the corresponding author.

Acknowledgments: The authors would like to thank the Department of Architecture and Built Environment, University of Nottingham, Ningbo China, and the School of Energy and Environment, City University of Hong Kong, for providing the materials used for the experiments and simulations.

Conflicts of Interest: The authors declare no conflict of interest.

Appendix A

The example building for each archetype, along with the floor plan, can be seen in Table A1.

Table A1. The example building for each archetype, along with the floor plan.


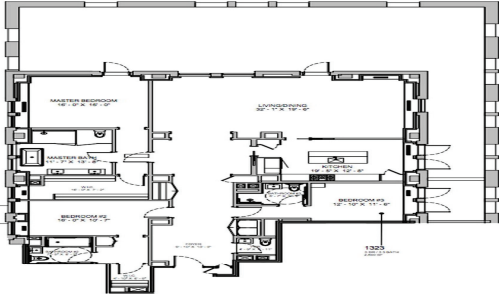
Archetype	Example Building	Floor Plan
1		

Table A1. Cont.






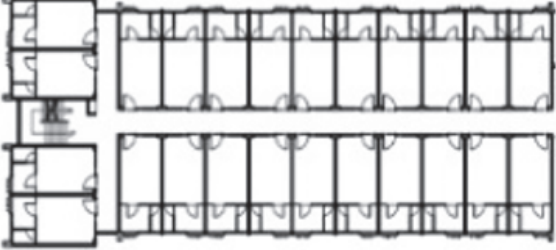
Archetype	Example Building	Floor Plan
2		
3		
4		

Table A1. Cont.


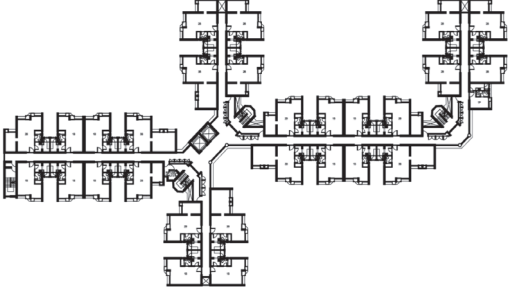

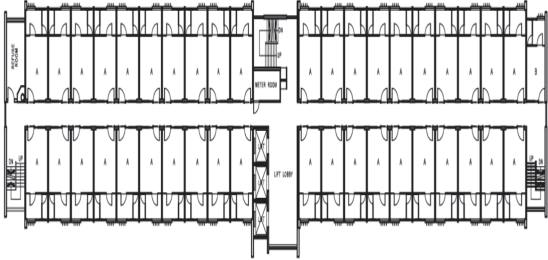

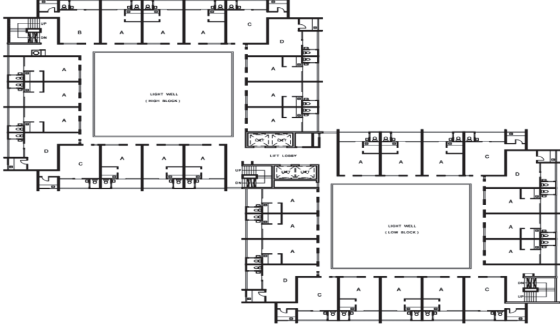

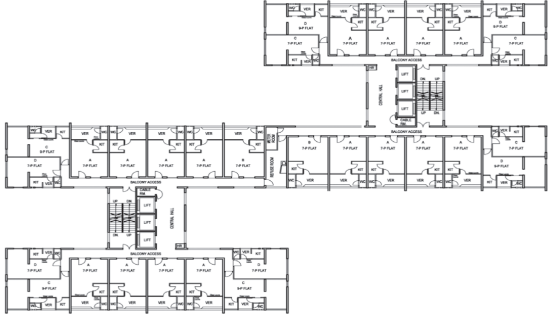
Archetype	Example Building	Floor Plan
5		
6		
7		
8		

Table A1. Cont.


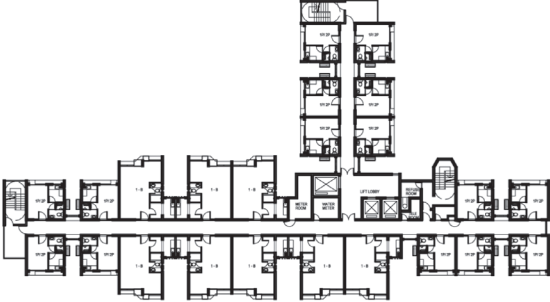

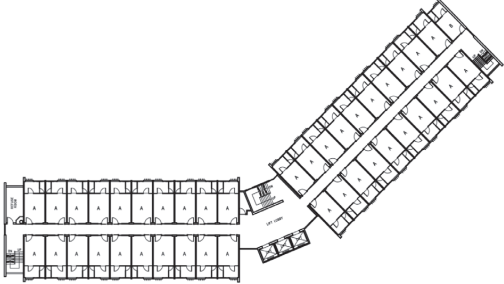

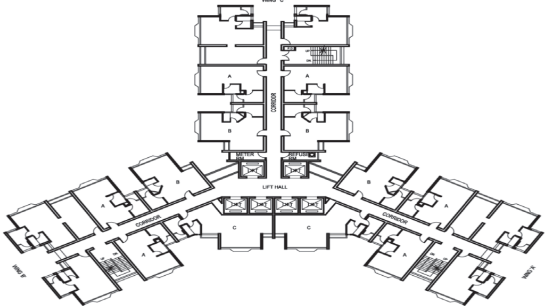

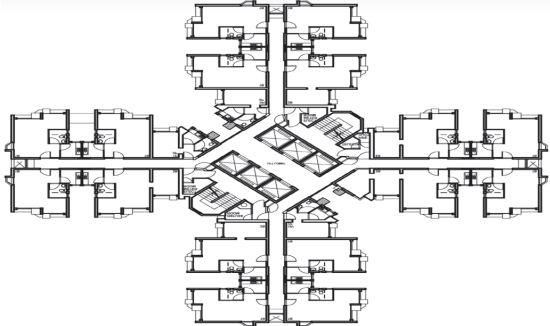

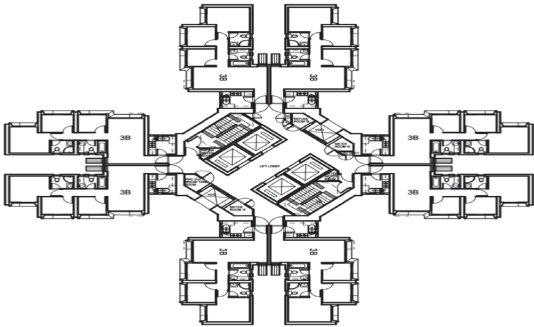




Archetype	Example Building	Floor Plan
9		
10		
11		
12		

Table A1. Cont.

Archetype	Example Building	Floor Plan
13		
14		
15		

Appendix B

Figure A1 shows the proportion of individual archetypes in the Hong Kong housing stock, broken down by district.

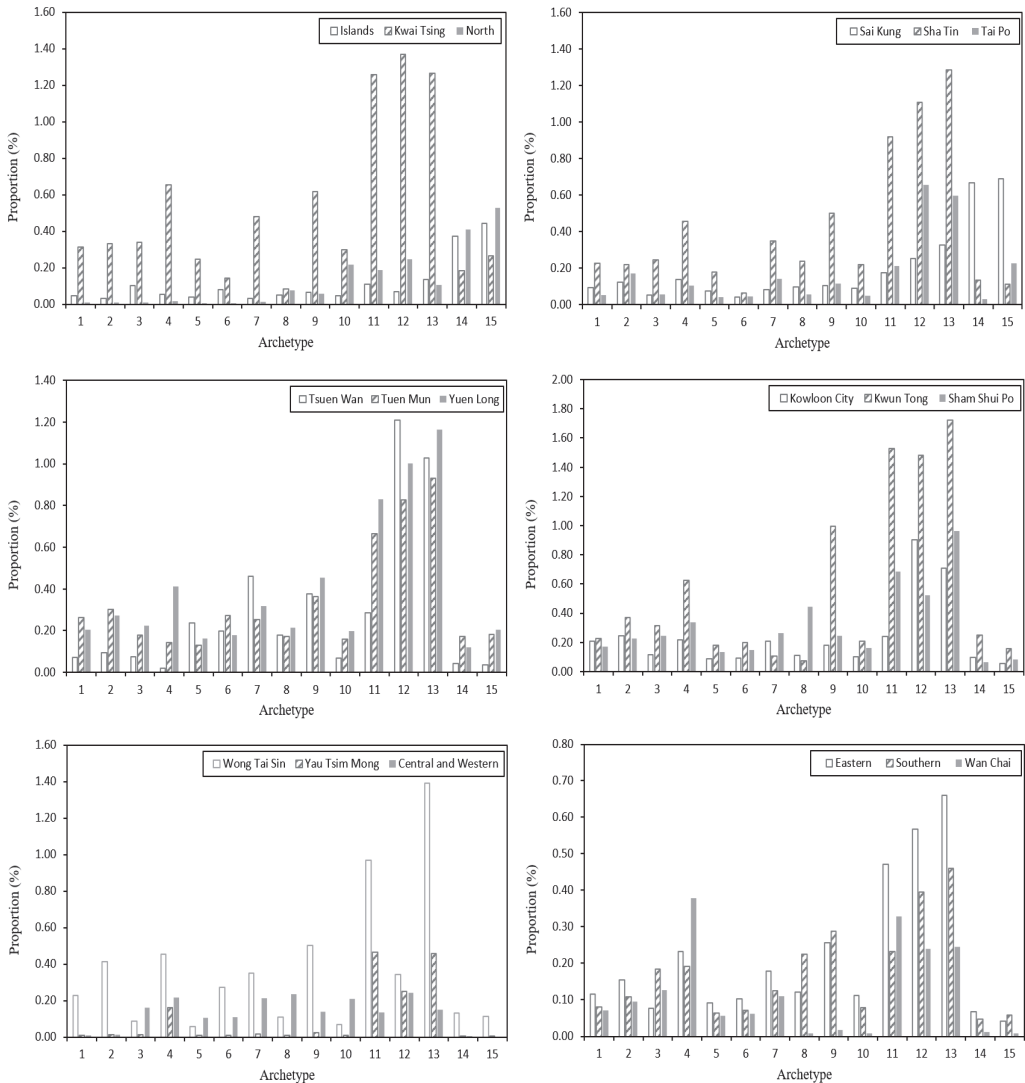


Figure A1. The proportion of individual archetypes in the housing stock, broken down by district.

Appendix C

According to the Buildings Department (BD), a dwelling can enjoy adequate cross ventilation if it meets the following geometrical requirements [49]:

1. The cross-ventilation path between the primary window-opening and secondary window-opening should be composed of no more than two straight lines (i.e., one turn only);
2. The angle of the turn should not be greater than 90° ;
3. The length of the cross-ventilation path should be less than 12 m. For buildings with concave surfaces, the External Plane (EP) (Figure A2) with a width greater than 4.5 m

has similar flow characteristics to the free airstream. A Secondary Window Plane (SWP) with a width of 2.3 m occurs when the width of the EP is less than 4.5 m. A window located in the SWP is considered as the acceptable secondary window-opening. If the window is located outside the SWP, then the ventilated area should be extended by a Notional Plane (NP) (with a width equal to that of the secondary window opening), which connects the secondary window-opening and the SWP. The depth of the NP is added to the length of the cross-ventilation path;

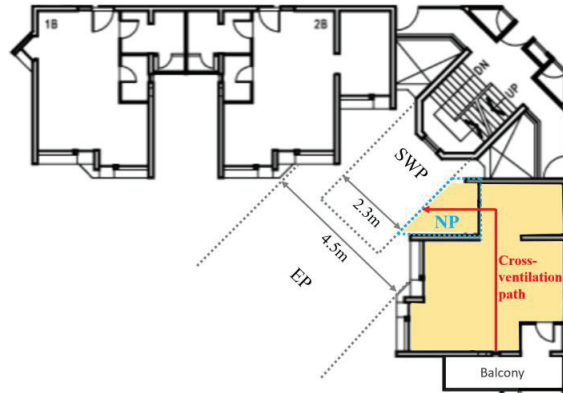


Figure A2. Schematics of the external plane, secondary window plane, and notional plane for buildings with concave surfaces.

1. The primary and secondary window-opening should be located apart with a reasonable distance. To assess this, a rectangle bounding the ventilated space is divided into two equal pieces through the longer side. The two windows should be located in different pieces of the rectangle.

The assessments of the cross-ventilation potential for the 15 archetypes can be seen in Table A2.

Table A2. The assessments of the cross-ventilation potential for the modelled 15 archetypes.

Archetype	Requirements Met	Schematics	Remarks
1	(1), (2), (3), (4)		Each room (including the living room and bedrooms) meets all the geometrical requirements, and therefore, has a good ability to cross-ventilate.

Table A2. Cont.

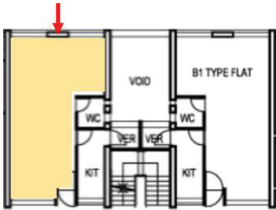

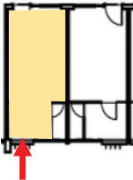
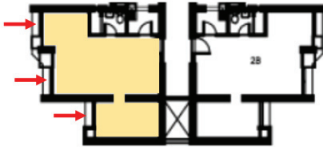
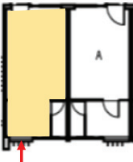
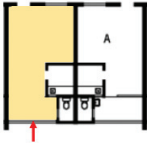
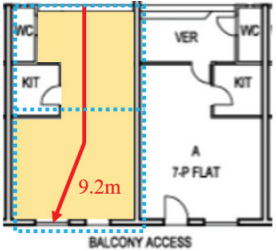
Archetype	Requirements Met	Schematics	Remarks
2	None		Each room has no significant secondary window opening and is, therefore, not likely to have adequate cross ventilation.
3	None		Each flat has no significant secondary window opening and is, therefore, not likely to have adequate cross ventilation.
4	None		Each flat has no significant secondary window opening and is, therefore, not likely to have adequate cross ventilation.
5	None		Each flat has no significant secondary window opening and is, therefore, not likely to have adequate cross ventilation.
6	None		Each flat has no significant secondary window opening and is, therefore, not likely to have adequate cross ventilation.
7	None		Each flat has no significant secondary window opening and is, therefore, not likely to have adequate cross ventilation.
8	(1), (2), (3), (4)		The ventilated space (including the living room and bedrooms) of individual flats meets all the geometrical requirements, and therefore, has a good ability to cross-ventilate.

Table A2. Cont.

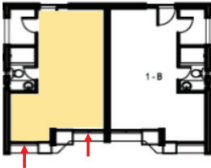
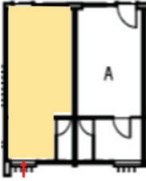
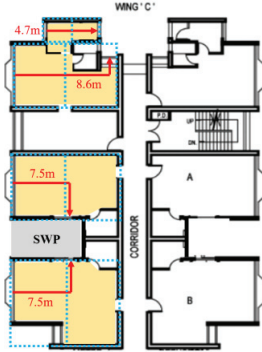
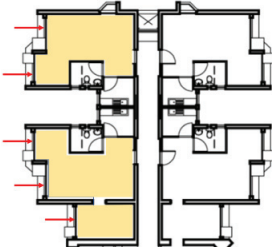
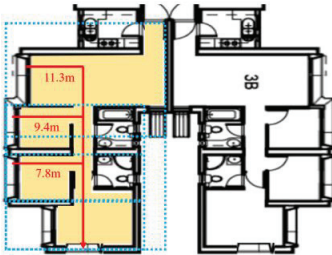
Archetype	Requirements Met	Schematics	Remarks
9	None		Each flat has no significant secondary window opening and is, therefore, not likely to have adequate cross ventilation.
10	None		Each flat has no significant secondary window opening and is, therefore, not likely to have adequate cross ventilation.
11	(1), (2), (3), (4)		The ventilated space (including the living room and bedrooms) of individual flats meets all the geometrical requirements, and therefore, has a good ability to cross-ventilate.
12	None		Each flat has no significant secondary window opening and is, therefore, not likely to have adequate cross ventilation.
13	(1), (2), (3), (4)		The ventilated space (including the living room and bedrooms) of individual flats meets all the geometrical requirements, and therefore, has a good ability to cross-ventilate.

Table A2. Cont.

Archetype	Requirements Met	Schematics	Remarks
14	(1), (2), (3), (4)		The ventilated space (including the living room and bedrooms) of individual rooms meets all the geometrical requirements, and therefore, has a good ability to cross-ventilate.
15	(1), (2), (3), (4)		The ventilated space (including the living room and bedroom) of individual rooms meets all the geometrical requirements, and therefore, has a good ability to cross-ventilate.

Appendix D

The descriptive statistics of the key environmental variables for individual districts can be seen in Table A3.

Table A3. The descriptive statistics of the key environmental variables for individual districts.

		Outdoor Temperature (°C)	Outdoor Relative Humidity (%)	Wind Speed (m/s)	Global Solar Radiation (W/m ²)	Ambient Outdoor PM _{2.5} Concentration (µg/m ³)		
						Ground-Floor	Middle-Floor	Top-Floor
Islands								
All year	Mean	23.6	74.0	7.4	163.7	20.7	7.8	5.9
	Median	23.9	76.0	4.2	3.9	15.0	4.0	1.7
	Min	7.6	19.0	0	0.1	0	0	0
	Max	35.1	99.0	16.8	1171.6	209.0	61.5	28.4
Kwai Tsing								
All year	Mean	23.2	79.0	3.6	163.7	24.1	8.8	6.6
	Median	23.5	82.0	2.1	3.9	20.7	5.4	2.2
	Min	4.5	15.0	0	0.1	0	0	0
	Max	35.6	99.0	12.7	1171.6	109.0	30.0	13.8
North								
All year	Mean	23.4	80.0	5.4	163.7	20.2	7.2	5.3
	Median	24.0	81.0	2.3	3.9	19.0	4.1	1.2
	Min	5.2	18.0	0	0.1	0	0	0
	Max	36.2	99.0	13.6	1171.6	139.0	40.9	18.9

Table A3. Cont.

		Outdoor Temperature (°C)	Outdoor Relative Humidity (%)	Wind Speed (m/s)	Global Solar Radiation (W/m ²)	Ambient Outdoor PM _{2.5} Concentration (µg/m ³)		
						Ground-Floor	Middle-Floor	Top-Floor
Sai Kung								
All year	Mean	23.2	81.0	3.7	163.7	16.8	6.9	5.2
	Median	23.5	84.0	2.0	3.9	14.0	4.3	1.8
	Min	7.8	20.0	0	0.1	0	0	0
	Max	36.8	99.0	9.6	1171.6	87.0	26.2	12.1
Sha Tin								
All year	Mean	23.7	77.0	4.4	163.7	24.0	9.0	6.8
	Median	24.0	80.0	2.3	3.9	17.2	4.6	1.9
	Min	8.0	16.0	0	0.1	0	0	0
	Max	36.8	98.0	10.2	1171.6	126.0	37.1	17.1
Tai Po								
All year	Mean	23.2	81.0	5.0	163.7	20.2	7.5	5.7
	Median	23.6	84.0	2.1	3.9	19.1	5.1	2.1
	Min	7.8	21.0	0	0.1	0	0	0
	Max	36.3	99.0	8.2	1171.6	139.0	40.9	18.9
Tsuen Wan								
All year	Mean	22.5	81.0	6.2	163.7	23.2	8.7	6.6
	Median	22.8	83.0	2.5	3.9	19.0	5.1	2.1
	Min	6.8	18.0	0	0.1	0	0	0
	Max	35.3	99.0	11.2	1771.6	210.0	61.8	28.5
Tuen Mun								
All year	Mean	23.6	77.0	4.7	163.7	26.3	9.8	7.5
	Median	24.0	80.0	1.6	3.9	25.0	6.7	2.8
	Min	5.5	14.0	0	0.1	0	0	0
	Max	36.5	99.0	8.5	1171.6	153.0	45.0	20.8
Yuen Long								
All year	Mean	23.7	80.0	5.3	163.7	20.5	7.7	5.8
	Median	24.1	83.0	2.0	3.9	17.0	4.6	1.9
	Min	4.8	20.0	0	0.1	0	0	0
	Max	36.8	99.0	12.2	1171.6	106.0	31.2	14.4
Kowloon City								
All year	Mean	23.6	79.0	4.1	163.7	24.3	9.1	6.9
	Median	23.9	80.0	1.5	3.9	22.0	5.9	2.5
	Min	6.4	15.0	0	0.1	1.0	0	0
	Max	37.2	99.0	8.9	1171.6	108.0	31.8	14.7
Kwun Tong								
All year	Mean	23.8	79.0	4.1	163.7	24.3	9.1	6.9
	Median	24.0	80.0	1.5	3.9	22.0	5.9	2.5
	Min	5.8	15.0	0	0.1	1.0	0	0
	Max	37.0	99.0	8.9	1171.6	108.0	31.8	14.7
Sham Shui Po								
All year	Mean	24.3	78.0	6.7	163.7	22.9	8.6	6.5
	Median	24.5	80.0	3.2	3.9	17.9	4.8	2.0
	Min	9.8	21.0	0	0.1	0	0	0
	Max	37.3	99.0	11.8	1171.6	123.0	36.2	16.7

Table A3. Cont.

		Outdoor Temperature (°C)	Outdoor Relative Humidity (%)	Wind Speed (m/s)	Global Solar Radiation (W/m ²)	Ambient Outdoor PM _{2.5} Concentration (µg/m ³)		
						Ground-Floor	Middle-Floor	Top-Floor
Wong Tai Shin								
All year	Mean	23.7	79.0	4.1	163.7	24.3	9.1	6.9
	Median	24.1	80.0	1.5	3.9	22.0	5.9	2.5
	Min	8.4	15.0	0	0.1	1.0	0	0
	Max	37.9	99.0	8.9	1171.6	108.0	31.8	14.7
Yau Tsim Mong								
All year	Mean	23.6	76.0	6.6	163.7	27.3	10.3	7.7
	Median	24.0	79.0	2.1	3.9	23.5	6.3	2.6
	Min	6.1	16.0	0	0.1	0	0	0
	Max	36.9	99.0	10.4	1171.6	146.0	43.0	19.8
Central and Western								
All year	Mean	23.6	80.0	5.1	163.7	24.0	9.0	6.8
	Median	23.8	82.0	2.6	3.9	20.4	5.5	2.3
	Min	6.7	23.0	0	0.1	0	0	0
	Max	35.8	99.0	11.9	1171.6	134.0	39.4	18.2
Eastern								
All year	Mean	23.3	82.0	6.3	163.7	23.0	8.6	6.5
	Median	23.7	85.0	2.1	3.9	18.7	5.0	2.1
	Min	6.3	26.0	0	0.1	0	0	0
	Max	36.2	99.0	12.8	1171.6	112.0	32.9	15.2
Southern								
All year	Mean	23.7	77.0	5.5	163.7	20	7.5	5.7
	Median	24.0	79.0	1.9	3.9	17.2	4.6	1.9
	Min	7.2	19.0	0	0.1	0	0	0
	Max	35.3	99.0	9.6	1171.6	105.0	30.9	14.3
Wan Chai								
All year	Mean	24.5	80.0	5.1	163.7	25.8	9.7	7.3
	Median	24.7	82.0	2.6	3.9	23.6	6.3	2.6
	Min	9.9	23.0	0	0.1	1.0	0	0
	Max	37.6	99.0	11.9	1171.6	139.0	40.9	18.9

References

1. EMSD. *Hong Kong Energy End-Use Data 2019*; Electrical and Mechanical Services Department: Hong Kong, China, 2019.
2. Cooling-More Efforts Needed. Available online: <https://www.iea.org/reports/cooling> (accessed on 2 September 2022).
3. Ji, Q.; Bi, Y.; Makvandi, M.; Deng, Q.; Zhou, X.; Li, C. Modelling Building Stock Energy Consumption at the Urban Level from an Empirical Study. *Buildings* **2022**, *12*, 385. [\[CrossRef\]](#)
4. Burnett, J.; Bojić, M.; Yik, F. Wind-induced pressure at external surfaces of a high-rise residential building in Hong Kong. *Buuld. Environ.* **2005**, *40*, 765–777. [\[CrossRef\]](#)
5. Li, J.; Ng, S.T.; Skitmore, M. Review of low-carbon refurbishment solutions for residential buildings with particular reference to multi-story buildings in Hong Kong. *Renew. Sustain. Energy Rev.* **2017**, *73*, 393–407. [\[CrossRef\]](#)
6. Kwok, Y.T.; de Munck, C.; Lau, K.K.-L.; Ng, E. To what extent can urban ventilation features cool a compact built-up environment during a prolonged heatwave? A mesoscale numerical modelling study for Hong Kong. *Sustain. Cities Soc.* **2021**, *77*, 103541. [\[CrossRef\]](#)
7. Jia, J.; Lee, W. Drivers of moderate increase in cooling energy use in residential buildings in Hong Kong. *Energy Build.* **2016**, *125*, 19–26. [\[CrossRef\]](#)
8. Du, J.; Pan, W. Evaluating energy saving behavioral interventions through the lens of social practice theory: A case study in Hong Kong. *Energy Build.* **2021**, *251*, 111353. [\[CrossRef\]](#)

9. Kwok, Y.T.; Lau, K.K.-L.; Lai, A.K.L.; Chan, P.W.; Lavafpour, Y.; Ho, J.C.K.; Ng, E.Y.Y. A comparative study on the indoor thermal comfort and energy consumption of typical public rental housing types under near-extreme summer conditions in Hong Kong. *Energy Procedia* **2017**, *122*, 973–978. [[CrossRef](#)]
10. Liu, T.; Lee, W. Evaluating the influence of transom window designs on natural ventilation in high-rise residential buildings in Hong Kong. *Sustain. Cities Soc.* **2020**, *62*, 102406. [[CrossRef](#)]
11. Kwok, Y.T.; Lai, A.K.L.; Lau, K.K.-L.; Chan, P.W.; Lavafpour, Y.; Ho, J.C.K.; Ng, E.Y.Y. Thermal comfort and energy performance of public rental housing under typical and near-extreme weather conditions in Hong Kong. *Energy Build.* **2017**, *156*, 390–403. [[CrossRef](#)]
12. Chung, W.; Kam, M.; Ip, C. A study of residential energy use in Hong Kong by decomposition analysis, 1990–2007. *Appl. Energy* **2011**, *88*, 5180–5187. [[CrossRef](#)]
13. Cheng, Y.; Cao, K.; Woo, C.; Yatchew, A. Residential willingness to pay for deep decarbonization of electricity supply: Contingent valuation evidence from Hong Kong. *Energy Policy* **2017**, *109*, 218–227. [[CrossRef](#)]
14. Power, A. Does demolition or refurbishment of old and inefficient homes help to increase our environmental, social and economic viability? *Energy Policy* **2008**, *36*, 4487–4501. [[CrossRef](#)]
15. Yu, C.; Du, J.; Pan, W. Improving accuracy in building energy simulation via evaluating occupant behaviors: A case study in Hong Kong. *Energy Build.* **2019**, *202*, 109373. [[CrossRef](#)]
16. Dahanayake, K.C.; Chow, C.L. Comparing reduction of building cooling load through green roofs and green walls by EnergyPlus simulations. *Build. Simul.* **2018**, *11*, 421–434. [[CrossRef](#)]
17. Liu, S.; Kwok, Y.T.; Lau, K.K.-L.; Chan, P.W.; Ng, E. Investigating the energy saving potential of applying shading panels on opaque façades: A case study for residential buildings in Hong Kong. *Energy Build.* **2019**, *193*, 78–91. [[CrossRef](#)]
18. Brimblecombe, P.; Ning, Z. Effect of road blockages on local air pollution during the Hong Kong protests and its implications for air quality management. *Sci. Total Environ.* **2015**, *536*, 443–448. [[CrossRef](#)]
19. Mason, T.G.; Schooling, C.M.; Chan, K.P.; Tian, L. An evaluation of the air quality health index program on respiratory diseases in Hong Kong: An interrupted time series analysis. *Atmos. Environ.* **2019**, *211*, 151–158. [[CrossRef](#)]
20. Fan, Z.; Pun, V.C.; Chen, X.-C.; Hong, Q.; Tian, L.; Ho, S.S.-H.; Lee, S.-C.; Tse, L.A.; Ho, K.-F. Personal exposure to fine particles (PM_{2.5}) and respiratory inflammation of common residents in Hong Kong. *Environ. Res.* **2018**, *164*, 24–31. [[CrossRef](#)] [[PubMed](#)]
21. Chen, X.-C.; Chow, J.C.; Ward, T.J.; Cao, J.-J.; Lee, S.-C.; Watson, J.G.; Lau, N.-C.; Yim, S.H.L.; Ho, K.-F. Estimation of personal exposure to fine particles (PM_{2.5}) of ambient origin for healthy adults in Hong Kong. *Sci. Total Environ.* **2018**, *654*, 514–524. [[CrossRef](#)]
22. Ejiowomu, O.A.; Shamsideen Oshodi, O.; Oladokun, M.; Bukoye, O.T.; Emekwuru, N.; Sotunbo, A.; Adenuga, O. Modelling and Forecasting Temporal PM_{2.5} Concentration Using Ensemble Machine Learning Methods. *Buildings* **2022**, *12*, 46. [[CrossRef](#)]
23. Dai, H.K.; Chen, C. Air infiltration rates in residential units of a public housing estate in Hong Kong. *Build. Environ.* **2022**, *219*, 109211. [[CrossRef](#)]
24. Yang, Y.; Tang, R.; Qiu, H.; Lai, P.-C.; Wong, P.; Thach, T.-Q.; Allen, R.; Brauer, M.; Tian, L.; Barratt, B. Long term exposure to air pollution and mortality in an elderly cohort in Hong Kong. *Environ. Int.* **2018**, *117*, 99–106. [[CrossRef](#)] [[PubMed](#)]
25. Tang, R.; Tian, L.; Thach, T.-Q.; Tsui, T.H.; Brauer, M.; Lee, M.; Allen, R.; Yuchi, W.; Lai, P.-C.; Wong, P.; et al. Integrating travel behavior with land use regression to estimate dynamic air pollution exposure in Hong Kong. *Environ. Int.* **2018**, *113*, 100–108. [[CrossRef](#)] [[PubMed](#)]
26. Lin, H.; Ma, W.; Qiu, H.; Wang, X.; Trevathan, E.; Yao, Z.; Dong, G.-H.; Vaughn, M.G.; Qian, Z.; Tian, L. Using daily excessive concentration hours to explore the short-term mortality effects of ambient PM_{2.5} in Hong Kong. *Environ. Pollut.* **2017**, *229*, 896–901. [[CrossRef](#)] [[PubMed](#)]
27. Taylor, J.; Shrubsole, C.; Davies, M.; Biddulph, P.; Das, P.; Hamilton, I.; Vardoulakis, S.; Mavrogianni, A.; Jones, B.; Oikonomou, E. The modifying effect of the building envelope on population exposure to PM_{2.5} from outdoor sources. *Indoor Air* **2014**, *24*, 639–651. [[CrossRef](#)]
28. Taylor, J.; Mavrogianni, A.; Davies, M.; Das, P.; Shrubsole, C.; Biddulph, P.; Oikonomou, E. Understanding and mitigating overheating and indoor PM_{2.5} risks using coupled temperature and indoor air quality models. *Build. Serv. Eng. Res. Technol.* **2015**, *36*, 275–289. [[CrossRef](#)]
29. Chan, L.; Kwok, W. Vertical dispersion of suspended particulates in urban area of Hong Kong. *Atmos. Environ.* **2000**, *34*, 4403–4412. [[CrossRef](#)]
30. Taylor, J.; Davies, M.; Mavrogianni, A.; Shrubsole, C.; Hamilton, I.; Das, P.; Jones, B.; Oikonomou, E.; Biddulph, P. Mapping indoor overheating and air pollution risk modification across Great Britain: A modelling study. *Build. Environ.* **2016**, *99*, 1–12. [[CrossRef](#)]
31. Dai, X.; Liu, J.; Li, X.; Zhao, L. Long-term monitoring of indoor CO₂ and PM_{2.5} in Chinese homes: Concentrations and their relationships with outdoor environments. *Build. Environ.* **2018**, *144*, 238–247. [[CrossRef](#)]
32. Shrubsole, C.; Ridley, I.; Biddulph, P.; Milner, J.; Vardoulakis, S.; Ucci, M.; Wilkinson, P.; Chalabi, Z.; Davies, M. Indoor PM_{2.5} exposure in London’s domestic stock: Modelling current and future exposures following energy efficient refurbishment. *Atmos. Environ.* **2012**, *62*, 336–343. [[CrossRef](#)]
33. Cheung, P.K.; Jim, C. Impacts of air conditioning on air quality in tiny homes in Hong Kong. *Sci. Total Environ.* **2019**, *684*, 434–444. [[CrossRef](#)] [[PubMed](#)]

34. Cao, J.J.; Lee, S.-C.; Chow, J.C.; Cheng, Y.; Ho, K.F.; Fung, K.; Liu, S.X.; Watson, J. Indoor/outdoor relationships for PM2.5 and associated carbonaceous pollutants at residential homes in Hong Kong—case study. *Indoor Air* **2005**, *15*, 197–204. [[CrossRef](#)] [[PubMed](#)]
35. Chao, C.Y.; Wong, K.K. Residential indoor PM10 and PM2.5 in Hong Kong and the elemental composition. *Atmos. Environ.* **2002**, *36*, 265–277. [[CrossRef](#)]
36. Tong, X.; Wang, B.; Dai, W.-T.; Cao, J.-J.; Ho, S.S.H.; Kwok, T.C.Y.; Lui, K.-H.; Lo, C.-M.; Ho, K.F. Indoor air pollutant exposure and determinant factors controlling household air quality for elderly people in Hong Kong. *Air Qual. Atmos. Health* **2018**, *11*, 695–704. [[CrossRef](#)]
37. Fazli, T.; Stephens, B. Development of a nationally representative set of combined building energy and indoor air quality models for U.S. residences. *Build. Environ.* **2018**, *136*, 198–212. [[CrossRef](#)]
38. Taylor, J.; Shrubsole, C.; Symonds, P.; Mackenzie, I.; Davies, M. Application of an indoor air pollution metamodel to a spatially-distributed housing stock. *Sci. Total Environ.* **2019**, *667*, 390–399. [[CrossRef](#)]
39. Crawley, D.B.; Lawrie, L.K.; Winkelmann, F.C.; Buhl, W.; Huang, Y.; Pedersen, C.O.; Strand, R.K.; Liesen, R.J.; Fisher, D.E.; Witte, M.J.; et al. EnergyPlus: Creating a new-generation building energy simulation program. *Energy Build.* **2001**, *33*, 319–331. [[CrossRef](#)]
40. HA. *Complete List of PRH/TPS Estates*; Hong Kong Housing Authority: Hong Kong, China, 2018.
41. BD. *Database of Private Buildings in Hong Kong*; Buildings Department: Hong Kong, China, 2018.
42. Building Directory—Hong Kong. Available online: <https://www.emporis.com/city/101300/hong-kong-china> (accessed on 20 July 2022).
43. Cheung, C.; Fuller, R.; Luther, M. Energy-efficient envelope design for high-rise apartments. *Energy Build.* **2005**, *37*, 37–48. [[CrossRef](#)]
44. Fong, K.; Lee, C. Investigation of separate or integrated provision of solar cooling and heating for use in typical low-rise residential building in subtropical Hong Kong. *Renew. Energy* **2015**, *75*, 847–855. [[CrossRef](#)]
45. HA. *Standard Block Typical Floor Plans*; Hong Kong Housing Authority: Hong Kong, China, 2018.
46. CSD. *Housing and Property*; Census and Statistics Department: Hong Kong, China, 2018.
47. Wan, K.; Yik, F. Building design and energy end-use characteristics of high-rise residential buildings in Hong Kong. *Appl. Energy* **2004**, *78*, 19–36. [[CrossRef](#)]
48. CentaMap. Available online: <http://hk.centamap.com/gc/home.aspx> (accessed on 20 July 2022).
49. BD. *Guidelines on Design and Construction Requirements for Energy Efficiency of Residential Buildings*; Buildings Department: Hong Kong, China, 2014.
50. Lam, J.C. Residential sector air conditioning loads and electricity use in Hong Kong. *Energy Convers. Manag.* **2000**, *41*, 1757–1768. [[CrossRef](#)]
51. HK-BEAM. *Hong Kong Building Environmental Assessment Method: HK-BEAM Version 5/04 Existing Buildings*; HK-BEAM Society: Hong Kong, China, 2004.
52. Wan, K.; Yik, F. Representative building design and internal load patterns for modelling energy use in residential buildings in Hong Kong. *Appl. Energy* **2004**, *77*, 69–85. [[CrossRef](#)]
53. Lam, J.C. An analysis of residential sector energy use in Hong Kong. *Energy* **1996**, *21*, 1–8. [[CrossRef](#)]
54. ISO 13790; Energy Performance of Buildings, Calculation of Energy Use for Space Heating and Cooling. International Organization for Standardization: Geneva, Switzerland, 2008.
55. O'Brien, W.; Kapsis, K.; Athienitis, A.K. Manually-operated window shade patterns in office buildings: A critical review. *Build. Environ.* **2013**, *60*, 319–338. [[CrossRef](#)]
56. Weerasuriya, A.; Zhang, X.; Gan, V.J.; Tan, Y. A holistic framework to utilize natural ventilation to optimize energy performance of residential high-rise buildings. *Build. Environ.* **2019**, *153*, 218–232. [[CrossRef](#)]
57. Mei, S.-J.; Hu, J.-T.; Liu, D.; Zhao, F.-Y.; Li, Y.; Wang, Y.; Wang, H.-Q. Wind driven natural ventilation in the idealized building block arrays with multiple urban morphologies and unique package building density. *Energy Build.* **2017**, *155*, 324–338. [[CrossRef](#)]
58. Yang, L.; Li, Y. Thermal conditions and ventilation in an ideal city model of Hong Kong. *Energy Build.* **2010**, *43*, 1139–1148. [[CrossRef](#)]
59. Zhou, H.; Lu, Y.; Liu, X.; Chang, R.; Wang, B. Harvesting wind energy in low-rise residential buildings: Design and optimization of building forms. *J. Clean. Prod.* **2017**, *167*, 306–316. [[CrossRef](#)]
60. Zhong, H.-Y.; Zhang, D.-D.; Liu, Y.; Liu, D.; Zhao, F.-Y.; Li, Y.; Wang, H.-Q. Wind driven “pumping” fluid flow and turbulent mean oscillation across high-rise building enclosures with multiple naturally ventilated apertures. *Sustain. Cities Soc.* **2019**, *50*, 101619. [[CrossRef](#)]
61. Ai, Z.; Mak, C. Wind-induced single-sided natural ventilation in buildings near a long street canyon: CFD evaluation of street configuration and envelope design. *J. Wind Eng. Ind. Aerodyn.* **2018**, *172*, 96–106. [[CrossRef](#)]
62. Wang, R.; Ren, C.; Xu, Y.; Lau, K.K.-L.; Shi, Y. Mapping the local climate zones of urban areas by GIS-based and WUDAPT methods: A case study of Hong Kong. *Urban Clim.* **2018**, *24*, 567–576. [[CrossRef](#)]
63. Tan, Y.; Liu, G.; Zhang, Y.; Shuai, C.; Shen, G.Q. Green retrofit of aged residential buildings in Hong Kong: A preliminary study. *Build. Environ.* **2018**, *143*, 89–98. [[CrossRef](#)]
64. Climatological Information Services. Available online: <https://www.hko.gov.hk/en/cis/climat.htm> (accessed on 20 July 2022).

65. Inquire and Download Air Quality Monitoring Data. Available online: <https://cd.epic.epd.gov.hk/EPICDI/air/station/?lang=en> (accessed on 20 July 2022).
66. PD. *Land Utilization in Hong Kong*; Planning North Point: Hong Kong, China, 2009.
67. ASHRAE. *ASHRAE Fundamentals Handbook 2017*; American Society of Heating, Refrigeration and Air Conditioning Engineers: Atlanta, GA, USA, 2017.
68. CIBSE. *Environmental Design: CIBSE Guide A*; The Chartered Institution of Building Services Engineers: London, UK, 2006.
69. ASHRAE. *ASHRAE Standard 160P: Criteria for Moisture Control Design Analysis in Buildings*; American Society of Heating, Refrigeration and Air Conditioning Engineers: Atlanta, GA, USA, 2009.
70. Wong, I.; Baldwin, A.N. Investigating the potential of applying vertical green walls to high-rise residential buildings for energy-saving in sub-tropical region. *Build. Environ.* **2016**, *97*, 34–39. [[CrossRef](#)]
71. Zhang, L. Energy requirements for conditioning fresh air and the long-term savings with a membrane-based energy recovery ventilator in Hong Kong. *Energy* **2001**, *26*, 119–135. [[CrossRef](#)]
72. Chen, X.; Yang, H.; Sun, K. A holistic passive design approach to optimize indoor environmental quality of a typical residential building in Hong Kong. *Energy* **2016**, *113*, 267–281. [[CrossRef](#)]
73. Chen, X.; Yang, H. Combined thermal and daylight analysis of a typical public rental housing development to fulfil green building guidance in Hong Kong. *Energy Build.* **2015**, *108*, 420–432. [[CrossRef](#)]
74. EMSD. *Code of Practice for Energy Efficiency of Building Services Installation*; Electrical and Mechanical Services Department: Hong Kong, China, 2018.
75. HKG. *Building (Planning) Regulations (Chapter 123)*; Hong Kong e-Legislation: Hong Kong, China, 1984.
76. Haldi, F.; Robinson, D. Interactions with window openings by office occupants. *Build. Environ.* **2009**, *44*, 2378–2395. [[CrossRef](#)]
77. Zhong, X.; Ridley, I.A. Verification of behavioural models of window opening: The accuracy of window-use pattern, indoor temperature and indoor PM2.5 concentration prediction. *Build. Simul.* **2020**, *13*, 527–542. [[CrossRef](#)]
78. Fabi, V.; Andersen, R.V.; Corgnati, S.; Olesen, B.W. Occupants’ window opening behaviour: A literature review of factors influencing occupant behaviour and models. *Build. Environ.* **2012**, *58*, 188–198. [[CrossRef](#)]
79. Dols, W.S.; Emmerich, S.J.; Polidoro, B.J. Coupling the multizone airflow and contaminant transport software CONTAM with EnergyPlus using co-simulation. *Build. Simul.* **2016**, *9*, 469–479. [[CrossRef](#)]
80. Jones, B.; Das, P.; Chalabi, Z.; Davies, M.; Hamilton, I.; Lowe, R.; Milner, J.; Ridley, I.; Shrubsole, C.; Wilkinson, P. The Effect of Party Wall Permeability on Estimations of Infiltration from Air Leakage. *Int. J. Vent.* **2013**, *12*, 17–30. [[CrossRef](#)]
81. Dimitroulopoulou, C.; Ashmore, M.; Hill, M.; Byrne, M.; Kinnersley, R. INDAIR: A probabilistic model of indoor air pollution in UK homes. *Atmos. Environ.* **2006**, *40*, 6362–6379. [[CrossRef](#)]
82. Long, C.M.; Suh, H.H.; Catalano, P.J.; Koutrakis, P. Using Time- and Size-Resolved Particulate Data To Quantify Indoor Penetration and Deposition Behavior. *Environ. Sci. Technol.* **2001**, *35*, 2089–2099. [[CrossRef](#)] [[PubMed](#)]
83. SketchUp Plugin Index. Available online: <http://sketchupplugins.com/plugins/nrel-openstudio/> (accessed on 20 July 2022).
84. JEPlus—An EnergyPlus Simulation Manager for Parametrics. Available online: <http://www.jeplus.org/wiki/doku.php?id=start> (accessed on 20 July 2022).
85. SAS Trials. Available online: https://www.sas.com/en_us/trials.html (accessed on 20 July 2022).
86. CSD. *2018 Population Census Summary Report*; Census and Statistics Department: Hong Kong, China, 2018.
87. Tan, Y.; Luo, T.; Xue, X.; Shen, G.Q.; Zhang, G.; Hou, L. An empirical study of green retrofit technologies and policies for aged residential buildings in Hong Kong. *J. Build. Eng.* **2021**, *39*, 102271. [[CrossRef](#)]
88. EMSD. *Hong Kong Energy End-Use Data 2018*; Electrical and Mechanical Services Department: Hong Kong, China, 2018.
89. Wan, M.P.; Wu, C.L.; To, G.N.S.; Chan, T.C.; Chao, C.Y.H. Ultrafine particles, and PM2.5 generated from cooking in homes. *Atmos. Environ.* **2011**, *45*, 6141–6148. [[CrossRef](#)]
90. El Orch, Z.; Stephens, B.; Waring, M.S. Predictions and determinants of size-resolved particle infiltration factors in single-family homes in the U.S. *Build. Environ.* **2014**, *74*, 106–118. [[CrossRef](#)]
91. Rim, D.; Wallace, L.A.; Persily, A.K. Indoor Ultrafine Particles of Outdoor Origin: Importance of Window Opening Area and Fan Operation Condition. *Environ. Sci. Technol.* **2013**, *47*, 1922–1929. [[CrossRef](#)] [[PubMed](#)]



Article

Energy Poverty and Personal Health in the EU

John M. Polimeni ^{1,*}, Mihaela Simionescu ² and Raluca I. Iorgulescu ²

¹ Department of Pharmacy Practice, Albany College of Pharmacy and Health Sciences, Albany, NY 12208, USA

² Institute for Economic Forecasting-NIER, Romanian Academy, 050711 Bucharest, Romania

* Correspondence: john.polimeni@acphs.edu; Tel.: +1-518-694-7384

Abstract: The aim of this paper is to assess the impact of energy poverty on health in the EU-27 countries for the period from 2003–2020 using Panel Autoregressive Distributed Lag models and generalized ridge regressions. Arrears on utility bills exerts positive long-run effects on capacity to keep the home adequately warm, current health expenditures, and self-perceived health as bad or very bad, but a negative long-run influence on energy import dependency. In the long-term, the population being unable to keep their home adequately warm positively affects self-perceived health as bad and very bad and negatively influences number of cooling days. Current health expenditure has a long-run influence on self-perceived health as bad and very bad and the number of heating days. Positive short-run impacts were observed for energy import dependency, arrears on utility bills, and number of heating days on current health expenditure and the population unable to keep their home adequately warm. People at risk of poverty or social exclusion in different zones had a significant impact on energy poverty indicators. A separate analysis is made for those EU states with the highest energy import dependency and the implications of the results are discussed.

Keywords: energy poverty; health; energy import dependence; panel ARDL model

1. Introduction

Access to energy is vital for reducing poverty, economic development, and better living conditions. Energy is necessary for cooking, lighting, and heating and cooling. As such, energy poverty is often thought to be caused by low incomes, energy efficiency, and energy prices [1–3] and has a great influence on the lives of millions of people [4]. The literature has often focused on energy prices, lack of energy resources, and low incomes [1,5–11]. As a result, energy poverty is sometimes defined as the inability to afford the required level of heating in the home [1,10,12,13]. With climate change, extreme heating also requires access to energy for cooling purposes [3,14]. Streimikiene et al. [15] illustrated the importance of considering energy poor households in climate change policies aimed at achieving a carbon free energy transition by 2050 because these households often have behavioral barriers to climate change mitigation. Furthermore, Nawaz [16] showed that climate shocks lead to health poverty and higher per capita health expenditures. Others have defined energy poverty as the inability of a household to obtain the required level of energy services for a home [17,18]. Thus, energy poverty is multidimensional with an objective component, where a household's net income after energy costs is below the national poverty line and energy costs are above the national average, and a subjective component, where the members of the household state they are not warm enough in the cold season [19–22]. Typically, the literature has focused on energy prices and affordability [1,11–13]. However, the concept of energy poverty has evolved as a lack of energy impacting economic and human development such that an energy-poor society will suffer from issues such as bad health, poverty, and illiteracy [22]. This multidimensional perspective does examine numerous indicators, such as health, poverty, education, and the environment. Recent literature has explored the impact of energy poverty on health, particularly in developing countries [22–25].

Citation: Polimeni, J.M.; Simionescu, M.; Iorgulescu, R.I. Energy Poverty and Personal Health in the EU. *Int. J. Environ. Res. Public Health* **2022**, *19*, 11459. <https://doi.org/10.3390/ijerph191811459>

Academic Editors: Andrew S. Hursthouse, Francesco Nocera, Roberto Alonso González Lezcano and Rosa Giuseppina Caponetto

Received: 5 August 2022

Accepted: 8 September 2022

Published: 12 September 2022



Copyright: © 2022 by the authors. Licensee MDPI, Basel, Switzerland. This article is an open access article distributed under the terms and conditions of the Creative Commons Attribution (CC BY) license (<https://creativecommons.org/licenses/by/4.0/>).

The extent of the problem is large, becoming a priority for institutions such as the World Bank and the United Nations. Energy poverty impacts the health of approximately 34 million people [26,27] and is a major problem throughout the European Union. Yet, there remains a vastly inadequate understanding of energy poverty [22]. This paper considers energy poverty to be much more complex than the previously stated definitions; a bi-directional causal relationship where energy poverty is caused by low income, poor energy efficiency, energy prices, and healthcare costs from poor health status, and energy poverty can create poor health status and low educational status [10,25]. Simply put, if an individual does not have adequate heating, cooling, or refrigeration capability, then they are more susceptible to illness; if that person is sick and incapable of working, then they will not be able to earn income to pay for energy resources. This vicious cycle is bi-directional and, hence, the importance of understanding the energy poverty-health relationship.

Energy poverty was mainstreamed in the EU in 2009 when the third Energy Package was ratified and further developed with the 2018 Clean Energy for all Europeans policy [27]. Many of the Central and Eastern European nations have a large stock of inefficient buildings and lower than average household incomes [27] that can be attributed to their centrally planned economies of the past. The transitional stage, started in 1990, has brought new challenges such as the liberalization of the electricity and gas markets, which has increased energy prices considerably, putting cost pressures on energy consumers [20,28]. Furthermore, many social assistance programs were defunded or eliminated, such as consumer subsidies, price controls, and state support of housing, transportation, and services [27,29,30]. Populations, especially children, the unemployed, the elderly, and low-income individuals and families, are especially vulnerable as a result.

This paper extends the previous literature by exploring the bi-directional causal relationship of energy poverty, poor health, and affordable housing and energy prices. The results indicate that this relationship does, in fact, exist and provides insight for public policy to be developed that will effectively combat energy poverty in the EU. The novelty of the paper is also brought by the methodological approach. In addition to panel data models for all the EU-27 countries to assess the impact of personal health on energy poverty, a cross-country analysis is conducted for the countries with the highest energy import dependency. Consequently, besides overall recommendations for the entire EU, a particular profile is built for some of the countries with vulnerabilities in terms of energy import dependency that need more specific policies.

The rest of the paper is as follows. Section 2 provides a literature review. Section 3 presents the materials and methods used, followed by Section 4, which outlines the theoretical framework employed. Section 5 presents the results. Lastly, Sections 6 and 7 end the paper with a discussion of the results and conclusion.

2. Literature Review

Energy poverty was first considered as fuel poverty, examining how livelihoods were impacted as a result [22,31]. Leach [32] showed energy poverty causes low-income households to spend a higher percentage of their household income on energy than middle-income households, and Boardman [33] quantified the percentage for energy poverty as 10% or more. Hills [11] and Moore [34] both built upon these findings to create new metrics of energy poverty. However, each of these measures apply more for advanced economies where affordability is the main issue rather than developing economies where affordability and accessibility are the problem. Therefore, energy poverty is a much more complex issue.

Energy poverty is multidimensional. Boardman [33] states that the interaction of the socioeconomic status of the household, the energy efficiency of the house, and energy prices are the multidimensional factors impacting energy poverty. Nussbaumer and Bazilian [20] developed a multidimensional energy poverty index, building upon the IEA energy development index, to capture a household's inability to access energy. Recalde [35] hypothesized that the multidimensional factors are deeper and should include structural determinants such as energy, housing, and labor policies, as well as economic and market

policies. As a result, energy poverty can have impacts beyond just affordability, accessibility, and usage for heating, lighting, and other necessities.

Energy poverty is not an insular issue, and it is often related to employment status, and food, housing, and utilities costs [18,36,37]. As a result, energy poverty can have significant health implications [3,38–41]. In fact, there is extensive evidence of the effects of energy poverty on human health [3,42,43]. Gonzalez-Equino [4] found that energy poverty and health are linked because access to clean energy is necessary to maintain or improve the health of individuals [22]. The direct health effects of energy poverty are increased mortality and morbidity rates through respiratory, cardiac, and cardiovascular diseases [3,44,45], impaired mental well-being, and the intensification of existing health problems. Cold temperatures in a household suppress the immune system, increasing the likelihood of infections and minor illnesses. Indirect health impacts include the impairment of childhood learning, emotional well-being, and resilience. Furthermore, dietary choices and opportunities are reduced, and accidents and injuries at home are more likely. Children, women, and the elderly are most susceptible, as are low-income households. Building on this research, Xiao et al. [46] showed that energy poverty has a negative impact on individual development and learning behavior, and that learning behavior and health conditions are correlated with energy poverty.

Energy poverty is a major problem in Europe. The European Commission has made solving energy poverty a key pillar in their transition to green energy [41]. The situation is only likely to worsen due to a transition to green energy, geopolitical energy dynamics, and reliance on Russia for natural gas supplies. There are considerable gaps in the literature about the impact of energy poverty on health at the European level. Only recently has the literature on energy poverty in Europe become more prevalent, focusing on understanding the socio-demographic factors causing energy poverty, emphasizing vulnerabilities related to income, gender and age [8,41,47–49], whereas other studies have explored the roles of energy prices and lack of energy efficiency [41,50–52]. There are geographic differences as well; energy poverty is largely more problematic in the Mediterranean and Eastern EU member states [17]. Eastern and Southern European countries are found to be more vulnerable because of higher levels of income poverty, inefficient housing quality, poor infrastructure, and governmental instability [31,41,53]. Energy poverty in the north is typically due to a combination of high energy prices, low incomes, and low energy efficiency. There have been few comparative studies to understand the relationship between energy poverty, health, and well-being in Europe [3,53–55]. A few studies have shown that energy poverty negatively impacts health in Southern European countries, focusing on a single or few health outcomes [3,17,35,56–58]. Bouzarovski and Tirado Herrero [59] found significant regional differences in energy poverty within Poland, Hungary, and the Czech Republic.

Thomson and Snell [3] did a comparative study of thirty-two European countries to illustrate the negative effects of energy poverty on respiratory and circulatory systems, as well as poor emotional well-being. Karpinska and Smiech [60] did a comparative analysis of energy poverty transitions (moving from a state of energy poverty to energy secure, and vice versa) and persistence of consumers in seventeen European countries. They found the probability of being in an energy poverty state is greater than 51%, for households in Bulgaria, Greece, Lithuania, and Romania close to the energy poverty trap. Oliveras and Peralta [17] found uneven patterns of energy poverty in Southern European countries in gender and social class using more healthcare services and medications.

As a result of the policies set forth by the EU, Romania has as one of the five main goals of the Romanian Energy Strategy 2016–2030 [19] to reduce energy poverty and protect vulnerable people. A major obstacle in achieving these goals is that 90% of the residential floor area was built before 1989 [27,61] when there was no incentive to build with good insulation or energy efficiency measures because housing was highly subsidized and energy costs were low [27,62]. Although efforts have been made recently to improve the energy efficiency of apartment blocks within urban areas in Romania, many still are energy inefficient, as are houses in more rural areas. The energy inefficient dwellings cause

households to reduce their energy consumption to save money, such as reducing their room temperature for heating or not using cooling for warm days [27,63].

This paper builds on these findings with the unique approach of exploring bi-directional causality. The next section describes the data and research methodology used which outlines the approach to show a bi-directional causal relationship between energy poverty, poor health, and affordable housing and energy prices.

3. Materials and Methods

A panel data approach is used to gain insight into energy poverty in the EU. A cross-country analysis is conducted to study insights for countries with high energy import dependence. Panel data models are built for the EU-27 countries (2003–2020), whereas a separate cross-country analysis is conducted for Italy, Malta, Cyprus, Luxembourg, and Ireland because they have the highest energy import dependency.

Panel Autoregressive Distributed Lag models (panel ARDL) are estimated under the hypotheses of heterogeneity, cross-dependence, and non-integration. The time series approach is developed on low volume samples, so Bayesian nonparametric models such as ridge regression are used for Romania, for example. The data used were obtained from Eurostat and the World Bank. The dependent variables are self-perceived health as bad or very bad (total), cooling days, heating days, energy import dependence, and the share of housing costs in disposable household income. The explanatory variables include arrears on utility bills (total) (arrears), current health expenditure (% of GDP), population unable to keep home adequately warm (population), and people at risk of poverty or social exclusion in cities, towns and rural zones.

Self-perceived health as bad or very bad is used because it is a good indicator of overall personal health and a forecaster of morbidity and mortality [17]. The number of cooling days is important for those individuals living in warmer climates [58] as an indicator for health issues such as heatstroke or other heat related ailments. The number of heating days is necessary to include due to the strong relationship between cold temperatures and illness, such as colds, cardiovascular, and respiratory diseases [59]. Energy import dependence is employed to understand how vulnerable to supply disruptions EU countries are and how any interruptions could worsen energy poverty. The share of housing costs in disposable income is an important factor in whether a household is in energy poverty [8,60,64]. The indicator people at risk of poverty or social exclusion have been shown to be a determinant in energy poverty [65–71]. The population unable to keep their home adequately warm is an important indicator of energy poverty [72–75]. Current health expenditure as a percentage GDP [76] is included in the analysis to indicate how a country's healthcare resources are related to energy poverty. People or households that are in arrears on their utility bills are often affected by energy poverty [47,65,77–80]. These variables are used in the models below.

4. Theoretical Framework

The basic panel ARDL model is based on self-perceived health as bad or very bad, arrears on utility bills, and population unable to keep home adequately warm as the explanatory variables.

Equation (1) is the representation of the panel ARDL model used to explain the logarithm of self-perceived health at time t (dependent variable). The explanatory variables are the logarithm of the variables: self-perceived health; arrears on utility bills; and population unable to keep home adequately warm at time $(t - l)$. The natural logarithm is applied to all data series to have interpretations in terms of elasticities.

$$\log(\text{self perceived health}_{it}) = \alpha_i + \sum_{l=1}^p \beta_0 \log(\text{self perceived health}_{it-l}) + \sum_{l=0}^q \beta_1 \log(\text{arrears}_{it-l}) + \sum_{l=0}^q \beta_2 \log(\text{population}_{it-l}) + e_{it} \quad (1)$$

where i is index for country and t is index for time, e_{it} is the error, α_i are the coefficients that vary across countries, and $\beta_0, \beta_1, \beta_2$ are parameters.

After parameterization, Equation (1) becomes:

$$\Delta \log(\text{self perceived health } h_{it}) = \alpha_i + \Phi_i(\log(\text{self perceived health } h_{it-1})) - \theta_1 \log(\text{arrears}_{it-1}) - \theta_2 \log(\text{population}_{it-1}) + \sum_{l=1}^{p-1} \lambda_{il} \Delta \log(\text{self perceived health}_{it-l}) + \sum_{l=0}^{q-1} \lambda'_{il} \Delta \log(\text{arrears}_{it-l}) + \sum_{l=0}^{q-1} \lambda''_{il} \Delta \log(\text{population}_{it-l}) + e_{it} \tag{2}$$

where Δ is the variational operator (this operator is applied to each variable of the corresponding data series in the first difference; i.e., the value of the indicator at time t minus value of the indicator at time $(t - 1)$), α_i , Φ_i are coefficients that vary across countries, and $\lambda_{il}, \lambda'_{il}, \lambda''_{il}$ are coefficients that vary across countries and in time. $\lambda, \lambda', \lambda''$ represent short-term parameters associated to the lagged endogenous variables, arrears on utility bills, and population unable to keep home adequately warm respectively. θ_1 and θ_2 are the long-term coefficients for arrears on utility bills and population unable to keep home adequately warm. The speed of adjustment is measured by Φ_i .

A particular type of panel ARDL model is considered based on the pooled mean group (PMG) estimator that considers heterogeneous short-run equilibrium across countries in the sample and homogenous long-run equilibrium across these countries [81]. In the short-run, there are different responses to external shocks of various countries, but in the long-run, the tendency is one of stabilization. The main benefit of the PMG estimator is given by its ability to diminish endogeneity.

Table 1 provides the descriptive statistics for the variables in the panel data models. The maximum value for total arrears on utility bills was registered by Greece in 2014, whereas Denmark reached the minimum value in 2008, before the world financial crisis. Malta was the country with the highest energy import dependence registered in 2013, whereas the lowest value was observed for Denmark in 2005. Croatia registered the maximum value for self-perceived health as bad or very bad in 2010, whereas the minimum was observed in Ireland in 2007.

Table 1. Descriptive statistics.

Variable	Mean	Standard Deviation	Minimum Value	Maximum Value
Arrears on utility bills (total)	10.44	8.36	4.7	65.4
Heating days	2821.02	1148.24	322.36	6179.75
Cooling days	119.14	182.12	0	812.18
Energy import dependency	57.08	26.57	−50.62	104.14
Share of housing costs in disposable household income (%)	38.41	10.72	11.8	76.5
People at risk of poverty or social exclusion in cities (%)	22.39	5.92	10.4	56.9
People at risk of poverty or social exclusion in towns (%)	22.87	9.03	9.3	62.3
People at risk of poverty or social exclusion in rural environment (%)	22.90	8.66	9	64.4
Population unable to keep home adequately warm	11.39	11.98	0.3	69.5
Self-perceived health as bad or very bad (total)	10.58	4.75	2.5	26.8
Current health expenditure (% of GDP)	8.13	1.72	4.70	11.58

Source: own calculations in Stata 15.

Traditional regression models could provide spurious results on the empirical data because of assumptions that, in most cases, are not verified by economic data series. Therefore, an accurate analysis should be based on a regression model describing all possible data models. A solution to this problem is given by the Bayesian nonparametric

approach that allows the construction of flexible models as an infinite mix of regression models based on minimal data assumptions.

Unlike the least squares estimator in the linear regression model, the linear ridge regression model constructs estimates by reduction. In this case, the prediction error and the mean square error are usually improved.

Given the theoretical background of a Bayesian linear regression model described by O’Hagan and Forster [82], for a given data set $D_n = (X, y)$ with $X = (x_{ip})_{n \times p}$ and $y = (y_1, \dots, y_n)^T$ and a normal-inverse gamma conjugate distribution for prior density (β, σ^2) , we have:

$$f(y|X, \beta, \sigma^2) = n_n(y|X, \beta, \sigma^2 I_n) = \pi(\beta, \sigma^2) = n_p(\beta|m, \sigma^2 V) ig(\sigma^2|a, b) = \text{nig}(\beta, \sigma^2|m, V, a, b) \tag{3}$$

where $n_n(\cdot|\mu, \Sigma)$ is the probability density function (pdf) for a normal multivariate distribution, $n_p(\cdot|\mu, \sigma^2)$ is the pdf for a normal univariate distribution, $ig(\cdot|a, b)$ is the pdf for an inverse gamma distribution (a is the form and b is the rate, $1/b$ is the scale), $\text{nig}(\beta, \sigma^2|m, V, a, b)$ is the pdf for a NIG (normal inverse gamma) distribution (the product between a gamma inverse distribution and a normal multivariate as in Lindley and Smith [83]), and $f(y|X, \beta, \sigma^2)$ is the likelihood function.

The posterior distribution is a combined likelihood function based on sample data and prior distribution.

If the prior distribution (β, σ^2) is NIG, in a marginal approach, β has an a priori Student distribution of mean m and the covariance matrix $V1(\beta) = \frac{b}{a-1}V$ and $2a$ degrees of freedom. σ^2 presents a prior inverse gamma distribution of average $\frac{b}{a-1}$ and variance $\frac{b^2}{(a-1)^2(a-2)}$.

According to Karabatsos [84], the ridge regression model (RR model) is a linear regression model of Bayesian type with normal a priori distribution $n_p(\beta|0, \sigma^2 \lambda^{-1} I_p)$ for β , conditioned by σ^2 . If (β, σ^2) has a normal-inverse gamma distribution $\text{nig}(\beta, \sigma^2|0, \lambda^{-1} I_p, a, b)$, all inference procedures corresponding to the traditional Bayesian linear model are also applied for the ridge regression.

Ridge regression allows for a fast estimation of the coefficients by the least squares method, even if the number of explanatory variables (p) is very large and when their number is greater than the number of observations. This approach, which involves many parameters, is also fulfilled in nonparametric Bayesian models. In fact, the specification of models with many parameters (to infinity) is done to obtain a robust and flexible statistical inference. Griffin and Brown [85] showed that Bayesian ridge regression is based on a simple anterior structure and has a good predictive performance in many cases. According to Polson and Scott [86], dimensional linear regression models could be described by Levy processes.

Estimates and the posterior probability are calculated for the standardized parameter to fall within a standard deviation of 0. Beta represents the standardized coefficients (posterior means), based on the centered mean and the normalized explanatory variables of mean 0 and variance 1. The coefficients are between -1 and 1 when all explanatory variables are uncorrelated (there is no multicollinearity).

PP1SD represents the posterior probability that a standardized coefficient is at maximum a standard deviation of zero. An explanatory variable significantly influences the dependent variable if PP1SD is less than 0.5.

b represents the non-standardized coefficients on the original scale of the variables. Coefficients are obtained based on standardized beta values:

$$b = \left[\bar{y} - \frac{\bar{X} \cdot \beta}{SD(X)}, \frac{\beta}{SD(X)} \right] \tag{4}$$

where b are the non-standardized coefficients, β are the standardized coefficients, X are the means of the explanatory variables in the model, and $SD(X)$ are the standard deviation of the explanatory variables in the model.

The standardized beta values are automatically computed and by applying Formula (4), the non-standardized coefficients on the original scale of the variables are computed.

The first value in b is the intercept (constant), and the other values are slopes. The mean X is a line vector that contains the means of the explanatory variables. The standard deviation $(X)'$ is a column vector containing the standard deviations of the explanatory variables.

5. Results

5.1. Panel Data Models

The hypothesis of heterogeneity is checked because the sample includes both developed and developing countries in the EU that present different patterns of economic, energy, and social development. According to the CD Pesaran test for cross-sectional dependence, if all the p -values are lower than 0.05, then the assumption of cross-section independence is rejected at the 5% level of significance (see Table 2). This cross-sectional dependence might be explained by the common regulations applied to all EU countries.

Table 2. The results of CD Pesaran’s test.

Variable	Calculated Statistics *
Arrears on utility bills; total population (%)	21.76
Heating days	46.30
Cooling days	32.76
% Population unable to keep home adequately warm	10.73
Energy import dependency	11.36
Self-perceived health as bad or very bad; total population (%)	4.55
Share of housing costs in disposable household income (%)	18.33
People at risk of poverty or social exclusion in cities (%)	9.21
People at risk of poverty or social exclusion in towns (%)	11.47
People at risk of poverty or social exclusion in rural environment (%)	11.47
Current health expenditure (% of GDP)	20.63

Note: * indicates that all the p -values are less than 0.05. Source: own calculations in Stata 15.

Next, the data are transformed using their logarithmic forms that allow interpretations in terms of elasticities. Under the assumption of heterogeneity, the Im-Pesaran-Shin test is used since the panel is unbalanced. The null hypothesis of this test considers that all the panels present unit roots. As shown in Table 3, the data series are stationary for heating days, cooling days, people at risk of poverty or social exclusion in towns and people at risk of poverty or social exclusion in rural environment.

Table 3. The results of Im-Pesaran-Shin test for unit roots in panel data.

Variable (in Log)	Calculated Statistics (p -Values)
Arrears on utility bills; total population (%)	−0.2600 (0.3974)
Heating days	−7.3388 (<0.05)
Cooling days	−9.2174 (<0.05)
Population unable to keep home adequately warm (%)	−0.0732 (0.4708)

Table 3. Cont.

Variable (in Log)	Calculated Statistics (p-Values)
Share of housing costs in disposable household income (%)	0.4908 (0.5567)
People at risk of poverty or social exclusion in cities (%)	−0.2292 (0.4093)
People at risk of poverty or social exclusion in towns (%)	−2.1715 (<0.05)
People at risk of poverty or social exclusion in rural environment (%)	−2.1805 (<0.05)
Self-perceived health as bad or very bad; total population (%)	0.1196 (0.5476)
Energy import dependency	−0.3141 (0.7234)
Current health expenditure (% of GDP)	−1.1948 (0.1161)

Source: own calculations in Stata 15.

Since the evidence of stationarity is mixed, the existence of cointegration is checked for the series with the same order of integration. The Westerlund test for cointegration is considered under the null hypothesis that some panels are cointegrated and, respectively, all the panels are cointegrated (see Table 4).

Table 4. The Westerlund test for cointegration.

Dependent Variable	Explanatory Variables	Some Panels Are Cointegrated Computed Statistics (p-Value)	All the Panels Are Cointegrated Computed Statistics (p-Value)
Share of housing costs in disposable household income (%)	Arrears on utility bills	2.3843 (0.0086)	−0.3998 (0.3446)
	Population unable to keep home adequately warm	0.8504 (0.1975)	0.8036 (0.2108)
Self-perceived health as bad or very bad; total population (%)	Current health expenditure	−0.6484 (0.2584)	−0.9792 (0.1637)
	Energy import dependency		

Source: own calculations in Stata 15.

The results indicate no clear evidence for cointegration and panel ARDL models are built in all the cases. Since the Hessian is unstable or asymmetric in some cases, health expenditure is not considered as a control variable in a few of the models. The PMG estimators presented in Table 5 suggest a long-run relationship between the dependent variables and regressors. In the case of a deviation from the long-run, the speed of adjustment to the equilibrium is given by the error correction term in absolute value. The highest rate of correction was registered in the model explaining cooling days, whereas the lowest one in the model explains self-perceived health as bad or very bad.

The results suggest both short-run and long-run impacts on health at the 95% confidence level. The long-run connections will be examined first. If a person or household is arrears on their utility bills, cannot keep their home adequately warm, or has increased current health expenditures then the long-run impact on self-perceived health as bad or very bad worsens. Furthermore, being arrears on utility bills is also related to a household spending more of their disposable income on housing, and a greater number of heating days. However, there is a negative long-run impact of arrears on utility bills on energy import dependency. Other long-run effects were found in the analysis. The results suggest that there is a positive long-run influence of the population unable to keep their home adequately warm on self-perceived health as bad and very bad and a negative long-run impact on number of cooling days. There is also a long-run impact that was found for

current health expenditure on self-perceived health as bad and very bad and the number of heating days.

Table 5. PMG estimators for the EU-27 countries (2003–2020).

Connection	Variables (in Log)	Dependent Variable (p-Value)				
		Self-Perceived Health as Bad or Very Bad (Total)	Energy Import Dependency	Share of Housing Costs in Disposable Household Income	Heating Days	Cooling Days
Long-run relationship	Arrears on utility bills	0.149 (0.000)	−0.167 (0.000)	0.362 (0.000)	0.046 (0.000)	−0.028 (0.534)
	Population unable to keep home adequately warm	0.121 (0.000)	0.006 (0.624)	−0.055 (0.042)	0.007 (0.502)	−0.117 (0.056)
	Current health expenditure	1.729 (0.000)	-	-	0.131 (0.017)	-
Error correction term		−0.219 (0.000)	−0.429 (0.000)	−0.493 (0.000)	−0.974 (0.000)	−1.035 (0.000)
Short-run relationship	Arrears on utility bills	0.021 (0.625)	0.066 (0.006)	−0.048 (0.43)	−0.059 (0.090)	−0.380 (0.411)
	Population unable to keep home adequately warm	0.043 (0.150)	0.004 (0.888)	0.065 (0.258)	0.098 (0.009)	0.214 (0.425)
	Current health expenditure	−0.315 (0.023)	-	-	0.235 (0.082)	-
	Constant	−0.469 (0.000)	1.922 (0.000)	1.390 (0.000)	7.324 (0.000)	3.876 (0.000)
Residuals	I(0)	I(0)	I(0)	I(0)	I(0)	I(0)

Source: own calculations in Stata 15.

Several short-run influences were also found. There is a positive short-run impact of being arrears on utility bills on energy import dependency and a negative short-run effect on the number of heating days. In addition, in the short-run, those individuals self-identifying as having bad or very bad health perceive their health as improving with an increase in current health expenditures. Positive short-run influences were found for both current health expenditure and the population unable to keep their home adequately warm on the number of heating days.

These long-run and short-run results are expected. An individual or household that cannot pay their utility bills on-time, cannot keep their house to an adequate heating temperature, or has higher health expenditures will have worse health over time [3,18,24]. Moreover, logic dictates that being in arrears on utility bills suggests more disposable income is spent on housing and that there might be more cold days requiring heating. As a result, less disposable income is available to pay bills such as utilities. The bi-directional causal relationships are evident in these results. In the short-run, however, increases in health expenditures can improve health, whereas long-term health expenditures indicate more serious health issues. Furthermore, increased expenses or an inability to pay expenses and keep a home warm will negatively impact health. If there is an inability to keep a home adequately warm, the ability to keep a home sufficiently cool will also decrease, as does the share of housing costs in disposable income.

When additional control variables are checked for robustness (people at risk of poverty or social exclusion in towns, cities and rural zones), the long-run relationships are kept, as

shown in Table 6. People at risk of poverty or social exclusion in cities and towns exerted a positive long-run influence on the share of housing costs in disposable household income and cooling days and a negative impact on heating days. People at risk of poverty or social exclusion in rural zones had a direct long-term impact on self-perceived health as bad or very bad, share of housing costs in disposable household income, and cooling days. In the short-term, people at risk of poverty or social exclusion in towns or rural zones had a positive influence on cooling days and a negative impact on self-perceived health as bad or very bad. These results should be expected as poverty and social exclusion are associated with lower incomes [7,87], severely impacting the ability to address health issues, or the ability to pay for appropriate levels of heating and cooling for the household.

In addition to the panel data analysis, a cross-country study is deemed necessary since the overall conclusions for the entire sample might not be applied for each country. Particular attention should be paid to countries with high energy import dependency for which the impact of previous regressors on dependent variables is assessed.

5.2. Cross-Country Analysis

A cluster analysis based on the average values of energy import dependency and a k-means method was done to identify countries with high values of this indicator and states with lower values (Table 7).

A separate individual analysis based on generalized ridge regressions was made for a few countries with the highest energy import dependency, represented in cluster 1: Malta, Cyprus, Italy, Luxembourg, and Ireland.

In Italy (Table 8), being more in arrears on utility bills and an increase in the number of people unable to keep their home adequately warm increases the negative perception on health, whereas being more in arrears on utility bills and a decrease in the number of people unable to keep their home adequately warm contributes to higher energy import dependency. Energy poverty affects approximately three million poor households in Italy [88]. Thus, these results are consistent with expectations as energy poverty, poverty, and inequality are synonymous with one another, and nearly 1.7 million households live in absolute poverty in Italy [89].

The results for Ireland (Table 9) indicate that self-perceived health rated as bad or very bad is explained by the population unable to keep their home adequately warm and people at risk of poverty or social exclusion in towns and a rural environment. Energy import dependency is determined by arrears on utility bills and people at risk of poverty or social exclusion in cities. Furthermore, the share of housing costs in disposable household income is explained by the people at risk of poverty or social exclusion in rural zones.

More people unable to keep their home adequately warm and more people at risk of poverty or social exclusion in rural zones increases the chances that a person will perceive their health as bad or very bad in Ireland. On the other hand, more people at risk of poverty or social exclusion in towns decrease the chances to perceive unsatisfactory health. This result might suggest that poor people in Irish towns feel healthier than those in villages due to better quality of medical services for these people. When arrears on utility bills in Ireland increases, the energy import dependency decreases, whereas more people at risk of poverty or social exclusion in cities increases energy import dependency. More people at risk of poverty or social exclusion in Irish rural zones contributes to the increase in the share of housing costs in disposable household income in Ireland. A generally accepted theory that holds in Ireland is that energy poverty arises out of low income and inefficient homes [90,91], seemingly confirmed by the results of the analysis presented here, as housing in rural areas tends to be less energy efficient and of lower building quality.

Table 6. Robustness: PMG estimators for additional variables in the case of EU-27 countries (2003–2020).

Connection	Variables (in Log)	Dependent Variable (p-Value)												
		Self-Perceived Health as Bad or Very Bad (Total)	Energy Import Dependency	Share of Housing Costs in Disposable Household Income	Heating Days	Cooling Days								
	Arrears on utility bills	0.095 (0.000)	-0.022 (0.267)	-0.002 (0.916)	-0.167 (0.000)	-0.193 (0.000)	0.070 (0.000)	0.112 (0.000)	0.19 (0.000)	0.037 (0.004)	0.037 (0.004)	-0.069 (0.231)	-0.124 (0.056)	
	Population unable to keep home adequately warm	0.043 (0.046)	-	0.020 (0.209)	0.005 (0.711)	-0.00006 (0.997)	-0.0006 (0.997)	-0.195 (0.000)	-	-0.149 (0.000)	0.031 (0.006)	0.031 (0.006)	-0.209 (0.010)	-0.167 (0.014)
	Current health expenditure	-0.244 (0.02)	-	-	-	-	-	-	-	-0.511 (0.000)	-	-	-	-
Long-run relationship	People at risk of poverty or social exclusion in cities	0.044 (0.507)	-	-	0.009 (0.831)	-	0.561 (0.000)	-	-0.042 (0.000)	-	-	0.304 (0.090)	-	
	People at risk of poverty or social exclusion in towns	-	0.331 (0.000)	-	-	0.049 (0.308)	-	0.103 (0.000)	-	0.002 (0.924)	-	-	0.284 (0.042)	
Error correction term	People at risk of poverty or social exclusion in rural zones	-	-	0.651 (0.000)	-	-	0.047 (0.307)	-	0.103 (0.0000)	-	0.002 (0.924)	-	-	
		-0.356 (0.000)	-0.366 (0.000)	-0.305 (0.000)	-0.378 (0.000)	-0.376 (0.000)	-0.467 (0.000)	-0.671 (0.000)	-0.508 (0.009)	-0.928 (0.000)	-0.928 (0.000)	-1.020 (0.000)	-1.021 (0.000)	

Table 6. Cont.

Connection	Variables (in Log)	Dependent Variable (p-Value)							
		Self-Perceived Health as Bad or Very Bad (Total)	Energy Import Dependency	Share of Housing Costs in Disposable Household Income	Heating Days	Cooling Days			
	Arrears on utility bills	0.006 (0.857)	0.046 (0.113)	0.089 (0.006)	0.089 (0.006)	−0.103 (0.005)	−0.007 (0.733)	−0.686 (0.080)	−0.546 (0.224)
	Population unable to keep home adequately warm	0.076 (0.105)	0.006 (0.839)	−0.002 (0.956)	0.197 (0.019)	0.206 (0.003)	-	0.219 (0.538)	0.216 (0.376)
	Current health expenditure	−0.062 (0.682)	-	-	-	0.500 (0.013)	-	-	-
Short-run relationship	People at risk of poverty or social exclusion in cities	−0.092 (0.251)	−0.188 (0.501)	-	0.008 (0.929)	0.070 (0.565)	-	0.653 (0.384)	-
	People at risk of poverty or social exclusion in towns	-	-	−0.049 (0.486)	-	−0.074 (0.115)	0.070 (0.304)	-	0.968 (0.032)
	People at risk of poverty or social exclusion in rural zones	-	−0.142 (0.001)	-	−0.046 (0.485)	0.008 (0.929)	-	−0.073 (0.114)	0.968 (0.032)
	Constant	−0.800 (0.000)	1.688 (0.000)	1.671 (0.000)	0.959 (0.000)	4.583 (0.007)	7.132 (0.000)	3.079 (0.000)	3.249 (0.000)
Residuals	I(0)	I(0)	I(0)	I(0)	I(0)	I(0)	I(0)	I(0)	I(0)

Table 7. Cluster Membership.

Country	Cluster Distribution Cluster	Distance
Greece		0.934
Austria		3.420
Lithuania		3.989
Slovakia		5.396
Spain		5.928
Belgium		8.033
Germany		8.261
Portugal		8.714
Italy		10.110
Hungary	1	11.603
Ireland		13.857
Latvia		15.205
Finland		19.576
Croatia		19.902
Slovenia		19.942
France		21.122
Cyprus		26.185
Luxembourg		26.741
Malta		29.782
Romania		2.107
Poland		3.209
Czechia		3.473
Estonia	2	8.409
Sweden		8.606
Netherlands		13.094
Bulgaria		15.874
Denmark		33.741

Source: own calculations in SPSS.

In the case of Cyprus (Table 10), the population unable to keep their home adequately warm is positively correlated with self-perceived health as bad or very bad, whereas more people at risk of poverty or social exclusion in towns and rural zones reduces the perceptions of bad or very bad health. More people unable to keep their home adequately warm and more people at risk of poverty or social exclusion in cities increases energy import dependency. More people arrears on bills and more people at risk of poverty or social exclusion in cities increases the share of housing costs in disposable household income. Cyprus has one of the higher percentages of arrears on utility bills in the EU [92] and a large percentage of households with poor energy affordability [93] and buildings that have poor quality of construction and an aging building stock [92].

More arrears on utility bills and more people unable to keep their home adequately warm contributes to the negative perception on health in Luxembourg (Table 11). Energy import dependency increases when arrears on utility bills grow and the population unable to keep their home adequately warm and people at risk of poverty or social exclusion in villages decreases. More people unable to keep their home adequately warm and more people at risk of poverty or social exclusion in towns increases the share of housing costs in disposable household income. These results build upon the findings of Michel [94] and are expected as Luxembourg has one of the most expensive housing markets in the EU.

In Malta (Table 12), more arrears on utility bills and more people at risk of poverty or social exclusion in towns improves the personal perception on health as being bad and very bad. One likely explanation for this is that people use their income to pay for their healthcare needs which can be expensive, thus, making a preference choice for healthcare overpaying for utilities. Nevertheless, energy poverty in Malta has increased a lot over the study time-period [77].

Table 8. The results of generalized ridge regressions for Italy.

Variables (in Log)	Dependent Variable Unstandardized Coefficients (PP1SD)			
	Self-Perceived Health as Bad or Very Bad (Total)	Energy Import Dependency	Share of Housing Costs in Disposable Household Income	Heating Days
Arrears on utility bills	0.516 (0.003)	0.035 (0.263)	-0.0001 (0.668)	-0.035 (0.601)
Population unable to keep home adequately warm	0.385 (0.201)	-0.067 (0.236)	-0.0001 (0.668)	0.006 (0.667)
People at risk of poverty or social exclusion in cities	-0.335 (0.631)	-0.088 (0.572)	0.0001 (0.668)	0.019 (0.476)
People at risk of poverty or social exclusion in towns	0.428 (0.647)	-0.032 (0.661)	0.0001 (0.668)	0.123 (0.642)
People at risk of poverty or social exclusion in rural zones	-0.430 (0.649)	-0.034 (0.664)	0.0001 (0.668)	0.125 (0.643)

Source: own calculations in MATLAB. Bold numbers are significant.

Table 9. The results of generalized ridge regressions for Ireland.

Variables (in Log)	Dependent Variable Unstandardized Coefficients (PP1SD)			
	Self-Perceived Health as Bad or Very Bad (Total)	Energy Import Dependency	Share of Housing Costs in Disposable Household Income	Heating Days
Arrears on utility bills	-0.022 (0.664)	-0.193 (0.348)	0.162 (0.558)	0.025 (0.555)
Population unable to keep home adequately warm	0.145 (0.401)	-0.037 (0.644)	0.100 (0.614)	0.011 (0.502)
People at risk of poverty or social exclusion in cities	-0.112 (0.626)	0.849 (0.021)	0.206 (0.635)	0.023 (0.634)
People at risk of poverty or social exclusion in towns	-0.487 (0.001)	-0.011 (0.666)	0.205 (0.610)	0.009 (0.657)
People at risk of poverty or social exclusion in rural zones	1.522 (0.002)	-0.083 (0.656)	0.253 (0.452)	-0.0009 (0.673)

Source: own calculations in MATLAB. Bold numbers are significant.

Table 10. The results of generalized ridge regressions for Cyprus.

Variables (in Log)	Dependent Variable Unstandardized Coefficients (PP1SD)			
	Self-Perceived Health as Bad or Very Bad (Total)	Energy Import Dependency	Share of Housing Costs in Disposable Household Income	Heating Days
Arrears on utility bills	0.015 (0.665)	-0.003 (0.647)	0.181 (0.481)	-0.003 (0.665)
Population unable to keep home adequately warm	0.492 (0.153)	0.046 (0.221)	0.329 (0.610)	-0.040 (0.554)
People at risk of poverty or social exclusion in cities	-0.082 (0.662)	0.053 (0.346)	0.179 (0.324)	-0.055 (0.596)
People at risk of poverty or social exclusion in towns	-0.499 (0.006)	0.01 (0.582)	0.471 (0.552)	0.004 (0.666)
People at risk of poverty or social exclusion in rural zones	-0.500 (0.006)	0.011 (0.582)	0.489 (0.556)	0.003 (0.667)

Source: own calculations in MATLAB. Bold numbers are significant.

Table 11. The results of generalized ridge regressions for Luxembourg.

Variables (in Log)	Dependent Variable Unstandardized Coefficients (PP1SD)			
	Self-Perceived Health as Bad or Very Bad (Total)	Energy Import Dependency	Share of Housing Costs in Disposable Household Income	Heating Days
Arrears on utility bills	0.080 (0.096)	0.004 (0.464)	-0.048 (0.597)	0.194 (0.573)
Population unable to keep home adequately warm	0.077 (0.265)	-0.003 (0.480)	0.119 (0.201)	0.116 (0.591)
People at risk of poverty or social exclusion in cities	0.047 (0.652)	-0.006 (0.634)	0.179 (0.598)	-0.221 (0.658)
People at risk of poverty or social exclusion in towns	0.070 (0.612)	-0.003 (0.152)	0.049 (0.261)	0.034 (0.611)
People at risk of poverty or social exclusion in rural zones	0.060 (0.666)	-0.003 (0.622)	0.078 (0.595)	0.184 (0.587)

Source: own calculations in MATLAB. Bold numbers are significant.

Table 12. The results of generalized ridge regressions for Malta.

Variables (in Log)	Dependent Variable Unstandardized Coefficients (PP1SD)				
	Self-Perceived Health as Bad or Very Bad (Total)	Energy Import Dependency	Share of Housing Costs in Disposable Household Income	Cooling Days	Heating Days
Arrears on utility bills	-0.176 (0.310)	0 (0.667)	0 (0.667)	0 (0.667)	0 (0.667)
Population unable to keep home adequately warm	0.054 (0.542)	0 (0.667)	0 (0.667)	0 (0.667)	0 (0.667)
People at risk of poverty or social exclusion in cities	-0.174 (0.615)	0 (0.667)	0 (0.667)	0 (0.667)	0 (0.667)
People at risk of poverty or social exclusion in towns	-0.027 (0.456)	0 (0.667)	0 (0.667)	0 (0.667)	0 (0.667)
People at risk of poverty or social exclusion in rural zones	0.148 (0.577)	0 (0.667)	0 (0.667)	0 (0.667)	0 (0.667)

Source: own calculations in MATLAB. Bold numbers are significant.

6. Discussion

The energy import dependency of the EU has the potential to severely increase energy poverty for its member states. A large percentage of energy imported to the EU comes from Russia. Should there be a dispute, politically or militarily, Russia could easily decrease or stop the flow of natural gas, for example, hurting countries in the Eastern portion of the EU, particularly Germany. The energy supply issue has been shown to be a problem for the EU in the Russia-Ukraine war. The supply of energy will become a bigger issue in the winter months as citizens of the EU will require natural gas to heat their homes.

Additionally, the EU has set policy to reduce their reliance on fossil fuels to decrease carbon emissions. To achieve this goal, the EU will need to substantially increase the use of renewable energy. This, in turn, will cause more volatility in energy markets in the short to medium run as the transition to green energy occurs. Consequently, the transition could negatively impact vulnerable households and individuals and their health. To offset these potential negative impacts from energy import dependency and the transition to green energy, the EU must increase their production of energy and increase budget allocations for public health and payments to offset energy costs. An increase in energy production would decrease their reliance on energy imports while simultaneously keeping the most vulnerable energy consumers from harm from higher energy prices and less supply. Moreover, as energy production is ramped up, public health budgets and allocations for energy assistance must be increased to offset any negative health impacts to residents and to prevent them.

As the EU transitions to green energy, the transition either must be rapid, which is unlikely to be feasible, or done in stages to reduce the harmful side-effects to vulnerable energy consumers. If the transition is otherwise, vulnerable energy consumers would need compensation to offset higher energy costs. These payments would add significantly to the budgets of EU countries, putting additional pressures on economies and deficits. As a result, energy poverty could be a ticking time bomb for the EU.

In response, countries across Europe have initiated public programs to protect the most vulnerable energy consumers, instituting policies to counteract high energy prices, such as tax reductions and cash payments to low-income households. Investments in energy efficiency improvements can reduce household energy consumption, resulting in energy poverty rates [95]. New construction regulations and investments in building renovations improving the minimum energy performance for buildings can help address some of these issues. Al-Tal et al. [96] showed that energy efficiency is vital in reducing energy poverty. Additionally, as suggested by Bukari et al. [97], since energy poverty increases household health expenditures, broadening the scope of health insurance in EU countries will be helpful in addressing negative health outcomes caused by energy poverty. However, the biggest investment, which has lagged for many years in the EU because of a lack of will by EU politicians, will be in developing more energy supply. Nawaz [16] suggested similarly, that to promote a health society, governments will need to increase the provision of energy services. In the short-run, this may require the use of energy resources that are unattractive to EU governments and, perhaps, citizens, but will likely be a necessary evil as the transition to green energy occurs.

7. Conclusions

Energy poverty in Europe is widespread, complex, and created by a combination of factors such as high energy prices, low incomes, and poor energy efficiency. The results of this research has expanded the findings of Halkos and Gkampoura [80] that electricity prices, unemployment, and the percentage of people at risk of poverty are drivers for energy poverty, whereas GDP per capita has an inverse relationship with energy poverty. The results have also expanded upon the findings of the literature cited earlier in this paper showing the bi-causal relationship between energy poverty and health. Our findings show that energy poverty leads to consumer vulnerability, impacting the state of a person's health. These results have many implications as extreme heat and cold temperatures become more commonplace, disproportionately impacting the most vulnerable households,

particularly the elderly, women, and the poor. Furthermore, household demand for energy is price-inelastic in the long-run [95]. Therefore, there will be higher levels of energy poverty resulting in higher poverty, reduced food consumption, and increased health issues because households must spend a greater proportion of their income on energy.

Despite the many contributions to the literature this research makes, the paper does not lack inherent limitations. Most importantly, the research presented in this paper was limited by the availability of data. Future research will explore creating an energy poverty index to capture all the meaningful energy poverty indicators into one measurement. This index will ensure that energy poverty can be fully analyzed, whereas individual indicators may not be captured in a significant relationship. This paper has shown the connection between energy poverty, poor health, and affordable housing and energy prices, filling a gap in the literature. The results of this study are important as they illustrate who might be the most vulnerable, enabling decision makers to develop better public policy to combat energy poverty in the EU. Since countries with high energy import dependency are more likely to enhance energy poverty, specific solutions should be adopted for Malta, Cyprus, Italy, Luxembourg, and Ireland based on national policies that might exceed the European framework. From this point of view, our paper is a step-forward in the research of energy poverty in Europe by providing the most effective recommendations for the most vulnerable countries.

Author Contributions: Formal analysis, M.S.; Writing—original draft, J.M.P.; Writing—review & editing, R.I.I. All authors whose names appear on the submission have made substantial contributions to the study conception and design. All authors have read and agreed to the published version of the manuscript.

Funding: This research received no external funding.

Institutional Review Board Statement: Not applicable.

Informed Consent Statement: Not applicable.

Data Availability Statement: The data used were obtained from Eurostat and the World Bank.

Conflicts of Interest: The authors declare no conflict of interest.

References

1. Boardman, B. Fuel Poverty Synthesis: Lessons Learnt, Actions Needed. *Energy Policy* **2012**, *49*, 143–148.
2. Fahmy, E.; Gordon, D.; Patsios, D. Predicting Fuel Poverty at a Small-area Level in England. *Energy Policy* **2011**, *39*, 4370–4377. [[CrossRef](#)]
3. Thomson, H.; Snell, C.; Bouzarovski, S. Health, Well-being and Energy Poverty in Europe: A Comparative Study of 32 European Countries. *Int. J. Environ. Res. Public Health* **2017**, *14*, 584. [[CrossRef](#)] [[PubMed](#)]
4. Gonzalez-Equino, M. Energy Poverty: An Overview. *Renew. Sustain. Energy Rev.* **2015**, *47*, 377–385. [[CrossRef](#)]
5. Birol, F. Energy Economics: A Place for Energy Poverty in the Agenda? *Energy J.* **2007**, *28*, 1–6. [[CrossRef](#)]
6. Bouzarovski, S.; Petrova, S.; Sarlamanov, R. Energy Poverty Policies in the EU: A Critical Perspective. *Energy Policy* **2012**, *49*, 76–82. [[CrossRef](#)]
7. Chester, L.; Morris, A. A New Form of Energy Poverty is the Hallmark of Liberalised Electricity Sectors. *Aust. J. Soc. Issues* **2016**, *46*, 435–459. [[CrossRef](#)]
8. Meyer, S.; Laurence, H.; Bart, D.; Middlemiss, L.; Marechal, K. Capturing the Multifaceted Nature of Energy Poverty: Lessons From Belgium. *Energy Res. Soc. Sci.* **2018**, *40*, 273–283. [[CrossRef](#)]
9. Okushima, S. Measuring Energy Poverty in Japan, 2004–2013. *Energy Policy* **2016**, *98*, 557–567. [[CrossRef](#)]
10. Primc, K.; Slabe-Erker, R.; Majcen, B. Energy Poverty: A Macrolevel Perspective. *Sustain. Dev.* **2019**, *27*, 982–989. [[CrossRef](#)]
11. Waddams, C.; Deller, D. *Affordability of Utilities' Services: Extent, Practice, Policy*; Centre on Regulation in Europe: Brussels, Belgium, 2015.
12. Hills, J. Getting the Measure of Fuel Poverty: Final Report of the Fuel Poverty Review. In *CASE Report*; London School of Economics and Political Science: London, UK, 2012.
13. Koh, L.; Marchand, R.; Genovese, A.; Brennan, A. Fuel Poverty: Perspectives from the Front Line. In *Fuel Poverty Series*; University of Sheffield, Centre for Energy, Environment and Sustainability: Sheffield, UK, 2012.
14. Bouzarovski, S.; Petrova, S. A Global Perspective on Domestic Energy Deprivation: Overcoming the Energy Poverty–Fuel Poverty Binary. *Energy Res. Soc. Sci.* **2015**, *10*, 31–40. [[CrossRef](#)]

15. Streimikiene, D.; Lekavicius, V.; Balezentis, T.; Kyriakopoulos, G.L.; Abrham, J. Climate Change Mitigation Policies Targeting Households and Addressing Energy Poverty in European Union. *Energies* **2020**, *13*, 3389. [[CrossRef](#)]
16. Nawaz, S. Energy Poverty, Climate Shocks, and Health Deprivations. *Energy Econ.* **2021**, *100*, 105338. [[CrossRef](#)]
17. Oliveras, L.; Peralta, A.; Palencia, L.; Gotsens, M.; Lopez, M.J.; Artazcoz, L.; Borrell, C.; Mari-Dell’Olmo, M. Energy Poverty and Health: Trends in the European Union Before and During the Economic Crisis, 2007–2016. *Health Place* **2021**, *67*, 102294. [[CrossRef](#)] [[PubMed](#)]
18. Carrere, J.; Peralta, A.; Oliveras, L.; Lopez, M.J.; Mari-Dell’Olmo, M.; Benach, J.; Novoa, A.M. Energy Poverty, Its Intensity and Health in Vulnerable Populations in a Southern European City. *Gac. Sanit.* **2021**, *35*, 438–444. [[CrossRef](#)] [[PubMed](#)]
19. Clodnitchi, R.; Busu, C. Energy Poverty in Romania—Drivers, Effects and Possible Measures to Reduce Its Effects and Number of People Affected. *Proc. Int. Conf. Bus. Excell.* **2017**, *11*, 138–145. [[CrossRef](#)]
20. Nussbaumer, P.; Bazilian, M.; Modi, V. Measuring Energy Poverty: Focusing on What Matters. *Renew. Sustain. Energy Rev.* **2012**, *16*, 231–243. [[CrossRef](#)]
21. Pelz, S.; Pachauri, S.; Groh, S. A Critical Review of Modern Approaches for Multidimensional Energy Poverty Measurement. *Wiley Interdiscip. Rev. Energy Environ.* **2018**, *7*, e304. [[CrossRef](#)]
22. Lin, B.; Okyere, M.A. Multidimensional Energy Poverty and Mental Health: Micro-Level Evidence from Ghana. *Int. J. Environ. Res. Public Health* **2020**, *17*, 6726. [[CrossRef](#)]
23. Nationen, V. *The Sustainable Development Goals*; United Nations Publications: New York, NY, USA, 2017.
24. Zhang, D.; Li, J.; Han, P. A Multidimensional Measure of Energy Poverty in China and Its Impacts on Health: An Empirical Study Based on the China Family Panel Studies. *Energy Policy* **2019**, *132*, 283–289. [[CrossRef](#)]
25. Oum, S. Energy Poverty in the Lao PDR and Its Impacts on Education and Health. *Energy Policy* **2019**, *132*, 247–253. [[CrossRef](#)]
26. European Commission. *Commission Staff Working Document Assessment National Energy and Climate Plan of Romania*, Brussels; European Commission: Brussels, Belgium, 2020.
27. Schneller, A.; Hoffmann, J.; Sinea, A. *Alleviating Energy Poverty in Romania and Beyond: Strategy Proposals for the Local and National Level*; Adelphi: Berlin, Germany, 2021.
28. Leca, A. Romania Needs a Strategy for Thermal Energy. *Manag. Mark.* **2015**, *10*, 3–11. [[CrossRef](#)]
29. Bouzarovski, S. When Homes Become Prisons: The Relational Spaces of Postsocialist Energy Poverty. *Environ. Plan. A: Econ. Space* **2007**, *39*, 1908–1925.
30. Bouzarovski, S. *Energy Poverty in Eastern Europe: Hidden Geographies of Deprivation*; Routledge: London, UK, 2007.
31. Lewis, P. *Fuel Poverty Can Be Stopped*; National Right to Fuel Campaign: Bradford, UK, 1982.
32. Leach, G. The Energy Transition. *Energy Policy* **1992**, *20*, 116–123. [[CrossRef](#)]
33. Boardman, B. *Fuel Poverty: From Cold Homes to Affordable Warmth*; Belhaven Press: London, UK, 1991.
34. Moore, R. Definitions of Fuel Poverty: Implications for Policy. *Energy Policy* **2012**, *49*, 19–26. [[CrossRef](#)]
35. Recalde, M.; Peralta, A.; Oliveras, L.; Tirado-Herrero, S.; Borrell, C.; Palencia, L.; Gotsens, M.; Artazcoz, L.; Mari-Dell’Olmo, M. Structural Energy Poverty Vulnerability and Excess Winter Mortality in the European Union: Exploring the Association Between Structural Determinants and Health. *Energy Policy* **2019**, *133*, 110869. [[CrossRef](#)]
36. Hulse, K.; Saugeres, L. *Housing Insecurity and Precarious Living: An Australian Exploration*; Australian Housing and Urban Research Institute Limited: Melbourne, Victoria, Australia, 2008.
37. Hernandez, D. Understanding ‘Energy Intensity’ and Why it Matters to Health. *Soc. Sci. Med.* **2016**, *167*, 357. [[CrossRef](#)]
38. Simcock, N.; Thomson, H.; Petrova, S.; Bouzarovski, S. *Energy Poverty and Vulnerability: A Global Perspective*; Routledge: London, UK, 2019.
39. Sunderland, L.; Jahn, A.; Hogan, M.; Rosenow, J.; Coward, R. *Equity in the Energy Transition: Who Pays and Who Benefits?* Regulatory Assistance Project (RAP): Brussels, Belgium, 2020.
40. Bouzarovski, S.; Thomson, H. Energy Vulnerability in the Grain of the City: Toward Neighborhood Typologies of Material Deprivation. *Ann. Am. Assoc. Geogr.* **2018**, *108*, 695–717. [[CrossRef](#)]
41. Bouzarovski, S.; Thomson, H.; Cornelis, M. Confronting Energy Poverty in Europe: A Research and Policy Agenda. *Energies* **2021**, *14*, 858. [[CrossRef](#)]
42. Lacroix, E.; Chaton, C. Fuel Poverty as a Major Determinant of Perceived Health: The Case of France. *Public Health* **2015**, *129*, 517–524. [[CrossRef](#)]
43. Liddell, C.; Guiney, C. Living in a Cold and Damp Home: Frameworks for Understanding Impacts on Mental Well-being. *Public Health* **2015**, *129*, 191–199. [[CrossRef](#)] [[PubMed](#)]
44. Marmot Review Team. *The Health Impacts of Cold Homes and Fuel Poverty*; Friends of the Earth and the Marmot Review Team: London, UK, 2011.
45. Peate, I. Keeping Warm: Health Risks and Vulnerable People. *Nurs. Resid. Care* **2008**, *10*, 606–610. [[CrossRef](#)]
46. Xiao, Y.; Wu, H.; Wang, G.; Wang, S. The Relationship Between Energy Poverty and Individual Development: Exploring the Serial Mediating Effects of Learning Behavior and Health Condition. *Int. J. Environ. Res. Public Health* **2021**, *18*, 8888. [[CrossRef](#)] [[PubMed](#)]
47. Aristondo, O.; Onaindia, E. Inequality of Energy Poverty Between Groups in Spain. *Energy* **2018**, *153*, 431–442. [[CrossRef](#)]
48. Galvin, R. Letting the Gini Out of the Fuel Poverty Battle? Correlating Cold Homes and Income Inequality in European Union Countries. *Energy Res. Soc. Sci.* **2019**, *58*, 101255. [[CrossRef](#)]

49. Petrova, S.; Simcock, N. Gender and Energy: Domestic Inequities Reconsidered. *Soc. Cult. Geogr.* **2019**, *22*, 849–867. [\[CrossRef\]](#)
50. Bollino, C.A.; Botti, F. Energy Poverty in Europe: A Multidimensional Approach. *PSL Q. Rev.* **2017**, *70*, 473–507.
51. Aranda, J.; Zabalza, I.; Conserva, A.; Millan, G. Analysis of Energy Efficiency Measures and Retrofitting Solutions for Social Housing Buildings in Spain as a Way to Mitigate Energy Poverty. *Sustainability* **2017**, *9*, 1869. [\[CrossRef\]](#)
52. Boemi, S.N.; Papadopoulos, A.M. Energy Poverty and Energy Efficiency Improvements: A Longitudinal Approach of the Hellenic Households. *Energy Build.* **2019**, *197*, 242–250. [\[CrossRef\]](#)
53. Healy, J. *Fuel Poverty and Policy in Ireland and the European Union*; Policy Institute, Trinity College Dublin: Dublin, Ireland, 2003.
54. Rudge, J.; Gilchrist, R. Excess Winter Morbidity Among Older People at Risk of Cold Homes: A Population-based Study in a London Borough. *J. Public Health* **2005**, *27*, 353–358. [\[CrossRef\]](#)
55. Braubach, M.; Jacobs, D.E.; Ormandy, D. *Environmental Burden of Disease Associated With Inadequate Housing*; WHO Regional Office for Europe: Copenhagen, Denmark, 2011.
56. Oliveras, L.; Artazcoz, L.; Borrell, C.; Palencia, L.; Lopez, M.J.; Gotsens, M.; Peralta, A.; Mari-Dell’Olmo, M. The Association of Energy Poverty with Health, Health Care Utilisation and Medication Use in Southern Europe. *SSM-Popul. Health* **2020**, *12*, 100665. [\[CrossRef\]](#) [\[PubMed\]](#)
57. Bosch, J.; Palencia, L.; Malmusi, D.; Mari-Dell’Olmo, M.; Borrell, C. The Impact of Fuel Poverty Upon Self-reported Health Status Among the Low-income Population in Europe. *Hous. Stud.* **2019**, *34*, 1377–1403. [\[CrossRef\]](#)
58. Thomson, H.; Simcock, N.; Bouzarovski, S.; Petrova, S. Energy Poverty and Indoor Cooling: An Overlooked Issue in Europe. *Energy Build.* **2019**, *196*, 21–29. [\[CrossRef\]](#)
59. Bouzarovski, S.; Tirado Herrero, S. The Energy Divide: Integrating Energy Transitions, Regional Inequalities and Poverty Trends in the European Union. *Eur. Urban Reg. Stud.* **2017**, *24*, 69–86. [\[CrossRef\]](#)
60. Karpinska, L.; Smiech, S. Conceptualising Housing Costs: The Hidden Face of Energy Poverty in Poland. *Energy Policy* **2020**, *147*, 111819. [\[CrossRef\]](#)
61. Buildings Performance Institute Europe. *Renovating Romania: A Strategy for the Energy Renovation of Romania’s Building Stock*; Buildings Performance Institute Europe: Bruxelles, Belgium, 2014.
62. Urge-Vorsatz, D.; Tirado Herrero, S. Building Synergies Between Climate Change Mitigation and Energy Poverty Alleviation. *Energy Policy* **2012**, *49*, 83–90. [\[CrossRef\]](#)
63. Sinea, A.C.; Vornicu-Chira, A. *Energy Poverty in Central and Southeast Europe*; Center for the Study of Democracy: Cluj-Napoca, Romania, 2020.
64. Grdenic, G.; Delimar, M.; Robic, S. Framing the Context of Energy Poverty in Croatia: A Case-Study From Zagreb. *Energy Policy* **2020**, *147*, 111869. [\[CrossRef\]](#)
65. Piowar, A. Outline of the Problem of Energy Poverty in Poland—Trend and Extent. In Proceedings of the International Scientific Conference Hradec Economic Days, Hradec Králové, Czech Republic, 2–3 April 2020; pp. 634–641.
66. Piowar, A.; Dzikic, M. Poverty and Social Exclusion: Is This a Problem in Rural Areas in the Visegrad Group Countries? *Eur. Res. Stud. J.* **2020**, *23*, 45–54. [\[CrossRef\]](#)
67. Spirkova, D.; Zubkova, M.; Babelova, J.; Caganova, D. Socio-Economics Aspects of Housing Quality in the Context of Energy Poverty. In Proceedings of the First EAI International Summit, Smart City 360°, Bratislava, Slovakia, 22–24 November 2016.
68. Maxim, A.; Costica, M.; Apostoiaie, C.-M.; Maxim, A. Energy Poverty in Southern and Eastern Europe: Peculiar Regional Issues. *Eur. J. Sustain. Dev.* **2017**, *6*, 247–260. [\[CrossRef\]](#)
69. Maxim, A.; Mihai, C.; Apostoiaie, C.-M.; Popescu, C.; Istrate, C.; Bostan, I. Implications and Measurement of Energy Poverty Across the European Union. *Sustainability* **2016**, *8*, 483. [\[CrossRef\]](#)
70. Bouzarovski, S.; Tirado Herrero, S. Energy Poverty in Central and Eastern Europe. In *Post-Socialist Urban Infrastructures*; Tuvikene, T., Sgibnev, W., Neugebauer, C.S., Eds.; Routledge: London, UK, 2019.
71. Castano-Rosa, R.; Sherriff, G.; Solis-Guzman, J.; Marrero, M. The Validity of the Index of Vulnerable Homes: Evidence From Consumers Vulnerable to Energy Poverty in the U.K. *Energy Sources Part B Econ. Plan. Policy* **2020**, *15*, 72–91. [\[CrossRef\]](#)
72. Pociño, M.D. *Energy Poverty in Portugal: Which Households Are the Most Vulnerable?* Universidade Nova de Lisboa: Lisbon, Portugal, 2020.
73. Kontonasiou, E.; Atanasiu, B.; Mariottini, F. Tackling Fuel Poverty with Building Renovation. In Proceedings of the ECEEE 2015 Summer Study—First Fuel Now, Toulon, France, 1–6 June 2015.
74. Hegeđus, K.; Endrođi-Kovacs, V. Energy Poverty in Hungary. *Koz-Gazd.* **2019**, *14*, 190–201.
75. Tutak, M. Analysis of Similarities between the European Union Countries in Terms of Sustainable Energy and Climate Development. *MAPE* **2021**, *4*, 86–96. [\[CrossRef\]](#)
76. Pan, L.; Biru, A.; Lettu, S. Energy Poverty and Public Health: Global Evidence. *Energy Econ.* **2021**, *101*, 105423. [\[CrossRef\]](#)
77. Halkos, G.; Gkampoura, E.-C. Evaluating the Effect of Economic Crisis on Energy Poverty in Europe. *Renew. Sustain. Energy Syst.* **2021**, *144*, 110981. [\[CrossRef\]](#)
78. Papada, L.; Kaliampakos, D. Measuring Energy Poverty in Greece. *Energy Policy* **2016**, *94*, 157–165. [\[CrossRef\]](#)
79. Neacsu, A.; Panait, M.; Muresan, J.D.; Voica, M.C. Energy Poverty in European Union: Assessment Difficulties, Effects on the Quality of Life, Mitigation Measures. *Some Evidences from Romania.* *Sustainability* **2020**, *12*, 4036.
80. Primc, K.; Slabe-Erker, R.; Majcen, B.; Slabe-Erker, R. Social Policy or Energy Policy? Time to Reconsider Energy Poverty Policies. *Energy Sustain. Dev.* **2020**, *55*, 32–36. [\[CrossRef\]](#)

81. Asteriou, D.; Pilbeam, K.; Pratiwi, C.E. Public Debt and Economic Growth: Panel Data Evidence for Asian Countries. *J. Econ. Financ.* **2021**, *45*, 270–287. [[CrossRef](#)]
82. O'Hagan, A.; Forster, J.J. *Kendall's Advanced Theory of Statistics, Volume 2B: Bayesian Inference*; Arnold: London, UK, 2004.
83. Lindley, D.V.; Smith, A.F. Bayes Estimates for the Linear Model. *J. R. Stat. Soc. Ser. B (Methodol.)* **1972**, *34*, 1–18. [[CrossRef](#)]
84. Karabatsos, G. Fast Marginal Likelihood Estimation of the Ridge Parameter(s) in Ridge Regression and Generalized Ridge Regression for Big Data. *arXiv* **2014**, arXiv:1409.2437.
85. Griffin, J.E.; Brown, P.J. Some Priors for Sparse Regression Modelling. *Bayesian Anal.* **2013**, *8*, 691–702. [[CrossRef](#)]
86. Polson, N.G.; Scott, J.G. On the Half-Cauchy Prior for a Global Scale Parameter. *Bayesian Anal.* **2012**, *7*, 887–902. [[CrossRef](#)]
87. Herrero, S.T. Energy Poverty Indicators: A Critical Review of Methods. *Indoor Built Environ.* **2017**, *26*, 1018–1031. [[CrossRef](#)]
88. Faiella, I.; Lavecchia, L. Energy Poverty. How Can you Fight It, If you Can't Measure It? *Energy Build.* **2021**, *233*, 110692. [[CrossRef](#)]
89. Bardazzi, R.; Bortolotti, L.; Pazienza, M.G. To Eat and Not to Heat? Energy Poverty and Income Inequality in Italian Regions. *Energy Res. Soc. Sci.* **2021**, *73*, 101946. [[CrossRef](#)]
90. Bouzarovski, S. Energy Poverty in the European Union: Landscapes of Vulnerability. *WIREs Energy Environ.* **2014**, *3*, 276–289. [[CrossRef](#)]
91. Healy, J.D.; Clinch, J.P. Quantifying the Severity of Fuel Poverty, Its Relationship with Poor Housing and Reasons for Non-investment in Energy-saving Measures in Ireland. *Energy Policy* **2004**, *32*, 207–220. [[CrossRef](#)]
92. Kyprianou, I.; Serghides, D.; Varo, A.; Gouveia, J.P.; Kopeva, D.; Murauskaite, L. Energy Poverty Policies and Measures in 5 EU Countries: A Comparative Study. *Energy Build.* **2019**, *196*, 46–60. [[CrossRef](#)]
93. Kyprianou, I.; Serghides, D. Dealing With Energy Poverty in Cyprus—An Overview. *Int. J. Sustain. Energy* **2020**, *39*, 308–320. [[CrossRef](#)]
94. Michel, M. *Energy Poverty in Europe—A Forsaken Problem with Many Facets: A Case Study of Energy-Poor Households in Luxembourg*; Technische Universität Wien: Vienna, Austria, 2021.
95. Council of Europe Development Bank (CEB). *Energy Poverty in Europe: How Energy Efficiency and Renewables Can Help*. In *CEB Studies*; Council of Europe Development Bank (CEB): Paris, France, 2019.
96. Al-Tal, R.; Murshed, M.; Ahmad, P.; Alfar, A.J.K.; Bassim, M.; Elheddad, M.; Nurmakhanova, M.; Mahmood, H. The Non-Linear Effects of Energy Efficiency Gains on the Incidence of Energy Poverty. *Sustainability* **2021**, *13*, 11055. [[CrossRef](#)]
97. Bukari, C.; Broermann, S.; Okai, D. Energy Poverty and Health Expenditure: Evidence from Ghana. *Energy Econ.* **2021**, *103*, 105565. [[CrossRef](#)]

Article

Identifying Potential Indicators of Neighbourhood Solar Access in Urban Planning

Agnieszka Czachura *, Niko Gentile, Jouri Kanters and Maria Wall

Division of Energy and Building Design, Department of Building and Environmental Technology, Lund University, P.O. Box 118, SE-221 00 Lund, Sweden

* Correspondence: agnieszka.czachura@ebd.lth.se

Abstract: Solar access describes the capacity of urban spaces to receive sunlight and daylight. Rapid urbanization and unbridled densification pose a threat to sustainable solar access, reducing the penetration of sunlight and daylight into cities. To effectively assess solar access at such an early design stage, at the urban planning level, it is critical that evaluation metrics are simple and reliable. This paper examines a cross section of solar metrics, from simple to more complex ones, to find potential solar performance indicators for urban planning evaluations. The metric datasets were created based on iterations of homogeneous neighbourhood designs, based on the three commonest typologies in the Swedish context: courtyard, slab, and tower. The results were validated using case studies sampled from districts of Malmö. The findings indicate that simple geometrical and latitudinal metrics may be suitable for assessing the solar access of urban designs due to high correlation with built density. Potential performance indicators aimed at indoor and outdoor evaluation of daylighting (VSC, SVF) and sunlighting (ASH_F, RD_G) in urban planning stages were suggested. Possible methods of applying the provided metric database into assessments were proposed. Future work should find evidence-based thresholds for the metric values to establish performance benchmarks.

Keywords: solar access; daylight; sunlight; Kendall correlation; regression analysis; urban planning; performance indicator; neighbourhood scale

Citation: Czachura, A.; Gentile, N.; Kanters, J.; Wall, M. Identifying Potential Indicators of Neighbourhood Solar Access in Urban Planning. *Buildings* **2022**, *12*, 1575. <https://doi.org/10.3390/buildings12101575>

Academic Editors: Roberto Alonso González Lezcano, Francesco Nocera and Rosa Giuseppina Caponetto

Received: 31 August 2022

Accepted: 28 September 2022

Published: 30 September 2022



Copyright: © 2022 by the authors. Licensee MDPI, Basel, Switzerland. This article is an open access article distributed under the terms and conditions of the Creative Commons Attribution (CC BY) license (<https://creativecommons.org/licenses/by/4.0/>).

1. Introduction

Sunlight is a valuable resource in cities, as it contributes to multiple sustainability and wellbeing goals. Solar energy impacts the building heat and energy balance, plays a major role in energy conservation strategies [1–3], and is essential for integrating on-site solar energy systems [4–6]. Furthermore, sunlight has the potential to improve mood [7,8], increase immune response [9], and kill germs [10], contributing to good health and the wellbeing of residents. The amount of sunlight reaching urban areas is commonly known as solar access. It defines the capacity of outdoor and indoor living spaces to receive sunlight.

The United Nations (UN) predicts that, by 2050, two-thirds of world's population will live in cities [11]. Cities will have to accommodate future inhabitants through new developments and densification projects, which has been observed in the past few decades already [12]. The rapid urbanization and increased densification of inhabited land pose a threat to sustainable solar access, reducing the availability of sunlight and daylight in cities. A study investigating daylighting in Swedish multi-family dwellings demonstrated that houses built in the years 1940–1960 received the highest solar access, which in later decades decreased due to an evident densification trend [13]. These authors also showed that increased urban density reduces chances to comply with daylight regulation.

Urban planners decide the form and layout of urban environments which define urban density and the amount of solar access. Studies have shown that urban planners often lack the expertise to carry out daylight assessments [14,15]. At such an early design stage, they also have insufficient data input for advanced simulation methods, missing crucial

information about, for example, window placements, material properties, roofscapes, balconies, and internal layouts. There is a need for simpler methods and assessment metrics that could be implemented in early planning and massing stages when available input data is limited [16,17].

A previous review on solar performance metrics for urban planning indicated that simpler metrics are more suited for early design stages due to their lower complexity and level of data input required [18]. The review identified relevant metrics and found those metric classes that may be adequate for urban planning purposes: geometrical, latitudinal, and external climatic. While the metrics' suitability was assessed based on literature, little is still known about the metrics' relationships, impact, and correlations. Many previous studies focused on examining differences between urban design typologies rather than metrics and their best application [19–22].

Research into the domain of solar performance metrics for urban planning focuses mainly on: (a) evaluation of metrics and their relationships to increase confidence and knowledge in their application in solar performance assessments, (b) benchmarking metric values to establish performance criteria that can be used in design evaluations, and (c) establishing working paradigms for urban solar assessment methods with the use of multiple metrics and relevant criteria. The present paper deals with the first objective (a) and provides a database foundation for the second objective (b). Finding suitable metrics will help in establishing solar assessment paradigms for urban planning practice. Because metrics that are suitable for urban planning tend to be simple (carrying limited information), assessment workflows might need to integrate a combination of several metrics into the method.

The purpose of this paper is to analyse a selection of existing and newly developed solar metrics as potential candidates as performance indicators in design assessments. Metric datasets were evaluated for their relationship to each other and their suitability for early design assessments. The question to be addressed is whether simpler metrics can substitute for more complex ones in measuring solar access, and how can these metrics be applied in solar neighbourhood assessments. This paper focuses on metrics which are numeric and whose function is designated as comparative [18], meaning that they can provide reduced bias in the assessments of multiple different designs.

2. Methods

A selection of solar performance metrics was calculated using a large dataset of homogenous computer-based neighbourhood design iterations and a small set of existing neighbourhood case studies, which were used for the purpose of validating the outcomes based on the larger virtual design dataset. The methodology section consists of four parts: (a) modelling the neighbourhood design iterations, (b) selection of case studies, (c) solar performance metrics, and (d) data analysis. Previous work on solar performance metrics used in urban morphology studies provided grounding to the present study and informed the selection of solar metrics for the analysis [18]. The scope of this study was limited to residential multi-family neighbourhoods in the northern latitudes with a focus on the Swedish context.

2.1. Neighbourhood Design Iterations

The selection of typical Swedish neighbourhood typologies for this study was conducted based on the existing Swedish residential stock of multi-family apartment blocks. Most of the Swedish residential stock (52%) consists of multi-dwelling buildings, and their proportion is increasing [23]. In the years 2011–2020, there were three times as many dwellings built as multi-family buildings than those of single- or double-dwelling building type. A survey into Swedish urban morphology revealed that the most prevalent multi-family building types can be reduced to courtyard, slab, and tower typologies [24]. In Malmö, slab and courtyard typologies appear to be the most dominant (Figure 1); other forms such as tower, L-shaped, and U-shaped exist but are less common. Although towers were found less frequently in Malmö, they appear more frequently in higher density cities,

including the Swedish capital city, Stockholm. Thus, for this study, three neighbourhood typologies were selected for generating design iterations and further solar performance analysis: courtyard, slab, and tower (Figure 2A–C).



Figure 1. Examples of existing urban neighbourhoods and building types in Malmö, where slab and courtyard typologies prevail. Imagery ©2022 Google, Imagery ©2022 Lantmäteriet/Metria, Maxar Technologies, Map data ©2022.

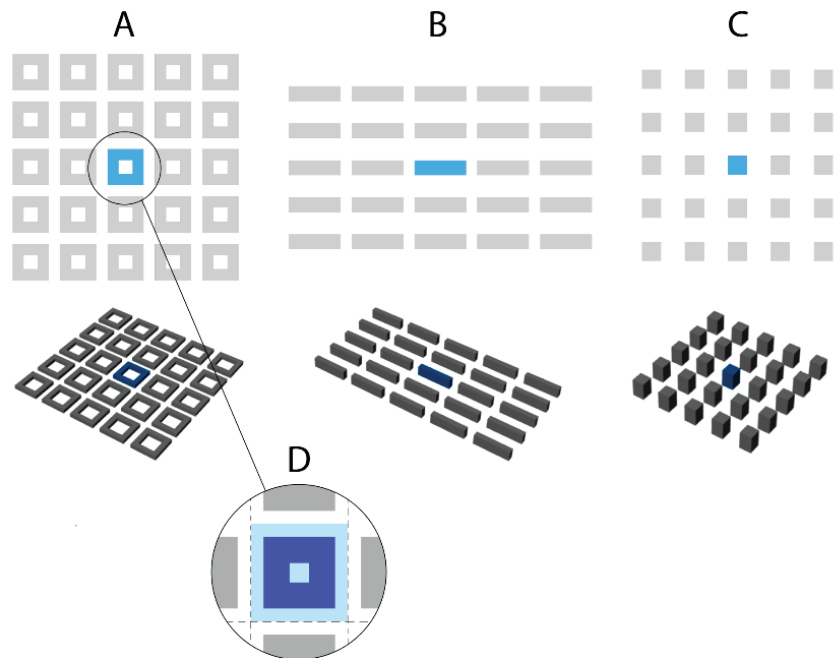


Figure 2. Exemplary iterations of the three studied neighbourhood typologies in top and perspective views: (A)—courtyard grid, (B)—slab grid, (C)—tower grid, and (D)—example of an analysed representative unit, comprising of one building and its plot (top view).

In order to facilitate the iterative modelling process, the neighbourhoods were modelled as homogeneous. Buildings within a neighbourhood were evenly spaced and arranged in a large, 5×5 unit orthogonal grid to include context shading (Figure 2A–C). Since the neighbourhoods were modelled homogeneously, only the central building unit and the immediate area around it were analysed for solar access i.e., the middle unit was considered

representative of the entire neighbourhood (Figure 2D). Vegetation and urban infrastructure were not included. Buildings were modelled without roof or façade details, which in digital city modelling is known as Level of Detail 1 (LoD1) [25]. The 3D models of design iterations were generated using Rhinoceros 7 [26] with Grasshopper [27].

Neighbourhood design iterations were created assuming ranges of geometrical design constraints. The dimensional constraints of the modelled neighbourhood geometries were intended to provide an adequate representation of the typical Swedish residential stock and a reasonable framework for the metric datasets. The discrete (countable) parameters are listed in Table 1, and the corresponding dimensions are marked in Figure 3. The number of design iterations changes in respect to the taxonomical class of calculated metrics; geometrical (G-) metrics have a smaller number of individual iterations because the building orientation variable is unapplicable for these metrics. Wall thickness (0.5 m) and storey height (3.0 m) were set as fixed values to calculate floor areas and space volumes. The plot offset was the distance from building façade edge facing outwards to the plot edge. For slab iterations, the offset distance was measured from the longer façade edge, and the distance from the short edge to the plot edge was equal to half the offset. This was found to be a common spatial feature in real slab neighbourhood cases.

Table 1. Range (X-Y) and number (N, in brackets) of discrete variables used in neighbourhood design iterations and the total number of iterations.

Typology	Variables					Total No. of Design Iterations [G-Metrics/Other Metrics]
	Dimension, B [m]	Plot Offset [m]	Building Depth, D [m]	Storeys	Rotations [°]	
Courtyard	12–92 (11)	8–32 (7)	16 (1)	2–10 (5)	0–45 (2)	385/770
Slab	32–128 (13)	8–32 (7)	16 (1)	2–10 (5)	0–90 (3)	455/1365
Tower	16–20 (3)	4–32 (15)	=B	2–20 (10)	0–45 (2)	450/900

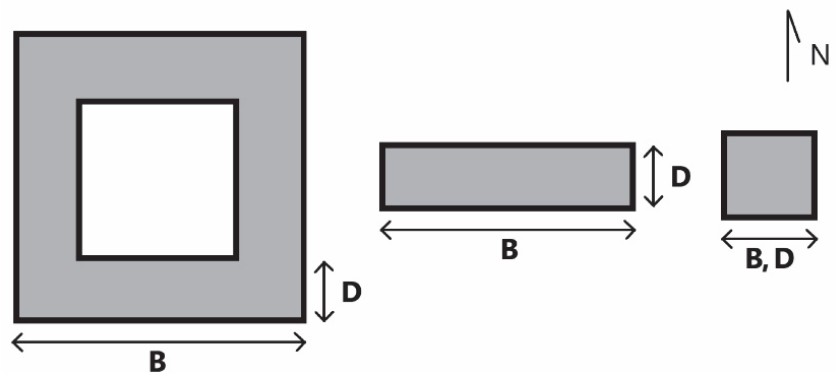


Figure 3. Courtyard, slab, and tower typologies (from left to right) presented in top view at 0° rotation: The letters ‘B’ and ‘D’ denote the dimension variables specified in Table 1.

The original dataset included more extreme cases (e.g., towers having 20 storeys and only 8 m span between buildings). However, iteration cases with a density indicator and a floor area ratio (FAR), larger than 4 were removed, as they represented highly unrealistic urban scenarios [28,29]. Even in the high-density city of New York, the maximum FAR averages 2.4 [30]. The FAR distribution of the original dataset is highly skewed (Figure 4). Neighbourhood design iterations with FAR above 4 were outliers of the dataset, as seen from the box plot in Figure 4. Removing the outliers provides a more balanced dataset.

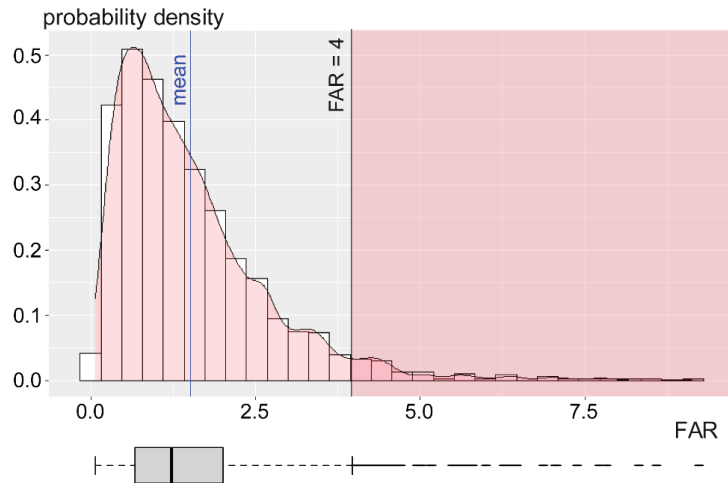


Figure 4. Population density of the FAR metric with original mean line (blue) and removed portion of iteration cases (where FAR > 4). A box plot of the FAR dataset is included at the bottom.

2.2. Case Studies

Case studies of seven existing neighbourhoods situated in Malmö, Sweden, were used to validate the iterative design datasets that were generated from hypothetical neighbourhoods (Section 2.1). The case studies were comprised of the same typologies as the iterations and included three courtyard neighbourhoods, three slab neighbourhoods, and one tower neighbourhood. The tower typology is underrepresented in the urban context of Malmö, therefore only one tower neighbourhood was included. The selected case studies are presented in Figures 5 and 6.

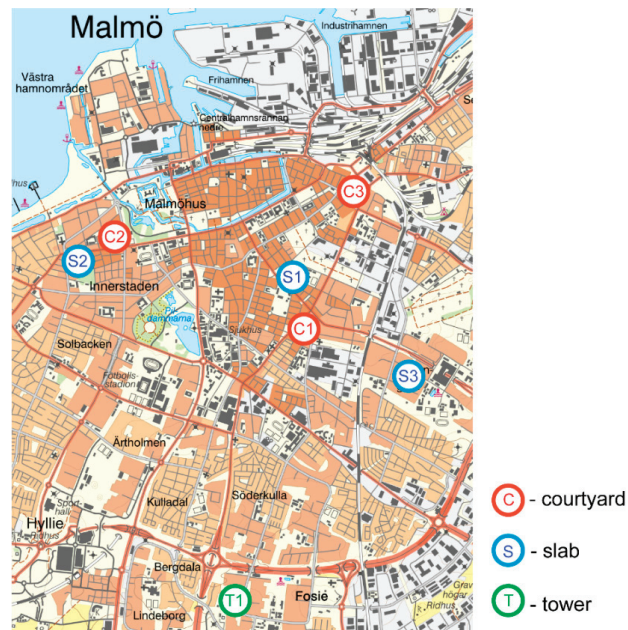


Figure 5. Map of Malmö with neighbourhood case study locations. Background map (1:50,000, raster) © Lantmäteriet (2022).

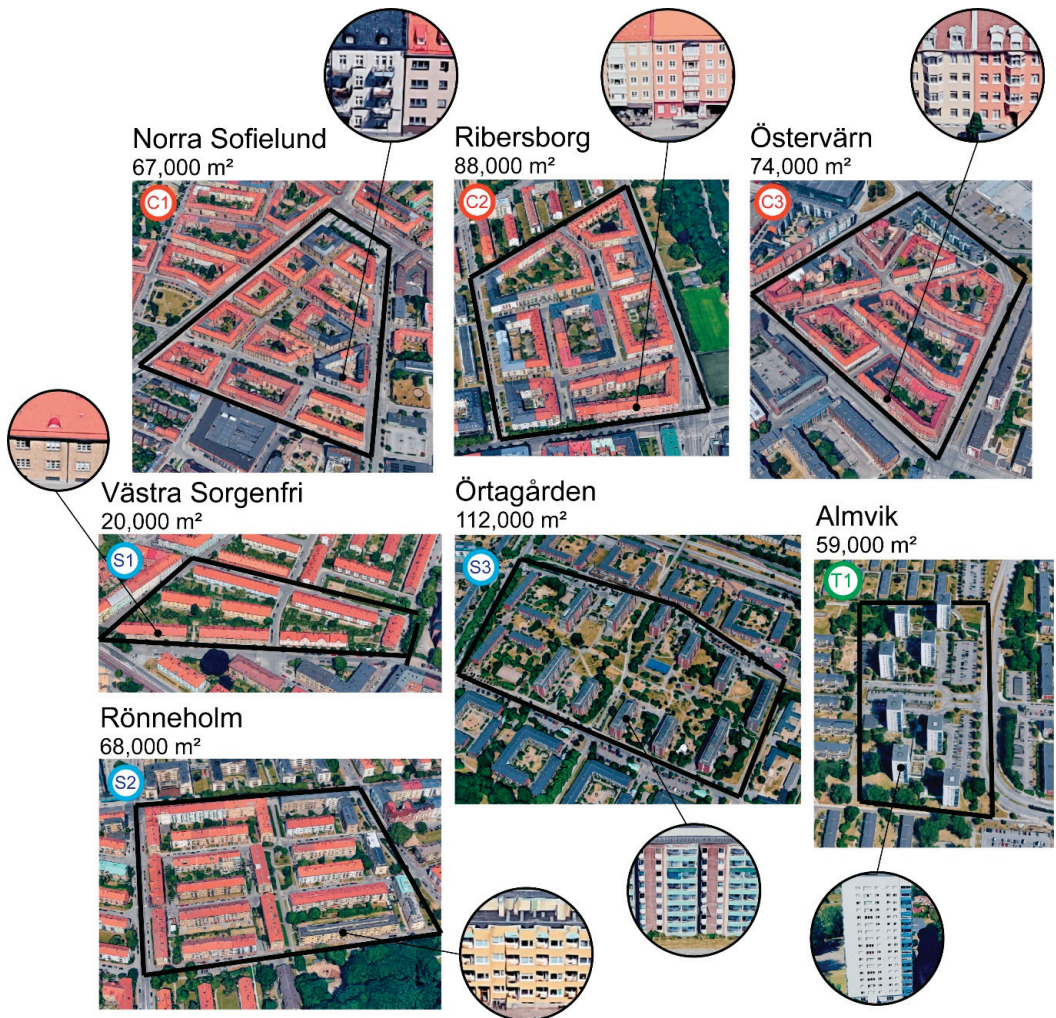


Figure 6. Malmö neighbourhood case studies used in analysis. Case study codes link to markings in the map in Figure 5. Imagery ©2022 Google, Imagery ©2022 Lantmäteriet/Metria, Maxar Technologies, Map data ©2022.

The identification of suitable neighbourhood areas for case studies was governed by preassigned selection criteria. The definition of a neighbourhood is vague; many varying neighbourhood concepts exist, and the classification of the extents of one neighbourhood tends to be blurry. The concept of a “neighbourhood unit” was used in this paper as a framework for the identification of neighbourhood boundaries [31–33]. However, the factors that define a neighbourhood should remain flexible, diverse, and sensitive to the local context [34,35]. Swedish cities differ slightly from the West European cities as they developed in a more decentralized fashion, and they tend to be less densely populated [36]. They also seem to lack a precise definition of a neighbourhood [37]. The selection criteria were thus adapted to reflect the understanding of a neighbourhood in the Swedish context. The criteria were also intended to match the attributes assigned to the hypothetical neighbourhood design iterations in order to provide a suitable validation framework for the solar metrics. The following selection criteria were used:

- The neighbourhood shall not be intersected by large traffic roads,
- The neighbourhood must be comprised of residential multi-storey buildings and include one of the three analysed typologies (courtyard, slab, tower),
- The neighbourhood shall be nearly homogenous (composed of the same typology),
- The neighbourhood shall be surrounded by built context of similar height,
- The case studies shall come from different administrative districts (sv: delområde).

The neighbourhoods were modelled in Rhinoceros 7. Geodata used for generating 3D models was obtained from Lantmäteriet [38]. The modelling details were similar to those of the iteration dataset: the geometries were simplified to LoD1, which means that roof and ground surfaces were horizontal and flat. Façade details, such as windows and balconies, were not included in the model, and neither were the vegetation and urban infrastructure elements.

2.3. Solar Performance Metrics

The selection of metrics for the analysis was based on an earlier review [18], and the metrics are listed in Table 2. All metrics belong to one of three classes of metrics: geometrical (G-metrics), latitudinal (L-metrics), and external climatic (EC-metrics). These three classes appear most suitable for solar assessments in urban planning stages due to the lower level of complexity compared with internal climatic metrics [18]. Only metrics with comparative and conforming functions [18] were used. Most of the metrics were sourced from previous literature, though there were also new metrics generated for this study; these were marked in Table 2 with an asterisk. Two types of urban surfaces were analysed for solar access depending on the assumed outdoor or indoor performance perspective, i.e., ground and facades (Figure 7). The analysis surfaces are given in the ‘Subject’ column of Table 2 and indicated with ‘G’ or ‘F’ suffix in metric acronyms. Roofs were not considered in this study because of their flat horizontal shape and the homogeneity of neighbourhood building heights in the iteration cases, which means that the roofs are receiving maximal solar access, and little variation due to design choices can be achieved. Metrics were simulated using Ladybug and Honeybee [39] in Grasshopper for Rhinoceros 7 [26].

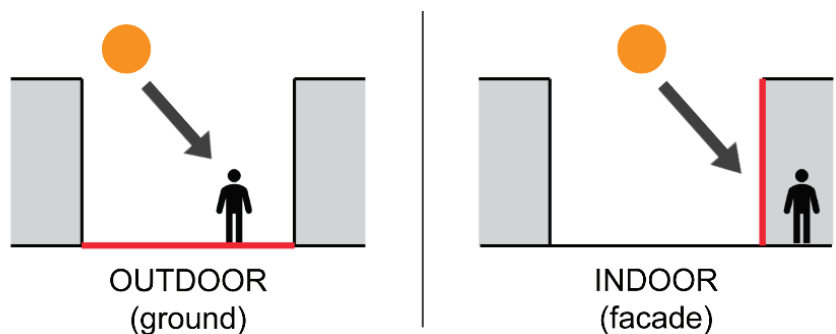


Figure 7. Two types of analysis surfaces (ground—left, façade—right) used to assess the outdoor and indoor environment.

G and L metrics that were calculated on façades (VSC, TH_F, ASH_F, RD_F) were simulated for a single string of points located on the façade at the height of 1.4 m and spaced 1 m apart (Figure 8), as solar access at the ground floor guarantees even better solar access at upper levels. Façade-based EC metrics measure surface irradiation, which affects the building’s overall thermal balance and solar energy potential, and thus, assessing the entire surface was deemed necessary to assess the radiation aspects. The radiation metrics were simulated for the entire façade surfaces (Figure 8).

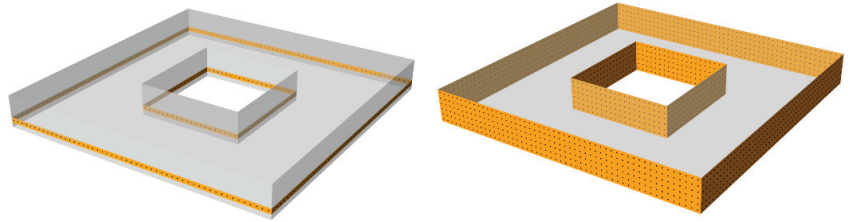


Figure 8. Two kinds of simulation point grids for façade-based metrics. **Left:** single string of points at 1.4 m height. **Right:** the whole façade made into a point grid.

Table 2. List of metrics selected for analysis. Metrics that were not sourced from literature were marked with an asterisk.

	Acronym	Name	Subject	Calculation or Simulation Method [Unit]
G-metrics	FAR	Floor Area Ratio	whole	Ratio of gross floor area to plot area [m^2/m^2 ; used as unitless]
	VAR	Volume Area Ratio	whole	Ratio of gross building volume to plot area [m^3/m^2 ; used as unitless]
	SAR *	Surface Area Ratio	whole	Ratio of gross external building surface area to plot area [m^2/m^2]
	OSR	Open Space Ratio	whole	Ratio of open space area to gross floor area [m^2/m^2]
	SVF	Sky View Factor	ground	Grid-based (1 m), 145 sky patches, cosine-weighted sky dome [%]
	VSC	Vertical Sky Component	façade (string)	At 1.4 m height, 1024 sky patches, CIE overcast sky [%]
L-metrics	APS	Area of Permanent Shadow	ground	Grid-based (1 m), ray intersection, fraction of the grid open to no direct sunshine on 21 March
	TH_G	Two-Hour area	ground	Grid-based (1 m), ray intersection, fraction of the grid open to 2 or more hours of direct sunshine on 21 March
	TH_F *	Two-Hour area	façade (string)	Grid-based (1 m), ray intersection, fraction of the grid open to 2 or more hours of direct sunshine on 21 March
	ASH_G *	Annual Sunlight Hours	ground	Grid-based (1 m), average direct solar access as fraction of all annual hourly sun vectors
	ASH_F *	Annual Sunlight Hours	façade (string)	Grid-based (1 m), average direct solar access as fraction of all annual hourly sun vectors
	RD_G *	Reference Day (Sunlight Hours)	ground	Grid-based (1 m), ray intersection, average hours of direct sunshine on 21 March [h]
	RD_F *	Reference Day (Sunlight Hours)	façade (string)	Grid-based (1 m), ray intersection, average hours of direct sunshine on 21 March [h]
EC-metrics	APSH	Annual Probable Sunlight Hours	façade (string)	Grid-based (1 m), average direct solar access as fraction of all annual hourly sun vectors (relative to cloud coverage: e.g., 40% cloudiness for a given hour gives 0.6 h of direct sun)
	RAD_F	Solar radiation (mean)	façade	Grid-based (1 m), annual solar radiation mean per façade area [kWh/m^2]
	nRAD_F	Solar radiation (norm.)	façade	Grid-based (1 m), total annual radiation normalized by gross floor area [kWh/m^2]
	nPV_F	PV potential	façade	Grid-based (1 m), surface area with solar radiation above $600 \text{ kWh}/\text{m}^2$ normalised by floor area [m^2/m^2]

There are different levels of site and layout factors that influence metrics, depending on their class, which are presented in Table 3. Location has impact on L- and EC-metrics; G-metrics are unaffected by location. Two European climates were investigated in the iterations analysis: Stockholm (59.65° N , 17.95° E) and Frankfurt (50.05° N , 8.60° E). Both locations belong to the transitional temperate zone of warm climate according to the classification by the European Environment Agency [40] yet are located at the northern and southern end of its reaches, which affects the amount of potential solar access. The case studies were simulated for the same locations. IWEC (international weather for energy

calculations) EPW (energy plus weather) annual weather files were used for both Stockholm and Frankfurt [41].

Table 3. The main influencing factors of each solar metric class.

G-Metrics	L-Metrics	EC-Metrics
geometrical dimensions	geometrical dimensions latitude orientation	geometrical dimensions latitude orientation insolation (climate)

2.4. Data Analysis

Metric datasets were analysed for correlations. The analysis method was two-fold: first, a Kendall correlation analysis was performed to assess the strength of associations based on its τ_B value, and then a pairwise graphical evaluation of metric relationships was conducted to assess the functions' linearity and variance.

The datasets did not meet the necessary conditions for linear regression and Pearson correlation analyses. However, for those cases of pairwise metric relationships that resembled a linear function, Pearson correlation (r value) and linear regression analyses were conducted. These analyses were carried out for illustrative purposes and should be treated with caution since required assumptions were not met. Statistical analyses were performed in RStudio [42].

The suitability iteration-based datasets were validated by comparing them with case study datasets for each metric pair. The test hypothesis was that the slope and intercept of the iteration-based regression line of a given solar metric would fall within a 95% confidence interval (CI) of the slope and intercept ranges of the case studies.

Pre-analysis of simulated datasets indicated that it is sufficient to focus on only one climate location and analyse metric relationships for that climate. Thus, for the ease of analysis, Frankfurt was selected as the base climate for analysis and results presentation in this paper. All datasets from this study were made available for further inspection and reuse and were uploaded to a scientific data sharing repository [see the Data Availability Statement].

3. Results

3.1. Metric Correlation

The results of the Kendall correlation analysis are presented in Figure 9. G-metrics show good correlation among themselves and with the comparative L- and EC-metrics. On the other hand, the correlation data hints that conforming metrics (metrics that are based on compliance to a threshold, e.g., pass/fail) do not correlate well with other metrics nor with each other. Furthermore, normalised radiation metrics did not prove high correlation to other metrics. The correlation study gave an initial indication of the strength of metrics' pairwise relations, which allowed for the identification of metrics with high correlation scores for further graphical analysis and interpretation. In Figure 9, the high scoring metrics were highlighted (in bold).

Additionally, a Pearson correlation was conducted to examine the linearity of metric relationships. It indicated that functions of metric pairs FAR-VAR and SVF-VSC might be linear because in addition to the high Kendall correlation, their Pearson correlation results were also close to 1.

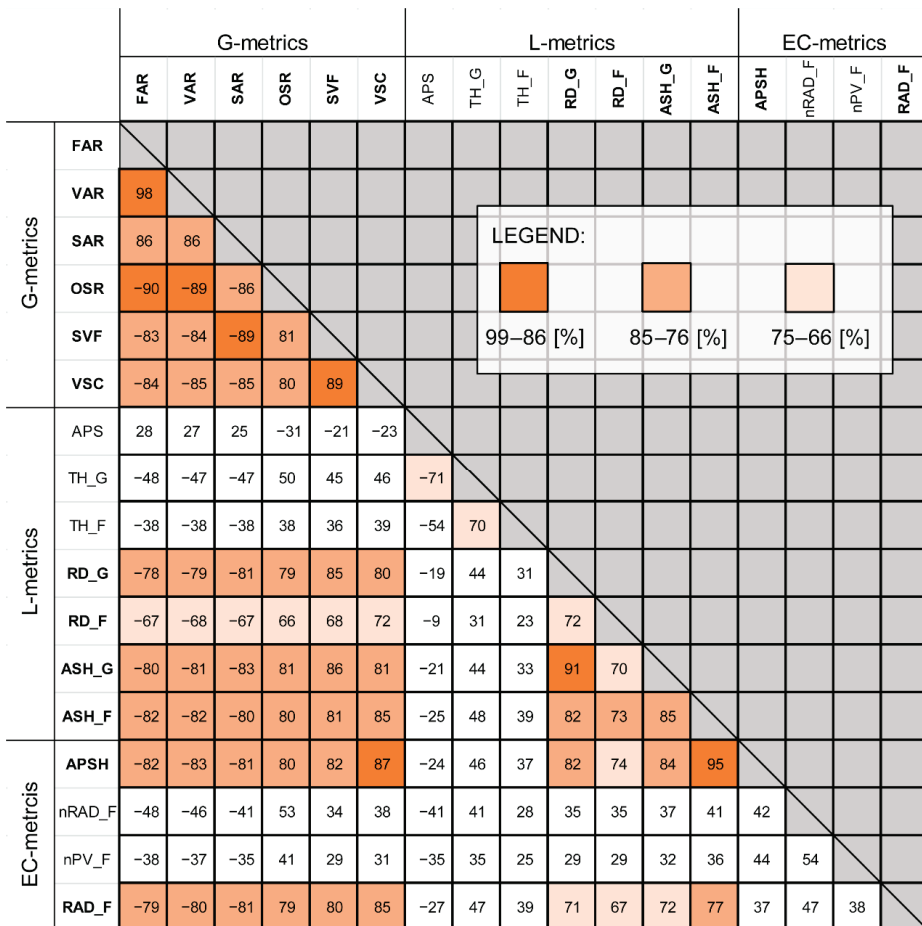


Figure 9. Correlation (Kendall) of metrics from iteration-based datasets simulated for Frankfurt and Stockholm presented in percentage format. τ_B values equal to 100% indicate perfect agreement. Metrics were described in Table 2.

3.2. Urban Density

Two metrics pertaining to urban density were studied: FAR and VAR. They demonstrated a high Kendall correlation ($\tau_B = 0.98$) and a potentially linear relationship ($r = 1.00$).

Figure 10 presents VAR as a function of FAR. The design iterations (black dots) show a nearly perfect linear function, while the case studies (red dots) diverge from the linear regression line. It is observed that the case studies do not fit the function well; that is because the case study storey heights varied, while storey height in design iterations was a constant.

Equation (1) explains the linear relationship between FAR and VAR, assuming that the storey height (h_s) is constant.

$$VAR = FAR \cdot h_s, \tag{1}$$

Figure 10 suggests that VAR is a better indicator of urban density for assessing real neighbourhood examples for solar access because it is free of the independent variable: storey height. Indeed, FAR has been used in studies where urban density is an indirect indication of population density, such as in land or property value, and in transportation studies [30,43,44]. VAR might be a better indicator of urban density for solar access considerations because it pertains to volumes of buildings rather than population. Therefore,

throughout this study, for the purpose of relating metrics to the urban density of the designs, the VAR metric was used as a density indicator.

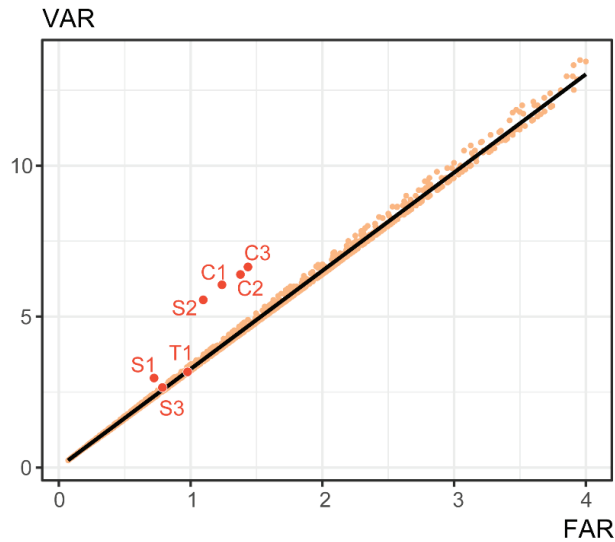


Figure 10. Iteration-based linear regression analysis of urban density metrics, FAR and VAR. Case studies are marked in red with labels (codes explained in Figures 5 and 6).

Figure 11 presents the VAR iteration-based dataset distribution and the density of the case studies (blue dots). The iteration-based distribution is positively skewed. Although the case studies were randomly selected, their densities distribute roughly symmetrically on the opposite sides of the mean line and form two clusters. An explanation for this could be found in the consistency of spatial or temporal aspects in the urban planning practices in Malmö city.

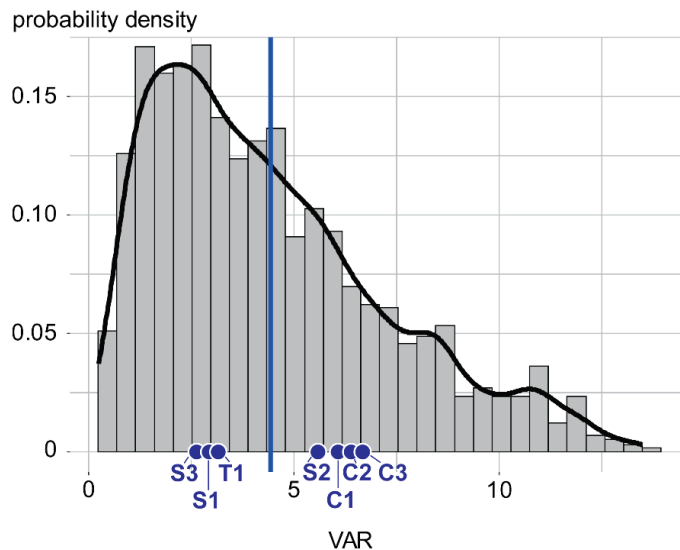


Figure 11. Probability distribution of VAR dataset. Blue line marks the dataset mean, and blue dots mark the case study values (codes explained in Figures 5 and 6).

3.3. G-Metrics

In this section, the results presented as metric datasets in graphs are identical for both simulated locations, Stockholm and Frankfurt, as G-metrics are only influenced by the geometry layout (see Table 3 in Section 2.3).

The G-metrics demonstrate a high Kendall correlation (Figure 9). The Pearson correlation analysis on these metrics resulted in equally high scores on the level of $r \approx 0.95$, except for the OSR metric. Graphs in Figure 12, which display pairwise plots, show a nearly linear relationship for most of the G-metric pairs.

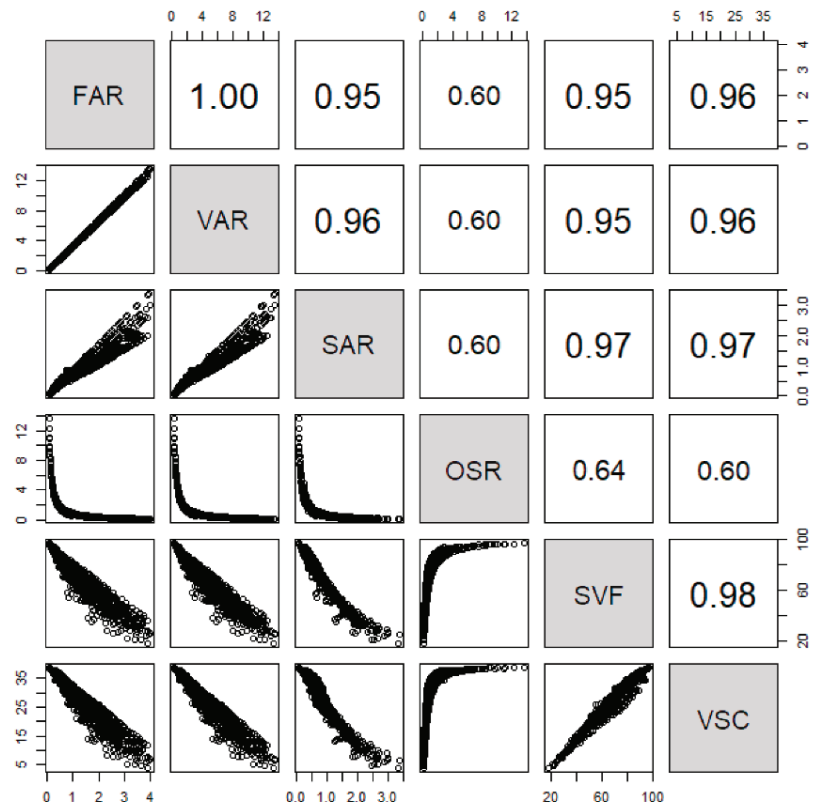


Figure 12. Summary of pairwise relationships between G-metrics with graphical plots (lower half) and Pearson correlation results (upper half).

Among the morphological G-metrics, FAR, VAR, and SAR have similar correlation scores and appearance of graphs, which may indicate that they play a similar role in assessment and could be used interchangeably. SAR as a function of either of the density metrics, FAR or VAR, forms a fan-shaped data graph, meaning that the variance becomes larger the higher the metric values. The OSR metric, albeit having similar correlation scores, has a reciprocal graph shape. Since OSR is a ratio that takes similar inputs as FAR, it is considered inferior to FAR because of the unfavourable graph appearance.

To further investigate the relationships between G-metrics, a linear regression analysis was conducted. Metrics SVF and VSC were tested against density VAR (Figures 13 and 14) and against each other (Figure 15). The case studies fit well within the iteration-based datasets, as they appear close to the regression lines and within the simulated iterative designs. The graphs in Figures 13 and 14 show fan-shaped relationships, which implies a heterogenous variance in the data. The SVF-VSC graph (Figure 15) shows a linear function with lower variance, though the function loses linearity at the data tails.

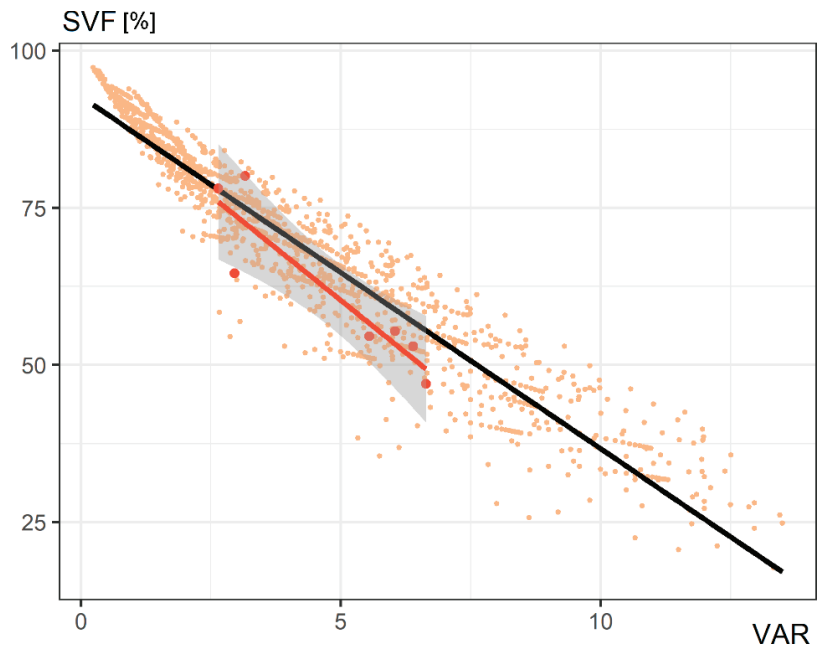


Figure 13. Linear regression function of metrics VAR and SVF based on neighbourhood iterations (black line) and case studies (red line), including the 95% CI for the case studies regression line indicated by the grey area.

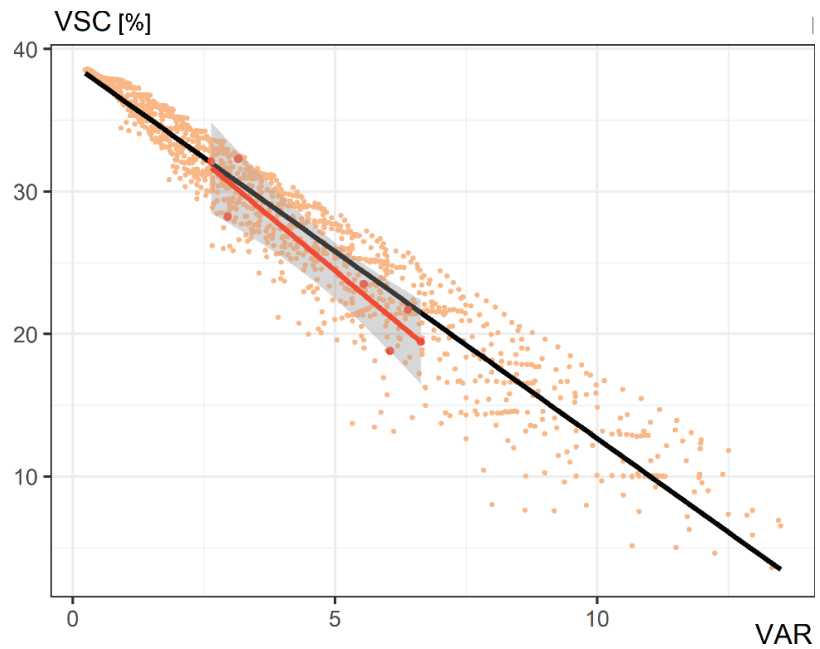


Figure 14. Linear regression function of metrics VAR and VSC based on neighbourhood iterations (black line) and case studies (red line), including the 95% CI for the case studies regression line indicated by the grey area.

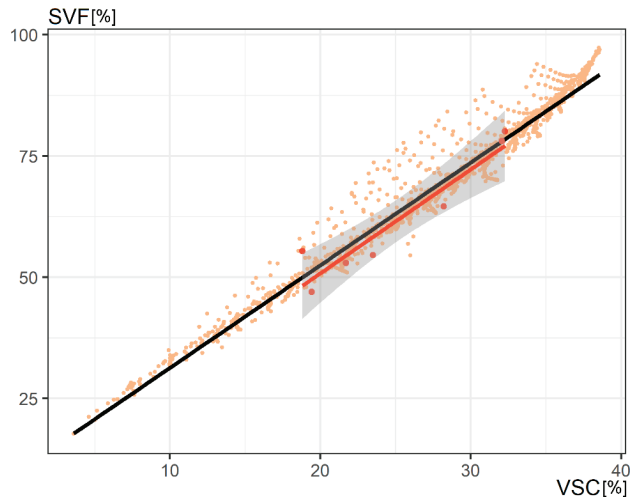


Figure 15. Linear regression function of metrics VSC and SVF based on neighbourhood iterations (black line) and case studies (red line), including the 95% CI for the case studies regression line indicated by the grey area.

3.4. L-Metrics

L-metrics communicate solar access based on a set time period. The length of the reference time period affects the intensity of the computer simulation. To simplify the calculation, legislation normally recommends checking solar access for only a single reference day [45]. Looking at two L-metrics, RD_G and ASH_G, which were simulated at the ground surface but assume different time periods (reference day and a whole year), their graph shows linear characteristics (Figure 16). This relationship hints that the single-day-based RD_G metric may be used instead of the annually based ground ASH_G metric, which assumes a longer simulation period and thus takes more time to simulate. Additionally, the case studies regression line is nearly colinear with the iteration-based regression line, which validates the occurring relationship between RD_G and ASH_G.

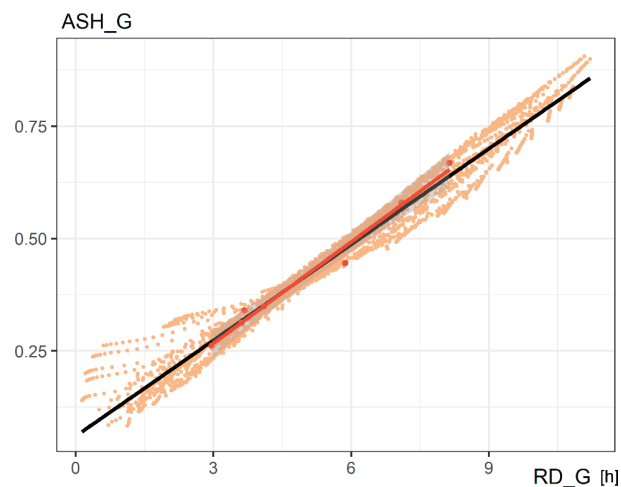


Figure 16. Linear regression function of ground-based L-metrics RD_G and ASH_G based on neighbourhood iterations (black line) and case studies (red line), including the 95% CI for the case studies regression line indicated by the grey area.

The ground-based L-metrics (RD_G and ASH_G) show a non-linear relationship with density expressed by VAR (Figure 17). However, linear regression lines drawn for the case studies seem to approximate the respective parts of the iteration-based functions. In particular, the case studies regression line for the RD_G metric appears to be a close approximation of the original iteration-based trendline. Notably, graphs showing relation of density to ASH_G and RD_G have a similar shape (Figure 17), which is in line with their high mutual correlation and linear relationship in Figure 16.

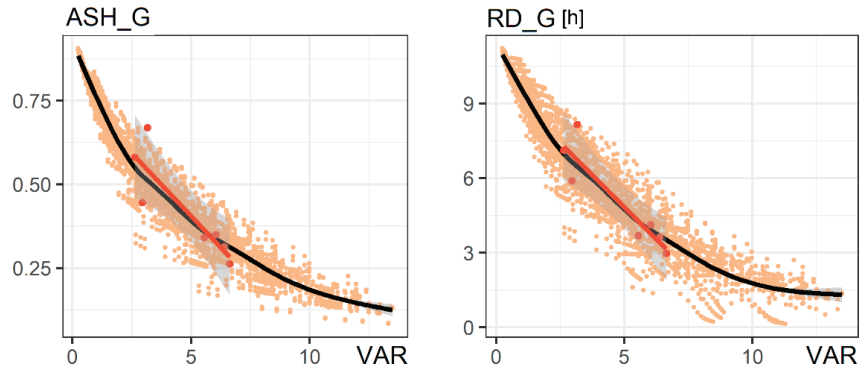


Figure 17. Non-linear regression functions of density metric VAR with L-metrics ASH_G (left) and RD_G (right) based on neighbourhood iterations (black line) and case-study-fitted linear regression line (red) with 95% CI in grey. The case study linear regression approximates the respective section of the non-linear regression from iterations.

Looking at the same metrics (RD and ASH) but calculated for the facades, the relationship does not show the same high-definition linearity, and a larger variance is present in the datasets (Figure 18). Similarly, the relation of RD_F to VAR is dispersed and non-linear (Figure 19). The dispersion and lack of continuity in the data could be attributed to the orientation of the analysis surfaces. Facades are vertical surfaces, which see only half of the sky dome for any given façade orientation, as opposed to the ground surface, which sees the whole sky dome. For the iteration-based neighbourhood cases, four facades facing four different directions (right-angled) were considered. Slab typology is more sensitive to rotation because it has two lines of symmetry (the square courtyard and tower have four), and this sensitivity can be seen in the graph (Figure 19). Furthermore, RD_F is a simpler version of the direct sunlight hours metric and is only based on a single reference day (21 March), as opposed to the whole year in the calculation of ASH_F; the simulation uses 12 hourly solar vectors for calculation of the sunlight hours. The sparse number of vectors means that the measurement may lack continuity, as time is divided into few discrete intervals. This can create a stepwise appearance of the datasets in the graph. The difference is apparent when comparing the relationships of the two façade L-metrics (RD and ASH) to VAR (Figures 19 and 20). The ASH_F metric not only shows higher correlation scores (Figure 9), but its relation graph also has a nearly linear data distribution (Figure 20), particularly for the lower densities.

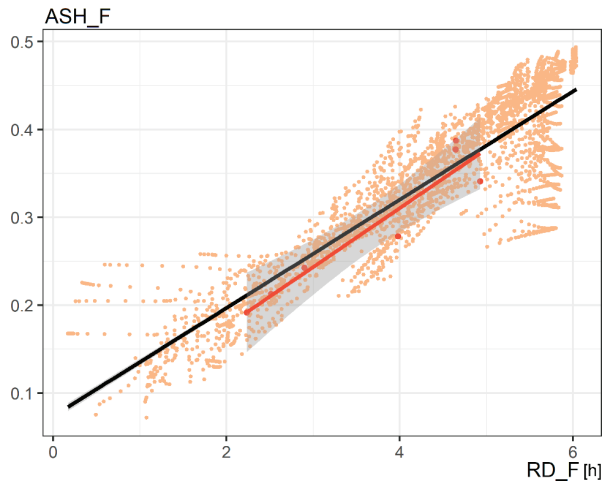


Figure 18. Linear regression function of façade-based L-metrics RD_F and ASH_F based on neighbourhood iterations (black line) and case studies (red line), including the 95% CI for the case studies regression line indicated by the grey area.

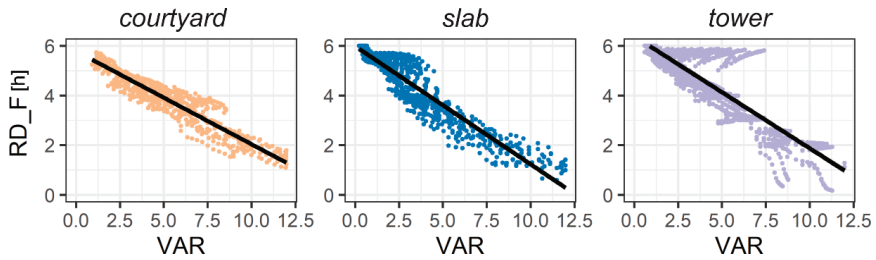


Figure 19. Linear regression functions of metrics VAR and RD_F based on neighbourhood iterations (black line), presenting results for each neighbourhood typology in a separate graph.

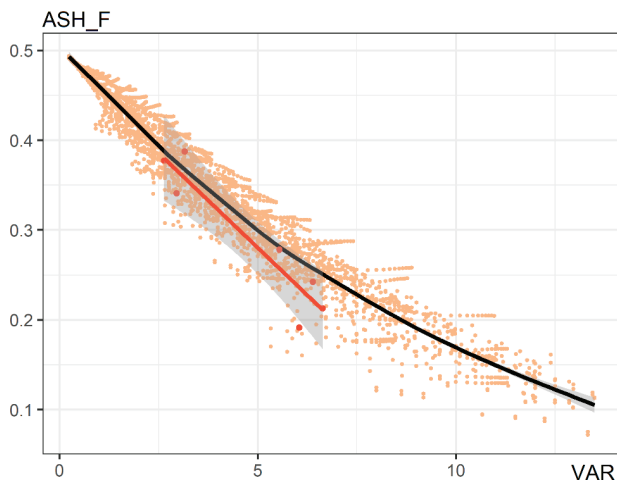


Figure 20. Non-linear regression function of density metric VAR with L-metric ASH_F based on neighbourhood iterations (black line) and case-study-fitted linear regression line (red) with 95% CI in grey.

3.5. EC-Metrics

APSH was the only metric in the EC-metric class that was not based on radiation; it was built on the hourly scores of the ASH_F metric with added information about cloud coverage, which was taken directly from the weather file. The correlation results for APSH (Figure 9) show almost identical scores as the simpler ASH_F metric. The correlation between ASH_F and APSH was at the level of 0.95, and their relationship was linear. This suggests that the simpler L-metric ASH_F may be used instead of the APSH, as there is no need to introduce an extra level of complexity with APSH.

Figure 21 shows an example of how a graph with a normalized (in this case per floor area) or conforming (threshold based) radiation metric tends to look. The data distribution is scattered and clustered in a stepwise manner due to the initial discrete parameter settings. The normalized metrics also show low correlation levels with other metrics (Figure 9).

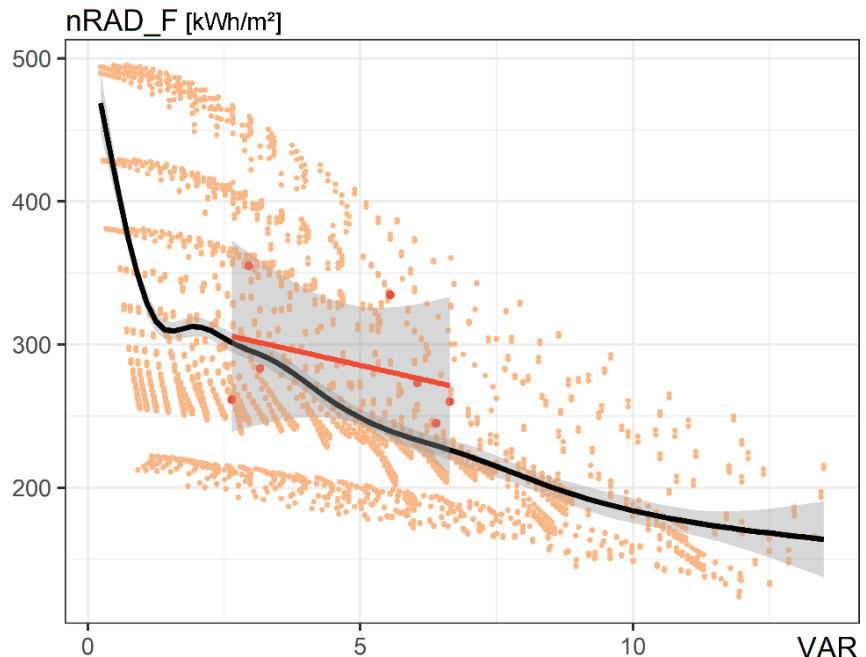


Figure 21. Non-linear regression function of density metric VAR and normalised EC-metric (black line) with case-study-fitted linear regression line (red) and 95% CI in grey. The graph indicates a low correlation with the scattering and clustering of data points.

Considering the comparative façade radiation metric, RAD_F, the example pairwise graph in Figure 22 relating RAD_F metric with density shows that the case studies' data points diverge from design iterations, as they scored significantly lower values of RAD_F. Façade irradiation was overestimated for the uniform, perfectly square, and evenly distributed neighbourhood typologies (iterations), while for the case studies, in which façades had non-right angles and more geometrical complexity, the scores were largely reduced. Compared with lower complexity metrics that were seen to have a good match between iterations and case studies, it seems that radiation metrics are more sensitive to changes in layout, surroundings, building forms and façade details. Furthermore, the lack of uniformity in building heights within case studies might have an additional impact on radiation estimates. The results suggest that, despite clearly defined curves of the iteration-based metric functions, these relationships do not hold for real neighbourhood cases.

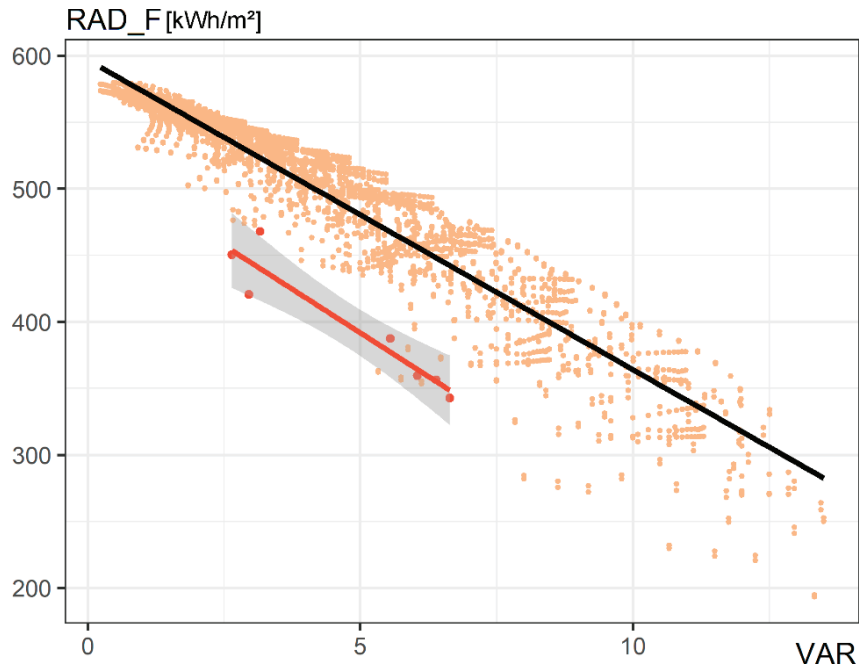


Figure 22. Linear regression function of metrics VAR and RAD_F based on neighbourhood iterations (black line) and case studies (red line), including the 95% CI for the case studies regression line indicated by the grey area.

Comparing the linear regression lines of the iterations and the case studies, it can be noted that their functions appear parallel. This may suggest that the regression lines based on the two datasets have a similar slope, just a different intercept (Figure 22). If the rate of change is similar, it may be justified to use the simpler metrics, such as VSC or ASH, to inform the selection of better performing designs. Although they might not be able to provide a precise estimation of radiation on facades, they may point towards designs that will provide a better radiation score in comparison to other proposals.

Table 4 presents 95% CIs of linear regression coefficients in some pairs of metrics. It confirms the observation on the regression slopes of the pairs containing the EC radiation metric. For all metrics pairs but the EC ones, the iteration-based CIs are narrower than the case study intervals (due to the higher number of degrees of freedom) and fall within the CIs of the case study regression coefficients. For those metrics pairs that include an EC metric, the intercept of the iteration-based cases does not fall within the case study interval, but the slope does. This means that the rate of change is expected to be the same, but the values will be reduced for more realistic neighbourhood geometries. The homogeneity of iteration design cases inflates the radiation results, and the CIs indicate an average reduction of 12% due to higher geometrical complexity. Reduction factors are typically applied for radiation estimates with urban designs of low LoD [46].

Table 4. Confidence intervals (CIs) of 95% level for linear regression model coefficients of iteration- (I) and case study- (CS) based metric datasets. A metric pair is validated when CI for I data fits within the CI of CS data.

Metric Pair	Data	Intercept		Slope	
		Lower CI	Higher CI	Lower CI	Higher CI
SVF-VAR	I	92.4	92.9	−5.65	−5.56
	CS	76.3	110.8	−10.08	−3.24
VSC-VAR	I	38.8	39.0	−2.65	−2.61
	CS	33.8	45.8	−4.25	−1.87
SVF-VSC	I	9.84	10.4	2.10	2.12
	CS	−13.1	29.0	1.32	2.96
ASH_G-VAR	I	0.731	0.740	−0.061	−0.059
	CS	0.548	1.013	−0.121	−0.029
RD_G-VAR	I	9.36	9.49	−0.84	−0.81
	CS	7.41	12.6	−1.54	−0.52
ASH_F-VAR	I	0.472	0.476	−0.032	−0.032
	CS	0.402	0.580	−0.060	−0.025
RD_F-VAR	I	6.06	6.14	−0.44	−0.42
	CS	5.00	7.94	−0.87	−0.29
RAD_F-VAR	I	595.3	598.3	−23.6	−23.0
	CS	470.1	576.2	−36.8	−15.8
ASH_G-RD_G	I	0.058	0.063	0.071	0.071
	CS	−0.017	0.101	0.064	0.086
RAD_F-VSC	I	252.0	256.0	8.71	8.85
	CS	134.1	237.0	6.43	10.44

4. Discussion

This study showed that many simple metrics can potentially be suitable for solar evaluations at the urban planning stages due to good correlations. The solar access assessments may have varying objectives, and the two main paths of evaluation have been found to be the daylighting and sunlighting provision. For each of these assessment targets, the most suitable metrics were identified and listed in Table 5. Sections 4.1 and 4.2 discuss the aspects of indoor and outdoor solar access assessments in relation to sunlight and daylight.

Table 5. Suggested metrics that may be suitable for early assessments of solar access at the urban planning level.

	Indoors	Outdoors
Daylighting	VSC	SVF
Sunlighting	ASH_F	RD_G

4.1. Solar Access Indoors

4.1.1. Daylight

The daylight factor (DF) is a common indicator of indoor daylighting. It is a G-metric, which means it is independent of location and climate inputs. The Swedish Building Code (SS-EN 17037) specifies that daylight in buildings should be measured using the DF metric simulated for a single point in a room [45]. The point, which is located halfway into the room from the aperture, 1 m away from the darkest wall, and 0.8 m above the ground, should score a DF of at least 1%. Driven by this legal constraint, urban planners in Sweden prioritise the daylighting objective when planning for solar access [16].

VSC can be used as an early indicator of daylighting at the façade level when aperture location and internal layouts are not yet established. Like the DF, the VSC is a G-metric, which is simulated for the CIE overcast sky model. The present study showed that the VSC correlates well with metrics of different complexities (e.g., Figure 14), also those which relate to sunlight (Figure 23). The Building Research Establishment (BRE) recommends a VSC level of at least 27% when conventional window design is used and cautions that a room with a VSC lower than 15% would likely need large windows to ensure good daylighting [47]. BRE states that VSC levels between 15% and 27% may provide enough daylighting if proper layout and fenestration design strategies are applied. However, it is important to note that the recommended VSC levels were given for the UK context, where national daylighting requirements are not mandated (BS-EN 17037 was withdrawn). It is thus yet uncertain how these recommended VSC levels would translate to meet the Swedish daylighting requirements.

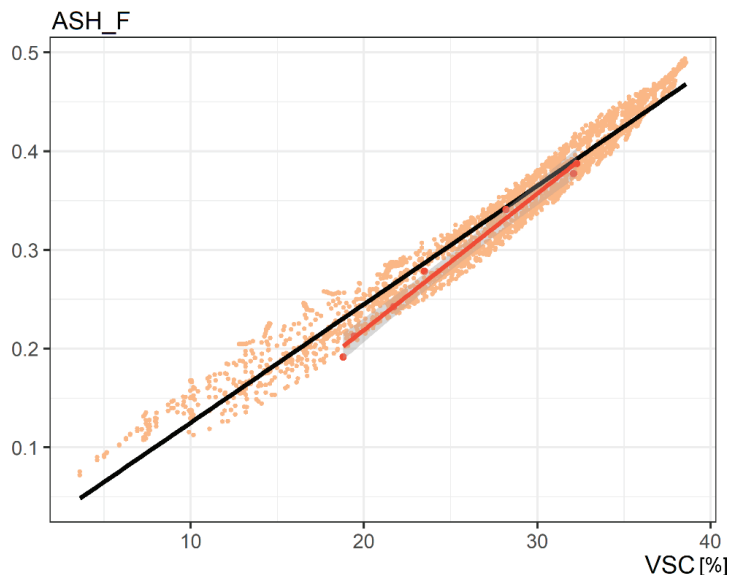


Figure 23. Linear regression function of façade-based metrics VSC and ASH_F based on neighbourhood iterations (black line) and case studies (red line), including the 95% CI for the case studies regression line indicated by the grey area.

The VSC metric dataset created in this study can be used to guide urban planners towards good daylight potential. We suggest two alternative methods to apply this dataset in practice, which are derived from a fixed variable: urban density as VAR. This means that, prior to the assessments, urban planning authorities must decide on the planned population density of a developed area. Assuming the amount of occupied floor area per inhabitant, the population density can be translated into urban density e.g., VAR. Knowing the target range of VAR, urban planners may use the simulated VSC dataset to retrieve a list of possible design cases from highest to lowest performing ones for the assigned density (Figure 24). Further on, introducing the area of the developed plot, the list can be reduced to include only those cases that fit a given plot (Figure 24). Alternatively, the method can provide urban planners with a range of expected VSC values to inform their design (Figure 25). In this case, the urban planners must perform VSC analysis themselves, and then use the VSC range as a guiding tool. It is important to mark that the method is intended for comparative design assessments, i.e., to determine which design proposals perform best, and not to accurately predict performance scores. This is future work which requires the identification of value benchmarks for performance levels backed by empirical evidence.

STEP 1: URBAN DENSITY

STEP 2: PLOT SIZE

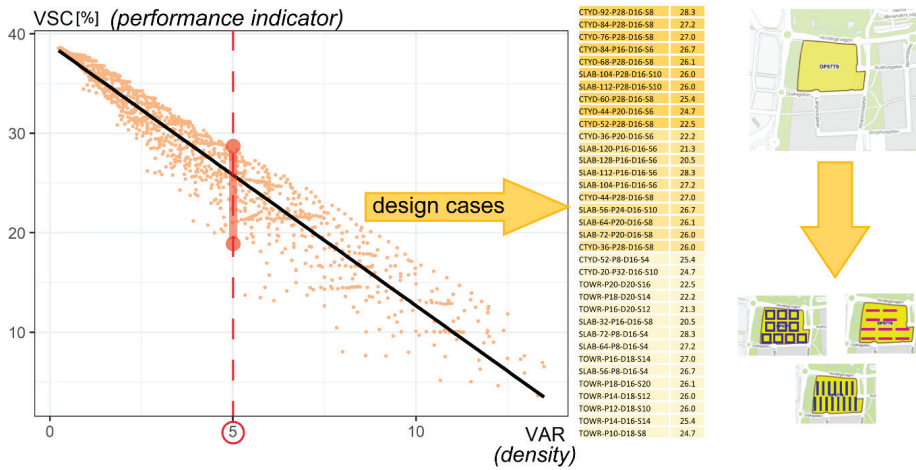


Figure 24. A suggestion for using the metric datasets in solar assessment of neighbourhood design in urban planning. In this example, the objective is daylighting of facades. Assuming target density and using the plot as an input, urban planners get suggestions for the best design options.

STEP 1: URBAN DENSITY

STEP 2: VALUE RANGE

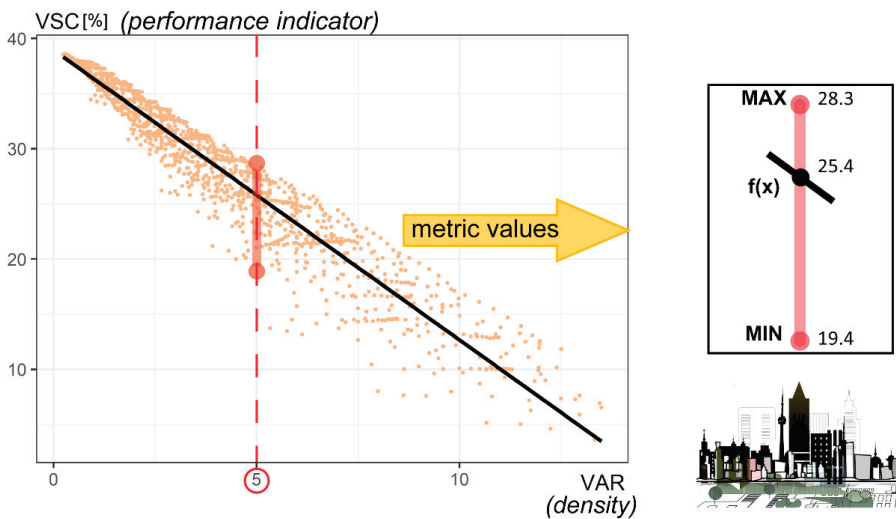


Figure 25. An alternative suggestion for using the metric datasets in solar assessment of neighbourhood design in urban planning. Assuming target density, the urban planners are presented with the expected ranges of metrics as a reference to compare range values with the results of their designs.

4.1.2. Sunlight

Access to direct sunlight in dwellings in Sweden is acknowledged in building legislation; however, it is not regulated as strictly as daylight. The Swedish Building Regulations [48] state that a minimum one room in a dwelling which people frequent more than occasionally should have access to sunlight, but how this should be enforced or measured is not specified. The European Daylighting Standard [45], on the other hand, provides a more concrete assessment method. It uses an L-metric, direct sunlight hours,

calculated for a point on the façade and for a single reference day between 1 February and 21 March. The exposure-to-sunlight levels are given from minimum: 1.5 h, through medium: 3 h, to maximum: 4 h. The European Standard sunlight metric is thus of conforming function, using a time constraint of one day. The stated sunlight stipulation is thus far just a recommendation.

The results of this study showed that some metrics have lower correlation to other solar metrics, and their pairwise relationships may have a dispersed appearance. Thus, may be less suitable for early assessment purposes. In particular, the conforming metrics were poorly correlated with other metrics, presenting high variance and lack of order in the data. Furthermore, the comparison of façade-based sunlight metrics, ASH_F and RD_F (Figure 18) was favourable to the annual time constraint, as it provides higher correlations, more continuous relationships with other metrics, and better linearity (Figures 20 and 23). The present study showed that the single-day RD_F metric has a large variance in the data in relation to other metrics. Current sunlight recommendations are based on a single day metric, and the present study showed that this time constraint may be less suitable in assessments due to the directionality of façade surfaces and a low number of simulated solar vectors. As a result of that, for example, the recommendation disqualifies dwellings from having all habitable rooms directly facing the North. There is insufficient evidence regarding user preferences with regard to solar access. These considerations may call into question the current assessment method for sunlight exposure, which is based on a poorly correlated conforming and single-day-based metric.

Conforming metrics, albeit their poor correlation, play an important role in assessments and should not be discounted. However, to apply design criteria using fixed thresholds with confidence, datasets need to have assigned evidence-based benchmarks, and the evidence on the amount of sunlight needed is currently lacking. More technical- and observation-based evidence on solar access at the façade level is needed in support of sustainable design objectives.

4.2. Solar Access Outdoors

Solar access in urban settings is often assessed at the outdoor ground level for visualization purposes (e.g., shadowing on the ground), but it has not yet been legislated. Ensuring solar access outdoors may be important for wellbeing, energy applications, and greenery growth. The results of this study showed that there is a good correlation and linear relationship between façade-based and ground-based G-metrics, i.e., VSC and SVF (Figure 15). Similarly, there is a strong correlation between ASH on the ground (ASH_G) and ASH at the façade level (ASH_F) (Figure 26). An interpretation of this result is that the indication of performance quality obtained from analysing only one type of target surface, either ground or façade, may be applicable to both indoor and outdoor environments.

The provision of solar access outdoors is also important in the aspects of urban heat island and microclimate. This study suggests that SVF is a promising early design indicator of daylighting performance of outdoor solar access. Since SVF has been previously linked to urban heat island mitigation [49], it strengthens the argument for implementing this metric into early solar access evaluations. Future work should establish limiting values for outdoor solar access SVF recommendations relative to the mitigation of the unwanted heat retention in cities.

An example of how the ground- and façade-based solar access data may be used in urban design assessments is presented in Figure 27. There are differences between different typologies depending on the target analysis surface used. The comparative solar performance graphs may be used as a tool to inform urban planners about the differences in performance of certain typologies and the trade-offs when considering different objectives. Currently, due to the legislative emphasis on the indoor environment, the priority in design assessments might be given to those typologies that score better solar access metrics at the façade level, e.g., slab; however, if significance was given to solar access outdoors, the courtyard typology could be more preferable.

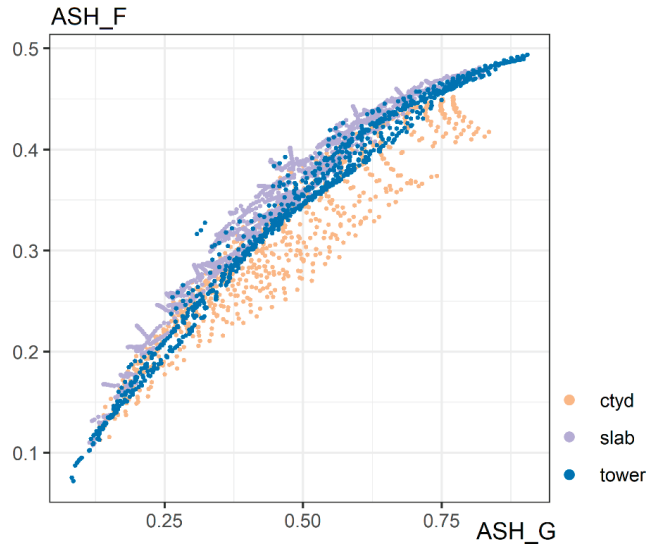


Figure 26. Relationship graph of metrics ASH_G and ASH_F, comparing the same metric calculated for ground and facades and presenting data points for the three analysed typologies.

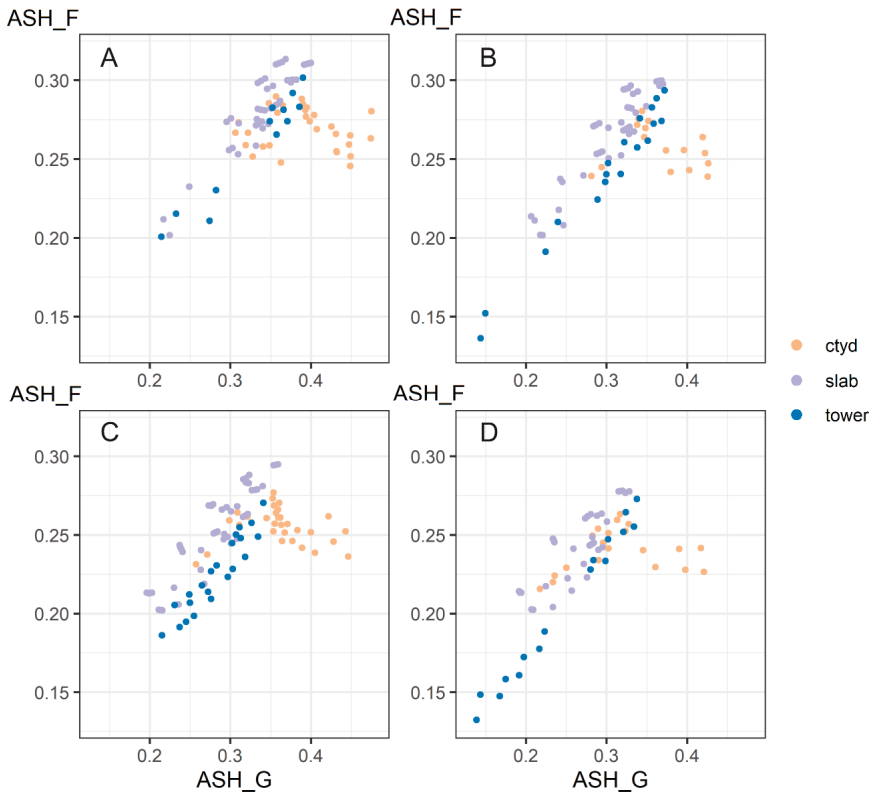


Figure 27. Selected neighbourhood cases presented as relation graphs based on the ASH on ground and façade. The graphs show cases with FAR in range of (A): (1.4–1.49), (B): (1.5–1.59), (C): (1.6–1.69), (D): (1.7–1.79).

4.3. Limitations and Future Work

This study was limited to particular neighbourhood typologies. The prerequisites for the selection of neighbourhood case studies, as well as the assumptions for modelling neighbourhood design iterations, gave constraints to the resulting metric datasets. In the future, these datasets could be expanded by adding neighbourhood cases of a wider variety, including diverse typologies and non-homogenous designs. A more complete database of solar metrics will support the decision-making process and improve solar-driven urban planning assessment methods, such as the two alternative approaches suggested in Section 4.1.1. An extended database could also open up possibilities for more advanced prediction models based on data statistics and machine learning.

The study focused on the European climates, and the solar performance metrics were selected assuming the northern latitude context for performance assessments. The solar access design objectives of northern locations may differ for other climates; for instance, in the hot climate regions, sunlight might be considered a liability, and access to it may have to be restricted in the design planning. The effect of different climates and latitudes should be studied further to also consider the impact of solar access on the microclimate.

Some metrics in this paper were calculated as an average value for the entire analysis area. This kind of assessment may be simplifying and reducing the design performance score. In some cases, in design assessments, it may be more valuable to have the metric displayed visually over the entire analysis area in order to be able to check for critical spots, especially in case of a non-homogenous neighbourhood.

Future work should establish relevant performance benchmarks for the suitable metrics that were presented in this study. Another point of perspective is also needed: occupants' perception of sunlight, both indoors and outdoors. There is scarce empirical evidence to support existing recommendations. This input will be instrumental in creating holistic methods of solar access evaluation, as it can help establish solar access targets assuming wellbeing as one of the urban design drivers alongside energy sustainability.

5. Conclusions

This study evaluated solar performance metrics, their graphical relations, and statistical correlations. The study was based on homogenous neighbourhood designs and focused on the context of northern Europe. The neighbourhood designs were validated via comparison with six case studies.

The outcomes of this study suggest that simple geometrical and latitudinal metric classes are valid candidates for potential solar performance indicators in the urban planning level of building design stages, whereas the external climatic metrics deem too complex. It was shown that, in some cases, the simpler metrics are even better suited for evaluating the performance of simple building blocks, i.e., the level of detail used in the early urban planning stage. More complex metrics were indeed more sensitive to geometrical details of the urban models and building facades.

In particular, it is concluded that VSC and SVF (for daylighting) and ASH_F and RD_G (for sunlight) are good candidate metrics for describing solar access indoors and outdoors, respectively.

The urban design and metric database created in this study may be useful for establishing assessment paradigms and prediction models. The database of metric values can be used in solar assessments of urban designs, may be used in prediction models, and can be of interest for future studies involving design optimization using advanced machine learning techniques. More diverse design solutions may be added to the datasets for increased validity and reliability. Some examples of urban-level solar assessment methods applying appropriate metrics specific for a given solar design objective were presented in this study.

Selecting appropriate metric thresholds is a challenge for the next phases of research into solar performance indicators. Performance benchmarks should be supported by evidence-based research, balancing energy and wellbeing objectives of sustainable neighbourhoods.

Author Contributions: Conceptualization, A.C., N.G., J.K. and M.W.; methodology, A.C., N.G., J.K. and M.W.; software, A.C.; validation, A.C., N.G., J.K. and M.W.; formal analysis, A.C.; investigation, A.C.; resources, J.K. and M.W.; data curation, A.C.; writing—original draft preparation, A.C.; writing—review and editing, A.C., N.G., J.K. and M.W.; visualization, A.C.; supervision, N.G., J.K. and M.W.; project administration, J.K. and M.W.; funding acquisition, M.W. and J.K. All authors have read and agreed to the published version of the manuscript.

Funding: This research was funded by the Swedish Energy Agency (Energimyndigheten)—grant number 49518-1.

Data Availability Statement: The data presented in this study are openly available in the Swedish National Data Service at <https://doi.org/10.5878/jf63-ay82> (accessed on 30 August 2022), reference number SND-ID: 2022-137.

Acknowledgments: This project contributes to the International Energy Agency Solar Heating & Cooling programme (IEA SHC) Task 63 “Solar Neighborhood Planning”. The authors wish to acknowledge the experts in IEA SHC Task 63 for the fruitful discussions during the Task activities.

Conflicts of Interest: The authors declare that they have no conflict of interest.

References

- Littlefair, P. Passive Solar Urban Design: Ensuring the Penetration of Solar Energy into the City. *Renew. Sustain. Energy Rev.* **1998**, *2*, 303–326. [[CrossRef](#)]
- Beckers, B. *Solar Energy at Urban Scale*; John Wiley and Sons: Hoboken, NJ, USA, 2013; ISBN 9781848213562.
- Knowles, R.L. The Solar Envelope: Its Meaning for Energy and Buildings. *Energy Build.* **2003**, *35*, 15–25. [[CrossRef](#)]
- IEA SHC. Task 51 Solar Energy in Urban Planning. In *Approaches, Methods and Tools for Solar Energy in Urban Planning*; IEA SHC: Cedar, MI, USA, 2018.
- Peronato, G.; Rastogi, P.; Rey, E.; Andersen, M. A Toolkit for Multi-Scale Mapping of the Solar Energy-Generation Potential of Buildings in Urban Environments under Uncertainty. *Sol. Energy* **2018**, *173*, 861–874. [[CrossRef](#)]
- Sarralde, J.J.; Quinn, D.J.; Wiesmann, D.; Steemers, K. Solar Energy and Urban Morphology: Scenarios for Increasing the Renewable Energy Potential of Neighbourhoods in London. *Renew. Energy* **2015**, *73*, 10–17. [[CrossRef](#)]
- Bilu, C.; Einat, H.; Zimmet, P.; Vishnevskia-Dai, V.; Kronfeld-Schor, N. Beneficial Effects of Daytime High-Intensity Light Exposure on Daily Rhythms, Metabolic State and Affect. *Sci. Rep.* **2020**, *10*, 19782. [[CrossRef](#)] [[PubMed](#)]
- Knoop, M.; Stefani, O.; Bueno, B.; Matusiak, B.; Hobday, R.; Wirz-Justice, A.; Martiny, K.; Kantermann, T.; Aarts, M.P.J.; Zemmouri, N.; et al. Daylight: What Makes the Difference? *Light. Res. Technol.* **2020**, *52*, 423–442. [[CrossRef](#)]
- Holick, M.F. Sunlight and Vitamin D for Bone Health and Prevention of Autoimmune Diseases, Cancers, and Cardiovascular Disease. *Am. J. Clin. Nutr.* **2004**, *80*, 1678S–1688S. [[CrossRef](#)] [[PubMed](#)]
- Fahimipour, A.K.; Hartmann, E.M.; Siemens, A.; Kline, J.; Levin, D.A.; Wilson, H.; Betancourt-Román, C.M.; Brown, G.; Fretz, M.; Northcutt, D.; et al. Daylight Exposure Modulates Bacterial Communities Associated with Household Dust. *Microbiome* **2018**, *6*, 175. [[CrossRef](#)]
- United Nations-Department of Economic and Social Affairs-Population Division. *World Urbanization Prospects. The 2018 Revision*; United Nations: New York, NY, USA, 2019.
- Angel, S.; Lamson-Hall, P.; Blei, A.; Shingade, S.; Kumar, S. Densify and Expand: A Global Analysis of Recent Urban Growth. *Sustainability* **2021**, *13*, 3835. [[CrossRef](#)]
- Bournas, I.; Dubois, M.-C. Daylight Regulation Compliance of Existing Multi-Family Apartment Blocks in Sweden. *Build. Environ.* **2019**, *150*, 254–265. [[CrossRef](#)]
- Kanters, J.; Wall, M. Experiences from the Urban Planning Process of a Solar Neighbourhood in Malmö, Sweden. *Urban Plan. Transp. Res.* **2018**, *6*, 54–80. [[CrossRef](#)]
- Lobaccaro, G.; Croce, S.; Lindkvist, C.; Munari Probst, M.C.; Scognamiglio, A.; Dahlberg, J.; Lundgren, M.; Wall, M. A Cross-Country Perspective on Solar Energy in Urban Planning: Lessons Learned from International Case Studies. *Renew. Sustain. Energy Rev.* **2019**, *108*, 209–237. [[CrossRef](#)]
- Kanters, J.; Gentile, N.; Bernardo, R. Planning for Solar Access in Sweden: Routines, Metrics, and Tools. *Urban Plan. Transp. Res.* **2021**, *9*, 348–368. [[CrossRef](#)]
- Nault, E.; Peronato, G.; Rey, E.; Andersen, M. Review and Critical Analysis of Early-Design Phase Evaluation Metrics for the Solar Potential of Neighborhood Designs. *Build. Environ.* **2015**, *92*, 679–691. [[CrossRef](#)]
- Czachura, A.; Kanters, J.; Gentile, N.; Wall, M. Solar Performance Metrics in Urban Planning: A Review and Taxonomy. *Buildings* **2022**, *12*, 393. [[CrossRef](#)]
- Morganti, M.; Salvati, A.; Coch, H.; Cecere, C. Urban Morphology Indicators for Solar Energy Analysis. *Energy Procedia* **2017**, *134*, 807–814. [[CrossRef](#)]
- Shi, Z.; Fonseca, J.A.; Schlueter, A. A Parametric Method Using Vernacular Urban Block Typologies for Investigating Interactions between Solar Energy Use and Urban Design. *Renew. Energy* **2021**, *165*, 823–841. [[CrossRef](#)]

21. Zhang, J.; Heng, C.K.; Malone-Lee, L.C.; Hii, D.J.C.; Janssen, P.; Leung, K.S.; Tan, B.K. Evaluating Environmental Implications of Density: A Comparative Case Study on the Relationship between Density, Urban Block Typology and Sky Exposure. *Autom. Constr.* **2012**, *22*, 90–101. [\[CrossRef\]](#)
22. Chen, K.W.; Norford, L. Evaluating Urban Forms for Comparison Studies in the Massing Design Stage. *Sustainability* **2017**, *9*, 987. [\[CrossRef\]](#)
23. Statistics Sweden (SCB) Nearly 5.1 Million Dwellings in Sweden. Available online: <https://www.scb.se/en/finding-statistics/statistics-by-subject-area/housing-construction-and-building/housing-construction-and-conversion/dwelling-stock/pong/statistical-news/dwelling-stock-december-31-2021/> (accessed on 10 May 2022).
24. Rådberg, J.; Friberg, A. *Svenska Stadstyper: Historik, Exempel, Klassificering*; Kungliga tekniska högskolan, Institutionen för arkitektur och stadsbyggnad: Stockholm, Sweden, 1996; ISBN 9171706992.
25. Nouvel, R.; Schulte, C.; Eicker, U.; Pietruschka, D.; Coors, V. CityGML-Based 3D City Model for Energy Diagnostics and Urban Energy Policy Support. In Proceedings of the BS2013: 13th Conference of International Building Performance Simulation Association, Chambéry, France, 26–28 August 2013; pp. 218–225.
26. McNeel, R. Associates Rhinoceros 3D, Version 7. Available online: <https://www.rhino3d.com/> (accessed on 6 December 2021).
27. McNeel, R. Associates Grasshopper—Algorithmic Modeling for Rhino. 2022. Available online: <https://www.grasshopper3d.com/?overrideMobileRedirect=1> (accessed on 6 December 2021).
28. American Society of Planning Officials. *Information Report No. 111: Floor Area Ratio*; American Society of Planning Officials: Chicago, IL, USA, 1958.
29. Krehl, A.; Siedentop, S.; Taubenböck, H.; Wurm, M.; Behnisch, M.; Meinel, G.; Kainz, W. A Comprehensive View on Urban Spatial Structure: Urban Density Patterns of German City Regions. *ISPRS Int. J. Geo-Inf.* **2016**, *5*, 76. [\[CrossRef\]](#)
30. Moon, B. The Effect of FAR (Floor Area Ratio) Regulations on Land Values: The Case of New York. *Pap. Reg. Sci.* **2019**, *98*, 2343–2354. [\[CrossRef\]](#)
31. Perry, C. The Neighborhood Unit: A Scheme of Arrangement for the Family-Life Community. In *The Regional Plan of New York and Its Environs*; Russell Sage Foundation: New York, NY, USA, 1929; Volume VII, ISBN 9781136205668.
32. Mumford, L. The Neighborhood and the Neighborhood Unit. *Town Plan. Rev.* **1954**, *24*, 256–270. [\[CrossRef\]](#)
33. Mehaffy, M.W.; Porta, S.; Romice, O. The “Neighborhood Unit” on Trial: A Case Study in the Impacts of Urban Morphology. *J. Urban* **2015**, *8*, 199–217. [\[CrossRef\]](#)
34. Byun, N.; Choi, Y.; Choi, J. Neighborhood Unit: Effective or Obsolete? *J. Asian Archit. Build. Eng.* **2014**, *13*, 617–624. [\[CrossRef\]](#)
35. Olson, P. Urban Neighborhood Research: Its Development and Current Focus. *Urban Aff. Rev.* **1982**, *17*, 491–518. [\[CrossRef\]](#)
36. Gallion, A.B.; Eisner, S. *The Urban Pattern: City Planning and Design*, 5th ed.; Van Nostrand Reinhold: New York, NY, USA, 1985; ISBN 0442227310.
37. Dahlberg, G.-B.; Ödmann, E. *Stadsutveckling Och Planering i Sverige*; Läromedelsförl. i samverkan med Byggforskningen; T/Statens råd för byggnadsforskning: Stockholm, Sweden, 1969.
38. Lantmäteriet Geodataportalen. Available online: <https://www.lantmateriet.se/sv/geodata/Geodataportalen/> (accessed on 30 August 2022).
39. Ladybug Tools Ladybug Tools | Home Page. Available online: <https://www.ladybug.tools/> (accessed on 11 October 2021).
40. European Environment Agency (EEA). Main Climates of Europe. Available online: <https://www.eea.europa.eu/data-and-maps/figures/climate> (accessed on 30 August 2022).
41. ASHRAE. *International Weather for Energy Calculations (IWEC Weather Files) Users Manual and CD-ROM*; ASHRAE: Atlanta, GA, USA, 2001.
42. RStudio Team. *RStudio: Integrated Development Environment for R*; RStudio, PBC: Boston, MA, USA, 2021.
43. Joshi, K.K.; Kono, T. Optimization of Floor Area Ratio Regulation in a Growing City. *Reg. Sci. Urban Econ.* **2009**, *39*, 502–511. [\[CrossRef\]](#)
44. Kono, T.; Kusum Joshi, K. A New Interpretation on the Optimal Density Regulations: Closed and Open City. *J. Hous. Econ.* **2012**, *21*, 223–234. [\[CrossRef\]](#)
45. SSI. *CEN SS-EN 17037:2018+A1:2021; Daylight in Buildings*. Swedish Standards Institute: Stockholm, Sweden, 2021.
46. Lobaccaro, G.; Lisowska, M.M.; Saretta, E.; Bonomo, P.; Frontini, F. A Methodological Analysis Approach to Assess Solar Energy Potential at the Neighborhood Scale. *Energies* **2019**, *12*, 3554. [\[CrossRef\]](#)
47. Littlefair, P.J.; King, S.; Howlett, G.; Ticleanu, C.; Longfield, A. *Site Layout Planning for Daylight and Sunlight (BR 209)*, 3rd ed.; S&P Global: New York, NY, USA, 2022; ISBN 978-1-84806-483-6.
48. Boverket. *Boverkets Byggregler (BFS 2019:2)—Föreskrifter Och Allmänna Råd*; Boverket: Karlskrona, Sweden, 2011.
49. Oke, T.R. Canyon Geometry and the Nocturnal Urban Heat Island: Comparison of Scale Model and Field Observations. *J. Climatol.* **1981**, *1*, 237–254. [\[CrossRef\]](#)



Article

How to Efficiently Reduce the Carbon Intensity of the Heavy Industry in China? Using Quantile Regression Approach

Bin Xu

School of Management, China Institute for Studies in Energy Policy, Collaborative Innovation Center for Energy Economics and Energy Policy, Xiamen University, Xiamen 361005, China; xubin9675@163.com

Abstract: This decoupling between carbon dioxide emissions and the heavy industry is one of the main topics of government managers. This paper uses the quantile regression approach to investigate the carbon intensity of China's heavy industry, based on 2005–2019 panel data. The main findings are as follows: (1) incentive-based environmental regulations have the greater impact on the carbon intensity in Jiangsu, Shandong, Zhejiang, Henan, Liaoning, and Shaanxi, because these provinces invest more in environmental governance and levy higher resource taxes; (2) the impact of mandatory environmental regulations on carbon intensity in Beijing, Tianjin, and Guangdong provinces is smaller, since these three provinces have the fewest enacted environmental laws and rely mainly on market incentives; (3) conversely, foreign direct investment has contributed most to carbon intensity reduction in Tianjin, Beijing, and Guangdong provinces, because these three have attracted more technologically advanced foreign-funded enterprises; (4) technological progress contributes more to the carbon intensity in the low quantile provinces, because these provinces have more patented technologies; (5) the carbon intensity of Shaanxi, Shanxi, and Inner Mongolia provinces is most affected by energy consumption structures because of their over-reliance on highly polluting coal.

Keywords: carbon intensity; the heavy industry; quantile regression analysis

Citation: Xu, B. How to Efficiently Reduce the Carbon Intensity of the Heavy Industry in China? Using Quantile Regression Approach. *Int. J. Environ. Res. Public Health* **2022**, *19*, 12865. <https://doi.org/10.3390/ijerph191912865>

Academic Editors: Roberto Alonso González Lezcano, Francesco Nocera and Rosa Giuseppina Caponetto

Received: 5 July 2022

Accepted: 22 September 2022

Published: 8 October 2022



Copyright: © 2022 by the author. Licensee MDPI, Basel, Switzerland. This article is an open access article distributed under the terms and conditions of the Creative Commons Attribution (CC BY) license (<https://creativecommons.org/licenses/by/4.0/>).

1. Introduction

Global warming has caused huge damage to the natural ecological environment on which human beings depend [1]; the culprit behind global warming is the accumulation of carbon dioxide. The negative impact of global warming has made all countries realize the necessity of jointly dealing with CO₂ emissions. The international community has developed a series of agreements to urge countries worldwide to cut CO₂ emissions in steps, such as the Copenhagen Accord (2009) and the Paris Agreement (2015) [2].

Currently, China's CO₂ emissions rank first in the world [3], and statistics show that China's total of CO₂ emissions in 2021 was 10.6 billion tons. The heavy industry contributed 55% of China's CO₂ emissions during the period 2005–2019. Carbon intensity is a key factor affecting CO₂ emissions of the heavy industries [4]. The motivation for this article is to investigate the effects of the influencing factors on the carbon intensity of the heavy industries, and to propose targeted countermeasures. The research results can provide empirical support for local governments to formulate industrial policies and can offer new paths for achieving carbon neutrality goals.

The importance of carbon intensity has attracted many scholars to conduct in-depth research into it. Analysis of the existing relevant literature found that these studies have the following two notable characteristics: (1) Existing studies have investigated the impact of environmental regulations on carbon intensity, but they do not break down environmental regulations. These regulations can be further subdivided into mandatory environmental regulations and incentive-based environmental regulations [5]. Moreover, the ways in which these two environmental regulations affect carbon intensity are markedly different; (2) Most literature investigates carbon intensity in the industrial sector using the ordinary

least squares. However, a prerequisite for the ordinary least squares to obtain robust parameters is that the sequence of economic variables is normally distributed. In fact, economic phenomena are complex and the data of economic variables have obvious characteristics of “sharp peak” and “thick tail”. This results in the series of economic variables being skewed. Using the ordinary least squares to estimate non-normally distributed variable data will lead to serious adverse consequences, such as increased variance and biased parameter estimators.

The possible contributions of this paper are mainly the following two points: (1) Considering the availability of data, this paper divides environmental regulations into mandatory environmental regulations and incentive-based environmental regulations. This paper investigates the impact of these two environmental regulations on carbon intensity separately. The findings help local governments to flexibly use corresponding environmental policies to promote carbon intensity reduction; (2) Preliminary test results show that the series of economic variables in this paper are not normally distributed. Quantile regression models do not require that the series of economic variables follow a normal distribution. Under the condition that the series of economic variables is not normally distributed, the results of quantile regression are more robust than those of the ordinary least squares [6]. Quantile regression can estimate the effects of influencing factors on carbon intensity at different levels, including maximum, minimum and median values. The ordinary least squares can only give an average effect of influencing factors on carbon intensity. Thus, the research results can provide empirical support for local governments to formulate effective emission reduction policies.

Apart from the introduction, this paper has the following sections: the literature review is placed in Section 2; the theoretical model and the construction of the empirical model are placed in Section 3; the empirical results are placed in Section 4; the discussion section is placed in Section 5; the results of the robustness test are presented in Section 6; policy recommendations are placed in Section 7; and the Limitation of the study and future recommendations are placed in the last section.

2. Literature Review

This section selects several representative influencing factors of carbon intensity for comment. China is now the world’s largest CO₂ emitter; in order to achieve low-carbon growth, the Chinese government has taken many measures to control fossil energy use and reduce CO₂ emissions, such as expanding investment in environmental governance and promulgating environmental laws. Most of these measures fall into the category of environmental regulations. Therefore, this section first reviews the existing literature on environmental regulations.

(1) Mandatory environmental regulations. In a survey in China, Liang et al. [7] found that mandatory environmental regulations promoted the improvement of environmental efficiency and the decrease in carbon intensity. The scale of China’s manufacturing industry was the largest in the world, and its carbon intensity was high [8]. Jiang et al. [9] pointed out that mandatory environmental regulations had not played a role in improving energy-saving technologies and reducing carbon intensity. However, Wang and Zhu [10] reached the opposite conclusion. Using a spatial econometric model, they found that mandatory environmental regulations helped to reduce carbon intensity. The main reason was that mandatory environmental regulations prompted heavy industrial enterprises to move from the provinces with strict environmental regulations to the provinces with low environmental regulations. A difference-in-difference model survey indicated that mandatory environmental regulations were beneficial for reducing the carbon intensity of the heavy industry [11]. The main reason was that mandatory environmental regulations increased the pressure on industrial enterprises, prompting industrial enterprises to change environmental strategies [12].

Compared with mandatory environmental regulations, incentive-based environmental regulations were flexible. Therefore, incentive-based environmental regulations could play a better role in environmental governance.

(2) Incentive-based environmental regulations. Incentive-based environmental regulations include many means of environmental governance, such as resource tax, carbon tax, carbon emission permits, and wastewater discharge permits [13]. However, the main task of developing countries was to facilitate the rapid economic development and social employment [14]. Therefore, many developing countries implemented loose incentive-based environmental regulations [15]. This attracted many investment projects in the heavy industries, such as the petrochemical, plastics processing, and metallurgy industries [16]. The lax incentive-based environmental regulations had made many heavy industrial companies pay little attention to improving energy efficiency and had resulted in high carbon intensity [17]. During the 12th and 13th Five-Year Plans, China's incentive-based environmental regulations had continuously strengthened and played a critical role in reducing carbon intensity [18]. Using a stochastic frontier approach, Yao et al. [19] found that incentive-based environmental regulations had prompted industrial enterprises to increase investment in technology research and development. Technological innovation could not only decrease the use of fossil energy but also expand the application of abatement equipment, thereby contributing to the reduction of carbon intensity.

Environmental regulations were mainly formulated by the governments. Energy prices were not only affected by domestic factors, but also by international factors. The heavy industry was energy-intensive and sensitive to energy prices. Soaring oil prices would prompt industrial enterprises to expand clean energy use, helping to reduce carbon intensity. The existing literature on the relationship between energy prices and carbon intensity is reviewed below.

(3) Energy prices. The production activities of the heavy industries often required a large amount of energy input [20]. Rising fossil energy prices turned to increase cost for heavy industry producers [21]. To reduce production costs and enhance market competitiveness, heavy industry production companies had begun to focus on improving energy efficiency and reducing carbon intensity [22]. Natural gas was a clean energy source, and many countries strongly encouraged natural gas consumption [23]. Government departments had expanded financial subsidies that had lowered natural gas prices. The decline in clean energy prices incentivized heavy industry producers to gradually increase the use of clean energy, thereby promoting carbon emission reductions and mitigating carbon intensity [24]. In recent years, major energy-consuming countries have accelerated the development of wind power and photovoltaic power [25]. Governments have also provided financial subsidies for wind power and photovoltaic power generation, thereby reducing renewable energy prices [26]. This induced heavy industry to expand the use of clean electricity, contributing to CO₂ emission reduction and carbon intensity mitigation.

Energy prices could affect the energy structure of the heavy industries. A sharp drop in oil prices would help increase the share of fossil fuels in energy structure, resulting in a high carbon intensity. A literature review of the relationship between energy structure and carbon intensity is given below.

(4) Energy structure. In general, the heavy industry still relied mainly on highly polluting coal to meet energy needs [27]. Coal had a high carbon content, as its excessive use resulted in the emission of carbon dioxide and high carbon intensity [28]. Using comparative analysis, Rojas-Cardenas et al. [29] examined the carbon intensity in Mexico and the world's energy-consuming countries; they showed that the carbon intensity of Mexico's steel industry was low, since the main source of energy consumption was clean natural gas. Similarly, Switzerland's heavy industrial production plants increased biomass energy use and significantly reduced the share of coal in energy consumption [30]. The carbon intensity of China's heavy industrial sector had historically been high, mainly because many heavy industries still relied on high-emission coal [31]. A coal-dominated energy mix remained a major obstacle to cutting down carbon intensity [32].

In the long run, technological progress was an important factor of carbon intensity. More low-carbon technologies would certainly help mitigate carbon intensity. The literature on the relationship between technological progress and carbon intensity was described as follows.

(5) Technological progress. Employing the decomposition approach, Song et al. [33] studied the heavy industry and showed that technological advances could help reduce carbon intensity. Moreover, the level of technology had obvious regional heterogeneity. It was because there were significant regional differences in R&D funding and technological talent [34]. This made the contribution of technological innovation to carbon intensity in different regions significantly different [35]. Findings from the Swedish steel industry showed that updating furnace technology and equipment could significantly improve energy efficiency and reduce coal use, thereby contributing to the mitigation of carbon intensity [36]. The European steel industry analysis also found that updating blast furnace combustion technology and carbon capture technology could significantly reduce carbon intensity [37].

Technological progress could help industrial enterprises to update energy utilization technology and reduce energy intensity, thereby contributing to the reduction of carbon intensity. The literature on the relationship between energy intensity and carbon intensity is reviewed below.

(6) Energy intensity. The heavy industry was an energy-intensive industry, as its energy intensity was significantly higher than that in other industries such as the light industries, services, and agriculture [38]. Under the background of China's energy consumption mainly relying on highly polluting fossil energy, high energy intensity made the reduction in carbon intensity a difficult task [39]. Shandong and Liaoning provinces were two major industrial provinces in China, where many heavy industrial enterprises gathered [40]. Therefore, reducing energy intensity was key in facilitating the decline of carbon intensity. A survey of the heavy industries in India yielded similar findings that energy intensity was one of the key factors influencing the changes in carbon intensity [41].

Reviewing the above research literature, it is found that most of the sources use mean models to analyze the impact of environmental regulations and other determinants on carbon intensity. The obtained research results have little reference value for local governments to manage the environment and reduce carbon intensity. Therefore, this paper first subdivides environmental regulations into incentive-based environmental regulations and mandatory environmental regulations. Quantile regression methods were then used to investigate the impact of these two environmental regulations and other determinants on carbon intensity. The quantile regression can estimate the heterogeneous impact of the influencing factors on carbon intensity, including the effect of the maximum, minimum, and median values.

3. Method and Model Specification

3.1. The Basic Principle of Quantile Regression

Economic and financial variable series are often characterized by spikes and thick tails. The strength of the influence of the independent variable on the maximum, minimum, and intermediate values of the dependent variable may vary significantly. The traditional mean models (e.g., linear panel data model, and distributed lag model) can only obtain the average influence of the explanatory variables on the dependent variable. For example, carbon intensity varies from province to province, and the effects of explanatory variables on the provinces with high carbon intensity are different from those with low carbon intensity.

Quantile regression can overcome the shortcomings of the mean models. The advantages of quantile regression models are as follows: (1) Quantile regression does not require the series of economic variables to follow a normal distribution. Economic phenomena are volatile, so the series of economic variables are often non-normally distributed. When the series of economic variables is not normally distributed, the estimated results of quantile regression are more robust than those of the mean models; (2) Quantile regression can

give the comprehensive influence of the explanatory variables on the dependent variables, including the influence of maximum, minimum and median values [42]. Thus, the quantile regression has obvious advantages over traditional mean models. The mathematical formula of quantile regression approach is shown in Equations (1) and (2) below:

$$y_i = x_i' \beta_\theta + \mu_{\theta i}, 0 < \theta < 1 \quad (1)$$

$$\text{Quant}_\theta(y_i | x_i) = x_i \beta_\theta \quad (2)$$

where the vector of explanatory variables is signified by X , the dependent variable is signified by Y , Quantile regression is expressed by quant. The specific theory of quantile regression can refer to Koenker and Hallock [43]. This paper uses the bootstrap method to estimate the parameters of the quantile regression model. The specific estimation process of the bootstrap method can refer to Efron [44].

3.2. Theoretical Mechanism and Model Specification

According to the status of China's heavy industry and literature review, this paper selects the main influencing factors of carbon intensity. The theoretical mechanism between carbon intensity and influencing factors is explained as follows:

(1) Energy structure. The heavy industry is highly energy-intensive. Although many heavy industrial enterprises are continuously expanding the use of clean energy, coal still occupies a large proportion of energy structure in the heavy industry [45]. The carbon intensity of coal is high, and the coal-dominated energy mix makes it difficult to reduce carbon intensity. Drawing on the experience of existing research, this paper applies the rate of coal consumption to measure energy structure (%);

(2) Technological progress. Technological innovation and application are important means of solving environmental problems. Technological progress will help break through the key core technologies of the heavy industry and improve energy efficiency [46]. In addition, technological progress is conducive to the large-scale application of new clean energy such as shale gas extraction, wind power, and photovoltaic power generation. Advances in cleaner production technology help reduce CO₂ emissions in the production process or end-of-line treatment. From the perspective of production scale, technological progress can help improve the marginal productivity of factors, drive enterprises to expand output, and make up for the increase in cost. Neither productivity improvements nor the use of carbon abatement technologies can help cut down the carbon intensity of the industrial sector. This paper adopts the ratio of technology R&D input to GDP to represent the variable value of technological progress (%);

(3) Incentive-based environmental regulations. Environmental pollution is mainly caused by industrial production activities such as CO₂ emissions and smog pollution. In order to reduce environmental pollution, government departments must play a regulatory role. Incentive-based environmental regulations are a means for government departments to control environmental pollution through market means, such as technological R&D, carbon emission permit system, and carbon emission trading markets [47]. There are two theories about the relationship between incentive-based environmental regulations and carbon intensity. The first theory holds that incentive-based environmental regulations will increase the production cost of enterprises, divert entrepreneurial energy, and affect the profitability of enterprises. This restricts industrial enterprises from expanding investment in technology research and development, and low technology levels are not conducive to reducing carbon intensity. The second theory holds that incentive-based environmental regulations promote enterprise innovation, which in turn reduces energy consumption and improves product quality. Therefore, incentive-based environmental regulations can help reduce CO₂ emissions and mitigate carbon intensity;

(4) Mandatory environmental regulations. Mandatory environmental regulations are used to control environmental pollution in the form of laws or rules: (1) Stringent environmental regulations have a major impact on CO₂ emissions and carbon intensity.

High-polluting industrial enterprises often face serious consequences such as high financial penalties, production stoppages, and factory closures. This caused a huge panic in the heavily polluting enterprises, which reduces the expected rate of return and restricts the expansion of reproduction. It is not conducive to improving corporate energy efficiency and reducing carbon intensity; (2) Mandatory environmental regulations require industrial enterprises to disclose environmental information through the Environmental Protection Law. As a result, environmental information transparency of industrial enterprises has been improved. Information disclosure reduces the asymmetry of environmental information between industrial enterprises and relevant stakeholders and strengthens external supervision. This forces industrial companies to focus on energy consumption and CO₂ emissions, which in turn contributes to a reduction in carbon intensity;

(5) Foreign direct investment. China’s heavy industry is changing from an extensive growth mode to an intensive growth mode. To achieve green and sustainable growth, the Chinese government has continuously strengthened foreign investment reviews. Introduced investment projects often have advanced technology and management models [48]. Expanding foreign direct investment can attract advanced manufacturing companies from developed countries into the Chinese market. The advanced management experience and production technology of foreign-funded enterprises have spillover effects. Thus, it can lead to an improvement in technologies, and promote a decline in carbon intensity among domestic heavy industry enterprises. Foreign direct investment is measured by the amount of foreign investment actually introduced (100 million yuan (CNY));

(6) Oil prices. International oil price fluctuations are normal. If oil prices rise sharply, the heavy industry expands the use of alternative energy sources, such as clean gas and biofuels [49]. Conversely, the decline in international oil prices will prompt energy-intensive heavy industry companies to expand oil use. Over-reliance on carbon-rich oil leads to high carbon intensity in the industrial sector. The oil trading volume of the West Texas, Brent, and Dubai oil markets has accounted for the largest proportion of the total oil transactions. This paper calculates the average price of oil transactions in these three oil markets, and uses it to measure the international oil price (CNY/ton);

(7) Economic growth. The economic growth of many countries has experienced a path from extensive growth to intensive growth. After high-input, high-output growth in the early stages, the Chinese government has realized that extensive growth is unsustainable. On the one hand, the Chinese government actively promotes the high-tech industries such as high-end equipment manufacturing. On the other hand, the government strictly controls the scale of heavy industry. The development of these industries can improve technologies and expand the supply of renewable energy, thereby promoting mitigation in carbon intensity [50].

The above theoretical analysis has shown that the selected socio-economic factors closely relate to carbon intensity. Therefore, this paper takes these factors into the analytical framework and constructs an empirical model of carbon intensity (Equation (3)).

$$LCI_{it} = C + \beta_1 LENS_{it} + \beta_2 LTEC_{it} + \beta_3 LIER_{it} + \beta_4 LMER_{it} + \beta_5 LFDI_{it} + \beta_6 LPRI_{it} + \beta_7 LGDP_{it} + \mu_{it} \tag{3}$$

where *L* means that the variable data is logarithmically processed. *ENS* means energy structure, the carbon intensity is measured by *CI*, technological progress is represented by *TEC*, incentive-based environmental regulations are represented by *IER*, mandatory environmental regulations are represented by *MER*, *FDI* means foreign direct investment, *PRI* means oil prices, and *GDP* means economic growth. The constant term is delegated by *C*, and the disturbance term is delegated by μ . The specific form of quantile regression is shown in Equation (4).

$$Q_{\tau}(LCI_{it}) = C_{\tau} + \beta_{1\tau} LENS_{it} + \beta_{2\tau} LTEC_{it} + \beta_{3\tau} LIER_{it} + \beta_{4\tau} LMER_{it} + \beta_{5\tau} LFDI_{it} + \beta_{6\tau} LPRI_{it} + \beta_{7\tau} LGDP_{it} + \mu_{it} \tag{4}$$

where τ signifies the quantile point. This paper selects 5 representative quantiles, which are 10th, 25th, 50th, 75th, and 90th.

3.3. Variable Selection and Data Source

The sample in this paper is the annual panel data of China’s 30 provinces from 2005 to 2019 (Table S1). (1) Explained variable: Carbon intensity of the heavy industry (10,000 t/100 million CNY). Carbon intensity = the heavy industry’s CO₂ emissions/the output of the heavy industry. CO₂ emissions are obtained by multiplying different types of fossil energy by their carbon emission coefficients and then adding them up. Emission output is distinct from carbon intensity. Emission output = the heavy industry’s output/the heavy industry’s CO₂ emissions. It can be seen that emission output is equivalent to a reciprocal of carbon intensity. Much literature has used carbon intensity to measure the low-carbon level of industrial development or economic growth [51,52]. Drawing on the existing literature, this paper uses carbon intensity to measure the carbon level of the heavy industry.

(2) Explanatory variables: First, the energy consumption structure is represented by the proportion of coal consumption (%). Second, technological progress is expressed by the ratio of technological innovation funding to GDP (%). Third, Foreign direct investment is expressed in the amount of foreign capital introduced (100 million CNY). Fourth, oil prices. The representative international oil markets mainly include the Dubai Petroleum Exchange Market in the UAE, the Brent Petroleum Exchange Market in the United Kingdom, and the West Texas Petroleum Exchange Market in the United States. This article uses the average oil prices of the three major oil markets as the variable value of oil prices (CNY/ton). Fifth, incentive-based environmental regulations are delegated by the ratio of investment in environmental governance to GDP (%). Sixth, this paper uses the number of environmental laws enacted by the government to represent mandatory environmental regulations (Piece). Seventh, economic growth. GDP per capita can objectively measure the level of regional economic development. Carbon intensity, economic growth, oil prices, and foreign direct investment have been deflated to remove the effects of inflation. The raw data for the economic variables come from the Wind database (<https://www.wind.com.cn/>, (accessed on 1 January 2021)). The definitions and units of the variables used are presented in Table 1. The statistical results of the variable series are presented in Table 2.

Table 1. Definition and unit of variables in this paper.

Variable	Definition	Unit
CI	Carbon intensity	Ton/10 ⁴ CNY
ENS	Energy consumption structure	%
TEC	Technological progress	%
IER	Incentive-based environmental regulations	%
MER	Mandatory environmental regulations	Piece
FDI	Foreign direct investment	100 million CNY
PRI	Oil prices	CNY/ton
GDP	Economic growth	CNY

Table 2. The statistical description of variables.

Variable	Units	Mean	Std.dev.	Min	Max	Obs
CI	Ton/10 ⁴ CNY	4.17	2.98	0.44	19.05	450
ENS	%	69.23	23.87	6.67	99.90	450
TEC	%	0.92	0.56	0.02	3.24	450
IER	%	15.75	12.12	2.22	84.70	450
MER	Piece	66.68	61.49	1.0	394.0	450
FDI	100 million CNY	446.0	478.7	0.31	2247.7	450
PRI	CNY/ton	387.0	84.2	240.0	527.4	450
GDP	CNY	42,638	27,018	5052	164,220	450

Notes: Obs represents observation.

4. Results

4.1. Unit Root Test

Since the 1960s, the development of econometrics has entered a fast lane. Econometric methods have become mainstream economics, sociology, and management research methods. However, the premise of econometric model regression is that the variable series is stationary. The unit root test is generally used to judge whether an economic series is stationary. If the socio-economic variable sequence has unit roots, it becomes a non-stationary sequence. Many existing studies have proved that a unit root process in an economic sequence implies non-stationarity and that a pseudo-regression problem in regression analysis may occur. The unit root test has now become an indispensable step in econometric analysis. If the probability value of the statistic value of the unit root test is less than 10%, it means that the tested economic variable sequence is stationary. On the contrary, it means that the series of variables is non-stationary. This paper uses the IPS, ADF, ADF-Fisher, Breitung test, Fisher-PP, and CIPS tests to examine the economic series used. Different from other testing methods, the CIPS test can determine whether the series of economic variables is stationary on the basis of considering the possible cross-sectional correlation. In order to improve the reliability of the test results, this paper uses these six methods to perform unit root tests. The formula for the main tests is listed in Appendix A. The results in Table 3 show that all economic series are not stationary.

Table 3. Results of unit root tests.

Series	LLC	Breit	PP	IPS	ADF	CIPS	Obs
LCI	−9.86 ***	0.47	226.41 ***	−4.97 ***	128.88 ***	−2.345	450
LENS	−0.86	2.13	80.81 **	−6.93 ***	65.34	−2.887 **	450
LTEC	0.47	5.18	19.96	5.11	29.40	−2.337	450
LIER	−5.23 ***	−0.19	73.58	−1.92 **	78.65 *	−1.941	450
LMER	−3.74 ***	4.16	100.62 ***	0.47	72.85	−3.058 ***	450
LFDI	−0.81	3.92	62.22	0.44	71.21	−2.058	450
LPRI	−0.92	−2.69 ***	68.67	−1.44 *	58.28	−2.003	450
LGDP	−1.97 **	6.11	22.00	4.71	24.18	−1.484	450

Notes: The above results of the test, under the condition that the constant and trend terms are included. At the 10% significance level, passing a significant test is indicated by *; At the 5% significance level, passing a significant test is indicated by **; At the 1% significance level, passing a significant test is indicated by ***. The above results are implemented by Stata software.

4.2. Cointegration Tests

Cointegration theory was first proposed by Engle and Granger [53]. It lays a theoretical foundation for finding equilibrium relations between two or more non-stationary variables and establishing error correction models with cointegration relations. Cointegration is the sequence when multiple economic variables show as non-stationarity, but a specific linear combination of these variables shows stability. Under these circumstances, a long-term stable relationship can exist between these variables. The methods suitable for testing the cointegration relationship of panel data mainly include the Pedroni test and the Kao test. Based on the logarithmic variable data, this paper uses these two methods to perform cointegration tests (Table 4). The probability values of the statistical values in Table 4 are all less than 10%, indicating that there is a causal nexus between carbon intensity and its determinants.

Table 4. Result of panel cointegration test.

Method	Statistics	Statistical Value (<i>p</i> -Value)
Kao test	Augmented Dickey–Fuller	2.395 ***
	Unadjusted Modified Dickey–Fuller	−1.700 **
Pedroni test	Modified Phillips–Perron	8.443 ***
	Phillips–Perron	−10.436 ***
	Augmented Dickey–Fuller	−9.505 ***

Notes: The above results are implemented by Stata software. ** and *** indicate the significance levels of 5% and 1%, respectively.

4.3. Multicollinearity Test

Econometric theory states that multicollinearity problems will arise if the explanatory variables are closely related. Multicollinearity includes perfect multicollinearity and approximate multicollinearity. Perfect multicollinearity will have some serious consequences, such as non-existence of parameter estimates and infinite variance of parameter estimates. Approximate multicollinearity produces undesirable results as follows: (1) the variance of the parameter estimates increases; (2) the confidence intervals of the parameter estimates become larger; and (3) the t-test of the estimated parameters may not be significant. The methods of multicollinearity test mainly include: (1) simple correlation coefficient method; (2) variance inflation factor (VIF) method; and (3) Klein’s discriminant rule. The VIF method has the advantages of easy operation and objective test process. Therefore, this paper uses the VIF method to perform a multicollinearity test. The formula of VIF is as follows:

$$VIF_j = \frac{1}{(1 - R_j^2)} \tag{5}$$

where R_j^2 represents the goodness of fit. J indicates that the j -th explanatory variable is used as the dependent variable for regression estimation. If $VIF_j \geq 10$, it indicates there is a severe multicollinearity between the explanatory variable and other explanatory variables. Moreover, this multicollinearity has serious adverse effects on the results of the ordinary least squares estimation. Conversely, if VIF_j is less than 10, it indicates that the multicollinearity is weak and will not have a serious adverse effect on the estimation results. The results in Table 5 show that all the values of VIF are less than 10, indicating that model 4 does not have severe multicollinearity.

Table 5. Results of the variance inflation factor (VIF).

Explained Variable	R ²	VIF	Judgement Result
LENS	0.229	1.297	<10
LTEC	0.583	2.398	<10
LIER	0.266	1.362	<10
LMER	0.358	1.558	<10
LFDI	0.357	1.555	<10
LPRI	0.126	1.144	<10
LGDP	0.572	2.336	<10

4.4. Tests of Normal Distribution

For traditional econometric models, an important prerequisite for obtaining good estimates is that the variable sequence obeys a normal distribution. However, many research results have shown that the series of economic variables is often non-normally distributed. Under the condition that the economic series is not normally distributed, the result of quantile regression is more robust. Therefore, before the model regression, this paper uses the Q-Q diagram (i.e., quartile–quartile) to test whether the economic series used is normally distributed. The results in Figure 1 show that the blue variable curve does not completely fit the X = Y line, which indicates that these economic series are not normally

distributed. In this case, it is more reasonable to use quantile regression to investigate carbon intensity.

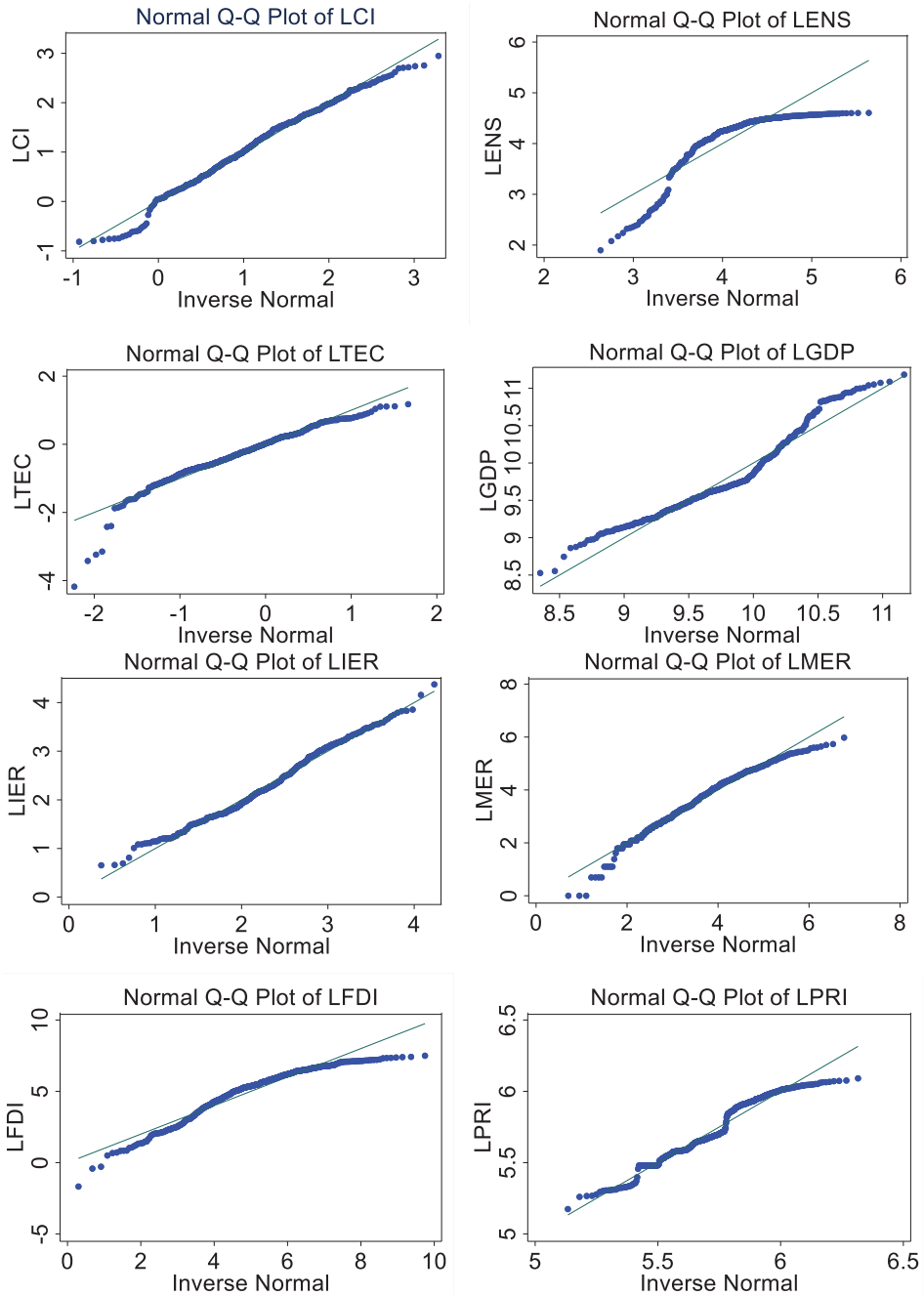


Figure 1. Q-Q diagram of economic variable series.

4.5. Quantile Regression Results

According to the level of carbon intensity, this paper divides the 30 administrative units into 6 groups (Table 6). The results of quantile regression are listed in Table 7, and the graph of quantile regression results is placed in Figure 2. In addition, this paper also uses the mean models for regression, and compares its results with that of quantile regression (Table 7):

Table 6. Grouped results of 30 provinces according to the level of carbon intensity.

Quantile Group	Provinces
lower 10th	Tianjin, Beijing, Guangdong
10th–25th	Jiangsu, Shandong, Fujian, Jiangxi
25th–50th	Hunan, Zhejiang, Henan, Hainan, Guangxi, Chongqing, Hebei, Gansu
50th–75th	Anhui, Yunnan, Liaoning, Shaanxi, Hubei, Xinjiang, Guizhou, Shanxi
75th–90th	Qinghai, Jilin, Inner Mongolia, Sichuan
upper 90th	Shanghai, Ningxia, Heilongjiang

Table 7. Quantile regression result.

Variables	Quantile Regression					Median
	10th Quant	25th Quant	50th Quant	75th Quant	90th Quant	
Constant	1.786	6.270 ***	8.529 ***	11.094 ***	14.501 ***	8.529 ***
LENS	0.677 ***	0.022	−0.328 **	−0.852 ***	−0.948 ***	−0.328 ***
LTEC	−0.287 ***	−0.327 ***	−0.336 ***	−0.275 ***	−0.170 **	−0.336 ***
LIER	0.285 ***	0.418 ***	0.479 ***	0.418 ***	0.383 ***	0.479 ***
LMER	−0.010 ***	−0.053 *	−0.102 ***	−0.136 ***	−0.151 **	−0.102 ***
LFDI	−0.072 ***	−0.031 **	0.041 *	−0.038 ***	−0.052 **	−0.041 **
LPRI	0.115 **	0.079 ***	−0.106 **	−0.117 **	−0.151 *	−0.106 *
LGDP	−0.489 ***	−0.688 ***	−0.652 ***	−0.584 ***	−0.820 ***	−0.652 ***
Pseudo R ²	0.390	0.313	0.316	0.309	0.306	0.316

Notes: Median regression is represented by median. *, ** and *** indicate the significance levels of 10%, 5% and 1%, respectively.

(1) Incentive-based environmental regulations. The carbon intensity in the 10th–25th, 25th–50th, and 50th–75th quantile groups receives a larger impact from incentive-based environmental regulations, with coefficients of 0.418, 0.479 and 0.418, respectively. These quantile groups mainly include Jiangsu, Shandong, Fujian, Hunan, Zhejiang, Henan, Hebei, Guangxi, Liaoning, Hebei, and Shanxi provinces. These provinces are home to many industrial enterprises, such as coal processing plants, petrochemical, iron and steel, and cement enterprises. To achieve low-carbon growth, local governments strengthen environmental regulations. Strict environmental regulations have prompted industrial companies to upgrade technology and equipment, which further cut down carbon intensity;

(2) Mandatory environmental regulations. Carbon intensity receives a negative effect from mandatory environmental regulations, as its regression coefficients ranging from the lower 10th quantile group to the upper 90th quantile group are −0.010, −0.053, −0.102, −0.136, and −0.151, respectively. A negative coefficient indicates that increasing the formulation and implementation of environmental laws has the effect of reducing carbon intensity. Furthermore, mandatory environmental regulations have a greater impact on carbon intensity in the 25th–50th, 50th–75th, and 75th–90th quantile groups. This is mainly because these provinces have enacted more environmental laws to deal with industrial pollution;

(3) The regression coefficients of energy consumption structure in the 25th–50th, 50th–75th, and 75th–90th quantile groups are negative, −0.328, −0.852, and −0.948, respectively. This result implies that changes in energy structure have contributed to the decline in carbon intensity. This is because the rate of clean energy in total energy consumption continues to expand, which is conducive to reducing CO₂ emissions. These groups include

Yunnan, Sichuan, Guangxi, Shanxi, Shaanxi, Inner Mongolia, Liaoning and Jilin. There are many rivers in Yunnan, Sichuan, and Guangxi, and the vertical drop of the rivers is large. The central government and local governments continued to increase hydropower development, and their hydropower output increased rapidly. Local industrial enterprises expand the use of hydropower, which improves energy structure and further drives down carbon intensity. Shanxi, Shaanxi and Inner Mongolia are major coal producing provinces. The local government encourages coal-to-gas production. Local industrial companies expand gas use, which helps reduce carbon intensity;

(4) The parameter estimates of technological progress in all quantile groups are negative, namely -0.287 , -0.327 , -0.336 , -0.275 , and -0.170 , respectively. This means that technological innovation is conducive to reducing carbon intensity. Technology is an important contributor to achieving carbon intensity reduction. In recent years, economic development has enabled government finance and industrial enterprises to allocate more funds to scientific and technological innovation. The number of granted patents has grown rapidly, and the application of patented technology helps industrial companies reduce carbon intensity;

(5) Foreign direct investment is negatively related to carbon intensity, which means that expanding foreign investment can contribute to the decline of carbon intensity. To improve the technical level of industrial enterprises, the government vigorously introduces foreign investment projects with advanced technology and less pollution. These technologically advanced and low-energy-consuming projects have driven domestic industrial enterprises to upgrade their technologies and equipment, reducing carbon intensity;

(6) The parametric estimates of oil prices are negative in the high quantile groups, indicating that oil prices have contributed to the decline in carbon intensity. International oil prices have generally risen, although with occasional sharp fluctuations. This brings a heavy economic burden to local industrial enterprises and is not conducive to the long-term stable development of this industry. Therefore, local governments actively develop clean energy and accelerate the replacement of oil resources. Expanded use of clean energy reduces CO₂ emissions, thereby contributing to a reduction in carbon intensity;

(7) Economic growth. The regression coefficients of economic growth in all groups are negative, -0.489 , -0.688 , -0.652 , -0.584 , and -0.820 , respectively. This denotes that economic growth is contributing to a reduction in carbon intensity. The coefficient values are all between -1 and 0 . It indicates that for every 1% increase in economic growth, carbon intensity decreases by less than 1%. The decline in carbon intensity is less than the increase in economic growth, and the main reasons for this are as follows: the mode of economic growth is undergoing a transition from an extensive economic growth to green economic growth; governments at all levels vigorously develop the high-tech industries and tertiary industries, and strictly control the scale of heavy industry; technological innovation and equipment renewal brought about by the development of high-tech industries are applied in the heavy industries, which promotes the reduction in carbon intensity; and economic growth still emits carbon dioxide, but the carbon intensity of economic growth is gradually decreasing.

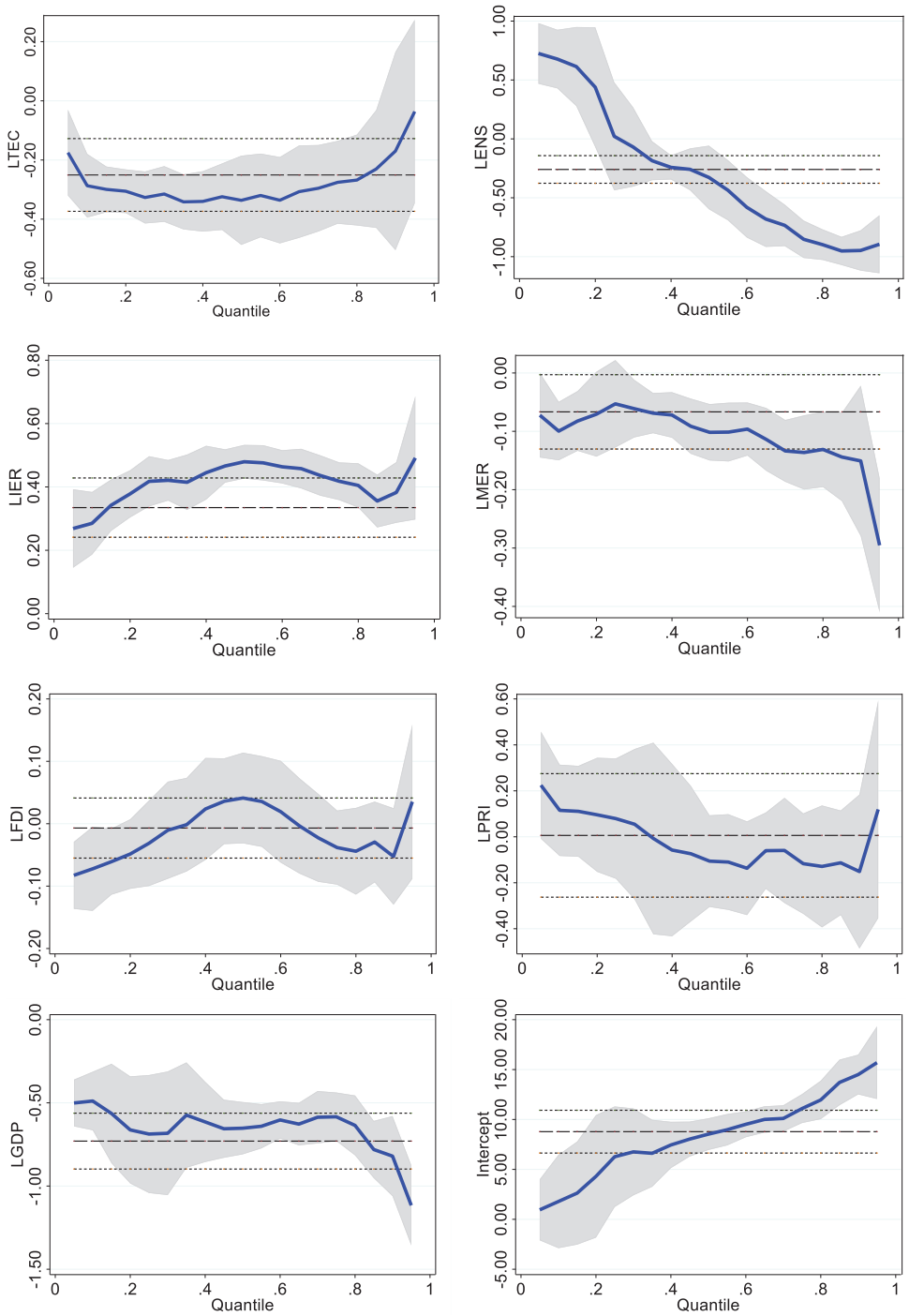


Figure 2. Plot of quantile estimates of carbon intensity.

5. Robustness Test

To test the reliability of the estimated results of carbon intensity, this paper adopts the method of changing variables' values to test the robustness. In Section 4.5, the value of foreign direct investment (FDI) is measured by total foreign direct investment, and technological progress is measured by the share of R&D investment in GDP. This section uses FDI per capita as the variable value of FDI and uses the number of patents per 10,000 people to measure technological progress. Then the paper uses the quantile regression model for regression estimation. The results in Table 7 show that the signs of the regression coefficients for foreign direct investment (LFDI) and technological progress (LTEC) are consistent with the results in Table 6. Combining the results in Tables 7 and 8, it can be seen that the quantile regression has high robustness, and the estimation results are reliable.

Table 8. Robustness test: the results of quantile estimation.

Variables	Quantile Regression					Median
	10th Quant	25th Quant	50th Quant	75th Quant	90th Quant	
Constant	1.915	5.120 **	7.724 ***	9.799 ***	15.237 ***	7.724 ***
LENS	0.337 ***	0.078	−0.358 *	−0.889 ***	−0.866 ***	−0.358 ***
LTEC	−0.307 ***	−0.289 ***	−0.204 ***	−0.187 ***	−0.054	−0.204 ***
LIER	0.189 *	0.258 ***	0.313 ***	0.395 ***	0.367 ***	0.313 ***
LMER	−0.033	−0.054	−0.083 ***	−0.113 ***	−0.205 ***	−0.083*
LFDI	−0.107 ***	−0.086 **	0.028	−0.048	−0.043	−0.028
LPRI	0.340 **	0.287 *	−0.287 **	−0.173	−0.084	−0.287
LGDP	−0.001	−0.170	−0.336 ***	−0.353 ***	−0.994 ***	−0.336 **
Pseudo R ²	0.423	0.341	0.327	0.321	0.304	0.428
Obs	450	450	450	450	450	450

Notes: *, ** and *** indicate the significance levels of 10%, 5% and 1%, respectively.

6. Discussion

Several of the above empirical results deserve further discussion.

6.1. The Carbon Intensity in the 10th–25th, 25th–50th, and 50th–75th Quantile Groups Are More Affected by Incentive-Based Environmental Regulations

This result differs from the conclusion of Yang et al. [54]. Using a nonlinear mediating effect model, they found a positive U-shaped nonlinear relationship between environmental regulations and carbon intensity. The provincial differences in environmental governance investment and resource tax can explain this result. (1) Environmental governance investment. An important feature of the incentive-based environmental regulations is the economic leverage it carries out when influencing pollutant emissions of industrial enterprises. Government departments affect the decision-making of industrial enterprises via the utilization of prices, taxes, charges, subsidies, credits, etc. The implementation of incentive environmental policies leads to an increase in the production cost of industrial enterprises. The larger the energy consumption scale of the enterprise, the greater the cost. This forces industrial companies to expand technological research and equipment upgrades, thus promoting a decline in carbon intensity. Statistics show that from 2005 to 2019 the average investment in industrial pollution control in the 10th–25th, 25th–50th, and 50th–75th quantile groups was 4.04 billion CNY, 1.90 billion CNY, and 1.85 billion CNY, respectively, which was higher than that in the lower 10th quantile group (1.77 billion CNY), the 75th–90th quantile group (1.43 billion CNY) and the upper 90th quantile group (1.14 billion CNY). More pollution control investment can not only update production technology, but also help to expand the use of carbon abatement equipment. The 10th–25th, 25th–50th, and 50th–75th quantile groups have more investment in environmental governance. This helps industrial enterprises to carry out technological innovation and mitigate carbon intensity.

(2) Resource tax. The resource tax turns the cost of environmental pollution into the internal cost for industrial enterprises. The resource tax is flexible and can effectively give full play to the subjective initiative of enterprises and promote their green transformation [55]. An example is the government environmental protection agency's levy resource tax on coal mining companies. The imposition of resource tax has led to rising coal prices and increased production costs for industrial enterprises. Governments are concerned about economic development and strengthening environmental supervision. Many heavy industrial enterprises are distributed in the 10th–25th, 25th–50th, and 50th–75th quantile provinces, such as Henan, Hebei, Shandong, Liaoning, Shaanxi, Hubei, Shanxi, and Guizhou. The formulated resource tax controls the serious environmental pollution and CO₂ emissions caused by industrial production. The resource tax levied by the above quantile provinces is more. This urges local industrial enterprises to update technology and equipment; therefore, the carbon intensity of the 10th–25th, 25th–50th, and 50th–75th quantile provinces is affected more by incentive environmental regulation.

6.2. Mandatory Environmental Regulations Significantly Impact Carbon Intensity in the Lower 10th Quantile Group

This result differs from the findings of Hou et al. [56]. Using a dynamic threshold effect model, they investigated China's industrial sector and found that environmental regulations affect carbon intensity through industrial structure transformation. Strict environmental regulations are not conducive to reducing carbon intensity. The provincial differences in the number of environmental decrees could explain the result in this paper. Mandatory environmental regulations are a direct regulatory tool, and an important means to achieve the purpose of environmental governance and are an administrative-led environmental governance mechanism. Under the direct regulation mode, the government relies on its power to directly regulate energy use and pollution emissions. In the process of economic construction, the role of the government is not only a "night watchman", but an "active participant". The Chinese government participates in environmental governance by formulating relevant environmental laws and regulations. In general, mandatory environmental regulations are more restrictive to industrial enterprises. If the pollutant discharge of industrial enterprises exceeds the standard, there will be serious consequences such as severe administrative penalties, fines, suspension of production activities or business closures [57]. An analysis of the statistics found that from 2005 to 2019, the governments in the lower 10th quantile provinces enacted the smallest environmental laws, with an average of 42 environmental laws per year. Other provinces have enacted more environmental ordinances. From the 10th–25th quantile group to the upper 90th quantile group, the average environmental regulations were 112, 78, 63, 51, and 46, respectively. The lower 10th quantile group includes Beijing, Tianjin, and Guangdong provinces; these three provinces are economically developed and have strong economic strength. Local government departments prefer to use incentive-based environmental regulations to promote industrial enterprises to upgrade technology and reduce CO₂ emissions, such as clean energy subsidies and R&D capital investment. Therefore, the contribution of imperative environmental regulations to the carbon intensity in the lower 10th quantile group is relatively small.

6.3. Technological Progress Contributes More to the Carbon Intensity in the Lower 10th, 10th–25th, and 25th–50th Quantile Groups

This result differs from the findings of Gu et al. [58], who do not give provincial differences in the impact of technological progress on carbon intensity. The results of this paper are mainly attributable to the obvious differences in the number of patents and energy intensity. (1) Provincial differences in the number of patents. For a long time, the heavy industries have been high energy-intensive, and their main source of energy consumption is high-emission coal. In order to control CO₂ emissions, governments at all levels and industrial enterprises have increased investment in research and development. Statistics show that from 2005 to 2019 the average growth rate of government financial investment in science and technology reached 15.0%. The growth rate of technological research and

development expenditures of industrial enterprises was 18.4%. Rapidly increasing R&D investment helps to obtain more patented technologies, such as energy-saving, carbon emission reduction, carbon capture, and renewable energy technologies. The statistics show that from 2005 to 2019 the average numbers of patents granted in the lower 10th, 10th–25th, and 25th–50th quantile groups were 158,146 pieces, 140,986 pieces, and 54,871 pieces, respectively. However, the number of patents granted in the 50th–75th, 75th–90th, and upper 90th quantile groups in these provinces was 32,672 pieces, 24,130 pieces, and 35,954 pieces. The number of patents granted in the lower quantile provinces was higher. The lower 10th, 10th–25th, and 25th–50th quantile groups have more advanced patented technologies, such as high-efficiency and energy-saving melting technology, and blast furnace energy-saving equipment. The promotion of many advanced patented technologies helps to reduce coal use and control CO₂ emission growth, thereby contributing to the reduction in carbon intensity. Therefore, technological progress contributes more to the decline in carbon intensity in these quantile groups.

(2) Provincial differences in energy intensity. Energy intensity is an important path through which technological progress affects carbon intensity [59]. Technological progress helps industrial companies use more advanced energy-efficient equipment, thereby reducing energy intensity. Coal and oil have long been the main sources of heavy industrial enterprises. Low energy intensity helps reduce fossil energy use, further contributing to a reduction in carbon intensity. Statistics show that from 2005 to 2019, the energy intensity of the lower 10th quantile provinces, 10th–25th quantile provinces, and 25th–50th quantile provinces were the lowest, at 0.39 ton/10,000 CNY, 0.74 ton/10,000 CNY, and 1.04 ton/10,000 CNY, respectively. However, the energy intensity of 50th–75th quantile provinces, 75th–90th quantile provinces, and upper 90th quantile provinces was 1.81 ton/10,000 CNY, 2.34 ton/10,000 CNY, respectively. Low energy intensity means that the same output can be obtained with less energy consumption. The energy intensity of the lower 10th quantile provinces, 10th–25th quantile provinces, and 25th–50th quantile provinces is the lowest, resulting in technological progress having the greatest impact on carbon intensity.

6.4. Foreign Direct Investment Has a Larger Impact on Energy Intensity in the Lower 10th Quantile Group

This result differs from the findings of Cai et al. [60]. They divide foreign direct investment into outward foreign direct investment (OFDI) and inward foreign direct investment (IFDI), finding that OFDI leads to an increase in carbon intensity and IFDI helps reduce carbon intensity. The differences in foreign direct investment can explain this result in this paper. The “pollution shelter hypothesis” holds that foreign direct investment will cause polluting industries to migrate to developing countries due to the loosening of environmental regulations, and this will exacerbate environmental pollution in developing countries. Since the economic reforms in 1980, China has been one of the most active host countries for foreign direct investment inflows. Foreign direct investment activates the market economy, promotes social employment, and drives Chinese domestic industrial enterprises to focus on technological innovation. While China has become the “processing factory of the world,” it also produces many CO₂ emissions. In recent years, Chinese governments have strictly monitored foreign-funded projects and vigorously introduced foreign-funded projects with advanced technology [61]. Through technology spillovers, foreign direct investment drives Chinese domestic industrial enterprises to upgrade their technologies and equipment, promoting a reduction in carbon intensity. Statistics show that from 2005 to 2019, the average foreign direct investment in the lower 10th quantile group was 380.7 billion CNY, much more than that in the 10th–25th quantile group (268.0 billion CNY), the 25th–50th quantile group (73.3 billion CNY), the 50th–75th quantile group (56.4 billion CNY), the 75th–90th quantile group (36.2 billion CNY), and the upper 90th quantile group (176.1 billion CNY). The lower 10th quantile group brings

in the most investment, making a foreign direct investment the largest contributor to the reduction in carbon intensity.

6.5. Energy Consumption Structure Significantly Reduces the Carbon Intensity in the 50th–75th, 75th–90th, and Upper 90th Quantile Groups

The results of this paper show that the energy consumption structure has a positive impact on the carbon intensity of some quantile provinces and exerts a negative impact in other provinces. This result differs from the findings of Yu et al. [62], who found that the improvement of energy consumption structure is helpful to reduce carbon intensity. The provincial differences in coal consumption can explain the above results in this paper. China's coal reserves are abundant and easy to exploit. The open-pit coal mines are distributed in many provinces in China, such as Inner Mongolia, Shanxi and Shaanxi provinces. Heavy industry production requires much energy, and to ensure adequate energy supply most of the heavy industries get situated in areas rich in coal resources or areas with convenient shipping, such as Anshan City in Liaoning Province, Panzhihua City in Sichuan Province, Shanghai City, and Huainan in Anhui province. For a long time, heavy industry enterprises have mainly used coal for production activities. The heavy use of coal has made the heavy industry the number one source of CO₂ emissions, which results in carbon intensity being high [63]. Reducing coal use and increasing clean energy consumption can significantly reduce carbon intensity. For example, many local governments have expanded energy subsidies to support natural gas and biomass use. The implementation of these measures has gradually reduced the proportion of coal. Many provinces in the 50th–75th, 75th–90th, and upper 90th quantile groups have numerous heavy industrial enterprises, such as Liaoning, Shanxi, Shanxi, Jilin, Heilongjiang, and Shaanxi provinces. These provinces are large coal-producing areas, providing sufficient energy sources to develop the heavy industry. In the context of carbon emission reduction targets, these provinces have significantly reduced direct coal combustion and increased the use of clean energy. For example, Shanxi, Shaanxi, and Inner Mongolia provinces vigorously developed a coal-to-gas technology and expanded the production scale of coal-to-liquids gas. The energy structure has been significantly improved so that the energy consumption structure contributes more to reducing carbon intensity.

7. Conclusions and Policy Implications

7.1. Conclusions

After performing the normality test, this paper investigates carbon intensity using a quantile regression model. The results obtained are as follows: (1) the carbon intensity in the 10th–25th, 25th–50th, and 50th–75th quantile groups is more affected by incentive-based environmental regulations, because the provinces in these groups invest more environmental governance funds and collect more resource taxes; (2) mandatory environmental regulations played a significant role in reducing carbon intensity and contributed the most to the decline in carbon intensity in the lower 10th quantile group; (3) technological progress contributes more to the carbon intensity in the low quantile provinces such as Guangdong, Beijing, Tianjin, Fujian, and Hainan; (4) foreign direct investment has a larger impact on energy intensity in Tianjin, Beijing, and Guangdong provinces, because these provinces bring in more foreign-funded enterprises; and (5) the energy structure played a role in significantly reducing the carbon intensity in the high quantile groups.

7.2. Policy Implications

7.2.1. The Lower 10th, 75th–90th, and Upper 90th Quantile Groups Should Improve the Environmental Tax System and Expand Environmental Governance Input

The coefficients of incentive-based environmental regulations in all quantile groups are all positive, indicating that incentive-based environmental regulations have not played a significant role in reducing carbon intensity. Therefore, all quantile groups should further increase environmental governance investment and raise the standard of environmental tax.

(1) The governments could formulate corresponding pollution tax standards based on each region's economic development. The standard of pollutant discharge fees should be higher than the income from enterprises stealing pollutants. This can prompt manufacturers to pay attention to pollution taxes and take specific actions to reduce CO₂ emissions, such as biofuels and pure electric vehicles. In addition, the environmental protection department could further improve the environmental monitoring system and strictly review the pollution discharge of all enterprises to ensure that the environmental protection tax is fully collected. (2) The government expands channels and increases pollution control investment. Fiscal funds for pollution control are often insufficient, which leads to unsatisfactory industrial pollution control. Government departments can adopt flexible mechanisms to encourage private capital to enter the field of environmental governance. For example, the government encourages private enterprises to participate in the construction of industrial parks, professionally deal with industrial CO₂ emissions, and obtain corresponding economic income. (3) Local governments should give full play to the leverage of financial funds and use limited financial funds to leverage more social capital into the fields of pollution control and environmental protection. This can give play to the multiplier effect of financial funds and achieve the impact of attracting more investment with the least amount of funds. Taking into account the main role of enterprises in pollution prevention and control, the government should guide enterprises to increase investment in environmental protection. For example, the tax department can lower the tax rate to encourage enterprises to increase investment in environmental protection equipment and improve production technology.

7.2.2. The Lower 10th Quantile Group Can Strengthen the Supervision of the Implementation of Mandatory Environmental Regulations

The coefficients of mandatory environmental regulations in all quantile groups are negative, indicating that the implementation of environmental laws has played a significant role in reducing carbon intensity. However, the absolute value of the coefficient for the lower 10th quantile group is the smallest, indicating that mandatory environmental regulations contribute the least to the reduction in carbon intensity. Therefore, the local government should further strengthen the formulation of environmental laws and strict environmental assessment systems. (1) In implementing command-type environmental regulations, the government should focus on implementing policies flexibly. It can focus on opening up more market areas and increasing market competition, forcing heavily polluting enterprises to transform faster. The government can formulate cleaner production demonstration projects and green technology promotion catalogs. Industrial enterprises with demonstration projects can enjoy a certain percentage of tax relief and financial subsidies. (2) The central government should improve the performance appraisal system and strictly assess the main responsibility of local governments for environmental protection. Local governments can establish a dynamic assessment mechanism for regional environmental quality and increase the weight of environmental protection in the assessment of local officials. During the promotion process of officials, the government adds the step of evaluating environmental performance. The government should bundle environmental protection with the "political life" of officials, which can ensure the continuity of local environmental protection goals.

7.2.3. The Government Should Take Various Measures to Increase Investment in Technology R&D

The absolute value of the coefficient of technological progress in the 50th–75th, 75th–90th, upper 90th quantile groups is smaller than that in the lower 10th, 10th–25th and 25th–50th quantile groups. It indicates that the contribution of technological progress to reducing the carbon intensity of the 50th–75th, 75th–90th, upper 90th quantile groups is relatively small. Therefore, these quantile groups should increase technological personnel training and research and development investment to improve the technical level. (1) The government should provide credit guarantees to encourage financial institutions to inject funds into technological innovation. Technological innovation activities are high risk and

high investment, and many companies do not have sufficient funds for technological innovation. Therefore, the financial support of financial institutions is crucial. The government provides guarantees for financial loans, which can ensure that R&D institutions receive much-needed funds. In addition, the government has formulated preferential policies to facilitate the entry of technology-based enterprises into the financial market. This has helped tech companies tap into the bond and stock markets and be well funded. (2) The government should increase support for the research and development of low-carbon technology. Firstly, the government can improve the scientific research platform and increase the guidance of research and development policies. For example, the government establishes a platform for enterprises and research institutes to communicate with each other. This helps research institutions to promote the acquired low-carbon technologies to the market as soon as possible. Second, the taxation department collects environmental protection tax and uses a certain percentage of the tax to subsidize green technology innovation. This can improve the enthusiasm of enterprises to engage in technology research and development and encourages industrial enterprises to update emission-reduction equipment. (3) The government should formulate differentiated carbon emission reduction targets and paths. Resource-based provinces can accelerate the transformation of the “extensive” development mode to the “high-efficiency, clean, and low-carbon” mode. The government accelerates the optimization of energy structure and promotes the transformation of technological progress to a low-carbon direction. Non-resource-based provinces should vigorously promote the development of energy technology and develop high-tech industries. Accelerating the optimization of the industrial structure can improve energy efficiency and promote carbon emission reduction in the heavy industry.

7.2.4. The 10th–25th, 25th–50th, 50th–75th, 75th–90th, and Upper 90th Quantile Groups Are Supposed to Strengthen the Management of Foreign-Funded Projects

The impact strength of foreign direct investment on carbon intensity in the 10th–25th, 25th–50th, 50th–75th, 75th–90th, and upper 90th quantile groups is low. Therefore, these quantile groups should take various measures to introduce more high-tech projects. (1) Local governments should reject the introduction of energy-intensive projects such as steel projects, petrochemicals, and non-ferrous metal processing projects. For heavy industrial projects that need to be introduced urgently, the government can control them through carbon taxes, carbon permits, and carbon emission trading. This helps control heavy industry scale, remove excess capacity, and improve energy efficiency. (2) The government should further adjust and optimize the structure of foreign direct investment and introduce foreign direct investment with low-carbon and new energy technologies. The government should formulate policies to give full play to the technology spillover effect of foreign direct investment to improve the low-carbon technology of domestic industrial enterprises. For example, the government can encourage foreign-funded enterprises to merge or acquire small and medium-sized industrial enterprises. This will help improve the technology and equipment level of the overall industrial sector as soon as possible and reduce energy consumption and carbon intensity. (3) The government should encourage domestic companies to establish joint ventures with foreign companies. This can expand the introduction of foreign capital and enable domestic enterprises to master advanced management models and technologies as soon as possible. Furthermore, the central government encourages the central and western regions to expand the introduction of foreign capital. (4) In the process of introducing foreign capital, local governments had better pay attention to the different CO₂ emissions in different industries. The government can increase investment in higher education and research institutes to improve technology absorptive capacity. This can give full play to the technological spillover effect of foreign direct investment and drive industrial enterprises to update emission reduction technologies.

7.2.5. The Lower 10th, and 10th–25th Quantile Groups Should Adopt Incentives to Urge Heavy Industry Producers to Expand the Use of Low-Carbon Energy

The coefficients of energy consumption structure in the lower 10th, and 10th–25th quantile groups are positive numbers (i.e., 0.677 and 0.022), indicating that energy consumption structure is not conducive to reducing carbon intensity. Therefore, these quantile groups should actively promote industrial enterprises to expand the use of clean energy. (1) The local governments should encourage heavy industry producers to expand the use of coal gas. China has abundant coal resources and under the conditions that the coal-to-gas technology has matured, the government can encourage coal gas production and adopt an energy subsidy policy to encourage heavy industry producers to expand the use of coal gas. (2) The government ought to mobilize various resources to increase natural gas extraction and imports. For example, the government should adjust policies to allow private enterprises to extract natural gas. It will speed up natural gas extraction and increase natural gas production. Meanwhile, government departments should increase natural gas imports by sea and land. On the one hand, the western region should expand natural gas cooperation with Central Asian countries and expand natural gas imports. This can meet the natural gas consumption needs of heavy industrial enterprises in the central and western regions. On the other hand, the eastern coastal areas should increase their natural gas import by sea routes, such as Australia, Indonesia, and Qatar. (3) The government should accelerate the development of natural gas-fired power generation and mobilize the enthusiasm of natural gas production enterprises, power generation enterprises and power grid enterprises. The government expands the laying of natural gas transmission pipelines in areas where industrial enterprises gather and expands the scope of application of natural gas in the industrial sector. The financial department provides financial support to encourage industrial enterprises to update equipment, improve the efficiency of natural gas use, and increase the enthusiasm of implementing “from coal to natural gas”. Local governments should rationally plan the distribution of industrial parks and the sites of renewable energy production enterprises. The western region is rich in solar energy and wind power resources. The local governments can build industrial parks near photovoltaic production bases to conveniently deliver the clean electricity produced to industrial enterprises.

8. Limitation of the Study and Future Recommendation

8.1. Limitation of the Study

This paper uses the panel quantile regression model to investigate the carbon intensity of China’s heavy industry, and the estimated results show the heterogeneous effects of influencing factors on the carbon intensity across quantile provinces. However, the quantile regression model is still a linear regression model. Existing research results show that the relationship between economic variables is more likely to be nonlinear; this is because economic phenomena are complex and changeable. The quantile regression model cannot estimate the possible non-linear relationship between the explanatory variable and the dependent variable. This is a shortcoming of this article.

8.2. Future Recommendation

The nonparametric econometric models are data-driven. In nonparametric econometric models, the relationship between the explanatory variable and the explained variable is determined by the variable data itself, and there is no artificial setting. Therefore, the nonparametric econometric model can realistically simulate the real relationship between the influencing factors and carbon intensity. In the future, we will construct a new nonparametric econometric model and use it to examine the carbon intensity of China’s heavy industry. The research results can provide empirical support for the government to formulate targeted energy policies according to different development stages.

Supplementary Materials: The following supporting information can be downloaded at: <https://www.mdpi.com/article/10.3390/ijerph191912865/s1>, Table S1: The original data of “How to efficiently reduce the carbon intensity of the heavy industry in China? using quantile regression approach”.

Funding: The paper is supported by the National Natural Science Foundation of China (No. 71974085), and Central University Scientific Research Projects (No. 20720221050).

Institutional Review Board Statement: Not applicable.

Informed Consent Statement: Not applicable.

Data Availability Statement: Readers can request the original data of the article by email.

Conflicts of Interest: The author declares no conflict of interest.

Appendix A

Panel unit root test methods mainly include IPS (Im–Pesaran–Shin), Fisher-ADF, LLC (Levin–Lin–Chu), and Breitung tests.

(1) The equation of the LLC test is as follows:

$$\Delta y_{n,t} = \alpha y_{n,t-1} + \sum_{i=1}^p a_{n,i} \Delta y_{n,t-1} + d'_{n,t} b_n + e_{nt} \tag{A1}$$

where a is the autoregressive coefficient, and p is the lag order.

(2) Breitung test. Assuming that Δy_{nt} and $y_{n,t-1}$ are regressed on their lag term ($\Delta y_{n,t-1}, \Delta y_{n,t-2}, \dots, \Delta y_{n,t-p}$), the residuals obtained are $e_{1,nt}$ and $e_{2,nt}$, respectively. Then, the residuals are subjected to orthogonal dispersion transformation, and the following formula is obtained:

$$e_{nt}^* = \left(\frac{T-t}{T-t+1} \right)^{1/2} \left(e_{nt}^{**} - \frac{1}{T-t} \sum_{l=t+1}^T e_{nl}^{**} \right) \tag{A2}$$

Finally, perform the following regression:

$$e_{nt}^* = \alpha e_{nt}^{**} + r_{nt} \tag{A3}$$

(3) The equation of IPS test is as follows:

$$\Delta y_{nt} = \alpha_n y_{n,t-1} + \sum_{i=1}^p a_{ni} \Delta y_{n,t-1} + d'_{nt} b_n + v_{nt}, t = p_n + 2, p_n + 3, \dots, T \tag{A4}$$

(4) The assumptions of the Fisher-ADF test are as follows:

$$H_0 : \alpha_n = 0 \quad n = 1, 2, \dots, N \quad H_1 : \begin{cases} \alpha_n < 0 & n = 1, 2, \dots, N_0 \\ \alpha_n = 0 & n = N_0 + 1, N_0 + 2, \dots, N \end{cases} \tag{A5}$$

The formula for the test statistic is as follows:

$$\bar{t} = \frac{1}{N} \sum_{n=1}^N t_n \tag{A6}$$

Each test method has unique characteristics and a different range of applications. The ADF test is suitable for testing economic series with higher order autoregression.

References

- Zhang, R.; Wei, Q.; Li, A.; Ren, L. Measuring efficiency and technology inequality of China’s electricity generation and transmission system: A new approach of network Data Envelopment Analysis prospect cross-efficiency models. *Energy* **2022**, *246*, 123274. [CrossRef]
- Xu, B.; Lin, B. Investigating spatial variability of CO₂ emissions in heavy industry: Evidence from a geographically weighted regression model. *Energy Policy* **2021**, *149*, 112011. [CrossRef]
- Sheng, B.; Xu, B.; Pan, Y.; Chen, H. How to efficiently promote distributed energy resources in China: Using a nonparametric econometric method. *J. Clean. Prod.* **2021**, *285*, 125420. [CrossRef]

4. Bekun, F.V. Mitigating emissions in India: Accounting for the role of real income, renewable energy consumption and investment in energy. *Int. J. Energy Econ. Policy* **2022**, *12*, 188–192. [[CrossRef](#)]
5. Amerio, A.; Brambilla, A.; Morganti, A.; Aguglia, A.; Bianchi, D.; Santi, F.; Capolongo, S. COVID-19 lockdown: Housing built environment's effects on mental health. *Int. J. Environ. Res. Public Health* **2020**, *17*, 5973. [[CrossRef](#)] [[PubMed](#)]
6. Sun, C.; Zhu, B.; Zhu, S.; Zhang, L.; Du, X.; Tan, X. Risk Factors Analysis of Bone Mineral Density Based on Lasso and Quantile Regression in America during 2015–2018. *Int. J. Environ. Res. Public Health* **2021**, *19*, 355. [[CrossRef](#)] [[PubMed](#)]
7. Liang, Z.; Zhang, M.; Mao, Q.; Yu, B.; Ma, B. Improvement of eco-efficiency in China: A comparison of mandatory and hybrid environmental policy instruments. *Int. J. Environ. Res. Public Health* **2018**, *15*, 1473. [[CrossRef](#)] [[PubMed](#)]
8. Zhan, L.; Guo, P.; Pan, G. The effect of mandatory environmental regulation on green development efficiency: Evidence from China. *Environ. Sci. Pollut. Res.* **2022**, 1–11. [[CrossRef](#)]
9. Jiang, Z.; Wang, Z.; Li, Z. The effect of mandatory environmental regulation on innovation performance: Evidence from China. *J. Clean. Prod.* **2018**, *203*, 482–491. [[CrossRef](#)]
10. Wang, Z.; Zhu, Y. Do energy technology innovations contribute to CO₂ emissions abatement? A spatial perspective. *Sci. Total Environ.* **2020**, *726*, 138574. [[CrossRef](#)] [[PubMed](#)]
11. Ouyang, X.; Fang, X.; Cao, Y.; Sun, C. Factors behind CO₂ emission reduction in Chinese heavy industries: Do environmental regulations matter? *Energy Policy* **2020**, *145*, 111765. [[CrossRef](#)]
12. Aragón-Correa, J.A.; Marcus, A.A.; Vogel, D. The effects of mandatory and voluntary regulatory pressures on firms' environmental strategies: A review and recommendations for future research. *Acad. Manag. Ann.* **2020**, *14*, 339–365. [[CrossRef](#)]
13. Bekun, F.V.; Gyamfi, B.A.; Onifade, S.T.; Agboola, M.O. Beyond the environmental Kuznets Curve in E7 economies: Accounting for the combined impacts of institutional quality and renewables. *J. Clean. Prod.* **2021**, *314*, 127924. [[CrossRef](#)]
14. Jayachandran, S. Social norms as a barrier to women's employment in developing countries. *IMF Econ. Rev.* **2021**, *69*, 576–595. [[CrossRef](#)]
15. Wang, J.; Li, Z.; Ye, H.; Mei, Y.; Fu, J.; Li, Q. Do China's coal-to-gas policies improve regional environmental quality? A case of Beijing. *Environ. Sci. Pollut. Res.* **2021**, *28*, 57667–57685. [[CrossRef](#)]
16. Shvetsova, O.A.; Lee, J.H. Minimizing the environmental impact of industrial production: Evidence from south Korean waste treatment investment projects. *Appl. Sci.* **2020**, *10*, 3489. [[CrossRef](#)]
17. Hu, Y.; Ren, S.; Wang, Y.; Chen, X. Can carbon emission trading scheme achieve energy conservation and emission reduction? Evidence from the industrial sector in China. *Energy Econ.* **2020**, *85*, 104590. [[CrossRef](#)]
18. Tan, X.; Choi, Y.; Wang, B.; Huang, X. Does China's carbon regulatory policy improve total factor carbon efficiency? A fixed-effect panel stochastic frontier analysis. *Technol. Forecast. Soc. Chang.* **2020**, *160*, 120222. [[CrossRef](#)]
19. Yao, X.; Zhang, X.; Guo, Z. The tug of war between local government and enterprises in reducing China's carbon dioxide emissions intensity. *Sci. Total Environ.* **2020**, *710*, 136140. [[CrossRef](#)]
20. Ulmann, V.; Kralickova, A.; Dziejzinska, R. Mycobacteria in water used for personal hygiene in heavy industry and collieries: A potential risk for employees. *Int. J. Environ. Res. Public Health* **2015**, *12*, 2870–2877. [[CrossRef](#)]
21. Zhang, R.; Wei, Q.; Li, A.; Chen, S. A new intermediate network data envelopment analysis model for evaluating China's sustainability. *J. Clean. Prod.* **2022**, *356*, 131845. [[CrossRef](#)]
22. Li, P.; Xin, J.; Bai, X.; Wang, Y.; Wang, S.; Liu, S.; Feng, X. Observational studies and a statistical early warning of surface ozone pollution in Tangshan, the largest heavy industry city of North China. *Int. J. Environ. Res. Public Health* **2013**, *10*, 1048–1061. [[CrossRef](#)] [[PubMed](#)]
23. Xu, B.; Chen, J. How to achieve a low-carbon transition in the heavy industry? A nonlinear perspective. *Renew. Sustain. Energy Rev.* **2021**, *140*, 110708. [[CrossRef](#)]
24. Alshammari, Y.M. Scenario analysis for energy transition in the chemical industry: An industrial case study in Saudi Arabia. *Energy Policy* **2021**, *150*, 112128. [[CrossRef](#)]
25. Lin, B.; Xu, B. How does fossil energy abundance affect China's economic growth and CO₂ emissions? *Sci. Total Environ.* **2020**, *719*, 137503. [[CrossRef](#)] [[PubMed](#)]
26. Liu, D.; Liu, Y.; Sun, K. Policy impact of cancellation of wind and photovoltaic subsidy on power generation companies in China. *Renew. Energy* **2021**, *177*, 134–147. [[CrossRef](#)]
27. Mujtaba, A.; Jena, P.K.; Bekun, F.V.; Sahu, P.K. Symmetric and asymmetric impact of economic growth, capital formation, renewable and non-renewable energy consumption on environment in OECD countries. *Renew. Sustain. Energy Rev.* **2022**, *160*, 112300. [[CrossRef](#)]
28. Sueyoshi, T.; Zhang, R.; Qu, J.; Li, A. New concepts for environment-health measurement by data envelopment analysis and an application in China. *J. Clean. Prod.* **2021**, *312*, 127468. [[CrossRef](#)]
29. Rojas-Cardenas, J.C.; Hasanbeigi, A.; Sheinbaum-Pardo, C.; Price, L. Energy efficiency in the Mexican iron and steel industry from an international perspective. *J. Clean. Prod.* **2017**, *158*, 335–348. [[CrossRef](#)]
30. Toktarova, A.; Karlsson, I.; Rootzén, J.; Göransson, L.; Odenberger, M.; Johnsson, F. Pathways for low-carbon transition of the steel industry—a Swedish case study. *Energies* **2020**, *13*, 3840. [[CrossRef](#)]
31. Yue, H.; Worrell, E.; Crijns-Graus, W. Impacts of regional industrial electricity savings on the development of future coal capacity per electricity grid and related air pollution emissions—A case study for China. *Appl. Energy* **2021**, *282*, 116241. [[CrossRef](#)]

32. Wen, S.; Jia, Z.; Chen, X. Can low-carbon city pilot policies significantly improve carbon emission efficiency? Empirical evidence from China. *J. Clean. Prod.* **2022**, *346*, 131131. [[CrossRef](#)]
33. Song, W.; Mao, H.; Han, X. The two-sided effects of foreign direct investment on carbon emissions performance in China. *Sci. Total Environ.* **2021**, *791*, 148331. [[CrossRef](#)]
34. Jia, Z.; Wen, S.; Sun, Z. Current relationship between coal consumption and the economic development and China's future carbon mitigation policies. *Energy Policy* **2022**, *162*, 112812. [[CrossRef](#)]
35. Jia, Z.; Wen, S.; Liu, Y. China's urban-rural inequality caused by carbon neutrality: A perspective from carbon footprint and decomposed social welfare. *Energy Econ.* **2022**, *113*, 106193. [[CrossRef](#)]
36. Bhaskar, A.; Assadi, M.; Nikpey Somehsaraei, H.N. Decarbonization of the iron and steel industry with direct reduction of iron ore with green hydrogen. *Energies* **2020**, *13*, 758. [[CrossRef](#)]
37. Wen, L.; Li, Z. Provincial-level industrial CO₂ emission drivers and emission reduction strategies in China: Combining two-layer LMDI method with spectral clustering. *Sci. Total Environ.* **2020**, *700*, 134374. [[CrossRef](#)]
38. Wang, L.; Xi, F.; Yin, Y.; Wang, J.; Bing, L. Industrial total factor CO₂ emission performance assessment of Chinese heavy industrial province. *Energy Effic.* **2020**, *13*, 177–192. [[CrossRef](#)]
39. Duan, H.; Dong, X.; Xie, P.; Chen, S.; Qin, B.; Dong, Z.; Yang, W. Peaking Industrial CO₂ Emission in a Typical Heavy Industrial Region: From Multi-Industry and Multi-Energy Type Perspectives. *Int. J. Environ. Res. Public Health* **2020**, *19*, 7829. [[CrossRef](#)]
40. Wang, Q.; Wang, S. Why does China's carbon intensity decline and India's carbon intensity rise? A decomposition analysis on the sectors. *J. Clean. Prod.* **2020**, *265*, 121569. [[CrossRef](#)]
41. Bhat, A.A.; Mishra, P.P. Evaluating the performance of carbon tax on green technology: Evidence from India. *Environ. Sci. Pollut. Res.* **2020**, *27*, 2226–2237. [[CrossRef](#)]
42. Habyarimana, F.; Zewotir, T.; Ramroop, S. Structured additive quantile regression for assessing the determinants of childhood anemia in Rwanda. *Int. J. Environ. Res. Public Health* **2017**, *14*, 652. [[CrossRef](#)]
43. Koenker, R.; Hallock, K.F. Quantile regression. *J. Econ. Perspect.* **2001**, *15*, 143–156. [[CrossRef](#)]
44. Efron, B. Second thoughts on the bootstrap. *Stat. Sci.* **2003**, *18*, 135–140. [[CrossRef](#)]
45. Berner, A.; Bruns, S.; Moneta, A.; Stern, D.I. Do energy efficiency improvements reduce energy use? Empirical evidence on the economy-wide rebound effect in Europe and the United States. *Energy Econ.* **2022**, *110*, 105939. [[CrossRef](#)]
46. Bruns, S.; Moneta, A.; Stern, D.I. *Macroeconomic Time-Series Evidence That Energy Efficiency Improvements Do Not Save Energy*; CAMA Working Paper No. 21/2019; SSRN: Rochester, NY, USA, 2019.
47. Xu, B.; Xu, L.; Xu, R.; Luo, L. Geographical analysis of CO₂ emissions in China's manufacturing industry: A geographically weighted regression model. *J. Clean. Prod.* **2017**, *166*, 628–640. [[CrossRef](#)]
48. Jia, Z.; Wen, S.; Lin, B. The effects and reacts of COVID-19 pandemic and international oil price on energy, economy, and environment in China. *Appl. Energy* **2021**, *302*, 117612. [[CrossRef](#)]
49. Csereklyei, Z.; Stern, D.I. Flying more efficiently: Joint impacts of fuel prices, capital costs and fleet size on airline fleet fuel economy. *Ecol. Econ.* **2020**, *175*, 106714. [[CrossRef](#)]
50. Stern, D.I. The environmental Kuznets curve after 25 years. *J. Bioecon.* **2017**, *19*, 7–28. [[CrossRef](#)]
51. Cheng, Y.; Yao, X. Carbon intensity reduction assessment of renewable energy technology innovation in China: A panel data model with cross-section dependence and slope heterogeneity. *Renew. Sustain. Energy Rev.* **2021**, *135*, 110157. [[CrossRef](#)]
52. Pan, X.; Guo, S.; Xu, H.; Tian, M.; Pan, X.; Chu, J. China's carbon intensity factor decomposition and carbon emission decoupling analysis. *Energy* **2022**, *239*, 122175. [[CrossRef](#)]
53. Engle, R.F.; Granger, C.W. Co-integration and error correction: Representation, estimation, and testing. *Econom. J. Econom. Soc.* **1987**, *55*, 251–276. [[CrossRef](#)]
54. Yang, G.; Zha, D.; Wang, X.; Chen, Q. Exploring the nonlinear association between environmental regulation and carbon intensity in China: The mediating effect of green technology. *Ecol. Indic.* **2020**, *114*, 106309. [[CrossRef](#)]
55. Xu, R.; Xu, B. Exploring the effective way of reducing carbon intensity in the heavy industry using a semiparametric econometric approach. *Energy* **2022**, *243*, 123066. [[CrossRef](#)]
56. Hou, J.; Teo, T.S.; Zhou, F.; Lim, M.K.; Chen, H. Does industrial green transformation successfully facilitate a decrease in carbon intensity in China? An environmental regulation perspective. *J. Clean. Prod.* **2018**, *184*, 1060–1071. [[CrossRef](#)]
57. Xu, B.; Xu, R. Assessing the role of environmental regulations in improving energy efficiency and reducing CO₂ emissions: Evidence from the logistics industry. *Environ. Impact Assess. Rev.* **2022**, *96*, 106831. [[CrossRef](#)]
58. Gu, W.; Chu, Z.; Wang, C. How do different types of energy technological progress affect regional carbon intensity? A spatial panel approach. *Environ. Sci. Pollut. Res.* **2020**, *27*, 44494–44509. [[CrossRef](#)]
59. Andrée, B.P.J.; Chamorro, A.; Spencer, P.; Koomen, E.; Dogo, H. Revisiting the relation between economic growth and the environment; a global assessment of deforestation, pollution and carbon emission. *Renew. Sustain. Energy Rev.* **2019**, *114*, 109221. [[CrossRef](#)]
60. Cai, L.; Firdousi, S.F.; Li, C.; Luo, Y. Inward foreign direct investment, outward foreign direct investment, and carbon dioxide emission intensity-threshold regression analysis based on interprovincial panel data. *Environ. Sci. Pollut. Res.* **2021**, *28*, 46147–46160. [[CrossRef](#)]

61. Xu, B.; Luo, Y.; Xu, R.; Chen, J. Exploring the driving forces of distributed energy resources in China: Using a semiparametric regression model. *Energy* **2021**, *236*, 121452. [[CrossRef](#)]
62. Yu, S.; Zheng, S.; Li, X. The achievement of the carbon emissions peak in China: The role of energy consumption structure optimization. *Energy Econ.* **2018**, *74*, 693–707. [[CrossRef](#)]
63. Xie, K.; Li, W.; Zhao, W. Coal chemical industry and its sustainable development in China. *Energy* **2010**, *35*, 4349–4355. [[CrossRef](#)]

Article

Managing Transport Processes in Thermal Cracking to Produce High-Quality Fuel from Extra-Heavy Waste Crude Oil Using a Semi-Batch Reactor

Riyadh Almkhtar ¹, Sally I. Hammoodi ², Hasan Shakir Majdi ³ and Khalid A. Sukkar ^{1,*}

¹ Department of Chemical Engineering, University of Technology-Iraq, Al-Sanna St., P.O. Box 19006, Baghdad 10066, Iraq

² Midland Oil Company, Ministry of Oil, P.O. Box 19244, Baghdad 10081, Iraq

³ Chemical and Petroleum Industries Engineering Department, Al-Mustaqbal University College, Hilla 51015, Iraq

* Correspondence: khalid.a.sukkar@uotechnology.edu.iq

Abstract: Soil pollution from waste crude oil in emergency pits is a major problem at petroleum industry sites. In this work, extra-heavy waste crude oil was recovered from emergency pits and underwent many pre-purification processes to remove water and impurities. This type of oil was subjected to thermal cracking reactions in a semi-batch reactor constructed from stainless steel, with a volume of 500 mL. The cracking reactions were tested at operating temperatures of 400, 425, and 450 °C, with operating pressures of 1, 3, 5, and 7 bar. The results indicated that during thermal cracking, the reaction mechanism was highly dependent on the heat and mass transfer processes that occurred in the reactor. It was noted that the interaction between the optimal reaction temperature and operating pressure enhanced the product distribution and formation of high-quality liquid fuel with low gaseous and coke formations. The highest API of 30.5 was achieved for the liquid product at an operating temperature of 400 °C and a pressure of 3 bar. Additionally, an evaluation of the thermal cracking mechanism found that the transport processes that occurred in the reactor were the chief factor in providing a high-performance thermal cracking process.

Keywords: transport phenomena; mass transfer; emergency pits; soil pollution; light fuel production; reaction mechanism

Citation: Almkhtar, R.; Hammoodi, S.I.; Majdi, H.S.; Sukkar, K.A. Managing Transport Processes in Thermal Cracking to Produce High-Quality Fuel from Extra-Heavy Waste Crude Oil Using a Semi-Batch Reactor. *Processes* **2022**, *10*, 2077. <https://doi.org/10.3390/pr10102077>

Academic Editors: Roberto Alonso González Lezcano, Francesco Nocera and Rosa Giuseppina Caponetto

Received: 6 September 2022

Accepted: 1 October 2022

Published: 14 October 2022



Copyright: © 2022 by the authors. Licensee MDPI, Basel, Switzerland. This article is an open access article distributed under the terms and conditions of the Creative Commons Attribution (CC BY) license (<https://creativecommons.org/licenses/by/4.0/>).

1. Introduction

Upgrading the purification processes to deal with extra-heavy waste crude oil poses a major challenge in the petroleum industry to produce high-quality liquid fuel from environmental pollutant materials [1–3]. Huge quantities of extra-heavy waste crude oil have been produced from the petroleum activities at petroleum sites. All of these wastes have been collected in large emergency pits near the petroleum site and regarded as a high source of pollution for the soil and groundwater [4–7]. Usually, heavy crude oil is a complex mixture that includes normal paraffins, aromatics, and naphthenes. Moreover, this waste causes extended economical loss and environmental and human health problems [8–11]. Therefore, the recovery of these materials and upgrading their structure using the thermal cracking process provides a key solution to this problem [12–16].

The thermal cracking process is a very effective technology for providing fractions of low boiling points for different industrial applications. This process is usually operated at a range of high temperatures and pressures to convert high-molecular-weight hydrocarbons into smaller ones [2,13,17]. Typically, heavy crude oil contains significant quantities of asphaltic compounds that can lead to serious technical problems in unit operations [14]. Most asphaltenes consist of high-molecular-weight polyaromatic compounds carrying long aliphatic hydrocarbons and alicyclic substituents. Ghashghaee and Shirvani [3], Wang et al. [7], and Corma et al. [18] indicated that the main benefit of the thermal cracking process

is to produce light and middle distillates from heavy petroleum crude and products such as reduced crude, fuel oil, vacuum residue, and asphaltic and waxy oil. Salehzadeh et al. [13] showed that the major parameter controlling the thermal cracking process of heavy crude oil is temperature, with the optimal range between 350–500 °C [7]. Additionally, the thermal cracking process is highly affected by the operating pressure: as the pressure increases, so do the thermal cracking reactions [1,3].

According to the literature, cracking reactions are complex and undergo more interactions due to the large number of chemical reactions that occur inside the reactor [10,17]. Therefore, the composition of waste crude oil, reaction temperature, pressure, and gas flow rate are the chief variables that determine the quality of the produced liquid fuel [18]. Usually, such waste oil contains high quantities of heavy hydrocarbon materials, including asphaltene [19–22] and resins [23]. Therefore, the thermal cracking process must be properly controlled to successfully manage the process of liquid fuel production with low amounts of undesired by-products (i.e., gases and coke) [24–28]. Evaluating the changes in the product specifications during the cracking reactions is necessary due to the complexity of upgrading these reactions [29–34].

Furthermore, many authors have identified the influence of operating conditions on the distribution of thermal cracking products. Several publications have shown that product quality is mainly dependent on the chemical composition, specifications, and asphaltene content [35–40]. AlHumaidan et al. [41] investigated the thermal cracking reactions of vacuum residues of heavy crude oil in a semi-batch reactor. They noted the formation of cracked oil, gaseous products, and pitch from the reaction and observed a clear increase in the produced saturate fraction due to the cracking process. Rueda and Gray [42] indicated that thermal cracking technology is a valuable process that reduces the viscosity of heavy crude oil. They pointed out that the produced liquid fuel from thermal cracking can be transported via pipeline with high flexibility without the need for added solvents. Al-Absi and Al-Khattaf [43] compared the results of the thermal and catalytic cracking processes that were carried out for a crude oil of API = 34. They found that for both processes, the production of light olefins, gaseous products, and coke formation increased with increasing operating temperatures. The authors noted that the catalytic cracking process was preferable to the thermal one because the first process relies on the free radical mechanism, but the later uses the carbenium ion mechanism. Wang et al. [44] studied the influence of saturates, aromatics, resins, and asphaltene compounds on the activity of heavy crude oil cracking reactions. The authors observed that resins and asphaltenes produced high yields of residues of about 22 and 45%, respectively. Voronetskaya and Pevneva [45] tested the thermal cracking of heavy oil resins and asphaltenes in a batch reactor at an operating temperature of 450 °C. They found significant structural variations in these materials, with a high production rate of solid condensation compounds.

Heavy crude oil is characterized by its high content of asphaltic compounds, which form about 5–15 wt% depending on the nature of the crude oil [39,46]. This material consists of complex hydrocarbon frameworks, with the main constituents of asphalt being bitumens [23,47]. Moreover, the term “asphaltic bodies” is widely used to describe the amount of precipitated asphalt in hydrocarbon fuel or lubricating oil. Thus, the mass of the asphalt can be determined by subjecting the fuel to a centrifugal process to remove the asphaltic bodies as precipitated compounds [48–52]. Additionally, the thermal cracking reaction usually occurs by the free radical mechanism. This mechanism consists of a series of reaction stages involving the initiation of the hydrocarbon chain, the H₂ abstraction process, radical decomposition, radical addition, and finally, a termination stage [26,43].

Previous studies have rarely dealt with the treatment of waste crude in an emergency pit [7,8]. These pits usually cause high environmental and human health risks. Additionally, most studies have identified the performance of the thermal cracking process according to the change in product distribution [8,34,51]. However, these studies do not explain the influence of transport processes and reaction mechanisms on the chemical quality of the products [5,42,52]. Therefore, the main aim of the present study was to investigate the

removal of extra-heavy crude oil from an emergency pit and then evaluate the production ability of high-quality liquid fuel from low-value waste via an efficient, controlled thermal cracking process.

2. Materials and Methods

2.1. Materials

In the present work, extra-heavy waste crude oil was used as a raw material in a cracking reaction. This type of oil was collected from an emergency pit in one of the petroleum sites outside the boundaries of Baghdad (East Baghdad Oil Field). Figure 1 presents some photographs of this emergency pit, whereas Figure 2 shows the fluid nature of the collected extra-heavy waste crude oil. Using ASTM D445, the kinematic viscosity of the extra-heavy waste crude oil was measured to be 172.3 cSt at 25 °C.



Figure 1. Photographs of the emergency pit at East Baghdad Oil Field, showing the extra-heavy waste crude oil.



Figure 2. The fluid nature of the collected extra-heavy waste crude oil.

2.2. Thermal Cracking Apparatus

The thermal cracking reaction was carried out in a semi-batch reactor. Figure 3 illustrates the thermal cracking apparatus, whereas Figure 4 shows a photograph of the semi-batch reactor. The reactor was constructed from stainless steel and was 500 mL in size. The reactor was heated uniformly by an electrical heater that surrounded the reactor. In addition, the reaction temperature inside the reactor was controlled with the aid of a highly sensitive temperature control system using a K-type thermocouple sensor with a digital temperature controller. The operating pressure was measured and controlled via a sensitive pressure gauge with an accurate needle. Moreover, the apparatus was supplied with a chiller system to cool the products in the reactor. The apparatus also had a nitrogen gas cylinder with a calibrated flow meter. Moreover, the reactor and all connected sections were insulated with a layer of fiberglass material to prevent heat loss from the apparatus.

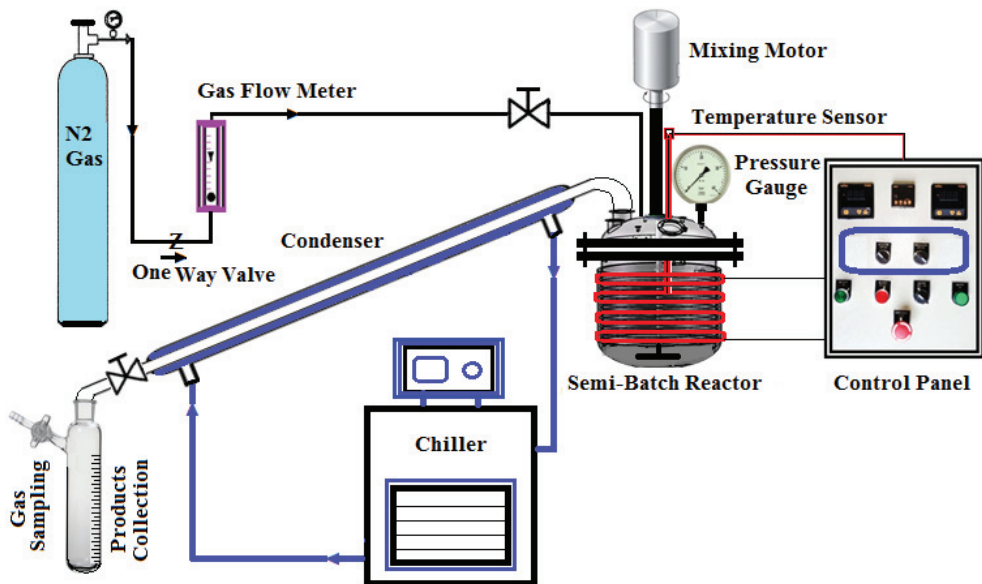


Figure 3. Schematic diagram of the waste crude oil cracking apparatus.



Figure 4. Photograph of the semi-batch reactor used for the thermal cracking process.

2.3. Cracking Reaction Procedure

The thermal cracking reaction for the extra-heavy waste crude oil was conducted in a semi-batch reactor. For each reaction run, 100 mL of feedstock was charged inside the reactor and cracked thermally under different operating temperatures and pressures. The cracking process was evaluated at various reaction temperatures (i.e., 400, 425, and 450 °C). To evaluate the influence of the operating pressure on the cracking process, each reaction was achieved at a selected set of operating pressures (i.e., 1, 3, 5, and 7 bar). Moreover, before starting the reaction process, the apparatus was supplied with nitrogen gas at a flow rate of 20 mL/min for 10 min to remove any traces of oxygen in the system. The reaction time continued for 3 h under continuous stirring using an electrical stirring motor and shaft system inserted inside the reactor with a constant mixing velocity of 120 rpm under sealing conditions. Then, the products were cooled using a chilling system, after which they were accumulated in a cylindrical collection system designed for this purpose. Next, the amount of produced liquid fuel was determined. Additionally, after completing the thermal cracking reaction, the reactor was opened and the amount of the precipitated coke was determined. Then, the amount of produced gases was estimated by subtracting the amount of liquid fuel and solid coke from the parent amount of feed to the reactor.

Furthermore, the product specifications and characterization were evaluated using many measuring techniques, such as Fourier-transform infrared (FTIR) spectroscopy (8400S/Shimadzu, Kyoto, Japan). Additionally, a thermogravimetric analysis (TGA) (TG-760 thermobalance, Stanton Redcroft, London, UK) was used to evaluate the thermal behavior of the parent extra-heavy waste crude oil. Then, to perform the TGA analyses, 8 mg of parent crude oil was distributed in alumina crucibles with a capacity of 100 µL. The oxygen was fed to the device at a volumetric flow rate of 50 mL/min and a heating rate of 20 °C/min. Additionally, the parent crude oil viscosity was measured using a Brookfield-DV3TLVKJ viscometer (USA). Finally, the crude oil density (specific gravity) was measured using a special hydrometer (L50SP, Stevenson Reeves Ltd., Edinburgh, Scotland). Then, the API gravity value was determined according to the general equation of API gravity [20,49].

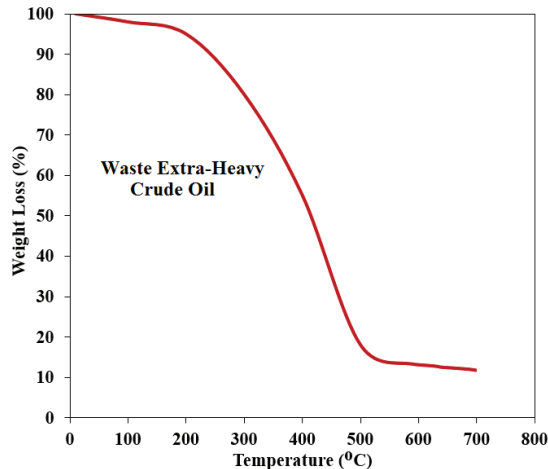
3. Results and Discussion

3.1. Thermogravimetric Analysis (TGA)

Table 1 illustrates the measured values of the physical properties of the parent waste of the extra-heavy crude oil. From the API value (6.83), it is clear that this crude oil was extra heavy and highly viscous. Moreover, the thermal characteristics of this extra-heavy crude oil were analyzed using thermogravimetric measurements to determine the best operating temperature for the cracking reaction. Figure 5 shows the TGA thermogram of the parent extra-heavy waste crude oil at different operating temperatures. The TGA results pointed to the presence of two reaction zones. The first reaction zone was related to a distillation process combined with a low-temperature oxidation (LTO) process of the compounds of the crude oil. This zone was achieved in a temperature range between 25 and 400 °C. However, the second reaction zone took place at an operating temperature higher than 400 °C due to the high-temperature oxidation (HTO) process employed for the remainder of the crude oil. The same trend was noted by Avendaño et al. [29]. Additionally, the results indicated that the operating temperature played a key role in the quality of the extra-heavy oil. It was noted that up to 95 °C, no coke formation precipitated. The weight of the coke precipitated at 180 °C was about five times higher than that at 140 °C.

Table 1. Specifications of the extra-heavy waste crude oil.

Property	Standard	Value
API Gravity at 15 °C	ASTM D5002	6.83
Specific Gravity at 15 °C (g/cm ³)	ASTM D-1298	0.98
Water Content (Vol%)	ASTM D1744	8.00
Sediment (Vol%)	ASTM D4807	0.50
Sulfur Content (wt%)	ASTM D4294	3.60
Salt Content (ppm)	ASTM-D3230	400

**Figure 5.** Thermogravimetric analysis of the extra-heavy waste crude oil.

To understand the thermal cracking process of crude oil, its mass-loss behavior provided a clear picture of the distribution of the produced gases included in the thermal cracking reactions. Corma et al. [18] and Hao et al. [20] indicated that the thermal cracking conditions (e.g., operating temperature, pressure, and heating rate value) play a significant role in controlling the reaction performance and product distribution. Heavy crude oil is composed of various kinds of fractions, such as saturates compounds, volatile aromatics, asphaltenes, and resins. The effective solubility and polar activity of hydrocarbons usually determines the main features of the fractions. Then, from a thermal point of view, asphaltene hydrocarbons possess high thermal resistance caused by various operational problems in the petroleum processing units. The asphaltic compounds consist of a complex hydrocarbon matrix. Therefore, the asphaltic bodies look like colloids dispersed in petroleum. Accordingly, asphaltene is usually precipitated in storage tanks and pipelines due to its ability to precipitate according to this mechanism [6,29,30,40].

3.2. Influence of the Temperature on the Cracking Reaction

The cracking reaction of extra-heavy waste crude oil using a semi-batch reactor was investigated at temperatures of 400, 425, and 450 °C and operating pressures of 1, 3, 5, and 7 bar. Figures 6–8 illustrate the influence of the thermal cracking temperature and operating pressure on the quantity of produced gases, liquid hydrocarbon, and solid residue, respectively. Figure 6 demonstrates that the amount of gaseous products (C₁–C₃) was highly influenced by the operating temperature and pressure. The highest gas production was observed at an operating temperature of 450 °C and a pressure of 7 bar, whereas the lowest gas production rate was noted at 425 °C. These results are attributed to the ability of C₅–C₁₂ hydrocarbons in the crude oil structure to crack, which forms more gaseous products. Additionally, the results indicated that at the lower thermal cracking temperature of 400 °C, slight levels of waste crude oil cracking were noted at a reaction time of 2 h.

Feedstock cracking was enhanced by increasing the operating temperature, as gaseous products increased to 28 and 52% at 425 and 450 °C, respectively. In addition, the feedstock molecules underwent major changes as the cracking temperature was raised, causing a clear breakdown of long-chain molecules into smaller hydrocarbons (gases). Moreover, the breaking down of the paraffinic compounds present in asphaltenes and also the cracking of smaller compounds will contribute to the formation of more cracking gases. The observed results were similar to the results reported by Ghashghaee and Shirvani [3], Yu et al. [12], Cheshkova et al. [25], and Wang et al. [44].

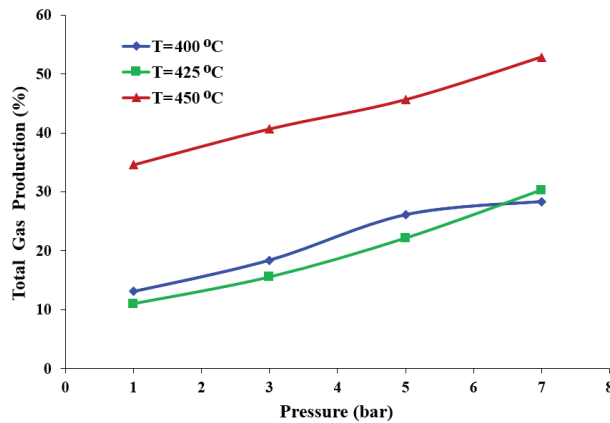


Figure 6. Influence of the thermal cracking temperature and operating pressure on the quantity of the produced gases.

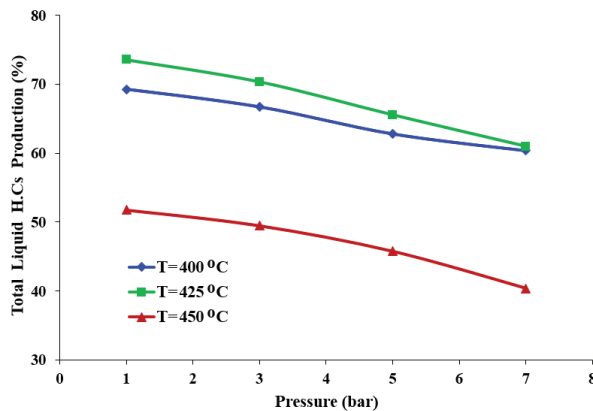


Figure 7. Influence of the thermal cracking temperature and operating pressure on the quantity of the produced liquid hydrocarbons.

Hochberg et al. [19], Jin et al. [33], and Wang et al. [44] showed that the general products of cracking reactions are usually paraffins, olefins, and aromatic compounds. Additionally, light gases (e.g., methane, ethane, and propane) are the main gases generated from thermal cracking reactions, although other gases including CO, CO₂, and H₂ have formed [18,26,40]. The composition of these gases highly depends on the operating pressure and temperature [39,45]. Thus, the suggested thermal cracking process in the present work can be regarded as an efficient solution for the reuse of extra-heavy waste crude oil from emergency pits. Additionally, light hydrocarbons can be produced without any environmental and economic problems. The controlled thermal degradation of crude oil in this process will enhance the physical specifications of the product. The amount of

produced light liquid fuel in the present work was about >61% at a temperature of 400 °C and pressure of 3 bar. The comparison of the results of the present work with that of other previous work indicated that the amount of light fuel is less than this value. Alsobaai [19] found the produced fuel from thermal cracking of heavy crude oil was in the range of 27–44%. Additionally, Guerra [26] and Afanasjeva et al. [28] observed that thermal cracking generates light crude oil of about 30 and 36%, respectively. According to the investigation of Wang et al. [44], the thermal cracking process of crude oil can produce more than 30 wt% of coke. However, in the present work, the coke formation is in the range of 10–18 wt%. Accordingly, it can be said that the amount of coke formation from the cracking process does not only depend on operating temperature, but also on crude oil specification. Crude oil with a higher mass of asphaltene formed more coke and residue.

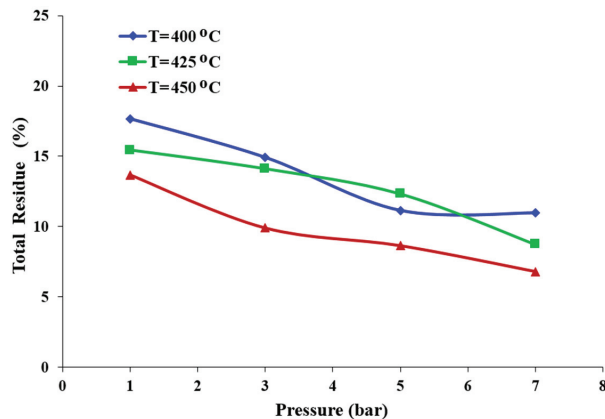


Figure 8. Influence of the thermal cracking temperature and operating pressure on the quantity of the precipitated residue.

Waste crude oil has been produced everywhere in petroleum production processes and petroleum refineries [30,46]. The collection of these wastes in an emergency pit has caused environmental problems that are fatal to humans and has also polluted groundwater [6,8]. However, the present work provides efficient solutions to this problem using thermal cracking technology, where high-quality crude oil was produced using waste crude oil. The environmental problems in petroleum sites can be resolved significantly, and emergency pits can then be removed from such sites.

3.3. Effect of the Pressure and Temperature on the Quality of the Liquid Product

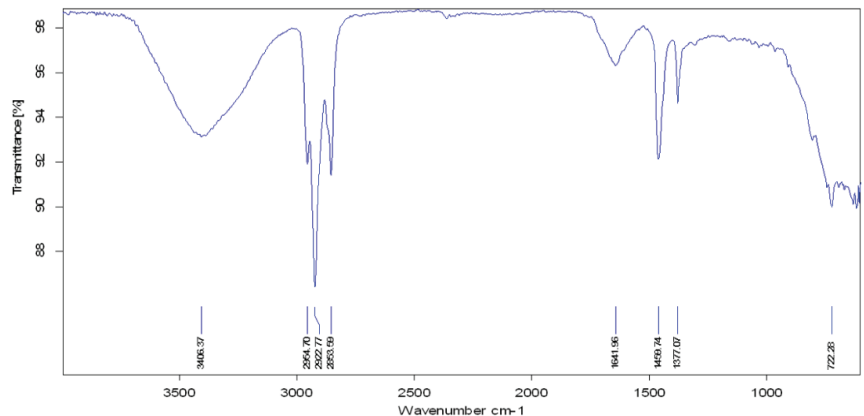
This study measured the effect of the operating pressure on the produced liquid hydrocarbons during the thermal cracking of waste crude oil. Table 2 shows the influence of the operating pressure of the produced liquid hydrocarbons at different operating temperatures. As the operating pressure increased, the API gravity of the produced liquid hydrocarbons increased up to 5 bar for all samples at various operating temperatures. At 400 °C, the highest value of the API gravity was 30.5 for the produced liquid fuel at a pressure of 3 bar. Moreover, as the operating pressure increased, the API gravity decreased slightly. Additionally, at a thermal cracking temperature of 425 °C, the API gravity reached its highest value of 28.65 at a pressure of 5 bar. On the other hand, Table 2 shows that there was no significant effect of pressure on the API value at a temperature of 450 °C. This behavior is attributed to the nature of the thermal cracking reaction mechanism, in which at a high thermal cracking temperature (450 °C), the cracking reaction produced more gases than liquid fuel [1,25,42]. This mechanism is related to the bond breaking of most high-molecular-weight hydrocarbons and the formation of C₁, C₂, and C₃ gaseous products. The same observation was noted by Kok [4], Al Darouich et al. [27], Jiao et al. [37], and Kaminski and Husein [40].

Table 2. Effect of the pressure and temperature on the API gravity of liquid products.

Temperature (°C)	Pressure (Bar)	API
400	1	28.29
	3	30.50
	5	29.29
	7	27.2
425	1	26.91
	3	27.34
	5	28.65
	7	27.15
450	1	27.88
	3	26.00
	5	26.93
	7	26.88

3.4. FTIR Analysis

The functional groups of the parent extra-heavy waste crude oil were evaluated using Fourier-transform infrared (FTIR) analysis. This analysis is the most applied method to obtain accurate information about the nature of the crude oil and the composition of the affected functional groups. Figures 9–12 present the spectra results of the parent and the produced liquid fuel. Figure 9 illustrates the functional groups attached to the parent extra-heavy waste crude oil. The two notable peaks at 2922.77 and 2853.95 cm^{-1} represent the aliphatic C–H group and were produced from the symmetric and asymmetric vibration activity. Additionally, a clear aromatic vibration band was noted at 1641.96 cm^{-1} , related to the aromatic compounds. Moreover, the resulting band at 722.28 cm^{-1} corresponds to the crystallinity of the wax that appeared in the crude oil structures [20]. Additionally, the bands that lie between 900.05 and 810.38 cm^{-1} usually appear in asphaltenic compounds and resins in heavy types of crude oil [20,29,39].

**Figure 9.** Major functional groups of the parent extra-heavy waste crude oil.

Figures 10–12 show the functional groups attached to the structure of the produced liquid fuel from the thermal cracking process at 3 bar and at 400, 425, and 450 °C, respectively. These samples underwent clear shifting in their general bands in comparison with the parent extra-heavy crude oil. This shifting is attributed to the thermal cracking reaction processes. To evaluate the effect of the operating temperature on the TGA results, a comparison between different bands was achieved, as shown in Table 3. This table clearly illustrates that the main characteristic bands of crude oil appeared at 2923.27 cm^{-1} and 2853.88 cm^{-1} . Moreover, the aromatic ring compounds disappeared in products at the

three operating temperatures due to the removal of the asphaltic material, which was converted into coke by the thermal cracking process. Additionally, the O–H stretching disappeared from the light crude structure because of the high operating temperature. Furthermore, the $-\text{CH}_2$ bending that was noted at 722 cm^{-1} varied slightly in all samples. These figures unambiguously indicate the presence of a general band of light crude oil. This band is related to the carboxylic acids and aromatic hydrocarbons at 1743 cm^{-1} and 1698 cm^{-1} , respectively. Additionally, Figures 10–12 show the disappearance of the OH^- group (3406.37 cm^{-1} in the parent feed in Figure 9) in the produced liquid fuel samples at different operating temperatures due to the liberation of physical and chemical water from the crude oil structures [7,39].

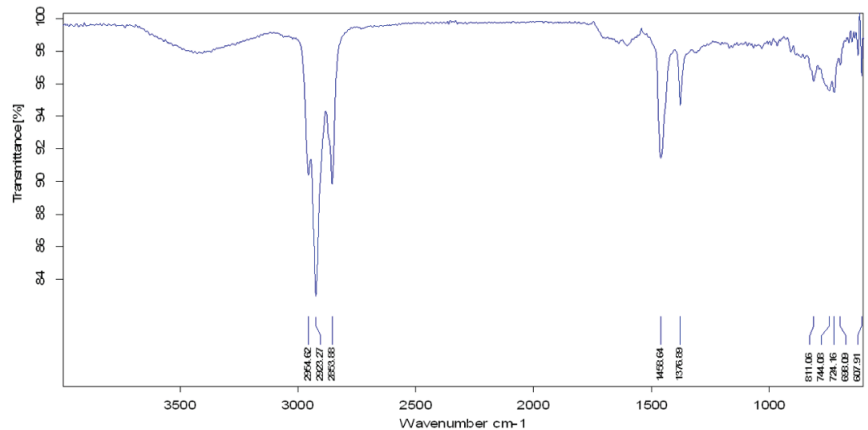


Figure 10. FTIR spectroscopy of the produced liquid fuel at $T = 400\text{ }^{\circ}\text{C}$ and 3 bar.

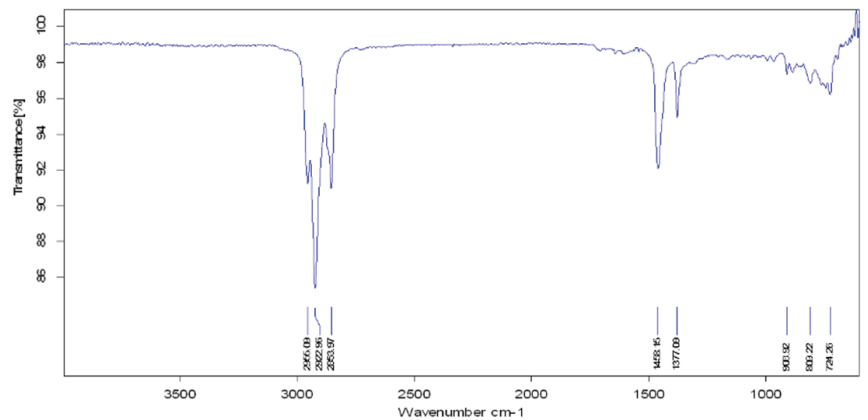


Figure 11. FTIR spectroscopy of the produced liquid fuel at $T = 425\text{ }^{\circ}\text{C}$ and 3 bar.

Additionally, a precipitated coke formed in the reactor after the reaction time was complete. Then, the FTIR spectroscopy showed a significant disappearance of all the produced fuels at the later bands between 900.05 and 810.38 cm^{-1} (Figures 10–12). These results are attributed to the precipitation of most of the asphaltenic and resin compounds in the reactor in the form of coke. According to the results of Salehzadeh et al. [13], Li et al. [15], and Cheshkova et al. [25], the asphaltene compounds represent the general body of coke formed by the thermal cracking reactions. Additionally, the gaseous products from the thermal cracking reaction were $\text{C}_1\text{--C}_3$, CO , CO_2 , and H_2 gas. The quality and

quantity of the produced gases are highly dependent on the type of crude oil and its composition [28,34,41].

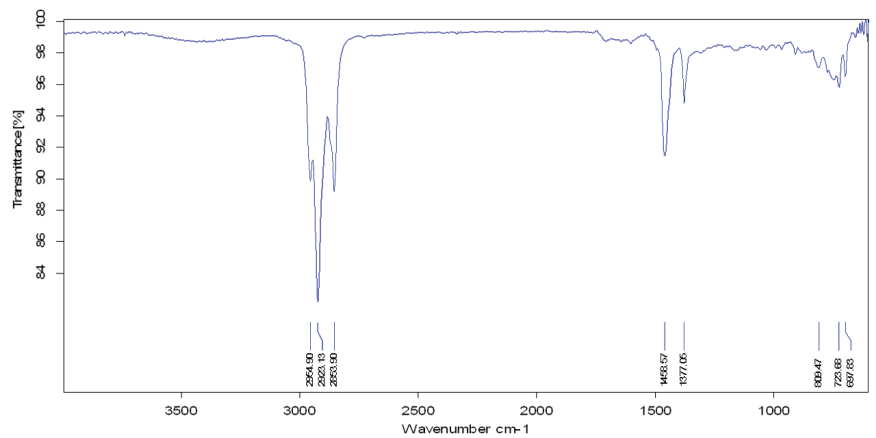


Figure 12. FTIR spectroscopy of the produced liquid fuel at $T = 450\text{ }^{\circ}\text{C}$ and 3 bar.

Table 3. Comparison between the main TGA results of the produced liquid fuels at different thermal cracking temperatures.

Functional Group	Parent Waste Crude Oil	Produced Fuel at 400 °C	Produced Fuel at 425 °C	Produced Fuel at 450 °C
Aliphatic C–H	2922.77 cm^{-1}	2923.27 cm^{-1}	2922.96 cm^{-1}	2923.13 cm^{-1}
	2853.95 cm^{-1}	2853.88 cm^{-1}	2853.97 cm^{-1}	2853.90 cm^{-1}
C–H Deformation of –CH ₂ and –CH ₃	1459.74 cm^{-1}	1458.64 cm^{-1}	1458.15 cm^{-1}	1458.57 cm^{-1}
C–H Symmetric Deformation of –CH ₂	1377.07 cm^{-1}	1376.89 cm^{-1}	1377.09 cm^{-1}	1377.06 cm^{-1}
Aromatic Ring	1641.96 cm^{-1}	-	-	-
O–H Stretching	3406.37 cm^{-1}	-	-	-
–C–H Bending	722.28 cm^{-1}	724.16 cm^{-1}	724.26 cm^{-1}	723.68 cm^{-1}

3.5. Transport Processes and Reaction Mechanism

The transport processes that occur in the thermal cracking reactions of crude oil are complex and require a deep understanding. A high rate of heat transfer will be achieved inside the reactor due to the thermodynamic performance of the cracking reactions (endothermic reactions). Usually, the activation energy of this type of reaction is dependent on the nature of the bond to be broken during the reaction path. Accordingly, the heat will be transferred from the reactor wall into the crude oil mixture depending on the required operating temperature. Nargessi and Karimzadeh [5], Ishiyama et al. [16], and AlHumaidan et al. [41] have stated that the transferred energy is mainly distributed between the reactor wall and crude oil mixture. In addition, the amount of energy transfer in the reactor plays a major role in determining the quality of the product distribution. Evaluating the mass transfer variation in the system will contribute to a clear understanding of the real reaction mechanism and performance in the thermal cracking process. The thermal cracking process normally undergoes faster mass changes due to the higher rate of hydrocarbon cracking occurring in the reactor. Therefore, three main parts of the products were achieved in the present semi-batch reactor: liquid hydrocarbon, a gaseous product, and precipitated coke.

Some researchers have found that increasing the contact between the reaction mixture highly influences the heat and mass transfer processes inside the reactor [17,41,45]. However, the enhancement in the heat transfer rate is related to there being more contact surface

area due to the agitation process. Figure 13 summarizes the main reaction sequences that occurred in the semi-batch reactor for the waste crude oil thermal cracking process. The general reaction mechanism of thermal cracking is dependent on the free radical mechanism [26]. This mechanism is supported by three basic operations: initiation, propagation, and termination, as shown in Table 4. Experimental work related to this mechanism by Guerra [26], as well as by Al-Absi and Al-Khattaf [43], has shown that all of these processes together form the total picture of thermal cracking products. When compared with the catalytic cracking process, thermal cracking does not occur by ionic intermediates [27,42]. Instead, in this case, the C–C bonds were broken, leaving each C atom to be finished by a single electron [12,40]. This produces free radicals, which allows different products to be synthesized from the results of thermal cracking reactions.

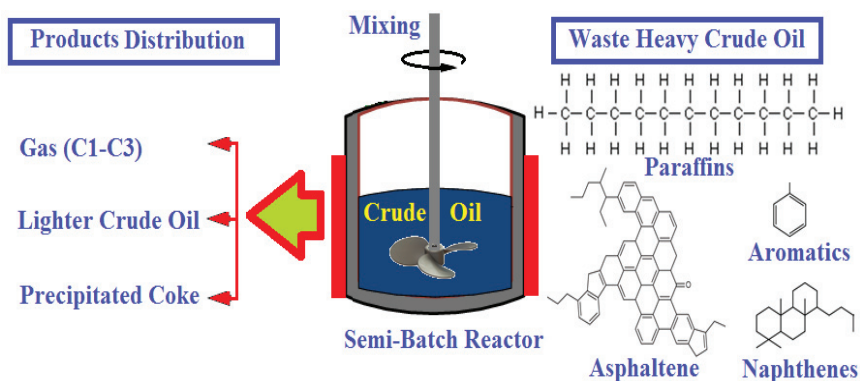


Figure 13. Reaction stages of the waste crude oil thermal cracking process.

Table 4. Radical mechanism that occurs during thermal cracking reactions [26].

Reaction Type	Description
Initiation Stage	Alkane + Heat \longrightarrow 2 Radicals
Propagation Stage	Alkane + Radical \longrightarrow (Radical + H) + Radical
	Radical \longrightarrow Radical + Olefin
Termination Stage	Radical + Radical \longrightarrow Hydrocarbons Products

Finally, extra-heavy waste crude oil is an undesirable material formed during petroleum production activities. The high viscosity of this material is attributed to the existence of long-chain hydrocarbons. In this study, the specifications of the thermal cracking product were improved in comparison with those of the parent waste crude oil. Thus, the proper management of transport processes in the reaction vessel during thermal cracking will enhance the conversion of extra-heavy waste crude oil into light oil with a higher value. It was found that the heat and mass transfer determines the quality of product, with reaction kinetics and thermodynamics playing a primary role in the yield of light crude oil. Therefore, the results showed the ability of the thermal cracking reaction of crude oil to maximize both the economic and environmental benefits of this process.

4. Conclusions

The pollution problem of accumulated extra-heavy waste crude oil in an emergency pit was solved successfully using thermal cracking technology. This work assessed the applicability of converting extra-heavy waste crude oil of API = 6.83 into a light liquid fuel of API = 30.5 via controlled thermal cracking reactions in a semi-batch reactor. This produced a high yield of high-quality synthesized crude oil with low coke deposition. The results indicated that the cracking temperature and operating pressure are the major

parameters that determine the quality of the produced fuel. High liquid products (>61%) were achieved under the optimal operating conditions of 400 °C and 3 bar. Moreover, it was found that there was no significant effect of the pressure on the API value at a temperature of 450 °C. This behavior is attributed to the nature of the thermal cracking reaction mechanism, in which at a high thermal cracking temperature (450 °C), the cracking reaction produced more gases than liquid fuel. Furthermore, comparisons of the produced liquid fuels with the parent extra-heavy crude oil at different operating temperatures indicated that these fuels underwent clear shifting in their general FTIR bands due to the thermal cracking reaction processes. Additionally, the standard functional groups of light crude oil were achieved in the produced fuels. A mass transfer and reaction mechanism of thermal cracking was suggested to explain the increased efficiency of producing liquid hydrocarbons by this process. The improvement in liquid fuel quality was related to the chemical reactions of converting high-molecular-weight compounds into those with low-molecular weights with limited mass transfer resistance. Thus, by this mechanism, free radicals were produced, and different products can be synthesized from the results of such thermal cracking reactions. Furthermore, utilizing extra-heavy waste crude oil provides a new source of petroleum fractions from low-value material that is both economical and has a flexible production rate.

Author Contributions: Conceptualization, R.A. and K.A.S.; methodology, S.I.H.; formal analysis, R.A. and S.I.H.; investigation, K.A.S.; data curation, S.I.H.; writing—original draft preparation, R.A.; writing (review and editing), K.A.S.; visualization, R.A.; supervision, H.S.M.; project administration, H.S.M. and K.A.S. All authors have read and agreed to the published version of the manuscript.

Funding: This research received no external funding.

Institutional Review Board Statement: Not applicable.

Informed Consent Statement: Not applicable.

Data Availability Statement: Not applicable.

Acknowledgments: The authors are thankful to the Design & Production Research Unit/Department of Chemical Engineering, University of Technology-Iraq and Al-Mustaqbal University College, Babylon, Iraq for their scientific support of this project.

Conflicts of Interest: The authors declare no conflict of interest.

References

- Al-Absi, A.A.; Aitani, A.M.; Al-Khattaf, S.S. Thermal and catalytic cracking of whole crude oils at high severity. *J. Anal. Appl. Pyrolysis* **2020**, *145*, 104705. [[CrossRef](#)]
- Lozano-Navarro, J.I.; Palacio-Pérez, A.; Suárez-Domínguez, E.J.; Pérez-Sánchez, J.F.; Díaz-Zavala, N.P.; Melo-Banda, J.A.; Rodríguez-Valdés, A. Modification of the viscosity of extra-heavy crude oil using aqueous extracts of common geranium (*Pelargonium hortorum*). *J. Petrol. Sci. Eng.* **2022**, *215*, 110583. [[CrossRef](#)]
- Ghashghae, M.; Shirvani, S. Two-step thermal cracking of an extra-heavy fuel oil: Experimental evaluation, characterization, and kinetics. *Ind. Eng. Chem. Res.* **2018**, *57*, 7421–7430. [[CrossRef](#)]
- Kok, M.V. Characterization of medium and heavy crude oils using thermal analysis techniques. *Fuel Process. Technol.* **2011**, *92*, 1026–1031. [[CrossRef](#)]
- Nargessi, Z.; Karimzadeh, R. Analysis of heat and mass transfer and parametric sensitivity in an experimental fixed-bed reactor for the catalytic cracking of heavy hydrocarbons based on modeling and experiments. *Ind. Eng. Chem. Res.* **2021**, *60*, 4831–4846. [[CrossRef](#)]
- Gabbar, H.A.; Aboughaly, M. Conceptual process design, energy and economic analysis of solid waste to hydrocarbon fuels via thermochemical processes. *Processes* **2021**, *9*, 2149. [[CrossRef](#)]
- Wang, F.; Yu, Y.; Biney, B.W.; Zhang, Z.; Liu, H.; Chen, K.; Wang, Z.; Guo, A. Relationship between olefins and coking propensity of heavy residual oil derived from vacuum residue thermal cracking products. *Fuel* **2022**, *331*, 125737. [[CrossRef](#)]
- Eklund, R.L.; Knapp, L.C.; Sandifer, P.A.; Colwell, R.C. Oil spills and human health: Contributions of the Gulf of Mexico Research Initiative. *GeoHealth* **2019**, *3*, 391–406. [[CrossRef](#)] [[PubMed](#)]
- Paulauskiene, T.; Uebe, J.; Kryzevicius, Z.; Kaskova, V.; Katarzyte, M.; Overlingé, D. Removal of petroleum hydrocarbons from brackish water by natural and modified sorbents. *J. Mar. Sci. Eng.* **2022**, *10*, 597. [[CrossRef](#)]

10. Subramanian, D.; Wu, K.; Firoozabadi, A. Ionic liquids as viscosity modifiers for heavy and extra-heavy crude oils. *Fuel* **2015**, *143*, 519–526. [\[CrossRef\]](#)
11. Dim, P.; Hart, A.; Wood, J.; Macnaughtan, B.; Rigby, S.P. Characterization of pore coking in catalyst for thermal down-hole upgrading of heavy oil. *Chem. Eng. Sci.* **2015**, *131*, 138–145. [\[CrossRef\]](#)
12. Yu, J.; Quan, H.; Huang, Z.; Li, P.; Chang, S. Synthesis of a heavy-oil viscosity reducer containing a benzene ring and its viscosity reduction mechanism. *ChemistrySelect* **2022**, *7*, 202102694. [\[CrossRef\]](#)
13. Salehzadeh, M.; Kaminski, T.; Husein, M.M. An optimized thermal cracking approach for onsite upgrading of bitumen. *Fuel* **2022**, *307*, 121885. [\[CrossRef\]](#)
14. Li, X.; You, L.; Kang, Y.; Liu, J.; Chen, M.; Zeng, T.; Hao, Z. Investigation on the thermal cracking of shale under different cooling modes. *J. Nat. Gas Sci. Eng.* **2022**, *97*, 104359. [\[CrossRef\]](#)
15. Goncharov, A.V.; Krivtsov, E.B. Calculation of the rate constants of thermal cracking and condensation reactions of high-sulfur tar asphaltenes. *Solid Fuel Chem.* **2022**, *56*, 108–115. [\[CrossRef\]](#)
16. Ishiyama, E.M.; Kennedy, J.; Pugh, S.J. Fouling management of thermal cracking units. *Heat Transf. Eng.* **2017**, *38*, 694–702. [\[CrossRef\]](#)
17. Almukhtar, R.S.; Abdulllah, S.I.H. Characterization of liquid produced from catalytic pyrolysis of mixed polystyrene and polyethylene terephthalate plastic. *Eng. Technol. J.* **2018**, *36*, 27–32.
18. Corma, A.; Sauvinaud, L.; Mathieu, Y.; Al-Bogami, S.; Bourane, A.; Al-Ghrami, M. Direct crude oil cracking for producing chemicals: Thermal cracking modeling. *Fuel* **2018**, *211*, 726–736. [\[CrossRef\]](#)
19. Alsobaai, A.M. Thermal cracking of petroleum residue oil using three level factorial design. *J. King Saud Univ.-Eng. Sci.* **2013**, *25*, 21–28. [\[CrossRef\]](#)
20. Hao, J.; Che, Y.; Tian, Y.; Li, D.; Zhang, J.; Qiao, Y. Thermal cracking characteristics and kinetics of oil sand bitumen and its SARA fractions by TG–FTIR. *Energy Fuels* **2017**, *31*, 1295–1309. [\[CrossRef\]](#)
21. Kumar, S.; Mahto, V. Emulsification of Indian heavy crude oil in water for its efficient transportation through offshore pipelines. *Chem. Eng. Res. Des.* **2016**, *115*, 34–43. [\[CrossRef\]](#)
22. Pei, S.; Huang, L.; Zhang, L.; Ren, S. Experimental study on thermal cracking reactions of ultra-heavy oils during air injection assisted in-situ upgrading process. *J. Petrol. Sci. Eng.* **2020**, *195*, 107850. [\[CrossRef\]](#)
23. Li, Y.; Wang, Z.; Hu, Z.; Xu, B.; Li, Y.; Pu, W.; Zhao, J. A review of in situ upgrading technology for heavy crude oil. *Petroleum* **2021**, *7*, 117–122. [\[CrossRef\]](#)
24. Al-Khodori, A.; Yusra, A.; Albayati, T.M. Adsorption desulfurization of actual heavy crude oil using activated carbon. *Eng. Technol. J.* **2020**, *38*, 1441–1453. [\[CrossRef\]](#)
25. Cheshkova, T.V.; Grinko, A.A.; Min, R.S.; Sagachenko, T.A. Structural transformations of heavy oil asphaltenes in the course of heat treatment. *Petrol. Chem.* **2022**, *62*, 214–221. [\[CrossRef\]](#)
26. Guerra, A. Modeling Mild Thermal Cracking of Heavy Crude Oil and Bitumen with VLE Calculations. Ph.D. Thesis, Université d'Ottawa (University of Ottawa), Ottawa, ON, Canada, 2018.
27. Al Darouich, T.; Behar, F.; Largeau, C. Pressure effect on the thermal cracking of the light aromatic fraction of Safaniya crude oil—Implications for deep prospects. *Org. Geochem.* **2006**, *37*, 1155–1169. [\[CrossRef\]](#)
28. Afanasjeva, N.; González-Córdoba, A.; Palencia, M. Mechanistic approach to thermal production of new materials from asphaltenes of Castilla crude oil. *Processes* **2020**, *8*, 1644. [\[CrossRef\]](#)
29. Avendaño-Salazar, C.A.; Ramírez-Jaramillo, E.; De la Cruz, J.L.M.; Albitar, A. Thermogravimetric and differential thermogravimetric analysis of effect of areal compositional gradient on combustion kinetics of Mexican extra-heavy crude oil. *Oil Gas Sci. Technol.* **2020**, *75*, 25. [\[CrossRef\]](#)
30. Khelkhal, M.A.; Lapuk, S.E.; Buzuyurov, A.V.; Krapivnitskaya, T.O.; Peskov, N.Y.; Denisenko, A.N.; Vakhin, A.V. Thermogravimetric study on peat catalytic pyrolysis for potential hydrocarbon generation. *Processes* **2022**, *10*, 974. [\[CrossRef\]](#)
31. Hart, A.; Greaves, M.; Wood, J. A comparative study of fixed-bed and dispersed catalytic upgrading of heavy crude oil using-CAPRI. *Chem. Eng. J.* **2015**, *282*, 213–223. [\[CrossRef\]](#)
32. Sukkar, K.A. Evaluation of transport processes in a catalytic reforming reactor with high performance nanocatalysts. *IOP Conf. Ser. Mater. Sci. Eng.* **2021**, *1067*, 012149. [\[CrossRef\]](#)
33. Jin, F.; Jiang, T.; Yuan, C.; Varfolomeev, M.A.; Wan, F.; Zheng, Y.; Li, X. An improved viscosity prediction model of extra heavy oil for high temperature and high pressure. *Fuel* **2022**, *319*, 123852. [\[CrossRef\]](#)
34. Davudov, D.; Moganloo, R.G. A systematic comparison of various upgrading techniques for heavy oil. *J. Petrol. Sci. Eng.* **2017**, *156*, 623–632. [\[CrossRef\]](#)
35. Fattah, M.Y.; Abdulkhabeer, W.; Hilal, M.M. Characteristics of asphalt binder and mixture modified with waste polypropylene. *Eng. Technol. J.* **2021**, *39*, 1224–1230. [\[CrossRef\]](#)
36. Jaber, T.N.; Sukkar, K.A.; Karamalluh, A.A. Specifications of heavy diesel lubricating oil improved by MWCNTs and CuO as nano-additives. *IOP Conf. Ser. Mater. Sci. Eng.* **2019**, *579*, 012014. [\[CrossRef\]](#)
37. Jiao, S.; Li, S.; Pu, H.; Dong, M.; Shang, Y. Investigation of pressure effect on thermal cracking of n-decane at supercritical pressures. *Energy Fuels* **2018**, *32*, 4040–4048. [\[CrossRef\]](#)
38. Pleyer, O.; Kubičková, I.; Vráblík, A.; Maxa, D.; Pospíšil, M.; Zbuzek, M.; Schlehöfer, D.; Straka, P. Hydrocracking of heavy vacuum gas oil with petroleum wax. *Catalysts* **2022**, *12*, 384. [\[CrossRef\]](#)

39. Hao, J.; Feng, W.; Qiao, Y.; Tian, Y.; Zhang, J.; Che, Y. Thermal cracking behaviors and products distribution of oil sand bitumen by TG-FTIR and Py-GC/TOF-MS. *Energy Convers. Manag.* **2017**, *151*, 227–239. [[CrossRef](#)]
40. Kaminski, T.; Husein, M.M. Partial upgrading of Athabasca bitumen using thermal cracking. *Catalysts* **2019**, *9*, 431. [[CrossRef](#)]
41. AlHumaidan, F.; Hauser, A.; Al-Rabiah, H.; Lababidi, H.; Bouesri, R. Studies on thermal cracking behavior of vacuum residues in Eureka process. *Fuel* **2013**, *109*, 635–646. [[CrossRef](#)]
42. Rueda-Velásquez, R.I.; Gray, M.R. A viscosity-conversion model for thermal cracking of heavy oils. *Fuel* **2017**, *197*, 82–90. [[CrossRef](#)]
43. Al-Absi, A.A.; Al-Khattaf, S.S. Conversion of Arabian light crude oil to light olefins via catalytic and thermal cracking. *Energy Fuels* **2018**, *32*, 8705–8714. [[CrossRef](#)]
44. Wang, J.X.; Wang, L.L.; Wang, T.F.; Peng, X.Q. Effects of SARA fractions on pyrolysis behavior and kinetics of heavy crude oil. *Petrol. Sci. Technol.* **2020**, *38*, 945–954. [[CrossRef](#)]
45. Voronetskaya, N.G.; Pevneva, G.S. Structural transformations of heavy oil resins and asphaltenes upon thermal cracking. *Solid Fuel Chem.* **2021**, *55*, 165–170. [[CrossRef](#)]
46. Mateus, L.; Taborda, E.A.; Moreno-Castilla, C.; López-Ramón, M.V.; Franco, C.A.; Cortés, F.B. Extra-heavy crude oil viscosity reduction using and reusing magnetic copper ferrite nanospheres. *Processes* **2021**, *9*, 175. [[CrossRef](#)]
47. Hammoodi, S.I.; Almkhtar, R.S. Thermal Pyrolysis of Municipal Solid Waste (MSW). *IOP Conf. Ser. Mater. Sci. Eng.* **2019**, *579*, 012018. [[CrossRef](#)]
48. Shakor, Z.M.; AbdulRazak, A.A.; Sukkar, K.A. A detailed reaction kinetic model of heavy naphtha reforming. *Arabian J. Sci. Eng.* **2020**, *45*, 7361–7370. [[CrossRef](#)]
49. Jalal, N.I.; Ibrahim, R.I.; Oudah, M.K. Flow improvement and viscosity reduction for crude oil pipelines transportation using dilution and electrical field. *Eng. Technol. J.* **2022**, *40*, 66–75. [[CrossRef](#)]
50. Abbas, A.D.; Sukkar, K.A. Rheological behaviour modification of Basrah crude oil by graphene additions at different temperatures in petroleum pipeline. *AIP Conf. Proc.* **2022**, *2443*, 030048.
51. Lababidi, H.M.; Sabti, H.M.; AlHumaidan, F.S. Changes in asphaltenes during thermal cracking of residual oils. *Fuel* **2014**, *117*, 59–67. [[CrossRef](#)]
52. Pevneva, G.S.; Voronetskaya, N.G.; Grin'ko, A.A.; Golovko, A.K. Influence of resins and asphaltenes on thermal transformations of hydrocarbons of paraffin-base heavy crude oil. *Pet. Chem.* **2016**, *56*, 690–696. [[CrossRef](#)]

Article

The Study of Quality of Life as a Guide to Urban Regeneration Analysis of Estepona's New City Hall as a Sustainable Model

Juan M. Ros-García

Principal Investigator Agenda Urbana y Retos Sociales Group, Department of Architecture and Design, Institute of Technology, Universidad San Pablo-CEU, CEU Universities, Urbanization, Av. de Montepíncipe, s/n, Boadilla del Monte, 28668 Madrid, Spain; jmros.eps@ceu.es

Abstract: Given the immersion of cities in a global situation of social emergency since the latest environmental and health events, current research on increasing the quality of life of citizens has become a priority in the attempt to provide the set of sustainable strategic conditions that must be met in favour of the necessary urban regeneration associated with the improvement of the habitable environment. Thus, being directly concerned by this matter, the construction of new buildings will have to follow concordant dynamics aiming at the improvement of the quality of life of their users and of the city as a whole, thus contributing to their mandatory healthy, habitable and equitable nature. It is necessary to redefine in the design of buildings certain potential criteria with a positive effect on the quality of life. These can be grouped into the following five key factors that define architectural work in relation to its habitability conditions: identity, character, image, materiality and implementation. These quality-of-life descriptors are assessed in a particular building, which serves as a real case study as follows: the new town hall of Estepona (Malaga, Spain). The aim is to provide an answer to the potential use of indicators that determine the improvement of the quality of life provided by a building in the city as a whole. The fact that it is a public building also turns it into a model of management that is consistent with the requirements of sustainable environmental progress in the general interest of a socially just city.

Keywords: sustainable architecture; environmental buildings; quality of life; healthy architecture; urban regeneration

Citation: Ros-García, J.M. The Study of Quality of Life as a Guide to Urban Regeneration Analysis of Estepona's New City Hall as a Sustainable Model. *Buildings* **2022**, *12*, 1699. <https://doi.org/10.3390/buildings12101699>

Academic Editors: Roberto Alonso González Lezcano, Francesco Nocera and Rosa Giuseppina Caponetto

Received: 21 September 2022
Accepted: 14 October 2022
Published: 15 October 2022



Copyright: © 2022 by the author. Licensee MDPI, Basel, Switzerland. This article is an open access article distributed under the terms and conditions of the Creative Commons Attribution (CC BY) license (<https://creativecommons.org/licenses/by/4.0/>).

1. Introduction

The relationships between the inhabitants and the city as interconnected entities were analysed against the orthodoxy of the modern movement by Reyner Banham in his book *Los Angeles: The Architecture of Four Ecologies* (1971) as the result of the following four topographical subsystems: the beach area (surfurberia), the motorway network (autopia), the plains and the hills with their large mansions, on each of which the variables of geography, climate, economy, demographics, technology and culture acted [1]. This reference allows us to enter into contemporary urban ecology as a current issue that we are interested in developing. Moreover, the above reference is shown as a similar configuration to the structure of the urban region under analysis in this case study, currently understanding the value that restorative qualities acquire in contact with the natural physical environment as an additional resource to promote positive interactions with the city (Kleinschroth and Kowarik 2020; Slater et al., 2020) [2,3].

Thus, in the face of widespread environmental awareness and the need for urgent measures, the architectural quality of the built objects in the city and the perception of improved quality of life as a healthy experience for the individual need to be identified in a coordinated manner in order to make it possible to “meet the needs of the present without compromising the ability of future generations to meet their own needs” [4] (p. 15). In “*Our Common Future*” 1987 report of the World Commission on Environment and Development

of the United Nations Assembly, this is confirmed by the possibility of achieving economic growth based on sustainable development policies, a development that protects human progress into the future and the expansion of environmental resources [4].

The disproportionate growth of town planning, together with a detachment from the natural environment, has caused numerous negative effects on people's physical and mental health (Pelczynski, 2019; Taylor and Kuo, 2006) [5,6]. The aim is to understand the factors that operate in favour of well-being and the perception of life quality (Corraliza and Collado, 2011), such as the moderating effect of enjoying greater contact with green areas [7]. The so-called welfare city (Barton & Grant, 2017) is based on a rethinking of the relationships between inhabitants, the urban environment and nature that are set to endure and prevail over temporary emergencies (Figure 1) [8]. Notably, the "Limits to Growth" report of 1972, commissioned by the Club of Rome, demonstrated the vulnerability of the global production system, warning about the irreversible environmental consequences of the unlimited development model and the unsustainable increase in the ecological footprint based on the depletion of natural resources and its negative impact on the future urban environment [9].

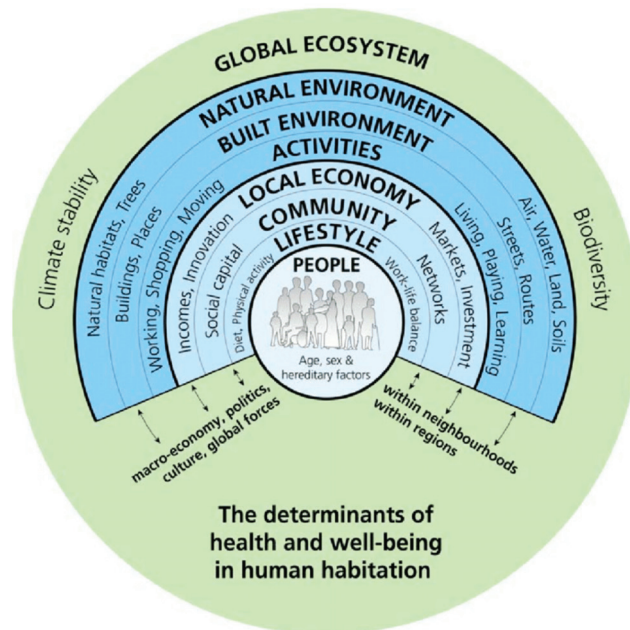


Figure 1. The Settlement Health Map. Source: Barton & Grant, 2006 [8].

Consequently, the architectural project as a proposal in the built environment must meet—among others—the requirements of environmental energy autonomy without interfering with the qualities of the landscape and incorporating sustainable practises that improve the efficiency and consumption of resources aimed at the building's own uses. This means that open space considerations will be taken into account as indivisible parts of the built space, with no negative impact on matters related to land's natural values (Higueras-García, E.; Ezquiaga-Domínguez, J.M., 2022) [10].

The definition of quality of life currently represents a topic of growing interest, and its association with urban regeneration has implications in the fields of health, architecture, economics, humanities, urban design, education and culture, amongst others (Figure 2).

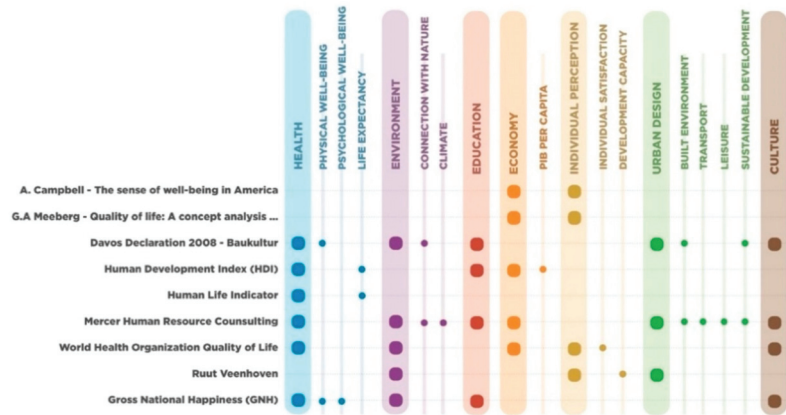


Figure 2. Summary diagram of factors influencing quality of life according to the literature of this study. Source: Compiled by the author.

Since the approach to quality of life as a social attribute gained momentum in the sixties of the twentieth century, when authors such as A. Campbell (1981) and G. A. Meeberg (1993) proposed the weight of individual qualitative variables as a necessary complement to the original metrics for economic status, it can be stated that the interest in adequately and scientifically characterising the concept has been evolving towards more integrative criteria and diverse characteristics [11]. Beyond the subjective indicators relating to the individual psychological perception of the concept of quality of life, which would complete the variation in the degree of satisfaction once added to the objective data, in order to defend the need to introduce psychological indicators in the determination of the variance in quality of life, the healthy characteristics of the physical environment, associated with the urban environment, with proven influence in obtaining high standards of recognition of the quality of life can be found (Nasution, 2019) [12].

The World Health Organization Quality of Life (WHOQOL) working group, created in 1995 by the World Health Organization (WHO) for research on the quality of life and the description of its weighting possibilities, introduced the correlation between objectively measurable multidimensional parameters and the perceived self-report of personal satisfaction as a methodological criterion for the potential comparison between different states of quality of life [13].

In this sense, the HDI indicator (Human Development Index), established by the United Nations Development Programme (UNDP-1990) and referring to each country, is frequently used [14]. It relates the three major demanded areas, assuming their interconnection, that is, health (life expectancy), education (schooling) and the economy (GDP per capita), to assess an assessable and comprehensive relative average state, based on the specific instruments of each one of them in relation to the fulfilment of certain standards and expectations. The Human Life Indicator, developed by the International Institute for Applied Systems Analysis (IIASA), is a new international comparative ranking for quality of life that has been imposed as an alternative and replacement for the HDI indicator. The Human Life Indicator, recently developed by the International Institute for Applied Systems Analysis (IIASA), is an alternative to the Human Development Index (HDI) by the United Nations. Its argument is based on the relative deviation of the birth-mortality extremes, averaging the percentages of greater longevity with respect to premature deaths [15].

Recently, there has been growing awareness of a substantial factor, which although it is not new, does seem to be at the heart of much of the debate. Indeed, the Davos Declaration (January 2018) *Towards a high-quality Baukultur for Europe* links the concept of “quality of life”, as the ultimate goal to be achieved, to factors that have a direct impact on

the design of the built and natural environment and on the sustainable development of cities. The Davos Declaration (2018) introduces the concept of “architectural quality” as a necessary guarantee, with national legislative status, to obtain a degree of the universal right to quality of life. An intangible, value-judgement parameter is reintroduced, pending classification as a new complex variable in the conceptual equation [16].

Similarly, in March 2019, Mercer Human Resource Consulting presented its latest global quality of life ranking for 215 cities worldwide (out of a total of 440 cities analysed), in order to guide large institutions and multinational corporations in moving their employees away from their original homes to the most attractive destinations. In a new attempt to define the high-impact components of people’s everyday lifestyles, the report assessed 10 categories and 39 different factors, grouped into economic, socio-political, cultural, environmental, health and education, services and transport, leisure, natural environment, consumer goods and housing contexts [17].

From a holistic point of view of development focusing on the achievement of public welfare policies, the Dutch researcher and sociologist Ruut Veenhoven (1942) mainly introduces the habitability of the environment as a condition of external quality and the individual’s capacity for development as a variable of internal quality, which directly relates opportunities with the results obtained expressed in practical utility and subjective appreciation [18]. Veenhoven proposes a comprehensive framework of multidimensional relationships for the reliable measurement and study of the quality of life of different societies in the same sense as the United Nations’ President, Ban Ki-moon, associated it with the right to happiness in the spirit of the Millennium Development Goals (MDGs) in the resolution adopted by the 2011 General Assembly session. Lhatu Wangchuk, Bhutan’s ambassador to the UN, representing King Jigme Singye Wangchuck, led the initiative by advocating at the 74th plenary session (14 January 2011) the yearning and need to achieve a fulfilling, meaningful and happy life as a fundamental goal for social development, based on a new satisfaction indicator for the quality of life, called the Gross Domestic Happiness Index (GDPI), away from more conventional socio-economic models of wealth. The factors to be considered for the sustainable development of the GDPI with strong qualitative weighting are the following: psychological well-being, health promotion, education, good governance, impact on the community’s vitality, environmental conservation and cultural promotion.

Thus, the extent to which existing cities, as dynamic physical frameworks of potential transformation, present themselves as places that facilitate accessibility, comfort, utility, diversity, security, prosperity, etc., will determine their capacity to provide a quality of life to the population. Citizens need to be aware of the dependent factors that increase or decrease their personal assessment in relation to levels of quality of life in their urban context.

Health risks associated with urban inequalities have been explored and reported in the document jointly published by the World Health Organization and the United Nations Human Settlements Programme (2010) [19]. Multiple scientific studies place health equality on the political agenda of European cities, highlighting the relevance of aspects relating to the physical environment, mainly the built environment. They aim to analyse different patterns of health inequalities in urban areas and to describe policies to reduce them in European cities [20]. Moreover, in the socio-economic environment in order to achieve a higher quality of life (Northridge, 2003; Evans, 2003; Haines et al., 2012; Borrell et al., 2013; Carnemolla, 2016; Chen, 2017) [21–26]. The study of urban regeneration associated with quality of life as a topic of international interest that is key to sustainable urban development, with a particular focus on health promotion. In particular, the population’s globally acquired awareness of climate change issues at the same time as the so-called Social Determinants of Health (SDH) has led to an increased sensitivity to the use of strategies that can be integrated into an ever-changing built environment [27]. Health, understood as the predominance of positive social well-being, according to the OECD report (2002), is framed as a strategic objective of global policy in order to design urban centres that improve health and well-being. The objective of promoting policies and actions for healthy and sustainable

development at the local level, which emphasizes equality in health and the principles of the European policies “Health for All and Health 2020” as the objective of improving quality of life, is especially meaningful [28].

2. Materials and Methods

In order to recognise the influencing factors that intervene in the condition of habitability with regard to the perception of quality of life, the starting point is on the one hand the bibliographical study of references of publications in journals of scientific impact and consolidated authors on the subject of quality of life, sustainability and urban regeneration as research tools, as well as the indicators proposed by governmental, European or world organisations on the subject. On the other hand, in terms of the new town hall building of Estepona as a case study of habitability conditions, the original technical architectural documentation of the project, the data used in the numerical simulation analysis of the design for decision-making and the construction process represent primary sources of information, as well as the precise information on the structure, installations, materials and the execution of the different stages of the work.

As a final reference support, we have availed of the documentation generated by the specialised consultancy in charge of verifying the degree of compliance with the certification criteria required by the Leadership in Energy and Environmental Design (LEED) accreditation seal and the results evaluation report (Figure 3).



Figure 3. LEED Certification Review Report accreditation document, provided by GBCe in the design phase, prior to the commissioning of the reference work, case study “New City Hall of Estepona”, in accordance with the rating systems created and maintained by the U.S. CITY HALL OR TOWN HALL, PREGUNTAR Green Building Council® (USGBC®). The LEED certification programme is administered by Green Business Certification Inc (GBCI®) [29].

Nevertheless, it is necessary to recall here the opinion supported by Ken Yeang's research on Ecological Design Theory that the "active solution", from solar panels, air conditioning, building automation systems, double skin facades, as well as building accreditation ratings such as LEED, do not exclusively make up what should be understood as a total Sustainable Design. Instead, passive systems integrated into the design and connected to the natural environment are the key to sustainable design and necessary for the well-being of users (Yeang, 1995) [30].

In order to establish the degree of quality of life of a community in a specific physical framework, understood as a state of dynamic integral well-being in all its expressions, it would be necessary to have objective relative variables, which would make it possible to assess the levels of satisfaction achieved and to compare the margins for standardised improvement beyond a qualitative perception (Pérez Maldonado, 1999) [31].

The quality of life identified with a given place is the result of applying degrees of compliance and levels of individual satisfaction to various objective common universal indicators, which have the property of fixing their interaction in a perceived and verifiable daily experience mainly in the domains of economy, health, culture and environment.

In this sense, it is necessary to highlight the current importance of Dr. Sabine O'Hara's work on the Theory of Economic Development, which from the University of the District of Columbia focuses on the quality of life and economic opportunity of local communities through the development of material and social assets, intellectual and physical multidimensional capabilities. These development assets are expressed in the following five pillars of economic development: education, health, environmental quality and leisure, social and cultural services. These five pillars can be considered qualitative, yet measurable outcomes associated with a high quality of life and a high capacity for economic development and progress towards an equitable city (O'Hara, 2018) [32].

For the evaluation of the criteria present in the design of the building that serves as a real case study, the new town hall of Estepona (Malaga-Spain), which has a positive effect on the quality of life, the following five key factors or descriptors are proposed that characterise the architectural work in its habitability condition: *Identity, Character, Image, Materiality and Implementation* (Figure 4).

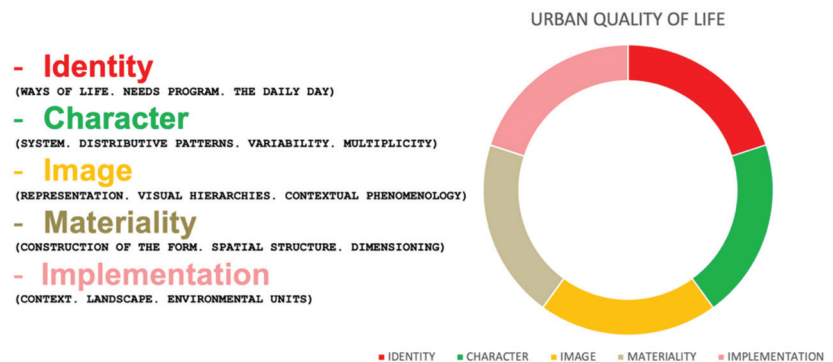


Figure 4. Key factors defining quality of life in architectural work. Source: Created by the author.

The condition of habitability has a subjective dimension associated with the personal meaning that each person can give to the objects and architecture in a given spatial context. Studies such as that of Csikszentmihalyi and Rochberg-Halton (1981) determine how the personalisation of spaces and objects is a means of expression, with which users can feel a greater degree of satisfaction with the environment by finding their own meaning based on life experience, establishing an emotional link with the place, which reinforces the sense of belonging projected towards the community, in what could be called the *identity of the architectural work* (Factor ONE) [33].

The condition of architectural habitability is not only defined by obtaining protection through thermal and acoustic comfort, but also by factors of architectural influence consistent with functionality and space (Landázuri and Mercado, 2004), in what could be called the *character of the architectural work* (Factor TWO) [34].

The need to add a phenomenological view to the condition of habitability, situated in a materialist subject-world ontology, inserting everyday ideation and conduct into the existential context of people's lives, into their immediate relationship with the contingent reality of their built space (Merleau-Ponty, 1974), is what could well be named the *image of the architectural work* (Factor THREE) [35].

Ever since Hungarian researcher Viktor Olgyay set out in 1963 in his book *Architecture and Climate. Bioclimatic design manual for architects and urban planners*, an authentic multidisciplinary theory applied to architectural design based on the achievement of hygrothermal comfort in four representative climatic regions (temperate zone, cold zone, warm-arid zone and warm-humid zone), based on the analysis of the site, it seeks the least environmental impact generated by the different defining elements of the built work conditioned by a specific physical environment [36]. Since then, the contextual correspondence that should be established between architecture (form) and energy (climate) to achieve a satisfactory result of *materiality* (Factor FOUR) in favour of the promotion of health, one of the most studied factors in relation to the improvement of the quality of life has been the physical conditioning of the environment, as an external factor to the individual, and the associated individual satisfaction and perception, as an internal factor. A few years later, in 1969, architect and professor of urban design Baruch Givoni (PhD in Public Health from the Faculty of Medicine of the University of Jerusalem in 1963) contributed with his book *Man, Climate and Architecture* to the parameterised definition of bioclimatic architecture as a contextual working tool of passive design for the healthy control of the indoor built environment, without excessive increase in additional energy consumption [37]. The novelty of its 1969 publication date is the incorporation of architectural design recommendations based on its well-known "Building Bioclimatic Chart", to ensure indoor comfort conditions. For the first time in 1971, British architect Carl Mahoney (together with John Martin Evans and Otto Königsberger) edited his own charts and recommendations for climate-appropriate architectural design [38]. As a result of the impact of his research, Givoni founded PLEA (*Passive Low Energy Architecture*) in 1982, an international association for the promotion of bioclimatic architecture, which is still active internationally in urban development. In both cases, the management of the balanced exchange of energy that occurs between the individual and the built object in relation to the physical environment is the key to developing the architectural project as a reference manual for improving the user's quality of life, based on the active promotion of health from a comfortable space.

Both the particular meaning attributed to urban environment by people subject to its condition of habitability, as well as the sensory bases of the related cognitive processes, represent from an environmental psychology point of view, an essential factor for the information that the individual needs to process as a member of the community. Research by T. Gärling (1998) on the different types and functions of environmental uncertainty basically concludes that people are optimisers of environmental uncertainty and that by minimising it, the level of environmental stress that is sought to obtain adequate levels of appreciation for the quality of life can be reduced into what could be called the *implementation of the architectural work* (Factor FIVE) [39].

With the aim of promoting healthy environments for the population, the Ministry of Health (Spanish Government), in coordination with the Ministry for Ecological Transition and Demographic Challenge, is implementing the Strategic Plan for Health and Environment (PESMA) until 2026, aimed at protecting the population from environmental risks. The Strategic Plan for Health and the Environment was approved at the extraordinary session of the Plenary Session of the Interterritorial Council of the National Health System and the Sectorial Conference on the Environment (November 2021) [40]. The Plan addressed the actions to be taken to reduce the impact of the main environmental factors

and determinants on health. Thus, as part of a policy of control over the environmental dynamics of the city and with the aim of helping resolve new lines of development in the architecture-health binomial, a series of project parameters are undertaken in the research process that would make it possible to determine a synthetic index of comparative relative territorial vulnerability, for the evaluation of the necessary urban regeneration. This brief preview of design criteria is just an initial sample of what we would like to achieve in order to establish sustainable and healthy parameters for generating new ways of building, as well as directly improving the healthy user experience. These parameters must intervene and be quantified in the definition of appropriate architectural solutions for habitability, in which abrupt changes in temperature and excessive consumption of metabolic energy are avoided; noise pollution is reduced; the incorporation of natural cooling systems is harmoniously regulated; the management of light and control of energy use and the consumption of resources and environmental pollution reduced. This implies an effective control over the architectural factor as a social determinant of health, and therefore a decrease in health inequalities and an increase in quality of life. In this sense, the proposed basic architectural parameters for healthy living incorporated into the design process would be the following:

a. Hygrothermal regulation

Integral approach that contemplates the characterisation of thermodynamic volume, for the control of internal humidity, so as to ensure the absence of any thermal discomfort of the users, for the human body to reach thermal balance between heat input and heat loss without the need to activate its natural thermoregulation mechanisms (metabolism, sweating . . .).

b. Energy exchange

Maximum efficiency derives from energy characteristics of the environment, taking into account the climatic conditions and the specific circumstances of the physical environment.

c. Indoor air quality

The use of natural ventilation is enhanced through design strategies by adapting the architectural envelope and interior layout to achieve optimal air renewal. It will be complemented by mechanical ventilation strategies to direct air flows from outside and clean areas through natural vegetation filters to those areas that may have higher concentrations of moisture or pollutants, ensuring a continuous renewal of clean air.

d. Form factor, proprioception and occupation

The form factor is the relationship between the built volume and the enveloping surface, referring to climatic harnessing; together with proprioception, understood as the capacity to adopt the relative position of the body schema with the physical space under the conditions of an ergonomic system, and occupancy, referring to overcrowding. It primarily affects the parasympathetic nervous system and the immune system, turning the interior space into a risky breeding ground for the spread of infectious diseases.

e. Sound perception

Human perception of sound involves both the acoustic qualities of sound (pitch, intensity, tone and duration) and the acoustic qualities of space (reflection, absorption, etc.).

f. Construction and material efficiency

Via the life cycle analysis of materials and construction processes employed, there is a guarantee on the use of technologies and delivery systems that require as little energy and raw materials as possible, while generating as little waste and toxic emissions as possible at all stages of their life cycle as follows: extraction of raw materials; processing and manufacture; distribution and transport; commissioning; use and waste management

g. Living nature

Effective use of vegetation in the indoor and outdoor environment of the building as a filter for air pollutants, a natural cooling system and thermal protection, as well as efficient water management with the aim of recreating part of the natural environment.

h. Lighting and colour

Healthy design promotes the use and control of natural lighting with its daily and seasonal changes. Artificial light is synchronised with these oscillations to adapt to the circadian rhythms of the human being, avoiding disturbances of the biological rhythms and promoting a continuous state of well-being. Visual variables of light (intensity, hardness and colour), visual variables of focus (amount of light, light fall-off, coverage, shadows, glare and colour) and vision factors (visual accommodation, adaptation and visual acuity) are taken into consideration. The design variables that are directly controlled in healthy architecture are the following: luminous intensity; illuminance; luminance; contrast and glare

Although, as described, the disciplinary exchange between human health and the built environment has been progressively accepted as a driver to reasonably advance the town planning agenda (Kent and Thompson, 2012) [41], nowadays, one of the direct consequences presented particularly by the COVID-19 pandemic, originating from the SARS-CoV-2 virus, is an opportunity to implement health promotion and disease prevention strategies, as well as the adoption of norms for living with a new urban order. The new norms of social behaviour imposed by health restrictions during the pandemic have led to changes in the spatial relations of coexistence, with direct impact on the urban environment (Frumkin, 2021) [42].

Now more than ever the term ‘affordance’, coined by the environmental perception psychologist Gibson (1979) [43], which refers to the perceived opportunities and constraints regarding a person’s actions in a given environment, can be revised to also incorporate the emotional, social and socio-cultural opportunities and constraints offered by a changing environment (Heft, 2001) [44].

It would be a paradoxical way of activating public space in a private manner, a kind of oxymoron of the city. Understanding the physical city not only as a right but also as a reward, the new great challenge will be to generate aseptic spaces of functional autonomy, harmless to excessive socialisation and environmental balance, based on a re-encounter with nature (Moraci, 2020) [45], interconnected by healthy sustainable mobility, no longer binding 70% of public space to be reserved for road traffic, all of this pointed out by the configuration of the well-known superblocks, once the need for large journeys has been reduced, in the face of the complementary irruption of the digital city. Superblock is known as a new basic urban organisation unit successfully developed, among others, in the Gracia neighbourhood (Barcelona), recognised as good practice by UN-Habitat (2010). Based on a new perimeter structure in the road network, with low environmental impact, it manages to improve public space and mobility for pedestrians, the new player of the intermediate scale of the city. UN-Habitat (2020) defines the components of the Right to the City as those that the entire population can exercise [46]. Lefebvre (1967) defined it as a framework resulting from an anti-capitalist political debate, centred on the necessary contemporary urban transformation, extended to all citizens [47].

Subsequently, various authors introduced new components of social change based on theories of environmental balance. Abraham et al. (2009) classifies the various types of close landscapes that can be therapeutic for certain health and well-being conditions of people [48]. For example, urban parks can promote the social integration of citizens; or a landscape with visually stimulating elements such as water or vegetation can help reduce stress and improve an individual’s emotional well-being (Bowler et al., 2010) [49]. Public spaces within the city can be conducive to the development of a more physically and socially active lifestyle, compared to areas with a shortage of open spaces (Lestan, 2014) [50].

The definition of the built environment that provides quality of life under the challenge of the new post-covid premises, (Oppio, Forestiero, Sciacchitano and Dell’Ovo, 2021), arises from a space that evolves towards maximum diversity, that absorbs events, not exclusive uses, whose project is not based on a recognisable closed form, but rather establishes a

trajectory, whose construction belongs to a particular instant in its maximum expression of adaptation [51]. The post-covid space is thus presented as awaiting an open-ended process of ongoing temporal reconfiguration in everyday constructed spaces for emotional re-balancing, in which the somewhat understandable haphophobic reaction to physical group proximity is overcome, critically engaging with the so-called spaces of fear' and their role in fragmenting and eroding the civic function of urban space (Tulumello, 2015) [52].

3. Results

The third ecological model of human development presented by Hancock (1993) places health as an intersection between the community, the environment and the economy, with specific conditions to be met in each of these three domains in order to achieve a positive quality of life development [53]. This model could be reinterpreted as the degree of coincidence between social sustainability (enabling communities), environmental sustainability (embodied in the environment) and economic sustainability (available in resources) (Figure 5).

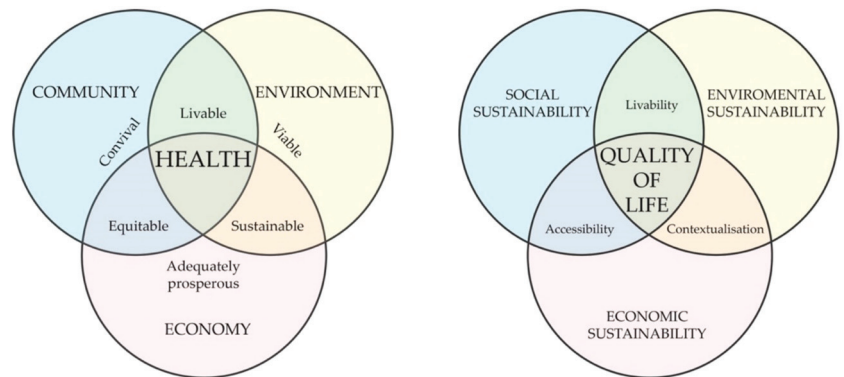


Figure 5. Comparison of the Hancock model (source: Hancock, 1993) [53] (on the left), with the proposed model (on the right) based on the definition of sustainability from the Brundtland Report (*Report of the World Commission on Environment and Development: Our Common Future*. Document A/42/427 General Assembly United Nations (UN), New York, USA 1987) [4]. Source: Created by the author.

This new model of integration between sustainability and quality of life supports the studies of authors such as Mohit (2013), who in his study on quality of life in natural and built environments states that maintaining a balance between the social, economic and environmental components of development is crucial to ensure sustainable development and to guarantee a better quality of life [54].

At the same time, societal recovery from the recent pandemic offers a number of lessons that will continue to emerge over the coming years (Capolongo et al. 2020; Milner et al. 2021; Rojas-Rueda and Morales-Zamora 2021) [55–57]. It also offers a historic opportunity (Frumkin, 2021) as follows [42]: to firmly ground the creation of new places for human needs, justice and environmental sustainability; to adopt indicators and metrics that reflect emerging priorities; to improve the efficiency and equality of urban governance; to harness technology to create places that are healthier and more resilient than ever before.

In this context, understanding that sustainability should be considered a transversal factor for urban transformation, focusing on finding the architectural design factors that influence the quality of life of the user provided by their environment, the objective is to establish a framework of study with key issues and positive indicators through a representative case, the new town city hall building of Estepona Town Hall (Malaga), from which the quality of life enhanced by a particular building can be evaluated with respect to the city (Ros-García, J.M. 2021) [58].

Estepona is a Spanish town in the province of Malaga, in the western Costa del Sol area. It is located on the southern border of the European Union, on the Mediterranean coast, just 50 km from the African coast. Both the natural, social and economic aspects, as well as its position between the Strait of Gibraltar and the dynamic city of Malaga, define Estepona as a geographical point of great strategic interest. The city enjoys a very mild Mediterranean climate, with mild winters and hot summers, with an annual average of 2850 h of sunshine. The population is growing steadily, with a current census of 71,925 inhabitants, according to the Spanish National Institute of Statistics (INE, 2021), with an average age of 41.6. Estepona's unique coastal landscape is complemented inland by the forested backdrop of the Sierra Bermeja, with an altitude of 1500 metres just 15 km from the coast, which provides an enormous variety of environments and microclimates, promoting the special biodiversity of a large number of plant and animal species.

Since 2011, the municipality of Estepona has been characterised as a major driver of urban transformation, as demonstrated by its concept of integral sustainability, in favour of improving the quality of life and actively promoting the health of its inhabitants. Its urban environment has been significantly improved over the last decade, thanks to the "Estepona, Garden of the Costa del Sol" project, financed by the European Regional Development Fund (ERDF) and the Integrated Sustainable Urban Development Strategies (EDUSI) through the creation of citizen-friendly green spaces and infrastructures as the main objective, which has transformed the city, with more than 130 naturalised pedestrian streets, as part of the process of revitalisation and economic regeneration of the historic centre of the municipality. The project addresses the five challenges (economic, environmental, climatic, demographic and social) affecting urban areas and promotes links between urban and rural environments in accordance with Article 7 of the ERDF Regulation (Regulation (EU) No 1301/2013 of 17 December 2013. Through the Sustainable Energy and Climate Action Plan (SECAP), Estepona Town Council promotes sustainable development policies and encourages local policies to adapt and fight against climate change, in compliance with the commitments acquired with the Spanish Federation of Municipalities and Provinces (FEMP) in the Spanish Network of Cities for Climate.

At the same time, the Territorial Information and Management System (SITES) has been implemented as an innovative model of e-administration for intelligent and coordinated municipal data management for the governance of all public services to citizens. As a novelty, it allows the use of the territory as an integrating element in the management of the various urban inventories for all municipal activity. In addition, the Estepona Town Council considers the Citizen Participation area of vital importance to offer a coordinated planning service for the whole city, from which the decisions and environmental or geo-referenced infrastructures of the municipality can be resolved. The Estepona Town Council joined the Network of Local Entities for the development of the 2030 Agenda in June 2020, and since that date, it has been working on the integration of the Sustainable Development Goals for municipal strategic planning.

The intention is to convert the urban area of intervention, where the construction of the new town city hall building of Estepona is located, into the focus of environmental centrality and qualitative articulation of the city. For the architectural project and subsequent execution of the construction of the new town city hall building of Estepona, different analysis and dynamic simulation models have been considered in terms of functionality, sustainability and energy efficiency, key issues and positive indicators that can be identified as determining factors for the enhancement of the perceived quality of life in the city. Its novelty also lies in the fact that it is the only new town city hall that has actually been newly built in 2022 in Spanish territory for municipalities with more than 20,000 inhabitants, which is why it is of the greatest relevance, thus reinforcing its selection as a particular case study. The location of the new town hall building is situated on a plot at the heart of Estepona town centre on Avenida Juan Carlos I, on the western border with the redeveloped old town (Figure 6).



Figure 6. Cont.



Figure 6. (above) Aerial view of Estepona town centre where the project is located. Combined density ($\text{m}^2/\text{hectares}$) = Total floor area (m^2)/Total buildable land (hectares) Combined density ($\text{m}^2/\text{hectares}$) = $487,463.60/32.50 = 14,998.88 \text{ m}^2/\text{hectares}$. (middle) View of the original state of the plot on which the current building is located. The boundary of the plot's urban performance represented by a red line. (below) Location plan with the footprint of the building in relation to the plot in black dashed line. Source: Castaño & Associates. LEED Rating System Report [59].

As it is a consolidated urban area with existing infrastructure, the distance between the services is reduced, facilitating movement and access on foot or by bicycle, encouraging daily physical activity by users, with the resulting limitation of greenhouse gas emissions, air pollution and other environmental damage associated with public health. Typologically, it is a free-standing building with a total of eight floors above ground level for administrative use and a basement floor for parking services, with a built surface area of approximately one thousand square metres per floor (9300 m^2 in total above ground level), a double-skin façade and a landscaped roof (Figure 7).

Strategically, the use of the form factor concept as a first approach to controlling the building's heat energy exchange with the outside from a bioclimatic point of view should be highlighted. Orientation and passive design strategies play an important role in the suitability of the adopted solution, significantly reducing the need for active strategies to ensure the responsible use of energy resources. In terms of construction, industrial standardisation is promoted by selecting methodologies such as DfMA (Design for Manufacture and Assembly), which refers to the set of guidelines drawn up to guarantee that a product is designed with the aim of maximising the efficiency of its manufacture, assembly and life cycle, thus minimising the impact of both the materials and construction systems and the construction processes, which grant it the corresponding quality standards "Environmental Product Declaration" (Model EPDs) issued by official certification agencies [60].



Figure 7. Double façade system with the external envelope made of lattice work. Modular geometric pattern used. South-facing elevation (**above**). Source: Castaño & Associates. LEED Rating System Report [59]. (**below**) Source: Pictures created by the author.

The concept of sustainable building, advocated by associations such as the Green Building Council (GBC), on which the most important urban transformations are based, is no longer just a necessary requirement, but a form of progress linked to quality of life. In this way, some criteria, used by the aforementioned GBC association, have been selected from the diagnostic and evaluation tool. Environmental, social and economic behaviours are analysed in a total of 15 collected impacts. Health and comfort have a weight of 9.38%, the highest percentage value of all those considered [61], for a cross-cutting approach to sustainable development that allows the quantification of improvements in the following three key areas: environmental, social and economic, by testing a real multi-level impact framework, in order to favourably evaluate the interior habitability of the town hall building of the new town council of Estepona (Malaga).

From an environmental viewpoint, in order to meet the EU's target of zero net emissions by 2050, it is necessary to improve energy efficiency in order to reduce emissions by encouraging the use of renewable energies. At the same time, within the framework of BUILD UPON [62], the European Commission stimulates citizen-focused urban energy improvement processes, creating jobs and local investment. The BUILD UPON project,

funded by the EU's Horizon 2020, is led by a consortium of eight national green building country councils, with GBC Spain as coordinator. It develops strategies and solutions that enable cities across Europe to join forces with national governments and industries to decarbonise their existing building stock by 2050. Based on the Renovation Wave action plan, the aim is to ensure indoor air quality and thermal comfort in buildings. Through measurable indicators of progress for the city's renewal strategies, specific objectives such as reducing emissions, increasing employment and improving health are coordinated with each other (Figure 8).

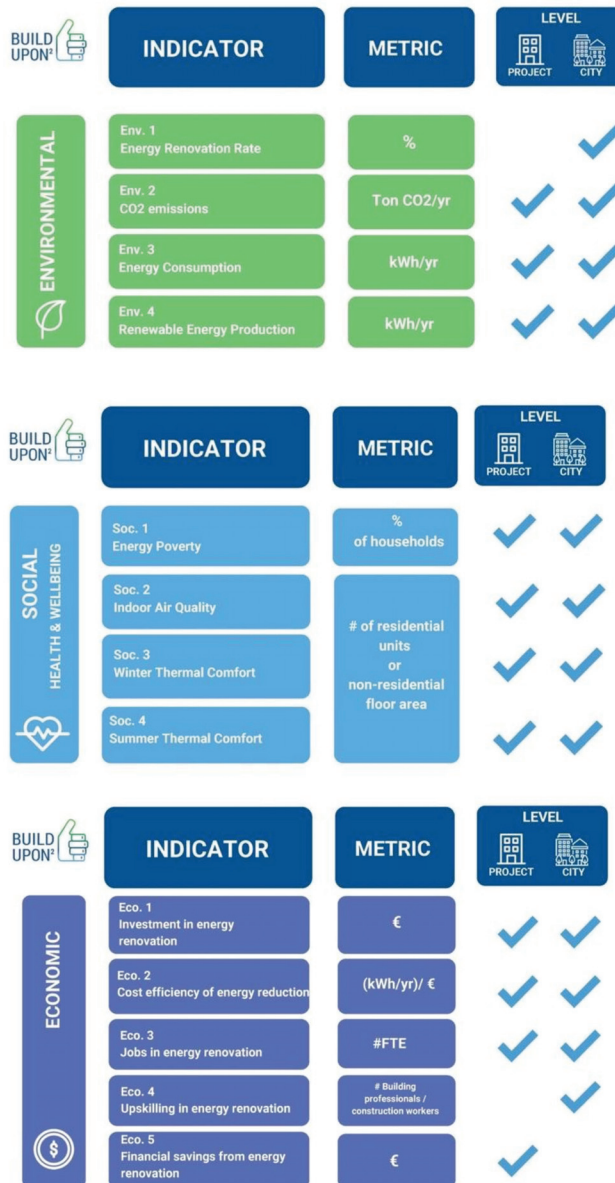


Figure 8. Methodology of core indicators proposed for the reporting and monitoring of the *Build Upon Energy Renewal Framework* [62].

Based on this methodology, variables such as thermal, acoustic and lighting comfort, air quality, and spatial functionality in its different areas are selected as defining parameters of any sustainable building for the analysis of this proposed case study.

Thus, light control is based on the entry of filtered natural light through an external latticework envelope that prevents glare and protects the indoor environment from excessive heating due to direct solar radiation through the second glass curtain wall layer. The section on lighting control in this study is a specific part of the project known as “*Integration of data in a territorial information system for the sustainable use of the lighting heritage in favour of the quality of urban life and economic development*” submitted to the 2021 call for funding of “strategic projects oriented towards the ecological transition and the digital transition” of the Ministry of Science and Innovation (Spanish Government) [63]. Its main objective is to guarantee optimum lighting conditions that promote health, quality of life and safety in the city, while respecting its natural heritage and current urban beautification, with the lowest energy consumption.

In the case of thermal comfort, priority is given to the possibility of individual control of air conditioning and heating (89% of individual spaces allow for individual control). Indoor air quality is provided by specialised ventilation systems. Mechanical ventilation has been identified as the appropriate ventilation strategy for the entire construction project. As the project is located in Estepona (southern Spain), it will meet the minimum outdoor air requirements of the following:

- Annex B of the European Committee for Standardisation (CEN) standard EN 15251-2007, Environmental input parameters for the design and assessment of the energy performance of buildings addressing indoor air quality, thermal environment, lighting and acoustics;
- Standard CEN EN 13779-2007, Ventilation for non-residential buildings, Performance requirements for ventilation and room conditioning systems, excluding Section 7.3, Thermal environment; 7.6, Acoustic environment; A.16; A.17.

For this purpose, a mechanical system consisting of three outdoor air energy recovery units (from manufacturer Swegon) has been considered to cover, on demand, the required outdoor air intake flow for all occupied spaces. All three units have at least F7 air filters as a form of air cleaning, taking into account the outdoor air category (Section 6.2.3) and the indoor air quality level (IDA 2, according to national regulations). The system has no air recirculation (100% outdoor air) and an energy recovery efficiency of 85%. Indoor spaces with an occupancy density of 3.7 square metres per person not to exceed 700 ppm above outdoor air levels (set out in CEN Standard 13779-2007, Annex A), have CO₂ sensors set according to ASHRAE 62.1-2010, Appendix C and a CO₂ generation rate per person of 0.31 l/min for an activity level of 1.2 met (office). However, as Standard CEN 13779-2007, Annex A, is more restrictive than the previous code in terms of CO₂ concentration, the set point has been set at 500 ppm, triggering an alarm when the CO₂ concentration exceeds this point by more than 10%, thus complying with the requirements of the standard.

Most of the materials used comply with the requirements set out in the applicable regulatory code as follows:

- The emission of total volatile organic compounds (TVOC) is under 0.1 mg/m²h;
- Formaldehyde emissions are less than 0.02 mg/m²h;
- Ammonia emissions are under 0.01 mg/m²h;
- The emissions of carcinogenic compounds (IARC) are under 0.002 mg/m²h;
- Materials are non-odorous (dissatisfaction with odour is less than 10%).

Total air flow into the building (ground floor—7th floor) through mechanical ventilation according to project design calculations is 13,611 l/s.

$$Q_{tot} = n - q_p + A - q_B = 857 \text{ persons} - 71/\text{s-pers} + 6474.70 \text{ m}^2 - 0.35 \text{ l/s-m}^2 = 8265.15 \text{ l/s}$$

$$Q_{tot} (\text{design}) = 136,11.111 \text{ l/s}$$

An electrical control system is fully integrated into each air ventilation unit. The microprocessor-based equipment controls and regulates temperatures, airflows and other functions.

The factors in the building’s surroundings that contribute to the better external habitability of the building as a qualitative public space that contribute to greater social cohesion are also taken into account. Thus, 60% of the plot area is allocated to free spaces for public use (1895 m²), in which unique areas of sustainable and energy-efficient urban furniture are located for resting (*Burbuhuts system*) by means of water sprays, which provide citizens with healthy wellbeing while practising physical exercise and allow the city to become more humanized. The purpose is to use the energy of human propulsion in mini-bike pedelecs as a renewable source applied to producing cumulative energy. Through the physical and sporting activity of pedalling, energy is generated, which, by means of two alternators, is fed into batteries where it is accumulated for recreational use and later used for energy in the form of outdoor conditioning by water misting and lighting (Figure 9) [64].

More than 25% of the open spaces are occupied by vegetation (507 m²) and by innovative street furniture aimed at promoting physical activity (Figure 9).

Estepona’s Town Hall is a public building, the purpose of which is to welcome and integrate the entire population, which is why it incorporates facilities accessible to everyone. It is located in a part of the city with good connections to public transport, cycling facilities and parking (Figure 10). Two bus stops are located at a distance of fewer than five hundred metres from the plot, where seven different bus lines are available. The outdoor square in which the building is located has access ramps to the various levels, providing total accessibility to the entire plot.

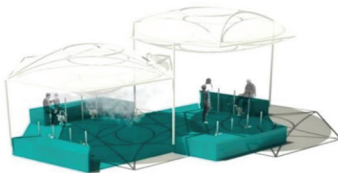
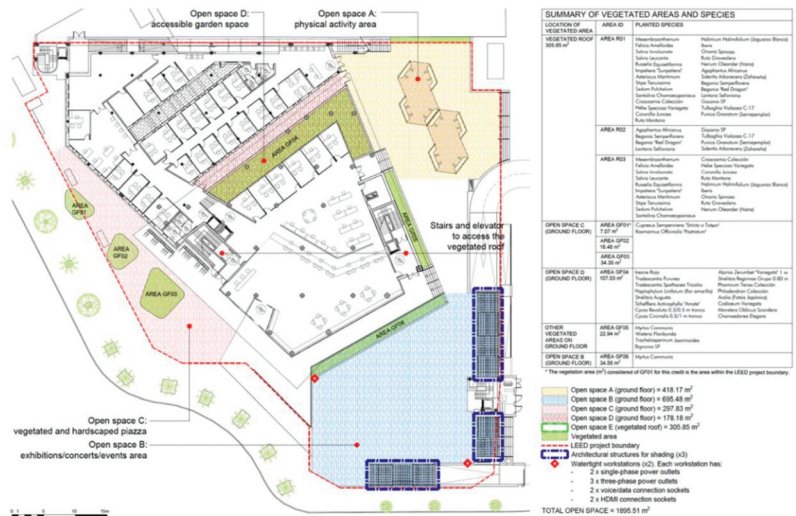


Figure 9. Cont.

achieve a transmission heat increase in summer, bringing significant benefits in terms of comfort, running costs and operational CO₂ emissions.



Figure 10. The project is located in such a way that all the functional entrances are within a 200-yard (180-m) walking distance or cycling distance from the bicycle network of the town. Besides, this bicycle network connects to at least 10 diverse uses. Source: Bicycle Network. Castaño & Associates. LEED Rating System Report [59].

Thus, the following measures are highlighted, depending on whether they are considered passive strategies or based on installation equipment:

- Reinforced concrete structure that improves the overall thermal mass levels of the building;
- Thermal insulation in the outer layer of the opaque façade (SATE system) that protects against sudden changes in temperature;
- A green roof improves the thermal performance of the building, acting as natural insulation;
- High-performance window frames with low-emissivity double glazing with a value of $U_g = 1.0 \text{ W/m}^2\text{K}$ and solar factor $g = 40\%$;
- External façade enveloping latticework that reduces solar incidence increase and generates a perimetral thermal cushion of protection by way of shading. At the same time, it prevents glare from impacting indoors without obstructing the view to the outdoor area;

- The use of energy-efficient LED lighting, combined with dynamic control via light sensors, reduces both space cooling requirements and the total installed light output;
- *Passivhaus* certified mechanical ventilation equipment with high efficiency (over 82% and F7 and F9) and heat recovery, ensuring consistent high-quality indoor air;
- The installation of energy-efficient lifts (energy efficiency class B according to VDI 4707) saves energy and reduces heat increase in lift shafts and stairwells;
- Energy is supplied to the building by an electricity trading company providing energy from renewable sources, with guaranteed labelling and transfers of guarantees of origin from the National Commission for Markets and Competition (CNMC).

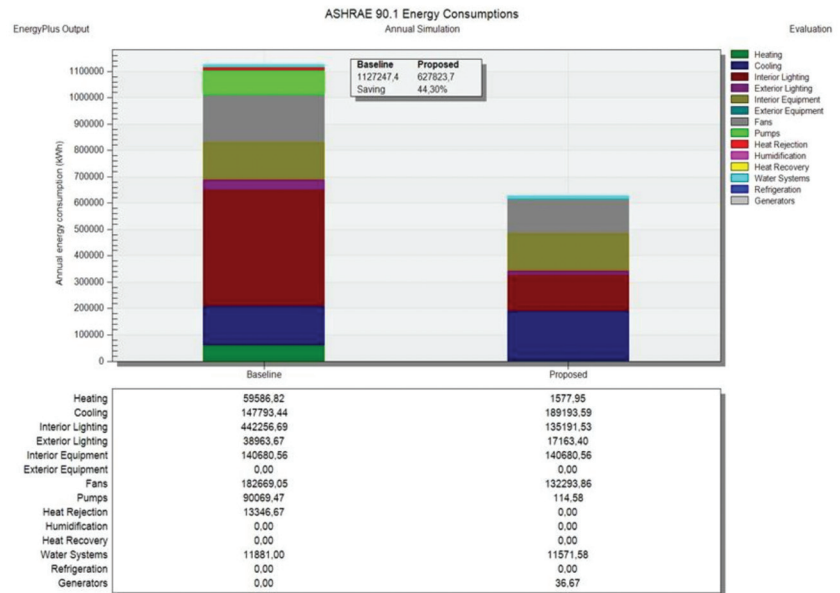


Figure 11. Annual simulation of energy consumption. Comparison chart according to ASHRAE standard 90.1. Program Version: EnergyPlus, Version 9.4.0. Report: Annual Building Utility Performance Summary. Timestamp: 2021-12-17 Input Verification and Results Summary. Component Sizing Summary. Climatic Data Summary. Envelope Summary. Lighting Summary. Equipment Summary. HVAC Sizing Summary. System Summary. Outdoor Air Summary. Energy Meters. Standard 62.1 Summary. LEED Summary. Economics Results Summary Report. Tariff Report. Source: Castaño & Asociados. Passivhaus engineering consultancy [66].

In relation to the demand for drinking water, the building's consumption is reduced to a minimum by installing the most water-efficient toilets and taps available. After simulating the water consumption of the building, considering the hours of operation of the building (Monday to Friday, 8 a.m. to 3 p.m.) and the occupancy of the building (300 employees and 280 visitors during peak hours), an annual consumption with a percentage reduction in indoor water use of 48.86% compared to the standard commercial range was obtained (Figure 12).

In relation to the demand for outdoor water consumption, from the beginning of the design phase of the project and considering the climate and the relatively low annual rainfall in the town of Estepona, it was agreed that native plant varieties with a wide variety of shapes, sizes, colours and flowering periods be selected, with very low water demand, for the 473.42 m² of landscaped space distributed between the outdoor space on the ground floor and the roof garden. The design of the urban public outdoor space surrounding the building environment considers the minimisation of the *heat island effect* by avoiding the absorption of the sun's heat by radiation into the atmosphere, based on light-coloured

paving with a high *solar reflectance index* (SRI = 65; SR = 0.56). This avoids an increase in regional average warming. The selection of suitable luminaires in a carefully considered location avoids the upward effect, glare and intrusion, thus reducing light source pollution, and also allows the ability to have a twilight sensor control system.

Summary for Design and Construction Rating Systems						
Note: All information on this tab is READ-ONLY. To edit, see the previous tab(s).						
Refresh Groups						
Group Name	Baseline Case (liters/year)			Design Case (liters/year)		
	Annual Flush Volume	Annual Flow Volume	Annual Consumption	Annual Flush Volume	Annual Flow Volume	Annual Consumption
Group 1	1,388,919.40	767,981.50	2,156,900.90	622,896.12	480,067.50	1,102,963.62
Annual baseline water consumption (liters/year)						2,156,900.90
Annual design water consumption (liters/year)						1,102,963.62
Percent water use reduction (%)						48.86%

Figure 12. Annual simulation of water consumption. Comparative table. Source: Castaño & Asociados. Passivhaus engineering consultancy [66].

Finally, the need for the disposal of the waste generated has been identified as recyclable into different types of waste, and to be stored in the correct selective manner according to the number of occupants and spaces (Figure 13).



Figure 13. Location of waste collection points according to type of use and workstations. Upper floor of the Plenary Hall (first floor). Office type floor (Third Floor). Source: Castaño & Associates. LEED Rating System Report [59].

It is estimated that the costs for obtaining an improvement in functionality in the integrated variables for quality of life, according to the parameters indicated in the proposed methodology, represent approximately an added amount of 20% of the initial expenditure in its planning phase, with a payback period in energy consumption savings of a maximum of 5 years within a planned development of high technical efficiency. However, in terms of health compensation, we can quantify them from the outset for the users due, among

other reasons, to the reduction of pollutant emissions into the environment as important mitigation measures against climate change.

4. Discussion

The direct results of the current research study conclude that, supported by the numerous scientific references and the abundant methodology applied to the reference-built work and study, they respond favourably in a coordinated way to the key dynamics explained, which interact on the condition of habitability and on the stated descriptors of urban quality of life. Urban regeneration linked to the improvement of the living environment is associated with the compliance of a set of sustainable and measurable strategic conditions, which define a positive effect on the quality of life. The study of urban regeneration associated with quality of life is a topic of international interest that is key to sustainable urban development, with a particular focus on the promotion of health.

Thus, it is possible to establish a direct association between these architectural factors, present in the design and subsequent construction phase, with their capacity to enhance the quality of urban life based on the promotion of the users' health in the context to which they belong. The evaluation of the proposed case study of the new town hall of Estepona (Malaga), which operates on the five reference factors (*Identity, Character, Image, Materiality* and *Implementation*), reflects a behaviour capable of enhancing the quality of life of the city as a whole.

The methodology defined by the analysis of the five triggers of architectural design starts from an approach of habitability recognisable in every work of built value. At the same time, the impact that urban development produces on the natural physical environment must necessarily consider the conditions that the climate establishes in the form and constructive reason of the architectural object. It is then a question of identifying a two-way path, which, acquiring its concrete meaning in local action for the quality of life towards environments conducive to the integral health of citizens, is firmly framed in a scenario of global thinking, assimilable to any joint action project committed to the three recognised areas of sustainability (social, environmental and economic) enunciated as early as 1987 by the Brundtland Report (Report of the World Commission on Environment and Development: Our Common Future. General Assembly United Nations) [4].

The application of the conclusions resulting from the project and the implementation of its operational management model may result in energising the natural capacity of areas currently undergoing urban transformation while contributing to correcting the current environmental deficit of urban developments towards an improvement in quality of life.

The proposed basic architectural parameters for healthy habitability incorporated into the design process, which provide key issues and positive indicators in terms of functionality, sustainability and energy efficiency, through the representative case study, imply an effective control over the architectural factor as a social determinant of health, and consequently, a decrease in health inequalities and an increase in quality of life (Figure 14).

The COVID-19 pandemic, caused by the SARS-CoV-2 virus, has made it possible to implement health promotion strategies with the adoption of modifications in spatial relations of coexistence aimed at knowing how to activate the public space in a private way, with direct repercussions on the urban environment in the transformation towards the conservation and improvement of the quality of urban life. The great new challenge is to generate aseptic spaces of functional autonomy, harmless to excessive socialisation and environmental balance, based on a re-encounter with nature once the need for long journeys has been reduced, in the face of the complementary irruption of the digital city.

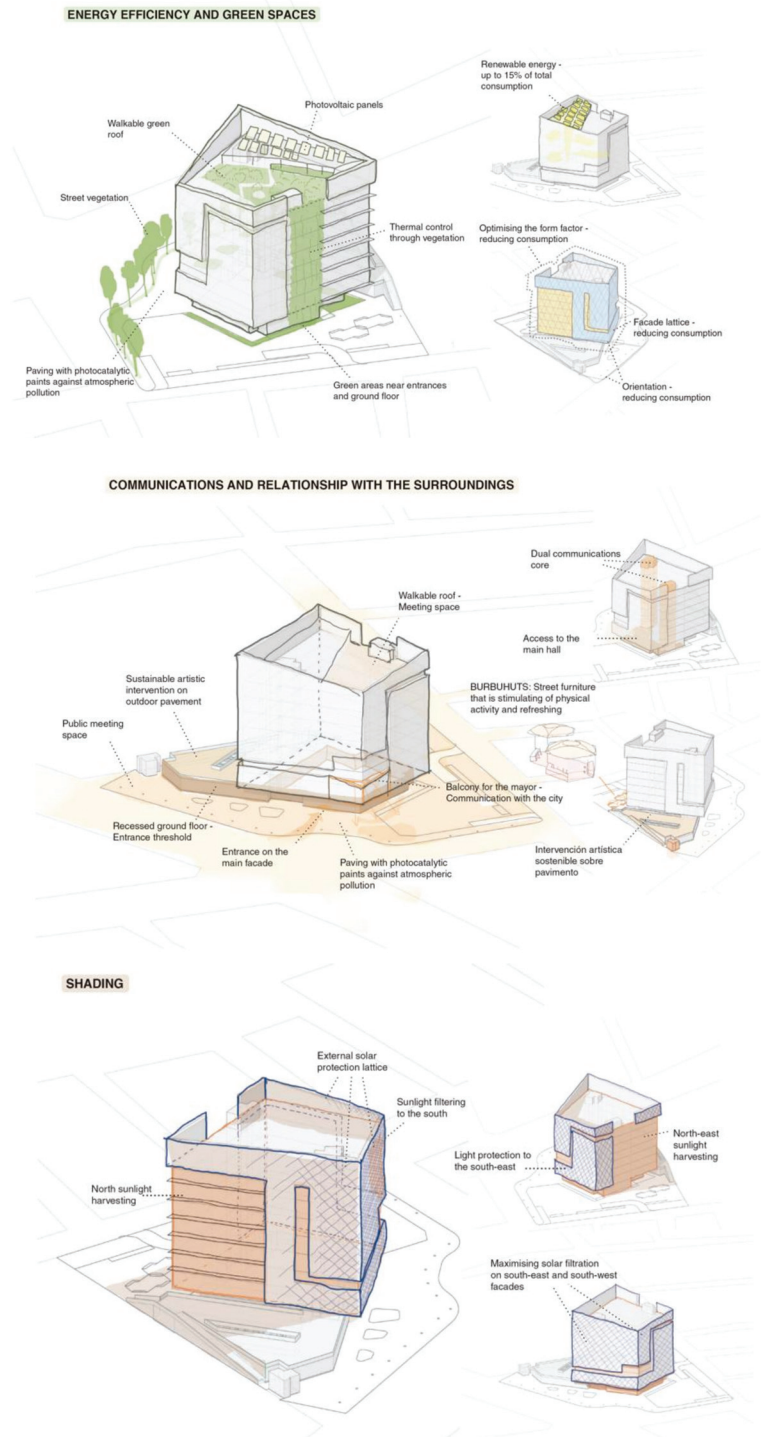


Figure 14. Cont.

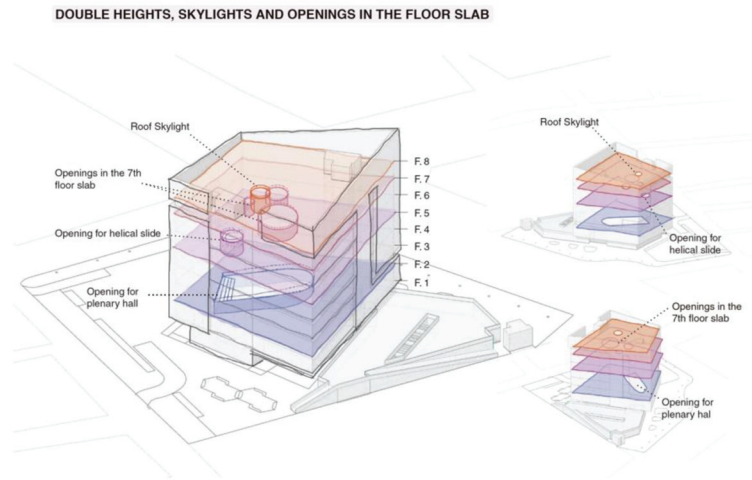


Figure 14. Volumetric diagrams of measures taken and actions relating to the following indicators: energy efficiency and green spaces; communications and relationship with the surroundings; shading; double heights, skylights and openings in the floor slab. Source: Created by the author.

The fact that the case under analysis is a public building also turns it into a coherent management model that can be extrapolated to the requirements of sustainable environmental progress in the general interest of a socially just city.

The degree of utilisation of available resources for the implementation of processes to improve the quality of life not only allows us to identify potential saving points, favouring the so-called energy transition, but also means investing in the progress of opportunities for equitable socioeconomic conditions of the population, where the relationship between the quality of life and the cost that supports it compensates for the effort required for its continuous improvement.

Funding: This research was funded by Universidad San Pablo-CEU, CEU Universities, Bridge Project in Consolidation Call 2021-22, Group AURS _EPS, grant number Oracle MCP21V08.

Institutional Review Board Statement: Not applicable.

Informed Consent Statement: Not applicable.

Data Availability Statement: Not applicable.

Acknowledgments: This article acknowledges and thanks, during all the construction phases of the new Estepona (Málaga, Spain) town hall building, (the project, calculation, material execution and supervision), the contribution and collaboration of all the technicians involved (Escarcena L.; González-Mera, J.; Martín J.; Murcia L.; Villena S.; Yebra M.), the construction team of the construction company ACP Infraestructuras (De la Peña G.; Fontan J.M.; Gallego A.), the assistance provided by the consultancy Castaño & Asociados, and as owner of the property, the City Council of Estepona (Malaga, Spain). Finally, in particular, José María García Urbano, Mayor of Estepona, for being the main promoter of the idea.

Conflicts of Interest: The funders had no role in the design of the study; in the collection, analyses, or interpretation of data; in the writing of the manuscript; or in the decision to publish the results.

References

1. Banham, R. Los Angeles. In *The Architecture of Four Ecologies*; Harper & Row: New York, NY, USA, 1971.
2. Kleinschroth, F.; Kowarik, I. COVID19 crisis demonstrates the urgent need for urban greenspaces. *Front. Ecol. Environ.* **2020**, *18*, 318–319. [[CrossRef](#)] [[PubMed](#)]

3. Slater, S.J.; Christiana, R.W.; Gustat, J. Recommendations for keeping parks and green space accessible for mental and physical health during COVID-19 and other pandemics. *Prev. Chronic Dis.* **2020**, *17*, E59. [CrossRef]
4. Report of the World Commission on Environment and Development: Our Common Future. Document A/42/427 General Assembly United Nations (UN), New York, USA, 1987. Available online: https://www.are.admin.ch/dam/are/en/dokumente/nachhaltige_entwicklung/dokumente/bericht/our_common_futurebrundtlandreport1987.pdf.download.pdf/our_common_futurebrundtlandreport1987.pdf (accessed on 20 September 2022).
5. Pelczynski, J.; Tomkowicz, B. Densification of cities as a method of sustainable development. In Proceedings of the IOP Conference Series: Earth and Environmental Science, Prague, Czech Republic, 9–13 September 2019; Volume 362, p. 012106. [CrossRef]
6. Taylor, A.F.; Kuo, F.E. Is contact with nature important for healthy child development? State of the evidence. In *Children and Their Environments: Learning, Using and Designing Spaces*; Spencer, C., Blades, M., Eds.; Cambridge University Press: Cambridge, UK, 2006; pp. 124–140.
7. Corraliza, J.A.; Collado, S. La naturaleza cercana como moderadora del estrés infantil. *Psicothema* **2011**, *23*, 221–226. [PubMed]
8. Barton, H.; Thompson, S.; Burgess, S.; Grant, M. *The Routledge Handbook of Planning for Health and Well-Being Shaping a Sustainable and Healthy Future*; Routledge: London, UK, 2017.
9. Meadows, D.H.; Meadows, D.L.; Randers, J.; Behrens, W.W. *The Limits to Growth. A Report for the Club of Rome 's Project on the Predicament of Mankind*; Universe Books: New York, NY, USA, 1972; Available online: <https://www.donellameadows.org/wp-content/userfiles/Limits-to-Growth-digital-scan-version.pdf> (accessed on 20 September 2022).
10. Higuera-García, E.; Ezquiaga-Dominguez, J.M. Barrios saludables, desde la renovación y el diseño de su espacio público: Ciudad y Territorio. *Estud. Territ.* **2022**, *LIV*, 113–130. [CrossRef]
11. Campbell, A. *The Sense of Well-Being in America*; McGraw-Hill: New York, NY, USA, 1981.
12. Nasution, A.D.; Salleh, A.G.; Wahid, J. Quality of Life: Public open space effects. *Asian J. Environ. Behav. Stud.* **2018**, *3*, 124–132. [CrossRef]
13. The Whoqol Group. The World Health Organization Quality of Life Assessment (WHOQOL): Development and general psychometric properties. *Soc. Sci. Med.* **1998**, *46*, 1569–1585. [CrossRef]
14. Human Development Index (HDI). Established by the United Nations. Development Programme (UNDP-1990). Available online: <https://hdr.undp.org/data-center/human-development-index#/indicies/HDI> (accessed on 2 June 2022).
15. Ghislandi, S.; Sanderson, W.C.; Scherbov, S. A simple measure of human development: The Human Life Indicator. *Popul. Dev. Rev.* **2018**, *45*, 219–233. [CrossRef]
16. Davos Declaration 2018. High-Quality Baukultur for Europe. Available online: <https://davosdeclaration2018.ch/en/dd/nav/index/davos-declaration> (accessed on 2 June 2022).
17. Mercer Human Resource Consulting 2019. Available online: <https://www.xpatweb.com/uncategorized/mercers-quality-of-living-city-ranking/> (accessed on 2 June 2022).
18. Veenhoven, R. *The Four Qualities of Life Ordering Concepts and Measures of the Good Life*; Happiness Studies Book Series; Springer: Dordrecht, The Netherlands, 2013; pp. 195–226.
19. United Nations Human Settlements Programme; WHO Centre for Health Development. Hidden Cities: Unmasking and Overcoming Health Inequities in Urban Settings: Executive Summary. Kobe, Japan, 2010. Available online: <https://apps.who.int/iris/handle/10665/44468> (accessed on 20 September 2022).
20. INEQ-CITIES. Socio-Economic Inequalities in Mortality: Evidence and Policies in European Cities. Executive Agency for Health and Consumers, European Union Commission. 2008. Available online: <https://www.ucl.ac.uk/ineqcities/> (accessed on 20 September 2022).
21. Northridge, M.E. Sorting out the Connections between the Built Environment and Health: A Conceptual Framework for Navigating Pathways and Planning Healthy Cities. *J. Urban Health Bull. N. Y. Acad. Med.* **2003**, *80*, 556–568. [CrossRef]
22. Evans, G. The Built Environment and Mental Health. *J. Urban Health Bull. N. Y. Acad. Med.* **2003**, *80*, 536–555. [CrossRef] [PubMed]
23. Haines, A.; Bruce, N.; Cairncross, S.; Davies, M.; Greenland, K.; Hiscox, A.; Lindsay, S.; Lindsay, T.; Satterthwaite, D.; Wilkinson, P. Promoting Health and Advancing Development through Improved Housing in Low-Income Settings. *J. Urban Health* **2012**, *90*, 810–831. [CrossRef] [PubMed]
24. Borrell, C.; Pons-Vigués, M.; Morrison, J.; Díez, È. Factors and Processes Influencing Health Inequalities in Urban Areas. *J. Epidemiol. Community Health* **2013**, *67*, 389–391. [CrossRef] [PubMed]
25. Carnemolla, P.; Bridge, C. Accessible housing and health-related quality of life: Measurements of wellbeing outcomes following home modifications. *Int. J. Archit. Res. ArchNet-IJAR* **2016**, *10*, 38. [CrossRef]
26. Chen, S.; Ni, Y.; Zhang, L.; Kong, L.; Lu, L.; Yang, Z.; Yang, L.; Zhang, X.; Zhu, Y. Noise Exposure in Occupational Setting Associated with Elevated Blood Pressure in China. *BMC Public Health* **2017**, *17*, 107. [CrossRef] [PubMed]
27. Commission on Social Determinants of Health. Closing the Gap in a Generation: Health Equity through Action on the Social Determinants of Health: Final Report: Executive Summary. World Health Organization. 2008. Available online: <https://apps.who.int/iris/handle/10665/69832> (accessed on 20 September 2022).
28. World Health Organization. Regional Office for Europe. Health 2020: A European Policy Framework Supporting Action across Government and Society for Health and Well-Being (Short Version) . World Health Organization. Regional Office for Europe. 2013. Available online: <https://apps.who.int/iris/handle/10665/131300> (accessed on 20 September 2022).

29. AENOR Internacional SAU Global EPD. Environmental Product Declaration. ECO Platform. In Accordance with UNE-EN ISO 14025; UNE-EN 15804 Standards. Available online: <https://www.en.aenor.com/certificacion/certificacion-de-producto/declaraciones-ambientales-de-producto/declaraciones-globalepd-en-vigor> (accessed on 20 September 2022).
30. Yeang, K. *Designing with Nature: The Ecological Basis for Architectural Design*; McGraw-Hill Inc.: New York, NY, USA, 1995.
31. Pérez Maldonado, A. *La Construcción de Indicadores Bio-Ecológicos Para Medir la Calidad del Ambiente Natural urbano*; Facultad de Arquitectura y Arte, Universidad de los Andes: Mérida, Venezuela, 1999.
32. O'Hara, S. *The Five Pillars of Economic Development*; University of the District of Columbia: Washington, DC, USA, 2018; Available online: <https://docs.udc.edu/causes/Five-Pillars-DC-Final-05-2018.pdf> (accessed on 20 September 2022).
33. Csikszentmihalyi, M.; Rochberg-Halton, E. *The Meaning of Things: A Study of Domestic Symbols and the Self*; Cambridge University Press: Cambridge, MA, USA, 1981.
34. Landázuri Ortiz, A.M.; Mercado Doménech, S.J. Algunos factores físicos y psicológicos relacionados con la habitabilidad interna de la vivienda. *Medio Ambiente Comport. Hum.* **2004**, *5*, 89–113.
35. Merleau-Ponty, M. *Fenomenología de la Percepción*; Planeta Agostini: Barcelona, Spain, 1985.
36. Olgyay, V. *Architecture and Climate. Bioclimatic Design Manual for Architects and Urban Planners*; Gustavo Gili: Barcelona, Spain, 1998.
37. Givoni, B.A. *Man, Climate and Architecture*; Elsevier Architectural Science Series; University of Sydney: Sydney, Australia, 1969.
38. Koenigsberger, O.H.; Mahoney, C.T.; Evans, M. *Climate and House Design*; United Nations: New York, NY, USA, 1971.
39. Gärling, T.; Biel, A.; Gustafsson, M. Different kinds and roles of environmental uncertainty. *J. Environ. Psychol.* **1998**, *18*, 75–83. [[CrossRef](#)]
40. Strategic Plan for Health and Environment (PESMA). National Health System and the Sectorial Conference on the Environment. Ministry of Health, Ministry for Ecological Transition and Demographic Challenge Spanish Government. 2021. Available online: [https://www.miteco.gob.es/es/prensa/ultimas-noticias/el-gobierno-presenta-el-plan-estrat%C3%A9gico-salud-y-medio-ambiente-\(pesma\)-destinado-a-proteger-a-la-poblaci%C3%B3n-de-los-riesgos-medioambientales/tcm:30-533340](https://www.miteco.gob.es/es/prensa/ultimas-noticias/el-gobierno-presenta-el-plan-estrat%C3%A9gico-salud-y-medio-ambiente-(pesma)-destinado-a-proteger-a-la-poblaci%C3%B3n-de-los-riesgos-medioambientales/tcm:30-533340) (accessed on 2 June 2022).
41. Kent, J.; Thompson, S. Health and the built environment: Exploring foundations for a new interdisciplinary profession. *J. Environ. Public Health* **2012**, *2012*, 958175. [[CrossRef](#)] [[PubMed](#)]
42. Frumkin, H. COVID-19, the Built Environment, and Health. *Environ. Health Perspect.* **2021**, *129*, 075001. [[CrossRef](#)] [[PubMed](#)]
43. Gibson, J.J. *The Ecological Approach to Visual Perception*; Houghton Mifflin: Boston, MA, USA, 1979; p. 332.
44. Heft, H. *Ecological Psychology in Context: James Gibson, Roger Barker, and the Legacy of William James's Radical Empiricism*; Psychology Press: New York, NY, USA, 2001; p. 476. [[CrossRef](#)]
45. Moraci, F.; Errigo, M.F.; Fazia, C.; Campisi, T.; Castelli, F. Cities under Pressure: Strategies and Tools to Face Climate Change and Pandemic. *Sustainability* **2020**, *12*, 7743. [[CrossRef](#)]
46. World Cities Report 2020. The Value of Sustainable Urbanization. United Nations Settlements Programme UN-Habitat. Available online: <https://unhabitat.org/World%20Cities%20Report%202020> (accessed on 20 September 2022).
47. Lefebvre, H. *Le Droit a la Ville*; Editions Anthropos: Paris, France, 1968; p. 166.
48. Abraham, A.; Sommerhalder, K.; Abel, T. Landscape and well-being: A scoping study on the health-promoting impact of outdoor environments. *Int. J. Public Health* **2009**, *55*, 59–69. [[CrossRef](#)] [[PubMed](#)]
49. Bowler, D.E.; Buyung-Ali, L.M.; Knight, T.M.; Pullin, A.S. A systematic review of evidence for the added benefits to health of exposure to natural environments. *BMC Public Health* **2010**, *10*, 456. [[CrossRef](#)]
50. Lestan, K.; Eržen, I.; Golobič, M. The Role of Open Space in Urban Neighbourhoods for Health-Related Lifestyle. *Int. J. Environ. Res. Public Health* **2014**, *11*, 6547–6570. [[CrossRef](#)] [[PubMed](#)]
51. Oppio, A.; Forestiero, L.; Sciacchitano, L.; Dell'Ovo, M. How to assess urban quality: A spatial multicriteria decision analysis approach. *Valori Valutazioni* **2021**, *28*, 21–30. [[CrossRef](#)]
52. Tulumello, S. From “spaces of fear” to “fearscapes”: Mapping for reframing theories about the spatialization of fear in urban space. *Space Cult. J.* **2015**, *18*, 257–272. [[CrossRef](#)]
53. Hancock, T. Health, Human Development and the Community Ecosystem: Three Ecological Models. *Health Promot. Int.* **1993**, *8*, 41–47. [[CrossRef](#)]
54. Mohit, M.A. Quality of Life in Natural and Built Environment—An Introductory Analysis. *Procedia Soc. Behav. Sci.* **2013**, *101*, 33–43. [[CrossRef](#)]
55. Capolongo, S.; Rebecchi, A.; Buffoli, M.; Appollono, L.; Signorelli, C.; Fara, G.M.; D'Alessandro, D. COVID-19 and Cities: From Urban Health strategies to the pandemic challenge. A Decalogue of Public Health opportunities. *Acta Biomed.* **2020**, *91*, 13–22. Available online: <https://www.mattioli1885journals.com/index.php/actabiomedica/article/view/961523750/abm.v91i2.9615> (accessed on 20 September 2022). [[PubMed](#)]
56. Milner, J. Emerging from COVID-19: Lessons for action on climate change and health in cities. *J. Urban Health* **2021**, *98*, 433–437. [[CrossRef](#)] [[PubMed](#)]
57. Rojas-Rueda, D.; Morales-Zamora, E. Built Environment, Transport, and COVID-19: A Review. *Curr. Environ. Health Rep.* **2021**, *8*, 138–145. [[CrossRef](#)]
58. Ros-García, J.M. *Estepona Activa*; Conarquitectura Ediciones: Madrid, Spain, 2021.
59. Castaño & Associates. *LEED Rating System Report*; Castaño & Associates: Sevilla, Spain, 2021.

60. VERDE Edificios 2020. Guía de Evaluación GBCE Green Building Council España Madrid. Available online: https://gbce.es/archivos/ckfinderfiles/VERDE/VERDE_Edificios_2020_-_Guia_de_evaluacion.pdf (accessed on 20 September 2022).
61. BUILD UPON Project, EU's Horizon 2020, Sponsor Agreement no. 840926-BUILD UPON2-H2020-LC-SC3-EE-16-2018). Available online: <https://www.worldgbc.org/build-upon2-project> (accessed on 20 September 2022).
62. World Green Building Council 2021. Available online: <https://www.worldgbc.org/our-renovation-strategy-framework> (accessed on 20 September 2022).
63. Ros-García, J.M.; Lora-Tamayo, M. Integration of Data in a Territorial Information System for the Sustainable Use of the Lighting Heritage in Favour of the Quality of Urban Life and Economic Development. Strategic Projects Oriented towards the Ecological Transition and the Digital Transition. Ministry of Science and Innovation, Spanish Government. Knowledge Generation Projects 2021. File number TED2021-130556B-I00. Available online: https://www.aei.gob.es/sites/default/files/convocatory_info/2022-06/TED2021_PROPUESTA_RELACION_NO_ALCANZAN_UMBRAL_fda.pdf (accessed on 20 September 2022).
64. Ros-García, J.M.; Iglesias Sanz, C.M.; González-Lezcano, R. Modular Structure of Biosaludable Urban Conditioning by Pedaling Mini-Bike. Fundación Universitaria San Pablo-CEU Universities ES1177985U-2017. Available online: <https://worldwide.espacenet.com/patent/search/family/058163374/publication/ES1177985U?q=pn%3DES1177985U> (accessed on 20 September 2022).
65. Brusilovsky, B. *Accesibilidad Cognitiva: Modelo para Diseñar Espacios Accesibles*; Colección Democratizando la Accesibilidad Vol. 6. Ed. Asociación Accesibilidad para Todos; La Ciudad Accesible: Granada, Spain, 2015; p. 322.
66. Castaño & Asociados. Estepona new Town Hall. Sustainability Report. Passivhaus engineering consultancy, LEED Summary, Sevilla, Spain, March 2022. Available online: <https://castanoyasociados.com/> (accessed on 20 September 2022).

Article

A Shift Schedule to Optimize Pure Electric Vehicles Based on RL Using Q-Learning and Opt LHD

Xin Yu, Ling Zhao *, Kun Zhang and Hongqiang Guo

School of Mechanical and Automobile Engineering, Liaocheng University, Liaocheng 252059, China

* Correspondence: zhaoling@lcu.edu.cn

Abstract: Range anxiety is a problem that restricts the development of pure electric vehicles. For this reason, much research starts from a shift schedule and strives to improve mileage. However, the proposed shift schedules have poor adaptive ability and are not suitable for dynamic conditions. In this paper, a shift schedule based on reinforcement learning (RL) is proposed, which uses Q-learning for optimization. However, the massive state variables and huge Q table in the state space put forward higher requirements on the computing power and storage space of the controller. Traditionally, the application of RL algorithms needs to rely on expensive GPU devices. To reduce high costs, we use an innovative treatment method, the optimal Latin hypercube design (Opt LHD), which is used for sampling, and state reduction is performed on the state space. Based on the above, the mileage is effectively improved by applying the shift schedule based on RL.

Keywords: pure electric vehicle; shift schedule; reinforcement learning; Q-learning; optimal Latin hypercube design

1. Introduction

The shift schedule affects the performance of the pure electric vehicle, such as power consumption economy and driving comfort. Research on shift schedule is conducive to further tapping the energy-saving potential of the pure electric vehicle, reducing the energy consumption and increasing the cruising range. Therefore, the study of the shift schedule plays an important role in pure electric vehicles.

J. Ruan et al. designed two customized shift schedules for DCT and CVT to improve economic performance [1]. Han K et al. proposed a collaborative optimization method for transmission design and shift schedule, which can effectively reduce energy consumption and improve the regenerative braking energy recovery efficiency [2]. Nguyen CT et al. developed an optimal shift schedule for acceleration and braking conditions based on a four-gear transmission with two motors. This shift schedule considers the motor efficiency and torque distribution, and also considers the influence of transmission ratio between different gears. Aiming at the hysteresis zone of the upshift and downshift curves, they developed a coordinated control strategy, which can achieve simultaneous upshift and downshift, effectively eliminating the shift interval and improving the shift quality [3]. To improve energy consumption, Kolmanovsky I et al. proposed a method for hierarchical optimization of the vehicle speed and shift schedule by using short-range traffic information flow. In this method, the integrated control problem is decomposed into pure continuous and discrete sub-problems, which overcomes the problem of calculating the integrated variable speed optimal control due to the different signal types of the vehicle speed signal and the gear signal [4]. Sujan VA et al. invented an adjustable shift schedule. The specific principle is to determine the loss power to overcome vehicle resistance according to the vehicle operation data. Based on the determined loss power, the vehicle operation parameters are optimized to compensate the loss of power. The shift schedule is dynamically adjusted to achieve the optimal shift and improve the adaptability to the dynamic unknown working conditions [5].

Citation: Yu, X.; Zhao, L.; Zhang, K.; Guo, H. A Shift Schedule to Optimize Pure Electric Vehicles Based on RL Using Q-Learning and Opt LHD. *Processes* **2022**, *10*, 2132. <https://doi.org/10.3390/pr10102132>

Academic Editors: Roberto Alonso González Lezcano, Francesco Nocera and Rosa Giuseppina Caponetto

Received: 20 May 2022

Accepted: 18 October 2022

Published: 19 October 2022



Copyright: © 2022 by the authors. Licensee MDPI, Basel, Switzerland. This article is an open access article distributed under the terms and conditions of the Creative Commons Attribution (CC BY) license (<https://creativecommons.org/licenses/by/4.0/>).

Jiang et al. used the volume Kalman filter estimation algorithm to accurately identify vehicle mass and road slope of the pure electric bus and use them as shift parameters. They proposed a four-parameter economical (EC) shift schedule considering vehicle speed, throttle opening, vehicle mass and road slope. The shift schedule not only considers the state of the vehicle itself, but also considers the influence of the vehicle mass change and the road slope on the driving gear, which further reduces the energy consumption of the vehicle, effectively avoids the frequent shift, and improves the riding comfort [6]. To integrate the power performance and economy of the vehicle, Huang et al. used the NSGA-II algorithm to conduct multi-objective optimization of transmission ratio of each gear, and solved the pareto optimal solution of the combination of transmission ratio. They designed a shift schedule based on dynamic programming (DP) with the goal of minimizing power consumption [7]. Sun et al. formulated a dynamic shift schedule according to the load characteristic diagram of the motor, which can significantly improve the working efficiency of the motor [8]. Lin et al. proposed a hybrid shift schedule for mechanical automatic transmission of pure electric city buses. By collecting and analyzing relevant data through bench test and real vehicle road test, the difference of driving conditions, shift characteristic points, and actual simplified transmission efficiency of urban routes are extracted. From the off-line global optimization results solved by DP algorithm, the comprehensive shift curve is extracted, and the typical features are fused together in a compatible way, so that it has better energy consumption performance under different working conditions in the city, and the universality of shift schedule is improved [9]. Qin et al. designed a shift schedule based on model predictive control. The changing trend of future working conditions is considered in the shift schedule, and the future vehicle speed change is predicted by neural network, and the trained neural network is used as the prediction model. Based on the optimal shift schedule designed by DP algorithm, and taking the shift schedule as the rolling optimization part of the model predicted shift schedule, the model predicted shift schedule was established. It not only saves energy consumption, but also reduces the shift frequency [10]. Li et al. proposed an algorithm to identify vehicle mass and road slope using the recursive least squares method, and based on this, designed a five-parameter shift schedule considering vehicle speed, acceleration, accelerator pedal (AP) opening, vehicle mass, and road slope. In addition to considering vehicle state and external environmental factors, the shift schedule also introduces the acceleration, which can reflect the dynamic performance of the vehicle, fully considers the driving intention of the driver, effectively improves the energy consumption performance, and realizes intelligent shift [11].

The research on the shift schedule of the pure electric vehicle mainly focuses on optimization, and a few shift schedules increase the shift parameters to improve the identification of the vehicle to the working condition, so that the ECU can make the optimal shift decision. The studies mentioned above improved vehicle performance. However, their essence does not get rid of the limitation of schedule-based shifts. Under the dynamic conditions, its energy consumption performance depends on the model prediction accuracy and identification accuracy. If the model is inaccurate or not accurate enough, the effect of shifting gears according to the shift schedule will be greatly reduced, which will inevitably lead to an increase in energy consumption.

Thus, this paper proposes a shift schedule based on RL to solve the problem of poor energy consumption under dynamic conditions. The principle of RL is that in an unknown environment, an agent can continuously improve its own behavior through continuous interaction with the external environment. The optimal control of the system can be realized by this operation, which is not limited by model accuracy and identification accuracy [12]. Although the RL using Q-learning can achieve the optimal learning effect, the massive state variables in the state space and the huge Q table put forward higher requirements on the computing power and storage space of the controller. Applications need to rely on expensive GPU devices, so the cost is high and the requirements are not met. Thus, the Opt LHD is used for sampling and state reduction is performed on the state space. Using Opt LHD sampling can reduce the number of tests, relieve the computational burden of

the computer, and effectively reduce the computing power requirement on the premise of ensuring the uniformity and stability of the sampling.

The main research contents of this paper are as follows: The construction of the longitudinal dynamics model of the pure electric vehicle, the design of the EC shift schedule based on the vehicle speed and the AP opening, the design of the intelligent shift schedule based on RL, and the hardware of the pure electric vehicle in-loop simulation test. The remaining part of the paper is organized as follows. In Section 2, the vehicle dynamics model is built. Section 3 illustrates the design of the shift schedule based on RL. In Section 4, the in-loop simulation experiments are introduced. Finally, the conclusions are drawn in Section 5.

2. Modeling of the Pure Electric Vehicle

Modeling plays an important role in reducing R&D costs and improving development efficiency to build the pure electric vehicle model. The more accurate the model, the higher the reliability of the simulation experiment. The model of the pure electric vehicle includes the battery model, motor model, power train model, vehicle dynamics model, and driver model.

2.1. Driver Model

The driver model is mainly used to simulate the driver's AP and brake pedal. The operating conditions are used as a reference, and the vehicle speed of the model simulation is used as a feedback. The AP opening and the brake pedal (BP) opening are the output in real time, and the driver model is based on PID control theory.

2.2. Motor Model

This paper adopts experimental data modeling [13]. The data modeling is based on the efficiency MAP of the motor and the external characteristic curves of the motor under different loads. In addition, the method of interpolation look-up table is used to determine the output of the motor under different working conditions. Figure 1 shows a MAP diagram of the motor efficiency. Figure 2 shows a graph of the motor speed and torque external characteristic curve.

In the modeling process, the input torque of the motor is related to the pedal opening. In general, the output torque of the motor has a linear relationship with the pedal opening, which is

$$T_{in} = f_1(\alpha, n_m) \quad (1)$$

where T_{in} denotes the output torque of the motor, and the unit is Nm; α is the AP opening, and the range is 0–1; n_m is the meaning of the motor speed, and the unit is rpm; f_1 presents the torque interpolation function of the motor.

The input power of the motor can be expressed as

$$P_{in} = \frac{T_{in}n_m}{9550} \quad (2)$$

where P_{in} is the input power of the motor, and the unit is kW.

In addition, because the motor has a certain power loss, its input power and output power are different. Moreover, the efficiency of the motor is different, and the degree of power loss is also different. The efficiency of the motor can be expressed as a function of the motor speed and motor torque, which is

$$\eta_m = f_2(T_{in}, n_m) \quad (3)$$

where η_m denotes the efficiency of the motor; f_2 represents the efficiency interpolation function of the motor.

The output power of the motor is

$$P_{out} = P_{in}\eta_m \tag{4}$$

where P_{out} is the output power of the motor, and the unit is kW.

When the vehicle is braking, the braking energy recovery of the motor also needs to be considered. Driving the motor can be regarded as doing negative work, which can be regarded as a process of charging the battery, and the tentative charging efficiency is 0.3.

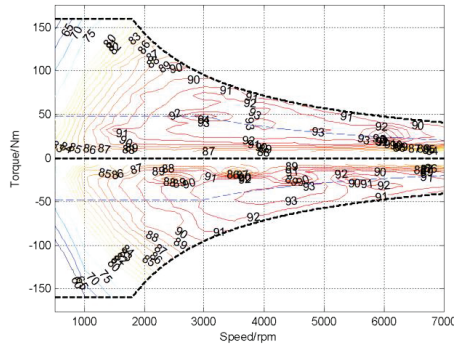


Figure 1. Motor efficiency.

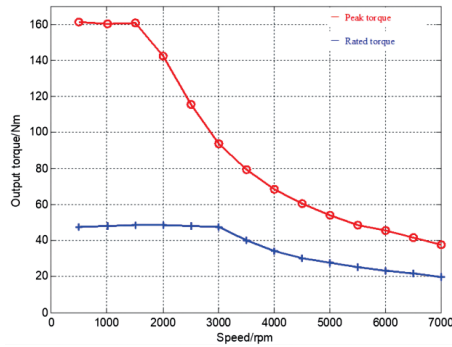


Figure 2. External characteristic curve.

2.3. Battery Model

This paper involves the study of the shift schedule of the pure electric vehicle, and the battery model considers parameters such as battery current, voltage, and SOC state estimation. Therefore, it is decided to use a relatively simple electrical model that is convenient for simulation analysis as a theoretical reference for modeling. Its equivalent circuit is shown in Figure 3.

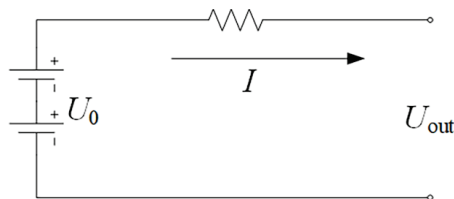


Figure 3. Equivalent circuit of the battery.

According to Figure 3, the output voltage of the battery can be expressed as

$$U_{out} = U_0 - IR \quad (5)$$

where U_{out} denotes the output voltage of the battery, and the unit is V; U_0 is the voltage of the battery, and the unit is V; I is the meaning of the output current of the battery pack; R represents the internal resistance of the battery, and the unit is Ω .

The output power of the battery is the input power of the motor. Combined with the output voltage of the battery, the output current of the battery can be calculated as

$$\begin{cases} P_{out} = P_{in} \\ I = \frac{U_0 - \sqrt{U_0^2 - 4RP_{in}}}{2R} \end{cases} \quad (6)$$

Assuming that the initial SOC value of the battery is 0.8, the SOC estimation of the battery adopts the ampere-hour integral method [14], which can be expressed as

$$SOC_{t+1} = SOC_t - \frac{I}{3600Q_0} \quad (7)$$

where SOC_{t+1} is the meaning of the battery SOC in the next second, and the unit is %; SOC_t represents the battery SOC at the current moment, and the unit is %; t is the time, and the unit is s; Q_0 denotes the battery capacity, and the unit is AH.

2.4. Power Train Model

The motor involved in this paper is mechanically connected to the AMT without a clutch. Therefore, it can be considered that there is no loss in the process of torque transmission, and the output torque of the motor is the input torque of the power train. Therefore, the output torque of the power train can be expressed as

$$T_{trans} = T_{in}i_gi_0\eta \quad (8)$$

where T_{trans} is the output torque of the transmission, and the unit is Nm; i_g denotes the transmission ratio of each gear; i_0 is the meaning of the main reducer transmission ratio; η represents the transmission efficiency of the AMT system.

The output speed can be expressed as

$$n_{trans} = \frac{n_m}{i_gi_0} \quad (9)$$

The gear selection and the transmission ratio of each gear are given by the shift schedule in the function module.

2.5. Vehicle Dynamics Model

The tractive force of the vehicle is

$$F_t = F_f + F_w + F_j + F_i \quad (10)$$

where F_t denotes the traction required for driving; F_f is the rolling resistance; F_w is the meaning of the air resistance; F_j represents the acceleration resistance; F_i is the slope resistance.

The driving resistance, air resistance, acceleration resistance, and gradient resistance can be expressed as:

$$\begin{cases} F_f = m g f \\ F_w = \frac{C_D A v^2}{21.15} \\ F_j = \delta m \frac{dv}{dt} \\ F_i = m g \sin \theta \end{cases} \quad (11)$$

where m denotes the vehicle mass, and the unit is kg; g is the gravitational acceleration, and the unit is m/s^2 ; f is the meaning of the rolling resistance coefficient; C_D represents the air drag coefficient; A is the vehicle windward area, the unit is m^2 ; δ represents the automobile rotating mass conversion factor; θ is the slope angle.

The true vehicle speed can be derived from the combination of Equations (11) and (12).

$$v = \int \frac{F_q - F_f - F_w - F_i}{\delta m} dt \quad (12)$$

3. Design of Shift Schedules

3.1. Design of EC Shift Schedule

The EC shift schedule is designed with economy as the goal, and the working efficiency of the motor is maintained in the high-efficiency region by selecting the appropriate shift point, so as to improve the driving range [15]. The current EC shift schedule control parameters generally use a pedal opening and vehicle speed. The design principle is to compare the working efficiency of the motor in different gears under the same pedal opening, and the efficiency intersection point of adjacent gears is the shift point at the pedal opening. The efficiency point is obtained as follows.

The relationship between the motor speed and the vehicle speed is

$$u = \frac{0.377n_m r}{i_g i_0} \quad (13)$$

Simultaneous Equations (1), (3), and (13) can obtain the relationship between motor efficiency and AP opening, vehicle speed, and transmission ratio.

$$\eta_m = f_2(f_1(\alpha, \frac{u i_g i_0}{0.377r}), \frac{u i_g i_0}{0.377r}) \quad (14)$$

The efficiency surface of each gear is shown in Figure 4. The shift points of each gear are the points where the motor efficiency of the previous gear decreases and the motor efficiency of the next gear increases.

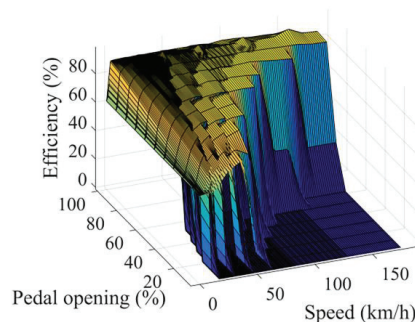


Figure 4. The efficiency surface of each gear.

By changing the pedal opening within 0 and 1, the shift points at different openings can be extracted. To prevent the frequent shift problem caused by the pedal opening or vehicle speed near the shift point, 5 km/h is used as the shift speed difference. The EC shift schedule curve can be obtained, as shown in Figure 5. The six curves in the figure represent the downshift curve from 2nd gear to 1st gear, the upshift curve from 1st gear to 2nd gear, the downshift curve from 3rd gear to 2nd gear, the upshift curve from 2nd gear to 3rd gear, the downshift curve from 4th gear to 3rd gear, and the upshift curve from 3rd gear to 4th gear.

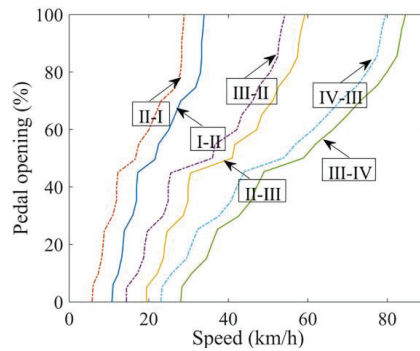


Figure 5. EC shift schedule curve.

As can be seen from Figure 4, although the EC shift schedule meets the requirements of the long battery life, the motor efficiency at the shift point is low (about 80%).

3.2. Design of the Shift Schedule Based on RL

3.2.1. Establishment of States and Actions of RL Algorithms

Energy consumption is directly related to the efficiency of the motor, and the efficiency of the motor is directly related to its speed and torque. According to Equation (13), the motor speed is directly related to the vehicle speed. Therefore, the vehicle speed needs to be designed as one of the state variables. To describe the vehicle state finely and consider the representation of the state variables in the later stage, the vehicle speed range from 0 to 100 km/h is uniformly discretized into 99 specific states, which is

$$v(t) = [0, 1.02, \dots, 100] \quad (15)$$

where $v(t)$ is the vehicle speed at time t .

Secondly, the motor speed is also related to the transmission ratio, so the current gear is also selected as a state variable. Since the research object is equipped with a 4-gear AMT, the first gear transmission ratio is extremely large, which is only used for large torque output, and is generally used for heavy loads and climbing. In normal driving conditions, the 2nd gear can be used to meet the needs. This paper does not consider the change of the slope and the mass of the vehicle, so it is decided to use three gears. The gear state can be described as

$$gear(t) = [2, 3, 4] \quad (16)$$

where $gear(t)$ is the gear at time t .

In addition, the energy consumption of the vehicle depends to a large extent on the proficiency of a person's driving skills. In the absence of unexpected emergencies, frequent rapid acceleration or rapid deceleration will lead to poor energy efficiency. Therefore, the acceleration also needs to be designed as a state variable. According to the offline measurement of a large number of urban working conditions, the acceleration interval is taken as -2 to 2 m/s, and it is also uniformly discretized into 99 state points, which is

$$acc(t) = [-2, -1.96, \dots, 0, \dots, 1.96, 2] \quad (17)$$

where $acc(t)$ is the acceleration at time t .

In summary, the state set can be expressed as

$$S = s(t) = [gear(t), v(t), acc(t)] \quad (18)$$

The state set S can be expressed as a three-dimensional state space, and the number of states in the state space reaches $99 \times 3 \times 99 = 29,403$.

To realize intelligent shift, the action of the RL is designed as the target gear, and it is designed as a discrete one-dimensional space; that is, the target gear is discrete in three points, which is

$$A = a(t) = [2, 3, 4] \quad (19)$$

where $a(t)$ represents the target gear at time t .

Each state variable in the state space corresponds to three different Q values. Therefore, the number of Q values in the Q table is $29,403 \times 3 = 88,209$. The state-action value function is stored by the Q table learned, and its state-action will be on the order of tens of thousands.

In addition, the Opt LHD sampling is adopted to reduce the state space.

3.2.2. RL State Space Reduction

When there is a lot of experimental data, Opt LHD sampling can reduce the number of experiments, relieve the computational burden of the computer, and effectively reduce the computing power requirement under the premise of ensuring the uniformity and stability of the sampling. To make the state variables of the shift schedule based on RL fill the entire state space as much as possible, this paper conducts sampling based on the idea of maximizing and minimizing distance. The specific steps are as follows: First, the scope of the state space is determined. Secondly, the minimum distance between each state variable and adjacent state variables is used as the characteristic distance, and the number of states in the state space after sampling is determined according to the requirements of the experimental design. Then, based on the number of states in the state space after sampling, the maximum distance between adjacent state variables is determined and sampled, so as to reduce the state space, and the maximum and minimum distance can be expressed as

$$\min_{1 \leq i, j \leq n, i \neq j} d(x_i, x_j) \quad (20)$$

$$d(x_i, x_j) = d_{ij} = \left[\sum_{k=1}^m |x_{ik} - x_{jk}|^t \right]^{1/t}$$

where $d(x_i, x_j)$ represents the distance between two sample points (x_i, x_j) .

The principle of determining the number of samples in this paper is to ensure the normal operation of the TCU, and the maximum number that can be programmed into the TCU shall prevail. The sampling results are shown in Figure 6.

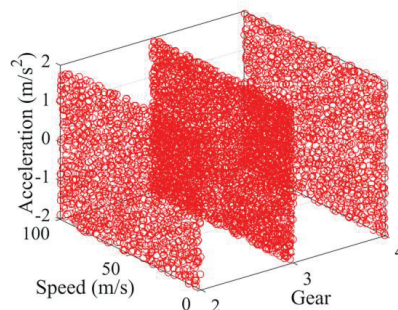


Figure 6. Opt LHD sampling diagram.

Although the degree of refinement of the state description after sampling is reduced, the requirements for controller computing power and storage space are greatly reduced, and the uniformity and stability of sampling also ensure that the reduced state variables are representative.

3.2.3. Return Function of the Shift Schedule Based on RL

The reward function $R(s(t), a(t))$ in this paper is as follows

$$R(s(t), a(t)) = \begin{cases} \frac{100}{Efficient(t)-efficient(t)} + \frac{1}{SOC_1(t)-SOC_2(t)}, Efficient(t) - efficient(t) \geq 0.05 \& \& SOC_1(t) > SOC_2(t); \\ \frac{100}{Efficient(t)-efficient(t)} + \frac{1}{SOC_1(t)-SOC_2(t)}, Efficient(t) - efficient(t) \geq 0.05 \& \& SOC_1(t) < SOC_2(t); \\ 1000 * (Efficient(t) - efficient(t)) + \frac{1}{SOC_1(t)-SOC_2(t)}, Efficient(t) > efficient(t) \& \& Efficient(t) - efficient(t) < 0.05 \& \& SOC_1(t) > SOC_2(t); \\ 1000 * (Efficient(t) - efficient(t)) + \frac{10}{SOC_2(t)-SOC_1(t)}, Efficient(t) > efficient(t) \& \& Efficient(t) - efficient(t) < 0.05 \& \& SOC_1(t) < SOC_2(t); \\ 0, Efficient(t) = efficient(t) \& \& SOC_1(t) = SOC_2(t); \\ \frac{10}{SOC_1(t)-SOC_2(t)}, Efficient(t) = efficient(t) \& \& SOC_1(t) > SOC_2(t); \\ \frac{10}{SOC_1(t)-SOC_2(t)}, Efficient(t) = efficient(t) \& \& SOC_1(t) < SOC_2(t); \\ \frac{10}{Efficient(t)-efficient(t)} + \frac{1}{SOC_1(t)-SOC_2(t)}, Efficient(t) < efficient(t) \& \& SOC_1(t) < SOC_2(t); \\ \frac{10}{Efficient(t)-efficient(t)} + \frac{1}{SOC_1(t)-SOC_2(t)}, Efficient(t) < efficient(t) \& \& SOC_1(t) > SOC_2(t); \end{cases} \quad (21)$$

where $Efficient(t)$ denotes the efficiency of the motor after shifting at time t ; $efficient(t)$ is the meaning of the motor efficiency that keeps the original gear at time t ; $SOC_1(t)$ is the battery SOC after shifting at time t ; $SOC_2(t)$ represents the battery SOC of the original gear and is maintained at time t .

From Figure 5, it can be seen that the difference between the efficiency at the motor shift point and the maximum efficiency of the motor is about 15%. Under the premise of considering the economy and taking into account the shift frequency at the same time, after many tests, the efficiency difference is finally designed to be 5%.

3.2.4. Establishment of the Shift Schedule Based on RL

In this paper, the action set is designed as the target gear, so the RL algorithms of Q-learning are mainly used to find the best target gear. Therefore, under each time step, the optimal control strategy $\pi^*(s(t), a(t))$ can be expressed as

$$\pi^*(s(t)) = \operatorname{argmax}_{a_t} Q(s(t), a(t)) \quad (22)$$

where $Q(s(t), a(t))$ is the meaning of the Q value to perform the action $a(t)$ in the current state $s(t)$. In this paper, the optimal Q value is defined as

$$Q^*(s(t), a(t)) = R(s(t), a(t)) + \gamma \max_{a' \in A} Q^*(s'(t), a'(t)) \quad (23)$$

where $R(s(t), a(t))$ is the meaning of the reward obtained after performing the current action $a(t)$; γ denotes the discount factor, $\gamma \in [0, 1]$; $\max_{a' \in A} Q^*(s'(t), a'(t))$ represents the maximum value of all actions at the next moment corresponding to the Q table in the next state $s'(t)$.

Furthermore, the update of the Q table can be expressed as

$$Q(s(t), a(t)) = Q(s(t), a(t)) + \alpha (R(s(t), a(t)) + \gamma \max_{a'} Q(s'(t), a'(t)) - Q(s(t), a(t))) \quad (24)$$

where α is the recession factor, $\alpha \in [0, 1]$.

This paper adopts the more common strategy $\epsilon - greedy$ in RL to select actions. To put it simply, strategy $\epsilon - greedy$ is a regulation strategy for the tendency of an agent to choose two optimization methods when choosing an action [16], which can be specifically expressed as

$$\pi^*(a(t)|s(t)) = \begin{cases} a = \operatorname{random}(A) & \text{if } ee \leq \epsilon \\ a = \max_a Q(s(t), a(t)) & \text{if } ee > \epsilon \end{cases} \quad (25)$$

where ϵ is the random exploration probability, ee is the meaning of the random number, and the unit is $[0 \sim 1]$.

In the early stages of offline training, to improve the learning efficiency, ϵ takes a larger value, so that the optimization method is more inclined to random exploration, so as to

find as many better actions as possible. With the continuous progress of offline training, the value of ϵ gradually decreases, so that the optimization method gradually tends to the optimal method of the Q table until the Q table converges. The offline training process of the Q table is shown in Figure 7.

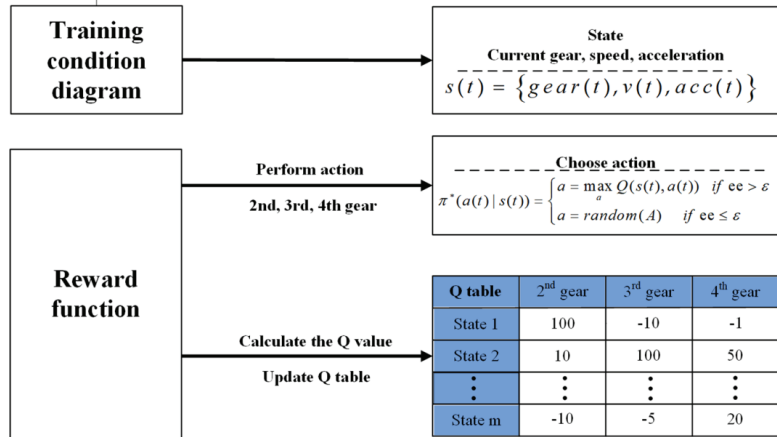


Figure 7. Q table offline training.

At each step, the RL agent determines the current state with the current gear, acceleration, and vehicle speed. Next, select the corresponding action based on the $\epsilon - greedy$ strategy and execute it to obtain the reward value in the current state. Then, calculate the Q value under the current action and update the Q table according to the reward value and the historical cumulative reward. Finally, the next state is updated based on the state parameters such as the current gear, and the above steps are repeated to update the Q value under the next state and action until the training ends, and the Q table is derived.

The purpose of offline training is to ensure that the vehicle can drive in the most economical gear in different states as much as possible. Therefore, the working conditions of the offline training should cover the entire state space as much as possible to ensure that the vehicle can drive in the optimal gear in any state. In this paper, four sets of internationally recognized test conditions are used to train the Q meter offline. The four groups of working conditions are the urban working condition WVUCITY for low-speed driving, the suburban working condition WVUSUB for medium-speed driving, the high-speed working condition HWFET for high-speed driving, and the mixed working condition UDSS [17]. The main eigenvalues are shown in Table 1.

Table 1. Characteristic values of each working condition.

Working Condition	Time	Distance	v_{max}	a_{max}
WVUCITY	1408 s	5.29 km	57.65 km/h	1.14 m/s ²
WVUSUB	1665 s	24.81 km	72.10 km/h	1.30 m/s ²
HWFET	766 s	16.41 km	96.40 km/h	1.43 m/s ²
UDSS	1370 s	11.99 km	91.25 km/h	1.48 m/s ²

It can be seen from Table 1 that the four groups of operating conditions almost cover the state of the full speed section. Therefore, using four sets of working conditions as training conditions can ensure that the coverage of the state space can reach the expectation.

Figures 8–11 shows the results obtained by training the four groups of working conditions in the order of urban working conditions → suburban working conditions → high-speed working conditions → mixed working conditions.

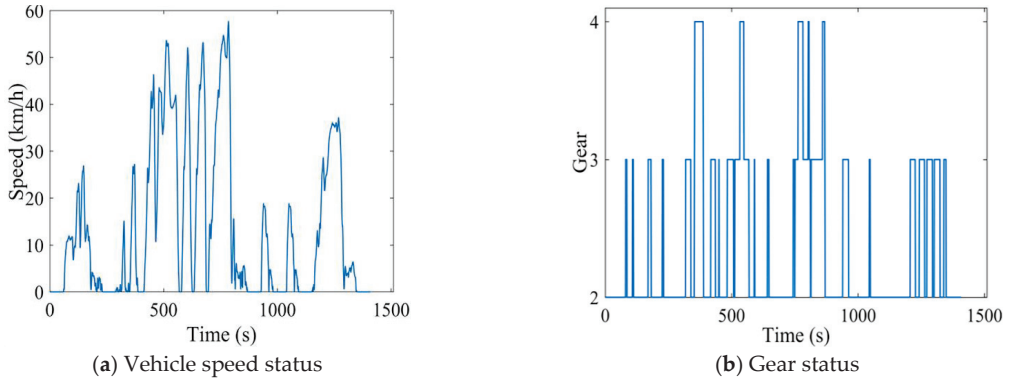


Figure 8. WVUCITY working condition.

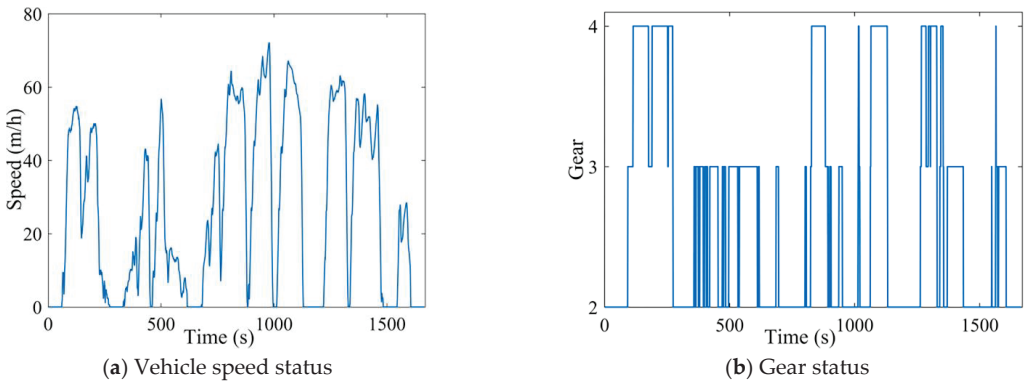


Figure 9. WVUSUB working condition.

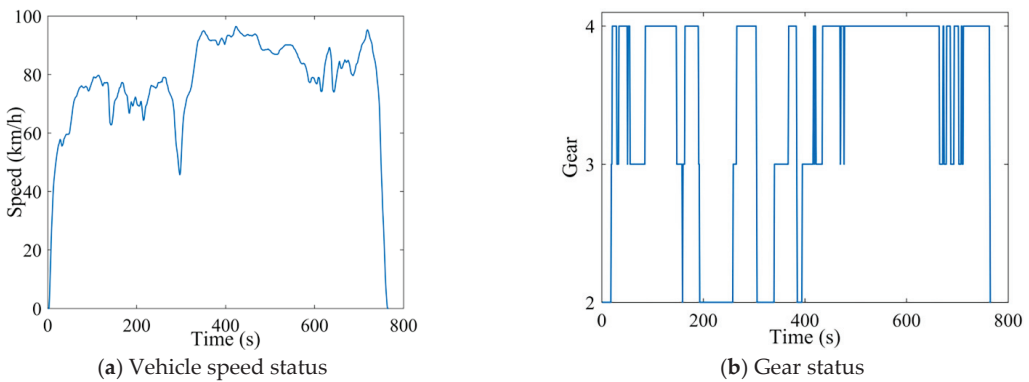


Figure 10. HWFET working condition.

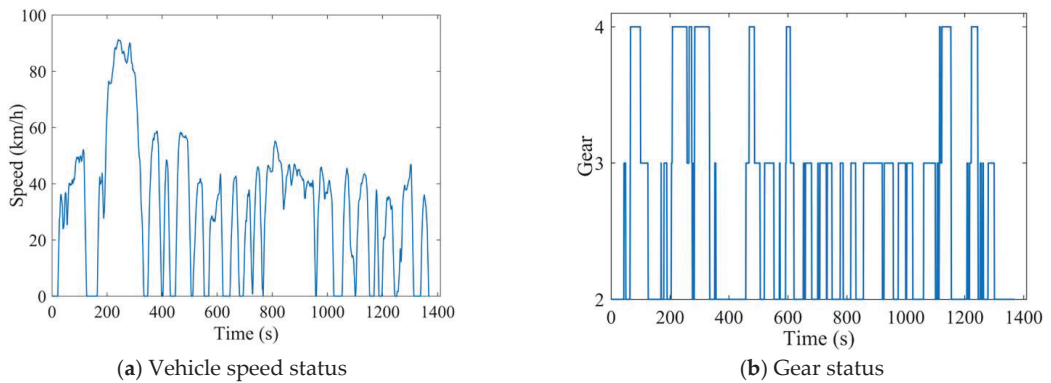


Figure 11. UDDS working condition.

In Figure 8a, for the front and rear of the WVUCITY condition, the vehicle speed is generally lower. In the middle section, there are several violent accelerations and decelerations, and the vehicle speed is high. Therefore, in Figure 8b, the front and rear are mostly driven in 2nd/3rd gear, and sometimes it is raised to 4th gear in the middle. However, due to the large change in vehicle speed at this stage, the gear is not maintained for a long time. The urban training Q table is taken as a reference, the suburban working conditions are trained, and the results are shown in Figure 9. In Figure 9a, at around 200 s, there are two periods when the vehicle speed exceeds 50 km/h in the WVUSUB condition. The gear in Figure 9b is also raised to 4th gear. However, at 400~600 s, according to the operating condition information in Figure 9a, when the vehicle speed exceeds 50 km/h, it does not shift to 4th gear. It may be because the corresponding state point is not collected when Opt LHD is used for sampling, so that in this state, the AMT selects the operation to maintain the original gear.

The results of continuing to train the high-speed case are shown in Figure 10. Under high-speed conditions, the frequency of shift is significantly reduced because the vehicle runs at a high speed throughout the entire journey, and there is almost no rapid acceleration or rapid deceleration.

After the training of the first three working conditions, as shown in Figure 11, it is the training result under the mixed working conditions. It can be found that although the vehicle speed fluctuation is relatively severe, the real-time performance of the gear is better in the low, medium, and high speed stages.

3.2.5. Model Simulation Verification

To test the performance of the shift schedule based on RL in terms of energy consumption economy, the next step is to conduct software-in-the-loop simulation tests for two shift schedules based on the pure electric vehicle model. Considering the usage scenarios and uses of the research object, it was decided to adopt the China light vehicle test cycle (CLTC) specified in the national standard of the People's Republic of China as the test condition [18]. The CLTC is shown in Figure 12.

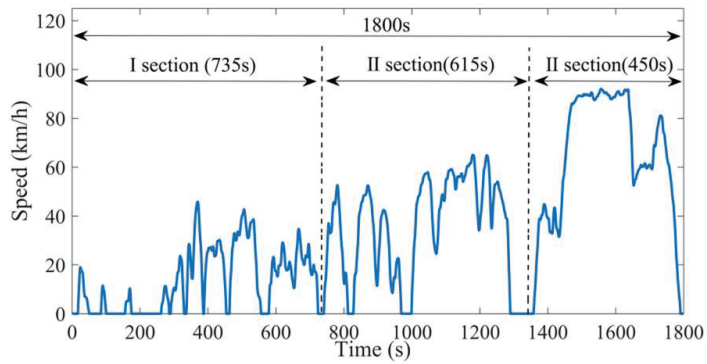


Figure 12. CLTC condition.

The CLTC working condition information is taken as the expected vehicle speed. After it is given to the driver model, the output AP opening is shown in Figure 13, and the acceleration and vehicle speed following output by the driving model are shown in Figures 14 and 15 respectively.

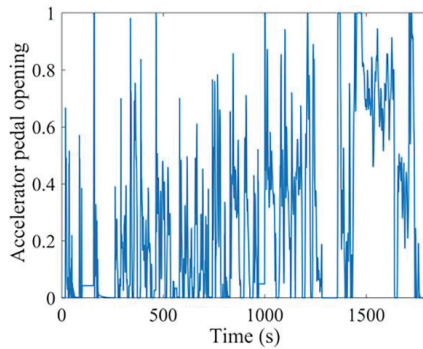


Figure 13. AP opening.

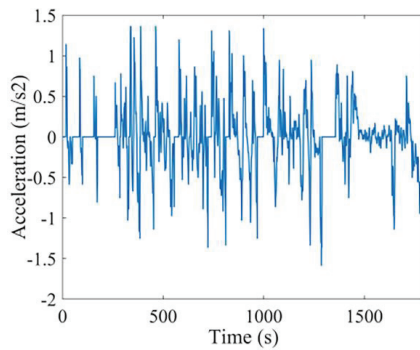


Figure 14. Acceleration.

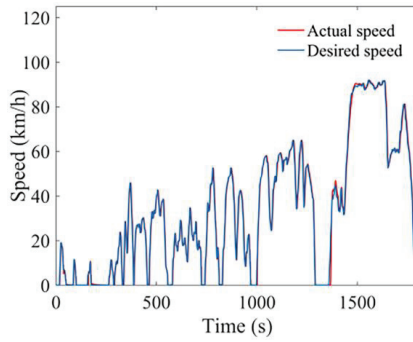


Figure 15. Speed following situation.

As can be seen from Figure 13, due to the rapid fluctuation of operating conditions, the change of the AP opening is also more frequent. Figure 14 also proves that there will be rapid acceleration during driving. The pedal opening will appear to be deeply depressed to ensure the power of the vehicle. It can be seen from Figure 15 that the actual vehicle speed can follow the target vehicle speed well, which further ensures the reliability and accuracy of the subsequent simulation. Based on the above working condition information, the two shift schedules are brought into the vehicle model for simulation [19]. The gear comparison diagram is shown in Figure 16, and the SOC result comparison diagram is shown in Figure 17.

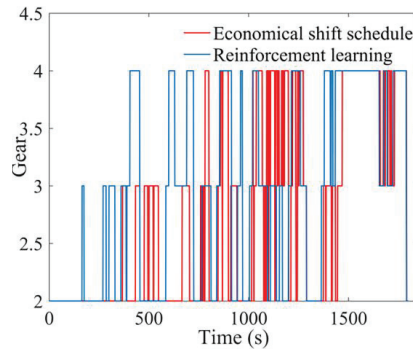


Figure 16. Gear comparison.

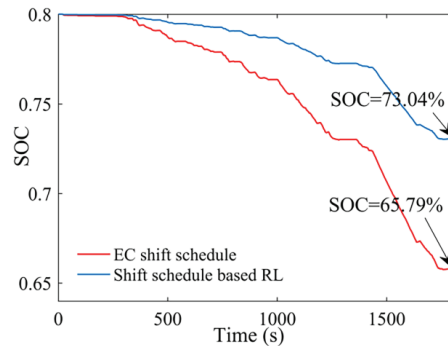


Figure 17. SOC result comparison.

Combined with the simulation conditions, it can be seen from Figure 16 that in the low-speed road section, the vehicle speed is generally low, and the vehicle is driven in a low gear under the EC shift schedule. The shift schedule based on RL adopts shifting gears to deal with the change of working conditions. This is due to the change of the state of the vehicle resulting in the change of the optimal gear, which shows that the shift schedule based on RL has a certain adaptability [20]. In the medium-speed section, due to the severe fluctuation of working conditions, frequent shift occurs under the EC shift schedule, while the problem of frequent shift does not occur under the shift schedule based on RL, which also proves the rationality of the design of return function in the previous paper. In the high-speed road section, due to the sudden deceleration in the second half of the high-speed working condition, the shift schedule based on RL and the EC shift schedule are adopted to change the gear position. Combining with Figure 17, it can be seen that both of them have different degrees of braking energy recovery, which is in line with practical applications. At the same time, the whole cycle is about 16.4 km in length. In terms of data, under the EC shift schedule, the SOC remains 65.79%. Under the shift schedule based on RL, the SOC remains 73.04%, and the energy consumption is reduced by about 7.27%.

On the whole, shift schedule based on RL can effectively reduce the energy consumption of the pure electric vehicle and improve the cruising range.

4. Hardware-in-the-Loop Experiment

4.1. Introduction to Hardware-in-the-Loop Platforms

The pure electric vehicle performance comprehensive test platform takes PXI as the core, and integrates six hardware modules: Driving simulator (Modified version based on cs75 console, Chang'an Automobile, Chongqing, China), battery pack (RiseSun MGL, Beijing, China), wheel speed simulator, motor, AMT (self-development) and chassis dynamometer. The human-computer interaction platform developed based on LabVIEW and the virtual environment built based on CarSim together constitute the software system of the hardware-in-the-loop experimental platform [21]. The experimental platform architecture is shown in Figure 18.

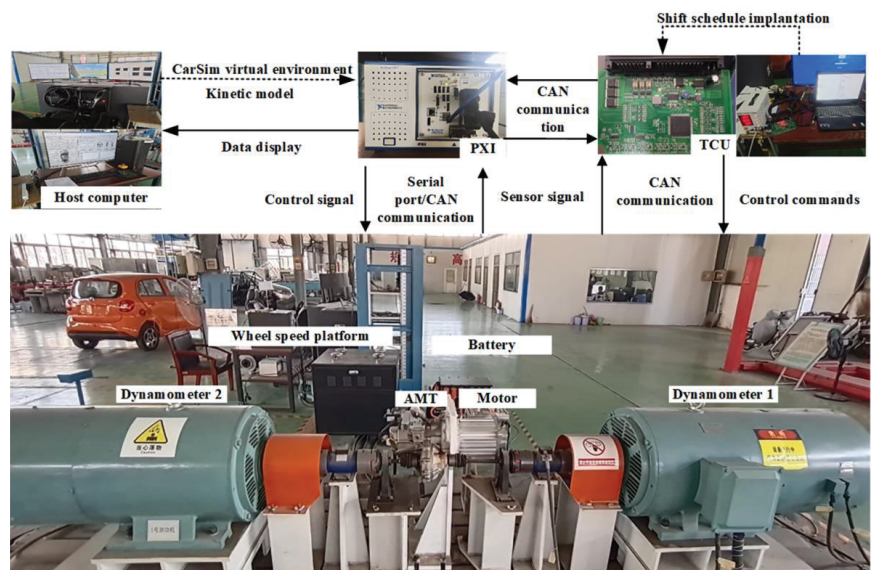


Figure 18. Hardware-in-the-loop experimental platform.

The platform is mainly divided into three parts, which are the host computer, the lower computer and the underlying actuator. The host computer is the PC side of the computer and runs the human-computer interaction software written by LabVIEW. The communication function between the PC and PXI is realized through the local area network to ensure the real-time transmission and display of data. In addition, the virtual environment built based on CarSim is also displayed and runs on the PC side. The lower computer is PXI, which realizes the signal interaction with the underlying actuator through CAN communication, and feeds back the signal of the underlying actuator to the host computer. The longitudinal dynamics model of the vehicle runs in the lower computer.

The underlying actuator mainly uses the AMT's gear selection motor and drive motor. According to the obtained vehicle status signal, the TCU judges the target gear, coordinates and controls the response of the motor and the gear selection motor, and then realizes the switching of gears. The TCU feeds back real-time signals to the lower computer through CAN communication, and the host computer reads the real-time data fed back to the lower computer by the underlying actuator through the local area network to realize the closed-loop simulation of the system. In addition, driving simulators, battery packs, wheel speed simulators, and chassis dynamometers can also be considered as categories of underlying actuator. The driving simulator is used to output the AP/BP opening signal and the shift handle position signal. The power battery pack provides power for the entire hardware-in-the-loop test platform, and feeds back the SOC to the host computer in real time. The wheel speed simulator is used to simulate the wheel speed. The chassis dynamometers are used to simulate the driving resistance of the car during driving.

4.2. Hardware-in-the-loop Experiments and Analysis

Dynamic Shift Experiment

This section compares and verifies the two shift schedules through dynamic shift experiments.

To ensure the consistency of the experimental conditions and eliminate the interference of human factors on the experimental results as much as possible, this paper conducts experiments based on fixed operating conditions, and comprehensively considers the application scenarios of vehicles mainly in China. Therefore, the experiment is carried out using China Typica, a typical domestic working condition. The China Typica working condition is shown in Figure 19.

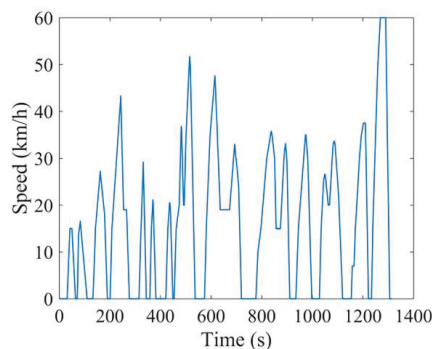


Figure 19. China Typica working condition.

In this test, the driver model running on the lower computer outputs the AP/BP opening, and the driving simulator is only used to realize the position control of the shift handle.

Figures 20–25 show the experimental results of the EC shift schedule based on the hardware-in-the-loop platform and the experimental results of the shift schedule based on RL. The two state parameters of the EC shift schedule are vehicle speed and pedal

opening. When the hardware in the loop platform is tested, the working condition is read by the host computer software and directly sent to the driver model of the lower computer for operation.

As shown in Figure 20, the change of the pedal opening is in line with the changing trend of the working conditions. There is good feedback in the rapid acceleration and rapid deceleration segments, indicating that the output parameters of the driver model are accurate and real-time.

The reliable driver model ensures the smooth progress of the dynamic shift schedule experiment, and its gear map and SOC change map are shown in Figures 21 and 22. In the low-speed section, although the vehicle speed fluctuates violently, the two state parameters do not reach the shift threshold, the AMT does not shift under the EC shift schedule. In the medium-speed section, when the vehicle speed exceeds 30 km/h, the AP opening exceeds at 50%, and the AMT will shift to the 3rd gear. Only when the vehicle speed exceeds 50 km/h and the AP opening exceeds 70%, the AMT will shift to the 4th gear. There were only three times of driving in 4th gear during the whole journey, and in high probability cases, they were all in low gears and driving with a large AP opening. Figure 22 reflects the SOC change under the EC shift schedule. The SOC change under this condition is 4.87%. The acceleration is calculated comprehensively based on the virtual load dynamically imposed by the chassis dynamometer, and the output is shown in Figure 23. It can be seen from the figure that the acceleration varies between -1 and 1 m/s. At the same time, the acceleration shows an instantaneous sudden change and short-term maintenance. The comparative analysis shows that this is also consistent with the characteristics of rapid acceleration and rapid deceleration under the China Typica working condition, which can reflect the state change of the vehicle to a certain extent.

Figure 24 reflects the gear map under the shift schedule based on RL. It is not difficult to see that the shift frequency is significantly increased compared with the EC shift schedule, and the frequency of switching back and forth between 2nd/3rd gear is mostly increased. This is because the Q table that stores the reinforcement learning shift rule defines the optimal gear in each vehicle state based on the motor efficiency. By analyzing the China Typica working condition, it is not difficult to find that the vehicle speed in this working condition mostly fluctuates between 0 and 40 km/h, and switching between 2nd/3rd gear is a normal phenomenon. In addition, in the range of 1200–1300 s, there is a maximum vehicle speed (60 km/h) under this working condition, but during the experiment, it did not increase to 4th gear in this state. Through the collected vehicle state parameters, the state of the vehicle is not found by searching the Q table. The reason for this situation is that the Opt LHD sampling results in the reduction of state variables, so when the vehicle reaches this state, the operation of maintaining the original gear is adopted by default.

The shift schedule based on RL designed in this paper is based on economy. The SOC change map as shown in Figure 25. The change of SOC is 1.69%. Compared with the EC shift schedule, the energy consumption is reduced by about 3.18%, which proves the feasibility and application potential of the shift schedule based on RL.

Experiment results of the EC shift schedule:

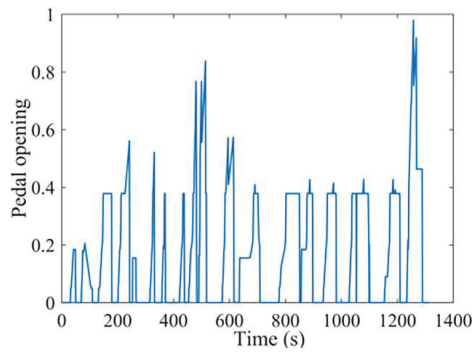


Figure 20. Pedal opening.

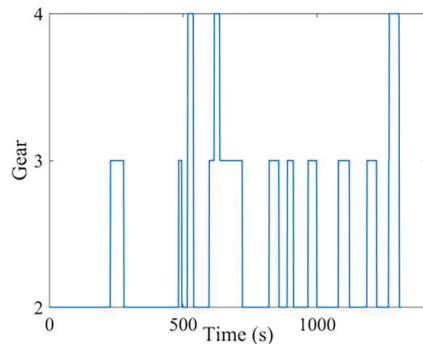


Figure 21. Gear of the EC shift schedule.

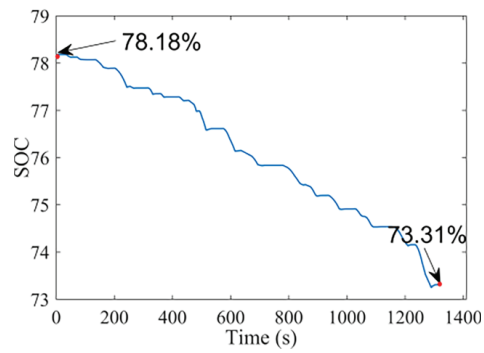


Figure 22. SOC of EC shift schedule.

Experiment results of the shift schedule based on RL:

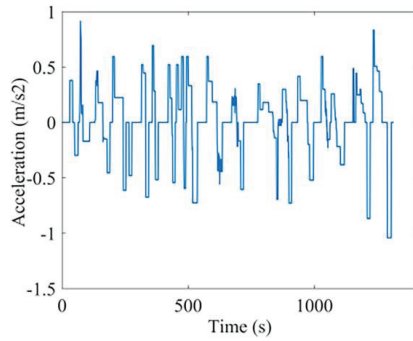


Figure 23. Acceleration.

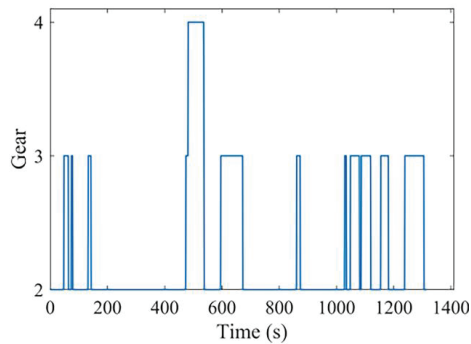


Figure 24. Gear of the shift schedule based on RL.

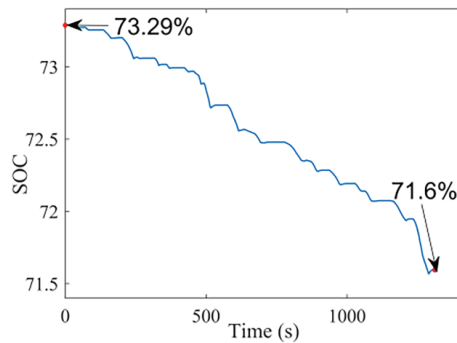


Figure 25. SOC of the shift schedule based on RL.

5. Conclusions

In this paper, a multi-speed AMT pure electric vehicle is taken as the research object, and a shift schedule based on RL is proposed to improve vehicle energy performance. The main conclusions are as listed as follows:

- (1) The proposed shift schedule can continuously self-learn according to the reward and punishment mechanism designed by the reward function and match the best gear according to the principle of economy. It solves the problem of high energy consumption caused by poor adaptability of traditional shift schedules.

- (2) The Opt LHD was introduced to reduce the state space of the Q table of the shift schedule, and solved the problem that the shift schedule could not be embedded in the TCU due to the “dimension disaster”. Using Opt LHD sampling can reduce the number of trials, ease the computational burden of the computer, and effectively reduce the computing power demand.
- (3) Compared with the EC shift schedule, energy consumption is reduced by about 3.18% by using the shift schedule based on RL. The feasibility and application potential of the shift schedule based on RL have been proven.

Overall, the method proposed in this paper taps the energy economy potential of multi-speed pure electric vehicles. The shift schedule based on RL proposed in this paper provides a new case for the combination of machine learning and shift schedule, and also provides a new idea for reducing the energy consumption of electric vehicles. Researchers can use other machine learning methods to optimize the shift schedule, which is not limited to RL. However, the proposed method has some shortcomings. First of all, due to the consideration of the impact of shift frequency on ride comfort, the design of the reward function is not based on the highest efficiency, but is designed in the form of a difference. Although shift frequency is reduced, energy consumption has been improved. Secondly, due to the problem of controller computing power, the state space of the Q table should not be too large. Therefore, the number of state variables is limited, and the accuracy of the Q table to describe the vehicle state needs to be further improved. In the future, through continuous research, the above problems will be solved.

Author Contributions: Conceptualization, X.Y. and K.Z.; methodology, H.G.; software, H.G.; validation, X.Y., K.Z. and L.Z.; formal analysis, X.Y.; investigation, X.Y.; resources, H.G.; data curation, L.Z.; writing—original draft preparation, X.Y.; writing—review and editing, X.Y.; visualization, X.Y.; supervision, L.Z.; project administration, L.Z.; funding acquisition, L.Z. All authors have read and agreed to the published version of the manuscript.

Funding: This research was funded by the Natural Science Foundation of Shandong Province (No. ZR2020ME128), 2022 Liaocheng University Student Innovation and Entrepreneurship Training Program (No. CXC2022378) and Key Funding Projects of Liaocheng University (No. 14211). And the APC was funded by High level start-up fee of Science and Technology Department (No. 318051903).

Institutional Review Board Statement: Not applicable.

Informed Consent Statement: Not applicable.

Data Availability Statement: Data sharing is not applicable to this article as no datasets were generated or analysed during the current study.

Conflicts of Interest: The authors declare no conflict of interest.

References

1. Ruan, J.; Walker, P.; Zhang, N. A comparative study energy consumption and costs of battery electric vehicle transmissions. *Appl. Energy* **2016**, *165*, 119–134. [[CrossRef](#)]
2. Han, K.; Wang, Y.; Filev, D.; Dai, E.; Kolmanovsky, I.; Girard, A. Optimized design of multi-speed transmissions for battery electric vehicles. In Proceedings of the 2019 American Control Conference (ACC), Philadelphia, PA, USA, 10–12 July 2019; pp. 816–821.
3. Nguyen, C.T.; Walker, P.D.; Zhang, N. Optimization and coordinated control of gear shift and mode transition for a dual-motor electric vehicle. *Mech. Syst. Signal Process.* **2021**, *158*, 107731. [[CrossRef](#)]
4. Han, K.; Li, N.; Kolmanovsky, I.; Girard, A.; Wang, Y.; Filev, D.; Dai, E. Hierarchical optimization of speed and gearshift control for battery electric vehicles using preview information. In Proceedings of the 2020 American Control Conference (ACC), Denver, CO, USA, 1–3 July; 2020; pp. 4913–4919.
5. Sujjan, V.A. System and Methods of Adjusting a Transmission Shift Schedule. U.S. Patent 9,989,147, 5 June 2018.
6. Yuanguang, J.; Haonan, L.; Jiankun, P.; Zhanjiang, L. Research of the AMT Multi Parameter Fusion Shift Rule of Pure Electric Bus. *Mech. Transm.* **2019**, *43*, 21–26. [[CrossRef](#)]
7. Huang, W.; Huang, J.; Yin, C. Optimal design and control of a two-speed planetary gear automatic transmission for electric vehicle. *Appl. Sci.* **2020**, *10*, 6612. [[CrossRef](#)]
8. Sun, G.B.; Chiu, Y.J.; Lu, G.W.; Xiong, M. The Study of Dynamic Programming with Fuzzy Logic Energy Design and Simulation of Gear Shift for Electric Vehicles. *J. Netw. Intell.* **2019**, *4*, 88–99.

9. Lin, C.; Zhao, M.; Pan, H.; Yi, J. Blending gear shift strategy design and comparison study for a battery electric city bus with AMT. *Energy* **2019**, *185*, 1–14. [[CrossRef](#)]
10. Hang, Q.; Hongwen, H.; Mo, H. Electric Vehicle Shift Strategy Based on Model Predictive Control. *J. Chongqing Univ. Technol.* **2021**, *35*, 90–95.
11. Li, H.; He, H.; Peng, J.; Li, Z. Five-parameter shift strategy of automatic mechanical transmission for electric bus. *DEStech Trans. Env. Energ. Earth Sci.* 2019. [[CrossRef](#)]
12. Li, G.; Görges, D. Ecological adaptive cruise control for vehicles with step-gear transmission based on RL. *IEEE Trans. Intell. Transp. Syst.* **2019**, *21*, 4895–4905. [[CrossRef](#)]
13. Wenguang, L.; Shanshan, B.; Chang, X. Shifting Strategy for Two-Speed AMT of Electric Vehicle. *J. Chongqing Univ. Technol.* **2021**, *35*, 41–49.
14. Liu, Z.; Li, Z.; Zhang, J.; Su, L.; Ge, H. Accurate and efficient estimation of lithium-ion battery state of charge with alternate adaptive extended Kalman filter and ampere-hour counting methods. *Energies* **2019**, *12*, 757. [[CrossRef](#)]
15. Zhu, B.; Zhang, N.; Walker, P.; Zhou, X.; Zhan, W.; Wei, Y.; Ke, N. Gear shift schedule design for multi-speed pure electric vehicles. *Proc. Inst. Mech. Eng. Part D J. Automob. Eng.* **2015**, *229*, 70–82. [[CrossRef](#)]
16. Samadi, E.; Badri, A.; Ebrahimpour, R. Decentralized multi-agent based energy management of microgrid using RL. *Int. J. Electr. Power Energy Syst.* **2020**, *122*, 106211. [[CrossRef](#)]
17. Yi, J.; Li, X.; Xiao, M.; Xu, J.; Zhang, L. Construction of nested maximin designs based on successive local enumeration and modified novel global harmony search algorithm. *Eng. Optim.* **2017**, *49*, 161–180. [[CrossRef](#)]
18. Chen, J.; Su, Y. Fuel Consumption and Nox Emissions from Vehicle Over the Wltc and Cltc_C. Available online: <https://ssrn.com/abstract=4046059> (accessed on 17 October 2022).
19. Powell, B.K.; Bailey, K.E.; Cikanek, S.R. Dynamic modeling and control of hybrid electric vehicle powertrain systems. *IEEE Control. Syst. Mag.* **1998**, *18*, 17–33.
20. Lewis, F.L.; Vrabie, D. RL and adaptive dynamic programming for feedback control. *IEEE Circuits Syst. Mag.* **2009**, *9*, 32–50. [[CrossRef](#)]
21. Sun, Y.; Ru, Y.; He, X.; Dong, C. Research on Testing System and Test Method for Charging Facilities of Electric Vehicles. In Proceedings of the 2018 5th IEEE International Conference on Cloud Computing and Intelligence Systems (CCIS), Nanjing, China, 23–25 November 2018; pp. 1048–1052.



Article

Telling You More Fluently: Effect of the Joint Presentation of Eco-Label Information on Consumers' Purchase Intention

Xingyuan Wang, Yingying Du *, Yun Liu and Shuyang Wang

School of Management, Shandong University, Jinan 250100, China

* Correspondence: yingdu@mail.sdu.edu.cn

Abstract: An eco-label is an important tool for identifying green products in the marketplace. Most eco-labels, however, present a single icon that is simple and carries limited information, thus creating cognitive barriers for consumers. As a result, eco-labels might not always effectively promote green consumption. Based on dual coding theory and the spatial contiguity effect, this study investigated the effect of the “joint presentation of eco-label information” (JPEI), which adds (functional/emotional) descriptive text to eco-labels, on improving consumers' cognitive fluency in eco-labels and subsequent purchase intention. We conducted three studies and found that, compared with the “single presentation of eco-label information” (SPEI), JPEI improved the cognitive fluency of consumers with low eco-label knowledge. Furthermore, spatially contiguous JPEI was more effective than spatially partitioned JPEI for consumers with low eco-label knowledge. In addition, we specifically explored the information types of JPEI that were effective for consumers with low eco-label knowledge. Low-construal consumers had higher cognitive fluency and higher purchase intentions under functional JPEI, and high-construal consumers had higher cognitive fluency and higher purchase intentions under emotional JPEI. The results of this study enrich eco-label research and can provide theoretical guidance for marketing practices in eco-labels.

Keywords: eco-label; joint presentation of eco-label information; cognitive fluency; spatial contiguity; construal level

Citation: Wang, X.; Du, Y.; Liu, Y.; Wang, S. Telling You More Fluently: Effect of the Joint Presentation of Eco-Label Information on Consumers' Purchase Intention. *Int. J. Environ. Res. Public Health* **2022**, *19*, 13713. <https://doi.org/10.3390/ijerph192013713>

Academic Editors: Roberto Alonso González Lezcano, Francesco Nocera and Rosa Giuseppina Caponetto

Received: 29 September 2022

Accepted: 17 October 2022

Published: 21 October 2022



Copyright: © 2022 by the authors. Licensee MDPI, Basel, Switzerland. This article is an open access article distributed under the terms and conditions of the Creative Commons Attribution (CC BY) license (<https://creativecommons.org/licenses/by/4.0/>).

1. Introduction

Eco-labels are used on product packaging to convey that a product has green attributes. Although eco-labels are widely used in green marketing, some studies have identified obstacles to their effective application [1]. Because of the simple format of most eco-labels, the limited information they convey [2], and the varied types of eco-label icons (the 2021 Eco-Label Index identified 455 different labels in 199 countries; <http://www.ecolabelindex.com/>, accessed on 30 June 2022), consumers often have difficulty recognizing and understanding eco-label information [3,4]. One eye-tracking study, for example, found that participants recognized and understood only two of 110 eco-labels [5]. It has also been found that eco-labels are mainly effective for consumers who already possess environmental awareness [6] and less effective for those who do not. Eco-labels are only effective when consumers can readily understand their meanings [2]. However, many consumers have cognitive difficulties related to eco-labels. A previous study in China also concluded that the eco-label system is very complex for consumers and that there is a need to improve consumers' understanding of eco-labels [7].

Recent research on eco-labels has focused on their effects on consumers' attitudes, purchase intentions, purchase behaviors, and willingness to pay a premium for green products [3,8–11]. Such effects are mainly related to the visibility of eco-label designs [12,13], eco-label certification sources [14], eco-label formats [15], consumers' knowledge of eco-labels or ecology [10,16], product quality inferences and product evaluation influenced by eco-labels [17,18], and consumers' attitudes toward eco-labels [19,20]. While some studies

have acknowledged the difficulties some consumers face in understanding eco-labels [3–5]—that is, their cognitive fluency in eco-labels—there remains a gap in the literature regarding how to address the problem [12]. To address the cognitive problem of eco-labels, we will mainly discuss the following aspects.

First, we take insights from dual coding theory (DCT), which proposes that verbal (e.g., text) and nonverbal (e.g., icon or image) codes corresponding to the same object can have additive effects on cognition [21]. Many eco-labels are presented as single icons and are nonverbal codes, which was conceptualized as “single presentation of eco-label information” (SPEI) in this study. We propose the eco-label format of “joint presentation of eco-label information” (JPEI), which adds descriptive text as verbal codes to single-icon eco-labels to improve consumers’ cognition and understanding of eco-labels. Regarding the information types to add for the descriptive text, we referred to the classification of information types in green advertising and divided the descriptive text into functional and emotional types [22], thus forming emotional JPEI and functional JPEI. However, studies on DCT have found that the effect of dual coding is related to individual characteristics, such as individuals’ prior knowledge [23]. Based on this, we took consumers’ eco-label knowledge as a moderator and explored whether JPEI was more effective than SPEI for improving consumers’ cognitive fluency in eco-labels.

Second, if, as predicted, JPEI is indeed more effective than SPEI for consumers’ cognition, how should JPEI be spatially located? In the extending research on DCT, scholars have proposed that individuals can cognize better when corresponding verbal and non-verbal codes are presented close to each other rather than far apart, which is known as the “spatial contiguity effect” [24]. This effect is also related to individuals’ prior knowledge [25]. Thus, we used consumers’ eco-label knowledge as a moderator to explore how the spatial distance of JPEI (spatially contiguous vs. spatially partitioned) can improve cognitive fluency in eco-labels. In addition, we explored whether increased cognitive fluency leads to higher purchase intentions.

Third, if JPEI is effective for consumers with a specific eco-label knowledge level, then we need to consider when to use functional JPEI or emotional JPEI. To examine this, we referred to construal level theory for insights into the effectiveness of functional vs. emotional JPEI. Specifically, we explored how functional JPEI and emotional JPEI can be matched to consumers’ construal level to generate higher cognitive fluency and purchase intentions.

This work enriches research on green consumption, especially eco-labels. We proposed the concept of “joint presentation of eco-label information” (JPEI), and examined the effects of spatial distance and information types in JPEI, which fills the research gap of eco-labels in cognitive perspective. Additionally, we constructed a framework in which eco-label presentation influences consumers’ purchase intentions. Our research also provides guidance for the future use of eco-labels.

2. Literature Review and Hypothesis Development

Ecolabels are symbols designed to identify and distinguish products that have a positive environmental effect [1]. While green products typically use eco-labels to communicate green attributes, there are barriers to consumers’ cognition [26]. This is mainly because there are many types of eco-label icons, some of them are very simple in format, and they convey limited information [2,14,17]. Eco-labels do not effectively transmit green information between buyers and sellers [27]. Carrero et al. [28] and Taufique et al. [13] noted that consumers have difficulty understanding and recognizing eco-labels, especially those who have low eco-label knowledge [29], making it difficult for eco-labels to serve their purpose in the purchasing process [30]. Therefore, how to make it easier for consumers to understand and recognize eco-labels is an important research topic. Cognitive fluency reflects the ease with which the meaning of information enters one’s mind [31]. This reflects the ease of higher-level processing, such as understanding the meaning of stimuli [32], which is often associated with purchase intentions [33]. Thus, our study explored whether

JPEI can influence product purchase intentions by improving consumers' cognitive fluency of eco-labels.

While previous studies have recognized that eco-label formatting affects purchase decisions, there is little research in this area [12]. An existing study found that icon-based eco-labels attracted more visual attention than text-based ones and that visual attention to icon-based eco-labels increased consumer bids [12]. In research on other types of labels, Jaud and Melnyk [34] showed that wine labels combining text with matching images were better than text-only labels and labels where images and text do not match. No studies, however, have specifically examined the effect of eco-labels with a combined format on consumers' cognition. Some research in the field of advertising has explored the effect of combinations of different information formats. Kim et al. and Sahin et al. found that combinations of logo-text or image-text designs were better than single-format designs [35,36]. Furthermore, some studies have suggested that when people combine images and textual information, their comprehension behavior is largely text driven; that is, people first use the text to construct an initial representation and then combine it with information from the images [37,38]. This suggests that descriptive eco-label text can facilitate consumers' understanding. Rihn et al. [12] also proposed that textual eco-labels may be useful for educating consumers about less familiar logos. In the next section, we will specifically elaborate on how JPEI enhances consumer purchase intentions through cognitive fluency.

2.1. Eco-Label Information Presentation, Consumers' Eco-Label Knowledge and Cognitive Fluency

Based on DCT, when individuals apply verbal and non-verbal coding in information processing, the joint processing of the two can enable more efficient interactions between them and improve individuals' learning and cognition [39]. Research on DCT has also suggested that nonverbal coding is more detrimental to cognitive learning than verbal coding [40]. When nonverbal coding is difficult to understand, the corresponding verbal coding can form a reference link with the nonverbal coding to help improve cognition [39]. However, nonverbal coding is cognitively efficient when individuals have a priori knowledge about nonverbal coding [41]. We therefore introduced consumers' eco-label knowledge as a moderator.

We defined consumers' eco-label knowledge as the level of information about a particular eco-label that consumers perceived to be stored in their memory [42]. Consumers' knowledge can influence consumers' perceptions of their ability to process relevant information [43]. Consumers with high and low knowledge differ in the presentation structure of their target. Specifically, those with low knowledge have a fragmented and shallow cognitive schema and do not have well-developed criteria for making decisions based on existing knowledge [44,45]; thus, they need to search for more external information to support their understanding [46]. Consumers with high knowledge are more likely to process information using prior knowledge and decision criteria readily available to them and are therefore less likely to rely on external heuristic cues [47].

In this study, the eco-label icon is nonverbal coding, and the eco-label descriptive text is verbal coding. Consumers with low eco-label knowledge have difficulty automatically activating eco-label processing, but consumers with high eco-label knowledge can [48]. We infer that JPEI can make consumers with low eco-label knowledge more fluent in their eco-label cognition because it provides more information [27] and allows for the joint processing of dual coding (i.e., an eco-label icon and its descriptive text). However, consumers with high eco-label knowledge are more likely to make purchasing decisions by simply identifying the eco-label icon [10] without relying on additional descriptive text. Thus, we propose the following interaction effects (see Figure 1a):

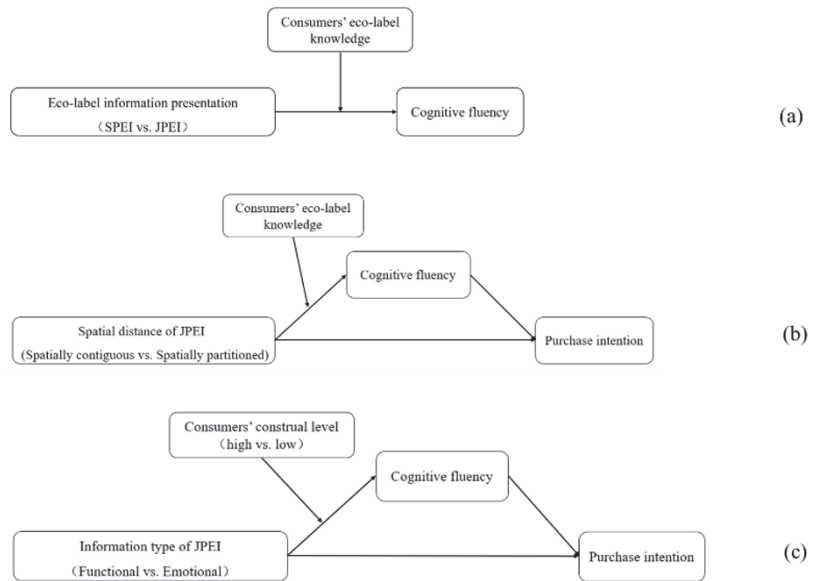


Figure 1. Conceptual model (Note: (a) shows H1a and H1b; (b) shows H2a and H2b; (c) shows H3a and H3b).

H1a. For consumers with low eco-label knowledge, JPEI can increase their cognitive fluency in eco-labels compared to SPEI.

H1b. For consumers with high eco-label knowledge, there are no significant differences in the effects of SPEI and JPEI on their cognitive fluency in eco-labels.

2.2. Spatial Distance of JPEI, Consumers' Eco-Label Knowledge, Cognitive Fluency and Purchase Intentions

In this study, spatial distance refers to an interval of geometric distance between design elements [49]; it can be either spatially contiguous or spatially partitioned [50]. Research on multimedia learning suggests the spatial distance between image and text affects cognitive or learning effects [51], and proposes the theory of “spatial contiguity effect” [52]. When images and text are both needed to understand a concept, spatial contiguity between them can reduce the time individuals spend searching for information, and they can retain more information in their short-term memory [53], which better facilitates learning [54]. When information is spatially partitioned, individuals become prone to attentional separation [50], in which case their cognitive load increases owing to the need to mentally combine different sources of information [55], which can result in reduced cognitive effects [52]. However, Mayer proposed that the spatial contiguity effect should consider the prior knowledge of individuals [25]. Spatial distance has less effect on individuals with higher prior knowledge [56]. This is because the eye movement paths of individuals with high prior knowledge are characterized by higher saccade lengths [57]. Thus, individuals with high prior knowledge are better able to visually and cognitively connect spatially distant elements to fully comprehend the information [53].

For consumers with low eco-label knowledge, spatially contiguous JPEI can facilitate consumers' visual search for information, and a good referential link between an eco-label and descriptive text will also improve cognitive fluency [56]. When JPEI is spatially partitioned, consumers need to process information from different locations, thus experiencing split attention and a greater cognitive load [52], which results in relatively low cognitive fluency. However, consumers with high eco-label knowledge rely less on other information

cues and more on their prior knowledge to process eco-labels [46]. Furthermore, even if consumers with high eco-label knowledge see the descriptive text, they can quickly link the eco-label and the text cognitively to complete their information processing [53]. Based on this, we predict that spatial distance will not have a significant effect on their cognitive fluency. Previous studies have found that cognitive fluency can positively influence consumers' purchase intentions [33]. Separately, Sigurdsson et al. also found that having an understanding of eco-labels can have a positive effect on purchase intentions [3]. Thus, we propose the following interaction effects (see Figure 1b):

H2a. *For consumers with low eco-label knowledge, spatially contiguous JPEI will enhance their cognitive fluency in eco-labels compared to spatially partitioned JPEI and then lead to higher purchase intentions.*

H2b. *For consumers with high eco-label knowledge, there will be no significant difference in the effect of spatially contiguous JPEI and spatially partitioned JPEI on cognitive fluency and, subsequently, purchase intentions.*

2.3. Information Type of JPEI, Consumers' Construal Level, Cognitive Fluency and Purchase Intentions

Construal level refers to the extent to which an individual is in an abstract mind-set (i.e., focused on objects' superordinate and central features) versus a concrete mind-set (i.e., focused on objects' subordinate and specific features) [58]. The theory proposes that one's construal level affects the processes of receiving, processing, and responding to information, as well as persuasion [59]. When the information type matches individuals' construal level, the matching information will produce a more fluent encoding process, which will positively affect individuals' purchase decisions [60,61]. At a low construal level, people typically focus on more specific information from a detailed perspective; at a high construal level, people focus on more abstract information from a central, essential perspective [62]. Some research on branding and advertising has shown that consumers with a high construal level prefer emotional information, while those with a low construal level prefer functional information [62,63]. We likewise believe that consumers' construal level will be associated with the effectiveness of the information type in eco-labels.

Functional JPEI provided practical information about eco-labels' environmental attributes [64], while emotional JPEI made emotional appeals about eco-labels to promote pro-environmental behavior [65]. Functional JPEI provides more concrete, realistic, and detailed information, which is more in line with the cognitive habits of low-construal consumers; emotional JPEI provides more abstract information and expresses a good vision, and is more in line with the cognitive habits of high-construal consumers [63]. Thus, functional JPEI should lead to more fluent eco-label cognition for low-construal consumers, and emotional JPEI should lead to more fluent eco-label cognition for high-construal consumers. In the above analysis, we have proposed that fluent cognition of eco-label information will positively affect consumers' purchase intentions [3,33]. Thus, we propose the following interaction effects (see Figure 1c):

H3a. *For low-construal consumers, functional JPEI will lead to higher cognitive fluency than emotional JPEI, which in turn will lead to higher purchase intentions.*

H3b. *For high-construal consumers, emotional JPEI will lead to higher cognitive fluency than functional JPEI, which in turn will lead to higher purchase intentions.*

Figure 1 depicts the conceptual model based on all of the above hypotheses.

3. Overview of Studies

Three experiments were designed to test the hypotheses. In Study 1, a two-piece (eco-label information presentation: SPEI vs. JPEI) \times continuous (consumers' eco-label knowledge) between-subjects design was conducted to test whether JPEI could improve consumers' cognitive fluency in eco-labels, using consumers' eco-label knowledge as the moderator. Based on Study 1, Study 2 also used consumers' eco-label knowledge as the moderator to test whether spatial contiguous JPEI would more effectively improve cognitive fluency compared to spatial partitioned JPEI and whether that improvement would positively affect purchase intentions. A two-piece (spatial distance of JPEI: spatially contiguous vs. spatially partitioned) \times continuous (consumers' eco-label knowledge) between-subjects design was adopted in Study 2. Study 3 used consumers' construal level as the moderator to test which information type of JPEI (functional vs. emotional) is more effective in increasing cognitive fluency among consumers with low eco-label knowledge and whether it would subsequently increase purchase intentions. A two-piece (JPEI information type: functional vs. emotional) \times two-piece (consumers' construal level: high vs. low) between-subjects design was used. The experimental stimulus used in Studies 1 and 2 was the FSC eco-label, and Study 3 used the "Euro-leaf" eco-label. We also performed a pre-test to justify the selection of stimuli in the experiments.

4. Study 1

Study 1 tested whether JPEI could improve participants' cognitive fluency in eco-labels more than SPEI under the boundary condition of participants' eco-label knowledge.

4.1. Method

4.1.1. Participants and Design

A total of 240 participants were randomly recruited from Credamo (www.credamo.com, accessed on 30 June 2022) and offered a reward (see Supplementary Material E, in Supplementary Materials, for demographic profiles of participants). Credamo is considered to have significant reliability [66], and a number of studies using Credamo have been published in leading journals (e.g., [67,68]). We adopted a 2 (eco-label information presentation: SPEI vs. JPEI) \times continuous (consumers' eco-label knowledge) between-subjects design. To increase authenticity, we selected a commonly used tissue as the stimulus and used the virtual brand "ECO" tissue to exclude interference from the brand factor. We selected "FSC" certification as the eco-label, because Tan et al. found that 21% of participants knew the FSC eco-label in Chongqing shopping for wood flooring products [69]. Currently, more consumers are familiar with the FSC eco-label. We conducted a pre-test to justify the eco-label selection. Regarding the added descriptive text, as mentioned previously, it could be either functional or emotional, and we tested the design in the pre-test.

We recruited 120 participants for the pre-test (see Supplementary Material E for demographic profiles of participants). First, the participants were asked to look at the image of the FSC eco-label and then answer the question, "Do you recognize the FSC eco-label?" (1 = yes, 2 = no). The results showed that approximately half (56.7%) of the participants recognized the FSC eco-label, indicating that the stimulus was reasonably selected.

Second, we performed a manipulation test on functional ($n = 60$) and emotional ($n = 60$) descriptive text. For functional descriptive text, following Matthes et al. [22] regarding functional claims, it was "This product has been certified by 'FSC Forest Stewardship Council' certification. Made from 100% FSC-certified, well-managed forests. Meets the FSC certification criteria for environmental suitability and community benefit." For emotional descriptive text, again following Matthes et al. [22], the text included emotional appeals as well as exclamation points at the end of sentences, which help mobilize emotions [70,71]. Referring to Aagerup et al. [72], emotional eco-label descriptive text was "Want a better environment and a more sustainable society? Then choose products certified by the 'FSC Forest Stewardship Council'! Keep forests alive forever and give future generations a better future!". After presenting the materials to the participants, the participants answered the

question, “Does the descriptive text reflect more of a specific environmental function or more of the emotional appeal of the FSC eco-label?” (1 = more specific environmental function; 7 = more emotional appeal) [72]. The results indicated that our manipulation of the descriptive text was successful ($M_{\text{functional}} = 3.43$, $SD = 2.070$; $M_{\text{emotional}} = 5.32$, $SD = 1.546$; $t(59) = -5.506$, $p < 0.001$).

4.1.2. Procedure

We first measured participants’ FSC eco-label knowledge after they viewed the FSC eco-label image. Chang’s mature scale of product knowledge was adapted [73], which included four items ($\alpha = 0.913$). Then, participants were asked to look at an image of ECO tissue packaging (see Supplementary Material A). For the SPEI group, the packaging had an FSC eco-label. For the JPEI group, the FSC eco-label was accompanied by the same functional descriptive text as in the pre-test (we also tested the emotional descriptive text; see Supplementary Material A: Follow-up Study).

After presenting the materials to the participants, we used the mature scale of Lee and Aaker to measure cognitive fluency [74], which included three items ($\alpha = 0.872$) (see Supplementary Material D). In addition, participants’ environmental attitudes might have affected the results; so, we measured the participants’ environmental concerns, also using mature four-item scales [22] ($\alpha = 0.749$). A seven-point Likert scale was used for all items, with 1 indicating “strongly disagree” and 7 indicating “strongly agree.” Finally, demographic variables such as gender and age were measured.

4.2. Results

There were no significant differences in environmental concern ($M_{\text{SPEI}} = 5.633$, $SD = 1.010$; $M_{\text{JPEI}} = 5.700$, $SD = 0.874$; $t(238) = -0.547$, $p > 0.05$), indicating that it did not affect our results. Eco-label information presentation is a categorical variable (SPEI = 0; JPEI = 1), and consumers’ eco-label knowledge is a continuous variable; thus, we used SPSS 25.0 PROCESS 3.3 (bootstrapping = 5000, 95% CI, Model 1) to test for interaction effects [75]. The results showed that both eco-label information presentation ($b = 1.027$, $SE = 0.352$, $t = 2.918$, $p < 0.01$) and consumers’ eco-label knowledge ($b = 0.642$, $SE = 0.126$, $t = 5.081$, $p < 0.001$) had a significant effect on cognitive fluency. The interaction between eco-label information presentation and consumers’ eco-label knowledge on cognitive fluency is also significant ($b = -0.185$, $SE = 0.078$, $t = -2.364$, $p < 0.05$). We further analyzed the moderating effect using the Johnson–Neyman technique [76]. Supporting H1a and H1b, the results showed that eco-label information presentation had a significant positive effect on cognitive fluency when consumers’ eco-label knowledge was equal to or lower than 4.2895 ($p = 0.002$ to 0.05); when consumers’ eco-label knowledge was higher than 4.2895, the effect of eco-label information presentation on cognitive fluency was not significant ($p = 0.05$ to 0.952 , $B_{\text{JN}} = 4.2895 = 0.233$, $SE = 0.118$) (see Figure 2).

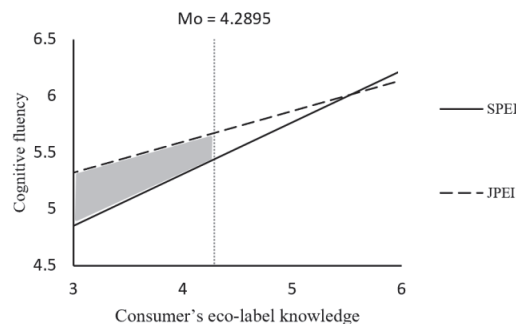


Figure 2. The interactive effect of eco-label information presentation and consumer’s eco-label knowledge (Study 1). Note: the shaded area is the Johnson–Neyman significant area.

4.3. Discussion

The results of Study 1 demonstrated that adding descriptive text to an eco-label (i.e., JPEI) improved the cognitive fluency of participants with low eco-label knowledge. However, for those with high eco-label knowledge, there was no difference between the presence or absence of descriptive text. To enhance the robustness of our results, we conducted another study. In the follow-up to Study 1 (see Supplementary Material A), we used a design similar to that of Study 1 but with a different information type for JPEI (the descriptive text was emotional). The results also supported H1a and H1b.

While this can suggest ways to improve eco-label cognition, enhancing the efficacy of descriptive eco-label text still needs investigation. Specifically, does the spatial distance between the eco-label and text affect cognition? What type of information should be used to make descriptive text more effective for those with low eco-label knowledge? Further, will enhanced cognitive fluency in eco-labels increase participants' willingness to purchase? These questions were addressed in the two studies that follow.

5. Study 2

Study 2 used consumers' eco-label knowledge as the moderator and investigated the effect of spatial distance on cognitive fluency. Specifically, we studied the differential effects of spatially contiguous and spatially partitioned JPEI on participants' cognitive fluency and whether such differences in cognitive fluency led to differences in purchase intentions.

5.1. Method

5.1.1. Participants and Design

Participants were randomly recruited from Credamo and offered a reward. A 2 (spatial distance of JPEI: spatially contiguous vs. spatially partitioned) \times continuous (consumers' eco-label knowledge) between-subjects design was adopted and 206 participants were recruited (see Supplementary Material E for demographic profiles of participants).

5.1.2. Procedure

The stimuli were similar to those in Study 1, still using the virtual brand ECO tissue and the FSC eco-label. The same scale as in Study 1 was used to measure participants' knowledge of the FSC eco-label ($\alpha = 0.939$). In the spatially contiguous JPEI group, the FSC eco-label was placed together with the functional descriptive text, both in the upper right-hand corner of the tissue packaging. In the spatially partitioned JPEI group, the FSC eco-label and functional descriptive text were separated, with the FSC eco-label in the lower left-hand corner and the text in the upper right-hand corner (see Supplementary Material B). We verified the spatial distance manipulation by asking for the distance between the FSC eco-label image and the descriptive text (1 = very close, 7 = very far away). The participants responded to the mature purchase intention scale adapted from Dodds et al. [77] ($\alpha = 0.798$). Then, cognitive fluency ($\alpha = 0.914$) and environmental concern ($\alpha = 0.636$) were measured in the same way as in Study 1 (see Supplementary Material D). All were measured on a seven-point Likert scale, with 1 indicating "strongly disagree" and 7 indicating "strongly agree". Finally, demographic variables were measured.

5.2. Results

5.2.1. Manipulation Test

Participants perceived the spatially partitioned group as more distant than the spatially contiguous group ($M_{\text{partitioned}} = 5.30$, $SD = 1.237$; $M_{\text{contiguous}} = 3.70$, $SD = 1.520$; $t(204) = 8.277$, $p < 0.01$). There were no significant differences in environmental concern between the two groups ($M_{\text{partitioned}} = 5.842$, $SD = 0.774$; $M_{\text{contiguous}} = 5.921$, $SD = 0.634$; $t(204) = -0.812$, $p > 0.05$).

5.2.2. Cognitive Fluency

Spatial distance is a categorical variable (spatially partitioned = 0; spatially contiguous = 1), and consumers' eco-label knowledge is a continuous variable; so, we used SPSS 25.0 PROCESS 3.3 (bootstrapping = 5000, 95% CI, Model 1) to test for interaction effects [75]. The results showed that both spatial distance ($b = 1.522$, $SE = 0.378$, $t = 4.023$, $p < 0.001$) and consumers' eco-label knowledge ($b = 0.559$, $SE = 0.055$, $t = 10.104$, $p < 0.001$) had a significant effect on cognitive fluency. The interaction effect between spatial distance and consumers' eco-label knowledge on cognitive fluency was also significant ($b = -0.239$, $SE = 0.080$, $t = -2.967$, $p < 0.01$). The Johnson–Neyman technique [76] showed that spatial distance had a significant positive effect on cognitive fluency when consumers' eco-label knowledge was equal to or lower than 5.1825 ($p = 0$ to 0.05). When consumers' eco-label knowledge was higher than 5.1825, the effect of spatial distance on cognitive fluency was not significant ($p = 0.05$ to 0.924, $B_{JN} = 5.1825 = 0.285$, $SE = 0.145$) (see Figure 3a).

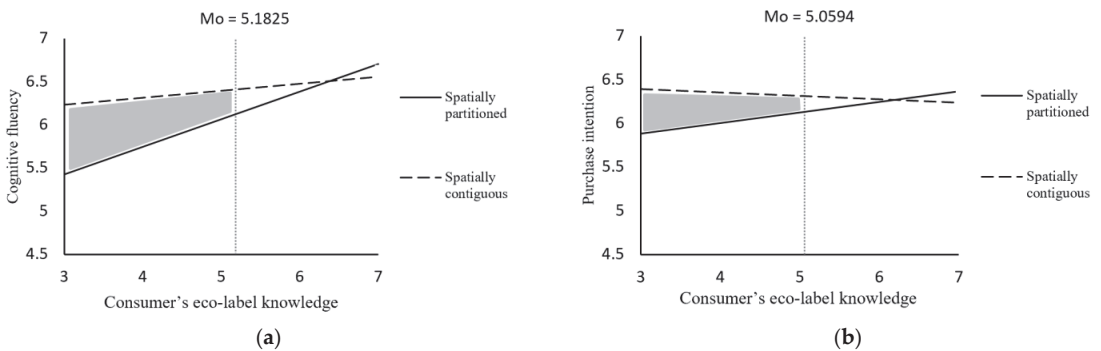


Figure 3. The interactive effect of JPEI spatial distance and consumers' eco-label knowledge (Study 2). Note: (a) shows the interaction effect with cognitive fluency as the dependent variable; (b) shows the interaction effect with purchase intention as the dependent variable. The shaded area is the Johnson–Neyman significant area.

5.2.3. Purchase Intention

The same method was used, and the results showed that both spatial distance ($b = 0.994$, $SE = 0.253$, $t = 3.936$, $p < 0.001$) and consumers' eco-label knowledge ($b = 0.281$, $SE = 0.037$, $t = 7.604$, $p < 0.001$) had a significant effect on purchase intentions. The interaction effect between spatial distance and consumers' eco-label knowledge on purchase intentions was also significant ($b = -0.160$, $SE = 0.054$, $t = -2.979$, $p < 0.01$). The Johnson–Neyman [76] results showed that spatial distance had a significant positive effect on purchase intentions when consumers' eco-label knowledge was equal to or lower than 5.0594 ($p = 0$ to 0.05); when consumers' eco-label knowledge was higher than 5.0594, the effect of spatial distance on purchase intentions was not significant ($p = 0.05$ to 0.957, $B_{JN} = 5.0594 = 0.185$, $SE = 0.094$) (see Figure 3b).

5.2.4. Moderated Mediation

We used PROCESS 3.3 in SPSS 25.0 to check whether cognitive fluency played a mediating role [75]. Bootstrapping analysis (samples = 5000, 95% CI, Model 7) showed that the mediation of cognitive fluency was significant (indirect effect = -0.066 , $SE = 0.030$, 95% CI = -0.130 to -0.013 , excluding 0). Specifically, when participants had low eco-label knowledge, the spatial distance of JPEI had a significant effect on purchase intentions through cognitive fluency (indirect effect = 0.236 , $SE = 0.085$, 95% CI = 0.084 to 0.418 , excluding 0); when participants had high eco-label knowledge, the spatial distance of JPEI had a nonsignificant effect on purchase intentions through cognitive fluency (indirect effect

= 0.021, SE = 0.032, 95% CI = -0.042 to 0.086, including 0), thus supporting H2a and H2b (see Figure 4).

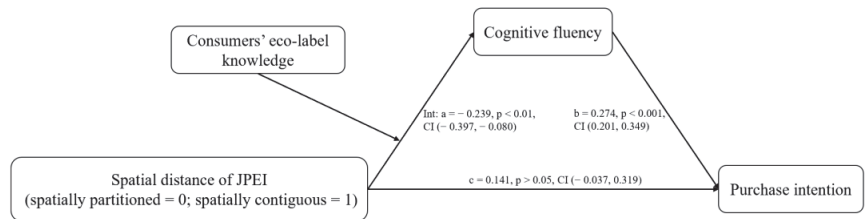


Figure 4. Results for the moderated mediation effect (Study 2).

5.3. Discussion

Study 2 demonstrated that when participants had low eco-label knowledge, spatially contiguous JPEI led to higher cognitive fluency and purchase intentions. When participants had high eco-label knowledge, spatially contiguous JPEI and spatially partitioned JPEI showed no significant differences. In addition, we verified it again using the emotional descriptive text and reached the same conclusion (see Supplementary Material B: Study 2 Follow-up A).

In this study, we placed the eco-label image on the lower left-hand corner of the package and the descriptive text on the upper right-hand corner of the package, but the observed effect may be explained by the specific location of the information rather than by the spatial distance. Thus, we conducted two additional studies, which made some changes in spatially partitioned JPEI group. One study placed both the eco-label and the descriptive text at the top of the package but separated them in terms of position. The other study placed the eco-label on the top right-hand corner of the package and the descriptive text on the bottom left-hand corner of the package. The results were consistent with those of Study 2 (see Supplementary Material B: Study 2 Follow-up B and C).

The first two studies revealed that for consumers with low eco-label knowledge, the eco-label should not only be accompanied by descriptive text but that they should also be placed in close proximity to each other. We also showed that both functional and emotional descriptive text can improve cognition for consumers with low eco-label knowledge. In the next study, we explored when to use functional descriptive text or emotional descriptive text.

6. Study 3

Study 3 tested the interaction effect between the JPEI information type and consumers' construal level on cognitive fluency among consumers with low eco-label knowledge. It also tested how changes in cognitive fluency lead to changes in purchase intentions.

6.1. Method

6.1.1. Participants and Design

A total of 314 participants were randomly recruited from Credamo and were offered a reward (see Supplementary Material E for demographic profiles of participants). A 2-piece (JPEI information type: functional vs. emotional) × 2-piece (consumers' construal level: high vs. low) between-subjects design was used. The product was the virtual brand "GRE" oatmeal, which was common in the participants' daily lives. The eco-label was the "Euro-leaf" organic certification, which has been mandatory in Europe since 2010. A survey in China found that only 16.5% of participants recognized it [78]. We therefore used the Euro-leaf eco-label as the stimulus to better illustrate the effect of JPEI on increasing participants' cognitive fluency among low eco-label knowledgeable consumers. We also conducted a pre-test to investigate cognition of the eco-label in China. Construal level manipulation was also tested in the pre-test.

We recruited 120 participants for the pre-test (see Supplementary Material E for demographic profiles of participants). First, the participants were asked to look at the image of the Euro-leaf eco-label and then answer the question, “Do you recognize the eco-label” (1 = yes, 2 = no). The results showed that 18.3% of the participants recognized the eco-label, indicating that cognition of the eco-label is low in China and that most consumers had low knowledge of the eco-label.

Second, we primed the participants’ construal level, using the method proposed by Freitas et al. [79]. “Why” is generally associated with a high construal level, and “how” is generally associated with a low construal level. Four consecutive “why” ($n = 60$) and “how” ($n = 60$) questions were asked on the topic of “improving and maintaining physical health”. That is, the second question is based on the answer to the first question and continues with the “why” or “how” question, and the third question is based on the answer to the second question and so on. There were some participants who entered into a more abstract way of thinking after the four consecutive “why” questions; this was the high-construal group. Other participants entered into a more concrete and specific way of thinking after four consecutive “how” questions; this was the low-construal group. Then, the participants completed the Behavior Identification Form for the manipulation test [80]. Specifically, the participants were asked to choose one of two possible options (one represents a high construal level, and the other represents a low construal level) for 10 behaviors [81]. We coded an answer as 0 (1) if the participant chose the low (high) construal level option (see Supplementary Material D). A higher score means a higher construal level. We found that the participants who answered “why” had a higher construal level, and those who answered “how” had a lower construal level ($M_{\text{low}} = 2.15$, $SD = 2.090$; $M_{\text{high}} = 3.03$, $SD = 2.365$; $t(59) = 2.241$, $p < 0.05$).

Finally, a manipulation test of the functional descriptive text ($n = 60$) and emotional descriptive text ($n = 60$) was conducted. Similar to the descriptive text in Study 1, the functional descriptive text was “The product has passed ‘EU organic certification’. Contain at least 95% organic ingredients. Meet ‘Euro-leaf’ eco-label’s principles of natural production and ecological balance.” The emotional descriptive text was “Do you want a healthier, greener lifestyle? Then choose products that have passed ‘Euro-leaf’ organic certification! Let’s live in harmony with nature!” (see Supplementary Material C). The results showed that the manipulation of the descriptive text was successful ($M_{\text{functional}} = 3.22$, $SD = 1.263$; $M_{\text{emotional}} = 5.17$, $SD = 1.137$; $t(59) = -7.268$, $p < 0.001$).

6.1.2. Procedure

Participants were asked to answer four consecutive “why” or “how” questions to prime them into the corresponding construal level. Then, the functional JPEI group viewed the “GRE” oatmeal packaging with the Euro-leaf eco-label and functional descriptive text; the emotional JPEI group viewed the “GRE” oatmeal packaging with the Euro-leaf eco-label and emotional descriptive text. Participants were then administered the same measures as in Studies 1 and 2 for cognitive fluency ($\alpha = 0.860$), purchase intentions ($\alpha = 0.854$), and demographic variables.

6.2. Results

6.2.1. Cognitive Fluency

We conducted two-way ANOVA in SPSS 25.0 with cognitive fluency as the DV and information type and construal level as the IV. The interaction between information type and participants’ construal level in relation to cognitive fluency was significant ($F(1, 310) = 25.481$, $p < 0.001$, $\eta_p^2 = 0.076$). As shown in Figure 5a, for participants with a low construal level, functional JPEI had higher cognitive fluency than emotional JPEI ($M_{\text{functional}} = 5.750$, $SD = 0.865$; $M_{\text{emotional}} = 5.071$, $SD = 1.099$; $F(1, 310) = 12.595$, $p < 0.001$, $\eta_p^2 = 0.039$). For participants with a high construal level, cognitive fluency was higher for emotional JPEI than for functional JPEI ($M_{\text{emotional}} = 5.890$, $SD = 0.988$; $M_{\text{functional}} = 5.352$, $SD = 1.107$; $F(1, 310) = 13.446$, $p < 0.001$, $\eta_p^2 = 0.042$).

6.2.2. Purchase Intention

We conducted two-way ANOVA in SPSS 25.0 with purchase intention as the DV and information type and construal level as the IV. The interaction effect between information type and participants' construal level on purchase intentions was significant ($F(1, 310) = 31.535, p < 0.001, \eta_p^2 = 0.092$). As shown in Figure 5b, for participants with a low construal level, functional JPEI showed a higher purchase intentions than emotional JPEI ($M_{\text{functional}} = 5.622, SD = 0.813; M_{\text{emotional}} = 4.976, SD = 0.938; F(1, 310) = 14.903, p < 0.001, \eta_p^2 = 0.046$). For participants with a high construal level, emotional JPEI showed a higher purchase intentions than functional JPEI ($M_{\text{emotional}} = 5.623, SD = 0.934; M_{\text{functional}} = 5.084, SD = 0.899; F(1, 310) = 17.586, p < 0.001, \eta_p^2 = 0.054$).

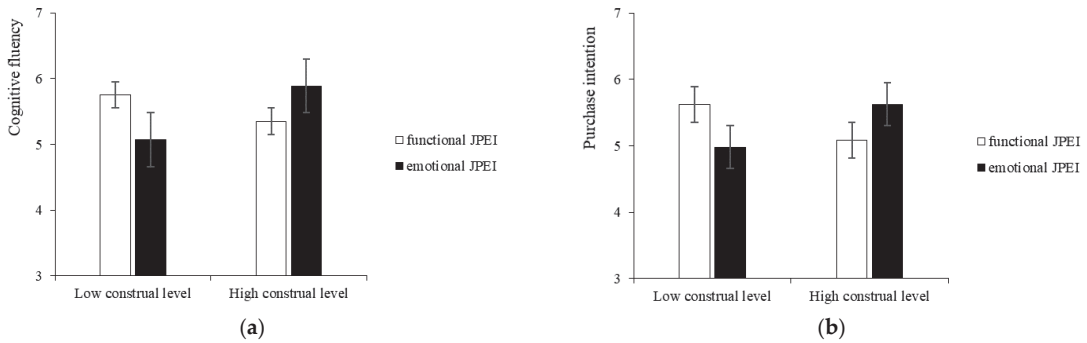


Figure 5. The interactive effect of the information type of JPEI and consumer's construal level (Study 3). Note: (a) shows the interaction effect with cognitive fluency as the dependent variable; (b) shows the interaction effect with purchase intention as the dependent variable.

6.2.3. Moderated Mediation

We used PROCESS 3.3 in SPSS 25.0 to analyze the mediating role of cognitive fluency [75]. Bootstrapping analysis (samples = 5000, 95% CI, Model 7) showed that the mediating effect of cognitive fluency was significant (indirect effect = 0.679, SE = 0.141, 95% CI = 0.408 to 0.963, excluding 0). Specifically, in the low-construal group, information type had a significant effect on purchase intentions through cognitive fluency (indirect effect = -0.379, SE = 0.106, 95% CI = -0.590 to -0.174, excluding 0). In the high-construal group, information type also had a significant effect on purchase intentions through cognitive fluency (indirect effect = 0.300, SE = 0.088, 95% CI = 0.132 to 0.480, excluding 0). These results support H3a and H3b (see Figure 6).

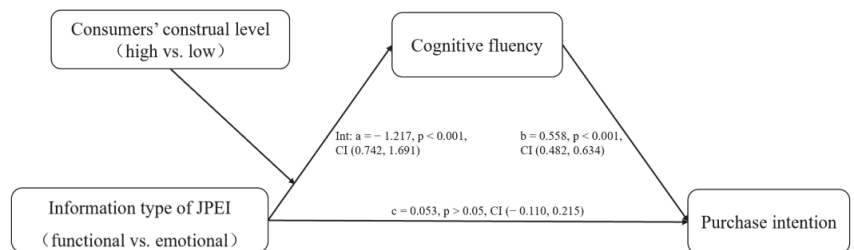


Figure 6. Results for the moderated mediation effect (Study 3).

6.3. Discussion

Study 3 demonstrated that matching the JPEI information type and consumers' construal level could improve their cognitive fluency in eco-labels and subsequently increase their purchase intentions. Specifically, participants with a low construal level had higher

cognitive fluency and purchase intentions when faced with functional JPEI; participants with a high construal level had higher cognitive fluency and purchase intentions when faced with emotional JPEI. This study provides evidence for what types of information should be added to eco-labels for consumers with low eco-label knowledge. The results of all hypothesis testing in this study are shown in Table 1.

Table 1. Summary of the findings.

Hypotheses	Study	Results
Eco-label information presentation (SPEI vs. JPEI) * consumers' eco-label knowledge → Cognitive fluency		
H1a: Significant difference for low eco-label knowledge consumers	Study 1	✓
H1b: No difference for high eco-label knowledge consumers	Study 1	✓
Spatial distance of JPEI (spatially contiguous vs. spatially partitioned) * consumers' eco-label knowledge → Cognitive fluency → Purchase intentions		
H2a: Significant difference for low eco-label knowledge consumers	Study 2	✓
H2b: No difference for high eco-label knowledge consumers	Study 2	✓
Information type of JPEI (functional vs. emotional) * consumers' construal level (high vs. low) → Cognitive fluency → Purchase intentions		
H3a: Functional JPEI for low-construal consumers	Study 3	✓
H3b: Emotional JPEI for high-construal consumers	Study 3	✓

Note: * means interactive effect.

7. General Discussion

7.1. Theoretical Contribution

First, we propose a new form of eco-label information presentation, which enriches the empirical research in the field of eco-labels. This study divided eco-label information presentation into two categories: SPEI and JPEI. This fills the gap in the research on eco-label information presentation or eco-label format while also enriching research on DCT. Some consumers have difficulty processing and understanding eco-labels [82]. However, there is insufficient research on how to solve this problem. We introduced DCT into the eco-label field and proposed adding descriptive text to eco-labels based on the cognitive perspective. Participants' understanding of eco-labels was improved through the dual-coding JPEI approach. Previous research has similarly found that consumers usually prefer specific, detailed eco-information [83,84]. JPEI can also give consumers specific, detailed information, which reduces cognitive difficulty of eco-labels, especially for those who lack eco-label knowledge.

Second, we identified a spatial contiguity effect of JPEI, which not only provides a theoretical basis for the spatial distribution of eco-label information presentation, but also expands the application field of the spatial contiguity effect. In the past, the spatial contiguity effect has been mainly applied to multimedia learning [52,56], psychology [85], and other fields. We applied this theory to eco-labels to demonstrate the optimal spatial distance in JPEI. Previous research on eco-label positioning focused on the position of eco-labels on packaging based on the visibility perspective. For example, Gutierrez et al. [86] found that placing an eco-label in the center of a package better attracted visual attention. Carrero et al. [28], meanwhile, suggested that placing an eco-label in front of or near the nutritional information could make eco-labels more noticeable. Those studies, however, were mainly based on SPEI (i.e., a single eco-label icon), and they addressed visual attention to the eco-label but not the cognition of the eco-label. They also neglected the effect of the distance between the eco-label icon and other eco-label elements. We have, to some extent, filled this research gap. This study can also be extended to research on brand logos or other visual symbols. For example, based on our conclusions, for a brand logo with low popularity, it should be accompanied by a textual description of the brand, and the two should be placed close to each other.

Finally, we found a matching effect between the JPEI type and consumers' construal level when consumers' eco-label knowledge was low, which not only provides theoretical

support for the design of eco-label information presentation content, but also extends the application of construal level theory. Previous research on eco-label information has compared the effectiveness of text and icons. For example, Rihn et al. [12] found that eco-label icons attract more visual attention and a relatively higher payment premium than textual eco-labels. However, no previous studies have explored the combined effect of icons and text or the explanatory role of eco-label text. Aiming to fill this gap, we classified descriptive eco-label text into functional and emotional categories and matched them with consumers' construal levels to explore the effects on cognition and consumption behavior.

7.2. Managerial Implications

First, eco-label certification institutions should add descriptive text to help inform consumers and reduce their search costs. When a new eco-label is introduced to a market or region, consumers have less knowledge about it and have more difficulty recognizing and understanding it if the format is simple and information is limited. JPEI can not only increase the cognition of eco-labels but also educate consumers, thus promoting green consumption. Eco-label certification institutions should ensure the spatial contiguity of the eco-label and text when designing eco-labels. Additionally, eco-label certification institutions should use different types of information—namely, functional and emotional—to match different construal levels among consumers.

Second, governments should call on certification institutions to optimize eco-label design and convey more eco-label information to consumers. We showed that increasing consumers' cognitive fluency in eco-labels can positively affect purchase intentions. Thus, popularizing eco-label knowledge and simplifying eco-label cognition for consumers can promote green consumption.

Finally, companies can choose eco-labels with more descriptive text, or they can independently add text adjacent to eco-labels when designing packaging to reduce consumers' cognitive difficulties. Companies should also consider consumers' construal level when establishing descriptive eco-label text. For consumers with a low construal level, functional text should be added; for those with a high construal level, emotional text should be used. Construal level can be either a long-term mindset or an induced temporary mindset [63]. Companies can use machine learning to quickly and effectively identify consumers with different construal levels based on their online behavior data [87]. Companies can also collect information from consumers and build consumer profiles to help identify consumers with different construal levels [60,88]. Alternatively, some elements can be used to induce consumers to form a specific construal level, such as using language or imagery that indicates the present or the future [63] or manipulating the visual height of advertising images [89].

7.3. Limitations and Future Research

This study has some limitations. First, we use a subjective measure for eco-label knowledge, and it is difficult to know whether the text information improved actual comprehension of the eco-label information. Future studies could use an objective measure of consumer eco-label knowledge to verify if the same results can be obtained. Second, our study was conducted in China, so it is uncertain whether the results can be generalized to other countries. Future studies could revalidate our results in other countries. Third, we mainly focused on eco-labels with low cognition, which may be in the early stages of development or newly introduced in a certain country, region, or market. We therefore need to further explore whether adding descriptive eco-label text will increase consumers' cognitive load and cause some negative effects when eco-labels have reached the mature stage of development. Fourth, the descriptive eco-label text used in this study mainly included information such as the full name of the eco-label, certification institutions, certification standards, or principles. We need to explore whether too much descriptive text increases cognitive load or whether too little fails to improve cognitive fluency. In addition, given the limited space on packaging, would a QR code associated with the eco-label be

more practical? Or would it not produce equivalent effects for low-knowledge consumers? Fifth, the complexity of other elements on the package can also affect how consumers respond to JPEI. For example, too many other information elements may interfere with the consumers' processing of JPEI. Finally, some demographic variables may influence consumers' willingness to purchase green products, such as gender, age, and education. This study did not take them into account as covariates in our model. Future studies could add this aspect to be considered.

8. Conclusions

This study's findings can provide insights for improving the use of eco-labels. From the producer's perspective, eco-labels are a tool for communicating the green attributes of products and services. However, from the consumer's perspective, many eco-labels do not communicate effectively. We therefore proposed JPEI, which can improve consumers' cognitive fluency in eco-labels. Study 1 confirmed H1a and H1b, that is, for consumers with low eco-label knowledge, JPEI enhanced cognitive fluency more so than SPEI. Study 2 further verified the effect of spatial distance (H2a and H2b). For consumers with low eco-label knowledge, spatially contiguous JPEI could improve cognitive fluency more than spatially partitioned JPEI. This in turn significantly affected purchase intentions, but there was no significant difference for consumers with high eco-label knowledge. Study 3 explored the effect of the JPEI type among consumers with low eco-label knowledge (H3a and H3b). Functional JPEI matched more with low-construal consumers, and emotional JPEI matched more with high-construal consumers. Such matching improved participants' cognitive fluency in eco-labels and increased their willingness to purchase the product.

Supplementary Materials: The following supporting information can be downloaded at: <https://www.mdpi.com/article/10.3390/ijerph192013713/s1>. Supplementary Material A: The Stimuli of Study 1 and Follow-up Study; Supplementary Material B: The Stimuli of Study 2 and Follow-up studies; Supplementary Material C: The Stimuli of Study 3; Supplementary Material D: Measurement Items; Supplementary Material E: Demographic Variables; Figure S1: The interactive effect of eco-label information presentation and consumer's eco-label knowledge (the follow-up of Study 1); Figure S2: The interactive effect of JPEI spatial distance and consumer's eco-label knowledge on cognitive fluency (Study 2 Follow-up A); Figure S3: The interactive effect of JPEI spatial distance and consumer's eco-label knowledge on purchase intention (Study 2 Follow-up A); Figure S4: Results of moderated mediation effect (Study 2 Follow-up A); Figure S5: The interactive effect of JPEI spatial distance and consumer's eco-label knowledge on cognitive fluency (Study 2 Follow-up B); Figure S6: The interactive effect of JPEI spatial distance and consumer's eco-label knowledge on purchase intention (Study 2 Follow-up B); Figure S7: Results of moderated mediation effect (Study 2 Follow-up B); Figure S8: The interactive effect of JPEI spatial distance and consumer's eco-label knowledge on cognitive fluency (Study 2 Follow-up C); Figure S9: The interactive effect of JPEI spatial distance and consumer's eco-label knowledge on purchase intention (Study 2 Follow-up C); Figure S10: Results of moderated mediation effect (Study 2 Follow-up C); Table S1. Demographic Variables.

Author Contributions: Conceptualization, X.W., Y.D., Y.L. and S.W.; methodology, X.W. and Y.D.; software, X.W., Y.D. and Y.L.; validation, X.W., Y.D., Y.L. and S.W.; formal analysis, X.W., Y.D., Y.L. and S.W.; investigation, X.W., Y.D., Y.L. and S.W.; resources, X.W.; data curation, X.W., Y.D., Y.L. and S.W.; writing—original draft preparation, X.W., Y.D. and Y.L.; writing—review and editing, X.W., Y.D., Y.L. and S.W.; visualization, X.W., Y.D., Y.L. and S.W.; supervision, X.W. and Y.D.; project administration, X.W.; funding acquisition, X.W. All authors have read and agreed to the published version of the manuscript.

Funding: This research was funded by Humanities and Social Science Planning Fund Project of the Ministry of Education of China, grant number 22YJA630092; Key Technology Research and Development Program of Shandong, China, grant number 2016CYJS1A01-3.

Institutional Review Board Statement: Because of the observational nature of the study, and in the absence of any involvement of therapeutic medication, no formal approval of the Institutional Review Board of the local Ethics Committee was required. Nonetheless, all subjects were informed about the

study, and participation was on a fully voluntary basis. Participants were assured of confidentiality and anonymity of the information associated with the surveys.

Informed Consent Statement: Informed consent was obtained from all subjects involved in the study.

Data Availability Statement: Due to the confidentiality of the subjects' privacy, data can be obtained by contacting the authors.

Conflicts of Interest: The authors declare no conflict of interest.

References

1. Donato, C.; Adigüzel, F. Visual Complexity of Eco-Labels and Product Evaluations in Online Setting: Is Simple Always Better? *J. Retail. Consum. Serv.* **2022**, *67*, 102961. [[CrossRef](#)]
2. Horne, R.E. Limits to Labels: The Role of Eco-Labels in the Assessment of Product Sustainability and Routes to Sustainable Consumption. *Int. J. Consum. Stud.* **2009**, *33*, 175–182. [[CrossRef](#)]
3. Sigurdsson, V.; Larsen, N.M.; Pálsdóttir, R.G.; Folwarczny, M.; Menon, R.G.V.; Fagerström, A. Increasing the Effectiveness of Ecological Food Signaling: Comparing Sustainability Tags with Eco-Labels. *J. Bus. Res.* **2022**, *139*, 1099–1110. [[CrossRef](#)]
4. Taufique, K.M.R.; Polonsky, M.J.; Vocino, A.; Siwar, C. Measuring Consumer Understanding and Perception of Eco-Labeling: Item Selection and Scale Validation. *Int. J. Consum. Stud.* **2019**, *43*, 298–314. [[CrossRef](#)]
5. Song, L.; Lim, Y.; Chang, P.; Guo, Y.; Zhang, M.; Wang, X.; Yu, X.; Lehto, M.R.; Cai, H. Ecolabel's Role in Informing Sustainable Consumption: A Naturalistic Decision Making Study Using Eye Tracking Glasses. *J. Clean. Prod.* **2019**, *218*, 685–695. [[CrossRef](#)]
6. Bratt, C.; Hallstedt, S.; Robèrt, K.-H.; Broman, G.; Oldmark, J. Assessment of Eco-Labeling Criteria Development from a Strategic Sustainability Perspective. *J. Clean. Prod.* **2011**, *19*, 1631–1638. [[CrossRef](#)]
7. Liu, Q.; Yan, Z.; Zhou, J. Consumer Choices and Motives for Eco-Labeled Products in China: An Empirical Analysis Based on the Choice Experiment. *Sustainability* **2017**, *9*, 331. [[CrossRef](#)]
8. Higgins, K.; Hutchinson, W.G.; Longo, A. Willingness-to-Pay for Eco-Labelled Forest Products in Northern Ireland: An Experimental Auction Approach. *J. Behav. Exp. Econ.* **2020**, *87*, 101572. [[CrossRef](#)]
9. Sörqvist, P.; Marsh, J.E.; Holmgren, M.; Hulme, R.; Haga, A.; Seager, P.B. Effects of Labeling a Product Eco-Friendly and Genetically Modified: A Cross-Cultural Comparison for Estimates of Taste, Willingness to Pay and Health Consequences. *Food Qual. Prefer.* **2016**, *50*, 65–70. [[CrossRef](#)]
10. Waris, I.; Ahmed, W. Empirical Evaluation of the Antecedents of Energy-Efficient Home Appliances: Application of Extended Theory of Planned Behavior. *MEQ* **2020**, *31*, 915–930. [[CrossRef](#)]
11. Zhang, X.; Yin, H.; Zhao, R. Consumer Willingness to Pay for Eco-Labels in China: A Choice Experiment Approach. *J. Manag. Anal.* **2021**, *8*, 673–692. [[CrossRef](#)]
12. Rihn, A.; Wei, X.; Khachatryan, H. Text vs. Logo: Does Eco-Label Format Influence Consumers' Visual Attention and Willingness-to-Pay for Fruit Plants? An Experimental Auction Approach. *J. Behav. Exp. Econ.* **2019**, *82*, 101452. [[CrossRef](#)]
13. Taufique, K.M.R.; Siwar, C.; Talib, B.; Sarah, F.H.; Chamhuri, N. Synthesis of Constructs for Modeling Consumers' Understanding and Perception of Eco-Labels. *Sustainability* **2014**, *6*, 2176–2200. [[CrossRef](#)]
14. Brécard, D. Consumer Confusion over the Profusion of Eco-Labels: Lessons from a Double Differentiation Model. *Resour. Energy Econ.* **2014**, *37*, 64–84. [[CrossRef](#)]
15. Nugraha, W.S.; Chen, D.; Yang, S.-H. The Effect of a Halal Label and Label Size on Purchasing Intent for Non-Muslim Consumers. *J. Retail. Consum. Serv.* **2022**, *65*, 102873. [[CrossRef](#)]
16. Taufique, K.M.R.; Vocino, A.; Polonsky, M.J. The Influence of Eco-Label Knowledge and Trust on pro-Environmental Consumer Behaviour in an Emerging Market. *J. Strateg. Mark.* **2017**, *25*, 511–529. [[CrossRef](#)]
17. Delmas, M.A.; Lessem, N. Eco-Premium or Eco-Penalty? Eco-Labels and Quality in the Organic Wine Market. *Bus. Soc.* **2015**, *56*, 318–356. [[CrossRef](#)]
18. Donato, C.; D'Aniello, A. Tell Me More and Make Me Feel Proud: The Role of Eco-Labels and Informational Cues on Consumers' Food Perceptions. *Brit. Food J.* **2021**, *124*, 1365–1382. [[CrossRef](#)]
19. Dhir, A.; Sadiq, M.; Talwar, S.; Sakashita, M.; Kaur, P. Why Do Retail Consumers Buy Green Apparel? A Knowledge-Attitude-Behaviour-Context Perspective. *J. Retail. Consum. Serv.* **2021**, *59*, 102398. [[CrossRef](#)]
20. Kumar, S.; Murphy, M.; Talwar, S.; Kaur, P.; Dhir, A. What Drives Brand Love and Purchase Intentions toward the Local Food Distribution System? A Study of Social Media-Based REKO (Fair Consumption) Groups. *J. Retail. Consum. Serv.* **2021**, *60*, 102444. [[CrossRef](#)]
21. Paivio, A. Dual Coding Theory: Retrospect And Current Status. *Can. J. Psychol./Rev. Can. De Psychol.* **1991**, *45*, 255–287. [[CrossRef](#)]
22. Matthes, J.; Wonneberger, A.; Schmuck, D. Consumers' Green Involvement and the Persuasive Effects of Emotional versus Functional Ads. *J. Bus. Res.* **2014**, *67*, 1885–1893. [[CrossRef](#)]
23. Vekiri, I. What Is the Value of Graphical Displays in Learning? *Educ. Psychol. Rev.* **2002**, *14*, 261–312. [[CrossRef](#)]
24. Mayer, R.E.; Gallini, J.K. When Is an Illustration Worth Ten Thousand Words? *J. Educ. Psychol.* **1990**, *82*, 715–726. [[CrossRef](#)]
25. Mayer, R.E. Using Multimedia for E-learning. *J. Comput. Assist. Learn.* **2017**, *33*, 403–423. [[CrossRef](#)]

26. D'Souza, C.; Taghian, M.; Lamb, P. An Empirical Study on the Influence of Environmental Labels on Consumers. *Corp. Commun. Int. J.* **2006**, *11*, 162–173. [[CrossRef](#)]
27. van Amstel, M.; Driessen, P.; Glasbergen, P. Eco-Labeling and Information Asymmetry: A Comparison of Five Eco-Labels in the Netherlands. *J. Clean. Prod.* **2008**, *16*, 263–276. [[CrossRef](#)]
28. Carrero, I.; Valor, C.; Diaz, E.; Labajo, V. Designed to Be Noticed: A Reconceptualization of Carbon Food Labels as Warning Labels. *Sustainability* **2021**, *13*, 1581. [[CrossRef](#)]
29. Sharma, N.K.; Kushwaha, G.S. Eco-Labels: A Tool for Green Marketing or Just a Blind Mirror for Consumers. *Electron. Green J.* **2019**, *1*. [[CrossRef](#)]
30. Thøgersen, J. Psychological Determinants of Paying Attention to Eco-Labels in Purchase Decisions: Model Development and Multinational Validation. *J. Consum. Policy* **2000**, *23*, 285–313. [[CrossRef](#)]
31. Schwarz, N. Metacognitive Experiences in Consumer Judgment and Decision Making. *J. Consum. Psychol.* **2004**, *14*, 332–348. [[CrossRef](#)]
32. Lee, A.Y.; Labroo, A.A. The Effect of Conceptual and Perceptual Fluency on Brand Evaluation. *J. Mark. Res.* **2004**, *41*, 151–165. [[CrossRef](#)]
33. Zou, J.; Tang, Y.; Qing, P.; Li, H.; Razzaq, A. Donation or Discount: Effect of Promotion Mode on Green Consumption Behavior. *Int. J. Environ. Res. Public Health* **2021**, *18*, 1912. [[CrossRef](#)]
34. Jaud, D.A.; Melnyk, V. The Effect of Text-Only versus Text-and-Image Wine Labels on Liking, Taste and Purchase Intentions. The Mediating Role of Affective Fluency. *J. Retail. Consum. Serv.* **2020**, *53*, 101964. [[CrossRef](#)]
35. Kim, S.-B.; Kim, K.J.; Kim, D.-Y. Exploring the Effective Restaurant CrM Ad: The Moderating Roles of Advertising Types and Social Causes. *Int. J. Contemp. Hosp. Manag.* **2016**, *28*, 2473–2492. [[CrossRef](#)]
36. Sahin, S.; Baloglu, S.; Topcuoglu, E. The Influence of Green Message Types on Advertising Effectiveness for Luxury and Budget Hotel Segments. *Cornell. Hosp. Q.* **2020**, *61*, 443–460. [[CrossRef](#)]
37. Lee, K.; Choi, J. Image-Text Inconsistency Effect on Product Evaluation in Online Retailing. *J. Retail. Consum. Serv.* **2019**, *49*, 279–288. [[CrossRef](#)]
38. Lee, W.-K.; Wu, C.-J. Eye Movements in Integrating Geometric Text and Figure: Scanpaths and Given-New Effects. *Int. J. Sci. Math. Educ.* **2018**, *16*, 699–714. [[CrossRef](#)]
39. Mayer, R.E.; Sims, V.K. For Whom Is a Picture Worth a Thousand Words? Extensions of a Dual-Coding Theory of Multimedia Learning. *J. Educ. Psychol.* **1994**, *86*, 389–401. [[CrossRef](#)]
40. Griffin, M.M.; Robinson, D.H. Role of Mimeticism and Spatiality in Textual Recall. *Contemp. Educ. Psychol.* **2000**, *25*, 125–149. [[CrossRef](#)]
41. Schwartz, N.H.; Ellsworth, L.S.; Graham, L.; Knight, B. Accessing Prior Knowledge to Remember Text: A Comparison of Advance Organizers and Maps. *Contemp. Educ. Psychol.* **1998**, *23*, 65–89. [[CrossRef](#)] [[PubMed](#)]
42. Dodd, T.H.; Laverie, D.A.; Wilcox, J.F.; Duhan, D.F. Differential Effects of Experience, Subjective Knowledge, and Objective Knowledge on Sources of Information Used in Consumer Wine Purchasing. *J. Hosp. Tour. Res.* **2005**, *29*, 3–19. [[CrossRef](#)]
43. Wang, H.; Ma, B.; Bai, R. How Does Green Product Knowledge Effectively Promote Green Purchase Intention? *Sustainability* **2019**, *11*, 1193. [[CrossRef](#)]
44. Chuang, S.-C.; Tsai, C.-C.; Cheng, Y.-H.; Sun, Y.-C. The Effect of Terminologies on Attitudes Toward Advertisements and Brands: Consumer Product Knowledge as a Moderator. *J. Bus. Psychol.* **2009**, *24*, 485–491. [[CrossRef](#)]
45. Kumar, P.; Polonsky, M.; Dwivedi, Y.K.; Kar, A. Green Information Quality and Green Brand Evaluation: The Moderating Effects of Eco-Label Credibility and Consumer Knowledge. *Eur. J. Mark.* **2021**, *55*, 2037–2071. [[CrossRef](#)]
46. Hong, J.; Sternthal, B. The Effects of Consumer Prior Knowledge and Processing Strategies on Judgments. *J. Mark. Res.* **2010**, *47*, 301–311. [[CrossRef](#)]
47. Naderi, I.; Paswan, A.K.; Guzman, F. Beyond the Shadow of a Doubt: The Effect of Consumer Knowledge on Restaurant Evaluation. *J. Retail. Consum. Serv.* **2018**, *45*, 221–229. [[CrossRef](#)]
48. Taufique, K.M.R.; Siwar, C.B.; Talib, B.B.A.; Chamhuri, N. Modelling Consumers' Environmental Responsibility and Understanding of Eco-Labels: A Conceptual Framework for Empirical Research in Malaysia. *Int. J. Green Econ.* **2014**, *8*, 199. [[CrossRef](#)]
49. Zhang, Z.; Qiao, S.; Chen, Y.; Zhang, Z. Effects of Spatial Distance on Consumers' Review Effort. *Ann. Tour. Res.* **2022**, *94*, 103406. [[CrossRef](#)]
50. Florax, M.; Ploetzner, R. What Contributes to the Split-Attention Effect? The Role of Text Segmentation, Picture Labelling, and Spatial Proximity. *Learn. Instr.* **2010**, *20*, 216–224. [[CrossRef](#)]
51. Ginn, P. Integrating Information: A Meta-Analysis of the Spatial Contiguity and Temporal Contiguity Effects. *Learn. Instr.* **2006**, *16*, 511–525. [[CrossRef](#)]
52. Schroeder, N.L.; Cenkcı, A.T. Spatial Contiguity and Spatial Split-Attention Effects in Multimedia Learning Environments: A Meta-Analysis. *Educ. Psychol. Rev.* **2018**, *30*, 679–701. [[CrossRef](#)]
53. Glaser, M.; Knoos, M.; Schwan, S. The Closer, the Better? Processing Relations between Picture Elements in Historical Paintings. *J. Eye Mov. Res.* **2020**, *13*, 1–14. [[CrossRef](#)]
54. Cierniak, G.; Scheiter, K.; Gerjets, P. Explaining the Split-Attention Effect: Is the Reduction of Extraneous Cognitive Load Accompanied by an Increase in Germane Cognitive Load? *Comput. Hum. Behav.* **2009**, *25*, 315–324. [[CrossRef](#)]

55. Hu, J.; Zhang, J. The Effect of Cue Labeling in Multimedia Learning: Evidence From Eye Tracking. *Front. Psychol.* **2021**, *12*, 736922. [[CrossRef](#)]
56. Mayer, R.E. The Promise of Multimedia Learning: Using the Same Instructional Design Methods across Different Media. *Learn. Instr.* **2003**, *13*, 125–139. [[CrossRef](#)]
57. Pihko, E.; Virtanen, A.; Saarinen, V.-M.; Pannasch, S.; Hirvenkari, L.; Tossavainen, T.; Haapala, A.; Hari, R. Experiencing Art: The Influence of Expertise and Painting Abstraction Level. *Front. Hum. Neurosci.* **2011**, *5*, 94. [[CrossRef](#)]
58. Trope, Y.; Liberman, N. Construal-Level Theory of Psychological Distance. *Psychol. Rev.* **2010**, *117*, 440–463. [[CrossRef](#)]
59. Dhar, R.; Kim, E.Y. Seeing the Forest or the Trees: Implications of Construal Level Theory for Consumer Choice. *J. Consum. Psychol.* **2007**, *17*, 96–100. [[CrossRef](#)]
60. Dogan, M.; Erdogan, B.Z. Effects of Congruence between Individuals’ and Hotel Commercial’s Construal Levels on Purchase Intentions. *J. Hosp. Market. Manag.* **2020**, *29*, 987–1007. [[CrossRef](#)]
61. Wright, S.; Manolis, C.; Brown, D.; Guo, X.; Dinsmore, J.; Chiu, C.-Y.P.; Kardes, F.R. Construal-Level Mind-Sets and the Perceived Validity of Marketing Claims. *Market. Lett.* **2012**, *23*, 253–261. [[CrossRef](#)]
62. Kim, K.; Lee, S.; Choi, Y.K. Image Proximity in Advertising Appeals: Spatial Distance and Product Types. *J. Bus. Res.* **2019**, *99*, 490–497. [[CrossRef](#)]
63. Gong, S.; Sheng, G.; Peverelli, P.; Dai, J. Green Branding Effects on Consumer Response: Examining a Brand Stereotype-Based Mechanism. *J. Prod. Brand Manag.* **2021**, *30*, 1033–1046. [[CrossRef](#)]
64. Hartmann, P.; Apaolaza Ibáñez, V.; Forcada Sainz, F.J. Green Branding Effects on Attitude: Functional versus Emotional Positioning Strategies. *Mark. Intell. Plan.* **2005**, *23*, 9–29. [[CrossRef](#)]
65. Searles, K. Feeling Good and Doing Good for the Environment: The Use of Emotional Appeals in pro-Environmental Public Service Announcements. *Appl. Environ. Educ. Commun.* **2010**, *9*, 173–184. [[CrossRef](#)]
66. Gong, S.; Lu, J.G.; Schaubroeck, J.M.; Li, Q.; Zhou, Q.; Qian, X. Polluted Psyche: Is the Effect of Air Pollution on Unethical Behavior More Physiological or Psychological? *Psychol. Sci.* **2020**, *31*, 1040–1047. [[CrossRef](#)] [[PubMed](#)]
67. Gai, P.J.; Puntoni, S. Language and Consumer Dishonesty: A Self-Diagnosticity Theory. *J. Consum. Res.* **2021**, *48*, 333–351. [[CrossRef](#)]
68. Zhou, Y.; Fei, Z.; He, Y.; Yang, Z. How Human–Chatbot Interaction Impairs Charitable Giving: The Role of Moral Judgment. *J. Bus. Ethics* **2022**, *178*, 849–865. [[CrossRef](#)]
69. Tan, Q.; Imamura, K.; Nagasaka, K.; Inoue, M. Effects of Eco-Label Knowledge on Chinese Consumer Preferences for Certified Wood Flooring: A Case Study in Chongqing City. *Forest. Prod. J.* **2019**, *69*, 329–336. [[CrossRef](#)]
70. Kwon, O.; Kim, C.; Kim, G. Factors Affecting the Intensity of Emotional Expressions in Mobile Communications. *Online Inform. Rev.* **2013**, *37*, 114–131. [[CrossRef](#)]
71. McAndrew, F.T.; De Jonge, C.R. Electronic Person Perception: What Do We Infer About People from the Style of Their E-Mail Messages? *Soc. Psychol. Pers. Sci.* **2011**, *2*, 403–407. [[CrossRef](#)]
72. Aagerup, U.; Frank, A.-S.; Hultqvist, E. The Persuasive Effects of Emotional Green Packaging Claims. *Brit Food J.* **2019**, *121*, 3233–3246. [[CrossRef](#)]
73. Chang, C. The Interplay of Product Class Knowledge and Trial Experience in Attitude Formation. *J. Advert.* **2004**, *33*, 83–92. [[CrossRef](#)]
74. Lee, A.Y.; Aaker, J.L. Bringing the Frame into Focus: The Influence of Regulatory Fit on Processing Fluency and Persuasion. *J. Personal. Soc. Psychol.* **2004**, *86*, 205–218. [[CrossRef](#)] [[PubMed](#)]
75. Hayes, A.F. *Introduction to Mediation, Moderation, and Conditional Process Analysis: A Regression-Based Approach*; Guilford Publications: New York, NY, USA, 2017; ISBN 978-1-60918-230-4.
76. Spiller, S.A.; Fitzsimons, G.J.; Lynch, J.G.; McClelland, G.H. Spotlights, Floodlights, and the Magic Number Zero: Simple Effects Tests in Moderated Regression. *J. Mark. Res.* **2013**, *50*, 277–288. [[CrossRef](#)]
77. Dodds, W.B.; Monroe, K.B.; Grewal, D. Effects of Price, Brand, and Store Information on Buyers’ Product Evaluations. *J. Mark. Res.* **1991**, *28*, 307–319. [[CrossRef](#)]
78. Shimokawa, S.; Hu, D.; Li, D.; Cheng, H. The Urban–Rural Gap in the Demand for Food Safety in China: The Role of Food Label Knowledge. *Agric. Econ.* **2021**, *52*, 175–193. [[CrossRef](#)]
79. Freitas, A.L.; Gollwitzer, P.; Trope, Y. The Influence of Abstract and Concrete Mindsets on Anticipating and Guiding Others’ Self-Regulatory Efforts. *J. Exp. Soc. Psychol.* **2004**, *40*, 739–752. [[CrossRef](#)]
80. Vallacher, R.R.; Wegner, D.M. Levels of Personal Agency: Individual Variation in Action Identification. *J. Pers. Soc. Psychol.* **1989**, *57*, 660–671. [[CrossRef](#)]
81. Septianto, F.; Lee, M.S.W.; Putra, P.G. Everyday “Low Price” or Everyday “Value”? The Interactive Effects of Framing and Construal Level on Consumer Purchase Intentions. *J. Retail. Consum. Serv.* **2021**, *58*, 102317. [[CrossRef](#)]
82. Cohen, M.A.; Vandenberg, M.P. The Potential Role of Carbon Labeling in a Green Economy. *Energy Econ.* **2012**, *34*, S53–S63. [[CrossRef](#)]
83. Cho, Y.-N. Different Shades of Green Consciousness: The Interplay of Sustainability Labeling and Environmental Impact on Product Evaluations. *J. Bus. Ethics* **2015**, *128*, 73–82. [[CrossRef](#)]
84. Engels, S.V.; Hansmann, R.; Scholz, R.W. Toward a Sustainability Label for Food Products: An Analysis of Experts’ and Consumers’ Acceptance. *Ecol. Food Nutr.* **2010**, *49*, 30–60. [[CrossRef](#)]

85. Roodenrys, K.; Agostinho, S.; Roodenrys, S.; Chandler, P. Managing One's Own Cognitive Load when Evidence of Split Attention Is Present. *Appl. Cogn. Psych.* **2012**, *26*, 878–886. [[CrossRef](#)]
86. Gutierrez, A.M.J.; Chiu, A.S.F.; Seva, R. A Proposed Framework on the Affective Design of Eco-Product Labels. *Sustainability* **2020**, *12*, 3234. [[CrossRef](#)]
87. Wang, X.; Liu, Y.; Wang, S.; Chen, H.A. Keep It Vague? New Product Preannouncement, Regulatory Focus, and Word-of-Mouth. *J. Retail. Consum. Serv.* **2022**, *65*, 102847. [[CrossRef](#)]
88. Yao, F.-S.; Shao, J.-B.; Zhang, H. Is Creative Description Always Effective in Purchase Intention? The Construal Level Theory as a Moderating Effect. *Front. Psychol.* **2021**, *12*, 619340. [[CrossRef](#)]
89. Roose, G.; Vermeir, I.; Geuens, M.; Van Kerckhove, A. A Match Made in Heaven or down under? The Effectiveness of Matching Visual and Verbal Horizons in Advertising. *J. Consum. Psychol.* **2019**, *29*, 411–427. [[CrossRef](#)]



Article

Global Ban on Plastic and What Next? Are Consumers Ready to Replace Plastic with the Second-Generation Bioplastic? Results of the Snowball Sample Consumer Research in China, Western and Eastern Europe, North America and Brazil

Ewa Kochanska ^{1,*}, Katarzyna Wozniak ¹, Agnieszka Nowaczyk ¹, Patrícia J. Piedade ², Marilena Lino de Almeida Lavorato ³, Alexandre Marcelo Almeida ⁴, Ana Rita C. Morais ⁵ and Rafal M. Lukasiak ²

¹ Research and Innovation Center Pro-Akademia, 9/11 Innowacyjna Str., 95-050 Konstancin Łódzki, Poland

² Unidade de Bioenergia e Biorrefinarias, Laboratório Nacional de Energia e Geologia I.P., Estrada do Paço do Lumiar 22, 1649-038 Lisboa, Portugal

³ BISA Benchmarking Inteligência Sustentável, Av. Nove de Julho—Bela Vista, São Paulo CEP 01313-001, Brazil

⁴ Commitment Prestação Serviços, São Paulo CEP 05844-120, Brazil

⁵ School of Engineering, The University of Kansas, 4165E Learned Hall, Lawrence, KS 66045, USA

* Correspondence: ewa.kochanska@proakademia.eu

Citation: Kochanska, E.; Wozniak, K.; Nowaczyk, A.; Piedade, P.J.; de Almeida Lavorato, M.L.; Almeida, A.M.; Morais, A.R.C.; Lukasiak, R.M. Global Ban on Plastic and What Next? Are Consumers Ready to Replace Plastic with the Second-Generation Bioplastic? Results of the Snowball Sample Consumer Research in China, Western and Eastern Europe, North America and Brazil. *Int. J. Environ. Res. Public Health* **2022**, *19*, 13970. <https://doi.org/10.3390/ijerph192113970>

Academic Editors: Roberto Alonso González Lezcano, Francesco Nocera, Rosa Giuseppina Caponetto and Paul B. Tchounwou

Received: 5 September 2022

Accepted: 18 October 2022

Published: 27 October 2022



Copyright: © 2022 by the authors. Licensee MDPI, Basel, Switzerland. This article is an open access article distributed under the terms and conditions of the Creative Commons Attribution (CC BY) license (<https://creativecommons.org/licenses/by/4.0/>).

Abstract: Plastic can be used for many things and at the same time is the most versatile material in our modern world. However, the uncontrolled and unprecedented use of plastic comes to its end. The global ban on plastic brings significant changes in technology but even more so in civil perception—changes taking place before our eyes. The aim of this study was to find answers to the questions about the readiness of consumers for a global ban on plastic. Within the research, the differences in consumer acceptance in countries in Europe, South and North America and Asia and the expression of social readiness to change attitudes towards plastic food packaging were analyzed. This work sketches the legal framework related to limiting the use of one-use food packaging made of fossil raw materials at the level of the European Union, Poland and Portugal but also at the level of the two largest economies in the world, China and the United States, as well as lower-income countries, e.g., Ukraine and Brazil. The survey results were analyzed using descriptive and inferential statistics. The performed study demonstrates that, in all the surveyed countries, appropriate legal acts related to the reduction of plastic in everyday life are already in place. Furthermore, this work demonstrates the full understanding of plastic banning in all surveyed countries. Consumers are aware that every effort should be made to prevent the world from drowning in plastic waste. Society is, in general, open to the use of bioplastics produced from the second-generation resource if second-generation bioplastics contribute to environmental and pollution reduction targets.

Keywords: bioplastic; food waste; consumer acceptance; snowball sampling

1. Introduction

As a global society, we are drowning in plastic garbage. There is so much of it in our cities, forests, seas and even in the air that the United Nations has declared a state of a plastic disaster on Earth [1]. The General Assembly of the United Nations asks the dramatic question: “Planet or Plastics?” and shows the rising numbers of the plastics catastrophe: 500,000,000,000 plastic bags are used each year, 13,000,000 tons of plastic leak into the ocean each year, 17,000,000 barrels of oil are used for plastic production each year, 1,000,000 plastic bottles are bought every minute and 50% of consumer plastics are single-use [1]. According to Atlas of Plastic [2], the planet could reach more than 600 million tons of plastic produced annually by 2025. The vast majority of it ends up as waste. Therefore, there are significant efforts made to find environmentally friendly materials that can replace the crude-oil-origin plastics but are, at the same time, as functional and cheap as classical

ones. Yet, the main challenge towards this goal is to develop the final environmentally friendly product and to produce it from raw materials other than cereals or potatoes, which should primarily be dedicated to food or feed uses. The circular economy concept refers to an economy that uses a systems-focused approach and involves industrial processes and economic activities that are restorative or regenerative by design and aim to keep products, components and materials at their highest utility and value at all times [3]. Therefore, according to the circular economy concept, the waste is at the center of the intensive research for a technology dedicated to bioplastics production.

Due to the fact that the largest user of plastic is the packaging sector, and food packaging accounts for about 40% of it [4], it is crucial to understand the needs of this sector in bioplastic development. Although bioplastic has been known as an environmentally friendly material for more than 70 years [5], still, the definition from a technical and material point of view is neither simple nor unambiguous. The term of “bioplastics” is used interchangeably with “biodegradable polymers”. Bioplastics are defined as materials produced from raw materials other than fossil fuels, especially crude oil, coal and lignite, and which are degraded naturally with the assistance of microorganisms in aerobic or anaerobic processes [6]. According to the European Bioplastics association [7], from a technical point of view, bioplastics can be divided into three main groups, as sketched in Figure 1:

1. Bio-based or partially bio-based but non-biodegradable materials such as bio-based polyethylene (PE), polypropylene (PP) or poly(ethylene terephthalate) (PET) (so-called “drop-ins”) and bio-based technical performance polymers such as poly(trimethylene terephthalate) (PTT) or thermoplastic copolyester elastomer (TPC-ET);
2. bio-based and biodegradable material, such as poly(lactic acid) (PLA), poly(hydroxyalkanoate) (PHA) and poly(butylene succinate) (PBS);
3. fossil-based but biodegradable material, such as poly(butylene adipate terephthalate) (PBAT).

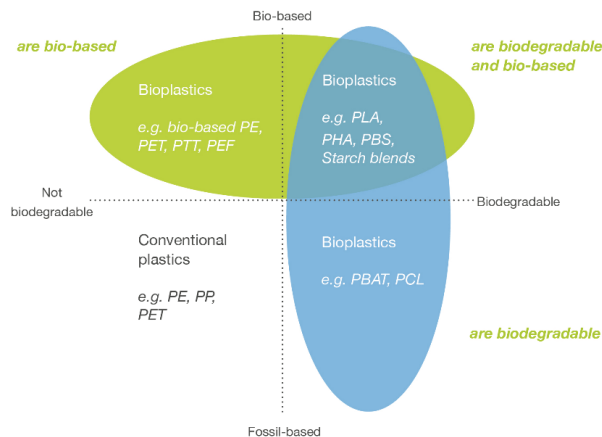


Figure 1. Material coordinate system of bioplastics [8].

As long as food and feed-like raw materials should be avoided for bioplastics production, there exists a strong need to seek alternative feedstock [9]. As stated above, one of the solutions might be to use wastes. However, the recent changes in the view of the economy as circular [3] renders the determination of some materials as wastes very complex and never straightforward [10]. Some materials called wastes in the past, e.g., organic fractions of municipal wastes, agriculture leftovers, etc., lost their attributes as they became relevant feedstocks for the energy and fine chemical sectors [11]. The food wastes bring another uncertainty in terms of definition. The food wastes are defined as the surplus of traded

food that leads to its waste in the stages of retail sale, catering and households, which is understood as a reduction in the weight of food that was destined for consumption by humans [12]. The importance of the prevention of food losses and the creation of food waste is expressed in the “Farm to Fork Strategy” [13]. The European Commission states that the avoidance of the food loss and waste is key to achieving sustainability. Consumers, as the participants of the food chain production, are to play an important role in the implementation of this strategy. It is worth stressing that, in Europe, around 40% of food waste occurs at the consumer level [13]. The use of the intelligent and active food packaging [14] might be considered a useful tool to sort out this problem. Yet, the use of food wastes to deliver new food packaging materials requires a lot of effort in ensuring the consumer perception as well as legislative adaptations regarding the use of waste-derived plastics. Present-day food marketing focuses on the positive impact on health or well-being and on paying attention to the environmentally friendly approach and technology used to produce the food [15–20]. However, a ground-breaking approach to build up the social acceptance in food marketing is appealing to the idea of recycling food waste and bringing food waste back into the food loop. Another challenge is to highlight the environmental benefits to make them vital to the ordinary citizen, convincing her/him to accept bio-packaging for food at a higher price than cheaper traditional fossil counterparts. It is especially relevant as “sustainable” decision making is not always effective [21,22]. For example, unwrapping the food may be fueling, rather than combating, Europe’s food waste problem. [23]. According to this study, both packaging and waste doubled in the EU between 2004 and 2014. The solution does not seem to be to stop using packaging but rather to create better packaging characterized by lower environmental and social impacts.

Therefore, the main goal of this work is to answer the three main questions given in the title: Is there a global ban on plastic? What is the general social behavior in relation to the global exclusion of single-use plastics? Are consumers ready to replace plastic with the second-generation bio counterparts? This work addresses these challenges, especially in the context of better understanding to what extent consumers are guided in their everyday choices by concern regarding the environment and whether they would be willing to adopt new solutions based on waste in food packaging.

2. Material and Methods

The online survey methodology was used to achieve the objectives of this study. The snowball sampling method for collecting data within the research was implemented. The snowball sampling method [24], or, the sampling method with a chain reference, is widely used where the group covered by the research is imprecise or difficult to specify, e.g., when the sampling group should be composed of all inhabitants of the earth, excluding only small children for whom parents make decisions, and the question of when to select the most reliable persons/objects as the reliable and representative research test group is problematic [25]. Simultaneously, defined as a probability-free sampling technique, this method takes samples, as indicated by the researchers. In the case of this work, recommendations for the recruitment of the questionees were provided by the authors of this work. In the first step, by indicating their own questionees, they were asked to forward the link to the questionnaires and the survey to other friends, thus creating a sampling with a chain reference [26].

This approach allowed for taking advantage of information and communication technologies, especially in terms of timesaving. In addition, in the COVID-19 pandemic time, an online survey allowed for the avoidance of direct contact between the questionees and interviewers. A potential disadvantage of the online survey is a risk of fraud by, e.g., multiple answers by the same questionee or using bots as questionees. Considering that there is no competing interest for any anonymous questionee, the risk of potential fraud was judged as minimal. Hence, contemplating these aspects, the survey was performed using the Edito CMS platform to conduct activities related to the content sharing. The survey questionnaire was created in the Dynamic Surveys module, which is a part of the

Edito CMS platform. A questionnaire was designed as a single choice, and the questionee has an option to not respond to one or more questions.

The survey was made available on the RIC Pro-Akademia website and was prepared in English, Polish, Portuguese, Russian and Ukrainian by native speakers. The online survey was conducted worldwide between 16 June 2021 and 17 September 2021.

The survey was divided into three parts. The first part was the introductory note, which is as follows: The survey is carried out by the Pro-Akademia Research and Innovation Center in Konstantynów Łódzki. Its results will be included in the project for the production of modern, biodegradable food packaging. We want to investigate whether consumers of bread, cakes and cookies follow the idea of environmental protection in their consumer choices and whether they would be willing to support innovative environmental solutions. Bioplastic can be the best ecological alternative to plastic, mainly produced from crude oil. It can be produced from plant raw materials or from waste biomass and therefore can be safer for users and the environment.

The second part was focused on acquiring fundamental information about the socio-economic status of the questionee. The last part, composed of eight questions, was directly related to the use of bioplastics as food packaging material. The list of questions and possible answers is presented in Table 1.

Table 1. The list of questions and available answers of the online survey.

Question	Answer
Gender	Female Male Other Prefer not to answer
Age	Under 21 years old 21–64 years old Over 65 years old
Level of education	Primary Vocational Secondary Higher No answer
Economic status	Very good Good Average Bad Prefer not to answer
Place of residence	Village Town with up to 50,000 inhabitants City with 50,000 to 150,000 inhabitants City with 150,000 to 500,000 inhabitants City with more than 500,000 inhabitants
Who in your household makes purchasing decisions	Mostly me Me and another person Mostly another person
Are you interested in receiving survey results? If so, please provide your e-mail address.	Free text
Country of the questionee	Free text

Table 1. Cont.

Question	Answer
1. Would you support replacing traditional plastic food packaging with bioplastic packaging?	Yes No I have no opinion
2. Did you know that bioplastics can be made from leftover of bakery and confectionery products (e.g., bread, cakes ...)?	Yes No
3. Would it bother you to know that the bioplastic packaging, in which the bread is wrapped, is made of bakery and confectionery leftovers?	Yes No I have no opinion
4. Would you expect a clear notice on the bioplastic packaging that will allow you to choose between traditional plastic and biodegradable plastic?	Yes No I have no opinion
5. How much more would you be able to pay for a product packed in bioplastic?	Not able to extra cost Below 10% Between 10% and 20% Between 20% and 30% Between 30% and 40% More than 40%
6. Did you know that bioplastic can extend the life of a product and preserve its visual and taste properties?	Yes No
7. Would you share the knowledge about such packaging with others?	Yes No I have no opinion
8. Would you encourage others to use modern, environmentally friendly packaging?	Yes No I have no opinion

The international authorship allowed for gathering the legal framework for the surveyed countries in the local language.

Statistical Data Analysis

The survey data were analyzed using descriptive and inferential statistics. Both statistical approaches were implemented using Microsoft Excel software. The inferential statistics were used to test the significance of the hypothesis and the results to validate that the drawn conclusions reflect the reality on the ground, not random chance. Multiple regressions were used to examine the relationships. The statistical significance of regression coefficients and effects were assessed using analysis of variance (ANOVA), with a p -value < 0.05 considered statistically significant.

3. Results and Discussion

To better understand the consequences and potential of a global ban on plastic and the more extensive use of bioplastics, this work scrutinized the legal frameworks and analyzed the general social acceptance for alternatives of single-use plastics in food and beverages in the most representative surveyed countries.

3.1. Legal Framework

3.1.1. European Union

In the European Union (EU), the key regulation in terms of plastics is the EU Directive 2019/904 on the reduction of the impact of certain plastic products on the environment [27]. This directive, also often called the Single-use Plastics (SUP) Directive, has introduced various measures for reducing the quantity of plastic goods being produced, along with measures for encouraging redesign and collection for recycling. However, it is important

to realize that this is not the first approach to controlling the use of single-use plastics. The preceding directive was the Plastic Bags Directive (EU Directive 2015/720) [28] that was also an amendment to the Packaging and Packaging Waste Directive (94/62/EC) [29]. The last one was the first attempt to deal with the unsustainable consumption and use of lightweight plastic carrier bags (i.e., plastic carrier bags with a wall thickness below 50 microns), which, at that time, was already one of the top ten littered items in Europe [30]. Such lightweight plastic carrier bags are often used only once and, at the same time, they take up to 20 years to break down in the marine environment [31]. They often end up in terrestrial or marine animals' digestion systems or break up into microplastics that ultimately go into the human and animal food chain [32]. Currently, the SUP Directive imposes many extended restrictions on the use of plastic for, e.g., cups for beverages, including their covers and lids; food containers intended for immediate consumption, either on-the-spot or take-away-ready for immediate consumption, etc. However, what is even more relevant is that the Single-Use Plastics Directive introduces a complete ban for a wide variety of plastic products, e.g., cotton bud sticks, cutlery (forks, knives, spoons, chopsticks), plates, straws, beverage stirrers, sticks to be attached to and to support balloons, food and beverage containers and cups made of expanded polystyrene with or without a cover, cap and lid. Additionally, the same directive puts enhanced responsibility on the producers. Producers are responsible for the introduction of certain types of plastics and should cover the costs that fall into one of the three categories, namely, the costs of the awareness-raising measures regarding those products; the costs of waste collection for those products that are discarded in public collection systems, including the infrastructure and its operation and the subsequent transport and treatment of that waste; and, finally, the costs of cleaning up the litter resulting from those products and the subsequent transport and treatment of that litter. In other words, the producers are forced to pay the potential environmental damages or seek more environmentally benign materials.

Although the proposed changes are in line with the objectives of a more sustainable and less fossil-carbon-dependent future, numerous aspects still must be properly regulated. One of these is the life cycle assessment (LCA) of fossil- and bio-based feedstocks used for plastics production. For example, European Bioplastics [33] claims that the approach of the Joint Research Center of the European Commission (JRC) in the LCA study [34] lacks important elements that are crucial for a fair, comparative assessment of bio-based and fossil-based plastics. The proposed methodology's approach of omitting the added value of biogenic carbon sequestration is a main criticism addressed by European Bioplastics, and, as a result, the proposed LCA approach clearly favors conventional plastics made from fossil resources. Furthermore, European Bioplastics complains that the indirect land use change rules [35] provide less strict requirements for fossil-based plastics. This results in an inconsistent inclusion of indirect effects, establishing different burdens of proof. The methodology also does not reflect the existence of multiple end-of-life realities and fails to treat all recycling options, including organic recycling, equally [36]. This single example depicts that a lot must still be done to properly address the changes in the plastic area in European and, later, in national legislative frameworks.

Following their obligations, some EU member states already started the implementation of the SUP Directive to the national legal system. Such examples are Portugal and Poland.

3.1.2. Portugal

In case of Portugal, the first stage of the SUP Directive transposition was to forbid the use and availability of single-use plastic tableware in the activities of the catering and/or beverage sectors and in the retail trade, which was to be in place starting on 2 September 2020 [37]. Due to the COVID-19 pandemic situation, this ban was postponed and entered into force on 31 March 2021. The second and the last part of the transposition was the entry in force, on 1 November 2021, of a new law. The objective of this law is to prohibit the placing of certain single-use plastic products on the market, such as those already

mentioned for the EU legal framework [38]. At the same time, this new regulation sets two goals for reducing the consumption of cups for beverages and packaging for ready-to-eat foods by 80% by 31 December 2026 and by a 90% by 31 December 2030, compared to the values of 2022. To accomplish these goals, some measures are also planned to be implemented. One of them, in response to the need for the development of a circular economy and for addressing challenges related to the excessive use of single-use plastics during the COVID-19 pandemic crisis, is the creation of a system promoting the multiple use of food containers used for take-away or home delivery [39]. The implementation of this system is foreseen to be carried out either at the national scale or by individual food retailers or restaurants.

3.1.3. Poland

In Poland, due to the necessity to implement the requirements of the SUP Directive, on 3 July 2021, the Polish Minister of Climate and Environment published a draft act amending the act on the obligations of entrepreneurs with regard to the management of certain types of waste and the product fee [40]. The new act aims to fully transcribe the SUP directive in terms of a ban on single-use plastic products and the responsibilities of the entrepreneurs placing selected products on the market.

3.1.4. Ukraine

During the 30th Ecology All-Ukrainian Forum on 7 June 2021, President Volodymyr Zelenskiy signed the Law on “Restricting the Trade in Plastic Bags in the Territory of Ukraine” No. 1489-IX, adopted by the Verkhovna Rada on 1 June 2021 [41]. The Plastic Act—the so-called “plastics policy” of the Ukrainian government—is aimed at ordering the issue of the use of plastics in Ukraine and identifying areas for improvement of the legislation, considering the specificity of domestic development related to the European approach to plastic waste management and the positive experiences of the other countries and leading companies as well. The Ukrainian government states that for the effective implementation of the Plastics Act in Ukraine, it is necessary to clarify the applicable national standards and harmonize them with European ones—first, with regard to the biodegradation and labeling of plastic bags. At the same time, attention is drawn to the fact that reducing the amount of plastic waste should go hand-in-hand with the search for substitutions for plastics, including alternative products and technologies, and changes in consumer habits. State legal regulations cover the issue of the reduction of plastic waste in several dimensions: (i) in terms of implementation—it is planned to create a state support mechanism for the replacement of the fossil plastics by the alternative environmentally friendly bioplastics, the implementation of technologies reducing the content of plastic in the final product and the effective enforcement of the principle of “polluter pays”; (ii) in terms of distribution, making retailers responsible for avoiding plastic in their distribution processes and (iii) in the field of recycling—the creation of a support system for plastics processing companies in order to implement the latest ecological recycling solutions into the Ukrainian economy.

3.1.5. Brazil

In terms of the use of plastic materials and its potential recycling, in Brazil, no dedicated legal framework exists today. Plastic is considered as any other waste and falls under the solid residues law called the National Politics of Solid Residues that was established in 2010 [42]. Only now, following the examples of other countries, has Brazil considered the importance of creating a dedicated law regarding the use of disposable plastic [43].

3.1.6. USA

In the last decade, regulations on the manufacturing and use of plastics, as well as subsidies to promote the recycling of plastic wastes, have been increasing in the USA [44]. Single-use plastics and carry-out bags have been banned in several American states, in-

cluding Hawaii in 2011, California in 2014 and New York, Delaware, Oregon, Maine, Connecticut and Vermont in 2019. In addition, single-use straws and polystyrene have been restricted in Vermont since 2019, while the Hastings-on-Hudson city (at New York state) banned the use of polystyrene in 2014. Fees up to USD 1.00 have been imposed on carry-out bags, depending on their thickness. Interestingly, a solution was put in place in the state of Maine, where, since 1991, retail stores can make a plastic bag available to a customer as long as all plastic bags within 20 feet of the entrance are collected and then recycled [45]. Other American states, such as Arizona, North Dakota, Minnesota, Oklahoma, Iowa, Missouri, Michigan, Indiana, Mississippi and Florida, acted to prohibit local governments from banning plastic bags and containers [45]. It is important to acknowledge that, since the start of the COVID-19 pandemic, many US states such as Massachusetts, New York and New Hampshire have rolled back the policies restricting the use of single-use plastic bags [46,47].

3.1.7. China

China has started to move away from the use of plastic straws and one-use plastic bags [48]. On 1 January 2021, a plastic prohibition went into effect in China, banning restaurants nationwide from using single-use plastic straws and shops in major cities from supplying plastic carrier bags. These are some of the restrictions on the production, sale and use of single-use plastic products set out in a policy on further strengthening the removal process of pollution from plastics issued jointly by the National Development and Reform Commission (NDRC) and the Ministry of Ecology and Environment on 16 January 2020 [49]. The NDRC obliges provinces across the country to implement, step by step, the national policy depicted within the five-year roadmap to reduce the use of single-use plastic products by the end of 2025. Non-degradable plastic bags will be banned in malls, supermarkets, pharmacies, bookstores and bars/eateries in all cities by the end of 2022. Only fresh produce markets are exempt from the ban until 2025. Restaurants across the country are already banned from using non-degradable plastic straws and plastic tableware. Take-away food packaging in cities must be cut by 30% by 2025. Hotels and private lodgings across China are forced to eliminate plastic items entirely by 2025 [50].

On top of that, plastic is banned in postal and courier services as well [51]. The specific developed areas of China, including Beijing, Shanghai, Jiangsu, Zhejiang, Fujian and Guangdong, are banned from using non-degradable plastic packaging until the end of 2022. This ban will be in force nationwide by 2025. Furthermore, according to the opinions of the NDRC, the production of cosmetics containing plastic microbeads is also excluded, and the sale of such products will be completely forbidden by the end of 2022 [49].

Under the Chinese act on solid waste, local authorities can impose a fine of CNY 10,000 to 100,000 (approximately USD 1545 to USD 15,460) for those who do not comply with the national restrictions on the use of non-degradable plastic bags and other single-use plastic products [52].

3.2. Consumer Acceptance for Alternatives to Single-Use Plastics in the Food and Beverage Sectors

3.2.1. European Union

The study performed by Pro Carton demonstrates that more than 60% of Europeans pay attention to the environmental impact of the packaging while purchasing a product [53]. Moreover, European customers are also influenced by the media coverage about the pollution, especially when it comes to marine pollution or microplastics that end up on consumers' plates. Among alternatives to plastic, the most common are, e.g., glass and aluminum, especially for beverages, or paper-based materials for other uses. Another option, especially in the beverage industry, is the use of biodegradable plastics. Dominant producers in this market make significant efforts to demonstrate their commitment to using bottles made of renewable materials. These tendencies are consistent with changes in the social perception. During the COVID-19 pandemic, between 45% and 69% of Europeans, depending on the country, declared that they are recycling more than they did in 2020 [53].

These data demonstrate that the general perception of society is changing and that the declared acceptance of alternatives to single-use plastics in Europe is rising and is one of the major concerns of European society nowadays.

3.2.2. Portugal

In Portugal, the average citizen produces 40.3 kg of plastic waste per year, which is 17% above the EU average [54]. The plastic packaging represents 8% of the overall Portuguese waste [54]. Only 13% of waste is separated for recycling and less than 20% is used for energetic valorization [55]. This means that the most predominant treatment in Portugal is landfilling (33%). This number can reach up to 58% when considering the reuse from other operations [56].

Between 2019 and 2020, the Portuguese recycling rate increased by 13%, which demonstrates an increase in awareness of the importance of recycling among the Portuguese population [56]. However, this is still not enough to mitigate the plastic problem in the country. Municipalities and companies have increased their recycling and reuse campaigns by creating drop-off containers for particular types of wastes such as coffee capsules, cooking oils, textiles and electronics, and, in some districts, PET bottles can be traded for price discounts [54]. Although these actions have led to an increase in recycling numbers, the trend is to enforce a reduction in the overall consumption by, for example, trading disposable capsules for long-term steel ones, hygiene liquid products for bars of soap, cleaning products for dissolvable tablets, etc. [55]. However, the main concern of plastic waste is food packaging. Although there is an increase in the sale of bulk food in supermarkets, reducing plastic packaging can lead to an increase in food waste, which, in Portugal, is already one-third of the overall food produced [57]. Therefore, bioplastics can play a major role in this reduction; however, bioplastics have also raised a few concerns, e.g., in the context of the environmental issues, especially regarding the insufficient information about the bioplastic reuse and correct separation approaches [58]. Nevertheless, Portugal is investing in bioplastics at both the research and implementation levels. For example, a consortium of 38 companies and investigation centers is planning to invest EUR 57.4 million in the construction of four factories, an R&D center and a logistics center for the production of insects and chitosan and the development of 43 insect-based materials and services, including bioplastics. At the same time, this investment will create 140 new direct jobs [59].

3.2.3. Poland

Polish consumers have focused on recycling and reducing the use of plastic for many years [60]. The report prepared by Kantar, Europanel and GfK shows that, from year to year, Poles take more and more actions to ban plastic [61]. In addition, due to the COVID-19 pandemic, almost overnight, an overturned hierarchy of priorities among Polish consumers could be observed. The safe, quick and comfortable shopping became the key trend, but, despite the fear of being affected by SARS-CoV-2 and the tremendous number of plastic products created by the pandemic regime (e.g., disposable gloves, masks or one-use food packaging), the majority of Polish consumers declare that they have environmentally friendly attitudes, which have been created over recent years [4]. The percentage of Polish consumers who take specific measures to reduce plastic waste increased from 18% in 2019 to 21% in 2020 [62]. At the same time, the number of consumers who can be considered as a group disregarding the plastic pollution hazard as a serious environmental problem has decreased from 41% to 35%. Additionally, the plastic waste pollution remains the main global environmental problem for Poles. On their list of the greatest threats to the environment, the problem of the uncontrolled, catastrophic amount of plastic rubbish is in first place [62]. Occupying the following places on this list are climate change, air pollution and food waste. As many as 48% of consumers in Poland feel personally affected by environmental problems. Because of that, 31% of Poles have stopped buying certain one-use plastic products, 55% have used refill and reused packaging, if available, and 54% try to avoid plastic when buying fruits and vegetables. In addition, 83% of shoppers use

their own shopping bag, and 77% skip plastic cutlery and plates for a party or barbecue. The biggest change in the attitudes of Poles took place regarding biodegradable cotton buds: even though the price of them is higher compared with that of the standard plastic buds, 34% of buyers declared to choose them, compared to 23% a year ago [62].

The Kantar's "Who Cares? Who Does?" report from 2021 shows that 92% of Poles declared that they segregate plastic packaging always or often. To the question of who is most responsible for the elimination of single-use plastic packaging, 47% of Polish consumers answered that producers are, 29% answered that authorities and law regulators are, 4% answered that retailers and distributors are and 20% answered that it is society and consumers through their everyday purchasing decisions [61].

3.2.4. Ukraine

Despite the extremely difficult political, economic and social situation, Ukrainian society is interested in environmental issues [63,64]. There is a public discussion on the "Ukrainian National Solid Waste Management Strategy". More and more initiative groups and NGOs are being formed around the problems of environmental protection. Zero Waste Alliance Ukraine, an active member of the global environmentally friendly social movement, is represented by the Zero Waste Europe organization and was founded in 2018 by three Ukrainian non-governmental organizations—Zero Waste Lviv, Ozero (now the Zero Waste Society) from Kyiv and Kharkiv Zero Waste. Zero Waste Alliance Ukraine runs information and advocacy campaigns such as WeChooseReuse, EnvironMenstrual Week, Plastic-Free July, Brand Audit, etc. Nevertheless, there is still work to be done to raise awareness of the widespread social movement regarding the defense of the environment, as the country is still under continuous political and economic threats.

3.2.5. Brazil

Although there exists a general understanding of the importance of plastic pollution (Figure 2), there is no specific research on social acceptance for alternatives to single-use plastics in the food and beverage sectors. Most of the activities in this respect are related to the private sector. Private initiatives in the plastics sector and institutions have promoted better environmental awareness of this important material. For example, the aim of the Brazilian Association of Flexible Packaging Industry (ABIEF) is to develop plastic recycling programs and thus promote environmental education, seeking to recognize the plastic production chain as a value chain. Another institution, Plactivida, a social service organization, sees plastic as a relevant tool for sustainable development.



Figure 2. The banners at the Fortaleza (Ceará, Brazil) beach, made by aware citizens. Left photo: "By 2050, there will be + waste in the ocean than fishes"; Right photo: "New rule: every time you go to the beach, collect at least 3 plastics from the sand". Photos taken on 6 March 2019 by a co-author of this work, R. M. Lukasik.

The Benchmarking Brazil Program, a respected sustainability seal that, since 2003, selects and certifies good practices of Brazilian organizations, catalogs approximately

400 cases that are considered benchmarking references for the quality of the practices adopted. Among them, the managerial themes of Productive Arrangements, Waste and R&D were those that registered innovative practices regarding renewable raw materials and waste management with social inclusion. Despite a large number of social movements regarding this subject, a lot must still be done to achieve a considerable impact at the national level.

3.2.6. USA

In the USA, in addition to the increased generation of waste plastic bags, the relaxation of some policies, e.g., rolling back the policies restricting the use of single-use plastic bags due to the COVID-19, is likely to have long-term consequences on consumers' attitudes towards re-introducing the single-use culture for consumers [46,47]. Improvements in the US plastic policies affecting the social awareness are strongly required, namely, in terms of popularity and transparency. It is clear that there is a lack of public awareness of plastic pollution; thus, the development of outreach and education throughout the population is quite important.

3.2.7. China

Rapid economic growth and increasing prosperity in China are reflected in the rising problem of the amount of plastic waste that lingers in China. The social acceptance for littering everywhere, the absence of plastic recycling or reusing systems and the fact that China is the world's biggest plastic producer and consumer takes the problem of plastic waste to the form of a national environmental disaster. When assessing social acceptance for pro-environmental activities in China, it is not possible to apply the same measures and directly compare with Western countries. These actions, including the ban on plastic, are generally initiated by the government, although grassroots, local social initiatives are also being observed [65–67]. In May 2018, the “Beautiful China Initiative” was announced, and it is a long-term environmental protection strategy aimed at fighting air, water and soil pollution and mitigating the effects of climate change, the depletion of resources and the habitats' exhaustion [68]. The solid waste recycling industry in China has grown rapidly over the past five years [69]. The industry's revenues have grown at a dizzying pace of 9.6% annually in the last 5 years, and for the current year, 2021, an increase of 10.2% compared to the previous year is expected. China's plastic waste recycling market is worth USD 22.7 billion [69]. Despite these very positive signals, a lot still has to be done to change the social perception of this aspect.

3.3. Online Survey Results

The online survey was conducted worldwide. The spread of answered surveys between countries is presented in Table 2. In total, 391 surveys were received from 16 different countries, while 9.5% were submitted with no country specified. Although the number of online surveys answered was low, the general trends discussed below can be drawn from the work of J. A. Angrist and G. W. Imbens, the Nobel prize winners in Economy for 2021, who demonstrated that the use of natural experiments in empirical social economics has ushered in the analysis of causal relationships [70]. Furthermore, the use of inferential statistics helped to extrapolate the drawn conclusion to the population size, i.e., the general audience.

By analyzing the number of questionnaires, it can be said that the representative countries were: EU countries—Poland and Portugal, China—the economy experiencing the fastest pace of development for the last decade [71], USA—the country with the highest level of Actual Individual Consumption (AIC) per capita in the world [72], Brazil—the country which faces many environmental problems of crucial importance for the entire world [73] and Ukraine, which is a characteristic example of a low-income post-communist country [74].

Table 2. The number of questionnaires by countries of questionees.







Country	Questionnaires
Ukraine	95
Poland	76
Portugal	58
Brazil	51
China	43
USA	7
Cyprus	5
Greece	5
Mexico	5
Germany	2
Russia	2
Finland	1
The Netherlands	1
Ireland	1
Italy	1
Spain	1
No country indicated	37

3.3.1. Characteristics of Questionees

Regarding the sex and age of the questionees, 66.5% were women ($n = 260$). A total of 80.3% of questionees ($n = 314$) were between 21 and 65 years old, and only 6.4% ($n = 25$) were above 65 years of age. The age structure corresponds to the world population age structure [75] and demonstrates that the vast majority of the questionees were of the age of the actual active consumers.

Taking into consideration the place of residence (Table 3), the majority (68.3%, $n = 267$) of questionees live in cities with a population of over 150,000 inhabitants. Taking into consideration the major differences in size and population between countries, it is hard to generalize regarding the representation of the questionees for each country individually. Nevertheless, from the survey point of view, it is important to stress that inhabitants of villages and towns constitute a considerable sample (above 17%, $n = 68$). This is in agreement with the worldwide structure of population, as currently 54% of people live in urban areas, and by 2050, the UN foresees that this number will increase to 68% [76]. Therefore, the results can be considered as representative of the public in the surveyed countries and in general.

Table 3. The place of residence of questionees.

Place of Residence	Number of Inhabitants							Other Countries	No Country Indicated	Total
village		3	14	3	1	2	0	1	6	30
town	<50 k	5	5	13	4	4	1	3	3	38
	50 k–150 k	4	15	12	6	10	1	6	2	56
city	150 k–500 k	42	2	7	13	8	3	2	8	85
	>500 k	41	40	23	27	19	2	12	18	182

Other relevant aspects in the analysis of the consumer preferences are the level of education and the economic status. The results are given in Figure 3.

The analysis of the answers depicts that most answers came from questionees with secondary (17.4%, $n = 68$) or higher education (73.4%, $n = 287$). This share distribution was generally observed for all surveyed countries, with the exception of China, where secondary or higher education was claimed by 23.2% ($n = 10$) and 41.9% ($n = 18$), respectively. At the same time, primary education was claimed by more than $\frac{1}{4}$ of questionees (27.9%, $n = 12$), while overall, the share of questionees with a primary education was as low—5.4% ($n = 21$).

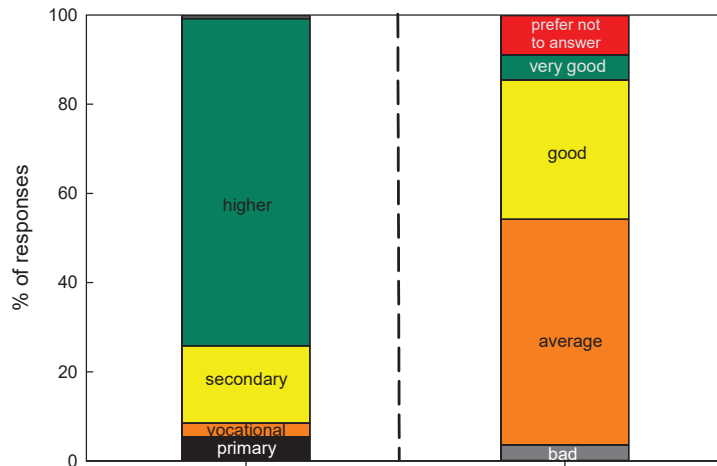


Figure 3. The level of education (left bar) and economic status (right bar) structure of questionnaires.

In terms of economic status, there exists a general agreement between Ukraine, Portugal and Brazil. Between 49% and 58% of questionnaires declared the average economic status. In China, the dominant share of questionnaires (79.6%, $n = 34$) declared an average economic status, whereas, in Poland, the highest share of questionnaires (51.3%, $n = 39$) declared a good economic status. In general terms, an average economic status was declared by 50.6% ($n = 198$), followed by 31.2% ($n = 122$) of questionnaires who considered their economic status as good. An important conclusion to be drawn is that the questionnaires from different countries may consider the same economic status differently. For the ones from the USA, the country with the highest level of AIC per capita in the world, the average economic status may have a very different meaning compared to the meaning it has for the questionnaires from the low-income countries, as the comparison is not accompanied by any numerical indicator but only by the very subjective opinion of the questionnaire. Nevertheless, the explained differences, especially in terms of place of living, education and economic status, influence the profile of the typical questionnaire. However, overall, the average questionnaire was a woman ($n = 260$, $SD = 91.3$) between 21 and 65 years of age ($n = 314$, $SD = 159.6$) with higher education ($n = 287$, $SD = 129.0$) and an average economic status ($n = 198$, $SD = 79.7$) who lives in city with more than 500k inhabitants ($n = 164$, $SD = 54.3$).

3.3.2. Social Perception of Bioplastics

This part of the survey consisted of eight questions, and the results are discussed below.

1. Would you support replacing traditional plastic food packaging with bioplastic packaging?

The survey showed that there is a global consumer acceptance (91.2% positive answers, $n = 301$) for moving away from traditional plastic food packaging made from fossil fuels and replacing them with bioplastics. For all questionnaires, the problem of avoiding single-use plastic food packaging and generally limiting plastics in everyday life is important and necessary from a social and environmental point of view. The highest (100% ($n = 7$)) acceptance for the replacement of fossil plastics with their bio counterparts was noticed for answers from the USA. An almost equally high acceptance, 96% ($n = 92$), was found for Ukraine, 90% ($n = 69$) Poland, (89% ($n = 52$)) Portugal, (88% ($n = 45$)) Brazil and (85% ($n = 36$)) China, as shown in Figure 4.

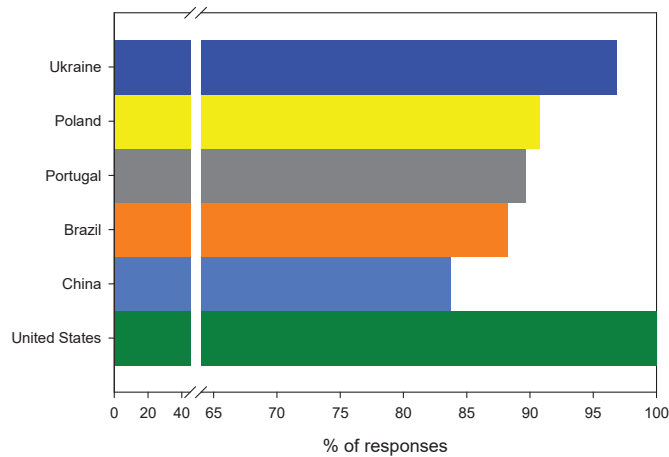


Figure 4. The distribution of positive answers to the question: Would you support replacing traditional plastic food packaging with bioplastic packaging?

Although the collected results demonstrate a general agreement, it is worth verifying the hypothesis about a difference in social acceptance between questionees from European ($M = 92.4\%$, $SD = 3.9\%$, $n = 3$) and non-European countries ($M = 90.6\%$, $SD = 8.4\%$, $n = 3$) or between those from developed (Poland, Portugal, USA— $M = 93.5\%$, $SD = 5.7\%$, $n = 3$) and developing countries (Ukraine, Brazil, China— $M = 89.6\%$, $SD = 6.7\%$, $n = 3$). Neither the first hypothesis (t ($df = 4$) = 0.33, $p = 0.38$ (1 tail)) nor the second one (t ($df = 4$) = 0.77, $p = 0.24$ (1 tail)) found its confirmation in the statistical analysis; hence, it can be concluded that there is indeed universal agreement on this matter for all questionees. Furthermore, these data are also coherent with those reported in the literature [77]. In addition, Scarpi et al. found that the widespread agreement on the change towards bioplastics can be associated with new moral norms and a new business-to-business (B2B) or business-to-consumer (B2C) relationship for circular economy success.

- Did you know that bioplastics can be made from leftovers of bakery and confectionery products (e.g., bread, cakes ...)?

In the case of the first question, there was a generalized agreement between questionees; however, in the case of the second question, the responses were not fully conclusive. As much as 58.3% ($n = 192$) of questionees were not aware that bioplastics can be made from leftovers. Only Brazilian and Portuguese questionees were more aware about this, whereas, in all other countries, the dominant response was negative, reaching as high as 62.8% ($n = 27$) and 67.4% ($n = 64$) for China and Ukraine, respectively, as outlined in Figure 5. The t-test confirmed that the results obtained from the Chinese and Ukrainian questionees ($M = 65.1\%$, $SD = 3.3\%$, $n = 2$) are indeed statistically different (t ($df = 4$) = 2.84, $p = 0.2$ (1 tail)) from the answers of questionees from the remaining countries ($M = 53.0\%$, $SD = 5.3\%$, $n = 4$). Therefore, by analyzing the social structure of questions, it can be concluded that the noticeable difference can be associated with the fact that a considerable share of Chinese questionees have only primary education, and, in the case of Ukraine, there is still a low level of social awareness linked to an underdeveloped legal framework. Hence, it is important to verify if there is a relation between the level of education of questionees and a distribution of negative answers to question 2. For this purpose, the linear response surface model was used, which is described by the following equation:

$$Y = \beta_0 + \beta_1 X_1 + \beta_2 X_2 + \beta_3 X_3 + \beta_4 X_4,$$

where Y is the percentage of negative answers to question 2, X_1 to X_4 are the shares of questionees with primary, vocational, secondary and higher education, respectively, and β_s is the regression coefficients. β_0 represents the analyzed response in the center of the experimental domain. The statistical significance of regression coefficients and the effects were assessed using analysis of variance, and the results are given in Table 4.

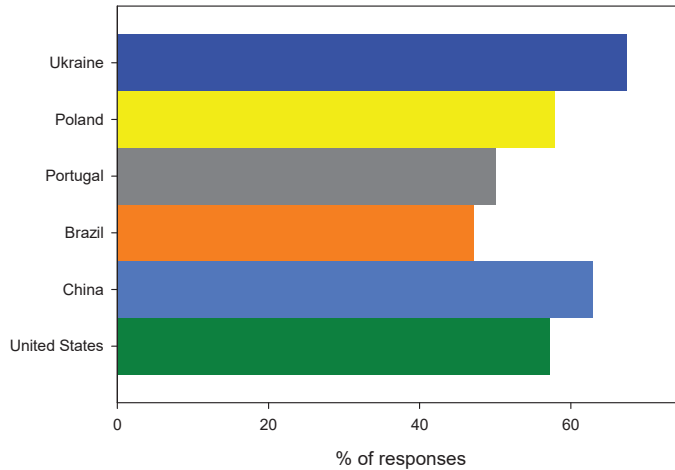


Figure 5. The distribution of negative answers to the question: Did you know that bioplastics can be made from leftovers of bakery and confectionery products (e.g., bread, cakes . . .)?

Table 4. ANOVA statistical analysis for the response surface linear model of the % of negative answers to the question “Did you know that bioplastics can be made from leftovers of bakery and confectionery products (e.g., bread, cakes . . .)?” in the function of the education of questionees.

	Model	β_1	β_2	β_3	B_4	R^2	Adjusted R^2
Coefficient		221.98	−2049.61	129.74	22.03	0.999	0.995
F value	2472.61	995.72	6238.98	1240.82	242.18		
p-value	0.015	0.020	0.008	0.018	0.041		

The p -value of the adjusted model ($p = 0.015$) implied that the model was significant. Therefore, the statistical analysis demonstrated that the model was well adapted to the response ($R^2 = 0.999$ and adjusted $R^2 = 0.995$). All terms were the statistically significant model terms ($p < 0.05$). Regression coefficients were compared with each other to indicate the relative importance of each significant variable in the model equation. The regression coefficients showed that vocational education has an almost 10-fold higher negative effect than the primary education of questionees. The less influencing regression coefficient is the one associated with higher education, which is close to 100 times lower than β_2 . Therefore, the statistical analysis of the employed regression model confirms the hypothesis that there is a significant relation between the level of education and the perception that bioplastics can be made from leftovers of bakery and confectionery products.

3. Would it bother you to know that the bioplastic packaging, in which the bread is wrapped, is made of bakery and confectionery leftovers?

The analysis of answers to this question draws interesting conclusions. Although the vast majority of questionees (78.1%, $n = 258$) lack concerns regarding the new, waste-based bioplastics, there are some substantial differences between countries, as portrayed in Figure 6. The questionees from Portugal (100%, $n = 58$), Brazil (96.1%, $n = 49$) and Poland (85.5%, $n = 65$) are the most open-minded, and they accept the use of bakery

and confectionary waste as a resource for a food packaging material production. The questionees from the USA (71.4%, $n = 5$) and Ukraine (69.5%, $n = 66$) were less willing to accept such a solution. For a great number of Chinese questionees (34.9%, $n = 15$), bioplastics made from leftovers raises doubts and opposition. Hence, it can be hypothesized that, in comparison to questionees from other countries ($M = 93.9\%$, $SD = 7.5\%$, $n = 3$), American, Ukrainian and Chinese ($M = 58.6\%$, $SD = 20.6\%$, $n = 3$) questionees demonstrate distinctive confidence regarding the safety and health issues of new products, combined with a low awareness about the technology advances. The inferential statistics allowed us to confirm this hypothesis (t ($df = 4$) = -2.79 , $p = 0.02$ (1 tail)); thus, it can be concluded that the visions of questionees from the USA, Ukraine and China are indeed significantly different from those from the remaining countries.

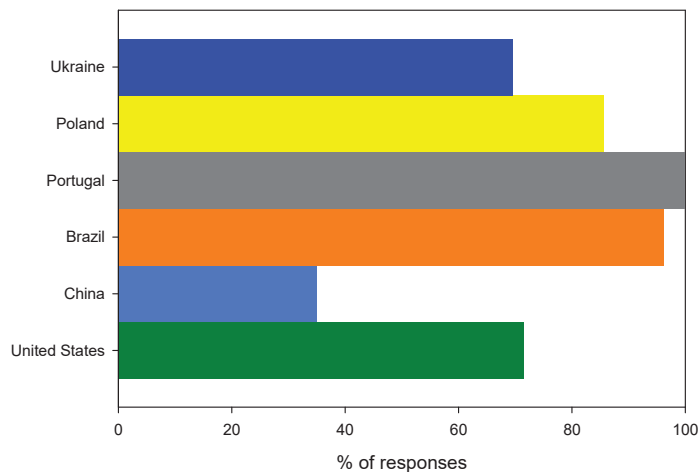


Figure 6. The distribution of positive answers to the question: Would it bother you to know that the bioplastic packaging, in which the bread is wrapped, is made of bakery and confectionery leftovers?

Koenig-Lewis et al. [78] addressed this aspect from a different perspective. They examined the association of biopackaging with the type of food. Surprisingly, the biodegradable plastic used for unhealthy food did not affect the purchasing habits. The opposite effect was observed when healthy food was purchased. In this case, the biodegradable packaging was selected more often. Considering the results of Koenig-Lewis and the results given in this work, it can be concluded that biopackaging might be a perfect solution for healthier foods, e.g., salad. Other studies confirmed a strong connection between the health consciousness and the impact of the purchase intention of food in compostable packaging [79,80].

4. Would you expect a clear notice on the bioplastic packaging that will allow you to choose between traditional plastic and biodegradable plastic?

By analyzing results of question 4, it can be concluded that the concerns about, e.g., the safety and health issues might in fact be the actual reason for the rather low acceptance of new bioplastics as a packaging material. Chinese questionees, followed by American and Ukrainian questionees, want to be fully aware of what they are buying, as can be observed in Figure 7. The observed results may suggest that this question is directly linked to the previous one. Therefore, again, it is relevant to verify to what extent the questionees from these three nations have a distinctive confidence regarding the bioplastic products. In fact, the statistical analysis confirmed the hypothesis (t ($df = 4$) = 2.86 , $p = 0.02$ (1 tail)) that Chinese, American and Ukrainian ($M = 87.7\%$, $SD = 14.7\%$, $n = 3$) questionees have a distinct perception and wish to be clearly informed about the bioplastic products compared to the majority of Polish, Portuguese and Brazilian ($M = 78.7\%$, $SD = 4.1\%$, $n = 3$) questionees.

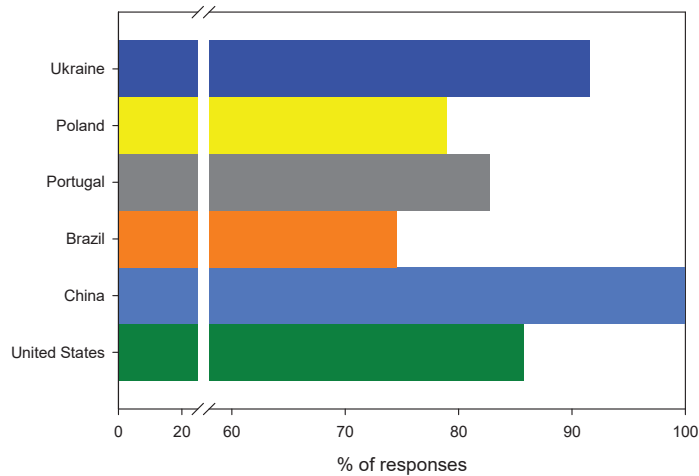


Figure 7. The distribution of positive answers to the question: Would you expect a clear notice on the bioplastic packaging that will allow you to choose between traditional plastic and biodegradable plastic?

A clear and unambiguous notice about the product origin is the responsibility of companies/brands and governments. Therefore, this question can be seen in a broader context, e.g., to what extent governments and companies can do more to help the environment. Pro Carton, in their survey, showed that both the industrial sector and administration can be much more involved in and responsible for informing and promoting environmentally friendly packaging. According to their studies, an overwhelming majority of Europeans (76%) strongly agreed/agreed with this aspect. Furthermore, as many as 61% of Europeans approved the introduction of additional taxes to force brands and retailers to adopt more environmentally oriented norms and behaviors [53,81].

5. How much more would you be able to pay for a product packed in bioplastic?

An interesting conclusion, especially for producers and vendors, comes from the answers to question 5. Although the most obvious answer is the one indicating the lowest acceptable premium price, numerous studies on consumer declarations vs. purchasing decisions show that declarations do not always translate into purchasing decisions [78,82–84]. Hence, this question allowed us to compare the declaration of the awareness of environmental risks and the readiness to replace traditional plastic food packaging with bioplastic (answers to the question 1) with the levels of consumer consciousness, sensibility regarding environmental aspects and mental openness for changes.

In general, the vast majority of questionees ($n = 240$) were ready to pay only up to a 10% premium price for new biopackaging, as shown in Figure 8. In all countries, the willingness to pay 10% extra for this kind of material is rather similar, with the exception of Brazil and Ukraine, whose respondents demonstrated that they are not able to pay extra fees. The responses from Brazilian questionees were more uniformly distributed among answers, i.e., 46% ($n = 23$) of questionees were able to pay up to 10% more, 20% of questionees ($n = 10$) were able to pay between 10% and 20% more, 4% of questionees ($n = 2$) were able to pay between 20% and 30% more and 8% of them ($n = 4$) were able to pay between 30% and 40% more than they do for traditional plastics.

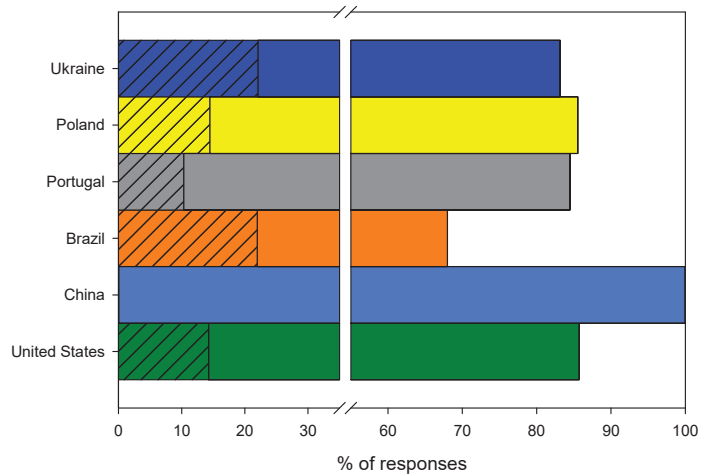


Figure 8. The distribution of answers of “not able to pay extra” (coarse bar) and “below 10%” (full bar) for the question: How much more would you be able to pay for a product packed in bioplastic? The data are given in a stacked form.

As stated above, Brazilian and Ukrainian questionees (22%, $n = 11$ and $n = 21$, respectively) were the least willing to be charged additionally for bioplastics. The answers of the Brazilians are really puzzling considering that almost 1/3 of Brazilians ($n = 16$) were able to pay more than 10% for bioplastics. This shows that the questionees representing Brazilian society were very distinct. On the other hand, similar to Ukraine, many households in Brazil are low-income, even if they self-declare as having an average or good economic status, as claimed in this work. The statistical analysis allowed for the confirmation (t ($df = 4$) = 2.41, $p = 0.04$ (1 tail)) of the veracity of the hypothesis that, in comparison to other nations ($M = 9.8\%$, $SD = 6.8\%$, $n = 4$), Brazilians and Ukrainians ($M = 22.1\%$, $SD = 0.1\%$, $n = 2$) have significantly different shares of the population who are not willing to pay any extra cost. So, it can be hypothesized that, to some extent, the economic status of each questionee defines a potential aptitude to pay or not pay the extra cost for bioplastic. This hypothesis was examined, and, for this purpose, the linear response surface model was used, which is described by the following equation:

$$Y = \beta_0 + \beta_1 X_1 + \beta_2 X_2 + \beta_3 X_3 + \beta_4 X_4,$$

where Y is the share of those not willing to pay any extra cost, X_1 to X_4 are the shares of questionees with very good, good, average and bad self-declared economic status, respectively, and β_s is the regression coefficients. β_0 represents the analyzed response in the center of the experimental domain. The statistical significance of regression coefficients and the effects were assessed using analysis of variance, and results are given in Table 5.

Table 5. ANOVA statistical analysis for the response surface linear model of the share of questionees not willing to pay any extra cost for bioplastic implementation in the function of the self-declared economic status of questionees.

Model	β_1	β_2	β_3	β_4	R^2	Adjusted R^2
Coefficient	−503.73	195.79	−150.97	706.62	1.000	0.999
F value	6327.97	3044.93	8207.04	11,527.27	16,469.54	
p-value	0.009	0.012	0.007	0.006	0.005	

The p -value of the adjusted model ($p = 0.009$) implied that the model was significant. Therefore, the statistical analysis demonstrated that the model was well adapted to the response ($R^2 = 1.000$ and adjusted $R^2 = 0.999$). All terms were statistically significant model terms ($p < 0.05$). Regression coefficients were compared with each other to indicate the relative importance of each significant variable in the model equation. The regression coefficients showed that a self-declared bad economic status indeed has the highest positive effect towards not paying any extra cost. The regression coefficient representing the questionees with a very good economic status validated the fact that they are strongly willing to pay (the second highest regression coefficient with a positive value). The regression coefficients representing questionees with good and average economic statuses are similar in terms of coefficient value; however, apparently, the β_2 is positive, i.e., questionees with a good economic status are less willing to pay any additional cost for bioplastics. Regardless of this, the statistical analysis of the employed regression model confirms the hypothesis that there is a clear relation between the self-declared economic status and the share of questionees with no ability to pay an extra cost for the use of bioplastics instead of fossil counterparts.

Similar conclusions can be drawn from the studies conducted by Pro Carton. This survey showed that society is only willing to pay the lowest possible amount of extra costs for packaging material, and only if this would mean a lower environmental impact of the final product [53]. As many as 61% of questionees declared that they were able to pay up to 10% more, and this share is, in general, consistent for all age groups included in this study.

6. Did you know that bioplastic can extend the life of a product and preserve its visual and taste properties?

The collected responses to question 6 indicate that a great proportion of questionees have almost no knowledge about the potential positive impact of bioplastic food packaging on the food packed in it. The highest knowledge of the functionality of bioplastic food packaging in extending the life of a food product and preserving its visual and taste properties was observed in the answers from Portugal (44.8%, $n = 26$). The Chinese (39.5%, $n = 17$), Ukrainian (26.3%, $n = 25$) and Brazilian (23.5%, $n = 13$) questionees were aware of the positive values of bioplastic, but the Poles (19.7%, $n = 15$) and Americans (14.3%, $n = 1$) apparently know the least about it (Figure 9). Hence, it can be hypothesized that Portuguese, Chinese, Ukrainian and Brazilian ($M = 34.0\%$, $SD = 9.6\%$, $n = 4$) questionees demonstrate different degrees of knowledge compared to Poles and Americans ($M = 17.0\%$, $SD = 3.8\%$, $n = 4$). Indeed, the statistical analysis results (t ($df = 4$) = -2.29 , $p = 0.04$ (1 tail)) confirmed that there is a significant difference in the understanding of this subject. Independently of this, the rather low understanding of this issue confirms that there is a lot to be done in terms of the better promotion of bioplastics not only as a solution for environmental problems but also as a solution for the reduction of food wastes and for better-quality food products.

7. Would you share the knowledge about such packaging with others?

As many as 86.7% ($n = 286$) of questionees declared that they were ambassadors of the biodegradable food packaging material. The Portuguese (96.5%, $n = 56$) turned out to be the most involved in sharing the new knowledge, while the Ukrainians (78.0%, $n = 74$) and Americans (71.4%, $n = 5$) seem to have the lowest willingness to transfer the information to others, as shown in Figure 10. Although the differences between Ukrainians and Americans ($M = 74.7\%$, $SD = 4.6\%$, $n = 2$) and the questionees from the remaining countries ($M = 90.8\%$, $SD = 4.6\%$, $n = 4$) are statistically significant (t ($df = 4$) = -4.0 , $p = 0.01$ (1 tail)), they are still small and can be generalized as positive feedback. On the other hand, it can be seen as overoptimistic, as it is only related to a declaration, with no actual action involved from the questionees' side. Nevertheless, it can be seen as a positive sign of social awareness in this context.

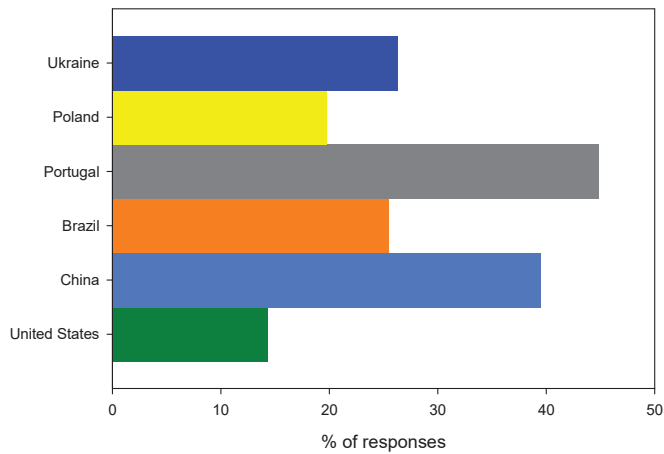


Figure 9. The distribution of positive answers to the question: Did you know that bioplastic can extend the life of a product and preserve its visual and taste properties?

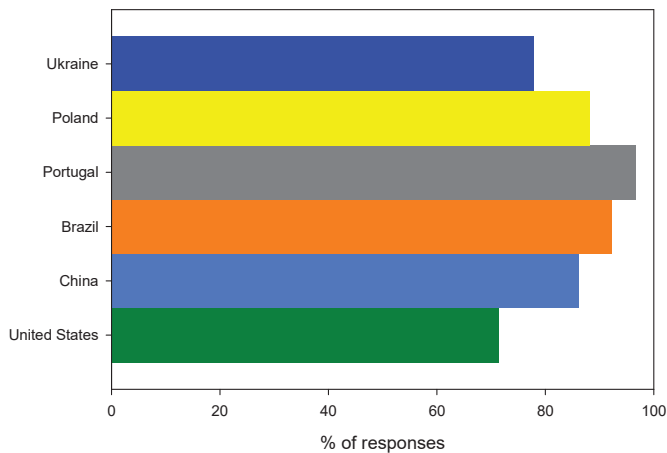


Figure 10. The distribution of positive answers to the question: Would you share the knowledge about such packaging with others?

8. Would you encourage others to use modern, environmentally friendly packaging?

Similar to the previous question, 89.1% ($n = 294$) of all questionees declared green self-identity and stated that they would promote the use of modern friendly packaging. These results are rather puzzling considering the previous questions related to the potential use of bioplastics for food wrapping as well as paying a potential extra cost for bioplastics, where the answers were quite modest compared to those to this question. It can be hypothesized that the questionees are not consistent in answering questions about similar matters. The last question received a very positive response: 100% ($n = 7$) of American questionees, 98.3% ($n = 57$) of Portuguese questionees, 96.1% ($n = 49$) of Brazilian questionees, 88.2% ($n = 67$) of Polish questionees, 86.0% ($n = 37$) of Chinese questionees and 81.1% ($n = 77$) of Ukrainian questionees said that they would promote this biomaterial in their circle of friends and encourage others to use it, as shown in Figure 11.

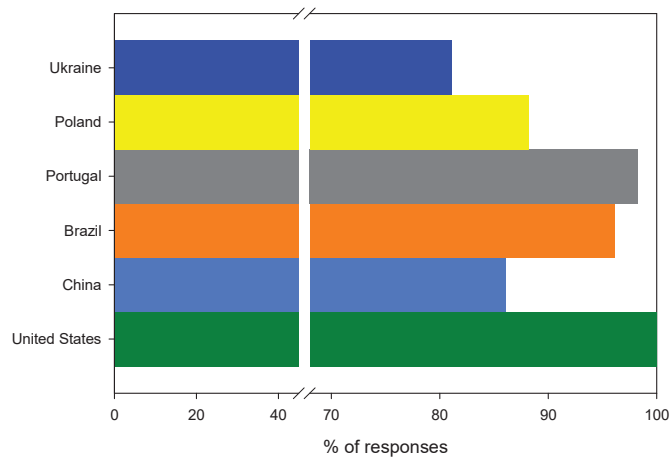


Figure 11. The distribution of positive answers to the question: Would you encourage others to use modern, environmentally friendly packaging?

The last two questions, although strongly declarative from the questionee side, demonstrate that society is aware of the plastic problems. Similar conclusions were found by Scarpi et al., who reported that the increased awareness of sustainability issues has increased the number of people following lifestyles oriented toward sustainable consumption [77]. This indicates that, behind the reported commitment to switch towards bioplastics and to promote their use, there exists a real change in the social perception.

4. Conclusions

This study is not meant to be conclusive. Rather, several limitations illuminate useful directions for future research and further implementation. The replacement of traditional single-use plastics with bioplastics for food packaging produced using the second-generation resources is a long-lasting process of creation. The specific, semi-qualitative research method—the snowball sample applied to a group of 391 questionees from 14 countries in the virtual space—allowed us to collect interesting conclusions and make the first comparative analyses. The sample size was not strictly defined, as the questionnaire was disseminated on the internet. In all the countries covered by the study, work on the construction of the basic frameworks is underway. It considers (i) the legal framework, including tax and incentive systems for producers and consumers, (ii) technologies for producing environmentally friendly, biodegradable materials with characteristics and functionalities comparable to or even better than traditional plastic and (iii) global social acceptance and consumer acceptance for pro-environmental activities and products. However, as the survey conducted in Brazil, China, Poland, Portugal, Ukraine and the USA showed, consumers' knowledge about the possibility of using the second-generation feedstocks, such as waste from bakeries or confectionery production, is considerably low. On the other hand, the consumers in the surveyed countries do not mind that the material produced from waste comes into contact with food, although some doubts in this respect are expressed, predominantly by Chinese questionees, followed by the ones from the USA and Ukraine. Most questionees in almost all surveyed countries are willing to pay only up to 10% more for new packaging. However, as many as 22% of questionees from Ukraine do not want to pay extra for biodegradable packaging at all. It is interesting that the questionees from China understand better than the questionees from other countries and accept that the bioplastic packaging must cost more; therefore, they are able to pay a higher price for this. In summary, this study shows that most consumers in all surveyed countries are ready to share the knowledge about new bioplastic food packaging materials and encourage others to move away from traditional plastic ones.

Author Contributions: Conceptualization: E.K. and R.M.L.; Methodology: E.K. and R.M.L.; Software: K.W., A.N.; Validation: E.K., P.J.P., M.L.d.A.L., A.M.A., A.R.C.M., and R.M.L.; Formal analysis: E.K. and R.M.L.; Investigation: E.K., P.J.P., M.L.d.A.L., A.M.A., A.R.C.M., and R.M.L.; Resources: K.W., A.N.; Data curation: K.W., A.N.; Writing—original draft preparation: E.K., P.J.P., M.L.d.A.L., A.M.A., A.R.C.M., and R.M.L.; Writing—review and editing: E.K. and R.M.L.; Visualization: R.M.L.; Supervision: E.K., R.M.L.; Project administration: E.K.; Funding acquisition: E.K. All authors have read and agreed to the published version of the manuscript.

Funding: Research and Innovation Centre Pro-Akademia.

Institutional Review Board Statement: Not applicable.

Informed Consent Statement: Not applicable.

Data Availability Statement: The datasets used and analyzed during the current study are available from the corresponding author on reasonable request.

Conflicts of Interest: The authors declare no conflict of interest.

References

1. United Nations. How do we #BeatPlasticPollution. 2021. Available online: <https://www.un.org/pga/73/plastics/> (accessed on 23 September 2021).
2. Fuhr, L.; Franklin, M. Plastic Atlas—Facts and Figures about the World of Synthetic Polymers, Heinrich Böll Foundation and Break Free from Plastic, Berlin, Germany. 2019. Available online: <https://za.boell.org/en/2019/11/06/plastic-atlas-facts-and-figures-about-world-synthetic-polymers> (accessed on 26 September 2021).
3. Morone, P.; Yilan, G. A paradigm shift in sustainability: From lines to circles. *Acta Innov.* **2020**, *36*, 5–16. [CrossRef]
4. Kocharńska, E.; Łukasik, R.; Dzikuć, M. New Circular Challenges in the Development of Take-Away Food Packaging in the COVID-19 Period. *Energies* **2021**, *14*, 4705. [CrossRef]
5. Endres, H.-J. Bioplastics. In *Biorefineries*; Springer: New York, NY, USA, 2017; Volume 166, pp. 427–468. [CrossRef]
6. Abhilash, M.; Thomas, D. Biopolymers for Biocomposites and Chemical Sensor Applications. In *Biopolymer Composites in Electronics*; Elsevier Inc.: Amsterdam, The Netherlands, 2017. [CrossRef]
7. European Bioplastics. 2021. Available online: <https://www.european-bioplastics.org/> (accessed on 26 September 2021).
8. European Bioplastics. What are Bioplastics? Material Types, Terminology, and Labels—An Introduction. 2018. Available online: <https://www.european-bioplastics.org/bioplastics/> (accessed on 26 September 2021).
9. Distaso, M. Potential contribution of nanotechnology to the circular economy of plastic materials. *Acta Innov.* **2020**, *37*, 57–66. [CrossRef]
10. Bojarska, J.; Złoty, P.; Wolf, W.M. Life cycle assessment as tool for realization of sustainable development goals—Towards sustainable future of the world: Mini review. *Acta Innov.* **2021**, *38*, 49–61. [CrossRef]
11. Lopes, T.F.; Łukasik, R.M. Economic, social and environmental impacts attained by the use of the effluents generated within a small-scale biorefinery concept. *Acta Innov.* **2020**, *36*, 57–63. [CrossRef]
12. Parfitt, J.; Barthel, M.; Macnaughton, S. Food waste within food supply chains: Quantification and potential for change to 2050. *Philos. Trans. R. Soc. B Biol. Sci.* **2010**, *365*, 3065–3081. [CrossRef]
13. European Commission. Farm to Fork Strategy. 2020, p. 23. Available online: https://ec.europa.eu/food/horizontal-topics/farm-fork-strategy_en (accessed on 30 September 2021).
14. Barska, A.; Wyrwa, J. Konsument Wobec Opakowań Aktywnych I Inteligentnych Na Rynku Produktów Spożywczych. *Probl. Agric. Econ.* **2016**, *349*, 143–161. [CrossRef]
15. Ashfaq, J.; Channa, I.A.; Shaikh, A.A.; Chandio, A.D.; Shah, A.A.; Bughio, B.; Birmahani, A.; Alshehri, S.; Ghoneim, M.M. Gelatin and Papaya-Based Biodegradable and Edible Packaging Films to Counter Plastic Waste Generation. *Materials* **2022**, *15*, 1046. [CrossRef]
16. Shaikh, S.; Yaqoob, M.; Aggarwal, P. An overview of biodegradable packaging in food industry. *Curr. Res. Food Sci.* **2021**, *4*, 503–520. [CrossRef]
17. Żołek-Tryznowska, Z.; Holica, J. Starch films as an environmentally friendly packaging material: Printing performance. *J. Clean. Prod.* **2020**, *276*, 124265. [CrossRef]
18. Channa, I.A.; Ashfaq, J.; Gilani, S.J.; Chandio, A.D.; Yousuf, S.; Makhdoom, M.A.; bin Jumrah, M.N. Sustainable and Eco-Friendly Packaging Films Based on Poly (Vinyl Alcohol) and Glass Flakes. *Membranes* **2022**, *12*, 701. [CrossRef]
19. Mishra, S.K.; Dahiya, S.; Gangil, B.; Ranakoti, L.; Agrawal, N. Mechanical properties of fibre/ filler based poly(Lactic Acid) (Pla) composites: A brief review. *Acta Innov.* **2021**, *41*, 5–18. [CrossRef]
20. Gairola, S.P.; Tyagi, Y.; Gangil, B.; Jha, K. Physio-mechanical & wear performance of banana fiber/walnut powder based epoxy composites. *Acta Innov.* **2021**, *41*, 42–55. [CrossRef]
21. White, A.; Lockyer, S. Removing plastic packaging from fresh produce—What’s the impact? *Nutr. Bull.* **2020**, *45*, 35–50. [CrossRef]

22. White, H. Evidence Review: Plastic Packaging and Fresh Produce, Banbury, UK, 2018. Available online: www.wrap.org.uk (accessed on 26 September 2021).
23. Schweitzer, J.-P.; Gionfra, S.; Pantzar, M.; Mottershead, D.; Watkins, E.; Petsinaris, F.; ten Brink, P.; Ptak, E.; Lacey, C.; Janssens, C. Unwrapped: How Throwaway Plastic is Failing to Solve Europe's Food Waste Problem (and what we need to do instead), Brussels, Belgium. 2018. Available online: www.rethinkplasticalliance.eu/ (accessed on 26 September 2021).
24. Naderifar, M.; Goli, H.; Ghaljaei, F. Snowball Sampling: A Purposeful Method of Sampling in Qualitative Research. *Strides Dev. Med. Educ.* **2017**, *14*. [CrossRef]
25. Handcock, M.S.; Gile, K.J. Comment: On the Concept of Snowball Sampling. *Sociol. Methodol.* **2011**, *41*, 367–371. [CrossRef]
26. Kirchherr, J.; Charles, K. Enhancing the sample diversity of snowball samples: Recommendations from a research project on anti-dam movements in Southeast Asia. *PLoS ONE* **2018**, *13*, e0201710. [CrossRef]
27. European Commission. Directive (EU). 2019/904 of the European Parliament and of the Council of 5 June 2019 on the Reduction of the Impact of Certain Plastic Products on the Environment. *Off. J. Eur. Union.* **2019**, *155*, 1–19. Available online: <https://eur-lex.europa.eu/eli/dir/2019/904/oj> (accessed on 26 September 2021).
28. European Commission. Directive (EU) 2015/720 of the European Parliament and of the Council of 29 April 2015 amending Directive 94/62/EC as regards reducing the consumption of lightweight plastic carrier bags. *Off. J. Eur. Union.* **2015**, *115*, 11–15. Available online: <https://eur-lex.europa.eu/legal-content/EN/TXT/?uri=CELEX:32015L0720> (accessed on 26 September 2021).
29. European Commission. Directive 94/62/EC of the European Parliament and Council of 20 December 1994 on packaging and packaging waste. *Off. J. Eur. Communities* **1994**, *1993*, 10–23. Available online: <https://eur-lex.europa.eu/legal-content/EN/ALL/?uri=CELEX:31994L0062> (accessed on 26 September 2021).
30. European Commission. The Plastic Bags Directive, (n.d.). Available online: https://ec.europa.eu/environment/topics/plastics/plastic-bags_en (accessed on 6 November 2021).
31. US National Oceanic and Atmospheric Administration. Woods Hole Sea Grant. 2021. Available online: <https://seagrant.whoi.edu/> (accessed on 26 September 2021).
32. Toussaint, B.; Raffael, B.; Angers-Loustau, A.; Gilliland, D.; Kestens, V.; Petrillo, M.; Rio-Echevarria, I.M.; Van den Eede, G. Review of micro- and nanoplastic contamination in the food chain. *Food Addit. Contam. Part A* **2019**, *36*, 639–673. [CrossRef]
33. European Bioeconomy Alliance. EUBA Position on the JRC LCA Methodology. *Eur Bioplastics* **2021**, 1–2. Available online: https://docs.european-bioplastics.org/publications/EUBA_Position_on_JRC_LCA_Methodology.pdf (accessed on 5 December 2021).
34. Nessi, S.; Sinkko, T.; Bulgheroni, C.; Garcia-Gutierrez, P.; Giuntoli, J.; Konti, A.; Sanye-Mengual, E.; Tonini, D.; Pant, R.; Marelli, L.; et al. Life Cycle Assessment (LCA) of Alternative Feedstocks for Plastics Production Part 1: The Plastics LCA Method. 2020. Available online: <https://publications.jrc.ec.europa.eu/repository/handle/JRC125046#:~:text=ThePlasticsLCAMethodprovides,studiesattheEUlevel> (accessed on 16 November 2021).
35. Peters, D.; Spottle, M.; Hahl, T.; Kuhner, A.-K.; Cuijpers, M.; Stomph, T.J.; van der Werf, W.; Grass, M. Methodologies for the Identification and Certification of Low ILUC Risk Biofuels. 2016. Available online: https://energy.ec.europa.eu/methodologies-identification-and-certification-low-iluc-risk-biofuels_en (accessed on 23 September 2021).
36. European Bioplastics. Bio-based Coalition Criticizes EU Methodology for LCAs Favouring Fossil-based Over Bio-based Plastics. 2021. Available online: <https://www.european-bioplastics.org/bio-based-coalition-criticizes-eu-methodology-for-lcas-favouring-fossil-based-over-bio-based-plastics/> (accessed on 6 September 2021).
37. Assembleia da República, Lei no 76/2019 of 2 September 2019. pp. 31–34. Available online: <https://dre.pt/dre/LinkFicheiroAntigo?ficheiroId=124347446> (accessed on 26 September 2021).
38. Assembleia da República, Decreto Lei no 78/2021 of 24 September. 2021. Available online: <https://dre.pt/dre/detalhe/decreto-lei/78-2021-171871496> (accessed on 26 September 2021).
39. Fundo Ambiental, Aviso no 19975/2021, Diário da República n.o 206/2021, Série II de 2021-10-22. 2021, pp. 287–305. Available online: https://dre.pt/web/guest/home/-/dre/173286479/details/9/maximized?serie=II&parte_filter=31&day=2021-10-22&date=2021-10-01&dreId=173280803 (accessed on 26 September 2021).
40. Minister Klimatu i Środowiska, Projekt ustawy o zmianie ustawy o obowiązkach przedsiębiorców w zakresie gospodarowania niektórymi odpadami oraz o opłacie produktowej oraz niektórych innych ustaw. 2021. Available online: <https://legislacja.rcl.gov.pl/projekt/12345305/katalog/12777253#12777253> (accessed on 10 September 2021).
41. Parliament of Ukraine, Law of Ukraine of June 1, 2021 No. 1489-IX about Restriction of Turnover of Plastic Packets in the Territory of Ukraine. 2021, pp. 300–303. Available online: <https://cis-legislation.com/document.fwx?rgn=132826> (accessed on 26 September 2021).
42. Presidência da República, Política Nacional de Resíduos Sólidos—Lei no 12.305/10. 2010. Available online: http://www.planalto.gov.br/ccivil_03/_Ato2007-2010/2010/Lei/L12305.htm (accessed on 10 September 2021).
43. Oceana, Legislações de outros países apontam caminho para redução de plástico descartável. 2021. Available online: <https://brasil.oceana.org/blog/legislacoes-de-outros-paises-apontam-caminho-para-reducao-de-plastico-descartavel/> (accessed on 26 September 2021).
44. U.S. Actions to Address Plastic Pollution, Washington DC. 2022. Available online: <https://www.state.gov/u-s-actions-to-address-plastic-pollution/> (accessed on 26 September 2021).

45. Nacional Conferences of State Legislatures, National Conference of State Legislatures—State Plastic Bag Legislation. 2021. Available online: <https://www.ncsl.org/research/environment-and-natural-resources/plastic-bag-legislation.aspx> (accessed on 26 September 2021).
46. Silva, A.L.P.; Prata, J.C.; Walker, T.R.; Campos, D.; Duarte, A.C.; Soares, A.M.; Barcelò, D.; Rocha-Santos, T. Rethinking and optimising plastic waste management under COVID-19 pandemic: Policy solutions based on redesign and reduction of single-use plastics and personal protective equipment. *Sci. Total Environ.* **2020**, *742*, 140565. [CrossRef]
47. Prata, J.C.; Silva, A.L.; Walker, T.R.; Duarte, A.C.; Rocha-Santos, T. COVID-19 Pandemic Repercussions on the Use and Management of Plastics. *Environ. Sci. Technol.* **2020**, *54*, 7760–7765. [CrossRef]
48. Qi, W.; Jinping, Q.; Bi, S.; Ning, C.; Min, N.; Shuangqiao, Y. Prevention and Control of Waste Plastics Pollution in China. *Chin. J. Eng. Sci.* **2021**, *23*, 160–166. [CrossRef]
49. Chinese National Development and Reform. *Single-Use Plastic Straw and Bag Ban Takes Effect*; Chinese National Development and Reform: Beijing, China, 2021.
50. Liu, J.; Yang, Y.; An, L.; Liu, Q.; Ding, J. The Value of China’s Legislation on Plastic Pollution Prevention in 2020. *Bull. Environ. Contam. Toxicol.* **2021**, *108*, 601–608. [CrossRef]
51. Duan, H.; Song, G.; Qu, S.; Dong, X.; Xu, M. Post-consumer packaging waste from express delivery in China. *Resour. Conserv. Recycl.* **2019**, *144*, 137–143. [CrossRef]
52. Standing Committee of the National People’s Congress. *Law of the People’s Republic of China on the Prevention and Control of Environment Pollution Caused by Solid Wastes (2020 Revision)*; Standing Committee of the National People’s Congress: Beijing, China, 2014; Volume 341902, pp. 1–35.
53. Pro Carton. *The Second European Consumer Packaging Perceptions Study*; Perspectives Global: Great Britain, London, 2021; Available online: www.procarton.com (accessed on 1 September 2021).
54. Prata, J.C.; Silva, A.L.P.; Duarte, A.C.; Rocha-Santos, T. The road to sustainable use and waste management of plastics in Portugal. *Front. Environ. Sci. Eng.* **2021**, *16*, 1–16. [CrossRef]
55. Costa, A.R.; Nabais, R.; Mota, A. Combater o plástico descartável. 2021. Available online: <https://www.deco.proteste.pt/casa-energia/manutencao-casa/noticias/combater-plastico-descartavel> (accessed on 16 September 2021).
56. Visão Verde. Portugal Produz Resíduos de Plástico Acima da Média Europeia, Conclui Estudo. 2021. Available online: https://visao.sapo.pt/visao_verde/ambiente/2021-11-06-portugal-produz-residuos-de-plastico-acima-da-media-europeia-estudo/ (accessed on 4 September 2021).
57. Barros, I. Quais as Soluções Empresariais Para uma Sociedade de Baixo Carbono? 2019. Available online: <https://www.ambientemagazine.com/quais-as-solucoes-empresariais-para-uma-sociedade-de-baixo-carbono/> (accessed on 6 September 2021).
58. Capital Verde, Bioplásticos Podem Não ser a Melhor Solução para Substituir o Plástico. 2021. Available online: <https://eco.sapo.pt/2021/06/25/bioplásticos-podem-nao-ser-a-melhor-solucao-para-substituir-o-plastico/> (accessed on 26 September 2021).
59. Pinto, I. Indústria dos Insetos: Consórcio Quer Investir 57 Milhões e Criar 140 Postos de Trabalho Até 2025. 2019. Available online: <https://www.dinheirovivo.pt/empresas/insectera-consorcio-quer-investir-57-milhoes-e-criar-140-postos-de-trabalho-ate-2025-14324032.html> (accessed on 26 September 2021).
60. CBOS. Swiadomość Ekologiczna Polakow. 2020. Available online: https://www.cbos.pl/SPISKOM.POL/2000/K_161_00.PDF (accessed on 26 September 2021).
61. Kantar. Who Cares, Who Does. 2021. Available online: <https://www.kantar.com/campaigns/who-cares-who-does-in-the-fmcg-industry> (accessed on 26 September 2021).
62. Czuchaj-Lagód, K.; Green Generation. Wspólnie na Rzecz Ziemi. 2020. Available online: https://eizba.pl/wp-content/uploads/2020/01/GreenGeneration_WspolnieNaRzeczZiemi.pdf (accessed on 12 September 2021).
63. Musina, L. Report on Green Transformation in Ukraine. 2016. Available online: http://www.eap-green.org/resources/2016_GreenTransformationinUkraineENG.pdf (accessed on 26 September 2021).
64. Ishchenko, M.; Iarova, A.; Adamovska, V.; Astafieva, K.; Holoborodko, T.; Lapshyna, D.; Holovchenko, Y. Waste management in Ukraine: Organizational aspects. *E3S Web Conf.* **2021**, *280*, 11004. [CrossRef]
65. Kou, H.; Zhang, S.; Liu, Y. Community-Engaged Research for the Promotion of Healthy Urban Environments: A Case Study of Community Garden Initiative in Shanghai, China. *Int. J. Environ. Res. Public Health* **2019**, *16*, 4145. [CrossRef]
66. Yin, J.; Zhang, Y. Institutional Dynamics and Corporate Social Responsibility (CSR) in an Emerging Country Context: Evidence from China. *J. Bus. Ethic.* **2012**, *111*, 301–316. [CrossRef]
67. Guttman, D.; Young, O.; Jing, Y.; Bramble, B.; Bu, M.; Chen, C.; Furst, K.; Hu, T.; Li, Y.; Logan, K.; et al. Environmental governance in China: Interactions between the state and “nonstate actors”. *J. Environ. Manag.* **2018**, *220*, 126–135. [CrossRef]
68. Fang, C.; Wang, Z.; Liu, H. Beautiful China Initiative: Human-nature harmony theory, evaluation index system and application. *J. Geogr. Sci.* **2020**, *30*, 691–704. [CrossRef]
69. Ibis World, Solid Waste Recycling Industry in China—Market Research Report, 2021. Available online: <https://www.ibisworld.com/china/market-research-reports/solid-waste-recycling-industry/> (accessed on 6 December 2021).
70. The Royal Swedish Academy of Sciences. Natural Experiments Help Answer Important Questions for Society. 2021. Available online: <https://www.nobelprize.org/prizes/economic-sciences/2021/press-release/> (accessed on 12 December 2021).

71. World Bank, GDP, PPP (constant 2017 international \$), 2021. Available online: <https://data.worldbank.org/indicator/NY.GDP.MKTP.PPKD> (accessed on 12 December 2021).
72. World Bank, Purchasing Power Parities and the Size of World Economies, Washington. 2020. Available online: <http://hdl.handle.net/10986/33623> (accessed on 26 September 2021).
73. WWF. Environmental Problems in Brazil. 2021. Available online: www.panda.org (accessed on 3 December 2021).
74. Kuczabski, A.; Michalski, T. Ukrainian Post-Communist Transformation: Causes, Consequences and Threats. *Quaest. Geogr.* **2014**, *33*, 171–180. [[CrossRef](#)]
75. Ritchie, H.; Roser, M. Age Structure. 2019. Available online: <https://ourworldindata.org/age-structure> (accessed on 26 September 2021).
76. United Nations. 2018 Revision of the World Urbanization Prospects, United Nations. 2018. Available online: <https://population.un.org/wup/> (accessed on 28 September 2021).
77. Scarpi, D.; Russo, I.; Confente, I.; Hazen, B. Individual antecedents to consumer intention to switch to food waste bioplastic products: A configuration analysis. *Ind. Mark. Manag.* **2020**, *93*, 578–590. [[CrossRef](#)]
78. Koenig-Lewis, N.; Grazzini, L.; Palmer, A. Cakes in plastic: A study of implicit associations of compostable bio-based versus plastic food packaging. *Resour. Conserv. Recycl.* **2021**, *178*, 105977. [[CrossRef](#)]
79. Donato, C.; Barone, A.M.; Romani, S. The satiating power of sustainability: The effect of package sustainability on perceived satiation of healthy food. *Br. Food J.* **2021**, *123*, 162–177. [[CrossRef](#)]
80. Bui, M.; Tangari, A.H.; Haws, K.L. Can health “halos” extend to food packaging? An investigation into food healthfulness perceptions and serving sizes on consumption decisions. *J. Bus. Res.* **2017**, *75*, 221–228. [[CrossRef](#)]
81. Adamkiewicz, J.; Kochanska, E.; Adamkiewicz, I.; Lukasik, R.M. Greenwashing and sustainable fashion industry. *Curr. Opin. Green Sustain. Chem.* **2022**, 100710. [[CrossRef](#)]
82. Vantomme, D.; Geuens, M.; De Houwer, J.; De Pelsmacker, P. Implicit Attitudes Toward Green Consumer Behaviour. *Psychol. Belg.* **2005**, *45*, 217–239. [[CrossRef](#)]
83. Rhein, S.; Schmid, M. Consumers’ awareness of plastic packaging: More than just environmental concerns. *Resour. Conserv. Recycl.* **2020**, *162*, 105063. [[CrossRef](#)]
84. Medina, C.A.G.; Martinez-Fiestas, M.; Viedma-Del-Jesús, M.I.; Aranda, L.A.C. The processing of price during purchase decision making: Are there neural differences among prosocial and non-prosocial consumers? *J. Clean. Prod.* **2020**, *271*, 122648. [[CrossRef](#)]

Article

Machine Learning and Deterministic Methods for Detection Meteorological Phenomena from Ground Measurements: Application for Low-Level Jet and Sea-Breeze Identification in Northern France

Sayahnya Roy ^{1,2}, Alexei Sentchev ¹, Marc Fourmentin ² and Patrick Augustin ^{2,*}

¹ CNRS, UMR 8187—LOG—Laboratoire d’Océanologie et de Géosciences, University Lille, University Littoral Côte d’Opale, F 62930 Wimereux, France

² UR 4493—LPCA—Laboratoire de Physico-Chimie de l’Atmosphère, University Littoral Côte d’Opale, F 59140 Dunkerque, France

* Correspondence: augustin@univ-littoral.fr

Abstract: This study focused on the detection of mesoscale meteorological phenomena, such as the nocturnal low-level jet (NLLJ) and sea breeze (SB), using automatic deterministic detection wavelet technique algorithms (HWTT and SWT) and the machine learning recurrent neural network (RNN) algorithm. The developed algorithms were applied for detection of NLLJ and SB events from ultrasonic anemometer measurements, performed between January 2018 and December 2019 at a nearshore experimental site in the north of France. Both algorithms identified the SB and NLLJ days successfully. The accuracy of SB event detection by the RNN algorithm attained 95%, and we identified 67 and 78 SB days in 2018 and 2019, respectively. Additionally, a total of 192 and 168 NLLJ days were found in 2018 and 2019, respectively. To demonstrate the capability of the algorithms to detect SB and NLLJ events from near-ground ultrasonic anemometer measurements, analysis of the simultaneous wind lidar measurements available for 86 days were performed. The results show a good agreement between the RNN-based detection method and the lidar observations, detecting 88% of SB. Deterministic algorithms (HWTT and SWT) detected a similar number of NLLJ events and provided high correlation (0.98) with the wind lidar measurements. The meteorological phenomena studied can significantly affect the energy production of offshore wind farms. It was found that the maximum hourly average peak power production could be to 5 times higher than that of the reference day due to higher wind speed observed during NLLJ events. During SB events, hourly average peak power production could be up to 2.5 times higher. In this respect, the developed algorithms applied for analysis, from near-ground anemometer measurements, may be helpful for monitoring and forecasting the meteorological phenomena capable of disturbing the energy production of offshore wind turbines.

Citation: Roy, S.; Sentchev, A.; Fourmentin, M.; Augustin, P. Machine Learning and Deterministic Methods for Detection Meteorological Phenomena from Ground Measurements: Application for Low-Level Jet and Sea-Breeze Identification in Northern France. *Atmosphere* **2022**, *13*, 1873. <https://doi.org/10.3390/atmos13111873>

Academic Editor: Massimiliano Burlando

Received: 23 September 2022

Accepted: 7 November 2022

Published: 10 November 2022



Copyright: © 2022 by the authors. Licensee MDPI, Basel, Switzerland. This article is an open access article distributed under the terms and conditions of the Creative Commons Attribution (CC BY) license (<https://creativecommons.org/licenses/by/4.0/>).

Keywords: sea breeze; nocturnal low-level jet; machine learning algorithm; wind; phenomenon automatic detection algorithm

1. Introduction

A number of meteorological phenomena, such as the nocturnal low-level jet (NLLJ) and sea breeze (SB), are observed in the lower atmospheric boundary layer in coastal regions. During these events, changes in wind speed, direction, and turbulence parameters occur at a time scales smaller than one hour. As a result, NLLJ and SB may have some impacts on the power production of wind turbines and air quality [1–3].

During SB events, the wind speed increases and the wind blows from the sea towards the land. This phenomenon occurs due to an adverse atmospheric pressure gradient generated by the temperature difference between the land and sea during the daytime. SB

evolution depends on a large range of geophysical factors including topography, Coriolis force, heat diffusion, solar radiation, synoptic forcing, and sea surface temperature [4–6].

In coastal regions, LLJ, characterized by a maximum in the wind speed profile in the lower troposphere [7,8], can have different driving mechanisms [9]. According to Schulz-Stellenfleth et al. [10], LLJ can be attributed to frictional decoupling from the underlying surface or baroclinicity due to the temperature contrast between the land and sea. Over the southern North Sea, relatively warm continental air advected over the cooler sea surface supports the development of surface temperature inversion, leading to the decoupling of the surface friction and acceleration of an air mass [11,12]. Moreover, the surface roughness difference between the land and sea favors the air flow acceleration [13]. Over the southern part of the North Sea, LLJ mainly occurs during the nighttime hours [13].

Recently, the power production of offshore wind turbines has become a large source of renewable energy capable of minimizing global carbon emissions. Since the SB is an important event of the coastal and offshore wind climate, it may significantly affect the resource assessment during the initial pre-construction phase of a wind farm. Indeed, the effect of the SB on offshore wind power production is not negligible; for example, along the Gujarat coast (India), the SB contributed 6.2% of the annual energy generation at the nearshore locations [14]. In the Llobregat Delta (NE of the Iberian Peninsula), Mazon et al. [2] found that a range of 42 to 55% of total wind energy was generated during the SB period, which accounts for 22% of the total time in a year. The resource assessment studies highlighted the importance of sea breezes, because they occur frequently during peak energy demand periods (summer afternoons) across many coastlines designated for offshore wind energy [15,16]. Some studies conducted in the European North Sea reported an enhancement in energy production due to SB [17,18]. Around the southern North Sea, Steele et al. [17] estimated wind energy enhancement of 10% due to the presence of the coastal jet, depending on the sea-breeze type and coastline characteristics. The SB may affect LLJ formation. During the North Sea OBLEX-F1 campaign, SB circulations have been observed that vanished before jet detection [9]. This process was previously observed by Angevine et al. [19], where an LLJ evolved after an SB breakdown [19]. During the OBLEX-F1 campaign, most LLJ detections occurred between the evening and the morning [9]. As population density and economic activity in the coastal zone increase [20], this nocturnal phenomenon can have some important impact on air quality [21–24] and on power production of wind turbines, especially during the high-electricity-consumption evening period (peak period), corresponding to the evening hours (after sunset) when there is a lot of demand [25]. To meet the nighttime power requirement from offshore wind turbines, NLLJ events can be effective in coastal regions.

Therefore, there is a strong motivation to fully understand the offshore wind and to develop algorithms capable of efficiently, easily, and quickly detecting SB and NLLJ from near ground, in situ measurements. In the literature, several methods have been developed for time series classification, such as feature-based [26] and transformation-based ensembles [27,28], supervised machine learning algorithms [29], and deep learning [30,31]. However, to the best of our knowledge, no study has focused on SB day classification algorithms using machine learning and NLLJ using deterministic methods applied mainly to in situ wind measurements near the ground.

The present study focused on the development of cutting-edge classification algorithms for SB and NLLJ, using time series of wind speed, wind direction, and turbulence kinetic energy measured by an ultrasonic anemometer in the coastal region of northern France. Moreover, we checked the performance of these algorithms by comparing them with lidar measurements. The second objective of this study was to develop a new machine learning algorithm using a recurrent neural network (RNN) to detect SB days and algorithms to detect NLLJ using discrete wavelet transform. The measurement techniques and the methodology for analysis and classification are presented in Section 2, and results are summarized in Section 3, followed by the conclusion in Section 4.

2. Materials and Methods

Measurements were taken in Dunkerque for a period of 2 years, using a 20 Hz ultrasonic anemometer (Figure 1). This measurement device provides 15 min averaged data. In the frame of EPhEMER project (Etude des Phénomènes météorologiques et leurs impacts sur la production Eolienne en MER) and during an intensive observation period (IOP) of 86 days (from July to October 2021), another ultrasonic anemometer located in the front of the coastal line (15 m AGL) and two Vaisala WindCube lidars (WLS7 and WLS100) were deployed to assess the impact of NLLJ and SB on wind turbines.

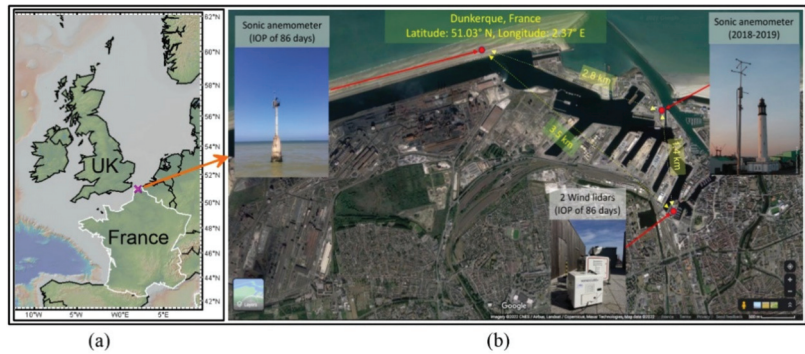


Figure 1. Measurement location map of North West of Europe (a); location in Dunkerque of the different experimental devices used in the measurement campaign (2 ultrasonic anemometers and 2 wind lidars) (b).

2.1. Calculation of Turbulence Parameters

u_R , v_R , and w_R are respectively the zonal, meridional, and vertical components of wind velocity measured using the ultrasonic anemometer. The wind flow directions are detailed in [32]. To avoid the effects of the meteorological coordinate system on the turbulence parameters, we adopted a new coordinate system where the mean flow is aligned with the x-axis [32,33]. In the new coordinate system, the instantaneous streamwise, transverse, and vertical wind velocity components (u , v , and w) were decomposed into a mean part and fluctuating part as:

$$u = \bar{u} + u', \quad v = \bar{v} + v', \quad w = \bar{w} + w', \quad (1)$$

where \bar{u} , \bar{v} , and \bar{w} are mean velocity components (15 min averaged), and u' , v' , and w' are the corresponding velocity fluctuations.

The turbulence kinetic energy (TKE) is defined as:

$$TKE = \frac{1}{2} (\overline{u'^2} + \overline{v'^2} + \overline{w'^2}), \quad (2)$$

The integral length scale can be calculated from the autocorrelation function using the Taylor frozen turbulence hypothesis [34] as:

$$L_u = u \int_0^\infty C_{u,x}(t) d\Delta t, \quad (3)$$

where $C_{u,x}(t)$ is the autocorrelation function, given as:

$$C_{u,x}(\Delta t) = C_{u,x}(\Delta x) = \frac{u'(t) \cdot u'(t - \Delta t)}{u'^2}, \quad (4)$$

and Δt is the time period, defined as:

$$\Delta t = \frac{\Delta x}{u}, \tag{5}$$

2.2. Detection Methods

To detect the SB and NLLJ, we developed four automatic detection algorithms: (i) Sign Change of Sea-Breeze Component (SCSBC) and (ii) machine learning recurrent neural network (RNN) for SB detection; (iii) Haar wavelet threshold technique (HWTT) and (iv) Symlets wavelet slope technique (SWT) for NLLJ detection.

In the SCSBC algorithm, four filters were used to identify SB days (steps 1 to 4 in Figure 2). Step 1 separates the extreme events. Step 2 rejects those days where wind direction changes more than 90 degrees in less than 1 h. In Step 3, for a period from 08:00 to 11:00 UTC, a shift in wind direction from offshore to onshore was recognized from an alteration of the sign of the normalized SB component ($SBC = (U \times \sin(-W_D))/U$, where W_D is the wind direction and U is the horizontal wind speed). A change from a negative to a positive value of SBC signifies the occurrence of an SB [35]. In the last step, a positive slope of the temperature gradient confirms the authenticity of the SB.

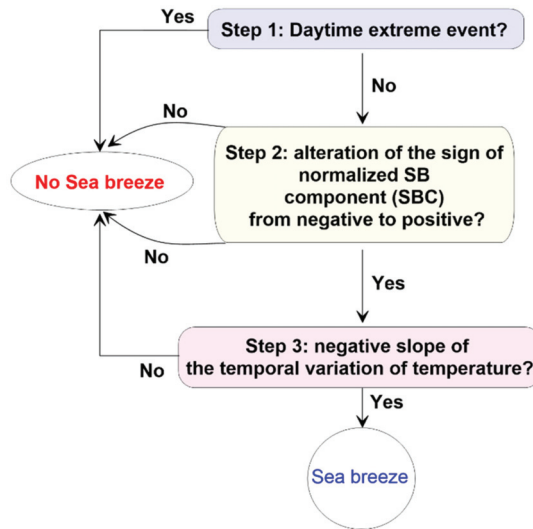


Figure 2. Flow chart for the SCSBC sea-breeze identification method.

In the RNN framework for SB detection, long short-term memory (LSTM) neural networks are a typical form of RNN. Hidden units in LSTM are capable of recalling the long-term reliance on sequential data (e.g., time series data), thus enhancing the efficiency for classifying the SB and non-SB days. Figure 3 shows the LSTM framework. Since SB days are frequent during the summer, we used six months (from April to September) of data in the input layer. The SBC in each day is treated as features, which consist of 15 min averaged wind direction for a period of 24 h. A total of 182 sequential feature vectors are used to train the network. The cell state in one LSTM block is updated by four interacting layers, namely, forgetting gate, input gate, cell state updating, and output gate. Equations involved in these gates are detailed in [3]. Note that a number of trials with hidden units was made to optimize the hyperparameter. We found that 96 hidden units is best to achieve an optimal prediction of SB days. The output from LSTM passes through a fully connected layer (2 classes). The output from the fully connected layer is followed by an output layer consisting of a softmax activation function, resulting in binary classification (i.e., 1 for SB or 0 for non-SB).

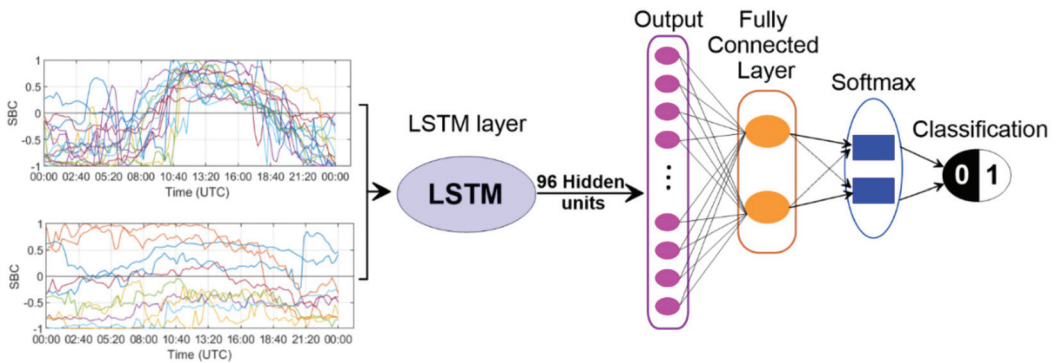


Figure 3. Machine learning recurrent neural network for the sea-breeze identification method (RNN).

We used a cross-entropy loss function to train classifiers. To optimize the backpropagation, the adaptive momentum estimator (ADAM) was used. The initial learning rate of ADAM was 0.001. To achieve a maximum accuracy a minibatch of 27 sequences, 300 epochs (6 iterations per epoch) were used. To train the network, we used 182 sequences from the year 2018. To test the network output, the same number of sequences from 2019 was used.

For HWTT for NLLJ detection, we used 5 filters (steps 1 to 2.3) to identify the NLLJ events (Figure 4). Since the LLJ is a nighttime event, Step 1 eliminates the extreme events. The turbulence kinetic energy (TKE) was calculated in Step 2. The decomposition of TKE was performed by the Haar wavelet function [1,36] in Step 2.1. In Steps 2.2 and 2.3, a large value of the dilation coefficient from sunset until early morning signifies the occurrence of NLLJ.

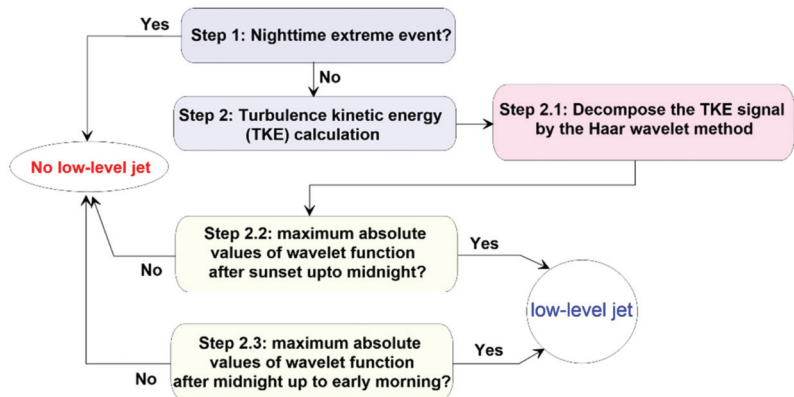


Figure 4. Flow chart for the low-level jet identification method using the Haar wavelet function (HWTT).

For the SWT for NLLJ detection (Figure 5), Steps 1 and 2 used in this algorithm are exactly the same as those for HWTT. However, the decomposition of the TKE signal was performed by discrete wavelet transform. Symlets mother wavelet function [37] was used to decompose the TKE signal into 4 levels of time resolution (15 min to 1 h). We tried to identify the NLLJ with all resolutions of decomposed TKE signals and found that a 1 h resolution (level 4) of the TKE signal provides optimal classification. The slope of this decomposed TKE was computed from sunset until early morning. In Steps 2.2 and 2.3, if the slope is positive from evening to midnight, and negative from midnight to early morning, it is considered a NLLJ event; otherwise, it is a non-NLLJ event.

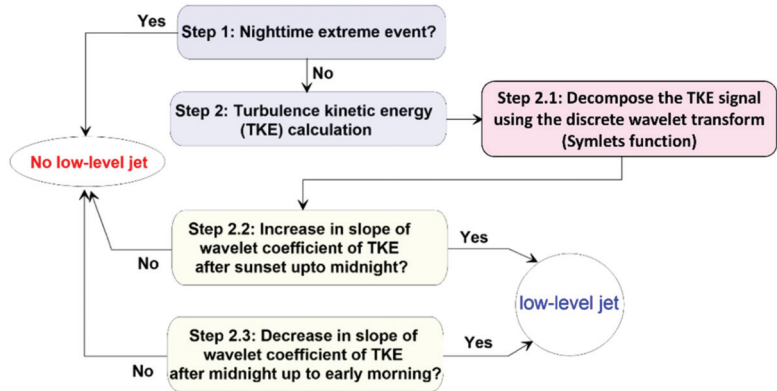


Figure 5. Flow chart for the low-level jet identification method using Symlets wavelet function and the slope of wavelet coefficients (SWT).

3. Results

3.1. Sea-Breeze Classification Results

The daytime heating creates thermal contrast between the land and sea, resulting in a concentrated wind flow from the sea toward land. We identified 67 and 78 SB days in 2018 and 2019, respectively, during the summertime (Figure 6) using the SCSBC algorithm.

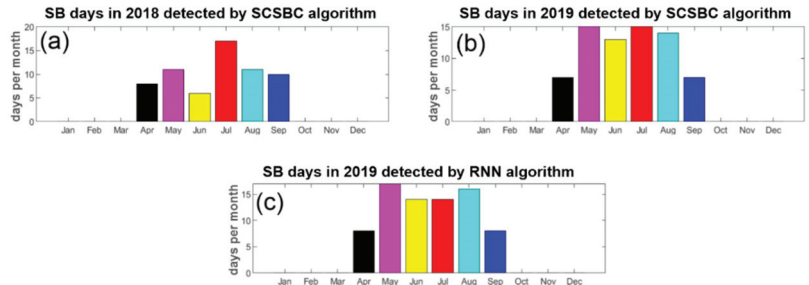


Figure 6. Identification of SB days using SCSBC algorithm from wind measurements in 2018 (a); 2019 (b). SB days identified by RNN algorithm, 2019 (c).

Furthermore, we developed an RNN algorithm using an LSTM block capable of detecting SB days. To train the network, we used the categorical SBC data from 2018. The RNN was used to classify the SB days in 2019. To validate the machine learning RNN performance, we used actual data of SBC from 2019 (Figure 7).

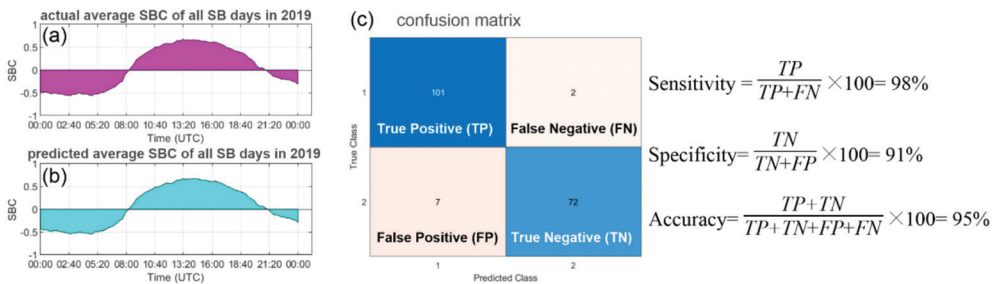


Figure 7. Performance test of RNN algorithm for SB day identification in 2019, actual average SBC of all SB days (a); predicted average SBC of all SB days (b); confusion matrix and accuracy (c).

The average actual and predicted SBC for all SB days are shown in Figure 6. In order to check the classification performance of the RNN algorithm, three statistical metrics, namely, sensitivity, specificity, and classification accuracy, were used. The sensitivity is defined as the ratio between the classified true positive (i.e., both observation and prediction samples are positive) and the total number of samples in true class 1, whereas false negative stands for the observed samples that are positive but prediction samples are negative. Specificity can be stated as the proportion of true negative (i.e., both observation and prediction samples are negative) and the total number of samples in true class 2, whereas false positive means the observed samples are negative but prediction samples are positive. The accuracy is calculated as the ratio of true positive and negative samples to all classes. The proposed RNN algorithm is good enough, having 98% sensitivity, 91% specificity, and 95% classification accuracy. The performance of the RNN algorithm can be enhanced with a greater number of observations.

Figure 8 shows the time average of the wind speed of all SB days. For both years, the range of variation in the average wind speed ($L_{WS} = 2.9$ m/s to $H_{WS} = 4.9$ m/s) was to be similar, where L_{WS} and H_{WS} are low and high wind speed, respectively. The maximum wind speed during the SB days occurs roughly from 13:00 UTC to 17:30 UTC. We observed that the maximum average wind speed during SB events is around 5 m/s (10 m AGL).

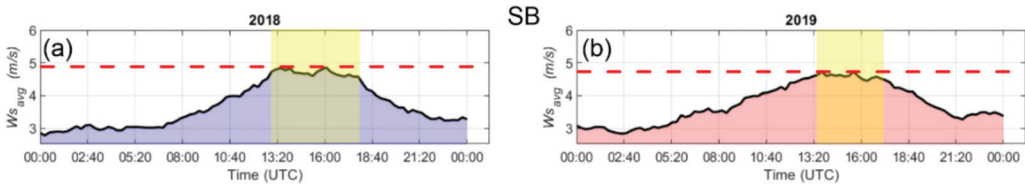


Figure 8. Time average of wind speed for all SB days during 2018 (a); 2019 (b).

3.2. Nocturnal Low-Level Jet Classification Results

A concentrated wind flow after sunset is known as the NLLJ. Since the NLLJ is a nighttime phenomenon, it can increase offshore wind power production during the night. Therefore, it is important to detect NLLJ phenomena in coastal regions for offshore wind turbines. We devised two automatic NLLJ detection algorithms, HWTT and SWT. Since the performance of both algorithms is quite similar, only the NLLJ classification by SWT is shown in Figure 9.

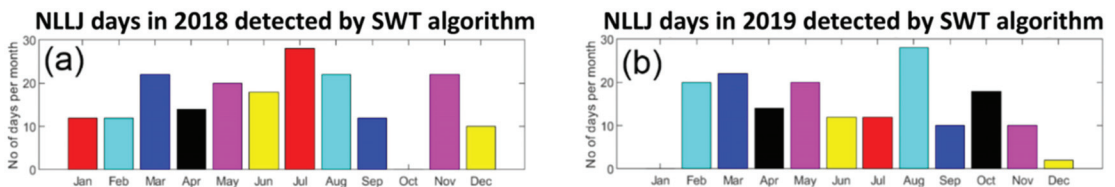


Figure 9. Identification of NLLJ days using SWT algorithm from wind measurements in 2018 (a); 2019 (b).

Except for October 2018 and January 2019, we found a significant occurrence of NLLJ in every month. A total of 192 and 168 NLLJ days were found in 2018 and 2019, respectively.

Figure 10 shows the hourly average of wind speed for all NLLJ days. The NLLJ events start during the evening; the wind speed increases until midnight, and then decreases. The range of average wind speed, near ground, was $L_{WS} = 3.9$ m/s to $H_{WS} = 4.9$ m/s in 2018 during NLLJ events. However, the range of average wind speed was $L_{WS} = 4.3$ m/s to $H_{WS} = 5.2$ m/s in 2019 during NLLJ events. We found that near the ground, the average wind speed increases by 1 m/s due to NLLJ during nighttime.

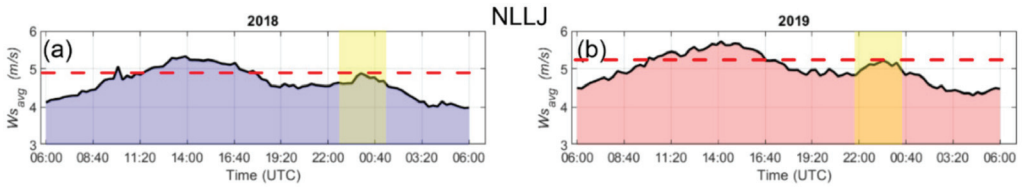


Figure 10. Time average of wind speed for all NLLJ days in 2018 (a); 2019 (b).

3.3. Validation of the Algorithms Detection

The algorithms of LLJ and SB detection were developed using only ultrasonic anemometer measurements during 2018–2019. However, in order to validate the algorithms, we exploited a statistically relevant database obtained from Vaisala WindCube lidar WLS100 measurements during an IOP of 86 days from 23 July 2021 to 16 October 2021. Hence, wind lidar measurements were used as a reference to validate the algorithms.

The RNN algorithm was validated by the SCSBC during 2019 and we ran it for the IOP. In this study, the SB criteria to determine the SB events from wind lidar measurements were the shift in wind direction from the land to the sea (<1 h) and/or the presence of the gravity current coming from the sea (NW to NE) with a change in wind direction [1]. During the IOP, 25 SB events were observed (two SB days from 23 to 31 July, eight days in August, 13 days in September, and two days in October 2021). The results obtained by the RNN algorithm are in good agreement with the observations, with 22 SB events detected (two SB days from 23 to 31 July, eight days in August, 10 days in September, and two days in October 2021).

Concerning NLLJ observations, NLLJ days were identified in the horizontal wind speed lidar profile, with a maximum wind (in this study below 1000 m), and decreasing wind speeds of at least 2 m/s both below and above that height [38]. NLLJ days occurred 28% of the time (582 of 2064 measurements), corresponding to 69 NLLJ events (162 of 250). During the IOP, the mean NLLJ core height was 260 m and the maximum observation height was between 500 and 800 m, corresponding to less than 10% of the NLLJ core height detected. The average NLLJ speed (wind speed at jet core height) was 10 m/s, with a standard deviation of 3 m/s. Around 75% of LLJ core came from the land to seaward, with a maximum of 20 m/s (Figure 11a), and a range of NLLJ speed between 8 and 14 m/s (Figure 11b).

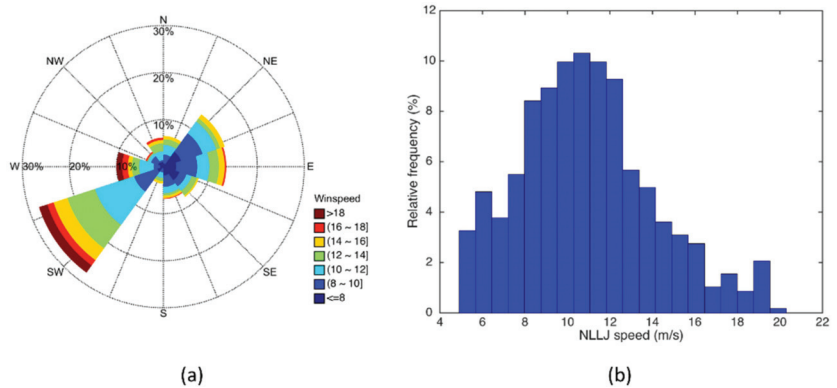


Figure 11. (a) Windrose of NLLJ core; NLLJ speed is shown in m/s and the percentage corresponds to the occurrence of NLLJ speed and direction relative to the total amount of NLLJ observed; (b) relative frequency distribution of NLLJ speed.

HWTT and SWT algorithms both detected 70 NLLJ events. The results show that 92% of events deduced from the HWTT algorithm are in good agreement with observations.

However, the algorithm detected 70 NLLJ events, corresponding to one event more than those observed, which can be attributed to the difficulty of validating this NLLJ event during a cloudy night, which limits the maximum range of wind lidar measurements. Moreover, 573 h of NLLJ were detected by the algorithm versus 582 h of NLLJ observations. The comparison between arrival times of NLLJ observed by the lidar and deduced from the algorithm shows a linear regression equation with an intercept of -0.05 , corresponding to a delay of about 1 h. The NLLJ time arrival agreed well with the observations. Moreover, comparison between the NLLJ breakdown times shows a linear regression equation with an intercept of $+0.04$. This means that the algorithm no longer detects the NLLJ with a gap of 1 h before the NLLJ breakdown times. Although the SW LLJ direction dominates during this IOP, both results cannot be explained by the separation distance between the anemometer and the wind lidar (located south from the anemometer). However, both results are in good agreement, with a correlation coefficient R^2 of 98% between the NLLJ detected from HWTT and wind lidar measurements.

3.4. Influence of NLLJ and SB on Power Production by Wind Turbines

In order to illustrate the impacts of NLLJ and SB on wind turbines, the hourly average of the horizontal wind speed for each altitude below 1000 m, measured by the wind lidar during NLLJ event days (Figure 12a) and SB event days (Figure 12b) of the IOP, was plotted. The date of 7 October 2021 was selected as a representative reference day without NLLJ and SB events below 300 m (Figure 12c).

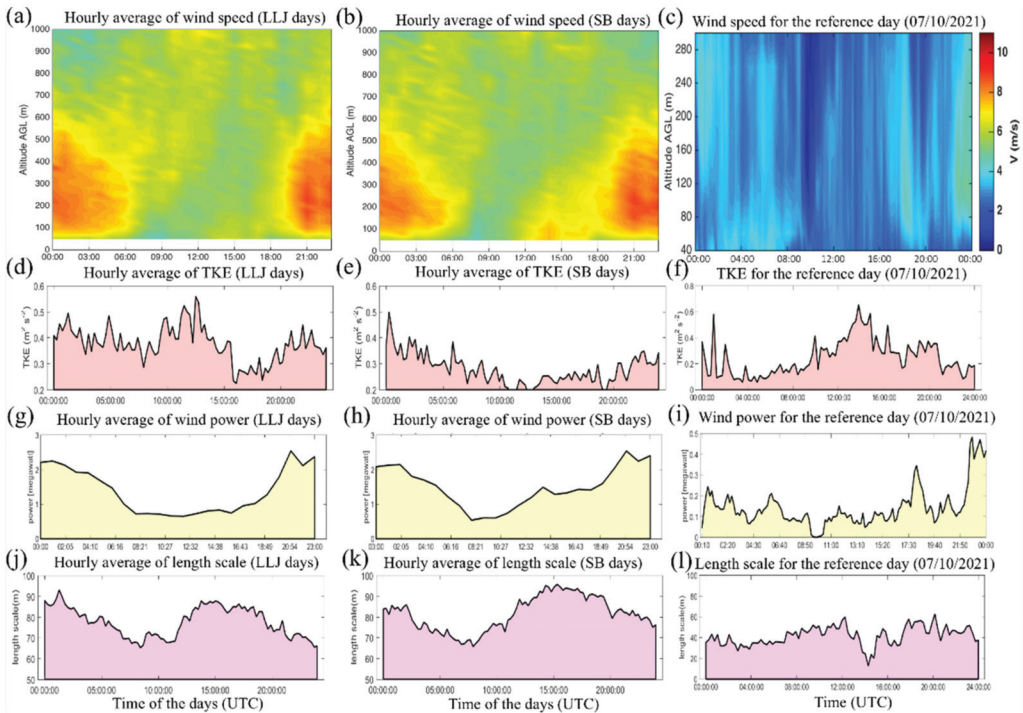


Figure 12. Time height section of hourly average horizontal wind speed using lidar measurements for NLLJ events from WLS100 (a); SB events from WLS100 (b); and for the reference day from WLS7 (c). Time evolution of hourly average TKE at 10 m (AGL) for NLLJ events (d); for SB events (e); and TKE for the reference day (f). Time evolution of hourly average potential power calculated using rotor equivalent wind speed for NLLJ events (g); for SB events (h); and for the reference day (i). Time evolution of hourly average length scale (L_H) for NLLJ events (j); for the SB events (k); and for the reference day (l).

Figure 12a reveals the presence of NLLJ between 00:00 to 6:00 UTC and 18:00 to 00:00 UTC located below 600 m. During NLLJ event days, the wind speed is relatively low during the daytime, unlike for the rest of the day, during which the NLLJ jet speed can reach more than 8 m/s. The NLLJ jet core is roughly located between 75–600 m with a jet speed height around 250 m. However, the majority of the jet core seems to decrease in the early morning before dissipating during daytime. The relatively high values of TKE observed near ground during the night can be explained by the presence of wind shear located below the jet core, which generates turbulence (Figure 12d).

Regarding SB events (Figure 12b), the results appear similar to those obtained for NLLJ events but with a more pronounced wind speed zone between 10:00 and 17:00 below 200 m. This zone corresponds to SB occurrence and seems to have an influence on the NLLJ development: the latter starts about 1 h earlier compared to days without SB events. This effect was observed in previous studies which revealed that, during low synoptic wind speeds, SB can occur, creating a LLJ [9,19,39]. This one-hour earlier arrival time of NLLJ may be explained by the fact that during SB events, the TKE is relatively low (Figure 12e), in comparison to the NLLJ event days (Figure 12d) and the reference day (Figure 12f); this may favor earlier formation of an inversion layer formation. Indeed, the daytime TKE low values may be due to the advection of cooling air coming from the sea toward the land. Therefore, the SB gravity current may support the development of surface temperature inversion, leading to the decoupling effect, which may favor the formation of the NLLJ.

The wind power production was estimated for a wind turbine with a height range of about 100–150 m. The power was calculated as:

$$Power = \frac{\pi}{2} r^2 U_{Res}^3 \rho \varphi, \tag{6}$$

where r is the rotor radius, U_{Res} is the rotor equivalent wind speed, ρ is air density, and φ is the efficiency factor; we used $\varphi = 40\%$ for all calculations.

The rotor equivalent wind speed can be calculated as [40]:

$$U_{Res} = \left(\sum_{i=1}^{n_h} U_i^3 \frac{\mathring{A}_i}{\mathring{A}} \right)^{1/3}, \tag{7}$$

where n_h is the measurement height, U_i is the average wind speed for the i^{th} segment, \mathring{A} is the total rotor swept area, $\mathring{A}_i (= \int_{H_i}^{H_{i+1}} \mathring{C}(H) dH)$ is the area of the i^{th} segment, where $\mathring{C}(H) = 2\sqrt{r^2 - (H - H_{hub})^2}$, r is the rotor radius, and H_{hub} is the hub height.

Figure 12g shows that the hourly average maximum power (≈ 2.5 megawatts) can be achieved at 21:00 UTC during the NLLJ events. Hence, the maximum hourly average estimated peak power generation is approximately 5 times higher than that of the reference day (Figure 12i). The hourly average SB events are mainly observed between 10:00 and 17:00 UTC. Then, during the SB events, the hourly average estimated peak power generation can be up to 2.5 times higher than that of the reference day.

The hourly average integral length scale (L_u), deduced near ground, has a similar evolution as that of the hourly average power production during the NLLJ (Figure 12j) and SB (Figure 12k) events, and the reference day (Figure 12l). L_u is the length of the largest eddy at the measurement location. An increment in L_u was observed within the NLLJ shear layer and the SB gravity current at the beginning of the NLLJ and SB occurrences. Moreover, the L_u during the NLLJ is 1.25 times larger than that of SB, which is 1.5 times larger than L_u of the reference day. By comparing all parameters used in this study, it was found that the ultrasonic anemometer measurements are useful for identifying NLLJ and SB events.

4. Conclusions

In this study, we assessed the wind measurements with the aim to identify SB and NLLJ meteorological events in the north of France. Measurements were mainly taken using an ultrasonic anemometer in the coastal region of Dunkerque. We developed four algorithms to identify NLLJ and SB days: Sign Change of Sea-Breeze Component (SCSBC), recurrent neural network (RNN) for SB, Haar wavelet threshold technique for NLLJ (HWTT), and Symlets wavelet slope technique for NLLJ (SWT).

These algorithms successfully identified the SB and NLLJ days. Some significant results obtained from the analysis are the following:

1. The proposed RNN algorithm is good enough for SB identification, having 98% sensitivity, 91% specificity, and 95% classification accuracy.
2. The results obtained from the RNN algorithm are in good agreement with the independent lidar observations and show that 88% of SB events were detected during the 86-day IOP.
3. Regarding NLLJ, the proposed algorithms (HWTT and SWT) detected a similar number of NLLJ events, with a R^2 of 0.98 between the NLLJ detected from HWTT and that from wind lidar measurement.
4. During the NLLJ events, the estimated maximum hourly average peak power generation was approximately 5 times higher than that of the reference day, and the peak power generation was 2.5 times higher during the SB events.
5. The integral length scale during the NLLJ was found to be 1.25 times larger than that during SB events. Furthermore, the integral length scale during the SB was 1.6 times larger than that expected for a reference day.

Author Contributions: Conceptualization, P.A. and A.S.; methodology, S.R., P.A., M.F. and A.S.; software, S.R., M.F., P.A.; validation, S.R., P.A., M.F. and A.S.; formal analysis, S.R., P.A., M.F. and A.S.; investigation, S.R., P.A., M.F. and A.S.; data curation, S.R., P.A., M.F. and A.S.; writing—original draft preparation, S.R., P.A. and A.S.; writing—review and editing, S.R., P.A., M.F. and A.S.; visualization, S.R., P.A., M.F. and A.S.; supervision, P.A. and A.S.; project administration, P.A. and A.S.; funding acquisition, P.A. and A.S. All authors have read and agreed to the published version of the manuscript.

Funding: This research was funded by EDF Renouvelables/EMD, by the Université du Littoral Côte d’Opale, by the Pôle de Recherche MTE, by the SFR Campus de la Mer, by the Institut de Recherches Pluridisciplinaires en Sciences de l’Environnement, by the Région «Hauts de France» and the Ministère de l’Enseignement Supérieur et de la Recherche (CPER IREnE and Climibio), by the European Fund for Regional Economic Development, by the Labex CaPPA (Chemical and Physical Properties of the Atmosphere), which is funded by the French National Research Agency through the PIA (Programme d’Investissement d’Avenir) under contract “ANR-11-LABX-0005-01”.

Acknowledgments: The authors would like to thank the Ministère de la Mer, the Direction interrégionale de la mer Manche Est - Mer du Nord, the Phares et Balises de Dunkerque for the permission to operate the field campaign in the front of coastal line of Dunkerque. The authors graciously acknowledge the efforts of our collaborators Caroline Piguet, Cedric Dalozzo (EDF Renouvelables), Anaïs Zamiara, Sébastien Lefèbvre (SFR Campus de la Mer), Véronique Vanvincq (UCEIV, Pôle MTE), Arnaud Cuisset, Dominique Schneider, Benoit Escorne (Pôle MTE), Julien Ratynski (LPCA), Fabien Marteel and Jérôme Parmentier (Service Technique du CGU de Dunkerque).

Conflicts of Interest: The authors declare no conflict of interest.

Abbreviations

NLLJ	Nocturnal Low-Level Jet
SB	Sea Breeze
AGL	Above Ground Level
RNN	Recurrent Neural Network
IOP	Intensive Observation Period
TKE	Turbulence Kinetic Energy
HWTT	Haar Wavelet Threshold Technique
SWT	Symlets Wavelet slope Technique
SCSBC	Sign Change of Sea-Breeze Component
LSTM	Long Short-Term Memory
ADAM	ADaptive Momentum estimator

References

- Augustin, P.; Billet, S.; Crumeyrolle, S.; Deboudt, K.; Dieudonné, E.; Flament, P.; Fourmentin, M.; Guilbaud, S.; Hanoune, B.; Landkocz, Y.; et al. Impact of Sea Breeze Dynamics on Atmospheric Pollutants and Their Toxicity in Industrial and Urban Coastal Environments. *Remote Sens.* **2020**, *12*, 648. [\[CrossRef\]](#)
- Mazon, J.; Rojas, J.I.; Jou, J.; Valle, A.; Olmeda, D.; Sanchez, C. An Assessment of the Sea Breeze Energy Potential Using Small Wind Turbines in Peri-Urban Coastal Areas. *J. Wind Eng. Ind. Aerodyn.* **2015**, *139*, 1–7. [\[CrossRef\]](#)
- Roy, S.; Sentchev, A.; Fourmentin, M.; Augustin, P. Turbulence of Landward and Seaward Wind during Sea-Breeze Days within the Lower Atmospheric Boundary Layer. *Atmosphere* **2021**, *12*, 1563. [\[CrossRef\]](#)
- Augustin, P.; Delbarre, H.; Lohou, F.; Campistron, B.; Puygrenier, V.; Cachier, H.; Lombardo, T. Investigation of Local Meteorological Events and Their Relationship with Ozone and Aerosols during an ESCOMPTE Photochemical Episode. *Ann. Geophys.* **2006**, *24*, 2809–2822. [\[CrossRef\]](#)
- Crumeyrolle, S.; Augustin, P.; Rivellini, L.-H.; Choël, M.; Riffault, V.; Deboudt, K.; Fourmentin, M.; Dieudonné, E.; Delbarre, H.; Derimian, Y.; et al. Aerosol Variability Induced by Atmospheric Dynamics in a Coastal Area of Senegal, North-Western Africa. *Atmos. Environ.* **2019**, *203*, 228–241. [\[CrossRef\]](#)
- Miller, S.T.K. Sea Breeze: Structure, Forecasting, and Impacts. *Rev. Geophys.* **2003**, *41*, 1011. [\[CrossRef\]](#)
- Banta, R.M.; Pichugina, Y.L.; Brewer, W.A. Turbulent Velocity-Variance Profiles in the Stable Boundary Layer Generated by a Nocturnal Low-Level Jet. *J. Atmos. Sci.* **2006**, *63*, 2700–2719. [\[CrossRef\]](#)
- Baas, P.; Bosveld, F.C.; Baltink, H.K.; Holtslag, A.A.M. A Climatology of Nocturnal Low-Level Jets at Cabauw. *J. Appl. Meteorol. Climatol.* **2009**, *48*, 1627–1642. [\[CrossRef\]](#)
- Wagner, D.; Steinfeld, G.; Witha, B.; Wurps, H.; Reuder, J. Low Level Jets over the Southern North Sea. *Meteorol. Z.* **2019**, *28*, 389–415. [\[CrossRef\]](#)
- Schulz-Stellenfleth, J.; Emeis, S.; Dörenkämper, M.; Bange, J.; Cañadillas, B.; Neumann, T.; Schneemann, J.; Weber, I.; zum Berge, K.; Platis, A.; et al. Coastal Impacts on Offshore Wind Farms—A Review Focussing on the German Bight Area. *Meteorol. Z.* **2022**, *31*, 289–315. [\[CrossRef\]](#)
- Davis, P.A. Development and Mechanisms of the Nocturnal Jet. *Meteorol. Appl.* **2000**, *7*, 239–246. [\[CrossRef\]](#)
- Larsén, X.G.; Fischereit, J. A Case Study of Wind Farm Effects Using Two Wake Parameterizations in the Weather Research and Forecasting (WRF) Model (V3.7.1) in the Presence of Low-Level Jets. *Geosci. Model Dev.* **2021**, *14*, 3141–3158. [\[CrossRef\]](#)
- Rausch, T.; Cañadillas, B.; Hampel, O.; Simsek, T.; Tayfun, Y.B.; Neumann, T.; Siedersleben, S.; Lampert, A. Wind Lidar and Radiosonde Measurements of Low-Level Jets in Coastal Areas of the German Bight. *Atmosphere* **2022**, *13*, 839. [\[CrossRef\]](#)
- Kumar, R.; Stallard, T.; Stansby, P.K. Large-scale Offshore Wind Energy Installation in Northwest India: Assessment of Wind Resource Using Weather Research and Forecasting and Levelized Cost of Energy. *Wind Energy* **2021**, *24*, 174–192. [\[CrossRef\]](#)
- Seroka, G.; Fredj, E.; Kohut, J.; Dunk, R.; Miles, T.; Glenn, S. Sea Breeze Sensitivity to Coastal Upwelling and Synoptic Flow Using Lagrangian Methods. *J. Geophys. Res. Atmos.* **2018**, *123*, 9443–9461. [\[CrossRef\]](#)
- Garvine, R.W.; Kempton, W. Ssessing the Wind Field over the Continental Shelf as a Resource for Electric Power. *J. Mar. Res.* **2008**, *66*, 751–773. [\[CrossRef\]](#)
- Steele, C.J.; Dorling, S.R.; Von Glasow, R.; Bacon, J. Modelling Sea-Breeze Climatologies and Interactions on Coasts in the Southern North Sea: Implications for Offshore Wind Energy. *Q. J. R. Meteorol. Soc.* **2015**, *141*, 1821–1835. [\[CrossRef\]](#)
- Holtslag, M.C.; Bierbooms, W.A.A.M.; van Bussel, G.J.W. Validation of Surface Layer Similarity Theory to Describe Far Offshore Marine Conditions in the Dutch North Sea in Scope of Wind Energy Research. *J. Wind Eng. Ind. Aerodyn.* **2015**, *136*, 180–191. [\[CrossRef\]](#)
- Angevine, W.M.; Tjernström, M.; Žagar, M. Modeling of the Coastal Boundary Layer and Pollutant Transport in New England. *J. Appl. Meteorol. Climatol.* **2006**, *45*, 137–154. [\[CrossRef\]](#)
- Filho, L.M.; Roebeling, P.; Villasante, S.; Bastos, M.I. Ecosystem Services Values and Changes across the Atlantic Coastal Zone: Considerations and Implications. *Mar. Policy* **2022**, *145*, 105265. [\[CrossRef\]](#)

21. Tsiringakis, A.; Theeuwes, N.E.; Barlow, J.F.; Steeneveld, G.-J. Interactions Between the Nocturnal Low-Level Jets and the Urban Boundary Layer: A Case Study over London. *Bound. Layer Meteorol.* **2022**, *183*, 249–272. [[CrossRef](#)]
22. Sullivan, J.T.; Rabenhorst, S.D.; Dreessen, J.; McGee, T.J.; Delgado, R.; Twigg, L.; Sumnicht, G. Lidar Observations Revealing Transport of O₃ in the Presence of a Nocturnal Low-Level Jet: Regional Implications for “next-Day” Pollution. *Atmos. Environ.* **2017**, *158*, 160–171. [[CrossRef](#)]
23. Corsmeier, U.; Kossmann, M.; Kalthoff, N.; Sturman, A. Temporal Evolution of Winter Smog within a Nocturnal Boundary Layer at Christchurch, New Zealand. *Meteorol. Atmos. Phys.* **2006**, *91*, 129–148. [[CrossRef](#)]
24. Tucker, S.C.; Banta, R.M.; Langford, A.O.; Senff, C.J.; Brewer, W.A.; Williams, E.J.; Lerner, B.M.; Osthoff, H.D.; Hardesty, R.M. Relationships of Coastal Nocturnal Boundary Layer Winds and Turbulence to Houston Ozone Concentrations during TexAQ5 2006. *J. Geophys. Res.* **2010**, *115*, D10304. [[CrossRef](#)]
25. Hill, S.L.; Desobry, F.; Garnsey, E.W.; Chong, Y.-F. The Impact on Energy Consumption of Daylight Saving Clock Changes. *Energy Policy* **2010**, *38*, 4955–4965. [[CrossRef](#)]
26. Nanopoulos, A.; Alcock, R.; Manolopoulos, Y. Feature-Based Classification of Time-Series Data. *Int. J. Comput. Res.* **2001**, *10*, 49–61.
27. Lines, J.; Taylor, S.; Bagnall, A. Time Series Classification with HIVE-COTE: The Hierarchical Vote Collective of Transformation-Based Ensembles. *ACM Trans. Knowl. Discov. Data* **2018**, *12*, 1–35. [[CrossRef](#)]
28. Koley, B.; Dey, D. An Ensemble System for Automatic Sleep Stage Classification Using Single Channel EEG Signal. *Comput. Biol. Med.* **2012**, *42*, 1186–1195. [[CrossRef](#)]
29. Sokolov, A.; Dmitriev, E.; Gengembre, C.; Delbarre, H. Automated Classification of Regional Meteorological Events in a Coastal Area Using In Situ Measurements. *J. Atmos. Ocean. Technol.* **2020**, *37*, 723–739. [[CrossRef](#)]
30. Wang, Z.; Yan, W.; Oates, T. Time Series Classification from Scratch with Deep Neural Networks: A Strong Baseline. In Proceedings of the 2017 International Joint Conference on Neural Networks (IJCNN), Anchorage, AK, USA, 14–19 May 2017; pp. 1578–1585.
31. Cui, Z.; Chen, W.; Chen, Y. Multi-Scale Convolutional Neural Networks for Time Series Classification. *arXiv* **2016**. [[CrossRef](#)]
32. Roy, S.; Sentchev, A.A.; Schmitt, F.G.; Augustin, P.; Fourmentin, M. Impact of Nocturnal Low-Level Jet and Orographic Waves on the Turbulent Motions and Energy Fluxes in the Lower Atmospheric Boundary Layer. *Bound. Layer Meteorol.* **2021**, *180*, 527–542. [[CrossRef](#)]
33. Golzio, A.; Bollati, I.M.; Ferrarese, S. An Assessment of Coordinate Rotation Methods in Sonic Anemometer Measurements of Turbulent Fluxes over Complex Mountainous Terrain. *Atmosphere* **2019**, *10*, 324. [[CrossRef](#)]
34. Hill, R.J. Corrections to Taylor’s Frozen Turbulence Approximation. *Atmos. Res.* **1996**, *40*, 153–175. [[CrossRef](#)]
35. Kirankumar, N.V.P.; Jagadeesh, K.; Niranjana, K.; Rajeev, K. Seasonal Variations of Sea Breeze and Its Effect on the Spectral Behaviour of Surface Layer Winds in the Coastal Zone near Visakhapatnam, India. *J. Atmos. Sol. Terr. Phys.* **2019**, *186*, 1–7. [[CrossRef](#)]
36. Baars, H.; Ansmann, A.; Engelmann, R.; Althausen, D. Continuous Monitoring of the Boundary-Layer Top with Lidar. *Atmos. Chem. Phys.* **2008**, *8*, 7281–7296. [[CrossRef](#)]
37. Al-kadi, M.I.; Reaz, M.B.I.; Mohd Ali, M.A. Compatibility of Mother Wavelet Functions with the Electroencephalographic Signal. In Proceedings of the 2012 IEEE-EMBS Conference on Biomedical Engineering and Sciences, Langkawi, Malaysia, 17–19 December 2012; pp. 113–117.
38. Andreas, E.L.; Claffy, K.J.; Makshtas, A.P. Low-Level Atmospheric Jets and Inversions Over The Western Weddell Sea. *Bound. Layer Meteorol.* **2000**, *97*, 459–486. [[CrossRef](#)]
39. Svensson, N.; Arnqvist, J.; Bergström, H.; Rutgeresson, A.; Sahlée, E. Measurements and Modelling of Offshore Wind Profiles in a Semi-Enclosed Sea. *Atmosphere* **2019**, *10*, 194. [[CrossRef](#)]
40. Wagner, R.; Cañadillas, B.; Clifton, A.; Feeney, S.; Nygaard, N.; Poodt, M.; Martin, C.S.; Tüxen, E.; Wagenaar, J.W. Rotor Equivalent Wind Speed for Power Curve Measurement—Comparative Exercise for IEA Wind Annex 32. *J. Phys. Conf. Ser.* **2014**, *524*, 12108. [[CrossRef](#)]

Article

The Impact of Building Clean Energy Consumption on Residents' Subjective Well-Being: Evidence from China

Zhiqun Sun ¹, Yanbo Wu ^{2,*}, Hao Sun ³, Dian Zhou ¹, Yang Lou ¹ and Lei Qin ³¹ School of Human Settlements and Civil Engineering, Xi'an Jiaotong University, Xi'an 710049, China² School of Business, Monash University, Melbourne, VIC 3161, Australia³ School of Business, Anhui University of Technology, Ma'anshan 243032, China

* Correspondence: ywuu0208@student.monash.edu

Abstract: This study used micro data from the Chinese General Social Survey (CGSS) in 2018 to explore the impact of China's residential clean energy consumption on residents' subjective well-being. Our research results show that: the more clean energy consumption is present in housing, the stronger the residents' sense of happiness; furthermore, it can be seen from the results of marginal effects that the increase in residential clean energy consumption increases the probability of residents choosing "relatively happy" and "extremely happy". Moreover, the heterogeneity analysis found that the increase in residential clean energy consumption increased the happiness of people with housing and low education, and also increased the happiness of residents in central China and middle-aged and elderly residents; the intermediary analysis shows that the use of clean energy in housing improves the health of residents, and improves their quality of life while increasing their expenditure. In addition, central heating affects the relationship between residential clean energy consumption and residents' well-being. Further analysis shows that there is no non-linear relationship between the increase in residential clean energy consumption and residents' happiness. This study enriches the research on residential clean energy and provides policy suggestions for improving residents' living standards and welfare.

Keywords: clean energy; subjective well-being; energy consumption; health; China residents

Citation: Sun, Z.; Wu, Y.; Sun, H.; Zhou, D.; Lou, Y.; Qin, L. The Impact of Building Clean Energy Consumption on Residents' Subjective Well-Being: Evidence from China. *Buildings* **2022**, *12*, 2037. <https://doi.org/10.3390/buildings12112037>

Academic Editors: Roberto Alonso González Lezcano, Francesco Nocera, Rosa Giuseppina Caponetto and Alessandro Cannavale

Received: 28 October 2022

Accepted: 16 November 2022

Published: 21 November 2022

Publisher's Note: MDPI stays neutral with regard to jurisdictional claims in published maps and institutional affiliations.



Copyright: © 2022 by the authors. Licensee MDPI, Basel, Switzerland. This article is an open access article distributed under the terms and conditions of the Creative Commons Attribution (CC BY) license (<https://creativecommons.org/licenses/by/4.0/>).

1. Introduction

Energy is a basic element for human survival and development, and residential energy consumption is an important part of China's energy demand [1]. Demand for energy has increased with the development of the Chinese economy [2]. On the one hand, traditional energy is nonrenewable. With the continuous exploitation and use of human beings, traditional fossil energy will eventually be exhausted [3]. On the other hand, traditional fossil energy produces a large amount of greenhouse gases such as CO₂ during combustion, and when fossil energy is not completely burned, it produces harmful gases such as SO₂ and CO [4]. Under the background of green and sustainable development, clean energy has become an ideal substitute for traditional fossil energy [5]. In addition, the Chinese government promised in the "Paris Climate Summit" to achieve peak carbon emissions by 2030 and carbon neutrality by 2060 [6]. In order to fulfill its commitments, reducing the use of traditional energy and increasing clean energy consumption are important measures taken by the Chinese government to reduce carbon dioxide emissions [7]. As shown in Figure 1, from 2000 to 2019, China's per capita domestic energy consumption increased from 132 kg to 438 kg coal equivalent, an increase of 3.2 times. For Chinese residents, on the one hand, the energy consumption of Chinese residents is still dominated by traditional sources (e.g., coal, firewood). The efficiency of solid fuels is low, heat is insufficient, and many harmful gases are produced during combustion, which is not conducive to the health of residents while polluting the environment [8]. However, the use of low-quality energy

aggravates economic poverty [9]. To obtain basic energy consumption, low-income people often need to spend a lot of time collecting straw or wood, which to a certain extent, occupies the working time of residents and the time for children to learn, ultimately leading to a negative feedback cycle between energy shortage and economic poverty [10]. The United Nations Sustainable Development Goal 7 (SDG 7) emphasizes that “everyone has access to affordable, reliable and sustainable modern energy” [11]. The Chinese government has also established the “Energy Consumption Revolution (ECR)” as a basic strategy for China’s energy development and formulated specific plans [12]. Furthermore, with the promotion of infrastructure construction in China, China has achieved full coverage of electricity, and energy infrastructure such as natural gas pipelines, are also under construction. China’s residential energy consumption mode has gradually changed from traditional to clean energy, and its energy use mode has improved [13]. The use of clean energy differs from traditional energy sources. Can clean energy overcome the limitations of traditional energy in improving residents’ happiness and effectively enhancing their well-being? Moreover, owing to obvious regional development differences in China, is there any difference in the impact of clean energy consumption on residents’ well-being? As one of the important starting points of the clean energy policy, the current academic community has not yet established a clear answer to this question. This study attempts to answer these two questions and focuses on the impact of clean energy consumption on residents’ health.

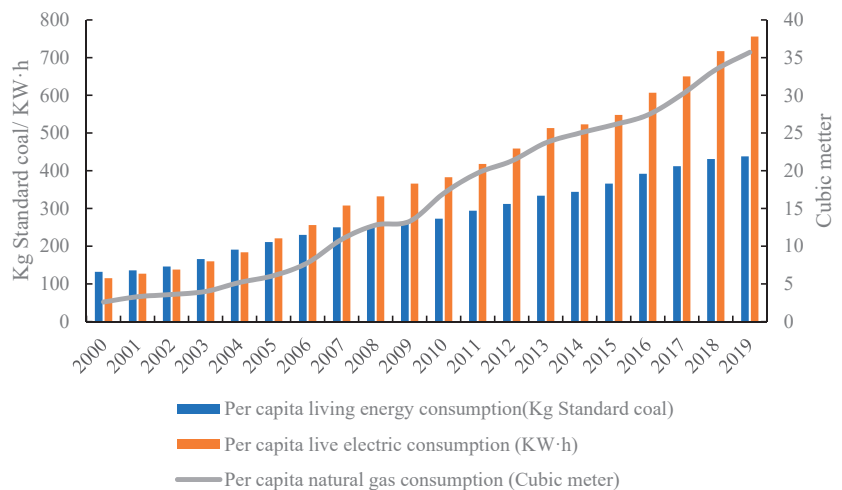


Figure 1. Domestic energy consumption of Chinese residents.

In recent years, discussions on the factors influencing residents’ well-being have become widespread among scholars. At present, there are two theories to measure residents’ well-being: on the one hand, it is the objectivist welfare theory. Objectivist welfare theory advocates measuring welfare by income, wealth, and commodity ownership [14]. In addition, social environment and behavioral culture are also factors that affect residents’ well-being; on the other hand, the utilitarian utility welfare theory takes utility as the index to evaluate welfare. Utility is equivalent to subjective psychological evaluations such as happiness or happiness and satisfaction with life, including sensory enjoyment and pain, as well as spiritual pleasure and torture [15]. Personal happiness is a complex combination of multiple levels and elements. The distribution of happiness is similar to that of human needs, conforming to Maslow’s hierarchy of needs theory. Many scholars have characterized residents’ welfare by their subjective psychological evaluation and carried out research, age difference [16], gender difference [17], employment status [18] and income inequality [19] affect residents’ happiness; Herman et.al. (2013) found that residents’ health status significantly affects their life satisfaction. The healthier the residents are, the higher

their life satisfaction will be [20]. Based on the above literature, this study uses residents' subjective well-being to represent their welfare.

Currently, research on residential clean energy consumption and residents' subjective well-being is mainly concentrated in developed countries. Binder and Blankenberg's (2017) research on British households found that residents' clean energy consumption was positively correlated with their life satisfaction [21]. Spanish research shows that clean energy has made important contributions to the sustainable development of local society, economy, and environment, and has improved the living standard and happiness of local residents [22]. Welsch and Biermann's survey of European residents showed that an increase in the share of wind energy and solar energy will improve residents' sense of happiness [23]. Moreover, residential clean energy consumption will promote household living standards through lighting, cooking and other behaviors, thus improving residents' life satisfaction [24]. In addition, some scholars' research on 27 countries such as the United States and Germany shows that the use of clean energy is significantly positively correlated with residents' life satisfaction [25]. However, few scholars have studied the impact of China's residential clean energy consumption on residents' subjective well-being. Therefore, improving the consumption of clean energy in residential buildings is not only an important proposition to realize China's energy transformation, but also an objective need to improve residents' living standards and welfare. Therefore, studying the clean energy consumption of buildings in China is of practical significance.

In summary, this study explores the impact of clean energy consumption in China's housing on residents' subjective well-being from the actual situation in China, using micro data from the Chinese General Social Survey (CGSS) in 2018. The marginal contributions of this study are as follows: first, this paper analyzes the impact of residential clean energy consumption on residents' welfare from the theoretical and empirical perspectives, and also effectively identifies the mechanism of the impact of residential clean energy consumption on residents' welfare from the perspective of utility function, which provides a new way for China to implement the "energy consumption revolution" policy to improve residents' welfare; secondly, this paper extends the research perspective from macro energy consumption behavior to micro household energy consumption behavior, and measures the impact of China's residential energy consumption on residents' welfare; thirdly, this study brings the heterogeneity characteristics of residents' age, education background and region into the analysis framework to explore the characteristics of residential clean energy consumption on subjective well-being of different residents. Furthermore, compared with other micro survey data, this paper makes in-depth research and innovative use of the data of CGSS (2018) energy module, filling the lack of research on clean energy in China's housing due to the lack of micro data, in order to better analyze China's residential energy problems.

2. Theoretical Analysis

Based on China's national conditions, this study defines residents' welfare as utility from the perspective of welfare economics, constructs a theoretical model in line with China's actual situation, and analyzes the impact of residential clean energy consumption on residents' well-being. To better analyze the relationship between the two, this study makes the following assumptions: (1) there are two types of consumption, building clean energy consumption (C_g) and other total consumption (C); (2) all the income gained in one's life is used for consumption; (3) the use of residential clean energy can obtain economic benefits, and the higher the use of residential clean energy, the higher the benefits that can be obtained.

The general utility function is considered an increasing function of the utility consumption level, that is, $U = U(y)$. Based on the above assumptions, this study constructs the resident utility function as:

$$U(C, C_g) = \ln C + \beta \ln C_g \quad (1)$$

where β represents the weight of clean energy consumption on utility. For individual residents, the constraints are:

$$C \times P_1 + C_g \times P_2 = Y + \Delta C_g \quad (2)$$

P_1 indicates the price level of the total consumption in the market. P_2 indicates the price level of clean energy consumption; Y represents the absolute income level of an individual in his life; ΔC_g represents the economic benefits of using clean energy. Individuals choose the best clean energy consumption (C_g) and other total consumption (C) to maximize the weighted utility function, that is,

$$\text{Max}U(C, C_g) \quad (3)$$

$$\text{s.t. } C \times P_1 + C_g \times P_2 = Y + \Delta C_g \quad (4)$$

s.t. is the constraint condition, using the Lagrangian method:

$$L = \ln C + \beta \ln C_g + \lambda (C \times P_1 + C_g \times P_2 - Y - \Delta C_g) \quad (5)$$

thus,

$$C = \frac{Y + \Delta C_g}{P_1 + \beta P_2} \quad (6)$$

$$C_g = \frac{\beta(Y + \Delta C_g)}{P_2(1 + \beta)} \quad (7)$$

Therefore, the maximum utility value that individuals can get is:

$$U_{max} = \ln \left(\frac{Y + \Delta C_g}{P_1 + \beta P_2} \right) + \beta \ln \left[\frac{\beta(Y + \Delta C_g)}{P_2(1 + \beta)} \right] \quad (8)$$

Based on this, this study proposes the following hypothesis: there is a positive relationship between building clean energy consumption and residents' well-being.

3. Data and Model Setting

3.1. Data Source and Sample Selection

The data used in this study were obtained from the Chinese General Social Survey (CGSS) conducted in 2018, which was implemented by the China Research and Data Center of Renmin University of China. This data covers 28 provinces, autonomous regions and municipalities in China except Hainan, Tibet, Xinjiang, Hong Kong, Macao and Taiwan. The population surveyed included urban and rural residents aged ≥ 18 years. The sample was representative and could be used for reliable statistical analyses. The survey items mainly included basic characteristics of respondents, the social attitude of the interviewees, including self-rating of social status and happiness of life, and energy use of the interviewees, including energy expenditure, heating, etc. Combined with the research theme of this study, the data were collated, and samples lacking basic variables (such as happiness and household expenditure) and invalid samples were deleted. The final valid samples were 3012.

Compared with the samples used in the existing research, the data used in this study have the following advantages in research on building clean energy and residents' well-being in China: (1) CGSS (2018) is one of the most detailed data on energy consumption in China, including electricity, natural gas, gas, central heating and other data; (2) CGSS (2018) carried out a detailed survey on residents' sense of happiness, health, education, and social status, making our later mechanism analysis more reliable.

3.2. Research Design and Variable Processing

In economic research, subjective well-being is often used to measure residents' welfare [26]. This is because we can avoid the shortcomings of using income to represent

residents' welfare, because it is not necessarily that residents with higher income have higher welfare. The higher the income, the greater the desire, and utility may be reduced, leading to a reduction in welfare. In addition, measuring welfare using objective indicators such as income or wealth can ultimately be transformed into whether life is happy. When residents' income or wealth meets their desires, they are happy [27]. As a subjective concept, it is difficult to objectify happiness; therefore, the questionnaire was reasonable and feasible [28]. This study's explained variable used residents' happiness to represent their subjective well-being. We used the question from the Chinese General Social Survey (CGSS) data: "in general, do you think your life is happy?" to measure Chinese residents' happiness. $Happiness_i$ takes values from 1 to 5, where 1 means "extreme unhappiness", 2 indicates "relatively unhappiness", 3 means "feel general", 4 indicates "relatively happiness", and 5 means "extreme happiness".

The explanatory variable of this paper is the consumption of clean energy ($Cese_i$). We use Xu and Ge (2022) to define modern clean energy [29], calculate the monthly consumption of electric energy, natural gas and liquefied petroleum gas used by the surveyed residents, add them up and convert them into annual consumption. This study used the natural logarithm of annual consumption as the explanatory variable.

The control variables were divided into two levels: personal and family. Individual characteristics included age, gender, education, marriage, residence account, political affiliation, race; while family characteristics included homeownership, residential area, family size, and family economic status.

The intermediary variables in this study were health and household expenditures. Health represents the health status of the respondents, and household expenditure is the annual household expenditure of the respondents. The data indicators of the regulating variables were obtained from the CGSS questionnaire "do you have central heating in your home?", we set central heating to 1 and no central heating to 0. See Table 1 for variable definitions. Figure 2 shows that there is a positive correlation between clean energy consumption and happiness of Chinese residents.

Table 1. Variable definition.

Variable	Variable Assignment Description	
Explained variable $Happiness_i$	Extremely unhappy = 1, relatively unhappy = 2, acceptable = 3, relatively happy = 4, extremely happy = 5	
Explanatory variable Clean energy consumption ($Cese_i$)	Natural logarithm of annual clean energy consumption	
Individual characteristic variables	Age	The specific figures filled in by the respondents in the questionnaire shall prevail
	Gender	Female = 0, Male = 1
	Education degree	Unschool = 0, elementary school = 6, middle school = 9, high school = 12, junior college = 15, undergraduate = 16, master or doctoral = 19
	Marriage	Unmarried = 0, married = 1
	Residence account	Rural account = 0, city account = 1
	Political affiliation	Other = 0, party member of CPC = 1
Family characteristic variables	Race	Other = 0, Han race = 1
	Homeownership	Otherwise = 0, housing owner = 1
	Residential area	Natural logarithm of residential area
	Family size	The specific figures filled in by the respondents in the questionnaire shall prevail
Family economic status	Family economic status	Far below average level = 1, below average level = 2, average level = 3, above average level = 4, well above average level = 5
	Health	Extremely unhealthy = 1, relatively unhealthy = 2, acceptable = 3, relatively healthy = 4, extremely healthy = 5
Mediating variables	Household expenditures	Natural logarithm of annual household expenditures
Moderator variable	Central heating	No central heating = 0, have central heating = 1

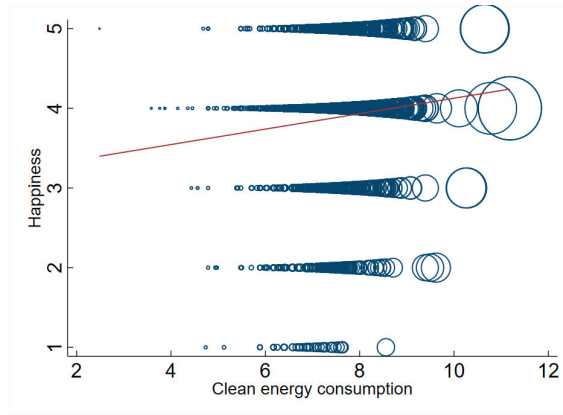


Figure 2. Happiness and clean energy consumption.

3.3. Model Analysis

Considering that the variable $Happiness_i$ is restricted to ordered data, if OLS estimation is adopted, it is biased and inconsistent. Therefore, based on theoretical analysis, we adopt an ordered probit for the estimation. The empirical model used in this study is as follows:

$$Happiness_i = \alpha_0 + \alpha_1 Cese_i + \alpha_2 X_i + \theta_i + \mu_i \tag{9}$$

In Equation (9), $Happiness_i$ represents the happiness of resident i , which is the explained variable; $Cese_i$ is an explanatory variable that represents clean energy consumption; X_i is a series of control variables, including personal and family characteristics; θ_i is the regional fixed effect; ϵ_i is the random interference term. Assumptions $\mu \sim N(0, 1)$ distribution, the Oprobit model can be expressed as:

$$\begin{aligned} P(Happiness = 1 | x) &= P(Happiness^* \leq r_0 | x) = \phi(r_0 - \alpha_1 Cese_i - \alpha_2 X_i - \theta_i) \\ P(Happiness = 2 | x) &= P(r_0 < Happiness^* \leq r_1 | x) \\ &= \phi(r_1 - \alpha_1 Cese_i - \alpha_2 X_i - \theta_i) - \phi(r_0 - \alpha_1 Cese_i - \alpha_2 X_i - \theta_i) \\ \dots \\ P(Happiness = 5 | x) &= P(r_3 \leq Happiness^* | x) = 1 - \phi(r_3 - \alpha_1 Cese_i - \alpha_2 X_i - \theta_i) \end{aligned} \tag{10}$$

In Equation (10), $r_0 < r_1 < r_2 < r_3$ is the parameter to be estimated; and the value of $Happiness_i$ is 1 to 5. The maximum likelihood method was used to estimate the model parameters by constructing the likelihood function of happiness for each respondent.

3.4. Descriptive Statistics

To obtain a preliminary understanding of the studied samples, we first conducted a descriptive analysis of the relevant variables, and the results are shown in Tables 2 and 3. We found that the mean value of the variable “happiness” was 3.8678, indicating that the happiness of the surveyed residents was between “relatively happiness” and “acceptable”, close to “relatively happiness”; secondly, the variable “gender” is 0.4641, which shows that the proportion of men and women interviewed is approximately equal, which is relatively representative; moreover, we have noticed that the education level of residents is 8.3434, indicating that compulsory education is basically universal in China, but the education level of Chinese residents still needs to be improved. Meanwhile, “marriage” represents whether the residents interviewed are married. 78.85% of the respondents in the sample are married. The value of the variable “residence account” is 0.4180, indicating that nearly 42% of the residents interviewed are urban residence account. In addition, 91.27% of the respondents own houses, which indicates that the housing ownership rate of Chinese residents is extremely high, and the policy of “having a place to live” is basically realized.

Furthermore, the variable “family size” is 2.8390, which indicates that Chinese families are basically composed of parents and one child, and the only child has become the mainstream. Finally, the “family economic status” value is 2.5710, which reflects that most respondents believe that their economic status is between the below average level and the average level.

Table 2. Descriptive statistics of binary variables.

Variable	Mean	Std. Dev	Min	Max	0 (%)	1 (%)
Gender	0.4641	0.4988	0	1	53.59%	46.41%
Marriage	0.7885	0.4084	0	1	21.15%	78.85%
Residence account	0.4180	0.4933	0	1	58.20%	41.80%
Political affiliation	0.0966	0.2955	0	1	90.34%	9.66%
Race	0.9240	0.2651	0	1	7.60%	92.40%
Homeownership	0.9127	0.2823	0	1	8.73%	91.27%
Central heating	0.2095	0.3321	0	1	79.05%	20.95%

Table 3. Descriptive statistics of other variables.

Variable	Mean	Std. Dev	Min	P50	P75	Max
Happiness	3.8659	0.8207	1	4	4	5
Clean energy consumption	7.3099	0.8009	2.4849	7.3340	7.7857	11.1845
Age	51.8373	15.9224	18	52	64	93
Education degree	8.3434	4.7950	0	9	12	19
Residential area	4.6292	0.9423	1.9459	4.6001	4.8828	9.2102
Family size	2.8390	1.4216	1	3	4	14
Family economic status	2.5710	0.7119	1	3	3	5
Health	3.5252	1.0869	1	4	4	5
Household expenditures	10.0647	1.1141	1.3863	10.1659	10.7852	14.4307

4. Analysis of Empirical Results

4.1. Benchmark Regression

Table 4 presents the regression results for the Oprobit model. Column (1) only controls for the explanatory variables and regional fixed effects and examines the direct impact of Chinese residents’ clean energy consumption on their happiness. The regression results show that there is a positive relationship between residents’ clean energy consumption and their well-being, and it is significant at the 1% statistical level. Column (2) adds individual characteristic variables on the basis of Column (1), and the explanatory variables are significant at the 1% level. Column (3) all control variables are included in the model, and the regression results are significant at the 5% level, and are basically consistent with the operation results of the first two models. For each control variable, according to the estimated results in Column (3) of Table 4, we can see from the regression coefficient of age and its square that there is a significant U-shaped relationship between age and happiness. At the same time, there is gender difference in residents’ well-being, and the well-being of men is lower than that of women. There is a significant positive correlation between the political identity of party members and residents’ happiness. In addition, we found that family size was positively correlated with residents’ happiness; the higher the economic status of the family, the better the living conditions of residents, and they will feel happier. In general, the influence direction and significance level of the explanatory variables do not change significantly between the columns, indicating that the model estimation is relatively robust. This further shows that there is a significant positive relationship between residents’ clean energy consumption and happiness.

Table 4. Benchmark regression.

Variables	Explained Variable: Happiness		
	(1)	(2)	(3)
Clean energy consumption	0.125 *** (0.033)	0.120 *** (0.035)	0.071 ** (0.035)
age		−0.049 *** (0.010)	−0.042 *** (0.010)
Square of age		0.501 *** (0.097)	0.442 *** (0.095)
Gender		−0.102 *** (0.046)	−0.089 ** (0.047)
Education degree		0.003 (0.005)	−0.006 (0.005)
Marriage		0.216 *** (0.076)	0.123 (0.077)
Residence account		0.038 (0.061)	−0.002 (0.064)
Political affiliation		0.159 *** (0.055)	0.117 * (0.064)
Race		0.006 (0.119)	0.004 (0.110)
Homeownership			0.132 (0.093)
Residential area			0.030 (0.023)
Family size			0.041 ** (0.020)
Family economic status			0.400 *** (0.041)
Regional fixed effect	Yes	Yes	Yes
/cut1	−1.637 *** (0.244)	−2.545 *** (0.415)	−1.626 *** (0.389)
/cut2	−0.820 *** (0.252)	−1.713 *** (0.441)	−0.744 * (0.413)
/cut3	−0.173 (0.243)	−1.056 ** (0.428)	−0.050 (0.407)
/cut4	1.601 *** (0.250)	0.740 * (0.438)	1.811 *** (0.410)
Observations	3012	3012	3012

Robust standard errors in parentheses, *** $p < 0.01$, ** $p < 0.05$, * $p < 0.1$.

4.2. Marginal Utility

Since the regression coefficient value of the Order probit model has no reference significance, we can only obtain limited information from the regression results, such as the significance level and sign direction. Therefore, this section further calculates the marginal effect of the order probit regression. The calculation method is as follows:

$$\frac{\partial P(y = i | x)}{\partial P x_i} \Bigg|_{x = \bar{x}} \quad (i = 1, 2, 3, 4, 5) \quad (11)$$

x represents all control variables and regional fixed effects except the explanatory variables in the two-stage regression. Formula (11) indicates that when other variables are at their mean value and remain fixed, the change in x_i per unit will lead to a change in the probability of taking $i = 1, 2, 3, 4, 5$ as the explanatory variable.

Because the explanatory variable \widehat{Cecce} of the two-stage regression is the fitting value of the one-stage probit regression, \widehat{Cecce} can be regarded as a continuous variable. When the

probability of $Cece = 1$ changes, the change in the marginal probability of the explanatory variable $i = 1, 2, 3, 4, 5$ is taken as:

$$\frac{\partial P(y = i | x)}{\partial P(Cece = 1 | x)} \Big|_{x = \bar{x}} = \frac{\partial P(y = i | x) / \partial \widehat{Cece}}{\partial P(Cece = 1 | x) / \partial \widehat{Cece}} \Big|_{x = \bar{x}} \quad (i = 1, 2, 3, 4, 5) \quad (12)$$

Table 5 presents the marginal effects of column (3) of Table 3. From the perspective of the marginal effect of explanatory variables, when all other variables are at the mean value and remain unchanged, the probability of clean energy consumption $P(Cece = 1 | x)$ increases every Δ , and the probability of happiness value “extremely unhappy” $P(happiness = 1 | x)$ decreases by 0.002150 Δ , and so on. The probability $P(happiness = 2 | x)$ of value “relatively unhappy” decreases by 0.007405 Δ ; the probability $P(happiness = 3 | x)$ of value “acceptable” decreases 0.009807 Δ ; the probability $P(happiness = 4 | x)$ of the value “relatively happy” increases 0.002444 Δ ; and the probability $P(happiness = 5 | x)$ of the value “extremely happy” increases 0.016918 Δ . According to the results of marginal effects, the increase in clean energy consumption increases the probability of residents choosing “relatively happy” and “extremely happy”, and reduces the probability of residents choosing “extremely unhappy”, “relatively unhappy” and “acceptable”.

Table 5. Marginal utility.

Variable Happiness	dy/dx	Explanatory Variable: Clean Energy Consumption			Significance
		Standard Error	Z Statistics	p-Value	
1	−0.002150	0.001090	−1.97	0.049	**
2	−0.007405	0.003738	−1.98	0.048	**
3	−0.009807	0.004772	−2.06	0.040	**
4	0.002444	0.001218	2.01	0.045	**
5	0.016918	0.008263	2.05	0.041	**

Robust standard errors in parentheses, ** $p < 0.05$.

4.3. Robustness Check

To further ensure the reliability of the research conclusions, we conducted a robustness test on the regression model from the perspectives of samples and models. Table 6 presents the results. First, we changed the explained variable, replacing “happiness” with “social stratum”. Since there is a strong correlation between social status and happiness [30], we choose to replace happiness with social status as the explained variable. The data indicators are from the CGSS question volume “what do you think of your current social status?”; the variable value ranges from 1 to 10, and all control variables and provincial fixed effects are introduced to conduct an ordered probit regression on the model. The regression results are still significant at the 1% significance level, as shown in Table 6 (1). Second, we replaced the regression model for the robustness test, using the ordered logit model and Tobit model for regression, and the empirical steps were consistent with the benchmark regression. Columns (2) and (3) of Table 6 show the regression results. The explanatory variables are significant at the 5% levels, which is consistent with the above results, indicating that the estimation results are robust.

4.4. Placebo Test

Owing to differences in the economic development of China’s provinces, different regions have different characteristics. Although the regional fixed effect is controlled for in the regression equation, it may have different effects on interviewees with different educational backgrounds, genders and other aspects. To test the effectiveness of the above research results, this study uses the method of randomly generating experimental groups to complete the placebo test, to verify the impact of clean energy consumption on the difference in residents’ well-being. First, we randomize the core explanatory variable

“clean energy consumption”, and then put it into the regression model to generate an estimation coefficient $\hat{\beta}$. This process was repeated 1000 times, and finally 1000 $\hat{\beta}$ was obtained; Figure 3 shows $\hat{\beta}$ distribution. The $\hat{\beta}$ distribution is close to the standard normal distribution, and the mean value is close to 0, indicating that the estimation equation passed the placebo test, indicating that the impact of clean energy consumption on residents’ well-being is robust, and excluding the interference of other random factors on the results.

Table 6. Robustness check.

Variables	Explained Variable: Social Stratum		Explained Variable: Happiness	
	(1)	(2)	(3)	
	Ordered Probit	Ordered Logit	Tobit	
Clean energy consumption	0.092 *** (0.030)	0.119 ** (0.060)	0.046 ** (0.022)	
Individual characteristic variables	Yes	Yes	Yes	
Family characteristic variable	Yes	Yes	Yes	
Regional fixed effect	Yes	Yes	Yes	
Observations	3012	3012	3012	

Robust standard errors in parentheses, *** $p < 0.01$, ** $p < 0.05$.

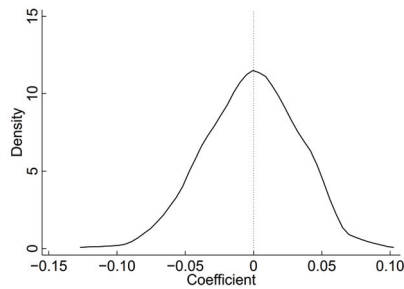


Figure 3. Placebo test.

5. Heterogeneity Analysis

5.1. By Age

The impact of energy consumption on different people is not identical [31]. With increasing age, the age energy consumption curve shows almost linear growth [32]. The results in Table 7 show that for different age groups of the study, there is a heterogeneous effect of clean energy consumption on residents’ well-being, and the older the age, the higher the significance of the effect of clean energy consumption on residents’ well-being. On the one hand, young people under the age of 35 are more willing to reduce the dependence on their original families and establish their own families. They tend to live in smaller families with a low capacity for energy consumption, which does not reflect that clean energy can improve their quality of life, thus improving their sense of happiness; on the other hand, for middle-aged and elderly people over 35 years old, most of them are married and have children, and perform more energy consuming activities such as cooking and washing, which increases the energy consumption of the middle-aged and elderly groups. Furthermore, these behaviors improve the quality of life of middle-aged and elderly individuals and increase their life satisfaction. Moreover, with increasing age and the gradual degradation of physical functions, middle-aged and elderly people have a slightly higher demand for comfort in their living environment. They pay more attention to products closely related to their own health [33]. The use of clean energy can make them healthier and increase their sense of well-being.

Table 7. Heterogeneity analysis from the perspectives of age.

Variables	Explained Variable: Happiness		
	(1) 18–35	(2) 35–60	(3) More Than 60
Clean energy consumption	−0.018 (0.064)	0.102 * (0.058)	0.092 ** (0.042)
Individual characteristic variables	Yes	Yes	Yes
Family characteristic variable	Yes	Yes	Yes
Regional fixed effect	Yes	Yes	Yes
Observations	541	1506	965

Robust standard errors in parentheses, * $p < 0.1$, ** $p < 0.05$.

5.2. By Homeownership and Education Degree

The difference between residents' housing and educational backgrounds may also bring about the heterogeneous impact of clean energy consumption on well-being. This section further discusses whether housing and educational differences exist in the impact of clean energy consumption on residents' well-being. The regression results in columns (1) and (2) of Table 8 show a significant positive relationship between clean energy consumption and the happiness of residents with housing. The relationship between happiness of residents without housing and clean energy consumption was not significant. We believe that for residents without housing, they may consume more in other aspects, are insensitive to energy consumption, and have greater randomness. The way for residents with housing to enjoy clean energy is more convenient. Simultaneously, clean energy can improve the quality of life of residents in housing and make them feel happier. In addition, the results in Columns (3) and (4) of Table 8 indicate that for the low educated group, clean energy consumption can significantly promote happiness, while those with high education are not significant. We refer to people with a college degree or above as people with a high educational background, while people with other educational backgrounds are those with a low educational background. Compared with people with low education background, people with high education background have a higher income level, and their quality of life has greater advantages compared with people with a low education background. The marginal utility of clean energy consumption on the quality of life of highly educated people is relatively small. Generally, the quality of life of the lower education group is probably less than that of the higher education group. Therefore, the marginal utility of consuming clean energy is relatively high for the lower education group, which can increase their life satisfaction.

Table 8. Heterogeneity analysis from the perspectives of homeownership and education degree.

Variables	Explained Variable: Happiness			
	(1) Homeownership	(2) Non-Homeownership	(3) Lower Education	(4) Higher Education
Clean energy consumption	0.086 ** (0.037)	−0.107 (0.093)	0.076 ** (0.037)	−0.004 (0.083)
Individual characteristic variables	Yes	Yes	Yes	Yes
Family characteristic variable	Yes	Yes	Yes	Yes
Regional fixed effect	Yes	Yes	Yes	Yes
Observations	2749	263	2578	434

Robust standard errors in parentheses, ** $p < 0.05$.

5.3. By Region

There are differences in the economic development of the eastern, central, and western regions of China, and the demand for energy in each region is different [34], which causes a large gap in the impact of clean energy consumption on the well-being of residents in the eastern, central and western regions of China. Table 9 reports the estimation results

grouped into the central, western, and eastern regions. Robust standard errors were used for each estimation equation. For the central region, the regression results show a significant positive correlation between clean energy consumption and residents' well-being, which is significant at the 5% statistical level. This indicates that clean energy in the central region can promote the happiness of residents. Moreover, compared to the basic regression results using the national sample, the coefficient of clean energy consumption in the regression results of the central region is larger, which shows that the happiness enhancement effect of clean energy consumption in the central region is higher than the average level in China. In addition, residents' clean energy consumption was not significant in the eastern and western regions, which indicates that the use of clean energy in these regions did not produce a significant happiness enhancement effect.

Table 9. Heterogeneity analysis from the perspectives of region.

Variables	Explained Variable: Happiness		
	(1) Mid	(2) West	(3) East
Clean energy consumption	0.103 ** (0.051)	−0.018 (0.061)	0.089 (0.063)
Individual characteristic variables	Yes	Yes	Yes
Family characteristic variable	Yes	Yes	Yes
Regional fixed effect	Yes	Yes	Yes
Observations	1064	767	1181

Robust standard errors in parentheses, ** $p < 0.05$.

We believe that whether clean energy consumption can play a significant role in improving residents' well-being is limited by economic development and income levels. Compared to the central region, economic development in the western region is relatively backward, the income level is low, and people are more urgent to improve their material living conditions. The impact of material factors such as income on happiness is often more prominent than the ecological environment factors. While the economic development level of the eastern region is the highest in China, the income level of residents is also high, and the price sensitivity is low. They may not care about the happiness brought about by clean energy consumption. The income, housing, and GDP per capita of residents in the central region are at a moderate level, and they are able to consume clean energy. At the same time, because the income of residents in the central is not as high as that of residents in the East, they focus on clean energy to improve their quality of life and improve their subjective well-being.

6. Mechanism Inspection and Further Analysis

The above analysis shows that clean energy consumption has a significant positive impact on residents' well-being. What type of path does clean energy use affect residents' welfare? Therefore, this study uses the intermediary and regulatory effect models to identify the mechanism of the impact of clean energy on residents' welfare.

At present, the existing literature has shown that energy consumption will cause a series of health and inequality problems [35], among which residents' health and other factors will affect their subjective well-being [36]. In addition, Middlemis et al. (2015) showed that it would cost more to obtain clean energy if one wanted to obtain a healthy body [37]. In addition, owing to the special geographical location of China, the temperature gap between the north and south is large. Most northern regions have implemented central heating policies, and there are many financial subsidies for central heating in northern cities. Residents have low energy consumption in winter, which may play a regulatory role in the process of improving their happiness. Based on the analytical framework of social psychology mediation and regulatory effects, we built a conceptual model of the clean energy consumption mechanism that affects residents' well-being (Figure 4).

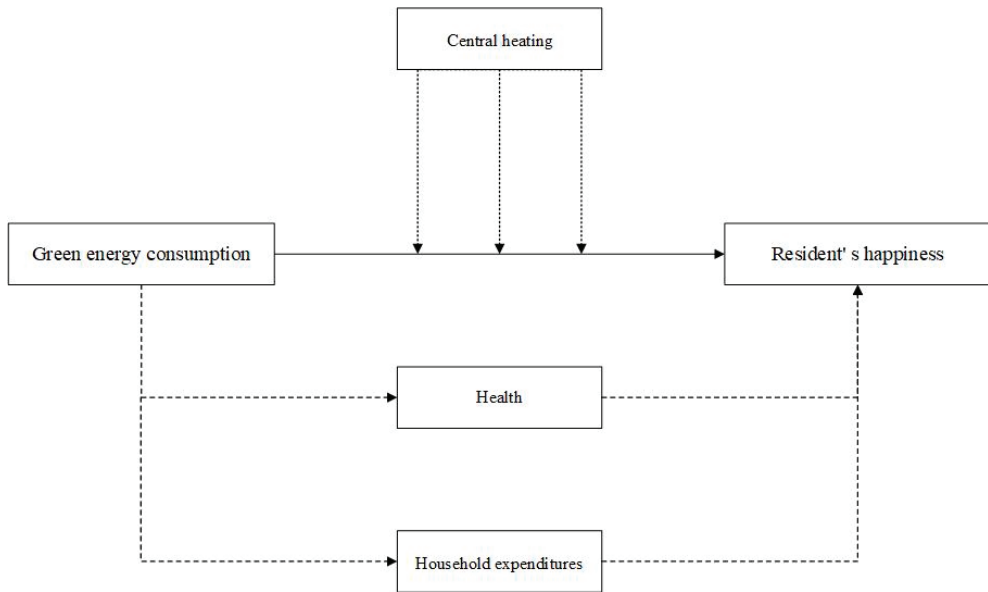


Figure 4. The mechanism of clean energy consumption revolution effect on resident' happiness.

6.1. Intermediary Effect Test

To empirically analyze whether clean energy has an impact on residents' well-being by affecting their health and consumption, we refer to Mehmetoglu's (2018) intermediary effect test procedure [38] to test whether residents' clean energy consumption affects their well-being by affecting their health and household expenditure. The intermediary effect model was set as follows:

$$Happiness_i = \beta_0 + dGese_i + \varepsilon_i \quad (13)$$

$$Mid_i = \beta_0 + aGese_i + \varepsilon_i \quad (14)$$

$$Happiness_i = \beta_0 + bMid_i + d'Gese_i + \varepsilon_i \quad (15)$$

In Formula (13), $Happiness_i$ regresses $Gese_i$ and estimates the coefficient d . d is the total effect of clean energy consumption on the well-being of the i th resident. If the statistics are significant, it means there is a mediation effect; in Formula (14), Mid_i regresses $Gese_i$ and estimates the coefficient a . a is the impact of clean energy consumption on intermediary variables, which must be statistically significant to prove the relationship between explanatory variables and intermediary variables. Mid_i is the intermediate variable. In Formula (15), $Happiness_i$ regresses Mid_i , while controlling $Gese_i$, and the estimation coefficient b must be statistically significant. b and d' represent the direct effects of the intermediary variables and clean energy consumption on the well-being of the i th resident. If d' is not significantly 0, then Mid_i is a partial intermediary effect. By substituting Formula (14) into Formula (15), we can conclude that the intermediary effect of clean energy consumption is $a \times b$. Then, we use Equation (16) to test the mediation effect $a \times b$. If $z > \pm 1.96$, the intermediary effect $a \times b$ at the statistical level of 0.05 is significant [39], that is, the indirect impact of clean energy consumption on residents' well-being through intermediary variables.

$$z = \frac{a \times b}{\sqrt{b^2 s_a^2 + a^2 s_b^2}} \quad (16)$$

In Formula (16), a and s_a^2 (standard error of a) come from Formula (14); b and s_b^2 (standard error of b) come from Formula (15).

Table 10 presents the regression results of the mediation model. First, the paths $X \rightarrow M$ and $M \rightarrow Y$ of the variables “health” and “household expenditures” are significant, indicating that the mediation effect exists, and the Z value of the variable and the direct effect $X \rightarrow Y$ are significant, indicating that the variables “health” and “household expenditures” are part of the mediation, that is, residents’ health and household income play a part of the mediation effect between clean energy consumption and happiness. By calculating the intermediary effect value, we find that the intermediary effect of “health” is 0.030, accounting for 31.9% of the total effect. The intermediary effect of “household expenditures” is 0.035, accounting for 36.8% of the total effects. This shows that in the process of clean energy consumption affecting residents’ happiness, residents’ health and household expenditure play an intermediary role. In general, with an increase in clean energy consumption, residents have become healthier. At the same time, the increase in household expenditures has improved the quality of life of residents and their sense of happiness.

Table 10. Mediation Analysis.

Variables	X→M	M→Y	X→Y	Indirect Effect	Standard Error	Z Value	p-Value	Significance	RIT
Health	0.143 ***	0.211 ***	0.064 ***	0.030	0.005	6.657	0.000	***	31.9%
Household expenditures	0.355 ***	0.098 ***	0.060 ***	0.035	0.007	4.965	0.000	***	36.8%

Robust standard errors in parentheses, *** $p < 0.01$.

6.2. Regulatory Effect

Column (1) of Table 11 shows whether the presence or absence of the heating interaction item (*Treat*) affected residents’ clean energy consumption and happiness. The results show that the interaction coefficient is negative, and significant at the 10% level. This shows that if residents enjoy central heating, the higher their clean energy consumption, the weaker is their sense of well-being. In other words, heating plays a negative role in regulating the impact of clean energy consumption on residents’ sense of well-being. Because central heating can reduce residents’ energy consumption [40], if residents enjoy central heating while their clean energy consumption increases, this will increase their expenditure, reduce their sense of well-being and reduce their welfare.

Table 11. Moderator and further analysis.

Variables	Explained Variable: Happiness			
	(1)	(2)	(3)	(4)
Clean energy consumption	0.085 ** (0.035)	−0.117 (0.335)	−0.112 (0.339)	−0.083 (0.323)
Square of clean energy consumption	-	0.017 (0.023)	0.016 (0.024)	0.011 (0.023)
Treat	−0.074 * (0.045)	-	-	-
Individual characteristic variables	Yes	No	Yes	Yes
Family characteristic variable	Yes	No	No	Yes
Regional fixed effect	Yes	Yes	Yes	Yes
Observations	3012	3012	3012	3012

Robust standard errors in parentheses, ** $p < 0.05$, * $p < 0.1$.

6.3. Further Analysis: Test of Non-Linear Effect

The main effect analysis above shows that, after controlling for a series of other variables, residential clean energy consumption has a significant positive effect on residents’

well-being. However, the greater the clean energy consumption, the greater the consumption expenditure of residents, which inhibits residents' happiness. Therefore, this section explores whether there is an inverted U-shaped relationship between residential clean energy consumption and residents' happiness; that is, after residents use residential clean energy to reach a certain extreme value, their happiness declines with the increase in clean energy consumption. Columns (2), (3) and (4) in Table 11 present the regression results. The values of the secondary terms of residential clean energy consumption and residential clean energy consumption are not significant, indicating that there is no nonlinear relationship between residential clean energy consumption and residents' well-being, that is, there is no inverted U-shaped relationship. This demonstrates that residents have not yet felt the negative impact of excessive clean energy consumption, and that the increase in residential clean energy consumption is constantly improving the quality of life of residents. This proves that the Chinese government must vigorously develop clean energy to enhance the happiness of Chinese residents.

7. Conclusions and Policy Implication

7.1. Conclusions

This study used data from the Chinese General Social Survey (CGSS) in 2018 to explore the impact of residential clean energy consumption on residents' well-being. Our research results show the following: there is a significant positive relationship between clean energy consumption and residents' well-being; furthermore, it can be seen from the results of marginal effects that the increase in clean energy consumption increases the probability of residents choosing "relatively happy" and "extremely happy". Moreover, in the heterogeneity analysis, for the groups with housing and low education background, there is a significant positive relationship between residential clean energy consumption and residents' well-being, and the impact on the middle and elderly groups is more significant. The intermediary analysis shows that the use of clean energy in housing improves the health of residents, and improves their quality of life while increasing their expenditure. In addition, central heating affects the relationship between residential clean energy consumption and residents' well-being. Further analysis shows that there is no nonlinear relationship between the increase in residential clean energy consumption and residents' happiness. This study conducted a series of robustness tests on the empirical results, including a placebo test, and the estimated results were robust.

7.2. Policy Implication

The results of this study have several important policy implications. Therefore, this study proposes corresponding policy suggestions from the following aspects. First, the government should actively promote the construction of residential clean energy infrastructure, such as natural gas pipelines, to achieve "household ventilation", so that residents can obtain clean and efficient living energy. In addition, through the relocation policy in combination with the poverty alleviation work, the residents living in remote mountain areas will be relocated to areas with high access to clean energy, reducing the cost of energy infrastructure construction. Secondly, when formulating policies to popularize clean energy for housing, we should adjust measures to local conditions and implement differentiated policies. Furthermore, we should vigorously publicize the advantages of clean energy, actively promote the policies of "replacing coal with electricity", "replacing coal with gas", and "clean heating in winter", and appropriately subsidize residents' use of clean energy in their homes. Third, the government should not only improve residents' ability to obtain clean energy for housing, but also cooperate with several measures to improve residents' welfare. Additionally, we will accelerate the construction of leisure and entertainment facilities to increase residents' leisure activities. Moreover, providing basic health services for residents who cannot use clean energy temporarily, formulating policies to reduce air pollution, ensuring residents' health, and preventing residents from feeling less happy due to health problems.

Author Contributions: Conceptualization, Z.S. and Y.W.; methodology, Y.L., Y.W. and H.S.; software, H.S. and L.Q.; validation, Z.S., Y.W. and H.S.; formal analysis, H.S. and Y.W.; investigation, D.Z. and L.Q.; resources, Z.S.; data curation, D.Z. and L.Q.; writing—original draft preparation, Y.W. and H.S.; writing—review and editing, Z.S., D.Z. and L.Q.; visualization, Y.L. and L.Q.; supervision, Y.W.; project administration, D.Z., Y.W. and H.S.; funding acquisition, Z.S. and D.Z. All authors have read and agreed to the published version of the manuscript.

Funding: Youth Program of National Natural Science Foundation of China (52208032).

Data Availability Statement: The data presented in this study are available on request from the corresponding author.

Acknowledgments: The authors thank anonymous reviewers and editors for their insightful comments and suggestions.

Conflicts of Interest: The authors declare no conflict of interest.

References

1. Wu, Y.; Wu, Y.; Zhang, Y.; Wang, X.; Song, Z. The Effect of Building Electricity Consumption on Residents' Subjective Well-Being: Evidence from China. *Buildings* **2022**, *12*, 710. [CrossRef]
2. Huang, H.; Hong, J.; Wang, X.; Chang-Richards, A.; Zhang, J.; Qiao, B. A spatiotemporal analysis of the driving forces behind the energy interactions of the Chinese economy: Evidence from static and dynamic perspectives. *Energy* **2022**, *239*, 122104. [CrossRef]
3. Valero, A.; Valero, A.; Calvo, G. Summary and critical review of the International Energy Agency's special report: The role of structural minerals in clean energy transitions. *Rev. Metal.* **2021**, *57*, 197. [CrossRef]
4. Sohail, M.T.; Ullah, S.; Majeed, M.T.; Usman, A.; Andlib, Z. The shadow economy in South Asia: Dynamic effects on clean energy consumption and environmental pollution. *Environ. Sci. Pollut. Res. Int.* **2021**, *28*, 29265–29275. [CrossRef] [PubMed]
5. Malinowski, M. "Green Energy" and the Standard of Living of the EU Residents. *Energies* **2021**, *14*, 2186. [CrossRef]
6. Wang, X.; Huang, H.; Hong, J.; Ni, D.; He, R. A spatiotemporal investigation of energy-driven factors in China: A region-based structural decomposition analysis. *Energy* **2020**, *207*, 118249. [CrossRef]
7. Ben Mbarek, M.; Saidi, K.; Rahman, M.M. Renewable and non-renewable energy consumption, environmental degradation and economic growth in Tunisia. *Qual. Quant.* **2018**, *52*, 1105–1119. [CrossRef]
8. Zhang, X.; Wu, L.; Zhang, R.; Deng, S.; Zhang, Y.; Wu, J.; Li, Y.; Lin, L.; Li, L.; Wang, Y.; et al. Evaluating the relationships among economic growth, energy consumption, air emissions and air environmental protection investment in China. *Renew. Sustain. Energy Rev.* **2013**, *18*, 259–270. [CrossRef]
9. Zahoor, Z.; Khan, I.; Hou, F. Clean energy investment and financial development as determinants of environment and sustainable economic growth: Evidence from China. *Environ. Sci. Pollut. Res.* **2021**, *29*, 16006–16016. [CrossRef]
10. Liddell, C.; Morris, C. Fuel Poverty and Human Health: A Review of Recent Evidence. *Energy Policy* **2010**, *38*, 2987–2997. [CrossRef]
11. United Nations. *The Sustainable Development Goals Report*; United Nations: New York, NY, USA, 2021; p. 2020.
12. Schwab, K. The fourth industrial revolution: What it means, how to respond. *Econ. Cult. Hist. Jpn. Spotlight Bimon.* **2016**, 3–5. Available online: https://www.jef.or.jp/journal/pdf/208th_Cover_01.pdf (accessed on 8 June 2022).
13. Nie, P.; Li, Q.; Sousa-Poza, A. Energy poverty and subjective well-being in China: New evidence from the China Family Panel Studies. *Energy Econ.* **2021**, *103*, 105548. [CrossRef]
14. Ejrnæs, A.; Greve, B. Your position in society matters for how happy you are. *Int. J. Soc. Welf.* **2017**, *26*, 206–217. [CrossRef]
15. Anand, P.; Hunter, G.A.; Smith, R. Capabilities and Well-Being: Evidence Based on the Sen–Nussbaum Approach to Welfare. *Soc. Indic. Res.* **2004**, *74*, 9–55. [CrossRef]
16. Bittmann, F. Beyond the U-Shape: Mapping the Functional Form Between Age and Life Satisfaction for 81 Countries Utilizing a Cluster Procedure. *J. Happiness Stud.* **2020**, *22*, 2343–2359. [CrossRef]
17. Tesch-Römer, C.; Motel-Klingebiel, A.; Tomasik, M.J. Gender Differences in Subjective Well-Being: Comparing Societies with Respect to Gender Equality. *Soc. Indic. Res.* **2007**, *85*, 329–349. [CrossRef]
18. Binder, M.; Coad, A. Heterogeneity in the Relationship between Unemployment and Subjective Wellbeing: A Quantile Approach. *Economica* **2015**, *82*, 865–891. [CrossRef]
19. Deaton, A. Income, health, and well-being around the world: Evidence from the Gallup World Poll. *J. Econ. Perspect. A J. Am. Econ. Assoc.* **2008**, *22*, 53–72. [CrossRef]
20. Herman, K.M.; Hopman, W.M.; Rosenberg, M.W. Self-rated health and life satisfaction among Canadian adults: Associations of perceived weight status versus BMI. *Qual. Life Res.* **2013**, *22*, 2693–2705. [CrossRef]
21. Binder, M.; Blankenberg, A. Green lifestyles and subjective well-being: More about self-image than actual behavior? *J. Econ. Behav. Organ.* **2017**, *137*, 304–323. [CrossRef]
22. Río, P.; Burguillo, M. An empirical analysis of the impact of renewable energy deployment on local sustainability. *Renew. Sustain. Energy Rev.* **2009**, *13*, 1314–1325.

23. Welsch, H.; Biermann, P. Electricity supply preferences in Europe: Evidence from subjective well-being data. *Resour. Energy Econ.* **2014**, *38*, 38–60. [[CrossRef](#)]
24. Welsch, H.; Biermann, P. Energy Affordability and Subjective Well-Being: Evidence for European Countries. *Energy J.* **2017**, *38*, 159–176. [[CrossRef](#)]
25. Welsch, H.; Kühling, J. Pro-environmental behavior and rational consumer choice: Evidence from surveys of life satisfaction. *J. Econ. Psychol.* **2010**, *31*, 405–420. [[CrossRef](#)]
26. Easterlin, R.A. Explaining happiness. *Proc. Natl. Acad. Sci. USA* **2003**, *100*, 11176–11183, PMID:PMC196947. [[CrossRef](#)] [[PubMed](#)]
27. Ferrer-i-Carbonell, A. Income and Well-Being: An Empirical Analysis of the Comparison Income Effect. *J. Public Econ.* **2005**, *89*, 997–1019. [[CrossRef](#)]
28. Ferreira, S.; Moro, M. On the use of subjective well-being data for environmental valuation. *Environ. Resour. Econ.* **2010**, *46*, 249–273. [[CrossRef](#)]
29. Xu, Z.; Ge, R. The Impact of Energy Consumption Revolution on Farmers' Happiness: An Empirical Analysis from China. *Front. Public Health* **2022**, *10*, 778002, PMID:PMC8960032. [[CrossRef](#)] [[PubMed](#)]
30. Argyle, M. Causes and correlates of happiness. In *Well-Being: The Foundations of Hedonic Psychology*; Kahneman, D., Diener, E., Schwarz, N., Eds.; Russell Sage Foundation: New York, NY, USA, 1999.
31. Aristondo, O.; Onaindia, E. Inequality of energy poverty between groups in Spain. *Energy* **2018**, *153*, 431–442. [[CrossRef](#)]
32. Estiri, H.; Zagheni, E. Age matters: Ageing and household energy demand in the United States. *Energy Res. Soc. Sci.* **2019**, *55*, 62–70. [[CrossRef](#)]
33. Gyberg, P.; Palm, J. Influencing households' energy behaviour—How is this done and on what premises? *Energy Policy* **2009**, *37*, 2807–2813. [[CrossRef](#)]
34. Wu, Y.; Huang, H.H.; Hong, J.; Wang, X.; Wu, Y.; Wu, Y. Transfer patterns and driving factors of China's energy use in trade: Evidence from multiregional input–output analysis and structural decomposition analysis. *Energy Rep.* **2022**, *8*, 10963–10975. [[CrossRef](#)]
35. Walker, G.; Day, R. Fuel poverty as injustice: Integrating distribution, recognition and procedure in the struggle for affordable warmth. *Energy Policy* **2012**, *49*, 69–75. [[CrossRef](#)]
36. Smith, J.; Borchelt, M.; Maier, H.; Jopp, D.S. Health and Well-Being in the Young Old and Oldest Old. *J. Soc. Issues* **2002**, *58*, 715–732. [[CrossRef](#)]
37. Middlemiss, L.; Gillard, R. Fuel poverty from the bottom-up: Characterising household energy vulnerability through the lived experience of the fuel poor. *Energy Res. Soc. Sci.* **2015**, *6*, 146–154. [[CrossRef](#)]
38. Mehmetoglu, M. medsem: A Stata package for statistical mediation analysis. *Int. J. Comput. Econ. Econom.* **2018**, *8*, 63–78.
39. Iacobucci, D.; Saldanha, N.; Deng, X. A meditation on mediation: Evidence that structural equations models perform better than regressions. *J. Consum. Psychol.* **2007**, *17*, 139–153. [[CrossRef](#)]
40. Walker, G. Decentralised systems and fuel poverty: Are there any links or risks? *Energy Policy* **2008**, *36*, 4514–4517. [[CrossRef](#)]

Article

Analysis of the Cooling and Humidification Effect of Multi-Layered Vegetation Communities in Urban Parks and Its Impact

Yu Zhang¹ and Meiqi Dai^{1,2,*}¹ College of Forestry, Central South University of Forestry and Technology, Changsha 410000, China² College of Tourism, Central South University of Forestry and Technology, Changsha 410000, China

* Correspondence: mqdai2022@163.com

Abstract: As urbanization continues to accelerate, the urban heat island effects have become one of the most important issues affecting the urban environment and people's living experience. Numerous studies have shown that urban parks and green spaces can effectively alleviate the problem of the urban heat island effect and provide cooling and humidifying effects. Vegetation communities are a fundamental part of urban parklands, and multi-layered vegetation communities are considered to have better cooling and humidifying effects. Previous studies have focused on comparative analyses between different cover types of vegetation communities but have not explored the differences in the cooling and humidifying effects of multi-layered vegetation communities of the same cover type. Therefore, the Olympic Forest Park in Beijing was selected as the subject of this study, and multi-layered vegetation-covered (tree-shrub-grass) with different degrees of densities and uncovered squares were selected for the control and comparison. The cooling and humidifying effects of multi-layered vegetation communities with different canopy densities at different times of the day through field measurements were studied, and the influencing factors for this were analyzed. The results show that the tree cover is the core factor affecting temperature; the degree of the canopy density of multi-layered vegetation communities is significantly and positively correlated with the intensity of cooling and humidification, and the cooling and humidifying effect of multi-layered vegetation communities increases as the degree of canopy density increases. The results of this study can provide some references for the planning and design of urban parks and green spaces.

Keywords: urban park; multi-layered vegetation communities; cooling and humidifying effects; canopy density

Citation: Zhang, Y.; Dai, M. Analysis of the Cooling and Humidification Effect of Multi-Layered Vegetation Communities in Urban Parks and Its Impact. *Atmosphere* **2022**, *13*, 2045. <https://doi.org/10.3390/atmos13122045>

Academic Editors: Roberto Alonso González Lezcano, Francesco Nocera and Rosa Giuseppina Caponetto

Received: 10 November 2022

Accepted: 3 December 2022

Published: 7 December 2022

Publisher's Note: MDPI stays neutral with regard to jurisdictional claims in published maps and institutional affiliations.



Copyright: © 2022 by the authors. Licensee MDPI, Basel, Switzerland. This article is an open access article distributed under the terms and conditions of the Creative Commons Attribution (CC BY) license (<https://creativecommons.org/licenses/by/4.0/>).

1. Introduction

Urbanization, which is growing rapidly, is important for improving human development. However, urbanization can also lead to serious environmental problems, such as the urban heat island (UHI) effect [1]. A gradual increase in the UHI effect has been observed in both large and medium-sized cities [2]. The UHI effect can lead to many problems, including thermal discomfort and even health risks for urban dwellers [3]. The ambient air temperature has a significant impact on human physiological activity, with high air temperatures causing increased discomfort and illness, as well as reducing human productivity [4], increasing energy consumption and air pollution [5], and altering species composition and distribution [6]. The UHI effect has become one of the most important factors affecting the livability of urban environments and has a potential impact on the quality of life of urban residents.

A growing body of research has demonstrated that urban green spaces provide multiple benefits for improving urban sustainability and livability [7–10]. Green spaces include parks and reserves, sports fields, riparian areas (such as streams and riverbanks), greenways and trails, community gardens, street trees, and nature reserves, as well as less traditional

spaces such as green walls and green alleys [11]. Urban parks are the largest patches of urban green space, with important ecological functions and significant impacts on the local and micro-scale climate [12–14]. Previous empirical studies have shown that parks are not only cold and wet areas in cities but can also have a cooling and humidifying effect on their immediate vicinity [15–18]. This gives rise to an “oasis effect” known as the “Park Cool Island” (PCI) [19,20]. Large urban parks, through the cooling and humidifying effects exerted by plants, enhance thermal comfort and reduce the UHI effect [21,22].

Plants in urban parks are usually planted in groups [23]. In China, the plant patterns follow the concept of “learning from nature”, with a large number of decorative plant species planted nearby, creating a complex flora in most urban parks [24]. The vegetation community absorbs and reflects large amounts of solar radiation through its branches and leaves, and the dense canopy acts as a shade. At the same time, plant evapotranspiration carries water into the air, converting and consuming ambient heat, thus, regulating the air temperature and relative humidity under the tree canopy and in its surroundings [25–27]. Available studies show that the cooling effect of evergreen plants is highest for conifers, followed by deciduous broadleaf bushes; broadleaf evergreens come third, and finally, palm clusters have the lowest cooling effect [12,28,29]. Vegetation communities consisting of trees, shrubs, and grasses produce more significant cooling and humidifying effects than lawns [30–33]. The vertical structure of the community refers to the variation in the vertical direction of the community in space, which is manifested in the stratification of plants in the community and is one of the most important manifestations of the morphological characteristics of the community. The plant communities are classified according to their structure as Tree-Shrub-Grass (TSG), Tree-Shrub (TS), Tree-Grass (TG), Shrub-Grass (SG), and Ground Cover/Grass (G) communities. The vertical structure of the communities can be divided into three patterns, TSG is a multi-layer plant community (MPC), TS, TG, and SG are double-layer plant communities (DPC), and G is a single-plant community (SPC) [34]. Most scholars believe that different community types have different cooling and humidifying effects, and those multi-layered vegetation communities consisting of Tree-Shrub-Grass have higher green biomass and, therefore, better cooling effects [35–37]. Previous studies have shown that trees can influence air temperature and relative humidity through shading, transpiration, and evaporative cooling, so parkland strips of trees, shrubs, and grasses can have a more pronounced impact than lawns [30,38]. Multi-layered communities dominated by trees are significantly better at regulating temperature and humidity than other types of communities [39,40].

Previous studies have shown that tree cover is a key factor influencing air temperature [41]. Compared to exposed areas, a natural shade can produce cooler and more comfortable human sensations [42,43]. In the southern subtropics, canopy density, solar radiation, wind speed, and canopy area all have significant effects on cooling, with canopy area and canopy density having significant effects on humidification and thermal comfort [12]. Researchers in Changchun, China, confirmed that the canopy density, leaf area index, and tree-height were the most significant drivers of the cooling effect [32]. From 9:00 a.m. to 12:00 p.m., the canopy density and leaf area index better reflects the cooling and humidifying effect [44], and canopy density is an important indicator for studying the cooling and humidifying effect of urban parks. In a comparative analysis of hot and cold spots for air temperature in 10 city parks in Singapore, shade was found to be an important factor in lowering temperatures [45]. In a study using Landsat data on tree species richness and diversity to predict the urban heat island effect mitigation in green spaces, it was shown that the average canopy width and tree density in green spaces could explain some of the variations in the cooling extent, and that, in terms of plant community structure, the trees with the widest canopies could produce more shade and potentially more evapotranspiration in summer and autumn. The study used dummy variable regression to measure the community structure of different types of vegetation forming tree-shrubs-herbs and tree-herbs in urban agglomerative green infrastructure and found that canopy density was significantly and positively correlated with cooling and humidifying effects [21]. The

specific contribution of the vegetation community structure to the cooling effect needs to be further explored, and the existing research focuses mainly on the comparative analysis of the cooling and humidifying effects between the different vegetation types or between three different patterns of communities in the vertical structure of the community, without exploring the differences in the cooling and humidifying effects of multi-layered vegetation communities of the same vegetation type. Therefore, in this study, the cooling and humidifying effects of multi-layered vegetation communities with different degrees of canopy density in urban parks were investigated and analyzed to understand the cooling effect of green spaces covered by multi-layered vegetation communities in urban parks at the micro-scale and to understand their changing trends and cooling intensities. There are two main scales of research on the cooling effect of the parkland: local or mesoscale studies based on satellite imagery and meteorological data. These studies apply the metrics of parkland cooling intensity to quantify the cooling effect of the parkland. Another type of small-scale study is the application of simulation models constructed through field observations and simulation tools such as ENVI-met or the Ladybug tool (LBT) [8]. Compared to spatial datasets derived from satellite imagery, field observations provide a more direct and accurate characterization of the dynamic relationship between parkland and atmospheric temperatures.

Therefore, in order to compare with previous studies and obtain more direct and accurate data results, this study proposes to achieve the following research objectives through field measurements:

(1) Study the effect of vegetation cover on the cooling and humidifying effect of the microclimate in urban parks during hot and dry summers.

(2) Analysis of the cooling and humidifying effects of multi-layered vegetation communities in urban parks with different degrees of canopy density and their effects.

It is hoped that the research will improve our understanding of the cooling effect of vegetation communities in urban green spaces and that the study of the vegetation structure on a small scale will help landscape gardeners and urban planners to make effective and efficient design and planning decisions, thus maximizing the cooling effect of green spaces in urban parks, improving microclimate conditions and human outdoor comfort, and giving full play to the role of urban parks as “urban cooling islands”.

2. Materials and Methods

2.1. Study Area

The study was conducted in the Chinese capital, Beijing (39°56′ N, 116°20′ E), which is located in the northwestern part of the North China Plain and has a warm temperate continental semi-humid monsoon climate with four distinct seasons, moderate precipitation, an average annual temperature of 11.5 °C, and 2841.4 h of sunshine throughout the year, with the hottest month of the year occurring in July.

The Olympic Forest Park (40°01′3.00″ N, 116°23′2.98″ E) is located on the northern side of Beijing’s central axis, with a total area of 1135 hm² (Figure 1). It is currently the largest national sports and leisure park in the northern region of Beijing, with the largest area covered by forest vegetation. The park is rich in forest resources, and the vegetation coverage is mainly trees and shrubs, with a greening rate of 95.61%, making it a national 5 A tourist attraction. In this study, the plot was selected in the central part of the city park because of the richness and diversity of the greenery and vegetation in this part of the park, which makes it easy to study.

2.2. Date Measurement

In this study, four equal-sized plots (50 m × 50 m), numbered 1, 2, 3, and 4 were selected for field measurements in the central part of the Olympic Park; the plots were composed of a multi-layered vegetation group of trees + shrubs + grasses, with densities of 8% (1), 16% (2), 31.2% (3), and 69.9% (3), respectively. The cooling effect of the park green space was studied according to the air temperature variation between different plots and

the relative humidity variation. Canopy density refers to the ratio of the total area projected on the ground when the sun shines directly on the canopy of a tree to the area of the forest floor and is expressed as a percentage. In addition, for the control experiment, an open field of equal size, numbered 0, was selected as a control site for this study. All plots and control site is located at a large distance from the surrounding buildings and are free from motor vehicle access, thus ensuring that the data from this measurement are true, reliable, and comparable. Detailed information is shown in Table 1.

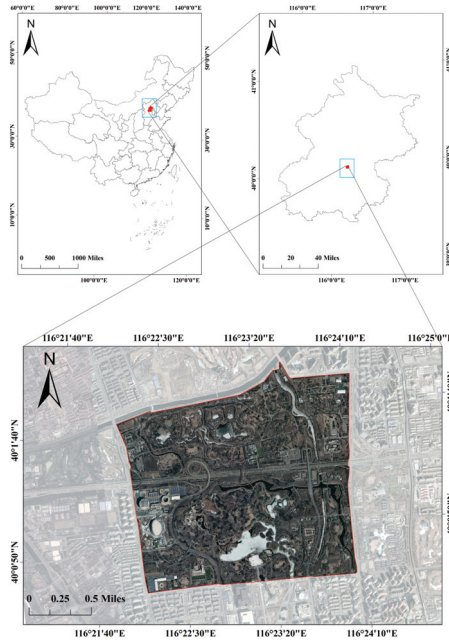


Figure 1. Map showing the experimental plot area—The Olympic Forest Park.

Table 1. Information on control site and plots of multi-layered vegetation communities (trees + shrubs + grasses) in forest parks with different canopy densities.

No.	Canopy Density (%)	Area	Types	Vegetation Types
1	8	50 m × 50 m	Tree-shrub-grass	Tree: <i>Salix babylonica</i> L., <i>Acer</i> spp., <i>Magnolia grandiflora</i> L., <i>Pinus tabulaeformis</i> Carr.,
2	16	50 m × 50 m		Shrub: <i>Rosa chinensis</i> Jacq., <i>Ligustrum × vicaryi</i> Hort.
3	31.2	50 m × 50 m		Grass: <i>Lolium perenne</i> L., <i>Poa annua</i> L.
4	69.9	50 m × 50 m		
0	0	50 m × 50 m	Impervious surface	No vegetation

2.2.1. Measurement of Air Temperature and Humidity by Using Kestrel 5000

Given the need for simultaneous observations at different plots, the Kestrel 5000 handheld meteorological instrument was chosen for the study to monitor the plot and record at regular intervals at fixed points. The Kestrel 5000 offers high accuracy, high performance, and portability, with the main parameters being air temperature and relative humidity at the plots and control site. All data measurements were taken from July to September 2020 in clear weather. Diagonal measurements were taken at 10 m intervals in different plots, with a fixed points monitoring method, and the height was set at 1.5 m of human breathing height. The air temperature and relative humidity were recorded accurately with an instrument from 8:00 am to 18:00 pm, and a set of data was measured every 2 h, 6 standard time slots in total, to ensure the reliability of the data. Each plot and the control site were measured three times or more to obtain the average value.

2.2.2. Measurement of Canopy Density Parameters

In this study, each of the plots that we selected had a similar proportion of shrubs and grasses, with differences in the canopy of trees. The canopy density of the plots was estimated visually by looking up at the canopy at diagonally spaced observation points and recording the number of plots that could be shaded by the projection of direct sunlight on the canopy, and dividing by the total number of points to calculate the size of the canopy density [46,47].

The data for the cooling effect of the different plots were processed by taking the arithmetic mean of the air temperature and relative humidity data obtained during the same period as the final air temperature and relative humidity of the observed plots. These data were compared with the control 0, and the cooling and humidification intensity of the plots compared with the control 0 was calculated as a measure of the cooling and humidification effect of the plots. The results were plotted as air temperature, a relative humidity trend, a cooling intensity trend, and a relative humidity intensity trend to give a more visual representation of the cooling and humidification effects on different plots [48,49].

The intensity of cooling at the plot: air temperature measured at control 0 minus the air temperature at the plot.

$$\Delta T = T_0 - T \quad (1)$$

Intensity of humidification in the plot: the relative humidity of the air in the plot minus the relative humidity of the air at control 0.

$$\Delta RH = RH - RH_0 \quad (2)$$

The values of ΔT and ΔRH represent the difference in temperature and humidity between a plot and the control site, respectively, i.e., the intensity of cooling and humidification that can be derived from the calculation; T and RH indicate the air temperature and relative humidity measured by a plot at a given time, respectively; T_0 and RH_0 represent the temperature and humidity values at control 0, respectively. If $\Delta T > 0$, it means that the temperature of the plot is lower than that of the control site, which means that the park green area has a certain cooling effect and ΔT as a larger value means that the cooling effect of the plot is more obvious, while the opposite means that the cooling effect is weaker. If $\Delta RH > 0$, it means that the relative humidity of the air in the plot is higher than the relative humidity of the control site, indicating that the park green space has a certain humidifying effect; the larger the value of ΔRH , the more obvious the humidifying effect, and vice versa, the weaker the effect.

3. Results

3.1. Air Temperature Variation at the Plots and Control Site

As can be seen from Figure 2, the pattern of the temperature change in the plots with different degrees of canopy density during the observation period is basically the same as that of the control site, showing an inverted "U" shaped trend of increasing and then decreasing. At 14:00, the maximum temperature was reached at all sample and control site, with the unvegetated control 0 temperature reaching 34.2 °C; The highest temperature in the plots with the multi-layered vegetation cover was the lowest canopy density plot 1. The value of 33.76 °C as the lowest temperature occurred at 8:00. The control 0 was 28.05 °C, and plot 4 was 28.02 °C, with small differences in the temperature, but at all times, the four plots with a multi-layered vegetation community cover had lower temperatures than the uncovered plots. This is a good indication of the significant cooling effect of vegetation cover during the day. This indicates that the higher the degree of canopy density of the same type of multi-layered vegetation community in a park green space, the lower the temperature; in the sample plots with a multi-layered vegetation cover, the temperature was above 30 °C for more than 8 h in Plot 1, 2, 3, and only above 6 h in Sample 4. The higher the canopy density, the shorter the duration of the high temperature in the sample plots. This means that the higher the vegetation cover of the parkland, the higher the

canopy density of the multi-layered vegetation, the lower the microclimate temperature, and the shorter the duration of high temperatures, the more effectively the parkland can reduce temperatures.

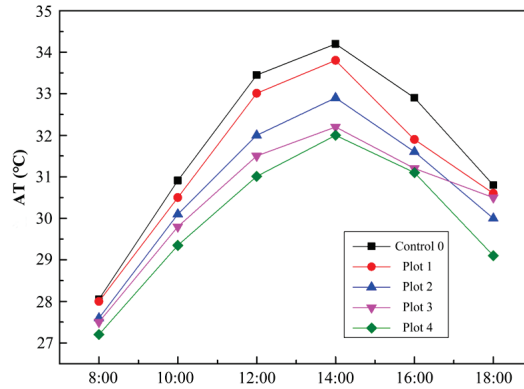


Figure 2. The air temperature changes at different plots.

3.2. Changes in Relative Humidity at the Plots and Control Site

As can be seen from Figure 3, the trend in the relative humidity at each plot and the control site is consistent, showing an inverted “U” pattern of rising and then falling, with the lowest point at all plots and the control site occurring around 14:00, in the opposite direction to the trend in air temperature. The relative humidity ranged from 42.58% to 69.91% in all the sample plots, significantly higher than the 36.26% to 56.89% in the control plots. This shows that the vegetation cover can have a significant humidifying effect. Previous studies have shown that the optimum air humidity for the human body is between 40% and 80%; when the relative humidity is below 40%, the air is relatively dry, and the resistance of the respiratory system is weakened, the incidence of various infectious diseases is significantly increased and respiratory diseases are easily induced and aggravated, which is also detrimental to the human body [50]. The non-vegetated control 0 showed a relative humidity below 40%, while the vegetated plots did not show this during the dry and hot summer months. In plot 4, the most densely vegetated plot, relative humidity above 55% was maintained at all times. This suggests that the higher the vegetation cover, the higher the relative humidity of the plots, and that green spaces were effective in raising the relative humidity of the air.

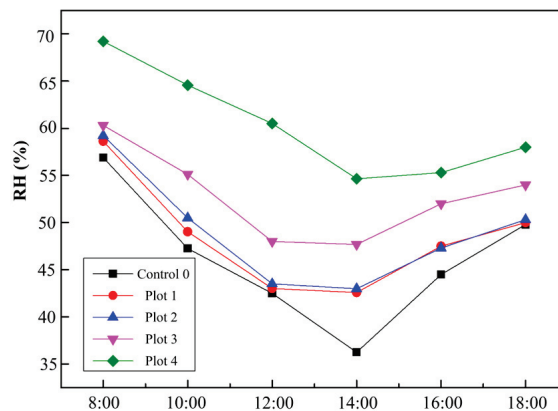


Figure 3. Relative humidity changes at different plots.

3.3. Comparison of the Cooling Effect of Plots with Different Degrees of Canopy Density

Figure 4 shows a comparison of the cooling intensity of plots with different degrees of canopy density. As can be seen from the figure, from 8:00 to 18:00, the temperature difference between all the measured plots and the control site is greater than 0. This result proves that urban park green spaces can significantly reduce the ambient temperature. Compared to the square floor tiles without vegetation coverage, the cooling intensity of each plot ranged from 0.05 °C to 2.44 °C during the observation time, with an average cooling intensity of 1.12 °C. From 10:00 to 16:00, the temperature difference between each plot and the control site began to increase, reaching the maximum temperature difference (2.44 °C) at 12:00, indicating that the urban park green space has the strongest ability to regulate temperatures during the highest temperature period of the day.

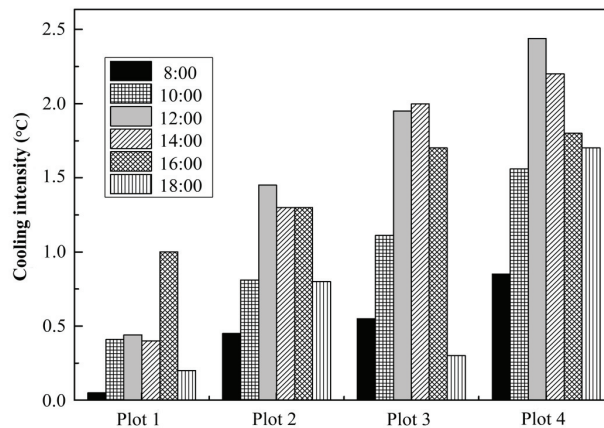


Figure 4. Comparison of different cooling effects between 8 o'clock and 18 o'clock.

The temperature difference between each plot and the control site was obvious during the observation period, and the cooling intensity was in the order of plot 4 > plot 3 > plot 2 > plot 1, with the greatest cooling intensity in plot 4, which had the highest canopy density. The maximum value was reached at 12:00. As can be seen from Figure 3, at any given moment, the cooling intensity was greatest in plot 4, which had the highest canopy density, and the cooling effect was best; the least intense cooling was in plot 1, which had the lowest canopy density. This result shows that the amount of vegetation coverage has a significant effect on the cooling effect of parks; the more vegetation coverage and the greater the degree of canopy density, the better the cooling effect of park green space, and the degree of canopy density of multi-layered communities in urban parks has a significant positive correlation with the cooling effect.

3.4. Comparison of the Humidifying Effect of Plots with Different Degrees of Canopy Density

Figure 5 shows a comparison of the intensity of humidification in plots with different degrees of canopy density. As can be seen from Figure 5, the difference in the relative humidity between plots 1 to 4 and control 0 was greater than 0 during the measurement period, and the difference in the relative humidity between each plot and the control site was significant. This result proves that urban parks with vegetation coverage can significantly enhance the relative humidity within the environment. The order of humidification intensity for each plot was 4 > 3 > 2 > 1, with the greatest intensity in plot 4, which had the greatest canopy density. Compared to the control 0, the moisture gain intensity of each plot ranged from 0.5% to 17.33% during the observation period, with an average moisture gain intensity of 6.46%; the moisture gain intensity of the park green space increased and then decreased over time, with the moisture gain intensity of each plot increasing from 10:00 to 16:00 and reaching the maximum moisture difference (18.38%) at 14:00.

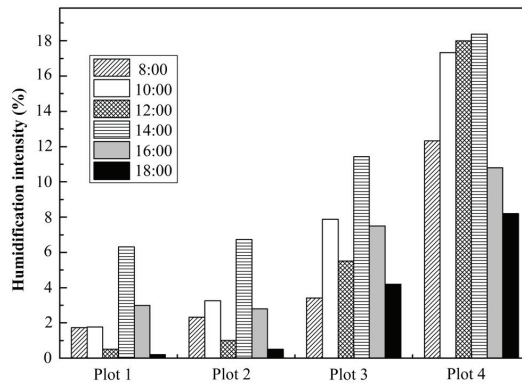


Figure 5. Comparison of different humidification effects between 8 and 18 o'clock.

The above results show that urban park plant communities have the greatest ability to humidify and regulate the environment during the time of day when the relative humidity is at its highest. During the observation period, the relative humidity magnitude of the urban park plots with different degrees of canopy density was higher than that of the control 0. At any moment, the highest degree of canopy density, plot 4, had the highest intensity of humidification and the best humidification effect. The least intensive moisture gain was in plot 1, which had the lowest canopy density. This result shows that vegetation coverage has a significant effect on the humidifying effect of parks, and the higher the degree of canopy density, the better the humidifying effect of green areas in parks, and the degree of canopy density of multi-layered vegetation communities in urban parks has a significant positive correlation with the humidifying effect.

4. Discussion

4.1. Analysis of the Effect of Vegetation Cover on Microclimate Cooling and Humidification in Urban Parks

The finding that urban parks can significantly improve urban air temperatures has been confirmed in many regional and urban studies [12,16–18]. In this study, after monitoring the air temperature variation patterns in Beijing Olympic Forest Park plots with different degrees of canopy density at fixed points, it was found that the temperature of the park green areas with vegetation cover was always lower than that of the control site in the open square floor tiles without vegetation cover during the observation time from early morning to late evening. During the observation period, the pattern of temperature change in each plot was the same as that of the control site, showing an inverted “U” shape trend increasing first and then decreasing; in terms of the cooling intensity, the order of cooling intensity was: plot4 > plot 3 > plot 2 > plot 1 > control 0. Compared with the square tiles without vegetation cover, the cooling intensity of multi-layered vegetation community sample sites during the observation period ranged from 0.05 to 2.44 °C, with an average cooling intensity of 1.12 °C. This result shows that the vegetation cover of urban parks can have a significant cooling effect, but there are some differences in the cooling intensity of the park plots at different times of the day and different degrees of canopy density. This result is consistent with the findings of Chang et al., who measured and compared the cooling effect in 61 parks in Taipei City and found that the cooling effect in parks was greatest at midday in summer, with an intensity of 0.81 °C, which is slightly lower than the results of this study [51]. The reason for this is probably related to the location of the observation plots and the different degrees of park closeness. The higher the degree of closeness, the more the multi-layered vegetation community absorbs and reflects a large amount of solar radiation through its branches and leaves, and the dense tree canopy acts as shade, which can largely shade the park during daylight hours, enhancing the cooling effect of the park [52,53]. The temperature of a substance is mainly determined by the

heat capacity of the substance itself, which is higher in the leaves of plants than in the impermeable ground. Therefore, for the same amount of solar radiation and time, the temperature of an area covered with plants rises more slowly, mainly because the plant leaves can photosynthesize [54,55].

During the observation period, the relative humidity in the vegetated parkland was consistently higher than in the non-vegetated open plaza ground control. The trend in the relative humidity was consistent between the plots and the control site, showing a 'U' shaped pattern of decreasing and then increasing, with the lowest point occurring at around 14:00 in all plots and the control site, in contrast to the temperature trend. Compared to the control site, the intensity of moisture increased at each plot during the observation period and ranged from 0.5% to 17.33%, with an average intensity of 6.46%; during the measurement time (8:00–18:00), the intensity of the moisture at the park green first increased and then decreased, and the intensity of the moisture increased at each plot from 10:00–16:00, reaching the maximum moisture difference (18.38%) at 14:00. The order of moisture gain intensity at each plot from highest to lowest was sample plot 4 > plot 3 > plot 2 > plot 1 > control 0; the greatest moisture gain intensity was at sample plot 4 with the lowest pressure, and the highest moisture gain intensity was at sample plot 4 with the lowest pressure. Due to the ample vegetation cover, the evaporation process of the plants and the evaporation of the soil radiates and converts solar energy into latent heat, which will not cause the air temperature to rise and is, thus, able to reduce the air temperature, which is one of the reasons why urban parks can have a cooling effect [56,57]. However, the evapotranspiration of plants requires a large amount of water, and the availability of sufficient water has a significant impact on the cooling and humidifying effect of the park. This study compares the changes in relative humidity of plant communities in parks with different degrees of canopy density over the observed time, and the results show that parks with higher degrees of canopy density have higher relative humidity and higher moisture retention; the comparison with the previous trend in temperature suggests that temperature keeps decreasing as the relative humidity increases, so it can be proved that evapotranspiration can influence temperature. As a result, plot 4, which had the highest canopy density, had the highest relative humidity and the lowest air temperature, and control 0, with no vegetation cover, had the lowest relative humidity and the highest air temperature. This finding echoes the findings of Chen and Wong, who investigated the cooling effect in two cities and found that city parks had the lowest temperatures and highest relative humidity in the area, and lower temperatures and relative humidity existed in the built-up areas outside the parks [13].

4.2. The Cooling and Humidifying Effect of Multi-Layered Vegetation Communities

Vegetation communities are an important object for studying the links between vegetation and microclimate in urban park cooling affect vegetation, as different vegetation communities can produce a range of microclimates. Previous studies have shown that the increase in relative humidity and reduction in air temperatures due to the evapotranspiration and shading of plants in multi-layered planting combinations is higher than in smaller vegetation communities and is most noticeable in summer [34,35]. In this study, multi-layered vegetation communities with different degrees of canopy density were selected from urban parks. It was found that the degree of the canopy density was significantly correlated with the intensity of cooling and humidification; the higher the degree of the canopy density, the better the effect of cooling and humidification; the higher the degree of canopy density, the slower the rate of warming and the shorter the duration of high temperature. Because the arboreal layer of the vegetation community has a higher green biomass than the other layer, it is the main contributor to cooling efficiency [36]. Multi-layered vegetation communities are more effective in blocking light penetration. With an adequate number of leaves, the forest grass community maintains a strong permeability, which facilitates air circulation under the canopy and shows an outstanding cooling effect, especially in breezy weather. The regulating effect of vegetation communities on environmental factors is not

a simple superposition of the regulating capacity of individual plants but rather reflects the total leaf volume and geometry of the vegetation community. Canopy structure has an important influence on energy conversion and sub-canopy airflow, thus affecting the microclimate [38].

In conclusion, the wetting effect of the greater canopy density plots is significantly better than that of the lesser canopy density plots and even better than that of the open squares without vegetation cover. This is mainly due to the fact that the larger the cover of the multi-layered vegetation community in the parkland, the higher the degree of canopy density and the bushier the trees and shrubs, and the more the canopy can shade more solar radiation so that the sunlight and thermal radiation radiated to the environment under the trees will be greatly reduced, and therefore, the temperature in the parkland will be relatively lower [58–61]. The greater the canopy density of the vegetation community, the more water is stored in the park, the less water is carried away by evapotranspiration, and the more water is retained, resulting in higher air humidity and a higher intensity of humidification, resulting in a better cooling effect. The high canopy density blocks light and has a significant effect on human physiological responses, making it feel cooler [55].

5. Conclusions

In this study, we took the Beijing Olympic Forest Park as an example and selected a sample of multi-layered vegetation communities with different degrees of vegetation cover and a square tile without vegetation cover in the park for control comparison. The conclusions of this paper are as follows:

(1) During the observation period, the pattern of the temperature change in each plot was the same as that in the control site, showing an inverted “U” pattern that increased and then decreased, while the trend of the relative humidity was the same between the plots and the control site, showing a “U” pattern which decreased and then increased, in contrast to the temperature trend. Compared with the square tiles without vegetation cover, the cooling intensity of the multi-layered vegetation community sample plots during the observation period ranged from 0.05 to 2.44 °C, with an average cooling intensity of 1.12 °C; compared with the control sites 0, the intensity of the moisture increased at each measurement plot during the observation period and ranged from 0.5% to 17.33%, with an average intensity of 6.46%. The cooling and moisture increase intensity of the sample plots with vegetation cover were higher than those without vegetation cover. The results indicate that vegetation cover types were cooler and wetter than non-vegetation cover types, suggesting that vegetation cover was the main factor influencing temperature.

(2) The study showed that during the measurement time (08:00–18:00), the temperature in the multi-layered vegetation community sample plots was lower than that in the control plots without vegetation cover, and the temperature in the sample plots decreased with increasing densities, ranking from highest to lowest: control 0 > plot 1 > plot 2 > plot 3 > plot 4; the relative humidity in all the multi-layered vegetation community sample plots was higher than that in the control plots with material cover at the time of observation. The relative humidity in the sample plots was higher than that in the control plots, and the relative humidity in the sample plots was higher than that in the non-vegetated open plaza. Multi-layered vegetation communities significantly affect the microclimate of urban parks. At the same observation time, the cooling and humidifying effect of high canopy density multi-layered vegetation communities was always higher than that of low canopy density ones, and the canopy density of urban park vegetation communities was significantly and positively correlated with the cooling effect and the humidifying effect. The higher the canopy densities, the better the cooling and humidifying effects and the shorter the duration of high temperatures.

This study compares the differences in cooling and humidifying effects between multi-layered vegetation communities with different degrees of canopy density in urban parks and open squares without vegetation cover at horizontal heights. The study selected sample plots with similar scrub, lawn, and tree densities, which could only cover tall

trees, but not low shrubs and grasses. The research on the cooling effect of more cover characteristic parameters of multi-layered vegetation communities can be strengthened, and more meteorological parameter indicators, such as wind speed can be introduced for comprehensive analysis. This study can provide a reference basis for the planning and design of urban parks in order to give full play to the heat island effect of urban parks.

Author Contributions: Conceptualization, M.D.; methodology, M.D.; investigation, Y.Z.; software, Y.Z.; resources, Y.Z.; writing—original draft preparation, Y.Z.; writing—review and editing, Y.Z. visualization, Y.Z. and M.D. All authors have read and agreed to the published version of the manuscript.

Funding: This research received no external funding.

Acknowledgments: We would like to thank our team of colleagues in the Central South University of Forestry and Technology. In addition, we would also like to thank the referees and the editors for their valuable comments for improving this manuscript.

Conflicts of Interest: The authors declare no conflict of interest.

References

- Grimm, N.B.; Faeth, S.H.; Golubiewski, N.E.; Redman, C.L.; Wu, J.; Bai, X.; Briggs, J.M. Global Change and the Ecology of Cities. *Science* **2008**, *319*, 756–760. [[CrossRef](#)] [[PubMed](#)]
- Oke, T.R. The Energetic Basis of the Urban Heat Island. *Q. J. R. Met. Soc.* **1982**, *108*, 1–24. [[CrossRef](#)]
- Martini, A.; Biondi, D.; Batista, A.C. Urban forest components influencing microclimate and cooling potential. *Rev. Árvore* **2017**, *41*, e410603. [[CrossRef](#)]
- Hami, A.; Abdi, B.; Zarehaghi, D.; Maulan, S.B. Assessing the Thermal Comfort Effects of Green Spaces: A Systematic Review of Methods, Parameters, and Plants' Attributes. *Sustain. Cities Soc.* **2019**, *49*, 101634. [[CrossRef](#)]
- Wang, X.; Cheng, H.; Xi, J.; Yang, G.; Zhao, Y. Relationship between Park Composition, Vegetation Characteristics and Cool Island Effect. *Sustainability* **2018**, *10*, 587. [[CrossRef](#)]
- White, M.A.; Nemani, R.R.; Thornton, P.E.; Running, S.W. Satellite Evidence of Phenological Differences Between Urbanized and Rural Areas of the Eastern United States Deciduous Broadleaf Forest. *Ecosystems* **2002**, *5*, 260–273. [[CrossRef](#)]
- Shekhar, S.; Aryal, J. Role of Geospatial Technology in Understanding Urban Green Space of Kalaburagi City for Sustainable Planning. *Urban For. Urban Green.* **2019**, *46*, 126450. [[CrossRef](#)]
- Qiu, K.; Jia, B. The Roles of Landscape Both inside the Park and the Surroundings in Park Cooling Effect. *Sustain. Cities Soc.* **2020**, *52*, 101864. [[CrossRef](#)]
- Grilo, F.; Pinho, P.; Aleixo, C.; Catita, C.; Silva, P.; Lopes, N.; Freitas, C.; Santos-Reis, M.; McPhearson, T.; Branquinho, C. Using Green to Cool the Grey: Modelling the Cooling Effect of Green Spaces with a High Spatial Resolution. *Sci. Total Environ.* **2020**, *724*, 138182. [[CrossRef](#)]
- Liu, S.; Zhao, J.; Xu, M.; Ahmadian, E. Effects of Landscape Patterns on the Summer Microclimate and Human Comfort in Urban Squares in China. *Sustain. Cities Soc.* **2021**, *73*, 103099. [[CrossRef](#)]
- Wolch, J.R.; Byrne, J.; Newell, J.P. Urban Green Space, Public Health, and Environmental Justice: The Challenge of Making Cities 'Just Green Enough'. *Landsc. Urban Plan.* **2014**, *125*, 234–244. [[CrossRef](#)]
- Zheng, J.; Tarin, M.W.K.; Chen, G.; Zhang, Q.; Deng, C. The Characteristics of Plant Clusters Influence on the Cooling Effect: A Case Study in a Subtropical Island Park, China. *Glob. Ecol. Conserv.* **2022**, *34*, e02055. [[CrossRef](#)]
- Yu, C.; Hien, W.N. Thermal Benefits of City Parks. *Energy Build.* **2006**, *38*, 105–120. [[CrossRef](#)]
- Úpmanis, H.; Eliasson, I.; Lindqvist, S. The Influence of Green Areas on Nocturnal Temperatures in a High Latitude City (Göteborg, Sweden). *Int. J. Climatol.* **1998**, *18*, 681–700. [[CrossRef](#)]
- Barradas, V.L. Air Temperature and Humidity and Human Comfort Index of Some City Parks of Mexico City. *Int. J. Biometeorol.* **1991**, *35*, 24–28. [[CrossRef](#)]
- Potchter, O.; Cohen, P.; Bitan, A. Climatic Behavior of Various Urban Parks during Hot and Humid Summer in the Mediterranean City of Tel Aviv, Israel. *Int. J. Climatol.* **2006**, *26*, 1695–1711. [[CrossRef](#)]
- Yan, H.; Wu, F.; Dong, L. Influence of a Large Urban Park on the Local Urban Thermal Environment. *Sci. Total Environ.* **2018**, *622–623*, 882–891. [[CrossRef](#)]
- Li, Y.; Fan, S.; Li, K.; Zhang, Y.; Dong, L. Microclimate in an Urban Park and Its Influencing Factors: A Case Study of Tiantan Park in Beijing, China. *Urban Ecosyst.* **2021**, *24*, 767–778. [[CrossRef](#)]
- Jauregui, E. Influence of a Large Urban Park on Temperature and Convective Precipitation in a Tropical City. *Energy Build.* **1990**, *15*, 457–463. [[CrossRef](#)]
- Cao, X.; Onishi, A.; Chen, J.; Imura, H. Quantifying the Cool Island Intensity of Urban Parks Using ASTER and IKONOS Data. *Landsc. Urban Plan.* **2010**, *96*, 224–231. [[CrossRef](#)]
- Wei, J.; Li, H.; Wang, Y.; Xu, X. The Cooling and Humidifying Effects and the Thresholds of Plant Community Structuring Parameters in Urban Aggregated Green Infrastructure. *Forests* **2021**, *12*, 111. [[CrossRef](#)]

22. Shi, D.; Song, J.; Huang, J.; Zhuang, C.; Guo, R.; Gao, Y. Synergistic Cooling Effects (SCEs) of Urban Green-Blue Spaces on Local Thermal Environment: A Case Study in Chongqing, China. *Sustain. Cities Soc.* **2020**, *55*, 102065. [[CrossRef](#)]
23. Zhao, D.; Lei, Q.; Shi, Y.; Wang, M.; Chen, S.; Shah, K.; Ji, W. Role of Species and Planting Configuration on Transpiration and Microclimate for Urban Trees. *Forests* **2020**, *11*, 825. [[CrossRef](#)]
24. Zheng, J.; Tarin, M.W.K.; Jiang, D.; Li, M.; Ye, J.; Chen, L.; He, T.; Zheng, Y. Which Ornamental Features of Bamboo Plants Will Attract the People Most? *Urban For. Urban Green.* **2021**, *61*, 127101. [[CrossRef](#)]
25. Dimoudi, A.; Nikolopoulou, M. Vegetation in the Urban Environment: Microclimatic Analysis and Benefits. *Energy Build.* **2003**, *35*, 69–76. [[CrossRef](#)]
26. Georgi, J.N.; Dimitriou, D. The Contribution of Urban Green Spaces to the Improvement of Environment in Cities: Case Study of Chania, Greece. *Build. Environ.* **2010**, *45*, 1401–1414. [[CrossRef](#)]
27. Oliveira, S.; Andrade, H.; Vaz, T. The Cooling Effect of Green Spaces as a Contribution to the Mitigation of Urban Heat: A Case Study in Lisbon. *Build. Environ.* **2011**, *46*, 2186–2194. [[CrossRef](#)]
28. Xue, X.; Zhang, J.; Sun, Y.; Zhuang, J.; Wang, Y. Study of Carbon Sequestration & Oxygen Release and Cooling & Humidifying Effect of Main Greening Tree Species in Shanghai. *J. Nanjing For. Univ. (Nat. Sci. Ed.)* **2016**, *40*, 81–86.
29. Wang, J.; Zhou, W.; Jiao, M.; Zheng, Z.; Ren, T.; Zhang, Q. Significant Effects of Ecological Context on Urban Trees' Cooling Efficiency. *ISPRS J. Photogramm. Remote Sens.* **2020**, *159*, 78–89. [[CrossRef](#)]
30. Han, H.J.; Zhou, Y.W. Cooling and Moisturizing Effect of Different Afforested Tree Species in July. *J. Hebei Agric. Sci.* **2007**, *5*, 28–30.
31. Petri, A.C.; Wilson, B.; Koeser, A. Planning the Urban Forest: Adding Microclimate Simulation to the Planner's Toolkit. *Land Use Policy* **2019**, *88*, 104117. [[CrossRef](#)]
32. Tang, Z.; Ren, Z.; Zheng, H.; He, X.-Y. Cooling Effects of Urban Forest Community Structure. *Chin. J. Appl. Ecol.* **2017**, *28*, 2823–2830.
33. Zhang, Z.; Lv, Y.; Pan, H. Cooling and Humidifying Effect of Plant Communities in Subtropical Urban Parks. *Urban For. Urban Green.* **2013**, *12*, 323–329. [[CrossRef](#)]
34. Pan, J.; Li, J.; Li, S.; Dong, L.; Wang, Y. Study on the Relationship between Plant Community and Spatial Differentiation of Negative Air Ions in Urban Green Space—A Case Study of Beijing Olympic Forest Park. *Chin. Landsc. Archit.* **2022**, *6*, 57–62.
35. Li, H.; Meng, H.; He, R.; Lei, Y.; Guo, Y.; Ernest, A.; Jombach, S.; Tian, G. Analysis of Cooling and Humidification Effects of Different Coverage Types in Small Green Spaces (SGS) in the Context of Urban Homogenization: A Case of HAU Campus Green Spaces in Summer in Zhengzhou, China. *Atmosphere* **2020**, *11*, 862. [[CrossRef](#)]
36. Tan, X.; Liao, J.; Bedra, K.B.; Li, J. Evaluating the 3D Cooling Performances of Different Vegetation Combinations in the Urban Area. *J. Asian Archit. Build. Eng.* **2022**, *21*, 1124–1136. [[CrossRef](#)]
37. Leuzinger, S.; Körner, C. Tree Species Diversity Affects Canopy Leaf Temperatures in a Mature Temperate Forest. *Agric. For. Meteorol.* **2007**, *146*, 29–37. [[CrossRef](#)]
38. Qin, Z.; Li, Z.; Cheng, F.; Chen, J.; Liang, B. Influence of Canopy Structural Characteristics on Cooling and Humidifying Effects of Populus Tomentosa Community on Calm Sunny Summer Days. *Landsc. Urban Plan.* **2014**, *127*, 75–82. [[CrossRef](#)]
39. Fowler, D.; Skiba, U.; Nemitz, E.; Choubedar, F.; Branford, D.; Donovan, R.; Rowland, P. Measuring Aerosol and Heavy Metal Deposition on Urban Woodland and Grass Using Inventories of 210PB and Metal Concentrations in Soil. In *Biogeochemical Investigations of Terrestrial, Freshwater, and Wetland Ecosystems across the Globe*; Wieder, R.K., Novák, M., Vile, M.A., Eds.; Springer: Dordrecht, The Netherlands, 2004; pp. 483–499, ISBN 978-94-010-3751-8.
40. Skelhorn, C.; Lindley, S.; Levermore, G. The Impact of Vegetation Types on Air and Surface Temperatures in a Temperate City: A Fine Scale Assessment in Manchester, UK. *Landsc. Urban Plan.* **2014**, *121*, 129–140. [[CrossRef](#)]
41. Cheung, P.K.; Jim, C.Y.; Siu, C.T. Effects of Urban Park Design Features on Summer Air Temperature and Humidity in Compact-City Milieu. *Appl. Geogr.* **2021**, *129*, 102439. [[CrossRef](#)]
42. Lin, T.-P.; Matzarakis, A.; Hwang, R.-L. Shading Effect on Long-Term Outdoor Thermal Comfort. *Build. Environ.* **2010**, *45*, 213–221. [[CrossRef](#)]
43. Rahman, M.A.; Dervishi, V.; Moser-Reischl, A.; Ludwig, F.; Pretzsch, H.; Rötzer, T.; Pauleit, S. Comparative Analysis of Shade and Underlying Surfaces on Cooling Effect. *Urban For. Urban Green.* **2021**, *63*, 127223. [[CrossRef](#)]
44. Liu, J.M.; Li, S.H.; Yang, Z.F. Temperature and Humidity Effect of Urban Green Spaces in Beijing in Summer. *Chin. J. Ecol.* **2008**, *27*, 1972–1978.
45. Hwang, Y.H.; Lum, Q.J.G.; Chan, Y.K.D. Micro-Scale Thermal Performance of Tropical Urban Parks in Singapore. *Build. Environ.* **2015**, *94*, 467–476. [[CrossRef](#)]
46. Xiao, X.D.; Dong, L.; Yan, H.; Yang, N.; Xiong, Y. The Influence of the Spatial Characteristics of Urban Green Space on the Urban Heat Island Effect in Suzhou Industrial Park. *Sustain. Cities Soc.* **2018**, *40*, 428–439. [[CrossRef](#)]
47. Wu, Z.; Zou, M.; Ai, L.; Feng, Y. The Heat Island Regulation Effects of Chongqing Parks in Summer. *Chin. Agric. Sci. Bull.* **2014**, *30*, 238–245.
48. Wang, C.; Zhao, C.; Chen, X.; Liu, D. Remote Sensing—Based Green Space Evolution in Tangshan and Its Influence on Heat Island Effect. *Remote Sens. Nat. Resour.* **2022**, *34*, 168–175.
49. Li, X.J.; Song, C.N.; Zhou, G.L.; Chao, W. Simplified Method for Simulating the FSI Effect of PCS Water Tank in a Nuclear Island Building. *J. Vib. Shock* **2019**, *38*, 6–12.

50. Ren, Q.; Xie, H.; Wang, H. Ecological Resource Assessment for Recreation and Leisure Tourism in Chishui City. *J. Green Sci. Technol.* **2022**, *24*, 148–151.
51. Chang, C.-R.; Li, M.-H.; Chang, S.-D. A Preliminary Study on the Local Cool-Island Intensity of Taipei City Parks. *Landsc. Urban Plan.* **2007**, *80*, 386–395. [[CrossRef](#)]
52. Wang, Y.; Akbari, H. The Effects of Street Tree Planting on Urban Heat Island Mitigation in Montreal. *Sustain. Cities Soc.* **2016**, *27*, 122–128. [[CrossRef](#)]
53. Yang, W.; Lin, Y.; Li, C.-Q. Effects of Landscape Design on Urban Microclimate and Thermal Comfort in Tropical Climate. *Adv. Meteorol.* **2018**, *2018*, 2809649. [[CrossRef](#)]
54. Kurban, A.S.; Papparelli, A.H.; Cunsulo, M.E. Aporte de la Forestación al Control del Clima Urbano en Zona Árida. *Av. En Energías Renov. Y Medio Ambiente* **2002**, *10*, 43–48.
55. Yoshida, A.; Hisabayashi, T.; Kashiwara, K.; Kinoshita, S.; Hashida, S. Evaluation of Effect of Tree Canopy on Thermal Environment, Thermal Sensation, and Mental State. *Urban Clim.* **2015**, *14*, 240–250. [[CrossRef](#)]
56. Rahman, M.A.; Moser, A.; Gold, A.; Rötzer, T.; Pauleit, S. Vertical Air Temperature Gradients under the Shade of Two Contrasting Urban Tree Species during Different Types of Summer Days. *Sci. Total Environ.* **2018**, *633*, 100–111. [[CrossRef](#)]
57. Wang, X.; Dallimer, M.; Scott, C.E.; Shi, W.; Gao, J. Tree Species Richness and Diversity Predicts the Magnitude of Urban Heat Island Mitigation Effects of Greenspaces. *Sci. Total Environ.* **2021**, *770*, 145211. [[CrossRef](#)]
58. Hua, L.; Sun, F.; Chen, J.; Tang, L. Quantifying the Cool-Island Effects of Urban Parks Using Landsat-8 Imagery in a Coastal City, Xiamen, China. *Acta Ecol. Sin.* **2020**, *40*, 8147–8157.
59. Mo, H.; Xiao, T.; Zhao, Y.; Zhu, Q.; Li, Z. The Impact of Urban Green Space on Cold Island Effect—A Case Study of Core Urban Changsha. *J. Nat. Sci. Hunan Norm. Univ.* **2019**, *42*, 18–22.
60. Lu, Q.; Yang, T.; Wang, Z.; Wang, X.; He, L. Characteristics of Micro Climate Effects of Wetlands. *Clim. Environ. Res.* **2020**, *25*, 399–409.
61. Zhao, R.; Shen, X.; Tian, G.; Guo, Y.; He, R. The Influence of Landscape Characteristics of a Park Green Space on the Park Cool Island Effect in Zhengzhou City. *Acta Ecol. Sin.* **2020**, *40*, 2886–2894.

Article

Evaluating Vehicle Energy Efficiency in Urban Transport Systems Based on Fuzzy Logic Models

Vasyl Mateichyk ^{1,*}, Nataliia Kostian ², Mirosław Smieszek ¹, Jakub Moszczyszewski ¹ and Liudmyla Tarandushka ²

¹ Department of Technical Systems Engineering, Rzeszow University of Technology, al. Powstancow Warszawy 10, 35-959 Rzeszow, Poland

² Department of Automobiles and Technologies for Their Operating, Cherkasy State Technological University, Shevchenko 333, 18006 Cherkasy, Ukraine

* Correspondence: vmate@prz.edu.pl

Abstract: This work solves the task of developing a fuzzy logic model for evaluating the energy efficiency of vehicles as part of the control unit of an intelligent transport system. Within the scope of this study, the previously obtained morphological model of the transport system was modified. A mathematical dependence is proposed to determine the vehicle energy efficiency indicator. This dependence characterizes the energy consumption of the vehicle in relation to the energy consumption of the vehicle under the reference operating conditions. Synthesis of system configurations was performed, and procedures were used to transform the morphological formulas of the received configurations into a base of logical derivation rules. Parameters of the membership functions of system parameters to fuzzy terms of the area of their definition are defined. Based on the results of the morphological analysis, two fuzzy derivation models were developed: the Mamdani type and the Sugeno type. The accuracy of the modeling was evaluated using different defuzzification algorithms in the control sample. The most accurate model is the fuzzy Mamdani model, with an accuracy value of 98.8%. Using the developed model, the nature of the mutual influence of the transport system parameters on the level of vehicle efficiency was assessed. The results of the study can be used to justify the choice of the vehicle under the specified operating conditions and in the settlement design of the road infrastructure.

Keywords: fuzzy logic model; membership function; morphological matrix; urban transport system; vehicle energy efficiency

Citation: Mateichyk, V.; Kostian, N.; Smieszek, M.; Moszczyszewski, J.; Tarandushka, L. Evaluating Vehicle Energy Efficiency in Urban Transport Systems Based on Fuzzy Logic Models. *Energies* **2023**, *16*, 734. <https://doi.org/10.3390/en16020734>

Academic Editors: Roberto Alonso González Lezcano, Francesco Nocera and Rosa Giuseppina Caponetto

Received: 5 December 2022

Revised: 2 January 2023

Accepted: 6 January 2023

Published: 8 January 2023



Copyright: © 2023 by the authors. Licensee MDPI, Basel, Switzerland. This article is an open access article distributed under the terms and conditions of the Creative Commons Attribution (CC BY) license (<https://creativecommons.org/licenses/by/4.0/>).

1. Introduction

The global trend of increasing motorization causes several problems, including those related to ensuring the rational functioning of city transport systems. Changes in one of the subsystems of the transport system require prompt adjustment of others. On the one hand, the renewal and growth of the car fleet require taking into account its characteristics when designing road infrastructure and implementing the latest traffic management tools. On the other hand, with the well-established structure of the already existing transport network, it is necessary to develop mechanisms for choosing the optimal type of transport depending on the operating conditions. In accordance with the goal of modernization, new technical and management solutions require the modernization of the knowledge base about system elements and states. In order to build the structure of the knowledge base and further determine the optimal solution to improve the technical system in the conceptualization phase, it is appropriate to use the method of morphological analysis, the stages of which are described in detail in the work [1]. At the same time, they build a morphological model (matrix) of the system. Based on the structure of the morphological matrix, the possible states of the system are synthesized. The disadvantage of the morphological model is the difficulty in transforming them into equivalent mathematical ones for further research.

Usually, the morphological features of the system are fully or partially represented by qualitative parameters. Therefore, when designing technical systems, it is convenient to use formal models: production, logical, network, and frame [2]. Thus, the authors of [1], based on the results of morphological analysis, built a base of production rules in the model of quality control of technological processes of car service systems. This model is based on the principles of fuzzy sets. The Sugeno fuzzy derivation algorithm used in [1] is shown to give a higher accuracy of the result compared to the Mamdani algorithm.

The paper [3] presents an intelligent method for controlling the movement of an electric vehicle. The method is based on the use of the Fuzzy Logic controller (FLC) as part of the driver model and the implementation of the genetic algorithm of swarm intelligence in the control design. This model allows for controlling the use of energy during movement and predicting the energy efficiency of the vehicle under the given conditions. The experimental results show that the use of the specified method provides energy savings while maintaining the performance of the electric vehicle.

The authors of [4] developed an intelligent system for preventing risky driving maneuvers based on soft computing technologies with the use of Mamdani-type fuzzy inference algorithms. The input parameters of the system are the structural properties of the road and the dynamic characteristics of the car, which are obtained using the inertial sensors of the smartphone, the GPS system, the accelerometer, and the gyroscope. The system is designed to work in real time and ensures an increase in the economy, environmental friendliness, and safety level of transport processes. However, among the multitude of input parameters, those that characterize settlement, weather conditions, and the peculiarities of driving during peak hours are missing. In the study [5], Soft Computing technology was used to design a classification system for two-lane roads. The work [6] is devoted to solving the problem of diagnosing driving skills in real conditions based on a fuzzy logic algorithm based on GPS data and video recordings. Fuzzy inference rules are built with traffic rules and expert driving criteria in mind.

The authors of [7] developed a fuzzy logic model for intelligent control and management of the behavior of electricity consumption of an electric car with battery power. The fuzzy model has two inputs: battery state and speed and three outputs according to the power consumption regulation functions of the car's auxiliary devices. The centroid method was used for the defuzzification of model outputs. Each of the parameters has only three implementation options. An optimal intelligent control strategy has been proven to make the engine operate in the high-efficiency zone most of the time, which can improve the energy recycling rate and reduce fuel consumption at a constant vehicle power. Experimental results show that when this energy consumption management system is used with auxiliary devices, it is possible to increase the battery range by 9.8–20.4%. Although the study was conducted for different driving cycles (European, Japanese), the control strategy was developed based on the technical characteristics of the LG-Proton IRIZ BEV and must be adjusted for other electric vehicle models.

In work [8], a simulation model of a hybrid tractor containing an optimization module was implemented to control energy consumption based on fuzzy logic. The optimal control strategy is determined by a genetic algorithm for Particle Swarm Optimization. The disadvantages of the classical algorithm for particle swarm optimization are given in [8], one of which is the probability of falling into a local extremum in the space of admissible solutions. To eliminate this shortcoming, the authors proposed a quantum modification of the classical algorithm. The simulation results of tractor operation in different work cycles show that the average fuel efficiency of the fuzzy logic control strategy after optimization improves by 6.9% compared to the strategy without optimization.

The results of the study [9] demonstrate the energy efficiency of multimode adaptive driving based on the use of fuzzy logic. The FLC controller contains one input (control loop) and three outputs: speed limit, β limit, and comfort level. The BEV battery electric vehicle model, which supports adaptive driving mode, has been tested for various weather

conditions that are most typical for Malaysia throughout the year. In adaptive mode, the driving parameters change automatically depending on the driving speed.

The authors of [10] presented a model in the form of a multilayer neural network with direct communication for forecasting the concentration of $PM_{2.5}$ based on traffic parameters in the area of crossroads, meteorological data, and background concentration of PM_{10} . The network was trained using the gradient descent method. Only a third of the statistical sample participated in the training process. This model is designed to expand the functionality of the intelligent system for monitoring traffic and harmful emissions in the city of Bielsko-Biala, Poland. The paper [11] presents an adaptive neuro-fuzzy inference system (ANFIS-PSO) for predicting the intensity of traffic flows in the example of the South African transport system. Training of the neuro-fuzzy system is implemented using the algorithm of Particle Swarm Optimization. The results of the study showed that the period of the day is a significant parameter affecting the movement of vehicles on freeways. The authors of [12] proposed the deep convolutional neural network for use in the process of technical diagnostics. Network optimization is carried out using the minibatch gradient descent method.

The variety of tasks successfully solved in the field of transport by Soft Computing methods testifies to their universality and feasibility of use in models of transport systems of cities, taking into account the nature of variability, partial uncertainty, and vagueness of statistical information. Soft Computing technologies are based on the principles of theories of fuzzy sets and neural networks, operate with fuzzy logic, and implement genetic algorithms. The integration of fuzzy logic controllers into the control units of the specified systems increased the efficiency of their functional elements. Furthermore, the development of the FLC strategy does not require precise analytical models.

In the last stage of the morphological analysis, the most rational states of the technical system are selected according to the given criterion. In research on optimizing the operation of the urban transport system, it is relevant to determine its best configurations based on the highest values of energy efficiency, productivity, and environmental safety. The effectiveness of the entire system can be evaluated based on partial performance indicators of its partitive functional elements or on the basis of an indicator that reflects the synergistic effect of the interaction of their morphological attributes. Since the number of emissions of harmful substances into the air is directly proportional to fuel consumption, and separate algorithms for evaluating the energy efficiency of road transport contain procedures for determining the work performed, the criterion of energy efficiency of transport can be considered a basic condition in the process of evaluating the configurations of the transport system synthesized based on the results of morphological analysis.

Currently, scientists offer several methods to evaluate the energy efficiency of road transport and strategies to increase its level. In work [13], the evaluation of its fuel economy, which is defined as the ratio of mileage to fuel consumption, is taken as an indicator of the efficiency of a vehicle. However, this estimate does not characterize the impact of vehicle loading. Studies [14,15] are devoted to evaluating the energy efficiency of public passenger transport. These works are limited to a given class of buses; at the same time, the results of their research can be adapted to other specifications of buses with internal combustion engines. The authors of [14] proposed a set of indicators that reflect the dependence of the energy efficiency of a city bus on the length of the haul, the coefficient of static use of passenger capacity, and the maximum power of the engine. Models of the energy efficiency of vehicles require an adequate assessment of vehicle energy consumption during operation. According to the authors [15], the fuel consumption of a city bus is determined using the VSP method, which is based on the defined index, which is affected by aerodynamic resistance, rolling resistance, road gradient, speed, and variable load on the bus. Polynomial, logarithmic, and exponential forms of analytical dependences are used to estimate the fuel consumption of an arbitrary vehicle in works [16–18], taking into account its instantaneous speed and modes of movement.

The authors of [19] proposed a strategy for managing thermal comfort in an electric vehicle based on the criterion of minimizing energy consumption in moderate and hot climates. Within the specified strategy, the energy required for traction and the energy required to maintain thermal comfort is determined on the basis of navigation data. The total traction energy is calculated as the sum of the traction energies of individual sections of the route, taking into account the average speed of the vehicle, its standard deviation, and the slope of the road in the sections. However, the average relative error can reach 10% in sections with a negative value of the road slope. In [19], a mathematical model was built for forecasting the energy required to maintain the rational operation of the HVAC in the air conditioning and ventilation modes. The model uses information about weather conditions and a scale of thermal comfort indices. The implementation of the algorithm of the proposed strategy was carried out in the MATLAB environment under different weather conditions, traffic flow intensity values, and the initial level of the battery charge. In the process of research [20], innovative technologies were developed to increase the energy efficiency of vehicles by reducing the weight of individual components and systems of vehicles and optimizing their operation using the example of the demonstration model of the QUIET battery electric vehicle of the Horizon 2020 European Union project. In [20], the results of the study [19] were also used and further developed. It has been proven that the issue of HVAC energy efficiency is relevant for electric vehicles with relatively low movement resistance.

In research [21], the consumption of fuel with given properties is determined based on the mass of emissions of carbon-containing gaseous components in exhaust gases using the carbon balance method. Usually, fuel consumption indicators are based on test results in driving cycles. A critical description of driving cycles used in different countries has been made. Its own unique vehicle test procedures have been developed to control fuel consumption. It is noted that the main problem in the design of fuel consumption control systems is the difficulty of formalizing a large number of variants of driving conditions, driving behavior, and weather conditions.

Articles [22,23] provide methods for managing the energy resource efficiency of a car in its life cycle. The authors of [22] proposed a complex indicator of the technical and energy and transport energy efficiency of a car. The built mathematical model of this indicator contains the energy mileage coefficient, the method of determining which is based on the comparison of the energy efficiency of the specified and reference cars during the performance of test and reference transport operations. The complex indicator in the study [22] takes into account the structural and parametric organization of vehicle design and road properties. However, this efficiency indicator is based on the average (for the test operation) and constant set (for the reference operation) value of the movement speed and its individual components require the determination of coefficients in accordance with the specifics of different vehicles and types of test operations. In [23], the energy efficiency of a vehicle is determined by taking into account the aging of materials during the stages of manufacture and operation for a vehicle with an internal combustion engine (CV), an electric vehicle (EV), a hybrid vehicle (HV) and a fuel cell vehicle (FCV). In addition, in [23], an indicator of the overall national energy efficiency of a car was proposed. This indicator is determined by the method of additive aggregation. The essence of the method is to find the sum of the products of the values of the energy efficiency indicators of the vehicle types under study and the share of their annual sales. It is observed that the difference between the values of the energy efficiency indicators of different types of vehicles decreases with an increase in the duration of the operation.

Articles [24–26] are devoted to the study of the energy efficiency of electric vehicles. The authors of [24] evaluate the energy efficiency of the Edison II electric car manufactured at the University of Zilina, Slovakia. Three modes of operation of the car were studied: battery charging, mode of wheel driving, and recuperation. Analytical dependences for energy calculation at various measurement points are presented on the basis of experimental data. It is shown that 47% of the energy is lost during transmission from the socket to the

electric motor shaft. It was determined that the amount of energy loss also depends on the design of the battery. The results of this study indicate that the formation of nitrogen oxides in the energy efficiency of Edison II will be greater than when using heavy trucks. The authors of [25] defined the energy efficiency index of the vehicle, which is the inverse of the energy load indicator Y_W [W/J]. In turn, the Y_W indicator depends on the maximum effective power of the engine, the total weight of the car, and the maximum speed of the car. It is shown that the energy load indicator Y_W compared to the specific engine power P_{sp} [kW/t], has a smaller variance. In paper [26], the energy efficiency of electric vehicles of seven categories was investigated. Separate linear regression dependences of the energy consumption of an electric vehicle on its mass, nominal engine power, and battery capacity were obtained, taking into account the modeling error. A multiple regression model was built to estimate energy consumption based on the specified indicators, year of manufacture, and vehicle category. The authors of [27] systematized the types of energy losses in vehicles and their elimination on the basis of improving the car design.

The results of the analysis of the results of recent studies are combined in Table 1.

Despite a significant number of studies in the direction of evaluating the energy efficiency of vehicles, the majority of them are aimed at optimizing this indicator by improving the design and operational characteristics of the vehicle. It remains relevant to identify potential external factors that, in combination with the technical and operational properties of the vehicle, affect its effectiveness, as well as the construction of generalized models that reflect the importance of this influence for research. In addition, among the latest studies, there is a lack of universal energy efficiency estimates for different categories of vehicles, which would take into account the parameters of all elements of the transport system and the changing conditions of its operation.

The purpose of the study is to evaluate the energy efficiency of vehicles taking into account the changing conditions of the transport system based on fuzzy output models. It is suggested that there is a close relationship between the results of the morphological analysis of the transport system and non-linear models for evaluating the energy efficiency of vehicles. The works discussed above reflected only separate stages of the morphological analysis of the studied systems. The formalization of the transition between the stages of morphological analysis and the construction of appropriate models will allow a comprehensive assessment of the level of energy efficiency of transport depending on the factors of all elements of the system.

Table 1. Generalized characteristics of the results of recent studies.

Methods and Technologies	Reference Number	Advantages	Disadvantages
Morphological analysis method	[1]	The principle of constructing a morphological matrix and morphological formulas is described	The transition to an equivalent mathematical model has not been formalized
	[2]	The stages of morphological analysis are described	The presented models only take into account the operational characteristics and design of the vehicle
	[3]	A model for forecasting energy efficiency was built	The model is only adequate for electric vehicles
	[4]	The developed intelligent system ensures an increase in the efficiency of transport processes	Traffic environment parameters, weather conditions and hours of the day are not taken into account
	[5]	The results can be used to define the attributes of the element of the “Road” system	Only Two-Lane Roads are considered
	[6]	Real driving conditions are considered; traffic rules are taken into account	An intelligent system is not universal; the energy efficiency of the vehicle is not taken into account
Soft Computing Technologies (fuzzy logic)	[7–9]	An intelligent system for controlling the energy consumption of vehicles has been developed, which allows to increase energy efficiency up to 20.4%	Only the vehicle parameters are taken into account (weather conditions are also taken into account in [8]); the system is intended for only one model of electric vehicle/hybrid vehicle; there is no argumentation for choosing the defuzzification method
	[10,11]	Attributes of the functional element of the “Transport flow” system are defined; in [11] an adaptive fuzzy neural network is used	In [10], the training sample is only a third of the initial sample; the modeling error (Mean Absolute Percentage Error) is significant and amounts to 24%. In [11], not all categories of vehicles were taken into account
	[12]	Used deep convolutional neural networks ensured an increase in the productivity of the machine learning system; the method can be used to determine the structure of the traffic flow	It requires significant financial resources to identify traffic flows on the entire street network of the city
Soft Computing Technologies (neural network)			

Table 1. Cont.

Methods and Technologies	Reference Number	Advantages	Disadvantages
Analytical and statistical methods of energy efficiency assessment	[13]	The indicator of energy efficiency of the vehicle was determined	The indicator does not take into account vehicle loading, environmental, traffic flow, roads parameters
	[14,15]	The indicator of energy efficiency of the vehicle was determined	Research is limited to a given class of bus
	[16–18]	Analytical estimates of the fuel consumption of arbitrary vehicle have been developed	The parameters of other (except vehicle) functional elements of the transport system are not taken into account
	[19,20]	models were built to forecast the energy required for efficient HVAC operation; the parameters of all functional elements of the system are taken into account	The average relative error can reach 10%; models are only adequate for electric vehicles
	[21]	Own unique vehicle test procedures for tracking fuel consumption have been developed	Dependence of the complexity of formalization of system parameters on their number
	[22,23]	Comprehensive indicators of energy efficiency of various categories of vehicles, taking into account their construction and road parameters, are proposed	Requires additional calculations in accordance with the specifics of various vehicles and types of test operations; in [23], the use of the indicator requires annual sales statistics
	[24–26]	Analytical dependencies of energy efficiency indicators were obtained; a comparison of the energy efficiency of different categories of electric vehicles was made	The energy efficiency of only electric cars was studied
[27]	The types of energy losses in vehicles and methods of their elimination are systematized	Only the parameters of the “vehicle” functional element are taken into account	

In order to achieve the goal, the following tasks must be solved:

- Formalize the mechanism of synthesis of transport system configurations;
- Synthesize various system configurations based on experimental data;
- Build a fuzzy inference model for evaluating the energy efficiency of the vehicle within the system;
- Determine rational modes of operation of the transport system.

According to the purpose of the research, the article consists of the following sections:

- The Section 1 provides a description of the results of the latest publications on the subject of the research and defines its purpose;
- In the Section 2, the morphological structure of the urban transport system with independent parameters is developed; its morphological model was built in the form of a morphological matrix; the criterion for evaluating the effectiveness of the vehicle is defined; a formalized transition from a morphological system model to a mathematical one is proposed;
- In the Section 3, the experimental part of the research is described, and its partial results are highlighted: the configurations of the transport system are synthesized, and the system of fuzzy rules of derivation is built for the evaluation of the energy efficiency of the vehicle under the given conditions of the transport system; the influence of the system parameters on the energy efficiency of the vehicle was investigated;
- The Section 4 presents the discussion and interpretation of the obtained results;
- The Section 5 summarizes the obtained results and outlines the vector of further research.

2. Materials and Methods

In order to ensure the rational operation of the urban transport system, it is necessary to have mechanisms and technologies to influence its essential parameters and focus on the problem of increasing the level of energy efficiency of vehicles (*LEE*). The algorithms of these mechanisms should be based on models characterizing the connection between system inputs and *LEE*. Such dependencies between parameters usually have a non-linear character.

This study is a continuation of the work [28] in which the functional elements of the intelligent transport energy efficiency management system (TrEECS) were identified on the basis of morphological analysis. The structure of the system is presented in Figure 1.

At the first level of the system, there are functional elements: vehicle (*V*), traffic flow (*TF*), road (*R*), and traffic environment (*Env*). At the second level, the morphological features (attributes) of these elements are defined. In the process of research [28], 10 independent parameters (the basis of the system) were selected from the set of 18 significant quantitative and qualitative parameters corresponding to morphological features. Figure 1 shows only the basic attributes. At the third level, for each attribute, its implementation options (domain, possible values) are listed. The method of determining the quantitative values of the limits of implementation options for each attribute is given in [28].

This hierarchy can be presented in the form of a morphological matrix (Table 2). Under each basic attribute (line 2 in Table 2), its implementation options x_{ij} (i —the attribute number; j —is the number the implementation option of the i -th attribute) are presented. All possible variants of one attribute make up its domain (cells of lines 3–8 of Table 2).

In Table 2, next to each verbal value of a qualitative characteristic, its quantitative counterpart is defined. For example, the attribute “1. Category” can take the following values: M1, M2, M3, N1, N2, N3. The first three categories correspond to passenger vehicles. M1 vehicles have no more than 8 seats. M2s have more than 8 seats, and the maximum weight does not exceed 5 tons. The maximum weight of M3 is more than 5 tons. Categories N1, N2, and N3 correspond to cargo vehicles. N1s have a maximum mass of less than 3.5 t. The maximum mass of N2 is more than 3.5 t but does not exceed 12 t. The maximum mass of N3 exceeds 12 t.

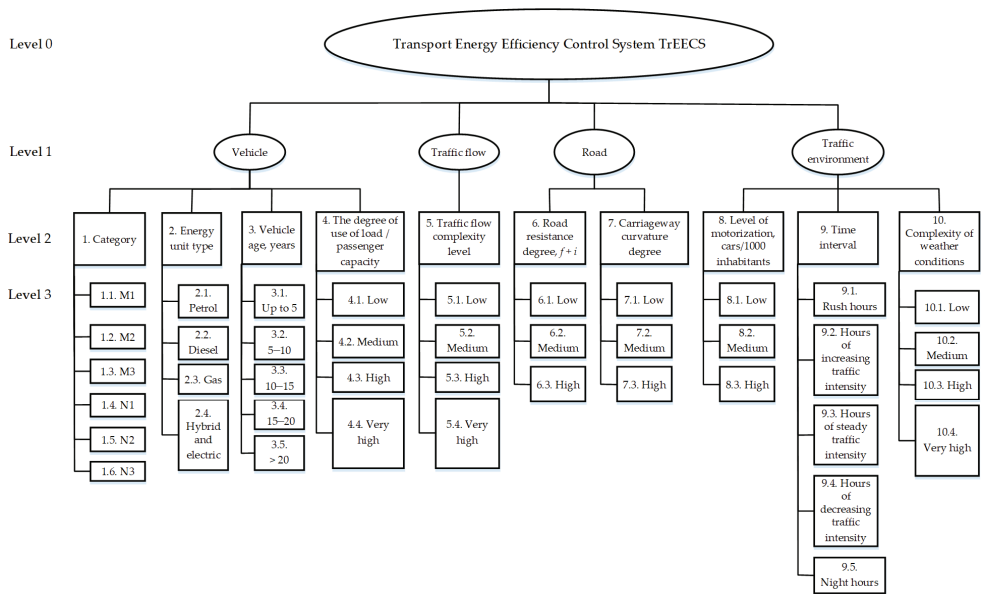


Figure 1. Structure of TrEECS.

This matrix (Table 2) is a modification of the matrix given in [28]. Dependent attributes were removed, and some value ranges were changed. Furthermore, based on the results of the [28], the order of implementation options for the separate attributes were inverted to reduce the number of negative correlations. Based on the real distribution of the values of the complexity level of the traffic flow, the ranges of its implementation options were changed compared to [28].

The synthesis of various configurations of the system takes place by combining various options for implementing its attributes. A separate configuration is given by a morphological formula. An example of a morphological formula is expression (1), which was constructed in the process of evaluating the energy efficiency of a SEAT Toledo passenger car (category M1 (x_{11}), gasoline (x_{21}), year of manufacture 2008 (x_{33}), the degree of use of passenger capacity—0.75 (x_{44})—heading in a stream with a low level of complexity 0.03 (x_{51}) on a road with an average degree of road resistance—0.09 (x_{62})—and an average degree of curvature (x_{72}) in an urban environment (Zamkovy Uzviz Street, Cherkasy) with an average level of motorization (200–300 cars/1000 inhabitants) (x_{82}), in the hours of reduced traffic intensity (20:00–21:00) (x_{94}) under weather conditions of high complexity (x_{103}):

$$[(x_{11} - x_{21} - x_{33} - x_{44}) + (x_{51}) + (x_{62} - x_{72}) + (x_{82} - x_{94} - x_{103})] = Y \quad (1)$$

Table 2. Modified morphological matrix of the TRECS system (built according to the results [28]).

Vehicle		Traffic Flow			Road			Traffic Environment		
1. Category	2. Energy Unit Type	3. Vehicle Age	4. The Degree of Use of Load/Passenger Capacity	5. Traffic Flow Complexity Level	6. Road Resistance Degree, $f + i$	7. Carriageway Curvature Degree	8. Level of Motorization, Cars/1000 Inhabitants	9. Time Interval	10. Complexity of Weather Conditions	
1.1. M1 1	2.1. Petrol 1	3.1. Up to 5 years 1	4.1. Low 0-0.4	5.1. Low 0-0.2	6.1. Low	7.1. Low	8.1. Low	9.1. Rush hours 1	10.1. Low 0-0.19	
1.2. M2 2	2.2. Diesel 2	3.2. 5-10 years 2	4.2. Medium 0.41-0.5	5.2. Medium 0.21-0.4	0.007-0.049	2maxR/3- maxR 1	<200 1	9.2. Hours of increasing traffic intensity 2	10.2. Medium 0.2-0.39	
1.3. M3 3	2.3. Gas 3	3.3. 10-15 years 3	4.3. High 0.51-0.7	5.3. High 0.41-0.7	6.2. Medium 0.05-0.099	7.2. Medium maxR/3- 2maxR/3 2	8.2. Medium 200-300 2	9.3. Hours of steady traffic intensity 3	10.3. High 0.4-0.69	
1.4. N1 4	3.4. 15-20 years 4									
1.5. N2 5	2.4. Hybrid and electric 4	3.5. More than 20 years 5	4.4. Very high 0.71-1	5.4. Very high 0.71-1	6.3. High 0.1-0.15	7.3. High 0-maxR/3 3	8.3. High > 300 3	9.4. Hours of decreasing traffic intensity 4	10.4. Very high 0.7-1	
1.6. N3 6								9.5. Night hours 5		

In the general case, the output of system Y is a vector consisting of indicators of environmental safety, energy efficiency, safety of transport processes, etc. In this study, the level of energy efficiency LEE is considered as the output of the TrEECS system, which for a given configuration is proposed to be determined as follows:

$$LEE = \frac{E_{basis}}{E_{fact}} = \frac{E_{basis}}{E_{basis}(1 + 0.01 \cdot K_e)} = \frac{1}{1 + 0.01 \cdot \left(\sum_{i=1}^n K_i - \sum_{j=n+1}^{n+m} K_j \right)} \quad (2)$$

where E_{basis} —energy consumed by the engine under ideal operating conditions, MJ; is determined according to the basic norms of fuel/energy consumption for a given vehicle model;

E_{fact} —energy actually consumed by the engine, MJ;

K_e —complex correction coefficient, %;

K_i — i -th correction factor that increases fuel consumption norms ($1 \leq i \leq n$), %;

K_j — j -th correction factor that reduces fuel consumption norms ($1 \leq j \leq m$), %.

The work [28] gives the values of the main correction coefficients used in the conditions of urban mobility.

Analytical dependence (2) is a universal formula that can be used to determine the energy efficiency of vehicles of different classes with a given type of power plant.

Thus, the selection of the best system configuration from a set of already synthesized ones is carried out according to the following criterion:

$$LEE = f(K_1, K_2, \dots, K_n, K_{n+1}, K_{n+2}, \dots, K_{n+m}) \rightarrow \max \quad (3)$$

However, the number of all possible TrEECS configurations, calculated using the combinatorics product rule, is 1.0368×10^6 . Processing such a volume of information requires significant resources and is not possible. In addition, the values of the correction coefficients are not known for all configurations. Therefore, the development of a mathematical fuzzy model with the possibility of further integration into the intelligent system of the control of energy efficiency of transport is relevant.

The fuzzy model of logical derivation represents a base of logical derivation rules (deduction rules) built on the results of the TrEECS morphological analysis. At the same time, each morphological formula of synthesized TrEECS configurations is uniquely matched by one logical derivation rule. System (4) characterizes the mechanism of transformation of a morphological formula into a rule as part of the model:

$$\left\{ \begin{array}{l} \Omega_{X_i} = \cup_{j=1}^{m_i} A_i^j, \text{ under the condition } \cap_{j=1}^{m_i} A_i^j = \emptyset \\ \quad \quad \quad A_i^j = \Psi_{x_{ij}} \\ \Theta_{LEE} = \cup_{s=1}^p B^s, \text{ under the condition } \cap_{s=1}^p B^s = \emptyset \\ \quad \quad \quad \text{Left}(F) \rightarrow \text{rule condition} \\ \quad \quad \quad \text{Right}(F) \rightarrow \text{the rule conclusion} \end{array} \right. \quad (4)$$

where Ω_{X_i} —area of determination of values of parameter X_i ;

A_i^j — j -th term (interval of definition area division) of i -th parameter;

m_i —the number of implementation options for the i -th feature;

$\Psi_{x_{ij}}$ —area of definition of the j -th variant of the implementation of the i -th feature;

Θ_{LEE} —area of definition of the LEE values;

B^s — s -th term of the resulting parameter LEE ;

$Left(F)$ —the left part of the morphological formula;

$Right(F)$ —the right part of the morphological formula.

In the next step, membership functions mf_j of system parameter values to fuzzy terms (intervals) of their definition area are constructed (Table 3).

Table 3. Parameters of the membership functions of the system input and output terms.

Inputs	Term A_i^j	Membership Function <i>mf</i> Parameters				Inputs/ Output	Term A_i^j	Membership Function <i>mf</i> Parameters			
		<i>a</i>	<i>b</i>	<i>c</i>	<i>d</i>			<i>a</i>	<i>b</i>	<i>c</i>	<i>d</i>
X ₁	A ₁ ¹	0	0.5	1.5	7	X ₆	A ₆ ¹	0	0.007	0.049	0.151
	A ₁ ²	0	1.5	2.5	7		A ₆ ²	0	0.05	0.099	0.151
	A ₁ ³	0	2.5	3.5	7		A ₆ ³	0	0.1	0.15	0.151
	A ₁ ⁴	0	3.5	4.5	7	X ₇	A ₇ ¹	0	0.5	1.5	4
	A ₁ ⁵	0	4.5	5.5	7		A ₇ ²	0	1.5	2.5	4
	A ₁ ⁶	0	5.5	6.5	7		A ₇ ³	0	2.5	3.5	4
X ₂	A ₂ ¹	0	0.5	1.5	5	X ₈	A ₈ ¹	0	0.5	1.5	4
	A ₂ ²	0	1.5	2.5	5		A ₈ ²	0	1.5	2.5	4
	A ₂ ³	0	2.5	3.5	5		A ₈ ³	0	2.5	3.5	4
	A ₂ ⁴	0	3.5	4.5	5		A ₉ ¹	0	0.5	1.5	6
X ₃	A ₃ ¹	0	0.5	1.5	6	X ₉	A ₉ ²	0	1.5	2.5	6
	A ₃ ²	0	1.5	2.5	6		A ₉ ³	0	2.5	3.5	6
	A ₃ ³	0	2.5	3.5	6		A ₉ ⁴	0	3.5	4.5	6
	A ₃ ⁴	0	3.5	4.5	6		A ₉ ⁵	0	4.5	5.5	6
	A ₃ ⁵	0	4.5	5.5	6		A ₁₀ ¹	0	0.05	0.19	1.01
X ₄	A ₄ ¹	0	0.01	0.4	1.01	X ₁₀	A ₁₀ ²	0	0.2	0.39	1.01
	A ₄ ²	0	0.41	0.5	1.01		A ₁₀ ³	0	0.4	0.69	1.01
	A ₄ ³	0	0.51	0.7	1.01		A ₁₀ ⁴	0	0.7	1	1.01
	A ₄ ⁴	0	0.71	1	1.01		B ¹	0	0.01	0.2	1.01
	A ₅ ¹	0	0.01	0.2	1.01		B ²	0	0.21	0.4	1.01
X ₅	A ₅ ²	0	0.21	0.4	1.01	LEE	B ³	0	0.41	0.6	1.01
	A ₅ ³	0	0.41	0.7	1.01		B ⁴	0	0.61	0.8	1.01
	A ₅ ⁴	0	0.71	1	1.01		B ⁵	0	0.81	1	1.01

In most of the fuzzy inference systems considered in the first section, triangular and trapezoidal membership functions of the terms to the parameter definition area of the fuzzy model are accepted. In some cases, Gaussian functions are used. The results of the study, which will be described in the next section, proved the feasibility of using the trapezoidal form of the membership function, given by the vector of parameters (*a, b, c, d, h*), height *h* = 1 [29]. On the basis of the implementation options values of the morphological features (Table 2) and system (4), parameters of the membership functions of the input and output values of the TrEECS are determined, which are presented in Table 3. When determining the parameters of the membership functions, the experience of experts in the field of organization and provision of road safety, including specialists of the civil service “Ukrtransbezpeka”, was taken into account. The parameters of the membership functions were adjusted according to the criterion of the smallest modeling error.

The general appearance of the logical derivation models of the Mamdani and Sugeno types of the TrEECS system is given by expressions (5), (6), respectively:

$$Rules_{Mamdani} = \left\{ rule_i : \&_{i=1}^{10} (X_i \in A_{ik}^j) \Rightarrow LEE_k \in B_k^s, i = \overline{1, m} \right\} \tag{5}$$

where X_i —value of the *i*-th TrEECS parameter;

A_{ik}^j —*j*-th term of the *i*-th parameter for the *k*-th system configuration;

LEE_k —level of energy efficiency of the vehicle in the k -th configuration;
 B_k^s — s -th term of the LEE_k value, m —number of TrEECS configurations.

$$Rules_{Sugeno} = \left\{ rule_i : \&_{i=1}^{10} (X_i \in A_{ik}^i) \Rightarrow LEE_k = LEE_{tabl}, i = \overline{1, m} \right\} \quad (6)$$

where LEE_{tabl} — LEE value obtained experimentally.

Thus, Formula (1) will be transformed into the following rule of logical derivation according to the Mamdani algorithm:

$$rule : (x_1 \in A_1^1) \& (x_2 \in A_2^1) \& (x_3 \in A_3^3) \& (x_4 \in A_4^4) \& (x_5 \in A_5^1) \& (x_6 \in A_6^2) \& (x_7 \in A_7^2) \& (x_8 \in A_8^8) \& (x_9 \in A_9^4) \& (x_{10} \in A_{10}^3) \Rightarrow LEE \in B^4 \quad (7)$$

Thus, the transition from the conceptual model of the system to the corresponding mathematical model can be represented by the following algorithm (Figure 2).

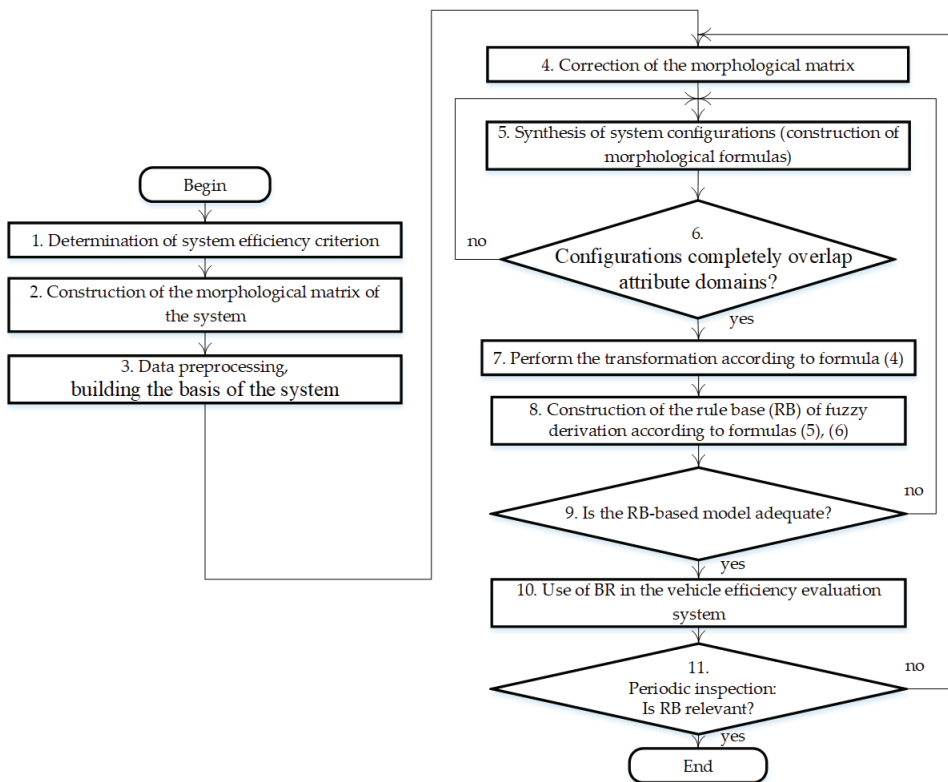


Figure 2. Scheme of the proposed approach.

The data preprocessing procedure (block 3 in Figure 2) is presented in [28].

The main condition for the completeness of statistical data is that they overlap all intervals of the area of definition of system attributes (the presence of all possible variants of their implementation). Therefore, loops 5–6 will be repeated until the condition of block 6 is met.

A sufficient number of statistical values of the resulting LEE parameter can be determined by Formulas (8) and (9):

$$N_{LEE} = \frac{t_k^2 \cdot \sigma^2}{\eta^2} \quad (8)$$

where t_α —confidence probability function, for confidence probability $\theta = 0.95$ function of confidence probability $t_\alpha = 1.96$;

σ —standard deviation;

η —extreme error allowed.

$$\eta = \Delta \cdot LEE_{avg} \quad (9)$$

where Δ —relative accuracy of accounting, assume $\Delta = 0.05$;

LEE_{avg} —average value of energy efficiency of vehicles.

In the next section, it is noted that for the initial sample, the examination of 25 transport system states, that is, 25 TrEECS configurations, proved to be sufficient. If as a result of the study, high accuracy of the modeling will not be achieved, then the study of other states of the system (synthesis of configurations) will be continued (loop 5–9 in Figure 2).

3. Results

3.1. Synthesis of System Configurations

Monitoring of the TrEECS states was carried out on the example of fragments of street and road networks in Kyiv, Lviv, Odesa, Cherkasy, Kaniv, Boryspil, Smila, Cherkasy Region, Zolotonosha, Cherkasy District (Ukraine) and the city of Rzeszów (Poland) under different time periods and weather conditions. The functional element “Vehicle” within the TrEECS was represented by the following car models: Renault Logan 1.2, Skoda Octavia A7 1.8, SEAT Toledo 1.6, ZAZ Lanos T150, Nissan Micra 1.2, Volkswagen Passat B5 GP 2.0, PAZ-4234, Ataman A092G6, Mercedes -Benz O530, Bogdan T70117, Mercedes Sprinter 214, IVECO Daily 35S170, FORD Transit 2.4D, MAN L 8.220, MAN TGL 8.180, VOLVO FH 460, which provided a complete set of options for the implementation of the three morphological attributes of the specified functional element. The methods for determining the TrEECS input parameters are given in [28].

In the process of researching TrEECS states, the specifics of traffic organization in different settlements are taken into account. Differences were recorded regarding the distribution of “peak” periods during the day and the level of passenger capacity utilization of public transport in Poland and Ukraine.

Based on the results of the TrEECS state monitoring in the sections of the investigated networks [28], 25 system configurations were synthesized, the morphological formulas of which are presented in Table 4. The left parts of the morphological formulas are constructed similarly to (1). The options for implementing the attributes of a separate functional element are listed in round brackets. It can be seen from the constructed 25 morphological formulas that the implementation options written in them completely overlap the areas of defining the attributes of the functional elements of the system. In addition, the required number of LEE values with a confidence probability $\theta = 0.95$ and relative accuracy of accounting $\Delta = 0.05$ is determined taking into account (8) by Formula (10):

$$N = \frac{1.96^2 \cdot 0.08^2}{(0.05 \cdot 0.657)^2} \approx 23 < 25. \quad (10)$$

Thus, 25 TrEECS configurations ensure the reliability of the initial statistical data sample.

System configurations with the lowest value of the sample variance were selected for the control sample [29]. The training sample was used for learning the constructed fuzzy logic models (Mamdani and Sugeno). The control sample was used to assess the accuracy of the developed models. The sample type is indicated in the last column of Table 4. The experimental values of the energy efficiency level LEE for the synthesized configurations were obtained using Formula (2). According to this method of calculating the output parameter, its scope is in a narrow range of values [0.5, 0.8]. To be consistent

with the area corresponding to the terms B^s (Table 3), the range of experimental LEE values is converted to a more acceptable interval $[0, 1]$ by expression (11):

$$LEE_{tabl} = (LEE - a) / (b - a) = (LEE - 0.5) / 0.3 \quad (11)$$

where LEE and LEE_{tabl} —experimental and reduced value of the energy efficiency level of the system, respectively;

a, b —the left and right boundaries of the LEE definition area, respectively.

The converted (tabular) output values of the system (LEE_{tabl}) are given in Table 4.

Table 4. Input data for building a fuzzy inference model.

Configuration Number	Left Part of the Morphological Formula	LEE_{tabl}	Sample Type
1	$[(x_{11} - x_{21} - x_{33} - x_{44}) + (x_{51}) + (x_{62} - x_{72}) + (x_{82} - x_{94} - x_{10\ 3})]$	0.648	training
2	$[(x_{11} - x_{23} - x_{35} - x_{42}) + (x_{51}) + (x_{62} - x_{72}) + (x_{82} - x_{94} - x_{10\ 2})]$	0.632	training
3	$[(x_{15} - x_{22} - x_{32} - x_{43}) + (x_{52}) + (x_{61} - x_{71}) + (x_{82} - x_{93} - x_{10\ 1})]$	0.556	training
4	$[(x_{13} - x_{22} - x_{34} - x_{44}) + (x_{52}) + (x_{61} - x_{71}) + (x_{82} - x_{93} - x_{10\ 1})]$	0.227	control
5	$[(x_{11} - x_{21} - x_{34} - x_{43}) + (x_{53}) + (x_{61} - x_{71}) + (x_{82} - x_{92} - x_{10\ 3})]$	0.632	control
6	$[(x_{13} - x_{24} - x_{32} - x_{44}) + (x_{51}) + (x_{61} - x_{71}) + (x_{83} - x_{91} - x_{10\ 2})]$	0.060	training
7	$[(x_{11} - x_{23} - x_{35} - x_{41}) + (x_{51}) + (x_{61} - x_{71}) + (x_{83} - x_{92} - x_{10\ 2})]$	0.681	training
8	$[(x_{11} - x_{21} - x_{31} - x_{41}) + (x_{52}) + (x_{62} - x_{71}) + (x_{81} - x_{93} - x_{10\ 1})]$	0.958	training
9	$[(x_{11} - x_{21} - x_{33} - x_{41}) + (x_{51}) + (x_{61} - x_{72}) + (x_{82} - x_{95} - x_{10\ 4})]$	0.859	training
10	$[(x_{12} - x_{22} - x_{33} - x_{44}) + (x_{51}) + (x_{61} - x_{72}) + (x_{82} - x_{93} - x_{10\ 2})]$	0.329	control
11	$[(x_{16} - x_{22} - x_{33} - x_{44}) + (x_{52}) + (x_{61} - x_{71}) + (x_{82} - x_{92} - x_{10\ 3})]$	0.017	training
12	$[(x_{14} - x_{22} - x_{34} - x_{43}) + (x_{52}) + (x_{61} - x_{71}) + (x_{81} - x_{91} - x_{10\ 1})]$	0.601	training
13	$[(x_{14} - x_{22} - x_{32} - x_{44}) + (x_{52}) + (x_{61} - x_{71}) + (x_{81} - x_{91} - x_{10\ 3})]$	0.430	training
14	$[(x_{13} - x_{22} - x_{35} - x_{42}) + (x_{51}) + (x_{61} - x_{71}) + (x_{81} - x_{94} - x_{10\ 3})]$	0.556	training
15	$[(x_{15} - x_{22} - x_{34} - x_{44}) + (x_{52}) + (x_{62} - x_{71}) + (x_{81} - x_{93} - x_{10\ 2})]$	0.175	training
16	$[(x_{11} - x_{23} - x_{35} - x_{41}) + (x_{52}) + (x_{62} - x_{71}) + (x_{81} - x_{94} - x_{10\ 2})]$	0.802	training
17	$[(x_{11} - x_{22} - x_{35} - x_{41}) + (x_{53}) + (x_{62} - x_{71}) + (x_{82} - x_{91} - x_{10\ 1})]$	0.632	training
18	$[(x_{11} - x_{21} - x_{33} - x_{42}) + (x_{52}) + (x_{62} - x_{71}) + (x_{82} - x_{94} - x_{10\ 1})]$	0.859	training
19	$[(x_{14} - x_{23} - x_{35} - x_{41}) + (x_{51}) + (x_{62} - x_{71}) + (x_{82} - x_{95} - x_{10\ 1})]$	0.897	training
20	$[(x_{14} - x_{22} - x_{34} - x_{44}) + (x_{53}) + (x_{61} - x_{71}) + (x_{82} - x_{93} - x_{10\ 2})]$	0.366	control
21	$[(x_{13} - x_{22} - x_{33} - x_{44}) + (x_{54}) + (x_{61} - x_{71}) + (x_{82} - x_{92} - x_{10\ 1})]$	0.145	control
22	$[(x_{11} - x_{21} - x_{33} - x_{41}) + (x_{54}) + (x_{61} - x_{73}) + (x_{82} - x_{93} - x_{10\ 1})]$	0.681	training
23	$[(x_{11} - x_{21} - x_{31} - x_{41}) + (x_{51}) + (x_{61} - x_{71}) + (x_{83} - x_{91} - x_{10\ 2})]$	0.714	training
24	$[(x_{14} - x_{22} - x_{32} - x_{43}) + (x_{51}) + (x_{63} - x_{73}) + (x_{82} - x_{93} - x_{10\ 4})]$	0.271	training
25	$[(x_{12} - x_{22} - x_{32} - x_{43}) + (x_{51}) + (x_{62} - x_{73}) + (x_{82} - x_{92} - x_{10\ 2})]$	0.329	training

3.2. Construction of TrEECS Nonlinear Models

In order to evaluate the LEE indicator, the TrEECS fuzzy control module has been developed, which consists of a rule base and blocks: Fuzzifier, The Inference Engine, and De-fuzzifier. The fuzzy control module was implemented in the Fuzzy Logic Toolbox environment of the Matlab package.

Based on the fuzzy logic models of Mamdani and Sugeno, two versions of the control unit were developed. The terms of the input parameters are given by trapezoidal membership functions. Model variants differ in the form of presentation of the area of the definition of the resulting parameter, presentation of the inference rules, and defuzzification

algorithms. In Mamdani's model, the membership functions of the *LEE* value ranges are used (Table 4). The type and parameters of the membership functions were experimentally selected. The Sugeno model uses an array of *LEE* values in the training sample. The view of the membership functions of the resulting parameter terms in the Mamdani model is shown in Figure 3.

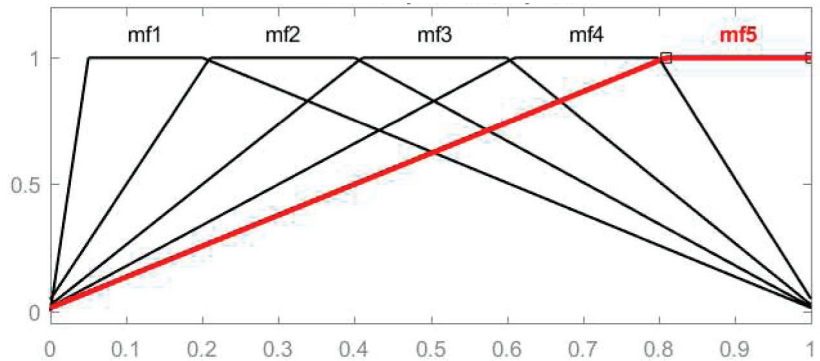


Figure 3. *LEE* membership functions in the Mamdani model.

The membership functions of the terms of the *LEE* parameter correspond to the following ranges of its values:

- Very low (mf1)—from 0 to 0.2;
- Low (mf2)—from 0.21 to 0.4;
- Middle (mf3)—from 0.41 to 0.6;
- High (mf4)—from 0.61 to 0.8;
- Very high (mf5)—from 0.81 to 1.

In order to achieve more accurate simulation results, the experimental data were divided into training and control samples in a ratio of 80:20, respectively. Accordingly, five configurations of the system were included in the control sample.

Based on the results of the morphological analysis, rule bases were built, which contain 20 derivation rules according to the size of the training sample. Since there are no repetitions in the rule bases, the weight of each rule is equal to 1. To determine the best model, the following defuzzification algorithms were implemented: bisector, centroid, the smallest of maximums, the mean of maximums, the weighted average, and the weighted sum. Evaluation of the simulation results was carried out for the values of the output parameter to which the inverse transformation of (11) was applied. The outputs of the system (*LEE*) in the control sample, the model values of the energy efficiency level (LEE_{model}) obtained by different algorithms, and their accuracy estimates are shown in Table 5.

The higher the level of overlap between the theoretically and practically obtained energy efficiency estimates, the higher the validity of the methodology. The level of agreement between the specified estimates can be analyzed by the value of the relative root-mean-square error of modeling (the last line in Table 5). According to Table 5, the relative root mean square error of model values of energy efficiency in the Sugeno system is achieved by the defuzzification method “the weighted average” and is 0.019 (1.9%).

The simulation results prove that the Mamdani model with the defuzzification algorithm “the smallest of maximums” is more adapted to the real operating conditions of the investigated transport systems. The relative standard deviation is 0.012 (1.2%). At the same time, the standard deviation of the model values from the experimental values is equal to 0.005. The specified model should be used to predict the level of vehicle energy efficiency.

Table 5. Simulation results using different defuzzification algorithms.

Configuration Number	Control Output Value LEE	Defuzzification Methods					
		Mamdani Type Model				Sugeno-Model	
		Bisector	Centroid	The Smallest of Maximums	The Mean of Maximums	The Weighted Average	The Weighted Sum
Model Output Value LEE_{model}							
4	0.568	0.668	0.665	0.623	0.691	0.691	0.727
5	0.690	0.659	0.658	0.584	0.692	0.688	0.706
10	0.599	0.635	0.640	0.509	0.586	0.650	0.682
20	0.610	0.656	0.654	0.623	0.691	0.643	0.768
21	0.543	0.650	0.651	0.506	0.641	0.650	0.604
Average value	0.60197	0.6536	0.65354	0.569	0.6599	0.66446	0.69722
Standard deviation σ							
4		0.009964	0.009374	0.003005	0.014962	0.015183	0.02535
5		0.000940	0.001034	0.011163	0.000005	0.000005	0.000251
10		0.001310	0.001705	0.008064	0.000177	0.002591	0.006839
20		0.002138	0.001975	0.000175	0.006520	0.001132	0.024915
21		0.011347	0.011539	0.001405	0.009510	0.011411	0.003675
Average value		0.00514	0.005126	0.004763	0.006235	0.006064	0.012206
Relative standard deviation Sr							
4		0.03086	0.02904	0.00931	0.04635	0.04703	0.07853
5		0.00198	0.00217	0.02347	0.00001	0.00001	0.00053
10		0.00365	0.00476	0.02249	0.00049	0.00722	0.01907
20		0.00575	0.00531	0.00047	0.01754	0.00304	0.06701
21		0.03842	0.03907	0.00476	0.03220	0.03863	0.01244
Average value		0.016132	0.016069	0.012099	0.019317	0.019188	0.035516

3.3. The Influence of TrEECS Parameters on the Vehicle Energy Efficiency

In order to study vehicle dynamics of changes in energy efficiency, it is advisable to use the mode of visualization of logical inference.

Analysis of the joint influence of the input parameters of the system on the indicator LEE was performed using a graphical method. At the same time, it is convenient to use the Sugeno model, which also showed a high accuracy of the model values of the energy efficiency level. According to the results of the previous study, it can be stated that the most significant factor in evaluating vehicle energy efficiency is the parameter x_4 – the degree of use of load/passenger capacity. Therefore, it is advisable to study the dynamics of the influence of combinations of the specified parameters and parameters of various functional elements of the system on the level of vehicle energy efficiency. Figure 4 shows the influence of the degree of use of load capacity of cars and the complexity of the traffic flow on the indicator LEE .

The dependence of $LEE(x_4, x_5)$ is non-linear. Figure 5 shows the projection of $LEE(x_4, x_5)$ onto the $x_4 \times x_5$ plane for buses (a) and trucks (b). The arrows in Figure 5 (gradient) point to the point (x_4^*, x_5^*) where the maximum value of LEE energy efficiency is reached. The maximum value of $LEE(x_4, x_5)$ is reached within the average level of its arguments (see Table 2): $x_4 \in [0.41, 0.5]$ and $x_5 \in [0.2, 0.4]$ regardless of the vehicle category (Figure 5).

When the vehicle category changes from a smaller value to a larger value (see Table 2), the gradient of the $LEE(x_4, x_5)$ decreases, and the area of LEE values close to the maximum narrows (Figure 4). Therefore, changing these system parameters has a greater effect on the energy efficiency of a bus than of a truck.

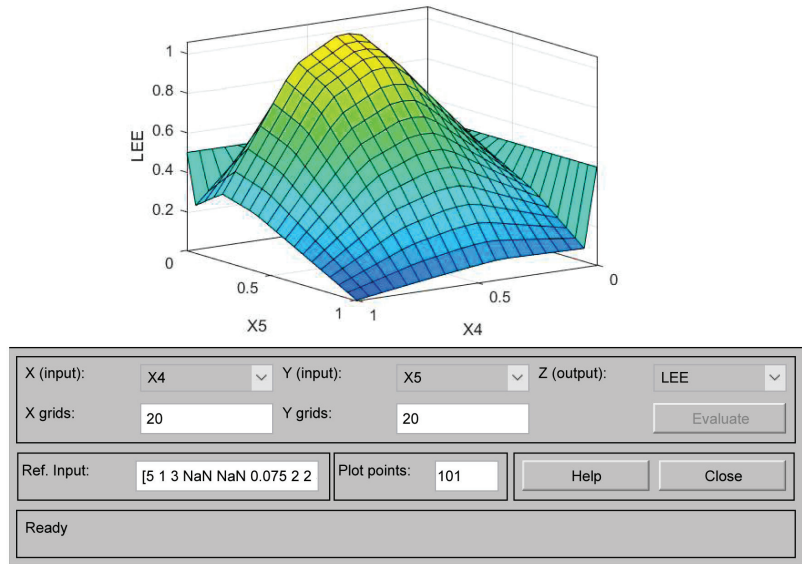


Figure 4. Dependence of $LEE(x_4, x_5)$ on the degree of use of load capacity (x_4) and traffic flow complexity level (x_5).

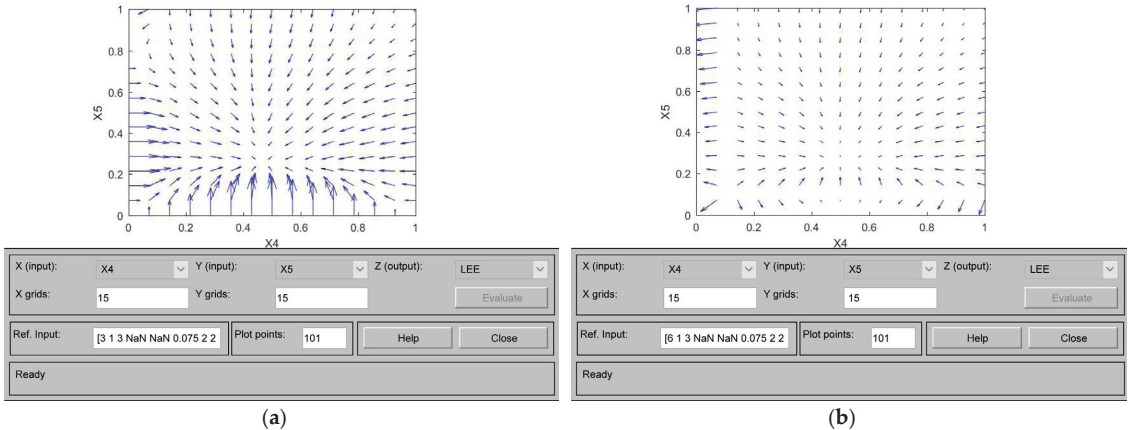


Figure 5. Optimal values of the $LEE(x_4, x_5)$: (a) bus, (b) truck.

The described trends regarding the dependence gradient $LEE(x_4, x_j)$, $1 \leq j \leq 9$, are preserved for other combinations of x_4 with the parameters of the functional elements of the transport system. Thus, the decrease in the $LEE(x_4, x_9)$ gradient reflects a decrease in the level of energy efficiency when the parameter $x_1 = 5$ (category N2) is changed to the value $x_1 = 6$ (category N3), provided that other parameters are the same (Figures 6 and 7).

As can be seen in Figures 6 and 7, the optimal value is $LEE_{N2}^* > LEE_{N3}^*$. The highest values of the vehicle energy efficiency level are observed in hours of constant intensity ($x_9 = 3$) and in hours of decreasing traffic intensity ($x_9 = 4$).

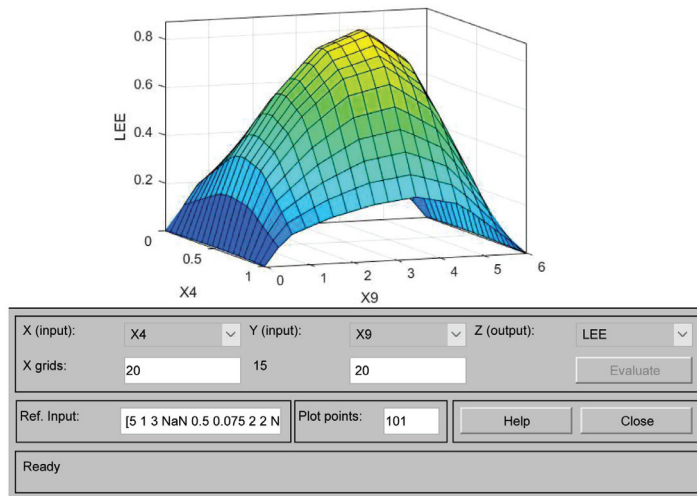


Figure 6. Dependence of $LEE(x_4, x_9)$ on the degree of use of load capacity (x_4) and time interval (x_9) for vehicle of category N2.

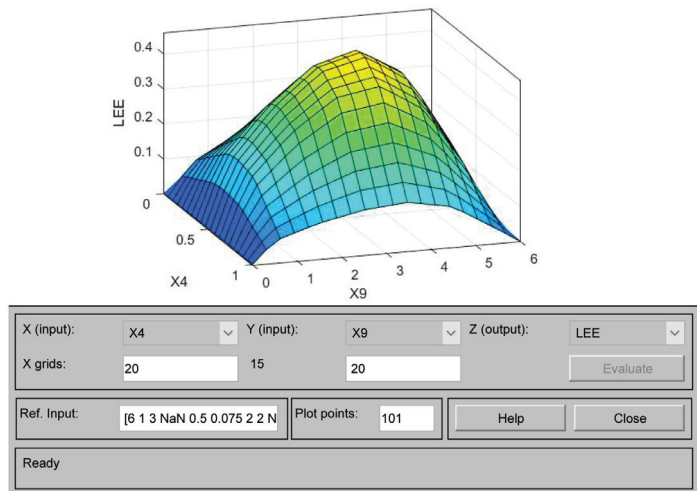


Figure 7. Dependence of $LEE(x_4, x_9)$ on the degree of use of load capacity (x_4) and time interval (x_9) for vehicle of category N3.

4. Discussion

Intelligent management of the urban transport system according to the selected criterion requires evaluation and formalization of the characteristics of the influence of the system on the components of the performance indicator. Estimating the energy efficiency of the vehicle is a basic subtask that is solved within the scope of implementing a significant number of methods to improve its environmental friendliness and productivity. In contrast to existing methods, determining the vehicle efficiency in the proposed way does not require a direct assessment of the energy consumption of the vehicle under study, but it can give a large error in the result. For the application of this method, additional studies are needed in the direction of clarification and completeness of the vector of correction coefficients, taking into account the peculiarities of the operation of the vehicle in different regions.

The results of the morphological analysis of the TrEECS system form the basis for the procedures for building a base of logical rules as part of the transport system control module. The construction and implementation of logical inference models partially smooth out the negative impact of the vague nature of the experimental data. The terms of the domains of each parameter are given by trapezoidal membership functions, the form of which is selected experimentally according to the criterion of the smallest modeling error. The developed system of Mamdani determines the value of the energy efficiency of the vehicle with an error of 1.2%, and the system of Sugeno—with an error of 1.9%—indicates the adequacy of the built models. The largest error is obtained for TrEECS configurations with a low level of energy efficiency. In the future, it is planned to adjust the obtained membership functions to ensure the accuracy of the model results within the given configurations.

On the developed models, it became possible to investigate the influence of transport system parameters on vehicle energy efficiency. It was determined that the parameter x_4 —the degree of use of load/passenger capacity—has the greatest weight in the evaluation of the indicator *LEE*. The results of the analysis of the level of dependence of the energy efficiency on the combination of this parameter and the level of complexity of the traffic flow showed that the weight of their total impact on *LEE* depends on the category of vehicle. The energy efficiency of buses is more affected by the combination (x_4, x_5) than that of trucks.

The initial sample was represented by a small number of new hybrid and electric cars and did not reflect their properties under the studied conditions. In the future, it is planned to expand the obtained base of rules of logical derivation, having previously checked that the new configurations do not affect the structure of the system base.

The aging of the vehicle park imposes certain limitations on the duration of the life cycle of the TrEECS model and requires periodic updating of the existing rule base by adjusting the vehicle age in the statistical sample and the values of the transition of the corresponding parameters to the next fuzzy term. The formalized stages of morphological analysis can be repeated to maintain an up-to-date base of derivatives. An up-to-date database will provide an assessment and forecast of the energy efficiency of vehicles in changing system conditions.

5. Conclusions

To evaluate the energy efficiency of vehicles of the TrEECS transport system, a morphological model of this system was built. The structure of the model contains four functional elements, 10 independent attributes of functional elements, and domains of their possible values. For the first time, a formalized mechanism of transition from the morphological model of the system to the corresponding fuzzy model of derivation is proposed. This will make it possible to periodically update the base of the intelligent transport system to maintain its relevance, taking into account new elements and factors.

The criterion of energy efficiency of vehicles based on dimensionless coefficients is determined. The proposed energy efficiency indicator characterizes the increase in energy consumption of vehicles relative to energy consumption under standard operating conditions. Unlike existing methods, this indicator is universal for vehicles of various categories and types, and its definition does not require a direct assessment of energy consumption.

On the basis of experimental data on the state of the TrEECS system, a synthesis of 25 system configurations was carried out on the example of nine settlements in Ukraine and Poland. Observation of the state of the relevant transport systems was carried out with the involvement of 16 units of equipment in different time and weather conditions. Mamdani and Sugeno, fuzzy derivation systems, were built for comprehensive evaluation of the energy efficiency of vehicles under given conditions. These systems are based on fuzzy models that take into account ten attributes of the vehicle, traffic flow, road, and traffic environment. At the same time, six defuzzification algorithms were used. The accuracy of the obtained models confirms their adequacy. The Mamdani system was the most adapted

to real conditions, with an energy efficiency estimation error of 1.2%. It is advisable to use this system in the control module of intelligent transport systems.

The impact of the TrEECS system parameters on the energy efficiency of the vehicle for the configurations of the control sample was evaluated. The degree of utilization of cargo/passenger capacity has the greatest influence. It was established that the total effect of combinations of this parameter with others depends on the vehicle category.

Further, it is planned to refine the correction coefficients for determining the energy efficiency indicator and expand the base of the transport system control module due to the study of new TrEECS configurations for electric vehicles. Further research also will be aimed at determining rational configurations of the TrEECS system based on multi-criteria optimization. The outputs of the corresponding model will be components of the complex efficiency criterion. The results of the study should be used in the design of effective mechanisms to manage the transport infrastructure of cities and road traffic in intelligent transport systems.

Author Contributions: Conceptualization, V.M. and M.S.; methodology, L.T. and N.K.; software, L.T. and N.K.; validation, L.T., N.K. and V.M.; formal analysis, L.T. and N.K.; investigation, N.K.; resources, J.M.; data curation, L.T. and N.K.; writing—original draft preparation, L.T., N.K., V.M. and M.S.; writing—review and editing, N.K.; visualization, V.M. and J.M.; supervision, V.M. and M.S.; project administration, V.M. and M.S. All authors have read and agreed to the published version of the manuscript.

Funding: This research received no external funding.

Data Availability Statement: Not applicable.

Conflicts of Interest: The authors declare no conflict of interest.

References

1. Tarandushka, L.; Mateichyk, V.; Kostian, N.; Tarandushka, I.; Rud, M. Assessing the quality level of technological processes at car service enterprises. *East.-Eur. J. Enterp. Technol.* **2020**, *2/3*, 58–75. [\[CrossRef\]](#)
2. Zinko, R.V. *Morphological Environment for the Study of Technical Systems: A Monograph*; Vydavnytstvo lvivskoi politekhniki: Lviv, Ukraine, 2014; p. 386. ISSN 978-617-607-638-4.
3. Al-Jazaeri, A.O.; Samaranyake, L.; Longo, S.; Auger, D.J. Fuzzy Logic Control for Energy Saving in Autonomous Electric Vehicles. In Proceedings of the 2014 IEEE International Electric Vehicle Conference, Florence, Italy, 17–19 September 2015. [\[CrossRef\]](#)
4. Barreno, F.; Santos, M.; Romana, M. Fuzzy Logic System for Risk and Energy Efficiency Estimation of Driving Maneuvers. In *14th International Conference on Computational Intelligence in Security for Information Systems and 12th International Conference on European Transnational Educational (CISIS 2021 and ICEUTE 2021)*; Springer: Cham, Switzerland, 2021; pp. 94–104. [\[CrossRef\]](#)
5. Barreno, F.; Santos, M.; Romana, M.G. Fuzzy-Logic Based Identification of Conventional Two-Lane Roads. In *15th International Conference on Soft Computing Models in Industrial and Environmental Applications (SOCO 2020) (SOCO)*; Springer: Cham, Switzerland, 2020; pp. 418–428. [\[CrossRef\]](#)
6. Pinilla, A.C.C.; Quintero, M.C.G.; Premachandra, C. Intelligent driving diagnosis based on a fuzzy logic approach in a real environment implementation. In Proceedings of the 2014 IEEE Intelligent Vehicles Symposium Proceedings, Dearborn, MI, USA, 8–11 June 2014; pp. 102–107. [\[CrossRef\]](#)
7. Abulifa, A.A.; Che Soh, A.; Hassan, M.K.; Raja Ahmad, R.M.K.; Mohd Radzi, M.A. Energy Management System in Battery Electric Vehicle Based on Fuzzy Logic Control to Optimize the Energy Consumption in HVAC System. *Int. J. Integr. Eng.* **2019**, *11*, 11–20. [\[CrossRef\]](#)
8. Yang, L.; Wang, Y.; Zhu, C. Study on Fuzzy Energy Management Strategy of Parallel Hybrid Vehicle Based on Quantum PSO Algorithm. *Int. J. Multimed. Ubiquitous Eng.* **2016**, *11*, 147–158. [\[CrossRef\]](#)
9. Mohd, T.A.T.; Hassan, M.K.; Aris, I.; Azura, C.S.; Ibrahim, B.S.K.K. Application of fuzzy logic in multi-mode driving for a battery electric vehicle energy management. *Int. J. Adv. Sci. Eng. Inf. Technol.* **2017**, *7*, 284–290. [\[CrossRef\]](#)
10. Brzozowski, K.; Ryguła, A.; Maczyński, A. An Integrated System for Simultaneous Monitoring of Traffic and Pollution Concentration—Lessons Learned for Bielsko-Biała, Poland. *Energies* **2021**, *14*, 8028. [\[CrossRef\]](#)
11. Olayode, I.O.; Severino, A.; Tartibu, L.K.; Arena, F.; Cakici, Z. Performance Evaluation of a Hybrid PSO Enhanced ANFIS Model in Prediction of Traffic Flow of Vehicles on Freeways: Traffic Data Evidence from South Africa. *Infrastructures* **2022**, *7*, 2. [\[CrossRef\]](#)
12. Zajačko, I.; Gál, T.; Ságová, Z.; Mateichyk, V.; Wiecek, D. Application of artificial intelligence principles in mechanical engineering. *MATEC Web Conf. Innov. Technol. Eng. Prod. (ITEP'18)* **2018**, *244*, 01027. [\[CrossRef\]](#)
13. Lim, J.; Lee, Y.; Kim, K.; Lee, J. Experimental Analysis of Calculation of Fuel Consumption Rate by On-Road Mileage in a 2.0 L Gasoline-Fueled Passenger Vehicle. *Appl. Sci.* **2018**, *8*, 2390. [\[CrossRef\]](#)

14. Khabutdinov, R.A.; Fedorenko, I.O. Analysis of the impact of transport energy efficiency indicators of the bus for urban passenger transportation. *Sci. Notes V.I. Vernadsky Taurida Natl. Univ. Ser. Tech. Sci.* **2021**, *32*, 259–266. (In Ukrainian) [[CrossRef](#)]
15. Śmieszek, M.; Mateichyk, V. Determining the fuel consumption of a public city bus in urban traffic. In *IOP Conference Series: Materials Science and Engineering, Proceedings of the 26th International Slovak-Polish Scientific Conference on Machine Modelling and Simulations (MMS 2021), Bardejovské Kúpele, Slovak Republic, 13–15 September 2021*; IOP Publishing Ltd.: Bristol, UK, 2021; Volume 1199. [[CrossRef](#)]
16. Dmytriiev, M.M. M 218-02070915-694:2011 *Methods for Assessing the Ingredient and Parametric Pollution of the Roadside Environment by the System Traffic Flow—Road*; National Transport University: Kyiv, Ukraine, 2011; p. 28.
17. Ahn, K.; Rakha, H.; Trani, A.; Van Aerde, M. Estimating vehicle fuel consumption and emissions based on instantaneous speed and acceleration levels. *J. Transp. Eng.* **2002**, *128*, 182–190. [[CrossRef](#)]
18. Du, J.; Rakha, H.A.; Filali, F.; Eldardiry, H. COVID-19 pandemic impacts on traffic system delay, fuel consumption and emissions. *Int. J. Transp. Sci. Technol.* **2021**, *10*, 184–196. [[CrossRef](#)]
19. Lahlou, A.; Ossart, F.; Boudard, E.; Roy, F.; Bakhouya, M. A Real-Time Approach for Thermal Comfort Management in Electric Vehicles. *Energies* **2020**, *13*, 4006. [[CrossRef](#)]
20. Patrone, G.L.; Paffumi, E.; Otura, M.; Centurelli, M.; Ferrarese, C.; Jahn, S.; Brenner, A.; Thieringer, B.; Braun, D.; Hoffmann, T. Assessing the Energy Consumption and Driving Range of the QUIET Project Demonstrator Vehicle. *Energies* **2022**, *15*, 1290. [[CrossRef](#)]
21. Klimenko, A.; Hill, N.; Windisch, E. Approaches to regulation of CO₂ emission and energy consumption indicators of new light duty vehicles in Ukraine. *Bull. Natl. Transp. Univ.* **2019**, *1*, 66–75. (In Ukrainian) [[CrossRef](#)]
22. Khabutdinov, R.A. System concept of energy-resource synergy and methodology of technological-innovative management on motor transport. *Bull. Natl. Transp. Univ.* **2020**, *1*, 365–374. (In Ukrainian) [[CrossRef](#)]
23. Kosai, S.; Nakanishi, M.; Yamasue, E. Vehicle energy efficiency evaluation from well-to-wheel lifecycle perspective. *Transp. Res. Part D Transp. Environ.* **2018**, *65*, 355–367. [[CrossRef](#)]
24. Synák, F.; Kučera, M.; Skrucaný, T. Assessing the Energy Efficiency of an Electric Car. *Communications* **2021**, *23*, 1–13. [[CrossRef](#)]
25. Podrigalo, M.A.; Abramov, D.V.; Tarasov, Y.V.; Kholodov, M.P.; Kaidalov, R.O.; Podrigalo, N.M.; Shein, V.S. Improvement evaluation methodology of vehicle load and energy efficiency. *Automob. Transp.* **2021**, *49*, 36–44. [[CrossRef](#)]
26. Weiss, M.; Cloos, K.C.; Helmers, E. Energy efficiency trade-offs in small to large electric vehicles. *Environ. Sci. Eur. [Online]* **2020**, *32*, 46. [[CrossRef](#)]
27. Mohanadass, A. Making the Most of the Energy We Have: Vehicle Efficiency. In *Advanced Energy Management, Modelling and Control for Intelligent and Efficient Transport Systems - Design, Modelling, Control and Simulation*; Truong Quang Dinh; IntechOpen: Coventry, UK, 2020; pp. 1–19. [[CrossRef](#)]
28. Smieszek, M.; Kostian, N.; Mateichyk, V.; Mościszewski, J.; Tarandushka, L. Determination of the Model Basis for Assessing the Vehicle Energy Efficiency in Urban Traffic. *Energies* **2021**, *14*, 8538. [[CrossRef](#)]
29. Snytiuk, V.Y. *Prognostication. Models. Methods. Algorithms*; Maklout: Kyiv, Ukraine, 2008; p. 364.

Disclaimer/Publisher’s Note: The statements, opinions and data contained in all publications are solely those of the individual author(s) and contributor(s) and not of MDPI and/or the editor(s). MDPI and/or the editor(s) disclaim responsibility for any injury to people or property resulting from any ideas, methods, instructions or products referred to in the content.



Article

Can Regional Eco-Efficiency Forecast the Changes in Local Public Health: Evidence Based on Statistical Learning in China

Xianning Wang ^{1,2,3}, Zhengang Ma ^{4,*}, Jiusheng Chen ¹ and Jingrong Dong ¹

¹ School of Economics and Management, Chongqing Normal University, Chongqing 401331, China

² Big Data Marketing Research and Applications Center, Chongqing Normal University, Chongqing 401331, China

³ Regional Economics Applications Laboratory (REAL), University of Illinois Urbana-Champaign, Champaign, IL 61801, USA

⁴ College of Life Sciences, Chongqing Normal University, Chongqing 401331, China

* Correspondence: zhengang@cqnu.edu.cn

Abstract: Regional eco-efficiency affects local public health through intermediaries such as economic and environmental impacts. Considering multiple factors, the implicit and uncertain relationship with regional characteristics, and the limited data availability, this paper investigated the forecasting of changes in local public health—including the number of visits to hospitals (VTH), outpatients with emergency treatment (OWET), number of inpatients (NI), number of health examinations (NOHE), and patients discharged (PD)—using calculated regional eco-efficiency with the Least Square-Support Vector Machine-Forecasting Model and acquired empirical evidence, utilizing the province-level data in China. Results: (1) regional eco-efficiency is a good predictor in both a single and multi-factor situation; (2) the prediction accuracy for five dimensions of the changes in local public health was relatively high, and the volatility was lower and more stable throughout the whole forecasting period; and (3) regional heterogeneity, denoted by three economic and demographic factors and three medical supply and technical level factors, improved the forecasting performance. The findings are meaningful for provincial-level decision-makers in China in order for them to know the current status or trends of medical needs, optimize the allocation of medical resources in advance, and enable ample time to tackle urgent emergencies, and, finally, the findings can serve to evaluate the social effects of improving regional eco-efficiency via local enterprises or individuals and adopting sustainable development strategies.

Keywords: the changes in local public health; forecasting; multiple factors; regional characteristics; statistical learning; regional eco-efficiency

Citation: Wang, X.; Ma, Z.; Chen, J.; Dong, J. Can Regional Eco-Efficiency Forecast the Changes in Local Public Health: Evidence Based on Statistical Learning in China. *Int. J. Environ. Res. Public Health* **2023**, *20*, 1381. <https://doi.org/10.3390/ijerph20021381>

Academic Editors: Roberto Alonso González Lezcano, Francesco Nocera and Rosa Giuseppina Caponetto

Received: 20 October 2022
Revised: 30 December 2022
Accepted: 6 January 2023
Published: 12 January 2023



Copyright: © 2023 by the authors. Licensee MDPI, Basel, Switzerland. This article is an open access article distributed under the terms and conditions of the Creative Commons Attribution (CC BY) license (<https://creativecommons.org/licenses/by/4.0/>).

1. Introduction

Economic and environmental factors affect local residents' health, and environmental and medical decision-makers attach importance to the trends of changes in local public health (CLPH) [1]. Early prediction of the changes in local public health can provide sufficient time to balance the supply and demand of medical resources such as by making people prepared to respond to medical emergencies [2] and optimizing the resource allocation of medical materials in advance, thereby dynamically promoting a local medical service level [3]. Regional eco-efficiency can serve as a flexible indicator that integrates the relevant economic or environmental factors, those which scholars indicate can be chosen as good exogenous predictors for public health. Based on the organic performance of input and output factors [4], regional eco-efficiency (REE) has been treated as an explicitly important indicator due to it integrating both economic and environmental impacts and being closely related to healthcare sustainability [5]. Therefore, is there any empirical evidence to show REE can forecast CLPH with acceptable accuracy?

This problem arouses many scholars' interests in these interdisciplinary issues [6], but the literature rarely shows adequate quantitative evidence. There are three main reasons for this. First, the factors that affect residents' health are multi-scale and multi-dimensional, including micro-level factors in individual health, macroeconomic factors, and environmental factors. Second, the description of a nonlinear relationship is uncertain, and simple linear regression cannot meet the needs of prediction. Third, the influence and heterogeneity of regional differences lead to the complexity of modeling. In the process of empirical operation, the above problems are transformed into one forecasting method with multiple factors, an implicit and uncertain relationship, regional characteristics, and limited data availability.

In the following literature review section, relevant studies have recognized and calculated the correlation between the two and the feasibility of prediction. This paper aimed to investigate this problem by building a new forecasting model based on statistical learning and obtain empirical evidence with Chinese regional data. This study can provide a new perspective and method to predict regional CLPH. In addition, in the collaborative process of promoting sustainable economic development by improving the REE, the related findings can strengthen inter- or intra-province cooperation with medical resources and improve risk management levels across different regions.

Relevant concepts about REE show that it is equipped with the capability and feasibility to forecast CLPH. As an instrument for sustainability analysis, it can reflect and judge the effectiveness of local economic activity, taking the nature of their goods or services into account [7]. Its definition, measurement, and main factors are closely associated with two kinds of forecasting variables: environmental change and economic factors. The former consists of the living conditions that directly affect the health levels of local inhabitants by impacting the air quality, water safety, solid waste disposal, and so on [8], and especially the energy efficiency and the accompanying pollutants [9]. The latter comprises the economic costs and individual financial capacities and determines the disease treatment of regional residents by impacting employment opportunities and disposable incomes. Therefore, in the economic, environmental, and medical health sciences and their intersectional fields there is inherent theoretical research or a basis to support that REE can act as one of the best leading indicators for CLPH.

Identifying what the implicit interaction between CLPH and spatial REE is an important prerequisite for making predictions; however, there is not a linear or convertible linear relationship because of outlier data, regional heterogeneity, the interactions of multiple influencing factors, etc. In view of the advantages of the Support Vector Machine (SVM), with its powerful identification ability within multi-dimensional complex data, it is a good choice to quickly identify the implicit relationship and accurately make predictions using the limited data sources and multiple factors.

Considering that alongside REE there are multiple factors affecting CLPH, such as an implicit and uncertain relationship, regional characteristics, and limited data availability, this paper investigated how to forecast CLPH using REE by building the Least Square-Support Vector Machine-Forecasting Model (LS-SVM-FM) and acquiring empirical evidence utilizing regional province-level data in China. Furthermore, on the bases of three forecasting error indicators, we measured the prediction accuracy for each region, such that we (1) chose VTH, OWET, NI, NOHE, and PD as proxy variables for CLPH, respectively; (2) calculated eco-efficiency with commonly required variables and collected data; (3) to reflect spatial heterogeneity, incorporated six control variables including economic and demographic factors [10] and medical supply and technical level factors; (4) compared the LS-SVM-FM without or with each control variable, respectively, and obtained the best forecasting model with a higher accuracy; (5) analyzed regional characteristics and forecasting variation in China with a comparison analysis; and (6) discussed the policy implications.

In Section 2, we conduct a literature review to have a clear understanding of existing problems for forecasting CLPH using REE. In Section 3, we present the model specification and the empirical setting of the LS-SVM-FM. Section 4 provides quantitative evidence

for forecasting CLPH using REE with Chinese provincial data, and a further comparison analysis of forecasting performance is conducted. Sections 5 and 6 show the summary and conclusion.

2. Literature Review

2.1. The Inner Relationship between CLPH and REE

The inner relationship between CLPH and REE originates from their basic concepts. REE is a concise and simplified comprehensive index and emphasizes the monetary costs of various resources and the environmental changes required for economic development. Meanwhile, CLPH is also closely and directly associated with this kind of economic and environmental change, with regards to the requirement of maximum profits and minimum pollution. In addition, a variety of factors, such as the consumption of energy, pollutant emissions in waste gas, pollutant emissions in waste water, industrial solid wastes, the increased value of industrial development, and so on [11,12], originate from the measurement of REE and impact CLPH simultaneously. The above internal connection is an important foundation for building a predictive model, and the related literatures provide a basis for theoretical feasibility.

(1) In the economic dimension [13–17], scholars have investigated how economic activities embedded in REE affect CLPH [18]. As the most basic and critical requirements, the physical health of residents necessitates food, exercise, spiritual guarantee, and so on, which are achieved under one important premise: that personal income level and economic development trends provide the fundamental roles [19]. Residents earn income through employment to purchase energy and nutrition, for continuous life and education services, etc. [20], and to afford the expenditure for necessary medical supplies, equipment, and services [21]. Macroeconomic trends serve as leading indicators for residents' disposable incomes on the micro-level, especially for healthcare [22–24]. In addition, many other social or economic activities, such as city planning [25,26], immigration [27], aging [23], or housing [28], affect the changes in local public health too. In addition, REE includes the continuing impact of economic activities, and it reflects the quantitative effects from the input–output perspective. For example, producers can optimize the decision-making process of resource allocation.

(2) In the environmental dimension [29,30], there is a variety of related literature that have probed and shown evidence that the surrounding environments incorporated into local eco-efficiency have impacted local public health. Calculations of REE already encompass environmental input–output factors, including both the BADS and GOODS [4], which have led to changes in local public health to some extent. For example, beyond a certain concentration range, the BADS, such as particulate matter (PM_{2.5}) or sulfur dioxide (SO₂), deteriorate the living environments of residents and pose a great hidden danger to public health. In particular, excessive PM_{2.5} or SO₂ have caused many diseases of the respiratory and nervous system with both short-term and long-term damage.

Firstly, as a hot topic, public health has also been suffering from the air pollutant emissions of the manufacturing industry [31–35]. The highly frequent appearance of haze episodes has brought huge stress to physical and psychological health and social daily operations. Yu, Wang [36] assessed this kind of negative impact in China by using satellite observations, and Gao, Woodward [37] conducted a review of the changes in haze pollution and local public health. There are many potential risks when the concentrations are big enough. PM₁₀, NO₂, O₃, and CO are bad for CLPH [31,38–40].

Secondly, solid or plastic waste is resistant to degradation, has low costs, and is rapidly growing, which squeezes living space and keeps deteriorating sanitary conditions [41–44] no matter what kind of waste, from economic activities or daily life. Using modified eco-efficiency indicators, Woon and Lo [45] focused on the public health and solid waste management of Hong Kong. Langdon, Chandra [46] pointed out that solid or plastic waste has led to contaminants entering the living environment. Solid or plastic waste has also caused public health to be exposed to heavy metals such as lead, mercury, cadmium, and

arsenic [47,48]. Moreover, solid or plastic waste affects the growth of plants and changes in local public health [49,50], and it is not conducive to the effective prevention of toxic substances and infectious diseases and weakens the effects of health work on medical institutions and CLPH [41,51].

Thirdly, excessive water pollution is another important derivative that affects changes in local public health during social or economic progress [52], and, although wastewater has been purified to be utilized again [53,54], chemical compounds—toxic micropollutants—hidden in the water pollutants have gradually evolved into a huge health risk [55,56]. Saha, Rahman [57] pointed out that through ingestion or dermal contact, local residents are likely to be diseased. CLPH have continued to deteriorate and have caused various diseases due to the pesticides or toxic metals in both the irrigation and drinking water systems [58].

2.2. The Keys to Forecast CLPH with REE

When forecasting CLPH using REE, there are the following issues that need to be settled. (1) There are many factors that make the relationship so complex. It is necessary to adopt a new technique (SVM) to map the linear, nonlinear, or some complex implicit relationship because CLPH are influenced by economic, environmental, and individual factors, as well as others (as discussed in the last section). Simultaneously, REE with six control variables works to add to the practical interpretability. (2) There is an implicit and uncertain relationship description when using REE to forecast CLPH, especially as this paper applied five indicators as proxy variables for CLPH and six control variables. Whether they are positive or negative impacts and linear or nonlinear, this needs more quantitative evidence. (3) Different regional characteristics require a quantitative comparison of prediction performances. Considering the regional heterogeneity, it is necessary to build or estimate a model for a single region. Moreover, since there are five proxy variables for residents' health status, there is a question worth discussing about the relatively higher prediction accuracy obtained via eco-efficiency and six other control variables. (4) There are limited sample data, and how to obtain better prediction accuracy with limited data is another question. Multiple factors and regions generally require more data to complete the fitting, obtain the optimal parameters, and further predict the data within or outside the sample on a secondary basis. It needs a strong learning ability and effective use of a small sample of information.

3. Data and Methods

3.1. Data and Variables

Considering the data availability of and lack of data on Tibet, Hong Kong, Macao, and Taiwan, in the empirical Section 3, all provinces or cities in China were taken into account. The time period is from 2002 to 2016. This paper adopted “SBM (Slacks-Based Measure)” [59] and DEA-SOLVER Pro 5.0 [60] to measure the REEs. The descriptive statistics of the main variables to calculate the REEs are listed in Table S1 and Figure 1. The results are consistent with most other studies [61]. The eastern values of REE are higher than the western values. The value of the eco-efficiency of the whole nation is up to 0.51 in 2016.

The data of VTH, OWET, NI, NOHE, and PD (mainly from hospitals) are from the Chinese Medical Health Statistics Yearbooks from 2003 to 2017. The main statistics descriptions can be obtained from Figure 2. Indicators related to REE and all the control variables were mainly collected from the China Statistical Yearbooks from 2002 to 2017. All the indicators related to value were excluded because of the effect of inflation on the prices in 1998.

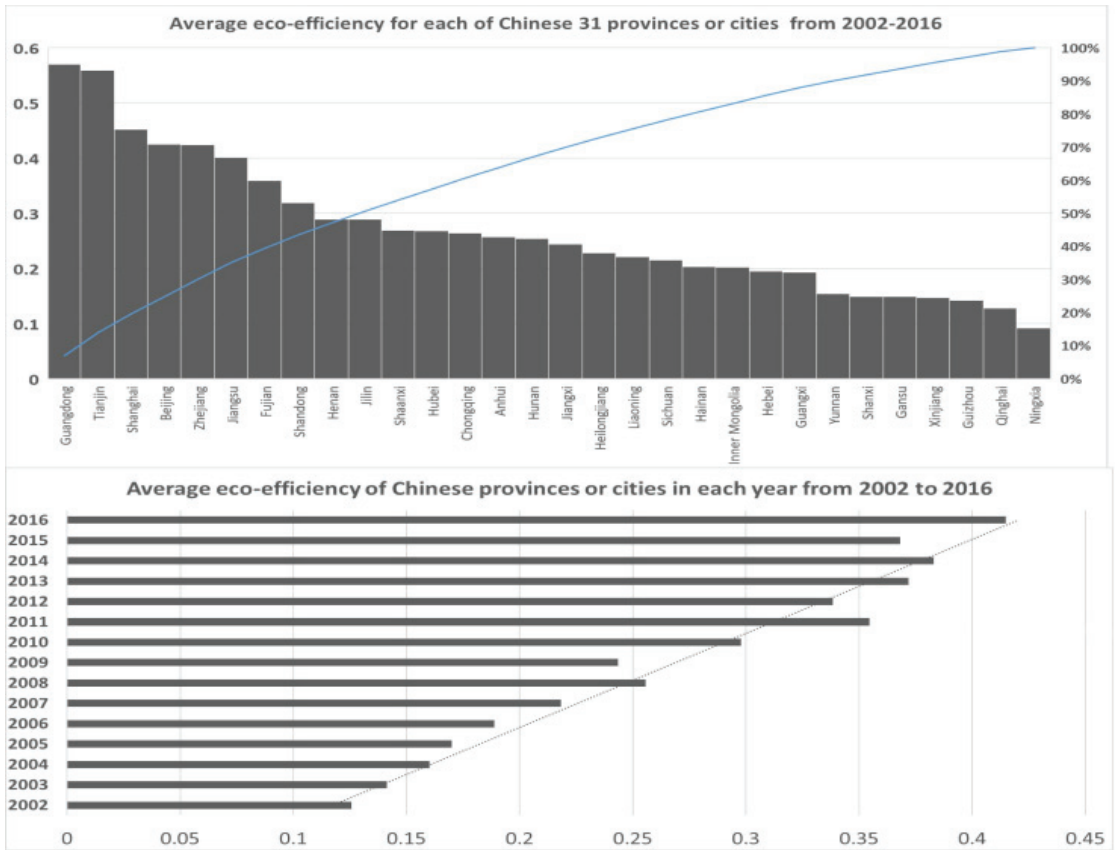


Figure 1. The values of REE in 30 provinces and cities of China.

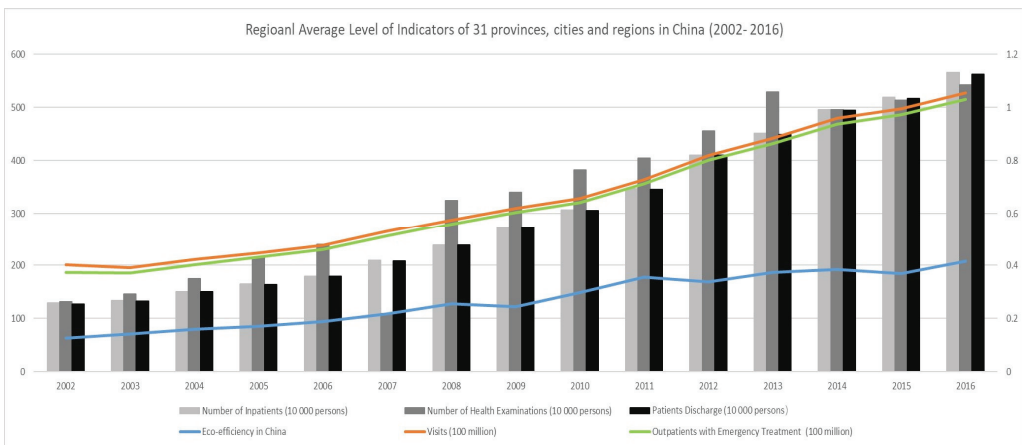


Figure 2. Regional average level of the used indicators in China.

In addition, due to the limitation in the same frequency processing of the data collection of the other variables in the forecasting model, the eco-efficiency calculation period is 2002–

2016 [62]. First of all, it was difficult to obtain the energy-related/CO₂-related input and output indicators (shown in Supplementary Materials: Table S1, including the main variables of the SBM to calculate the regional eco-efficiency) in some provinces and cities, such as Tibet, which limited our sample range. Secondly, there were many independent variables and dependent variables in the prediction model. This paper applied 5 indicators as proxy variables for CLPH and 6 control variables, including the development level of regional GDP, urbanization, population, and the number of local medical personnel, local licensed (assistant) doctors, and local health care institutions. In order to keep the time range of all the variables used consistent, we had to choose all data from 2002 to 2016. Although the eco-efficiency in 2017–2019 can be calculated, statistical data such as basic medical conditions (the statistical data of medical personnel, licensed doctors, or health care institutions) were scarce or had different statistical calibers, and we were limited to unifying the range of selected years. In addition, the impact of COVID-19 after 2019 can be seen as an uncertain external impact, which may need to be the focus of future research.

Figure 2 displays the regional average levels of all the used indicators in China. It can be seen that CLPH maintained a more moderate growth trend and so did the REE. However, from the theoretical explanation, they cannot be arbitrarily predicted using linear methods because there are many factors that determine the health levels of residents, for example, physical fitness, wealth, psychological factors, exercise methods, etc., which is consistent with the view in Section 2. Considering the implicit and uncertain relationship between REE and CLPH, regional characteristics, and low data availability, the following section draws on the advantages of the LS-SVM-FM in mapping and identifying the relationship (even if non-linear), which can ensure the fitting effect and prediction accuracy.

3.2. Method Design

SVM performs well in building models when there are many factors or a nonlinear data pattern with small samples in many literatures, including [63–67]. Based on these, this paper utilized its relevant methods to ensure the fitting effect and prediction accuracy.

(1) The implicit relationship could have a much clearer mapping in the high-dimensional hyper feature space by constructing a hyper plane and finding support vectors to represent all the information, which allowed us to predict with a small sample of data.

(2) Its diverse kernel functions (linear and nonlinear) could meet the need for complex forecasting alongside the commonly used linear models, which allowed us to predict with the complex or uncertain relationship of the forecasting model. In the high-dimensional feature space, the proposed method adopted the nonlinear kernel to map the non-linear function learned by a linear learning machine, the process of which is not limited to spatial dimensionality.

(3) Compared with other methods, taking the “Structural Risk Minimization Principle” as the principle, SVM enabled our method to be equipped with an improved classification power [68], which allowed us to acquire a better forecasting accuracy for each region in China with a good fitting [67].

(4) Most forecasting based on SVM such as the Least Square-Support Vector Machine (LS-SVM) has already been applied to time series data, and this study extended it to regional panel data by constructing the LS-SVM-FM.

Based on the classic LS-SVM, LS-SVR, and LS-SVR-DS, this paper built the LS-SVM-FM with different regions and multiple factors.

With the dependence on the two parameters σ and γ , the solution of the LS-SVR can be modified as the following equation:

$$y(X; \sigma, \gamma) = \sum_{i=1}^m \alpha_i(\sigma, \gamma) K(x_j, x_i) + b(\sigma, \gamma) \quad (1)$$

It is better to apply the optimal method to obtain what are the true values of those main parameters by minimizing the average of squared errors. It can be displayed as

$$\min_{\sigma, \gamma} G(\sigma, \gamma) = \frac{1}{m} \sum_{j=1}^m [y_j - y(x_j; \sigma, \gamma)]^2 = \frac{1}{m} \sum_{j=1}^m \left[y_j - \sum_{i=1}^m \alpha_i(\sigma, \gamma) K(x_j, x_i) - b(\sigma, \gamma) \right]^2 \quad (2)$$

In the empirical parts, the proposed LS-SVM-FM took the CLPH as Y , whose proxy variables are, separately, the VTH, OWET, NI, NOHE, and PD. x_1, x_2, x_3, \dots , and x_7 represent variable values of REE, and all 6 of the control variables are represented as X . The next section introduces the relevant data and variables in detail. The continued LS-SVM-FM is written as the following:

$$F_p(X|W) = Y_p(X) = \sum_{q=1}^7 \sum_{k=1}^N \alpha_{pqk} K_p(x_q, x_k) + b_p \quad (3)$$

It rewrites as

$$Y_p(X) = \sum_{q=1}^7 [\alpha_{p1} K_p(x_q, x_1) + \alpha_{p2} K_p(x_q, x_2) + \alpha_{p3} K_p(x_q, x_3) + \dots + \alpha_{pN} K_p(x_q, x_N)] + b_p \quad (4)$$

$p = 1, \dots, P$, where P denotes the number of regions or province or cities. Here, P is 30 and stands for the 30 provinces or cities in China. $p = 1, \dots, Q$, where Q denotes the number of variables. Here, Q is 7 and stands for the 7 different variables including REE and the control variables in China. $k = 1, 2, \dots, N$, where N is equal to 15, and k stands for the specific year from 2002 to 2016. There are four kinds of kernels. The Radial Basis Function (RBF) kernels $K(x, x_k) = \exp(-\|x - x_k\|^2 / 2\sigma^2)$ were chosen as the specific form, which has been unanimously recognized by scholars with the most frequent application, relatively [69].

3.3. Main Steps

Without an explicit close form on σ and γ of G , here, we provide the following algorithm of the search procedure [69].

Step 1. Initialize a search point $B_0 = (\sigma_0, \gamma_0)$ and $k = 1$.

Step 2. Let the point, $B_1 = (\sigma_0 + \lambda_\sigma, \gamma_0 + \lambda_\gamma)$, be alternative, in which λ_σ and λ_γ denote the random step sizes generated from the (0, 1) uniform distribution.

Step 3. Calculate $G(\sigma_0, \gamma_0)$ and $G(\sigma_0 + \lambda_\sigma, \gamma_0 + \lambda_\gamma)$ simultaneously by applying (2).

Step 4. Replace σ_0 with $\sigma_0 + \lambda_\sigma$ and γ_0 with $\gamma_0 + \lambda_\gamma$, if $G(\sigma_0 + \lambda_\sigma, \gamma_0 + \lambda_\gamma) \leq G(\sigma_0, \gamma_0)$. Otherwise, $\sigma_0 = \sigma_0$ and $\gamma_0 = \gamma_0$.

Step 5. When $G(\sigma_0, \gamma_0) \leq \varepsilon$ or $k \geq N$, the iteration can stop. Otherwise, set $k \geq k + 1$ and return to Step 2. The iteration can stop either when the forecasting accuracy can be achieved or the computation is finished within an exogenously prespecified iteration number N . When the algorithm stops, it finds the ‘optimal’ pair of (σ_0, γ_0) for the LS-SVM-FM, which minimizes the training error.

The main procedures are described as follows: (1) We applied each of the 30 province-level datasets in China to the LS-SVM-FM and performed in-sample learning and fitting to determine the parameter value and out-of-sample prediction and comparison to determine the prediction accuracy; (2) mean percentage error (MPE) and mean square or standard deviation of prediction error (MSE or SDE) were chosen to judge the prediction accuracy; (3) the VTH, OWET, NI, NOHE, and PD for CLPH were respectively taken as Y ; (4) REE and the control variables in China were adopted as X , and the LS-SVM-FM without or with each of the 6 control variables were compared, respectively, and we obtained the best forecasting model with a lower prediction error; and (5) the forecasting accuracy with the single factor and multiple factors in China was drawn from the comparison analysis [69].

$$(1) \text{ MPE} = \frac{\sum_{t=1}^T \frac{y_t - \hat{y}_t}{y_t}}{T}$$

$$(2) \text{ MSE} = \frac{\sum_{t=1}^T (y_t - \hat{y}_t)^2}{T}; \text{ SDE} = \sqrt{\frac{\sum_{t=1}^T (y_t - \hat{y}_t)^2}{T}}$$

y_T and y_t denote the known sample values of the year t . \hat{y}_T and \hat{y}_t denote the predicted sample values of the last year and the year of t using the LS-SVM-FM. $t = 1, 2, \dots, T$.

4. Results

4.1. Forecasting Accuracy with the Single Factor and Multiple Factors

Chinese data were applied to the LS-SVM-FM to obtain empirical evidence. To understand the prediction better and keep a reasonable explanation, each of the five proxy indicators of CLPH for the thirty different provinces and cities in China were forecasted, and we compared the prediction errors from the following three aspects: (I) utilizing the single-factor-REE to forecast the CLPH in China, naming the model LS-SVM-FM (1); (II) adopting the multi-factors-REE and three more economic and demographic factors, naming the model LS-SVM-FM (2); and (III) based on the LS-SVM-FM (2), incorporating three more medical supply and technical level factors, naming the model LS-SVM-FM (3).

The three models obviously showed whether the forecasting accuracy changed significantly when applied to more control variables and which model gained the lowest prediction errors of each selected region in China. Tables 1–6 display detailed corresponding information about the forecasting performances of LS-SVM-FM (1), LS-SVM-FM (2), and LS-SVM-FM (3).

Table 1. The First Part of Forecasting performance of LS-SVM-FM (1).

	Visits (100 Million)			Outpatients with Emergency Treatment (100 Million)			Number of Inpatients (10,000 Persons)		
	MPE	MSE	SDE	MPE	MSE	SDE	MPE	MSE	SDE
China	0.00192	0.91664	0.95741	0.00203	0.90207	0.94977	0.00377	405,619.57361	2466.63609
Beijing	0.00593	0.00166	0.04068	0.00413	0.00138	0.03716	0.00641	55.98069	28.97776
Tianjin	0.00347	0.00059	0.02431	0.00370	0.00060	0.02449	0.00429	23,26127	18.67937
Hebei	0.00621	0.00550	0.07414	0.00684	0.00532	0.07292	0.00596	1922.83207	169.83074
Shanxi	0.03625	0.00497	0.07052	0.03664	0.00439	0.06627	0.08777	4054.84798	246.62263
Inner Mongolia	0.01775	0.00161	0.04012	0.01747	0.00149	0.03857	0.01914	540.89685	90.07471
Liaoning	0.01685	0.00877	0.09366	0.01881	0.00904	0.09510	0.04576	7055.55512	325.32034
Jilin	0.00218	0.00019	0.01373	0.00178	0.00016	0.01264	0.00206	76.35504	33.84266
Heilongjiang	0.05188	0.01065	0.10321	0.05657	0.01089	0.10435	0.014120	10,230.06615	391.72821
Shanghai	0.00971	0.00575	0.07583	0.01049	0.00576	0.07593	0.00921	310.72021	68.27007
Jiangsu	0.00149	0.00193	0.04392	0.00248	0.00196	0.04428	0.00294	265.18282	63.06935
Zhejiang	0.00311	0.00343	0.05856	0.00330	0.00342	0.05845	0.00457	409.03585	78.32967
Anhui	0.00299	0.00124	0.03519	0.00207	0.00112	0.03340	0.00349	662.15291	99.66089
Fujian	0.00818	0.00237	0.04869	0.01005	0.00244	0.04940	0.01062	710.07202	103.20407
Jiangxi	0.00194	0.00036	0.01898	0.00191	0.00034	0.01834	0.00432	327.05850	70.04197
Shandong	0.00302	0.00569	0.07545	0.00382	0.00554	0.07442	0.00569	3580.87560	231.76094
Henan	0.00197	0.00172	0.04151	0.00126	0.00154	0.03920	0.00328	985.31963	121.57218
Hubei	0.00218	0.00055	0.02341	0.00158	0.00040	0.02000	0.00338	233.81192	59.22144
Hunan	0.00112	0.00053	0.02300	0.00111	0.00048	0.02195	0.00459	492.60320	85.95957
Guangdong	0.00243	0.01016	0.10081	0.00249	0.00987	0.09933	0.00309	1056.46133	125.88455
Guangxi	0.00156	0.00039	0.01964	0.00093	0.00031	0.01770	0.00610	299.17792	66.99006
Hainan	0.05362	0.00068	0.02611	0.05283	0.00066	0.02564	0.11745	292.27729	66.21298
Chongqing	0.00259	0.00033	0.01826	0.00177	0.00026	0.01622	0.00927	272.60830	63.94626
Sichuan	0.00290	0.00081	0.02839	0.00303	0.00076	0.02759	0.00086	520.90749	88.39464
Guizhou	0.00306	0.00011	0.01027	0.00587	0.00030	0.01744	0.01692	471.29101	84.07952
Yunnan	0.01100	0.00542	0.07364	0.01093	0.00509	0.07136	0.01956	3485.27203	228.64619
Shaanxi	0.01456	0.00387	0.06220	0.01480	0.00382	0.06181	0.03167	3495.36887	228.97715
Gansu	0.02359	0.00188	0.04336	0.02318	0.00164	0.04048	0.10303	3128.21615	216.61773
Qinghai	0.02693	0.00019	0.01381	0.03077	0.00017	0.01296	0.06899	148.65021	47.22026
Ningxia	0.00420	0.00006	0.00765	0.00435	0.00005	0.00731	0.00751	20.19197	17.40344
Xinjiang	0.04769	0.00653	0.08080	0.05348	0.00660	0.08124	0.13928	8130.00502	349.21351
Average	0.01235	0.00293	0.04633	0.01295	0.00286	0.04553	0.02961	1775.23518	128.99176

Table 2. The Second Part of Forecasting performance of LS-SVM-FM (1).

	Number of Health Examinations (10,000 Persons)			Patients Discharged (10,000 Persons)		
	MPE	MSE	SDE	MPE	MSE	SDE
China	0.05315	1,738,096.51187	1318.36888	0.00379	468,007.97061	684.11108
Beijing	0.05275	2321.08266	48.17762	0.00584	56.57502	7.52164
Tianjin	0.00583	54.18368	7.36096	0.00440	23.06877	4.80300
Hebei	0.10931	4276.50913	65.39502	0.00584	1830.36096	42.78272
Shanxi	1.16767	277,966.67011	527.22545	0.08932	3988.56250	63.15507
Inner Mongolia	0.09933	298.63334	17.28101	0.01811	510.15312	22.58657
Liaoning	0.03394	2655.96989	51.53610	0.04458	6920.06978	83.18696
Jilin	0.00325	21.97031	4.68725	0.00128	69.38246	8.32961
Heilongjiang	0.34022	6837.08484	82.68667	0.14290	10,187.72469	100.93426
Shanghai	0.35247	5197.56606	72.09415	0.00811	301.01225	17.34970
Jiangsu	0.54699	17,129.53347	130.87984	0.00296	281.25033	16.77052
Zhejiang	0.58323	20,354.73403	142.67002	0.00292	311.05583	17.63677
Anhui	0.09713	2662.96101	51.60389	0.00470	682.88916	26.13215
Fujian	0.11796	2643.99917	51.41983	0.01340	669.29284	25.87069
Jiangxi	0.00329	83.20221	9.12152	0.00469	329.00479	18.13849
Shandong	0.05606	10,654.74975	103.22185	0.00566	3597.07065	59.97558
Henan	0.08149	5035.28206	70.95972	0.00371	1019.82336	31.93467
Hubei	0.02445	1362.81613	36.91634	0.00401	247.69873	15.73845
Hunan	0.00602	433.10634	20.81121	0.00443	477.56503	21.85326
Guangdong	0.17755	75,738.38389	275.20608	0.00369	1185.90951	34.43704
Guangxi	0.02221	959.26509	30.97200	0.00543	292.49687	17.10254
Hainan	0.23382	79.71844	8.92852	0.11625	291.26718	17.06655
Chongqing	0.01628	300.69067	17.34043	0.00860	258.00590	16.06256
Sichuan	0.00255	198.86296	14.10188	0.00544	378.55165	19.45640
Guizhou	0.03541	727.41516	26.97064	0.01709	455.52373	21.34534
Yunnan	0.01910	1054.97890	32.48044	0.01991	3483.63044	59.02229
Shaanxi	0.15467	3689.90557	60.74459	0.03075	3476.96806	58.96582
Gansu	0.03230	649.66192	25.48847	0.10175	3061.53453	55.33114
Qinghai	0.10173	63.68169	7.98008	0.07157	152.00172	12.32890
Ningxia	0.02544	48.12243	6.93703	0.00763	19.27320	4.39013
Xinjiang	0.30604	13,059.15345	114.27665	0.14053	8078.00936	89.87775
Average	0.16028	15,218.66314	70.51584	0.02985	1754.52775	33.00289

Table 3. The First Part of Forecasting performance of LS-SVM-FM (2).

	Visits (100 Million)			Outpatients with Emergency Treatment (100 Million)			Number of Inpatients (10,000 Persons)		
	MPE	MSE	SDE	MPE	MSE	SDE	MPE	MSE	SDE
China	0.00035	0.03927	0.19816	0.00034	0.03387	0.18404	0.00048	18,889.43367	137.43884
Beijing	0.00338	0.00092	0.11736	0.00212	0.00058	0.02415	0.00240	32.24121	5.67813
Tianjin	0.00039	0.00002	0.01598	0.00038	0.00002	0.00399	0.00000	0.00000	0.00003
Hebei	0.00003	0.00000	0.00344	0.00000	0.00000	0.00017	0.00072	91.60878	9.57125
Shanxi	0.00148	0.00010	0.03899	0.00133	0.00009	0.00935	0.00013	1.21191	1.10087
Inner Mongolia	0.00114	0.00003	0.02198	0.00090	0.00002	0.00470	0.00079	13.90730	3.72925
Liaoning	0.00001	0.00000	0.00209	0.00000	0.00000	0.00002	0.00000	0.00000	0.00020
Jilin	0.00006	0.00000	0.00601	0.00068	0.00004	0.00641	0.00059	11.04432	3.32330
Heilongjiang	0.00000	0.00000	0.00000	0.00017	0.00002	0.00421	0.00039	21.98675	4.68900
Shanghai	0.00020	0.00005	0.02828	0.00023	0.00005	0.00740	0.00022	3.04555	1.74515
Jiangsu	0.00043	0.00057	0.09235	0.00072	0.00071	0.02667	0.00006	15.07263	3.88235
Zhejiang	0.00188	0.00136	0.14269	0.00218	0.00143	0.03786	0.00161	158.65937	12.59601
Anhui	0.00093	0.00009	0.03632	0.00063	0.00005	0.00690	0.00011	15.50991	3.93826
Fujian	0.00024	0.00004	0.02592	0.00022	0.00002	0.00499	0.00222	42.85782	6.54659
Jiangxi	0.00095	0.00007	0.03204	0.00085	0.00006	0.00758	0.00000	0.00000	0.00010
Shandong	0.00106	0.00086	0.11340	0.00126	0.00074	0.02718	0.00110	409.18927	20.22843
Henan	0.00031	0.00016	0.04969	0.00000	0.00000	0.00063	0.00105	189.65446	13.77151
Hubei	0.00114	0.00027	0.06360	0.00114	0.00026	0.01603	0.00293	196.14484	14.00517
Hunan	0.00004	0.00000	0.00752	0.00000	0.00000	0.00000	0.00022	23.05697	4.80177

Table 3. Cont.

	Visits (100 Million)			Outpatients with Emergency Treatment (100 Million)			Number of Inpatients (10,000 Persons)		
	MPE	MSE	SDE	MPE	MSE	SDE	MPE	MSE	SDE
Guangdong	0.00064	0.00265	0.19935	0.00061	0.00258	0.05083	0.00029	506.50071	22.50557
Guangxi	0.00000	0.00000	0.00000	0.00085	0.00013	0.01125	0.00042	45.89589	6.77465
Hainan	0.00010	0.00000	0.00300	0.00008	0.00000	0.00087	0.00081	0.72074	0.84896
Chongqing	0.00032	0.00001	0.01292	0.00102	0.00003	0.00591	0.00124	8.16018	2.85660
Sichuan	0.00076	0.00034	0.07123	0.00073	0.00030	0.01718	0.00094	240.77377	15.51689
Guizhou	0.00213	0.00009	0.03756	0.00124	0.00005	0.00681	0.00862	178.35468	13.35495
Yunnan	0.00015	0.00003	0.01959	0.00020	0.00003	0.00566	0.00065	46.15658	6.79386
Shaanxi	0.00026	0.00003	0.02008	0.00020	0.00002	0.00396	0.00013	1.56745	1.25198
Gansu	0.00025	0.00001	0.01051	0.00023	0.00001	0.00258	0.00286	19.70234	4.43873
Qinghai	0.00217	0.00001	0.00961	0.00340	0.00001	0.00295	0.00988	6.72635	2.59352
Ningxia	0.00064	0.00000	0.00833	0.00042	0.00000	0.00154	0.00027	0.18873	0.43443
Xinjiang	0.00016	0.00000	0.00800	0.00026	0.00002	0.00428	0.00006	0.16210	0.40262
Average	0.00071	0.00026	0.03993	0.00074	0.00024	0.01007	0.00136	76.00335	6.24600

Table 4. The Second Part of Forecasting performance of LS-SVM-FM (2).

	Number of Health Examinations (10,000 Persons)			Patients Discharged (10,000 Persons)		
	MPE	MSE	SDE	MPE	MSE	SDE
China	0.05708	1,675,850.37137	1294.54640	0.00054	21,295.74204	145.93061
Beijing	0.05268	2135.02766	46.20636	0.00242	24.89391	4.98938
Tianjin	0.00233	9.22267	3.03688	0.00000	0.00000	0.00001
Hebei	0.10389	3419.73632	58.47851	0.00096	99.69114	9.98455
Shanxi	0.98408	262,613.20253	512.45800	0.00009	0.65840	0.81142
Inner Mongolia	0.22479	701.77480	26.49103	0.00062	9.30115	3.04978
Liaoning	0.01316	1020.55332	31.94610	0.00000	0.00000	0.00003
Jilin	0.05828	302.46745	17.39159	0.00039	9.07593	3.01263
Heilongjiang	0.15970	1494.46364	38.65829	0.00028	18.70821	4.32530
Shanghai	0.33256	4048.37308	63.62683	0.00028	3.82234	1.95508
Jiangsu	0.57970	18,005.27888	134.18375	0.00010	21.60201	4.64780
Zhejiang	0.58310	18,751.62824	136.93658	0.00155	98.13550	9.90634
Anhui	0.10308	2622.21053	51.20752	0.00015	23.27889	4.82482
Fujian	0.09563	1881.63866	43.37786	0.00155	39.77409	6.30667
Jiangxi	0.02288	406.57600	20.16373	0.00094	18.46146	4.29668
Shandong	0.05166	8354.16534	91.40112	0.00063	407.54852	20.18783
Henan	0.01490	627.91876	25.05831	0.00107	183.87315	13.55998
Hubei	0.02629	1359.24663	36.86796	0.00332	218.08177	14.76759
Hunan	0.00733	371.56303	19.27597	0.00021	22.10366	4.70145
Guangdong	0.19417	83,228.00416	288.49264	0.00112	348.43544	18.66643
Guangxi	0.01360	526.90583	22.95443	0.00000	0.00000	0.00009
Hainan	0.22777	46.11755	6.79099	0.00078	0.74638	0.86393
Chongqing	0.02990	475.66845	21.80982	0.00103	7.68410	2.77202
Sichuan	0.02201	1746.69817	41.79352	0.00093	226.88005	15.06254
Guizhou	0.02494	450.87739	21.23387	0.00813	168.95577	12.99830
Yunnan	0.00770	345.33049	18.58307	0.00084	55.21420	7.43063
Shaanxi	0.00000	0.00000	0.00057	0.00013	1.65379	1.28600
Gansu	0.01446	173.65754	13.17792	0.00294	22.16623	4.70810
Qinghai	0.07494	26.13551	5.11229	0.00587	2.30415	1.51794
Ningxia	0.00038	0.26050	0.51040	0.00028	0.21509	0.46378
Xinjiang	0.05055	1352.35582	36.77439	0.00000	0.00000	0.00014
Average	0.13588	13,883.23530	61.13334	0.00122	67.77551	5.90324

Table 5. The First Part of Forecasting performance of LS-SVM-FM (3).

	Visits (100 Million)			Outpatients with Emergency Treatment (100 Million)			Number of Inpatients (10,000 Persons)		
	MPE	MSE	SDE	MPE	MSE	SDE	MPE	MSE	SDE
China	0.00008	0.01127	0.10614	0.00005	0.00699	0.08359	0.00027	28,446.81852	168.66185
Beijing	0.00338	0.00086	0.02939	0.00256	0.00056	0.02358	0.00208	26.96360	5.19265
Tianjin	0.00055	0.00004	0.00655	0.00047	0.00003	0.00576	0.00025	1.61696	1.27160
Hebei	0.00080	0.00017	0.01313	0.00024	0.00005	0.00674	0.00119	106.43587	10.31678
Shanxi	0.00003	0.00000	0.00023	0.00012	0.00000	0.00072	0.00012	28.64374	5.35198
Inner Mongolia	0.00148	0.00004	0.00592	0.00129	0.00003	0.00512	0.00059	11.76455	3.42995
Liaoning	0.00036	0.00009	0.00928	0.00030	0.00010	0.01004	0.00030	40.62011	6.37339
Jilin	0.00061	0.00003	0.00555	0.00136	0.00006	0.00795	0.00113	14.20003	3.76829
Heilongjiang	0.00000	0.00000	0.00000	0.00000	0.00000	0.00002	0.00226	86.19048	9.28388
Shanghai	0.00006	0.00003	0.00564	0.00005	0.00003	0.00535	0.00006	2.09720	1.44817
Jiangsu	0.00000	0.00000	0.00000	0.00000	0.00000	0.00021	0.00010	2.58493	1.60777
Zhejiang	0.00009	0.00008	0.00867	0.00011	0.00009	0.00944	0.00019	13.05925	3.61376
Anhui	0.00016	0.00002	0.00451	0.00015	0.00002	0.00450	0.00014	19.53235	4.41954
Fujian	0.00045	0.00006	0.00755	0.00051	0.00005	0.00691	0.00178	23.29297	4.82628
Jiangxi	0.00022	0.00002	0.00388	0.00021	0.00001	0.00355	0.00212	25.25358	5.02529
Shandong	0.00082	0.00073	0.02710	0.00039	0.00022	0.01474	0.00073	357.04299	18.89558
Henan	0.00013	0.00006	0.00777	0.00010	0.00005	0.00676	0.00052	76.89721	8.76911
Hubei	0.00066	0.00009	0.00961	0.00064	0.00007	0.00852	0.00061	40.09426	6.33200
Hunan	0.00127	0.00011	0.01051	0.00139	0.00011	0.01031	0.00172	103.22381	10.15991
Guangdong	0.00045	0.00181	0.04251	0.00045	0.00174	0.04169	0.00053	129.27407	11.36988
Guangxi	0.00040	0.00007	0.00836	0.00025	0.00004	0.00611	-0.00003	17.86174	4.22632
Hainan	0.00000	0.00000	0.00000	0.00016	0.00000	0.00089	0.00005	0.08138	0.28527
Chongqing	0.00007	0.00000	0.00109	0.00001	0.00000	0.00024	0.00059	2.22248	1.49080
Sichuan	0.00035	0.00017	0.01307	0.00036	0.00015	0.01243	0.00056	149.20399	12.21491
Guizhou	0.00186	0.00006	0.00762	0.00031	0.00001	0.00301	0.00084	25.19384	5.01935
Yunnan	0.00007	0.00001	0.00342	0.00010	0.00001	0.00352	-0.00002	42.26552	6.50119
Shaanxi	0.00024	0.00001	0.00372	0.00019	0.00001	0.00333	0.00073	8.27122	2.87597
Gansu	0.00200	0.00007	0.00817	0.00017	0.00000	0.00171	0.00001	0.02165	0.14714
Qinghai	0.00007	0.00000	0.00060	0.00183	0.00000	0.00205	0.01404	5.48537	2.34209
Ningxia	0.00151	0.00001	0.00283	0.00139	0.00001	0.00251	0.00146	2.26042	1.50347
Xinjiang	0.00000	0.00000	0.00000	0.00051	0.00002	0.00492	0.00116	31.90758	5.64868
Average	0.00060	0.00015	0.00822	0.00052	0.00012	0.00709	0.00119	46.45210	5.45703

When only using the REE to forecast the CLPH in China, performance comparisons within Tables 1 and 2 provide more information. Firstly, overall, REE can better predict the health status of regional residents of the five proxy variables in China. The MPE values all fall within the acceptable interval, and in particular, the average MPE values of the CLPH are 1.295%, 1.235%, 2.961%, 16.028%, and 2.985%, although the NOHE is bigger than 10%, and 12 of the 30 regions show a bigger than 10% prediction error. As with the literature mentioned above, REE owned the impacts from both economic and environmental aspects at the same time, and it is crucial and well-behaved for describing the health conditions of residents. Change in eco-efficiency affect living conditions and thus the changes in local public health. Therefore, it can be regarded as a good predictor, helping decision-makers to quantify future changes in residents' health in advance and, finally, adjust various medical supplies and technical preparations.

Secondly, the volatility of the forecasting error appears quite differently in each province or city, as represented by the bigger values of MSE and SDE for NI, NOHE, and PD compared with the other indicators. Their bigger MSE values are in part due to a smaller statistical unit, but SDE is much more convincing, with values of 128.99, 70.52, and 33.00. Another possibility is whether the model ignores important explanatory variables or other observed factors because local public health can actually be impacted by a number of factors no matter if on the individual or environmental level, as analyzed in the previous literature review.

Thirdly, regardless of the vertical comparison of a resident's health status or the horizontal comparison of different indicators, significant differences in forecasting accuracy between provinces and cities also exist, or the influence of regional heterogeneity on prediction accuracy is very obvious. Regional decision-makers should notice the phenomenon.

The specific situations of different provinces or cities are important clues for analyzing the above differences of LS-SVM-FM (1).

Table 6. The Second Part of Forecasting performance of LS-SVM-FM (3).

	Number of Health Examinations (10,000 persons)			Patients Discharged (10,000 persons)		
	MPE	MSE	SDE	MPE	MSE	SDE
China	0.05829	1,574,796.96650	1254.90915	0.00024	29,753.99626	172.49347
Beijing	0.05383	2194.24540	46.84277	0.00205	26.98889	5.19508
Tianjin	0.00539	44.62784	6.68041	0.00024	1.53127	1.23745
Hebei	0.10162	3338.60733	57.78068	0.00107	98.52758	9.92611
Shanxi	0.93100	264,433.55297	514.23103	0.00011	24.02664	4.90170
Inner Mongolia	0.00000	0.00000	0.00016	0.00037	6.94152	2.63468
Liaoning	0.01432	879.38933	29.65450	0.00036	43.02915	6.55966
Jilin	0.08450	532.94037	23.08550	0.00120	15.60832	3.95074
Heilongjiang	0.15653	1442.59133	37.98146	0.00212	77.74058	8.81706
Shanghai	0.35348	4291.54063	65.50985	0.00007	2.18768	1.47908
Jiangsu	0.58290	18,198.78578	134.90288	0.00000	0.00001	0.00307
Zhejiang	0.56100	17,154.77353	130.97623	0.00022	21.99573	4.68996
Anhui	0.10377	2265.71143	47.59949	0.00016	22.42324	4.73532
Fujian	0.09960	1620.21954	40.25195	0.00111	23.02546	4.79849
Jiangxi	0.02990	418.17833	20.44941	0.00379	87.44515	9.35121
Shandong	0.05872	8440.11959	91.87012	0.00079	390.75954	19.76764
Henan	0.09288	5285.62259	72.70229	0.00044	71.24126	8.44045
Hubei	0.02366	925.55176	30.42288	0.00067	47.80071	6.91381
Hunan	0.02203	868.42598	29.46907	0.00159	102.13969	10.10642
Guangdong	0.18586	78,816.83292	280.74336	0.00051	175.82555	13.25992
Guangxi	0.02157	688.26442	26.23479	−0.00005	24.98931	4.99893
Hainan	0.26425	53.91894	7.34295	0.00006	0.07449	0.27293
Chongqing	0.02812	453.15321	21.28740	0.00070	2.61682	1.61766
Sichuan	0.02669	2253.60230	47.47212	0.00064	151.31722	12.30111
Guizhou	0.00000	0.00000	0.00001	0.00078	25.06643	5.00664
Yunnan	0.00858	350.20840	18.71386	0.00005	48.79165	6.98510
Shaanxi	0.13403	1985.82231	44.56257	0.00071	8.36057	2.89147
Gansu	0.01780	182.81707	13.52099	0.00009	0.46562	0.68236
Qinghai	0.08828	25.76667	5.07609	0.00148	0.73092	0.85494
Ningxia	0.01259	13.25353	3.64054	0.00149	2.46583	1.57030
Xinjiang	0.05300	1411.59057	37.57114	0.00126	33.53680	5.79110
Average	0.13720	13,952.33714	62.88588	0.00080	51.25512	5.65801

By adding the relevant control variables to consider the multiple factors of the LS-SVM-FM at two times, it helps to understand the aspects confirmed in the above analysis. Tables 3 and 4 shows the forecasting performance of LS-SVM-FM (2), with REE and GDP per capita, urbanization level, population density; Tables 5 and 6 shows the forecasting performance of LS-SVM-FM (3), with medical supply and technical level factors, based on the former one. As presented in Tables 3–6, other information on economic population and supplementary information on medical supply and technical level helps to better understand the potential relationship between CLPH and REE in China when constructing an empirical forecasting model.

Firstly, incorporating the six control variables enables the model to obtain better results. LS-SVM-FM (3) and LS-SVM-FM (2) show better or higher forecasting accuracies than LS-SVM-FM (1). LS-SVM-FM (3) is the best one based on all the values of MPE, MSE, and SDE for CLPH in most provinces or cities in China. For example, the minimum averages of MPE are 0.06%, 0.05% 0.12%, 13.72%, and 0.08% and as are the values of MSE and SDE. This can be attributed to the control variables to provide better information for machine learning methods in order to identify more realistic mapping relationships in high-dimensional spaces.

Secondly, the main findings in Tables 3–6 present similar results as those in Tables 1 and 2. The other reason for the overall continuously improved prediction effect is that the radial basis kernel function better describes the above relationship, and it can take into account the linear and nonlinear relationships between multiple explanatory variables to the greatest possible extent. The 7 explanatory variables (eco-efficiency and 6 control variables) and the one-to-one regression for the 30 selected regions of China established high requirements for the sample size. Because there are only 15 years of data, the traditional panel model fitting and prediction effects were limited. However, the method proposed in this paper only needs to find the support vectors due to the advantage of the conversion of the high-dimensional space, but with extra data or information still needed. At the same time, the powerful calculation and learning capabilities make up for the limited data.

Thirdly, the NOHE of CLPH owns the bigger prediction errors for MPE, MSE, and DSE in the three models than the other four. Some points can explain some of the reasons. For example, the raw data of health examinations fluctuated greatly in 2007, especially in the Shaanxi Province. In addition, as well as the factors already considered, the health examinations may be related to the medical insurance system in China and medical process of medical and health institutions, and further research is required.

4.2. Forecasting Variation with the Single Factor and Multiple Factors

The previous section gave specific prediction accuracies and a corresponding direct analysis. However, when actually predicting the CLPH, in addition to the annual forecast performance and change, scholars also arouse attention to how the changes in forecast errors shift across the time dimension, including changes in averages (average degree) and changes in variance (variation degree), that is to say, how the MPE, MSE, and SDE change according to time. At the province level, it was shown that the values of the averages and standard deviations of MPE, MSE, and SDE for each of the five proxy variables of the changes in local public health levels in China. Furthermore, it can be learned that the concentration trend and degree of dispersion of the forecast error change, based on which the reliability and robustness of the models can be analyzed.

As is shown in Tables 5 and 6, for the forecasting variation of the LS-SVM-FM in China, LS-SVM-FM (3) outperformed LS-SVM-FM (1) and LS-SVM-FM (2) with the greatest number of average degrees and variation degrees for all five variables of the CLPH. The minimum value of each line is marked with bold font, which represents the overall variation in the forecast error at the province or city level. The prediction accuracies of some provinces or cities are very high, and for some others are very small, but the overall prediction accuracy is acceptable for LS-SVM-FM (1), LS-SVM-FM (2), and LS-SVM-FM (3). Taking LS-SVM-FM (3) as an example, the lowest value of average degree is about 0.00060 (change in MPE) for VTH of CLPH, 0.00012 (change in MSE) for OWET, and 0.007099 (change in SDE) for OWET, and the lowest values of variation degree are about 0.00061 (change in MPE) for OWET, 0.00032 (change in MSE) for OWET, and 0.00808 (change in SDE) for OWET.

By comparing the average degrees and variation degrees of prediction errors such as MPE, MSE, and SDE, from the global perspective, LS-SVM-FM (3), taking into account all six control variables, was more reliable and has a higher relative robustness than LS-SVM-FM (1) and LS-SVM-FM (2), although the other two models are also acceptable within a certain range of prediction accuracy. Meanwhile, the forecast volatility of NI, NOHE, and PD significantly expanded, so it is the best choice to make short-term or spot predictions on the above three dimensions of the CLPH.

5. Discussion

5.1. Main Revelation

REE affects the CLPH through intermediaries that are integrated and represented by the economic and environmental impacts from the inputs or outputs of computing the REE at the provincial level in China. Specifically speaking, green sustainable development is to improve eco-efficiency and encourage consumers, producers, and managers to avoid

excessive pollution [12]. The continuous increase in green behaviors in work and life has improved the living environment on which residents depend. Under the premise of ensuring environmental protection, economic achievements improve the disposable income for living standards and medical conditions and reduce pollution in living environments and guarantee a reduction in disease.

The calculated prediction results can be used as the basis for evaluating the specific social effects of adopting sustainable development strategies by local enterprises or individuals. Making residents' living or health conditions better is one of the most fundamental pursuits of a higher REE in each province or city. Local inhabitants are the ultimate maintainers and beneficiaries. Therefore, empirical findings by forecasting CLPH via REE could serve as a tool to evaluate the performance of REE-related policy formulation and activity implementation and find out the actual effects and deficiencies that need to be addressed to guide sustainable development practices.

The innate differences and respective characteristics between provinces in China are an important material for explaining the imbalance of spatial medical demand and supply distribution. For example, there are three economic and demographic factors and three medical supply and technical level factors to reflect regional heterogeneity. These factors show why the real situations of CLPH and the magnitudes of change are different across different provinces, and the above six factors explain the different effects of increasing REE promotion on local CLPH, although there are other individual, behavioral, climatic, psychological, and even political factors for CLPH such as nutrition, climate change, noise, institutional determinants, medical insurance, and so on. However, considering the quite limited data availability from micro-individual statistics, it is necessary to investigate what the interactions are between the economy, environment, and local public health at the overall macro- and meso-levels.

5.2. Policy Implications

To be more specific, this study is very helpful for decision-makers in each province of China to understand and optimize the allocation of medical resources. With the help of the early information on CLPH obtained with the right proposed model, which can forecast VTH, OWET, NI, NOHE, and PD with a high prediction accuracy in 30 provinces or cities of China, decision-makers can take this as the quantization basis to confront some urgent emergencies via a continuous supply of medical supplies. It is an important guarantee for changes in local public health.

Taking VTH as an example, in addition to the general medical supplies, different departments of VTH require independent professionals and medical resources, and more advanced forecasts provide time and a quantitative basis for the production, purchase, and storage of various medicines, disinfectants, or medical tools, from a general point of view. Combining the whole forecast for VTH with the ratios of all the sub-departments on average, there will be more evidence to distinguish the most important demand or emergency, and the expensive medical supplies to be purchased from others. As it is shown in Figures 3, S1 and S2, the Departments of Internal Medicine, Chinese Medicine, Surgery, Obstetrics and Gynecology, and Pediatrics ranked in the top five, which reflects the differentiated needs and the five most common problems in residents' health. It seems obvious that the medical resources required by the five departments vary greatly. The treatment methods of the Department of Chinese Medicine have more Chinese characteristics. The medicines are concentrated in Chinese herbal medicines. The production and use of medicines and rehabilitation training require special medical equipment (acupuncture equipment, medical Tuina, etc.). In addition, the requirements for medical equipment for testing, diagnosis, or even treatment between Departments of Internal Medicine and Surgery vary widely with a higher accuracy. The Department of Pediatrics have higher requirements for the various ingredients of drugs, which are different from those for adults, as are the mentioned medical staff and job requirements in different professional directions. Therefore, these top five need to be given enough attention according to the real conditions

of the 30 selected regions in China, and plans should be made about the following aspects, including enough medical workers, prepared medical resources, and earlier cooperation with upstream and downstream enterprises.

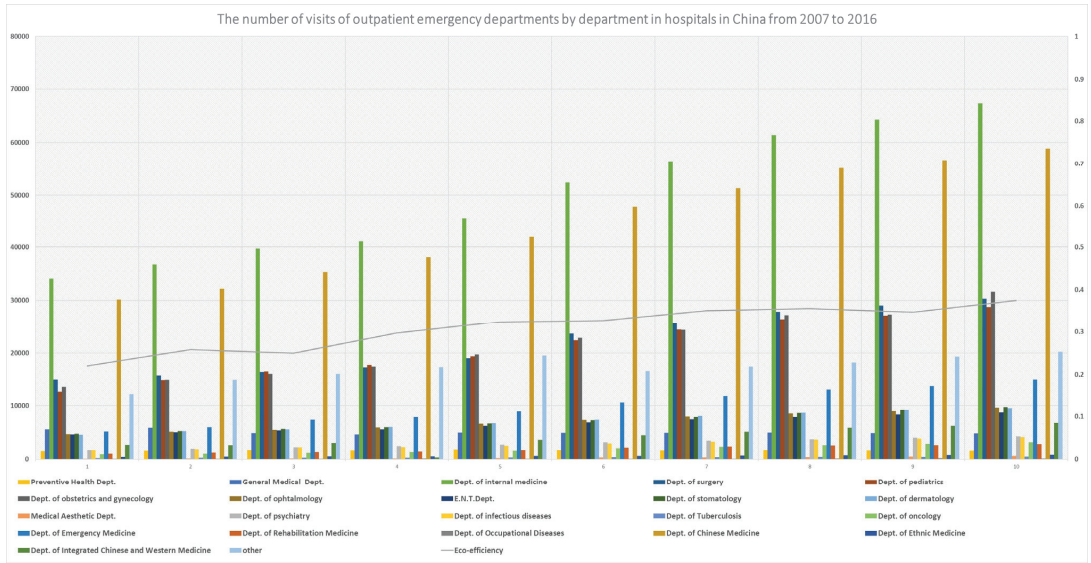


Figure 3. Comparison by department of visits to outpatient emergency departments in China.

From the perspective of risk and early warning, related forecasting results can be used as an important reference for early warning and risk identification in public health. Taking VTH as an example, more detailed comparisons of different sub-departments between regions are attached in the Supplementary Material. Obtaining the regional heterogeneity of CLPH in the figures through our predictions, based on the perspectives of local residents' eating habits, disposable incomes, and population density, decision-makers can formulate local medical material reserve methods and emergency medical incident response plans. As the figures show, for the top five sub-departments with high numbers of visits that are urgently needed in various regions, policy or tax support can be provided to promote the healthy development of the related industries in the long run. For short-term fluctuations in individual provinces or cities, certain consultation or coordination mechanisms can be adopted between other regions to deploy medical personnel and materials to increase efficiency and reduce the waste of resources, just as that in Guangdong, Shandong, and Shanxi. As a whole, forecasting results from the other four indicators—OWET, NI, NOHE, and PD—can also be utilized as with the above analysis with some specific auxiliary information. Accurate predictions from the above five dimensions can help to detect residents' medical conditions. The primary advantage of the above results is that they can optimize medical supplies and personnel in various regions in time and grasp the overall situation of different types of medical needs. For example, according to the need changes in OWET, inpatients, health examinations, and patients discharged, the medical industry can dynamically adjust the supply and reserves of materials, reduce inventory, and minimize waste and excessive use of medical resources, and especially important medicines and instruments that are in short supply and have a long production cycle.

From the perspective of decision optimization, through findings on the control variables and how to calculate the required indicators of regional eco-efficiency, we can learn a differentiated path to improve public health in different regions. When adopting economic policies and measures for local sustainable development for improving the REE, they should consider regional differences and be possible to adjust to the most urgent and

corresponding factors that affect CLPH in real-time, according to their own economic development level. Furthermore, it is helpful to strengthen regional cooperation to optimize the allocation of medical resources. These main findings can guide the industry or the government to strengthen the close cooperation between upstream and downstream enterprises in the medical industry. Accurate forecasting guarantees that there is enough time to carry out the following work: technical cooperation that breaks through key technical bottlenecks, resource coordination that reduces overall risks, and personnel exchanges that share prevention experience.

6. Conclusions

6.1. Main Findings

REE is a highly synthetic indicator with integrated economic and environmental impacts that is associated with local CLPH. Considering that there are multiple factors affecting CLPH in addition to REE, such as the implicit and uncertain relationship between the two, regional characteristics, and low data availability, this paper investigated how to forecast CLPH using REE by utilizing the LR-SVM-FM and acquire empirical evidence utilizing the regional province-level data in China.

Taking REE as the main predictor and province-level data in China, this paper investigated how five proxy variables of CLPH were predicted, with different control variables including more economic and demographic factors and three more medical supply and technical level factors. Some interesting empirical findings were that (1) REE is a good predictor for predicting residents' health, whether in a single-factor situation or a multi-factor situation. (2) The proxy indicators that measure the health status of residents have different prediction effects. The prediction accuracy of VTH, OWET, and NI is relatively high and the volatility is lower and more stable throughout the whole forecasting period. (3) Utilizing three economic and demographic factors and three medical supply and technical level factors can improve forecasting performance. (4) The LR-SVM-FM based on machine learning meets the forecasting needs: regional heterogeneity of provinces and cities in China, limited samples, uncertain functional relationships, etc.

As explained and proposed earlier, the results show that (1) REE is a comprehensive indicator that combines the dual impacts of the economy and the environment, which are also important factors that affect residents' health conditions. (2) The proposed prediction model relying on the machine learning method can better characterize the uncertain and complex relationship between different regions and multiple influencing factors with limited samples. (3) Six control variables from economic factors, technical factors, and demographic factors improve the model with a higher degree of explanation, which is more in line with the real phenomenon.

6.2. Future Research

This article tried to conduct interdisciplinary research by forecasting CLPH using regional eco-efficiency with integrated economic and environmental impacts. Future research based on this could include searching for more micro-individuals and psychological indicators, or happiness indexes, to improve prediction models; quantifying the impacts of regional interactions on the prediction effect; and understanding how medical emergencies and responses to them can be influenced by the prediction performance.

Supplementary Materials: The following supporting information can be downloaded at <https://www.mdpi.com/article/10.3390/ijerph20021381/s1>. Table S1: main variables of the SBM to calculate the regional eco-efficiency; Figure S1: the number of visits of outpatient emergency departments by sub-department in hospitals in China; and Figure S2: the number of visits of outpatient emergency departments by sub-department in hospitals in China.

Author Contributions: Conceptualization, X.W., Z.M. and J.C.; Data curation, X.W. and Z.M.; Formal analysis, X.W., Z.M. and J.D.; Funding acquisition, X.W. and Z.M.; Investigation, X.W. and Z.M.; Methodology, X.W. and Z.M.; Resources, X.W. and Z.M.; Supervision, X.W., Z.M., J.C. and J.D.;

Software, X.W., J.C. and Z.M.; Validation, Z.M., X.W. and J.D.; Visualization, X.W. and Z.M.; Writing—original draft preparation, X.W. and Z.M.; Writing—review and editing, X.W. and Z.M. All authors have read and agreed to the published version of the manuscript.

Funding: This research was funded by the Chongqing Social Science Planning Doctor and Cultivation Project (2020PY41) and the Project of National Natural Science Foundation of China under grant No. 71671019; the Chongqing Basic Research and Frontier Exploration Project of 2019 (Chongqing Natural Science Foundation), grant No. cstc2019jcyj-msxmX0592; the Science and Technology Research Project of Chongqing Municipal Education Commission, grant No. KJQN201900503; and the Chongqing Normal University Ph.D. Startup Fund Project, grant No. 19XLB001.

Institutional Review Board Statement: Not applicable.

Informed Consent Statement: Not applicable.

Data Availability Statement: Not applicable.

Conflicts of Interest: The authors declare no conflict of interest. The funders had no role in the design of the study; in the collection, analysis, or interpretation of data; in the writing of the manuscript; or in the decision to publish the results.

References

1. Koehler, D.A.; Bennett, D.H.; Norris, G.A.; Spengler, J.D. Rethinking environmental performance from a public health perspective—A comparative industry analysis. *J. Ind. Ecol.* **2005**, *9*, 143–167. [[CrossRef](#)]
2. Soltani, S.A.; Overcash, M.R.; Twomey, J.M.; Esmaili, M.A.; Yildirim, B. Hospital Patient-Care and Outside-the-Hospital Energy Profiles for Hemodialysis Services: Report of Two Cases. *J. Ind. Ecol.* **2015**, *19*, 504–513. [[CrossRef](#)]
3. Han, C.L.; Han, K.; Wang, S.S.; Hu, X.H. *Combination Forecast on Health Status of Residents in China*; IEEE: New York, NY, USA, 2016. [[CrossRef](#)]
4. Wang, K.; Wang, J.Y.; Hubacek, K.; Mi, Z.F.; Wei, Y.M. A cost-benefit analysis of the environmental taxation policy in China: A frontier analysis-based environmentally extended input-output optimization method. *J. Ind. Ecol.* **2020**, *24*, 564–576. [[CrossRef](#)]
5. Cimprich, A.; Santillan-Saldivar, J.; Thiel, C.L.; Sonnemann, G.; Young, S.B. Potential for industrial ecology to support healthcare sustainability: Scoping review of a fragmented literature and conceptual framework for future research. *J. Ind. Ecol.* **2019**, *23*, 1344–1352. [[CrossRef](#)]
6. Ramaswami, A.; Weible, C.; Main, D.; Heikkilä, T.; Siddiki, S.; Duvall, A.; Pattison, A.; Bernard, M. A Social-Ecological-Infrastructural Systems Framework for Interdisciplinary Study of Sustainable City Systems An Integrative Curriculum Across Seven Major Disciplines. *J. Ind. Ecol.* **2012**, *16*, 801–813. [[CrossRef](#)]
7. Niero, M.; Hauschild, M.Z.; Hoffmeyer, S.B.; Olsen, S.I. Combining Eco-Efficiency and Eco-Effectiveness for Continuous Loop Beverage Packaging Systems Lessons from the Carlsberg Circular Community. *J. Ind. Ecol.* **2017**, *21*, 742–753. [[CrossRef](#)]
8. Cucurachi, S.; Schiess, S.; Froemelt, A.; Hellweg, S. Noise footprint from personal land-based mobility. *J. Ind. Ecol.* **2019**, *23*, 1028–1038. [[CrossRef](#)]
9. Alstone, P.; Lai, P.; Mills, E.; Jacobson, A. High Life Cycle Efficacy Explains Fast Energy Payback for Improved Off-Grid Lighting Systems. *J. Ind. Ecol.* **2014**, *18*, 722–733. [[CrossRef](#)]
10. Ooi, G.L. Urbanization in southeast Asia—Assessing policy process and progress toward sustainability. *J. Ind. Ecol.* **2007**, *11*, 31–42. [[CrossRef](#)]
11. Liang, Z.; Zhang, M.; Mao, Q.; Yu, B.; Ma, B. Improvement of Eco-Efficiency in China: A Comparison of Mandatory and Hybrid Environmental Policy Instruments. *Int. J. Environ. Res. Public Health* **2018**, *15*, 1473. [[CrossRef](#)]
12. Wang, Y.; Sun, M.; Wang, R.; Lou, F. Promoting regional sustainability by eco-province construction in China: A critical assessment. *Ecol. Indic.* **2015**, *51*, 127–138. [[CrossRef](#)]
13. Ranis, G.; Stewart, F.; Ramirez, A. Economic growth and human development. *World Dev.* **2000**, *28*, 197–219. [[CrossRef](#)]
14. Kondilis, E.; Giannakopoulos, S.; Gavana, M.; Ierodiakonou, I.; Waitzkin, H.; Benos, A. Economic Crisis, Restrictive Policies, and the Population’s Health and Health Care: The Greek Case. *Am. J. Public Health* **2013**, *103*, 973–980. [[CrossRef](#)]
15. Johannesson, M.; Jonsson, B. Economic-evaluation in health-care—Is there a role for cost-benefit-analysis. *Health Policy* **1991**, *17*, 1–23. [[CrossRef](#)]
16. Simou, E.; Koutsogeorgou, E. Effects of the economic crisis on health and healthcare in Greece in the literature from 2009 to 2013: A systematic review. *Health Policy* **2014**, *115*, 111–119. [[CrossRef](#)]
17. Catalano, R.; Goldman-Mellor, S.; Saxton, K.; Margerison-Zilko, C.; Subbaraman, M.; LeWinn, K.; Anderson, E. The health effects of economic decline. *Annu. Rev. Public Health* **2011**, *32*, 431–450. [[CrossRef](#)]
18. Watt, R.G. Emerging theories into the social determinants of health: Implications for oral health promotion. *Community Dentist. Oral Epidemiol.* **2002**, *30*, 241–247. [[CrossRef](#)]
19. Chakraborty, S. Endogenous lifetime and economic growth. *J. Econ. Theory* **2004**, *116*, 119–137. [[CrossRef](#)]
20. Strauss, J.; Thomas, D. Health, nutrition, and economic development. *J. Econ. Lit.* **1998**, *36*, 766–817.

21. Ahnquist, J.; Wamala, S.P.; Lindstrom, M. Social determinants of health—A question of social or economic capital? Interaction effects of socioeconomic factors on health outcomes. *Soc. Sci. Med.* **2012**, *74*, 930–939. [[CrossRef](#)]
22. Lu, Z.N.; Chen, H.Y.; Hao, Y.; Wang, J.Y.; Song, X.J.; Mok, T.M. The dynamic relationship between environmental pollution, economic development and public health: Evidence from China. *J. Clean. Prod.* **2017**, *166*, 134–147. [[CrossRef](#)]
23. Harper, S. Economic and social implications of aging societies. *Science* **2014**, *346*, 587–591. [[CrossRef](#)] [[PubMed](#)]
24. Suhrcke, M.; Stuckler, D. Will the recession be bad for our health? It depends. *Soc. Sci. Med.* **2012**, *74*, 647–653. [[CrossRef](#)]
25. Giles-Corti, B.; Vernez-Moudon, A.; Reis, R.; Turrell, G.; Dannenberg, A.L.; Badland, H.; Foster, S.; Lowe, M.; Sallis, J.F.; Stevenson, M.; et al. City planning and population health: A global challenge. *Lancet* **2016**, *388*, 2912–2924. [[CrossRef](#)] [[PubMed](#)]
26. Dimitrova, R.; Danchoviski, V.; Egova, E.; Vladimirov, E.; Sharma, A.; Gueorguiev, O.; Ivanov, D. Modeling the Impact of Urbanization on Local Meteorological Conditions in Sofia. *Atmosphere* **2019**, *10*, 366. [[CrossRef](#)]
27. Castaneda, H.; Holmes, S.M.; Madrigal, D.S.; Young, M.E.D.; Beyeler, N.; Quesada, J. Immigration as a Social Determinant of Health. In *Annual Review of Public Health*; Fielding, J.E., Ed.; Annual Reviews: Palo Alto, CA, USA, 2015; Volume 36, pp. 375–392.
28. Ruel, E.; Oakley, D.; Wilson, G.E.; Maddox, R. Is Public Housing the Cause of Poor Health or a Safety Net for the Unhealthy Poor? *J. Urban Health* **2010**, *87*, 827–838. [[CrossRef](#)]
29. Haines, A.; Kovats, R.S.; Campbell-Lendrum, D.; Corvalan, C. Climate change and human health: Impacts, vulnerability and public health. *Public Health* **2006**, *120*, 585–596. [[CrossRef](#)]
30. Frumkin, H.; Bratman, G.N.; Breslow, S.J.; Cochran, B.; Kahn, P.H.; Lawler, J.J.; Levin, P.S.; Tandon, P.S.; Varanasi, U.; Wolf, K.L.; et al. Nature Contact and Human Health: A Research Agenda. *Environ. Health Perspect.* **2017**, *125*, 18. [[CrossRef](#)]
31. Li, Y.; Chiu, Y.-h.; Lu, L.C. Energy and AQI performance of 31 cities in China. *Energy Policy* **2018**, *122*, 194–202. [[CrossRef](#)]
32. Kelly, F.J.; Fussell, J.C. Air pollution and public health: Emerging hazards and improved understanding of risk. *Environ. Geochem. Health* **2015**, *37*, 631–649. [[CrossRef](#)]
33. Jerrett, M.; Arain, A.; Kanaroglou, P.; Beckerman, B.; Potoglou, D.; Sahuvaroglu, T.; Morrison, J.; Giovis, C. A review and evaluation of intraurban air pollution exposure models. *J. Expo. Anal. Environ. Epidemiol.* **2005**, *15*, 185–204. [[CrossRef](#)] [[PubMed](#)]
34. Turnock, S.T.; Butt, E.W.; Richardson, T.B.; Mann, G.W.; Reddington, C.L.; Forster, P.M.; Haywood, J.; Crippa, M.; Janssens-Maenhout, G.; Johnson, C.E.; et al. The impact of European legislative and technology measures to reduce air pollutants on air quality, human health and climate. *Environ. Res. Lett.* **2016**, *11*, 10. [[CrossRef](#)]
35. Wang, X.P.; Mauzerall, D.L. Evaluating impacts of air pollution in China on public health: Implications for future air pollution and energy policies. *Atmos. Environ.* **2006**, *40*, 1706–1721. [[CrossRef](#)]
36. Yu, T.; Wang, W.; Ciren, P.; Zhu, Y. Assessment of human health impact from exposure to multiple air pollutants in China based on satellite observations. *Int. J. Appl. Earth Obs. Geoinf.* **2016**, *52*, 542–553. [[CrossRef](#)]
37. Gao, J.H.; Woodward, A.; Vardoulakis, S.; Kovats, S.; Wilkinson, P.; Li, L.P.; Xu, L.; Li, J.; Yang, J.; Li, J.; et al. Haze, public health and mitigation measures in China: A review of the current evidence for further policy response. *Sci. Total Environ.* **2017**, *578*, 148–157. [[CrossRef](#)] [[PubMed](#)]
38. Pope, C.A.; Dockery, D.W. Health effects of fine particulate air pollution: Lines that connect. *J. Air Waste Manag. Assoc.* **2006**, *56*, 709–742. [[CrossRef](#)]
39. Bernstein, J.A.; Alexis, N.; Barnes, C.; Bernstein, I.L.; Bernstein, J.A.; Nel, A.; Peden, D.; Diaz-Sanchez, D.; Tarlo, S.M.; Williams, P.B. Health effects of air pollution. *J. Allergy Clin. Immunol.* **2004**, *114*, 1116–1123. [[CrossRef](#)]
40. Dominici, F.; Peng, R.D.; Barr, C.D.; Bell, M.L. Protecting Human Health from Air Pollution Shifting from a Single-pollutant to a Multipollutant Approach. *Epidemiology* **2010**, *21*, 187–194. [[CrossRef](#)]
41. Halden, R.U. Plastics and Health Risks. In *Annual Review of Public Health*; Fielding, J.E., Brownson, R.C., Green, L.W., Eds.; Annual Reviews: Palo Alto, CA, USA, 2010; Volume 31, pp. 179–194.
42. Thompson, R.C.; Moore, C.J.; vom Saal, F.S.; Swan, S.H. Plastics, the environment and human health: Current consensus and future trends. *Philos. Trans. R. Soc. B-Biol. Sci.* **2009**, *364*, 2153–2166. [[CrossRef](#)]
43. Thriene, B. Garbage incineration plants—Planning, organisation and operation from health point of view. *Gesundheitswesen* **2004**, *66*, 827–832. [[CrossRef](#)]
44. Chen, H.Y.; Teng, Y.G.; Lu, S.J.; Wang, Y.Y.; Wang, J.S. Contamination features and health risk of soil heavy metals in China. *Sci. Total Environ.* **2015**, *512*, 143–153. [[CrossRef](#)] [[PubMed](#)]
45. Woon, K.S.; Lo, I.M.C. An integrated life cycle costing and human health impact analysis of municipal solid waste management options in Hong Kong using modified eco-efficiency indicator. *Resour. Conserv. Recycl.* **2016**, *107*, 104–114. [[CrossRef](#)]
46. Langdon, K.A.; Chandra, A.; Bowles, K.; Symons, A.; Pablo, F.; Osborne, K. A preliminary ecological and human health risk assessment for organic contaminants in composted municipal solid waste generated in New South Wales, Australia. *Waste Manag.* **2019**, *100*, 199–207. [[CrossRef](#)] [[PubMed](#)]
47. Jarup, L. Hazards of heavy metal contamination. *Br. Med. Bull.* **2003**, *68*, 167–182. [[CrossRef](#)]
48. Tong, S.; von Schirnding, Y.E.; Prapamontol, T. Environmental lead exposure: A public health problem of global dimensions. *Bull. World Health Organ.* **2000**, *78*, 1068–1077.
49. Li, Z.Y.; Ma, Z.W.; van der Kuijp, T.J.; Yuan, Z.W.; Huang, L. A review of soil heavy metal pollution from mines in China: Pollution and health risk assessment. *Sci. Total Environ.* **2014**, *468*, 843–853. [[CrossRef](#)]

50. Hu, H.; Jin, Q.; Kavan, P. A Study of Heavy Metal Pollution in China: Current Status, Pollution-Control Policies and Countermeasures. *Sustainability* **2014**, *6*, 5820–5838. [[CrossRef](#)]
51. Rootes, C. Environmental movements, waste and waste infrastructure: An introduction. *Environ. Polit.* **2009**, *18*, 817–834. [[CrossRef](#)]
52. Saravanan, V.S.; Mavalankar, D.; Kulkarni, S.P.; Nussbaum, S.; Weigelt, M. Metabolized-Water Breeding Diseases in Urban India: Sociospatiality of Water Problems and Health Burden in Ahmedabad City. *J. Ind. Ecol.* **2015**, *19*, 93–103. [[CrossRef](#)]
53. Hanjra, M.A.; Blackwell, J.; Carr, G.; Zhang, F.H.; Jackson, T.M. Wastewater irrigation and environmental health: Implications for water governance and public policy. *Int. J. Hyg. Environ. Health* **2012**, *215*, 255–269. [[CrossRef](#)]
54. Qadir, M.; Wichelns, D.; Raschid-Sally, L.; McCormick, P.G.; Drechsel, P.; Bahri, A.; Minhas, P.S. The challenges of wastewater irrigation in developing countries. *Agric. Water Manag.* **2010**, *97*, 561–568. [[CrossRef](#)]
55. Afroz, R.; Banna, H.; Masud, M.M.; Akhtar, R.; Yahaya, S.R. Household's perception of water pollution and its economic impact on human health in Malaysia. *Desalin. Water Treat.* **2016**, *57*, 115–123. [[CrossRef](#)]
56. Pawlowicz, E.T. Organic pollution of water and human health. *Health Probl. Civiliz.* **2017**, *11*, 32–39. [[CrossRef](#)]
57. Saha, N.; Rahman, M.S.; Ahmed, M.B.; Zhou, J.L.; Ngo, H.H.; Guo, W.S. Industrial metal pollution in water and probabilistic assessment of human health risk. *J. Environ. Manag.* **2017**, *185*, 70–78. [[CrossRef](#)] [[PubMed](#)]
58. Azizullah, A.; Khattak, M.N.K.; Richter, P.; Hader, D.P. Water pollution in Pakistan and its impact on public health—A review. *Environ. Int.* **2011**, *37*, 479–497. [[CrossRef](#)]
59. Tone, K. A slacks-based measure of efficiency in data envelopment analysis. *Eur. J. Oper. Res.* **2001**, *130*, 498–509. [[CrossRef](#)]
60. Du, J.; Liang, L.; Zhu, J. A slacks-based measure of super-efficiency in data envelopment analysis: A comment. *Eur. J. Oper. Res.* **2010**, *204*, 694–697. [[CrossRef](#)]
61. Huang, J.; Xia, J.; Yu, Y.; Zhang, N. Composite eco-efficiency indicators for China based on data envelopment analysis. *Ecol. Indic.* **2018**, *85*, 674–697. [[CrossRef](#)]
62. Yang, L.; Zhang, X. Assessing regional eco-efficiency from the perspective of resource, environmental and economic performance in China: A bootstrapping approach in global data envelopment analysis. *J. Clean. Prod.* **2018**, *173*, 100–111. [[CrossRef](#)]
63. Tay, F.E.H.; Cao, L.J. Application of support vector machines in financial time series forecasting. *Omega-Int. J. Manag. Sci.* **2001**, *29*, 309–317. [[CrossRef](#)]
64. Vapnik, V.; Golowich, S.E.; Smola, A. Support vector method for function approximation, regression estimation, and signal processing. In *Advances in Neural Information Processing Systems 9: Proceedings of the 1996 Conference, Denver, CO, USA, 2–5 December 1996*; Mozer, M.C., Jordan, M.I., Petsche, T., Eds.; MIT Press: Cambridge, MA, USA, 1997; Volume 9, pp. 281–287.
65. Vlastakis, N.; Dotsis, G.; Markellos, R.N. Nonlinear modelling of European football scores using support vector machines. *Appl. Econ.* **2008**, *40*, 111–118. [[CrossRef](#)]
66. Cortes, C.; Vapnik, V. Support-vector networks. *Mach. Learn.* **1995**, *20*, 273–297. [[CrossRef](#)]
67. Suykens, J.A.K.; Vandewalle, J. Least squares support vector machine classifiers. *Neural Process. Lett.* **1999**, *9*, 293–300. [[CrossRef](#)]
68. Brooks, J.P. Support Vector Machines with the Ramp Loss and the Hard Margin Loss. *Oper. Res.* **2011**, *59*, 467–479. [[CrossRef](#)]
69. Wang, X.; Ma, Z.; Dong, J. Quantitative Impact Analysis of Climate Change on Residents' Health Conditions with Improving Eco-Efficiency in China: A Machine Learning Perspective. *Int. J. Environ. Res. Public Health* **2021**, *18*, 12842. [[CrossRef](#)]

Disclaimer/Publisher's Note: The statements, opinions and data contained in all publications are solely those of the individual author(s) and contributor(s) and not of MDPI and/or the editor(s). MDPI and/or the editor(s) disclaim responsibility for any injury to people or property resulting from any ideas, methods, instructions or products referred to in the content.

Article

Evaluating Smart Home Services and Items: A Living Lab User Experience Study

Eugene Seo¹ and Wanseok Yang^{2,*}¹ Department of Architecture, College of Engineering, Kwangwoon University, Seoul 01897, Republic of Korea² Department of Architecture and Architecture Engineering, Seoul National University, Seoul 08826, Republic of Korea

* Correspondence: diryws25@hanmail.net

Abstract: South Korea is expected to become a super-aged society by 2025, when more than 20% of its population will be aged 65 and over. One possible solution for minimizing the socioeconomic burden posed by this aging trend is smart home technology, which can be used to support older adults' daily routines. In this study, the aim is to suggest the direction of development on smart home technology and products to enhance our understanding of service and item needs for the optimal commercialization of smart homes for users. A living lab was set up to research the experience of using smart home technology in real environments. To obtain intuitive and specific evaluations, visitors of varying ages tested each item and living space and responded to a five-point scale questionnaire on importance (recognition) and performance (satisfaction). The recognition and satisfaction for each smart home item or service were then evaluated using basic statistical analysis, importance-performance analysis, and factor analysis using SPSS. It was determined that the importance and performance evaluations of smart home services and items differed by age group. The scores for the two categories exhibited evident similarities in the older adult group. More similarities were found in the evaluation of performance than importance across age groups. The results show that different age groups agree that the development of services/items that can constantly and automatically check residents' health status should be prioritized.

Citation: Seo, E.; Yang, W. Evaluating Smart Home Services and Items: A Living Lab User Experience Study. *Buildings* **2023**, *13*, 263. <https://doi.org/10.3390/buildings13010263>

Academic Editors: Roberto Alonso González Lezcano, Francesco Nocera, Rosa Giuseppina Caponetto and Koen Steemers

Received: 28 November 2022
Revised: 29 December 2022
Accepted: 13 January 2023
Published: 16 January 2023



Copyright: © 2023 by the authors. Licensee MDPI, Basel, Switzerland. This article is an open access article distributed under the terms and conditions of the Creative Commons Attribution (CC BY) license (<https://creativecommons.org/licenses/by/4.0/>).

Keywords: smart home; user evaluation; smart technology; smart item; IPA analysis; factor analysis

1. Introduction

South Korea is facing a fundamental demographic shift, with exceptional growth in the older adult population. In 2022, 9.018 million people, or 17.5% of the total population, were aged 65 or older [1]. Furthermore, South Korea has been ranked the fastest aging among 11 countries—the others being Japan, Canada, the United States, Italy, Australia, Spain, Germany, France, the United Kingdom, and Austria—with 7–14% (aging society) and 14–20% (aged society) of the population reaching the age of at least 65 in 18 years and 7 years, respectively [2]. According to the National Assembly Budget Office, owing to this rapid population aging, the cost of supporting older adults will increase from 21.8% in 2020 to 58.2% in 2040 [3]. The corresponding increase in pension and medical welfare spending will pose a heavy strain on society. Against this background, researchers and industries are studying various ways to offer older adults daily life support, one of which is the development of smart home technologies that automate the monitoring of daily living and wellbeing [4,5].

The concept of a smart home offering new services can be traced back to futuristic display homes in 1930s America, developed at a time when electricity consumption was unproblematic and presenting [6]:

... unprecedented levels of luxury, relaxation, and indulgence, with excessive the benefits of modern living with less effort from householders [7].

The concept remained a specialized one for some time, only able to take shape for a mass market in the final quarter of the 20th century as computing power became increasingly accessible and automated appliances more commonplace [6].

The barrier of entry for the usage of smart products with the latest technology tends to be high for older adults, whom many companies and studies are targeting as the main user class [8,9]. On the contrary, although the present youth and middle-aged groups can expect to have relatively high levels of familiarity with electronic devices even in old age, investigations into their demands and needs are presently lacking. The current study addresses these issues. The aim is to provide a better understanding of prospective users' needs for smart homes (services and devices). This study is an attempt to broaden the existing understanding through user evaluations of two categories, focusing on empirical evidence regarding users' perceptions and not just understanding the preference for smart homes and technology. For smart homes to succeed, we need to understand the recognition and demands of prospective users.

An accurate grasp of the support requirements and preferences of prospective users will help set the direction of development on smart products and technology, minimizing risks for both research and businesses. Thus, it is necessary to prepare for the upcoming aging society through extensive research not only on current older adults but also the middle-aged and youth.

The next three questions identify prospective users' perceptions of smart homes and broaden the understanding of the direction in which smart home services should develop:

Q1. *How do prospective users perceive various smart home technologies?*

Q2. *How do prospective users evaluate various smart home technologies?*

Q3. *Is the evaluation of smart home technology aligned with users' perceptions?*

Each of these questions is answered through the analysis of survey data ($n = 628$). A survey of smart home services and device assessment provides insight into how demand varies by prospective users. It showcases an important perspective in shaping age-friendly smart home services.

2. Literature Review and Methodology

2.1. Smart Homes

The smart home originated from building automation technology. The development of the first smart automation system paved the way for smart homes in 1966 [7]. Indeed, the affordability of innovative technology was improved with the development of the microcontroller in 1971 [10]. Additionally, the introduction of gerontechnology in the smart home field proved a milestone intervention in improving the quality of life of older adults in the 1990s [11,12].

Smart home technology became very popular at the dawn of the 21st century. The advancement in information and communications technology, artificial intelligence, and the Internet of Things (IoT) have resulted in a massive transformation of the housing sector. Nowadays, introducing technological support to homes has become a global phenomenon [13,14]. In the last decades, there have been many discussions regarding integrating smart home and service devices in the smart technology and smart home sector. Many researchers have expressed interest in developing smart spaces in living environments [15–18].

Despite the increasing number of studies, research in this field is confined to three themes. First, studies do not typically consider the multidimensionality of the concept of the smart home, leading to a one-sided representation of its implications, services, and user segments [4,19–21]. Chan et al. (2008) attempted to cover the technical state of various smart home projects and established a comprehensive understanding of the current and future challenges that smart homes and smart technologies brought to users. The authors pointed out the tendency to describe the potential benefits of technology while ignoring the users' viewpoint and following a product-centric approach. According to them, the

prevailing technological focus of existing research explains the low acceptance of smart homes in the market [20,22].

Second, studies tend to examine smart homes from a technological perspective, by focusing on the functions of devices and the infrastructure and architecture of automated homes [23–26]. Several technological aspects of the smart home are covered in recent papers, including the connection with IoT, reasoning systems, fog-based computing approach, and risks. Recently, one of the main advantages of smart home technologies highlighted across smart home research is the optimization of energy consumption [20,27–30] and the resulting environmental sustainability [19,31,32]. In particular, intelligent sensors, wireless fidelity, load modeling, real-time systems, and computational modeling are identified as emerging knowledge domains in the field of smart homes [13,33–35].

Third, the majority of studies discuss the potential advantages of smart home technology [36,37] while providing little empirical evidence regarding users' perceptions of challenges and benefits [20]. Despite all the potential and prospective growth, the spread of smart home technology, in general, has been slower than expected [14,27,38–43]. Thus, users' perceptions of smart homes need to be deeply investigated to accelerate their adoption and diffusion [14,20,28,40,44]. An intention–behavior gap has been identified in recent research, meaning there is a lacuna between consumers' estimation and their actual behavior regarding the purchase or use of smart home technologies [14,41,45,46]. Understanding users' adoption process beyond perceptions is, therefore, essential [43,47,48]. The author felt the need to include this dimension while conducting smart home living lab research. Therefore, this study is expected to deepen that understanding with the analysis of user perceptions and effects through the experiences of smart home services and devices.

2.2. Materials and Methods

After conducting a primary questionnaire survey regarding simple preferences for smart homes (services and items) [9], we considered a more detailed survey for this study, particularly regarding whether there may be a difference between the evaluation of preference and behaviors in future choices. This study was conducted using survey contents that distinguish importance (recognition of service/item) and performance (satisfaction upon which the choice of service/item is based). In other words, in the importance evaluation, although the user's general recognition affects the result, their decision regarding actual purchases may be different. Thus, even if the importance evaluation score is high, it may not be a proper user evaluation if only a few of them lead to choose (consumption, etc.).

For this series of studies, a selection of service cases on smart home items within the current technical scope was researched and collected; subsequently, a living lab where visitors could experience and evaluate the use of these items in a space resembling a real residence was created. This is because it can be difficult to perform an actual evaluation of product utility without experiencing its use. This approximately 200 square meter living lab was constructed in April 2018 at a university in South Korea. As shown in Figure 1, it consists of a bedroom, open living room, and kitchen, similar to the spatial structures of South Korean apartments. However, the bathroom was designed in such a way as to differentiate it from existing spaces to enable the proposal of new scenarios. Even though people do not actually reside in living labs, the spaces were planned according to the layout of the average home. The functionality of each space was then matched with applicable smart home services/items. The entire complex space consisted of “residing space+IoT+active smart service,” and the linked items were designed to allow visitors to experience the actual operation of the space. Thus, prospective users' evaluation was designed to be practical and experience-based to enable the effective assessment and prediction of actual smart service and item demand.

The smart home services and items were based on a thorough investigation of various cases, technologies, and items that have already been developed but have not yet been subjected to universalization. From these, services and items (front door, bedroom, toilet, hallway, kitchen, and living room) were selected based on the characteristics of daily

residential behavior (Table 1). These items and services for a comfortable and safe living can be classified according to four categories (Table 2) devised by the Korea Smart Home Industry Association: comfortable life, safe life, economic life, and joyful life. “Comfortable life” is relevant to convenience and management in daily life; “safe life” is relevant to health maintenance and emergency management; “economic life” is relevant to eco-friendliness, energy production, and efficiency; and “joyful life” is relevant to entertainment, such as sociocultural aspects and shopping.

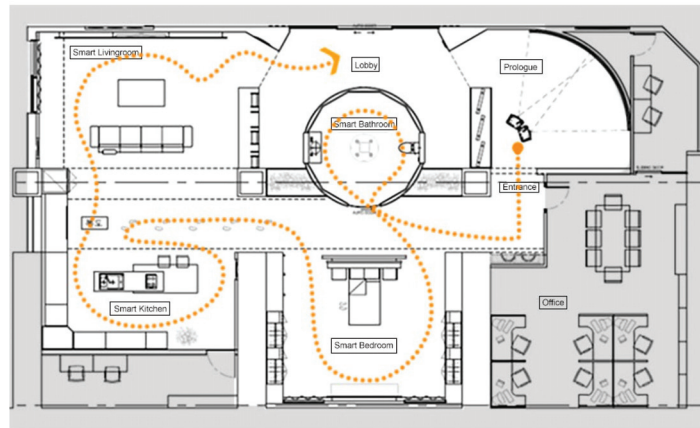


Figure 1. Smart home living lab (w/ tour path).

Table 1. Resident behavior.

Daily Behavior (Indoor)	
Eating	Getting Dressed
Meals	Clothes
Snacks	Laundry
Cooking	
Rest	Mobility
Sleeping	Walking
Napping	Standing (sitting)
Bathing and Hygiene	Communicate
Bathing	Talking
Showering	Using the Internet
Washing up	Other
Elimination	Exercise
Cleaning	Study/learning
	Taking medicine

The living lab items were as follows (Table 3): (1) daily living support services and items: check-in/last check at the entrance; smart lighting, bed, and curtains in the bedroom; water temperature display in the bathroom; and countertop height control in the kitchen, (2) health care services and items: body composition analysis/smart toilet in the bathroom; nutrition care (refrigerator) in the kitchen; and gait analysis in the corridor, and (3) emergency and safety response service and items: auto ventilation in the kitchen and fall management/pill reminder in the living room. Owing to the premise that the services and items in the living lab exhibit functions within a simulated residential space, there were limitations concerning the “economy” (eco-friendly, etc.) and “joy” (leisure, etc.) items among the aforementioned four categories [9].

Table 2. Smart home value classification [9].

Life	Category	Service
Comfort	Daily life support convenience management	<ul style="list-style-type: none"> Schedule for management and provision of daily life information, such as the weather. Support for various living conditions, such as finding lost items and doing household chores. Coordination of video calls with family and friends. Facilitation of leisure through digital devices. Management of lighting.
	Health care	<ul style="list-style-type: none"> Body signal detection, such as blood pressure, pulse, and blood sugar. Health measurement and management. Identification of disease and management of diabetes through bowel analysis. Provision of medication dosage and administration times.
Safety	Emergency and safety management	<ul style="list-style-type: none"> Smart door lock and active emergency response service. Control services for infants, older adults, people with disabilities, and pets.
	Eco-friendly energy management	<ul style="list-style-type: none"> Smart green home. Pro-energy power generation system. Smart home-based energy and management services.
Joy	Leisure Culture	<ul style="list-style-type: none"> Bidirectional shopping. Social activity/entertainment.

Importance–performance analysis (IPA) (Figure 2), an evaluation method that simultaneously compares and analyzes the importance and performance (satisfaction) assigned by the user with regard to the evaluation target, was employed. Since its introduction by James and Martilla (1977) as a methodology used mainly in the management field, IPA has been applied in research studies on services [49] and planning elements [50,51]. IPA can help grasp the relative value assigned by the user to the evaluated object, showing the satisfaction and importance of certain factors as perceived by future consumers based on the placement of each factor in one of four quadrants on an XY coordinate plane (Figure 2). Therefore, it is useful for distinguishing underdeveloped elements from those that have undergone excessive development (investment). In particular, it can help determine the areas for future maintenance and improvement through the evaluation of objects that have been used before.

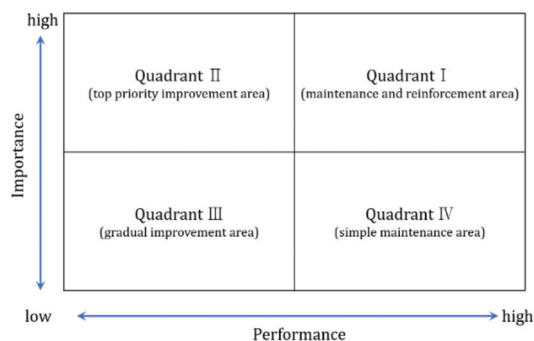





Figure 2. IPA quadrant sections.

Table 3. Smart items in the smart home living lab [9].

Location	Item Name	Item Contents	Importance (a)	Performance (b)	(b) SD	Energy Optimization
Entrance	(A) Check-in	Where walking aids, essential for older adults, are placed in designated locations, check-in services are provided. The lights are adjusted when people enter the house, and a guiding voice is heard.	4.02	3.29	1.455	▲
	(B) Last check	Before the user leaves the house, (B) informs the user of an item's location (w/ location sensor) that must be packed on screen at the entrance. The day's weather and primary schedule can also be checked on screen.	4.43	4.15	1.141	▲
	(C) Light control	When the resident falls asleep with the lights on, the lighting system senses this event and turns off the lights. When a resident goes to the bathroom during sleeping hours, or suddenly wakes up and moves, the light turns on at a muted level, to avoid blinding the resident in the dark.	4.36	4.22	1.082	▲
Bedroom	(D) Bed control	(D) is a motion bed, modified to fit the resident's body shape and posture, and facilitates sound sleep through links with sensors on the ceiling that detect sleep.	4.31	4.14	1.161	
	(E) Curtain control	The sensor recognizes when a resident enters the room and opens and sets the curtain in advance.	3.83	3.66	1.315	
	(F) Body composition analysis	When a resident stands in front of the bathroom sink, the floor sensor measures the body composition and compares it with (past) data. Through smart mirrors, the resident can obtain important health information, such as body composition analysis and health care advice.	4.54	4.36	1.007	
Bathroom	(G) Water temperature color	The sensor visually identifies the temperature, with red for hot water and blue for cold water. The resident can check for their desired temperature visually without touching the water.	3.96	3.78	1.294	
	(H) Smart toilet	The pressure sensor on the floor identifies the user and analyzes their excretion. With information accumulated every day, changes and abnormalities in the body can be immediately identified through smart mirrors.	4.41	4.27	1.082	
	(I) Countertop height control	During extended cooking and washing of dishes, the heights of the countertops adjust to suit users based on the floor pressure and the distance from the ceiling.	4.35	4.15	1.180	
Kitchen	(J) Auto ventilation	When the hood alone lacks ventilation, or if the resident does not detect air pollution, (J) automatically opens the window and operates the ventilation fan.	4.20	4.08	1.208	▲
	(K) Nutrition	A customized diet is recommended according to nutrition and ingestion conditions and based on food ingredients. (K) shows the nutrition information and recipes of recommended menus on a screen and helps encourage ideal eating habits and nutrition management. Provision of information, such as recipes and nutrients.	4.12	3.94	1.195	
Corridor	(L) Gait analysis	Pressure sensors on the floor, and motion sensors on the ceiling and walls, check the resident's gait. Users can check information using display items. The resident's gait width, pressure, and knee angle are checked to help prevent arthritis.	3.97	3.69	1.331	

Table 3. Cont.

Location	Item Name	Item Contents	Importance (a)	Importance (a) SD	Performance (b)	Performance (b) SD	Energy Optimization
Living room	(M) Fall management	(M) detects indoor falls and accidents and sends emergency rescue signals to the outside world. In case of an emergency, voice guidance activates a speaker throughout the house, and signals an emergency call for outside help. Emergency signals are sent, together with indoor video information by prior consent, which are linked to emergency number 119, and released from the security system to facilitate rescue efforts.	4.50	0.887	4.13	1.226	
	(N) Pill reminder	For proper medication management, the service informs the resident of their medication administration time. The location of the medicine bottle is also illuminated, and guidance on the type of medicine is provided by voice.	4.23	0.993	3.92	1.225	
Mean			4.23	1.01	3.99	1.21	
Daily life support service and product							
Health maintenance service and product							
Emergency and safety response service and product							

One of the challenges of this study is the evaluation of unfamiliar smart items or services that have never been used. We expected that the public (not experts) would have difficulty in separately evaluating importance and performance. Even after visitors have experienced the use of smart home services and items in the living lab, it would not be easy for them to distinguish between the concepts of importance and performance. Therefore, we attempted to overcome these limitations in the survey by delivering a simple but clear question: to control variables, a survey was conducted on the premise that smart services and items were at an “appropriate price level.”

Q1. “How important do you think this item is (for future housing)?”

Q2. “Are you willing to install this item in your home?”

The first question, regarding the importance of the product for future housing, can be understood as intuitive and a reflection of recognition by the visitor. The response was used as an indicator of ideal importance and general recognition among different age groups. The second question related to performance and visitor satisfaction (upon which the choice of service/item is based). The visitors would answer the second question by evaluating the product regarding their satisfaction and willingness to pay for it. Thus, in the IPA, the answer to the first question was used as a measure of importance and the answer to the second question served as a measure of performance.

Subsequently, factor analysis was conducted to reveal any differences between the importance and performance (I–P) evaluation. Factor analysis uses mathematical procedures for the simplification of interrelated measures to discover patterns in a set of variables [52]. Attempting to discover the simplest method of interpretation of observed data is known as parsimony, and this is essentially the aim of factor analysis [53]. Factor analysis operates on the notion that measurable and observable variables can be reduced to fewer unobservable latent variables that share a common variance, known as reducing dimensionality [54]. These unobservable factors are not directly measured but are essentially hypothetical constructs used to represent variables [55]. The two main factor analysis techniques are exploratory factor analysis (EFA) and confirmatory factor analysis. Confirmatory factor analysis attempts to confirm hypotheses and uses path analysis diagrams to represent variables and factors, whereas EFA tries to uncover complex patterns by exploring the dataset and testing predictions [52]. EFA is used when a researcher wants to discover the number of factors influencing variables and to analyze which variables “go together” [55]. A basic hypothesis of EFA is that there are “m” common “latent” factors to be discovered in the dataset, and the goal is to find the smallest number of common factors that will account for the correlations [56].

Factor analysis is now used in many fields, such as behavioral and social sciences, medicine, economics, and geography, because of technological advancements [57]. Large datasets that consist of several variables can be decreased by observing “groups” of variables (i.e., factors)—that is, factor analysis assembles common variables into descriptive categories [57]. Factor analysis is suitable for studies that involve a few or hundreds of variables, items from questionnaires, or a battery of tests that can be reduced to a smaller set, to get at an underlying concept and to facilitate interpretation [58]. As it is easier to focus on some key factors rather than having to consider too many variables that may be trivial, factor analysis is useful for placing variables into meaningful categories [57,58]. Many other uses of factor analysis include data transformation, hypothesis testing, mapping, and scaling [58]. The recommended sample size is at least 300 participants, and the variables that are subjected to factor analysis should each have at least 5–10 observations [59]. A factor loading for a variable is a measure of how much the variable contributes to the factor; thus, high factor loading scores indicate that the dimensions of the factors are better accounted for by the variables [57]. In this study, 628 samples were used and all items were analyzed based on a factor loading of 0.40 or more. With factor analysis, it could be inferred which factors and underlying concepts influenced the evaluation of the two questions.

3. Assessment

3.1. Statistical Preparation and Descriptive Statistics

Visitors to the living lab from September 2019 were asked to experience the use of its smart items, and then to evaluate their importance and performance based on a five-point scale. A total of 628 data points were collected, and the visitors were distinguished by age as follows (Table 4): the young (under 40 years old; 189 data points), the middle-aged (over 40 years old and under 59 years old; 279 data points), and older adults (over 60 years old; 160 data points). Individual or group visitors experienced the living lab based on the instructions of a guide in the order of entrance (in)–toilet–bedroom–corridor–kitchen–living room–entrance (out). After the guided tour, each visitor took a comfortable look at the smart home and had time to manipulate services and items. They then answered a questionnaire at the end of the experiment. In the subsequent analysis of the questionnaire, insincere responses, and those wherein all questions were graded with the same score, were excluded.

Table 4. Characteristics of visitor.

Categories		Number of Responses	Ratio
Total		628	100%
Age	20–39	189	30%
	40–59	279	44%
	60+	160	26%

As a result of the survey, the Cronbach’s α value of importance was 0.899, whereas that of performance was 0.916, indicating that the items were reliable. The average importance score, for a total of 14 smart home service and item questions, was 4.23 points, based on a five-point scale evaluation. Among these, the highest importance score was 4.53 points for (F) body composition analysis (bathroom), followed by 4.50 points for (M) fall management (living room) and 4.42 points for (B) last-check (entrance). The below-average scores were 4.20 points for (J) auto ventilation (kitchen), 4.12 points for (K) nutrition care (kitchen), 4.01 points for (A) check-in (entrance), 3.97 points for (L) gait analysis (kitchen), 3.96 points for (G) water temperature color (bathroom), and 3.83 points for (E) smart curtains (bedroom). The standard deviation for each item was 0.86–1.17 or less, indicating that the deviations between visitors were not significant and that the visitors had similar experiences and evaluations (Table 3).

Meanwhile, the average performance score, for a total of 14 smart home service and item questions, was 3.99 points, based on a five-point scale evaluation; this score was lower than that for importance. Among these, the highest performance score was 4.36 points for (F) body composition analysis (bathroom), followed by 4.27 points for (H) smart toilet (bathroom), and 4.22 points for (C) light control (bedroom). The below-average scores were 3.94 points for (K) nutrition care (kitchen), 3.92 points for (N) pill reminder, 3.78 points for (G) water temperature color (bathroom), 3.69 points for (L) gait analysis (kitchen), 3.66 points for (E) smart curtains, and 3.29 points for (A) check-in. The standard deviation for each item ranged from 1.00 to 1.45 or less and had a bigger range than that for the importance value. The largest difference between the importance and performance scores was 0.72 points for (A) check-in, whereas the smallest difference was 0.12 points for (J) auto ventilation. When age was not considered, the overall high-scoring items in the importance and performance categories were those related to health maintenance. By contrast, items with low scores were related to daily living support (Table 3).

3.2. IPA

IPA was performed based on the average values, that is, 4.2 and 3.7, of the importance and performance scores, respectively, to analyze the marketability of the services/items in the smart living lab (Figure 3). Quadrant I encompassed the categories of items requiring constant maintenance owing to their high importance and satisfaction: (B) last check, (C)

light control, (D) bed control, (F) body composition analysis, (H) smart toilet, (I) countertop height control, (M) fall management, and (N) pill reminder. Quadrant II encompassed high-importance but low-performance items. None of the products and services evaluated in this study were included in this quadrant. Quadrant III encompassed items characterized as having both low importance and low performance: (A) check-in, (E) curtain control, (G) water temperature color, and (L) gait analysis. Finally, Quadrant IV encompassed items with relatively high performance compared to their importance: (J) auto ventilation (boundary line) and (K) nutrition care.

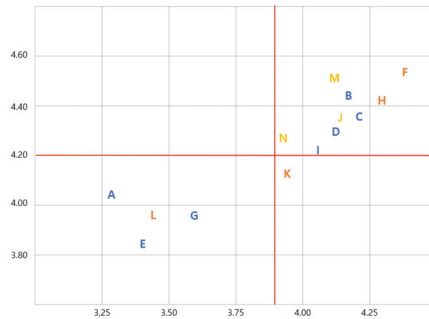


Figure 3. IPA (all age groups).

Subsequently, the entire IPA graph was distinguished by age group for a more accurate analysis, as follows.

- **Young Group (Table 5)**

Table 5. Statistics (young group).

	I-Value	p-Value	I-P
(A) Check-in	3.7	2.62	1.08
(B) Last check	4.19	4.16	0.17
(C) Light control	4.2	4.13	0.07
(D) Bed control	4.23	4.17	0.06
(E) Curtain control	3.67	3.48	0.19
(F) Body composition analysis	4.57	4.32	0.25
(G) Water temperature color	3.59	3.41	0.18
(H) Smart toilet	4.23	4.04	0.19
(I) Countertop height control	4.29	4.13	0.16
(J) Auto ventilation	4.00	3.92	0.08
(K) Nutrition care refrigerator	4.01	3.86	0.15
(L) Gait analysis	3.6	3.14	0.46
(M) Fall management	4.44	3.68	0.76
(N) Pill reminder	4.33	3.57	0.62
Daily-life support service and item			
Health maintenance service and item			
Emergency and safety response service and item			

The average score for importance was 4.07, whereas that for performance was 3.75. In the young group, item categories F, M, N, and I scored high in importance, whereas G, L, E, and A scored low in importance. In the same age group, item categories F, D, B, and I scored high in performance, whereas A, L, G, and E scored low in performance. Although the orders were different, item categories A, L, G, and E remained in the lower ranks for both importance and performance. Furthermore, L did not seem appealing to young visitors. Among all items, it consistently had the lowest score in the I-P evaluations.

For all items, importance scores were greater than performance scores, with A, M, N, and L exhibiting the largest differences between the two scores. The I–P value of these items (A, M, N, L) was more than twice the other values. More specifically, category A was for users of walking aids, M referred to detectors for residents at risk of falling, N was for users who need to constantly take their medicines without forgetting, and G referred to services that check for walking posture. Even though there were no distinctly common characteristics among these items and services, it may be speculated that the users of these items had a high possibility of being older adults. In other words, these can be said to be items with distinct characteristics that support frailness due to gerontification.

Based on the IPA results for the young group (Figure 4), Quadrant I encompassed B, C, D, F, H, and I, which include daily living support services and items and a few for health maintenance. Quadrant II, defined as a top-priority improvement area, encompassed M and N, which are emergency and safety response services and items. Quadrant III, defined as a gradual improvement area, encompassed A, E, G, and L, which include daily living support services and items and a few health maintenance services and items, as in quadrant I. Lastly, quadrant IV, defined as a simple maintenance area, encompassed J and K, which are health maintenance and emergency and safety response services and items.

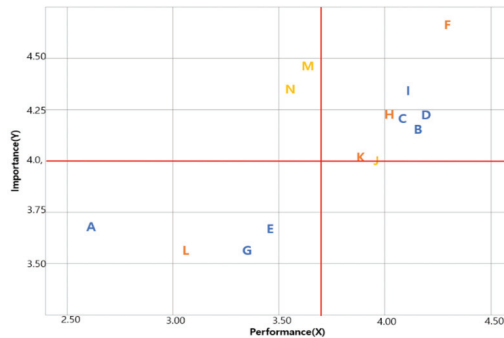


Figure 4. IPA (young group).

- Middle-aged Group (Table 6)

Table 6. Statistics (middle-aged).

	I-Value	p-Value	I–P
(A) Check-in	4.15	3.48	0.67
(B) Last check	4.44	4.06	0.38
(C) Light control	4.44	4.27	0.17
(D) Bed control	4.44	4.21	0.23
(E) Curtain control	3.97	3.79	0.18
(F) Body composition analysis	4.62	4.48	0.14
(G) Water temperature color	4.15	3.94	0.21
(H) Smart toilet	4.54	4.41	0.13
(I) Countertop height control	4.44	4.21	0.23
(J) Auto ventilation	4.27	4.18	0.09
(K) Nutrition care refrigerator	4.21	3.98	0.22
(L) Gait analysis	4.20	3.97	0.23
(M) Fall management	4.54	4.31	0.23
(N) Pill reminder	4.24	4.03	0.21

The average score for importance was 4.34, whereas that for performance was 4.10. In the middle-aged group, item categories F, M, H, and B scored high in importance, whereas L, A, G, and E scored low in importance. In the same age group, item categories F, H, M, and C scored high in performance, whereas L, G, E, and A scored low in performance.

Moreover, for all items, importance scores were greater than performance scores. The lower-ranking item categories for the middle-aged and young groups were the same (A, E, G, L); however, the upper-ranking item categories were different. A, E, and G were the least appealing items for the middle-aged group and consistently exhibited the lowest scores in the I–P evaluations. With regard to the I–P values, A and B exhibited the largest differences, more than twice the other values. Quite notably, the middle-aged and young groups were similar in this regard, that is, item category A had the largest I–P value.

Based on the IPA results for the middle-aged group (Figure 5), Quadrant I encompassed C, D, F, H, I, and M, which included daily living support services and items and a few for health maintenance. Quadrant II, defined as a top-priority improvement area, encompassed B as its sole item. Quadrant III, defined as a gradual improvement area, encompassed A, E, G, L, and N, mainly for daily living support. However, with regard to health maintenance and emergency and safety response services and items, the trends were mixed. Lastly, quadrant IV encompassed J as its sole item, which was also included in the same quadrant for the youth group.

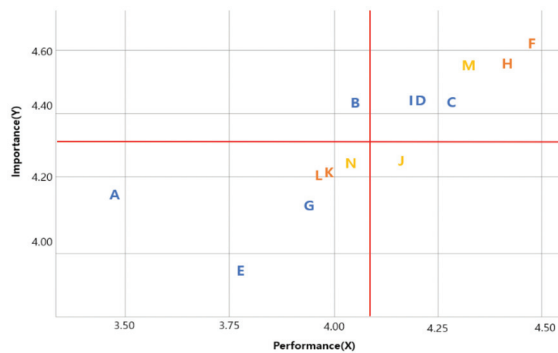


Figure 5. IPA (middle-aged group).

- **Older Adult Group (Table 7)**

Table 7. Statistics (older adults).

	I-Value	p-Value	I–P
(A) Check-in	4.15	3.72	0.43
(B) Last check	4.47	4.28	0.19
(C) Light control	4.36	4.2	0.16
(D) Bed control	4.15	3.91	0.24
(E) Curtain control	3.73	3.62	0.12
(F) Body composition analysis	4.33	4.19	0.14
(G) Water temperature color	4.07	3.88	0.19
(H) Smart toilet	4.34	4.26	0.08
(I) Countertop height control	4.36	4.05	0.31
(J) Auto ventilation	4.08	4.08	0
(K) Nutrition care refrigerator	4.09	3.89	0.2
(L) Gait analysis	3.94	3.8	0.14
(M) Fall management	4.47	4.31	0.16
(N) Pill reminder	4.07	4.12	−0.05

The average score for importance was 4.19, whereas that for performance was 4.02. In the older adult group, item categories B, M, C, I, and H scored high in importance, whereas G, N, L, and E scored low in importance. In the same age group, item categories M, B, H, and C scored high in performance, whereas G, L, A, and E scored low in performance. For this age group, it seemed that the two categories began to exhibit more evident similarities. In the older adult group, the importance value was not always greater than the performance

value, unlike in the other age groups. N and J were the item categories with the highest performance values, while E, L, and G were the least appealing and consistently exhibited the lowest scores in the I–P evaluations, as in the middle-aged group. Moreover, A and I exhibited the largest differences in I–P values. Quite notably, all three age groups had this characteristic in common, that is, item category A consistently exhibited the largest I–P value for all groups.

Based on the IPA results for the older adult group (Figure 6), Quadrant I encompassed B, C, F, H, I, and M, whereas quadrant II encompassed none of the tested items. Quadrant III, defined as a gradual improvement area, encompassed A, D, E, G, K, and L, mainly for daily living support. Lastly, quadrant IV encompassed J and N. Noticeably, item category J was consistently in this quadrant for all three age groups.

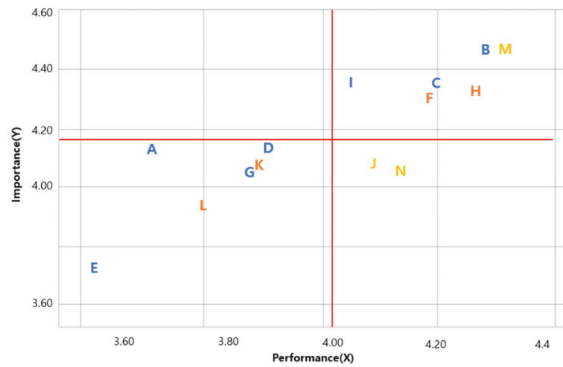


Figure 6. IPA (older adult group).

3.3. I–P Factor Analysis

Factor analysis was used to infer differences in evaluation by age group and varimax rotation was adopted to simplify the factor placement. To broaden the understanding of the difference between I–P evaluations, all items were analyzed based on a factor loading of 0.40 or more. The resulting Kaiser–Meyer–Olkin value was 0.908, and the significant probability for Bartlett’s test of sphericity was 0.000, appropriate for the model [60] (Table 8).

Table 8. Factor analysis (all age groups).

Importance	Performance	
	1	2
(N) Pill reminder	0.734	0.169
(H) Smart toilet	0.708	0.246
(M) Fall management	0.688	0.165
(F) Body composition analysis	0.675	0.256
(L) Gait analysis	0.642	0.251
(K) Nutrition care refrigerator	0.614	0.287
(E) Curtain control	0.075	0.765
(C) Light control	0.190	0.742
(D) Bed control	0.245	0.685
(A) Check-in	0.292	0.534
(B) Last check	0.283	0.525
(I) Countertop height control	0.369	0.512
(G) Water temperature color	0.469	0.476
(J) Auto ventilation	0.443	0.462
(F) Body composition analysis	0.772	0.285
(H) Smart toilet	0.758	0.185
(K) Nutrition care refrigerator	0.659	0.325
(N) Pill reminder	0.588	0.108
(J) Auto ventilation	0.555	0.342
(L) Gait analysis	0.549	0.090
(G) Water temperature color	0.525	0.317
(C) Light control	0.234	0.748
(E) Curtain control	0.148	0.741
(D) Bed control	0.430	0.674
(B) Last check	0.103	0.496
(I) Countertop height control	0.442	0.494
(A) Check-in	0.034	0.216
(M) Fall management	0.492	0.090

Extraction method: principal component analysis.
Varimax with Kaiser normalization.

Total	% variation	% cumulative	Total	% variation	% cumulative
3.585	25.61	25.61	3.548	25.341	25.341
3.181	22.72	48.33	2.566	18.326	43.668
			1.997	14.263	57.931

For All Groups: The results of factor analysis for all visitors are shown in Table 8. As all factors had a load value of 0.4 or higher, they could each be classified as a corresponding factor. With this result, it could be assumed that in their I–P evaluations, visitors perceived two categories related to “health” and “daily living.” Furthermore, health-related (including emergency response) services and items were considered a more significant factor than daily living related. However, J, G, and M were regarded as singularities in the attribute classification part of the factor analysis. In the importance factor analysis, it was understandable for J to be classified with a daily living support item group. On the contrary, the classification of G as a health-related item group was rather ambiguous.

Meanwhile, A and M were classified as third factors relevant to performance. It could be speculated that the third factors (A and M) were designed for older adults: specifically, those who use a walking aid and those who have a risk of falling indoors. In all groups, the results of the factor analysis relevant to importance showed that the classification of health-related (i.e., health maintenance, emergency response) and daily living support items affected the assessment.

Factor analyses for the age groups are as follows:

- **Young Group**

The results of the factor analysis for the young group are shown in Table 9. As B had a load value under 0.4 in the first analysis, it was eliminated, and the analysis was performed again. This group exhibited the largest number of factors out of the three age groups: a four-factor configuration for importance and three-factor configuration for performance. Daily living support items were demonstrated to be clearly independent in this factor analysis. Based on the most important first configuration, it can be inferred that the results of the factor analysis relevant to importance were more about emergency situations, whereas the results of the factor analysis relevant to performance were more about daily health care.

Table 9. Factor analysis (young group).

	Importance					Performance		
	1	2	3	4		1	2	3
N	0.736	−0.020	0.234	−0.045	F	0.830	0.087	0.119
M	0.679	0.035	0.108	−0.020	H	0.748	0.189	0.102
K	0.640	0.138	0.134	0.132	K	0.599	0.417	0.218
L	0.613	−0.057	0.260	0.237	D	0.522	−0.080	0.464
J	0.588	0.247	−0.126	0.299	M	0.143	0.817	0.056
E	−0.041	0.780	0.125	0.217	N	0.297	0.724	0.086
A	0.413	0.691	−0.029	−0.202	A	−0.122	0.681	0.255
C	−0.033	0.615	0.119	0.465	L	0.403	0.474	0.082
G	0.109	0.461	0.454	0.159	J	0.381	0.412	0.224
H	0.122	0.177	0.838	−0.031	C	0.017	0.121	0.820
F	0.306	−0.021	0.694	0.140	E	0.088	0.167	0.738
I	0.217	−0.014	0.119	0.761	I	0.255	0.080	0.587
D	0.054	0.290	0.015	0.700	G	0.204	0.281	0.426
Total	% variation		% cumulative		Total	% variation		% cumulative
2.478	19.060		19.060		2.426	18.658		18.658
1.877	14.435		33.495		2.402	18.474		37.132
1.603	12.334		45.829		2.16	16.641		53.773
1.585	12.191		58.019					

As a result of factor analysis relevant to performance, if health and emergency sectors were considered to have similar characteristics, D and A can be understood to be singularities. Given the results of the first configuration (of factor analysis relevant to performance), D may be regarded as a health-related service/item by the young group. On the contrary, the second-factor configuration in the factor analysis relevant to performance includes

services/items related to gerontification. Item categories A, M, N, and L were mentioned in the previous sections as a noticeable configuration related to the I-P value. They were mentioned as having “no distinctly common characteristics,” but it may be predicted that the older adults were the main target users. In this configuration, J was determined to be a singularity.

- **Middle-aged Group:**

The results of the factor analysis for the middle-aged group are shown in Table 10. As all factors had a load value of 0.4 or higher, they could each be classified as a corresponding factor. For this group, each factor configuration for importance and performance had one less factor than the young group, that is, three factors for importance and two for performance.

Table 10. Factor analysis (middle-aged group).

	Importance				Performance	
	1	2	3		1	2
H	0.847	0.202	0.030	C	0.755	0.115
F	0.735	0.307	0.119	D	0.737	0.254
M	0.670	0.149	0.223	E	0.705	0.119
N	0.628	0.286	0.321	K	0.670	0.312
L	0.615	0.235	0.316	F	0.647	0.411
K	0.542	0.272	0.312	H	0.629	0.367
C	0.278	0.799	0.009	J	0.614	0.360
D	0.316	0.766	−0.020	G	0.609	0.351
E	0.115	0.647	0.350	I	0.570	0.332
I	0.213	0.561	0.325	A	0.049	0.747
J	0.331	0.504	0.377	M	0.350	0.712
G	0.411	0.430	0.353	L	0.302	0.669
A	0.212	0.157	0.824	B	0.299	0.591
B	0.229	0.112	0.803	N	0.454	0.584
Total		% variation	% cumulative	Total	% variation	% cumulative
	3.400	24.286	24.286	4.458	31.842	31.842
	2.788	19.913	44.199	3.057	21.838	53.680
	2.186	15.618	59.817			

According to the configuration in the factor analysis relevant to importance, health-related items (H, F, M, N, L, K) and daily living support items (C, D, E, I, G, A, and B) were clearly independent among the middle-aged group. In the second configuration, J was distinguished by a singularity.

On the contrary, the results of the factor analysis relevant to performance were more complicated and mixed. In particular, the first-factor configuration for performance was difficult to infer. Meanwhile, the second-factor configuration for performance was almost the same as the second-factor configuration (performance: M, N, A, L, and J) for the young group, presumed to be related to gerontification. Item categories A, M, N, and L were mentioned in the previous sections as a noticeable configuration related to the I-P value and to the second-factor configuration of performance for the young group.

- **Older Adult Group**

The results of the factor analysis for the older adult group are shown in Table 11. As all factors had a load value of 0.4 or higher, they could each be classified as a corresponding factor. For this age group, the number of factors for importance and performance was the same as for the middle-aged group: three factors for importance and two for performance. The similarity between the two scoring categories was higher than for the other age groups.

Table 11. Factor analysis (older adult group).

	Importance			Performance		
	1	2	3	1	2	
K	0.823	0.097	0.153	F	0.801	0.152
F	0.787	0.202	0.167	K	0.752	0.154
G	0.732	0.246	0.225	G	0.749	0.266
H	0.574	0.500	0.287	N	0.716	0.186
L	0.533	0.332	0.195	H	0.706	0.304
I	0.494	0.313	0.390	L	0.667	0.238
N	0.292	0.786	0.047	M	0.612	0.408
M	0.247	0.780	0.196	I	0.607	0.374
J	0.207	0.648	0.325	J	0.571	0.482
E	0.137	0.104	0.787	D	0.565	0.562
A	0.265	0.046	0.660	E	0.208	0.755
C	0.218	0.398	0.616	B	0.249	0.751
D	0.433	0.261	0.586	A	0.104	0.664
B	0.056	0.467	0.555	C	0.465	0.572
Total		% variation	% cumulative	Total	% variation	% cumulative
	3.206	22.901	22.901	4.943	35.309	35.309
	2.673	19.096	41.998	3.059	21.852	57.161
	2.607	18.621	60.619			

For each item category, although the orders according to the factor values were slightly different, the overall factor classification compositions and trends were very similar. For the older adult group, factor analysis relevant to importance clearly revealed three categories (daily living, health maintenance, emergency and safety). In this factor analysis, daily living support items were clearly independent but were a third-factor configuration, not a priority consideration factor. Furthermore, G and I were distinguished from the daily living category. Instead, they were assigned to the health-related (including emergency) factor configuration. G refers to sensors that show the water temperature using color, whereas I refers to a height controller for countertops. Thus, it could be carefully inferred that older adults perceived these services as health-related, because these items provide aid for their vulnerability. Moreover, the first and second configurations in the factor analysis relevant to importance converged into the first configuration in the factor analysis relevant to performance.

4. Discussion

IPA helps understand, interpret, and amplify the “lived experiences” of the research participants and make their experiences meaningful. However, IPA has been criticized for being mostly descriptive and not sufficiently interpretative [61–63]. Thus, we tried to interpret unobservable latent variables that IPA analysis could not present with factor analysis.

In IPA analysis, we conceptually linked “importance” to “recognition” and “performance” to “satisfaction.” As mentioned previously, the two categories (importance and performance) began to exhibit more evident similarities with the aging of the prospective users. Therefore, as the users became older, their evaluations of importance and performance began to achieve consensus. Moreover, for all groups, H and M appeared at the top of importance evaluations, whereas C and F appeared at the top of performance evaluations. D had a high appeal for the youth and middle-aged groups, but not older adults. On the contrary, H and M had a high appeal for the middle-aged and older adult groups, but not for the young. Among all groups, the lower-ranking item categories were more similar than the higher-ranking item categories, and E, G, and L always appeared at the bottom ranks of the two scoring categories. However, A was always bottom ranked except in terms of importance for older adults. The results of the importance evaluations for the youth and middle-aged groups were similar to the results of the performance evaluation for the older

adult group: among the top five items, four were common with the young group, whereas five were common with the middle-aged group.

Furthermore, except for N in the older adult group, the importance score was always higher than the performance score. This trend indicates that evaluations made based on expected future importance tend to be more generous than those based on assumed consumption. The I–P values also became smaller as the users became older. The I–P value for the young group was 0.32, that for the middle-aged group was 0.24, and that for the older adult group was 0.16. This result shows that the two categories (importance and performance) began to exhibit more evident similarities as the users became older. A, L, and M were the item categories with the highest I–P values among the young and middle-aged groups, whereas A, D, and I were the item categories with the highest I–P values among the middle-aged and older adult groups. It is also noticeable that A exhibited the largest differences between the two categories for all groups.

For a more comprehensive understanding of these data, IPA was performed. In IPA, three out of four quadrants shared common items across the age groups.

Quadrant I encompassed (C) light control, (D) bed control, (F) body composition analysis, (H) smart toilet, (I) countertop height control, and (M) fall management. These smart home-related services and items exhibit high satisfaction and market demand, which are factors to consider in their commercialization more than in their development. In particular, item categories C, D, and F demonstrated high purchase intentions among the young and middle-aged groups. On the contrary, item categories C, F, H, and M demonstrated high purchase intentions among the middle-aged and older adult groups. By comparison, Quadrant II, usually considered an important part of market evaluation, encompassed no common items for immediate improvement.

Quadrant III encompassed (A) check-in, (E) curtain control, (G) water temperature color, and (L) gait analysis, whereas quadrant IV encompassed (J) auto ventilation. Specifically, item categories A, E, G, and L were generally of low appeal to evaluators of all ages. In particular, A and E scored lowest in both importance and performance. A and E were quadrant III's elements, indicating that these items have a low need for development and improvement, which are also the least important factors to consider in their development and commercialization. Considering the results simply and directly, it might be possible to conclude that these services are not important for all generations. However, from another perspective, further study is needed on whether the usability or appearance is insufficient or if there is another reason for these trends.

Lastly, quadrant IV encompassed J, which consistently scored low in importance but high in performance for all age groups. In South Korea, because of the recent universalization of air purifiers, J as a service seems to be less appealing. On the contrary, in the living lab, A, B, C, and J were designed to optimize energy consumption; however, this may not have made a significant difference to the experimental experience of the evaluators.

The fact that IPA focuses on cognition is problematic and limiting to our understanding because empirical research seeks to understand lived experiences but does not explain why they occur [64]. An authentic research inquiry seeking to understand the experiences of its participants will also seek to explore the conditions that trigger the association of experiences relating to past events, histories, or sociocultural domains. However, this study had limitations, and at the simplest level, the weaknesses of the study were based on factors such as duration of use. Thus, we adapted the factor analysis to build up the methodology firmly.

The next phase, comparing the factor analysis results among the age groups (Figure 7), was an attempt to infer the cause of the difference between the two scoring categories. Across all groups, the factor analysis relevant to importance firmly revealed the significance of health-related items. Daily living support items were ranked as a less important factor. However, the results of the performance analysis revealed mixed configurations of items related to daily living support, health, and emergencies, especially for the middle-aged and older adult groups. Overall, the factor configuration of the performance analysis showed a

mixture of various categories compared to the item composition of the importance analysis. In other words, it is possible to assume that the heterogeneity of the factor configuration as a result of the analysis of performance was the result of considering actual needs when the prospective user presupposed purchase.

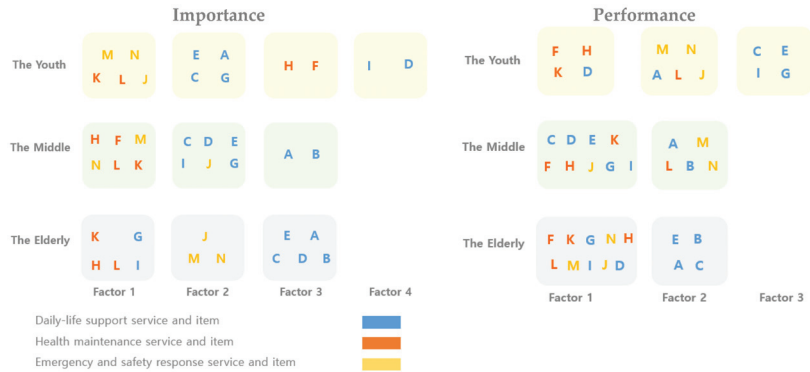


Figure 7. Age group-specific factors.

It was also found that the second-factor configuration (performance) for the young group was almost the same as the second-factor configuration for the middle-aged group, whereas these factors converged into a first-factor configuration in the performance evaluation by the older adult group. In the previous chapter, common item categories A, M, N, and L were noted as prominent constructs in relation to gerontification. Comparing the factor analysis of “importance and performance”, it can be inferred that notions of gerontification and needs of older adults influenced the judgment of prospective users.

5. Conclusions

IoT technologies and products have been rapidly changing our daily lives, with some of these technologies already permeating the houses of today. However, even though these products and services are being seen far more frequently than before, their use has not yet become successfully pervasive throughout our society. In a previous study, it was determined that there are many reasons that can affect surveys regarding user preference for smart technologies, and that people’s conceptual evaluations and practical choices tend to be different [9]. Among research efforts on future housing, many studies were based on this type of conceptual evaluation, determined through surveys [65–68]. Therefore, in this study, there was an attempt to evaluate a variety of smart home services, to better understand the recognition by and satisfaction of a user in a more empirical manner. Subsequently, “importance” was conceptually linked to “recognition” by the people and “performance” to “satisfaction” of the people. This was because evaluators marked the importance scores based on the recognition that the item will be important (for future housing) and marked the performance score based on whether their satisfaction was sufficient to motivate them into purchasing the item.

According to the statistical analysis, the two scoring categories tended to have a low similarity among the young group but began to exhibit evident similarities with the aging of the users. In other words, the importance and performance scores in the older adult group were more similar than in the other groups. On the contrary, the results of the importance evaluations for the young and middle-aged groups were analogous to the result for the older adult group, whereas those of the performance evaluations were not. Furthermore, the lower-ranking items for the I–P evaluations were consistently common among all age groups; by contrast, the upper-ranking items tended to differ. There were also clear similarities regarding which items did not appeal to any of the groups.

For further understanding, a factor analysis was performed. As mentioned previously, the scores for the two categories began to exhibit evident similarities with the aging of the users. Factor analysis was used to gain an understanding of the different structures among the factors underlying the measured items. It is noteworthy that the second-factor configuration (performance) for the young group was almost the same as the second-factor configuration for the middle-aged group. Furthermore, in relation to the aforementioned result, the third-factor configurations (performance) for all visitors offered a hint about the feature. If there were no similarities in the configurations (performance) for the two groups, we might think that the second-factor configuration was approximately about emergency response. However, with the results for the middle-aged and older adult groups, the feature of the configuration was deduced as relevant to older adults: gerontification and, more specifically, vulnerability. This is certainly related to health care or emergency response, based on the close intertwinement with the physically debilitating conditions that tend to be present in older adults. Such physically debilitating conditions cannot be a significant factor in performance evaluations (i.e., satisfaction is sufficient to motivate the purchase of the item) in the young and middle-aged groups. However, that factor converged into an underlying cause for first-factor configuration in performance evaluation by the older adult group. By comparison, among the young and middle-aged groups, services and items related to daily health maintenance and management tended to be more appealing. More generally, it is reasonable to infer that whereas health-related services and items are considered “important” by all groups, user vulnerability affects the priority of these services and items in terms of “performance.”

To sum up, for the design of future smart homes suitable for an aging society, the development of services/items that can constantly check the health status of the resident should be given priority. For smart homes with older residents, the development of services/items that can support them in their vulnerability should be emphasized. Eventually, more successful developments (i.e., that motivate the purchase of the item) should prioritize services and items that can actively support health-related vulnerabilities caused by aging. For a relatively young population, items with automatic detection and response functions in daily life are attractive. However, for this favorable impression to lead to a purchase, it is preferable that a health factor is included. In South Korea, most active health services have not yet been developed in different aspects because of restrictions related to medical services. To develop smart homes that are more practical and suitable for user needs in the future, follow-up studies should be conducted, and measures to overcome these limitations should be proposed.

Smart homes are an advancing wave of technological development whose success depends on a coalescence between the visions of technology developers for enhanced functionality and energy management, and the needs and demands of households in the complex places that are homes. Yet there is a wide and growing recognition of the need to develop a better picture of who users are and how they might use smart homes [69–71]. This study discusses evaluations by prospective users of smart home technology and products, to enhance the existing understanding of service and item needs for the optimal commercialization of smart homes for users. Smart home testing procedures typically attempt to capture the “user experience” in a lab or single-occupancy apartment and are often criticized for missing the intricacies of home life, where practices are shared and negotiated between residents and visitors with different priorities [6,69,70]. One cannot help but point out that this study has the same limitation. Experience in the smart home lab would be completely different from real life and it would be difficult to reflect on its complexity. The findings reported here cannot, therefore, be simply generalized to all types of smart home service and items contexts.

However, perhaps the main significance of this study is that it extends our understanding of “user evaluation vs. choice” and our understanding of different demands for smart home performance in each age group. Moreover, by comparing the results of factor analysis of each age group, it was possible to infer the users’ concealed considerations. It may even encourage ideas about properly complex but practical responses to the wicked

issues posed by our reliance on user evaluation. Careful development of services and items that satisfy these considerations and their outcomes will be a necessary part of designing and carrying out smart home performance.

Author Contributions: Conceptualization, E.S.; writing—original draft preparation, E.S.; writing—review and editing, E.S.; methodology, W.Y.; software, W.Y. All authors have read and agreed to the published version of the manuscript.

Funding: The present research paper has been conducted by the Research Grant of Kwangwoon University in 2022.

Data Availability Statement: Not applicable.

Acknowledgments: This work was supported by the Ministry of Land, Infrastructure, and Transport (of the Korean Government) [21RERP-B090228-07]. Thank all of the countless researchers who have been involved in the eight-year study; Bae Si-hwa, Lim Mi-sook, Hwang Jung-hyun, Choi Young-joon, Choi Hyun-chul, Ji Soo-in, Shon Dong-hwa, Park Eun-joon, Choi Dae-ho, Kim Hee-kyung, Kim Young-sun, and numerous graduate and undergraduate students.

Conflicts of Interest: The authors declare no conflict of interest.

References

1. Korean Statistical Information Service Population and Elderly Statistics. Available online: https://kostat.go.kr/portal/korea/kor_nw/1/1/index.board?bmode=read&aSeq=420896 (accessed on 1 October 2022).
2. Statistics Korea 2022 Elderly Statistics (Korea). Available online: https://kostat.go.kr/portal/korea/kor_nw/1/1/index.board?bmode=read&aSeq=420896 (accessed on 1 October 2022).
3. National Assembly Budget Office. *Public Finance of Korea 2018*; National Assembly Budget Office: Seoul, Republic of Korea, 2018.
4. Harmo, P.; Taipalus, T.; Knuutila, J.; Vallet, J.; Halme, A. Needs and solutions-home automation and service robots for the elderly and disabled. In Proceedings of the 2005 IEEE/RSJ International Conference on Intelligent Robots and Systems, Edmonton, AB, Canada, 2–6 August 2005; pp. 3201–3206.
5. Noury, N. ALLISA: Experimental platforms to evaluate remote care and assistive technologies in gerontology. In Proceedings of the 7th International Workshop on Enterprise networking and Computing in Healthcare Industry, Busan, Republic of Korea, 23–25 June 2005; pp. 67–72.
6. Darby, S.J. Smart technology in the home: Time for more clarity. *Build. Res. Inf.* **2018**, *46*, 140–147. [CrossRef]
7. Strengers, Y. *Smart Energy Technologies in Everyday Life: Smart Utopia?* Springer: Berlin/Heidelberg, Germany, 2013.
8. Belbachir, A.N.; Drobics, M.; Marschitz, W. Ambient Assisted Living for ageing well—an overview. *e & i Elektrotechnik Inf.* **2010**, *127*, 200–205.
9. Seo, E.; Bae, S.; Choi, H.; Choi, D. Preference and usability of Smart-Home services and items-A Focus on the Smart-Home living-lab. *J. Asian Archit. Build. Eng.* **2021**, *20*, 650–662. [CrossRef]
10. Coulby, G.; Clear, A.; Jones, O.; Young, F.; Stuart, S.; Godfrey, A. Towards remote healthcare monitoring using accessible IoT technology: State-of-the-art, insights and experimental design. *Biomed. Eng. Online* **2020**, *19*, 80. [CrossRef] [PubMed]
11. Moyle, W.; Murfield, J.; Lion, K. Therapeutic use of the humanoid robot, Telenoid, with older adults: A critical interpretive synthesis review. *Assist. Technol.* **2022**, 1–8. [CrossRef]
12. Bouma, H.; Fozard, J.L.; Bouwhuis, D.G.; Taipale, V. Gerontechnology in perspective. *Gerontechnology* **2007**, *6*, 190–216. [CrossRef]
13. Ohlan, R.; Ohlan, A. A comprehensive bibliometric analysis and visualization of smart home research. *Technol. Forecast. Soc. Chang.* **2022**, *184*, 121975. Available online: <https://www.sciencedirect.com/science/article/pii/S0040162522004966> (accessed on 1 November 2022). [CrossRef]
14. Ferreira, L.; Oliveira, T.; Neves, C. Consumer’s intention to use and recommend smart home technologies: The role of environmental awareness. *Energy* **2023**, *263*, 125814. Available online: <https://www.sciencedirect.com/science/article/pii/S036054422027001> (accessed on 1 November 2022). [CrossRef]
15. Gram-Hanssen, K.; Darby, S.J. “Home is where the smart is”? Evaluating smart home research and approaches against the concept of home. *Energy Res. Soc. Sci.* **2018**, *37*, 94–101. [CrossRef]
16. Del Rio, D.D.F.; Sovacool, B.K.; Bergman, N.; Makuch, K.E. Critically reviewing smart home technology applications and business models in Europe. *Energy Policy* **2020**, *144*, 111631. [CrossRef]
17. Sovacool, B.K.; Del Rio, D.D.F. Smart home technologies in Europe: A critical review of concepts, benefits, risks and policies. *Renew. Sustain. Energy Rev.* **2020**, *120*, 109663. [CrossRef]
18. Sahni, Y.; Cao, J.; Shen, J. Challenges and opportunities in designing smart spaces. In *Internet Everything. Internet of Things*; Springer: Singapore, 2018; pp. 131–152.
19. Balta-Ozkan, N.; Amerighi, O.; Boteler, B. A comparison of consumer perceptions towards smart homes in the UK, Germany and Italy: Reflections for policy and future research. *Technol. Anal. Strateg. Manag.* **2014**, *26*, 1176–1195. [CrossRef]

20. Marikyan, D.; Papagiannidis, S.; Alamanos, E. A systematic review of the smart home literature: A user perspective. *Technol. Forecast. Soc. Chang.* **2019**, *138*, 139–154. Available online: <https://www.sciencedirect.com/science/article/pii/S0040162517315676> (accessed on 1 November 2022). [[CrossRef](#)]
21. Yang, R.; Newman, M.W. Learning from a learning thermostat: Lessons for intelligent systems for the home. In Proceedings of the 2013 ACM International Joint Conference on Pervasive and Ubiquitous Computing, Zurich, Switzerland, 8–12 September 2013; pp. 93–102.
22. Chan, M.; Estève, D.; Escriba, C.; Campo, E. A review of smart homes—Present state and future challenges. *Comput. Methods Programs Biomed.* **2008**, *91*, 55–81. [[CrossRef](#)]
23. Peine, A. Understanding the dynamics of technological configurations: A conceptual framework and the case of Smart Homes. *Technol. Forecast. Soc. Chang.* **2009**, *76*, 396–409. [[CrossRef](#)]
24. Xu, K.; Wang, X.; Wei, W.; Song, H.; Mao, B. Toward software defined smart home. *IEEE Commun. Mag.* **2016**, *54*, 116–122. [[CrossRef](#)]
25. Sun, Y.; Li, S. A systematic review of the research framework and evolution of smart homes based on the internet of things. *Telecommun. Syst.* **2021**, *77*, 597–623. [[CrossRef](#)]
26. De Silva, L.C.; Morikawa, C.; Petra, I.M. State of the art of smart homes. *Eng. Appl. Artif. Intell.* **2012**, *25*, 1313–1321. [[CrossRef](#)]
27. Sanguinetti, A.; Karlin, B.; Ford, R.; Salmon, K.; Dombrovski, K. What’s energy management got to do with it? Exploring the role of energy management in the smart home adoption process. *Energy Effic.* **2018**, *11*, 1897–1911. [[CrossRef](#)]
28. Alam, M.R.; Reaz, M.B.I.; Ali, M.A.M. A review of smart homes—Past, present, and future. *IEEE Trans. Syst. Man Cybern. Part C (Appl. Rev.)* **2012**, *42*, 1190–1203. [[CrossRef](#)]
29. Zhou, B.; Li, W.; Chan, K.W.; Cao, Y.; Kuang, Y.; Liu, X.; Wang, X. Smart home energy management systems: Concept, configurations, and scheduling strategies. *Renew. Sustain. Energy Rev.* **2016**, *61*, 30–40. [[CrossRef](#)]
30. Minoli, D.; Sohraby, K.; Occhiogrosso, B. IoT considerations, requirements, and architectures for smart buildings—Energy optimization and next-generation building management systems. *IEEE Internet Things J.* **2017**, *4*, 269–283. [[CrossRef](#)]
31. Ahn, M.; Kang, J.; Hustvedt, G. A model of sustainable household technology acceptance. *Int. J. Consum. Stud.* **2016**, *40*, 83–91. [[CrossRef](#)]
32. Dangelico, R.M.; Pontrandolfo, P. From green product definitions and classifications to the Green Option Matrix. *J. Clean. Prod.* **2010**, *18*, 1608–1628. [[CrossRef](#)]
33. Yuan, X.; Han, P.; Duan, Y.; Alden, R.E.; Rallabandi, V.; Ionel, D.M. Residential electrical load monitoring and modeling—state of the art and future trends for smart homes and grids. *Electr. Power Compon. Syst.* **2020**, *48*, 1125–1143. [[CrossRef](#)]
34. Avdevičius, E.; Heider, F.; Eskander, M.; Schulz, D. Smart Grid Residential Load Modeling for Real-time Applications. In Proceedings of the NEIS 2021 Conference on Sustainable Energy Supply and Energy Storage Systems, Hamburg, Germany, 13–14 September 2021; pp. 1–8.
35. Badar, A.Q.; Anvari-Moghaddam, A. Smart home energy management system—a review. *Adv. Build. Energy Res.* **2022**, *16*, 118–143. [[CrossRef](#)]
36. Peek, S.T.; Wouters, E.J.; Van Hoof, J.; Luijkx, K.G.; Boeijs, H.R.; Vrijhoef, H.J. Factors influencing acceptance of technology for aging in place: A systematic review. *Int. J. Med. Inf.* **2014**, *83*, 235–248. [[CrossRef](#)]
37. Saroha, P.; Singh, G. A study on functional capabilities and recent advancements in smart home environment. *Mater. Today Proc.* **2022**, *69*, 609–613. Available online: <https://www.sciencedirect.com/science/article/pii/S2214785322063234> (accessed on 1 November 2022). [[CrossRef](#)]
38. Wilson, C.; Hargreaves, T.; Hauxwell-Baldwin, R. Benefits and risks of smart home technologies. *Energy Policy* **2017**, *103*, 72–83. [[CrossRef](#)]
39. Pal, D.; Funilkul, S.; Vanijja, V.; Papisatorn, B. Analyzing the elderly users’ adoption of smart-home services. *IEEE Access* **2018**, *6*, 51238–51252. [[CrossRef](#)]
40. Shin, J.; Park, Y.; Lee, D. Who will be smart home users? An analysis of adoption and diffusion of smart homes. *Technol. Forecast. Soc. Chang.* **2018**, *134*, 246–253. [[CrossRef](#)]
41. Visutsak, P.; Daoudi, M. The smart home for the elderly: Perceptions, technologies and psychological accessibilities: The requirements analysis for the elderly in Thailand. In Proceedings of the 2017 XXVI International Conference on Information, Communication and Automation Technologies (ICAT), Sarajevo, Bosnia and Herzegovina, 26–28 October 2017; pp. 1–6.
42. Schak, M.; Blum, R.; Bomsdorf, B. Smart Home for the Elderly—A Survey of Desires, Needs, and Problems. In Proceedings of the International Conference on Human-Computer Interaction, Virtual Event, 26 June–1 July 2022; pp. 107–121.
43. Al-Husamiyah, A.; Al-Bashayreh, M. A comprehensive acceptance model for smart home services. *Int. J. Data Netw. Sci.* **2022**, *6*, 45–58. [[CrossRef](#)]
44. Maswadi, K.; Ghani, N.A.; Hamid, S. Factors influencing the elderly’s behavioural intention to use smart home technologies in Saudi Arabia. *PLoS ONE* **2022**, *17*, e0272525. [[CrossRef](#)] [[PubMed](#)]
45. Schill, M.; Godefroit-Winkel, D.; Diallo, M.F.; Barbarossa, C. Consumers’ intentions to purchase smart home objects: Do environmental issues matter? *Ecol. Econ.* **2019**, *161*, 176–185. [[CrossRef](#)]
46. Takayama, L.; Pantofaru, C.; Robson, D.; Soto, B.; Barry, M. Making technology homey: Finding sources of satisfaction and meaning in home automation. In Proceedings of the 2012 ACM Conference on Ubiquitous Computing, Pittsburgh, PA, USA, 5–8 September 2012; pp. 511–520.

47. Gross, C.; Siepermann, M.; Lackes, R. The acceptance of smart home technology. In Proceedings of the International Conference on Business Informatics Research, Vienna, Austria, 21–23 September 2020; Springer: Berlin/Heidelberg, Germany, 2020; pp. 3–18.
48. Nikou, S. Factors driving the adoption of smart home technology: An empirical assessment. *Telemat. Inf.* **2019**, *45*, 101283. Available online: <https://www.sciencedirect.com/science/article/pii/S0736585319307750> (accessed on 1 November 2022). [[CrossRef](#)]
49. Chu, R.K.; Choi, T. An importance-performance analysis of hotel selection factors in the Hong Kong hotel industry: A comparison of business and leisure travellers. *Tour. Manag.* **2000**, *21*, 363–377. [[CrossRef](#)]
50. Bae, Y.; Byun, G.; Ha, M. Study on Environmental Project Factors in Peripheral Spaces around Children’s Parks within Low-rise Housing Areas by Using IPA Analysis-Focusing on user consciousness survey. *J. Archit. Inst. Korea Plan. Des.* **2019**, *35*, 73–81.
51. Yi, N. Importance-performance analysis (IPA) of service quality attributes of university foodservice-A comparison of male and female students’ perceptions in Daejeon. *Korean J. Hum. Ecol.* **2012**, *21*, 389–405. [[CrossRef](#)]
52. Child, D. *The Essentials of Factor Analysis*; Cassell Educational, Continuum International Publishing Group: London, UK, 1990.
53. Harman, H.H. *Modern Factor Analysis*; University of Chicago Press: Chicago, IL, USA, 1976.
54. Bartholomew, D.J.; Knott, M.; Moustaki, I. *Latent Variable Models and Factor Analysis: A Unified Approach*; John Wiley & Sons: Hoboken, NJ, USA, 2011.
55. Cattell, R. *The Scientific Use of Factor Analysis in Behavioral and Life Sciences*; Springer Science & Business Media: Berlin/Heidelberg, Germany, 2012.
56. McDonald, R.P. *Factor Analysis and Related Methods*; Psychology Press: New York, NY, USA, 2014.
57. Yong, A.G.; Pearce, S. A beginner’s guide to factor analysis: Focusing on exploratory factor analysis. *Tutor. Quant. Methods Psychol.* **2013**, *9*, 79–94. [[CrossRef](#)]
58. Rummel, R.J. *Applied Factor Analysis*; Northwestern University: Evanston, IL, USA, 1970.
59. Comrey, A.L.; Lee, H.B. *A First Course in Factor Analysis*; Psychology Press: New York, NY, USA, 2013.
60. Tobias, S.; Carlson, J.E. Brief report: Bartlett’s test of sphericity and chance findings in factor analysis. *Multivar. Behav. Res.* **1969**, *4*, 375–377. [[CrossRef](#)]
61. Larkin, M.; Watts, S.; Clifton, E. Giving voice and making sense in interpretative phenomenological analysis. *Qual. Res. Psychol.* **2006**, *3*, 102–120. [[CrossRef](#)]
62. Brocki, J.M.; Wearden, A.J. A critical evaluation of the use of interpretative phenomenological analysis (IPA) in health psychology. *Psychol. Health* **2006**, *21*, 87–108. [[CrossRef](#)]
63. Hefferon, K.; Gil-Rodriguez, E. *Interpretative Phenomenological Analysis*; American Psychological Association: Washington, DC, USA, 2011.
64. Tuffour, I. A critical overview of interpretative phenomenological analysis: A contemporary qualitative research approach. *J. Healthc. Commun.* **2017**, *2*, 52. [[CrossRef](#)]
65. Barbosa, N.M.; Park, J.S.; Yao, Y.; Wang, Y. “What if?” Predicting Individual Users’ Smart Home Privacy Preferences and Their Changes. *Proc. Priv. Enhancing Technol.* **2019**, *2019*, 211–231. [[CrossRef](#)]
66. Lee, E.; Park, S. A Preference-Driven Smart Home Service for the Elderly’s Biophilic Experience. *Sensors* **2021**, *21*, 5108. [[CrossRef](#)]
67. Shah, A.S.; Nasir, H.; Fayaz, M.; Lajis, A.; Ullah, I.; Shah, A. Dynamic user preference parameters selection and energy consumption optimization for smart homes using deep extreme learning machine and bat algorithm. *IEEE Access* **2020**, *8*, 204744–204762. [[CrossRef](#)]
68. Jeong, K.; Salvendy, G.; Proctor, R.W. Smart home design and operation preferences of Americans and Koreans. *Ergonomics* **2010**, *53*, 636–660. [[CrossRef](#)]
69. Wilson, C.; Hargreaves, T.; Hauxwell-Baldwin, R. Smart homes and their users: A systematic analysis and key challenges. *Pers. Ubiquitous Comput.* **2015**, *19*, 463–476. [[CrossRef](#)]
70. Beringer, R.; Sixsmith, A.; Campo, M.; Brown, J.; McCloskey, R. The “acceptance” of ambient assisted living: Developing an alternate methodology to this limited research lens. In Proceedings of the International Conference on Smart Homes and Health Telematics, Montreal, QB, Canada, 20–22 June 2011; Springer: Berlin/Heidelberg, Germany, 2011; pp. 161–167.
71. Solaimani, S.; Bouwman, H.; Baken, N. The smart home landscape: A qualitative meta-analysis. In Proceedings of the International Conference on Smart Homes and Health Telematics, Montreal, QB, Canada, 20–22 June 2011; Springer: Berlin/Heidelberg, Germany, 2011; pp. 192–199.

Disclaimer/Publisher’s Note: The statements, opinions and data contained in all publications are solely those of the individual author(s) and contributor(s) and not of MDPI and/or the editor(s). MDPI and/or the editor(s) disclaim responsibility for any injury to people or property resulting from any ideas, methods, instructions or products referred to in the content.

Review

Hypomagnetic Fields and Their Multilevel Effects on Living Organisms

Miroslava Sinčák and Jana Sedlakova-Kadukova *

Faculty of Natural Science, University of Cyril and Methodius in Trnava, Nam. J. Herdu 2, 91701 Trnava, Slovakia
* Correspondence: prof.jana.sedlakova@ucm.sk; Tel.: +421-905245200

Abstract: The Earth's magnetic field is one of the basic abiotic factors in all environments, and organisms had to adapt to it during evolution. On some occasions, organisms can be confronted with a significant reduction in a magnetic field, termed a "hypomagnetic field—HMF", for example, in buildings with steel reinforcement or during interplanetary flight. However, the effects of HMFs on living organisms are still largely unclear. Experimental studies have mostly focused on the human and rodent models. Due to the small number of publications, the effects of HMFs are mostly random, although we detected some similarities. Likely, HMFs can modify cell signalling by affecting the contents of ions (e.g., calcium) or the ROS level, which participate in cell signal transduction. Additionally, HMFs have different effects on the growth or functions of organ systems in different organisms, but negative effects on embryonal development have been shown. Embryonal development is strictly regulated to avoid developmental abnormalities, which have often been observed when exposed to a HMF. Only a few studies have addressed the effects of HMFs on the survival of microorganisms. Studying the magnetoreception of microorganisms could be useful to understand the physical aspects of the magnetoreception of the HMF.

Keywords: hypomagnetic field; magnetic zero; magnetoreception

Citation: Sinčák, M.; Sedlakova-Kadukova, J. Hypomagnetic Fields and Their Multilevel Effects on Living Organisms. *Processes* **2023**, *11*, 282. <https://doi.org/10.3390/pr11010282>

Academic Editors: Roberto Alonso González Lezcano, Francesco Nocera and Rosa Giuseppina Caponetto

Received: 13 December 2022
Revised: 9 January 2023
Accepted: 12 January 2023
Published: 16 January 2023



Copyright: © 2023 by the authors. Licensee MDPI, Basel, Switzerland. This article is an open access article distributed under the terms and conditions of the Creative Commons Attribution (CC BY) license (<https://creativecommons.org/licenses/by/4.0/>).

1. Introduction

Every living organism on Earth has adapted to the geomagnetic field during an evolutionary process lasting billions of years. The presence of a geomagnetic field (approximately 50 μT) is natural to each cell [1]. However, in a few circumstances, organisms can face the absence of magnetic fields. Understanding its effect can enhance our knowledge of magnetoreception mechanisms, with applications in space research, biotechnology or medicine. The terms "hypomagnetic", "conditionally zero magnetic field" or "magnetic vacuum" generally refer to fields with a magnetic flux density (B) below 100 nT [2], but according to some authors, we can speak of a magnetic field weaker than 5 μT as being hypomagnetic [3].

Hypomagnetic fields (HMFs) commonly occur in the interplanetary space of the solar system and fluctuate in the range of several nanoteslas (nT). For example, the lunar magnetic field is less than 300 nT, and the magnetic field on Mars is approximately 1 μT [3]. The planetary magnetic field of Mars is extremely small, and the planetary magnetic field of Venus is practically non-existing [4] (Figure 1).

New technologies are currently being developed to enable space exploration and interplanetary flights. In the future, organisms will be exposed to a HMF during space travels, which is significantly weaker than the geomagnetic field (GMF) and expected to have diverse biological effects. During these travels, organisms will be exposed to tedious periods of a HMF that is approximately 10,000 times weaker than the Earth's magnetic field, ranging from 0.1 to 1 nT [5]. However, attenuation of the Earth's magnetic field is not limited to staying in space but occurs in daily life, for example, in buildings with steel walls or steel reinforcement [2]. Building walls are a natural shield against low- and high-frequency electromagnetic fields. However, a magnetic field (such as a geomagnetic field)

is more difficult to shield. In contrast to radiofrequency and low-frequency electric fields, thin sheets of metal have no effect on magnetic fields [6]. However, there is evidence that buildings with steel in their construction magnetise and deform the natural geomagnetic field [5], causing an even 50-fold magnetic field attenuation according to the building size and the complexity of the steel [7].

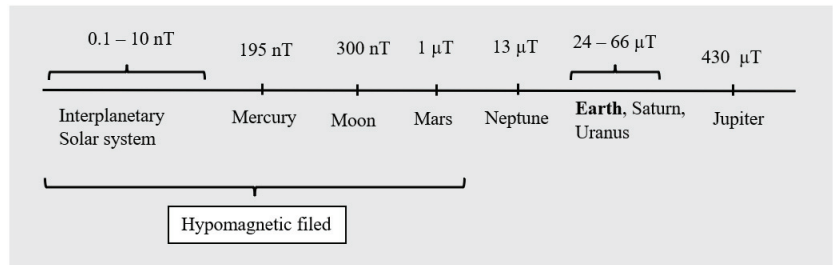


Figure 1. Presence of hypomagnetic field in the solar system [3].

Hypomagnetic fields can have various effects on organisms, although the underlying mechanisms remain unknown. Erdman et al. [8] suggest that the magnetoreception of the HMF differs among different organisms. The authors assume that the magnetoreception of the HMF is a nonspecific mechanism and manifests in highly different biological systems as mostly random reactions as a result of magnetic interaction with magnetic moments at a physical level. This moment, which is present in each molecule, could transfer the magnetic signal at the level of downstream biochemical events [2].

In this study, we summarise information about the observed biological effects of the HMF on eukaryotic and prokaryotic organisms and show the possible underlying mechanisms.

2. Materials and Methods

We used the scientific databases PubMed and ScienceDirect to select papers that contained the terms “hypomagnetic”, “magnetic zero”, “magnetic vacuum” or “magnetic shielding” in their titles, abstracts and keywords. This gave, after a subsequent semantic control, 65 experimental and theoretical articles that included original results suitable for further investigation. This type of search was repeated with each new relevant article iteratively until no new articles could be detected.

3. Mechanisms of Magnetoreception of HMFs

Magnetoreception is the universal ability of a biological system to detect magnetic and electromagnetic fields, although it may manifest itself differently in different organisms. Any changes in magnetic field intensity may affect the organisms in many ways, including the basic metabolism of prokaryotic and eukaryotic cells [8]. Magnetoreception relates not only to geomagnetic fields and higher magnetic and electromagnetic fields, but it also explains the perception of HMFs. The hypothesis of nonspecific nonthermal magnetoreception on the physical level has not been studied since none of those has yet been identified experimentally. Typical for hypomagnetic magnetoreception experiments is a high sensitivity to the physical, chemical and physiological conditions, as well as a low reproducibility [2] and a great variety of effects in different organisms. It has not yet been possible to establish any common conditions controlling the magnetic effects in different organisms or populations rather than in their individual forms [9]. Several mechanisms have been described that could explain the mechanism of magnetoreception, such as the cyclotron resonance model, macroscopic charged vortices in the cytoplasm and the parametric resonance model, among others [10]. The most likely physical mechanisms with expected biological responses are: (i) the radical pair mechanism, (ii) the universal physical mechanism and (iii) the molecular gyroscope mechanism. However, according

to Binhi and Prato [2], the radical pair mechanism is unlikely to explain all HMF effects on living organisms. The authors assume that the universal physical mechanism and the molecular gyroscope mechanism are more accurate.

These primary physical mechanisms can lead to secondary biophysical responses, which can include changes in ROS concentrations, Ca²⁺ ion homeostasis or influence enzymes that are involved in the electron transport chain in mitochondria or in cell cycle promotion.

1. Radical pair mechanism

Traditionally, radicals (for example, reactive oxygen species (ROS)) are considered harmful because they can cause cell death via oxidative intracellular damage in the metabolism of sugars, fats and nucleic acids. Several studies have also shown the importance of ROS in intracellular signalling cascades such as apoptosis initiation [11–13]. Radicals are magnetic because an electron (along with a proton and a neutron) has a property known as spin or, more precisely, a spin momentum [14].

The radical pair consists of two radicals that have been formed simultaneously, usually by a chemical reaction. The spins of two unpaired electrons can be either parallel to each other ($\uparrow\uparrow$ which gives $S = 1$) or anti-parallel ($\uparrow\downarrow$, which gives $S = 0$, where S is the spin quantum number). The two forms of the electron pair are therefore known as triplet ($S = 1$) and singlet ($S = 0$) [15]. Influencing either singlet or triplet formations of electron pairs could be associated with the presence of an external magnetic field and leads to a longer life of the radical pairs (triplet states) [16].

This mechanism can cause a difference in the stability of radical pairs and affects the shift of the chemical reaction equilibrium. Thus, during the formation of radical pairs, external magnetic fields change the recombination rate of these radical pairs, which in turn changes the concentration of radicals such as O₂ • and molecules such as H₂O₂ [17]. In general, the coupling between unpaired electrons and nuclei in each fragment of a radical pair can be achieved by magnetic fields in the range of 10 μ T–3 mT [18]. Magnetic fields could interact with the magnetic moments of radical pairs at physical levels, which are ubiquitous in macromolecules with unpaired electrons, protons, paramagnetic ions or other magnetic nuclei in biological cells, and then transmit the magnetic signal to subsequent biochemical events such as cell oxidative stress reactions. This procedure would therefore lead to highly different biological observables and mostly random reactions [19].

This mechanism does not have frequency selectivity because the development of a magnetosensitive spin state occurs over an extremely short life of the radical pair, usually in the order of 10^{-9} – 10^{-7} s [20]. Many authors explain the observed results by this mechanism [21–23].

2. Universal physical mechanism

The rotation of magnetic moments in a magnetic field precedes any biophysical or biochemical mechanism of magnetoreception and largely determines the spectral and nonlinear characteristics of the biological effect of the field. The mechanism is based on the external magnetic field, which influences the magnetic moment of the molecules and leads to the terminal relaxation of the magnetic moment [19]. Magnetic relaxation is known as the approach to equilibrium after a magnetic system was exposed to magnetic field change. Relaxation processes allow nuclear spins to return to equilibrium following a magnetic disturbance [24].

The biological effect is observed only when changes in the magnetic momentum dynamics go through the stages of transformation at the biochemical, physiological and biological levels of the system. A special characteristic of this mechanism is that it predicts the effects of weak magnetic fields but also those of electromagnetic fields induced by alternating electric currents (ACs) in the same biological system [2].

3. Molecular gyroscope mechanism

The molecular gyroscope mechanism can be explained as the rotation of large fragments of macromolecules or amino acid residues with a distributed electric charge. This movement can be influenced by a magnetic field.

In some stages of protein assembly, in the final stage of their synthesis, virtual cavities without water molecules, of the order of 1 nm or less, may occur in the protein [25]. In these cavities, amino acid residues (molecular gyroscopes) rotate over milliseconds, searching for the best position. As a result of such rotation, a magnetic moment interacts with an external magnetic field [2]. The magnetic field affects these rotations, which results in possible changes in protein folding. The folding of protein chains is an evolutionarily conserved process, and improper folding can prevent a protein from performing its specific function [26]. Mostly, random changes in the proteome of the cell can explain various biological responses after HMF exposure.

4. Influences of HMFs on Organisms

In many areas, the biological effects of HMFs are contradictory, which might be explained by the length of exposure to the HMF. The authors of [27] reported that exposure to a HMF for a shorter time (1 h) could promote cell respiration, but a longer exposure time (6 h) has an inhibitory effect.

Another parameter causing conflicting results may be the method of generating the HMF. The authors used either the shielding of the present HMF or its compensation by another magnetic field, which may have caused a different result. For example, the production of free radicals caused by direct-current (DC) HMFs differs from the effect of AC HMFs. A similar difference was observed when the HMF was induced by a static field or a variable frequency-alternating magnetic field [28].

The type of organism is an important factor of the HMF effect [29]. Not only does the biological effect of HMFs vary between plant and animal cells, but according to Binhi and Prato [2], there are different targets of HMFs for different organisms or even for individuals of the same species. The observed effect of the HMF differs between eukaryotic and prokaryotic organisms, even in plant and animal cells. Few effects of HMF exposure could be similar for various organisms and are on the level of individual ions and proteins; they are generally related to cell signalling.

Regarding the spectrum of the hypomagnetic effect in various types of organisms according to their basic differences in structure and life cycle, we will separately discuss plant, animal and prokaryotic organisms.

4.1. Animals and Animal Cell Cultures

The observed effects can differ at various levels of the organization of the living organism. According to the observations described in various studies, we will discuss cell transport and respiration in a separate subsection (Section 4.1.1), and subsequently, we will discuss animals at the level of the organism or organ systems (Section 4.1.2).

4.1.1. Cell Transport and Respiration

The effects of the HMF on a single-cell level may include the effect on ion transport and concentration as well as cellular respiration (Table 1).

Table 1. Impact of hypomagnetic field on cell transport and metabolism (B—magnetic flux density in Tesla (T)).

Impact on	Effect	Hypomagnetic Field Properties				References
		Organism	Mechanism	B (nT)	Duration	
Mineral density of bones	Reduction	Sprague-Dawley rats	Shielding	<300	3 days	[30]
The concentration of Fe, Mn, Cu, Cr	Reduction	Fur of laboratory rats Wistar	Shielding	<20	7 months	[31]

Table 1. Cont.

Impact on	Effect	Hypomagnetic Field Properties				References
		Organism	Mechanism	B (nT)	Duration	
Ca ²⁺ dependent proteases	Inactivation	Enzymes from fish and invertebrates	Compensation		1 h	[32]
The concentration of Co, Ni	No effect	Fur of laboratory rats Wistar	Shielding	<20	8 months	[31]
Mitochondrial activity	Reduction	Skeletal muscle cells	Compensation	<200	7 days	[33]
Mitochondrial activity	Reduction	Mouse (C57BL/6)	Compensation	0–500	30 days	[34]
ATP levels	Reduction	Skeletal muscle cells	Compensation	<30,000	3 days	[35]
Cell respiration	Reduction	<i>Drosophila melanogaster</i>	Compensation	1	6 h	[27]
Cell respiration	Promotion	<i>Drosophila melanogaster</i>	Compensation	1	1 h	[27]

The cellular transport mechanisms of various nutrients can be affected by near-zero magnetic field exposure. Some studies have reported changes in the Ca²⁺ ion concentration in the cytosol after being subjected to hypomagnetic conditions. The effect of the HMF on Ca²⁺ ion concentration in tissues is the basis of the parametrical resonance theory [35], which deals with magnetoreception; it is caused by the effect of HMF on Ca²⁺ ions and proteins with Ca²⁺ binding sites. This theory agrees with the results of Kantserova et al. [32], who showed that the production of Ca²⁺-dependent proteases was inactivated after HMF exposure. It can be assumed that the inhibition of Ca²⁺-dependent enzymes under hypomagnetic conditions may negatively affect the basic calcium-mediated transduction in the cell. In eukaryotic cells, the Ca²⁺ ion plays a role as a primary and secondary messenger, and Ca-dependent enzymes, including calcium-dependent kinases or proteases, may participate in cell membrane fusion, cell division and apoptosis [36].

Several studies have found that a stronger magnetic field ($\geq 100 \mu\text{T}$) can increase the levels of reactive oxygen species (ROS) [37–39], whereas the HMF can significantly decrease the level of ROS in cells [21,40]. There is experimental evidence of the correlation between HMF-induced changes in cellular ROS concentration and biological effects, such as cell growth in vitro [28]. Therefore, ROS may represent a potential target for the magnetic field, which may cause the modulus of biological functions [2]. The changes in ROS concentrations in the cell are directly related to the presence of free radicals, and the authors investigating ROS lean towards the theoretical radical pair mechanism as the magnetoreception mechanism of the HMF influence.

The main source of cellular ROS are the mitochondrial electron-transport chain complexes I, II and III, which are present in the inner mitochondrial membrane. Complexes I and II are the primary sources of O₂• under either physiological or pathological conditions [40]. For an individual cell, the rate of ROS generation varies depending on the availability of cellular O₂, the redox state of the electron carriers, the respiration rate, the state of the electron carrier, the mitochondrial inner membrane potential and the post-translational modifications of the respiratory protein chain [28]. Mitochondria are the organelles most sensitive to HMF exposure due to their electron-transparent matrix and lower mitochondrial membrane potential in both plant and animal cells [41,42].

Ogneva et al. [27] reported a decrease in *Drosophila melanogaster* sperm cell respiration as a consequence of affecting the I. mitochondrial electrical transport chain complex after 6 h in a HMF. Mitochondria may also undergo morphological rearrangements under HMF conditions. In another study, the size and relative volume of mitochondria in plant cells increased and cristae size decreased after hypomagnetic field exposure, as described in [41].

However, the mechanism by which the level of ROS is modulated by the magnetic field remains unclear. It is assumed that weak magnetic fields can alter the free radical level response and, consequently, affect specific cellular functions and inhibit or reduce cell growth [43]. In addition to metabolic changes, it is possible to consider changes at the morphological level, namely the accumulation of lipid bodies, the development of a lytic compartment (vacuoles and cytosomes) and the reduction of phytoferritin in plastids after HMF exposure [41].

4.1.2. Animals

On the level of the whole organism, studies dealing with HMFs mostly focus on animals, humans, tissue cultures and embryos. The most common areas of study are the influences of HMFs on prenatal development as well as cardiovascular and nervous systems (Table 2).

Table 2. Impact of hypomagnetic field on animal neural systems (B—magnetic flux density in Tesla (T)).

Impact on	Effect	Organism	Hypomagnetic Field Properties				
			Mechanism of Generation	B (nT)	Duration	References	
Neural system	ROS levels	Reduction	Mouse (C57BL/6 J), males	Shielding	170	Every 3 days/ 150 days	[23]
	ROS levels	Reduction	Peritoneal mice neutrophils	Shielding	20	1.5 h	[21]
	Growth	Promotion	Primary neural progenitor/mouse stem cells	Shielding	0–200	7 days	[42]
	ROS levels	Reduction	Human cells of neuroblast	Shielding	0–200	16 h	[44]
	ROS genes expression	Reduction	Mouse (C57BL/6 J), males	Shielding	170	3 day/150 days	[23]
	Gene expression	Reduction (down-regulation)	Human neuroblast cells	Compensation	<200	2 days	[45]
	Migratory properties	Reduction	Human cells of neuroblast	Shielding	0–200	48 h	[46]
	Proliferation	Promotion	Human cells neuroblast (SH-SY5Y)	Shielding	0–200	3 days	[46]
	Memory	Reduction	<i>Drosophila melanogaster</i>	Compensation	100–680	10–19 generations	[47]
	Proliferation	Promotion	Human neuroblastoma cells	Shielding	-	-	[48]
	Cognitive abilities	Reduction	Human (volunteers)	Compensation	400	45 min	[49]
	Proliferation	Promotion	Human neuroblastoma (SHSY5Y) cells	Shielding	<200	3 days	[50]
	Hippocampal neurogenesis	Inhibition	Mouse (C57BL/6 J), males	Shielding	170	every 3 day/ 150 days	[23]
Cardiovascular system	Blood pressure	Promotion	Human (volunteers)	Compensation	±10	60 min	[51]
	Blood circulation	Promotion	Human (volunteers)	Compensation	±10	60 min	[52]
	Haemolysis	Promotion	Human blood	Compensation	100	72 h	[53]
	Haemolysis	Promotion	Blood of rats	Compensation	192	6 h to 4 weeks	[54]
Life cycle and survival	Survival	Reduction	Milnesium inceptum	Shielding	-	21 days	[29]
	Survival	Reduction	Tardigada (Echiniscus testudo and Milnesium inceptum)	Shielding	-	21 days	[29]
	Life expectancy	Reduction	Daphnia magna	Compensation	15	Generational period	[55]
	Larval development	Inhibition	Mythimna separata	Compensation	<500	12 h	[56]
	Development of eggs and nymphs	Delayed	Nilaparvata lugens	Compensation	0–1060	Generational period	[57]

Table 2. Cont.

Impact on	Effect	Organism	Hypomagnetic Field Properties				
			Mechanism of Generation	B (nT)	Duration	References	
Life cycle and survival	Fertility	Reduction	Nilaparvata lugens	Compensation	0–1060	Generational period	[58]
	Production of abnormal embryos	Promotion	Xenopus larvae	Shielding	104 ± 12.6	4 days	[59]
	Fertility	Reduction (sterility)	NMRI mouse zygotes	Shielding	200	12 days	[60]
	Abortion	Promotion	Pregnant NMRI mice	Shielding	200	3–12 days	[60]
	Survival of cells exposed to X-rays	Promotion	Immortalised human bronchial epithelial cells	Shielding	<50	24 h	[61]
	Chromatic condensation	Changes	Human fibroblasts and lymphocytes	Compensation	1800	20–70 min	[62]

Hypomagnetic fields can delay the development of insect eggs and nymphs, reduce the fetal size and body length, reduce female fertility in adult insects [41] and reduce the life span of daphnia [56]. Yan et al. [22] also reported negative effects on the mating ratio and developmental stages of insects (*Mythimna separata*) and on the foraging orientation of *Nilaparvata lugens* [57], but a stimulating effect on positive phototaxis and flight capacity of *Sogatella furcifera* [58]. Similar to insects, adverse effects on embryonal development in *Xenopus laevis* have been observed [59], along with the induced loss of the ability to bear offspring in pregnant mice [60]. Adverse effects of the HMF were observed even in the case of extremophilic invertebrates from the phylum Tardigrada. The obtained results showed that even partial isolation from the geomagnetic field has a negative effect on the anhydrobiotic (resting) stage of both tested species (*Echiniscus testudo* and *Milcium inceptum*). Both species exhibited lower survival rates during entering anhydrobiosis, in the anhydrobiotic state, and upon returning to the active state. The authors also observed higher mortality in *E. testudo* compared to *M. inceptum*, which suggests that different species respond to hypomagnetic conditions in different ways [29]. Developmental abnormalities caused by HMFs may be related to epigenetic modifications of embryonic stem cells, such as abnormal DNA methylation. The results suggest that a suitable electromagnetic field may be necessary for favorable epigenetic remodelling and, thus, for differentiation during the embryonic stage [63].

An effect of HMFs on the nervous system has also been observed. The results suggest that specific brain structures represent neural substrates for the orientation of the magnetic compass in certain magnetosensory animals. In several experiments, HMFs accelerated the proliferation of neuroblastoma cells and neural progenitor/stem cells [42], and this proliferative effect may be related to decreased levels of cellular reactive oxygen species (ROS). After exposure of neuroblast cells to the HMF, a Warburg effect (commonly observed in cancer metabolism) was observed, when cell metabolism is induced by the repression of oxidative stress and the up-regulation of anaerobic glycolysis. In this case, the increased activity of LDH (lactate dehydrogenase), a key member of glycolysis, could be a direct response to a HMF [49]. The other explanation for the enhanced cell proliferation, according to Mo et al. [50], is the acceleration of proliferation by a forward shift of the cell cycle in the G1 phase. In contrast to the G1 phase, G2 and M phases were not affected during the experiment. The same results could be recorded when Belyaev et al. [62] observed that the effect of the zero magnetic field on chromatin condensation is more pronounced at the beginning of the G1 phase.

A comprehensive study examining the human transcriptome after exposure to a HMF (<200 nT) for 2 days showed a change in the gene expression of 2464 genes associated with the neural system. Mentioned genes were significantly grouped into a few key processes, for example, protein transport, macromolecule localization, RNA processing and brain

function. These results suggest the involvement of the MAPK pathway and cryptochrome in the early biological responses to the presence of a HMF [45].

In addition to the effects on the neural system, effects of the HMF on the cardiovascular system have been observed. Capillary blood velocity increased by 17%, cardio intervals increased by 88.7% [51], and capillary circulation rate increased by 22.4% [52] during HMF exposure. At the end of exposure, diastolic blood pressure dropped considerably relative to mid-exposure values, whereas systolic blood pressure, on the contrary, showed a significant increase [52]. One of the crucial parameters which influence the observed effects of HMFs is exposure time. Both previous studies claim to have simulated hypomagnetic conditions during interplanetary flight, but the time of HMF exposure was only 60 min. We assume that the time of exposure was not sufficient to demonstrate hypomagnetic conditions during a longer stay in space. In comparison, in two studies with a longer exposure time of 72 h [53] and up to 4 weeks [54], the authors recorded an increase in haemolysis and the weakening of the deformation and aggregation properties of human blood, along with a reduction in enzymatic activities. The reduction of these enzyme activities and the promotion of haemolysis can be related to increased protein denaturation and decreased efficiency of the proteolytic system [53].

4.2. Plants

Recent studies have shown that plants respond to near-zero magnetic fields through morphological and developmental changes, including delays in flowering time and germination [64], breath conductivity, chlorophyll content [65], photoreceptor involvement [66] and changes in auxin [67], and gibberellin concentrations [68] (Table 3).

Table 3. Impact of hypomagnetic field on plants (B—magnetic flux density in Tesla (T)).

Impact on	Effect	Organism	Hypomagnetic Field Properties			
			Mechanism of Generation	B (nT)	Duration	References
Growth	Reduction	<i>Glycine max</i>	Shielding	111 ± 15	24 h	[69]
Growth	Reduction	<i>Arabidopsis thaliana</i>	Compensation	0–1330	35 days	[70]
Growth	Reduction	<i>Arabidopsis thaliana</i>	Compensation	40–44	96 h	[71]
Epicotyl elongation	Promotion	<i>Pisum sativum</i>	Shielding	-	24 h	[72]
Gene expansion	Reduction	<i>Arabidopsis thaliana</i>	Compensation	0–1330	33 days	[68]
Activity of photoreceptors phyA	Reduction	<i>Arabidopsis thaliana</i>	Compensation	40	3 h	[64]
Activity of <i>phyB</i> photoreceptors	Promotion	<i>Arabidopsis thaliana</i>	Compensation	40	3 h	[64]
The content of auxin in flower	Reduction	<i>Arabidopsis thaliana</i>	Compensation	0–1330	33 days	[67]
Gene expression (associated with flowering)	Promotion	<i>Arabidopsis thaliana</i>	Compensation	50	33 days	[73]
Auxin content in roots	Promotion	<i>Arabidopsis thaliana</i>	Compensation	1–1330	33 days	[67]
Iron intake by roots	Reduction	<i>Arabidopsis thaliana</i>	Compensation	40–44	96 h	[71]
Concentration of Ca ²⁺ ions	Promotion	<i>Pisum sativum</i> (root system)	Shielding	0.5–2	3 days	[41]

The HMF can either have inhibitory or stimulating effects on plants, depending on the part of the growth to which the plant is exposed. Hypomagnetic fields can inhibit [41] but also promote vegetative growth, e.g., by increasing the percentage of the germination rate [69]. On the other hand, they may have a reducing effect on reproductive growth by inhibiting seed production [70]. The magnetic field, in this case, is thought to affect the activity of cryptochromes and their gene expressions [64,74]. Plant hormones are also involved in cryptochrome-mediated flowering. Exposure to HMFs reduces the gibberellin content and the expression of their biosynthetic genes in wild-type *Arabidopsis thaliana* but not in the cryptochrome mutant strain (*cry1/cry2*). Similar results have been obtained for another plant hormone, auxin [67].

As in the case of animal cells, changes in the ion concentrations of some nutrients (NH_4^+ , K^+ , Ca^{2+} , Mg^{2+} , Cl^- , SO_4^{2-} , NO_3^- and PO_4^{3-}) in plant cells after exposure of the *A. thaliana* root system to the HMF were recorded. A few minutes of exposure to a zero magnetic field resulted in a significant reduction in the intake of all studied nutrient ions, which can be explained by the existence of a plant magnetoreceptor responding to the HMF by modulating mineral nutrient transport genes. According to Narayan et al. [75], the response to an almost zero magnetic field is rapid, suggesting that some ion channels and all transport activities may not necessarily be related to gene expression. Ion channel changes have been reported in other studies and may influence flowering time [64], photoreceptor signaling [76], and seed germination [77].

In plant cells exposed to HMFs, the functional activity of the genome declined in the early pre-replication period. The HMF can intensify protein synthesis. At the ultrastructural level, changes in condensed chromatin distribution and nuclear compaction, the accumulation of lipid bodies, the development of the lytic compartment (vacuoles, cytosegresomas and paramural bodies), and the reduction of phytoferritin in plastids in meristem cells have been observed in pea roots [39].

In contrast to the animal cell, where the HMF stimulated proliferation and accelerated the passage through the G1 phase, the observed effect on the plant cell was the opposite. The HMF had a negative effect on the speed and progress of the cell cycle. The reproductive cycle of the cells slowed down due to the expansion of the G1 and G2 phases, whereas the other phases of the cell cycle remained relatively stable. The HMF also caused a remarkable decrease in proliferating plant cells (from 68% to 95%) [41].

Tsetlin et al. [78] also recorded remarkable results when they described a synergistic inhibitory effect of HMF and ionizing radiation (α and γ) on plant germination. This experiment simulated another environmental parameter to which the plants will be exposed during interplanetary flights.

4.3. Prokaryotes

Only a few studies have examined the effects of the HMF on microorganisms. Magnetotactic bacteria, i.e., bacteria capable of perceiving the Earth's geomagnetic field by means of magnetosomes, have been investigated most frequently [5] (Table 4).

Table 4. Impact of hypomagnetic field on procaryotic microorganisms (B—magnetic flux density in Tesla (T)).

Impact on	Effect	Organism	Field Properties			
			Mechanism	B (nT)	Duration	References
Growth and number of cells	Reduction	Magnetotactic bacteria (MO-1)	Shielding	2	2 days	[79]
Tolerance to antibiotics	Both reduction and promotion	<i>Escherichia coli</i>	Compensation	-	6 days	[80]
Tolerance to antibiotics	Both reduction and promotion	<i>Pseudomonas</i> and <i>Enterobacter</i> strains	Field compensation	-	6 days	[81]
Magnetosome size	Promotion	<i>Magnetospirillum magneticum</i> AMB-1	Compensation	500	16 h	[82]
Gene expression	Modification	<i>Magnetospirillum magneticum</i> AMB-1	Compensation	500	16 h	[82]

Studies on the magnetotactic bacterium *Magnetospirillum magneticum* AMB-1 have shown that after 16 h of magnetic compensation (500 nT), AMB-1 synthesises larger magnetosomes due to the up-regulation (stimulation) of genes encoding larger magnetosomes and the down-regulation (inhibition) of genes encoding smaller magnetosomes. The gene responsible for magA iron transport remained unchanged [82]. Inhibition of the growth and viability of magnetotactic bacteria (MO-1) after exposure to a 2-nT magnetic field for 2 days has also been noted [79].

In addition to magnetotactic bacteria, changes in antibiotic resistance in human pathogenic bacteria have been studied. The susceptibility of 26 strains of *Escherichia coli* to selected antibiotics was examined after HMF exposure. Susceptibility to antibiotics (ampicillin, ceftazidime, tetracycline, ofloxacin, and kanamycin) either increased or decreased in different strains, depending on the studied drug. The authors detected two types of *E. coli* strains: non-sensitive and sensitive to geomagnetic field compensation, which represents about one-third of the strains. Magneto-sensitive *E. coli* strains showed modified minimum inhibitory concentration (MIC) values to two of five tested antibiotics after HMF exposure [80]. According to Creanga et al. [81], half of the eight tested human pathogen strains (*Pseudomonas* and *Enterobacter* strains) were magnetosensitive and showed a change in antibiotic susceptibility (increase or decrease, depending on the tested antibiotics) from 2- to 16-fold.

Ilyin et al. [83] have recently isolated bacteria from the nasopharynx of cosmonauts after their return to Earth from a space mission. The authors observed multiple decreases in antibiotic resistance after exposure to space conditions. Although the effect of the HMF was not especially investigated in this study, its effect on bacterial life is undeniable and can be related to the observed changes in resistance.

The authors further suggest that the HMF can affect cell metabolism by changing the ion transport mechanism in cell plasma membranes in the prokaryotic cell, and this can be applicable in eucaryotic magnetoreception by influencing endoplasmic reticulum (including ribosomal membranes) and mitochondrial membranes [81].

5. Conclusions

So far, the impacts of HMFs on biological systems have been rarely investigated, and the exact mechanism of action remains unclear. The authors explain their results by several theoretical mechanisms, most often by the mechanism of radical pairs which influence the reactive oxygen species concentration. Experimental studies on HMFs yielded conflicting results on the development and functioning of the nervous and cardiovascular systems. However, HMFs are likely to have a negative effect on early developmental stages and fertility in both plants and animals. The conflicting results may have been due to the different exposure times, organism types, and methods of creating a HMF, which seem to be the key factors in the observed biological effects.

However, fewer studies have focused on the effect of the HMF on microorganisms. In our opinion, it is the research of prokaryotic models that can offer useful insight into the magnetoreception of the HMF. Based on this review, the level of magnetoreception can take place at the level of ions, protein complexes, or the cell membrane, and thus, the primary targets of the HMF could be similar for both prokaryotic and eukaryotic organisms.

Hypomagnetic fields seem to affect cell signaling on the level of ion transport and ROS, which has been demonstrated for disruptive embryonal development.

Author Contributions: M.S. wrote the paper; J.S.-K. edited the manuscript. All authors have read and agreed to the published version of the manuscript.

Funding: The work was supported by financial aid from the Slovak Grant Agency project No. VEGA 1/0018/22.

Data Availability Statement: The manuscript has no associated data.

Conflicts of Interest: The authors declare no conflict of interest or interpretation of data. The funders had no role in the design of the study; in the collection, analyses, or interpretation of data; in the writing of the manuscript; or in the decision to publish the results.

References

- Monteil, C.L.; Lefevre, C.T. Magnetoreception in Microorganisms. *Trends Microbiol.* **2019**, *28*, 266–275. [[CrossRef](#)] [[PubMed](#)]
- Binhi, V.N.; Prato, F.S. Biological effects of the hypomagnetic field: An analytical review of experiments and theories. *PLoS ONE* **2017**, *12*, e0179340. [[CrossRef](#)] [[PubMed](#)]
- Mo, W.; Liu, Y.; He, R. Hypomagnetic field, an ignorable environmental factor in space? *Sci. China Life Sci.* **2014**, *57*, 726–728. [[CrossRef](#)] [[PubMed](#)]
- Kivelson, M.G.; Bagenal, F. Planetary magnetospheres. In *Encyclopedia of the Solar System*, 3rd ed.; Elsevier: Amsterdam, The Netherlands, 2014; Chapter 7, pp. 137–157.
- Zhang, Z.; Xue, Y.; Yang, J.; Shang, P.; Yuan, X. Biological Effects of Hypomagnetic Field: Ground-Based Data for Space Exploration. *Bioelectromagnetics* **2021**, *42*, 516–531. [[CrossRef](#)]
- Pavlik, M. Compare of shielding effectiveness for building materials. *Prz. Elektrotechniczny* **2019**, *95*, 137–140. [[CrossRef](#)]
- Guo, C.; Liu, D. Quantitative Analyses of Magnetic Field Distributions for Buildings of Steel Structure. In Proceedings of the 2012 Sixth International Conference on Electromagnetic Field Problems and Applications, Dalian, China, 19–21 June 2012.
- Erdmann, W.; Kmita, H.; Kosicki, J.Z.; Kaczmarek, Ł. How the Geomagnetic Field Influences Life on Earth—An Integrated Approach to Geomagnetobiology. *Space Life Sci.* **2021**, *51*, 231–257. [[CrossRef](#)]
- Wajnberg, E.; Acosta-Avalos, D.; Alves, O.C.; de Oliveira, J.F.; Srygley, R.B.; Esquivel, D.M.S. Magnetoreception in eusocial insects: An update. *J. R. Soc. Interface* **2010**, *7*, S207–S225. [[CrossRef](#)] [[PubMed](#)]
- Binhi, V.N.; Savin, A.V. Molecular gyroscopes and biological effects of weak extremely low-frequency magnetic fields. *Phys. Rev. E* **2002**, *65*, 051912. [[CrossRef](#)]
- Dröge, W. Free Radicals in the Physiological Control of Cell Function. *Physiol. Rev.* **2002**, *82*, 47–95. [[CrossRef](#)]
- Gauron, C.; Rampon, C.; Bouzaffour, M.; Ipendey, E.; Teillon, J.; Volovitch, M.; Vríz, S. Sustained production of ROS triggers compensatory proliferation and is required for regeneration to proceed. *Sci. Rep.* **2013**, *3*, srep02084. [[CrossRef](#)]
- Van Huizen, A.V.; Morton, J.M.; Kinsey, L.J.; Von Kannon, D.G.; Saad, M.A.; Birkholz, T.R.; Czajka, J.M.; Cyrus, J.; Barnes, F.S.; Beane, W.S. Weak magnetic fields alter stem cell-mediated growth. *Sci. Adv.* **2019**, *5*, eaau7201. [[CrossRef](#)] [[PubMed](#)]
- Adams, B.; Sinayskiy, I.; Petruccione, F. An open quantum system approach to the radical pair mechanism. *Sci. Rep.* **2018**, *8*, 15719. [[CrossRef](#)] [[PubMed](#)]
- Hore, P.J.; Mouritsen, H. The Radical-Pair Mechanism of Magnetoreception. *Annu. Rev. Biophys.* **2016**, *45*, 299–344. [[CrossRef](#)] [[PubMed](#)]
- Ruiz-Gómez, M.J.; Sendra-Portero, F.; Martínez-Morillo, M. Effect of 2.45 mT sinusoidal 50 Hz magnetic field on *Saccharomyces cerevisiae* strains deficient in DNA strand breaks repair. *Int. J. Radiat. Biol.* **2010**, *86*, 602–611. [[CrossRef](#)]
- Barnes, F.; Greenbaum, B. Some Effects of Weak Magnetic Fields on Biological Systems: RF fields can change radical concentrations and cancer cell growth rates. *IEEE Power Electron. Mag.* **2016**, *3*, 60–68. [[CrossRef](#)]
- Brocklehurst, B.; Mclauchlan, K.A. Free radical mechanism for the effects of environmental electromagnetic fields on biological systems. *Int. J. Radiat. Biol.* **1996**, *69*, 3–24. [[CrossRef](#)]
- Binhi, V.N.; Prato, F.S. A physical mechanism of magnetoreception: Extension and analysis. *Bioelectromagnetics* **2016**, *38*, 41–52. [[CrossRef](#)] [[PubMed](#)]
- Otsuka, H.; Mitsui, H.; Miura, K.; Okano, K.; Imamoto, Y.; Okano, T. Rapid Oxidation Following Photoreduction in the Avian Cryptochrome4 Photocycle. *Biochemistry* **2020**, *59*, 3615–3625. [[CrossRef](#)] [[PubMed](#)]
- Novikov, V.V.; Yablokova, E.V.; Fesenko, E.E. The Effect of a “Zero” Magnetic Field on the Production of Reactive Oxygen Species in Neutrophils. *Biophysics* **2018**, *63*, 365–368. [[CrossRef](#)]
- Yan, M.-M.; Zhang, L.; Cheng, Y.-X.; Sappington, T.W.; Pan, W.-D.; Jiang, X.-F. Effect of a near-zero magnetic field on development and flight of oriental armyworm (*Mythimna separata*). *J. Integr. Agric.* **2021**, *20*, 1336–1345. [[CrossRef](#)]
- Zhang, B.; Wang, L.; Zhan, A.; Wang, M.; Tian, L.; Guo, W.; Pan, Y. Long-term exposure to a hypomagnetic field attenuates adult hippocampal neurogenesis and cognition. *Nat. Commun.* **2021**, *12*, 1174. [[CrossRef](#)] [[PubMed](#)]
- Gupta, A.; Stait-Gardner, T.; Price, W.S. Is It Time to Forgo the Use of the Terms “Spin-Lattice” and “Spin-Spin” Relaxation in NMR and MRI? *J. Phys. Chem. Lett.* **2021**, *12*, 6305–6312. [[CrossRef](#)] [[PubMed](#)]
- Zangi, R.; Hagen, M.; Berne, B.J. Effect of Ions on the Hydrophobic Interaction between Two Plates. *J. Am. Chem. Soc.* **2007**, *129*, 4678–4686. [[CrossRef](#)] [[PubMed](#)]
- Zhao, V.; Jacobs, W.M.; Shakhnovich, E.I. Effect of Protein Structure on Evolution of Cotranslational Folding. *Biophys. J.* **2020**, *119*, 1123–1134. [[CrossRef](#)]
- Ogneva, I.V.; Usik, M.A.; Burtseva, M.V.; Biryukov, N.S.; Zhdankina, Y.S.; Sychev, V.N.; Orlov, O.I. *Drosophila melanogaster* Sperm under Simulated Microgravity and a Hypomagnetic Field: Motility and Cell Respiration. *Int. J. Mol. Sci.* **2020**, *21*, 5985. [[CrossRef](#)]
- Zhang, B.; Tian, L. Reactive Oxygen Species: Potential Regulatory Molecules in Response to Hypomagnetic Field Exposure. *Bioelectromagnetics* **2020**, *41*, 573–580. [[CrossRef](#)]

29. Erdmann, W.; Idzikowski, B.; Kowalski, W.; Kosicki, J.Z.; Kaczmarek, Ł. Tolerance of two anhydrobiotic tardigrades *Echiniscus testudo* and *Milnesium inceptum* to hypomagnetic conditions. *PeerJ* **2021**, *9*, e10630. [[CrossRef](#)]
30. Jia, W.; Fan, Z.; Du, A.; Shi, L. Molecular mechanism of Mare Nectaris and magnetic field on the formation of ethyl carbamate during 19 years aging of Feng-flavor Baijiu. *Food Chem.* **2022**, *382*, 132357. [[CrossRef](#)]
31. Tombarkiewicz, B. Effect of long-term geomagnetic field deprivation on the concentration of some elements in the hair of laboratory rats. *Environ. Toxicol. Pharmacol.* **2008**, *26*, 75–79. [[CrossRef](#)]
32. Kantserova, N.P.; Krylov, V.V.; Lysenko, L.A.; Ushakova, N.V.; Nemova, N.N. Effects of Hypomagnetic Conditions and Reversed Geomagnetic Field on Calcium-Dependent Proteases of Invertebrates and Fish. *Izv. Atmos. Ocean. Phys.* **2017**, *53*, 719–723. [[CrossRef](#)]
33. Fu, J.-P.; Mo, W.-C.; Liu, Y.; Bartlett, P.F.; He, R.-Q. Elimination of the geomagnetic field stimulates the proliferation of mouse neural progenitor and stem cells. *Protein Cell* **2016**, *7*, 624–637. [[CrossRef](#)] [[PubMed](#)]
34. Hu, P.D.; Mo, W.C.; Fu, J.P.; Liu, Y.; He, R.Q. Long-term Hypogeomagnetic field exposure reduces muscular mitochondrial function and exercise capacity in adult male mice. *Prog. Biochem. Biophys.* **2020**, *47*, 426–438.
35. Lednev, V.V. Bioeffects of weak static and alternating magnetic fields. *Biofizika* **1996**, *41*, 224–232. [[PubMed](#)]
36. Krebs, J. Structure, Function and Regulation of the Plasma Membrane Calcium Pump in Health and Disease. *Int. J. Mol. Sci.* **2022**, *23*, 1027. [[CrossRef](#)] [[PubMed](#)]
37. Poniedziałek, B.; Rzymyski, P.; Karczewski, J.; Jaroszyk, F.; Wiktorowicz, K. Reactive oxygen species (ROS) production in human peripheral blood neutrophils exposed in vitro to static magnetic field. *Electromagn. Biol. Med.* **2013**, *32*, 560–568.
38. Vergallo, C.; Ahmadi, M.; Mobasher, H.; Dini, L. Impact of Inhomogeneous Static Magnetic Field (31.7–232.0 mT) Exposure on Human Neuroblastoma SH-SY5Y Cells during Cisplatin Administration. *PLoS ONE* **2014**, *9*, e113530. [[CrossRef](#)]
39. Tang, R.; Xu, Y.; Ma, F.; Ren, J.; Shen, S.; Du, Y.; Hou, Y.; Wang, T. Extremely low frequency magnetic fields regulate differentiation of regulatory T cells: Potential role for ROS-mediated inhibition on AKT. *Bioelectromagnetics* **2016**, *37*, 89–98. [[CrossRef](#)]
40. Angelova, P.R.; Dinkova-Kostova, A.T.; Abramov, A.Y. Assessment of ROS Production in the Mitochondria of Live Cells. In *Reactive Oxygen Species*; Humana: New York, NY, USA, 2021; pp. 33–42. [[CrossRef](#)]
41. Belyavskaya, N. Biological effects due to weak magnetic field on plants. *Adv. Space Res.* **2004**, *34*, 1566–1574. [[CrossRef](#)]
42. Fu, J.-P.; Mo, W.-C.; Liu, Y.; He, R.-Q. Decline of cell viability and mitochondrial activity in mouse skeletal muscle cell in a hypomagnetic field. *Bioelectromagnetics* **2016**, *37*, 212–222. [[CrossRef](#)]
43. Montoya, R.D. Magnetic fields, radicals and cellular activity. *Electromagn. Biol. Med.* **2017**, *36*, 102–113. [[CrossRef](#)]
44. Zhang, H.-T.; Zhang, Z.-J.; Mo, W.-C.; Hu, P.-D.; Ding, H.-M.; Liu, Y.; Hua, Q.; He, R.-Q. Shielding of the geomagnetic field reduces hydrogen peroxide production in human neuroblastoma cell and inhibits the activity of CuZn superoxide dismutase. *Protein Cell* **2017**, *8*, 527–537. [[CrossRef](#)] [[PubMed](#)]
45. Mo, W.; Liu, Y.; Bartlett, P.F.; He, R. Transcriptome profile of human neuroblastoma cells in the hypomagnetic field. *Sci. China Life Sci.* **2014**, *57*, 448–461. [[CrossRef](#)] [[PubMed](#)]
46. Mo, W.C.; Zhang, Z.J.; Wang, D.L.; Liu, Y.; Bartlett, P.F.; He, R.Q. Shielding of the geomagnetic field alters actin assembly and inhibits cell motility in human neuroblastoma cells. *Sci. Rep.* **2016**, *6*, 22624. [[CrossRef](#)] [[PubMed](#)]
47. Zhang, B.; Lu, H.; Xi, W.; Zhou, X.; Xu, S.; Zhang, K.; Jiang, J.; Li, Y.; Guo, A. Exposure to hypomagnetic field space for multiple generations causes amnesia in *Drosophila melanogaster*. *Neurosci. Lett.* **2004**, *371*, 190–195. [[CrossRef](#)] [[PubMed](#)]
48. Sarimov, R.M.; Binhi, V.N.; Milyaev, V.A. The influence of geomagnetic field compensation on human cognitive processes. *Biophysics* **2008**, *53*, 433–441. [[CrossRef](#)]
49. Wang, G.-M.; Fu, J.-P.; Mo, W.-C.; Zhang, H.-T.; Liu, Y.; He, R.-Q. Shielded geomagnetic field accelerates glucose consumption in human neuroblastoma cells by promoting anaerobic glycolysis. *Biochem. Biophys. Res. Commun.* **2022**, *601*, 101–108. [[CrossRef](#)]
50. Mo, W.-C.; Zhang, Z.-J.; Liu, Y.; Bartlett, P.F.; He, R.-Q. Magnetic Shielding Accelerates the Proliferation of Human Neuroblastoma Cell by Promoting G1-Phase Progression. *PLoS ONE* **2013**, *8*, e54775. [[CrossRef](#)]
51. Gurfinkel, Y.; At'Kov, O.; Vasin, A.; Breus, T.; Sasonko, M.; Pishchalnikov, R. Effect of zero magnetic field on cardiovascular system and microcirculation. *Life Sci. Space Res.* **2016**, *8*, 1–7. [[CrossRef](#)]
52. IuI, G.; Vasin, A.L.; Matveeva, T.A.; Sasonko, M.L. Evaluation of the hypomagnetic environment effects on capillary blood circulation, blood pressure and heart rate. *Aviakosmicheskaja I Ekol. Meditsina= Aerosp. Environ. Med.* **2014**, *48*, 24–30.
53. Ciorba, D.; Morariu, V.V. Life in zero magnetic field. III. Activity of aspartate aminotransferase and alanine aminotransferase during in vitro aging of human blood. *Electro- Magn.* **2001**, *20*, 313–321. [[CrossRef](#)]
54. Katiukhin, L.N. Rheological Properties of the Erythrocytes in Weakened Static Magnetic Field of the Earth In vitro Study. *J. Sci. Res. Rep.* **2019**, *22*, 1–12. [[CrossRef](#)]
55. Krylov, V.V.; Bolotovskaya, I.V.; Osipova, E.A. The response of European *Daphnia magna* Straus and Australian *Daphnia carinata* King to changes in geomagnetic field. *Electromagn. Biol. Med.* **2013**, *32*, 30–39. [[CrossRef](#)] [[PubMed](#)]
56. Wan, G.-J.; Yuan, R.; Wang, W.-J.; Fu, K.-Y.; Zhao, J.-Y.; Jiang, S.-L.; Pan, W.-D.; Sword, G.A.; Chen, F.-J. Reduced geomagnetic field may affect positive phototaxis and flight capacity of a migratory rice planthopper. *Anim. Behav.* **2016**, *121*, 107–116. [[CrossRef](#)]
57. Zhang, Y.; Pan, W. Removal or component reversal of local geomagnetic field affects foraging orientation preference in migratory insect brown planthopper *Nilaparvata lugens*. *PeerJ* **2021**, *9*, e12351. [[CrossRef](#)] [[PubMed](#)]

58. Wan, G.-J.; Jiang, S.-L.; Zhao, Z.-C.; Xu, J.-J.; Tao, X.-R.; Sword, G.A.; Gao, Y.-B.; Pan, W.-D.; Chen, F.-J. Bio-effects of near-zero magnetic fields on the growth, development and reproduction of small brown planthopper, *Laodelphax striatellus* and brown planthopper, *Nilaparvata lugens*. *J. Insect Physiol.* **2014**, *68*, 7–15. [[CrossRef](#)] [[PubMed](#)]
59. Mo, W.; Liu, Y.; Cooper, H.M.; He, R.-Q. Altered development of *Xenopus* embryos in a hypogeomagnetic field. *Bioelectromagnetics* **2011**, *33*, 238–246. [[CrossRef](#)]
60. Fesenko, E.E.; Mezhevikina, L.M.; Sipenko, M.A.; Gordon, R.Y.; Khutzian, S.S. Effect of the “zero” magnetic field on early embryogenesis in mice. *Electromagn. Biol. Med.* **2010**, *29*, 1–8. [[CrossRef](#)]
61. Xue, X.; Ali, Y.F.; Liu, C.; Hong, Z.; Luo, W.; Nie, J.; Li, B.; Jiao, Y.; Liu, N.-A. Geomagnetic Shielding Enhances Radiation Resistance by Promoting DNA Repair Process in Human Bronchial Epithelial Cells. *Int. J. Mol. Sci.* **2020**, *21*, 9304. [[CrossRef](#)]
62. Belyaev, I.Y.; Alipov, Y.D.; Harms-Ringdahl, M. Effects of zero magnetic field on the conformation of chromatin in human cells. *Biochim. Biophys. Acta (BBA)-Gen. Subj.* **1997**, *1336*, 465–473. [[CrossRef](#)]
63. Baek, S.; Choi, H.; Park, H.; Cho, B.; Kim, S.; Kim, J. Effects of a hypomagnetic field on DNA methylation during the differentiation of embryonic stem cells. *Sci. Rep.* **2019**, *9*, 1333. [[CrossRef](#)]
64. Agliassa, C.; Narayana, R.; Christie, J.M.; Maffei, M.E. Geomagnetic field impacts on cryptochrome and phytochrome signaling. *J. Photochem. Photobiol. B Biol.* **2018**, *185*, 32–40. [[CrossRef](#)]
65. Maffei, M.E. Magnetic field effects on plant growth, development, and evolution. *Front. Plant Sci.* **2014**, *5*, 445. [[CrossRef](#)]
66. Agliassa, C.; Mannino, G.; Molino, D.; Cavalletto, S.; Contartese, V.; Bertera, C.M.; Secchi, F. A new protein hydrolysate-based biostimulant applied by fertigation promotes relief from drought stress in *Capsicum annuum* L. *Plant Physiol. Biochem.* **2021**, *166*, 1076–1086. [[CrossRef](#)] [[PubMed](#)]
67. Xu, C.; Zhang, Y.; Yu, Y.; Li, Y.; Wei, S. Suppression of Arabidopsis flowering by near-null magnetic field is mediated by auxin. *Bioelectromagnetics* **2017**, *39*, 15–24. [[CrossRef](#)] [[PubMed](#)]
68. Xu, C.; Yu, Y.; Zhang, Y.; Li, Y.; Wei, S. Gibberellins are involved in effect of near-null magnetic field on Arabidopsis flowering. *Bioelectromagnetics* **2016**, *38*, 1–10. [[CrossRef](#)] [[PubMed](#)]
69. Mo, W.-C.; Zhang, Z.-J.; Liu, Y.; Zhai, G.-J.; Jiang, Y.-D.; He, R.-Q. Effects of a hypogeomagnetic field on gravitropism and germination in soybean. *Adv. Space Res.* **2011**, *47*, 1616–1621. [[CrossRef](#)]
70. Xu, C.; Wei, S.; Lu, Y.; Zhang, Y.; Chen, C.; Song, T. Removal of the local geomagnetic field affects reproductive growth in Arabidopsis. *Bioelectromagnetics* **2013**, *34*, 437–442. [[CrossRef](#)]
71. Islam, M.; Maffei, M.; Vigani, G. The Geomagnetic Field Is a Contributing Factor for an Efficient Iron Uptake in Arabidopsis thaliana. *Front. Plant Sci.* **2020**, *11*, 325. [[CrossRef](#)]
72. Negishi, Y.; Hashimoto, A.; Tushima, M.; Dobrota, C.; Yamashita, M.; Nakamura, T. Growth of pea epicotyl in low magnetic field implication for space research. *Adv. Space Res.* **1999**, *23*, 2029–2032. [[CrossRef](#)]
73. Xu, C.; Yin, X.; Lv, Y.; Wu, C.; Zhang, Y.; Song, T. A near-null magnetic field affects cryptochrome-related hypocotyl growth and flowering in Arabidopsis. *Adv. Space Res.* **2012**, *49*, 834–840. [[CrossRef](#)]
74. Xu, C.; Li, Y.; Yu, Y.; Zhang, Y.; Wei, S. Suppression of Arabidopsis flowering by near-null magnetic field is affected by light. *Bioelectromagnetics* **2015**, *36*, 476–479. [[CrossRef](#)] [[PubMed](#)]
75. Narayana, R.; Fliegmann, J.; Paponov, I.; Maffei, M.E. Reduction of geomagnetic field (GMF) to near null magnetic field (NNMF) affects Arabidopsis thaliana root mineral nutrition. *Life Sci. Space Res.* **2018**, *19*, 43–50. [[CrossRef](#)] [[PubMed](#)]
76. Vanderstraeten, J.; Gailly, P.; Malkemper, E.P. Low-light dependence of the magnetic field effect on cryptochromes: Possible relevance to plant ecology. *Front. Plant Sci.* **2018**, *9*, 121. [[CrossRef](#)]
77. Soltani, F.; Kashi, A.; Arghavani, M. Effect of magnetic field on Asparagus officinalis L. seed germination and seedling growth. *Seed Sci. Technol.* **2006**, *34*, 349–353. [[CrossRef](#)]
78. Tsetlin, V.; Moisa, S.; Levinskikh, M.; Nefedova, E. EFFECT OF VERY SMALL DOSES OF IONIZING RADIATION AND HYPOMAGNETIC FIELD CHANGE PHYSIOLOGICAL CHARACTERISTICS OF HIGHER PLANT SEEDS. *Aviakosmicheskaja I Ekol. Meditsina= Aerosp. Environ. Med.* **2016**, *50*, 51–58. [[CrossRef](#)]
79. Zhang, S.-D.; Petersen, N.; Zhang, W.-J.; Cargou, S.; Ruan, J.; Murat, D.; Santini, C.-L.; Song, T.; Kato, T.; Notareschi, P.; et al. Swimming behaviour and magnetotaxis function of the marine bacterium strain MO-1. *Environ. Microbiol. Rep.* **2013**, *6*, 14–20. [[CrossRef](#)] [[PubMed](#)]
80. Poiata, A.; Creanga, D.E.; Morariu, V.V. Life in zero magnetic field. *VE coli resistance to antibiotics. Electromagn. Biol. Med.* **2003**, *22*, 171–182. [[CrossRef](#)]
81. Creanga, D.; Poiata, A.; Morariu, V.; Tupu, P. Zero-magnetic field effect in pathogen bacteria. *J. Magn. Magn. Mater.* **2004**, *272–276*, 2442–2444. [[CrossRef](#)]
82. Wang, X.K.; Ma, Q.F.; Jiang, W.; Lv, J.; Pan, W.D.; Song, T.; Wu, L.-F. Effects of Hypomagnetic Field on Magnetosome Formation of *Magnetospirillum Magneticum* AMB-1. *Geomicrobiol. J.* **2008**, *25*, 296–303. [[CrossRef](#)]
83. Ilyin, V.K.; Orlov, O.I.; Morozova, Y.A.; Skedina, M.A.; Vladimirov, S.K.; Plotnikov, E.V.; Artamonov, A.A. Prognostic model for bacterial drug resistance genes horizontal spread in space-crews. *Acta Astronaut.* **2022**, *190*, 388–394. [[CrossRef](#)]

Disclaimer/Publisher’s Note: The statements, opinions and data contained in all publications are solely those of the individual author(s) and contributor(s) and not of MDPI and/or the editor(s). MDPI and/or the editor(s) disclaim responsibility for any injury to people or property resulting from any ideas, methods, instructions or products referred to in the content.



Article

Heat Hazard Control in High-Temperature Tunnels: Experimental Study of Coupled Cooling with Ventilation and Partial Insulation for Synergistic Geothermal Extraction

Junjian Wang ¹, Zijun Li ^{1,*}, Gang Li ² and Yu Xu ¹

¹ School of Resources and Safety Engineering, Central South University, 932 Lu Shan South Road, Changsha 410083, China

² Sinosteel Maanshan General Institute of Mining Research Co., Ltd., Maanshan 243000, China

* Correspondence: anquan@csu.edu.cn

Abstract: The problem of heat hazard in tunnel engineering has seriously affected the normal work of personnel and machinery. After combining the heat hazard control method of controlling the energy source and blocking the energy transfer, a technical scheme of precise thermal insulation at the working face in concert with geothermal energy extraction is proposed, forming a coupled cooling method of ventilation and partial thermal insulation. By building a scaled model test platform, the temperature field of the working area was analyzed, and the effect of factors, such as with or without a thermal insulation layer, ventilation velocity, and surrounding rock temperature on the cooling limit, was discussed. The feasibility of extracting energy and enhancing cooling through the heat exchange layer was judged. The results show that the partial thermal insulation can effectively weaken the heat dissipation of the surrounding rock and enhance the ventilation and cooling effect, which can reduce the average ventilation limit temperature of the working area by 1.6 °C. The addition of the heat exchange layer can further improve the tunnel environment on the basis of partial insulation, making the cooling limit temperature drop by another 3.1 °C, and the heat exchange layer can work for one year to extract geothermal energy 4.5×10^8 J. The coupled cooling scheme of ventilation and partial thermal insulation is practical and useful, which can provide technical ideas for improving the thermal environment of the tunnel.

Keywords: heat hazard control; partial thermal insulation; ventilation; coupled cooling; geothermal energy extraction

Citation: Wang, J.; Li, Z.; Li, G.; Xu, Y. Heat Hazard Control in High-Temperature Tunnels: Experimental Study of Coupled Cooling with Ventilation and Partial Insulation for Synergistic Geothermal Extraction. *Int. J. Environ. Res. Public Health* **2023**, *20*, 1941. <https://doi.org/10.3390/ijerph20031941>

Academic Editors: Roberto Alonso González Lezcano, Francesco Nocera and Rosa Giuseppina Caponetto

Received: 20 November 2022

Revised: 8 January 2023

Accepted: 16 January 2023

Published: 20 January 2023



Copyright: © 2023 by the authors. Licensee MDPI, Basel, Switzerland. This article is an open access article distributed under the terms and conditions of the Creative Commons Attribution (CC BY) license (<https://creativecommons.org/licenses/by/4.0/>).

1. Introduction

With the gradual deepening of mine mining depth [1–3] and the construction of high geothermal tunnels in plateau areas guided by the western development plan [4–6], heat hazard, a common geological disaster problem, has become a bottleneck restricting the operation of various underground space projects. On the one hand, the high temperature environment will cause huge physical and psychological harm to the staff, such as rapid heart rate [7], fatigue [8], inattention [9] and other adverse reactions, thereby significantly increasing the accident rate. On the other hand, it will also lead to difficulties in the operation of mechanical equipment to dissipate heat, resulting in mechanical aging and a reduction in production efficiency [10]. Therefore, it is urgent to solve the problem of heat hazard in excavation tunnels.

The traditional mine tunnel heat hazard control methods can be divided into two aspects: controlling the energy source and blocking the energy transfer. The main idea of controlling the energy source is to offset the heat source and conduct heat diversion through the cold source, or directly reduce the temperature of the underground heat source. The cold source heat transfer generally adopts the method of ventilation to convey low-temperature air flow to the working area to neutralize and divert the heat emitted by the surrounding rock.

Yaping Wang [11] analyzed the effects of different air velocities and air supply temperatures on the high-temperature environment of the tunnel and came up with the optimal air supply conditions that could satisfy the working surface temperature. Qi Chen et al. [12] explored the connection between wind flow velocity and the convective heat transfer coefficient in the construction of tunnel duct air supply, revealing the distribution of the convective heat transfer coefficient at tunnel corners to provide a theoretical basis for optimizing duct ventilation design. Kepeng Wang et al. [13] revealed the thermodynamic characteristics of a deep coal mine as an example and derived a method to calculate the cooling load of a deep tunnel working face. However, due to the long air transport distance in the deep tunnel, the air flow on the ground has a higher temperature when it reaches the working face. In engineering practice, ventilation is usually combined with refrigeration at the same time [14–16]. The widespread use of refrigeration equipment imposes a significant economic burden and has problems, such as difficulty in discharging heat from the facility. It is very important to reduce air cooling loss and improve ventilation efficiency to save project costs and improve the working environment quality.

With the gradual strengthening of environmental protection awareness in various countries, heat hazard control methods to directly reduce the temperature of underground heat sources have also been widely studied. As a high-quality clean energy, underground high temperature can reduce the heat dissipation of surrounding rock to the interior of the tunnel when extracted [17,18]. Guozhu Zhang et al. [19] developed a numerical model of the tunnel liner ground heat exchanger and evaluated the effect of ventilation on the thermal performance of the tunnel liner ground heat exchanger. Chao Yang et al. [20] proposed the idea of installing ground source heat pumps into underground tunnels and demonstrated the feasibility of this method to extract geothermal energy by numerical simulation and evaluated its economic benefits. Yu Xu et al. [21] proposed a synergetic mining of geothermal energy in deep mines to control heat hazard and established a fully coupled numerical model to determine that this technique can significantly improve thermal comfort and yield considerable geothermal energy in the tunnel.

The technical idea of blocking energy transfer is to isolate the high-temperature surrounding rock that causes heat hazard from the internal environment of the tunnel. It is a common method to spray thermal insulation material or set up thermal insulation layers on both sides of the tunnel to reduce the heat transfer efficiency. Guozhu Zhang et al. [22] proposed an air-layer structure to insulate the roadway, and the thermal performance of the insulated roadway with air-layer structure was evaluated by numerical simulation, which confirmed that the roadway with air-layer structure has better insulation effects. Fangchao Kang et al. [23] established a heat transfer model for high-temperature tunnels, compared the temperature fields of tunnels with and without insulation, and judged the many factors affecting the insulation effect. Weijing Yao et al. [24] studied the effect of thermal insulation on the radius of the heat transfer circle, the temperature field of surrounding rock, and the wall temperature by the ANSYS numerical simulation method, with sensitivity analysis of thermal insulation with different thermal conductivity and thickness. Nikodem Szlajak et al. [25] insulated the roof and sidewalls, comparing the climatic conditions in excavation tunnels with and without insulation, and the results showed that insulation is essential in high-temperature tunnels. However, there are few construction tests of tunnel insulation. Although the configured materials can play a good role in blocking energy transmission, the overall spraying or laying will greatly increase the process and economic burden in the early stage of project construction.

In previous studies, the engineering scale was usually large, and researchers discussed the influence of the thermal properties of surrounding rock on the overall tunnel heat transfer in a macroscopic way [26–28]. However, the influence of the thermal diffusion behavior of surrounding rock in local areas on spatial temperature distribution cannot be ignored [29], but the heat dissipation characteristics of the surrounding rock in excavation tunnels are rarely studied. In our previous research, it was found that the existence of auxiliary ventilation systems in excavation tunnels would bring differences in local thermal

diffusion [30,31]. It causes local high temperature in the working area of the excavation tunnel. Therefore, precise thermal insulation and cooling in areas with strong thermal diffusion is proposed as a simple, energy-saving, and efficient heat hazard control method. Based on the study of the thermal diffusion behavior of tunnel surrounding rock, this paper proposes a technical idea of accurate, partial thermal insulation for the working area with the most serious heat hazard and the largest number of workers from a local perspective. By combining the partial heat insulation with the auxiliary ventilation system in the excavation operation, together with the heat exchange system installed on the partial thermal insulation, the purpose of coupled cooling of ventilation and partial thermal insulation for synergistic geothermal energy extraction is realized. The establishment of partial insulation can effectively save the initial construction cost of the project and avoid the waste of materials caused by the overall laying. The precise thermal insulation of the work area can easily achieve a good effect of improving the tunnel environment, reduce the burden of refrigeration required by the ventilation system, and ensure a reasonable allocation of resources. In order to explore the characteristics and heat transfer laws of tunnel thermal environments under partial insulation conditions, a scaled model test platform of coupled cooling of ventilation and partial thermal insulation was built based on the law of similarity. The ventilation and cooling model of excavation tunnels was established by COMSOL Multiphysics, and the correctness of geometric and similar parameters selection in the scaled model test platform was verified. The influence law of partial insulation on the heat transfer of surrounding rock is obtained by analyzing the change of temperature in the tunnel with or without partial insulation. By adjusting the parameters of the ventilation and heat exchange layer, the efficiency of the ventilation coupled cooling and partial insulation was measured and the feasibility of the ventilation coupled cooling and partial insulation in the collaborative geothermal mining working face was judged, which provided a theoretical basis for further optimizing the working environment and saving energy.

2. Partial Thermal Insulation Technical Solutions and Advantages

2.1. Partial Thermal Insulation Design

In underground space engineering heat hazard, the surrounding rock is the main source of heat [32,33]. In the kilometer-deep mine tunnel, due to poor ventilation and continuous heat exchange between rocks, the local area is in a state of heat balance for a long time, and the initial rock temperature is stable at about 40 °C. Since the rock physical properties of the excavation tunnel in the same deep mine are similar (as shown in Table 1), the heat dissipation of surrounding rock in undeveloped local areas will not be too different.

Table 1. Thermal parameters of rocks.

Parameters	Value
Specific heat capacity of rock (J/(kg·°C))	1300
Heat conduction coefficient of rock (W/(m·°C))	3.5
Density of rock (kg/m ³)	2600
The initial temperature of rock (°C)	40–45

However, when the tunnel starts to be excavated, the heat dissipation of surrounding rocks in different areas is different. Due to the processes of rock cutting, drilling, and loading explosives, workers have to work 3–6 m away from the working face. In order to ensure the occupational safety of workers, auxiliary ventilation facilities must be added to ensure the cooling and dust removal needs. When ventilation facilities operate, air distribution becomes complicated, and there is a complex heat exchange process among the environment of the excavation tunnel, the high temperature surrounding rock, and the ventilation airflow. In the working area, high air velocity will lead to strong convective heat transfer, resulting in “heat recovery” [30,31,34]. This area is therefore the focus of precise insulation. Figure 1 shows the technical solution for partial insulation of underground space works.

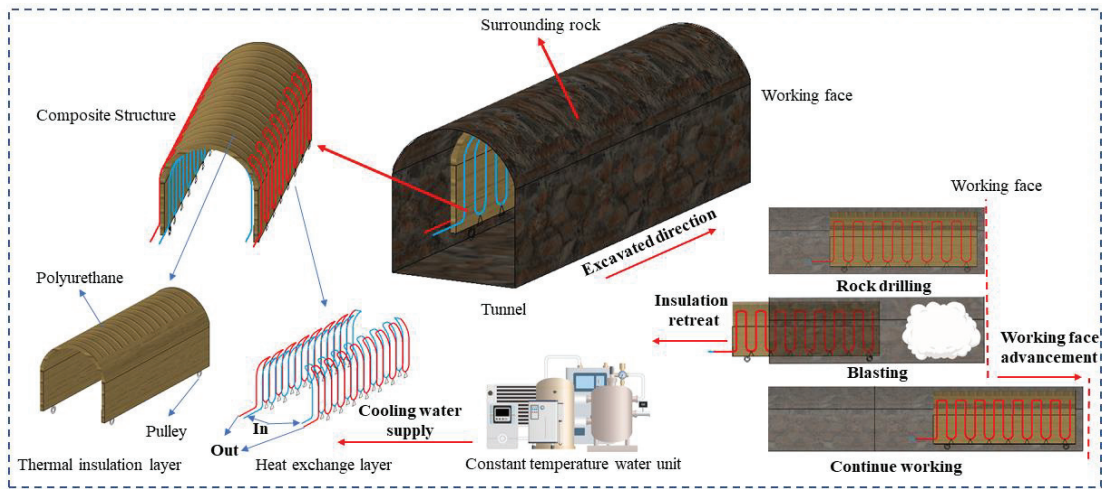


Figure 1. Movable thermal insulation layer structure and partial insulation method.

A movable thermal insulation layer (MTIL) is used in this study to achieve partial thermal insulation. Figure 1 shows the construction of a movable thermal insulation layer, which can be spliced into small sections in the design to ensure that the layer is adapted to a wider range of conditions. The heat exchange layer is arranged outside the insulation, using a thermostatic water unit to provide cold water as the medium for heat exchange. In this part, the main objective is to solve the heat hazard problem. The heat extraction aspect is considered when the water that can be provided in the mine allows the heat exchange layer to exchange heat effectively. And when the groundwater cannot meet the cooling requirements, the thermostatic water control device comes into play to provide a lower temperature heat exchange medium to achieve the cooling demands. The heat exchange medium is fed from the inside of the insulation for the first stage of heat transfer with the internal tunnel environment, thus reducing the ambient temperature inside the tunnel. The heat exchange medium is then transferred back to the outside of the insulation layer to reduce heat dissipation from the surrounding rock in the second phase of heat exchange with the surrounding rock, while allowing the heat exchange medium to be transported back to the end of the insulation layer for geothermal energy harvesting at the working face. A number of pulleys are arranged at the bottom of the insulation layer to achieve a movable function of the partial insulation structure, facilitating the pushing with the advance of the working face.

The movable thermal insulation layer is located at the working face with the workers when they are in the tunnel for processes, such as rock drilling and explosive loading. After these processes, the insulation is retreated with the staff to a safe area, and blasting is carried out. After blasting, the insulation continues to move forward with the slag-out process and so on to ensure that the temperature of the personnel working area is always within the allowable range of national standards.

2.2. Prospects, Values, and Limitations

The partial insulation discards the previous idea of laying insulation or spraying concrete throughout the tunnel and provides targeted cooling for the working area. From a technical point of view, partial insulation protects the areas where the heat exchange is most intense, blocking the heat dissipated by the surrounding rock while reducing the convective heat exchange between the air flow and the rock wall. The preserved air flow cools the internal environment of the tunnel more. In addition, there is little difference in the effectiveness of partial and total insulation in blocking heat transfer. From an economic

point of view, tunnels often extend hundreds or even thousands of meters, so for a single tunnel length of 100 m and commercially available insulating concrete of USD 187.5 per ton, the cost of insulation is approximately USD 30,000, whereas the cost of creating partial insulation is approximately 1 percent of that. Partial insulation not only saves a lot of materials, but also saves workers' time and effort when laying the whole insulation, which can better speed up the project.

Although the thermal insulation mortar used in the tunnels has a much lower thermal conductivity than ordinary concrete [35–38], it still falls short of commercially available building insulation materials [39,40]. However, building insulation materials are not suitable for underground space projects due to their high combustibility and low strength [41]. In the case of partial insulation, the insulation covers a small area and does not act as a support, which allows for a preferential selection of materials. The partial insulation can be disassembled and reused many times, even with expensive materials, without increasing costs.

With the gradual expansion of engineering (e.g., the increased depth of mining, the spread of tunnels to the plateau areas, the continuous expansion of the metro, etc.), the geothermal problem is gradually becoming more widespread, and the occupational health of workers is generally at risk. Although the partial insulation solution offers a simple and easy solution to improve the working environment, there are some problems with its implementation. Chief among these problems is the fact that the surrounding rock of the freshly excavated tunnel is not smooth, and the protruding rock is quite disruptive to the movement of partial insulation devices. Therefore, regular tunnels should be insulated with rigid materials according to the actual situation, and irregular tunnels should be designed with insulation curtains made of flexible materials, but the thermal insulation properties of both need further consideration and research. In addition, the partial insulation is not conducive to observing the dynamic changes in the surrounding rock because it does not assume a supporting role and covers a large area. Therefore, it is necessary to install monitoring holes or sensors on the insulation for real-time monitoring. In this study, such reconcilable realities have not been considered, but rather the focus has been on the functionality and efficiency of partial insulation. The neglected elements will be mentioned in the assumptions section.

3. Description of Similarity Experiment

When using mathematical methods to study some complex heat transfer processes, realistic or sufficiently accurate solutions are often not obtained because the set conditions are too ideal. Testing directly on the engineering site can have an impact on the productivity of the company, and it is impossible to determine the degree of influence of each factor and to make a single-factor summary of the law. The emergence of similarity theory has filled these gaps by offering the possibility of generalizing individual experimental results to similar phenomena. The following assumptions were made in this paper in order to reasonably simplify the test process:

- (1) The rock material is a homogeneous medium and the roughness is ignored.
- (2) Ignore the effect of humidity on heat transfer.
- (3) Ignore local heat dissipation by personnel and machinery.

3.1. Selection of Similarity Parameters

The similarity of the two phenomena presupposes that each element that makes up the model must be similar to its counterpart in the prototype, i.e., the physical field made up of a series of physical quantities must be correspondingly similar. The corresponding results for the prototype can be deduced from the results of the model tests. According to the similarity criterion, when two phenomena are similar, all the dimensionless combinations in the system of equations and singular value conditions of the two phenomena correspond to equal numbers and have the same dimensionless solution [42].

In the test, the heat exchange between the wind flow and the internal environment of the tunnel is mainly considered, so the selection of the similarity index involves fluid mechanics and heat transfer. During tunnel ventilation, the influence of pressure on the flow field is much greater than that of gravity, so the Froude number is ignored, and the main reference is the Reynolds number and the Archimedes number [43–45]. The medium in the tunnel where the heat transfer occurs is always air, so that the Prandtl number characterizing the physical properties of the fluid is almost constant [46,47]. In addition, the effects of buoyancy, inertial force, convective heat transfer, and thermal conductivity are also considered, and the Grashof number and Peclet number are analyzed [48,49]. The similarity indexes for fluid mechanics and heat transfer are selected as shown in Table 2.

Table 2. Similarity index for fluid mechanics and heat transfer.

Similarity Index	Representation
Reynolds number	Reflecting the ratio of inertial to viscous forces
Archimedes number	Reflecting the ratio of buoyancy to inertia force
Grashof number	Reflecting the ratio of buoyancy to viscous force
Prandtl number	Reflecting the relationship between momentum transfer and heat transfer

The main parameters of the scaled model tests are shown in Table 3.

Table 3. Scale model test parameters.

Parameter	Symbols	Scale	Relations
Length	$C_l = l_m:l_p$	1:10	-
Volume	$C_v = v_m:v_p$	1:1000	$C_v = C_l^3$
Velocity	$C_u = u_m:u_p$	10:1	-
Time	$C_t = t_m:t_p$	1:100	$C_t = C_l/C_v$
Density	$C_\rho = \rho_m:\rho_p$	1:1	-
Viscosity	$C_\mu = \mu_m:\mu_p$	1:1	-
Convective heat transfer coefficient	$C_h = h_m:h_p$	10:1	$C_h = C_\lambda/C_t$
Thermal conductivity	$C_\lambda = \lambda_m:\lambda_p$	1:1	-
Specific heat	$C_{cp} = C_{p_m}:C_{p_p}$	1:1	-
Temperature	$C_T = T_m:T_p$	1:1	-

A mathematical model was built with Comsol Multiphysics 6.0 to verify the feasibility of conducting scale model tests using the selected parameters. This study involves a multiphysics coupling of flow and heat transfer, and the governing equations were chosen as follows:

Fluid Mechanics Section:

- (1) Mass conservation equation and N-S equation [50,51]:

$$\frac{\partial \rho}{\partial t} + \nabla \cdot (\rho u) = 0, \tag{1}$$

$$\rho \left(\frac{\partial u}{\partial t} + u \cdot \nabla u \right) = -\nabla p + \nabla \cdot \left(\mu \left(\nabla u + (\nabla u)^T \right) - \frac{2}{3} \mu (\nabla \cdot u) I \right) + F, \tag{2}$$

where ρ is the density of fluid (kg/m³), t is the time (s), u is the velocity vector of fluid (m/s), p is the pressure of fluid (Pa), μ is the dynamic viscosity (Pa·s), I is the unit vector, and F is the momentum source term (kg/(m³·s)).

- (2) Realizable k-ε turbulence equation [52]:

$$\rho \frac{\partial k}{\partial t} + \rho u \cdot \nabla k = \nabla \cdot \left(\left(\mu + \frac{\mu_t}{\sigma_k} \right) \nabla k \right) + P_k + P_b - \rho \epsilon, \tag{3}$$

$$\rho \frac{\partial \varepsilon}{\partial t} + \rho u \cdot \nabla \varepsilon = \nabla \cdot \left(\left(\mu + \frac{\mu_t}{\sigma_\varepsilon} \right) \nabla \varepsilon \right) + C_{\varepsilon 1} \frac{\varepsilon}{k} P_k - C_{\varepsilon 2} \rho \frac{\varepsilon^2}{k}, \tag{4}$$

where $C_{\varepsilon 1}$, $C_{\varepsilon 2}$, σ_k , and σ_ε are realizable k - ε constants. C_μ is related to the mean strain rate and is defined by Equation (5):

$$C_\mu = \frac{1}{A_0 + A_S \frac{U^* k}{\varepsilon}}, \tag{5}$$

where A_0 , A_S , and U^* are functions of velocity gradients.

Heat transfer section:

(1) Heat transfer within the rock [53]:

$$\rho C_P \frac{\partial T_S}{\partial t} + \rho C_P u \cdot \nabla T_S = \nabla \cdot (K_S \Delta T_S) + (\nabla \cdot q) + Q, \tag{6}$$

where C_P is the specific heat capacity, J/(kg·K); T_S is the temperature of the solid, K; K_S is the thermal conductivity of the solid, W/(m·K); and Q is the heat resource, W/m³.

(2) Heat transfer between fluids [54]:

$$\rho C_P \frac{\partial T_g}{\partial t} + \rho C_P u \cdot \nabla T_g = \alpha_P \left(\frac{\partial p_A}{\partial t} + u \cdot \nabla p_A \right) - (\nabla \cdot q) + \tau : S + \nabla \cdot (K_g \Delta T_g) + Q, \tag{7}$$

where α_P is the coefficient of thermal expansion, 1/K; T_g is the temperature of air, K; P_A is the absolute pressure, Pa; τ is the viscous stress tensor, Pa; S is the strain rate tensor, 1/s; and K_g is the thermal conductivity of gas, W/(m·K).

(3) Heat exchange at fluid-solid coupling interfaces [55]:

$$q_c = h_k(T_g - T_s) + h_c(T_g - T_s), \tag{8}$$

where q_c is the heat flux by conduction and convection, W/m², and h_k and h_c are the heat conductivity coefficient and convective heat transfer coefficient, respectively, W/(m²·K).

To obtain a mesh-independent solution for the simulation results, the grid independence verification was carried out, and the results are shown in Table 4. As the number of grids increases, both the air temperature and ventilation volume tend to stabilize at the grid number of 38,000. Taking into account the accuracy of the solution and the speed of the calculation, the grid number was chosen to be 43,072.

Table 4. Grid Independence Verification.

Grid Number	Air Temperature (°C)	Ventilation Volume (m ³ /min)
1124	25.48	21.87
1476	25.11	21.63
1723	25.79	21.63
2106	25.52	21.47
2733	25.66	21.36
5585	24.35	23.11
13,102	24.34	23.61
38,100	26.70	27.05
43,072	26.72	27.17

Forty monitoring locations were evenly selected at the central axis of the tunnel, and the temperature errors between the model and the prototype are shown in Table 5.

The relative error is calculated by the following formula:

$$RE = \frac{P_v - M_v}{P_v} \times 100\%, \tag{9}$$

where RE is the relative error, %; P_v is the calculated value of the prototype, K ; and M_v is the calculated value of the model, K .

Table 5. Prototype and model relative error.

Monitoring Location Number	Relative Error (%)	Monitoring Location Number	Relative Error (%)
1	2.62×10^{-4}	21	-1.22×10^{-2}
2	-8.70×10^{-4}	22	-1.22×10^{-2}
3	-1.75×10^{-3}	23	-1.24×10^{-2}
4	-2.74×10^{-3}	24	-1.24×10^{-2}
5	-3.71×10^{-3}	25	-1.25×10^{-2}
6	-4.67×10^{-3}	26	-1.26×10^{-2}
7	-5.53×10^{-3}	27	-1.32×10^{-2}
8	-6.44×10^{-3}	28	-1.36×10^{-2}
9	-7.18×10^{-3}	29	-1.33×10^{-2}
10	-8.09×10^{-3}	30	-1.34×10^{-2}
11	-8.75×10^{-3}	31	-1.35×10^{-2}
12	-9.60×10^{-3}	32	-1.27×10^{-2}
13	-1.01×10^{-2}	33	-1.18×10^{-2}
14	-1.06×10^{-2}	34	-1.19×10^{-2}
15	-1.10×10^{-2}	35	-1.36×10^{-2}
16	-1.12×10^{-2}	36	-1.45×10^{-2}
17	-1.14×10^{-2}	37	-1.42×10^{-2}
18	-1.16×10^{-2}	38	-1.39×10^{-2}
19	-1.18×10^{-2}	39	-1.36×10^{-2}
20	-1.20×10^{-2}	40	-1.20×10^{-2}

As can be seen from Table 3, the relative error between the model and the prototype does not exceed 0.015%, with a maximum value of -0.014% . Errors of this magnitude are negligible in engineering, so it can be assumed that the parameters were chosen correctly and that the tests carried out in the model can provide a reference for discussing the phenomenon in the engineering prototype.

3.2. Composition of the Test Platform

The built test platform for the coupled cooling of ventilation and partial insulation scale model consists of three main components: the ventilation unit, the data acquisition unit, and the temperature control unit. The ventilation unit consists of the axial fan, tapering tube, reducer, ventilation ducts, and model tunnel; the data acquisition unit consists of the KEYSIGHT DAQ970A Data Acquisition System, Pt100 thermocouples, and Fluke 923 air velocity meter; and the temperature control unit consists of the electric heating belts, temperature controller, and insulation cotton for the tunnel exterior.

3.2.1. Test Platform Dimensions and Layout

The prototype referenced for the construction of the test platform is a conventional arch shape. The scaled model tunnel width is 0.3 m, the sides of the surrounding rock are 0.18 m high, and the arch height is 0.28 m. The tunnel monitoring area is the part of the length of 1 m from the working face. In addition, to prevent the influence of the tunnel exit boundary conditions on the monitoring area, the tunnel exit was extended to create a virtual tunnel up to 2 m. The ventilation duct has a diameter of 0.05 m and is suspended 0.025 m from the floor. The test model is heated by wrapping an electric heating belt evenly around the exterior of the surrounding rock and adjusting it to the required temperature by means of a thermostat. Wrap insulation cotton around the outside of the electric heating belt to ensure the stability of the temperature control and to avoid excessive errors caused by fluctuations in the external ambient temperature. A number of thermocouples were placed inside the model tunnel, connected to the data acquisition system for real-time

temperature monitoring, and the input air flow velocity was controlled in the ventilation system by means of air windows. The layout of the test platform is shown in Figure 2.

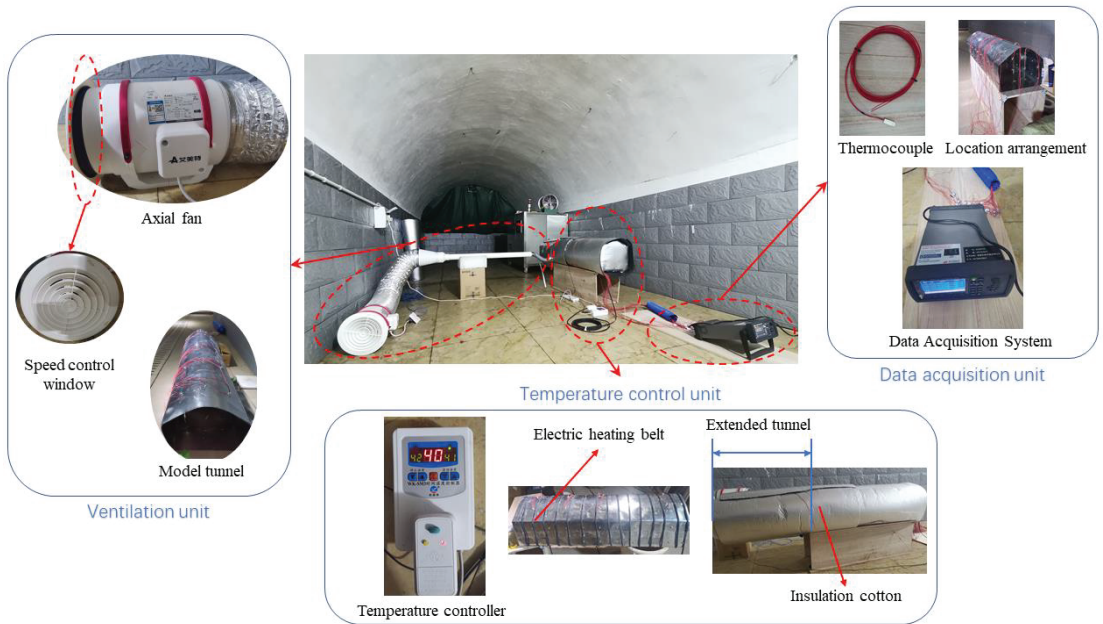


Figure 2. Scale model test platform for coupled cooling of ventilation and partial thermal insulation.

3.2.2. Monitoring Scheme

A total of 24 temperature-monitoring locations were set up on the test platform, including 18 temperature-monitoring locations for working areas (101–118) and 3 monitoring locations for surrounding rock walls (201-roof, 202-left wall, and 204-floor). The remaining 4 monitoring locations were the inlet of the fan (207), the extended tunnel (203), the outlet of the ventilation duct (205), and the test environment (206). The distribution of each temperature-monitoring location is shown in Figure 3.

Monitoring locations 101–108 are at a height of 0.2 m above the floor, and monitoring locations 109–118 are at a height of 0.1 m above the floor. The data scan interval for all monitoring locations is 1 s.

3.3. Test Strategy

The experiment investigates the effect of the presence or absence of insulation in a ventilation tunnel on the high-temperature environment and determines the feasibility and cooling efficiency of partial insulation devices. The presence or absence of insulation, ventilation time, air velocity, and surrounding rock temperature were used as study variables in the tests, with temperature variation in the tunnel as the target variable for analysis. In addition, extraneous variables, such as heating method, fan heat dissipation, and ambient temperature, were kept as consistent as possible to avoid any influence on the test results. Table 6 depicts the ambient temperature (including pre-test) at each test.

Before starting the experiment, set the velocity of the duct outlet to the required value and fix the position of the duct. Due to the different positions of the thermocouples and the fact that the heating of the surrounding rock is not absolutely uniform, the ambient temperature control in the tunnel is based on the monitoring point with the slowest temperature rise reaching the required value. In addition, the temperature controller is equipped with sensors arranged on the tunnel rock wall to control the heating efficiency

and keep the temperature of the surrounding rock within a certain range to ensure the accuracy of the experiment.

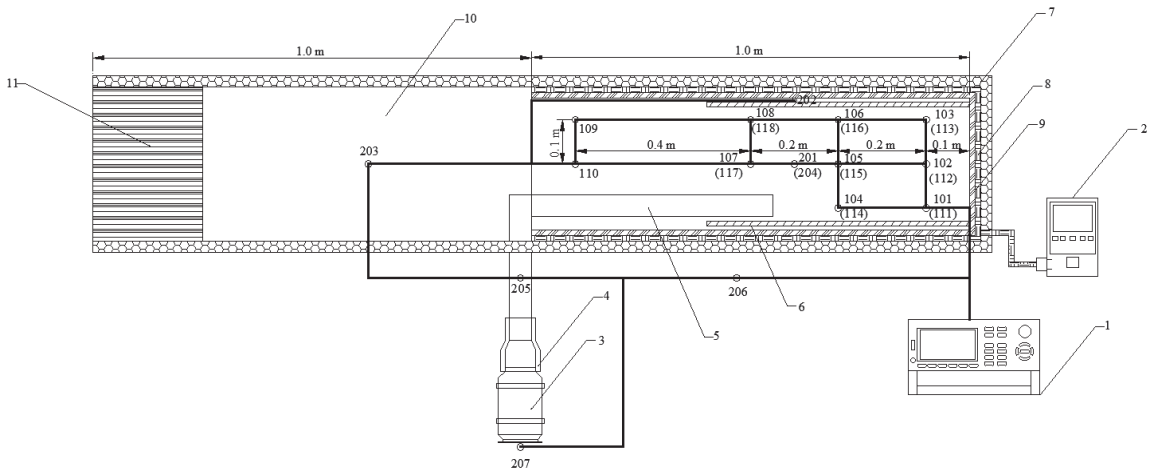


Figure 3. Distribution of temperature-monitoring locations on the test platform. 1—Data acquisition system; 2—Temperature controller; 3—Axial fan; 4—Reducer; 5—Ventilation duct; 6—Partial thermal insulation baffle; 7—Insulation cotton; 8—Electric heating belt; 9—Surrounding rock; 10—Virtual tunnel; 11—Tunnel movable exit.

Table 6. Temperature variation in the test ambient.

Test Number	1	2	3	4	5	6	7	8	9	10	11	12	13
Ambient temperature (°C)	16.5	16.5	16.6	16.6	16.5	17.1	16.7	16.7	17.0	16.5	16.2	16.4	16.5

4. Analysis of the Temperature Field in the Partial Insulated Tunnel

4.1. Partial Thermal Insulation Effect

To investigate the effect of partial insulation, heating tests were carried out in a tunnel with and without insulation. In this paper, the insulation was chosen to be made of polyurethane, in a length of 0.6 m, placed close to the working face and 0.01 m from the sides of the tunnel. Heating started 120 s after the data acquisition was started, and the heating process continued for 500 s. The results are shown in Figure 4, with data collected at monitoring location 101 in the insulation-covered area and location 203 in the uncovered area.

Figure 4a shows that the tunnel with the insulation layer heated up more slowly. For example, it took 545 s for a tunnel with insulation and only 480 s for a tunnel without insulation to reach 40 °C. This means that tunnels with insulation in the project will reach high temperatures almost 2 h later. The temperature difference with and without insulation is shown at the bottom of Figure 4a. At the beginning of the heating, the temperature difference was small, but as the heating continued, the temperature difference gradually increased and eventually tended to stabilize, with a final stable temperature difference of approximately 3.5 °C. Figure 4b shows that the opposite situation exists in the uncovered area as opposed to the covered area, where the temperature is higher in the uncovered area of the tunnel with partial insulation. This is due to the presence of the insulation affecting the direction of heat dissipation, with more heat escaping towards the rear of the tunnel along the gap between the insulation and the surrounding rock. After accounting, the average temperature of the working area of the tunnel without insulation reached 45.0 °C when heated continuously for 600 s, while the average temperature of the working area of the tunnel with insulation was only 41.6 °C.

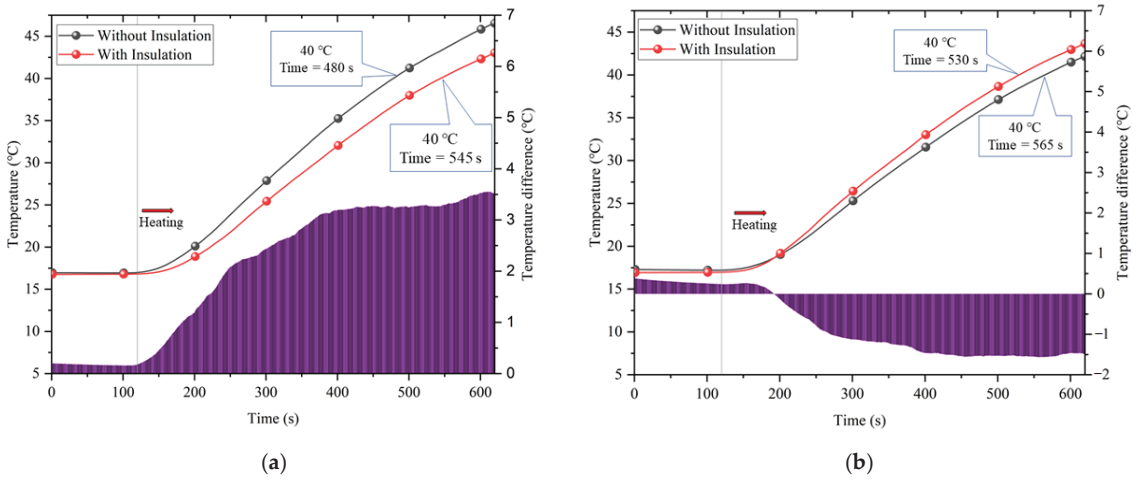


Figure 4. Comparison of partial insulation effects: (a) Covered area; (b) Uncovered area.

4.2. Temperature Field Distribution of Partially Insulated Tunnel

Due to differences in the position of the monitoring locations, the temperature at each location varies. Figure 5 shows the variation in temperature at the monitoring locations in the partially insulated tunnel.

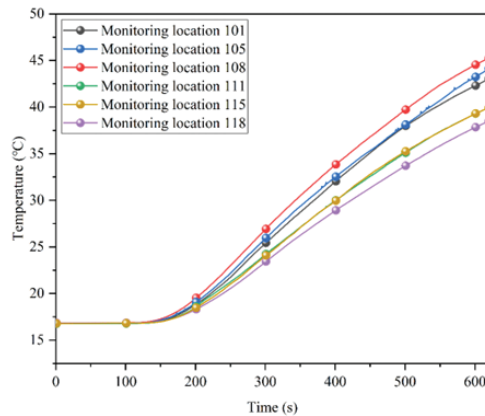


Figure 5. Partially insulated tunnel monitoring-point temperatures.

In Figure 5, it can be seen that the upper monitoring locations (i.e., monitoring locations 101–108) had higher temperature than the lower monitoring locations (i.e., monitoring locations 109–118). There are two main reasons for such difference: on the one hand, the heating time is short, and the heating is carried out continuously, the density of the air decreases as the temperature rises, and the hot air moves upwards to accumulate; on the other hand, the tunnel is arched, and the area of the top plate is much larger than the bottom plate, which has a larger area for heat dissipation, and the temperature is higher at the monitoring points near the top plate. The above phenomenon is not related to the placement of partial insulation, which has an effect on the temperature field distribution mainly on the temperature difference between the upper and lower monitoring locations. The temperature difference between vertical sections at some of the monitoring locations is shown in Figure 6.

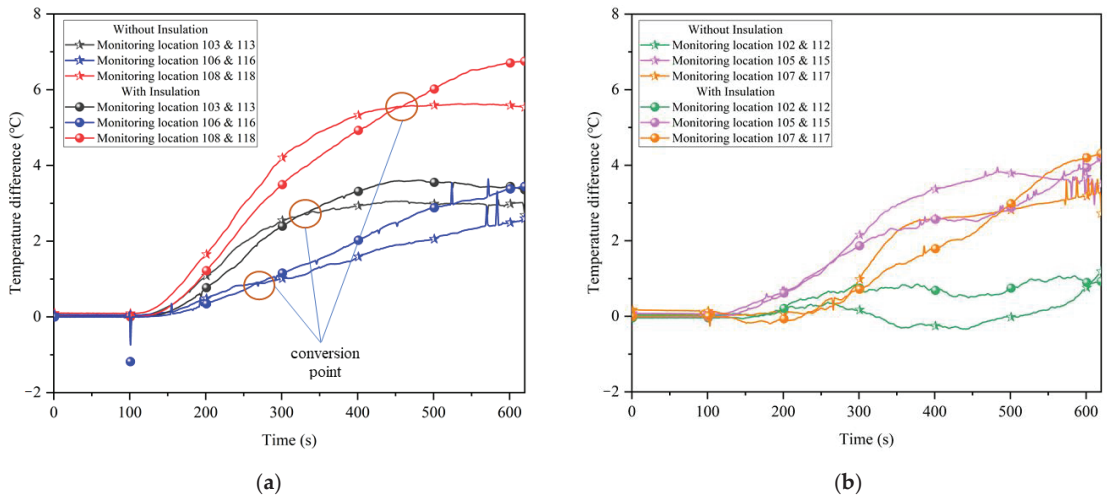


Figure 6. Temperature difference between vertical sections at selected monitoring locations: (a) Left side of tunnel; (b) Middle of tunnel.

Figure 6a shows that on the left side of the tunnel, the temperature difference between the upper and lower monitoring locations gradually shows an increasing trend with increasing heating time. In the early stages of heating, the different heat dissipation areas of the surrounding rock walls, and the fact that the walls reached similar temperature within a short period of time, resulted in a large difference in temperature between the upper and lower parts of the tunnel without insulation, while the tunnel with insulation had no significant difference in temperature between the upper and lower parts because the temperature diffusion was slower. After heating for a period of time, the conversion point was reached. As the upper monitoring locations were closer to the roof of the tunnel, they were more severely affected by heat dissipation, and the heat from the rock wall on both sides would spread upwards through the gap between the insulation and the surrounding rock, while the lower monitoring locations were located inside the insulation and were only affected by heat dissipation from the floor, so the insulation effect gradually manifested. The temperature difference between the upper and lower parts of the tunnel with insulation rises and exceeds that of the tunnel without insulation.

The conversion points represent the times when the insulation affects the change in temperature between the upper and lower monitoring locations, where monitoring locations 106 and 116 were located in the middle of the insulation and the conversion points arrived earlier. Monitoring locations 103 and 113 were slow to reach the conversion point due to their proximity to the working face and the effect of heat dissipation from the working face. Monitoring locations 108 and 118 were located at the back end of the insulation, where the insulation was weakened, thus reaching the conversion point the latest. Figure 6b shows the variation of the temperature difference between the upper and lower part of the tunnel at the central axis, which does not show the regular variation as in Figure 6a because the temperature at the center was less influenced by the insulation. The unevenness of the temperature of the surrounding rock in the test results is a diffusion of heat in the tunnel that is not linear. According to the second law of thermodynamics, the temperature at the center of the tunnel should develop towards a certain stable value. With insulation, the temperature difference between the center and rear monitoring locations (i.e., 105 and 115, 107 and 117) was much lower than without insulation. This means that the insulation makes the temperature spread more evenly in the center of the tunnel. The monitoring locations at 102 and 112 were close to the working face and were heavily

influenced by heat dissipation, resulting in a small temperature difference between the top and bottom, close to 0.

Combined with what is shown in Figure 4b, the general distribution of the temperature field under partial insulation can be derived. Due to the existence of gaps between the insulation layer and the surrounding rock, most of the heat is dissipated from above and behind the gaps, thus presenting a phenomenon that the upper temperature is greater than the lower temperature, and the front temperature difference is lower than the rear temperature difference in the partially insulated tunnel.

5. Analysis of the Coupling Effect of Ventilation and Partial Thermal Insulation

5.1. Effect on Cooling Limit

The following tests were carried out to investigate the effect of with or without partial insulation on the ventilation cooling limit. First, the virtual tunnel outlet was closed and heating was started. When the overall ambient temperature inside the tunnel was above 40 °C, the outlet was opened, and ventilation was started for a duration of 800 s. After this period, the heating and ventilation were stopped, and the insulation was removed. The heating and ventilation were repeated as described above. Using a model inlet air velocity of 7.5 m/s as an example, the temperature variation curve over time was obtained for some of the monitoring locations in the tunnel, as shown in Figure 7.

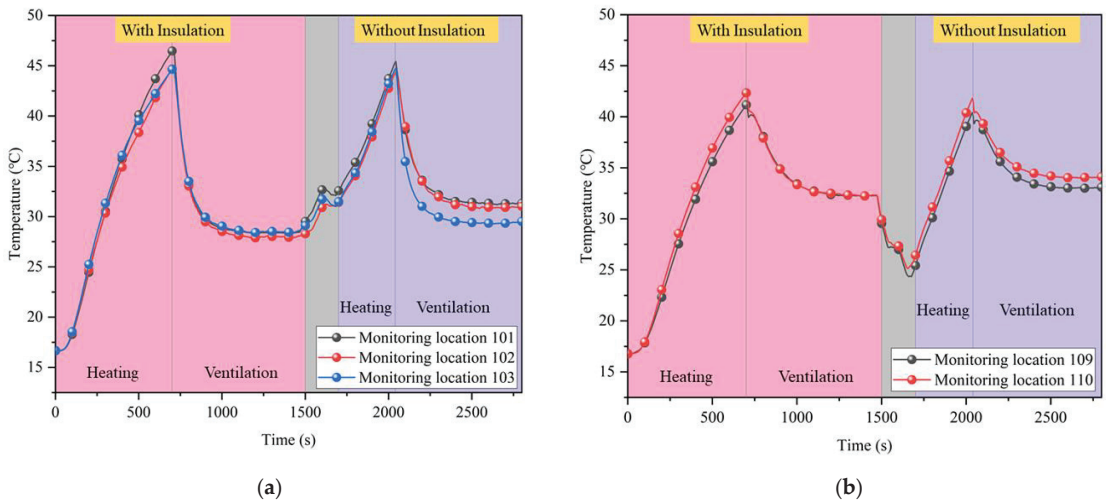


Figure 7. Temperature variation in the tunnel under coupled cooling test: (a) Inside the insulation area; (b) Outside the insulation area.

The first half of Figure 7a,b is both with insulation, which was removed after 1500 s of testing (i.e., the central grey area), and the second half is tested without insulation. Figure 7a shows that in the condition with partial insulation, the monitoring point reached a lower temperature at steady state than without insulation. This is because the insulation layer blocks the direct contact between the airflow and the high-temperature surrounding rock, reducing the loss of airflow cooling during convective heat transfer. In Figure 7b, with or without insulation had no significant effect on the cooling limit because the positions of the monitoring locations were outside the partial insulation. This also confirms that convective heat transfer between the airflow and the surrounding rock is not significant at the rear of the air shaft outlet.

In the case of partial insulation, the upper and lower monitoring locations end up with similar cooling limits, whereas without insulation, the lower monitoring locations near the

ducts can be reduced to lower temperature. The cooling limits for the upper and lower monitoring locations with and without insulation are shown in Figure 8.

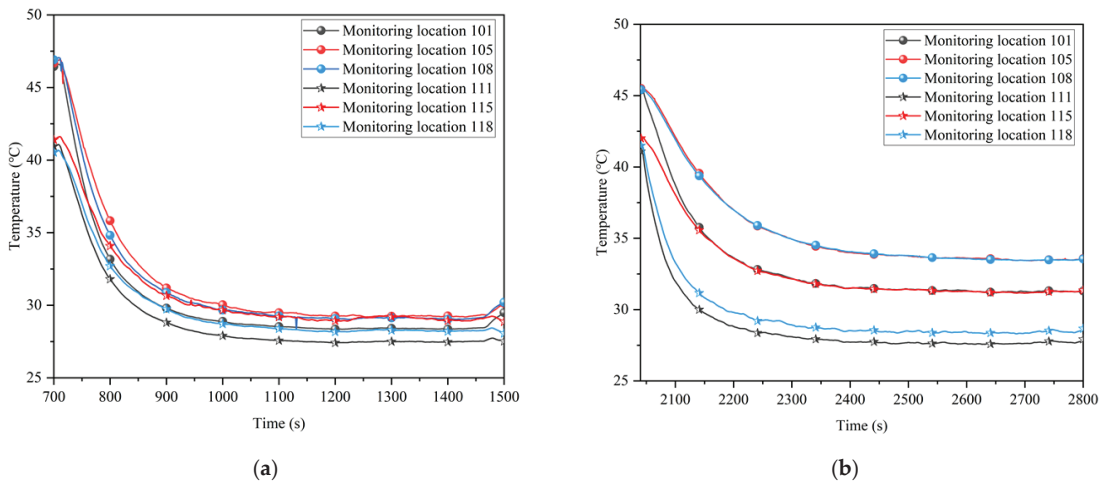


Figure 8. Comparison of cooling limits at upper and lower monitoring locations with and without insulation: (a) With insulation; (b) Without insulation.

As the air flow was only convective heat exchange with the working surface when there was insulation, more of the cooler volume was used to cool the tunnel environment, resulting in a lower overall temperature. Conversely, when there was no thermal insulation, the cooler air flow was used to offset the convective heat exchange with the surrounding rock and thus failed to cool the upper tunnel environment. The average temperature at each monitoring location in the partial insulation range was calculated to be 29.6 °C with insulation and 31.2 °C without insulation. The difference is 1.6 °C, while the difference in temperature limit at some monitoring locations is much higher than this value, up to 4.3 °C. Combined with the rate of temperature rise in the tunnel, this results in a cooling savings of approximately 2.6×10^6 J per day when using coupled cooling of partial insulation and ventilation.

5.2. Effect of Ventilation Speed

In order to explore the influence of air velocity on the partial insulation effect, the model air velocity was adjusted to 7.5 m/s, 8.5 m/s, and 9.5 m/s for experiments. To ensure that the ambient temperature was consistent in the test, the same steps as those in Section 5.1 were used, and the results are shown in Figure 9.

Figure 9 shows that the achievable cooling limit decreased with increasing air velocity and was more pronounced when without insulation. This indicates that the partial insulation effect decreased with increasing air velocity for the same initial temperature and rock temperature. The cooling effect at 8.5 m/s air velocity with insulation in the figure is almost equal to the cooling effect at 9.5 m/s air velocity without insulation. Therefore, when the minimum dust removal air velocity is met, the practical engineering can reduce the consumption of air volume by providing partial insulation.

5.3. Effect of Surrounding Rock Temperature

The temperature of the surrounding rock is one of the main factors affecting ventilation and cooling. The effect of the initial temperature of the surrounding rock on the coupling of ventilation and partial thermal insulation was investigated by controlling the temperature of the surrounding rock at 50, 45, 40, and 35 °C. The corresponding ambient temperatures in the tunnel were 47.9, 40.5, 38.1, and 33.7 °C, respectively. In this paper, the top plate

temperature was used as a reference for temperature control, and the test results are shown in Figure 10.

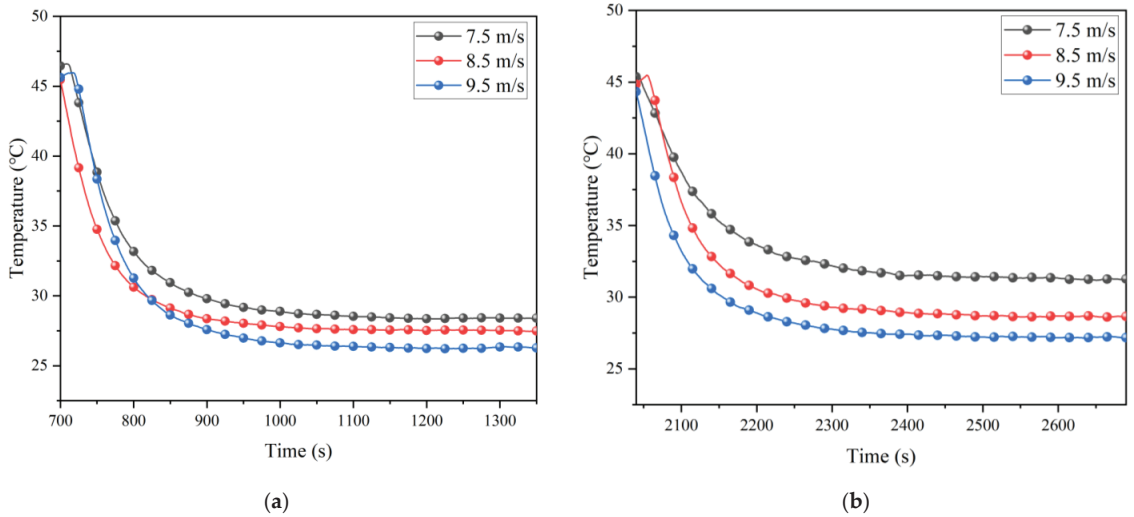


Figure 9. Average cool-down at different air velocities with and without insulation: (a) With insulation; (b) Without insulation.

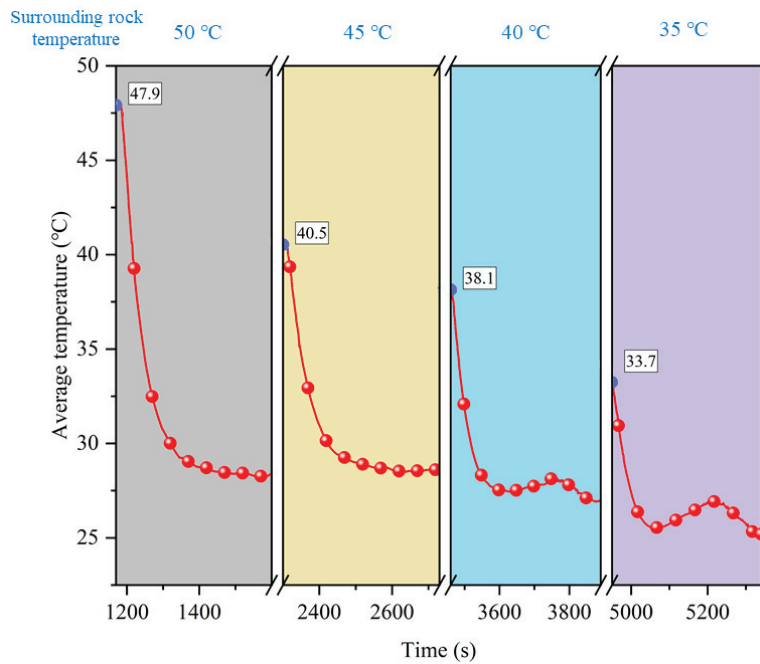


Figure 10. Cooling effect at different surrounding rock temperatures.

The effect of coupled ventilation and partial insulation for different rock temperatures is illustrated in Figure 10, where it can be seen that the cooling effect increases as the rock temperature decreases. This effect is reflected in two ways. Firstly, the tunnel with a low surrounding rock temperature can reach a lower temperature after cooling for the same

ventilation conditions. Secondly, at the start of ventilation, the temperature of a tunnel with a low rock temperature drops more quickly, and the cooling limit can be reached in a shorter period of time.

5.4. Effect of Single and Double Heat Exchange Layer on Cooling Effect

In this section, a heat exchange layer is attached to the original partial insulation layer to realize the coupled cooling of ventilation and partial insulation for synergistic geothermal extraction. In order to better reflect the working effect of the heat exchange layer, the inlet air temperature in this section is set higher than in the previous test, with an average of 26.6 °C. The ventilation speed is set to a constant 8.5 m/s. The average temperature variation with ventilation time in the working area of the tunnel with a single heat exchanger layer (the heat exchanger layer is only arranged inside the insulation layer), a double heat exchanger layer (the heat exchanger layer is arranged on both sides of the insulation layer), and without a heat exchanger layer is shown in Figure 11.

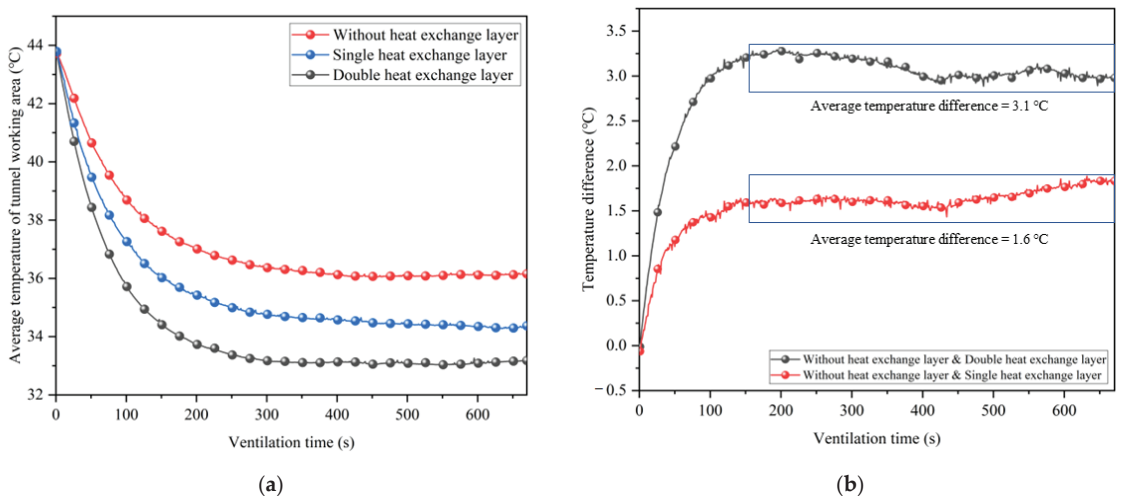


Figure 11. Comparison of the average temperature in the working area of different types of heat exchange layers: (a) Average temperature; (b) Temperature difference.

In Figure 11, the average temperature in the working area of the tunnel is highest when reaching thermal equilibrium without the additional heat exchange layer. The placement of the heat exchanger layer can effectively reduce the tunnel temperature further. From Figure 11b, it can be seen that a single heat exchange layer can reduce the thermal equilibrium temperature in the tunnel by 1.6 °C on average, and a double heat exchange layer can reduce the thermal equilibrium temperature in the tunnel by 3.1 °C. Despite the fact that the second heat exchange layer is installed on the outside of the insulation, the cooling effect is nearly doubled. To investigate the effect of single and double heat transfer layers on the temperature field of the working area in the tunnel, the equilibrium temperature of the working area in the tunnel under each case was organized into a cloud diagram, as shown in Figure 12.

As can be seen in Figure 12, the temperature in both the upper and lower parts of the working area decrease with the addition of heat transfer layers and the increase in the number of layers. The difference is that in the lower part of the working area, the shape of the temperature field does not change, and the area of high temperature is fixed in each case. Since the auxiliary ventilation ducts are installed in the lower part of the tunnel, the air velocity below the tunnel is larger, and the coupling effect is formed between the fresh air flow and the heat exchange layer, so the temperature field distribution is closely related

to the trajectory of the air flow. The upper part of the tunnel is more directly affected by the heat exchange layer, and the low-temperature heat exchange medium comes in contact with the hot air in the tunnel to lower the temperature. In general, the existence of the heat transfer layer can significantly improve the efficiency of the coupled cooling of ventilation and partial thermal insulation, while the cooling effect of the double heat exchange layer is much higher than that of the single heat exchange layer. Adding a heat exchange layer on the basis of partial thermal insulation can promote the further improvement of the heat environment in the tunnel. In addition, considering the purpose of synergistic geothermal energy extraction, the temperatures of the input and output water were monitored, and the results obtained are shown in Figure 13.

Figure 13 depicts a large difference in water temperature at the inlet and outlet of the heat exchanger layer, indicating that geothermal energy extraction can be achieved by attaching a heat exchanger layer to the partial insulation. In the initial stage of ventilation, the temperature of the collected return water is higher, which is due to the warming of the accumulated water in the heat exchange layer with the heating of the tunnel during the heating stage, resulting in a larger amount of heat energy extraction in the initial stage, while it gradually tends to stabilize afterwards. During the measurement, the heat energy extraction of the double heat exchange layer is higher, with an average temperature difference of 6.9 °C between the inlet and outlet water, while the single layer can reach only 3.3 °C. Combine the flow rate of the medium in the experimental heat exchange layer with a similar theory, for example, a single heat exchange layer can extract geothermal energy of 2.151×10^8 J and a double layer can extract geothermal energy of 4.5×10^8 J with one year of operation.

5.5. Effect of Heat Exchanger Pipe Arrangement Density on Cooling Effect

In addition to the number of heat transfer layers, considering that the density of heat transfer pipes arranged on one side of the insulation layer may also be an important parameter affecting the cooling and heat extraction effect, the following test was done: a denser heat transfer pipe was arranged on one side of the insulation layer, so that the length of the heat transfer pipe was the same as the total length of the pipes arranged on both sides in the double heat transfer layer for the cooling test. The average temperature of the working area and the temperature of the water extracted from the heat exchange layers are shown in Figure 14.

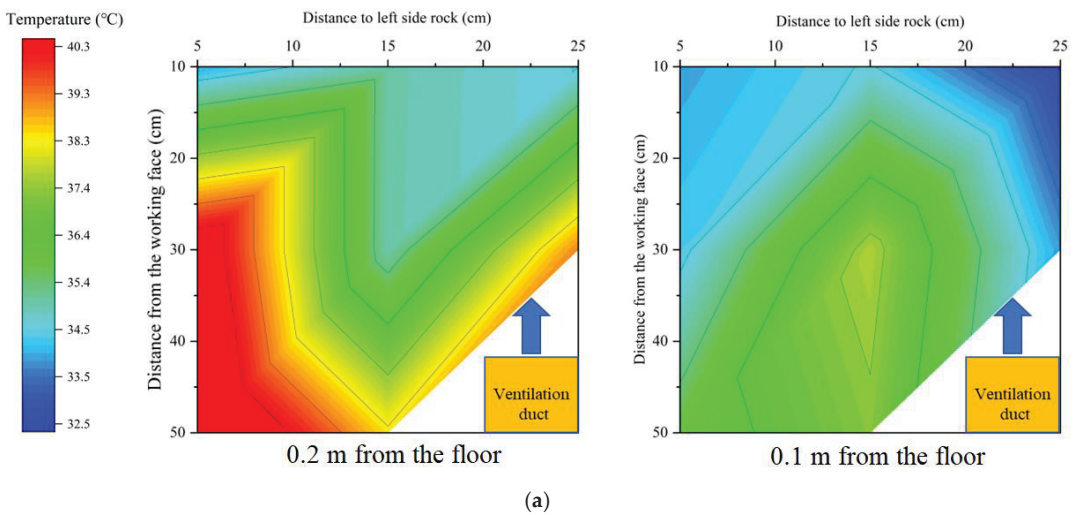


Figure 12. Cont.

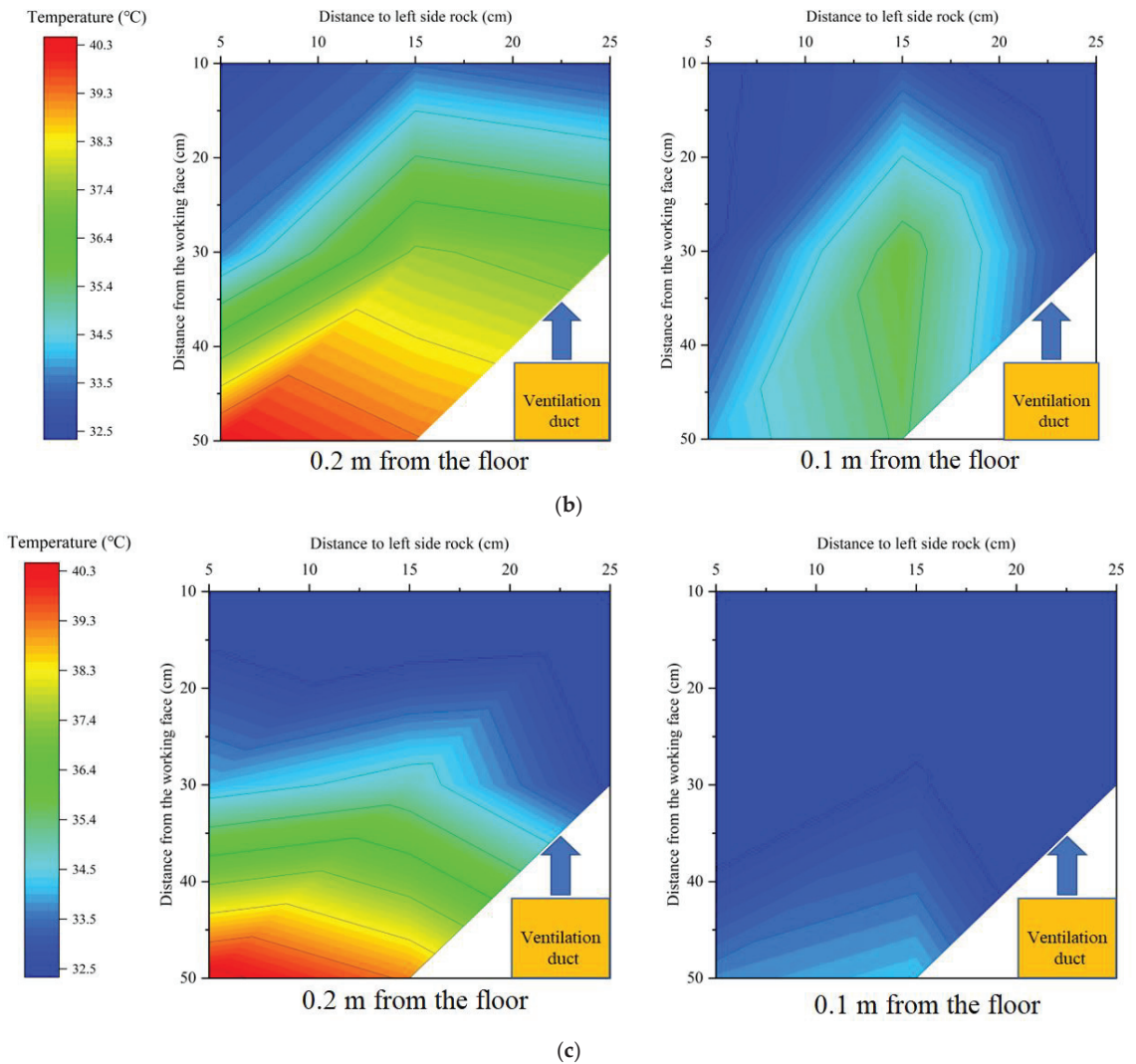


Figure 12. Working area temperature field under different heat exchange layer arrangement cases: (a) Without heat exchange layer; (b) Single heat exchange layer; (c) Double heat exchange layer.

In Figure 14a, the final cooling effect after increasing the density of the heat exchange pipes is similar to the setting of a double heat exchange layer. This indicates that it is mainly the effective heat transfer length that affects the heat transfer effect. However, in Figure 14b, the heat extraction effect of the double heat transfer layer is much higher than that of the large density heat transfer layer. This is due to the fact that one side of the double heat transfer layer is almost next to the surrounding rock, and the heat transfer effect is obvious while reducing the heat dissipation from the surrounding rock, so more heat can be extracted while achieving almost the same cooling effect. Therefore, when wanting to enhance the cooling effect by adjusting the heat exchange layer, the density of the heat exchange pipe arrangement should be increased, and if wanting to extract more geothermal energy, double insulation should be adopted to obtain more economic benefits without increasing additional pumping power.

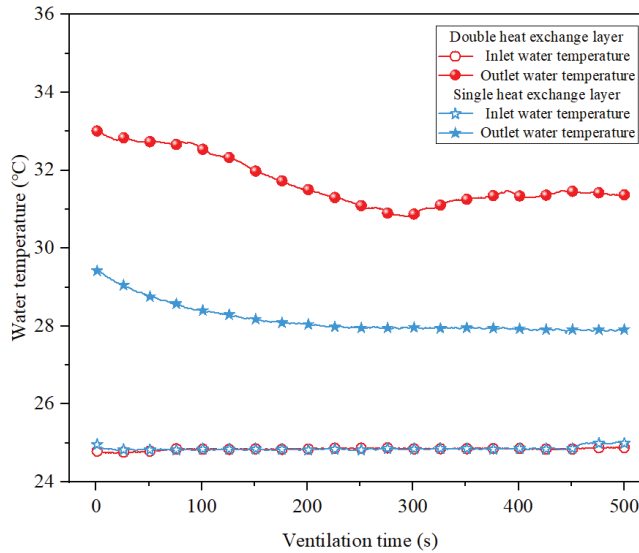


Figure 13. Variation of inlet outlet water temperature under different heat exchange layer cases.

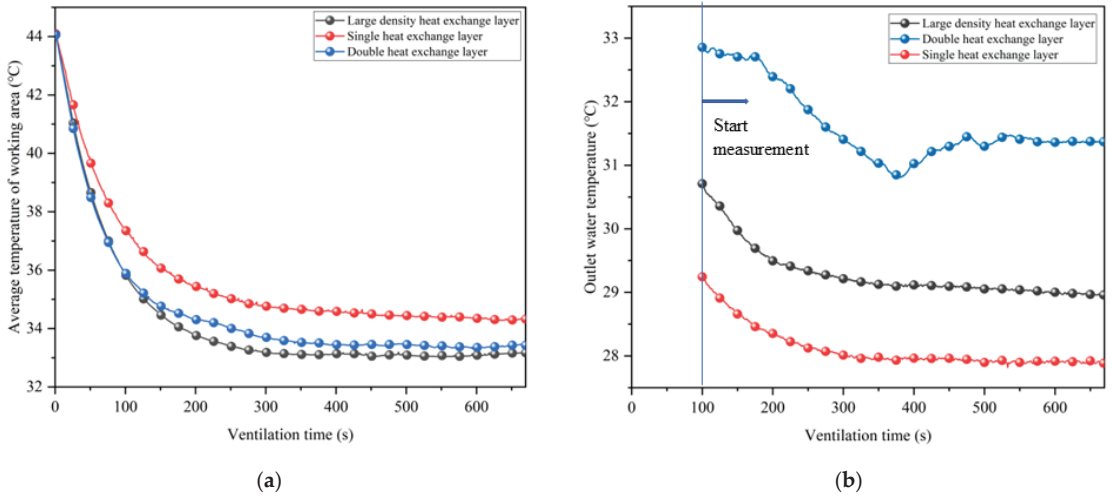


Figure 14. Average temperature of working area and water at different heat exchange pipe density: (a) Average temperature; (b) Water temperature.

6. Conclusions

Aiming at the heat hazard problem in underground tunnels, this paper proposed a new technical idea of coupled cooling of ventilation and partial insulation. Based on the similarity principle, the geometric parameters and similar parameters were determined and calculated, and the experimental platform of the ventilation and partial insulation coupling cooling scale model was established. The three-dimensional ventilation and cooling model of tunnel flow and heat transfer coupling was established by COMSOL, and the rationality of similar parameter selection was verified. By adjusting the parameters and modes of heat insulation, ventilation, and heat transfer, the feasibility of the coupling method of ventilation and local heat insulation and cooling is verified by experiments. The main conclusions are as follows:

- (1) The concept of coupled cooling of ventilation and partial thermal insulation is proposed. The precise insulation of the working area can effectively enhance the ventilation cooling effect and improve the tunnel environment, while saving insulation materials and reducing the unnecessary investment in the tunnel construction.
- (2) By constructing a test platform for coupled cooling of ventilation and thermal insulation, it was confirmed that the construction of partial insulation can improve the high-temperature environment in the working area. The construction of partial insulation makes the temperature field in the tunnel appear higher at the top than at the bottom and the difference lower at the front than at the back. When ventilation and partial heat insulation are coupled to reduce temperature, the partial thermal insulation layer can make the ventilation cooling limit decrease. The average temperature of the working area is reduced by 1.6 °C.
- (3) The ventilation velocity and the temperature of the surrounding rock are important factors affecting the coupled cooling effect of ventilation and partial thermal insulation. As the air velocity increases, the cooling effect gradually increases, and the thermal insulation effect gradually decreases. As the temperature of the surrounding rock increases, the efficiency of the coupled cooling of ventilation and partial thermal insulation decreases.
- (4) The further addition of a heat exchange layer on top of the insulation layer can achieve a better cooling effect and realize the synergistic exploitation of geothermal energy. The cooling effect is proportional to the length of the heat exchanger tube, and the best heat energy extraction effect is achieved by the double heat insulation layer, which can extract about 4.5×10^8 J of heat energy in 1 year of operation.

Author Contributions: J.W.: Writing—original draft, visualization, methodology, validation. Z.L.: Funding acquisition, project administration. G.L.: Visualization, review, and editing. Y.X.: Formal analysis. All authors have read and agreed to the published version of the manuscript.

Funding: This research was supported by the National Natural Science Foundation of China (Project No. 52274247), Natural Science Foundation of Hunan Province (Project No. 2022JJ30050), Changsha Municipal Natural Science Foundation (Project No. kq2202073), and Postgraduate Innovative Project of Central South University (Project No. 2021XQLH005).

Institutional Review Board Statement: Not applicable.

Informed Consent Statement: Not applicable.

Data Availability Statement: Not applicable.

Conflicts of Interest: The authors declare that there is no conflict of interest regarding the publication of this paper. The founding sponsors had no role in the design of the study; in the collection, analyses, or interpretation of data; in the writing of the manuscript; or in the decision to publish the results.

References

1. Zhu, S.; Cheng, J.; Song, W.; Borowski, M.; Zhang, Y.; Yu, B.; Wang, Y.; Qi, C.; Tukkaraja, P.; Hua, G.; et al. Using seasonal temperature difference in underground surrounding rocks to cooling ventilation airflow: A conceptual model and simulation study. *Energy Sci. Eng.* **2020**, *8*, 3457–3475. [[CrossRef](#)]
2. Chu, Z.; Zhou, G.; Rao, Z.; Wang, Y.; Zhao, X. Field measurement and assessment on airflow thermodynamic parameters in hot and humid underground tunnelling: A case study. *Tunn. Undergr. Space Technol.* **2022**, *121*, 104341. [[CrossRef](#)]
3. Xu, Y.; Li, Z.; Wang, J.; Chen, Y.; Li, R.; Wang, Q.; Jia, M. Ventilation and heat exchange characteristics in high geotemperature tunnels considering buoyancy-driven flow and groundwater flow. *Int. J. Therm. Sci.* **2022**, *173*, 107400. [[CrossRef](#)]
4. Wang, M.; Hu, Y.; Wang, Q.; Tian, H.; Liu, D. A study on strength characteristics of concrete under variable temperature curing conditions in ultra-high geothermal tunnels. *Constr. Build. Mater.* **2019**, *229*, 116989. [[CrossRef](#)]
5. Liu, W.; Liang, S.; Shi, C. Risk modelling and simulation of thermal safety in underground railway tunnel surrounding. *Accid. Anal. Prev.* **2022**, *168*, 106620. [[CrossRef](#)] [[PubMed](#)]
6. Lin, M.; Zhou, P.; Jiang, Y.; Zhou, F.; Lin, J.; Wang, Z. Numerical investigation on comprehensive control system of cooling and heat insulation for high geothermal tunnel: A case study on the highway tunnel with the highest temperature in China. *Int. J. Therm. Sci.* **2022**, *173*, 107385. [[CrossRef](#)]

7. Yunpeng, H.; Mingnian, W.; Qiling, W.; Dagang, L.; Jianjun, T. Field test of thermal environment and thermal adaptation of workers in high geothermal tunnel. *Build. Environ.* **2019**, *160*, 106174. [[CrossRef](#)]
8. Lee, J.; Lee, W.; Choi, W.-J.; Kang, S.-K.; Ham, S. Association between Exposure to Extreme Temperature and Injury at the Workplace. *Int. J. Environ. Res. Public Health* **2019**, *16*, 4955. [[CrossRef](#)]
9. Bidassej-Manilal, S.; Wright, C.Y.; Engelbrecht, J.C.; Albers, P.N.; Garland, R.M.; Matooane, M. Students' Perceived Heat-Health Symptoms Increased with Warmer Classroom Temperatures. *Int. J. Environ. Res. Public Health* **2016**, *13*, 566. [[CrossRef](#)]
10. Mohammadnia, A.; Ziapour, B.M.; Sedaghati, F.; Rosendahl, L.; Rezanian, A. Fan operating condition effect on performance of self-cooling thermoelectric generator system. *Energy* **2021**, *224*, 120177. [[CrossRef](#)]
11. Wang, Y. Case study on ventilation and cooling control technology of multi heat source coupling in long distance subsea tunnel construction. *Case Stud. Therm. Eng.* **2021**, *26*, 101061. [[CrossRef](#)]
12. Chen, Q.; Zhang, H.; Zhu, Y.; Chen, S.; Ran, G. Study on distributions of airflow velocity and convective heat transfer coefficient characterizing duct ventilation in a construction tunnel. *Build. Environ.* **2021**, *188*, 107464. [[CrossRef](#)]
13. Wang, K.; Li, Q.; Wang, J.; Yang, S. Thermodynamic characteristics of deep space: Hot hazard control case study in 1010-m-deep mine. *Case Stud. Therm. Eng.* **2021**, *28*, 101656. [[CrossRef](#)]
14. Qiaoyun, H.; Yi, Z.; Kongqing, L.; Shenghua, Z. Computational evaluation of cooling system under deep hot and humid coal mine in China: A thermal comfort study. *Tunn. Undergr. Space Technol.* **2019**, *90*, 394–403. [[CrossRef](#)]
15. Bornman, W.; Dirker, J.; Arndt, D.C.; Meyer, J.P. Integrated energy simulation of a deep level mine cooling system through a combination of forward and first-principle models applied to system-side parameters. *Appl. Therm. Eng.* **2017**, *123*, 1166–1180. [[CrossRef](#)]
16. Li, X.; Fu, H. Development of an Efficient Cooling Strategy in the Heading Face of Underground Mines. *Energies* **2020**, *13*, 1116. [[CrossRef](#)]
17. Luo, X.; Wang, Y.; Zhao, J.; Chen, Y.; Mo, S.; Gong, Y. Grey relational analysis of an integrated cascade utilization system of geothermal water. *Int. J. Green Energy* **2014**, *13*, 14–27. [[CrossRef](#)]
18. Buhmann, P.; Moormann, C.; Westrich, B.; Pralle, N.; Friedemann, W. Tunnel geothermics—A German experience with renewable energy concepts in tunnel projects. *Géoméch. Energy Environ.* **2016**, *8*, 1–7. [[CrossRef](#)]
19. Zhang, G.; Xia, C.; Zhao, X.; Zhou, S. Effect of ventilation on the thermal performance of tunnel lining GHEs. *Appl. Therm. Eng.* **2016**, *93*, 416–424. [[CrossRef](#)]
20. Yang, C.; Peng, F.-L.; Xu, K.; Zheng, L.-N. Feasibility study on the geothermal utility tunnel system. *Sustain. Cities Soc.* **2019**, *46*, 101445. [[CrossRef](#)]
21. Xu, Y.; Li, Z.; Chen, Y.; Jia, M.; Zhang, M.; Li, R. Synergetic mining of geothermal energy in deep mines: An innovative method for heat hazard control. *Appl. Therm. Eng.* **2022**, *210*, 118398. [[CrossRef](#)]
22. Zhang, G.; Cao, Z.; Wang, W.; Mei, X.; Zhao, X.; Shen, S.; Na, T. Field test and numerical investigation on thermal environment of tunnel with air layer structure. *Build. Environ.* **2021**, *203*, 108105. [[CrossRef](#)]
23. Kang, F.; Li, Y.; Tang, C. Numerical study on airflow temperature field in a high-temperature tunnel with insulation layer. *Appl. Therm. Eng.* **2022**, *179*, 115654. [[CrossRef](#)]
24. Yao, W.; Lyimo, H.; Pang, J. Evolution regularity of temperature field of active heat insulation roadway considering thermal insulation spraying and grouting: A case study of Zhujidong Coal Mine, China. *High Temp. Mater. Process.* **2021**, *40*, 151–170. [[CrossRef](#)]
25. Szlázak, N.; Obracaj, D.; Swolkień, J. Thermal Insulation of Excavations and Its Effect on Climate Conditions. *Energies* **2021**, *14*, 4170. [[CrossRef](#)]
26. Dalla Santa, G.; Galgaro, A.; Sassi, R.; Cultrera, M.; Scotton, P.; Mueller, J.; Bertermann, D.; Mendrinis, D.; Pasquali, R.; Perego, R.; et al. An updated ground thermal properties database for GSHP applications. *Geothermics* **2020**, *85*, 101758. [[CrossRef](#)]
27. Zhu, J.; Liu, Q.; Ju, Q.; Fan, J. Geothermal distribution and thermal damage prediction in Xutuan Coal Mine. *Coal Eng.* **2021**, *53*, 131–135. (In Chinese)
28. Amiri, L.; Ghoreishi-Madiseh, S.A.; Sasmito, A.P.; Hassani, F.P. Effect of buoyancy-driven natural convection in a rock-pit mine air preconditioning system acting as a large-scale thermal energy storage mass. *Appl. Energy* **2018**, *221*, 268–279. [[CrossRef](#)]
29. Galgaro, A.; Dalla Santa, G.; Cola, S.; Cultrera, M.; De Carli, M.; Conforti, F.; Scotton, P.; Viesi, D.; Fauri, M. Underground warehouses for food storage in the Dolomites (Eastern alps-Italy) and energy efficiency. *Tunn. Undergr. Sp. Tech.* **2020**, *102*, 103411. [[CrossRef](#)]
30. Xu, Y.; Li, Z.; Liu, H.; Jia, M.; Wang, Q.; Zhang, M.; Xu, Y. Modeling of the dynamic behaviors of heat transfer during the construction of roadway using moving mesh. *Case Stud. Therm. Eng.* **2021**, *26*, 100958. [[CrossRef](#)]
31. Li, Z.; Liu, H.; Xu, Y.; Li, R.; Jia, M.; Zhang, M. Numerical Analysis on the Thermal Performance in an Excavating Roadway with Auxiliary Ventilation System. *Int. J. Environ. Res. Public Health* **2021**, *18*, 1184. [[CrossRef](#)]
32. Wang, H.; Zhou, Q. Finite Element Analysis of Surrounding Rock with a Thermal Insulation Layer in a Deep Mine. *Math. Probl. Eng.* **2020**, *2020*, 5021853. [[CrossRef](#)]
33. Tu, R.; Huang, L.; Jin, A.; Zhang, M.; Hai, X. Characteristic studies of heat sources and performance analysis of free-cooling assisted air conditioning and ventilation systems for working faces of mineral mines. *Build. Simul.* **2021**, *14*, 1725–1736. [[CrossRef](#)]
34. Fang, Y.; Yao, Z.; Lei, S. Air flow and gas dispersion in the forced ventilation of a road tunnel during construction. *Undergr. Space* **2019**, *4*, 168–179. [[CrossRef](#)]

35. Hou, C.; Xin, S.; Zhang, L.; Liu, S.; Zhang, X. Foundation Research on Physicochemical Properties of Mine Insulation Materials. *Coatings* **2020**, *10*, 355. [[CrossRef](#)]
36. Zhang, Y.; Lu, S.; Zhang, X.; Gao, Y.; Jia, Y. Development of a novel heat barrier coating for deep mining application. *Aust. J. Mech. Eng.* **2018**, *16*, 112–116. [[CrossRef](#)]
37. Jiang, Y.; Xin, S.; Li, H.; Zhang, L.; Hou, C.; Zhang, Z.; Guo, J. Performance of Heat-Insulating Materials Doped with Basalt Fibres for Use in Mines. *Polymers* **2020**, *12*, 2057. [[CrossRef](#)]
38. Wang, Y.; Wang, C.; Gao, S.; Zheng, X.; Darkwa, J. The impact of thermal insulation on cooling energy consumption and optimal insulation thickness for underground tunnel. *Sustain. Energy Technol. Assess.* **2021**, *47*, 101495. [[CrossRef](#)]
39. Lakatos, Á.; Csík, A. Multiscale Thermal Investigations of Graphite Doped Polystyrene Thermal Insulation. *Polymers* **2022**, *14*, 1606. [[CrossRef](#)]
40. Tlajji, G.; Pennec, F.; Ouldboukhitine, S.; Ibrahim, M.; Biwolé, P. Hygrothermal performance of multilayer straw walls in different climates. *Constr. Build. Mater.* **2022**, *326*, 126873. [[CrossRef](#)]
41. Wang, J.; Wan, Z.; Zhang, H.; Wu, D.; Zhang, Y.; Wang, Y.; Xiong, L.; Wang, G. Application of Thermal Insulation Guniting Material to the High Geo-Temperature Roadway. *Adv. Civ. Eng.* **2020**, *2020*, 8853870. [[CrossRef](#)]
42. Jia, M.; Chen, Y.; Wu, L.; Wang, S.; Jian, C. Design of metal mine deep mining roadway thermal exchange simulation test platform. *Met. Mine* **2014**, *14*, 113–116. (In Chinese)
43. Zeng, Y.; Tao, L.; Ye, X.; Zhou, X.; Fang, Y.; Fan, L.; Liu, X.; Yang, Z. Temperature reduction for extra-long railway tunnel with high geotemperature by longitudinal ventilation. *Tunn. Undergr. Space Technol.* **2020**, *99*, 103381. [[CrossRef](#)]
44. Liu, K.; Guo, J.; Wan, L.; Xu, C. A model test study to optimize the ventilation system of a long expressway tunnel. *J. Wind. Eng. Ind. Aerodyn.* **2020**, *207*, 104393. [[CrossRef](#)]
45. Kalman, H.; Portnikov, D. Analyzing bulk density and void fraction: A. the effect of archimedes number. *Powder Technol.* **2021**, *381*, 477–487. [[CrossRef](#)]
46. Lee, J.-C.; Bang, K.-S.; Yu, S.-H.; Choi, W.-S.; Ko, S. Similarity analysis of thermal-fluid flow for thermal testing using scaled-down model of spent fuel storage cask. *Ann. Nucl. Energy* **2020**, *149*, 107791. [[CrossRef](#)]
47. Осипова, В.А. *Experimental Research on Heat Transfer*, 1st ed.; Higher Education Press (Chinese Translation): Beijing, China, 1982.
48. Shah, N.A.; Animasaun, I.; Ibraheem, R.; Babatunde, H.; Sandeep, N.; Pop, I. Scrutinization of the effects of Grashof number on the flow of different fluids driven by convection over various surfaces. *J. Mol. Liq.* **2018**, *249*, 980–990. [[CrossRef](#)]
49. Paradis, P.; Champlaud, H. New correlations for heat transfer in parallel-plate ducts at low Peclet number. *Int. J. Heat Mass Transf.* **2021**, *178*, 121595. [[CrossRef](#)]
50. Haymes, R.; Gal, E. Iterative multi-scale approach for heat conduction with free convection problem in periodic hollow structures. *Int. J. Therm. Sci.* **2020**, *158*, 106519. [[CrossRef](#)]
51. Xiu, Z.; Nie, W.; Yan, J.; Chen, D.; Cai, P.; Liu, Q.; Du, T.; Yang, B. Numerical simulation study on dust pollution characteristics and optimal dust control air flow rates during coal mine production. *J. Clean. Prod.* **2020**, *248*, 119197. [[CrossRef](#)]
52. Li, Z.; Wang, J.; Zhao, S.; Xu, Y. The effect of oxygen supply and oxygen distribution on single-head tunnel with different altitudes under mixed ventilation. *Indoor Built Environ.* **2022**, *31*, 972–987. [[CrossRef](#)]
53. Suresh, C.; Sundararajan, T.; Venkateshan, S.; Das, S.K.; Thansekhar, M. Heat transfer from a totally blocked fuel subassembly of a liquid metal fast breeder reactor: II. Numerical simulation. *Nucl. Eng. Des.* **2005**, *235*, 885–895. [[CrossRef](#)]
54. Freire, A.D.J.; Alexandre, J.L.C.; Silva, V.B.; Couto, N.D.; Rouboa, A. Compact buried pipes system analysis for indoor air conditioning. *Appl. Therm. Eng.* **2013**, *51*, 1124–1134. [[CrossRef](#)]
55. Chen, G.; Wang, Y.; Tang, L.; Wang, K.; Yu, Z. Large eddy simulation of thermally induced oscillatory flow in a thermoacoustic engine. *Appl. Energy* **2020**, *276*, 115458. [[CrossRef](#)]

Disclaimer/Publisher’s Note: The statements, opinions and data contained in all publications are solely those of the individual author(s) and contributor(s) and not of MDPI and/or the editor(s). MDPI and/or the editor(s) disclaim responsibility for any injury to people or property resulting from any ideas, methods, instructions or products referred to in the content.

MDPI
St. Alban-Anlage 66
4052 Basel
Switzerland
Tel. +41 61 683 77 34
Fax +41 61 302 89 18
www.mdpi.com

MDPI Books Editorial Office
E-mail: books@mdpi.com
www.mdpi.com/books





Academic Open
Access Publishing

www.mdpi.com

ISBN 978-3-0365-8227-6